Ground Vehicle Engineering Series

Driveline Systems of Ground Vehicles

Theory and Design



Alexandr F. Andreev
Viachaslau I. Kabanau
Vladimir V. Vantsevich

CRC Press
Taylor & Francis Group

Driveline Systems of Ground Vehicles

Theory and Design

Ground Vehicle Engineering Series

Driveline Systems of Ground Vehicles

Theory and Design

Alexandr F. Andreev

Viachaslau I. Kabanau

Vladimir V. Vantsevich

Vladimir V. Vantsevich, Scientific and Technical Editor

CRC Press
Taylor & Francis Group
Boca Raton London New York

CRC Press is an imprint of the
Taylor & Francis Group, an **informa** business

CRC Press
Taylor & Francis Group
6000 Broken Sound Parkway NW, Suite 300
Boca Raton, FL 33487-2742

© 2010 by Taylor and Francis Group, LLC
CRC Press is an imprint of Taylor & Francis Group, an Informa business

No claim to original U.S. Government works

Printed in the United States of America on acid-free paper
10 9 8 7 6 5 4 3 2 1

International Standard Book Number: 978-1-4398-1727-8 (Hardback)

This book contains information obtained from authentic and highly regarded sources. Reasonable efforts have been made to publish reliable data and information, but the author and publisher cannot assume responsibility for the validity of all materials or the consequences of their use. The authors and publishers have attempted to trace the copyright holders of all material reproduced in this publication and apologize to copyright holders if permission to publish in this form has not been obtained. If any copyright material has not been acknowledged please write and let us know so we may rectify in any future reprint.

Except as permitted under U.S. Copyright Law, no part of this book may be reprinted, reproduced, transmitted, or utilized in any form by any electronic, mechanical, or other means, now known or hereafter invented, including photocopying, microfilming, and recording, or in any information storage or retrieval system, without written permission from the publishers.

For permission to photocopy or use material electronically from this work, please access www.copyright.com (http://www.copyright.com/) or contact the Copyright Clearance Center, Inc. (CCC), 222 Rosewood Drive, Danvers, MA 01923, 978-750-8400. CCC is a not-for-profit organization that provides licenses and registration for a variety of users. For organizations that have been granted a photocopy license by the CCC, a separate system of payment has been arranged.

Trademark Notice: Product or corporate names may be trademarks or registered trademarks, and are used only for identification and explanation without intent to infringe.

Library of Congress Cataloging-in-Publication Data

Andreev, Aleksandr Fedorovich.
Driveline systems of ground vehicles : theory and design / authors, Alexandr F. Andreev, Viachaslau I. Kabanau, and Vladimir V. Vantsevich.
p. cm. -- (Ground vehicle engineering series)
"A CRC title."
Includes bibliographical references and index.
ISBN 978-1-4398-1727-8 (alk. paper)
1. Motor vehicles--Power trains. I. Kabanau, Viachaslau. II. Vantsevich, V. V. (Vladimir Vladimirovich) III. Title. IV. Series.

TL260.A532 2009
629.2'4--dc22 2009030197

Visit the Taylor & Francis Web site at
http://www.taylorandfrancis.com

and the CRC Press Web site at
http://www.crcpress.com

Dedication

In fond and respectful memory of Dr. Anatoliy Kh. Lefarov, engineer, scientist, and educator



My father, Anatoliy Khristoforovich Lefarov, was born on February 2, 1913, in a rural family of intellectuals. His father was an accountant and his mother was a teacher. From a young age, my father devoted his life to education and work. He graduated from a peasant's youth school in 1929 and from a technical school of agriculture in 1932. From 1934 onward, he worked as a grain-harvesting combine operator and as a driver of Caterpillar and International Harvester Farmall Tractors, first at the Evpatoria, and then at Simferopol farms that specialized in grain growing.

In recognition of the high quality of his professional work, the People's Agriculture Commissariat of the Crimean Autonomous Soviet Socialist Republic sent my father to Leningrad Industrial Institute (subsequently renamed as Leningrad Polytechnic Institute) in 1935, where he was successfully admitted.

Upon his admission to the institute, my father immediately devoted all his time and energy to his studies. His diligence, which consisted of studying 12–14 hour daily, did not fail to bear fruit. During the third year of his school, he became one of the best students in the institute and was awarded a higher-level stipend; he was later awarded the highest student honor at the time—the Stalin grantee.

Having graduated from the institute with honors in 1940, my father was assigned to work at the design department of the Gor'kiy Automotive Company (GAZ). He started his work under the guidance of one of the U.S.S.R. founders of the school of off-road equipment design—Vitaliy Andreyevich Grachev. It was precisely at this time that the direction of his scientific activity, which subsequently became his entire life purpose, germinated. Using his knowledge and through diligent work, he rapidly gained the respect of his coworkers and the leadership of the design office.

After Nazi Germany attacked the U.S.S.R. in 1941, my father was drafted and sent to the front. But he was soon recalled, as his engineering expertise was needed by the military, and he was returned to the GAZ design office. He continued working in this office donning the role of a senior designer. During the war, he designed and refined a number of mechanisms and assemblies of off-road wheeled and tracked vehicles for the military.

With the end of the war in 1945, my father, who was now a fully established expert, was transferred by the order of the Secretary of Automotive Industry of the U.S.S.R. to the Dnepropetrovsk Automobile Company (DAZ) as a deputy chief designer. Here fate again brought father together with his superior at the Gor'kiy Automotive Company, Vitaliy Andreyevich Grachev, who had been appointed as the chief designer of DAZ the previous year.

In DAZ, the following vehicles were designed under the guidance of V.A. Grachev with the direct participation of my father: the DAZ-150 4 ton self-loader, the DAZ-485 3-axle amphibian truck (LAT, large amphibian truck) for the military, the Ukraina passenger car, and other vehicles. But soon, by decree of the Soviet government the DAZ was switched to other manufacturing tasks and my father was sent to Minsk, the capital of Belarus, and appointed as the deputy chief design engineer at the Minsk Automotive Company (MAZ). In Minsk, he resumed his work with heavy-duty trucks, in particular, high-mobility trucks and tractors.

This was the time when the MAZ had just established a special design office (SKB-1 as further mentioned in the preface) for designing multiaxle rocket tractors. This office consisted of a large scientific, engineering, and manufacturing task force that subsequently not only established an entirely new direction in the design of military and civilian multi-wheel heavy-duty trucks but also became a prominent scientific and engineering school of the Soviet Union. This office was headed by Boris L'vovich Shaposhnik, a leading design engineer, and my father became his first deputy. The SKB-1 was established in 1954; the project of the base four-axis chassis MAZ-535 was already completed by 1955, and just a year later, the MAZ-537 tractor with a hydraulic gearbox, locked by a torque converter, lockable differentials, and independent suspension of all the wheels was also completed. In 1962, under the leadership and direct participation of my father, gear-type free-running differentials for heavy-duty MAZ tractors were designed. These differentials became an integral part of the driveline system of the well-known four-axle MAZ-543 chassis that went into production in 1962. The design of the differentials was so successful that they are still used on tractors that serve as carriers of various rocket launchers. Drs. Otto Ya. Zaslavskiy and Lev Kh. Gileles, who worked for many years with my father, write in their memoirs that my father had a sharp intellect, tact, and exceptional precision. This he most probably acquired from the old Russian engineering community and professors, some of whom remained in the Stalin years at Leningrad Polytechnic Institute, which was his alma mater. His colleagues made mention of the fact that he was the first one to point to the organic link between engineering developments and scientific studies, and was the first to call attention to the importance of intellectual property in modern society. He was the first staff member in the SKB-1 who was issued a certificate (Soviet equivalent of patent) for an invention. It is most likely that for these reasons my father performed experimental and analytic studies and wrote scientific works while being engaged in designing new vehicles. He authored articles and books and was the first in the SKB-1 to defend a PhD dissertation.

But father did not devote himself exclusively to military vehicles. He also worked actively on designing MAZ trucks, MAZ-501 and MAZ-509, and various modifications of the MAZ-537, for civil use. For example, he developed and put into production an original lightweight front axle for an all-wheel-drive timber carrier. The MAZ-501 automobile was the first automobile in the U.S.S.R. to employ a differential in the transfer case. This was a significant achievement for Dr. Lefarov as a designer. The locking differential designed and tested by my father under actual operating conditions started coming into use on MTZ-52 and MTZ-82 tractors of the Minsk Tractor Works, and also on the K-700 tractor of the Leningrad Tractor Company named after Kirov.

While working at the MAZ, my father, on the invitation of the administration of the College of Automobile and Tractor Engineering of Belarusian National Technical University (previously Belarusian Polytechnic Institute, BPI), Minsk, Belarus, became involved in teaching students—future experts in automobile and tractor engineering. He left his company in 1963 for the chair of the tractor engineering department of BPI.

In this institute, my father acquired students; he then established a school of study—a research group on multiwheel drive vehicles and driveline systems. His school investigated power distribution among the wheels connected with different types of driveline systems, and developed techniques of calculating the torque bias of self-locking differentials of different types. He also investigated the effect of many factors on the properties of locking and self-locking differentials.

The studies performed by father and his students were not restricted to two-axle automobiles and tractors, but concerned themselves with all multiaxle, many-wheel-drive vehicles. The main purpose of my father's school was, and still is, to find methods of optimizing the properties of systems of power distribution among the wheels and, in the final analysis, improving the overall mobility and other operational properties of wheeled vehicles operating under various road and off-road conditions.

As a result of the large volume of work performed at the SKB-1 and at the institute, my father defended his DSc dissertation (the highest degree in the U.S.S.R.) in 1976, and in 1977 he was conferred the rank of professor. For his contributions to the national machine-building industry, he was conferred the honorary title of Deserving Machine Builder of Belarus.

My father devoted all his life to work; more precisely, work was his entire life. He passed away on February 10, 1992, but left behind his scientific works, the automobiles and tractors that he designed, and, most importantly, his students who continue his work.

Dr. Victor A. Lefarov
Minsk, Belarus

Contents

Series Preface xiii
Preface xv
Acknowledgments xxi
Authors xxiii
List of Symbols xxv

1. Driveline Systems and Vehicle Performance 1
1.1 Brief Review of Driveline Systems History 1
1.1.1 First Wheeled Carriages 1
1.1.2 First Differential Transmissions 4
1.1.3 First Hybrid Cars and All-Wheel Drive Vehicles 7
1.1.4 Front-Wheel Drive Designs 7
1.1.5 First Mechanical Four-Wheel Drives 8
1.1.6 Invention of Pneumatic Tires and Design Measures for Improving the Poor-Terrain Mobility of Vehicles 9
1.1.7 Constant-Velocity Joints 12
1.1.8 All-Wheel and Multiwheel Drive Trucks and Passenger Cars 14
1.1.9 Power Dividing Units 28
1.2 Classification of Driveline Systems and Power Dividing Units 33
1.3 Wheel Dynamics and Energy Efficiency 56
1.3.1 Five Power-Loading Modes 56
1.3.2 Kinematic and Force Factors 61
1.3.2.1 Effective Rolling Radius and Slip Ratio 61
1.3.2.2 Wheel Force and Torque Factors 66
1.3.3 Wheel Power and Force Balance 70
1.3.4 Motion with a Slip Angle 75
1.3.4.1 Interaction between Longitudinal and Lateral Forces 75
1.3.4.2 Wheel Kinematic and Force Factors under Sideslip 77
1.4 Vehicle Energy/Fuel Efficiency and Driveline Systems Design 80
1.4.1 Mechanical Power Losses in Driveline Systems 82
1.4.2 Mechanical Power Losses in Wheel Systems 86
1.4.2.1 Tractive Operating Mode 86
1.4.2.2 Transportation Operating Mode 90
1.4.2.3 Combined Operating Mode 94
1.4.3 Fuel Efficiency of Multiwheel Drive Vehicles 96
1.5 Vehicle Performance and Driveline Systems Design 101
1.5.1 Traction and Velocity Properties of Vehicles 103
1.5.2 Mobility of Vehicles 106
1.5.3 Turnability 107
1.5.4 Stability of Motion 110
1.5.5 Handling of the Vehicle 112
1.6 Principles of Driveline System Design 114

2. Interwheel and Interaxle Open and Lockable Differentials 119
2.1 Kinematics and Dynamics of Differentials: The Gear-Ratio Concept 119
2.2 Kinematics of a Vehicle with an Interaxle Differential 132
2.2.1 Vehicle with Front-Steered Wheels 132
2.2.2 Vehicle with Front- and Rear-Steered Wheels 137
2.3 Tooth Forces in Bevel-Gear Differentials 139
2.3.1 Axial Forces in a Pinion-Side Gear Mesh 139
2.3.2 Total Axial Forces in Bevel Differentials 146
2.3.3 Force Evaluation: A Method for Practical Use 153
2.3.4 Experimental Results 157
2.3.5 Conclusion 159
2.4 Robustness of Differentials 161
2.5 Design of Axle/Interwheel Differentials 168
2.5.1 General Engineering Issues and Solutions 168
2.5.2 Design of Differential Geometry 185
2.5.2.1 Highway Heavy-Duty Trucks 189
2.5.2.2 Articulated Timber Carriers 191
2.5.2.3 Farm Tractors 195
2.5.3 Oil Lubrication Systems 202
2.6 Design of Interaxle Differentials and Transfer Cases 209
2.6.1 General Engineering Issues and Solutions 209
2.6.2 Design of Differential Geometry 219
2.6.3 Oil Lubrication Systems 227
2.6.3.1 Lubrication Systems for Interaxle Differentials of Driving Tandems 227
2.6.3.2 Lubrication Systems for Transfer Cases 233
2.7 Designing Locking Devices 238
2.8 Wheel Power Distribution and Vehicle Performance 249
2.8.1 Generalized Vehicle Parameters and Energy/Fuel Efficiency 249
2.8.2 Vehicle Tractive and Velocity Properties 264
2.8.3 Vehicle Turnability and Stability of Motion 268
2.9 Optimal and Reasonable Differential Gear Ratios: Control Principles 274

3. Automatic and Manual Positively Engaged Power-Dividing Units 289
3.1 Designs of Power-Dividing Units 289
3.2 Kinematic Discrepancy and Generalized Vehicle Parameters 301
3.2.1 Vehicles with 4×4 Wheel Formula 301
3.2.2 Vehicles with $2m \times 2n$ Wheel Formula 305
3.2.2.1 Vehicles with $2m \times 2n$ Wheel Formula in Rectilinear Motion 306
3.2.2.2 Vehicles with $2m \times 2n$ Wheel Formula with Steered Wheels in Curvilinear Motion 309
3.2.2.3 Articulated $2m \times 2n$ Vehicles with Steered Wheels 312
3.2.2.4 The Interwheel Positive Engagement 317
3.3 Wheel Slips and Circumferential Wheel Forces 318
3.3.1 4×4 Vehicles 319
3.3.2 $2m \times 2n$ Vehicles 326

3.4 Wheel Power Distributions and Vehicle Energy/Fuel Efficiency 330
3.4.1 Mechanical Power Losses in Wheel Systems 330
3.4.2 Mechanical Power Losses in Driveline Systems 338
3.4.3 Combined Power Losses in Driveline and Wheel Systems—Fuel Consumption 343
3.5 Wheel Power Distribution and Vehicle Performance 355
3.5.1 Vehicle Tractive and Velocity Operational Properties 355
3.5.2 Vehicle Turnability and Stability of Motion 358
3.6 Optimal and Reasonable Kinematic Discrepancy: Control Principles 368

4. Limited Slip Differentials 379
4.1 Torque Biasing and Locking Performance 379
4.2 Disk Differentials without Additional Lockers 385
4.3 Disk Differentials with Cam Lockers 391
4.4 Disk Differentials with V-Lockers 399
4.5 Worm-Gear Differentials 405
4.6 Cam-Plunger Differentials 413
4.7 Torque Sensitive Differentials 418
4.8 Speed Sensitive Differentials 432
4.9 Force Fluctuations in Disk Differentials 435
4.10 Tractive Performance and Yaw Moment of a Drive Axle 443
4.11 Asymmetrical Interaxle Differentials 448

5. Free-Running Differentials and Viscous Clutches 453
5.1 Design and Operating Principles of Free-Running Differentials 453
5.2 Applications of Free-Running Differentials 463
5.3 Viscous Clutches: Operation and Design Aspects 466

6. Combined Automated Mechanical Driveline Systems 475
6.1 Vehicle Operational Properties 475
6.1.1 Vehicles with Steered Wheels 475
6.1.2 Articulated Vehicles with Steered Wheels 486
6.2 A Method of Synthesizing Driveline Systems with Optimal Properties 492
6.3 Objective Function Analysis 496
6.4 Synthesis of the Properties of Interwheel Power-Dividing Units 510
6.5 Synthesis of Properties of Interaxle Power-Dividing Units 519
6.6 Synthesis of Properties of Interwheel and Interaxle Power-Dividing Units 531
6.6.1 The Mathematical Model of a Vehicle 531
6.6.2 Optimal Properties 539

7. Mechatronic Driveline Systems 555
7.1 Simple, Combined, and Integrated Driveline Systems—A Brief Overview 555
7.2 Inverse Wheel Dynamics and Control 560
7.3 Proactive Assessment of Terrain Conditions 568
7.4 Kinematics and Dynamics of Mechanical Subsystems 574

7.4.1 The Open Differential ... 577
7.4.2 Double Differentials ... 580
7.4.3 The Open Differential with Three-Link Planetary Rows ... 587
7.4.4 Single-Row Planetary Mechanism with Mating Pinions ... 591
7.5 Design of Simple and Combined Driveline Systems ... 596
7.6 Design of Integrated Driveline Systems ... 605
7.6.1 Optimal Power Distribution and Features of the System ... 606
7.6.2 Synthesis and Implementation of a Parallel Control Algorithm ... 620
7.6.2.1 Logical Control Languages ... 620
7.6.2.2 The Logical Control Algorithm ... 621
7.7 Hybrid Driveline Systems ... 626
7.7.1 Advanced Hybrid-Hydraulic Driveline Systems ... 626
7.7.2 Design Selection of the Kind and Standard Dimension of Hydraulic Units ... 639

8. Testing of Driveline Systems and Multiwheel Drive Vehicles ... 649
8.1 Laboratory Studies of the Locking Performance of Differentials ... 649
8.2 Laboratory Testing of Friction Clutches of Differentials ... 662
8.3 Laboratory Tests of Differential Lubrication Systems ... 667
8.4 4×4 Vehicle Chassis Dynamometer with Individual Roll Control ... 679
8.5 Field and Road Tests of Wheeled Vehicles ... 690

Problems and Questions ... 711

Bibliography ... 729

Index ... 743

Series Preface

Ground-vehicle engineering took shape as an engineering discipline in the twentieth century, and became the foundation for significant advancements and achievements, from personal transportation and agriculture machinery to lunar and planetary exploration. As we step into the twenty-first century faced with global economic challenges, there is a need to develop fundamentally novel vehicle engineering technologies, and effectively train future generations of engineers. The Ground Vehicle Engineering Series will unite high-caliber professionals from the industry and academia to produce top-quality professional/reference books and graduate-level textbooks on the engineering of various types of vehicles, including conventional and autonomous mobile machines, terrain and highway vehicles, and ground vehicles with novel concepts of motion.

The Ground Vehicle Engineering Series concentrates on conceptually new methodologies of vehicle dynamics and operation performance analysis and control, advanced vehicle and system design, experimental research and testing, and manufacturing technologies. Applications include, but are not limited to, heavy-duty multilink and pickup trucks; farm tractors and agriculture machinery; earthmoving machines; passenger cars; human-assist robotic vehicles; planetary rovers; military conventional and unmanned wheeled and track vehicles; and reconnaissance vehicles.

Dr. Vladimir V. Vantsevich
Series Editor

Preface

The dynamics and performance of a vehicle manifest themselves in the interaction of the vehicle with the surroundings and result from its properties such as energy/fuel efficiency, terrain mobility, tractive and velocity properties, vehicle turnability, stability of motion and handling, braking properties, and smoothness of ride. A distinctive feature in the design of vehicles with four or more driving wheels that is of great significance is that many of their properties depend markedly not only on the total power applied to all the driving wheels but also on the distribution of the total power among the wheels. Under given road or terrain conditions, the same vehicle with a constant total power at all the driving wheels, but with different power distributions among the driving axles and the left and right wheels of each axle, will perform differently; that is, the criteria of the above-mentioned vehicle properties will have different quantitative values. In practical engineering terms, this means that due to different power distributions among the driving wheels, a given vehicle will demonstrate variable fuel consumption, terrain mobility, and traction, and will accelerate differently and turn at different radii. Depending on the wheel power split, the vehicle can ''unexpectedly'' run into either understeering or oversteering and can sometimes become unstable, skidding in a lateral direction and eventually rolling over.

The power distribution among the driving wheels is largely determined by the vehicle's driveline system, which is generally defined as a part of the power train, located between the transmission and the driving wheels. A driveline system includes a set of mechanisms and subsystems which have been referred to in this book as power-dividing units (PDUs). Typically, a PDU has one input and two outputs. These units are employed in transfer cases, interaxle reduction gears, and driving axles. For a vehicle with one engine and with a conventional axle-type driveline system layout (which differs from the left–right side layout), the number of PDUs is equal to the number of the driving wheels less one. For example, a vehicle with four driving wheels will have three PDUs and a vehicle with eight driving wheels will have seven PDUs (see Figure 1).

It should be obvious to the reader that the number of combinations of mechanisms and subsystems that can be employed even in three PDUs of a vehicle with two driving axles is virtually limitless. In fact, a list of such mechanisms and subsystems may be compiled of open differentials and positively locked units, limited slip differentials with all kinds of torque biases, mechanically and electronically locked differentials, viscous couplings, NoSPINs, and also most current developments that are commonly referred to as torque-vectoring or torque-management systems.

This gives rise to two fundamental engineering problems: First, how to investigate the effect of different driveline systems on the properties of vehicles, their dynamics, and performance? Second, how to determine the optimal characteristics of the driveline system and its PDUs and then design them for a specific vehicle in a manner that would ensure a high level of dynamics and performance, mobility and fuel efficiency, traction and acceleration, and stability of motion and turnability?

Probably the first study of the effect of a driveline system on vehicle motion was the research paper of Prof. Nikolay E. Zhukovskiy, titled ''The theory of the instrument of engineer Romeyko-Gurko,'' published in 1903. The developments in the theory, design, and manufacture of vehicles with four or more driving wheels—all-wheel drive and multiwheel drive vehicles (see Section 1.2)—were to a large extent facilitated by

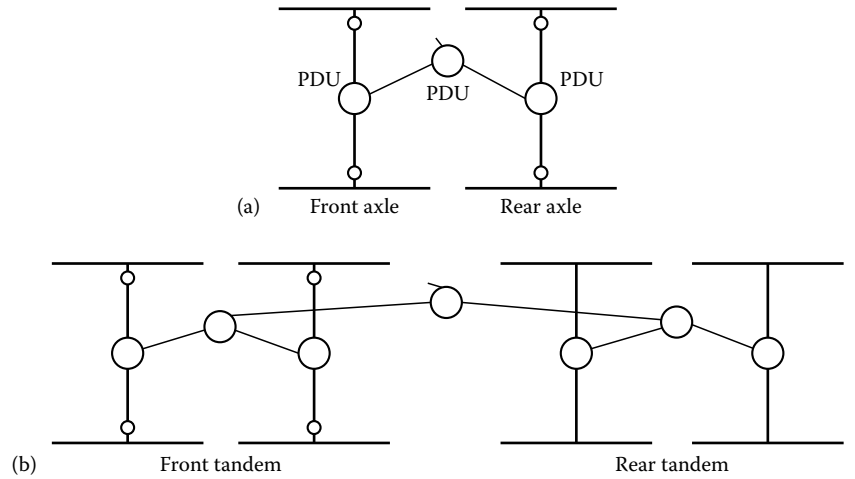


FIGURE 1
Driveline system layouts of (a) 4 × 4 and (b) 8 × 8 vehicles.

experience gathered during World War II: The shortage of arterial and high-type roads and the poor terrain mobility of vehicles determined how military applications progressed for many postwar years. After World War II, with the development of hard-surface roads, multiwheel drive vehicle layouts were actively designed and employed in the agriculture sector, and in construction, forestry, and the petroleum industry. At a later stage when space research and space flights began, planet rovers were also designed with all the wheels driven by torque. From the 1980s onward, passenger cars and sport-utility vehicles with four driving wheels became very popular. The twentieth century thus saw the emergence of multiwheel-drive vehicles of all types. In conjunction with this, the names of many engineers, researchers, and professors, who developed the theory of motion of vehicles and the practice of driveline system design, should be mentioned here. This is a very difficult task and I fully realize that I could fail to mention many of them. However, the following persons deserve special mention: Yakov S. Ageykin, Alexander S. Antonov, Dmitriy A. Antonov, Pavel V. Aksenov, Mieczyslaw G. Bekker, Nikolay F. Bocharov, G. Broulhiet, Colin Chapman, Evgeniy A. Chudakov, Keith Duckworth, J. R. Ellis, Yaroslav E. Farobin, Thomas G. Gillespie, Wunibald Kamm, Frederick W. Lanchester, Andrey S. Litvinov, William F. Milliken and Douglas L. Milliken, M. Mitschke, Tatsuro Muro, Maurice Olley, Hans B. Pacejka, Vladimir A. Petrushov, Yuliy V. Pirkovskiy, Vladimir F. Platonov, A.R. Reece, Robin Sharp, Anatoliy T. Skoybeda, Gleb A. Smirnov, Sergei B. Shukhman, Jaroslav J. Taborek, Igor S. Tsitovich, Jo Y. Wong, and Georgiy V. Zimelev.

Engineering designers and their design developments are now part of history; notable engineers among them include N.A. Astrov, Marius Berliet, William Besserdich, Carl Borgward, Henry Bussing, Carlo Cavalli, John W. Christie, V.E. Chvyalev, Wesley M. Dick, G.A. Fest, V.A. Grachev, Nikolay I. Korotonoshko, A.M. Kriger, I.P. Ksenevich, Nils Magnus, Alfred Masury, A.A. Lipgart, Ralf Nash, Ferdinand Porsche, Wilfredo Ricart, Delmar B. Roos, B.L. Shaposhnik, and M.S. Vysotskij. Vitali A. Grachev, chief design engineer, who has designed many forms of multiwheel drive vehicles, became legendary in the former U.S.S.R. among experts who designed military vehicles. Boris L. Shaposhnik established the Special Design Office, known by its Russian-language acronym, SKB-1, in Minsk, Belarus, where new-generation vehicles, such as multiwheel drive missile carriers,

were designed. Vladimir E. Chvyalev followed in the footsteps of B.L. Shaposhnik. He headed the design department of the Minsk Wheeled Tractors Company that grew out of SKB-1. Dr. Mikhail S. Vysotskij, academician at the National Academy of Sciences of Belarus and chief design engineer of automotive vehicles in Belarus led the design of heavy-duty vehicular trains. Even now, in spite of advancing years, he directs a scientific research institute of the National Academy of Sciences.

Another eminent individual in the field, Professor Anatoliy Kh. Lefarov, a design engineer, subsequently became a professor of Belarusian National Technical University (the current name), Minsk, Belarus; Dr. Lefarov was the deputy of chief design engineer, V.A. Grachev, and the first deputy of chief design engineer, B.L. Shaposhnik. During the 1960s, Dr. Lefarov established a research group in the field of multiwheel drive vehicles that designed various driveline systems and PDUs and performed analytic and experimental studies on the effect of driveline systems on the properties of vehicles.

We have been associated with Dr. Lefarov's research group for our entire professional lives. Dr. Kabanau was his first postgraduate student and then became the principal design engineer, who has to his credit designed many mechanisms and systems. Dr. Andreev is concerned with simulating the motion of vehicles and designing PDUs. Seventeen professionally fortunate years, which have rapidly slipped away, with our leader united me not only in a common endeavor but also in a binding friendship. Dr. Lefarov has shaped me not only as an expert but also as a human being. It so happened that after he passed away in 1992, I became the leader of our group.

The culmination of all of this has led to this book. This book comprehensively covers the subject matter from a historic overview, classification, and the nature of driveline influence on vehicle dynamics and performance (Chapter 1), through analytical fundamentals (Chapters 2 through 5) and optimization and control of wheel power distributions (Chapters 6 and 7), to mechanical and mechatronic design of advanced systems (Chapters 2 through 7) and experimental research and tests (Chapter 8). Also, I believe the readers will thoroughly enjoy the illustrations, hand-drawn by Dr. Kabanau.

In many ways, this book is unique; it is probably the only book that deals with the solution of the two fundamental engineering problems that were formulated earlier in the preface. Therefore, the reader can see that the book presents an analytical treatment of driveline systems research, design, and tests based on vehicle dynamics and performance requirements. Methodologically, this is described in two ways. First, the book introduces analytical tools for studying the driveline effects on power distribution among the driving wheels and then on the dynamics and performance of vehicles. Engineering applications of these tools, for instance, include the comparative analysis of several driveline systems with the purpose of selecting a driveline system that provides a given vehicle with better performance and also to evaluate same-class vehicles with different driveline systems. Additionally, the developed techniques adequately supplement the mathematical modeling of vehicle dynamics. Chapters 1 through 5 and Chapter 7 present the necessary material for such mathematical modeling of driveline systems that can be compiled of different types of PDUs. All analytical techniques were built based on the so-called generalized vehicle parameters, which integrate characteristics of PDUs with tire (or combined tire/soil) characteristics and, implicitly, suspension characteristics.

Second, the book develops methodologies for the synthesis of optimal characteristics of PDUs that can be applied to different types of vehicles. Thus, a researcher would not need to run a comparative analysis of hundreds of potential driveline systems to try to find a better one for the vehicle under design. Instead, optimal characteristics can be directly achieved and then optimal PDUs can be designed. Respective analytical techniques were

based on the principles of driveline system designs that were developed on the inverse vehicle dynamics approach and first introduced in this book. To learn more about the inverse vehicle dynamics approach and the optimization of power distribution among the driving wheels, the reader should start with Sections 1.5 and 1.6, then go through Sections 2.9 and 3.6, and finally to Chapters 6 and 7. The mechanical design of PDUs and control development issues are covered in Chapters 2 through 5, and also in Chapter 7.

The book is also unique in the sense that it was written virtually entirely on the basis of the results of investigations by its authors. All analytical tools, and computational, design, and test methods were verified through many engineering projects; some of the projects are presented in this book as illustrative examples to prove the applicability of the developed theories. The material in this book will provide the reader with answers to intriguing engineering problems such as achieving higher energy/fuel efficiency of a vehicle by driving either all the wheels or not all the wheels, obtaining oversteering characteristics by increasing the torque at the front-steered wheels, and many other such technical problems. Engineering workers will find interesting methods of design and experimental studies of new driveline systems that provide for optimal/specified vehicle properties. The presented methodologies and results on the optimization of wheel power distributions among the driving wheels can also be of interest to engineers working on vehicles with individual wheel drives and vehicles with hybrid driveline systems.

The reader will find only some of the references in the text to the detailed bibliography at the end of the book. The bibliography reflects that, to a large degree, the history of investigations in driveline system engineering and vehicle dynamics during the twentieth century and the start of the twenty-first century was compiled by studying a large number of publications and it should be regarded as a source of additional engineering data; after all, the experience of each expert is unique. We have conscientiously investigated publications on the theory of motion of all-wheel-drive vehicles and on driveline system design for many years and, if we missed some important investigations and did not include them in the bibliography, we apologize to the authors. We have also included some of our own publications in the bibliography that reflect not only the results of investigations but also, by representing a sequence, give an idea about the development of our scientific and engineering approaches to, and methods of, solutions for engineering problems.

The volume of the scientific and engineering information and the structure of its arrangement within the book are such that it could be used both by beginning design and test engineers as well as engineers with experience in the design and experimental studies of various PDUs, driveline systems, and multiwheel drive ground vehicles as a whole. The book will also be useful to research engineers involved in simulating motion and in testing multiwheel drive vehicles, because it illuminates many aspects of the mathematical simulation of the different driveline systems and dynamics of such vehicles, something that is usually not examined in classical textbooks on vehicle dynamics. The simulation of vehicle dynamics on the basis of the inverse dynamics approach is also a topic that is examined in this book for the first time. This method is also used for working out algorithms for the control of mechatronic driveline systems.

For many years, we developed and delivered university-level courses on the theory of vehicle motion and on the design of driveline systems. This book was written with reference to these courses and can therefore also be used as a textbook on advanced vehicle dynamics and on the design of driveline systems in master of science and PhD courses. Thereby, all the mathematical formulae in the book have been derived together with the necessary detailed explanations, something that makes the material easily comprehensible and convenient both for the student and the lecturer. The analytical results are illustrated by

quantitative examples (illustrative problems) and examples of developing driveline systems and PDUs. Using our experience, we devised engineering problems associated with the dynamics of vehicular motion, design, and testing of driveline systems. These problems developed for each chapter can be used in the course of studies as examination problems or homework assignments, and also by practicing engineers for better familiarization with the material in the book and for illustrating its underlying theoretical principles.

Dr. Vladimir V. Vantsevich
Southfield, Michigan

Acknowledgments

We regard it as a pleasure to express our appreciation to our colleagues whom we invited to participate and write sections of the book. More than 30 years of friendship and mutual work link me with Dr. Sergei I. Strigunov and Dr. Vladimir S. Voiteshonok. We studied together in the university and then worked with Dr. Lefarov. Dr. Strigunov presented the results of his studies and participated in writing Sections 3.1, 3.2, 3.3.1, 3.4, and 8.5. Dr. Voiteshonok contributed the results of his studies and participated in writing Sections 2.5.1, 3.6, and 8.5.

In the course of writing this book, we had the pleasure of continuing cooperation with my first PhD student and currently chief design engineer, Front Driving Axles and Wheel Systems at P/A Minsk Tractor Works, Belarus—Dr. Valeriy Yermalionak. Dr. Yermalionak participated in writing Sections 2.5.1, 2.6.1, and 2.7. He also supplied some material for Sections 1.2 and 4.4.

Dr. Siarhei V. Kharytonchyk, also my PhD student and currently the head of the computer center at the Joint Institute of Mechanical Engineering, National Academy of Sciences of Belarus, participated in the investigations that are jointly described in Section 7.6. Together with another PhD student, Dr. Gennady Valyuzhenich, we tested the differential lubrication systems, which we have described in Section 8.3.

I collaborated with Dr. Arkadij D. Zakrevskij, corresponding member of the National Academy of Sciences of Belarus, who works in the field of parallel logical control algorithms. Some of the results of his studies and their application to the design of mechatronic systems have been included in Section 7.6.2, which was jointly written.

It has been almost 15 years since I first collaborated with Dr. Gemunu S. Happawana, professor at California State University at Fresno, Fresno, California. Dr. Happawana participated in writing Sections 2.1, 6.5, and 7.6.1.

For many years, I was lucky to enjoy the friendship and professional collaboration of Dr. Yuliy V. Pirkovskiy, and, after his passing, of his successor Dr. Sergei B. Shukhman. I am glad that the book includes Sections 7.7.1 and 7.7.2, written by Dr. Shukhman and his colleague Dr. Evgenij I. Prochko.

We would like to express our gratitude to the heads of Lawrence Technological University, Southfield, Michigan—President Dr. Lewis N. Walker, Provost Dr. Maria J. Vaz, and Associate Provost Dr. Steven K. Howell—for their financial support for the translation of the manuscript.

This book was written during a transitional period of my life, when I was taking up work at Lawrence Technological University.

I wish to express my heartfelt gratitude for professional collaboration and friendship, technical and personal advice, and fruitful discussions to Dr. William Begell, Professor Eugene I. Rivin, Dr. Joseph and Mrs. Sally Wolf, Dr. Moisey and Mrs. Vera Shkolnikov, Dr. Lev Gileles and Dr. Otto Zaslavskiy, Dr. Simon and Mrs. Larisa Itskovich, Dr. Guennadi Koulechov and Svetlana Skalskaya, Robert Edmonson, Mr. John and Mrs. Carol Erickson, Mr. James and Mrs. Sandra Fisher, Mr. Patric and Mrs. Maryann Hermes, Joanne Kowalenok, Mr. Ephim and Mrs. Anna Schmidt, Mr. Volodymyr and Mrs. Lyubov Shesiuk, Dr. Jan and Mrs. Nadzia Zaprudnik, Dr. Vitaut Kipiel, Mr. Allen M. Krass, and many colleagues and friends in academia and industry, and my church.

We would like to express our gratitude to Dr. Mircea Gradu, Chrysler LLC; Celso Fratta, Eaton Corp.; Dr. Sankar Mohan, Magna Powertrain; and Dr. Alexandre F. Opeiko, Chrysler LLC, for their professional and constructive comments and suggestions.

The publication of this book owes a great deal to the painstaking labor of Dov Lederman, BME, interpreter, to whom we express our gratitude and appreciation.

The time spent in writing the book was irreversibly taken away from family time. We are immeasurably grateful to our spouses and children for their understanding of the importance of our contribution to the profession, and for their unwavering love and support.

When I was still a student, I once asked Dr. Lefarov why he had not written his autobiography. His reply was surprising and it took me years to understand and accept it. He said that his life as a person is not of much interest—after all it is very similar to the lives of millions of people in the country where we live. Dr. Lefarov added that it would be much more interesting to read our engineering books, which reflect not only the progress made in the field of engineering, but also, frequently, give insight about the lives of the authors at a professional, social, and sometimes even personal level. He did not leave any remarks concerning his life. These were written for this book by his son, Dr. Victor A. Lefarov.

As for engineering books, our new book is now held by the readers. The authors hope that this book will be useful. As Dr. Lefarov once said, the engineer must remember that any redundant line on the blueprint of an design may require an additional machine tool and maybe even an entire automatic production line. If the publication of this book reduces the number of ''redundant lines,'' that is, mistakes, and results in the appearance of more advanced driveline systems and causes more young engineering experts to become professionally associated with multiwheel drive vehicle engineering, the authors will have the satisfaction of having achieved their goal. Any remarks and comments will be gratefully received.

Dr. Vladimir V. Vantsevich
Southfield, Michigan

Authors



Alexandr F. Andreev has been an associate professor in tractor engineering at the College of Automobile and Tractor Engineering, Belarusian National Technical University, since 1975. He received his PhD in automobile and tractor engineering in 1972. Dr. Andreev has also worked as a leading researcher in vehicle dynamics and vehicle performance analysis of the Research and Design Group on Multi-Wheel Drive Vehicles since the founding of the group in 1963. His research concentrates on motion modeling, design, and computation of ground transport and tractive vehicles, and vehicle systems. Dr. Andreev served as the principal investigator to 11 research programs and projects, and contributed to 57 more projects with his innovative analytical models of vehicles in motion, driveline systems, and tire–ground interaction models. His designs of limited slip differentials have been employed in 4×4 farm tractors and multiwheel drive terrain trucks.

Dr. Andreev has written 19 internal research reports, and has published 4 technical books and graduate level texts on vehicle driveline system design and computation, hydraulic and pneumatic control systems, and hydro-drive design and engineering. He has authorized 22 research papers published in journals and conference proceedings, and has received 8 certified inventions.

Professor Andreev developed standards and curricula for MSc programs in tractor engineering, mobile track and wheeled vehicle engineering, and urban electric vehicle engineering. He served at the Higher Education Publishing House of Belarus for 15 years, and as the executive editor of two major research journals in Belarus: *Automobile and Tractor Engineering* and *Design, Computation and Operation of Automobiles and Tractors*.



Dr. Viachaslau I. Kabanau has been an associate professor at the College of Automobile and Tractor Engineering, Belarusian National Technical University, ever since he received his PhD in automobile and tractor engineering in 1966. He also served as the associate dean of the college for 10 years. Dr. Kabanau has worked as a leading researcher and the principal design engineer of the Research and Design Group on Multiwheel Drive Vehicles since the founding of the group in 1963. His research and design work focuses on vehicle driveline systems and mechanism design, and vehicle experimental research. Dr. Kabanau participated in and contributed with his original designs of transfer cases, differentials with lubrication systems, locking and free-running differentials to more than 20 R&D programs and projects on terrain and highway truck and farm tractor engineering. Dr. Kabanau has authorized 6 technical books, graduate level texts, and brochures; he has published 40 reviewed papers in research journals and conference proceedings, and

has received 11 certified inventions. He has also delivered a number of presentations and invited lectures to industry and universities.

Professor Kabanau actively developed innovative academic programs and courses in tractor engineering. His lecture courses on hydro dynamic drive engineering, vehicle experimental research and tests, vehicle art design, and ergonomics have been of immeasurable service to the College of Automobile and Tractor Engineering and also established him as an outstanding teacher and student project advisor.



Vladimir V. Vantsevich is a professor in mechanical engineering and the founding director of the MSc in Mechatronic Systems Engineering Program and the Laboratory of Mechatronic Systems at Lawrence Technological University, Michigan. He is also a cofounder and associate director of the Automotive Engineering Institute. Before joining Lawrence Tech, Dr. Vantsevich was a professor and the head of the Research and Design Group on Multiwheel Drive Vehicles that designed and developed a number of mechatronic and mechanical driveline systems for multipurpose vehicles in Belarus. He received his PhD and DSc (the highest degree in the former U.S.S.R.) in automobile and tractor engineering from the Belarusian National Technical University approved by the Higher Awarding Committee of the Russian Federation.

Professor Vantsevich's research area is inverse and direct dynamics of mechanical and mechatronic systems, and system modeling, design, and control. Applications include conventional and autonomous, multiwheel ground vehicles, and vehicle locomotion and driveline systems. He developed a novel research avenue—*inverse ground vehicle dynamics*—which is the basis of his optimization of power distribution among the driving wheels and control of vehicle performance including vehicle mobility, energy/fuel consumption, traction and acceleration performance, and stability of motion.

He is the author of 5 technical books and more than 100 research papers on inverse dynamics, vehicle performance and energy efficiency optimization and control, and design of driveline and autonomous wheel power management systems. Professor Vantsevich has participated in more than 110 science seminars, and has delivered lectures and technical presentations at academic institutions, professional societies, and to industry. He is a registered inventor of the U.S.S.R. and holds 30 certified inventions.

Professor Vantsevich is the founder and editor of a series of handbooks, textbooks, and references on ground vehicle engineering at Taylor & Francis Group/CRC Press. He is a member of the editorial boards of the *International Journal of Vehicle Autonomous Systems,* the *Journal of Multi-Body Dynamics* (Part K of the Proceedings of the Institution of Mechanical Engineers), and the *International Journal of Advanced Mechatronics and Robotics*. He is also an associate editor of the *International Journal of Vehicle Noise and Vibration*.

Professor Vantsevich was honored with a fellowship of the American Society of Mechanical Engineers and of the Belarusan Institute of Arts and Sciences, New Jersey. He is a member of the Association of Vehicle Autonomous Systems International, the Society of Automotive Engineers, the International Society for Terrain-Vehicle Systems, and the International Association for Vehicle System Dynamics.

List of Symbols

Symbol	Definition	First Mentioned and Explained in Section
a	Distance between the gravity center and the front axle of a vehicle with two axles	Section 2.2
$a_{dr}, a_n, a_f, a_d, a_b$	Tire off-set distance, the distance between the line of the normal reaction of a wheel and the wheel axis of rotation in the driven, neutral, free, diving, and braking modes	Section 1.3
a_x	Longitudinal acceleration of the center of the wheel; also vehicle acceleration in straight line motion	Sections 1.3 and 1.4
a_y	Vehicle lateral acceleration	Section 1.5
A	Geometric parameter of limited slip differential	Section 4.2
A_d	Conditional cross-sectional area of a bevel gear differential	Section 2.5
b	Distance between the gravity center and the rear axle of a vehicle with two axles	Section 2.2
b	Tooth width	
B	Geometric parameter of limited slip differential	Section 4.2
B_a	Width of the implement's sweep	Section 1.5
C	Geometric parameter of limited slip differential	Section 4.3
C_c	Constant specific for a particular limited slip differential	Section 4.7
C_{pi}	Suspension stiffness factor reduced to a wheel	Section 6.6
C_{ti}	Tire (tire and soil for deformable surfaces) normal stiffness factor	Section 6.6
d_a	Diameter of the addendum circle	Section 2.3
d_{go}, d_{gi}	Outer and inner friction diameters of a bevel side gear with the case of a differential	Section 2.5
d_{po}, d_{pi}	Outer and inner friction diameters of a pinion with the case of a differential	Section 2.5
d_{sc}	Spider pin diameter in contact with the case of a differential	Section 2.5
d_{sp}	Spider pin diameter in contact with the pinion	Section 2.5
D	Geometric parameter of limited slip differential	Section 4.3
D_a	Air drag	Section 2.5
D_a	Vehicle air dynamic force (air drag)	Section 1.4
E	Shift of center of turn	Section 1.5
f	Rolling resistance coefficient	Section 1.3
f_0	Rolling resistance coefficient at the creeper speed	Section 6.6
F_0	Force in the contact between the spider and the differential's housing	Section 2.5
F_l	Wheel lateral reaction	Section 1.3

F_l^a	Component of the wheel lateral reaction exerted by the interaxle power dividing unit	Section 2.8
F_l^{max}	Maximal wheel lateral reaction limited by the deformation properties of the tire and the soil	Section 1.3
F_l^w	Component of the wheel lateral reaction exerted by the interwheel power dividing unit	Section 2.8
F_a	D'Alambert's force	Section 1.4
F_b	Force in the contact between the spider and the pinion	Section 2.5
F_d	Vehicle drawbar pull load	Section 1.4
F_d	Drawbar pull	Section 2.5
$F_{frame\,x}$	A force acting on a wheel from the vehicle frame in x-direction (frame force)	Section 1.3
F_k	Radial force acting between cams of a side gear and an intermedium cam bushing	Section 4.3
F_x	Wheel circumferential (tangential) force	Section 1.3
$F_{x\Sigma}$	Vehicle total circumferential force	Section 1.4
F_x^{max}	Maximum circumferential wheel force that can be attained at the contact between the wheel and the surface of motion	Section 1.3
F_w	Wheel traction force (or net tractive force)	Section 1.3
F_ψ	Total force of resistance to vehicle motion	Section 1.5
g_d	Drawbar pull–specific fuel consumption	Section 6.4
g_e	Engine-specific fuel consumption	Section 1.4
h_z	Tire normal deflection	Section 1.3
i_M	Number of friction pairs in one disk clutch of a limited slip differential	Section 4.2
I_w	Moment of inertia of a wheel about the axis of rotation	Section 1.3
k	Factor from the exponential characteristic (1.26)	Section 1.3
K	Design parameter of a planetary gear set	Section 7.4
K_a	Longitudinal stiffness coefficient of the tires of the driving axle	Section 2.9
K_{a1}, K_{a2}	Coefficients for evaluating vibrations of the total axial force acting on a bevel side gear from the pinions	Section 2.3
K_d	Torque bias (locking coefficient) corresponding to dynamic friction coefficient	Section 4.1
K_{dp}	Torque bias (locking coefficient) corresponding to static friction coefficient	Section 4.1
K_{ext}	Locking coefficient variation factor	Section 4.9
K_{max}	Locking coefficient variation factor	Section 4.9
K_{mk}	Factor of optimal torque distribution among the wheels of a drive axle	Section 6.2
K_{mo}	Factor of optimal torque distribution among the drive axles	Section 6.2
K_{opt}	Coefficient of effectiveness of distributing the power between the wheels	Section 1.4
K_{pi}	Shock-absorber resistance factor reduced to a wheel	Section 6.6

K_{pu}	Single correction factor	Section 4.2
K_q	Driveline system quality factor	Section 1.4
K_r	Relative friction torque	Section 4.1
K_{s1}, K_{s2}	Coefficients for evaluating vibrations of the total axial force acting on a bevel pinion from the side gears	Section 2.3
K_{ti}	Tire (tire and soil for deformable surfaces) damping factor	Section 6.6
K_u	Mileage wear factor of a differential	Section 2.5
K_w	Coefficient of utilization of the traction weight	Section 1.1
K_{wp}	Vehicle weight/payload ratio	Section 1.1
K_x, K_w	Longitudinal stiffness coefficients of a tire	Section 1.3
K_y	Lateral slip resistance coefficient (also called the cornering stiffness of a tire)	Section 1.3
K_{y0}	Tangent of the curve $F_l = f(\alpha)$ at the coordinate origin	Section 1.3
K_M	Force-loading factor of a differential	Section 2.5
K_N	Energy-loading factor of a differential	Section 2.5
K_X, K_Y, K_A	Indices for assessing vehicle turnability	Section 1.5
K_μ	Gripping force utilization factor	Section 1.5
i_{ab}^H	Gear ratio of a planetary gear set	Section 7.4
l_a	Longitudinal coordinate of the center of gravity of a multiwheel drive vehicle	Section 6.5
l_i	Distance between the front axle and the ith axle of a vehicle, $i = 2, m$	Section 2.1
l_{sc}	Spider pin length in contact with the case of a differential	Section 2.5
l_{sp}	Spider pin length in contact with the pinion	Section 2.5
L	Wheelbase of a vehicle	Section 3.3
m	Number of the driving and driven (not coupled to the driveline system) axles of a vehicle	Section 1.2
m_a	Gross (full) mass of a truck	Section 2.5
m_{dr}	Mass taken by the drive wheels of a vehicle	Section 2.5
m_r	Kinematic discrepancy factor of a 4 × 4 vehicle	Section 3.2
m_{rR}	Kinematic discrepancy factor of a 4 × 4 vehicle	Section 3.2
m_{ru}	Kinematic discrepancy factor of a 4 × 4 vehicle	Section 3.2
m_{ruR}	Kinematic discrepancy factor of a 4 × 4 vehicle	Section 3.2
m_t	Tractor mass	Section 1.1
m_{te}	Outer module a side gear and a pinion measured at the large end of the teeth	Section 2.3
m_u	Kinematic discrepancy factor of a 4 × 4 vehicle	Section 3.2
m_{uR}	Kinematic discrepancy factor of a 4 × 4 vehicle	Section 3.2
m_{Hi}	Kinematic discrepancy factor of the ith driving axle	Section 3.2
m_R	Kinematic discrepancy factor of a 4 × 4 vehicle	Section 3.2
M_f^c	Rolling resistance moment caused by the normal reaction shift	Section 1.3
M_B	Yaw moment due to the inequality of the left and right circumferential forces	Section 2.8

M_{Bd}	Moment of resistance to turning of a drive axle with a limited slip differential after the differential actuated	Section 4.10
n	Number of the driving axles of a vehicle	Section 1.2
n_w	Number of revolutions of a wheel	Section 1.3
N_{PDU}	Number of power dividing unit in a driveline system	Section 1.2
p_0	Pressure in the contact between the spider and the differential's housing	Section 2.5
p_a	Pressure in the thrust washer of the bevel side gear	Section 2.5
p_b	Pressure in the contact between the spider and the pinion	Section 2.5
p_c	Pressure in the thrust washer of the bevel pinion	Section 2.5
p_w	Tire inflation pressure	Section 1.3
P_0	Input power supplied to a power dividing unit	Section 2.5
P_a	Power extended on increasing the kinetic energy of the wheel in translational motion	Section 1.3
P_{ax}	Mechanical power loss in engine and power for driving auxiliary devices	Section 1.4
P_b	Wheel brake power	Section 7.5
P_d	Drawbar pull power	Section 1.4
P_{drl}	Mechanical power loss in the driveline system	Section 1.4
P_e	Engine power	Section 1.4
P_e^{max}	Maximal engine power	Section 1.1
P_f	Wheel rolling resistance power	Section 1.3
$P_{f\Sigma}$	Vehicle rolling resistance power	Section 1.4
$P_{fc\Sigma}$	Power of resistance to the rolling of the wheels caused by the vehicle curb weight	Section 1.4
P_{fg}	Wheel rolling resistance power needed for overcoming force R_{xg}	Section 1.3
$P_{fg\Sigma}$	Power of resistance to the rolling of the wheels caused by the cargo being transported	Section 1.4
P_{frame}	Power transmitted from a wheel to the vehicle frame	Section 1.3
P_i	Geometric parameter of limited slip differential	Section 4.1
P_i^{in}	Engine indicator power	Section 1.4
P^{out}	Vehicle output power	Section 1.4
P_{trm}	Mechanical power loss in transmission	Section 1.4
P_{ts}	Mechanical power loss for deflecting tires and soil	Section 1.4
P_w^{in}	Wheel input power	Section 1.3
P_w^{out}	Wheel output power	Section 1.3
$P_{w\Sigma}^{in}$	Input power on the drive wheels	Section 1.4
p_x	Vehicle mobility indicator from the point of view of its traction	Section 1.5
P_M	Driveline input power	Section 1.4
P_ε	Power needed to increase the kinetic energy of the rotational motion of the wheel	Section 1.3
P_δ	Wheel slip power	Section 1.3
$P_{\delta\Sigma}$	Vehicle slip power	Section 1.4

p_μ	Vehicle mobility indicator from the point of view of its grip with the surface of motion	Section 1.5
q	Coefficient of power distribution to a drive axle	Section 1.4
q_d	Pressure on the plate disks of a limited slip differential	Section 4.9
q_k	Pressure in the contact of the pinion pin and the groove of the differential's case	Section 4.9
q_R	Vehicle turning radius variation factor	Section 1.5
$q_{\alpha T}$	Correction factor for reflecting the effect of traction force F_w on function $F_\mathrm{l} = f(\alpha)$	Section 1.3
Q_a	Total axial force acting on a bevel side gear from the differential's pinions	Section 2.3
$Q_\mathrm{a}^{'}$	Axial component of the resultant force on a bevel side gear from one pinion	Section 2.3
Q_avg	Average fuel consumption per 100 km of travel	Section 1.5
Q_h	Per hour fuel consumption	Section 1.4
Q_k	Axial (thrust) force acting between cams of a side gear and an intermedium cam bushing	Section 4.3
Q_m	Lubricant flow rate	Section 8.3
Q_s	Fuel consumption referred to the distance traveled by the vehicle	Section 1.4
Q_s	Total axial force acting on a bevel pinion from the differential's side gears	Section 2.3
Q_sp	Spring force	Section 4.7
r	Radius of an unloaded wheel (also, radius of a rigid wheel)	Section 1.3
r_a^0	Generalized rolling radius of a vehicle in the driven mode	Section 2.8
r_{ai}^0	Generalized rolling radius of the ith driving axle in the driven mode	Section 2.8
r_c	Pitch (average) radius of a pinion	Section 2.5
r_cf	Average friction radius of a bevel pinion	Section 2.5
r_cr	Radius of the carrier	Section 2.1
r_d	Dynamic loaded radius of a wheel	Section 1.3
r_g	Pitch (average) radius of a side gear	Section 2.1
r_gb	Medium friction radius at the end of the pressure cup and the pinion's shoulder	Section 4.4
r_gf	Average friction radius of a bevel side gear	Section 2.5
r_k	Medium radius of the end cams in a limited slip differential	Section 4.3
$r_{k\mathrm{p}}$	Medium radius of friction between the spider and a side gear	Section 4.3
r_0	Radius (arm) of the force F_0	Section 2.5
r_s	Static loaded radius of a wheel	Section 1.3
r_sp	Spider pin radius in the contact with pinion	Section 4.2
r_w	Effective rolling radius of a wheel in the driving and braking modes	Section 1.3
r_wp	Friction radius of the pinion at the differential's case	Section 4.2
r_w^f	Effective rolling radius of a wheel in the free mode	Section 1.3

r_w^0	Effective rolling radius of a wheel in the driven mode	Section 1.3
r_M	Medium friction radius of disk plates in limited slip differential	Section 4.2
R_a	Vehicle actual radius of turn	Section 1.5
R_t	Vehicle theoretical radius of turn	Section 1.3
R_{td}	Turn radius of a drive axle with a limited slip differential after differential actuated	Section 4.10
R_x	Rolling resistance force of a wheel	Section 1.3
R_{xc}	Wheel rolling resistance caused by the curb weight W_{wc}	Section 1.3
R_{xg}	Wheel rolling resistance caused by the payload weight W_{wg}	Section 1.3
$R_{xg\Sigma}$	Vehicle total rolling resistance caused by W_g	Section 1.4
R_z	Ground normal reaction onto a wheel	Section 1.3
s_δ	Tire slip ratio (slippage)	Section 1.3
$s_{\delta a}$	Generalized slippage of a vehicle	Section 2.8
$s_{\delta ai}$	Generalized slippage of the ith driving axle	Section 2.8
S_e	Handling sensitivity	Section 1.5
S_e^{dn}	Unsteady-state handling sensitivity	Section 1.5
S_e^{st}	Steady-state handling sensitivity	Section 1.5
S_t	Tooth thickness	Section 2.3
S_w	Wheel's travel	Section 1.3
t_b	Wheel tread (a distance between the wheels of an axle)	Section 2.2
t_p	Pure time of work of a farm tractor	Section 1.5
t_Σ	Total time of work of a farm tractor	Section 1.5
t_R	Time delay in vehicle's reaction to a quick turn of the steering wheel	Section 1.5
T	Output torque on one output shaft of a power dividing unit	Section 2.1
T_b	Brake torque	Section 1.3
T_{gb}	Torque of friction at the pressure cup	Section 4.4
T_i	Torque of the ith drive axle	Section 1.3
T_{int}	Elastic internal torque in a differential	Section 2.1
T_{lock}	Locking torque of a clutch	Section 2.7
T_0	Input torque of a power dividing unit	Section 2.1
T_r	Dynamic friction torque in limited slip differential	Section 4.1
T_{rp}	Torque of the primary friction in the clutches of a limited slip differential	Section 4.2
T_{rs}	Static friction torque in a limited slip differential	Section 4.1
T_{sb}	Torque of friction between the bushing and the differential's case (or the spider)	Section 4.3
T_{sp}	Friction torque between the pinion and the carrier pin	Section 4.2
T_w	Wheel drive torque	Section 1.3
T_{wp}	Friction torque between the pinion and the case of a differential	Section 4.2
u_a	Driving axle gear ratio	Section 2.5

u_d	Internal gear ratio of a differential	Section 2.1
u_{dd}	Internal gear ratio of a double differential	Section 7.4
u_d^*	Optimal internal gear ratio of a differential	Section 2.9
u_f	Final drive gear ratio	Section 2.1
u_i	Gear ratio from the central power dividing unit's (i.e., transfer case) input shaft to the wheels of the ith drive axle or to the interaxle differential of the ith drive axle (see a note on p. 302)	Section 2.8
u_k	Wheel–hub reduction gear ratio	Section 2.1
u_p	Torque distribution factor to link the differential gear ratio and the kinematic discrepancy factor	Section 3.3
u_{trm}	Vehicle transmission gear ratio	Section 6.1
u_w	Weight distributing factor	Section 2.8
V_a	Theoretical travel velocity of a vehicle	Section 3.2
V_{avg}	Vehicle average actual velocity	Section 1.5
V_c	Linear velocity of the pinion and the spider (on the friction surface)	Section 2.5
V_{cr}	Vehicle critical speed	Section 1.5
V_{mid}	Vehicle average design velocity	Section 1.1
V_t	Theoretical linear velocity of the wheel center (no slip occurs)	Section 1.3
V_x	Actual linear velocity of the wheel center (slip occurs). Also, vehicle actual velocity in straight line motion or along the longitudinal axis	Sections 1.3 and 1.4
V_δ	Tire slip velocity	Section 1.3
W_a	Vehicle gross (total) weight	Section 1.1
W_c	Vehicle curb weight	Section 1.1
W_{dr}	Adhesion weight, i.e., the weight devolving upon the driving wheels	Section 1.1
W_g	Vehicle payload	Section 1.1
W_w	Normal load of a wheel (wheel weight)	Section 1.3
W_{wc}	Wheel normal load without the useful load (curb weight)	Section 1.3
W_{wg}	Wheel normal load caused by the useful load (payload weight)	Section 1.3
x	Coefficient of initial contour displacement	Section 2.3
y_Δ	Perceptible displacement coefficient	Section 2.3
Y_w	Wheel lateral force	Section 1.3
z_c	Gear tooth number of a pinion of a differential	Section 2.1
z_c	Tooth number of a pinion of a differential	Section 2.3
z_{cr}	Tooth number of a spur gear equivalent to a bevel pinion	Section 2.3
z_g	Gear tooth number of a side gear of a differential	Section 2.1
z_g	Tooth number of a side gear of a differential	Section 2.3
z_{gr}	Tooth number of a spur gear equivalent to a bevel side gear	Section 2.3

Greeks

α	Wheel slip angle	Section 1.3
α_k	Pressure angle corresponding to a tooth point of contact and to the rotation center of a spur gear equivalent to a bevel side gear	Section 2.3
α_{kc}	Pressure angle corresponding to a point of tooth contact and to the rotation center of a spur gear equivalent to the pinion	Section 2.3
α_w	Pressure angle corresponding to the pitch point	Section 2.3
δ	Wheel steering angle	Section 1.3
δ_c	Pitch pinion angle	Section 2.3
δ_r	Vehicle mass factor	Section 6.3
ε_w	Wheel angular acceleration	Section 1.3
η_d	Mechanical efficiency in a reduction gear	Section 4.1
η_f	Vehicle rolling resistance efficiency	Section 1.4
η_{fw}	Wheel rolling resistance efficiency	Section 1.3
η_{fw}^{tr}	Wheel rolling resistance efficiency for evaluating the resistance exerted by the payload	Section 1.3
η_h	Fuel consumption variation factor	Section 3.4
η_M	Overall mechanical efficiency of the driveline system	Section 1.4
η_{Mi}	Mechanical efficiency of ith branch of the driveline system	Section 1.4
η_n	Mechanical efficiency of a differential	Section 2.5
η_{trm}	Mechanical efficiency of vehicle transmission	Section 6.1
η_t	Vehicle tractive efficiency	Section 1.4
$\eta_{x\Sigma}$	Vehicle running gear total efficiency	Section 1.4
η_x^t	Vehicle running gear tractive efficiency	Section 1.4
η_v	Vehicle velocity variation factor	Section 3.5
η_w^t	Wheel tractive efficiency	Section 1.3
η_w^{tr}	Wheel transportation efficiency	Section 1.3
η_x^{tr}	Vehicle running gear transportation efficiency	Section 1.4
η_δ	Vehicle slip efficiency	Section 1.4
$\eta_{\delta w}$	Wheel slip efficiency	Section 1.3
$\eta_{\Sigma w}$	Wheel total efficiency	Section 1.3
γ	Lead angle of the worm thread	Section 4.5
λ	Lagrange factor	
λ_i	Normal loading factor	Section 2.8
λ_w, γ_w	Longitudinal elasticity coefficient of a tire	Section 1.3
μ	Dynamic friction coefficient	Section 2.3
μ_l	Peak friction coefficient in lateral direction of a tire	Section 1.3
μ_{px}, μ_p	Peak friction coefficients in longitudinal direction of a tire (also grip coefficients)	Section 1.3
μ_s	Static friction coefficient	Section 4.1
μ_x	Current friction of grip coefficient (friction coefficient ''in use'')	Section 1.3
ν_c	Angle of pinion rotation	Section 2.3

$(\pi m - S_t)$	Width of space	Section 2.3
φ_k	Angle of the working edges of the cams. Slope of the V-shaped groove in the differential's case	Sections 4.3 and 4.4
θ	Wheel angle of rotation	Section 1.3
θ_n	Surface longitudinal angle of inclination	Section 1.4
ρ	Friction angle and dynamic friction coefficient	Section 2.3
ω_a	Angular velocity of a vehicle about the vertical axis	Section 2.8
ω_c	Angular velocity of a pinion about the carrier	Section 2.1
ω_{rel}	Relative angular velocity of a side-gear and the case of a differential	Section 2.1
ω_w	Wheel angular velocity	Section 1.3
ω_0	Angular velocity of the input element of a power dividing unit	Section 2.1
ω_{01}, ω_{02}	Angular velocities of the output shafts of an interaxle power dividing unit	Section 1.3
ω', ω''	Angular velocities of the output shafts of an interwheel power dividing unit	Section 2.1

Subscripts

r, l	right, left	Section 2.3
' and ''	Indices relating to the left/right or right/left wheels	

Note: This list contains symbols that are used through the whole book. Symbols, which are only used in a particular section, are not listed here.

1

Driveline Systems and Vehicle Performance

1.1 Brief Review of Driveline Systems History

1.1.1 First Wheeled Carriages

The first motorized wheeled carriage capable of moving under its own power was a steam-driven vehicle designed by a French army engineer, N. J. Cugnot (Figure 1.1). This vehicle was constructed in 1769.

With all its shortcomings, the steam-driven vehicle—Cugnot's chariot—had a rational design. It had the most simple driveline system combined with a most simple steering mechanism. All this stemmed from the fact that the force cylinder was most successfully located above the forward drive and, simultaneously, the steering wheel. The vehicle's weak spot consisted of its using a ratchet and pawl transmission mechanism that made it impossible for the vehicle to move uniformly. In addition, because of its imperfect steam engine, Cugnot's chariot stopped every 10 m to allow steam to accumulate in the boiler and to rise to the required level.

In 1801, an enterprising English inventor, Richard Trevithick, constructed the first steam-driven passenger stagecoach and organized, for the first time in history, mass construction of such coaches in the insular part of Great Britain. The rear driving axle of the coach with wheels rigidly fastened to it was driven by a pair of gears from an intermediate transmission shaft. The design of the wheels, taken from horse-driven carriages and their rigid coupling with the driving axle, was the weak link of the first such coaches. The driving wheels, with their smooth and narrow rim, had poor traction with the road and frequently skidded. This was remedied by equipping the driving wheels with an additional device, consisting of a set of pushers and detents—''claws''. Figure 1.2 presents another vehicle of a similar design of the claws. Performing reciprocating motion were a pair of claws hinged on rods that became alternately coupled with the road surface and assisted in rotating the driving wheels of the carriage without perceptible skidding.

Subsequently, in 1813, somebody by the name of Brunton invented pushers and used them as the principal and sole propulsion device on the primitive locomotive constructed by him (Figure 1.3a). Without exception, all the wheels in Brunton's locomotive were driven (no torque applied), and functioned as a support structure. It should be noted that at that time few believed in the traction ability of carriage wheels. Even such an experienced mechanic as Trevithick did not fully trust wheels with smooth rims. In particular, he did not trust the wheels of the locomotive that were supposed to roll on smooth rails. For this reason, he placed forged nails on the rims past the flanges of the driving wheels of his two first locomotives constructed in 1803 (Figure 1.3b). The nails

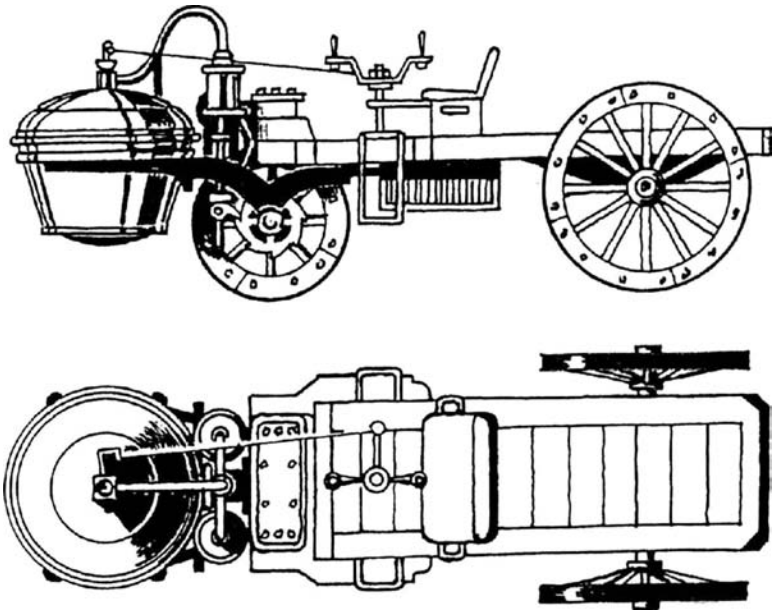


FIGURE 1.1
First self-propelled steam automobile designed by French army engineer N. J. Cugnot.

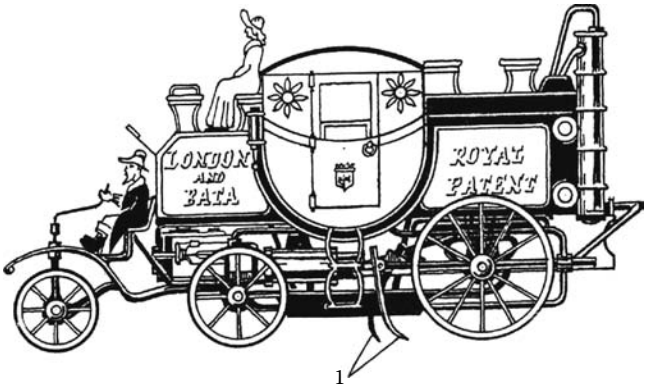


FIGURE 1.2
H. Herney's ''steamer'': 1, Coupling ''claw.''

stuck into wooden beams placed along the rails, thus significantly improving the coupling between the wheels and the additional support surface and, hence, improved their traction.

One of the nonrail carriages constructed with a drive similar to that of Brunton's locomotive was the carriage of D. Gordon. It was constructed in 1824, and consisted of a three-wheeled machine—a steam-driven stagecoach (Figure 1.4). All the wheels in this stagecoach were supporting driven wheels, whereas the propulsion was provided by a ''pusher-leg'' system with a complicated lever-type drive. In this manner, by placing additional devices in the form of ''pushers'' and ''claws,'' the designers of steam-driven carriages gradually and surely approached the invention of a wheel with a tread. It is

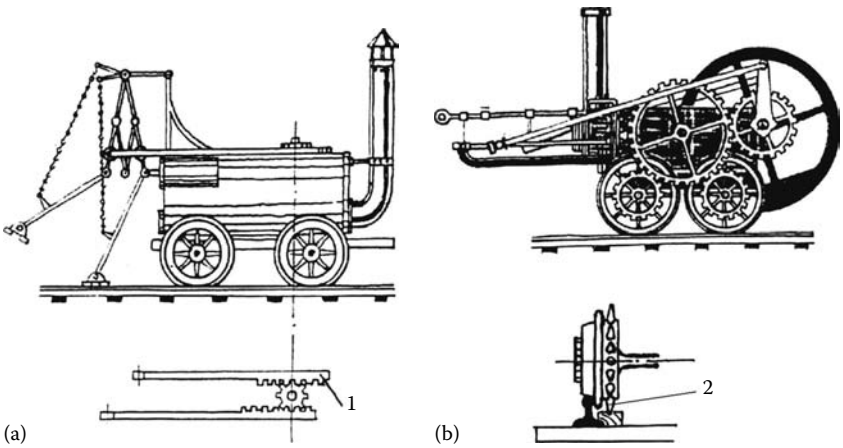


FIGURE 1.3
Locomotives: (a) Brunton's locomotive (1, drive of pusher ''legs''); (b) Trevithick's locomotive (2, wheel pair with nails on the rims).

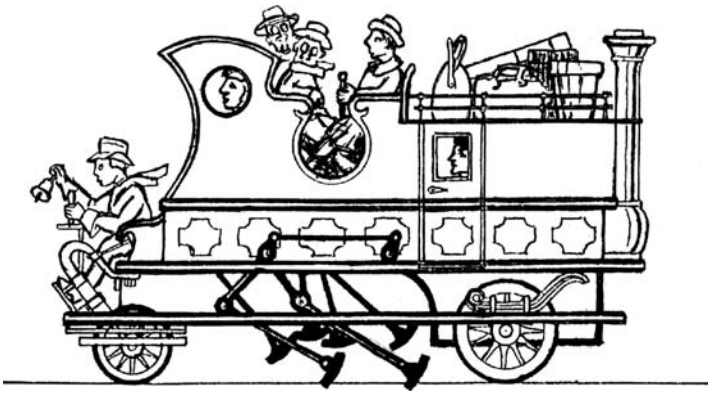


FIGURE 1.4
Gordon's three-wheeled stagecoach with a system of pusher ''legs.''

precisely such a wheel that, in the majority of cases, is capable of ensuring reliable traction between itself and the road surface.

In 1805, an American mechanic, Oliver Evans, constructed a suction dredge for cleaning up the Philadelphia harbor waterfront. According to the inventor, the dredge was supposed to deliver itself to its place of work. For this purpose, Evans equipped it, together with an aft propulsion screw, which served for floating, five wheels (Figure 1.5) that would allow it to move on land. The leading wheel together with the wheels of the front turning axle allowed the dredge to take turns, whereas the wheels of the rear driving axle provided the traction. The rear driving axle of the dredge was driven by a steam engine by means of a belt drive. The *Orukter Amphibolas* (which was the name of the dredge) was the first motorized amphibious vehicle.

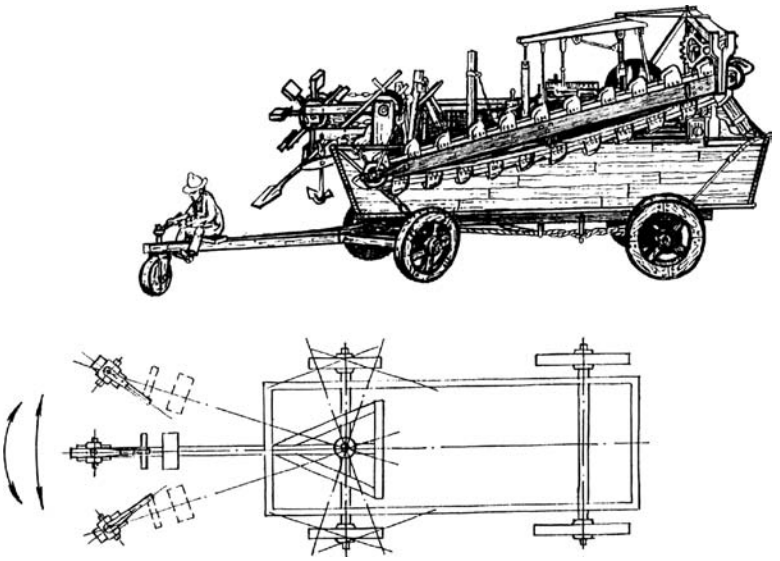


FIGURE 1.5
Oructur Amphiblus—dredge designed and constructed by Oliver Evans.

1.1.2 First Differential Transmissions

One of the problems that were encountered was that the driving wheels of the first steam-driven vehicles were rigidly coupled to their driving axles. Because of this, each of the driving wheels could not roll along its own path that were formed by irregularities in the road ahead each of them. Two wheels on a single rigid axle in translational motion traversed different paths over the same time interval. For this reason, one of the wheels skidded while the other slipped, which was detrimental to the machine's traction. Moreover, the rigid fastening of the wheels did not allow the driving wheels to roll at different angular velocities (over different paths) when the vehicle made turns. This situation brought about the invention of the differential transmission (henceforth referred to as differential).

The differential was invented by a French watchmaker, Onesiphore Pecquer, in 1827 and was installed by him in 1828 in his private steam-driven vehicle. From this time on, the differential started appearing in other steam-driven vehicles and, subsequently, in the drivelines of vehicles with engines driven by petroleum-derived fuels, i.e., in driveline systems of automobiles. The differential separated the driving axles of the machine into two half axles with driving wheels, allowing each of them to roll along its own path. This reduced the loss of power incurred in the skidding of wheels when their traction with the road surface was sufficient.

The first differentials were extremely simple. They divided into half the torque that became converted into the traction of the vehicle between the driving wheels of the axle. As a result of this, the torque to both driving wheels was that utilized by the wheel that had the poorer contact with the road surface. This is a negative property of the simple differential. It causes the vehicle to come to a full stop when one of its driving wheels spins on a slippery part of the road, i.e., it brings about complete loss of mobility by the vehicle. Such differentials are now known as open, or free differentials.

The mobility of a wheeled vehicle and, in particular, of an automobile refers to its ability to travel over poor roads and rough terrain while transporting loads, delivering the maximum possible work output. Automobile utilization practice puts precisely such requirements to the vehicles. In order to improve the vehicle's ability to travel over difficult surfaces, it is necessary to force the differential to divide the torque supplied by the engine among the driving wheels in such a manner that the wheels would exert a torque in accordance with the conditions of their gripping with the surface of motion. The solution to this problem began when automobile manufacturers started inventing various devices that lock the half-shafts of the driving axle, i.e., lock the differential itself. In this manner, the driveline systems acquired locking differentials of various design. This is discussed further down in this chapter. The properties of current differentials are presented in Chapters 2, 4, 5, and 7.

In 1878, a French engineer, Amede Bollee Sr., together with his son, also named Amede (Amede Bollee Jr.), constructed a steam-driven vehicle that they named *La Manselle* (Figure 1.6), which had an original packaging and a very simple layout. The driveline system of its driving wheels had, in addition to the previously mentioned gear and belt transmissions, a universal-joint drive coupled with a chain drive. Unfortunately, the drive

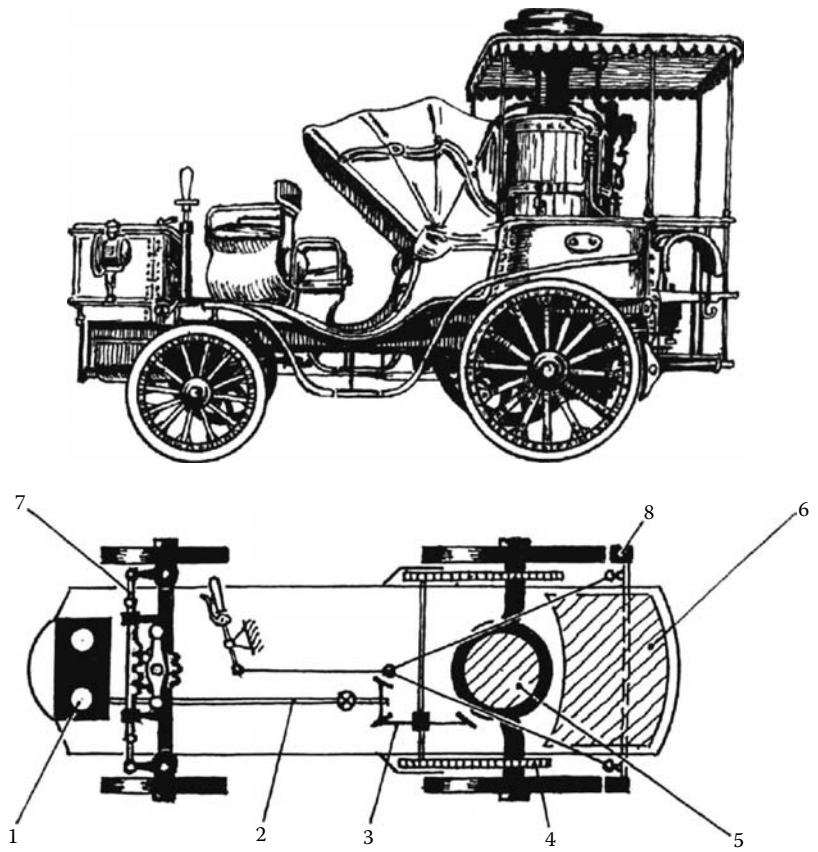


FIGURE 1.6
La Manselle constructed by Bollee Sr. and Bollee Jr.: 1, engine; 2, cardan propeller shaft; 3, final drive; 4, chain drive; 5, boiler; 6, water tank; 7, hinged steering-gear parallelogram; 8, shoe brakes.

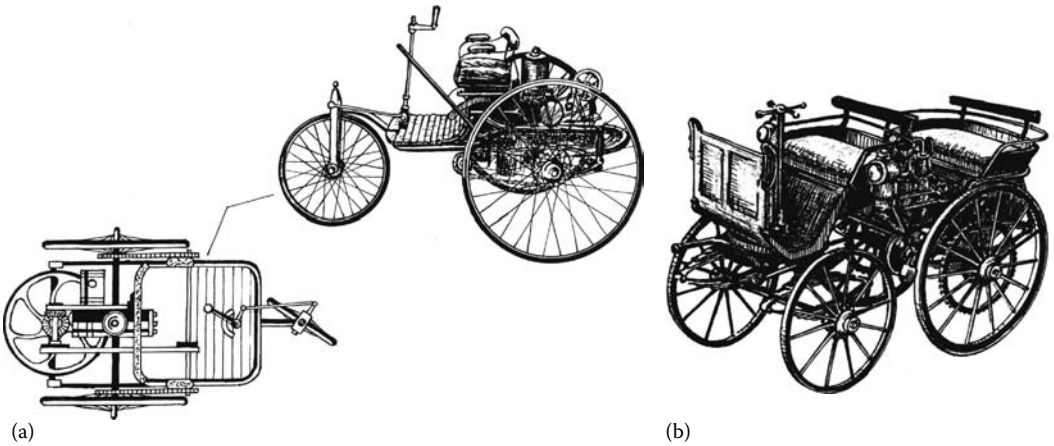


FIGURE 1.7
The first automobiles: (a) by Benz; (b) by Daimler.

of Bollee's steam-driven vehicle lacked the simplest of differentials that was already available at that time.

The first world-acclaimed automobiles manufactured by Carl Benz and Gottlieb Daimler also lacked differentials in the drives of their driving wheels. The driving wheels of the Benz automobile were driven by a chain transmission, whereas the Daimler car was equipped with a gear transmission (Figure 1.7).

The differential in the drives of automobiles built by these carmakers appeared somewhat later. Starting with the Panhard–Levassor automobiles produced in 1891 (Figure 1.8), differentials have gradually come into use in the drives of all vehicles, both on the intermediate axles and, directly, on the driving axles (Figure 1.9).

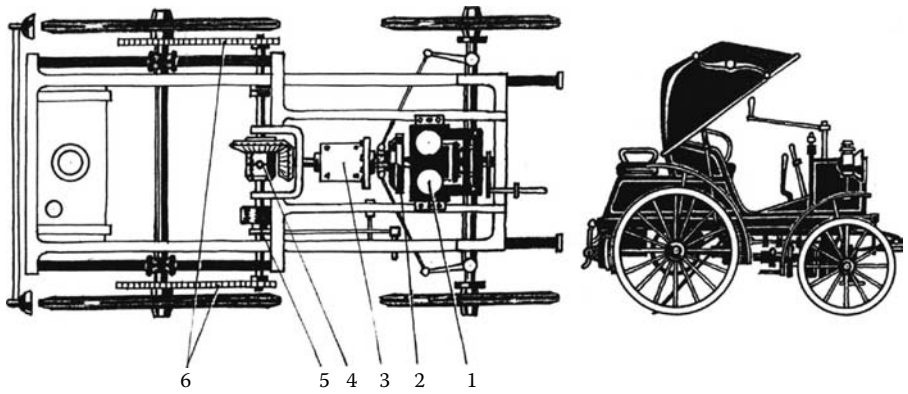


FIGURE 1.8
Schematic diagram and driveline of the Panhard–Levassor automobile (designed by Emile Levassor); 1, engine; 2, main clutch; 3, gearbox; 4, differential with final drive; 5, transmission brake; 6, chain drive.

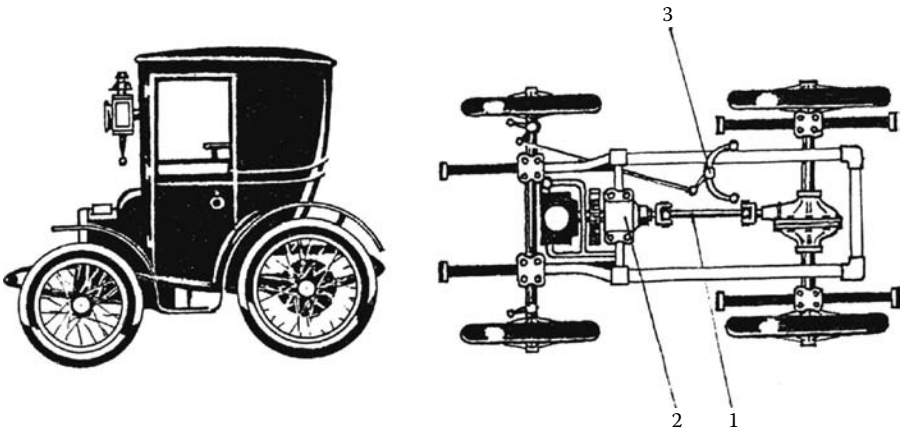


FIGURE 1.9
View and design of a Renault automobile: 1, cardan propeller shaft; 2, gearbox; 3, bicycle-type steering gear.

1.1.3 First Hybrid Cars and All-Wheel Drive Vehicles

In 1900, at the request of E. W. Hart, a resident of Luton, Austria, Ferdinand Porsche, an engineer employed by the Joined Lohner company, constructed a four-wheel drive automobile driven by electric motors built into the wheels. These motors were supplied with electricity from storage batteries that weighed 1800 kg. It turned out somewhat later that the weight of these batteries was an insurmountable obstacle to the making of such vehicles. For this reason, Porsche replaced the storage batteries by an internal combustion engine with an electric generator and, thus, obtained a ''hybrid drive'' automobile. In 1903, he was issued a number of patents on this automobile and started manufacturing such vehicles.

The first hybrid Porsche automobiles had only two driving wheels and, even if they were a great improvement over the four-wheel drive vehicle with storage batteries, their speed was insufficient for participating in races. And then Porsche, who was a devoted enthusiast of car races, redesigned his hybrid automobile as a four-wheel drive vehicle. This happened in 1903. In the same year, Porsche participated with this car in races that took place not too far from Vienna. It is quite possible that the Porsche–Lohner hybrid-drive automobile was the first 4×4 formula all-wheel drive car.

1.1.4 Front-Wheel Drive Designs

The first front-wheel drive (FWD) automobile appeared in 1903. This was a unique vehicle designed by an American, John Walter Christie (Figure 1.10). Its uniqueness consisted in the fact that the beam cross-member of the front nondrive axle consisted of the engine, which was located transversely to the longitudinal axis of the vehicle, with a crankshaft that was coupled through reduction gearing to the driving wheels. The rear axle of the vehicle was driven and steered.

Christie's FWD vehicle demonstrated the many advantages of this kind of drive over the rear-wheel drive that became standard at that time. It was found to impart good course stability to the car. Inspired by this, Christie established the Christie Direct Action Motor Car Company. This company produced only a limited number of cars with Christie's

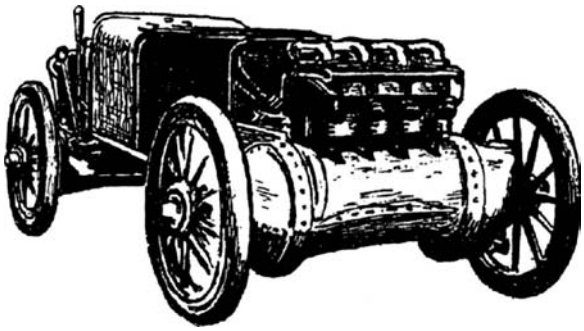


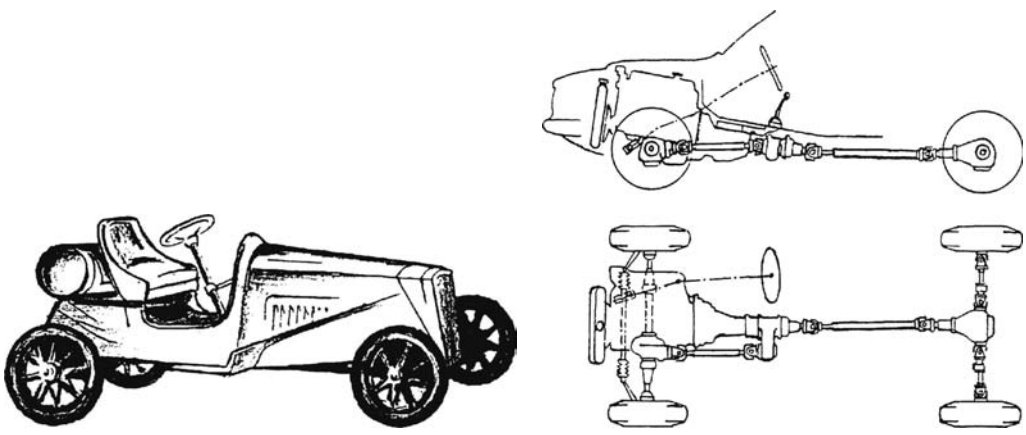
FIGURE 1.10
J. W. Christie's FWD automobile.

FWD, because they were not in great demand. For this reason, he had to switch to the manufacture of high-power two-wheel (single axle) tractors that served for pulling steam-driven fire pumps.

The development of FWD vehicles started in earnest during the 1920s and 1930s. Harry Miller and Leo Goosen constructed a pair of radical front-drive cars late in 1924. Miller managed to solve the problem of getting enough weight on the front driving wheels, given his rather long, north-south-mounted engine. Miller created an extremely compact transmission and differential in one case, the first transaxle.

1.1.5 First Mechanical Four-Wheel Drives

The first all-wheel drive automobile with a 4×4 formula and a purely mechanical drive appeared in 1903. It was exhibited at the Paris Automobile Salon by the Dutch Spyker company (Figure 1.11a). The drive of this car's wheels was designed in a manner that rapidly became classic (see Figure 1.11b). It had an additional gearbox and, in it, a locking



(a) (b)

FIGURE 1.11
All-wheel drive automobiles: (a) 4×4 automobile—the Dutch Spyker; (b) classical design of a 4×4 automobile in which the front wheels were engaged by the driver by means of a tooth-type clutch.

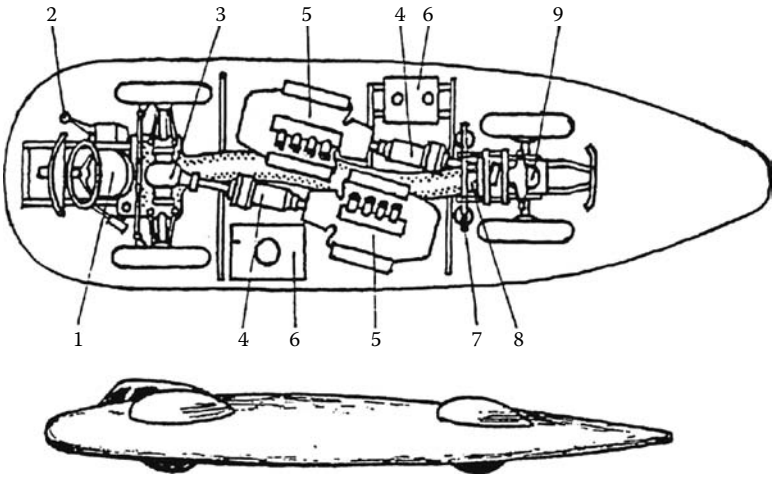


FIGURE 1.12
Railton's 1947 4 × 4 racecar. 1, driver's seat; 2, gearbox lever; 3, front axle; 4, gearbox and transmission brake; 5, engine; 6, fuel and oil tanks; 7, pneumatically controlled brake cylinder; 8, chassis with the central tube of the body skeleton; 9, rear axle.

dog clutch that could be used for coupling the engine to the front axle when it became necessary to increase the car's traction. The power to the steered and at the same time driving wheels of the front axle was transmitted by means of a universal-joint drive and single Hooke's joints with an improved spider.

It is interesting to note that, at approximately the same time, in 1906, the world's first armored car with two driving axles was constructed by Paul Daimler, the engineering director of the Austro-Daimler company.

In 1905, J. W. Christie constructed a 4 × 4 car in which the wheels of each of the axles were set into motion by a separate engine. This car was used by Christie personally to participate in the Vanderbilt Cup and other American auto races. The machine did not live up to expectations. The races were along an elliptical path with a large radii of curvature. Nevertheless, Christie's four-wheel drive vehicle took poorly even such turns because of the excessively large kinematic discrepancy between the rotation of the front and the rear wheels, each of which was powered by a separate engine, and also because of the use of single Hooke's joints in the drives of the front wheels.

A second attempt to construct a 4 × 4 car with two engines was undertaken in 1947 by an Englishman, Railton Reid. He used the same design for constructing a racing car (Figure 1.12). When driven by racing-car driver John Cobbs along a straight path, it attained a speed of 634.26 km/h. This was a new speed record. As to handling turns, this car suffered from the same shortcomings as Christie's vehicle.

1.1.6 Invention of Pneumatic Tires and Design Measures for Improving the Poor-Terrain Mobility of Vehicles

The invention of the pneumatic tire was an epoch making event for the development of the car and of wheel-drive designs. In 1888, John Boyd Dunlop, a veterinary surgeon, was issued the English Queen's patent for the bicycle pneumatic tire invented by him. Eleven years later, in 1899, the French brothers Edoard Michelin and Andre Michelin were

the first to ''shoe'' an electric racecar with pneumatic tires. As of that time, the two brothers, who established the Michelin Pneumatic Tire Company, subdivided the tire into a chamber and a cover so that it could be easily changeable. The cover had shallow grooves on the tire tread that, according to the inventors, should have ensured adhesion with the road surface. All this was indeed true under good road conditions. However, when a car equipped with tires having shallow grooves was called upon to travel under poor terrain conditions (sandy, swampy terrain), over wet dirt roads, and also over snow and ice encrusted roads, its wheels started spinning and the car completely lost its ability to travel. This forced car manufacturers and tire engineers to find a way to improve the mobility of their products. The first addressed this problem by looking for methods of locking the differentials and inventing self-locking differentials; this included inventing such means for increasing the gripping of the supporting surface by the driving wheels as chains wound on individual wheel rims and caterpillar tracks (Figure 1.13). The latter were termed half-track drives. The others—tire engineers—focused on improving the grooving pattern and the tire tread design.

Adolphe Kegresse, a Frenchman, employed as a mechanic at the Russian Imperial garage, was one of the first persons to invent and use the half-track drive for automobiles of the Russian Emperor. His invention was intended for improving the mobility of vehicles on snow-covered roads and unpaved stretches of land. Kegresse patented this invention in 1912.

Following Kegresse's caterpillar drive design, a composite rubber-metal caterpillar track, that was nicknamed ''overall,'' was designed in the United States. It was simply slipped

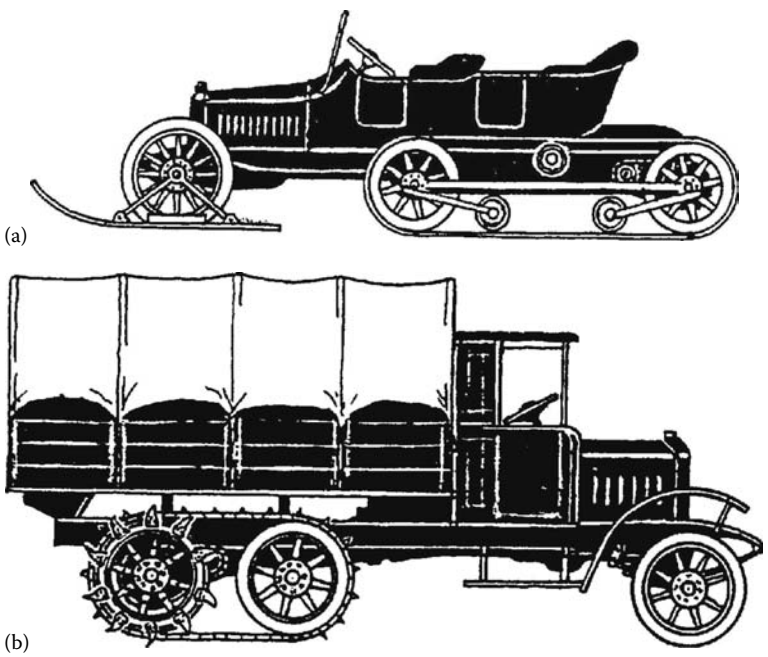


FIGURE 1.13
Half-track running gears: (a) by Adolphe Kegresse on the Russo-Balt automobile; (b) with ''overall'' caterpillar tracks and grousers made by the Henschel Company on the rear wheels of a truck.



FIGURE 1.14
Snowmobile, U.S.S.R., 1961.

over the pair of rear wheels of army and commercial six-wheeled trucks and also of armored vehicles. From this time, the half-track drive with an overall type caterpillar track came into use also in other countries, primarily on trucks. For example, in 1934, the Henschel company (Germany) used overall-type rubber-metal tracks, coupled with special metal grousers, on its trucks (see Figure 1.13b). German armored carriers equipped with half-track drives did not exhibit sufficient mobility, particularly in snow and mud. Attempts were made to design vehicles with half-track drives and skies instead of leading wheels (see Figure 1.14). It may apparently be stated that the half-track drive did not succeed in becoming an alternative to four-wheel drive vehicles with various types of driveline systems.

However, developments in tire design promoted the development of four-wheel drive vehicles. Their mobility was highly improved by the invention, during the 1920s, of low-pressure tires. These tires have a reduced rolling resistance and larger than ordinary contact patch between the soft tire and the surface, which improves the vehicle's mobility.

It can be claimed that tire designers started, during the 1940s, to actively improve the grooving patterns and design of the tire tread, which should highly improve the mobility of vehicles. As a result, there appeared high-mobility tires with developed tread (Figure 1.15) for use primarily in off-road vehicles. Intensive work was also done to design tires that would provide improved mobility to both off-road vehicles and those intended for paved-road travel. Here is an example.

A tire with a wide annular groove over the center of its tread was designed. The groove served for removing water from the pavement-tire contact patch. For this purpose, the groove actually divided the patch into two distinct contact spots. Its cone-shaped transverse grooves together with the longitudinal annular groove rapidly remove water from both contact spots. Both hard halves of the tread provide the tire with good directional stability.

There are also other approaches to improving tires for enhancing the mobility of vehicles. One such example designed in the 1990s has the wheel rim equipped with wedge-shaped flanges for preventing the beads of the tire from sliding into the rim. It has a device that



FIGURE 1.15
Drawings of high-mobility (all-terrain) tire treads: 1, straight herringbone; 2 and 3, skewed herringbone (''ribbed''); 4, split herringbone; 5, spiral (asymmetric about the longitudinal axis of the wheel); 6, herringbone; 7, semispiral (''skeleton''); 8, drawing with longitudinal slots; 9, split skewed herringbone.

signals a drop in the tire air pressure. The tire has two detents that take up the weight of the vehicle upon a drop in the inner-tube air pressure. The shape of the wedge-like connecting strips of the rim assists in holding the sidewall of the tire in it even when the air pressure drops to the atmospheric pressure. This tire-wheel arrangement allows driving a car with a fully or partially flat tire for 80–90 km. This arrangement is intended primarily for ensuring passenger safety when a tire goes flat. However, it can be easily seen that this system also protects the car from total mobility loss. Recently, in 2008, an active self-inflating tire system was introduced. The technical idea is based on peristaltic pump principles. To inflate the tire, the normal load and motion of the vehicle are used.

It may be concluded that improvement of tire design was one of the most significant conditions for the intensive development of multiaxle drive vehicles.

1.1.7 Constant-Velocity Joints

Another factor that delayed the appearance of not only front-drive but also all-wheel drive vehicles, in which the engine's power is utilized to a greater extent by being transformed into their traction capacities and acceleration performance, was the lack of constant-velocity joints.

The problem was that single Hooke's joints could not transmit uniform rotation to the steered wheels of the vehicle, particularly when taking a turn. For this reason, the invention of constant-velocity joints became one of the first priorities for vehicle designers from the very start of the twentieth century.

In 1925, a German design engineer and scientist, Richard Bussien, linked two single Hooke's joints, and thus transformed a nonconstant velocity joint into a new constant-velocity mechanism. He used his invention on a front-drive passenger car constructed by him and called it VORAN (Vorderrad Antrieb—FWD). It turned out that the rather bulky dual Hooke's joint that caused the steered wheel to have a too-large overhang

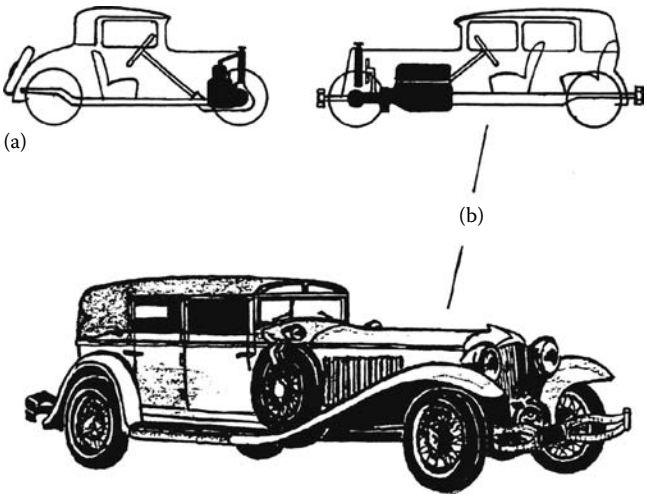


FIGURE 1.16
Front-wheel drive automobiles: (a) schematic of the Trakta vehicle (1926) designed by Jean-Albert Gregoire; (b) schematic and view of the Cord-L-26 automobile (1929) designed by E. L. Cord.

(kingpin offset) is not suitable for passenger cars. A steered wheel with a large kingpin offset exerts a greater resistance to turns and causes the machine difficult to steer. As a result, very few VORAN passenger cars were sold and their manufacture ceased.

Jean-Albert Gregoire, an engineering designer and entrepreneur, started to design in 1925 and constructed in 1926 a FWD vehicle that he called *Trakta* (Figure 1.16a). This was the first FWD vehicle with satisfactory handling. Satisfactory handling was achieved by a constant-velocity joint designed and constructed by Gregoire's companion, Pierre Fenay, a passionate devotee of the four-wheel driveline. Since Fenay's joint was used for the first time on the Trakta automobile, it has automatically acquired the car's name and it was patented in 1926 under the name Trakta.

The Trakta joint was much more compact than the constant-velocity dual Hooke's joint (Figure 1.17a). As was already said, shortly before this, Bussien attempted using the dual Hooke's joint for the steered driving wheels of a passenger car. This was not successful. Gregoire's Trakta avoided the fate of Bussien's automobile by using Fenay's joint.

The Fenay constant-velocity joint was followed by a similar joint designed in 1927 by a Czech engineer, Rzeppa, that was patented under the name of the Rzeppa joint and others (see Figure 1.17). Thus, between 1923 and 1930, there was a boom in inventing constant-velocity joints.

Toward the end of the 1930s and the beginning of the 1940s, the Trakta constant-velocity joint was used in the first of Erret Loban Cord's FWD vehicles. Cord's cars had an unusual appearance because of the very long engine hood (see Figure 1.16b). This was caused by the fact that the clutch mechanism as well as the gearbox were located in front of the engine, rather than at the back of it, as in the classical arrangement. This new driveline system turned out to be rather poor. It reduced the load on the front, both steered and driving axle, which impaired the vehicle's traction and its stability in taking turns. For this reason, front drive Cords did not last too long. But still, in spite of their short life, they left behind a rather happy memory. They are remembered as America's first cars with a fully shrouded radiator and having the longest engine hood.

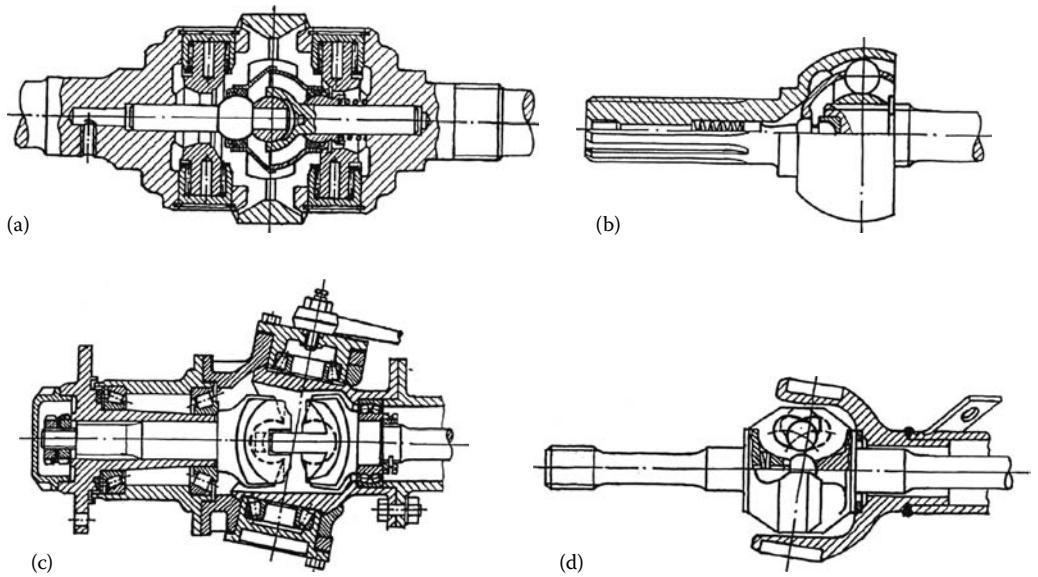


FIGURE 1.17
Equal-velocity joints: (a) Hooke's double joint; (b) Rzeppa's joint; (c) Bendix–Trakta joint; (d) Bendix–Weiss joint.

1.1.8 All-Wheel and Multiwheel Drive Trucks and Passenger Cars

As early as 1911, all-wheel drive automobiles designated as FWD started rolling out from the gates of the factory owned by Otto Zachow and William Besserdich. The FWD automobiles utilized the previously mentioned Dutch Spyker vehicle drive, but they differed by utilizing new ball joints in that part of the drive that provided for transmission of the engine power from the differential to the front, steered wheels of the car. These were by now constant-velocity joints. They were invented by one of the designers of the FWD vehicle—Otto Zachow. His joints, as opposed to the familiar single Hooke's joints, and the first Clarence Spyker joints, transmitted to the steered wheels of the car uniform rotation, this means that they were those first constant-velocity joints, which were badly needed by car manufacturers for setting up mass production of all-wheel drive vehicles. For this reason, starting with the FWD car, the U.S. automobile fleet started rapidly filling up with all-wheel drive vehicles.

In 1922, the French company Renault designed and started manufacturing the first in the world three-axle truck, the Renault MN. It was the first to use doubled wheels on all the axles, including the front steering axle.

The results of mobility tests of the Renault MN under difficult road conditions, even when using low-power engines (from 10 to 25 HP) that this machine used, exceeded all expectations. Three-axle trucks with doubled wheels were in no way inferior to the Citroen-Kegresse all-terrain (half-track) vehicles on poor roads and even exceeded them with respect to many performance indicators.

The only serious shortcoming of the Renault MN was its poor turnability. This stemmed from the fact that the forward, steering axle also had doubled wheels. Nevertheless, triple-axle trucks with doubled wheels enjoyed a very good reputation in spite of the doubled wheels on the steering axle. Their reputation improved even further when the Renault MN trucks completed a trip over African desert sands. The large supporting surface of the doubled wheels prevented the machines from sinking and digging deeply into the sand.

Up to 1931, it was up to the driver to decide whether to engage the front wheels. However, in the case of high-speed cars the advantage of all-wheel drive should be utilized permanently and independently of the driver. This can be achieved simplest by inserting into the drive between the driving axles of the car an open (also called free), symmetrical bevel-geared differential that divides the torque into half, i.e., by introducing a permanent drive between the two axles. This is the conclusion that was drawn by Ettore Bugatti, an Italian design engineer who lived in Elzas, France. Having ascertained from experience that the two driving wheels of a four-wheel automobile are not capable of fully utilizing the torque produced by a large-volume engine, he constructed three first 4×4 racing cars with a permanent interaxle drive of all four wheels, located between the two axles. His machines were known as *Bugatti-Type53*. The torque to the front steered wheels of these machines was transmitted by a double Hooke's joint. The Bugatti-Type53 machines had a reputation of being difficult to drive, as it became evident during their participation in races, because of the use of the double Hooke's joint. In connection with this, Bugatti's automobiles were used primarily for races on straight tracks that passed over rough terrain.

Starting with 1932, the English companies, Grey, Leyland, and Armstrong Siddeley, started constructing multiaxle, multiwheel drive and all-wheel drive trucks with complex arrangements for driving the axles and the driving bogies (or tandems). At that time, a vehicle similar to those mentioned above was constructed at the Yaroslavl Automotive Vehicles Plant in the U.S.S.R. (Figure 1.18). This was an all-wheel drive truck with an 8×8 wheel formula with steered and driving wheels in the front tandem and two driving nonsteered axles in the rear tandem. The steered wheels of each of the axles of the front tandem are coupled, as shown in Figure 1.18, to the differentials of their axles by means of drive shafts with Hooke's single universal joints. This stems from the fact that both axles of the front tandem are of the De Dion design. The drive of the ЯГ-12 vehicle, including the drive of the rear tandem, uses a total of 9 drive shafts with 18 Hooke's single universal joints. The second axle of the front tandem, as the first axle of the rear tandem, is of the drive-through type. They employ an original drive-through bevel-gear final drive shown in the figure. It should be noted that the ЯГ-12 machine, which was the name given to the above Yaroslavl plant product, left a good impression. It exhibited high mobility. It handled relatively easily up to 1.5 m wide trenches, fords, slopes of up to 30°, confidently moved over mud and deep snow; was capable of attaining speeds of 40–45 km/h on roads with minimum power consumption, at that time for this class of vehicles—52 L per 100 km of travel.

Ferdinand Porsche designed, in 1938, the folk passenger car the Volkswagen Beetle which was produced during World War II as a reconnaissance amphibian vehicle with a distinctive body. It was known as the ''pail-car'' (*Kubelwagen* in German) (Figure 1.19a). This was an all-wheel drive vehicle. It was the first car in which the drive of all the four wheels differed highly from the classical arrangement. The in-line four-cylinder engine of this vehicle was located in the rear part of the body. The engine, transmitted power to the rear driving wheels through a gearbox located past the engine—first to the rear axle and then from that axle to the front wheels—via a cardan drive. This 4×4 driveline system turned out to be simpler than the classical one. It still employed a dog clutch, that allowed the driver to couple also the front wheels to the engine, but it dispensed with a separate transfer case. This driveline system is called ''pure.'' It has attained final purity in the 1980s and 1990s. At that time, it will be put to use in the Audi Quattro car, where it was rotated through 180°, since the engine in the Audi Quattro is located ahead of the leading axle. Subsequently, Porsche himself continued using this driveline system in his all-wheel drive vehicles.

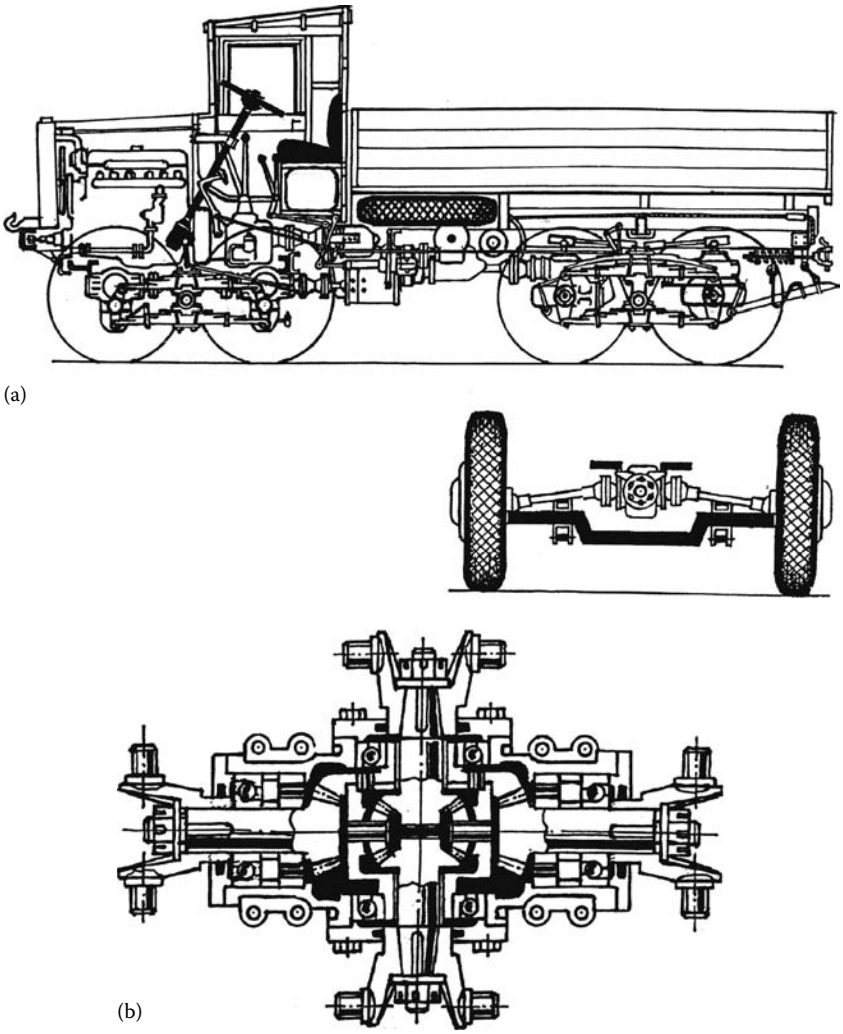


FIGURE 1.18
Design of the first Soviet-made four-axle, 8 × 8 formula truck, ЯГ-12, with two front-steered axles: (a) De-Dion-type steered and driving axle; (b) final drive of the drive-through axle.

While Porsche was working on his new 4 × 4 wheel driveline system, the U.S. industry continued producing such machines with the classical 4 × 4 driveline system. Thus, Karl Probst, an engineer working for the American Bantam company developed a design of a classical all-wheel driveline system for an army vehicle with a highly simple, open body (Figure 1.19b). The machine was manufactured and became a part of the U.S. army vehicle fleet. At first, it was called the ''Mobile Bantam,'' then ''Willys MB,'' and, finally, ''Ford GPV'' (Ford General Purpose Vehicle). During World War II, it was used, under the last name, as a light artillery towing tractor and staff car. Light artillery all-wheel drive vehicles with the classical driveline similar to the American ones were also produced in the Soviet Union under the brand name GAZ-67 (Figure 1.19c)

In 1947, an engineer, Spen King, employed by the British Rover Company designed a gas-turbine passenger car, the T3 Rover (Figure 1.20). This was a four-wheel drive

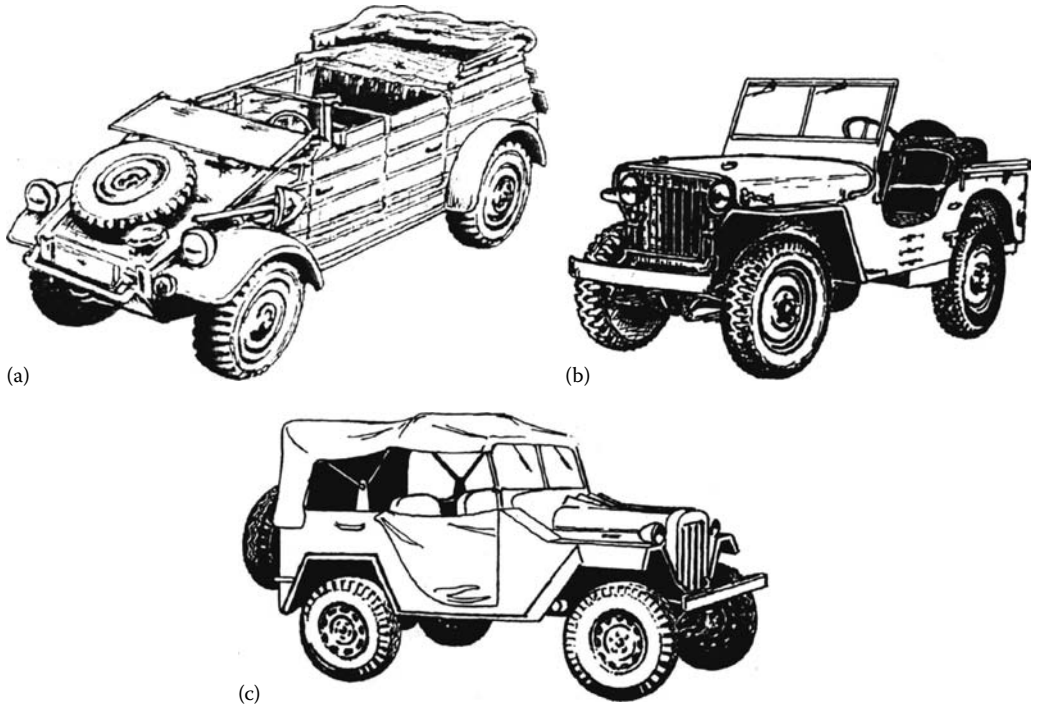


FIGURE 1.19
4×4 automobiles: (a) Kubelwagen with ''pure'' drive; (b) Ford GPV with classic drive; (c) GAZ-67 with classic drive.

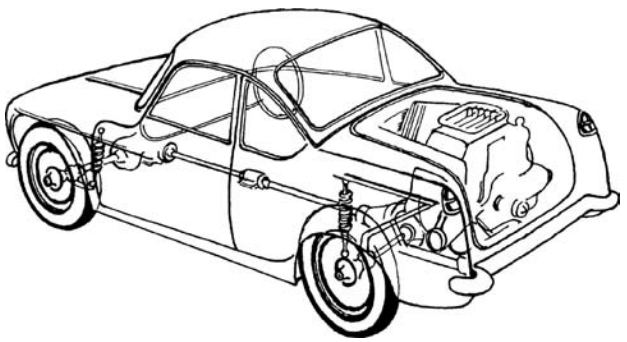


FIGURE 1.20
First gas-turbine 4×4 formula highway automobile—the T3 Rover (1947).

highway car. Its gas-turbine engine was located in the back. For this reason, the power from it was transmitted to the front axle from the rear axle. The two axles were coupled by an overrunning clutch. The kinematic discrepancy between the axles built into the driveline (analytic material on kinematic discrepancy is presented in Chapter 3), caused the clutch to disengage the front axle of the car when it took a turn. For this reason, the leading wheels could rotate when taking a turn at a higher speed than the rear wheels. At that time, it was a new progressive technical solution.

The driveline of the T3 Rover was very similar to that of the Kubelwagen. They differed from one another by the fact that the driveline of the former employed an overrunning clutch whereas of the latter—a dog clutch.

A system similar to that of the T3 Rover driveline, except that rotated through 180° because of its being located at the head of the engine and with an interaxle differential instead of the overrunning clutch, was used at the end of the 1970s the Audi-200 Turbo Quattro. It was noted by a large number of automobile manufacturers, impressed them, and has advanced it toward further development of a ''pure driveline.''

Starting with 1948, Rover started producing an all-wheel automobile with a permanent drive to the wheels under the name ''Landrover'' which, unlike the T3 Rover, had an ordinary internal combustion engine.

In the 1940s and 1950s, permanent four-wheel driveline systems of medium- and heavy-duty trucks came into extensive use. Dr. A. Kh. Lefarov headed a team during this time that designed a new 4×4 timber truck with an interaxle differential and redundant locking capacity, the first in the former Soviet Union (Figure 1.21).

Owing to consumer demand, the manufacture of the Buick 70 automobile began, starting in 1947, installing the Dynaflow hydrodynamic transmission, invented and constructed by G. W. Simpson. Starting with the next 1948 model, this transmission became a standard on all the Buick 70 cars. The Dynaflow transmission consisted of a torque converter and a mechanical planetary gearbox that provided one lower-speed gear and operation in reverse. The transmission was disconnected under ordinary driving conditions and was put into operation only under difficult road conditions and when using the engine for braking the automobile on descents to assist the brake operation. The car's motion under ordinary road conditions started with the torque converter converting the torque followed by its functioning as hydraulic clutch after the car attained the desired acceleration. This means that under ordinary conditions the transmission operated without shifting of gears, i.e., fully automatically. The Dynaflow transmission was followed by other similar devices. These were used not only in the drives of expensive passenger cars, but also in buses and in heavy-duty trucks.



FIGURE 1.21
MAZ-501, Belarus.

The construction of gas and oil mains, railroads, and highways, open-pit mining, mechanization of the timber industry, agriculture, and military needs call for the availability of high-performance all-terrain wheeled vehicles with high mobility and traction performance.

Such equipment can be designed by improving mobility of existing conventional vehicle designs as well as by special high mobility vehicles with original design solution of overall arrangement, units, and systems. High mobility vehicles are more suitable for the aforementioned tasks. This conclusion is to some extent supported by data in Table 1.1 that lists weight/payload ratios calculated from the expression

$$K_{wp} = W_c/W_g \tag{1.1}$$

where

W_c is the curb weight of the vehicle

W_g is the payload weight

The average value of K_{wp} of high-mobility machines is about 15% lower than that of those with improved mobility. At the same time the values of K_{wp} for both of these machines is higher than that of general-purpose vehicles.

Both the improved- and high-mobility machines typically employ multiwheel and all-wheel drivelines, with the number of driving axles being two or more. The use of such systems, driven by the need to further improve the mobility and capacity, increased greatly during the 1960s, which saw the appearance of 8×8 and 12×12 vehicles that provided capacities in excess of 50 ton (Figures 1.22 and 1.23).

Thus, the Semex-Tatra 4727OL pipe carrier had the 10×8 wheel formula; 10×6, 12×6, 14×8, and 16×8 chassis were utilized for Faun truck cranes. High-mobility chassis cranes with 8×8 and 12×12 wheel formulae were designed in the U.S.S.R. The Central Research Institute of Automobiles and Automobile Engines (NAMI, U.S.S.R.) designed an articulated dumpster consisting of a three-axle articulated truck tractor and a two-axle semitrailer. The Titan company (Germany) produced specialized automobiles with wheel formulas from 6×4 to 10×8 that were used as airport and in-plant truck tractors, communal vehicles and on oil fields.

The need to improve productivity by increasing the payload capacity under the existing limitations on the loading of road surfaces has resulted in an extensive use of multiwheel drive systems in ordinary and articulated trucks (combinations of a truck tractor and trailers and semitrailers) used for intercity transportation over upgraded roads. This not only reduces (or at least prevents increasing) the load on the wheels, but ensures high tractive and velocity operational properties in particular in the case of heavy- and extra-heavy duty highway trucks.

Statistical analysis of the use of various wheel formulae on highway heavy-duty trucks showed the following (Table 1.2). Two-axle drives (4×2 and 4×4) are used in lower-power vehicles as compared with automobiles designed to the 6×4 and 6×6 formulae. Here 4×4 vehicles having a somewhat lower mean engine power are used over a larger range of power classes than those 4×2 machines, which is seen from the values of the power of the coefficient of variations, equal to the ratio of the standard deviation to the mean value of the power. The same applies to 6×4 and 6×6 vehicles.

These statistical data are validated by results of the economic studies. Thus, all-wheel drive vehicles not only have longer service lives than 4×2 vehicles, but their resale value is also much higher. The depreciation costs for 10 years of operation of a 4×4 vehicle are, as a

TABLE 1.1

Truck Mass Parameters

Truck	Full Mass, ton	Wheel Formula	K_{wp}	Year of Truck's Data
Improved off-road mobility trucks, $K_{wp}^{average} = 1.398$				
GAZ-66	5.460	4 × 4	1.820	1982
ZIL-43273H	8.460	4 × 4	1.683	2006
Mercedes-Benz 1018A	10.500	4 × 4	0.736	2006
Mercedes-Benz 1318A	13.500	4 × 4	0.561	2006
ZIL-433440	10.715	6 × 6	1.777	2006
ZIL-131	11.685	6 × 6	1.337	1982
Ural 375D	13.025	6 × 6	1.605	1982
Ural 4320	13.245	6 × 6	1.645	1982
Ural 4320-41	15.400	6 × 6	1.567	2006
KrAZ-255Б1	19.525	6 × 6	1.604	1982
KrAZ-260	22.000	6 × 6	1.445	1982
KrAZ-6322	23.000	6 × 6	1.257	2006
MAZ-6317	24.050	6 × 6	1.370	1990
Steyr 26M 39	26.000	6 × 6	1.167	1994
High off-road mobility trucks, $K_{wp}^{average} = 1.215$				
Chrysler M-410	6.980	8 × 8	1.083	1967
Ford M-656	11.800	8 × 8	1.622	1967
Bussing NAG	17.000	8 × 8	1.427	1967
M.A.N.	22.000	8 × 8	1.193	1972
KamAZ-4310 + active semitrailer	23.175	10 × 10	1.295	1978
M977 A2	28.123	8 × 8	1.673	2006
M1074	39.200	10 × 10	1.376	1993
MAZ-543	40.500	8 × 8	1.025	1995
MAZ-79091	43.500	8 × 8	0.813	1995
MAZ-7916	82.000	12 × 12	0.640	1995
Road trucks, $K_{wp}^{average} = 0.802$				
GAZ-53A	7.400	4 × 2	0.849	1982
Mercedes-Benz 1018	10.500	4 × 2	0.544	2006
ZIL-130-76	10.525	4 × 2	0.754	1974
International 4300	10.660	4 × 2	1.255	2006
Mercedes-Benz 1018	13.500	4 × 2	0.495	2006
Mercedes-Benz 1328	13.820	4 × 2	0.531	2006
MAZ-53371	16.000	4 × 2	0.883	1982
KrAZ-5133B2	18.000	4 × 2	1.046	2006
Ural 377H	14.950	6 × 4	0.992	1982
KamAZ-5320	15.305	6 × 4	0.912	1982
ZIL-133ГЯ	17.835	6 × 4	0.783	1982
ZIL-6309HO	18.225	6 × 4	0.800	2006
KrAZ-257Б1	22.600	6 × 4	0.883	1982
KrAZ-65101	26.000	6 × 4	0.675	2006
KrAZ-65053	28.000	6 × 4	0.626	2006



FIGURE 1.22
MAZ-7310, 8 × 8.



FIGURE 1.23
MAZ-537, 12 × 12.

TABLE 1.2

Statistical Analysis of Heavy-Duty Highway Trucks

	Year of Production		
Wheel Formula	**1982**	**1990**	**2000**
4 × 2	147.5[a] / 34.0	167.6 / 36.1	186.4 / 34.8
4 × 4	126.7 / 42.8	155.3 / 44.0	178.6 / 43.1
6 × 4	191.0 / 17.0	237.3 / 18.3	254.2 / 19.2
6 × 6	190.1 / 26.6	211.8 / 28.3	228.7 / 27.6

[a] Mean power in numerator, kW; coefficient of variation in denominator, %.

rule, identical to those of a 4×2 vehicle operated for 8 years. It was also assumed reasonable that the value of a 4×4 machine be 25%–30% higher than that of a 4×2 vehicle. On the basis of transported freight above 10 ton the profit of a user can, in many cases, be greater from using a 6×4 vehicle than one with a 4×4 wheel formula. Truck tractors with 6×4 or 6×6 wheel formulae are extensively used in towing semitrailers with a full mass of 38–42 ton and more. These are MAZ-6422, Mercedes-Benz 2232, Scania-142N, and others.

Starting with 1940s trisection articulated machines consisting of a truck tractor, semitrailer and trailer came into extensive use in the United States. This arrangement is at present the most prevalent there, where at times four-section vehicles consisting of a truck tractor with a semitrailer and two trailers are also used. In Europe, the standard arrangement is a truck tractor towing two trailers.

The axles of the trailers and semitrailers may be powered. Thus, for example, Multidrive Ltd. (England) has designed transmissions for articulated carriers consisting of truck tractors and semitrailers with driving axles. The wheel formula of these carriers may be 8×6, 10×6 or bigger. Figure 1.24 shows an all-terrain truck tractor with a semitrailer with engine-powered wheels. The overall wheel formula of this carrier is 10×10.

Using a similar principle, the Krane Fruehauf Company has constructed a self-dumping carrier (truck tractor and a semitrailer) with a body volume of 25 m^3. The front wheels of the 6×2 truck tractor are steerable, whereas traction is supplied by the rear axle with double wheels. The front wheels of the semitrailer are also driving wheels. At the negligible penalty of the added weight of the transmission, the 38-ton carrier has a load-carrying capacity of 22.08 ton, which has corresponding to it a value of the weight/payload ratio (K_{wp}) of 1.721.

As a result of the tendency toward constant increasing the load-carrying capacity, many companies initiated, during the 1980–1990s, the manufacture of four- and five-axle vehicles. Companies such as Daimler-Benz, M.A.N., and Volvo also produce a wide range of such machines. Their 8×4 and 8×6 paved-road vehicles are usually operated



FIGURE 1.24
KrAZ-260D, 10×10.

at full mass of 32–35 ton and at times as high as 41 ton. The 8×8 all-wheel drive vehicles are usually designed for off-road work and have a full mass of 48–65 ton.

The increase in the number of axles improves the vehicle capacity. The total cost of transporting 1 ton of cargo by a four-axle vehicle is, as a rule, 30% lower than when using a three-axle truck.

The FTF Company (the Netherlands) was one of the first to produce five-axle vehicles with the 10×4 wheel formula (three steering axles). They could be provided with truck bodies or be used as truck tractors for pulling heavy loads. Chassis with the 10×4 wheel formula (three steering axles) are also used on Mercedes-Benz 4335 K dumpsters.

The Tatra Company has complemented the range of its multiaxle vehicles by the 10×8 five-axle vehicle. At full mass of 53 ton, the two leading axles carry 9 ton each, whereas the three rear axles—12, 12, and 11 ton.

Articulated carriers with truck tractors employing a large number of axles and with trailers that also employ a large number of axles have come into extensive use. In Sweden, articulated carriers with a full mass of 52 ton employ trailers with four axles. Articulated trucks in the Netherlands with a full mass of 50 ton employ 8×2 M.A.N. truck tractors.

A similar gradual increase in the use of multiaxle machines was and is observed in the manufacture of agricultural tractors. This was aided by the continuous rise in engine power and in the energy density of tractors. For example, the mean power of farm tractors produced in the United States increased approximately 3.5-fold during the last 35 years of the twentieth century. The power rating of class 1.4 Belarus tractors increased from 27.2 kW of the MT3-2 (in the 1950s) to 78.3 kW of the MT3-1025 as of today.

The first step in more completely utilizing the engine power was to increase the work velocities. Extensive experience in operating farm tractors with such energy density has validated this approach. At the same time, analysis shows that, as the engine power is increased, the rates at which the tractor velocities increase still decreases. Statistical studies of parameters of wheeled tractors with an energy density of about 20 kW/ton show that the dependence of the average design velocities V_{mid}, m/s, on the tractor mass m_{t}, ton, has the form

$$V_{\text{mid}} = 3.032 m_{\text{t}}^{0.321} \tag{1.2}$$

where $V_{\text{mid}} = 0.5(V_{\min} + V_{\max})$.

The rate of rise in V_{mid} decreases with increasing weight and power of the tractors and, starting with approximately $P_{\text{e}}^{\max} = 120$ kW and $m_{\text{t}} = 6$ ton, the average velocity remains virtually the same. This behavior of V_{mid} is attributable in the first place to the conditions under which agricultural operations are carried out, the increase in the resistance of soil-working implements with increasing vehicle velocity, etc.

The limitations on the velocity increase has shifted the efforts of utilizing the high engine power to increasing the width of worked soil and combining agricultural operations that allow to significantly increase the tractor's drawbar pull. At the same time, increasing the traction capacity increases the use of the adhesive weight (the weight taken up by the driving wheels) and, as a result, increases the power lost for slippage.

In addition, the use of heavy, wide span implements and combined agricultural operations significantly increases the normal loads on tractor wheels. The latter causes compaction and damage to the soil structure, reducing the yield. The yield of barley in track passages of MTZ-80 and K-700 tractors decreased by 12%–14% and that of potatoes—by 27%. In view of this, when outfitting tractors with their associated agricultural machinery it

becomes necessary to reduce the worked span, which decreases the traction and underutilizes the engine power.

Investigations and experience shows that the most cardinal way of increasing the tractor traction performance and utilizing the engine power is using all-wheel driveline systems.

The high traction performance of 4×4 tractors allows increasing the time available for agricultural work and enhancing the tractor's utilization on a year-round basis. In addition to improved traction, 4×4 tractors have velocities higher than their 4×2 counterparts do. Analysis shows that the average velocities of 4×4 tractors at nominal drawbar pulls are 10%–14.5% higher than the average velocities of 4×2 tractors.

A statistical analysis of more than 4000 agricultural tractors was undertaken. Comparison of power-distribution densities shows that a 4×2 tractor's power P_e^{max} the coefficient of variations reduced from 39.7% in 1970 to 24.8% in 1995, while 4×4 enjoyed growth of this parameter from 33.6% up to 37.8%. The coefficient of variation changes of that kind attest to a still bigger advantage of all-wheel drive tractors and a decrease of power P_e^{max} range in which 4×2 tractors are used. Studies of power distribution densities $f\left(P_e^{max}\right)$ of 4×2 and 4×4 tractors having identical and nonidentical wheels produced in the years to follow brought forth approximately similar results (Table 1.3).

This manner of changes in the coefficient of variations points to ever increasing use of all-wheel drive tractors and the reduction in the range of P_e^{max} within which 4×2 tractors are used. The higher capacity of 4×4 tractors as compared with 4×2 ones is responsible for the fact that all the currently manufactured and under-design wheeled tractors, including those with moderate capacities either have all-driving wheels or employ all-wheel drive modifications.

Positive locking units secure the best indicators of a tractor's tractive properties in the field. From the design point of view, this is done as follows. Interaxle drives employ positive locking axle engagement with the possibility of disengaging one of them or have interaxle differentials with a backup positive locking system installed in them. Locking and self-locking differentials are widely used in tractors' driving axles.

Two-axle drives have gradually penetrated also into passenger car designs. At the end of the 1950s, an original four-wheel driveline design was developed at the Ferguson Company. It included an interaxle differential with overrunning clutches (see Figure 1.25).

TABLE 1.3

Statistical Analysis of Agricultural Tractors

Year of Production	Agricultural Tractors		
	Agricultural Tractors 4×2	4×4 with Different Front and Rear Wheels	4×4 with the Same Front and Rear Wheels
1982	48.1[a] / 33.1	60.1 / 45.3	98.2 / 48.8
1984	46.0 / 28.4	60.1 / 46.3	93.0 / 53.9
1986	47.7 / 29.9	63.9 / 42.0	116.3 / 40.1
1989	51.2 / 28.1	64.8 / 41.8	98.3 / 56.3
1995	53.9 / 29.2	67.4 / 45.2	112.8 / 48.8

[a] Mean power in numerator, kW; coefficient of variation in denominator, %.

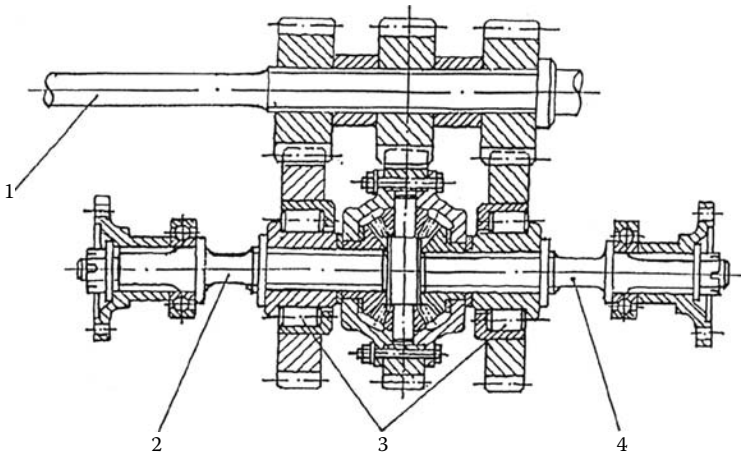


FIGURE 1.25
Concept of Ferguson's center differential and free-running clutches: 1, input shaft of transfer case; 2, output to front axle; 3, roller-type overrunning clutches; 4, output to rear axle.

Power to the interaxle differential in this drive was fed by the input shaft 1 of the gearbox through overrunning clutches 3 and transmitted it, dividing it into halves, through shaft 2 to the leading axle and through shaft 4 to the rear axle. The overrunning clutches allowed the leading axle wheels to turn freely when the vehicle took a turn. In addition, the clutches automatically locked the differential when the wheels of one of the axles slipped. Then one clutch locked the interaxle differential upon slipping of the front-axle wheels and the second—upon slipping of the rear-axle wheels.

Ferguson's design was developed further in the Jensen FF car, in which Jensen, an engineer with the Harry Ferguson Research Ltd., used a nonsymmetrical interaxle differential of the epicyclical type. He supplied 63% of the torque to the rear axle and 37%—to the front axle. This improved the road stability of the vehicle. Secondly, the overrunning blocking clutches were replaced by a multidisk clutch that operated on an organosilicon fluid. This was one of the first cases of utilizing a viscous clutch as a locking mechanism. This clutch perceptibly simplified the design of Jensen's driveline system. Finally, Jensen replaced the mechanical locking device employed in the Ferguson driveline by an electronic locking device.

The Ferguson and Jensen driveline designs started seriously attracting the attention of automobile manufacturers during the 1980s. As an example of a similar drive produced at that time, the ''Zahnradfabrik'' can be referred here (Figure 1.26).

The autumn of 1964 saw the start of the series production of the Porsche 911 all-wheel drive passenger car, designed by the son of the famous Porsche, whose first name was also Ferdinand and was known as Ferry Porsche. This machine was regarded as the best automobile of 1960–1969. The Porsche 911 had an air-cooled rear-mounted six-cylinder in-line engine rated at 130 HP. Its primary driving axle was in the rear. Power to the front steering axle was supplied with the same arrangement used previously on the Kubelwagen designed by Porsche Senior, with the only difference that the driveline of the Kubelwagen employed a dog clutch, whereas the Porsche 911 used a hydraulically controlled multidisk friction clutch. The engine, the gearbox, the rear-axle differential, the interaxle multidisk friction clutch together with the drive shaft for the front driving axle of this vehicle comprised a single compact subassembly. A permanent interaxle

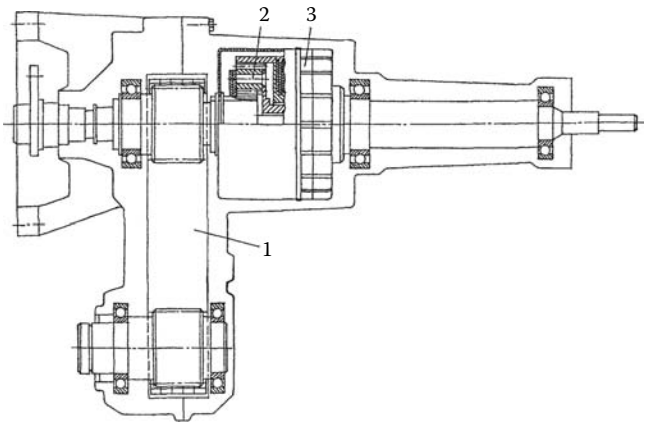


FIGURE 1.26
Kinematic diagram of a ZF A-95 transfer case: 1, front-axle chain drive; 2, planetary type central differential; 3, viscous clutch.

differential driveline was also employed by Porsche. Later, in 2005, there appeared the new, 977 version of the Porsche 911 with a multidisk viscous coupling which transfers from 5% to 40% of the tractive force to the front wheels.

Toward the end of the 1970s, the Matra Company that manufactured Formula 1 sports cars, attempted to design a mixed driveline for its all-wheel drive automobile. In it, the rear wheels were to be driven mechanically, whereas the front wheels, by means of a hydrostatic drive (see Figure 1.27).

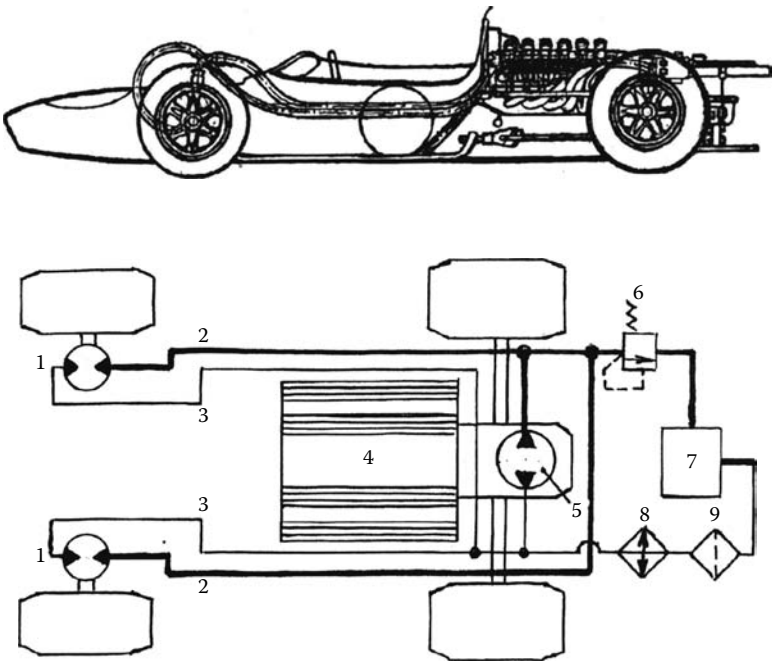


FIGURE 1.27
Tentative design of hydrostatic drive of the forward axle of a Matra sports car: 1, hydraulic motors; 2, hydraulic motor fluid supply lines; 3, hydraulic motor fluid drain lines; 4, internal combustion engine; 5, fluid pump; 6, pressure (safety) valve; 7, oil tank; 8, radiator; 9, filter.

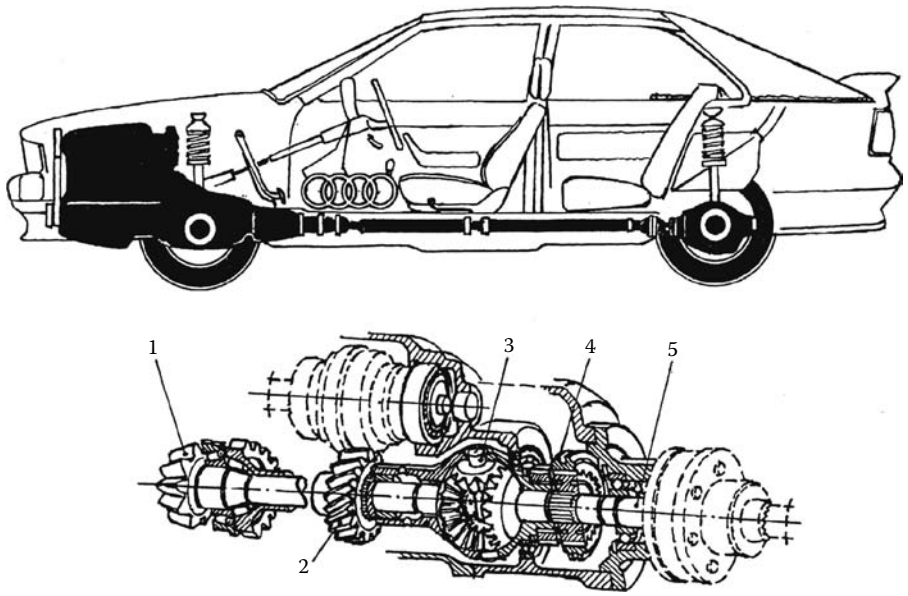


FIGURE 1.28
Schematic of permanent drive of Audi-200 Turbo Quattro: 1, pinion of final drive of the front axle; 2, gear pair connecting the case of the central differential with the output shaft of the gearbox; 3, central differential; 4, locking clutch; 5, differential output shaft—an element of the drive to the rear driving axle.

In 1980, the manufacture of the Audi-200 Turbo Quattro was started. The vehicle combined the response of a sports automobile and a high comfort and safety level. It owed this to turbocharging and other modern achievements of this time in vehicle manufacture that were embodied in it. The Audi-200 additionally boasted a ''pure,'' highly lightened drive of the wheel pairs (see Figure 1.28).

The interaxle (central) differential together with the front-axle differential were built into the Quattro's transmission. As a result, the driveline was ''pure'': there was no transfer case.

Irrespective of the merits of the first all-wheel drive passenger cars, there is no doubt that the Audi-200 was precisely the vehicle from which the boom in manufacturing similar cars by other makers started. Somewhat later, there appeared the VW Passat Variant Syncro with the same driveline arrangement. The all-wheel drive concept that was developed for the Lancia Delta Turbo 4×4 became an alternative to the Audi. In this vehicle, the engine and the transmission are located transversely, which made it possible to place the planetary interaxle differential in the housing of the final drive of the transversely placed power unit. The interaxle differential divides the power between the leading and trailing axles in a 58/42 proportion and the cardan shaft transmits rotation to the rear wheels. This arrangement also dispenses with the transfer case. The 2 VW Type was one of the first trucks with a ''pure'' drive in which the front steered and driving axle was coupled automatically to the engine by a viscous clutch. It should be noted that heavy-duty all-wheel drive trucks also entered the realm of the permanent drive. The operation of drive axles in these vehicles is often controlled by specially designed electronic systems. According to some estimates, the ratio between cars with 4×2 and 4×4 wheel formulae will soon be one to one.

1.1.9 Power Dividing Units

The use of all-wheel drives does not fully exhaust the potential for improving traction-velocity properties even though it is assumed that the coefficient of utilization of the traction weight of all-wheel drive vehicles is equal to unity. That is the entire weight participates in generating the traction power, as compared with ordinary-driveline (or nonall-wheel drive) vehicles, in which a part of the weight devolves upon the driven wheels

$$K_w = W_{dr}/W_a \tag{1.3}$$

where

W_a is the gross weight of the vehicle

W_{dr} is the adhesion weight, i.e., the weight devolving upon the driving wheels

Note that for ordinary-drive vehicles, $K_w < 1$.

Nevertheless, the possibility still exists that even the adhesion weight of all-wheel drive vehicles may be underutilized. This happens, for example, in the case of open differentials and when the wheels of the vehicles move under different road conditions, when the driving wheels with better conditions are not able to develop the required traction. For this reason, together with the active development of all-wheel and multiwheel designs, a continuous search is under way for designs of power dividing units (PDUs) that would be capable of dividing the power among the driving wheels in accordance with the tire surface grip.

A multidisk clutch that employed an organosilicon fluid—polymethylsiloxane (abbreviated to siloxane)—was patented in the United States in 1917 for use as a locking mechanism. As opposed to ordinary incompressible fluids, siloxane—the working fluid of the clutch—is a compressible (non-Newtonian) fluid. When this polymer is stirred, its spirally shaped macromolecules increase in volume with attendant increase in viscosity as a function of the shear strain (gradient of velocity between the layers). Figure 1.29a shows

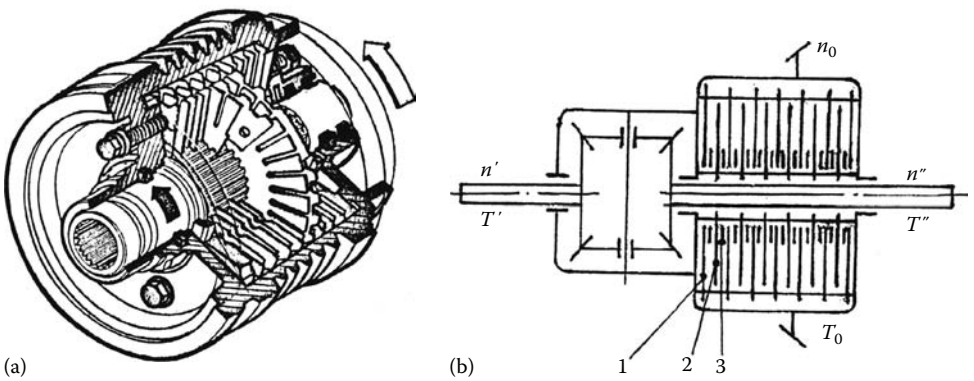


FIGURE 1.29
Viscous clutch and differential schematics: (a) viscous clutch; (b) differential with a viscous clutch, equipped with disks 1, coupled to the case; disks 2, coupled to the output shaft; 3, spacer rings.

an example of such a viscous clutch. It consists of a housing and shaft with which alternating driving and driven disks, made of soft 0.25–1.0 mm thick sheet steel are coupled by means of splines. A 0.1–0.2 mm clearance is left between the disks. In certain viscous clutches, spacing rings are used for maintaining the spacing between the disks constant. When no such rings are installed, the disks are polished and a 5–50 μm thick antiscuff coating is applied to their surfaces. The disks of the viscous clutch are perforated by slots and holes of different configurations to enhance their mechanical effect on the working fluid. The configuration (shape) of the slots and holes is selected experimentally. The leak-proof housing of the viscous clutch is filled to 90%–93% of its volume. The fluid-free parts of the volume serve as a ''safety chamber'' that does not allow the expanding siloxane to exert a destructive force on the viscous clutch.

The first viscous clutch was designed during the 1960s by T. Rolton and D. Gordner, who were on the staff of the Formula Ferguson Research Company. The design of the viscous clutch was similar to that described above. However, no such clutch was put into production during the year when it was designed since the Formula Ferguson Research Company closed down and the patent was transferred to the GKN Company. This company, together with the Zahndradfabrik corporation, formed the Viscodrive company in Germany that started producing viscous clutches for BMW cars (Germany) and for Ford automobiles. Viscodrive opened a branch in Japan that started producing viscous clutches for Toyota and Nissan automobiles. Honda obtained a license from GKN and started producing viscous clutches for its own cars. In 1979, mass production of viscous clutches, also under GKN license, was undertaken for Eagle car models of the American Motors by New Process Company, a Division of Chrysler. Viscous clutches were also produced by the Steyr-Daimler-Puch Company (Austria) for the Caravelle-Syncro Volkswagen minivan. The viscous clutch is used for automatically coupling one of the axles of the vehicle and also as a locking mechanism of differentials (Figure 1.29b).

The MacPower Divider self-locking differential was invented in the United States in 1929. It was used on 4×4 trucks as an interaxle PDU and from 1948, it also came into use as an interwheel differential for driving axles. In both cases, it improved mobility and traction performance of the vehicles.

Mule and Scarlock invented in 1932 a self-locking worm-gear differential. Initially nothing was known about its locking performance and no use was found for it. Then, after its properties were learned, it gradually came into use as an interwheel differential on heavy-duty trucks and on truck tractors. It came into wide use in the 1950s. It exhibited good performance in drives of tri-axle very heavy-duty trucks and special tractors used in quarries and in snow removing and similar machines. A modification of the worm-gear differential that lacked additional satellite gears with radial axes was extensively used in drives of vehicles produced by the Walter Company.

A double-acting overrunning clutch under the name of Tronton-Tandem was designed in the United States in 1937. This was a differential of a kind that provided for automatic uncoupling of the outer wheel from the drive at the time when the machine took a turn. Because of this property, it was used by different companies on 22 models of trucks rated at from 0.25 to 4 ton. The Tronton-Tandem was the second double-acting free-running differential. The first such was the Multi-Pull differential (Figure 1.30a).

Unlike the Tronton-Tandem, the Multi-Pull had a number of shortcomings and did not come into such extensive use as the former. A further development of the double-acting free-running clutch is exemplified by the NoSPIN differential designed by the engineering staff of the Detroit Automotive Products Corporation. This reliable mechanism is in

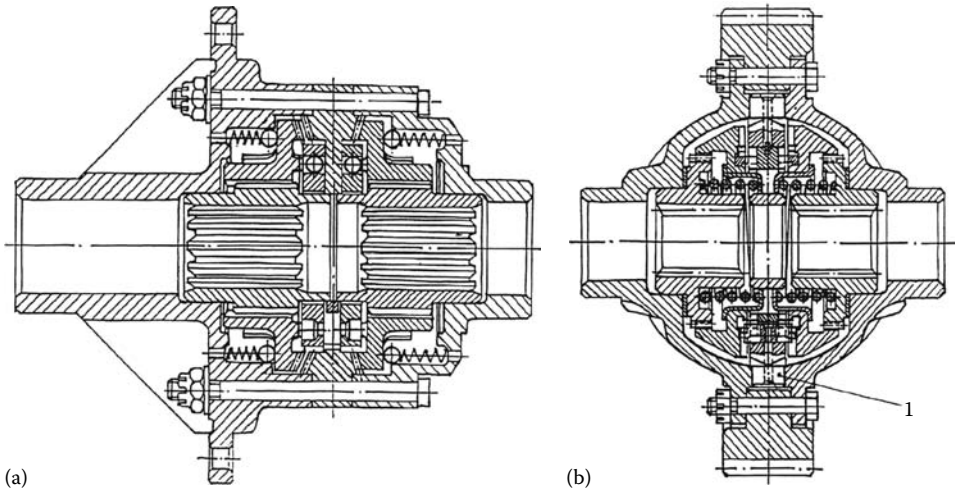


FIGURE 1.30
Overrunning self-locking differentials: (a) ''Multi-Pull''; (b) MAZ, Belarus.

production even currently. When it first appeared, the Ford Motor Company engineers used it as a basis for designing nine NoSPIN models for different vehicles from trucks to passenger cars. Differentials that operated on the NoSPIN principle were developed under the leadership of Dr. A. Kh. Lefarov (Figure 1.30b) and have been used in multiaxle vehicles of MAZ company (Figures 1.22 and 1.23).

The Thornton Power Lock self-locking differential that utilized friction disks (Figure 1.31a) was designed in the United States in 1956. Its locking properties were first tested out

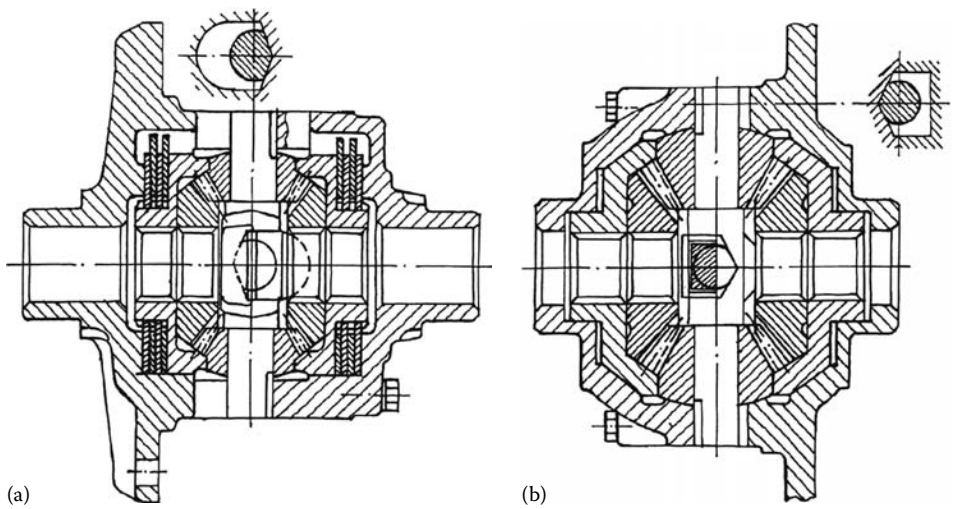


FIGURE 1.31
Thornton Power Lock self-locking differential: (a) with disk-type friction clutches (1956); (b) with cone-shaped friction clutches.

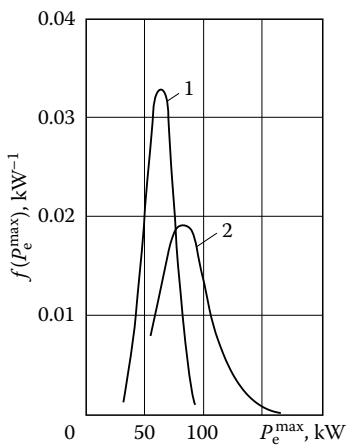
on certain models of Packard passenger cars and then, on popular demand, it was also installed in Studebacker cars. As of the middle of 1958, the Thornton Power Lock Company produced and installed about 200,000 differentials with friction disk clutches.

The Thornton Power Lock differential had, instead of the spider two pins located one across the other at a right angle with a pair of pinions on each of the pins. One pin presses by its ends, beveled at a certain angle, on the beveled slots in the apertures of the plain half of the differential case, whereas the other pin, with its ends, beveled at a certain angle, presses on the beveled slots in the apertures of the flange half the differential case. This allows the pins with their pinions to move each in its direction, relative to the principal axis (axis of rotation) of the differential and press either the friction cones (Figure 1.31b) or, by means of the pressure rings, the disk stacks (see Figure 1.31a) to the right and left halves of the differential housing. This will be accompanied by an increase in the friction torque inside the differential and this will cause the half axles to lock and the torque to be redistributed between the driving wheels of the axle. In addition, this provided for transmitting a higher torque to the wheel having the better adhesion with the supporting surface.

Self-locking differentials with a large variety of features came into extensive use. These differentials came into wide use in passenger cars, by customer order, starting with the middle of the 1980s. Analysis shows that these mechanisms were installed on vehicles with a wide range of power ratings: from 50 to 150 kW (Figure 1.32). Such a tendency is also retained in modern designs.

With increasing engine power and traction loads on axles, differential mechanisms with different locking methods came into increasing use in driving-axle reducers of highway truck tractors (particularly of heavy-duty highway trucks). Table 1.4 lists the percentage breakdown of various driving axle differentials installed on 1990 model year trucks.

Approximately the same tendency prevails until now. Approximately 60% of trucks use locking driving-axle differentials, 14% self-locking differentials, and the remaining 26% open differentials. These differentials are distributed among trucks of different power classes and different wheel formulae in the following manner. One half of trucks with a full mass of 2.5 ton and above with 4×2 and 4×4 wheel formulae have locking differentials on their rear axles, and approximately 17% of these trucks have self-locking differentials. The remaining 33% (usually these are light- and medium-duty trucks) are



N	Parameters
1	68.0*/22.7
2	89.9/22.3

FIGURE 1.32
Power distribution density (P_e^{max}) of 4×2 passenger car engines: (1) with open differentials; (2) with self-locking differentials on customer order; *the numerator gives the mean power, kW; and the denominator—the coefficient of variation, %.

TABLE 1.4

Power-Dividing Units on 1990 Trucks—Statistical Data

	Percentage of PDUs on Trucks with Full Mass of				
PDU in Driving Axles	**Less than 2.5 ton**	**2.5–4 ton**	**4.5–9 ton**	**9–12 ton**	**12 and More ton**
Open differentials	65%	65%	33%	—	—
Locking differentials	—	—	34%	100%	100%
Limited-slip differentials	35%	35%	33%	—	—

equipped with open differentials. About 90% of extra-heavy duty trucks with wheel formulae of 6×2, 6×4, 6×6, 8×6, and 8×8 use locking interwheel differentials. The remaining 10% use self-locking units.

Statistical analysis shows that the selection of a given PDU for use in agricultural tractors depends on the power, weight and geometries of the tractors as well as on general engineering considerations. In the overwhelming majority of cases, tractors with identical front and rear wheels use interaxle locking differentials. Tractors with smaller front-wheels have front axles with either free- or self-locking differentials. As a rule, locking or in some cases self-locking differentials are used in rear-driving axles of such tractors. Table 1.5 presents statistics on the power distribution densities of 4×4 tractors employing different types of front-axle differentials.

It is seen that the range of applicability of limited-slip differentials on tractors of different power classes is much broader than the range of applicability of free differentials. Locking differentials are used on tractors of the same power classes as limited-slip differentials. The locking action of the differentials is usually attained by hydraulic and much less frequently—by pneumatic control.

An overall assessment of the development of designs of components and systems for distributing power among axles and their wheels, shows that this development proceeded from the simple to the complex. It started in 1930–1940s with the development of mechanical self-locking differentials of the worm-gear type, differentials with friction clutches, speed-sensitive and torque-sensitive differentials, and continued during the 1970s and

TABLE 1.5

Statistical Analysis of Agricultural Tractors

	Differentials		
Year of Production	**Free**	**Self-Locking**	**Locking**
1982	49.8 / 36.8	76.1 / 48.2	—
1986	44.5 / 22.3	68.4 / 42.5	71.8 / 42.5
1989	48.7 / 31.9	70.6 / 44.9	68.3 / 43.1
1995	49.4 / 32.7	72.4 / 45.3	73.6 / 44.2

Note: Mean power in numerator, kW; coefficient of variation in denominator, %.

1980s with design of electromechanical locking and electronically controlled units. Special mention is deserved by the Auto-Lock system for locking the interaxle differential of the 6×4 truck (Rockwell International, New York), the 4MATIC electronic system for the Mercedes (Daimler-Benz, Stuttgart, Germany) passenger car, the locking device for a differential that is actuated by the difference in wheel speeds of agricultural tractors (SIGE) and many others.

Today, some automotive companies are introducing ''torque-bias coupling,'' ''torque-vectoring,'' and ''torque management'' devices to control power delivery to the front and rear axles and the left and right wheels (see Chapter 7). These driveline systems are actually mechatronic systems, and the introduction of such mechatronic designs is an epoch-making step in driveline system design. The mechatronic driveline systems are more ''flexible'' and proactive in distributing the engine power to the driving wheels than automated mechanical systems, e.g., the different limited-slip differentials, mechanically/electronically lockable differentials, viscous clutches, NoSPINs, on-demand systems and many others.

At the very beginning of the development of driveline systems and PDUs, the sole purpose was improving the mobility of the vehicles. Today an increasing number of OEMs and suppliers recognize the fact that vehicle operational properties such as tractive and velocity properties, stability of motion, turnability, handling, braking properties highly depend on characteristics of driveline systems that distribute power to the driving wheels. It is important to emphasize that the fuel economy and safety of vehicles that are vehicle consumer properties also depend to a large extent on driveline system designs. For this reason, driveline systems for distributing the power to the driving wheels should be designed with consideration of their combined effect on many of the vehicle operational and consumer properties.

This book is concerned with problems of driveline design precisely from the point of view of their combined effect on the performance and dynamics of wheeled vehicles.

1.2 Classification of Driveline Systems and Power Dividing Units

Depending on the manner of power transmission, all drives can be classified as electrical, hydraulic, mechanical, and hybrids. This section examines in detail mechanical driveline systems, including those of vehicles with different steering systems. Electronically controlled mechanical driveline systems are defined as mechatronic driveline systems. When speaking about mechanical and mechatronic driveline systems, many publications as a rule refer solely to the wheel formula, and at times adding information on types of the differentials. These data are clearly insufficient for complete description of driveline systems and for understanding their integration within the overall design of the vehicle. After all, frequently even vehicles of the same type use different mechanisms: symmetrical and asymmetrical differentials, positive locking engagement, self-locking differentials, limited slip differentials, free running clutches, viscous clutches, etc. This is particularly intrinsic to off-road vehicles. Thus, the driveline system the International Harvester XM-409 was fully differential with redundant locking. The 8×8 M.A.N. and Tatra-813 vehicles have the same driveline systems. In the latter, the distance between the axles of the front bogie (or tandem) is somewhat larger than that between the axles of the rear tandem. Many vehicles use mixed systems with different coupling-unit mechanisms. For example, the

central differential of the MAZ-79091 8×8 truck is a symmetrical, bevel-gear differential with redundant locking, the interaxle drive of the rear tandem is constantly locked and the interaxle drive of the front tandem and also the interwheel drives of the front tandem axles employ symmetrical open differentials. NoSPIN type differentials are used in the interwheel drives of the axles of the rear tandem. The wheel drives of the XM-453E1 truck with an 8×8 wheel formula and with tandem arrangement of the axles employ limited slip Power-Lock differentials.

The above example demonstrates the need for a tool that would provide a detailed description of the various existing driveline systems as a part of the overall design of the vehicles, from which it will be easier to understand the reasons for using the particular driveline system design. Design engineers need such a tool for describing and representing the driveline system that they design. The SAE J1952 Standard All-Wheel Driveline Systems Classification contains definitions to be used to outline the basic nomenclature and to classify all-wheel drive concepts. Some information is also contained in the *Terrain-Vehicle Systems Standards*, worked out by the International Society for Terrain-Vehicle Systems (ISTVS).

Historically, the terms and definitions pertaining to the classification of drive schemes were developed in the course of new driveline system design. The definitions of different types of drives were worked out primarily with consideration of marketing needs rather than from the point of view of the technical substance of the systems. For example, the term permanently engaged rear-wheel drive with the on-demand engagement of the front wheels by means of the transfer case is applied to 4WD. The same term, 4WD is applied to vehicles in which the two axles are coupled by an interaxle differential in the transfer case. This means that the same term is applied to vehicles, the driveline systems of which have an entirely different effect on vehicle performance. At the same time, the term AWD (all-wheel drive) is also applied to vehicles in which the interaxle differential is combined with the interwheel differential of the front axle. Following this logic, the same vehicle could be labeled as 4WD or AWD depending on the location of the interaxle differential—in the transfer case or together with the front-axle interwheel differential. However, the location of the interaxle differential does not affect the entire vehicle's performance.

In this book, driveline systems with two, four and more driving wheels are classified from the point of view of their effect on vehicle performance. The specifics of a given arrangement are reflected by means of additional indicators that integrate the driveline system with the overall vehicle design. The effect of the driveline system on vehicle performance depends on the characteristics of the locking properties of mechanisms and subsystems of the driveline system, i.e., their ability to distribute the power among the driving wheels. The overall vehicle design layouts first introduced by P. V. Aksenov include the type and location of the driving axles within the overall arrangement of all of the vehicle's axles, the steering system, type of suspension, and dimensions of the tires of the different axles of the vehicle. Consider details of the developed classifications.

The wheel formula of all types of drivelines is designated by a single expression $2m \times 2n$, in which n is the number of the driving axles to which the engine power is transmitted, whereas m is the total number of driving and driven (not coupled to the driveline system) axles. If $m = n$, then the vehicle is called an all-wheel drive vehicle. For example, 4×4, 6×6, 8×8, 10×10, 12×12, and 16×16 are all-wheel drive vehicles. Vehicles with different numbers of driving and driven axles, for which $m \neq n$, are known as multiwheel drive vehicles. Thus, for example, vehicles with wheel formulas 6×4, 8×4, 8×6, and 14×6 are multiwheel drive vehicles. The term nonall-wheel drive is applied to vehicles with two

driving wheels. These include FWD and RWD vehicles with 4×2 wheel formula; vehicles with wheel formulas of 8×2 and 6×2 are also nonall-wheel drive vehicles.

The relationship between the driveline system and the overall vehicle design is expressed by means of the following indicators.

The drive formula gives the location of the driving axles within the overall design of the vehicle. For example, the designation 0034 corresponds to an 8×4 vehicle with the third and forth axle powered. A 12×12 vehicle has a drive formula written as 123456, whereas a 6×2 vehicle with a rear-wheel drive is designated as 003.

The axle formula symbolizes the number of axles situated in a row. For example, a vehicle with four axles (let us say, 8×8, 8×6, 8×4) that form two tandems have an axle formula of 2-2, whereas vehicles with four axles in which the second and the third axles are located close to one another have the axle formula 1-2-1. If a vehicle has wheels of different dimensions on the different axles, then the height of numbers in the axle formula should be different. For example, an agricultural tractor with two axles and smaller tires on the front wheels has the axle formula 1-1.

The steering formula gives the ordinal number of the steered axle. For example, the steering formula for a vehicle with three axles in which the second and third axles form a tandem, whereas the front axle is steered, is 1-00. A vehicle with two axles, of which the front axle is steered, has a steering formula of 1-0. For articulated vehicles, additional designations are provided in the steering formula:

v, for an articulated trailer without control
$\frac{v}{c}$, for an articulated trailer with control
s, for a fifth wheel (a tractor-semitrailer combination)

For example, the steering formula $0\frac{v}{c}0$ corresponds to an articulated vehicle with two nonsteered axles and that is able to take turns by means of a controlled relative rotation of two segments of the vehicle about a vertical hinge. Steering systems are depicted graphically in Table 1.6.

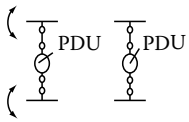
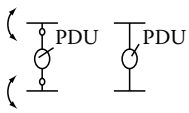
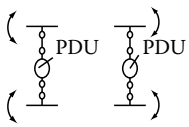
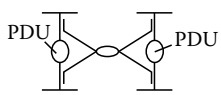
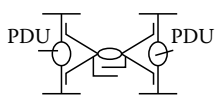
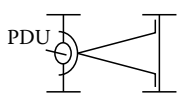
In this book, the systems that distribute the power to the wheels are defined by the concept of PDUs. Within the context of their effect on the vehicle performance, PDUs are classified by the attributes of their locking properties, i.e., on the basis of their effect on the distribution of power between the output shafts. The examples shown in Figure 1.33 illustrate types of PDUs, one of which requires additional explanation. These are planetary gear sets with two or more than two degrees of freedom and locking coupling. This is a new recently emergent type of PDUs that is used in sophisticated driveline systems. The designs of such PDUs include open differentials with additional planetary rows and locking couplings. The couplings consist of controllable friction, magneto-rheological or other clutches. This is concerned to one or another measure with virtually all types of PDUs shown in Figure 1.33.

To graphically represent the various PDUs, Table 1.7 presents designations for the most typical designs. Here there is no need to use different symbols for PDUs of the same type. For example, the same symbol $\otimes$ is used for all the limited slip differentials some of which are shown in Figure 1.33 for illustration purposes. Instead of using a large number of symbols, it is proper to write out which limited-slip differentials are used on the given vehicle. This approach is taken because a large number of designs with the most different features have already been produced and are under development.

In addition to PDUs, graphic representations of driveline units are described by Power Transfer Units (PTUs, see SAE J1952 Standard). However, in the present book the

TABLE 1.6

Steering Systems

Type of System	Designation	Steering Formula
Drive-steer and nonsteer articulated axles with independent suspension		1-0
Drive-steer and nonsteer conventional axles with dependent suspension		1-0
Drive-steer articulated axles with independent suspension		1-1
Lag hinge without steering: v		$0\overset{v}{-}0$
Lag hinge with steering: $\frac{v}{c}$		$0\frac{v}{c}0$
Fifth wheel hinge without steering: s *Notice*: Second axle is driven (nondriving)		$0\overset{s}{-}0$

definition of this term has been extended: PTUs are used for controlling power flow between their input and output elements. Typical graphical symbols of PTUs are presented in Table 1.8.

Using the PDUs and PTUs from Tables 1.7 and 1.8 it is possible to compose different driveline systems that shall be termed simple, combined, and integrated. Definitions of these systems are given in Figure 1.34. A simple driveline system may be exemplified by the drive of a 4×4 automobile with open differentials in the driving axles and an open differential in the transfer case. This means that in a simple driveline system identical mechanisms are used in all the PDUs. Should at least one of the differentials of the above vehicle be a limited-slip differential, then such a driveline system will be known as a combined system. If the vehicles under study are equipped, for example, by a traction control system, then their systems will be known as integrated, since the driveline system is functionally coupled to the braking system.

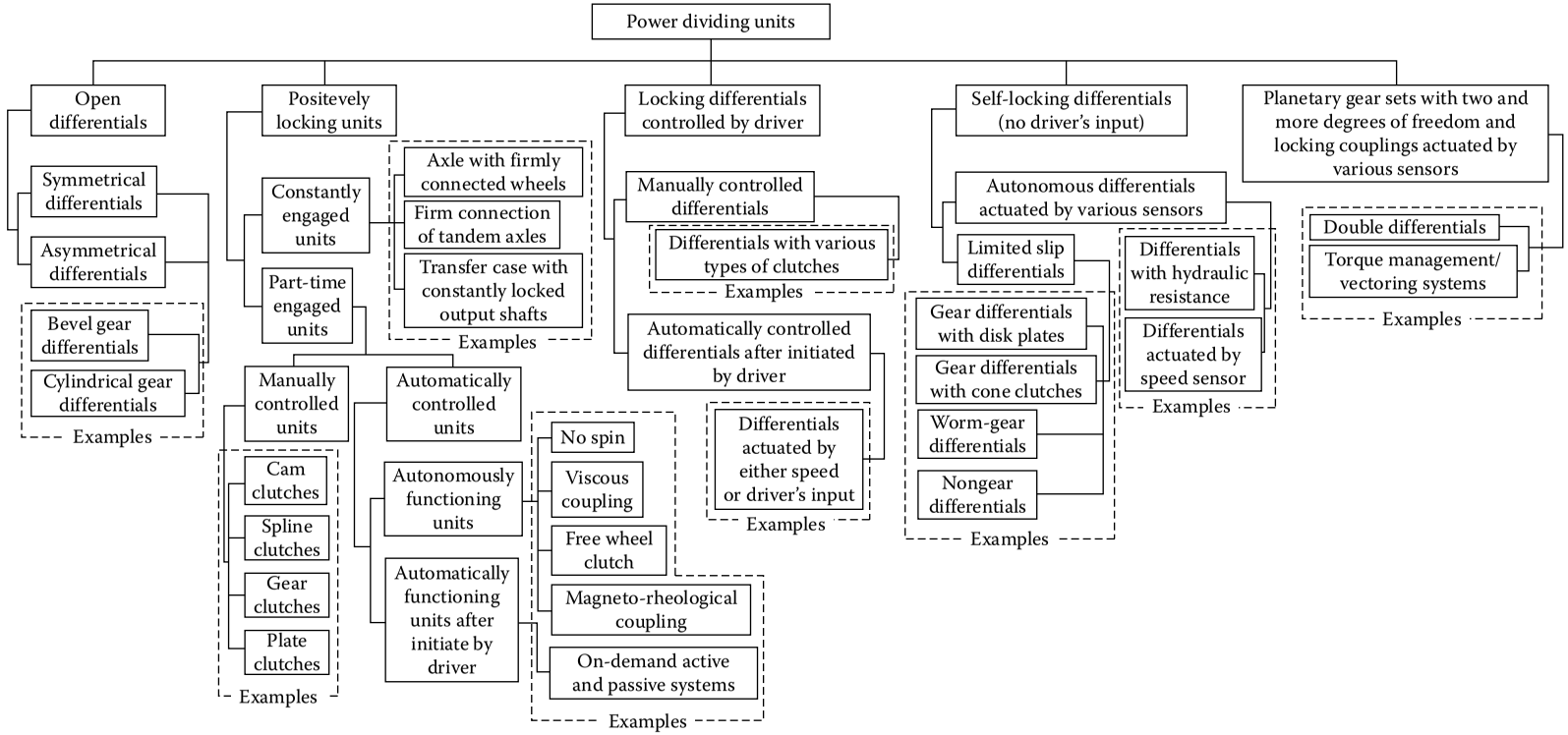


FIGURE 1.33
Major types of PDUs.

TABLE 1.7

Symbols of Mechanisms of Power Dividing Units

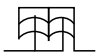
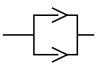
Mechanism in PDU	Designation
Symmetrical open (free) differential	
Symmetrical locking differential	
Asymmetrical open (free) differential	
Asymmetrical locking differential	
Symmetrical limited slip differential	
Asymmetrical limited slip differential	
Symmetrical differential with viscous or rheological clutch	
Asymmetrical differential with viscous or rheological clutch	
Overrunning self-locking differential (similar to NoSPIN)	
Automatic engagement/disengagement of one of the output shafts (e.g., on-demand systems)	
Freewheel (overrunning) clutch	
Constantly locking engagement of the output shafts	
Nonconstant engagement with manual disengagement of one of the output shafts	
Torque vectoring (torque management) device based on planetary gear sets with two and more degrees of freedom and locking couplings/mechanisms	

Notes:

1. Intelligence symbols  (SAE J1952 Standard) may be added to the basic symbol to indicate that the PDU responds automatically to signals from one or more external control systems.
2. Additional abbreviations explains  symbols. Examples: AL/AS, antilock and antispin brake; IA/IW, interaction between interaxle and interwheel PDUs. The following abbreviations describe an interaction between driveline system (DL) and other vehicle systems and sensors: DL/DT, drivetrain (engine and transmission) system; DL/ST, steering system; DL/SS, suspension system; DL/BR, brake system; DL/LoA, longitudinal acceleration sensors; DL/LaA, lateral acceleration; DL/YAW, yaw (rate) sensors; DL/RO, rollover sensors.

TABLE 1.8

Symbols of Power Transfer Units

Power Transfer Unit	Designation
Multiple plate clutch	
Multiple plate clutch with viscous or rheological fluid	
Automatic or manual disconnect (e.g. disconnect hub)	
Hydrostatic drive	
Electric drive	

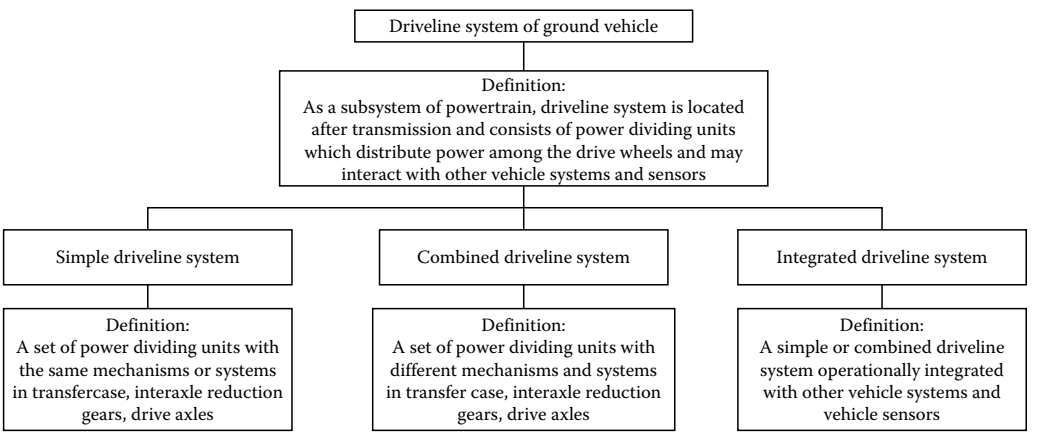


FIGURE 1.34
Simple, combined, and integrated driveline systems.

Note that the number of PDUs for a vehicle with a single engine and an axle system is always by one less than the number of the driving wheels. For example, a 12×12 vehicle has eleven PDUs. It is useful to note in connection with this that vehicles with a single driving axle may have either simple or integrated driveline systems, since they have only one PDU between the left and right driving wheels.

For characterizing wheel driveline systems as a part of the powertrain it is convenient to use powertrain layouts that are composed of gears, shafts, connected by couplings, locking clutches, splined and keyed joints, hinges and bearings. Table 1.9 lists the most typical elements. Certain other elements, not contained in Table 1.9, can be easily recognized in the layouts presented in the book.

TABLE 1.9

PTU Elements for Kinematic Diagrams

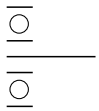
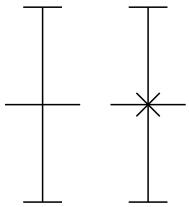
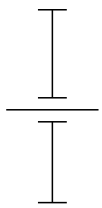
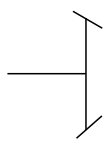
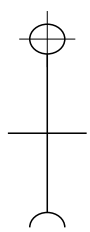
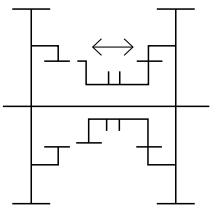
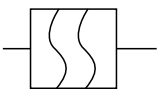
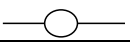
Power Transfer Unit Element	Designation
Shaft, axle	
Sliding bearing	
Rolling bearing	
Cylindrical gears firmly connected to shafts	
Cylindrical gears freely rotating on shafts	
Bevel gears firmly connected to shafts	
Worm—gear set	
Brake	

TABLE 1.9 (continued)

PTU Elements for Kinematic Diagrams

Power Transfer Unit Element	Designation
Gear-type coupling	
Cam-type coupling	
Universal joint	
Constant velocity joint	

Now examine examples of the use of the suggested classification of driveline systems in conjunctions with the general vehicle design.

Table 1.10 shows typical examples of general engineering layout and driveline systems of 4×4 agricultural tractors. A lockable interaxle driveline that provides for disengagement of one of the axles is widely employed both on articulated-frame tractors (e.g., K-710 or T-150K, positions 1 and 2 in Table 1.10) and tractors with steering wheels (MTZ—Minsk Tractor Works, LTZ—Lipetsk Tractor Works, positions 3, 6, and 7). Identical-wheel tractors (Profi Trac, position 4) are designed with interaxle symmetrical locking differentials. John Deere 3640 tractors with nonidentical front- and rear-axle wheels (position 5) make use of interaxle asymmetrical locking differentials. As to interwheel PDUs, the examples listed in Table 1.10 correspond to the above statistical data showing wide use of locking and self-locking (limited-slip) differentials.

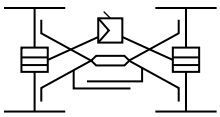
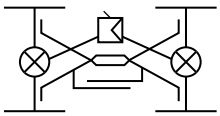
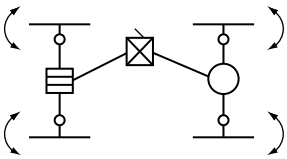
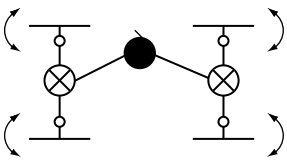
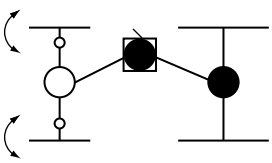
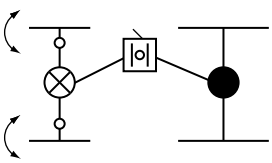
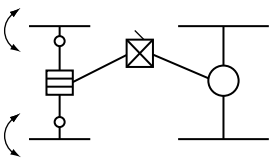
Figure 1.35 shows the kinematic layout of an articulated tractor listed under No. 1 in Table 1.10. This articulated tractor has overrunning self-locking differentials (similar to NoSPIN) in its driving wheels, which is shown by the ▯▯ designation. The primary traction axle here is the front one. The rear axle is engaged and disengaged by a mechanical clutch M (see Figure 1.35).

Figure 1.36 shows the kinematic layout of the powertrain of the T-150K articulated tractor (Table 1.10, position 2). The primary driving axle of this tractor is in the rear, whereas the front axle is coupled mechanically by means of gear 19 that is capable of sliding along the shaft. The tractor is equipped with limited-slip differentials with disk-type clutches in the driving axles.

The powertrain layout of the MTZ-82 tractor, position 6 in Table 1.10, is shown in Figure 1.37. The front-axle differential P with floating pinion fingers (see Chapter 4) is a limited-slip device, whereas the rear axle differential D is locked by hydraulically controlled

TABLE 1.10

4×4 Agricultural Tractors

No.	Chassis and Driveline System Layout	Wheel Formula	Drive Formula	Axle Formula	Steering Formula
1		4×4	12	1-1	$0\frac{v}{c}0$
2		4×4	12	1-1	$0\frac{v}{c}0$
3		4×4	12	1-1	1-2
4		4×4	12	1-1	1-2 1-0
5		4×4	12	1-1	1-0
6		4×4	12	1-1	1-0
7		4×4	12	1-1	1-0

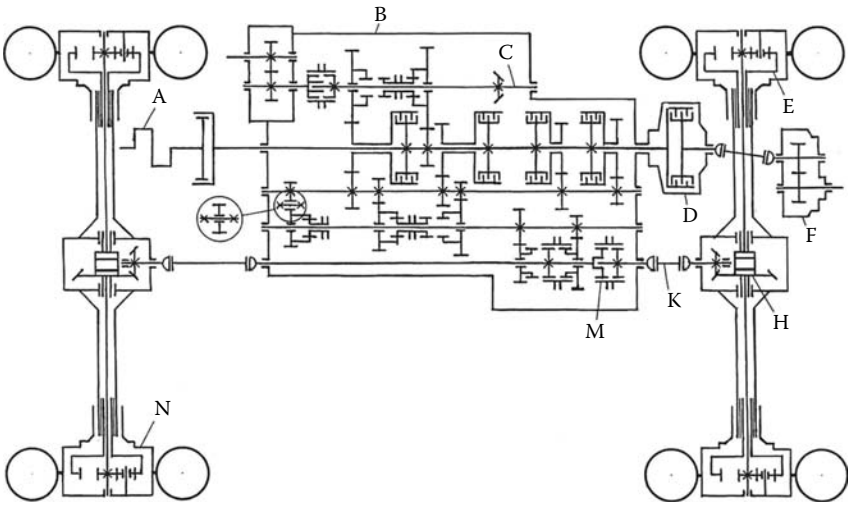


FIGURE 1.35
Tractor K-710: kinematic layout of powertrain. A, engine; B, transmission; C, pump shaft; D, power take off clutch; E, wheel-hub planetary gear set; F, power take off reduction gear; H, final drive with overrunning self-locking differential; K, drive shaft; M, positive locking engagement of the rear axle; N, front driving axle.

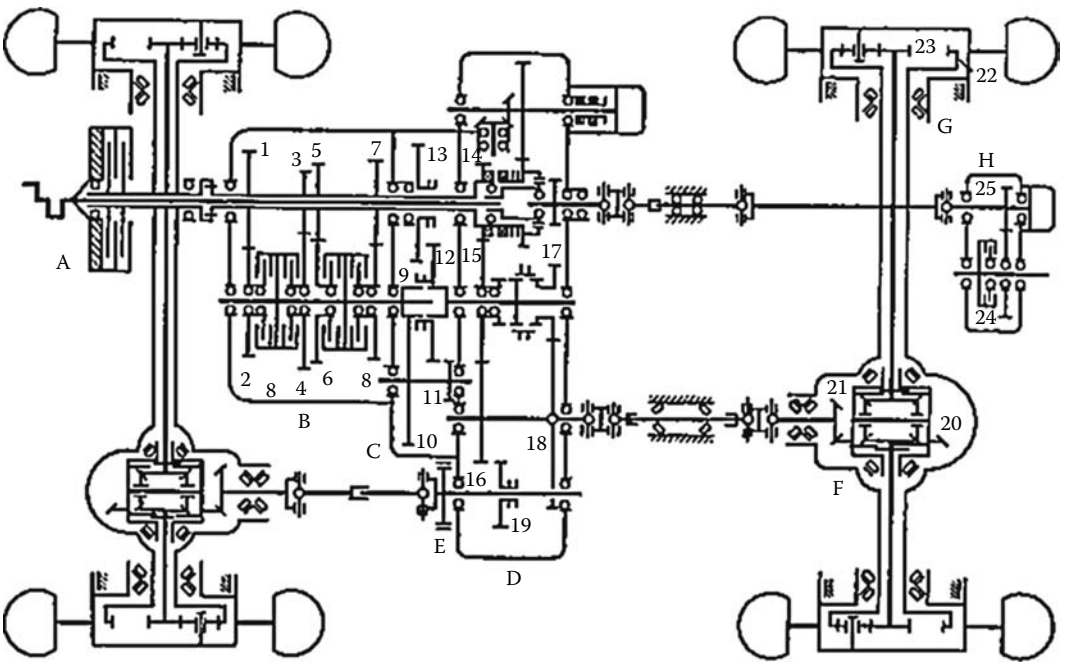


FIGURE 1.36
Tractor T-150K: kinematic layout of powertrain. A, engine with main clutch; B, transmission; C, reduction gear; D, transfer case; E, auxiliary brake; F, final drive with limited-slip differential in the rear axle; G, wheel-hub planetary gear set; H, power take off reduction gear.

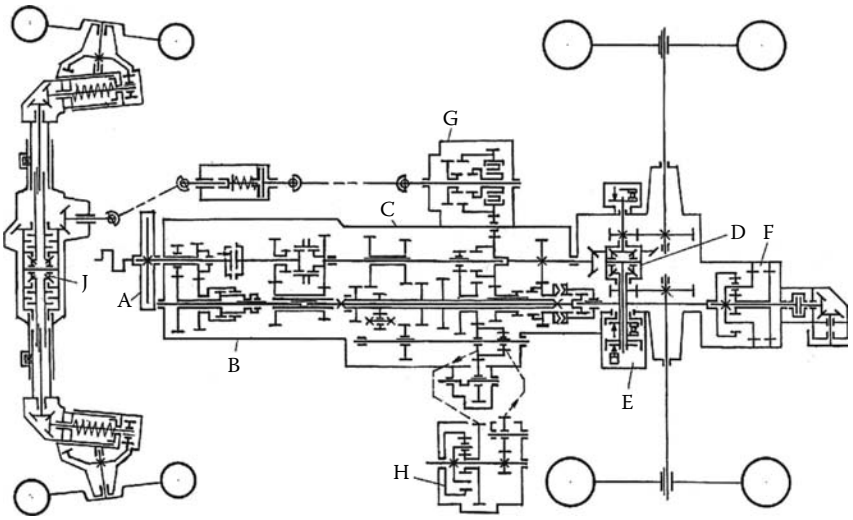


FIGURE 1.37
Tractor MTZ-82: powertrain kinematic layout. A, engine with main clutch; B, reduction gear; C, transmission; D, final drive with locking differential; E, disk brake and differential locking clutch; F, power take off reduction gear; G, transfer case with automatic positive engagement of front axle; H, reduction gear; J, limited slip differential of front axle.

clutch E. The front axle is engaged/disengaged automatically by means of a roller-type overrunning clutch, located in the transfer case G.

In addition to the fact that the kinematic powertrain layout shows clearly the location of the driveline system in the overall powertrain layout, these layouts have the added convenience of making it possible to compute the transmission ratios from the engine to the wheels when the different gears are engaged in transmission. For example, the engine power at the first gear of the T-150K tractor is transmitted to the rear wheels by gears 3, 4, 17, 18, 20, and 21 and the wheel-hub planetary reduction gear K. The gear ratio at the first gear is defined as the ratio of the number of teeth of the corresponding gears:

$$u_{\mathrm{I}} = (N_4/N_3)(N_{18}/N_{17})(N_{20}/N_{21})u_{\mathrm{k}},$$

where $u_{\mathrm{k}} = 1 + N_{22}/N_{23}$ is the gear ratio of the planetary reduction gear. When the front axle is engaged, a part of the engine power starts being transmitted from the shaft of gear 18 through gear 16 to gear 19 and then to the front wheels. The front and rear axles are then rigidly coupled via the gear trains. Analytical methods of determining the power to the front and rear wheels are of definite interest for assessing the performance of the vehicles. These problems are examined in Chapter 3.

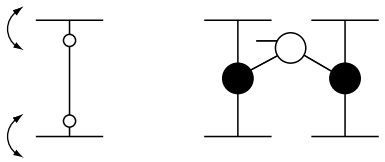
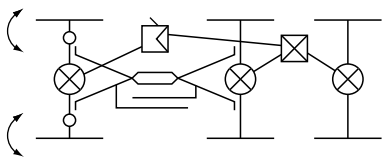
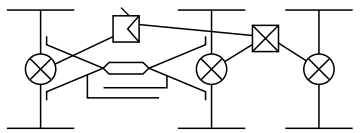
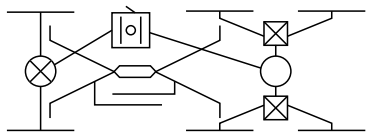
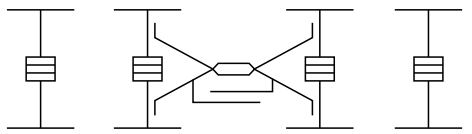
Analysis of the design of six-wheel tractors provides insight into the most typical designs and driveline systems (Table 1.11). For example, the 6×4 system is found in the Valmet 1502 tractor (Table 1.11 position 1).

6×6 tractors with a nonpermanently engaged front axle (known as part-time systems) may perform turns either by means of an articulated frame or by its combination with steered front wheels (Table 1.11, positions 2 and 3).

The 6×6 Locomo forestry tractors (Table 1.11, position 4) employ a differential drive between the side reduction gears of the forward rear and rearward rear axles.

TABLE 1.11

6×4, 6×6, and 8×8 Farm and Forestry Tractors

No.	Chassis and Driveline System Layout	Wheel Formula	Drive Formula	Axle Formula	Steering Formula
1		6×4	023	1-2	1-00
2		6×6	123	1-2	$1\frac{v}{c}00$
3		6×6	123	1-2	$0\frac{v}{c}00$
4		6×6	123	1-2	$0\frac{v}{c}00$
5		8×8	1234	2-2	$00\frac{v}{c}00$

The 8×8 Locomo forestry tractors (Table 1.11, position 5) make extensive use of NoSPIN differentials in their driving axles.

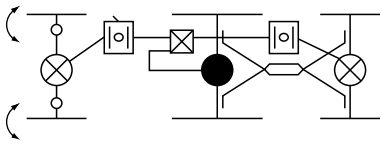
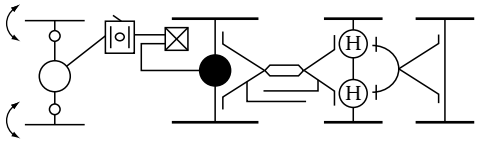
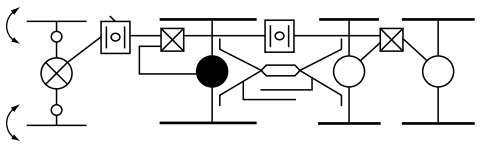
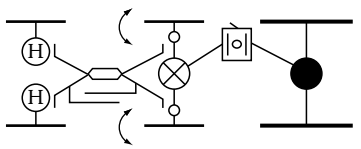
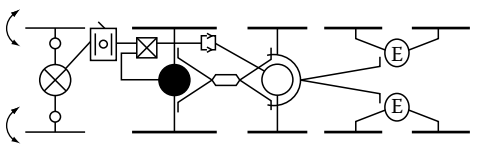
It should, however, be pointed out that there is a limit to increasing a tractor's traction and velocity performance by merely adding driving axles, something that would deliver more of the engine's power to the drawbar. This problem is solved by using a high-power tractor that, while towing a part of the trailer and/or semitrailer vehicular train also serves as a power module that supplies power to the wheels of another part of the train. These wheel drives are normally powered by a power takeoff shaft from the power module and less frequently by separate motors powered by the power module.

Table 1.12 presents examples of such vehicular trains comprised of a 4×4 power module and several trailers powered by it. Ordinarily the powered trailers are arranged in the rear of the power modules (Table 1.12, positions 1–3, 5). The front location (Table 1.12, position 4) is used when the power module provides power to agricultural implements that are propelled by power supplied by it.

In addition to driving the motorized towed units by means of a synchronous power takeoff shaft from the power module (Table 1.12, positions 1 and 3) these may be driven by

TABLE 1.12

Power-Module Driven Vehicular Trains

No.	Chassis and Driveline System Layout	Wheel Formula	Drive Formula	Axle Formula	Steering Formula
1		6×6	123	1-1-1	$1 - 0\frac{v}{-}0$ $1 - 0\frac{v}{c}0$
2		8×6	1230	1-1-1-1	$1 - 0\frac{v}{c}0\frac{s}{-}0$
3		8×8	1234	1-1-2	$1 - 0\frac{v}{c}00$
4		6×6	123	1-1-1	$0\frac{v}{c}2 - 0$
5		10×10	12345	1-1-1-2	$1 - 0\frac{v}{-}0\frac{s}{-}00$

hydraulic (positions 2 and 4) and electrical drives (position 5). It is seen from this that front-axle drive systems of mobile power modules and motorized towed units comprise complex, branched systems.

Figure 1.38 shows the different applications of power-module driven vehicular train No. 1 from Table 1.12.

Now examine the driveline system layouts of trucks. Table 1.13 shows trucks with only one and with many (but not all) driving axles, whereas Table 1.14 illustrates all-wheel drive trucks with different wheel formulae and other parameters that describe the relationship between the driveline system and the general design of the vehicle. It is seen how important it is to have driveline system layouts: vehicles with ideal wheel and drive formulae, with similar arrangement of the axles at the wheelbase and similar steering systems may have different systems of distribution of power between wheels, i.e., different driveline systems.

Kinematic layouts for each of the vehicles in Tables 1.13 and 1.14 are very useful in characterizing the place of drivelines systems in the overall layout of powertrains. For example, the kinematic layout of the powertrain for 4×4 trucks with nonpermanently engaged driveline systems (part-time systems, Table 1.14, position 1) is shown in Figure 1.39.

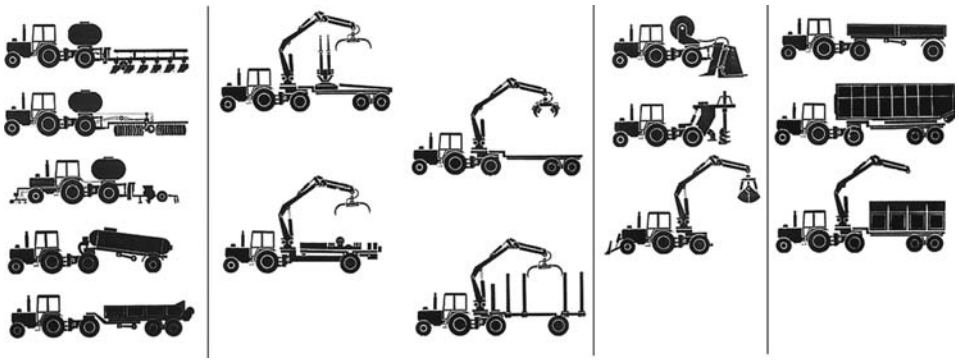
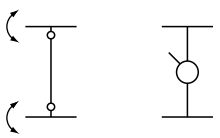
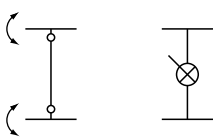
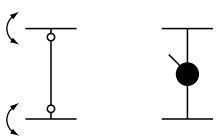
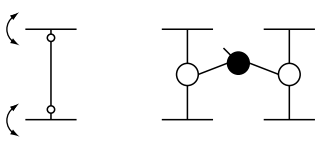
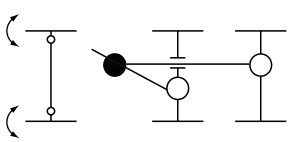
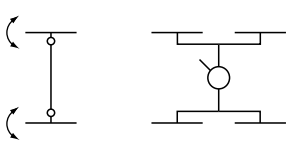


FIGURE 1.38
6 × 6 vehicular train applications: (a) agricultural sector; (b) forestry; (c) earth moving machinery; (d) transportation.

TABLE 1.13
Single-Axle and Multiaxle Drive Trucks

No.	Chassis and Driveline System Layout	Wheel Formula	Drive Formula	Axle Formula	Steering Formula
1		4 × 2	02	1-1	1-0
2		4 × 2	02	1-1	1-0
3		4 × 2	02	1-1	1-0
4		6 × 4	023	1-2	1-00
5		6 × 4	023	1-2	1-00
6		6 × 4	023	1-2	1-00

(*continued*)

TABLE 1.13 (continued)

Single-Axle and Multiaxle Drive Trucks

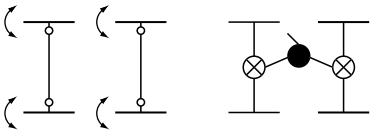
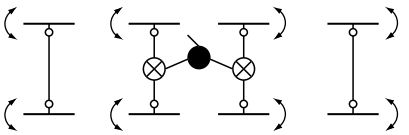
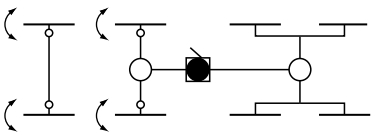
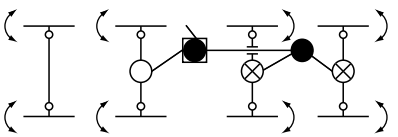
No.	Chassis and Driveline System Layout	Wheel Formula	Drive Formula	Axle Formula	Steering Formula
7		8 × 4	0034	2-2	12-00
8		8 × 4	0230	1-2-1	1-23-4
9		8 × 6	0234	2-2	12-00
10		8 × 6	0234	2-2	12-34

TABLE 1.14

All-Wheel Drive Trucks

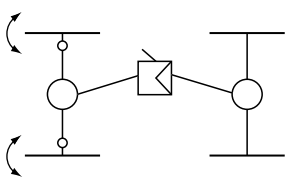
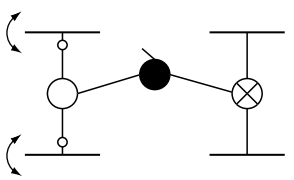
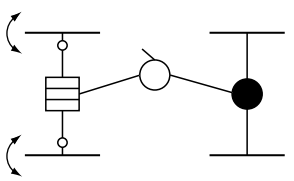
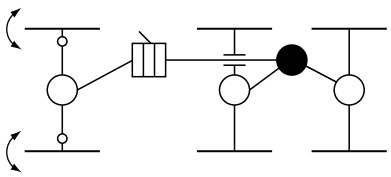
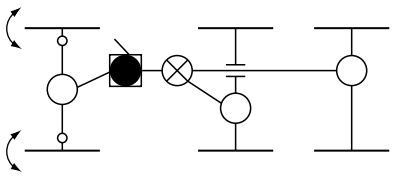
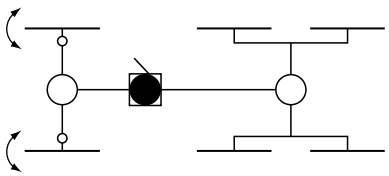
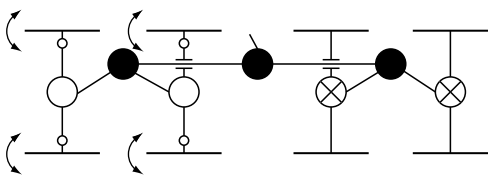
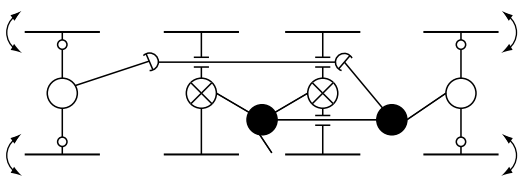
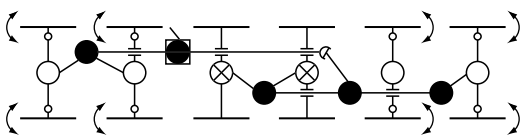
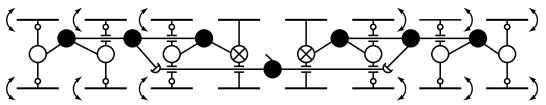
No.	Chassis and Driveline System Layout	Wheel Formula	Drive Formula	Axle Formula	Steering Formula
1		4 × 4	12	1-1	1-0
2		4 × 4	12	1-1	1-0
3		4 × 4	12	1-1	1-0

TABLE 1.14 (continued)

All-Wheel Drive Trucks

No.	Chassis and Driveline System Layout	Wheel Formula	Drive Formula	Axle Formula	Steering Formula
4		6 × 6	123	1-2	1-00
5		6 × 6	123	1-2	1-00
6		6 × 6	123	1-2	1-00
7		8 × 8	1234	2-2	12-00
8		8 × 8	1234	1-2-1	1-00-4
9		12 × 12	123456	2-2-2 1-1-1-1-1-1	12-00-56
10		16 × 16	12345678	2-2-2-2	12-30-06-78

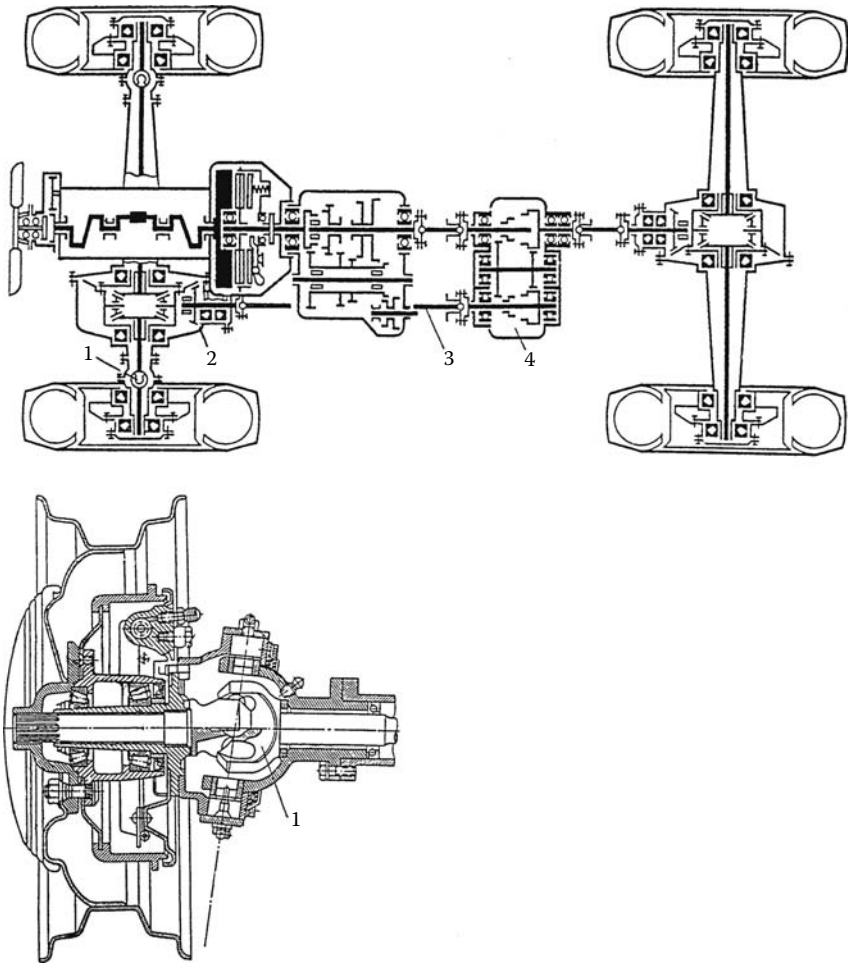


FIGURE 1.39
4 × 4 truck with a part time interaxle system. 1, constant velocity joint; 2, front axle; 3, drive shaft; 4, transfer case.

It is cumbersome, not as ''pure'' as the driveline of the 4 × 4 passenger cars of the start of the 1990s. However, in it one can clearly follow all the components, each of which performs certain functions. Such drives came into extensive use in light- and medium-duty and off-road automobiles and in special-purpose passenger cars (military and cars used in agriculture, on farms).

If reducing gearing is employed in the drive of light- and medium-duty vehicles, it is incorporated into the transfer case 4 to simplify the design and reduce the weight (see Figure 1.39). The transfer case as such serves in all cases for holding a mechanism for dividing the power between the axles. Figure 1.39 shows the drive of the front steered and driving axle with constant velocity joint 1 incorporated into it, front-axle differential 2 and universal-joint propeller shaft 3. This figure also shows the design of one of the constant velocity joints.

Figure 1.40 shows the kinematic layout of a 12 × 12 vehicle. It employs an interaxle, symmetrical locking differential 1 that divides the power between the three forward and three rear axles. An overrunning self-locking differential similar to NoSPIN 2 is located

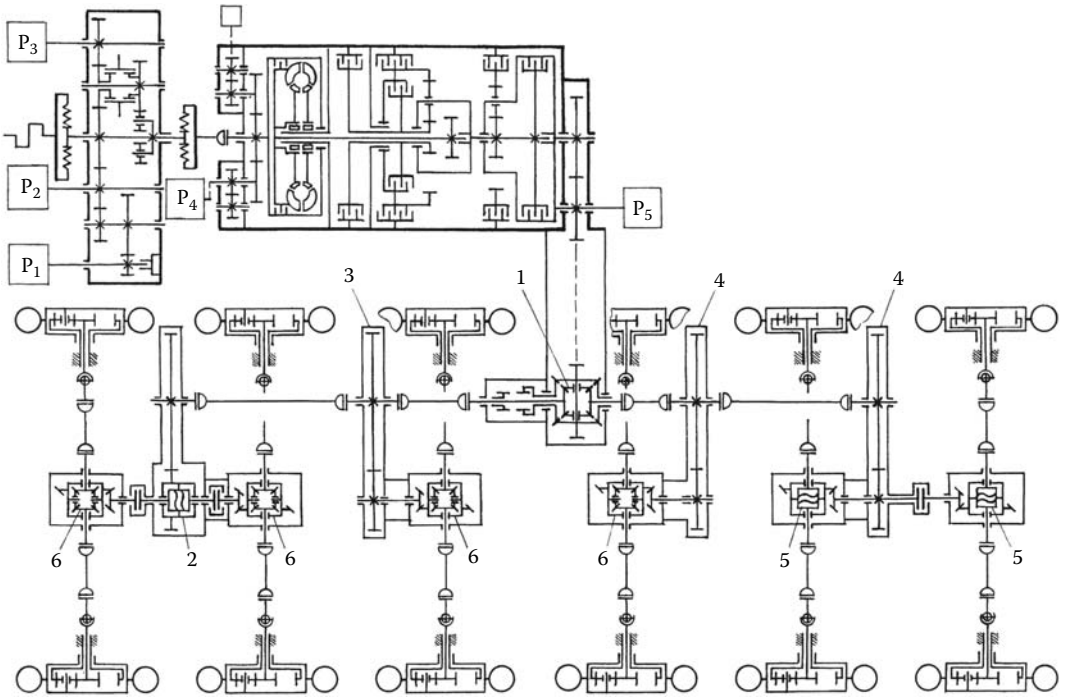


FIGURE 1.40
12 × 12 vehicle: powertrain kinematic layout. 1, transfer case differential; 2, NoSPIN similar differentials between the 1st and 2nd axles; 3, positive engagement between the first two axles and the 3rd axle; 4, positive engagement between the 4th, 5th, and 6th axles; 5, NoSPIN similar differential; 6, open differentials.

between the first and second axles. Positive engagement 3 is used between the first and second axles on one side and the third axle on the other side. Drive 4 for the fourth, fifth, and sixth axles is also locked. NoSPIN similar differentials 5 are used in the fifth and sixth axles. Axles 1 through 4 use open differentials 6.

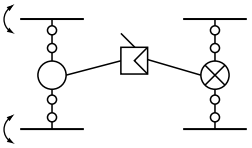
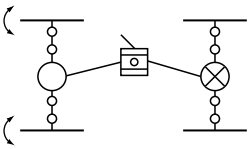
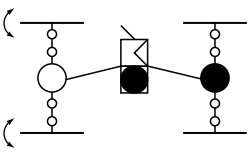
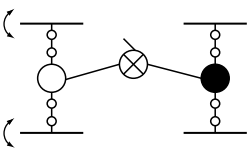
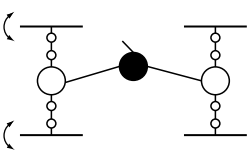
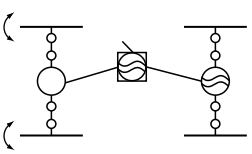
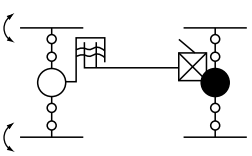
Table 1.15 lists the most typical layouts used for passenger cars and for SUVs. These layouts are usually employed on vehicles with longitudinal location of the engine. These vehicles have traditional transfer cases and employ interaxle PDUs located in the transfer case. These vehicles have identical wheel, drive, axle, and steering formulas. However, these driveline systems are either part-time or full-time systems. Vehicles 1 and 2 from Table 1.15 differ by the fact that the front axle is engaged either manually or automatically (for example, on-demand systems).

Layout 3 is known as the Mercedes-Benz 4MATIC. It can operate with two versions of drive-axle arrangements: (1) a part-time system in which the front axle is disengaged and a single rear axle provides the drive and (2) both axles are engaged by means of a locking interaxle asymmetrical differential.

A permanently engaged driveline system with a worm-gear type interaxle differential and with locking rear-axle differential used in the Audi Quattro is shown under number 4. Layouts numbered 5 and 6 are in extensive use. In layout 5, the interaxle differential may be lockable whereas the interwheel differentials are open. Layout 6 employs viscous clutches in the interaxle differential and in the rear-wheels differential (Ford Scorpio, Ford Sierra XR, BMW325LX). Layout 7 is used in Porsche 997, in which the rear driving

TABLE 1.15

4 × 4 Passenger Cars and SUVs

No.	Chassis and Driveline System Layout	Wheel Formula	Drive Formula	Axle Formula	Steering Formula
1		4 × 4	12	1-1	1-0
2		4 × 4	12	1-1	1-0
3		4 × 4	12	1-1	1-0
4		4 × 4	12	1-1	1-0
5		4 × 4	12	1-1	1-0
6		4 × 4	12	1-1	1-0
7		4 × 4	12	1-1	1-0

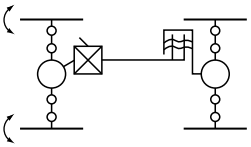
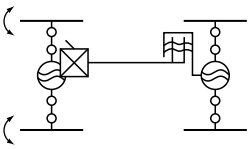
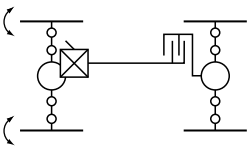
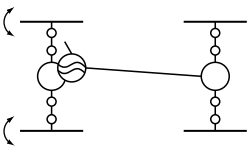
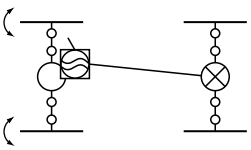
axle is the principal, whereas the front axle is engaged by means of a viscous clutch. The front-axle differential is open, whereas that of the rear axle is lockable.

Table 1.16 shows layouts of 4 × 4 vehicles based on FWD vehicles. They are distinguished by the fact that the interaxle PDU and the front axle PDU are located close to one another (layout 1) or together (layouts 2 to 5).

In layout 1, used in the Renault Espace Quadra and the R21 Nevada the power is transmitted from a longitudinally located engine to a gearbox that is also arranged

TABLE 1.16

4 × 4 Passenger Cars

No.	Chassis and Driveline System Layout	Wheel Formula	Drive Formula	Axle Formula	Steering Formula
1		4 × 4	12	1-1	1-0
2		4 × 4	12	1-1	1-0
3		4 × 4	12	1-1	1-0
4		4 × 4	12	1-1	1-0
5		4 × 4	12	1-1	1-0

longitudinally. Then the power is divided between the two axles. The rear-axle drive has a viscous clutch that serves for automatically engaging it to the engine.

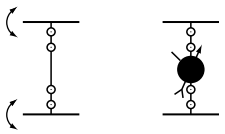
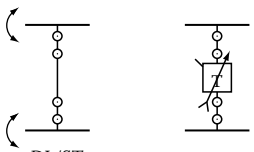
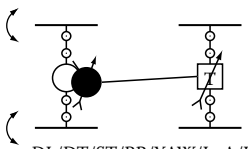
Layout 2 (Table 1.16) that is used on the Nissan Pulsar with a laterally positioned engine and gearbox (known as the transaxle), also has a viscous clutch in the rear-axle drive. The rear-axle differential is also equipped with a viscous clutch. Layout 3 is used in Volvo vehicles. It has an automatically operated hydraulic clutch for engaging the rear axle.

Layouts 4 and 5 with a permanently engaged driveline have interaxle differentials integrated into front-wheel differentials. This is brought about by the lateral arrangement of the engine and the gearbox. The interaxle differential in layout 4 is of the symmetrical type whereas layout 5 employs an asymmetrical interaxle differential. The rear-axle differential in layout 4 is open, whereas that in layout 5 is a limited-slip (worm-gear type) differential. Layout 4 is used on the Toyota Celica and layout 5 on the Lancia Delta/Prisma HF.

Recent developments in driveline system design pertain in a large measure to various integrated mechatronic systems. These systems are more flexible as compared with mechanical drives. Table 1.17 lists as an illustration several such designs. Mechatronic systems are analyzed in Chapter 7.

TABLE 1.17

Vehicles with Integrated Mechatronic Driveline Systems

No.	Chassis and Driveline System Layout	Wheel Formula	Drive Formula	Axle Formula	Steering Formula
1	 DL/YAW/RO	4 × 2	02	1-1	1-0
2	 DL/ST	4 × 2	02	1-1	1-0
3	 DL/DT/ST/BR/YAW/LoA/LaA	4 × 4	12	1-1	1-0

In all the vehicles analyzed above the overall driveline system is of one and the same type: the power supplied by the gearbox is first divided between the axles and then between the left and right wheels of each axle. The number of PDUs for such a driveline layout is equal to

$$N_{\text{PDU}} = 2n - 1 \tag{1.4}$$

where

n is the number of driving axles

$2n$ is the number of the driving wheels

Other driveline system layouts exist and are in use. For a number of years now use is made of the vehicle-sides layout: the power supplied from the gearbox is divided between the right and left sides of the vehicle and then between the wheels of each side.

Figure 1.41 shows a diagonal driveline of four wheels of a vehicle. Power to the left forward wheel is transmitted from shaft I_a by right spur-gear differential *II* and to the right front wheel from shaft II_a by left spur-gear differential *I*, whereas these same differentials transmit power from the shafts of reduction gearing II_b and I_b, respectively to the left and right rear wheels.

This driveline system includes two spur-gear differentials—the left *I* and the right *II*. In Figure 1.41 the gears of the left differential are designated by a single prime and those of the right by a double prime. The left differential provides engagement through gears $1''$ and $2''$ between the right-hand differential and shafts I_a and I_b, whereas the right

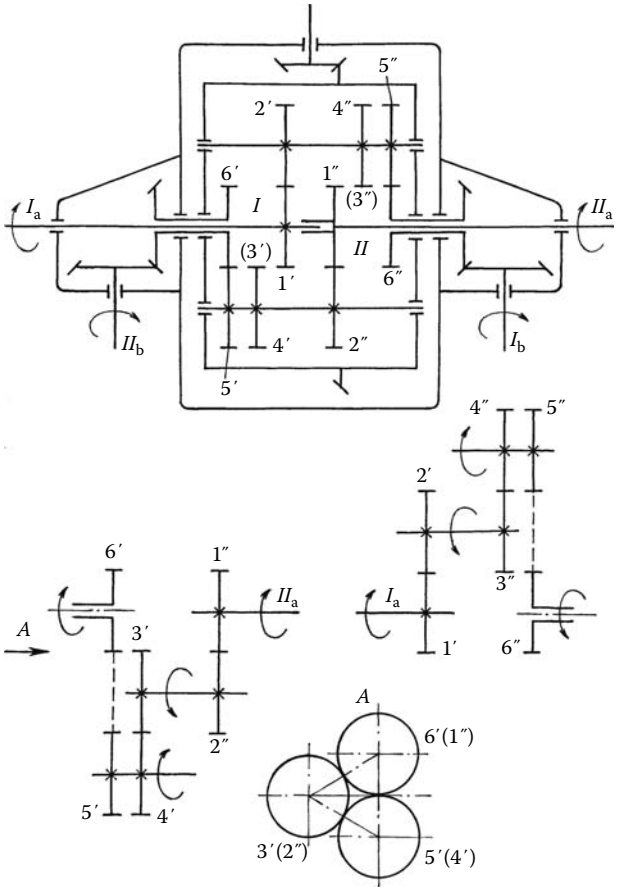


FIGURE 1.41
Diagonal driveline system.

differential by means of gears 1′ and 2′ between shafts II_a and II_b. This is clearly seen on the developments of both differentials located below the main layout. The refolded (nondeveloped) left differential viewed in direction *A* is shown in the figure under the same letter symbol. The gear designations in parentheses mean that these gears are retracted and are located beneath the gears the designations of which are not included in parentheses. The right differential is refolded in the box, just as the left differential. As compared with the classic layout of a driveline with free differentials, which corresponds to formula (1.4), this layout employs only two differentials.

This means that the clarification of driveline systems and PDUs described in the present section makes it possible to identify a given driveline system and to describe the PDUs that it incorporates together with the overall engineering design of the vehicles and the location of the driveline system in the overall powertrain layout.

Such a description of driveline systems is needed for comparing different driveline systems employed on similar vehicles and for subsequent analysis of its effect on vehicle performance. The development of methods for performing such an analysis is one of the principal topics of this book.

1.3 Wheel Dynamics and Energy Efficiency

Vehicle performance is determined to a large extent by the interaction between the tire and the supporting surface. Torque is supplied to the wheel by the vehicle's driveline system. The wheel speed depends also to a large extent on the characteristics of the vehicle's driveline system. This means that the driveline system plays an important role in the formation of vehicle performance. Here the characteristics of wheel dynamics and performance that are needed for: (1) gaining insight into the mechanism of the driveline system that affects vehicle performance, and (2) performing engineering calculations associated with assessing the effect of driveline systems on vehicle performance and determining the characteristics of the driveline system that make for optimal vehicle performance are considered.

1.3.1 Five Power-Loading Modes

Consider a pneumatic wheel in a steady planar motion (the specifics of unsteady motion shall be examined further down). The surface of motion can be either firm or deformable. Such a wheel is subjected to various and different combinations of forces that are applied to it by the vehicle frame. Also, the wheel can have driving and breaking torques that originate in the driveline system and in the brake mechanism. Please note that under certain conditions a braking torque can also be applied by the driveline system. These conditions will be discussed in Section 3.3.1.

Different combinations of forces and torques lead to different ground reactions. On the whole, these forces, reactions and torques are grouped into five power-loading modes. The modes are named power-loading modes since the wheel forces and torques produced by the respective linear and angular velocities of the wheel represent various components of the wheel power balance that will be considered in Section 1.3.3.

Driven rolling mode (driven loading mode, Figure 1.42a). The wheel moves under the action of the longitudinal force $F_{\text{frame}.x}$ applied to the axle in the direction of motion. This force counterbalances the longitudinal reaction R_x, which is called the rolling resistance force. The normal reaction R_z counterbalances the normal load of the wheel W_{w}, which includes the weight of the wheel itself. Primarily due to internal tire friction and friction in road-tire contact patch, the normal reaction R_z is shifted forward with respect to the normal wheel diameter by an offset distance a_{dr}. The total ground reaction passes through the wheel's center of rotation (see dotted line in Figure 1.42a). The wheel is in equilibrium.

Neutral mode (Figure 1.42b). Apply a small torque T_{w} to the wheel. Assume this torque is not enough to twist the tire and to overcome the rolling resistance. To move the wheel forward, a force $F_{\text{frame}.x}$ should be applied to the wheel center. Now, the wheel is rolling. The line of action of the total surface reaction passes above the wheel rotation axis. The moment exerted by this total reaction about the wheel center is balanced by the torque T_{w}.

Free mode (Figure 1.42c). In this mode, the torque T_{w} develops a longitudinal force F_x named the wheel's circumferential force. This force balances the rolling resistance R_x; therefore the longitudinal forces cancel one another and the wheel rolls under the action of the driving torque T_{w}, which counterbalances the rolling resistance moment M_{f}^{c} caused by the normal reaction shift

$$M_{\text{f}}^{\text{c}} = R_z a_{\text{f}} \tag{1.5}$$

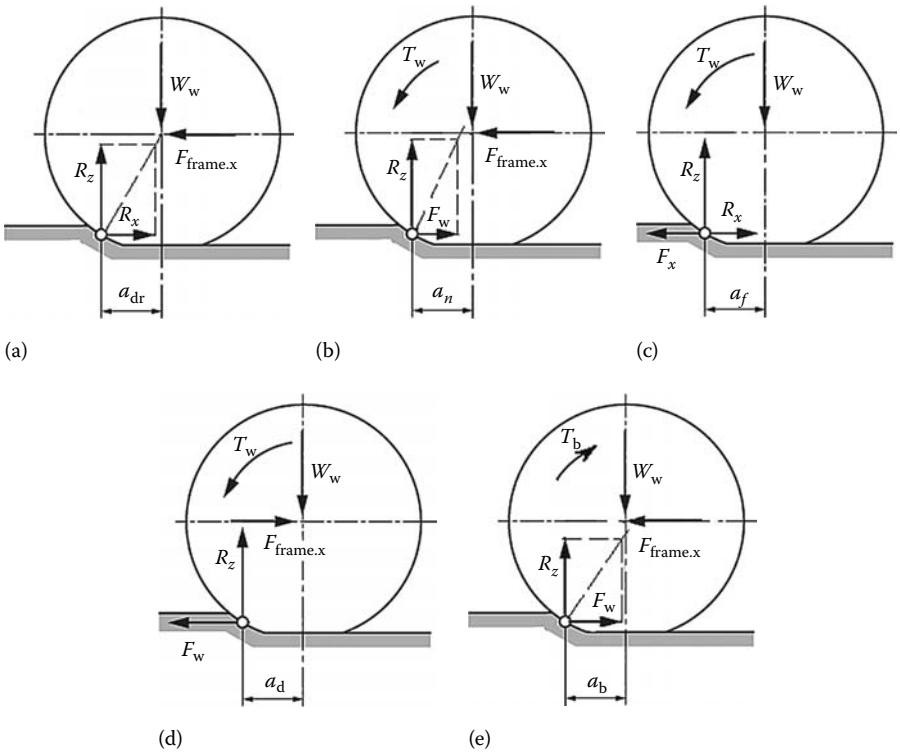


FIGURE 1.42
Five power-loading modes: (a) driven; (b) neutral; (c) free; (d) driving; (e) braking.

Driving mode (Figure 1.42d). The wheel torque T_w is large, and the circumferential force F_x developed by this torque is larger than the rolling resistance R_x. Therefore, the rest of the force F_x left from compensating the rolling resistance is a force F_w named the wheel traction force or the net tractive force

$$F_w = F_x - R_x \tag{1.6}$$

This force F_w can counterbalance the frame force $F_{frame.x}$ that is exerted by the vehicle frame in the direction opposite to the wheel motion.

Braking mode (Figure 1.42e). Braking torque T_b opposes the wheel rotation. Longitudinal force F_w is a braking force that counterbalances the vehicle frame force $F_{frame.x}$.

As was shown, the above five modes are characterized by different combinations of the wheel torque T_w and the net tractive force F_w. Figure 1.43 is a conceptual representation of all the five modes. This relationship is shown by a straight line that corresponds to the constant rolling resistance force $R_x = \text{const}$. In the driven mode (point 1) the torque is $T_w = 0$, whereas the force F_w is negative and equal to the wheel's rolling resistance force $F_w = R_x$. Segment 2 is the neutral rolling mode, the torque is positive, but is small and insufficient for setting the wheel into motion. This requires applying some longitudinal force $F_{frame.x}$ to the wheel's axis that will counterbalance the negative force F_w shown in Figure 1.43. Point 3 is typical of the free mode, $T_w > 0$ and $F_w = 0$. In the driving mode (segment 4), the torque T_w and force F_w are both positive. This positive force F_w balances

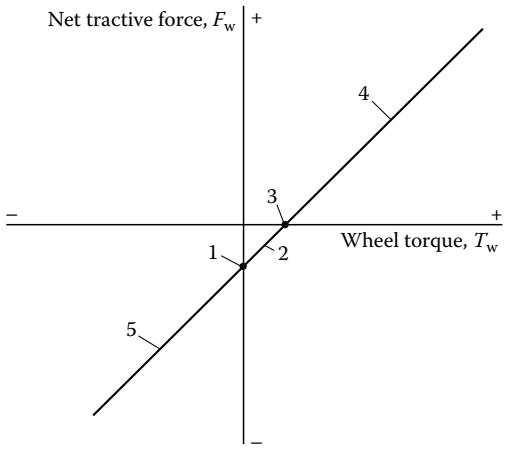


FIGURE 1.43
Torque T_w–net tractive force F_w diagram.

the force $F_{\text{frame}.x}$ exerted on the wheel by the vehicle's frame. At segment 5 the torque T_w and force F_w are negative; this is the braking mode.

The above five modes are typical of wheels of all-wheel-drive vehicles. The wheels of vehicles with a single drive axle may only have three modes in steady-state motion: driven, driving, or braking. Figure 1.44 presents free-body diagrams of front and rear wheels of a FWD vehicle. Torque T_w generates a circumferential force F_x that is expended in overcoming the rolling resistance of the front wheels and generating the traction force F_w. This force F_w is transmitted through the vehicle's frame to the rear wheels as force $F_{\text{frame}.x}$. Force $F_{\text{frame}.x}$ overcomes the rolling resistance R_x of the rear wheels. The neutral and free modes do not arise in 4×2 vehicles since their torques and forces on one axle are insufficient for setting the driven wheels of the second axle into motion.

As an example that illustrates all the five modes of all-wheel-drive vehicles, examine the bicycle model of a 4×4 vehicle with positive engagement of the front and rear axles

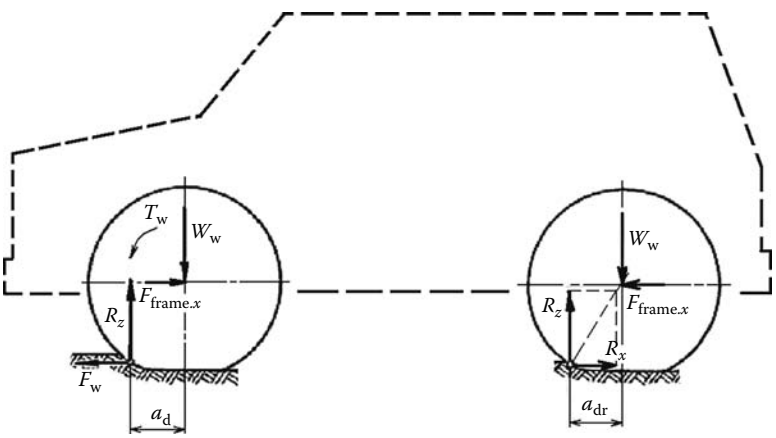


FIGURE 1.44
Front-wheel drive vehicle: free-body diagrams of the front and rear wheels.

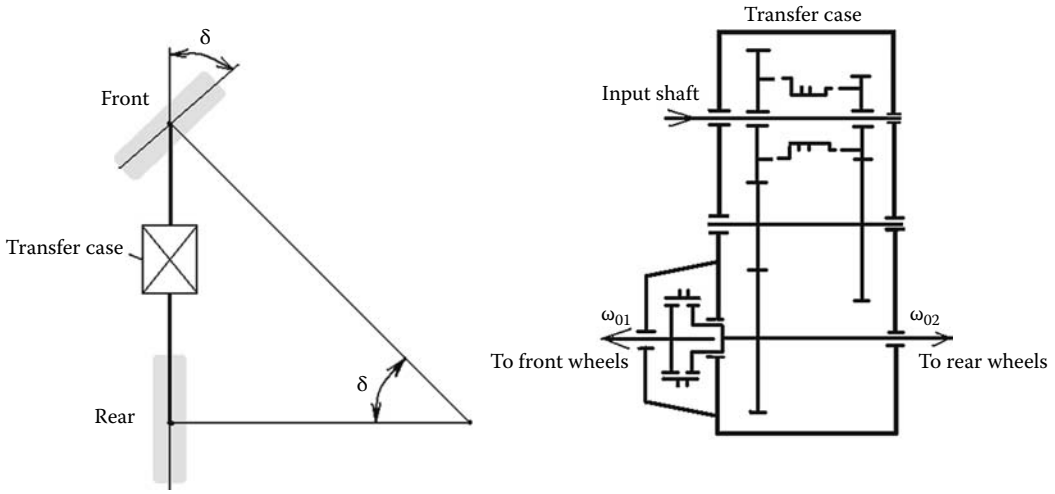


FIGURE 1.45
Bicycle model of a 4 × 4 vehicle with positive engagement of the driving axles taking a turn.

making a turn. Figure 1.45 shows such a vehicle; its transfer case locks the front and rear axles: the output shafts of the transfer case rotate at the same angular velocities, $\omega_{01} = \omega_{02}$.

Figure 1.46 shows the torques of the front and rear axles, T_1 and T_2, of this vehicle as a function of the steering angle δ of the front wheels (this angle can be determined from the vehicle geometry using the angles of the left and right wheels, δ″ and δ′). The five modes in which the wheels may find themselves are designated by numbers 1 to 5 that correspond to the five combinations of F_w and T_w from Figure 1.43. At small δ both axles are in the driving mode (number 4).

Forces F_w that the axles develop may be expended for towing a trailer or for accelerating the vehicle. As angle δ increases, torque T_1 of the front wheels decreases, whereas that of the rear wheels (T_2) increases (the reasons for this shall be discussed in Chapter 3). Point 3 corresponds to the free mode of the front wheels: they are set into motion by torque T_1 applied by the driveline system. No forces are acting between the front wheels and the vehicle's frame. The front wheels move in a manner ''detached'' from the vehicle's frame

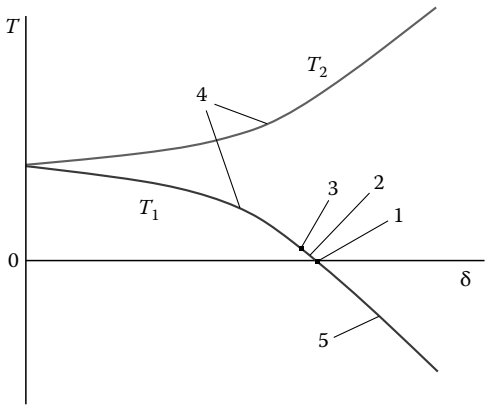


FIGURE 1.46
Front and rear torques of a 4 × 4 vehicle with positive engagement of the driving axles taking a turn.

(wheel lateral forces are not being discussed at this moment). At that time, the front wheels become ''idlers'' of a kind, without contributing to the vehicle's motion. Actually, however, front-wheel motion in the free mode is highly unstable, constantly changing either to the driving or the neutral mode (segments 4 and 2 in Figure 1.46).

In the neutral mode the torque T_1 is small and is insufficient for setting the front wheels into motion. Nevertheless, they move since they are subjected to the pushing force $F_{\text{frame}.x}$ by the vehicle's frame. This pushing force is developed by the rear wheels that are subject to appreciable loading by torque T_2 and move in the driving mode.

In point 1 on Figure 1.46 the no torque is imparted on the front wheels by the driveline system, $T_1 = 0$. The front wheels are caused to rotate by the pushing force $F_{\text{frame}.x}$ exerted by the vehicle's frame and developed by the rear wheels that continue to move in the driving mode under the action of the significant torque T_2. The front wheels are not disengaged from the driveline system and a further increase in the turn angle δ of the front wheels causes these wheels to enter the braking mode, $T_1 < 0$ (segment 5 in Figure 1.46). Moving the front wheels requires a significant pushing force that is supplied to the front wheels by the rear wheels by way of the vehicle frame. It is said that there exists circulation of parasitic power, which shall be examined in Chapter 3.

Still another example that illustrates the rolling modes may consist of an axle with a NoSPIN. Let us examine the motion of such an axle when it takes a turn (Figure 1.47). With decreasing radius of turn R, i.e., with increasing curvature $1/R$, torque T''_{w} of the inner wheel increases whereas that of the outer wheel T'_{w} decreases. Because of this the outer wheel shifts from the driving mode (segment 4) to the free mode (point 3) and then to the neutral mode (segment 2).

Then, when $T'_{\text{w}} = 0$, the NoSPIN disengages the outer wheel from the driveline system and it rolls in the driven mode. Further reduction in R does not change the wheel rolling mode: the outer wheel rolls in the driven mode (segment 1), whereas the inner wheel remains, as before in the driving mode (segment 4).

Understanding of wheel-loading modes and of the possible combinations of forces and torques is needed for gaining insight into the relationship between the kinematic and force factors of a wheel and then for describing the power balance of a wheel and of the effect of the driveline system on it. This material is given in Sections 1.3.2 and 1.3.3.

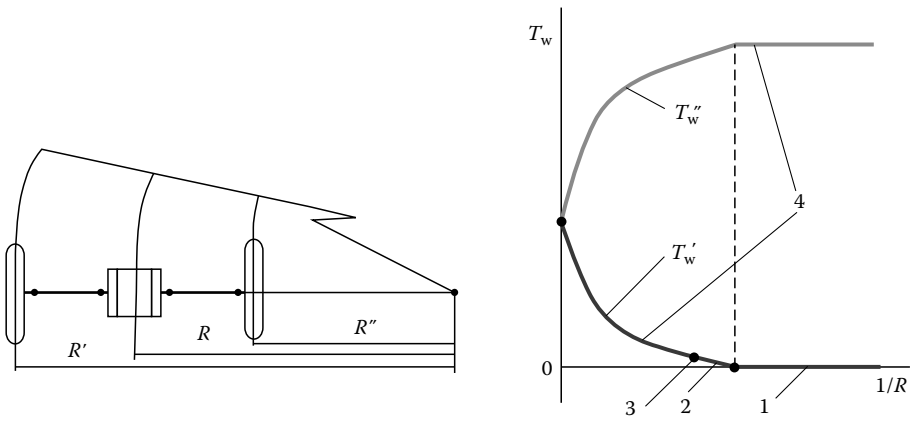


FIGURE 1.47
Axle with NoSPIN taking a turn.

1.3.2 Kinematic and Force Factors

The kinematic and force factors of a pneumatic wheel and their functional mathematical description are determined by the tire's ability to deform in the normal, tangential and lateral directions. To understand the manner in which the driveline system affects the vehicle performance, it is important to compile functional relationships that relate the kinematic and force factors of the wheel. This is, in fact, important, because the force factors of the wheel depend on the torque that is fed to the wheel by the driveline system.

The kinematic, together with the force factors, determine the power that is supplied to the wheel and its part that is lost in the wheel. It should be emphasized that these factors are highly affected by the properties of the surface of motion: the type and state of the solid cover; presence of a wet layer (water and snow) on a solid road and the physical and mechanical properties of the terrain under off-road conditions.

1.3.2.1 Effective Rolling Radius and Slip Ratio

This radius of a wheel with a pneumatic tire is one of the most important concepts of wheel kinematics needed for analyzing the distribution of power among the wheels. To introduce the concept of the effective rolling radius (or simply the rolling radius), consider a rigid wheel with radius r in planar motion on a perfectly firm flat road. Such a motion can be replaced by the rotation of the wheel about the instantaneous center of zero velocity A. The location of this center is determined by the wheel's rolling conditions. When the center A is located at the point of contact between the wheel and the road (Figure 1.48a), the absolute velocity of point A is zero (there is no relative motion between the wheel and the road in point A). When point A moves towards the center of the wheel (Figure 1.48b), the circumference of the wheel gains motion in the direction opposite to the direction of the wheel's center. The wheel is said to be slipping. When point A is below the road level (Figure 1.48c), the wheel's circumference and its center both move in the same direction. The wheel is skidding.

Consider now a wheel with an elastic tire moving at constant angular velocity ω_w from position 1 to position 2 (Figure 1.49a). The radius of such a wheel, obtained by dividing the wheel's displacement S_w by the number of revolutions n_w, is equal neither to the free radius r (measured on the wheel with no normal load) nor the static radius r_s (the distance between the road and the center of the stationary wheel with normal load) or the dynamic r_d radius (the distance between the road and the center of the wheel moving under normal load). This radius is the rolling radius (or the effective rolling radius) r_w that links the actual velocity V_x of the center of the wheel to the wheel's angular velocity ω_w:

$$r_w = \frac{V_x}{\omega_w} \tag{1.7}$$

Since the rolling radius r_w of a pneumatic wheel is not equal to its free radius r, a pneumatic wheel and a rigid wheel of the same radius r with no slip or skid will make different numbers of revolutions on the same traveled distance S_w (see Figure 1.49b).

The rolling radius is a hypothetical radius of a pneumatic wheel, since it cannot be directly measured on the wheel itself as can be done with the static and dynamic radii. Figure 1.50a shows the instantaneous center of zero velocity located at distance r_w down the center of the wheel when it travels the distance S_w between positions 1 and 2. It is seen that the same distance S_w will be traversed by a rigid wheel with $r = r_w$ moving without either slip or skid from 1 to 2 (Figure 1.50b).

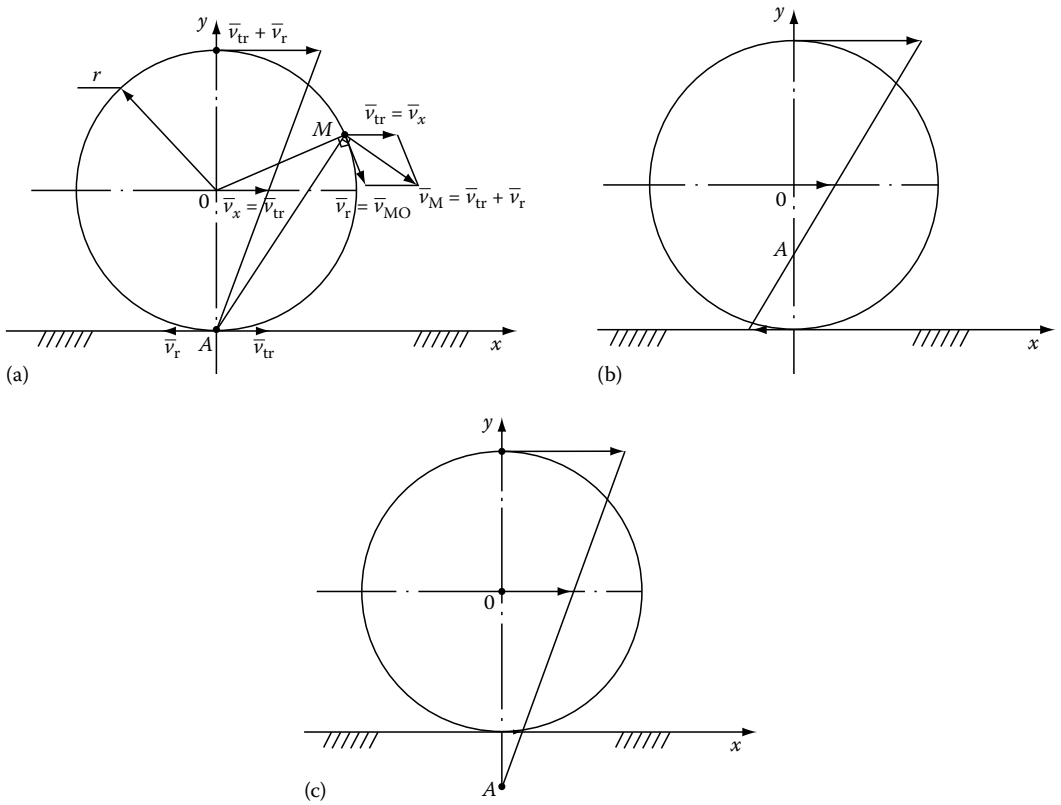


FIGURE 1.48
Rigid wheel kinematics.

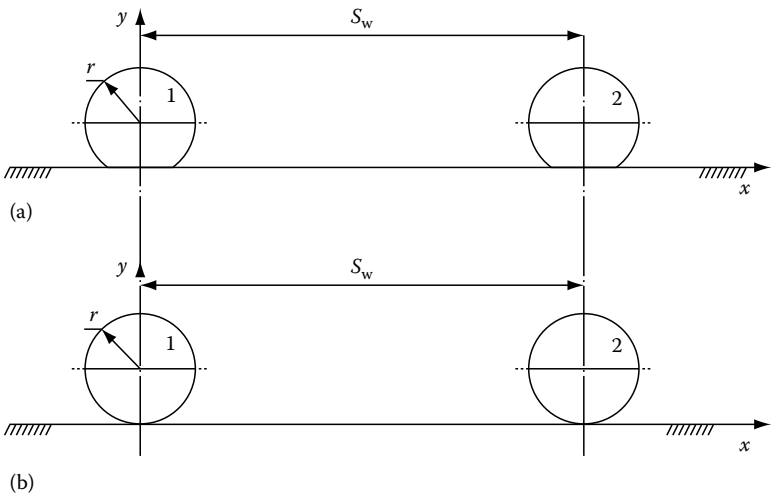


FIGURE 1.49
(a) Pneumatic and (b) rigid wheels.

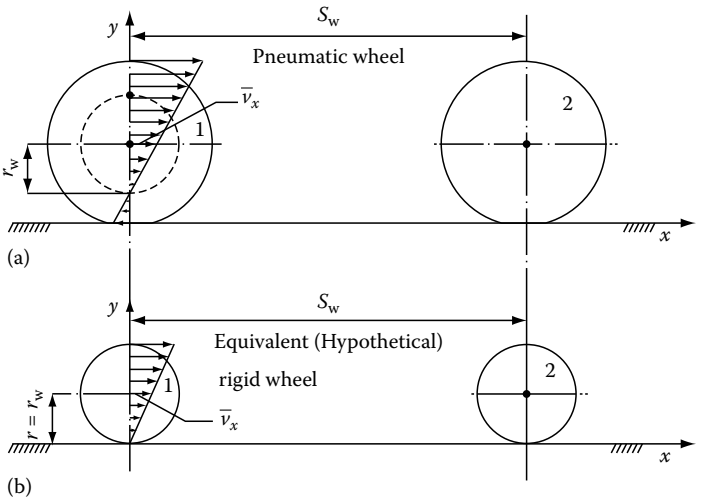


FIGURE 1.50
(a) Pneumatic and (b) equivalent rigid wheels.

The most important conclusion to emerge from such an observation is that the rolling radius of a wheel with an elastic tire is the radius of a hypothetical rigid wheel that has the same linear velocity V_x as the real pneumatic wheel (Figure 1.50a and b):

$$V_x = \omega_w r_w = \omega_w r \tag{1.8}$$

The rolling radius of a pneumatic wheel is not constant because the wheel will make different numbers of revolutions on the same travel when loaded by different combinations of moments and longitudinal forces at the wheel axis and at the tire-road/soil contact patch. There are five major combinations of forces and moments discussed in Section 1.3.1. These different torque-force combinations lead to: (1) longitudinal (tangential) deflections of the tire; (2) longitudinal (tangential) deflections of the soil on deformable surfaces; and (3) relative displacement between the tire and soil (skid).

As an example, Figure 1.51 illustrates the rolling radii that are different due to longitudinal (tangential) deflections of the tire and soil caused (a) by a given torque in the driving mode, $T_w > 0$, and (b) by the frame force in the driven mode when $T_w = 0$.

Any combination of (1), (2), and (3) changes the rolling radius and the angular velocity of a wheel. This leads to a definition of the slip ratio, as a measure of change in the linear velocity of the wheel center caused by changes in the rolling radius and in the angular velocity of the wheel due to any combination of the longitudinal deflections of the tire, tire and soil on deformable surfaces, and due to the skid between the tire and the soil:

$$s_\delta = \frac{V_t - V_x}{V_t} = \frac{V_\delta}{V_t} \tag{1.9}$$

here

V_t is the theoretical linear velocity of a wheel ($s_\delta = 0$)
V_x is the actual linear velocity of the wheel ($s_\delta > 0$)
$V_\delta = V_t - V_x$ is the slip velocity

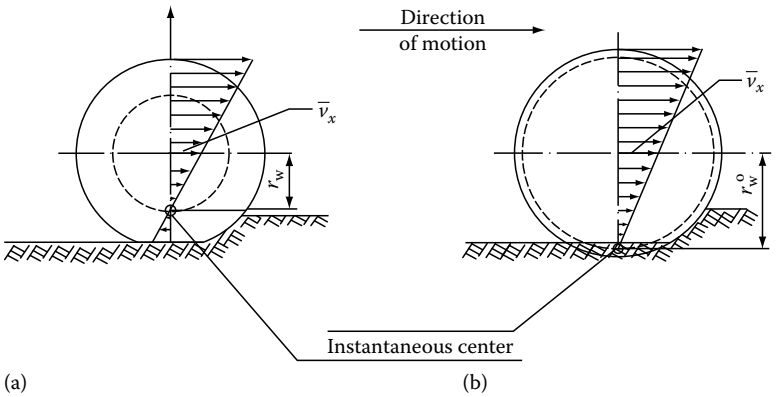


FIGURE 1.51
Rolling radii in (a) driving mode (at a given torque value) and (b) driven mode.

Equation 1.9 can be easily transformed to the expression

$$V_x = V_t(1 - s_\delta) \tag{1.10}$$

Formula (1.10) assesses the changes in the linear velocity of a wheel V_x due to wheel slip s_δ. When a wheel moves in the free mode and the slip ratio is zero, $s_\delta = 0$, the actual and theoretical velocities are equal, $V_x = V_t$, and the rolling radius is r_w^f. When the driving torque T_w increases and the slip ratio goes up, the rolling radius changes to r_w. If the wheel is spinning and the linear velocity $V_x = 0$, the rolling radius becomes $r_w = 0$ and the slip is $s_\delta = 1(100\%)$.

Theoretically, there are no longitudinal deflections of a tire and soil in the free mode of a wheel since there are no longitudinal forces in the tire/soil contact patch (see Figure 1.43c). Hence the theoretical velocity is $V_t = \omega_w r_w^f$ where r_w^f is the rolling radius in the free mode.

The free-mode wheel rolling radius r_w^f can be determined analytically using the diagram in Figure 1.52. It is assumed that wheel radius at the first instant of contact with the road is

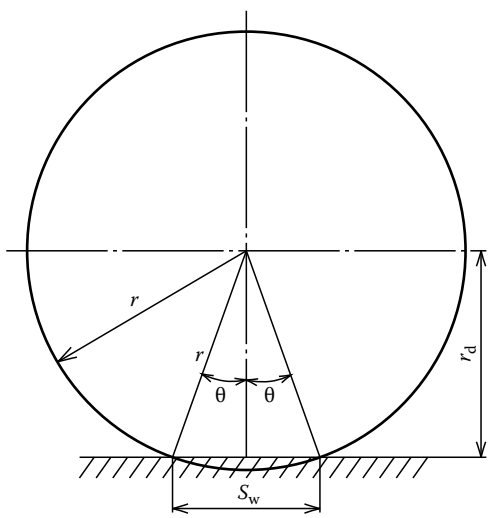


FIGURE 1.52
Wheel diagram.

equal to the free radius r. When the wheel turns in the free mode through an angle 2θ, the path of the wheel center is defined as

$$S_w = 2r \sin\theta \tag{1.11}$$

Expanding $\sin\theta$ in a series and retaining the first two terms, expression (1.11) can be rewritten to

$$S_w = 2r\left(\theta - \frac{\theta^3}{3!}\right) \tag{1.12}$$

The same travel S_w can be expressed in terms of the free-mode wheel rolling radius r_w^f:

$$S_w = 2r_w^f\theta \tag{1.13}$$

Equating the right-hand sides of Equations 1.12 and 1.13, it can be obtained as

$$r_w^f = r\left(1 - \frac{\theta^2}{3!}\right) \tag{1.14}$$

In expression (1.14) it is useful to eliminate the angle θ. For this the free radius r is expressed in terms of the dynamic radius r_d. It is seen from Figure 1.52 that

$$2r_w^f\theta = 2r_d \tan\theta \tag{1.15}$$

Expanding $\tan\theta$ in a series

$$\tan\theta = \theta + \frac{1}{3}\theta^3 + \frac{2}{15}\theta^5 + \cdots$$

and retaining the first two terms, it is obtained as

$$r_w^f = r_d\left(1 + \frac{\theta^2}{3}\right) \tag{1.16}$$

Eliminating the angle θ in expressions (1.14) and (1.16), one can find what is known as Dr. G. V. Zimelev's formula

$$r_w^f = \frac{3r_d}{\left(1 + \frac{2r_d}{r}\right)} \tag{1.17}$$

It was proven experimentally by Dr. G. A. Smirnov that Equation 1.17 allows calculating the values of radius r_w^f for the majority of tires that differ from experimental values by not more than 3%–8%.

However, it is more convenient to use the rolling radius in the driven mode r_w^0 instead of r_w^f for the following reasons. As established, the difference between the radii r_w^0 and r_w^f can be neglected for hard-surface roads and dry dirt roads and the radius r_w^0 can be used as the reference for zero slip ratio: $s_\delta = 0$, where $r_w = r_w^0$. When having reference to wheels rolling on deformable soils, instead of using the radius in the free mode r_w^f, the radius in the driven mode r_w^0 on asphalt can again be accepted for reference of zero slip ratio and for determining the theoretical wheel velocity V_t. Therefore, the radius in the driven mode r_w^0

on asphalt is accepted as the basic radius in this book for determining the theoretical velocity and the slip ratio of a wheel under any type of road and terrain conditions. This approach has the advantage that the radius r_w^0 can be determined indirectly and very easily by experiment as shown in Chapter 8.

The rolling radius r_w^0 in the driven mode on asphalt can also be determined analytically. It can be calculated from the same Equation 1.17 in the same manner as r_w^f. The error as a rule does not exceed 0.3%. Engineering literature contains rather extensive empirically obtained information on determining the effect of the normal load and of the air pressure in the tire on the value of r_w^0 on asphalt. It was shown experimentally that usually

$$r_w^0 = r - \left(\frac{1}{3} \cdots \frac{2}{3}\right) h_z \tag{1.18}$$

here, h_z is the normal deflection of the tire.

Finally, Equation 1.9 can be re-written as

$$s_\delta = \frac{V_t - \omega_w r_w}{V_t} \tag{1.19}$$

Here, r_w is determined in the driving mode and the theoretical velocity is determined based on the rolling radius r_w^0 in the driven mode rather than on the rolling radius r_w^f in the free mode. The advantage of the representation of the slip ratio in the form of Equation 1.19 shall also be demonstrated in Section 7.2.

1.3.2.2 Wheel Force and Torque Factors

Indeed, the rolling radius r_w depends on the applied torque, as previously mentioned. Dr. E. A. Chudakov was apparently the first to validate the first linear function $r_w = f(T_w)$ experimentally. It was later confirmed for wheel operating loads under road conditions and in some off-road operations:

$$r_w = r_w^0 - \lambda_w T_w \tag{1.20}$$

Here λ_w is the longitudinal elasticity factor of a tire on the road or the combined elasticity factor of a tire and soil in off-road travel. It will be proven in Section 1.3.3 (see Equation 1.35) that

$$F_x = \frac{T_w}{r_w^0} = R_x + F_{\text{frame}.x} \tag{1.21}$$

Introducing the tangential elasticity of the tire as

$$\gamma_w = r_w^0 \lambda_w \tag{1.22}$$

But upon substitution of Equation 1.21, Equation 1.20 can be transformed to

$$r_w^f = r_w^0 - \gamma_w R_x \tag{1.23}$$

at $F_{\text{frame}.x} = 0$ in the free wheel rolling mode. Then Dr. E. A. Chudakov's equation (Equation 1.20) becomes

$$r_w = r_w^f - \gamma_w F_{\text{frame}.x} \tag{1.24}$$

A wheel rolls with the rolling radius r_w^0 in the driven mode when the torque is zero, $T_w = 0$ (see Equation 1.20). If the torque is $T_w \neq 0$, but the resultant force in the tire/surface contact patch is $F_w = 0$ (also the force $F_{frame.x} = 0$; the free wheel-rolling mode), the slip ratio is zero and $r_w = r_w^f$ (see Equation 1.24). In the driving mode, when $T_w \neq 0$ and $F_w \neq 0$, both Equations 1.20 and 1.24 give identical values of the rolling radius r_w. Note that the factors, γ_w and λ_w, are measured in [m/N] and [m/Nm], respectively.

Dr. A. Kh. Lefarov divided both sides of Equation 1.20 by r_w^0, and thus obtained a new linear function between the slip ratio s_δ and the wheel circumferential force F_x:

$$\frac{T_w}{r_w^0} = F_x = \frac{1}{\lambda_w} \frac{r_w^0 - r_w}{r_w^0} = K_x s_\delta \tag{1.25}$$

Here K_x is the longitudinal stiffness, $K_x = 1/\lambda_w$; when the longitudinal elasticity, λ_w is given as [m/Nm]. As can be noted by the reader, the circumferential force F_x of the wheel in Equation 1.25 is determined from torque T_w using the driven-mode rolling radius r_w^0, rather than any other, for example the dynamic radius r_d. The necessity to use radius r_w^0 shall be proven in Section 1.3.3 (see Equations 1.34 and 1.35).

These linear functions represented by Equations 1.20 and 1.25 work well on firm roads and dense terrain. A large body of date is available in engineering literature on the longitudinal elasticity of tires that can be used for calculations using Equations 1.20 and 1.25.

It should be noted here that a large number of nonlinear functions relating the tire slip s_δ (or the radius r_w) to the circumferential force F_x (or the wheel torque T_w) is available for the case when wheels are under both operational and with full loads on soft and damp soils. These functions are nonlinear, which stems from the specifics of soft soil structure and its moisture content. Such nonlinear functions are derived mathematically using a tire-soil model of deflections or are found experimentally based on statistical analysis of experimental data. One of such function that has gained wide acceptance in research is presented below:

$$F_x = R_z \mu_{px} (1 - \exp(-k s_\delta)) \tag{1.26}$$

where

R_z is the normal tire reaction

μ_{px} is the peak friction coefficient (also called the grip coefficient)

k is an empirical factor that depends on the properties of the tire and the surface

The peak friction (grip) coefficient in Equation 1.26 is equal to the force ratio:

$$\mu_{px} = \frac{F_x^{max}}{R_z} \tag{1.27}$$

where F_x^{max} is the maximum circumferential wheel force that can be attained in the contact between the wheel and the surface of motion. Such an approach to determining the peak friction coefficient is usually typical of technical references pertaining to tractors and other off-road vehicles.

The peak friction coefficient is defined in automotive literature as the ratio

$$\mu_p = \frac{F_w^{max}}{R_z} \tag{1.28}$$

where F_w^{max} is the maximum wheel traction force.

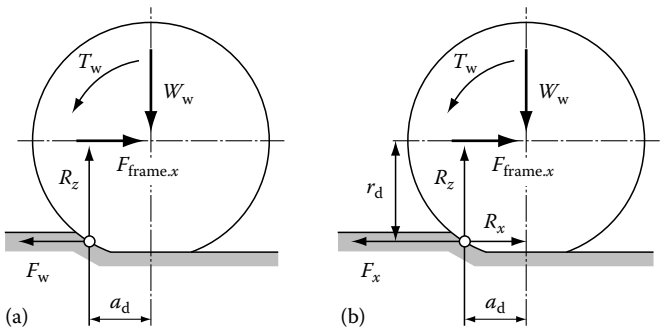


FIGURE 1.53
Equivalent free-body diagrams of a wheel in the driving mode.

It is seen by comparing Figure 1.53a and b and taking into consideration Equation 1.21 that the force F_x is larger than the wheel force F_w by the amount of rolling resistance R_x. For this reason μ_{px} is larger than μ_p. This must be remembered when using Equation 1.26. Utilizing Equation 1.21 and making use of the fact that $F_w = F_{frame.x}$, the following can be found:

$$\mu_{px} = \mu_p + f \tag{1.29}$$

where $f = R_x/R_z$ is the rolling resistance coefficient.

Another observation pertaining to expressions (1.27) and (1.28), in the wide body of engineering literature, in particular in Russian, the coefficients μ_{px} and μ_p are usually termed the grip coefficients or the peak adhesion coefficients. Such a definition fits precisely the interaction between the tire components and the supporting surface.

Divide both sides of Equation 1.26 by the normal road reaction R_z. This yields

$$\mu_x = \frac{F_x}{R_z} = \mu_{px}(1 - \exp(-ks_\delta)) \tag{1.30}$$

where μ_x is the current friction of grip coefficient (often called the friction coefficient ''in use''). This coefficient represents the percentage of the normal reaction R_z that is utilized in generating the circumferential force F_x needed for motion under the given conditions.

Figure 1.54 presents experimental data and graphs constructed on the basis of Table 1.18.

Experimental results show that the relationship between force F_x and slippage s_δ for many vehicles traveling over soil is close to linear up to some value of $s_{\delta 0}$ that shall be termed the characteristic value. If $s_\delta > s_{\delta 0}$, then $F_x = f(s_\delta)$ becomes nonlinear. For such cases it is convenient to use the expression

$$F_x = \mu_{px} R_z \left(1 - \frac{s_{\delta 0}}{2|s_\delta|}\left(1 - \exp\left(-\frac{2|s_\delta|}{s_{\delta 0}}\right)\right)\right)\text{signs}_\delta \tag{1.31}$$

or

$$\mu_x = \frac{F_x}{R_z} = \mu_{px}\left(1 - \frac{s_{\delta 0}}{2|s_\delta|}\left(1 - \exp\left(-\frac{2|s_\delta|}{s_{\delta 0}}\right)\right)\right)\text{signs}_\delta \tag{1.32}$$

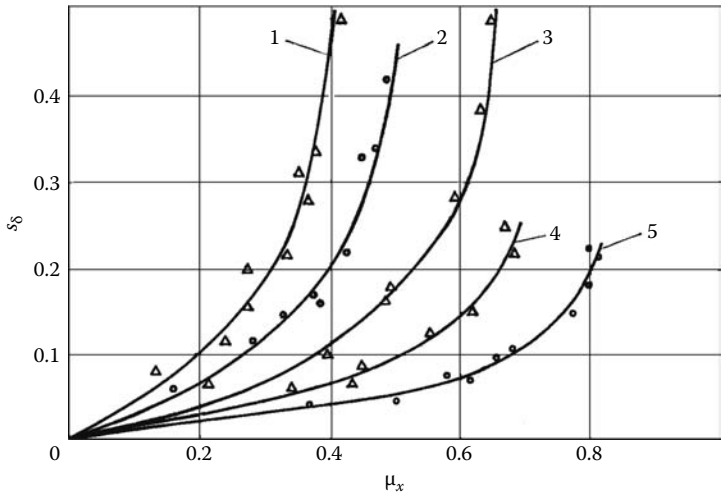


FIGURE 1.54
Experimental data approximated by formula (1.30): Tire 8.3/8-20, $p_w = 0.14$ MPa: 1, field; 2, harvest-field. Tire 15.5-38R, $p_w = 0.12$ MPa: 3, field. Tire 465-868R, $p_w = 0.10$ MPa: 4, field; 5, harvest-field.

TABLE 1.18

Tire-Surface Characteristics

Tire Model	Wheel Disk	Inflation Pressure MPa	Asphlat K_x, kN	Field Ready for Sowing	
				μ_{px}	k
15.5R38 F-2A	DW 14	0.14	77.45	0.622	5.671
	DW 14	0.08	101.28	0.722	6.596
	DW 11	0.08	108.22	0.686	6.436
I6.9R38 F-52	W15L	0.13	249.93	0.778	7.023
18.4R34 FB-11	DW16	0.13	324.68	0.726	6.647
	DW16	0.15	263.14	0.699	5.612
16.9R30 F-43	W15L	0.10	277.78	0.749	6.633
8.3-20 B-105A	W7	0.10	49.31	0.497	5.081
	W7	0.14	46.08	0.466	4.358
11.2-20 F-35	W8	0.10	58.83	0.544	4.580
	W8	0.14	50.91	0.508	4.112
11.2-20 R-296	W9	0.10	92.06	0.585	4713
	W9	0.14	60.09	0.553	4251
16.0-20 F-64	DW13	0.10	96.13	0.627	5.093

where
sign $s_\delta = 1$ for the driving mode
sign $s_\delta = -1$ for the braking mode

The numerical values of μ_{px} and $s_{\delta 0}$ can be determined from experimental data. As an example, Figure 1.55 shows experimental results on the 13.6R38 tire and data obtained from Equation 1.31. Better agreement between predicted and measured results is obtained in the case of deformable soil.

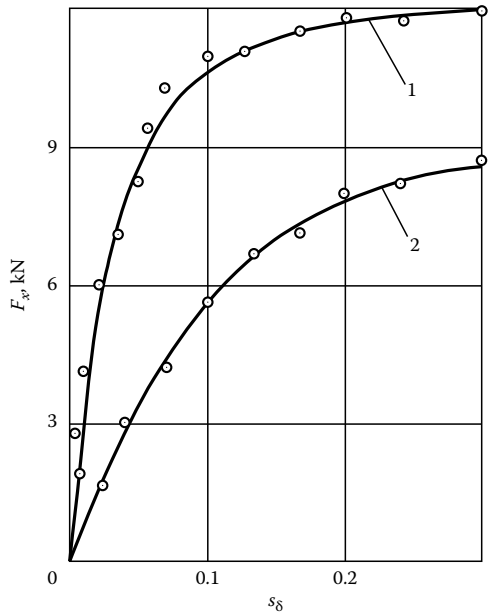


FIGURE 1.55
Tire 13.6R38, $p_w = 0.1$ MPa, $R_z = 10$ kN: 1, concrete; 2, field.

Equations 1.20, 1.25, 1.26, and 1.31 above illustrate the manner in which pneumatic wheel kinematics has a direct bearing on the wheel dynamics and then energy effectiveness of the wheel. Details on integrating wheel kinematics and wheel dynamics with its energy efficiency is given in the next section.

1.3.3 Wheel Power and Force Balance

Consider a pneumatic wheel rolling in the driving mode at constant rotational speed ω_w under the applied driveline torque T_w (Figure 1.53). As mentioned before, Figure 1.53a and b are mutually equivalent:

$$F_x = F_{\text{frame}.x} + R_x = F_w + R_x \tag{1.33}$$

The wheel can be described as a power-consuming system with input power P_w^{in}, output power P_w^{out}, and several components that account for the difference between these two (see Figure 1.56). All these terms comprise the wheel power balance

$$P_w^{in} = P_f + P_\delta + P_w^{out} \tag{1.34}$$

where

$P_w^{in} = T_w\omega_w$; $P_f = R_x V_x$ is the power expended in overcoming the rolling resistance force R_x (upon normal deflections of the tire and soil)

$P_\delta = F_x\omega_w\left(r_w^0 - r_w\right)$ is the slip power, i.e., the power lost in slippage (in deflecting the tire and the soil

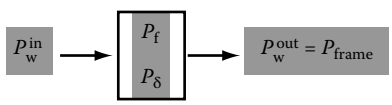


FIGURE 1.56
Wheel power-consuming system.

in the longitudinal direction) that results in loss of the linear velocity of the wheel given by the expression $V_\delta = V_t - V_x$ in Equation 1.9

$P_w^{out} = F_{frame.x} V_x$ is the output power that is transmitted from the wheel to the vehicle body

Substituting the expressions for power components in Equation 1.34, one can arrive at the following form of the wheel force balance:

$$F_x = \frac{T_w}{r_w^0} = R_x + F_{frame.x} \tag{1.35}$$

Equation 1.35 of the wheel power balance derived from the general power balance proves the need to use term r_w^0—the rolling radius in the driven mode—for determining the circumferential force F_x from the torque T_w. Usually this force is determined using the dynamic radius r_d, which follows from the free-body diagram of the wheel that is based on the Coulomb-friction approach. This is not entirely correct. The power balance gives a rather general approach to compare with Coulomb friction. This is because the power balance deals with the tire/surface deflections, as opposed to a static free-body diagram that treats the wheel as a rigid body even when it is actually deflected. For this reason the rolling radius r_w^0 is used throughout this book instead of the dynamic radius r_d.

Equations 1.34 and 1.35 are very important for understanding the influence of the driveline system on the vehicle energy efficiency and thence on the fuel consumption. Indeed, the force F_x that is produced by the wheel driveline torque T_w directly determines the slip power loss. This is shown by the component P_δ in power balance Equation 1.34. The force F_x produces the longitudinal deflections of the tire and the soil. These deflections lead to changes in the rolling radius r_w. The changes in r_w were defined as the tire slip in Section 1.3.2.

The driveline system is seen to affect the vehicle energy efficiency by way of the slip power. Proper design of PDUs of the driveline system allows controlling the slippage power expended by all the vehicle's wheels and to thus improve its energy and fuel efficiency.

The fraction of parasitic power losses in Equation 1.34 can be estimated using the wheel efficiency in the driving mode, which is known as the wheel tractive efficiency:

$$\eta_w^t = \frac{P_w^{out}}{P_w^{in}} = \frac{F_{frame.x} V_x}{F_x V_t} = \frac{F_{frame.x}}{F_x} \frac{V_x}{V_t} = \eta_{fw} \eta_{\delta w} \tag{1.36}$$

where

$\eta_{fw} = \dfrac{F_{frame.x}}{F_x} = \dfrac{F_x - R_x}{F_x} = 1 - \dfrac{R_x}{F_x}$ is the wheel rolling resistance efficiency

$\eta_{\delta w} = \dfrac{V_x}{V_t} = \dfrac{V_t - V_\delta}{V_t} = 1 - \dfrac{V_\delta}{V_t} = 1 - s_\delta$ is the wheel slip efficiency

Figure 1.57 illustrates the efficiency η_w^t as a function of the net-tractive force $F_w = F_{frame.x}$. It is seen that at $4 < F_w < 6.5$ kN there exist optimal values of the normal load W_w, that correspond to the maximum values of η_w^t.

The efficiency η_w^t is a measure of the energy effectiveness of the wheel when rolling in the driving mode, when $F_w = F_{frame.x} > 0$. In the free mode $F_{frame.x} = 0$ and hence $\eta_w^t = 0$ (see Equation 1.36). Formally this means that the wheel does not perform useful work in

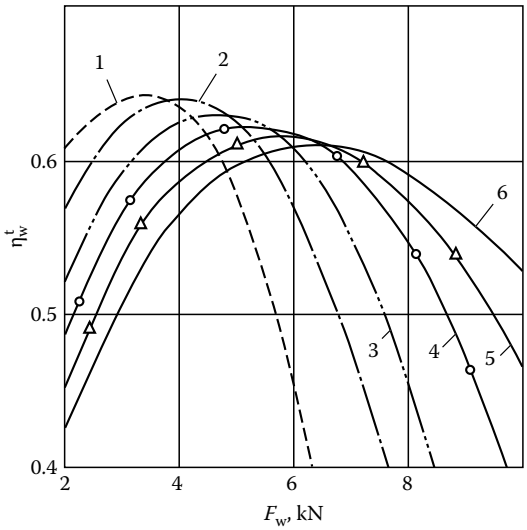


FIGURE 1.57
Tractive efficiency of a wheel with a 16.9R30 tire on soft soil. 1, $W_w = 10$ kN; 2, $W_w = 12$ kN; 3, $W_w = 14$ kN; 4, $W_w = 16$ kN ; 5, $W_w = 18$ kN; 6, $W_w = 20$ kN.

the free mode. This, however, is not so: the wheel may be transporting a payload. The energy assessment of a wheel in the free mode can be obtained using the transportation (or payload moving) efficiency. For this purpose, the following formula shall write the normal load on a wheel as

$$W_w = W_{wc} + W_{wg} \tag{1.37}$$

where
W_{wc} is the curb weight
W_{wg} is the payload weight

Hence the wheel rolling resistance force is

$$R_x = R_{xc} + R_{xg} \tag{1.38}$$

where
R_{xc} is the rolling resistance exerted by the curb weight W_{wc}
R_{xg} is the rolling resistance exerted by the payload weight W_{wg}

Component R_{xg} may be referred to the useful resistance and then the transportation efficiency can be defined as

$$\eta_w^{tr} = \frac{P_{fg}}{P_w^{in}} = \frac{R_{xg} V_x}{F_x V_t} = \frac{R_{xg}}{R_{xc} + R_{xg}} \frac{V_x}{V_t} = \eta_{fw}^{tr} \eta_{\delta w} \tag{1.39}$$

where
$\eta_w^{tr} = \frac{R_{xg}}{R_{xc}+R_{xg}}$ is the efficiency for evaluating the resistance exerted by the payload
$\eta_{\delta w}$ is the slip efficiency for evaluating the tire slip caused by the payload

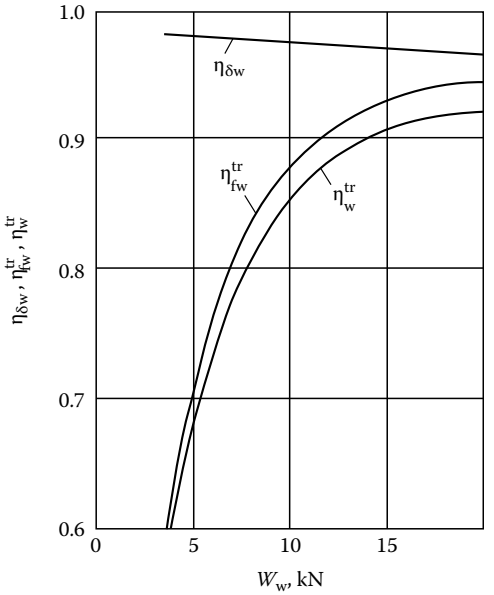


FIGURE 1.58
Transportation efficiency of a wheel with a 16.9R30 tire on soft soil.

Note that, as a result of the nonlinear rise in the rolling resistance upon increasing the normal load, it is first necessary to calculate R_x and R_{xc} and to then determine R_{xg} from Equation 1.38. The values of R_{xc} and R_{xg} thus found should be used for determining η_w^{tr} from Equation 1.39.

Figure 1.58 is a plot of η_w^{tr} and its components as a function of the normal load W_w that increases by an increase in its component W_{wg}. As expected, an increase in the payload causes some rise in the power lost in slippage and a reduction in $\eta_{\delta w}$. However, the rather insignificant reduction in $\eta_{\delta w}$ is compensated by a marked rise in η_{fw}^{tr}. As a result, η_w^{tr} also increases.

To obtain an energy evaluation of wheels loaded both by the payload W_{wg} and by the traction load $F_{frame.x}$, the total efficiency can be used:

$$\begin{aligned}\eta_{\Sigma w} &= \frac{P_w^{out}}{P_w^{in}} = \frac{P_{frame} + P_{fg}}{P_w^{in}} \\ &= \frac{P_{frame}}{P_w^{in}} + \frac{P_{fg}}{P_w^{in}} \\ &= \eta_w^t + \frac{R_{xg}}{R_{xc} + R_{xg} + F_w}(1 - s_\delta)\end{aligned} \tag{1.40}$$

Equation 1.40 is plotted in Figure 1.59. The total efficiency decreases with increasing F_w because of the rise in slippage s_δ. The total efficiency improves with increasing payload W_{wg}.

A rather useful comment should be made here. As seen from Equations 1.36, 1.39, and 1.40, the efficiencies structurally contain force and velocity components that represent the force and velocity power losses.

In the case of nonsteady motion, the power balance of a wheel in the driving mode can be written as (see Figure 1.60):

$$P_w^{in} = P_f + P_\delta + P_a + P_\varepsilon + P_w^{out} \tag{1.41}$$

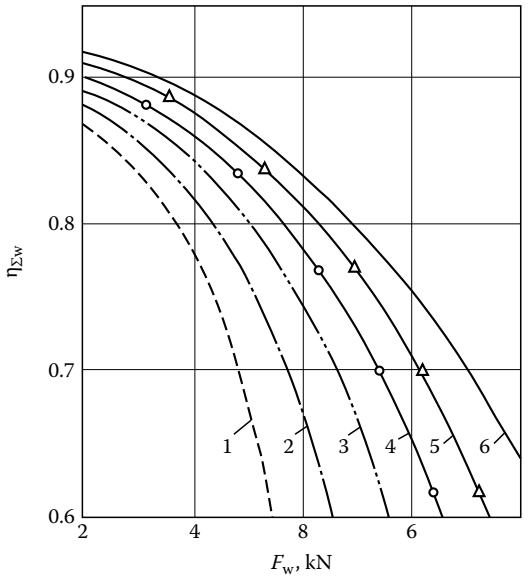


FIGURE 1.59
Total efficiency of a wheel with a 16.9R30 tire on soft soil. 1, $W_w = 10$ kN; 2, $W_w = 12$ kN; 3, $W_w = 14$ kN; 4, $W_w = 16$ kN; 5, $W_w = 18$ kN; 6, $W_w = 20$ kN.

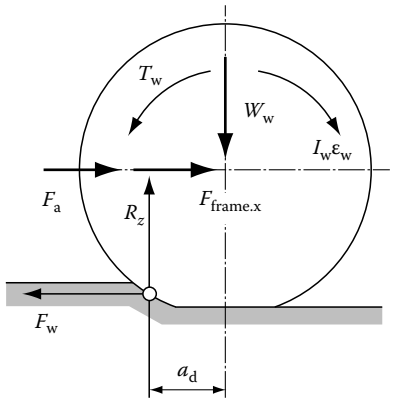


FIGURE 1.60
Wheel in nonsteady planar motion.

where there are contained two additional components: $P_a = \frac{W_w}{g} a_x V_x = F_a V_x$ is the power needed to increase the kinetic energy of a wheel in translational motion speeding up with acceleration a_x up to velocity V_x and $P_\varepsilon = I_w \varepsilon_w \omega_w$ is the power needed to increase the kinetic energy of the rotational motion of the wheel with the moment of inertia I_w when speeding up with the angular acceleration ε_w up to the rotational velocity ω_w.

Substituting the power components into Equation 1.41, it can be rewritten to the form

$$T_w = (R_x + F_{frame.x} + F_a) r_w^0 + I_w \varepsilon_w \tag{1.42}$$

that defines the torque applied by a driveline system to a wheel.

In conclusion, the material presented in Sections 1.3.1 through 1.3.3 explains the nature of a driveline system's influence on (1) the power-loading mode of a wheel, (2) the tire slippage as a complex process of longitudinal deflections and relative moment of a tire and soil, and (3) the slip power loss and energy efficiency of a wheel.

1.3.4 Motion with a Slip Angle

This section deals with two problems pertaining to the motion of a wheel with a side-slip angle that has a direct bearing on the driveline designs under considerations:

1. Mutual effect of longitudinal and lateral forces of the wheel
2. Relationship between the longitudinal force of the wheel and its rolling radius (slip ratio) at slip angle $\alpha \neq 0$

Usually in deriving a mathematical model of rolling of a sliding wheel the principal attention is focused on the first question whereas, unjustifiably so, much less attention is paid to the second one. Nevertheless, even the first question of interaction between longitudinal and lateral forces is in need of additional clarification.

1.3.4.1 Interaction between Longitudinal and Lateral Forces

Figure 1.61 shows a free-body diagram of a pneumatic wheel that depicts two sets of forces exerted on the wheel by the vehicle and by the road. The vehicle exerts a normal load, W_w, lateral force Y_w and also the longitudinal force $F_{frame.x}$ not shown, but applied at point O_w perpendicular to the page and toward the reader. Forces W_w, Y_w, and $F_{frame.x}$ can be regarded as active applied forces. They deform the tire and cause elementary forces to form upon contact between the tire and the road. These elementary forces can be reduced to three road reactions: normal reaction R_z, applied in point A of the tire-tread impression, longitudinal reaction F_w, known as the traction force and applied in point B and lateral reaction F_l applied in point C. It must be kept in mind that force factors R_z, F_w, and F_l are in substance reactions, even though they are frequently called forces.

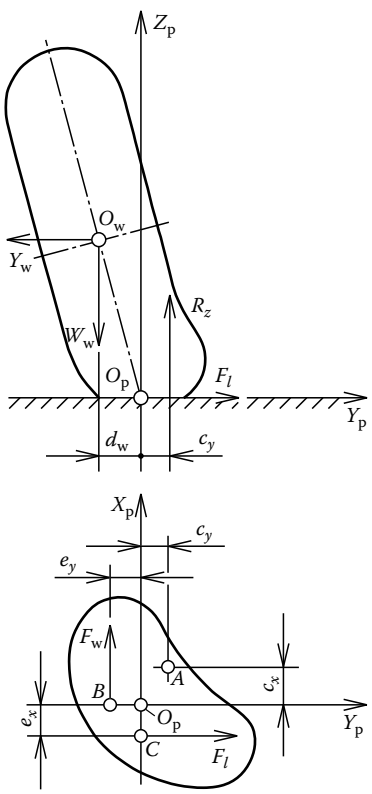


FIGURE 1.61
Wheel free-body diagram.

Changes in the driving/braking torques T_w and T_b applied to the wheel by the driveline system modify the value and direction of reaction F_w. Lateral reaction F_l is a function of lateral force Y_w. At the same time, the maximum values of reactions F_w^{max} and F_l^{max} are limited by the deformation properties of the tire and the soil. If the wheel is subjected simultaneously to longitudinal and lateral forces then reactions F_w and F_l are interrelated as

$$\sqrt{F_w^2 + F_l^2} = \mu_p R_z \tag{1.43}$$

This relationship was compiled on the assumption that the properties of contact between the tire and the surface of motion are isotropic, i.e., are the same in all directions.

It follows from this assumption that the grip coefficients in the longitudinal μ_p and the lateral μ_l directions are identical, i.e., that

$$\mu_p = \frac{F_w^{max}}{R_z}, \quad \mu_l = \frac{F_l^{max}}{R_z}, \quad \mu_p = \mu_l \tag{1.44}$$

Actually, however, coefficients μ_p and μ_l may not be identical and may be related in different ways. It is seen by comparing the values of longitudinal and lateral grip coefficients that, as a rule, $\mu_p < \mu_l$. The relationship between these two coefficients depends highly on the kind of the surface of motion.

To satisfy Equation 1.43 when the tangential reaction F_w increases with increasing numerical value of the wheel torque T_w, the lateral reaction F_l should decrease. This means that the available cornering force Y_w that can be absorbed by the wheel decreases. For example, at high traction forces F_w the appearance of a low-force side wind, i.e., applied force Y_w, may cause the wheel to slip in the lateral direction. This is particularly noticeable in accelerating on icy roads, when not only a side wind, but also rolling onto a small stone (surface irregularity) causes side slip. This is confirmed by Equation 1.43: $F_l = 0$ at $F_w = \mu_p R_z$, i.e., the wheel is unable to take up any lateral forces Y_w.

A large body of analytic results and experimental information is available in engineering literature on the effect of the tangential force of a wheel on its capacity to withstand side forces. As an illustration the nonlinear lateral slip theory developed by Dr. D. A. Antonov is referred to:

$$F_l = K_y \alpha = K_{y0} \prod_{i=1}^{9} q_{\alpha i} \alpha \tag{1.45}$$

where lateral force F_l is a function of slip angle α; K_y is known as the lateral slip resistance coefficient (also called the cornering stiffness of the tire), whereas K_{y0} is the tangent of function $F_l = f(\alpha)$ at the coordinate origin; $\prod_{i=1}^{9} q_{\alpha i}$ is the product of nine correction factors that correct Equation 1.45 upon change in the normal load, soil properties, irregularities of the surface of motion, wheel alignment, etc. One of the nine partial correction factors $q_{\alpha T}$ reflects the effect of traction force F_w. In the case of ultimate loading of the wheel contact patch this coefficient is determined from Equation 1.43 as a ratio of the value of K_y at force F_w to its value at $F_w = 0$:

$$q_{\alpha T} = \frac{K_y}{K_{yF_w=0}} = \frac{\sqrt{(\mu_p R_z)^2 - F_w^2}}{\mu_p R_z} = \sqrt{1 - \left(\frac{F_w}{\mu_p R_z}\right)^2} \tag{1.46}$$

It is seen from Equation 1.46 that the wheel's slip resistance is highest when $F_w = 0$. With the appearance and increase in force F_w (with increasing torque T_w) the value of $q_{\alpha T}$ decreases, i.e., the ability of the wheel to take up lateral forces decreases. At $F_w^{max} = \mu_p R_z$, when the wheel starts spinning, $q_{\alpha T} = 0$. The wheel is unable to develop even a small lateral reaction, $F_l = 0$. Hence the appearance of an even small lateral force Y_w causes the wheel to slip to the side.

In the case of slightly-loaded contact between the tire and the surface of motion, when

$$\sqrt{(F_w)^2 + (F_l)^2} \le 0.5 \mu_p R_z \tag{1.47}$$

the correction factor is determined from the expression

$$q_{\alpha T} = \frac{\sqrt{1 - \left(\frac{F_w}{\mu_p R_z}\right)^2}}{1 + 3\left(1 - \left|\frac{F_w}{\mu_p R_z}\right|\right)\left(0.08 + 0.17\frac{R_z}{W_w^{nom}}\right)\left(1 - \frac{F_l}{F_l^{max}}\right)\frac{F_w}{R_z}} \tag{1.48}$$

where W_w^{nom} is the nominal tire load, whereas $F_l^{max} = \sqrt{(\mu_p R_z)^2 - (F_w)^2}$.

This means that changes in the driving/braking torques T_w and T_b and the corresponding changes in longitudinal force F_w modify the value of correction factor $q_{\alpha T}$ and together with it the slip resistance factor K_y in Equation 1.45. Even on paved roads the value of K_y for driving wheels of cars may be 5%–30% lower than its value for driven wheels. At constant wheel lateral force a reduction in K_y in Equation 1.45 shall result in marked increase in α. Since the nature of the curvilinear motion of a vehicle depends highly on the difference between the slip angles of the front (α_1) and rear (α_2) axles, the effect of coefficients K_{y1} and K_{y2} on the dynamics of a vehicle taking a turn become understandable. The above material also explains the mechanism by means of which the driveline system affects the relationship between the lateral force of the wheel and its slip angle. This problem shall be developed further in Sections 2.8.3 and 3.5.2.

1.3.4.2 Wheel Kinematic and Force Factors under Sideslip

Section 1.3.2 examined equations relating the kinematic and force parameters of a wheel in planar motion. The question arises naturally as to the validity of these equations in the case of motion with a slip angle. To resolve this question the following must be clarified: the effect of sideslip on the value of the rolling radius r_w^0 in the driven mode, the tangential elasticity λ_w of the tire and the parameters μ_{px} and k in Equation 1.26.

Figure 1.62 shows the paths of motion AB and AC of the center of a driven wheel without and with slip. When moving along path AC (i.e., with slip angle) the elementary motion of the center of the wheel can be regarded as the resultant motion along the line of action of the longitudinal and lateral reactions of the road. For this reason the total travel AC is determined by segments AB and BC. If the radius r_w^0 is independent of α, then its value r_w^0 determined without slip ($\alpha = 0$) from point A to point B should be equal to the value of $r_{w\alpha}^0$ determined from segment AB when the wheel rolls with slip from point A to point C.

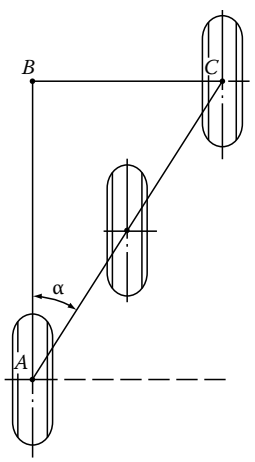


FIGURE 1.62
Layout of a wheel with slip angle α.

Figure 1.63 shows the results of testing a 5.00-10 tire on a stand with a rotating drum. The experiments were performed at preset angle α and the wheel rolling radius was determined from the traveled distance S_{AC}:

$$r_\alpha = \frac{S_{AC}}{2\pi n_w} \tag{1.49}$$

where

$S_{AC} = 2\pi r_r n_r$

r_r is the radius of the drum

n_r is the number of revolutions of the drum over path S_{AC}

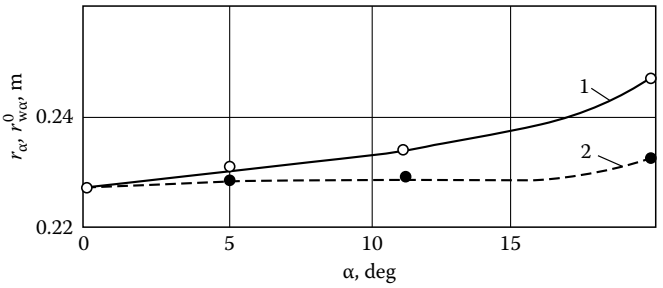


FIGURE 1.63
Tire 5.00-10; $p_w = 0.15$ MPa; $W_w = 2$ kN. 1, r_α; 2, $r^0_{w\alpha}$.

Multiplying the value of r_α from Equation 1.49 by cos α, the value of the rolling radius $r^0_{w\alpha}$ in the driven mode over segment *AB* is obtained. It is seen that $r^0_{w\alpha}$ deviates from r^0_w by not more than 1.5%. This result, as well as analysis of a large volume of experimental data allows the conclusion that the effect of lateral slip on the wheel-rolling radius in the driven mode can be neglected.

This, however, does not apply to the tangential elasticity of the tire (tire and soil) λ_w (or γ_w, see Section 1.3.2). The value of the latter increases highly with increasing α. Figure 1.64 shows the results of calculating $\gamma_{w\alpha}$ as a function of α performed for a 6.00-16 tire. The calculations were performed used two different formulae derived by Drs. A. S. Litvinov and Ya. E. Farobin. The results obtained by both methods are virtually identical.

One of the above-mentioned expressions derived by Drs. A. S. Litvinov and Ya. E. Farobin can be used for practical calculations

$$\gamma_{w\alpha} = \gamma_w / C_{cor}$$

here

$$C_{cor} = \frac{W_w \mu_p}{\sqrt{\left(\frac{F_w}{C_{cor}}\right)^2 + (K_{y0} \tan\alpha)^2}} \left[1 - \frac{0.25 W_w \mu_p}{\sqrt{\left(\frac{F_w}{C_{cor}}\right)^2 + (K_{y0} \tan\alpha)^2}}\right] \tag{1.50}$$

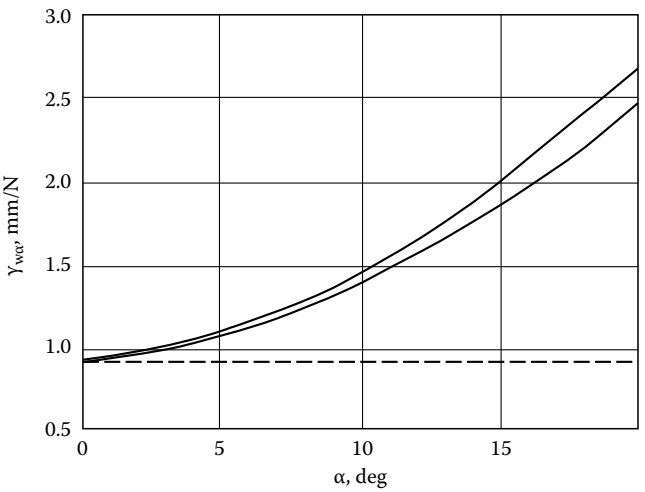


FIGURE 1.64
Longitudinal elasticity of a 6.00-16 tire.

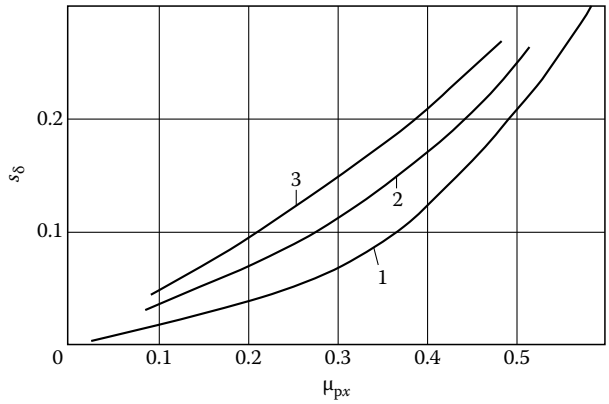


FIGURE 1.65
Computed slip curves of the 7.50-18AS with $\mu_{px} = 0.75$, $k = 5.5$. 1, $\alpha = 0$; 2, $\alpha = 10°$; 3, $\alpha = 15°$.

Experimental results show that the slip s_δ of a wheel increases with α at constant force F_x. A function $F_x = f(s_\delta, \alpha)$ was derived mathematically from basic Equation 1.26 and on assumption of isotropy of the properties of the surface of motion:

$$F_x = \frac{R_z \mu_{px} s_\delta}{\sqrt{s_\delta^2 + (1 - s_\delta)^2 \tan^2 \alpha}} \left[1 - \exp\left(-k\sqrt{s_\delta^2 + (1 - s_\delta)^2 \tan^2 \alpha}\right)\right] \tag{1.51}$$

Figure 1.65 displays curves plotted from Equation 1.51. Comparison of these data with experimental results from the research paper by G. Krick and other experimental data shows that Equation 1.51 is sufficiently accurate for engineering calculations. Please note that at $\alpha = 0$ Equation 1.51 takes the form of Equation 1.26 that relates F_x and s_δ when there is no side slip.

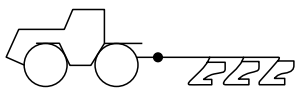
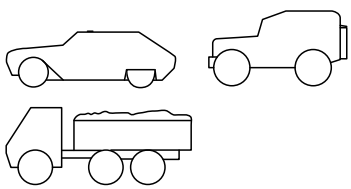
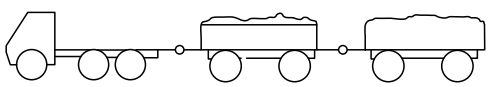
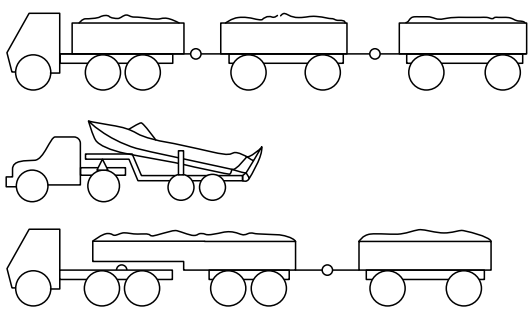
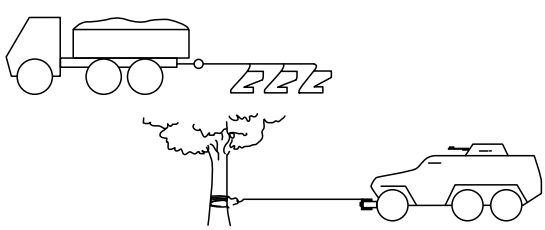
The material presented in this section is of great significance for analytic studies of the effect of driveline systems both on the dynamics of vehicles in curvilinear motion and on the energy effectiveness of vehicles in turns. The reason for this is as follows. Different driveline systems distribute the torque to the driving wheels when a vehicle takes a turn in different manners. For this reason, also the traction forces to which these wheels are subjected in turns are different. These different traction forces also affect differently the slip angle and the lateral forces of the wheels (see notation F_w in Equations 1.46 and 1.48 which are components of Equation 1.45). This determines to a large extent the path dynamics of the vehicle. The functional relationship between the kinematic and force parameters of the wheel changes simultaneously when taking a turn (see Equation 1.26 where the exponent does not contain α and Equation 1.51 in the present section where the exponent does include α). This occurs because of the tangential elasticity of the tire changes with changing α (see Figure 1.64). An increase in wheel slip s_δ when moving at a slip angle causes an increase in the power P_δ expended on slipping of the wheel. This follows from Equation 1.19 and Equation 1.34. This reduces the slip efficiency $\eta_{w\delta}$ and, in the final analysis, the wheel efficiency (see Equations 1.36, 1.39, and 1.40). The material and clarification of the mechanism of the effect of the driveline system on the interaction of a wheel with the support surface allows next to clarify the manner in which the driveline systems affect the energy effectiveness of the vehicle and, in the final analysis, the vehicle performance.

1.4 Vehicle Energy/Fuel Efficiency and Driveline Systems Design

The wheel drive energy of a moving vehicle is spent in overcoming all kinds of resistances to motion and performing useful work. This useful work is different in vehicles intended for different uses. Depending on the useful work that is performed, wheeled vehicles and the modes of their functions can be classified into three groups (see Table 1.19): traction vehicles (traction work mode), transportation vehicles (cargo transportation mode), and transportation-traction (combined) mode.

TABLE 1.19

Modes of Vehicle Operation

No	Vehicle	Modes		
		Tractive	Transportation	Combined
1		+	−	−
2		−	+	−
3		−	+	−
4		−	+	−
5		−	−	+

Traction vehicles are those whose useful work consists in overcoming the traction resistance. For example, the farm tractor (Table 1.19, position 1) performs useful work in plowing a field overcoming the traction resistance of the farm implement. Transportation vehicles (Table 1.19, positions 2 through 4) perform transportation work in transporting passengers and cargo (payload), which is also true of trucks and vehicular trains that transport cargo. Transportation-traction vehicles are loaded simultaneously by transported cargo and a traction effort (combined mode). An example of this is a vehicle with a cargo platform that has devices for attaching farm implements (Table 1.19, position 5). Military trucks operate in the transportation-traction mode when they are equipped with a self-recovery winch (Table 1.19, position 5).

The first step in investigating the energy effectiveness of a vehicle should consist in determining its mode of operation. The definition of the mode of operation should be approached with care, since certain vehicles may alternately function in several modes. For example, consider a single-bucket loader that scoops up material into the bucket while moving, raising the boom, and rotating the bucket. In the course of this process the loader overcomes the force of resistance of the material that acts on the edge of the bucket. One of the components of this resistance force, parallel to the surface of motion, is the drawbar pull that the loader develops. The mass of the material accumulated in the bucket (payload) increases simultaneously. At first sight it may appear that the loader operates in the combined mode. However, this is not so because transportation of the material in the bucket in the course of scooping up the material cannot be regarded as cargo. Conversely, the ever-increasing mass of material in the bucket increases the mass of the loader and the resistance to its motion. When scooping up the material the loader operates in the traction mode. After completing the scooping up of the material the loader transports the material in the bucket to the point of its unloading. In this case the loader operates in the transportation mode.

With reference to assessment of their energy and fuel effectiveness all three types of vehicles can be represented as power-consuming boxes to which the input power $P_{\mathrm{i}}^{\mathrm{in}}$ that is known as the indicator power of the engine. Consider now how this power is expended in the constant-speed motion of a vehicle over a horizontal surface, when the aerodynamic drag can be neglected. This power $P_{\mathrm{i}}^{\mathrm{in}}$ is expended in overcoming mechanical resistances (see Figure 1.66).

A part of this power P_{ax} is expended in mechanical losses in the engine itself and for driving auxiliary equipment and the steering controls (box a in Figure 1.66). Mechanical power losses P_{trm} (box b in Figure 1.66) take place in the transmission. Another part of the power is expended in mechanical losses P_{drl} in the driveline system (box c) and then for deforming the tires and the soil P_{ts} (box d). The remaining output power P^{out} is expended in (1) overcoming the traction resistance by traction vehicles; (2) transporting passengers and cargo by transportation vehicles; and (3) overcoming the traction resistance and transporting the cargo in the combined mode.

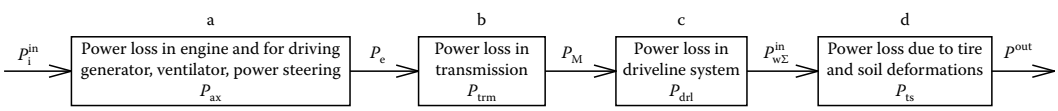


FIGURE 1.66
Power balance of a vehicle.

With reference to the nomenclature in Figure 1.66, the power balance of a vehicle becomes

$$P_{\mathrm{i}}^{\mathrm{in}} = P_{\mathrm{ax}} + P_{\mathrm{trm}} + P_{\mathrm{drl}} + P_{\mathrm{ts}} + P^{\mathrm{out}} \tag{1.52}$$

where

$$P_{\mathrm{ts}} = P_{\mathrm{f}\Sigma} + P_{\delta\Sigma} \tag{1.53}$$

Here $P_{\mathrm{f}\Sigma}$ is the power expended for overcoming the rolling resistance forces of all the wheels, whereas, $P_{\delta\Sigma}$ is the power lost in the slipping of the driving wheels.

It is entirely clear that the energy and fuel effectiveness of vehicles is determined to a large extent by the power ratio $P^{\mathrm{out}}/P_{\mathrm{i}}^{\mathrm{in}}$. The item of interest here is the effect of the driveline system on the energy/fuel effectiveness of vehicles. This effect is reflected by boxes c and d in Figure 1.66 and the components P_{drl} and P_{ts} in formulae (1.52) and (1.53). The physical substance of both these power-loss components shall be examined one after the other and methods of assessing them shall be worked out.

1.4.1 Mechanical Power Losses in Driveline Systems

The mechanical power losses P_{drl} in driveline systems can be subdivided into two groups:

1. Losses that do not depend on the distribution of power between the driving wheels, i.e., losses that are independent of the driveline system characteristics. These include losses in seals, hydraulic losses in mixing, spraying, and squeezing out of lubricating oil and also a part of power losses in bearings.
2. Losses that depend on the distribution of power between the driving wheels, i.e., losses that depend on the driveline system characteristics. The physical substance of losses making up this second group consists in the fact that the change in the load torques and angular velocities of PDU components changes the friction torques in gearing and modifies that part of losses in bearings that depend on the torque transmitted by the shaft. In this section, naturally, consideration is given to losses of the second group.

Consider a vehicle with n driving axles. The flows of power from the transfer case to the driving wheels shall be termed positive (Figure 1.67a). In certain cases there occur negative power flows from the wheels to the transfer case (Figure 1.67b). An example of negative torque on the front wheels of a 4×4 vehicle that causes power to flow from the front axle to the transfer case was presented in Section 1.3.1 (Figure 1.46). The reasons for such power circulation shall be analyzed in Chapter 3.

Let p_1 be the number of driving axles with positive power flow and p_2 the number of axles with negative power flow. It is obvious that

$$p_1 + p_2 = n \tag{1.54}$$

The power fed to the driving axles is designated as (see Figure 1.67)

$$P_{\mathrm{w}\Sigma}^{\mathrm{in}} = \sum_{i=1}^{n} P_{\mathrm{w}i}^{\mathrm{in}} \tag{1.55}$$

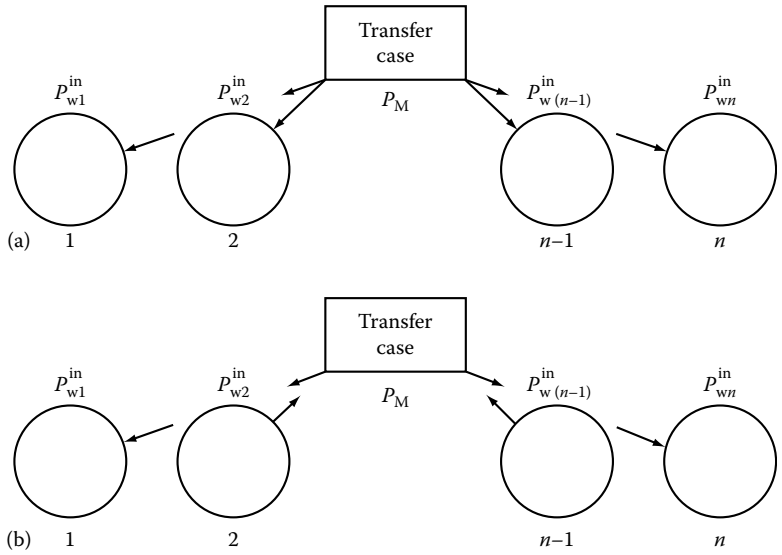


FIGURE 1.67
Vehicle with n driving axles.

If P_M is the power fed from the transmission to the driveline system (see Figures 1.66 and 1.67), then the mechanical power loss in the driveline system (see P_{drl} in Figure 1.66) can be assessed using the overall mechanical efficiency:

$$\eta_M = \frac{P_M - P_{drl}}{P_M} = \frac{P_{w\Sigma}^{in}}{P_M} = \frac{\sum_{i=1}^{n} P_{wi}^{in}}{P_M} \tag{1.56}$$

The components in the right-hand side of formula (1.56) shall be determined by writing the coefficient of distribution of power to the ith axle as

$$q_i = \frac{P_{wi}^{in}}{P_{w\Sigma}^{in}} = \frac{P_{wi}^{in}}{\sum_{i=1}^{n} P_{wi}^{in}} \tag{1.57}$$

where P_{wi}^{in} is the power supplied to the ith axle. It is obvious that

$$\sum_{i=1}^{n} q_i = \sum_{i=1}^{p_1+p_2} q_i = 1 \tag{1.58}$$

Power P_M in formula (1.56) is defined as

$$P_M = \sum_{i=1}^{p_1} P_{Mi}^{pos} + \sum_{i=1}^{p_2} P_{Mi}^{neg} \tag{1.59}$$

where P_{Mi}^{pos} and P_{Mi}^{neg} are the components of power P_M; power P_{Mi}^{pos} is fed from the transfer case to the ith axle, whereas power P_{Mi}^{neg} is fed from the ith axle to the transfer case. These components are defined using formulae (1.54), (1.55), and (1.57):

$$P_{Mi}^{pos} = \frac{P_{wi}^{in}}{\eta_{Mi}^{pos}} = \frac{q_i \sum_{i=1}^{n} P_{wi}^{in}}{\eta_{Mi}^{pos}} \tag{1.60}$$

$$P_{Mi}^{neg} = P_{wi}^{in}\eta_{Mi}^{neg} = \left(q_i \sum_{i=1}^{n} P_{wi}^{in}\right)\eta_{Mi}^{neg}$$

where η_{Mi}^{pos} and η_{Mi}^{neg} are the efficiencies of the branches of the driveline system with positive and negative power flows.

Using formulae (1.59) and (1.60) the expression for the total efficiency η_M from formula (1.56) finally becomes

$$\eta_M = \frac{1}{\sum_{i=1}^{p_1} \frac{q_i}{\eta_{Mi}^{pos}} + \sum_{i=1}^{p_2} q_i \eta_{Mi}^{neg}} \tag{1.61}$$

It is seen from formula (1.61) that the mechanical efficiency of the driveline system decreases with increasing number of negative power flows (the second component in the denominator).

If all the power flows are positive, then formula (1.61) becomes

$$\eta_M = \frac{1}{\sum_{i=1}^{n} \frac{q_i}{\eta_{Mi}}} \tag{1.62}$$

Formula (1.62) yields an important result. The distribution of power between driving axles and, accordingly, the driveline system, affect the overall efficiency η_M only when the mechanical efficiencies η_{Mi}, ($i = 1$ to n) of the driveline system branches are different. If, however, the mechanical efficiencies η_{Mi} of all the n branches of the driveline system are identical, then in accordance with formula (1.58), formula (1.62) becomes

$$\eta_M = \frac{\eta_{Mi}}{\sum_{i=1}^{n} q_i} = \eta_{Mi} \tag{1.63}$$

i.e., the total efficiency is equal to the efficiency of a single branch. In this case the distribution of power between the driving axles has no effect on η_M, since $\sum_{i=1}^{n} q_i$ is always equal to 1.

The above makes it necessary to determine η_{Mi}, ($i = 1$ to n) in formulae (1.61) and (1.62). Numerous investigations show that the value of η_{Mi}, over the range of potential velocities and force loads are not constant, but depend on the transmitted power. These results conform to the subdivision of mechanical power losses into two groups presented at the start of this section. For this reason the parameters q_i, η_{Mi}^{pos}, and η_{Mi}^{neg} in formula (1.61) are interdependent (which also applies to q_i and η_{Mi} in formula (1.62)). This complicates the application of formulae (1.61) and (1.62) in practice. A large number of investigators assume in practical calculations that η_{Mi} are constant, i.e., are independent of the power being transmitted. This assumption of constancy of η_{Mi} is utilized in the numerical example

presented further on of using formulae (1.61) through (1.63) for assessing the value of η_M of a vehicle with two driving axles ($n = 2$). When the flows of power to the driving wheels are positive and efficiencies η_{M1} and η_{M2} in the drives of the front and rear axles are equal to one another,

$$\eta_{M1} = \eta_{M2} = 0.91 \tag{1.64}$$

the driveline system has no effect on the mechanical power losses. In this case $\sum_{i=1}^{2} q_i = 1$ in formula (1.63) for any combinations of q_1 and q_2, i.e., 0.5 and 0.5, 0.3 and 0.7, 0.2 and 0.8, etc. According to formula (1.63)

$$\eta_M = \eta_{M1} = \eta_{M2} = 0.91 \tag{1.65}$$

The dash straight-line segment 1 in Figure 1.68 reflects the equalities expressed by formula (1.65).

Consider now the case when the power flows to the driving wheels are positive, but $\eta_{M1} \neq \eta_{M2}$. For example,

$$\eta_{M1} = 0.91; \quad \eta_{M2} = 0.86$$

In this case the total efficiency η_M should be determined from formula (1.62) upon proper selection of coefficients q_i ($i = 1, 2$) of the distribution of power between the driving axles. Solid line 2 in Figure 1.69 shows the total mechanical efficiency of a vehicle's driveline system over a range of q_1 and q_2 from 0 to 1 and from 1 to 0, respectively. Here the sum $(q_1 + q_2)$ is always equal to unity. The extreme points on line 2 correspond to a FWD (FWD, $q_1 = 1$, $q_2 = 0$, $\eta_M = 0.91$) and to a rear-wheel drive (RWD, $q_1 = 0$, $q_2 = 1$, $\eta_M = 0.86$). It is seen that a change in the manner of distribution of power between the driving axles affects the value of η_M. Increasing the contribution of the front axle, which has the higher efficiency η_{M1} in the traction balance of the vehicle (i.e., an increase in q_1) increases the value of η_M.

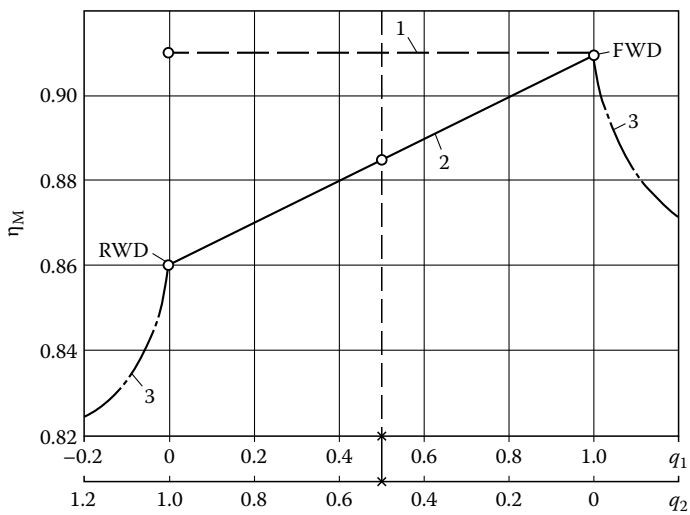


FIGURE 1.68
4×4 Vehicle: mechanical efficiency of a driveline.

Still another result follows from comparing lines 1 and 2 in Figure 1.68. An effort should be made in designing vehicles with two driving axles to make η_{M1} and η_{M2} equal to one another. In this case η_M is independent of the distribution of power among the axles, i.e., of the values of q_1 and q_2. This provides the designer with more freedom in designing the interaxle PDU.

The dash-dotted curves 3 in Figure 1.68 correspond to modes when one of the power flows is negative. As is seen from this figure, the appearance of negative power flows highly reduces the total mechanical efficiency of the driveline system. Further details pertaining to analysis of positive and negative power flows are given in Sections 3.3.1 and 3.4.2.

1.4.2 Mechanical Power Losses in Wheel Systems

Section 1.3.3 was concerned with methods of assessing the energy effectiveness of a single wheel in the traction, transportation and combined (transportation-tractive) modes. These methods are being extended to vehicles with any specified relationship between the total number m of axles and n of drive axles, i.e., to machines with wheel formula $2m \times 2n$, $m \leq n$.

All of a vehicle's wheels, connected by means of the driveline system, together with the vehicle frame and suspension comprise the vehicle's running-gear system. The wheels that are a part of the vehicle's running-gear system comprise its wheel system. The purpose of this section is to develop a method for assessing power loss in the vehicle's running gear system by showing the effect of power loss in the wheel system on the running gear efficiency and then on the vehicle efficiency.

It is assumed that the vehicle moves at constant velocity V_x over a horizontal solid or deformable surface. The conditions of gripping between the vehicle's wheels and the supporting surface may be either identical or different. For example, general-purpose plowing tractors have, in the course of plowing, stable but different gripping conditions of the left- and right-side wheels: the left wheels move over the stubble, whereas the right wheels move in the furrow formed by the plowing. When a car moves over a road under winter conditions, the gripping conditions may change due to the appearance of frozen road sections. Off-road vehicles of all kinds (combat and tactical military vehicles, rovers used on other plants, etc.) have unstable coupling conditions of the wheels with the ground due to the constantly changing terrain conditions. The methods present below may be used for vehicles of all kinds moving under any road/off-road conditions.

1.4.2.1 Tractive Operating Mode

In this mode (see Table 1.19, number 1) the main index of the energy effectiveness of vehicles that is extensively used in the theory of wheeled towing vehicles is the tractive efficiency η_t. A mathematical expression for η_t can be compiled on the basis of Figure 1.66:

$$\eta_t = \frac{P_d}{P_e} = \eta_{trm}\eta_M\eta_f\eta_\delta \tag{1.66}$$

In this expression P_e is the effective power of the engine, $P_d = P^{out} = F_d V_x$ is the drawbar pull power, which is the power expended for overcoming the useful draw pull load F_d

(induced, for example, by an agricultural implement). The components η_{trm} and η_M are the efficiencies representing the power losses in the transmission and in the driveline system. The coefficient η_f, known as the rolling resistance efficiency, reflects the loss of power in normal deformation of the tire (of the tire and the soil on deformable surfaces). The component η_δ in Equation 1.66 is known as the slip efficiency and reflects the power loss in the slipping of driving wheels.

In investigating the wheel system of tractive vehicles one analyzes the efficiency of the vehicle running gear system that, with reference to Figure 1.66, is defined as

$$\eta_x^t = \frac{P^{out}}{P_{w\Sigma}^{in}} = \frac{P_d}{P_{w\Sigma}} = \eta_f \eta_\delta \tag{1.67}$$

Here $P_{w\Sigma}^{in}$ is the power supplied to the driving wheels.

The cofactors in Equations 1.66 and 1.67 for 4×2 tractive vehicles with a single driving axle can be determined rather easily. The values of the efficiencies η_{trm} and η_M of the transmission and the driving system can be determined, among others, in terms of the efficiencies of geared couplings, universal-joint drives and bearings. In the classical theory of vehicle dynamics, the efficiencies η_f and η_δ of 4×2 vehicles are usually determined for an equivalent (bicycle) vehicle scheme, in which two of the axle's wheels are replaced by one equivalent wheel:

$$\eta_f = \frac{F_d}{F_x}, \quad \eta_\delta = 1 - s_\delta \tag{1.68}$$

where F_x and s_δ are the circumferential force and the slip coefficient (slip ratio) of the equivalent driving wheel (driving axle of the vehicle). The value of s_δ for a vehicle moving over high-grade roads with solid pavement may be 6%–8% due to tangential deformation of the tires or 20%–25% when moving over field conditions and unpaved roads due to tangential deformation of the tire and the soil and also due to the relative longitudinal movement of the tire and the soil.

The calculation of η_t and η_x^t for a vehicle with two or more driving axles, when it is necessary to perform separate calculations for the left and right wheels, is much more complicated. This is due in the first place to the fact that the loss of power in the wheel system of such vehicles depends not only on the overall traction load, but also on the manner in which it is distributed among the driving axles and the two driving wheels of each axle. The latter, in its turn, is determined to a large extent by the vehicle's driveline systems. This is hereby demonstrated.

The efficiency that reflects the power lost in slipping is written as

$$\eta_\delta = \frac{P_{w\Sigma}^{in} - P_{\delta\Sigma}}{P_{w\Sigma}^{in}} = 1 - \frac{\sum_{i=1}^{n} \left(P'_{\delta i} + P''_{\delta i}\right)}{\sum_{i=1}^{n} \left(P_{wi}^{in'} + P_{wi}^{in''}\right)}, \tag{1.69}$$

where the single and double primes pertain to wheels of the same axle; $P_{wi}^{in'('')} = F_{xi}^{'('')} V_{ti}^{'('')}$ is the power supplied to one of the wheels of the ith axle; $V_{ti}^{'('')}$ is the theoretical velocity of one

of the axle's wheels, without slipping, whereas $P_{\delta}^{'(")} = F_{xi}^{'(")} V_{ti}^{'(")} s_{\delta i}^{'(")}$ is the slipping power of one of the wheels of the ith axle.

Expressing the theoretical velocity of the wheel in terms of its slip ratio and of the actual velocity V_x of the vehicle,

$$V_{ti}^{'(")} = \frac{V_x}{1 - s_{\delta i}^{'(")}}$$

one can transform Equation 1.69 to

$$\eta_{\delta} = 1 - \frac{\sum_{i=1}^{n} \left(\frac{F_{xi}^{'} s_{\delta i}^{'}}{1 - s_{\delta i}^{'}} + \frac{F_{xi}^{"} s_{\delta i}^{"}}{1 - s_{\delta i}^{"}} \right)}{\sum_{i=1}^{n} \left(\frac{F_{xi}^{'}}{1 - s_{\delta i}^{'}} + \frac{F_{xi}^{"}}{1 - s_{\delta i}^{"}} \right)} \tag{1.70}$$

Equation 1.70 can be used for determining the vehicle's slipping efficiency, when the circumferential forces and the wheel slips are not the same for the wheels. For an equivalent scheme of a vehicle, in which both wheels of each axle are replaced by a single equivalent wheel, Equation 1.70 simplifies somewhat to

$$\eta_{\delta} = 1 - \frac{\sum_{i=1}^{n} \frac{F_{xi} s_{\delta i}}{1 - s_{\delta i}}}{\sum_{i=1}^{n} \frac{F_{xi}}{1 - s_{\delta i}}} \tag{1.71}$$

To make the computations less cumbersome and to gain insight into the physical substance of the effect of the driveline system on the power lost in a wheel system, one can write Equation 1.70 as

$$\begin{aligned} \eta_{\delta} &= \frac{\sum_{i=1}^{n} \left(F_{xi}^{'} + F_{xi}^{"} \right)}{\sum_{i=1}^{n} \left(F_{xi}^{'} + F_{xi}^{"} \right) + \sum_{i=1}^{n} \left(\frac{F_{xi}^{'} s_{\delta i}^{'}}{1 - s_{\delta i}^{'}} + \frac{F_{xi}^{"} s_{\delta i}^{"}}{1 - s_{\delta i}^{"}} \right)} \\ &= \frac{F_{x\Sigma}}{F_{x\Sigma} + \sum_{i=1}^{n} \left(\frac{F_{xi}^{'} s_{\delta i}^{'}}{1 - s_{\delta i}^{'}} + \frac{F_{xi}^{"} s_{\delta i}^{"}}{1 - s_{\delta i}^{"}} \right)} \end{aligned} \tag{1.72}$$

and for the equivalent vehicle scheme

$$\begin{aligned} \eta_{\delta} &= \frac{\sum_{i=1}^{n} F_{xi}}{\sum_{i=1}^{n} F_{xi} + \sum_{i=1}^{n} \frac{F_{xi} s_{\delta i}}{1 - s_{\delta i}}} \\ &= \frac{F_{x\Sigma}}{F_{x\Sigma} + \sum_{i=1}^{n} \frac{F_{xi} s_{\delta i}}{1 - s_{\delta i}}} \end{aligned} \tag{1.73}$$

The numerator and the first terms in the denominator in Equations 1.72 and 1.73 is known as the total circumferential force of the vehicle $F_{x\Sigma}$. This force that is developed by all the driving wheels and is hence equal to the sum of circumferential forces of the driving

wheels, should be equal to the sum of the applied resistances to the vehicle's motion (since otherwise the vehicle could not move):

$$F_{x\Sigma} = \sum_{i=1}^{n} \left(F'_{xi} + F''_{xi} \right) = \sum_{i=1}^{m} \left(R'_{xi} + R''_{xi} \right) + \sum_{j=1}^{s} F_j \tag{1.74}$$

The first term in the right-hand side of Equation 1.74 is the arithmetic sum of the rolling resistance forces of all of the vehicle's wheels; $\sum_{j=1}^{s} F_j$ is the algebraic sum of the forces acting on the vehicle. This sum may, among others, include the drawbar pull F_{d} produced by the farming implement, and also the air drag D_{a}. If the scope of the problem at hand is widened to include consideration of the power expended for ascending (descending) at angle θ_n, and also accelerated (decelerated) motion, then the sum $\sum_{j=1}^{s} F_j$ will contain the longitudinal component $\pm W_{\mathrm{a}} \sin \theta_n$ of the vehicle's weight and the D'Alambert force F_{a}. This means that the total circumferential force $F_{x\Sigma}$ of the vehicle that all the driving wheels together have to develop is a known quantity for the given set of conditions of motion. This result is important for understanding the mechanism by means of which the driveline system affects the slip efficiency in Equations 1.72 and 1.73, meaning also the energy effectiveness of the vehicle and its fuel economy. The form of Equations 1.72 and 1.73 shows that the energy effectiveness of a vehicle depends both on the total tractive load of the vehicle and on its distribution among the driving wheels. In fact, the total tractive load is determined by the total resistance to motion that is equal to the total circumferential force of the vehicle $F_{x\Sigma}$. The effect of the distribution of $F_{x\Sigma}$ among the driving wheels on the slip efficiency η_δ is reflected by the second term in the denominators of Equations 1.72 and 1.73. It is seen that the numerical value of η_δ depends on the fraction in the total force $F_{x\Sigma}$ devolving upon each driving wheel that develops the force $F'^{(\prime)}_{xi}$ and each its value of slip ratio $s'^{(\prime)}_{\delta i}$. Recall that the wheel's force F_x and the slip coefficient s_δ are functionally related to one another (see Section 1.3.2).

The numerical values of $F'^{(\prime)}_{xi}$ $(i = 1, n)$, the circumferential forces of the driving wheels, depend to a large extent on the parameters of PDUs that can be installed within the driveline system. For this reason the same vehicle will have different values of η_δ (i.e., will have different fuel consumptions), depending on the driveline system that it will use. For the same reason different vehicles of the same class with the same driveline system will not necessarily have the same values of η_δ. The values of this coefficient of these vehicles may be different because of differing values of $F_{x\Sigma}$ and its distribution among the wheels, which also depends on the mass and geometry of the vehicles, the parameters of the tires and soil, of the suspension, etc.

This naturally gives rise to the question as how to determine/calculate the circumferential forces F_{xi}, $i = 1, n$ of the driving wheels with allowance for the specifics of the driveline systems. Chapters 2 through 5 present methods of calculating F_{xi}, $i = 1, n$ for various driveline systems with different PDUs.

A technical approach may be drawn from analysis of Equations 1.69, 1.72, and 1.73. It is quite obvious that it is possible to determine a certain optimal distribution of power $P^{\mathrm{in}}_{\mathrm{w}\Sigma}$ between the driving wheels at which is attained the best energy effectiveness of the vehicle, i.e., the maximum value of η_δ. If one were to design a ''flexible'' controlled driveline system that would ensure an optimal or close to optimal distribution of power among the wheels, this would ensure the best fuel economy of the vehicle. These problems are discussed in Chapters 6 and 7.

Now return to Equation 1.67 and determine the rolling resistance efficiency η_f. Since a part of the power supplied to the wheel is spent in slip, the expression for efficiency η_f becomes

$$\eta_f = \frac{F_d}{\sum_{i=1}^{n}\left(F'_{xi} + F''_{xi}\right)} \tag{1.75}$$

When applied to an equivalent scheme of the vehicle, Equation 1.75 becomes

$$\eta_f = \frac{F_d}{\sum_{i=1}^{n} F_{xi}} \tag{1.76}$$

Using Equations 1.72, 1.73, 1.75, and 1.76 for calculating η_δ and η_f, one can obtain from Equation 1.67 the tractive efficiency η_x^t of the vehicle's running gear system. To determine η_t from Equation 1.66 one must have data on η_{trm} and η_M. To calculate the transmission power loss and determine η_{trm} one must use recommendations provided by a number of investigators. The total mechanical efficiency η_M of the driveline system can be calculated from equations from Section 1.4.1 and the recommendations of various investigators on determining the partial efficiencies η_{Mi} of the different driveline system components. As noted in Section 1.4.1, the values of η_{Mi} are determined by making allowance for losses in gear couplings, bearings, universal joints, etc.

The material presented above on the effect of driveline systems on the energy effectiveness of tractive vehicles shall now be extended to vehicles operating in the transportation and combined modes.

1.4.2.2 Transportation Operating Mode

This is a mode of operation of vehicles listed under numbers 2 to 4 in Table 1.19. These vehicles perform only transportation operations and it is impossible to assess their energy effectiveness on the basis of the tractive efficiency from Equation 1.66, since the drawbar pull F_d and with it the drawbar power P_d, are equal to zero. Whereas this statement is obvious in the case of passenger cars and trucks (vehicles 2 from Table 1.19), additional clarification is needed for vehicles numbered 3 and 4. Vehicle 3, consisting of a truck tractor and one or several trailers, and vehicles 4 with semitrailers and trailers should be treated as transport rather than tractive vehicles. These vehicles transport cargo in trailers and semitrailers, but are not involved in overcoming the drawbar pull generated by the trailers, semitrailers, and the transported cargo. This is actually so, since the towing of empty trailers and semitrailers cannot be regarded as useful work and it cannot be evaluated using the towing efficiency η_t from Equation 1.66. This problem can be solved by considering the transportation efficiency η_x^{tr} of the vehicle's running gear system by analogy with the transport efficiency η_w^{tr} of a single wheel from Section 1.3.3.

To obtain an energy effectiveness assessment of a vehicular wheel system when transporting cargo in the truck body (see number 2 in Table 1.19), the approach by V. N. Shalyagin is employed to multiwheel drive vehicles and the transportation efficiency of the running gear system is submitted as

$$\eta_x^{tr} = \frac{\sum_{i=1}^{m}\left(P'_{fgi} + P''_{fgi}\right)}{\sum_{i=1}^{n}\left(P_{wi}^{in'} + P_{wi}^{in''}\right)} \tag{1.77}$$

where the numerator represents that part of the power of resistance to the rolling of the wheels $P_{gf\Sigma}$ that is caused by the cargo being transported, i.e.,

$$P_{fg\Sigma} = \sum_{i=1}^{m} \left(P'_{fgi} + P''_{fgi} \right) = V_x \sum_{i=1}^{m} \left(R'_{xgi} + R''_{xgi} \right) \tag{1.78}$$

where R'_{xgi} and R''_{xgi} are the forces of rolling resistance of the wheels of the ith axle that stem from the weight of the cargo being transported W_g.

These forces are calculated from the expression

$$R'^{(\prime\prime)}_{xgi} = R'^{(\prime\prime)}_{xi} - R'^{(\prime\prime)}_{xci} \tag{1.79}$$

where $R'^{(\prime\prime)}_{xi}$ is the force of resistance to rolling that stems from that part of the curb weight W_c of the vehicle that is transmitted to wheel and also from a part of the weight of the useful cargo W_g; $R'^{(\prime\prime)}_{xci}$ is the force of resistance to rolling of the wheel that stems in part from curb weight W_c of the vehicle. Then Equation 1.77 will take the final form

$$\eta_x^{tr} = \frac{\sum_{i=1}^{m} \left(R'_{xgi} + R''_{xgi} \right)}{\sum_{i=1}^{n} \left(\frac{F'_{xi}}{1 - s'_{\delta i}} + \frac{F''_{xi}}{1 - s''_{\delta i}} \right)} \tag{1.80}$$

Analyzing the equivalent scheme of the vehicle, Equation 1.80 simplifies and becomes

$$\eta_x^{tr} = \frac{\sum_{i=1}^{m} R_{xgi}}{\sum_{i=1}^{n} \frac{F_{xi}}{1 - s_{\delta i}}} \tag{1.81}$$

As an illustration of the application of Equations 1.80 and 1.81, the values of η_x^{tr} were computed for a 4×4 vehicle with parameters close to that of Unimog U120/425. The calculations were performed for a change in the total weight W_a of the vehicle caused by the useful cargo W_g. It follows from Figure 1.69 that the value of η_x^{tr} increases proportionally to the transported mass. The zero value of η_x^{tr} corresponds to the curb weight of

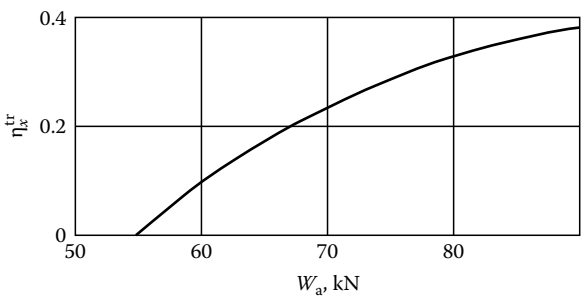


FIGURE 1.69
Transportation running gear efficiency of 4×4 vehicle on stubble vs. gross vehicle weight.

the vehicle W_c. Note that in this and other examples analyzed further down in this section, no reference is made to the calculation of the circumferential forces $F_{xi}^{\prime(\prime\prime)}$ or to the wheel slip forces $s_{\delta i}^{\prime(\prime\prime)}$. As previously mentioned, these problems shall be discussed in the subsequent chapters.

The transportation efficiency of the running gear system for the vehicle numbered 3 in Table 1.19 can be determined from an expression similar to Equation 1.80. Except that the rolling resistance forces, $R_{xgi}^{\mathrm{trl}^{\prime}}$ and $R_{xgi}^{\mathrm{trl}^{\prime\prime}}$, contained in the numerator should be referred to the trailers:

$$\eta_x^{\mathrm{tr}} = \frac{\sum_{j=1}^{c}\left[\sum_{i=1}^{l}\left(R_{xgi}^{\mathrm{trl}^{\prime}} + R_{xgi}^{\mathrm{trl}^{\prime\prime}}\right)\right]_j}{\sum_{i=1}^{n}\left(\frac{F_{xi}^{\prime}}{1-s_{\delta i}^{\prime}} + \frac{F_{xi}^{\prime\prime}}{1-s_{\delta i}^{\prime\prime}}\right)} \tag{1.82}$$

where l is the number of axles of the jth trailer and c is the number of trailers. Respectively, for the equivalent system,

$$\eta_x^{\mathrm{tr}} = \frac{\sum_{j=1}^{c}\left(\sum_{i=1}^{l} R_{xgi}^{\mathrm{trl}}\right)}{\sum_{i=1}^{n}\frac{F_{xi}}{1-s_{\delta i}}} \tag{1.83}$$

Equation 1.82 was employed for calculating the efficiency of the running gear system of the MTZ-102 farm tractor coupled with the 2PTS-4 two-axle trailer upon a change in the weight W_g of the cargo. An increase in W_g causes an increase in the total weight of the trailer and, accordingly in the rolling resistance forces R_{x1}^{trl} and R_{x2}^{trl}. These forces form the drawbar load of the tractor:

$$F_d = R_{x1}^{\mathrm{trl}} + R_{x2}^{\mathrm{trl}} \tag{1.84}$$

For this reason η_x^{tr} was calculated as a function of the drawbar pull F_d that reflects implicitly the variation in W_g. Curve 1 in Figure 1.70 is a plot of $\eta_x^{\mathrm{tr}} = f(F_d)$.

However, if this tractor is evaluated as solely a tractive vehicle, then for the same values of drawbar pull F_d it is possible to calculate the value of η_x^{t} of the tractor's running gear system from Equations 1.67, 1.72, and 1.75. The relationship $\eta_x^{t} = f(F_d)$ is plotted in Figure 1.70 (see curve 2). The solid lines of both curves in this figure correspond to real values of the load F_d that stem from increasing the mass of the cargo transported in the trailer.

As opposed to the tractive efficiency, the transportation efficiency η_x^{tr} reflects the actual energy efficiency of the running gear of a tractor in the transportation mode. Thus, when towing an empty trailer ($F_d \approx 2$ kN) $\eta_x^{\mathrm{tr}} = 0$, whereas $\eta_x^{t} = 0.4$. This occurs because in computing η_x^{t} the concept of useful resistance is applied to the total drawbar pull that stems from the mass of the trailer itself and of the cargo being transported. Actually, not the entire drawbar pull is useful, since the hauling of the empty trailer cannot be treated as useful work for which reason $\eta_x^{\mathrm{tr}} = 0$. For this reason the transportation running-gear efficiency η_x^{tr} should be used for evaluating a farm tractor when transporting a cargo.

If, in addition to the load-carrying trailers and semitrailers, the vehicle has a useful load in the form of passengers and/or cargo (see number 4 in Table 1.19) then the transport efficiency of its running gear system can be computed from the expression

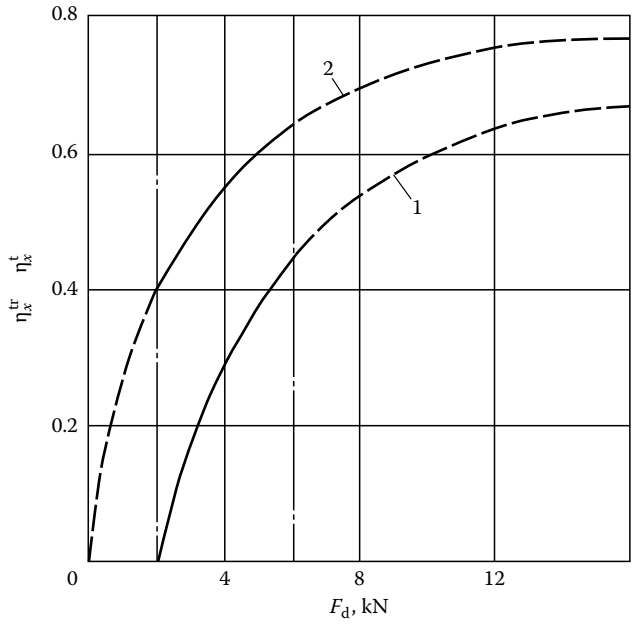


FIGURE 1.70
Running gear efficiencies of MT2-102 farm tractor with 2PTS-4 trailer vs. drawbar pull F_d: 1, transportation efficiency η_x^{tr}; 2, tractive efficiency η_x^t.

$$\eta_x^{tr} = \frac{\sum_{i=1}^{m}\left(R'_{xgi} + R''_{xgi}\right) + \sum_{j=1}^{c}\left[\sum_{i=1}^{l}\left(R_{xgi}^{trl'} + R_{xgi}^{trl''}\right)\right]_j}{\sum_{i=1}^{n}\left(\frac{F'_{xi}}{1-s'_{\delta i}} + \frac{F''_{xi}}{1-s''_{\delta i}}\right)} \tag{1.85}$$

For the equivalent scheme of the vehicle, Equation 1.85 becomes

$$\eta_x^{tr} = \frac{\sum_{i=1}^{m} R_{xgi} + \sum_{j=1}^{c}\left[\sum_{i=1}^{l} R_{xgi}^{trl}\right]_j}{\sum_{i=1}^{n}\left(\frac{F_{xi}}{1-s_{\delta i}}\right)} \tag{1.86}$$

As an illustration of the application of Equation 1.85 there was computed the transport efficiency of the running gear system of a 4×4 vehicle with parameters close to those of the Unimog U120/425 that moves over stubble while towing a trailer. The computations were made on the assumption that the masses of cargo added simultaneously to the bodies of the vehicle and the trailer are the same. This, naturally, increases the drawbar pull F_d and the total weight W_a of the tractor and trailer rig, as a function of which the curves in Figure 1.71 were plotted. The tractive efficiency η_x^t of the running gear system was computed from Equations 1.67, 1.72, and 1.75.

When an empty trailer is towed by an empty vehicle ($F_d = 1.8$ kN) no useful work is being performed ($\eta_x^{tr} = 0$), whereas $\eta_x^t = 0.24$.

It additionally follows from Figure 1.71 that an increase in the mass of cargo being transported is virtually not reflected in the number value of η_x^t which then barely increases. At the same time, η_x^{tr} shows how the effectiveness of the vehicle rises with the increasing mass of the cargo.

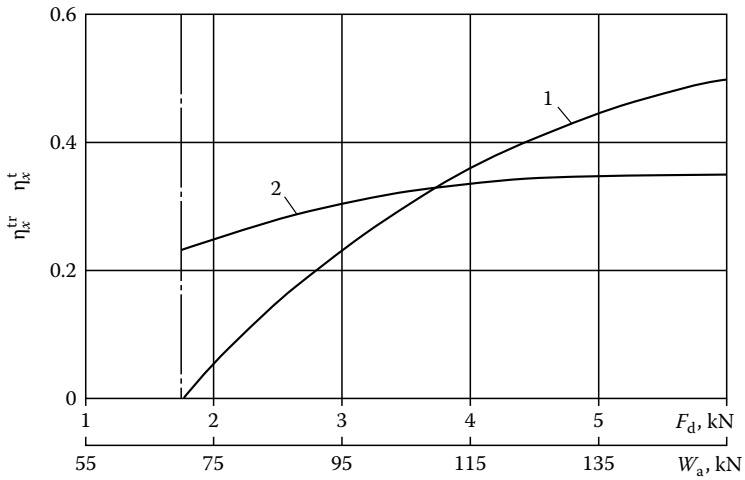


FIGURE 1.71
Running gear efficiencies of a 4×4 truck with a trailer vs. drawbar pull F_d and weight W_a: 1, transportation efficiency η_x^{tr}; 2, tractive η_x^t efficiency.

In addition, comparison of curve 1 in Figure 1.71 with Figure 1.69 shows that it is highly expedient to use tractor and trailer rigs instead of single-unit trucks. Thus, the maximum value of η_x^{tr} that corresponds to full loading of the truck and the trailer is 0.49 (Figure 1.69), whereas for a single-unit truck it is 0.38 (see Figure 1.69).

The above shows that the use of the efficiency η_x^{tr} makes it possible to compare the effectiveness of single-unit trucks and tractor and trailer rigs when hauling cargo. It is useful to reemphasize that the effect of driveline systems on η_x^{tr} of vehicles numbered 2 through 4 in Table 1.19 is reflected in the circumferential forces $F_{xi}^{'(''')}$ and the slip coefficients $s_{\delta i}^{'(''')}$ in the denominators of Equations 1.80, 1.82, and 1.85.

1.4.2.3 Combined Operating Mode

This is the operating mode of vehicles numbered 5 in Table 1.19. To assess the energy effectiveness of the running gear systems of such vehicles as a function of the distribution of power between the wheels, it is proposed to use the total efficiency of the running gear system

$$\eta_{x\Sigma} = \frac{P_d + \sum_{i=1}^{m}\left(P'_{fgi} + P''_{fgi}\right)}{\sum_{i=1}^{n}\left(P_{wi}^{in\,'} + P_{wi}^{in\,''}\right)} = \frac{F_d + \sum_{i=1}^{m}\left(R'_{xgi} + R''_{xgi}\right)}{\sum_{i=1}^{n}\left(\frac{F'_{xi}}{1-s'_{\delta i}} + \frac{F''_{xi}}{1-s''_{\delta i}}\right)} \tag{1.87}$$

and for the equivalent scheme of the vehicle:

$$\eta_{x\Sigma} = \frac{F_d + \sum_{i=1}^{m} R_{xgi}}{\sum_{i=1}^{n} \frac{F_{xi}}{1-s_{\delta i}}} \tag{1.88}$$

The expressions presented above for the efficiencies η_x^{tr}, η_x^{t}, and $\eta_{x\Sigma}$ correspond to uniform motion of vehicles over a horizontal surface. These expressions must be refined when it is required to determine the energy efficiency of vehicles moving over macroirregularities at angle θ_n of ascent and descent (road grades) and with longitudinal acceleration a_x. For example, for transport vehicles with useful cargo W_g (see Equation 1.80) such refinements must be introduced by referring to the useful resistance of the component $W_g \sin \theta_n$ that is parallel to the support surface and the part of the force of inertia of translational motion that stems from the mass of the cargo W_g/g:

$$\eta_x^{tr} = \frac{\sum_{i=1}^{m} \left(R'_{xgi} + R''_{xgi} \right) \pm W_g \sin \theta_n + \frac{W_g}{g} a_x}{\sum_{i=1}^{n} \left(\frac{F'_{xi}}{1 - s'_{\delta i}} + \frac{F''_{xi}}{1 - s''_{\delta i}} \right)} \tag{1.89}$$

where the plus sign corresponds to ascending motion and the minus sign represents descending motion. Other expressions obtained in this section for other vehicles from Table 1.19 may be refined similarly.

The engineering literature contains also other criteria for assessing the energy effectiveness of the motion of multiaxle vehicles. For example, the driveline system quality factor suggested by P. V. Aksenov, B. N. Belousov, and A. F. Starikov in our notation then will be

$$K_q = 1 - \frac{\sqrt{\sum_{i=1}^{n} \left(P_{\text{wopt}i}^{\text{in}'('')} - P_{\text{w}i}^{\text{in}'('')} \right)^2}}{\left(P_{\text{w}\Sigma}^{\text{in}} \right)_{\text{opt}}} \tag{1.90}$$

where $\left(P_{\text{w}\Sigma}^{\text{in}}\right)_{\text{opt}}$ is the total optimal power that should be supplied to all the wheels to ensure minimum loss in all the wheels in rolling resistance and slip; $P_{\text{wopt}i}^{\text{in}'('')}$ is the optimal power that should be supplied to one of wheels to ensure minimum loss in that wheel in rolling resistance and slip; and $P_{\text{w}i}^{\text{in}'('')}$ is the power supplied to a wheel by the actual vehicle driveline system. The quality factor for a vehicle with an ideal driveline system is $K_q = 1$, whereas for a vehicle with an actual driveline system it is $K_q < 1$.

Still another criterion for assessing the effectiveness of distributing the power between the vehicle's wheels consists of the coefficient proposed by Yu. V. Pirkovskij and S. B. Shukhman:

$$K_{\text{opt}} = \frac{P_{\text{w}\Sigma}^{\text{in}} - \left(P_{\text{w}\Sigma}^{\text{in}}\right)_{\text{opt}}}{P_{\text{w}\Sigma}^{\text{in}}} \tag{1.91}$$

where

$\left(P_{\text{w}\Sigma}^{\text{in}}\right)_{\text{opt}}$ is the same as in Equation 1.90

$P_{\text{w}\Sigma}^{\text{in}} = \sum_{i=1}^{n} P_{\text{w}i}^{\text{in}'('')}$ is the total power supplied to all of the vehicle's wheels by an actual driveline system

The expressions obtained in Section 1.4.2 have thus been shown to provide an assessment of the energy efficiency of the vehicle's running gear systems and then also in

multiaxle drive vehicles as a whole in performing transportation or towing work or both of them together. These equations describe the pertinent efficiencies in general form. To be able to use them for calculating the efficiencies of specific vehicles, one must have available numerical values of the circumferential forces of the wheels and their slip ratios, i.e., must know the manner in which these forces are distributed among the wheels. The latter, as noted, is determined largely by the vehicle's driveline system. For this reason, equations for calculating the towing, transportation and total efficiency must be obtained for each specific driveline system. These relationships are listed in Chapters 2 to 5. Section 1.4.3 is concerned with the effect of driveline systems on the fuel economy of vehicles.

1.4.3 Fuel Efficiency of Multiwheel Drive Vehicles

There is no consensus among experts concerning the effect of driveline system parameters on the vehicle's fuel consumption. Many are of the opinion that, for example, the use of two drive axles instead of one unalterably increases the vehicle's fuel consumption, irrespective of the parameters of PDUs and of driving conditions. Their main argument usually consists of the higher power consumption for providing motion to the drive components of the additional driving axle. Others claim, for example, that a permanently engaged drive with an open interaxle differential improves the fuel economy of a sedan as compared with a single-axle drive by up to 2 mpg on highways.

Still another interesting example of the effect of the driveline system on the fuel economy of SUVs is shown in Table 1.20 compiled on the basis of publications in engineering journals. Of four SUVs of similar class, three vehicles have a rear-axle drive, whereas one has a two-axle (four-wheel) driveline system by means of a Torsen interaxle differential.

It is rather obvious that comparison of these vehicles, that are equipped with different engines and have different mass and geometric parameters, is not quite proper. However, this example shows, as a minimum, that the use of two driving axles was not detrimental to the competitiveness of vehicle No. 1 as compared with other vehicles from Table 1.20.

The only correct data are those that were obtained for the same vehicle with different driveline systems. Such experimental data are listed in Table 1.21.

The MAZ-501 timber carrier conveying a load of timber and having a total mass of 25.5 ton was tested on a high-quality paved road. The fuel consumption over a measured 1 km stretch of road was measured for different vehicle speeds and recalculated to a 100 km trip. It is seen from Table 1.21 that the highest fuel economy is achieved when the vehicle uses

TABLE 1.20

SUVs with Different Fuel Efficiency

Parameter	Vehicle #1	Vehicle #2	Vehicle #3	Vehicle #4
Power, HP	275	286	283	279
Engine volume, cm^3	3998 V8	4398 V8	4293 V8	4266 V8
Curb mass, kg	1795	1820	1735	1680 (or 1880)
Front/rear curb weight distribution	60/40	52/48	54/46	54/46
Driveline system	4×4 with Torsen in transfer case	RWD	RWD	RWD
Total fuel consumption, L/100 km	13.1	13.6	14.0	13.6

TABLE 1.21

Timber Truck Fuel Consumption

	Fuel Consumption, L/100 km			
	Truck Speed, km/h			
Driveline System	**20**	**28**	**38**	**45**
4×4, Open interaxle differential	49	56	62	70
4×2, RWD	53	59	66	74
4×4, Interaxle differential fully locked	55	62	69	76

an open interaxle differential. When moving with one driving axle the fuel consumption increases by 5.5%–8% whereas locking of the interaxle differential increased the fuel consumption by 8.5%–12%. Additional journeys over a distance of 150 km also showed that the 4×4 driveline system with an open interaxle differential is the most fuel efficient. When using a single driving axle the fuel consumption increased by about 1.5%, whereas when the interaxle differential was locked it increased by 6.8%. Similar results were obtained for passenger and sports cars. Audi proved experimentally that its all-wheel drive Quattro has a better fuel efficiency than a FWD car with an identical power rating. This information can be found in Audi's recently published article written by M. Scarlett and listed in the bibliography list.

This section provides an analytical insight into the mechanism of the effect of the driveline system on the vehicle's fuel consumption. The material given below explains the reasons for increasing or decreasing the fuel consumption when using different driveline systems.

The fuel economy of a vehicle is represented by the fuel consumption referred to the distance traveled by the vehicle:

$$Q_{\mathrm{s}} = \frac{Q_{\mathrm{h}}}{V_x} = \frac{g_{\mathrm{e}} P_{\mathrm{e}}}{V_x}, \ \mathrm{g/km} \tag{1.92}$$

where

Q_{h} is fuel consumption, g/h

V_x is the vehicle velocity, km/h

g_{e} is the specific fuel consumption, g/(kW-h)

P_{e} is the effective power of the engine which can be represented using Figure 1.66 as follows:

$$P_{\mathrm{e}} = P_{\mathrm{trm}} + P_{\mathrm{drl}} + P_{\mathrm{ts}} + P^{\mathrm{out}} \tag{1.93}$$

Making use of formula (1.53), the power balance (1.93) takes the form

$$P_{\mathrm{e}} = P_{\mathrm{trm}} + P_{\mathrm{drl}} + P_{\delta\Sigma} + P_{\mathrm{f}\Sigma} + P^{\mathrm{out}} \tag{1.94}$$

With reference to Figure 1.66 and the material presented in Sections 1.4.1 and 1.4.2, expressions for the loss P_{drl} of mechanical power in the driveline system and the slip power $P_{\delta\Sigma}$ can compiled as follows:

$$P_{\mathrm{drl}} = P^{\mathrm{in}}_{\mathrm{w}\Sigma}(1 - \eta_{\mathrm{M}})/\eta_{\mathrm{M}} \tag{1.95}$$

$$P_{\delta\Sigma} = P_{w\Sigma}^{in}(1 - \eta_\delta) \tag{1.96}$$

where the power supplied to the driving wheels is

$$P_{w\Sigma}^{in} = \sum_{i=1}^{n} T_{wi}^{'('')}\omega_{wi}^{'('')} = \sum_{i=1}^{n} F_{xi}^{'('')}V_{ti}^{'('')} \tag{1.97}$$

In formulae (1.95) and (1.96) the efficiencies η_M and η_δ characterize the effect of the distribution of power among the driving wheels on the mechanical power losses in the drive and on the power lost in wheel slipping.

Substituting formulae (1.95) through (1.97) into expression (1.94), one obtains

$$P_e = P_{trm} + P_{w\Sigma}^{in}(1 - \eta_M)/\eta_M + P_{w\Sigma}^{in}(1 - \eta_\delta) + P_{f\Sigma} + P^{out} \tag{1.98}$$

and, accordingly, the fuel consumption Q_s from formula (1.92) is

$$Q_s = \frac{g_e}{V_x}\left[P_{trm} + \sum_{i=1}^{n} T_{wi}^{'('')}\omega_{wi}^{'('')}(1 - \eta_M)/\eta_M + \sum_{i=1}^{n} T_{wi}^{'('')}\omega_i^{'('')}(1 - \eta_\delta) + P_{f\Sigma} + P^{out}\right] \tag{1.99}$$

The second and third terms in the square brackets of formula (1.99) define the direct effect of the vehicle's driveline system on the fuel consumption Q_s. In fact, different driveline systems bring about different distributions of power to the driving wheels which, in its turn, affects the total mechanical efficiency η_M (see formula (1.61)) and the power loss in slipping (see formula (1.72)). This means that the efficiencies η_M and η_δ should be the objects of attention in assessing the effect of driveline systems on the fuel economy of vehicles. To provide for minimal fuel consumption the driveline system should ensure such distribution of power among the wheels $\left(T_{wi}^{'('')}\omega_{wi}^{'('')},\ i = 1, n\right)$ that provide for maximum values of η_M and η_δ under the given travel conditions.

The contribution of each of these efficiencies (η_M and η_δ) on the fuel consumption is different. At positive power flows from the transfer case to the driving wheels, the effect of η_M and η_δ on Q_s when moving on solid surfaces is commonly commensurable or sometimes the power losses P_{drl} may exceed $P_{\delta\Sigma}$ in all-wheel drive vehicles. To illustrate this, reference can be made to the previously mentioned article concerning the 4×4 Audi Quattro: while having a 1.5%–3% bigger power loss in its driveline system (as compared with the 4×2 version), this car demonstrated a better fuel efficiency due to less power loss in tire deflections. On a deformable surface the effect of $P_{\delta\Sigma}$ may be more perceptible and depends on the type of the driveline system. Specific examples shall be examined in the following chapters that reflect the authors' experience in evaluating and solving problems in the field of energy/fuel efficiency of vehicles with two and more driving axles; only general recommendations are of concern here.

Let the four identical wheels of a vehicle be subject to identical vertical loads and move under identical gripping conditions, i.e., have the same coefficients K_x of tangential stiffness of the tires. The total circumferential force of the vehicle is (for the case of the linear function (1.25))

$$F_{x\Sigma} = 4K_x s_{\delta 4\times 4} \tag{1.100}$$

Then the slipping efficiency is

$$\eta_{\delta 4\times 4} = 1 - s_{\delta 4\times 4} = 1 - \frac{F_{x\Sigma}}{4K_x} \tag{1.101}$$

If one of the vehicle's axles is disconnected, then for the same value of the circumferential traction force $F_{x\Sigma}$ in formula (1.100) the slip increases:

$$F_{x\Sigma} = 2K_x s_{\delta 4\times 2} \tag{1.102}$$

where $s_{\delta 4\times 2} > s_{\delta 4\times 4}$.

Then

$$\eta_{\delta 4\times 2} = 1 - s_{\delta 4\times 2} = 1 - \frac{F_{x\Sigma}}{2K_x} \tag{1.103}$$

It is seen by comparing formulae (1.101) and (1.103) that the efficiency $\eta_{\delta 4\times 4}$ is greater than $\eta_{\delta 4\times 2}$. An increase in η_δ has a positive effect on the fuel economy Q_s.

In the general case, for a given load $F_{x\Sigma}$ equal to the total resistance to the vehicle's motion, the value of η_δ will be the higher, the more the driving wheels. Still, consideration should be given to the effect of the driveline system on the power $P_{\delta\Sigma}$. This assertion is proven as follows. If it is assumed that the relationship between the wheel's circumferential power F_x and its slip s_δ is linear ($F_x = K_x s_\delta$) then the power lost in slipping of the front and rear wheels is the same (reference is made to an equivalent scheme of the vehicle):

$$\begin{aligned} P_{\delta 1} &= F_{x1} V_{\delta 1} = F_{x1} s_{\delta 1} V_t \\ P_{\delta 2} &= F_{x2} V_{\delta 2} = F_{x2} s_{\delta 2} V_t \\ P_{\delta\Sigma} &= P_{\delta 1} + P_{\delta 2} \end{aligned} \tag{1.104}$$

It follows from formula (1.104) that the products $F_{x1}s_{\delta 1}$ and $F_{x2}s_{\delta 2}$ at constant theoretical velocity V_t reflect to some scale the slip powers $P_{\delta 1}$ and $P_{\delta 2}$. Figure 1.72 is a plot of linear relationships $F_{x1(2)} = K_a s_{\delta 1(2)} = 2K_x s_{\delta 1(2)}$ (here, K_a is the longitudinal stiffness of two wheels of an axle). The areas

$$\begin{aligned} A_{a1} &= F_{x1} s_{\delta 1} = (15)(0.0625) = 0.9375 \\ A_{a2} &= F_{x2} s_{\delta 2} = (15)(0.0625) = 0.9375 \\ A_{a\Sigma} &= A_{a1} + A_{a2} = 1.875 \end{aligned} \tag{1.105}$$

of the two rectangles ////// and \\\\\\ in Figure 1.72a are proportional to powers $P_{\delta 1}$, $P_{\delta 2}$, and $P_{\delta\Sigma}$ from formulas (1.104) at equal slipping of both axles, $s_{\delta 1} = s_{\delta 2} = 0.0625$ and of the total circumferential force

$$F_{x\Sigma} = F_{x1} + F_{x2} = 15 + 15 = 30 \text{ kN}$$

If the driveline system is modified in such a manner that the circumferential forces of the axles will become unequal (see Figure 1.72b)

$$F_{x1} = 10 \text{ kN} \quad \text{and} \quad F_{x2} = 20 \text{ kN}$$
$$F_{x\Sigma} = F_{x1} + F_{x2} = 10 + 20 = 30 \text{ kN}$$

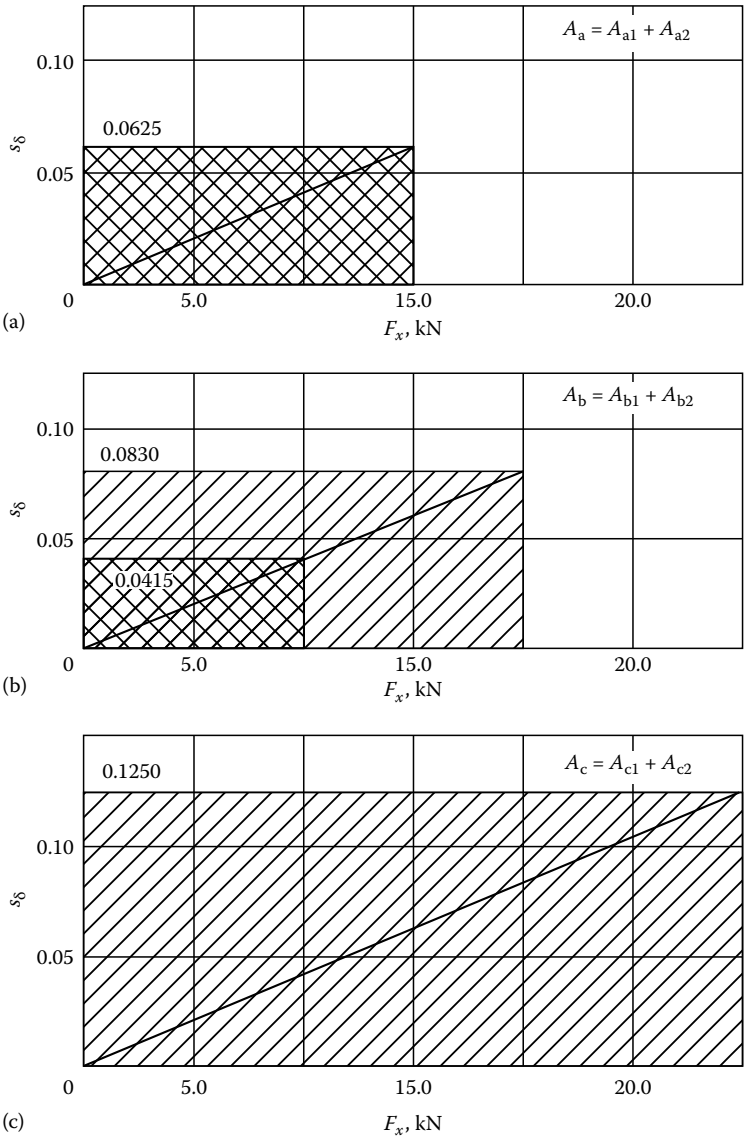


FIGURE 1.72
Slip power losses.

then the wheel slips also change

$$s_{\delta 1} = 0.0415 \quad \text{and} \quad s_{\delta 2} = 0.0830$$

This brings about a change in the numerical values of the areas:

$$\begin{aligned} A_{b1} &= F_{x1} s_{\delta 1} = (10)(0.0415) = 0.4150 \\ A_{b2} &= F_{x2} s_{\delta 2} = (20)(0.0830) = 1.660 \\ A_{b\Sigma} &= A_{b1} + A_{b2} = 2.075 \end{aligned} \tag{1.106}$$

Figure 1.72c corresponds to the case of a rear driving axle:

$$F_{x\Sigma} = F_{x2} = 30 \text{ kN}, \quad s_{\delta 2} = 0.1250$$

Then

$$\begin{aligned} A_{c1} &= F_{x1} s_{\delta 1} = 0 \\ A_{c2} &= F_{x2} s_{\delta 2} = (30)(0.1250) = 3.75 \\ A_{c\Sigma} &= A_{c1} + A_{c2} = 3.750 \end{aligned} \tag{1.107}$$

It is seen by comparing the values of $A_{a\Sigma}$, $A_{b\Sigma}$, and $A_{c\Sigma}$ from formulae (1.105) through (1.107) that the greatest slip power losses occur in vehicles with a single driving axle. The lowest slipping power losses take place in a vehicle with two driving axles at $s_{\delta 1} = s_{\delta 2}$ (this shall be analyzed subsequently in the course of a deeper mathematical analysis). Two-axle drive vehicles at $s_{\delta 1} \neq s_{\delta 2}$ occupy an intermediate position, i.e.,

$$A_{a\Sigma} < A_{b\Sigma} < A_{c\Sigma} \tag{1.108}$$

According to formulae (1.108), the component $\sum_{i=1}^{2} T_{wi}\omega_{wi}(1 - \eta_\delta)$ in formula (1.99) will affect the fuel consumption Q_s.

In summing up the above, an algorithm shall be presented below for assessing the effect of the driveline system on the vehicle's fuel consumption. At the first stage, it is required to calculate the circumferential forces, torques, angular velocities and slip of the wheels (the methods are presented in the subsequent chapters). Then the efficiencies η_M and η_δ are calculated using the formulae in Sections 1.4.1 and 1.4.2. Then formula (1.99) can be used for determining the driveline system influence on the fuel consumption. It should be remembered that the output power P^{out} in formula (1.98) is equal to the tractive (drawbar) power P_d for towing and transportation-traction vehicles from Table 1.19. For transportation vehicles, for which, $P_d = 0$, the output power is the rolling resistance power that stems from the weight of the cargo being transported, i.e.,

$$P^{out} = P_{fg\Sigma}$$

Here $P_{f\Sigma}$ in formula (1.98) should be replaced by the rolling resistance power that stems from the curb weight of the vehicle, i.e., $P_{fc\Sigma}$. Methods of calculating $P_{fg\Sigma}$ and $P_{fc\Sigma}$ were presented in Section 1.4.2.

1.5 Vehicle Performance and Driveline Systems Design

Traditionally, university courses in vehicle dynamics are concerned with the dynamic behavior of a vehicle in motion. In many respects those vehicle dynamics courses are a logical continuation of courses in Statics and Dynamics that are concerned with rigid bodies and systems.

Actually, however, vehicles are much more complex systems, the design of which requires much more than understanding their dynamic behavior in motion. Vehicle dynamics as the theory of a vehicle in motion must be concerned with the vehicle's

performance in the interaction with its functional surroundings. The vehicle performance is comprised of its engineering capacity and economic efficiency and is determined by its dynamics and properties. It is common to cluster vehicle properties into two major groups: (1) consumer properties (fuel economy, reliability, and safety, ecological and ergonomic properties) and (2) operational properties (mobility, traction and velocity properties, handling, stability of motion, turnability, braking properties, and ride smoothness).

The material presented in Section 1.4 on the effect of driveline systems on the energy effectiveness/fuel economy serves as confirmation of the need and utility to study vehicle dynamics as a set of properties, whose indicators determine the vehicle performance and the engineering and economic effectiveness. In fact, a design engineer must know what the aggregate of the above-listed properties is that the vehicle should posses in order to best perform the functions for which it is intended. Functionally vehicles were grouped into three categories, these being the traction, transportation and combined (transportation-traction) mode of operation (see Table 1.19).

The operational and consumer properties of vehicle depend on its mass and geometric parameters (such as weight, wheelbase and track, location of the center of gravity, etc.) and on the characteristics of the vehicle's systems (engine, transmission, driveline system, suspension, tires, braking and steering systems, etc.). Figure 1.73 shows a block diagram that illustrates the interrelationship between a vehicle's systems and its operational and consumer properties.

Vehicle parameters and systems	Vehicle operational properties							Consumer properties				
	Tractive and velocity properties	Mobility	Turnability	Stability of motion	Handling	Brake properties	Ride	Fuel consumption	Safety	Reliability	Comfort of driving/ ergonomic properties	Ecological properties
General mass and geometric parameters	+	+				+	+	+	+			
Engine and transmission	+							+		+		+
Driveline system	+	+	+	+	+			+	+	+	+	
Tires	+	+	+	+	+		+	+				+
Suspension system			+	+	+		+		+	+	+	
Steering system			+	+	+		+		+	+	+	
Braking system				+	+	+			+	+		

FIGURE 1.73
Vehicle properties vs. vehicle systems.

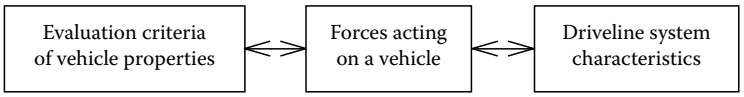


FIGURE 1.74
Relationship between vehicle properties and driveline-system characteristics.

The usefulness of this block diagram for a design engineer consists in providing a graphical idea of the properties that are affected by a given system. Thus, it must be remembered in designing simple driveline systems, that their characteristics affect the mobility and traction-velocity properties, handling, stability and turnability, and fuel economy of vehicles. The design of integrated driveline systems should include a study of additional properties of the vehicle. For example, the braking performance must be investigated in designing a control system of interaxle and interwheel PDUs and of the braking mechanisms (e.g., a traction control integrated with an antislip differential system).

This book is concerned with design of driveline systems on the basis of their direct effect on the vehicle operational properties and the fuel economy. Other consumer properties (ease of handling, safety, etc.) are referred to in the book indirectly, as a result of improving vehicle performance, primarily, stability of motion and turnability. It should be additionally noted that in certain cases, when a driveline system is analyzed for mobility and traction-velocity properties on deformable surfaces, one must also investigate ecological changes that stem from compacting and abrasion of the soil in the course of forming the track. This is of importance for farm tractors, since it involves preserving the fruit-bearing layer of the soil and the yield. In recent years ecologic factors are more increasingly taken into account in the design of military vehicles.

As previously noted, vehicle properties result from the interaction between the vehicle and its surroundings. This interaction manifests itself through forces acting on a vehicle. Such forces are the result of interaction between the vehicle and the support surface. For this reason it is important to establish functional relationships between these forces and the indicators/criteria of vehicle properties on one hand, and between forces acting on the vehicle and characteristics of the driveline system, on the other hand (see Figure 1.74).

In this case it becomes possible to assess the effect of the characteristics of the driveline system on the properties of the vehicle and, accordingly, to design more perfect drives that ensure better vehicle properties and performance. As an example, the formulae in Section 1.4.2 establish functional relationships between the indices of the energy effectiveness of vehicles and the wheel circumferential forces and slips.

The operational properties of vehicles that are a function of the driveline system characteristics (see Figure 1.73) are analyzed further down. These properties shall be defined and the criteria for evaluating them shall be examined.

1.5.1 Traction and Velocity Properties of Vehicles

The traction-velocity properties of vehicles determine the potential range of velocities and the limiting acceleration rates induced by the circumferential forces of the driving wheels, subject to limitations on the conditions of gripping between the wheels and the surface and limitations by the engine characteristics. The traction properties allow the vehicle to move on upgrades and to tow trailers, whereas the velocity properties make it possible to accelerate, move by inertia and move at high velocities.

The traction-velocity properties are assessed by means of various single indicators, each of which allows assessing these properties under some defined motion situation. Most frequently, use is made of the maximum velocity, the time of acceleration over a distance of 400 and 1000 m; the time for accelerating to a given velocity, typically 50, 60, and 100 mph. The velocity characteristic consists of acceleration-coasting distance; acceleration in picking up speed; maximum achievable upgrade; the velocity characteristic in speeding up in the highest gear, and certain others. All the above indicators define the average velocity V_{avg} that is a generalized indicator of traction-velocity properties.

The traction-velocity properties of vehicles are usually analyzed together with their fuel economy indicators. This is due to the fact that V_{avg}, as a generalized indicator of traction-velocity properties, and of the fuel consumption determine the principal criterion of the vehicles effectiveness—its general and specific output. In fact, the product of the mass of the payload W_{g}/g and the average vehicle speed may be used to determine the engineering efficiency of a vehicle, which is its transport capacity:

$$T_{\text{r}} = \frac{W_{\text{g}}}{g} V_{\text{avg}} \tag{1.109}$$

Here the transport capacity is measured in ton-km/h, where W_{g} is in kN; g is the acceleration of gravity in m/s^2 and V_{avg} is in km/h.

Accordingly, the specific output is defined as

$$ST_{\text{r}} = \frac{\left(\frac{W_{\text{g}}}{g} V_{\text{avg}}\right)}{Q_{\text{avg}}} \tag{1.110}$$

where ST_{r} is in [ton-km/h] $\frac{100}{L}$; Q_{avg} is average fuel consumption in liters per 100 km of travel, W_{g}, V_{avg}, and g are in the same units as in formula (1.109).

It should be noted that the specific transport capacity ST_{r} is similar to the transport efficiency suggested by Dr. Wong (2001):

$$\eta_{\text{tr}} = \frac{W_{\text{g}} V_x}{P_{\text{e}}} \tag{1.111}$$

where

P_{e} is the effective engine power (see Figure 1.66)

V_x is the actual forward speed of the vehicle

As was demonstrated in Section 1.4.3, the manner in which the power is distributed between the driving wheels has a perceptible effect on the circumferential forces and on the wheel slip ratios and hence on the power P_δ lost in slipping and on the fuel consumption referred to the distance traveled by the vehicle Q_{s} (and, of course, on the fuel consumption Q_{avg}). At the same time, the wheel slip determines the magnitude of V_{avg}. It can hence be concluded that circumferential forces of the wheels and their slips affect, by way of the vehicle's velocity and power loss, the traction-velocity properties and the fuel economy of the vehicle.

It is precisely in this manner that the driveline system affects the traction-velocity properties and the fuel economy of the vehicle. As an illustration, analyze the rectilinear uniform motion of a driving axle when the road-gripping conditions of the wheels are different. If the axle's differential is open, then the slip ratios of the two wheels will be different. Slipping is equal when the differential is locked. It is obvious that the velocity V_{avg} of the axle with an open differential is lower than in the case when it is locked. The circumferential forces of the axle's wheels also differ depending on whether the differential is open or locked (analytic expressions shall be given in Chapters 2 and 3). In view of the above, the indicators defined by formulae (1.109) through (1.111) may be used for assessing the effect of driveline systems on the traction-velocity properties of vehicles.

At the same time it should be noted that the structure of the specific capacity criterion is similar to that of efficiency. Hence subsequently the traction-velocity properties and fuel economy of multiwheel drive vehicles shall be assessed using the transportation efficiency η_x^{tr}. It should be noted that the efficiency η_x^{tr} is convenient not only for finding the optimal distribution of power among the driving wheels upon uniform motion of the vehicle, but also in investigating the traction-velocity performance of vehicles in the course of acceleration. In fact, criteria for assessing the acceleration should be formulated in such a manner that it would be possible to determine which of the vehicles being compared has the higher average velocity at the same acceleration time and the lower average fuel consumption over a given acceleration path. These requirements are satisfied by the efficiency η_x^{tr}. Formula 1.89 can be used for calculating the values of η_x^{tr} in accelerating.

The output of tractive vehicles also serves as the criterion of their engineering efficiency. The output of farm tractors, for example, is defined as

$$T_{\text{t}} = 0.1 B_{\text{a}} V_{\text{avg}} \frac{t_{\text{P}}}{t_{\Sigma}} \tag{1.112}$$

where

T_{t} is in hectare/h; a note: a hectare is a measure of area (1 hectare = 1.47 acre)
B_{a} is the width of the implement's sweep, m
V_{avg} is in km/h
t_{Σ} is the total time of work in h, including time t_{P} of pure work with the farm implement and the time for traversing the field from one point to another

For farm tractors frequent use is also made of an indicator equal to the ratio of the fuel consumption Q_{avg} to the output, i.e.,

$$T_{\text{o}} = \frac{Q_{\text{avg}}}{T_{\text{t}}} \tag{1.113}$$

The criteria represented by formulae (1.112) and (1.113) have the same structure as the expression for the efficiency, for which reason the tractive properties and the fuel economies of tractors are also assessed by the pertinent running-gear efficiency. Thus, farm tractors in fieldwork and industrial tractors coupled to working equipment should be assessed by the tractive efficiency η_x^{t} of the running gear. The traction-velocity properties of tractors employed for payload transportation should be assessed on the basis of the transportation efficiency η_x^{tr} of the running gear.

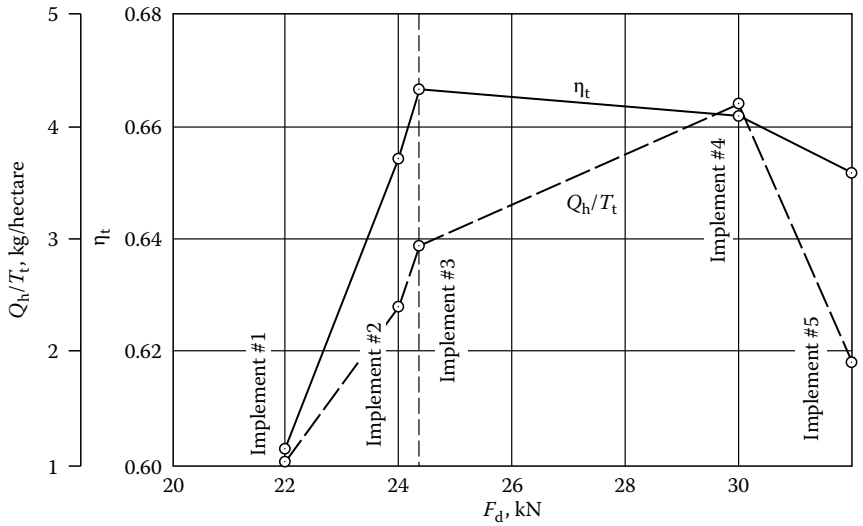


FIGURE 1.75
4×4 farm tractor, $P_e^{max} = 95.3$ kW, with five agricultural implements.

Additional studies were performed for obtaining an analytic assessment of the feasibility of using the efficiency instead of the specific output; the results are plotted in Figure 1.75.

This figure shows the analytically obtained values of the tractive efficiency η_t and of an indicator equal to the ratio of the fuel consumption per hour Q_h (kg/h) to the output T_t (hectare/h). It is seen that the shape of both curves is approximately the same, which confirms the feasibility of utilizing the running-gear efficiency for assessing the traction-velocity properties of vehicles. It should be emphasized here that the running-gear efficiency is a component of the efficiency η_t (see formulae (1.66) and (1.67)). It is also interesting to note that the rolling resistance efficiency and the slip efficiency, the product of which determines the running-gear efficiency, represent respectively the force and velocity components of power loss. This follows from formulae (1.67), (1.68), and (1.70) for all-wheel drive vehicles.

1.5.2 Mobility of Vehicles

The mobility of vehicles is their ability to move under road-less terrain conditions, while still performing their functions. Recall that vehicles were classified by their functional attributes into three groups (see Table 1.19). A distinction is made between the topographical and support-surface mobility. The topographical (geometric) mobility represents the ability of a vehicle to surmount various obstacles including ditches and trenches, hillsides, man-made obstacles (this applies to combat and tactical vehicles), etc. The support-surface mobility is determined by the ability of the vehicle to move over deformable surfaces and over snow. This book is concerned primarily with support-surface mobility.

The ability, in principle, of a vehicle to move is determined by the condition

$$\sum_{i=1}^{n} \left(F'_{xi} + F''_{xi} \right)_{max} \geq F_{\psi} \tag{1.114}$$

where F_ψ is the total force of resistance to motion; $\sum_{i=1}^{n}\left(F'_{xi}+F''_{xi}\right)_{\max}$ is the sum of the maximum possible circumferential forces of the driving wheels that the engine, transmission, driveline system and the wheels can supply under the conditions of motion, that are represented by the force F_ψ.

Condition 1.114 is more general than Equation 1.74, in which the sum of circumferential forces of the driving wheels was termed the total circumferential force of a vehicle $F_{x\Sigma}$. Condition 1.114 clearly illustrates the effect of the driveline system on the vehicle's mobility. If the characteristics of the driveline system provide for such a value of the total circumferential force $F_{x\Sigma}^{\max}$ that inequality (1.114) is satisfied, then the mobility of the vehicle is ensured in principle. In the opposite case, the vehicle loses its mobility and new characteristics for its driveline system must be found in order to satisfy condition (1.114).

In addition to inequality (1.114) various additional absolute and relative indicators are used. A relative assessment of mobility is obtained using the dimensionless ratios

$$p_x = 1 - \frac{F_\psi}{F_{x\Sigma}^{\max}} \quad p_\mu = 1 - \frac{F_\psi}{F_{x\Sigma}^{\mu}} \tag{1.115}$$

where $F_{x\Sigma}^{\mu}$ is the total circumferential force of the vehicle determined from the conditions of gripping between the wheels and the terrain, i.e.,

$$F_{x\Sigma}^{\mu} = \sum_{i=1}^{n}\left(\mu'_{\mathrm{p}xi}R'_{zi} + \mu''_{\mathrm{p}xi}R''_{zi}\right) \tag{1.116}$$

The index p_x represents the mobility of the vehicle from the point of view of its traction capacity. The greater $F_{x\Sigma}^{\max}$, the higher the vehicle's mobility. In the case of $F_{x\Sigma}^{\max} = F_\psi$, $p_x = 0$ and the vehicle's mobility is at minimum, i.e., the vehicle moves within the limits of its capability. A further small deterioration in the conditions of motion will cause complete loss of mobility. The parameter p_μ in formulae (1.115) represents the mobility capacity based on conditions of gripping between the wheels and the surface of motion.

Off-road travel of vehicles involves a significant reduction in their speed and output. For this reason mobility is assessed using absolute indicators such as V_{avg}, the outputs T_{r}, S_{tr}, T_{t} and the fuel consumption Q_{avg} (see formulae (1.109), (1.110), and (1.112)). As previously discussed, the running-gear efficiency may be used instead of these indicators.

1.5.3 Turnability

Turnability is the ability of a vehicle to change the curvature of its path of motion upon changes in its design parameters (in our case the driveline system) and operating factors (velocity, drawbar pull, conditions of gripping between the wheels, and the surface of motion, etc.). For example, locking of the interwheel differential causes the circumferential wheel forces to become unequal and brings about the appearance of a moment of resistance to turning in the plane of the road, which generates lateral forces and wheel side slip. This increases the turning radius R_{a} (the path curvature $1/R_{\mathrm{a}}$ decreases), the location of the instantaneous turn center and the path of the vehicle's motion change.

The turnability is accessed employing the concepts of ''understeering,'' ''neutralsteering,'' and ''oversteering'' that are determined from the relationship between the slip angles of the front (α_1) and the rear (α_2) axles (Figure 1.76).

The turnability is insufficient (understeering) if $\alpha_1 > \alpha_2$ and the actual turn radius of the vehicle R_{a} is greater than the theoretical radius R_{t}, determined by the Ackerman Geometry,

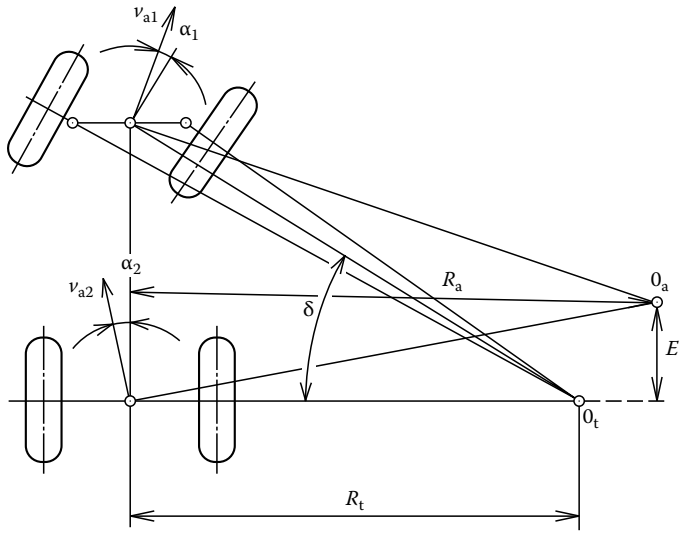


FIGURE 1.76
Vehicle taking a turn.

i.e., by the steering angles of the front wheels. Oversteering takes place at $\alpha_1 < \alpha_2$, when R_a becomes smaller than R_t. In the case of $\alpha_1 = \alpha_2$ the vehicle, so to speak exhibits neutral turnability (neutralsteering), $R_a = R_t$.

If the relationship between slip angles α_1 and α_2 is determined at values of operating factors that are fixed in time and at unchanged design parameters of the vehicle, one refers to the static turnability of the vehicle. An example of investigating the static turnability is determining the curvature, $1/R_a$, at a fixed value of the steering angle, δ, of the front axle and constant vehicle speed (note that angle δ is linked with the steering angles of the right and left wheels, δ'' and δ', respectively).

The dynamic turnability of a vehicle, as an ability to change the path of motion is determined upon change in the operating factors and design parameters of the vehicle in time. For example, the path curvature is investigated at a specified mode of change in the turn angles of steered wheels, with the wheel traction control system operating, under unstable road conditions or upon changes in the velocity of the vehicle.

Figure 1.77 illustrates the behavior of $1/R_a$ as a function of the steering angle δ of vehicles that exhibit different turnability modes. Straight line 1 is typical of a vehicle with neutral-steering, when the actual and theoretical turn radii are equal ($R_a = R_t$).

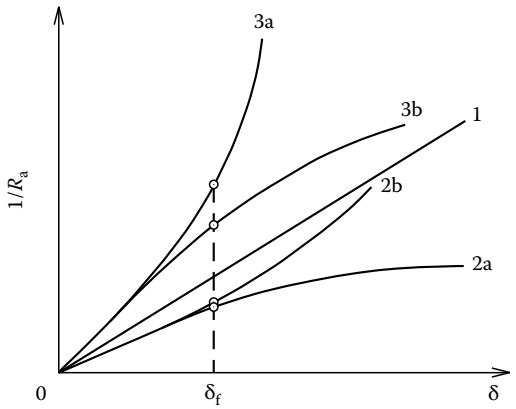


FIGURE 1.77
Curvature vs. steering angle.

Curves 2 and 3 are typical of vehicles with under- and oversteering. In fact, curves 3 correspond to smaller values of R_a, whereas curves 2 correspond to larger values of this radius as compared with R_t at a given value of angle δ_f. Convex curve 2a corresponds to a vehicle for which the understeering increases with increasing δ. Concave curve 2b indicates that with increasing δ understeering starts approaching neutralsteering. If curve 2b intersects straight line 1, this means that the vehicle's turnability performance changes from understeering to oversteering. Curve 3a is typical of vehicles with increasing oversteering, whereas curve 3b corresponds to a vehicle in which the oversteering diminishes and approaches the neutral with increasing δ.

A similar turnability analysis can be performed upon change in the vehicle's forward speed V_x. Figure 1.78 illustrates the effect of V_x on δ, the values of which are determined from the requirement of ensuring steady motion along a circle with a fixed radius.

Horizontal line 1 corresponds to neutral static turnability. An increase in V_x causes a rise in the lateral acceleration V_x^2/R_a and, accordingly, in the centrifugal force. The latter produces additional lateral loads on the wheels and increases their slip angles. Since, however, the slip angles of the front and rear axles are identical ($\alpha_1 = \alpha_2$), there is no need to change δ for maintaining the vehicle on a circle with a specified radius. It should be noted that actually line 1 is not rigorously horizontal due to inevitable changes in the real operating conditions.

Curve 2 in Figure 1.78 corresponds to continuously increasing understeering. An increase in V_x with its corresponding increase in α_1 and α_2, while maintaining the condition that $\alpha_1 > \alpha_2$, require increasing δ in order to hold the turning circle radius constant.

In the case of continuously increasing oversteering, when the difference between α_1 and α_2 increases continuously ($\alpha_1 \ll \alpha_2$), angle δ must just as continuously decrease so that the turning radius should remain the same while the velocity is increasing (curve 3 in Figure 1.78).

Curve 4 in Figure 1.78 corresponds to a vehicle with increasing understeering at low velocities. As V_x increases, the turnability of the vehicle approaches the neutralsteering mode. Curve 5 describes transition from over- to understeering. Apparently, the same vehicle may exhibit both under- and oversteering, depending on the conditions of motion.

It is convenient to assess under- and oversteering qualitatively by means of a turning radius variation factor representing the change in R_a relative to R_t:

$$q_R = \frac{R_a - R_t}{R_t} \tag{1.117}$$

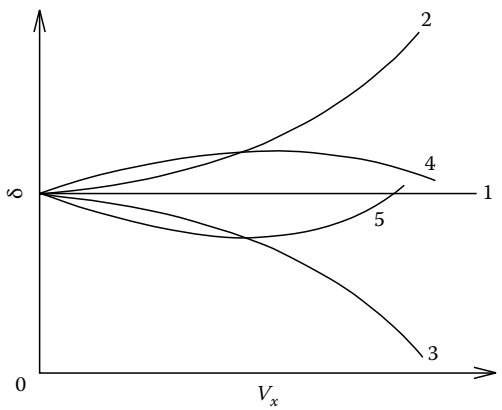


FIGURE 1.78
Steering angle vs. vehicle speed.

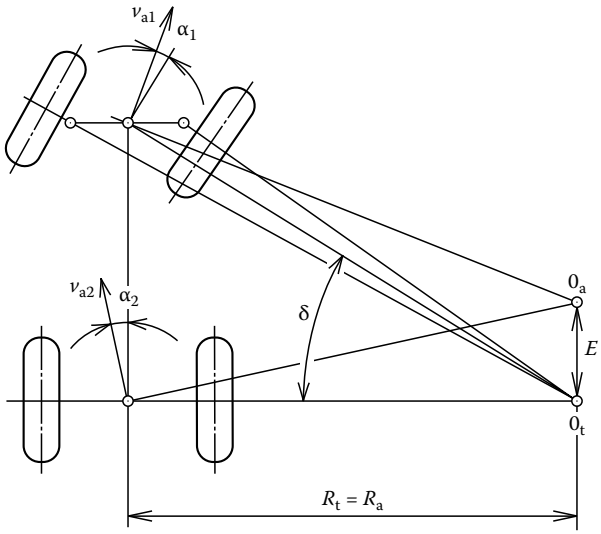


FIGURE 1.79
Vehicle with neutralsteering taking a turn.

The offset distance of the center of turn E (see Figure 1.76) may serve as still another criterion for assessing the turnability. Both these criteria q_R and E give an idea of the actual path curvature and the location of the real center of turn relative to the rear axle of the vehicle.

Some investigators define a vehicle with ''ideal'' turnability as that having neutral turnability (neutralsteering) on the basis of the fact that the actual turning radius R_a is equal to the theoretical R_t. However, then the turn center is shifted from point O_t to point O_a (see Figure 1.79).

This causes the location of the vehicle on the plane of motion to change, i.e., the path of motion becomes different than that specified by angle δ. The vehicle may simply not fit into the turn unless δ is changed. For this reason it is useful to be able to assess turnability by means of criteria not associated with the vehicle (as R_t, R_a, E are), but associated with the coordinate system fixed on the plane of motion (on the ground). These criteria may consist of coefficients (see also Figure 1.80) such as

$$K_X = \frac{X_a}{X_t}; \quad K_Y = \frac{Y_a}{Y_t}; \quad K_A = \frac{A_a}{A_t} \tag{1.118}$$

the values of which are determined, using parameters found in the absence of wheel slip (subscript t—''theoretical'') and for wheels rolling at a slip angle (subscript a—''actual'').

1.5.4 Stability of Motion

Stability of motion is the property of a vehicle to maintain specified differential parameters of motion or a specified course of variation in them, after the perturbing forces are removed. The term perturbing forces is here used to denote forces that have not been included in the vehicle's equation of motion due to lack of knowledge of their direction and their magnitudes.

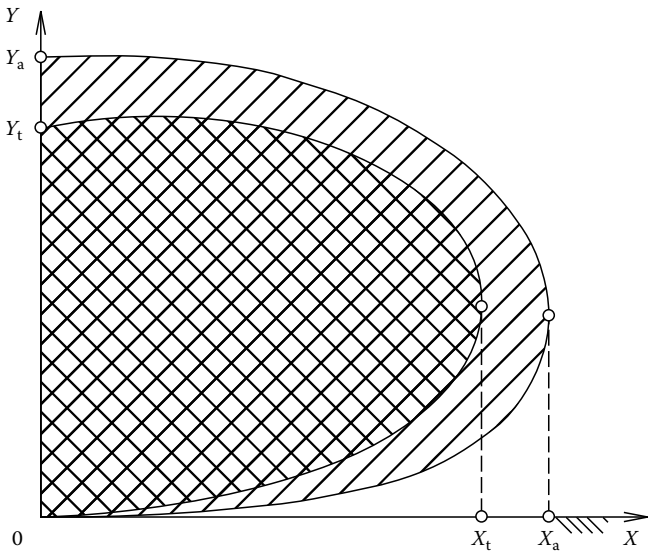


FIGURE 1.80
Wheel paths in XY coordinate system fixed to the ground: A_t, A_a.

This formulation is comprised of three principal elements that must be considered in investigating vehicle stability:

1. *Forces acting on a vehicle*. A vehicle is caused to move by all kinds of forces that include applied forces, gravity forces, inertia forces, and finally circumferential forces, the distribution of which among the wheels depends to large extent on the driveline system. The time of action of the forces is finite, but in investigating stability, their aftereffects should be considered even when some of them are no longer applied.
2. *Vehicle velocity*. Stability may be retained up to a certain velocity level that depends on road conditions, applied forces and design parameters of the vehicle. When this velocity is reached, the motion of the vehicle becomes unstable which means also that it is potentially dangerous for subsequent travel.
3. *The relationship governing the steering system*. This is usually specified; if not given, it is regarded as an exception. A note: active steering is not a subject of this book.

There are six generalized coordinates of a vehicle: three linear, along the x-longitudinal, y-lateral, and z-vertical axes, associated with the vehicle body and three angular turns about these axes. A vehicle may deviate from its specified path and lose stability in four of six generalized coordinates of the vehicle body: linear motion along the x-axis and along the z-axis of the vehicle are not included in this consideration.

A distinction is made between the following kinds of stability relative to these four coordinates:

1. Course stability, determined by the direction of the vehicle's longitudinal (x) axis.
2. Lateral stability, determined by lateral displacement along the y-axis.
3. Stability to longitudinal rollover about the y-axis and transverse rollover about the x-axis. In view of this, a distinction is made between longitudinal and transverse or lateral stability of a vehicle.

The course stability highly affects the motion of the vehicle along its specified path. In the case of unsatisfactory course stability, the driver must always be ready to change the direction of motion caused by deviation from the specified path. When the course stability is excessive, the driver must exert an additional effort to change the direction of motion.

Loss of lateral stability manifests itself in lateral slip (or skidding) of the vehicle that may subsequently result in rollover about the x-axis, i.e., loss of stability in transverse rollover.

Motion along the specified path is virtually independent of the stability to longitudinal rollover about the y-axis.

The critical velocity V_{cr}, upon reaching which the vehicle motion becomes unstable is the most prevalent criterion of stability assessment. The value of the vehicle's V_{cr} is usually examined from analysis of the values of coefficients of the gripping force utilization factor K_μ of all the driving wheels:

$$K_\mu = \frac{\sqrt{F_x^2 + F_l^2}}{\mu_{px} R_Z} \tag{1.119}$$

The lower the value of K_μ, the higher the gripping potential of the wheels and the greater the probability that the vehicle will move in the curved path set by the driver. It is usually assumed that lateral skid of a wheel occurs at $K_\mu > 0.5$.

The stability of motion is also assessed on the basis of the following

1. Angular velocity r of vehicle about the vertical axis, known as the yaw rate, rad/s or deg/s
2. Lateral velocity V_y and lateral acceleration a_y of the center of gravity
3. Lateral roll angle of the sprung mass γ_l

The effect of the driveline system on motion stability manifests itself in the fact that the redistribution of the circumferential forces among the driving wheels affects the lateral wheel forces F_l (see Section 1.3.4) and hence the value of K_μ from formula (1.119). This may cause skid of individual wheels and then of individual axles and of the entire vehicle.

Controlling the redistribution of circumferential forces between the axles and also between the left and right wheels, allows governing the yaw rate, the lateral velocity and lateral acceleration of the vehicle. These means make it possible to prevent a situation when the lateral roll angle γ_l would reach its critical value.

1.5.5 Handling of the Vehicle

Handling of the vehicle is here a term applied to the ability of the vehicle to respond to the steering input with the required precision and speed. The handling of a vehicle depends to a large extent on its turnability and stability. In fact, the precision and speed of responding to the steering input should differ depending on whether the vehicle is unstable or is overstable. Overstability also reduces the vehicle's ability to take a turn, which is detrimental to its turnability. Under these conditions the driver must devote additional emotional power to making the turn. This has a negative effect on the ease of handling and on safety that the consumer expects of the vehicle.

With reference to the above, handling, as an operating property of the vehicle may even be excluded from the list properties that depend on the driveline system design. It is

assumed here that the features of driveline systems that ensure the required stability and turnability of the vehicle simultaneously satisfy the handling requirement. Such an approach can be applied to off-road equipment that moves at relatively low velocities. If, however, it is necessary to assess the handling of a vehicle directly, this is done on the basis of the ratio of the yaw rate r to angle of turn δ of steering wheels, which is known as the handling sensitivity (i.e., the sensitivity of the vehicle to the steering input by the driver):

$$S_e = \frac{r}{\delta} \tag{1.120}$$

Figure 1.81 shows typical curves of handling sensitivity S_e as a function of the forward speed V_x.

Straight line 1 corresponds to a vehicle with neutral turnability (neutralsteering). If the vehicle exhibits oversteering (curve 2), then the value of S_e tends to infinity and the vehicle cannot be handled because of loss of stability: the speed attains the critical value of V_{cr}. In the case of understeering (curve 3) S_e attains some maximum value upon an increase in speed. Steady-state sensitivity is known as

$$S_e^{st} = \frac{1}{\delta R_a} \tag{1.121}$$

and unsteady-state (dynamic) sensitivity is

$$S_e^{dn} = \frac{\partial S_e^{st}}{\partial t} \approx \frac{S_e^{st}}{t_R} \tag{1.122}$$

where t_R is the time delay in the vehicle's reaction to a quick turn of the steering wheel (vehicle response time). The value of t_R depends on the play and elasticity of the steering system, the ability of the suspension and tires to generate lateral reactions F_l in the contact patches between the tires and the road. Driveline systems affect the lateral reactions of tires by means of redistribution of torque among the wheels and in this way they also affect the magnitude of time t_R.

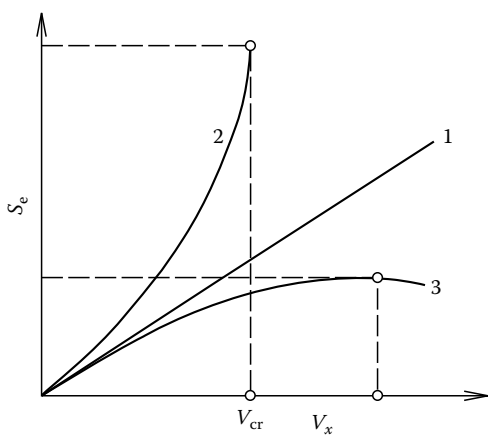


FIGURE 1.81
Handling sensitivity.

In addition to sensitivity S_e and the time t_R, the handling of a vehicle is assessed by the following

1. Speed of self-return of the steered wheels upon completing the turn
2. Steering-wheel torque as a function of the lateral acceleration a_y and path curvature $1/R_a$
3. Transient time t_s needed to stabilize the motion when completing lane change
4. Roll angle γ_l of the vehicle's sprung mass as a function of the lateral acceleration a_y

Some investigators classify the study of vehicle handling modes into three stages:

1. The primary handling stage that is primarily linear
2. The secondary handling stage, which is one in which the handling becomes substantially nonlinear
3. The final handling stage, which is the last stage that corresponds to higher lateral accelerations (from $0.5g$ for commercial vehicles to $0.8g$ for passenger cars and to even higher values for racing cars)

It follows from the material presented above that the driveline systems affect several operational and consumer properties of vehicles. Here each of these properties has several evaluation criteria. Very frequently, when designing a driveline system on the basis of a criterion (criteria) representing one of the properties it is possible to worsen other properties of the vehicle. For example, locking the differential of the driving axle improves the traction-velocity properties of the vehicle, but is detrimental to its turnability, since this causes a marked increase in the turning radius R_a. For this reason the finding of optimal and close to them characteristics for the driveline system should be treated as a multicriterion problem. The main principles of the design of driveline systems are treated in the next section.

1.6 Principles of Driveline System Design

This section focuses on the engineering principles of designing driveline systems, pertaining to determination of the optimal features of driveline systems and PDUs, investigation of the effect of driveline system on the vehicle performance and dynamics and also pertaining directly to engineering design of PDUs. No consideration is given here to the economic and manufacturing aspects of design, since it is assumed that they are considered concurrently with the design process.

Historically, driveline system design has been initially based on the method of comparative analysis. According to this approach, a number of driveline systems with various combinations of PDU mechanisms and systems could be researched analytically for a given vehicle or vehicles based on some criteria of the vehicle's properties from the point of view of its operation and customer satisfaction.

The ranges of the numerical values of these criteria are usually established and the values themselves are determined on the basis of computer simulation of the vehicle's

mathematical model with the given driveline system. Such an analysis of the vehicle criteria aids in applying analytical and experimental analysis to select the best of the several driveline systems under consideration for the given vehicle. Comparative analysis also enables engineers to analytically and experimentally compare different vehicles with the same or different driveline systems.

However, the application of the above design research approach in no way ensures that the selected driveline system endows the vehicle with the optimal/desired performance, within the specified range of values of these criteria. It is indeed possible that the best driveline system and the optimal combination of PDUs are to be found outside the researched selection of drivelines and sets of PDU mechanisms and subsystems. Hence, the method of comparative analysis does not provide prerequisites and conditions sufficient for developing better driveline systems.

The importance and the necessity of further development of advanced approaches and methodologies in the field of driveline systems design remain undiminished. The urgency of the need for a new scientifically founded methodology also stems from recent engineering advancements. Some automotive companies are presently working on torque-bias couplings, torque-vectoring, and torque management devices to control torque distribution to the drive axles and wheels. These are mechatronic systems, and designing mechatronic driveline systems is to be founded on a new methodological basis.

This section of the book describes a methodology that includes the key principles of all-wheel driveline system design and is based not on wheel torque vectoring but on wheel power management as a part of a broader analytical approach. The proposed principles pertain to the optimization of power distribution among the driving wheels in both rectilinear and curvilinear vehicle motion. This new methodology is based on inverse dynamics, consisting in treated aspects of vehicle dynamics as an inverse dynamics problem. Under this approach, forces acting on a mechanical system are determined for the given/required kinematic parameters, e.g., program of motion. To explain this in simple terms, the equation of motion of a body is given below in the form of Newton's second law:

$$\sum_{i=1}^{s} \overline{F_{\mathrm{i}}} = m\bar{a} \tag{1.123}$$

In applying inverse dynamics, the acceleration $\bar{a}$ is assigned first, and then the forces $\sum_{i=1}^{s} \overline{F_{\mathrm{i}}}$ acting on the body with mass m needed to provide it with the required acceleration are synthesized. As for vehicles, these forces are the foundation for researching vehicle operational properties, namely for optimizing the criteria for these properties and then for designing optimal driveline systems.

The following example will serve for illustrating many of the applications of inverse-dynamics analysis. Curve 1 in Figure 1.82 describes the variation in the vehicle's speed as it is being accelerated to the specified value. Let it be required to improve the vehicle acceleration performance in such a manner that the velocity V_x in the course of acceleration conform to curve 2. This requires that acceleration a_x defined by function $V_x = f(t)$ from curve 2, be used for determining the circumferential forces of the wheels $F_{xi}^{'(\prime\prime)}$, $(i = 1, n)$, from Equation 1.123. These forces should then be used for designing the vehicle's systems including the driveline system.

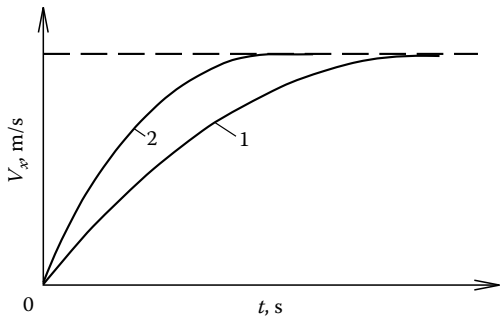


FIGURE 1.82
For acceleration performance analysis.

Summing up, the proposed methodology:

1. Provides a way to optimally manage power distribution to the wheels and to determine the optimal characteristics of driveline systems based on operational-properties criteria
2. Links these operational properties optimization to improvement of vehicle dynamics
3. Leads to the required/desired vehicle performance and engineering efficiency.

These principles can be formulated as follows

> Principle 1. Specify the required kinematic parameters of a vehicle in motion and treat vehicle dynamics as the inverse dynamics for the purpose of determining the total power required for the vehicle's motion. Find optimum combinations of the total power distribution to the driving wheels that conform to the specified kinematic parameters of the vehicle in the specified modes of operation and under the specified road/terrain conditions.

As seen from Principle 1, the kinematic parameters of motion should be assigned first for the given vehicle's operational modes and conditions of motion. Modes of operation and road/terrain conditions stem from the vehicle's intended use. Passenger cars and earth-moving machines work in different modes and under different conditions. The required kinematic parameters may be assigned based on the vehicle's design specification.

As discussed earlier, vehicle dynamics influences vehicle performance. To better represent this influence, Principle 1 proposes a new approach to determining the total power required for the vehicle motion and to optimizing power distribution to the driving wheels. The approach is based on treating vehicle dynamics as the inverse dynamics: forces acting on the driving wheels of a vehicle (see formulae (1.123) and (1.74)) are determined using the required kinematic parameters represented by the acceleration in the above formulae. These forces are used to determine the total power needed for the vehicle's motion and for finding the power distribution to the driving wheels.

> Principle 2. The optimum combinations of power distributions to the driving wheels should also be determined by providing the extrema values of vehicle operational properties criteria in the specified modes of operation and under the given road/terrain conditions. There are three modes of operation and these are presented in Table 1.19. A list of operational properties and their criteria were given in Section 1.5 (see Figure 1.73).

It is hereby suggested that a new term—''power vectoring'' or ''power management'' be used in determining the optimum power distribution to the driving wheels. Such an approach addresses both vehicle dynamics and vehicle performance issues. Indeed, optimum combinations of power distributions to the driving wheels, which conform to the extrema values of some vehicle performance criteria, can be used for synthesizing laws and algorithms for controlling driveline mechanisms and subsystems of a particular vehicle. Moreover, optimum power distributions to the driveline wheels create an efficient way for designing new-concept driveline systems and mechanisms.

It should be noted that the wheel power optimization in Principles 1 and 2 is a constrained multicriteria optimization. In practice, some wheel power distributions that are optimal from the point of tractive and velocity properties can be detrimental to other vehicle operational properties such as turnability and handling. Some power distributions may be optimal in terms of vehicle operational properties, but they could not satisfy the kinematic requirements put to vehicle motion. For this reason, when pursuing Principle 2, the task of determining the extrema values of the criteria can be replaced with finding the required/specified values of these criteria.

> Principle 3. Based on the optimal wheel distributions, synthesize and establish optimal characteristics for a hypothetical driveline system.

The driveline system has been termed hypothetical, because this principle is implemented at a stage when the vehicle does not yet have a driveline system. At this point, the only available information is the optimal wheel power distribution. This distribution is the basis for synthesizing optimal characteristics for so called hypothetical driveline systems.

Also, Principle 3 does not set up rules for designing a particular driveline system that could be either mechanical or a mechatronic one. Because of this, Principle 3 does not limit engineers, but gives them another degree of freedom in designing driveline systems with new characteristics. Indeed, these characteristics can be considered not only as torque biased, but also as control algorithms for individual wheel power control. Such new characteristics may lead to driveline system designs that are based on novel concepts of operation. At this stage, engineers and researches should thoroughly research achievements in fundamental science that can be used for driveline applications. As an example, viscous clutches can be regarded as a driveline application emerged from fundamental research of non-Newtonian fluids.

> Principle 4. Once the optimal driveline system characteristics are synthesized, design a driveline system, simple or combined or integrated, that implements the optimal or near optimal characteristics in a set of PDUs, which, if needed, interact with other vehicle systems.

The mechanisms that implement the optimal characteristics in given PDUs need not necessarily always be new designs. Sometimes, mechanisms with the required optimal or near optimal characteristics are available off the shelf. The optimality of these characteristics should be validated following the research done under Principle 4. Such validation can be performed by means of a performance analysis of a vehicle with the new optimal driveline system.

It is clear from principles 1 to 4 formulated above that a vehicle with the newly-designed driveline system will have an optimal power distribution to the driving wheels, and the vehicle will move with the required kinematic parameters in the given operational modes

<table>
<tr><td rowspan="2">Principle</td><td colspan="4">Algorithm major steps</td></tr>
<tr><td>#1</td><td>#2</td><td>#3</td><td>#4</td></tr>
<tr><td>#1</td><td>Based on inverse dynamics approach develop a math model of a vehicle without a driveline system and determine the total wheel power under the required vehicle kinematics</td><td rowspan="2">Optimize power distributions among the drive wheels using criteria of vehicle operational properties and vehicle kinematics requirements</td><td rowspan="3">Synthesize optimal characteristics for vehicle power dividing units</td><td rowspan="3">Design power dividing units which provide optimal characteristics found in step 3</td></tr>
<tr><td>#2</td><td></td></tr>
<tr><td>#3</td><td colspan="2"></td></tr>
<tr><td>#4</td><td colspan="3"></td></tr>
</table>

FIGURE 1.83
General algorithm for driveline system design.

and road/terrain conditions. Finally, the vehicle will manifest its optimal operational properties and performance and therefore, will operate at higher engineering efficiency level.

The four principles presented above include the following major key-points:

- Inverse vehicle dynamics approach to determining the total wheel power required for motion with the given kinematic parameters.
- Wheel power optimization based on the criteria of vehicle operational properties and vehicle kinematics requirements.
- Synthesis of optimal characteristics of vehicle PDUs.
- Design of a driveline system and PDUs that provides optimal distribution of power to the wheels and better vehicle performance, and the required/desired kinematic parameters of vehicle motion.

Principles 1 through 4 and the general algorithm from Figure 1.83 that represents the principles were verified and validated in many research projects.

Chapters 6 and 7 present various applications of the principles to mechanical and mechatronic driveline systems design. Chapters 2 through 5 present analytical methods and their applications to designing and researching various PDUs including open and locking differentials, viscous clutches, NoSPINs, on demand systems, etc. The material presented in these chapters is important for carrying out the fourth step of the algorithm from Figure 1.83.

2

Interwheel and Interaxle Open and Lockable Differentials

2.1 Kinematics and Dynamics of Differentials: The Gear-Ratio Concept

The objective conditions of vehicle travel require that its wheels move at different velocities. This is caused by the fact that the paths traveled by each of the wheels are not the same. The paths of travel of the different wheels both in the horizontal and vertical directions have different curvatures. Moreover, a slight inequality in the radii of the wheels stemming from allowances in tire manufacture and differences in the degree of wear of the individual tire treads, and differences in tire inflation pressure, loads on the wheels, and other factors cause the difference in velocities.

Inequality in the velocities of driven wheels is accommodated by seating them individually on the axle of rotation, whereas that of driving wheels, by the use of open differentials (further referred to as differentials). The differential as a power-dividing unit in general form is a mechanism with a single input link and two output links (Figure 2.1).

These links rotate about the principal axis of the differential. A torque, T_0, is supplied to the input link that rotates at velocity ω_0; the input power is hence $P_{in} = T_0\omega_0$. The output links rotate at angular velocities ω' and ω'' and are subjected to torques T' and T''; accordingly, the output powers at the differential's output shafts are $T'\omega'$ and $T''\omega''$.

Depending on the type of gears that are used, differentials are known as bevel-gear (Figure 2.2a and c) and spur-gear differentials (Figure 2.2b and d).

If the output torques are the same, $T' = T''$, then the differentials are known as symmetrical (Figure 2.2a and b), whereas when $T' \neq T''$, the differentials are known as asymmetrical (Figure 2.2c and d).

Unlike the bevel-gear differential, in the spur-gear differential the coupling between the side gears is attained by a pair of double planetary gears or pinions (Figure 2.2b). Each pinion is coupled by one of its rings to an output side gear that sits on an output shaft (or a half axle), whereas by its other ring—to its twin pinion. There may be two to four such pinions, sitting of pins, or spiders. Bevel-gear differentials have two or four pinions; three pinions are used very rarely.

It is seen by comparing the open-type bevel-gear and spur-gear differentials that the bevel-gear differential has the advantage of using fewer gears (there are no paired pinions) and of the smaller overall dimensions of the housing in the plane perpendicular to the principal axis, whereas the spur-gear differential, while being somewhat more complex, has the advantage of greater ease in manufacturing the gears, the absence of axial loads in the gearing, and smaller overall dimension in the direction of the principal axis (Figure 2.2).

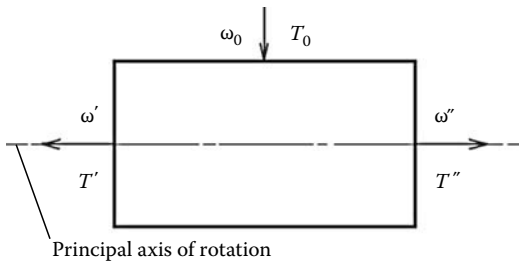


FIGURE 2.1
Block-diagram of a differential.

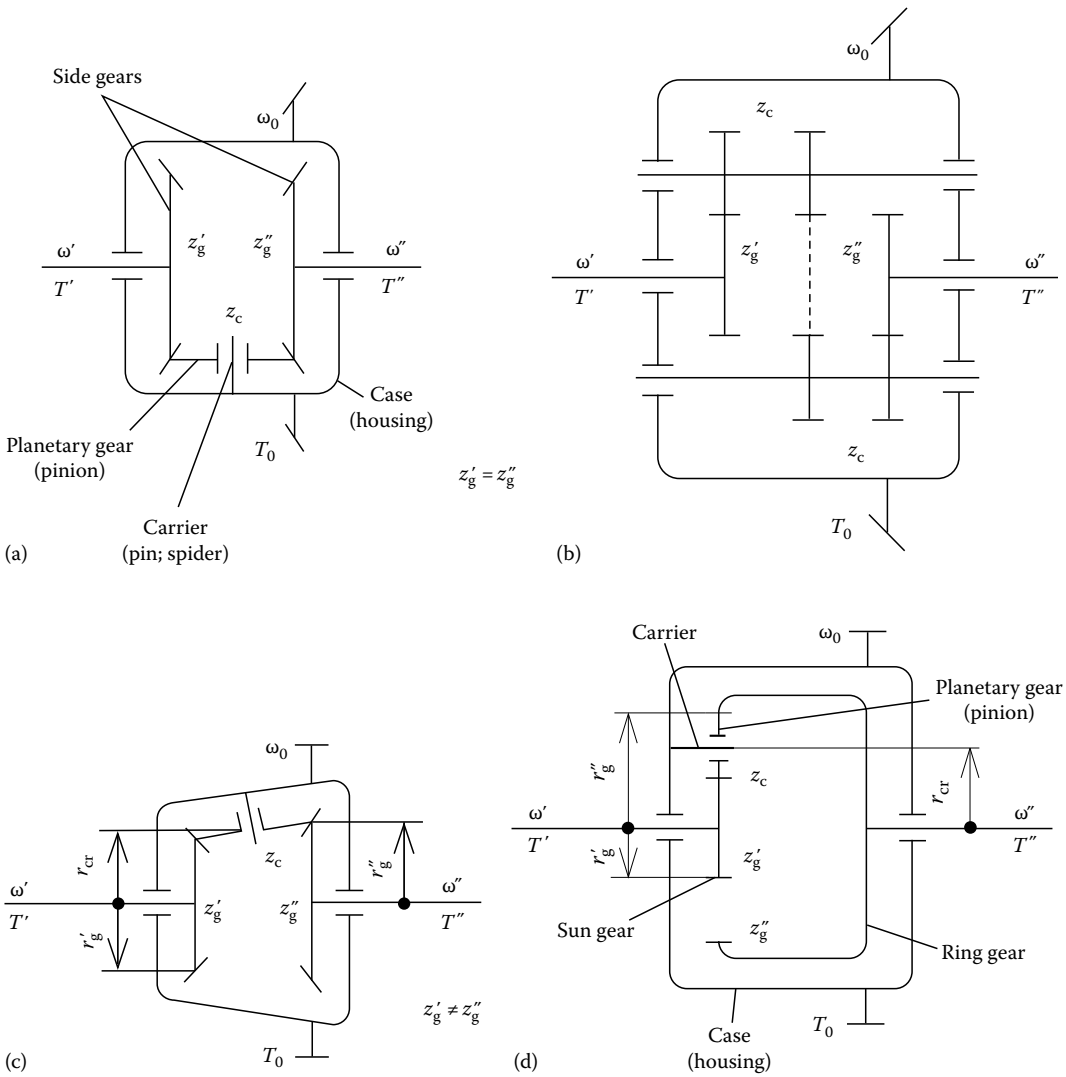


FIGURE 2.2
Diagrams of differentials. (a) Symmetrical bevel-gear mechanism; (b) symmetrical spur-gear mechanism; (c) asymmetrical bevel-gear mechanism; (d) asymmetrical spur-gear mechanism.

The power is transmitted from the input link of the differential to its output links in the following manner:

1. Differential housing → carrier → pinions → output-side gears (see Figure 2.2a through c)
2. Differential housing → carrier → pinions → sun and epicyclical (or ring) gears (Figure 2.2d)

Depending on their location in the vehicle, the differential may be:

1. Interwheel (installed in the driving axle and distributing power among its right and left wheels)
2. Interaxle (installed between two axles or between two clusters of axles or between one axle and a cluster of axles)
3. Interside (installed between the left and right sides of the vehicle)

Examples of several vehicles with different differentials are listed in Section 1.2.

The kinematics and dynamics of differentials are examined by introducing the concept of the internal gear ratio, u_d, of a differential (or simply the differential gear ratio). It is defined as the ratio of the number of teeth of the output-side gears coupled to the output shafts with the housing (carrier) stationary. For symmetrical differentials ($z'_g = z''_g$, see Figure 2.2a and b) the internal gear ratio is equal to

$$u_d = \frac{z_c}{z_g}\frac{z_g}{z_c} = 1 \tag{2.1}$$

For asymmetrical differentials (see Figure 2.2c and d):

$$u_d = \frac{z_c}{z'_g}\frac{z''_g}{z_c} = \frac{z''_g}{z'_g} > 1 \tag{2.2}$$

The differential is a mechanism with two degrees of freedom; this means that in order to define the kinematic parameters of the differential's links, it is necessary to specify two independent generalized coordinates. If the turn angles φ' and φ'' of the output shafts of the differential are taken as such independent generalized coordinates, then the turn angle of the input link (the differential housing) will consist of a function such as

$$\varphi_0 = f(\varphi', \varphi'') \tag{2.3}$$

The differentiation of both parts of (2.3) yields

$$\frac{d\varphi_0}{dt} = \left(\frac{\partial f}{\partial \varphi'}\right)\left(\frac{d\varphi'}{dt}\right) + \left(\frac{\partial f}{\partial \varphi''}\right)\left(\frac{d\varphi''}{dt}\right) \tag{2.4}$$

The partial derivatives are designated as

$$\frac{\partial f}{\partial \varphi'} = p', \quad \frac{\partial f}{\partial \varphi''} = p''$$

and formula (2.4) is then written as

$$\omega_0 = p'\omega' + p''\omega'' \tag{2.5}$$

Equality (2.5) obtained above is valid for any mechanism with two degrees of freedom. But the term differential applies only to mechanisms of the class under consideration for which the coefficients p' and p'' are constant. In other words, differential mechanisms implement a linear relationship between the angular velocity of one link with the velocities of two other links.

A general consideration of Equation 2.5 is given in Section 7.4. Here, open differentials with the housing (the carrier) as the input link are considered. To define coefficients p' and p'' assume that one of the output shafts is stopped, for example, $\omega'' = 0$. Then it follows from formula (2.5) that

$$\begin{aligned} \omega_0 &= p'\omega' \\ p' &= \frac{\omega_0}{\omega'} = i''_{0'} \end{aligned} \tag{2.6}$$

If the second output link is stopped, $\omega' = 0$, then

$$\begin{aligned} \omega_0 &= p''\omega'' \\ p'' &= \frac{\omega_0}{\omega''} = i'_{0''} \end{aligned} \tag{2.7}$$

In formulae (2.6) and (2.7), $i''_{0'}$ and $i'_{0''}$ are the velocity ratios between two links of the differential with the third link stopped. For example, $i''_{0'}$ means the velocity ratio between the differential housing (index zero, 0) and an output link (index′) when the other output link is stopped (index″). Formulae for calculating $i''_{0'}$ and $i'_{0''}$ are derived in the theory of planetary-gear drivetrains on the basis of design parameter K, which is known as the characteristic of the planetary-gear set. In the case of differentials, K is calculated as the gear ratio between the sun and ring gears with the carrier stopped. In other words, K is equal to the internal gear ratio of the differential introduced by formulae (2.1) and (2.2): $K = u_d$, i.e., $K \geq 1$ in all cases. It is known from the theory of planetary drivetrains that

$$\begin{aligned} i''_{0'} &= \frac{1}{1+K} = \frac{1}{1+u_d} \\ i'_{0''} &= \frac{K}{1+K} = \frac{u_d}{1+u_d} \end{aligned} \tag{2.8}$$

Using formulae (2.6) through (2.8), formula (2.5), which relates functionally the angular velocities of the three principal links of the differential, is now rewritten as

$$\omega_0 = \frac{\omega' + u_d\omega''}{1+u_d} \tag{2.9}$$

In the case of $u_d = 1$ for a symmetrical differential, formula (2.9) becomes

$$\omega_0 = \frac{\omega' + \omega''}{2} \tag{2.10}$$

Formulae (2.9) and (2.10) may also be derived by the direct use of u_d. Assume that the housing of the differential in Figure 2.2d has been stopped. Then, designating the angular

velocity of the sun gear as ω_{rel}, it is found that the angular velocity of the ring gear is ω_{rel}/u_d. If the differential housing is now freed from being restrained and its angular velocity is designated by ω_0, then the new values of the angular velocities of the sun and ring gears will be

$$\begin{aligned} \omega' &= \omega_0 + \omega_{rel} \\ \omega'' &= \omega_0 - \frac{\omega_{rel}}{u_d} \quad \text{or} \quad u_d\omega'' = u_d\omega_0 - \omega_{rel} \end{aligned} \tag{2.11}$$

Summing over formulae (2.11) yields formula (2.9).

As seen from the above analysis, the kinematics of differentials is more complicated than that of drives with a single input and single output link in which the angular velocity of the input and output links are uniquely related. For example, the angular velocity of a motorcycle wheel is directly proportional to the angular velocity of the engine's crankshaft, i.e., the drive of a single wheel has one degree of freedom. A vehicle with two driving wheels already needs one, and a vehicle with three wheels needs two differentials, etc. This means that the number of differentials needed by a vehicle with a fully differential drive should be by unity less than the number of driving wheels. If the vehicle employs two or more engines with independent drives of independent (intrinsic to each engine) driving wheels, then the number of differentials needed decreases. The drives of a vehicle in which the number of engines is equal to the number of driving wheels do not require differentials. This means that in the case of a single engine the driveline system of the driving wheels is a system that has as many degrees of freedom as the number of drive wheels.

No fixed relationship exists between the angular velocity of individual wheels and between the angular velocity of any wheel and the angular velocity of the engine crankshaft in differential drives of all-wheel and multiwheel drive vehicles. A rigorous relationship exists in this case only between the angular velocity of the engine crankshaft (more precisely, the angular velocity of the housing of the differential of the transfer case) and the sum of the angular velocities of the driving wheels, i.e.,

$$\sum_{i=1}^{n} q_i\left(\omega_i' + \omega_i''\right) = q_0\omega_0 \tag{2.12}$$

where

q_i and q_0 are constant factors determined by the gear ratio of the drive
ω_i' and ω_i'' are the angular velocities of the advancing and the lagging wheels of the ith axle when moving over a road with any curvature
n is the number of driving axles
ω_0 is the angular velocity of the housing of the transfer case differential

If the vehicle's differentials are symmetrical and the tires are of the same model, then formula (2.12) becomes

$$\sum_{i=1}^{n}\left(\omega_i' + \omega_i''\right) = 2\omega_0\left(\frac{n}{u}\right) \tag{2.13}$$

where u is the gear ratio of the drive from the transfer case differential to the wheels.

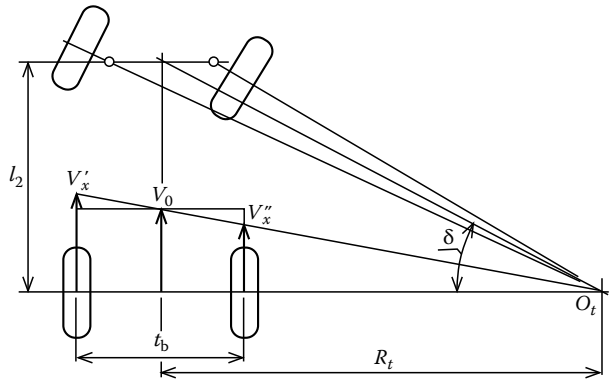


FIGURE 2.3
Rear wheel drive vehicle in turn.

The kinematic analysis of the differential is now continued. If $\omega' = \omega''$ then, as follows from (2.9) and (2.10), the angular velocities of the three links are identical

$$\omega_0 = \omega' = \omega'' \tag{2.14}$$

i.e., there is no relative rotation of the differential's components.

The equality of angular velocities expressed by (2.14) corresponds to the idealized case of rectilinear motion of a vehicle over a perfectly smooth road, with the same wheel radii and identical gripping conditions. However, there exists a continuous, even if insignificant, relative motion of the three links of differentials that occur in accordance with formulae (2.9) and (2.10).

When the vehicle moves along a curved path, the angular velocities of the wheels of the axle linked by an open differential is determined by formula (2.10) and by the geometry of the turn shown in Figure 2.3.

Assuming that the slippages of the left and right wheels of the rear-driving axle are identical, it is found that

$$\begin{aligned} \omega' &= \omega_0\left(1 + \frac{t_b}{2R_t}\right) = \omega_0\left(1 + 0.5\frac{t_b}{l_2}\tan\delta\right) \\ \omega'' &= \omega_0\left(1 - \frac{t_b}{2R_t}\right) = \omega_0\left(1 - 0.5\frac{t_b}{l_2}\tan\delta\right) \end{aligned} \tag{2.15}$$

As the steering angle of the front wheels δ increases, the difference in the angular velocities ω' of the outer and ω'' of the inner wheel also increases.

In calculating the velocity modes of differentials, it is important to be able to determine the relation of the angular velocity of the pinion relative to that of the carrier ω_c. For example, for symmetrical bevel-gear differentials, this relative velocity can be determined by setting equal the linear velocities V of the point of contact of the planetary gear and the side gear (see Figure 2.4):

$$V = \omega_c r_c = \omega_{rel} r_g \quad \text{or} \quad \omega_c z_c = \omega_{rel} z_g \tag{2.16}$$

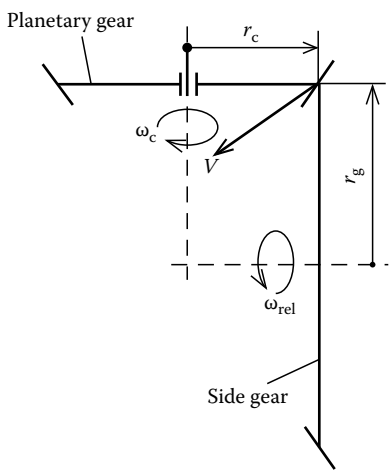


FIGURE 2.4
Diagram of relative angular velocities ω_c and ω_{rel}.

where the angular velocity of the side gear, ω_{rel}, relative to the differential's housing is determined from formulae (2.11) and (2.15) at $u_d = 1$,

$$\omega_{rel} = 0.5\omega_0 \frac{t_b}{R_t} = 0.5\omega_0 \frac{t_b}{l_2} \tan\delta \tag{2.17}$$

Then the angular velocity of the planetary gear about the carrier is

$$\omega_c = 0.5\omega_0 \frac{z_g}{z_c} \frac{t_b}{l_2} \tan\delta \tag{2.18}$$

Consider now an example of the use of formula 2.18.

Illustrative Example

The angular velocity, ω_0, of the housing of the interwheel differential may be expressed as

$$\omega_0 = \frac{V_0}{r_w} u_k \tag{2.19}$$

where

V_0 is the actual linear velocity of the axle center

r_w is the effective rolling radius in the driving mode (when slippage is negligible, suppose that $r_w = r_w^{0'} = r_w^{0''}$, where $r_w^{0'}$ and $r_w^{0''}$ are the effective rolling radii of the left and right wheels in the driven mode)

u_k is the wheel-hub reduction gear ratio

$u_k = 1$ for vehicles without wheel-hub reduction gear

Then formula (2.18) becomes

$$\omega_c = 0.5 \frac{V_0}{r_w^0} u_k \frac{z_g}{z_c} \frac{t_B}{l_2} \tan\delta \tag{2.20}$$

The values of ω_c were computed for open interwheel differentials of 14 heavy-duty highway trucks with gross mass of 18–38 ton, of which there were eight trucks with 4×2 tractor models and six trucks with 6×4 tractor models. It was assumed that their highway velocity is 65.5 km/h; the range of angles δ of the front-steered wheels was set at 0°–12°. Figure 2.5 shows the range of angular velocity, ω_c, vs. δ.

The ranges in Figure 2.5 stem from the fact that the tractors have different geometries and the parameters of their differentials are also different. The curves in Figure 2.4 have steeper slopes for trucks with wheel-hub reduction gear sets. Thus, the values of ω_c for 4×2 tractors with wheel-hub reduction gear sets are 2.57-fold higher than those of ω_c of tractors without wheel-hub reduction gear sets at $\delta = 12°$. The ratio of the average values of ω_c for 6×4 tractors with and without wheel-hub reduction gear sets is 4.25. At the same time, the average values of ω_c for 6×4 tractors with wheel-hub reduction gears is 1.68 higher than for 4×2 tractors also with wheel-hub reduction gear sets.

In the previously examined illustrative example, the rotation of the pinions about the pins of the spiders at angular velocity, ω_c, stems from the fact that the tractors travel over curved paths, when $\delta \neq 0$. However, if the gripping conditions of the wheels are not the

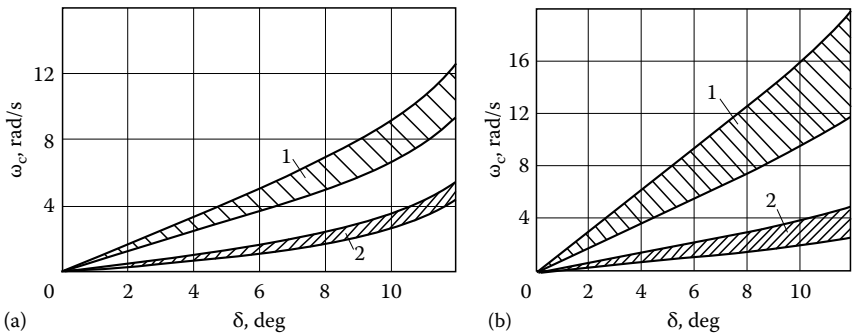


FIGURE 2.5
Angular velocity of a pinion ω_c vs. steering angle δ. Trucks with (a) 4 × 2 tractors; (b) 6 × 4 tractors. 1, driving axles with wheel-hub reduction gear; 2, driving axles without wheel-hub reduction gear.

same, then the values of ω_c will be much greater because of the large difference in the angular velocities of the wheels. This is presented in Table 2.1, which lists the angular velocities of the members of the driving tandem of a 6 × 4 tractor as a function of the possible combinations of slippages of the driving wheels.

It was assumed in all cases that $\omega_5'' = 0$. Figure 2.6 clarifies the designations of the driving-tandem members.

The next subject of analysis is the dynamics of open differentials. Start with a symmetrical bevel-gear differential (Figure 2.2a). The dynamics of symmetrical spur-gear differential is similar. It will be assumed, in determining the relationship between the torques of the three principal links (the housing and the two output shafts) that the housing is stationary. Then, treating the mechanism as a speed reducer at gear ratio equal to unity

TABLE 2.1
Angular Velocities in a Differential Driveline of a Two-Axle Tandem

		Driveline System Members							
No.	**Slipping Wheels**	**1**	**2**	**3**	**4**	**4′**	**4″**	**5**	**5″**
1	One wheel of the first axle slipping	ω_0	$2\omega_0$	0	$2\omega_0/u_f$	$4\omega_0/u_f$	0	0	0
2	Two wheels of the first axle slipping	ω_0	$2\omega_0$	0	$2\omega_0/u_f$	$2\omega_0/u_f$	$2\omega_0/u_f$	0	0
3	One wheel of each axle slipping	ω_0	ω_0	ω_0	ω_0/u_f	$2\omega_0/u_f$	0	ω_0/u_f	$2\omega_0/u_f$
4	Three wheels slipping (uncertain relationship)	ω_0	$2\omega_0 \ldots 0$	$0 \ldots 2\omega_0$	$0 \ldots 2\omega_0/u_f$	$0 \ldots 2\omega_0/u_f$	$0 \ldots 2\omega_0/u_f$	$2\omega_0/u_f \ldots 0$	$4\omega_0/u_f \ldots 0$
4a	Three wheels slipping ($\omega_{4'} = \omega_{4''} = \omega_{5'}$)	ω_0	$\frac{4}{3}\omega_0$	$\frac{4}{6}\omega_0$	$\left(\frac{4}{3}\omega_0\right)\Big/u_f$	$\left(\frac{4}{3}\omega_0\right)\Big/u_f$	$\left(\frac{4}{3}\omega_0\right)\Big/u_f$	$\left(\frac{4}{6}\omega_0\right)\Big/u_f$	$\left(\frac{4}{3}\omega_0\right)\Big/u_f$
4b	Three wheels slipping ($\omega_{5'} = 2\omega_{4'} = 2\omega_{4''}$)	ω_0	ω_0	ω_0	ω_0/u_f	ω_0/u_f	ω_0/u_f	ω_0/u_f	$2\omega_0/u_f$

Notes: The angular velocity $\omega_{5''}$ is supposed to be equal to zero for all items 1 through 4b; u_f is the gear ratio of the final drive.

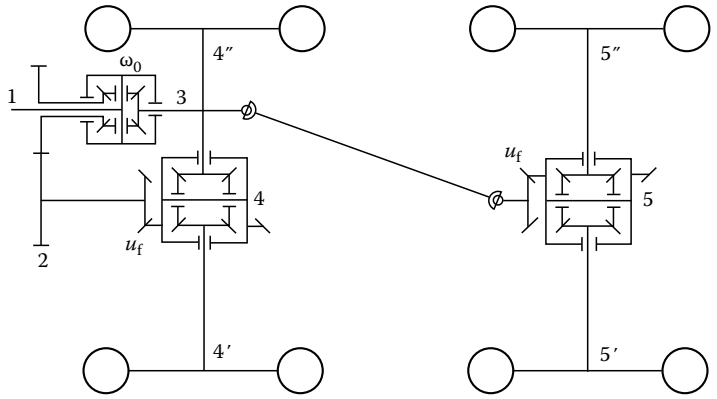


FIGURE 2.6
Kinematic layout of two-axle tandem.

($u_d = 1$), the torques at the shafts shall be equal (friction losses in the reducer are sufficiently small to be neglected). Since the angular velocities of the differential's output shafts are directed oppositely, the external torques at the shafts will be of the same direction. As a result, the dynamics of a three-link differential mechanism will be given by the expression

$$\begin{aligned} T' &= T'' \\ T' + T'' &= T_0 \end{aligned} \tag{2.21}$$

where
T' and T'' are the torques at the driving (leading) and driven (trailing) shafts
T_0 is the torque at the differential's housing

Formula (2.21) remains valid also when the differential's housing rotates, since the external torques do not change. Thus, the torques at the output shafts of a symmetrical differential are always equal, irrespective of the conditions under which the vehicle moves, which is an important property of the differential that determines to a large extent the vehicle's performance.

Now, let us analyze the dynamics of asymmetrical differentials shown in Figure 2.2c and d. The circumferential force $F = T_0/r_{cr}$ exerted by the carrier on the pinions is equal to the sum of circumferential forces F' and F'' exerted by the output gears on the pinions:

$$F = \frac{T_0}{r_{cr}} = F'' + F' \tag{2.22}$$

Neglecting the internal friction in the open differential, it may be assumed that

$$F'' = F' = 0.5F = 0.5\frac{T_0}{r_{cr}} \tag{2.23}$$

The torques at the output gears are determined, using (2.23), as follows:

$$\begin{aligned} T'' &= F''r''_{\mathrm{g}} = 0.5\frac{T_0}{r_{\mathrm{cr}}}r''_{\mathrm{g}} \\ T'' &= F'r'_{\mathrm{g}} = 0.5\frac{T_0}{r_{\mathrm{cr}}}r'_{\mathrm{g}} \end{aligned} \tag{2.24}$$

It is seen from Figure 2.2c and d that the radius r_{cr} can be calculated from the formula

$$r_{\mathrm{cr}} = 0.5(r''_{\mathrm{g}} + r'_{\mathrm{g}}) \tag{2.25}$$

The substitution of (2.25) into (2.24) and the replacement of the radii r''_{g} and r'_{g} by the number of teeth z''_{g} and z'_{g} (recall that the gears have the same pitch/module) yields expressions for the torques at the output links of an asymmetrical differential:

$$\begin{aligned} T'' &= T_0\frac{z''_{\mathrm{g}}}{z''_{\mathrm{g}} + z'_{\mathrm{g}}} \\ T' &= T_0\frac{z'_{\mathrm{g}}}{z''_{\mathrm{g}} + z'_{\mathrm{g}}} \end{aligned} \tag{2.26}$$

It is seen that the torques at the output shafts of asymmetrical differentials are not the same, $T'' \neq T'$. It can be noted that the ratio T''/T' is equal to u_{d}, the internal gear ratio, from formula (2.2):

$$\frac{T''}{T'} = \frac{z''_{\mathrm{g}}}{z'_{\mathrm{g}}} = u_{\mathrm{d}} \tag{2.27}$$

The importance of formula (2.27) for designing asymmetrical differentials should be emphasized: the ratio of output torques is constant and equal to gear ratio u_{d} irrespective of the gripping conditions of the wheels coupled to the output shafts of the mechanism. The distribution of the input torque $T_0 = T'' + T'$ between the output shafts of the differential may be changed by changing the tooth numbers z''_{g} and z'_{g} and accordingly, of the gear ratio u_{d}:

$$\begin{aligned} T'' &= T_0\frac{u_{\mathrm{d}}}{(1 + u_{\mathrm{d}})} \\ T' &= \frac{T_0}{(1 + u_{\mathrm{d}})} \end{aligned} \tag{2.28}$$

Formulae (2.21) and (2.28) together with formulae (2.9) and (2.10) provide an insight into the substance of the effect of open differentials on the traction and velocity properties of the vehicle. An example is hereby given.

Illustrative Example

Let a 4×2 vehicle with an open symmetrical differential in the rear axle move rectilinearly at constant velocity. The wheels of the driving axle are directly coupled to the side gears of the

differential. It is required to determine the maximum circumferential gripping forces of the wheels under identical and different road (gripping) conditions: $\mu'_{px} = \mu''_{px} = 0.7$; $\mu'_{px} = 0.1$ and $\mu''_{px} = 0.7$. It is also required to clarify the kinematics of the wheels. The normal loads on the left and right wheels are taken to be the same and the rolling radii in the driven mode are likewise the same: $W''_w = W''_w = W_w$; $r^{0'}_w = r^{0''}_w = r^0_w$.

SOLUTION

The maximum circumferential gripping force of a wheel is

$$F_{x\max} = \mu_{px} W_w \tag{2.29}$$

Consider the gripping conditions of the wheels are identical $\mu'_{px} = \mu''_{px} = 0.7$. Since the gripping conditions are identical and the road exerts the same resistance to the rotation of both wheels, the maximum forces $F''_{x\max}$ and $F'_{x\max}$ will be the same by virtue of the symmetry of the differential ($F' = F''$, $T' = T''$, see Figure 2.7a):

$$F''_{x\max} = F'_{x\max} = \mu_{px} W_w = 0.7 W_w \tag{2.30}$$

Then all the links of the differential and the wheels of the axle rotate at the same angular velocity: $\omega_0 = \omega'' = \omega'$.

The difference in the gripping conditions ($\mu''_{px} = 0.7$; $\mu'_{px} = 0.1$) causes the road to exert a different resistance to the motion of the wheels. An open differential, by virtue of its symmetry, provides for equality of the torques, $T' = T''$, and of the circumferential forces $F' = F''$ (see Figure 2.7b). The values of torques of the wheels shall hence be identical and their values will be determined by the wheel's gripping conditions with a lower friction coefficient μ'_{px}. The maximum circumferential wheel forces will, accordingly, also be equal:

$$F''_{x\max} = F'_{x\max} = \mu'_{px} W_w = 0.1 W_w \tag{2.31}$$

The wheel that rolls under better gripping conditions is not able to develop a force larger than $F''_{x\max}$, which is determined from formula (2.31). This wheel tends to stop $\omega'' < \omega_0$; the second wheel of the axle that rolls under poorer gripping conditions starts spinning, $\omega' > \omega_0$.

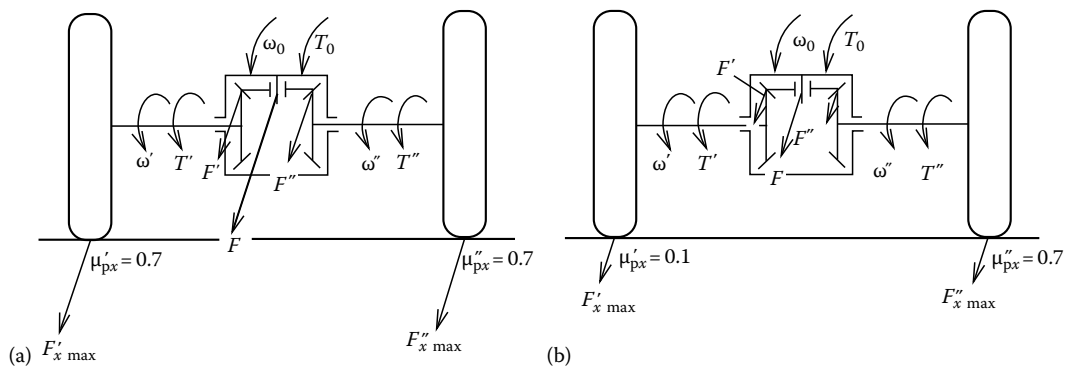


FIGURE 2.7
A driving axle with an open symmetrical bevel-gear differential. (a) Wheels rolling under the same road conditions; (b) wheels rolling under different road conditions.

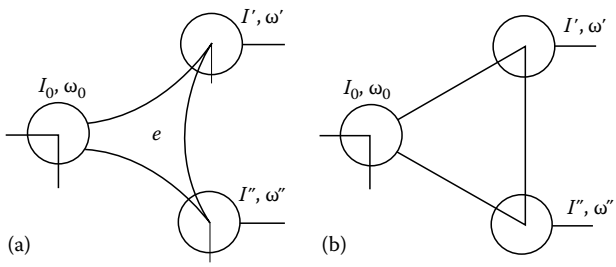


FIGURE 2.8
Dynamic diagrams of differentials: (a) compliant; (b) rigid.

The analysis of dynamics of differentials is continued. In problems of dynamics, calculation and assessment of the loading of driveline systems, consideration must be given to the inertia and elasticity of the components. Consider a mathematical model that describes the dynamics of a differential with allowance for the above factors. To obtain the needed formulae it is first necessary to compile the dynamic model of the differential. Dynamic systems comprise rotating lump masses connected by compliant or rigid inertia-less elements. Friction and reactive links associated with the vehicle's frame may be inserted into dynamic models. The form of a dynamic model of a differential depends on whether the compliance of the components is incorporated in it or the differential is regarded as perfectly rigid. In practical calculations, the differential can be regarded as rigid, since the stiffness of the gears and of other components is much greater than that of the shafts in the vehicle's driveline system. Figure 2.8 shows dynamic models of an open differential with and without allowance for compliances of its components.

Graphically, the dynamic diagrams look similar for symmetrical and asymmetrical models. The difference relates to determining the diagrams' parameters. The three rotating masses in Figure 2.8 correspond to a differential housing with a carrier and two output side gears; the planetary gears are regarded as inertia-less, and there is no friction. The speeds of rotation of the three masses may be different, for which reason the parameters of the dynamic models are reduced to the same shaft, i.e., to the same angular velocity. This reduction should be carried out by maintaining equality of the kinetic energies of the original and of the reduced mass, equality of the potential energies of deflections of the original and reduced compliant links and, finally, their scattering energies (dissipative functions) on the original and reduced link. The values of reduced parameters for the dynamic model of a differential in Figure 2.8 are defined as follows:
moments of inertia

$$I_* = \frac{I}{i^2} \tag{2.32}$$

angular velocity

$$\omega_* = \omega i \tag{2.33}$$

compliance

$$e_* = ei^2 \tag{2.34}$$

where i is the velocity ratio from the axis of reduction to the axis of the link being reduced; I, e, and ω are the eigenvalues of the moment of inertia, compliance and angular velocity of the link being reduced. Using formulae (2.32) through (2.34) the parameters reduced to the differential's housing (see Figure 2.8) are defined as

$I_0 = I_{0*}$—moment of inertia of the differential's housing and its associated carrier

$I''_* = \dfrac{I''}{(i'_{0''})^2}$ and $I'_* = \dfrac{I'}{(i''_{0'})^2}$ are moments of inertia of the output side gears, reduced to the differential's housing

$e_* = \dfrac{e_c}{a} + e_{''}(i'_{0'})^2 + e_{'}(i''_{0'})^2$ is total compliance

$\omega_{0*} = \omega_0$; $\omega'_* = \omega' i''_{0'}$; $\omega''_* = \omega''_* i'_{0''}$ are the angular velocities of the three links of the differential reduced to the housing

In these expressions e_c is the compliance of the pinion, a is the number of such gears and e'' and e' are the compliances of the teeth of the side gears.

The reduced torques are determined by equating the works of the reduced and original torques:

$$T_* = T/i \tag{2.35}$$

where T is the original (real) torque and T_* is the reduced torque. Using formula (2.35), the torque at the output shafts of the differential, reduced to its housing, are given by the expressions

$$\begin{aligned} T'_* &= T'/i''_{0'} \\ T''_* &= T''/i'_{0''} \end{aligned} \tag{2.36}$$

The compliance of the differential's components produces in it an elastic internal torque T_{int}, which in the computational model is applied to the differential's housing.

Velocity ratios $i''_{0'}$ and $i'_{0''}$ are defined by formulae (2.6) and (2.7). The numerical values of $i''_{0'}$ and $i'_{0''}$ are determined from formulae (2.9) and (2.10). For example, for an open symmetrical differential

$$i''_{0'} = i'_{0''} = 0.5$$

and for an open asymmetrical differential,

$$i''_{0'} = \frac{1}{1+u_d}; \quad i'_{0''} = \frac{u_d}{1+u_d}$$

With consideration of the rules above for reducing the equations of rotational motion of masses of a compliant differential shown schematically in Figure 2.8a, these expressions are

$$\begin{aligned} I_0\dot{\omega}_0 &= T_0 - T_{\text{int}} \\ I'\dot{\omega}' &= (i''_{0'})T_{\text{int}} - T' \\ I''\dot{\omega}'' &= (i'_{0''})T_{\text{int}} - T'' \\ e\dot{T}_{\text{int}} &= \omega_0 - i''_{0'}\omega' - i'_{0''}\omega'' \end{aligned} \tag{2.37}$$

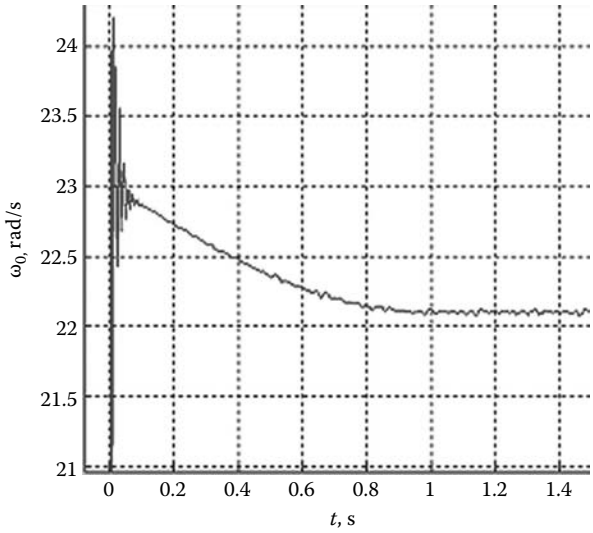


FIGURE 2.9
Angular velocity ω_0 of a truck's differential.

where T_0, T', and T'' are the torques applied to the links of the differential; here T_0 is the active torque, whereas T' and T'' are resistance torques.

Figure 2.9 shows an example of calculating the angular velocity ω_0 of the housing of an interwheel differential of a 4×2 truck upon an abrupt throw of the main clutch pedal and different gripping conditions of the driving wheels.

Mathematical models of differentials are also capable of including factors such as, for example, a change in the thickness and properties of the grease film in the teeth contacts, flows of lubricant oil inside the differential's housing, etc. The detailing level of the differential's model depends on the problem that has to be solved.

2.2 Kinematics of a Vehicle with an Interaxle Differential

As a part of the design and research of all-wheel drive vehicles, it becomes necessary to determine the relative angular velocities of the elements of the differential drive and the linear velocities of characteristic points of the vehicle. These problems are examined for the case of vehicles with two driving axles coupled by an interaxle open differential. The interwheel differentials of both axles are also open.

2.2.1 Vehicle with Front-Steered Wheels

The gear ratios of the driving axles are taken to be unity. This condition does not affect the course of study and its conclusions. The motion takes place on a straight horizontal surface. The wheels are subject to identical road conditions and the wheels themselves are identically the same.

On the above assumptions in straight-line motion, the angular velocity of the wheels, of the housings of interwheel differentials and drive shafts of the axles are the same and equal

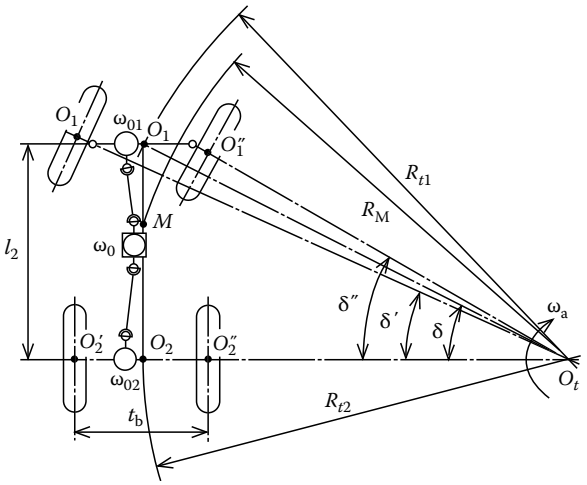


FIGURE 2.10
Vehicle with front-steered wheels taking a turn.

to the angular velocity ω_0 of the interaxle differential. The linear velocities V_a of the centers of wheels and axles are the same and equal to the speed at which the vehicle moves

$$V_a = \omega_0 r_w \tag{2.38}$$

where
r_w is the rolling radius that is assumed to be the same for all the wheels
ω_0 is the angular velocity of the interwheel differentials (the same for the front and rear differentials)

When the vehicle turns (Figure 2.10), it rotates about the turn center O_t at angular velocity ω_a. Then the linear velocities of points O_1 and O_2 can be defined as

$$\begin{aligned} V_{a1} &= \omega_a R_{t1} \\ V_{a2} &= \omega_a R_{t2} \end{aligned} \tag{2.39}$$

On the other hand, these velocities can be defined as the products of the angular velocities of the interwheel differentials, ω_{01} and ω_{02}, and the radius r_w

$$\begin{aligned} V_{a1} &= \omega_{01} r_w \\ V_{a2} &= \omega_{02} r_w \end{aligned} \tag{2.40}$$

The right-hand sides of formulae (2.39) and (2.40) are equated to one another

$$\begin{aligned} \omega_{01} r_w &= \omega_a R_{t1} \\ \omega_{02} r_w &= \omega_a R_{t2} \end{aligned} \tag{2.41}$$

and one of expression (2.41) is divided by the other:

$$\frac{\omega_{02}}{\omega_{01}} = \cos\delta \tag{2.42}$$

It is seen from expression (2.42) that the ratio of the angular velocities of the housings of the interwheel differentials is independent of the wheelbase, the wheel track, and other parameters and is hence valid for any vehicle with a design such as in Figure 2.10.

Assuming that the vehicle uses an asymmetrical interaxle differential with gear ratio u_d, it is possible to find the values of the angular velocities ω_{01} and ω_{02}. For this, it is necessary to solve simultaneously formulae (2.9) and (2.42) since the relationship between ω_{01} and ω_{02} should satisfy simultaneously both equations:

$$\frac{\omega_{01}}{\omega_0} = \frac{1+u_d}{1+u_d\cos\delta} > 1; \quad \frac{\omega_{02}}{\omega_0} = \frac{1+u_d}{u_d+1/\cos\delta} < 1 \tag{2.43}$$

These expressions show that when a differential drive is used, the linear velocities of the centers of the driving axles change, when taking a turn, relative to the rectilinear velocity. This is because the angular velocity ω_{02} of the center of the rear axle decreases ($\omega_{02} < \omega_0$) and that of the front axle increases ($\omega_{01} > \omega_0$). Here the value of ω_{01} moves away from that of ω_0, whereas that of ω_{02} comes closer to the value of ω_0, when the gear ratio u_d increases. When u_d decreases, the value of ω_{01} approaches whereas that of ω_{02} moves away from the value of ω_0. The absolute values of $\omega_{01}(V_{a1})$ and $\omega_{02}(V_{a2})$ increase and decrease with u_d.

It is of interest to determine the limiting values of ω_{01} and ω_{02} as u_d varies from zero to infinity. Resolving the indefiniteness in formulae (2.43), it is found that

$$\begin{aligned}\omega_{01} &= \omega_0\frac{1+u_d}{1+u_d\cos\delta} = \frac{\omega_0}{\cos\delta}\\ \omega_{02} &= \omega_0\frac{1+u_d}{u_d+1/\cos\delta} = \omega_0\end{aligned} \tag{2.44}$$

at $u_d \to \infty$.

It is seen from formulae (2.44) that at $u_d = \infty$, ω_{01}, and ω_{02} attain their highest possible values. This case corresponds to the motion of a vehicle with a single rear-driving axle.

Similarly,

$$\begin{aligned}\omega_{01} &= \omega_0\frac{1+u_d}{1+u_d\cos\delta} = \omega_0;\\ \omega_{02} &= \omega_0\frac{1+u_d}{u_d+1/\cos\delta} = \omega_0\cos\delta\end{aligned} \tag{2.45}$$

at $u_d \to 0$.

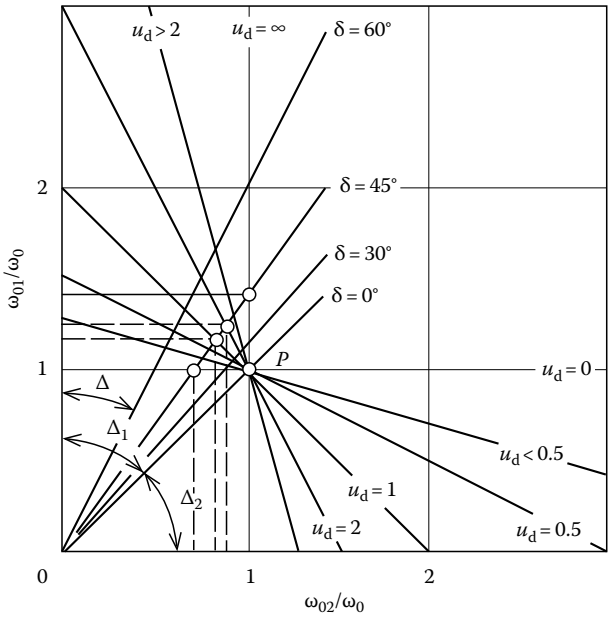


FIGURE 2.11
Relationship between ω_{01} and ω_{02} of the front and rear differentials.

It is seen from formulae (2.45) that the smallest possible values of ω_{01} and ω_{02} are attained at $u_d = 0$. This case corresponds to the motion of a vehicle with a single front driving–steered axle.

Figure 2.11 is a plot of the behavior of ω_{01} and ω_{02} for different values of the angle δ in the form of a bundle of straight line, passing through the coordinate origin. These curves were constructed using the expression

$$\frac{\omega_{02}}{\omega_{01}} = \cos\delta = \tan\Delta \tag{2.46}$$

where $\tan\Delta$ is an artificially introduced auxiliary function.

Point P is known as the scale point, corresponding to rectilinear motion of the vehicle when $\omega_{01} = \omega_{02} = \omega_0$ (irrespective of the value of u_d). The points of interaction of the bundles of straight lines from formulae (2.9) and (2.42) yield specific values of ω_{01} and ω_{02} at known u_d and δ. Figure 2.11 graphically reflects the conclusions drawn when analyzing formulae (2.43). For example, at $u_d = 2$ and $\delta = 45°$, $\omega_{01} = 1.24\omega_0$, whereas $\omega_{02} = 0.88\omega_0$. In the limit of $u_d = \infty$ the angular velocities are equal to $\omega_{01} = 1.41\omega_0$ and $\omega_{02} = \omega_0$. In the case of $u_d = 0$, it is found that $\omega_{01} = \omega_0$ and $\omega_{02} = 0.71\omega_0$. This means that ω_{01} increases with δ, whereas ω_{02} decreases. If it is assumed that $\delta = 90°$ (a hypothetical case), then $\omega_{02} = 0$, i.e., the turn center O_t coincides with center O_2 of the rear axle in Figure 2.10.

The above relationships for 4×4 vehicles with front-steered axle lie within the angle Δ_1. The same analysis can be performed for 4×4 vehicles with rear-steered and front-nonsteered driving axles. The corresponding curves for such a vehicle arrangement lie within the limits of angle Δ_2.

Since the linear velocity of point O_1 in Figure 2.10 increases as the vehicle turns, whereas that of O_2 decreases, then there obviously exists on the longitudinal axis of the vehicle a point M, the linear velocity of which does not change in the course of the turn and is always equal to the rectilinear velocity of the vehicle (upon unchanged ω_0). The variation of the

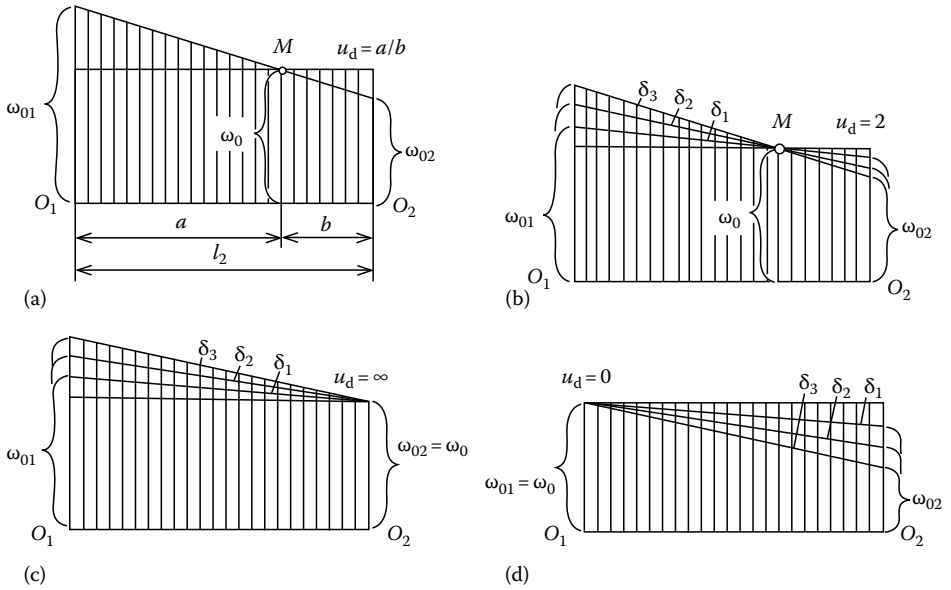


FIGURE 2.12
Plot of velocities of points on the longitudinal axis of a vehicle taking a turn.

linear and angular velocities of points O_1 and O_2 is linear, since the rolling radii of the front and rear axles were taken to be the same. It is hence possible to construct a diagram of the linear velocities of all points of the vehicle's longitudinal axis on the basis of two points (Figure 2.12a). The vectors of linear velocities are represented by angular velocities that are directly proportional to the former.

Find the ratio between segments a and b. It is found from similitude of the triangles in Figure 2.12a that

$$\frac{a}{b} = \frac{\omega_{01} - \omega_0}{\omega_0 - \omega_{02}} \tag{2.47}$$

Substitution into this expression of values of ω_{01} and ω_{02} from formulae (2.43) and regrouping, yields

$$\frac{a}{b} = u_d \tag{2.48}$$

It follows from formula (2.48) that the location of point M is independent of δ and on the vehicle dimensions. Its location is constant for a given vehicle and depends only on the gear ratio u_d of the interaxle differential. When this differential is symmetrical, $a = b$.

In designing interaxle differentials for road vehicles, the gear ratio u_d may be selected in proportion to the distribution of weight between the driving axles (for vehicles that operate more frequently on deformable surfaces different recommendations shall be examined in Section 2.9). In the case examined here, the vertical line passing through point M also passes through the vehicle's center of gravity:

$$u_d = \frac{a}{b} = \frac{W_2}{W_1} \tag{2.49}$$

where W_1 and W_2 are the weight loads on the front and on the rear axle. Under actual conditions, it is difficult to attain equality (2.49), since the gear ratio u_d in the interaxle differential is not always identical to the distribution of weights between the axles. The fact that the center of gravity of the vehicle coincides with point M is a positive factor that stabilizes the vehicle's load mode and, in the first place, the engine load. If this coincidence does not exist, then the center of gravity will decelerate or accelerate when taking a turn, i.e., there shall arise transient, unstable modes of motion and loads.

Figure 2.12b is a diagram of the velocities of points of the vehicle's axis for different values of angle δ of the steered wheels, whereas Figure 2.12c and d present diagrams of velocities when only the rear driving axle operates ($u_d = \infty$, Figure 2.12c) and when only one front driving wheel operates ($u_d = 0$, Figure 2.12d). At $u_d = \infty$ point M coincides with point O_2 whereas at $u_d = 0$—with point O_1 (see the location of points O_1 and O_2 in Figures 2.10 and 2.12).

2.2.2 Vehicle with Front- and Rear-Steered Wheels

The kinematics of a 4×4 vehicle with an interaxle differential and two-steered axles is the most general case. The kinematics of a vehicle with one front or one rear-steered axle is a particular case. The relationships between ω_{01} and ω_{02} are now clarified for the case of all-steered wheels (Figure 2.13).

The linear velocities V_{a1} and V_{a2} of points O_1 and O_2 and the corresponding angular velocities ω_{01} and ω_{02} are proportional to the radii of rotation about point O_t:

$$\frac{V_{a1}}{V_{a2}} = \frac{\omega_{01} r_w}{\omega_{02} r_w} = \frac{\omega_{01}}{\omega_{02}} = \frac{R_{t1}}{R_{t2}} = \frac{\cos \delta_2}{\cos \delta_1} \tag{2.50}$$

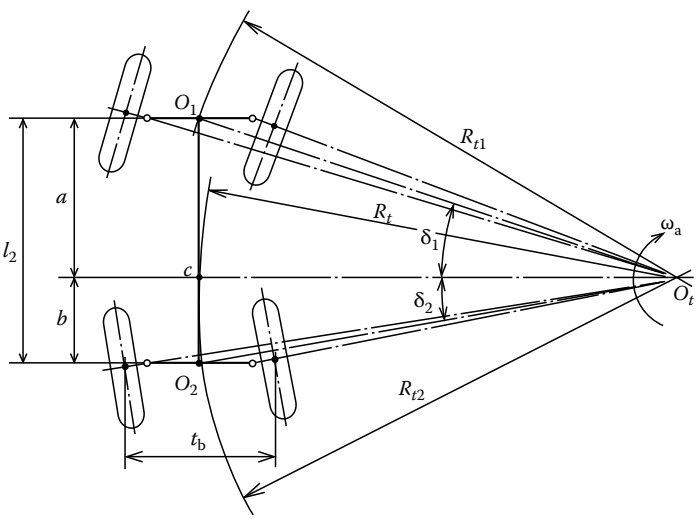


FIGURE 2.13
Vehicle with front and rear-steered wheels taking a turn.

whence

$$\omega_{01} = \omega_{02}\frac{\cos\delta_2}{\cos\delta_1}; \quad \omega_{02} = \omega_{01}\frac{\cos\delta_1}{\cos\delta_2} \tag{2.51}$$

Solution of these formulae together with formula (2.9) yields the values of ω_{01} and ω_{02} as a function of δ_1 and δ_2, u_d and ω_0:

$$\omega_{01} = \omega_0\frac{1+u_d}{1+u_d\frac{\cos\delta_1}{\cos\delta_2}}; \quad \omega_{02} = \omega_0\frac{1+u_d}{u_d+\frac{\cos\delta_2}{\cos\delta_1}} \tag{2.52}$$

Angles δ_1 and δ_2 are interrelated by an expression determined by the ratio of a to b and provided by the steering system,

$$K_l = \frac{b}{a} = \frac{\tan\delta_2}{\tan\delta_1} \tag{2.53}$$

or

$$\tan\delta_2 = K_l\tan\delta_1 \tag{2.54}$$

whence

$$\delta_2 = \arctan(K_l\tan\delta_1) \tag{2.55}$$

For this reason, when u_d and ω_0 are known the values of ω_{01} and ω_{02} are determined on the basis of the value of δ_1. Assuming that

$$\frac{\cos\delta_1}{\cos\delta_2} = \frac{\omega_{02}}{\omega_{01}} = \tan\beta \tag{2.56}$$

it is possible to plot the behavior of ω_{01} and ω_{02} for different values of δ_1 at a given specific value of K_l. For each value of K_l the above variation in ω_{01} and ω_{02} lies within some angle β (Figure 2.14).

At $K_l < 1$ the curves are located in the top half of the first quadrant, at $K_l > 1$ they are located in its bottom half. The closer K_l is to unity, the smaller is the angle β. At $K_l = 1$ ω_{01} and ω_{02} are equal to one another for any value of δ_1 and their behavior is defined by the straight line that divides the angle of the first quadrant into halves.

To obtain particular values of ω_{01} and ω_{02} as a function of ω_0 of a vehicle with known K_l, a bundle of straight lines based on formula (2.9) must be superimposed on the graph with a bundle of straight lines constructed from formula (2.56), similar to the manner that this was done in Figure 2.11. The points of intersection of the straight lines of these two bundles will then provide the specific values of ω_{01} and ω_{02}.

The analytic and graphic relationships and their associated methods descried above can be used in analyzing vehicles with a large number of differential-driven axles, i.e., for type 6×6, 8×8, etc., vehicles. This will yield the necessary formulae and graphs.

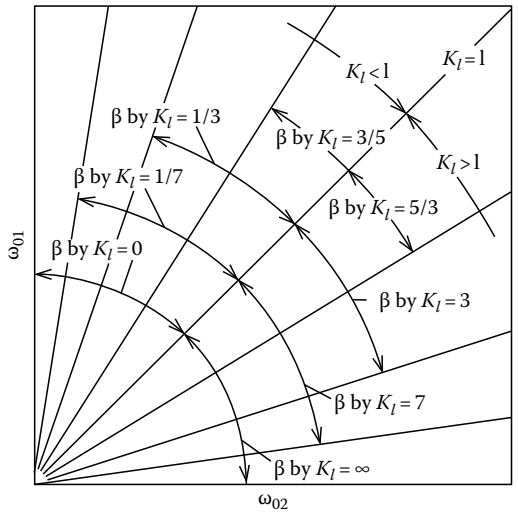


FIGURE 2.14
Angular velocities ω_{01} and ω_{02} of the front and rear differentials.

2.3 Tooth Forces in Bevel-Gear Differentials

Experimental studies and experience in operating differentials show that in certain cases their components exhibit elevated wear and interference. Cases were observed of partial or complete wearing away and vanishing of thrust washers located between a side gear and the differential's housing. These defects arose at moderate design pressures. It is obvious that one of the causes of this is the presence of significant internal forces in the differentials that were not incorporated in the calculations and, in fact exceed the design values. This section presents a detailed analysis of previously unknown forces and, on this basis, gives recommendations on the desired combinations of the number z_g of teeth of the side gears and z_c of the pinions in order to reduce the actual forces that act in differentials.

2.3.1 Axial Forces in a Pinion-Side Gear Mesh

Forces acting inside the bevel-gear differentials are determined by the forces that arise in the meshing of pinions and side gears. In particular, forces acting on the friction surface of the housing, thrust washers and side gears are composed of axial forces of individual meshings between the pinions and side gears. Hence, the discussion will be started by analyzing a method for determining the axial forces in the meshing of one pinion and one side gear.

Figure 2.15 shows a single pair of gears with spur bevel teeth—a pinion and a side gear. Section $A - A$ (at the left above) shows the location a of point A of contact between the tooth profiles on the pressure line B_1B_2 and the pitch point P that does not move and lies on the intersection of the line of centers O_1O_2 and the line B_1B_2. Section $A - A$ (at the right below) shows a diagram of forces exerted by the pinion on the side gear. Such a force diagram is standard in the theory of mechanisms and machines for the analysis of forces.

When calculating these forces, the force exerted by the pinion on the side gear is replaced by the force R acting at the pitch point in the direction of the pressure line (see Figure 2.15). This means that the force diagram does not account for both the movement of the point of

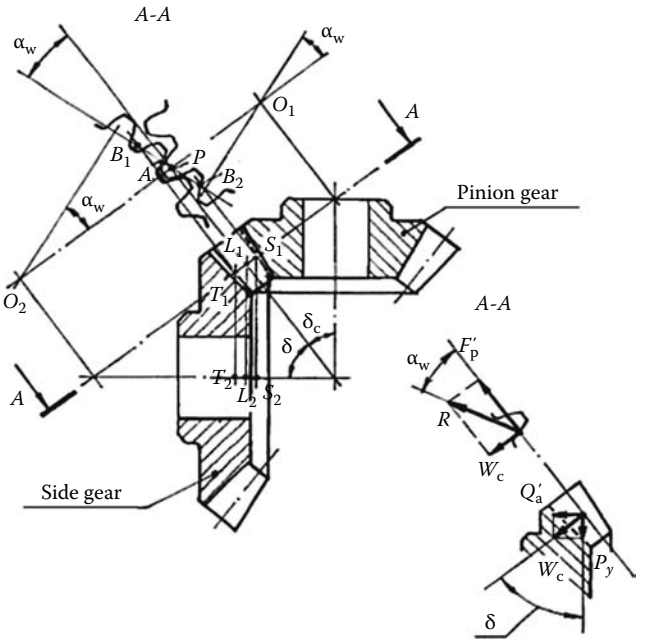


FIGURE 2.15
Schematic of a single pair of mating bevel gears.

contact along the pressure line and for friction in the mating gear teeth. As follows from Figure 2.15, the resultant force R is usually broken up into two components F'_p and W_c. Component F'_p acting on arm $L_1L_2 = r_g$ creates a torque that must be applied to drive the gear. In turn, force W_c can be resolved into the radial P_y and axial Q'_a components, respectively. The axial component Q'_a is supported by the differential's housing (usually, through a thrust washer). If this force is excessive, it can result in ''eating that thrust washer away'' and can cause some wear of the differential case half. The axial force is usually given as follows (see Figure 2.15):

$$Q'_a = F'_p \tan\alpha_w \cos\delta_c \tag{2.57}$$

If the pair of gears in Figure 2.15 belongs to a four-pinion bevel differential, the axial force is usually expressed as

$$Q'_a = \frac{T_0}{(4)(2)r_g} \tan\alpha_w \cos\delta_c = \frac{T_0}{8r_g} \tan\alpha_w \cos\delta_c \tag{2.58}$$

here, (4) stands for four pinions and (2) means that every pinion is engaged with two side gears. In case of a two-pinion differential, the above formula becomes

$$Q'_a = \frac{T_0}{4r_g} \tan\alpha_w \cos\delta_c \tag{2.59}$$

It follows from formulae (2.57), (2.58), and (2.59) that the axial force Q'_a is constant (if torque T_0 applied to the differential's housing is fixed), and this force does not depend on friction in the mating tooth profiles or on the motion of the point of contact along the pressure line.

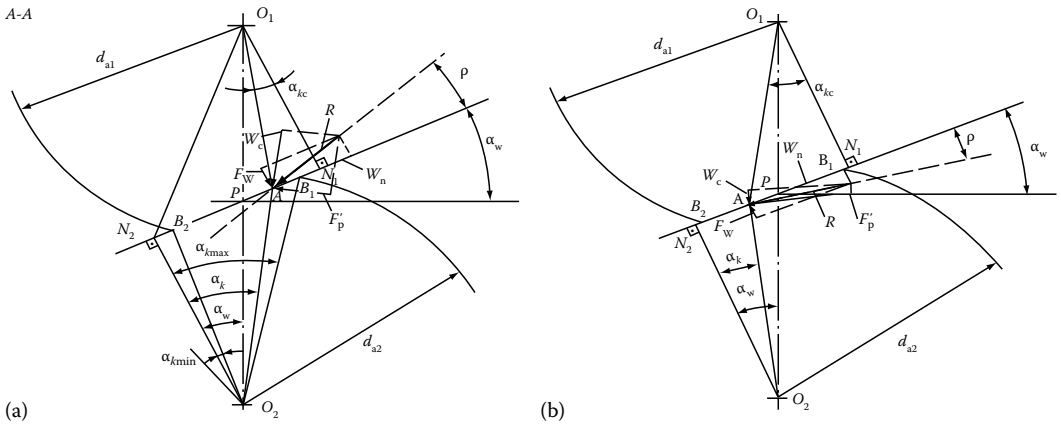


FIGURE 2.16
Schematic of forces in a pair of spur mating gears equivalent to bevel gears: (a) the point of contact is on PB_1; (b) the point of contact on PB_2.

A new approach, which takes these facts into account, is now considered. Figure 2.16 shows forces acting in the mating of spur gears.

Point of contact A moves along the line of action: contact begins at point B_1 and ends at B_2. Vector R fails to the line B_1B_2 by the angle ρ due to the influence of friction force F_w. These spur gears may be regarded as being equivalent to the bevel gears, shown in Figure 2.15.

The situation considered here is that of the load in a bevel gearing being transferred by a pair of tooth profiles. This is true because the contact ratio factor in differential gears is usually close to one.

It follows from Figure 2.16 that

$$W_c = F'_p \tan(\alpha_k \pm \rho) \tag{2.60}$$

here the plus and minus in ''±'' correspond to $\alpha_k > \alpha_w$ (Figure 2.16a) and $\alpha_k < \alpha_w$ (Figure 2.16b), respectively. As seen from Figure 2.16, line of force F'_p forms with line O_1O_2 an angle that is not equal to 90°. Therefore, the torque applied to the side gear is created not by the entire force F'_p, but by its component that crosses O_1O_2 and intersects the axis of the side gear at a right angle. The second component of F'_p reduces the axial force acting on the side gear. This reduction of the axial force can be neglected if it is to connect the side gear torque with the force F'_p instead of the component that crosses O_1O_2 and intersects the axis of the side gear at a right angle. Thus, there will be no error in making this assumption and hence,

$$W_c = F'_p \tan(\alpha_k \pm \rho) = \frac{T_0}{8r_{gt}} \tan(\alpha_k \pm \rho) \tag{2.61}$$

here size of the arm r_{gt} ranges between T_1T_2 and S_1S_2 (see Figure 2.15).

To determine the size of arm r_{gt}, the straight-line segments O_2N_2, O_2P, and AP from Figures 2.15 and 2.16b can be written as the expansions (when $\alpha_k < \alpha_w$)

$$\begin{aligned} O_2N_2 &= O_2P\cos\alpha_w, \\ O_2P &= \frac{r_g}{\sin\delta_c} \end{aligned} \tag{2.62}$$

and

$$AP = PN_2 - AN_2 = O_2P\sin\alpha_w - O_2N_2\tan\alpha_k = \frac{r_g(\sin\alpha_w - \cos\alpha_w\tan\alpha_k)}{\sin\delta_c} \tag{2.63}$$

The projection of AP onto line L_1L_2 is determined as

$$AP\sin\alpha_w\sin\delta_c = r_g\sin\alpha_w(\sin\alpha_w - \cos\alpha_w\tan\alpha_k) \tag{2.64}$$

On the basis of the above (at $\alpha_k < \alpha_w$)

$$r_{gt} = r_g - AP\sin\alpha_w\sin\delta_c = r_g[1 - \sin\alpha_w(\sin\alpha_w - \cos\alpha_w\tan\alpha_k)] \tag{2.65}$$

In general, when the pinion and side gear-tooth profiles run from the initial point B_1 in Figures 2.15 and 2.16 (contact begins at this point) to the final point, B_2 (contact ends at this point), values of r_{gt} are determined from the formula

$$r_{gt} = r_g[1 \pm \sin\alpha_w(\pm\cos\alpha_w\tan\alpha_k \mp \sin\alpha_k)] \tag{2.66}$$

Using formulae (2.61) and (2.66) and referring to Figures 2.15 and 2.16, the axial force applied to the side gear a differential gear by the pinion, is described by the formula
for a four-pinion differential

$$Q'_a = \frac{T_0}{8r_g}\frac{\tan(\alpha_k \pm \rho)\cos\delta_c}{[1 \pm \sin\alpha_w(\pm\cos\alpha_w\ \tan\alpha_k \mp \sin\alpha_w)]} \tag{2.67}$$

for a two-pinion differential

$$Q'_a = \frac{T_0}{4r_g}\frac{\tan(\alpha_k \pm \rho)\cos\delta_c}{[1 \pm \sin\alpha_w(\pm\cos\alpha_w\tan\alpha_k \mp \sin\alpha_w)]} \tag{2.68}$$

Formulae (2.67) and (2.68) have the same form as formulae (2.58) and (2.59) if $\alpha_k = \alpha_w$ and $\rho = 0$. Computations using formulae (2.67) and (2.68) require knowing the values of friction angle ρ (or of the friction coefficient, μ). The friction coefficient usually varies from 0.04 to 0.08 depending on the pressure in the tooth profiles, on the relative sliding speed of these profiles and on the type of oil. The computations were performed on the assumption that $\mu = 0.06$ ($\rho = 3.43°$).

As follows from formulae (2.67) and (2.68), even if friction is not taken into consideration, the axial force Q'_{a} is variable due to the variation in angle α_k from $\alpha_{k\max}$ (at the time of teeth engagement) to $\alpha_{k\min}$ (disengagement). The extreme values of the angle α_k are now determined by applying the sine theorem to triangle O_2PB_1, so that it can be written (see Figure 2.16a)

$$\frac{0.5d_{\mathrm{a}2}}{\sin(\pi+\alpha_{\mathrm{w}})}=\frac{PO_2}{\sin(180^\circ-90^\circ-\alpha_{\mathrm{w}}-\angle PO_2B_1)}$$

or

$$\frac{0.5d_{\mathrm{a}2}}{\cos\alpha_{\mathrm{w}}}=\frac{PO_2}{\cos(\alpha_{\mathrm{w}}+\angle PO_2B_1)} \tag{2.69}$$

Referring to Figure 2.16a, it can be written as

$$\alpha_{k\max}=\alpha_{\mathrm{w}}+\angle PO_2B_1 \tag{2.70}$$

Next taking into account formulae (2.62), (2.69) and (2.70) the angle

$$\alpha_{k\max}=\arccos\left(\frac{2r_{\mathrm{g}}\cos\alpha_{\mathrm{w}}}{d_{\mathrm{a}2}\sin\delta_{\mathrm{c}}}\right) \tag{2.71}$$

The diameter $d_{\mathrm{a}2}$ of the addendum circle is

$$d_{\mathrm{a}2}=m(z_{\mathrm{gr}}+2+2x-2y_\Delta)=\left(m_{\mathrm{te}}-\frac{b}{\sqrt{z_{\mathrm{g}}^2+z_{\mathrm{c}}^2}}\right)\left(\frac{z_{\mathrm{g}}}{\sin\delta_{\mathrm{c}}}+2+2x-2y_\Delta\right) \tag{2.72}$$

where

m and z_{gr} are the module and the tooth number of the spur gear in Figure 2.16 that is equivalent to the side gear in Figure 2.15
m_{te} is the outer module of bevel gears
b is the tooth width
x is the coefficient of initial contour displacement
y_Δ is the perceptible displacement coefficient

The coefficient y_Δ is equal to zero when high-altitude tooth correction is used. This correction is usually applied in bevel-gear differentials in which displacements of the involute rack for the pinion and the side gear are equal in magnitude and opposite in sign.

Substituting (2.72) into (2.71), a formula is obtained for computing the maximum value of $\alpha_{k\max}$:

$$a_{k\max}=\arccos\left\{\frac{r_{\mathrm{g}}\cos\alpha_{\mathrm{w}}}{\left(m_{\mathrm{te}}-\frac{b}{\sqrt{z_{\mathrm{g}}^2+z_{\mathrm{c}}^2}}\right)[0.5z_{\mathrm{g}}+(1-x-y_\Delta)\sin\delta_{\mathrm{c}}]}\right\} \tag{2.73}$$

A formula for computing the minimal value of α_k can be obtained by analogy in the form

$$a_{k\min} = \arccos\left\{ \frac{r_g \cos\alpha_w}{\left(m_{te} - \frac{b}{\sqrt{z_g^2+z_c^2}}\right)[0.5z_g - (1-x)\sin\delta_c]} \right\} \tag{2.74}$$

Formulae (2.73) and (2.74) set limits on the angle α_k when formulae (2.67) and (2.68) are used to calculate the axial forces Q'_a.

A functional relationship between angles α_k and α_{kc} from Figure 2.16 and the pinion rotation angle v_c must be derived to describe the axial force's change when the pinion rotates about its axis.

According to Figure 2.16 the straight-line segment AN_1 is

$$AN_1 = O_1N_1 tg\alpha_{kc}$$

or

$$AN_1 = PN_1 + PA = PN_1 + (N_2P - N_2A) = O_1N_1\tan\alpha_w + O_2N_2\tan\alpha_w - O_2N_2\tan\alpha_k$$

Equating the right-hand parts of these expressions to one another yields the expansion

$$\tan\alpha_{kc} = \tan\alpha_w\left(1 + \frac{O_2N_2}{O_1N_1}\right) - \frac{O_2N_2\tan\alpha_k}{O_1N_1} \tag{2.75}$$

Using formulae (2.62), expression (2.75) can be transformed to

$$\alpha_{kc} = \arctan[(1 + \mathrm{ctan}^2\delta_c)\tan\alpha_w - \mathrm{ctan}^2\delta_c\tan\alpha_k]$$

or

$$\alpha_k = \arctan[(1 + \tan^2\delta_c)\tan\alpha_w - \tan^2\delta_c\tan\alpha_{kc}] \tag{2.76}$$

It was assumed that angle v_c is equal to zero when point of contact A is situated in the pitch point P (see Figure 2.16). This means that $v_c = 0$ if $\alpha_{kc} = \alpha_w$. During the recession phase, when $\alpha_{kc} > \alpha_w$, contact occurs along the line PB_2 (again, see Figure 2.16b, point of contact A belongs to PB_2), and angle v_c follows from Figure 2.17

$$v_c = \alpha_{kc} - \alpha_w - \theta_0 + \theta_1$$

It is known that

$$\theta_0 = \mathrm{inv}\alpha_w = \tan\alpha_w - \alpha_w$$
$$\theta_1 = \mathrm{inv}\alpha_{kc} = \tan\alpha_{kc} - \alpha_{kc}$$

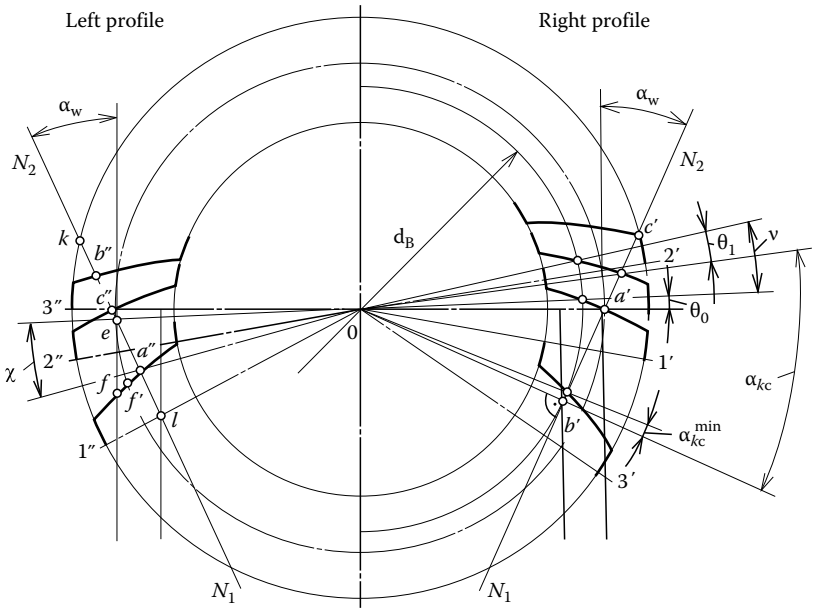


FIGURE 2.17
Schematic of a pinion with an even tooth number.

then

$$v_c = \tan\alpha_{kc} - \tan\alpha_w \quad \text{or} \quad \alpha_{kc} = \arctan(\tan\alpha_w + v_c) \tag{2.77}$$

Similarly, when $\alpha_{kc} < \alpha_w$

$$v_c = \tan\alpha_w - \tan\alpha_{kc} \quad \text{or} \quad \alpha_{kc} = \arctan(\tan\alpha_w - v_c) \tag{2.78}$$

The specific axial force $(8r_g/T_0)Q'_a$, calculated on the basis of formulae (2.67), (2.73), (2.74), and (2.76) through (2.78), is plotted in Figure 2.18 as a function of the angles v_c, α_k and α_{kc} (solid curve 1 represents $\rho = 3.43°$). The curve 2 conforms to results of calculations using those formulae when $\rho = 0$. The dashed line 3 reflects the results calculated from formula (2.58). Due to variation in angle α_k (when $\rho = 0$), the maximum value of the axial force exceeds its minimal value by a factor 1.64 and exceeds the value calculated by formula (2.58) by 1.34. If friction is taken into account ($\rho = 3.43°$), these force increments are more substantial amounting to 2.67 and 1.56, respectively. The stepped shape of the solid curve shown in Figure 2.18 is attributable to the change in the direction of the friction force when the contact point A is passing the pitch point P where $\alpha_w = \alpha_k = \alpha_{kc}$, $\rho = 0$. Another reason for this is that new pairs of teeth draw closer to the approach phase of contact. Thus, when the pinion rotates through the full angle the number of steps in the axial force is equal to the tooth number of the pinion.

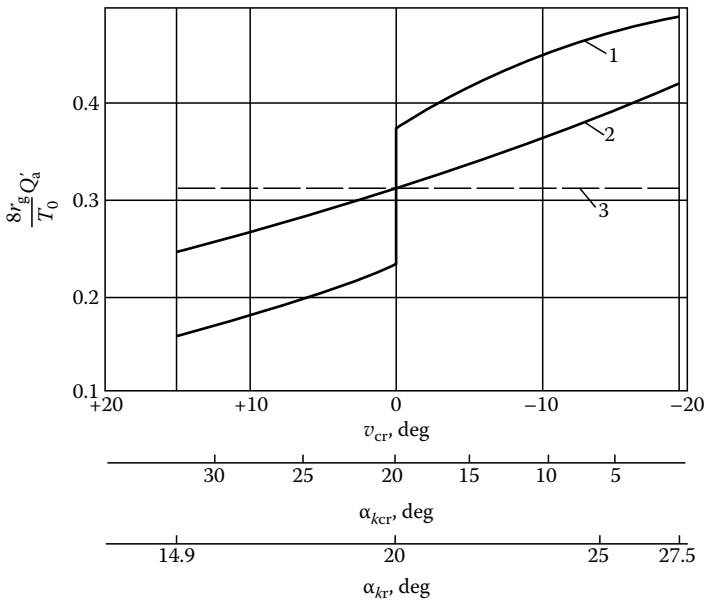


FIGURE 2.18
MTZ 102 tractor: specific axial force acting on a side gear from a pinion in rear axle differential.

2.3.2 Total Axial Forces in Bevel Differentials

The total axial forces that act on the left and right side gears are now determined:

$$Q_{ar} = \sum_{j=1}^{a} \left(Q'_{ar}\right)_j,$$
$$Q_{al} = \sum_{j=1}^{a} \left(Q'_{al}\right)_j \tag{2.79}$$

where a is the number of pinions; it is assumed here that $a = 2$ or 4 for two- or four-pinion differentials. Formulae (2.79) reflect the summation of all the axial forces exerted by the pinions on the side gears, but the axial force acting in one pinion side-gear set is not necessarily simply doubled (quadrupled). This is because the axial forces exerted by the pinions on the two side gears can be different at every moment. Indeed, the pairs of mating tooth profiles can have different locations on the pressure lines at the same point in time.

As our study has shown, tooth numbers of the side gear and the pinion determine the locations of all the mating tooth profiles on the lines of action. With reference to this statement, all bevel-gear differentials with two or four pinions have been classified into four groups, shown in Table 2.2.

As an illustration to Table 2.2, Figure 2.19 presents the developed forms of gear sets for four-pinion differentials in which two racks submit the side gears and the pinions are shown as bars. Similar forms for two-pinion differentials can be easily obtained by deleting two-pinions (for example, the first and the third ones beginning counting the pinions from whatever end).

Any bevel-gear differential will definitely fall into one of these four groups depending on the values of z_c and z_g/a. For example, a four-pinion differential with $z_c = 10$ and $z_g = 16$

TABLE 2.2

Four Groups of Bevel Gear Differentials

Group Number	z_c	z_g/a
I	Even number	Integer
II	Odd number	Integer
III	Odd number	Fractional number
IV	Even number	Fractional number

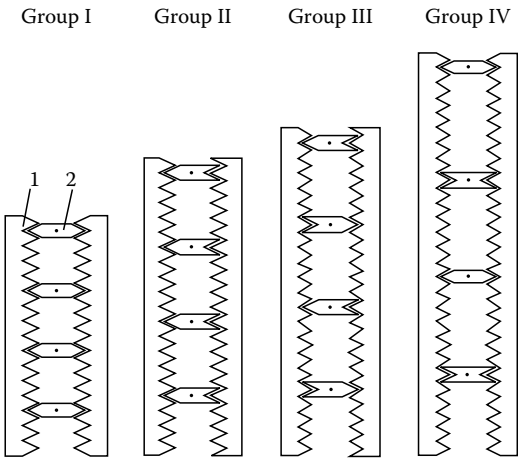


FIGURE 2.19
The only four possible forms of gear sets in four-pinion differentials: 1, side gear; 2, pinion.

belongs to Group I. A four-pinion differential with $z_c = 11$ and $z_g = 22$ belongs to Group III. A two-pinion differential with $z_c = 11$ and $z_g = 16$ belongs to Group II. As examples of a variety of differentials with different—but limited to four—combinations of tooth numbers, Table 2.3 presents data of 12 heavy-duty trucks.

Such a classification of bevel-gear differentials facilitates the analysis of the total axial forces acting on the side gears. An analysis of the forces was performed for differentials of each of the four groups. This has manifested and exhibited the complex behavior of total axial forces in toothed differential gearings. The essential results are presented below.

Group I. As seen from Figure 2.19, the total axial force that acts on one side gear can be determined by quadrupling (in four-pinion differentials) or by doubling (in two-pinion differentials) the axial force exerted by one pinion on one side gear. However, the magnitudes of the total axial forces acting on the left and right side gears are different at any point in time. This can be explained using Figure 2.17. When tooth profile 1′ of the pinion and a tooth profile of the right-side gear contact one another at point a′, the profile of the diametrically opposite tooth of the pinion is outside of the line of action. In this case, the load is transmitted to the left gear by tooth 1″, which has the angle

$$\alpha_k = \alpha_w - \chi$$

Therefore, angles α_{kr} and α_{kl} of the right and left side gears are different. Hence, the forces Q'_{ar} and Q'_{al} are also not equal to one another. This requires determining Q'_{al} and Q'_{ar}.

Assuming that triangle $a''eo$ is a right triangle, line segment ef can be found to be

$$ef = \pi m - S_{th} \tag{2.80}$$

TABLE 2.3

Tooth Numbers and Modules of Interwheel Differentials

Trucks	Number of Side Gear Teeth	Number of Pinion Teeth	Group Number	Outer Module
12-wheel trucks				
ZIL 130 B1	22	11	III	6.35
MAZ 200 B	22	11	III	8
MAZ 504 B	22	11	III	6
MAZ 5432	16	11	II	7
18-wheel trucks				
ZIL 133	22	11	III	6.35
KamAZ 54112	22	11	III	6.35
KrAZ 258	22	11	III	8
MAZ 64227	16	11	II	7
Scania 142H	18	11	III	7.75*
Volvo F12	16	9	II	8.25*
Mercedes-Benz 2232	16	10	I	5.75*
Renault R310T	16	11	II	7*

Note: *By measurement.

here S_{th} is the tooth thickness; $(\pi m - S_{th})$ is the width of the space. Application of the sine theorem to triangle $a''eo$ yields

$$a''e/\sin\chi = (0.5mz_{ce} - ef\sin\alpha_w)/\sin(0.5\pi - \alpha_w) \tag{2.81}$$

From formulae (2.80) and (2.81), the angle χ is as follows

$$\chi = \arcsin\left(\frac{(\pi m - S_{th})\cos^2\alpha_w}{0.5mz_{ce} - (\pi m - S_{th})\sin\alpha_w}\right) \tag{2.82}$$

It is seen from Figure 2.17 that angles v_{cr} and v_{cl} of the right and left pinion tooth profiles are different, but interdependent. The correlation between these angles is given in Table 2.4.

In Table 2.4, the angles v_{min} and v_{max} correspond to the angles $\alpha_{kc\,min}$ and $\alpha_{kc\,max}$ from formulae (2.73), (2.74), and (2.76). Using the data from Table 2.4 and formulae (2.67), (2.73), (2.74), and (2.76) through (2.78), it is possible to compute values of the axial forces exerted on the right and left side gears by one pinion.

The following also presents a graphical method for determining one of the above-mentioned axial forces if values of the other axial forces have been already computed using formula (2.67). When the right profile occupies position 1′ in Figure 2.17 and the ordinate of point a' in Figure 2.20a gives a value of the specific force $\left(\frac{8r_g}{T_0}\right)Q'_{ar}$, the specific force $\left(\frac{8r_g}{T_0}\right)Q'_{al}$ can be determined graphically.

This is done as follows: measure angle v_0 from point a' toward the right. Then draw in Figure 2.20 the vertical line e_1e_2 in such a manner as to provide for equality of the ordinates of points e_1 and e_2. The intersection of a vertical line drawn through point a', with a horizontal line segment drawn through point e_2, gives point a''. The ordinate of this

TABLE 2.4

Correlation between the Turn Angles of the Right and Left Profiles of the Pinion in Figure 2.17

v_r	**Right Pinion Tooth Profile: Position of the Point of Contact with the Right-Side Gear Profile**	v_l	**Right Pinion Tooth Profile: Position of the Point of Contact with the Left-Side Gear Profile**
0	At position a' (position 1′)	$v_l = v_0 = \tan\alpha_w - \tan(\alpha_w - \chi)$	At position a'' (position 1″)
$v_r < v_0$	On line $a'b'$	$v_l = v_0 - v_r$	On line $a''e$
$v_r = v_0$	On line $a'b'$	$v_l = 0$	At point e
$v_r > v_0$	On line $a'b'$	$v_l = v_r - v_0$	On line ke
$v_r = v_{min}$	At position b' (position 3′)	$v_l = v_{min} - v_0$	At position b'' (position 3″)
v_r	On line $a'c'$	$v_l = v_r + v_0 < v_{min}$	On line $a''b_2$
$v_r' > v_r'$	On line $a'c'$	$v_l = v_r' + v_0 = v_{min}$	At point b_2 (a new pair of teeth coming into contact)
$v_r'' > v_r'$	On line $a'c'$	$v_l = v_{max} - (v_r'' - v_r')$	On line ke
$v_r''' = v_{max}$	At position c' (position 2′)	$v_l = v_{max} - (v_{max} - v_r''')$	At position c'' (position 2″)

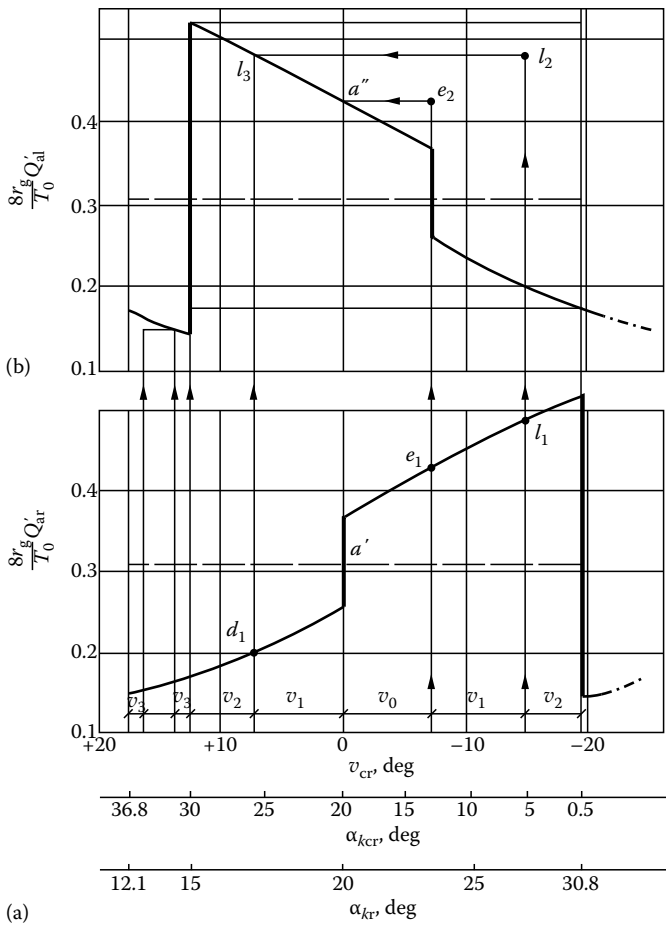


FIGURE 2.20
Front axle differential of MTZ 102 tractor (Group I): right (a) and left (b) specific axial forces. ——— by formula (2.67); —— —— by formula (2.58).

point is equal to the value of the specific force $\left(\frac{8r_g}{T_0}\right)Q'_{al}$ that acts on the left side gear when the right and left tooth profiles of the pinion are in position 1′ and 1″, respectively (see Figure 2.17). After moving the right pinion profile from 1′ and 2″, the magnitude of the force $\left(\frac{8r_g}{T_0}\right)Q'_{ar}$ is determined by the ordinate of point d_1 (see Figure 2.20a). In order to determine the magnitude of the specific force $\left(\frac{8r_g}{T_0}\right)Q'_{al}$ at this moment, the angle $(v_0 + v_1)$ is measured from point a' toward the right and then the vertical line segment l_1l_2 presents equal ordinates of points l_1 and l_2 in Figure 2.20a and b. Point l_3, the ordinate of which is equal to the magnitude of $\left(\frac{8r_g}{T_0}\right)Q'_{al}$, is obtained from the crossing of the horizontal and vertical line segments drawn through points l_2 and d_1, respectively. The other points, which belong to the stepped curve in Figure 2.20b, are obtained in a similar way. Finally, Figure 2.20a and b present specific forces exerted by one pinion on the right and left side gears. The total axial forces exerted by the four pinions on the two side gears are determined, as previously mentioned, by quadrupling the values in Figure 2.20a and b. As seen from Figure 2.20, there are considerable fluctuations in the total axial forces within the confines of the tooth pitch. Marked differences between real axial forces and those obtained from the conventional formula (2.58) can also be observed in Figure 2.20.

Group II. Refer to the sketch of a differential in Figure 2.19 and its pinion in Figure 2.21.

Since z_c is an odd number, the right profile is in position 1′, when the diametrically opposite left profile occupies position 1″. If the tooth profiles are shifted, the tooth width is not equal to the width of the space and point a'' misses line $a'o$ in Figure 2.21. However, this angular shift is about 1.5 degrees and may be neglected.

It follows from Figure 2.21 that the turn angles, v_{cr} and v_{cl}, have the same magnitude and different signs: $|v_{cr}| = |v_{cl}| = |v|$. Using angle v as the argument and applying formulae (2.67), (2.68), (2.73), (2.74), (2.76) through (2.78), one can determine the axial forces exerted by one pinion on the left and right side gears of a four- or two-pinion differential that

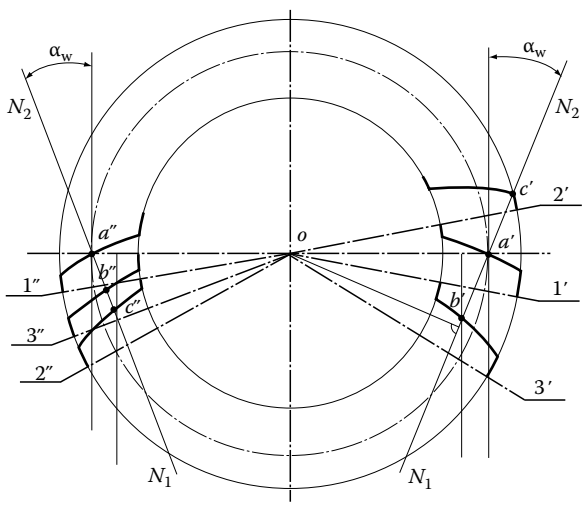


FIGURE 2.21
Schematic of a pinion with an odd tooth number.

belongs to Group II. Figure 2.22 presents a graphical approach to determining these axial forces.

To determine the axial force exerted by the pinion on the left side gear, the force on the right side gear should be calculated and plotted (see Figure 2.22a) using the above formulae. Then, picking point e with an arbitrary positive angle v_1 on Figure 2.22a, a vertical line is drawn to reach a horizontal segment line e_2e_3 at point e_3. Line segment e_2e_3 is obtained from a vertical line segment e_1e_2 with negative angle $-v_1$. As a result of this construction, points e_1 and e_3 are seen to determine the axial forces that are exerted on the right (Figure 2.22a, point e) and left (Figure 2.22b, point e_3) side gears by the very same pinion. All other points on the curve in Figure 2.22b may also be found by similar constructions.

According to the diagrams pertaining to Group II in Figure 2.19, the teeth of each pinion mesh simultaneously with the teeth of each side gear. Therefore, the total axial forces acting

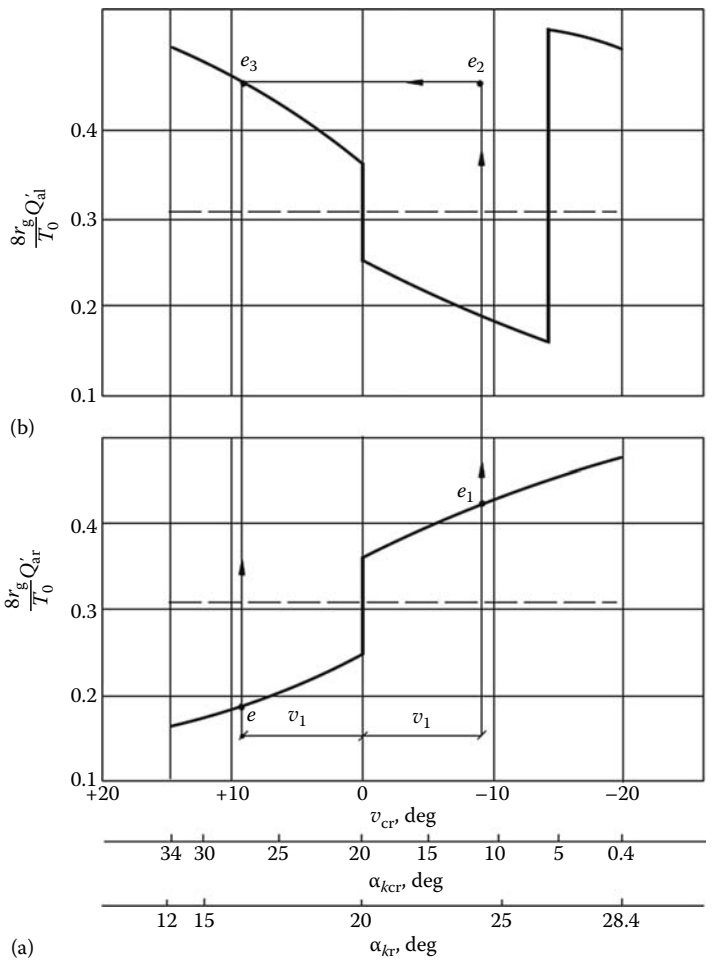


FIGURE 2.22
Axle differential of MAZ 500 truck (Group II): right (a) and left (b) specific axial forces. ——— by formula (2.67); —— —— by formula (2.58).

on the left and right side gears can be found by quadrupling the forces $\left(\frac{8r_g}{T_0}\right)Q'_{al}$ and $\left(\frac{8r_g}{T_0}\right)Q'_{ar}$ from Figure 2.22.

Group III. For differentials from this group, z_c is an odd number and z_g/a is a fractional number (see Table 2.2). The approach of Group II may be applied for finding the axial forces exerted by a pinion onto the left and side gears in a differential of Group III, since for both groups z_c is an odd number. Hence, the schematic diagram of a pinion in Figure 2.21 may be used to determine the locations of the diametrical tooth profiles of the pinion on the lines of action. The results are presented in Figure 2.23.

To determine the total axial forces acting on both side gears, consider Figures 2.19 and 2.24.

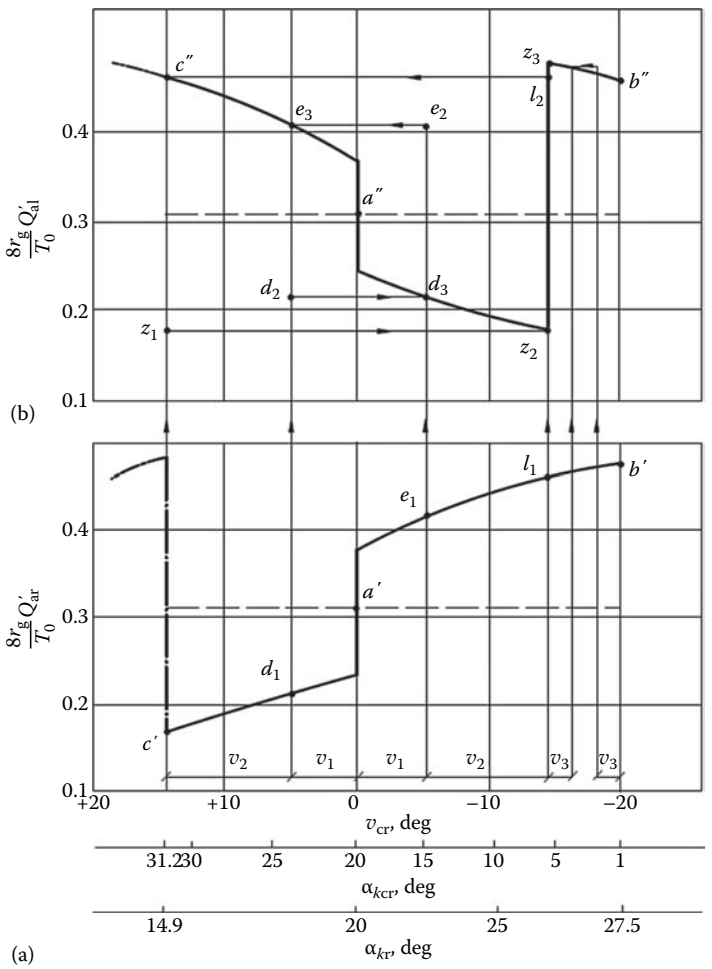


FIGURE 2.23
Rear axle differential of MTZ 102 tractor (Group III): right (a) and left (b) specific axial forces. ——— by formula (2.67); —— —— by formula (2.58).

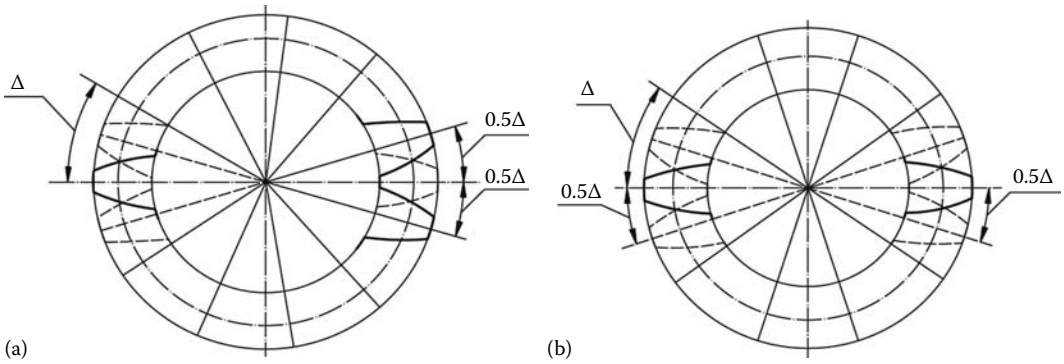


FIGURE 2.24
Tooth profiles of two adjacent pinions with an odd (a) and even (b) numbers of teeth z_c.

The latter figure gives tooth profiles of two adjacent pinions with odd and even values of z_c. As follows from Figures 2.19 and 2.24a, the relative displacement of the tooth profiles of adjacent pinions for a Group III differential is equal to a half of the circular pitch Δ. Hence shifting the curves in Figure 2.23 through an angle $v = 0.5\Delta$ yields the axial forces exerted onto the left and right side gears, by a pinion that is adjacent to the pinion that exerts forces in Figure 2.23. The results are shown in Figure 2.25.

The solid curves in Figure 2.25 represent the forces exerted by a pinion on both side gears. The dash-dotted lines give the axial forces exerted on the side gears by an adjacent pinion. To determine the total axial forces acting on the right side gear, the forces in Figure 2.25a should be added and the result should be doubled (see Figure 2.26a). By proceeding similarly with the forces in Figure 2.25b, the total axial force acting on the left side gear is found (Figure 2.26b).

Group IV. The number of the pinion teeth in this group may only be even (see Table 2.2). The axial forces exerted by a pinion on the side gears are then determined as for a differential of Group I (presented in Figure 2.20). The results can be seen in Figure 2.27.

To determine the total axial forces acting on both side gears, consider Figure 2.19 and Figure 2.24b. It is seen from these figures that the relative displacement of the tooth profiles of adjacent pinions for a Group IV differential is equal to a half of the circular pitch Δ. Hence, by shifting the curves in Figure 2.27 through an angle $v = 0.5\Delta$, the axial forces exerted by the other pinion, which is adjacent to the pinion that exerts forces in Figure 2.27, on the left and right gears may be determined. The results are displayed in Figure 2.28.

To determine the total axial force exerted on the right side gear, the forces in Figure 2.27a should be added to the forces in Figure 2.28a and the result should be doubled (see Figure 2.29a). By proceeding similarly with the forces in Figures 2.27b and 2.28b, the total axial force acting on the left side gear is found (Figure 2.29b).

The analysis presented above proves that the axial forces in bevel-gear differentials fluctuate perceptibly. The above results also point to the sizeable difference between real axial forces and those obtained on the basis of formula (2.58).

2.3.3 Force Evaluation: A Method for Practical Use

To evaluate the differences between the axial forces exerted on the side gears, the following coefficients have been introduced:

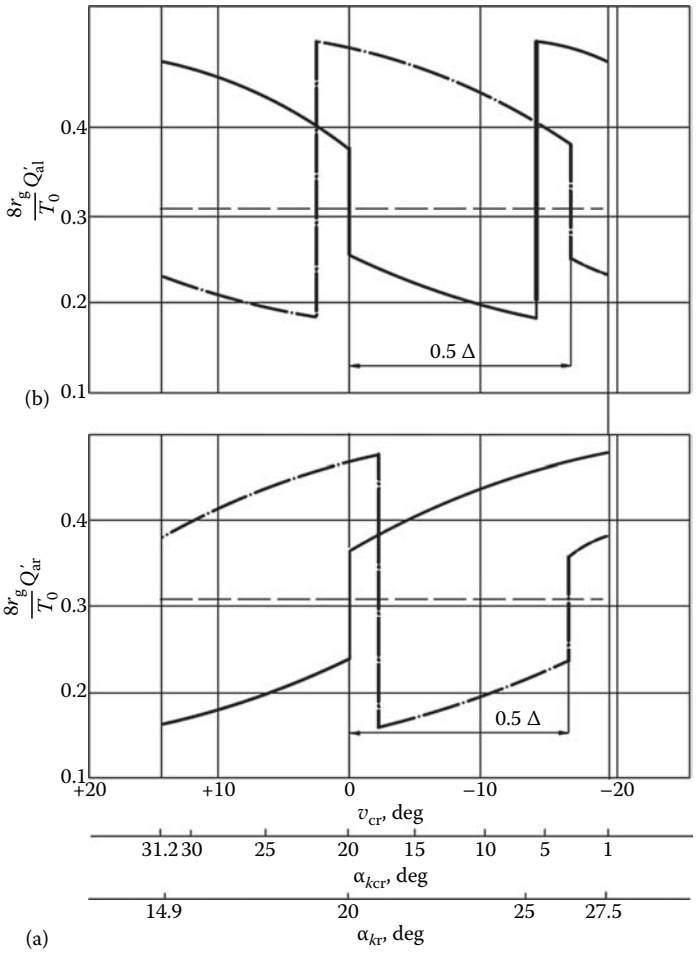


FIGURE 2.25
Rear axle differential of MTZ 102 tractor (Group III): right (a) and left (b) specific axial forces of two adjacent pinions. ——— and —·— by formula (2.67); — — by formula (2.58).

$$K_{a1} = \frac{Q_a^{max}}{Q_a}, \quad K_{a2} = \frac{Q_a^{max}}{Q_a^{min}} \tag{2.83}$$

where Q_a^{max} and Q_a^{min} are extreme values of the total axial force; Q_a is the value of the force calculated by quadrupling (for four-pinion differentials) its value from formula (2.58) and doubling its value from formula (2.59) for two-pinion differentials:

$$Q_a = \frac{T_0}{2r_g} \tan \alpha_w \cos \delta_c \tag{2.84}$$

The forces exerted by the side gears on the pinions also vary considerably from their values determined by conventional means. The new method that was developed for calculating

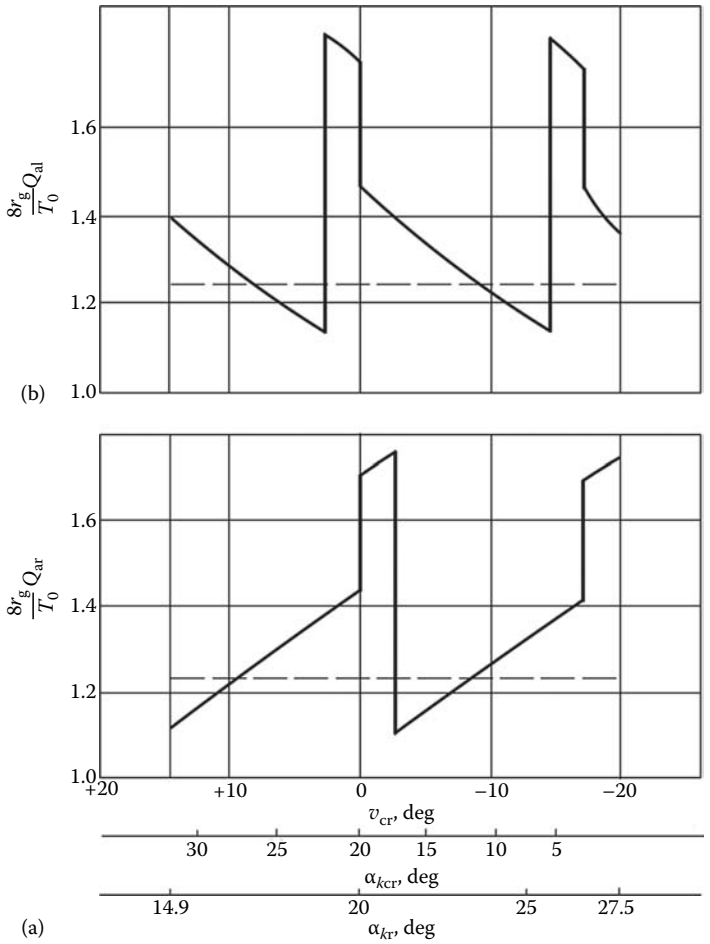


FIGURE 2.26
Rear axle differential of MTZ 102 tractor (Group III): right (a) and left (b) total specific axial forces. ——— by using formula (2.67); —— —— by quadrupling values from formula (2.58).

these forces is similar to the method described above for evaluating the axial forces exerted on the side gears. To evaluate the forces acting on the pinion, the following coefficients were used:

$$K_{s1} = \frac{Q_s^{max}}{Q_s} \quad K_{s2} = \frac{Q_s^{max}}{Q_s^{min}} \tag{2.85}$$

where Q_s^{max} and Q_s^{min} are extreme values of the forces; Q_s is the value given by the conventional formula (for a four-pinion differential)

$$Q_s = \frac{T_0}{4r_g} \tan \alpha_w \sin \delta_c \tag{2.86}$$

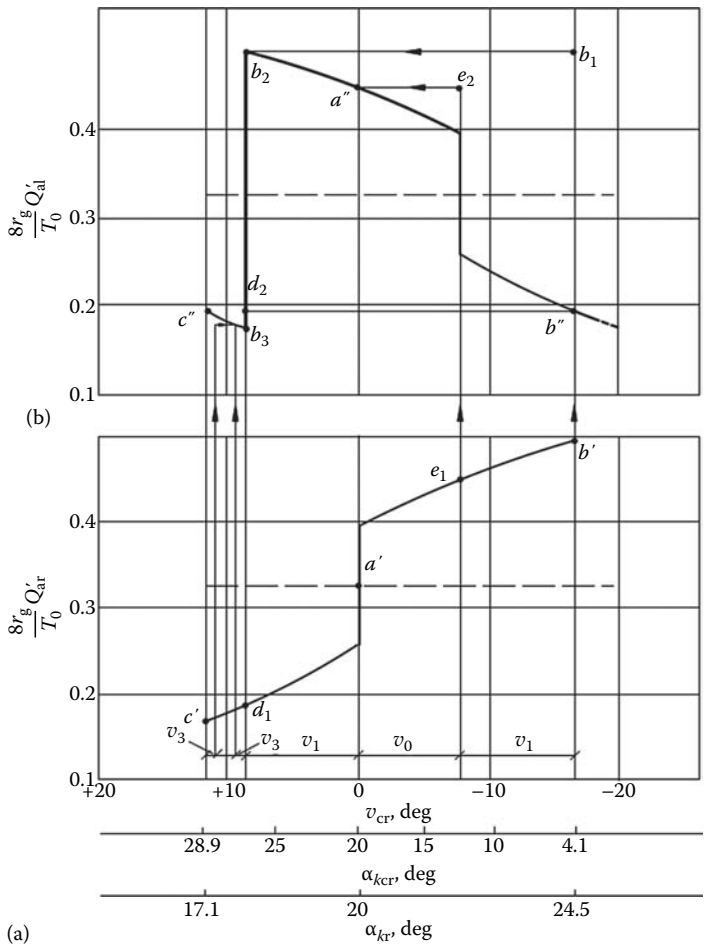


FIGURE 2.27
Axle differential of T 150K tractor (Group IV, $\alpha_w = 20°$): right (a) and left (b) specific axial forces. ——— by formula (2.67); —— —— by formula (2.58).

It has become evident by many computations that gears with different pitches and tooth numbers, belonging to the same group, that are used in differentials have close values of the coefficients K_{a1}, K_{a2}, K_{s1}, K_{s2}. Table 2.5 presents the magnitudes of these coefficients that can be used for calculating the extreme values of the total axial forces $Q_a^{max}, Q_a^{min}, Q_s^{max}, Q_s^{min}$ acting in any four-pinion differential.

To determine these values it is necessary to determine values of the axial forces Q_a and Q_s using the conventional formula (2.84) and (2.86) and to utilize the values of the coefficients from Table 2.5.

Comparison of values of the coefficients listed in Table 2.5 for all the groups of differentials thus allows selecting a preferred combination of tooth numbers for both pinion and side gears. This combination corresponds to differentials within group III in which amplitudes of the total axial forces are minimal. As an example, Table 2.6 gives some parameters and axial forces of the MAZ 64227 18-wheel truck's interwheel differential having various pinion and side gear tooth numbers.

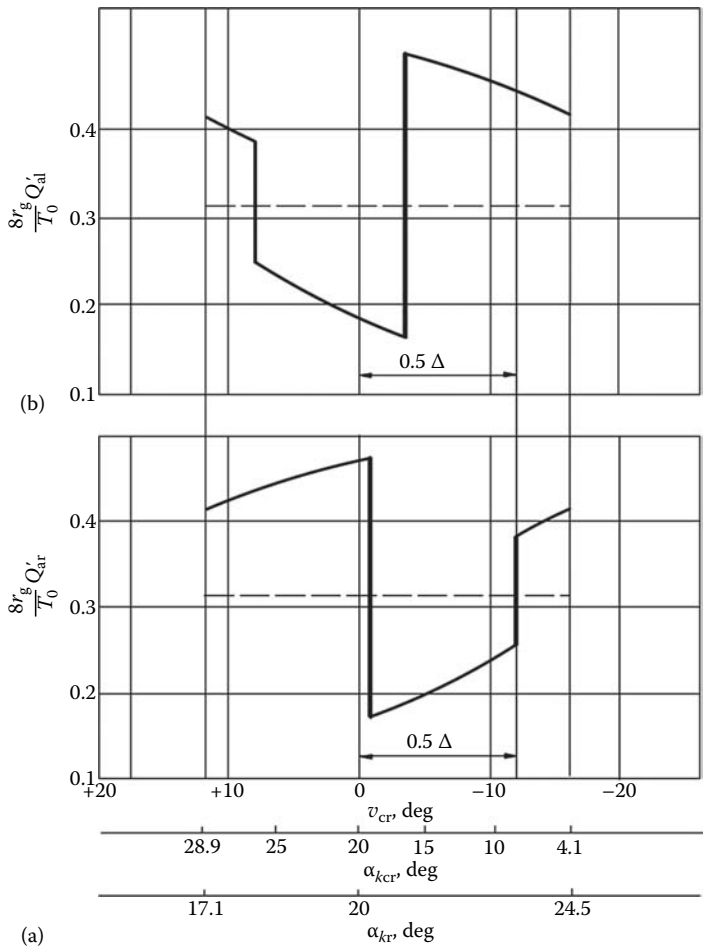


FIGURE 2.28
Axle differential of T 150K tractor (Group IV, $\alpha_w = 20°$): right (a) and left (b) specific axial forces of a pinion adjacent to the pinion in Figure 2.27. ——— by formula (2.67); —— —— by formula (2.58).

It is seen from Table 2.6 that changing the number of teeth number of the side gears from 16 to 18 leads to a substantial decrease in the axial forces.

2.3.4 Experimental Results

Laboratory-stand tests were performed to study the axial forces in a bevel-gear differential. The test stand that includes a machine for testing differentials and a laboratory testing equipment allows testing a differential with relative rotation of the three basic links while one output shaft is stopped and the other output shaft rotates twice as fast as the differential case (under load and without a load).

The method used for determining the axial forces was based on direct measurement of their values. To this end, two specially designed devices for measuring the total axial forces were installed between the side gears and the differential case halves (Figure 2.30).

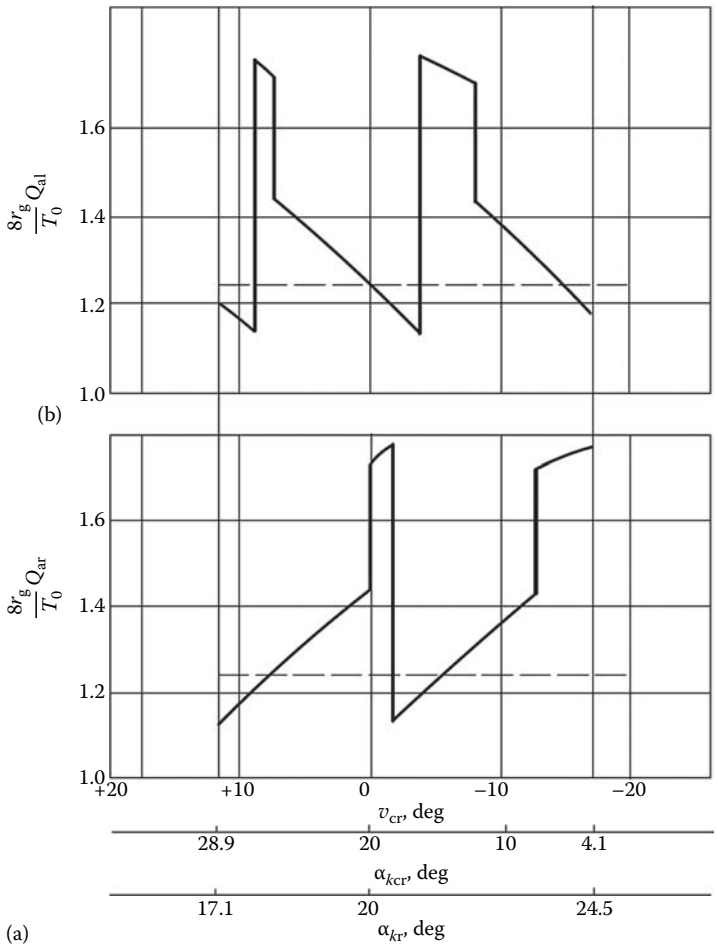


FIGURE 2.29
Axle differential of T 150K tractor (Group IV, $\alpha_w = 20°$): right (a) and left (b) total specific axial forces. ——— by using formula (2.67); —— —— by quadrupling values from formula (2.58).

TABLE 2.5
Coefficients for Force Computations

Group	K_{a1}	K_{a2}	K_{s1}	K_{s2}
I	1.69	3.59	1.29	2.54
II	1.60	3.63	1.42	1.46
III	1.40	1.54	1.38	1.44
IV	1.45	1.60	1.30	2.43

Figure 2.31 shows a sample of an oscillogram with sensor signals that are proportional to the total axial forces. The ordinates y_{max} and y_{min} correspond to the extreme values of the forces Q_a^{max} and Q_a^{min}.

TABLE 2.6

MAZ 64277 Interwheel Differential

Factors and Parameters	MAZ 64227 Conventional	MAZ 64227 Improved
Total resistance to the truck's motion (kN)	3.91	3.91
Side gear tooth number, z_g	16	18
Pinion tooth number, z_c	11	11
Group number (see Table 2.2)	II	III
Outer module, m_{ie}	7	7
Pressure angle, α_w	22°30′	22°30′
Total conventional axial force acting on the side gear, Q_a (kN)/pressure on diff. case caused by Q_a (MPa)	0.88/0.16	0.82/0.10
Total maximum axial force acting on the side gear Q_a^{max} (kN)/pressure on diff case caused by Q_a^{max} (MPa)	1.41/0.26	1.15/0.14
Total conventional axial force acting on the pinion, Q_s (kN)/pressure on diff. case caused by Q_s (MPa)	0.30/0.12	0.25/0.10
Total maximum axial force acting on the pinion Q_s^{max} (kN)/pressure on diff. case caused by Q_s^{max} (MPa)	0.43/0.17	0.36/0.14

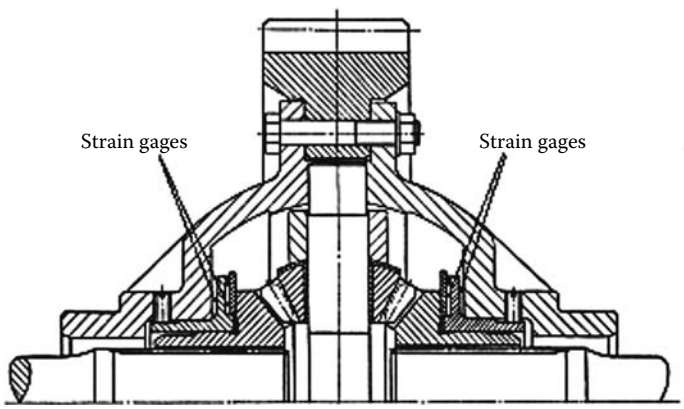


FIGURE 2.30
Devices for measuring total axial forces.

The coefficient K_{a2} is obtained by dividing y_{max} by y_{min}. For the tested differential (Group I from Table 2.2), the measured coefficient K_{a2} is equal to 3.38 and differs from its numerically determined value by 6.21% (the accuracy of ordinate measurements was 0.1 mm).

2.3.5 Conclusion

Another previously unknown phenomenon was discovered in bevel-gear differentials. This phenomenon is referred to as the fluctuating nature of the internal forces in involute tooth bevel gearings.

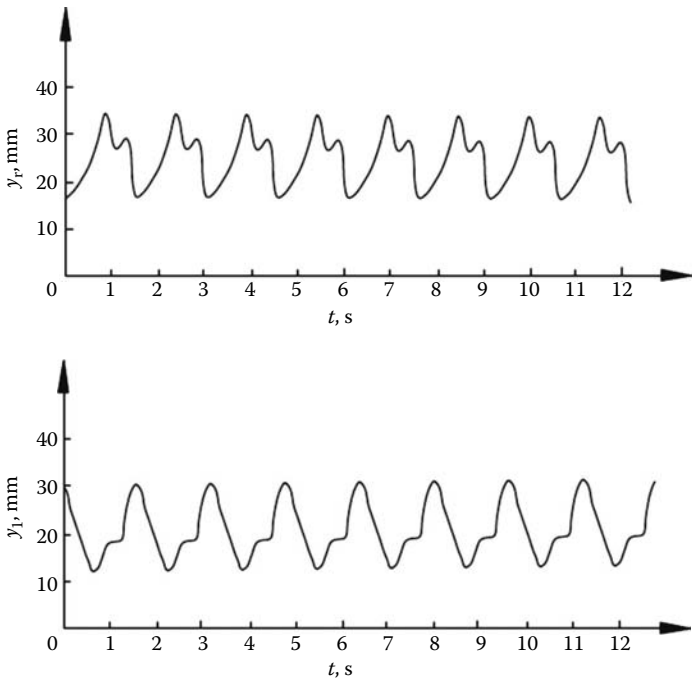


FIGURE 2.31
Example of oscillogram.

The motion of the points of contact of the gears along the lines of action, friction in mating gears and, finally, the discovered summation of the axial forces acting on all the differential bevel gearings that takes into account the four possible combinations of tooth numbers for differential pinions and side gears all lead to significant fluctuations in the real total axial forces, and cause them to be much greater than analytically predicted and, as a result, to have significantly greater maximal values than predicted by the standard method. The fluctuations of the real axial forces in toothed gearings cause increased pressure and accordingly damage the friction surfaces of the differential's parts.

The amplitudes of the total axial forces are minimal when the number of teeth of the pinion is odd and when a fractional number is obtained by dividing the number of teeth of one side gear by the number of the pinions a. The latter is equal to 2 or 4. A differential having tooth numbers for its pinions and side gear that satisfy this condition belongs to Group III according to the suggested classification (see Table 2.2).

Over the past century of designing differentials, designers were only concerned with ensuring conformity of the tooth number z_g of the side gear to the assembly condition. According to this condition, the result of dividing the sum of numbers of teeth of the two side gears by the number of the pinions $(z_g + z_g)/a$ must be an integer. Henceforth, in addition to this assembly condition, an engineer should choose the tooth numbers z_g and z_c in a way that will ensure obtaining a differential that falls within Group III. This will improve the operational reliability and also increase the durability of the differential and decrease vibrations and noise in this mechanism.

2.4 Robustness of Differentials

Differentials are used since the advent of self-driven wheeled vehicles. During this period the conceptual design of these devices did not undergo significant changes. The positive effect of the differential on the operating properties of vehicles made it one of the indispensable mechanisms in vehicular engineering.

In spite of this, improvement of differentials is still high on the engineering agenda. This is because the conditions under which differentials operate become increasingly more complex. For example, the use of three- and more unit vehicular trains (a tractor-semitrailer-trailer combination) caused a marked increase in the traction forces of the axles. With rising specific powers of the vehicles, their speeds and, in particular, with introduction of wheel-hub gear drives, the velocity mode of differential performance has become increasingly more complicated. All this has a negative effect on the reliability of the vehicle's operation. For example, the driving axles of a 6×4 truck with a total mass of 18.425 ton break down 3–3.5-fold more frequently than its transmission. Table 2.7 presents typical breakdowns of components of interwheel and interaxle differentials that were detected in operating 6×4 heavy-duty highway trucks.

The greatest number of differential failures is caused by component wear rather than by breakage. Actual breaking of pinion teeth and side gears is usually observed only following substantial wear of spider pins, pinion bushings and thrust washers that interferes with normal operation of bevel gearing. This may cause breaking of teeth and also skewing and seizing of pinions that causes the differential to ''lock'' and this brings about excessive wear of the tires. One of the causes of the excessive wear of thrust washers and sometimes of their complete wearing out and of the wear of the spider pins consists in significant axial forces, the nature of the inception of which was discussed in Section 2.3.

The elevated pressures that arise in the contact between the side gear and the differential's housing may cause a break in the lubricant film. This causes galling and sometimes the appearance of oxidation tint on the differential's parts, i.e., in local welding between the housing and the side gear. Reducing the pressure on the rubbing surfaces requires increasing the area of the friction surface within the differential dimensions.

As is well known, wear is caused not only by the force load, but also by the speed at which the rubbing surfaces move one relative to the other. Whereas the force load on the differential's components can be determined rather precisely, this does not apply to the relative motion between the differential's surfaces. This relative motion occurs when the vehicle is taking a turn and, in the case of separate skidding of wheels, when traveling over adverse road conditions. For this reason it is extremely difficult to determine the actual

TABLE 2.7

Typical Failure of Interwheel and Interaxle Differentials

Component	Failure
Side gear	Wear and breaking of teeth
Pinion	Wear and breaking of teeth
Spider/pinion pin	Wear of pins beneath pinions
Pinion bushing	Wear of rubbing surface
Pinion washer and side gear thrust washer	Wear of rubbing surface

velocity mode of the differential's components. This in fact is the reason why designers usually are concerned only with the analysis of the force loads.

However, operating experience shows that the velocity mode cannot be neglected. Thus for one failure of an interwheel differential of a 6×4 truck with a total mass of 18.425 ton there occur, as a rule, 5–6 failures of the interaxle differential. Here the interaxle differential is subject to lower pressures at its rubbing surfaces but to much higher sliding speeds. Section 2.1 presented a method for calculating the relative rotational speeds of the differential's components. Further, in the present chapter consideration shall be given to the assessment of differential design that allows for the contribution of the relative speed of component motion.

The effect of the velocity factor on wear in differentials can be reduced by improving the lubricant circulation by providing grooves on the rubbing surfaces, providing various grease traps and specially distributed holes.

The wear resistance of surfaces of a differential's housing in its contacts with thrust washers is sometimes improved by laser toughening. The improvement provided by this method was verified in stand tests.

The gears and pinions of differentials are subjected simultaneously to fatigue, abrasive, and oxidation wear. Fatigue pitting is the principal form of failure of teeth surfaces subject to contact loads. Particles that separate from the metal parts due to high contact loads form cracks on the teeth surfaces. Lubricants penetrate into these cracks and lock up in the cracks in the surface of the tooth of the mating gear. The lubricant acts as a wedge that produces a high pressure in the crack, widening it. Cracks may become as wide as 3–5 mm (M. F. Lavrinovich and M. M. Shusternyak).

Abrasive pitting of teeth is caused by road dust and products of wear of rubbing surfaces that penetrate into the lubricant. Even if the lubricant contains as little as 2% of dust, abrasive pitting develops at a higher rate than fatigue pitting. Abrasive particles remove surface layers of teeth by micro cutting, which causes nonuniform wear of tooth profiles.

Oxidation wear manifests itself in the appearance of galling and seizing of the working surfaces of teeth at high pressures, when the lubricant film breaks and oxide films are removed.

Failure of geared couplings is caused by the simultaneous effect of fatigue, abrasion and oxidation wear. Usually tooth wear reduction is achieved by chemical and thermal treatment. However, the serviceability and robustness of geared couplings may also be improved by design methods. One of these methods consists in correct selection of the combination of the number of teeth of the pinion and of the side gear, which makes possible to significantly reduce the actual axial forces in the differential (see Section 2.3). The use of flow-through lubrication (see Sections 2.5 and 2.6) allows directing the lubricant to specific parts of the differential and help to remove wear products of rubbing components and dust particles that pass through the packing.

The amount of dust that penetrates the driving axles can be reduced by paying proper attention to the design of sealing components. The initial properties of seals change because of aging of the rubber, its wear, and cracking. This disrupts the elastic contact between the seal and the shaft and causes oil leaks. The robustness of the seal–shaft pair depends on the shaft velocity, its wobble, hardness and surface roughness, and type of seal material.

One of the factors responsible for penetration of abrasive particles into the lubricant and with it into the differential is misalignment in the moving coupling between the sealing collar and the shaft. As an illustration, the interaxle differential of a 6×4 truck will be examined. One of the supports of the differential's housing contains a single-row ball

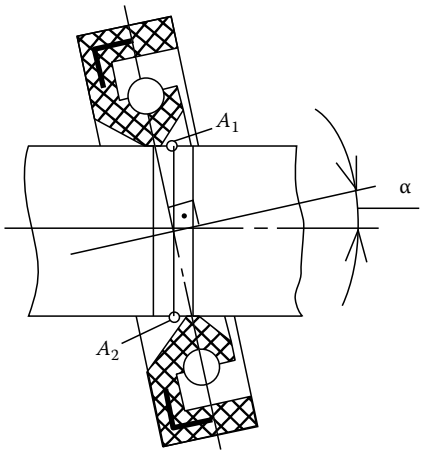


FIGURE 2.32
The sealing collar—differential-housing shaft pair.

bearing with maximum radial clearance of 0.033 mm. The second support consists of a splined joint between the housing and the hub of the final-drive pinion. This joint also has a clearance. The clearances in the supports increase in the course of operation, which causes misalignment between the axis of rotation of the housing of the interaxle differential and the axis of the sealing collar. Figure 2.32 illustrates this process.

In the course of rotation of the differential's housing, an abrasive particle that was initially located at A_1 moves to point A_2, i.e., inside the crankcase of the middle axle, in which the interaxle differential is located. Improving the precision of the couplings and modifying the design of the differential's sealing collar—shaft pair, should prevent the penetration of the abrasive into the lubricant.

As a rule, failure of the pinion spiders and pins is caused by wear of the surfaces of the pins beneath the pinions. The rate of wear tends to increase with increasing vehicle mileage. For example, for a 4×2 dumpster with a total mass of 10.850 ton the spider-pin wear was respectively 0.018, 0.05, and 0.18 mm after 20,000, 40,000, and 80,000 km.

Analysis of test results and operational data of various vehicles shows that the wear in the diameter of the spider pins may be as much as 0.5 to 0.7 mm after 200,000 km on the road for some vehicles and after as much as 1,000,000 km for others. Wear occurs over the entire length of the opening in the pinion.

Some companies improve the wear resistance of spiders by using what is called ''an inverse friction pair.'' This term applies to the situation when the pinion bushing is pressed onto the spider pin rather than into the pinion. As, a result, the sliding motion occurs over the bushing-pinion surfaces rather than over the bushing—spider-pin surfaces.

Lubrication of rubbing surfaces is of great significance for improving the robustness and serviceability of spiders. A flat must be provided on the spider pin and a groove in the pinion's sleeve (see Figure 2.33a and b).

The flat serves as a lubricant accumulator, whereas the groove distributes the lubricant over all the rubbing surfaces. In two-pinion differentials that have no pinion bushings, the grooves are made in the pin (Figure 2.33c). It is important to provide an opening that will allow the lubricant to enter the spider—pinion coupling at its base close to the principal axis of rotation of the differential. Circulation of lubricant through the differential is very important for removing products of wear that have a tendency to accumulate on the inner surfaces of the differential's housing. This accumulation of the products of wear interferes

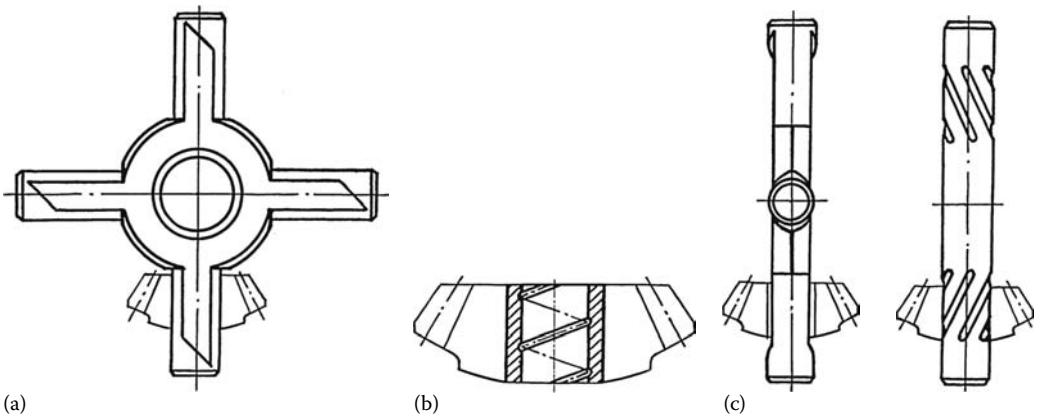


FIGURE 2.33
Rubbing elements: (a) spider–flats; (b) pinion bushing with groove; (c) pinion pin with grooves.

with the flow of lubricant to the pinion's washer and further to the pinion—spider contact. Lubricant circulation systems are described in Sections 2.5 and 2.6.

Sometimes wear is observed even in nonmoving couplings of the spider (of the pinion's pin) and the differential's housing. This is caused by fretting corrosion that arises because of micro-movements resulting from design axial misalignment, assembly and production inaccuracies. The micro movements may also be caused by nonuniformity in the distribution of contact loads.

Fretting corrosion usually starts at micro-movements of the order of 0.025 mm and more. Initially the surfaces are hardened by the interaction between their projections; this may be coupled by seizing of individual points (local welding). Subsequent fatigue processes form products of wear and skin holes on the contacting surfaces. At movements of the order of 0.07 mm and above significant fatigue damage develops at surfaces. This is accompanied by oxidation and formation of a corrosion medium caused by absorption of oxygen and moisture. The contact surface softens and flakes of metal peel off.

Reduction in the amplitude of these micro movements and, accordingly, improvement of the service life of the spider—housing contact can be achieved by ensuring that the axes of the openings in the differential's housing as well as the spider pins be made strictly perpendicular in the course of manufacture. In connection with this, the use of separate pinion pins instead of the spider is preferable, because this eliminates the mutual effect of nonperpendicularity of the axes on the micro motions in the carrier–housing contact. However, the use of separate pins instead of the spider causes the loading on the pinions to be nonuniform, which is a more significant limitation on the reliability and service life of the differential. The above is now analyzed in more detail.

Nonuniform distribution of the load on the differential's pinions causes a perceptible change in the loading modes of the teeth, increases the contact stresses in the moving spider-pin—pinion couplings and also increases contact stresses on the thrust washers of the pinions and of the side gears. Galling appears on the rubbing surfaces and they wear out rapidly. In certain cases, split bushings were pushed out from the pinions. In differentials in which the pinions had no bushings, the pinions were seized on their axles of rotation due to lubricant displacement.

Conditions necessary for uniform distribution of load between the pinions are: existence of (1) simultaneous contact between the teeth of all the pinions and the teeth of the side gears and (2) simultaneous contact between the pinions and spider pins. It is also important that the load-caused deformations of similar components be the same. For this reason, design must consider the stiffness of the carrier's pins, of the teeth of the pinion and of the side gears. The face stiffness of the thrust washers and the torsion stiffness of the differential's housing need not be considered because their deformations are negligible.

The side play between the teeth of pinions and side gears in an assembled differential is not a constant quantity both for all the pinions and for a single pinion in the course of rotation. The pinion with the minimum side play is the first to come into contact with the teeth of the side gear. It is obvious that in the case of side plays of different magnitude, the greatest load will be transmitted by the pinion with the smallest play. The pinion with the greatest play will take up the smallest load and may not be loaded at all.

The design of a differential assumes a rigorously uniform distribution of the pinions over a circle and, consequently, identical plays in the gear meshes and uniform loading of the pinions. Errors in component manufacture may result in nonuniformity of the plays that cause nonuniform loading of the pinions.

A marked contribution to nonuniform pinion loading is made by the error in the location of pinion axes of rotation. This error is composed of (1) shift Δ_1 of the pinions caused by nonperpendicularity of their axes of rotation (see Figure 2.34a) and (2) parallel shift Δ_2 of the pinion axis relative to the design location of the axes of holes in the differential's housing (Figure 2.34b).

Nonperpendicularity of the geometric axes of pinions is a function of the nonperpendicularity of the axes of holes in the differential's housing (see Figure 2.35a) and nonperpendicularity of the pins of the spider (see Figure 2.35b). An error in the location of pinions may appear when the real axis is not situated in the design location (Figure 2.35c).

If the pinions are seated on two separate pins, then the existence of a right angle between their axes is ensured by proper location of the pinholes in the course of manufacture. Deviations from right angularity are not detected in the course of assembly, since the two separate pins are always installed in their place. Deviation from right angularity can be detected in the course of assembly only when the errors are perceptible, i.e., when certain tooth meshes have no clearance. As noted, nonuniform distribution of forces between the

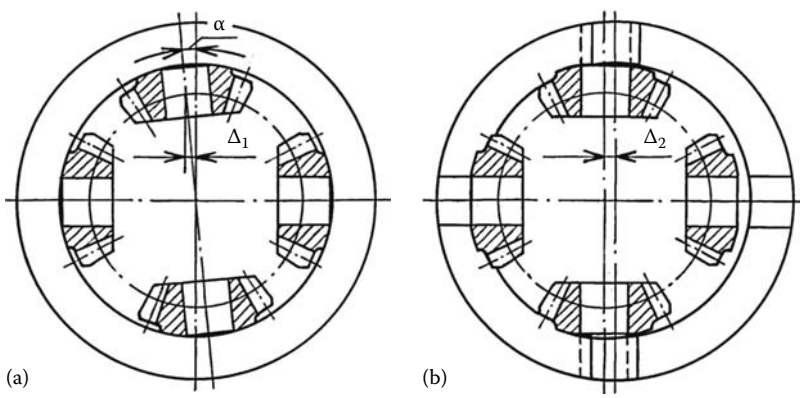


FIGURE 2.34
Errors Δ_1 and Δ_2 in the location of pinion axes.

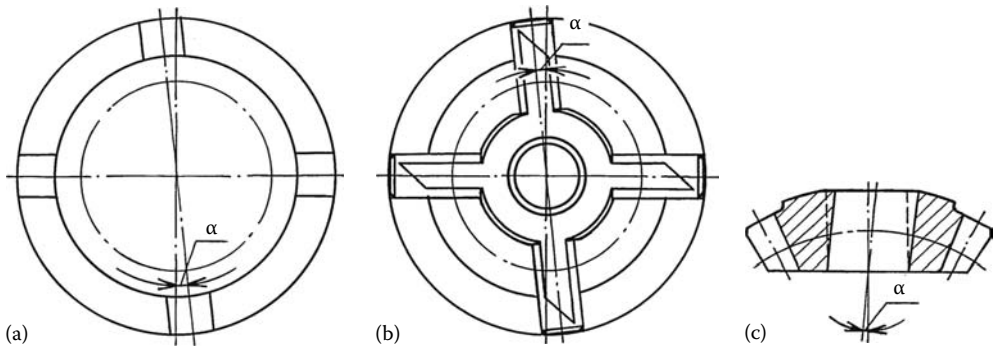


FIGURE 2.35
Factors responsible for errors in the location of pinion axes.

pinions has a negative effect of the strength of the differential's gear teeth and on the wear resistance of the rubbing pairs.

When a differential housing and a spider are assembled, the errors of the housing and of the spider add up. Since the housing is much more rigid than the spider, the spider pins are elastically deformed in the course of assembly to allow installing them in the holes in the housing (Figure 2.35a and b). If these errors are significant, the differential cannot be assembled at all. This means that nonperpendicularity in the location of pinion axes cannot markedly differ from the nonperpendicularity in the openings in the housing. This makes the spider more preferable than separate pinion pins, since it promotes more uniform distribution of load between the pinions.

The play in gear meshes and the distribution of load between the pinions is affected by the axial shifting of the pinions. This shift may be caused by imperfections in the shape of the hole in the differential's housing (its being elliptical, $\phi_1 \neq \phi_2$ in Figure 2.36, rather than round) and also by an error in the thickness of the pinion thrust washers and out-of-flatness of the thrust washers of the side gears.

In improving the serviceability of differentials by equalizing the loads on the pinions, an effort should be made to improve the load uniformity within a single pinion-carrier pin contact. This was possible in certain models of 80 HP tractors by increasing the nominal clearance in the pinion—carrier-pin coupling to 0.2 mm. A more uniform distribution of

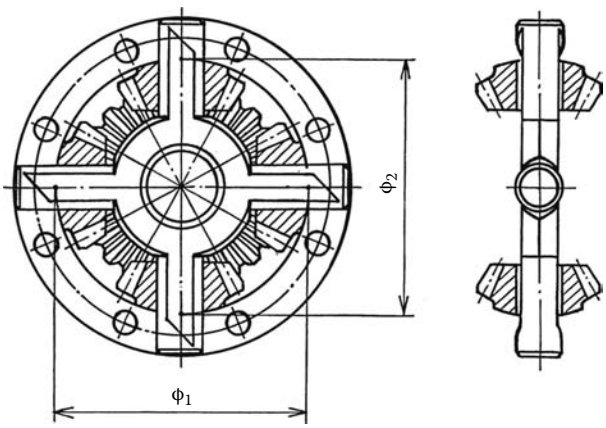


FIGURE 2.36
Ellipticity of the hole in the housing.

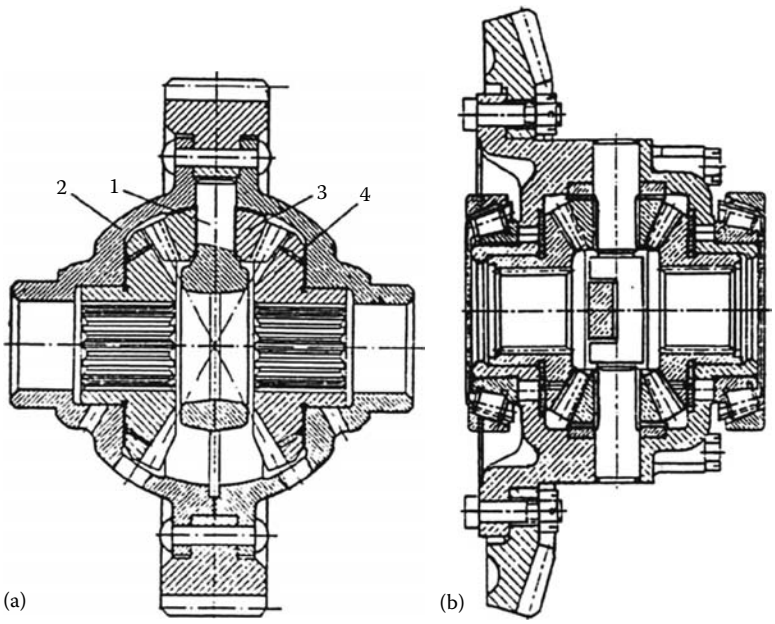


FIGURE 2.37
Open differentials: (a) spherical pinion washer (1, spider; 2, housing; 3, pinion; 4, side gear) and (b) flat pinion washer.

loads between the pinions was promoted by increasing the clearance between the hub of the side gear and the housing to 0.3 mm (P. I. Boikov, et al.).

Still another design feature of differentials should be mentioned. The face thrust surface of the pinion is made either spherical or flat (see Figure 2.37). Observations show that differentials with a spherical thrust surface exhibit a somewhat better serviceability, particularly with respect to the pinion—spider-pin pair, than differentials with flat thrust surfaces. Apparently the spherically shaped surface somewhat reduces the load on the pin by taking up a part of the circumferential force.

The data presented above prove that differential design must be carried out together with a thorough study of forces acting between the differential's components, in order to avoid overloading some while under-loading other components. This requires profound analysis of the features of the proposed conceptual design. Thus, for example, some designs of interaxle differentials of the driving tandems of 6×4 trucks unjustifiably use three support-point arrangements for shafts, the shortcoming of which is rather well known. This brings about the appearance of additional forces that overload both the shafts and their supports. For this reason, an effort should be made to use two-support shafts, which produces a favorable distribution of loads between the components.

Some vehicles suffer from failure of rolling-contact bearings in which the differentials are installed. These failures are not due to fatigue contact spalling of the races or of rolling components but to wear. It was noted that the races and the rolling component surfaces first lose their original roughness. Then their roughness increases and traces of plastic flow of metal and irregularities appear on them. This indicates that the races and the rolling components interact by way of abrading particles. The presence of such particles, even as small as 0.05 mm already causes the bearings to wear out. The way to remove the abrading particles is to use forced circulation lubrication, which also purifies the lubricant.

TABLE 2.8

Statistical Data on Interaxle Differentials of Highway Heavy-Duty Trucks

No.	Indicator	Side Gears	Pinions	Spider	Pinion Bushings	Thrust Washers	Teeth of Locking Device	Locking Device Fork	Tapered Roller Bearings in Middle Axle Drive	Cylindrical Roller Bearings in Rear Axle Drive
1	Percentile distribution of failures of differential parts in trucks	4.84	8.60	9.68	2.69	4.30	1.08	4.30	15.05	8.60
2	Percentile distribution of failures among individual components of differentials	8.18	14.55	16.37	4.55	7.27	1.81	7.27	25.45	14.55

Many of the failures of differentials described above were also investigated on the basis of data on many-years' operation of 186 highway heavy-duty trucks consisting of 6×4 tractors and semitrailers (the total mass ranged from 38 to 44 ton). Statistical analysis of the above data yielded the percentile distribution of failures of interaxle differential components. The results are presented in Table 2.8.

The data in row 1 give the percentile distribution of failures in vehicular trains. For example, failure of differentials associated with wear of pinion bushings was observed in 2.69% of the trucks in the sample. The data of row 2 in the table show the percentile distribution of failures among individual components of interaxle differentials that made it possible to map out the best ways of improving the designs of these mechanisms.

It should be emphasized in conclusion that the existence of failures in the operation of differentials is not a shortcoming inherent to these mechanisms, but stems from the ever-increasing loads and complication of their velocity modes. The following sections of this chapter are concerned with analytic methods, design methods, and the results of their application that allow addressing the force and velocity modes of differentials and to design them with better features and improved serviceability and robustness.

2.5 Design of Axle/Interwheel Differentials

2.5.1 General Engineering Issues and Solutions

The aspects of robustness of differentials analyzed in Section 2.4 point to the need to develop certain design approaches that would result in producing more refined designs. There is no doubt that each design engineer of differentials has his/her own approaches

that have evolved over many years in the field. This section presents some of these principles, actually recommendations that are examined within the context of designing the differential—the driving axle system.

Designs of differentials must conform to the following requirements:

- Conform to the functional intent under specified operating conditions
- Be strong, rigid, reliable and robust and have a sufficiently long operating life

Conformance of component design to the intent and operating conditions of the differential is ensured by proper selection of the configuration, dimensions, and mutual location of the elements of the components. In this respect, previously inexistent, original components, are designed ''on the spot.'' This is done on the basis of the designer's experience in utilizing designs of elements of typical components. To successfully design original components the designer must have sufficient experience in designing typical components such as gears, parts of bearings, springs, etc. Typical components, on the other hand, are usually designed using a prototype.

The strength of a component is determined by the material from which it is manufactured. It must be designed to withstand the actual working stresses in its cross section within the limits of permissible stresses. The strength of steel components depends to a large extent on the chemical and heat treatment, but depends to a not lesser degree on the proper selection of the shape of the load-bearing sections and dimensions of the design.

The stiffness requirement pertains to limiting the deflection and angle of rotation in sections within the limits of permissible stresses. Stiffness of components, for example, of steel, is ensured by the same factors as their strength. In addition, the stiffness of components is affected by properties (qualities) of the material such as elasticity and susceptibility to shear that are estimated by the pertinent moduli.

The strength and stiffness of components of a differential can be controlled by varying their dimensions and mass, varying the configuration of their cross section in the most dangerous location, i.e., by modifying the component's design. Changes in dimensions and mass of components may cause excessive material consumption and increase the cost of the differential. To prevent this from happening, the dimensions of the loaded sections should be specified most frugally without excessively increasing the safety factor. Additionally, the component stiffness should not be exaggerated. The latter is attained both by properly configuring the cross section and by selecting its design. For example, a T cross section (see Figure 2.38a) provides a greater stiffness than a round or square cross section. The stiffness of a component can be improved by special fins (ribs) on its surface that could simultaneously serve as a radiator for removing heat from the device or from its individual elements (see *A* in Figure 2.38b and c).

Among others, one of the ways of reducing the design stresses in shaft cross sections consists in avoiding cantilevered designs. If this is impossible, at least they should be made as short as possible. One of the effective methods of reducing the length of cantilevered shafts is ''building in'' the components seated on them. An example of this approach is one of the designs shown in Figure 2.38b and c. Building in the sheave made it possible to reduce the cantilevered part of the shaft from l_1 (see Figure 2.38a) to l_2 that was obtained in designs b and c. Another example of reducing the length of the cantilevered part of tubular shaft 3 located in sleeve 4 of the half-axle of the driving axle of a vehicle may consist of the building hub 1 into drum 2 of the wheel (see Figure 2.39).

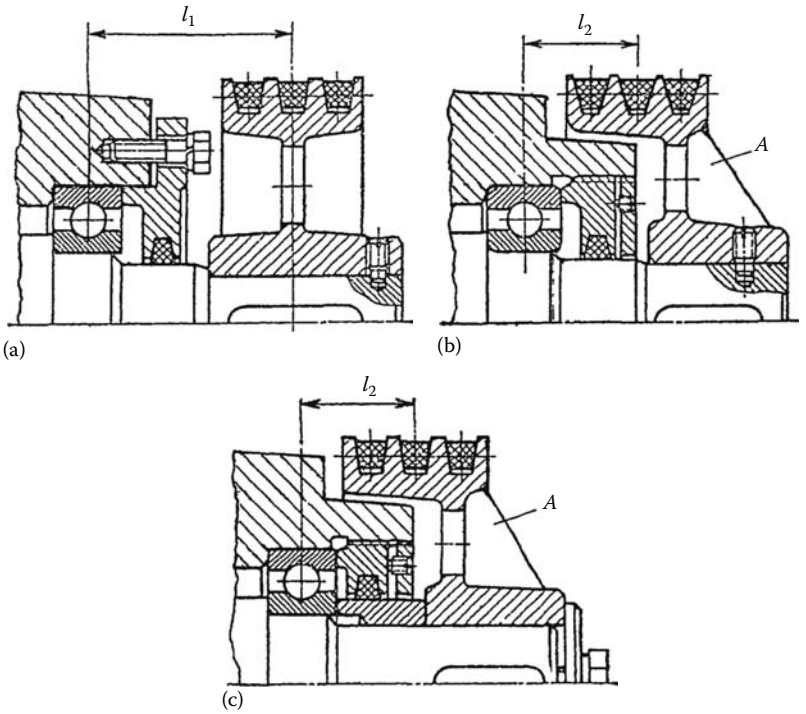


FIGURE 2.38
Examples of the location of the drive sheave on the cantilevered part of the shaft: (a) nonmanufacturable design; (b) built-in (manufacturable) design with the sheave prevented from axial motion by a screw; (c) manufacturable design with the sheave fastened by a bolt and an end washer. l_1 and l_2 are the arms of the flexural force exerted on the cantilevered part of the shaft; A is a stiffening rib.

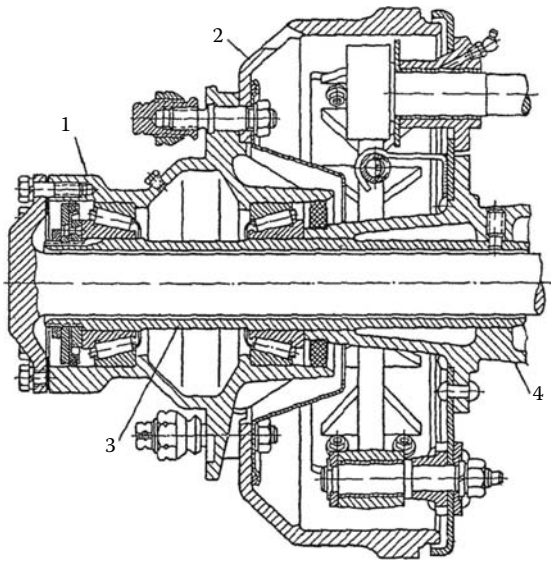


FIGURE 2.39
Design of hub built into the wheel's drum: 1, hub; 2, wheel's drum; 3, cantilevered tubular shaft; 4, sleeve of the axle's beam.

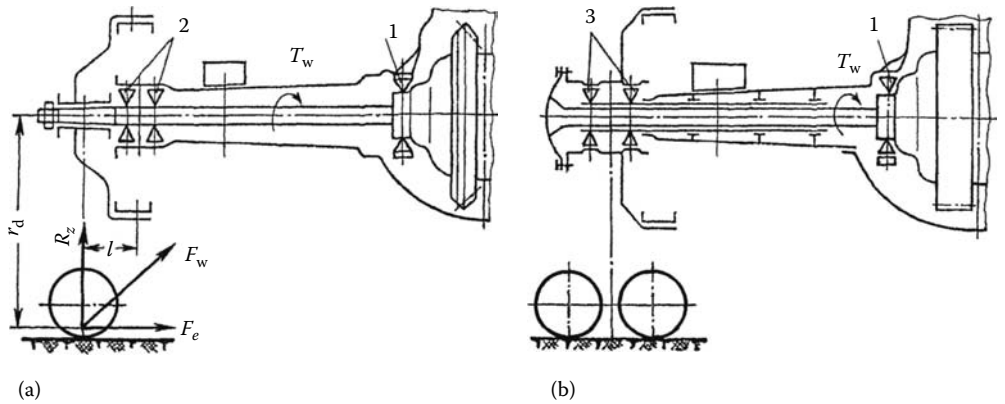


FIGURE 2.40
Designs of driving axles: (a) semi-floating; (b) full floating; 1, the differential's housing bearing; 2 and 3, wheel hub bearings; l is the arm of the flexural forces acting on the cantilevered part of the shaft.

Modification of the design of an element or component may allow shifting certain forms of load from one component to another that is stronger. As an illustration of utilizing this approach, consider the case of the semi-floating and floating driving axles shown respectively in Figure 2.40a and b.

The semifloating half-axle is connected by its inner end to the side gear of the differential, whose housing rotates in bearings 1 of the axle's casing, while being connected by its outer end that is supported on bearings 2 to the hub of the driving wheel. This half-axle is subjected to all the four loads shown in the schematic:

- Torque T_w
- Bending moment in the horizontal plane, $M_h = F_w l$
- Two bending moments in the vertical plane, $M_{v1} = R_z l$ and $M_{v2} = F_l r_d$

The full floating half-axle (see Figure 2.40b) is not supported by bearings 3 at its outer end that is rigidly fastened to the hub of the driving wheel. The support was transferred from the sleeve of the half axle to the tubular shaft built into the sleeve. Because of this, all the bending moments produced by forces acting on the driving wheel are transferred to the tubular shaft and the half-axle shaft is subjected only to torque T_w.

The stiffness of a cantilevered shaft can also be adjusted by using various installations of tapered bearings and selecting their dimension. Thus the axle drive bevel-gear shaft of the final drive is cantilevered, the stiffness can be improved both by increasing the distance between the bearings and by increasing the size of the bearing located directly at the gear ring. Here, in order to ensure the required stiffness of the element and to provide for low-noise operation, the distance between the bearings should at least be 2.5-fold greater than the distance from the middle of the gear's teeth to the closest bearing. All this is shown in Figure 2.41.

The stiffness of the element under consideration, primarily in the axial direction, can also be increased by additional pretensioning in the bearings of the drive gear. But it must be

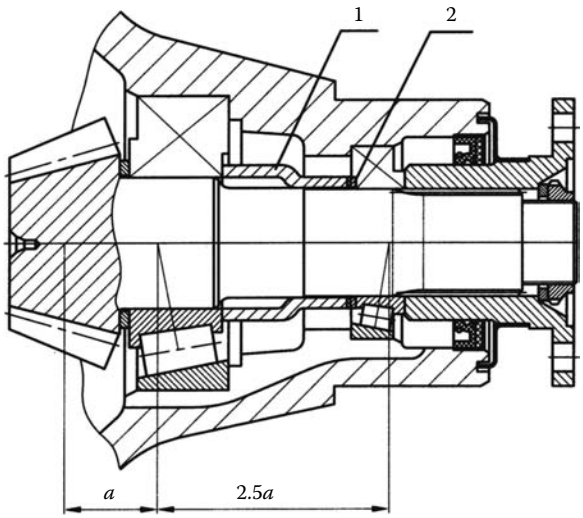


FIGURE 2.41
Cantilevered placement of the final drive pinion: 1, spacing bushing; 2, adjustment washers.

remembered here that the pretensioning should be such that it would not cause the temperature of the bearings to rise and reduce their robustness. Note that the level of pretensioning depends to a large extent on the design of the bearings themselves.

When torque is transmitted by means of rivets, bolts, studs, and similar joints, the connecting elements should be removed as far as possible from the hubs of the components being joined in order to reduce the load. Figure 2.42a shows the fastening of the driven

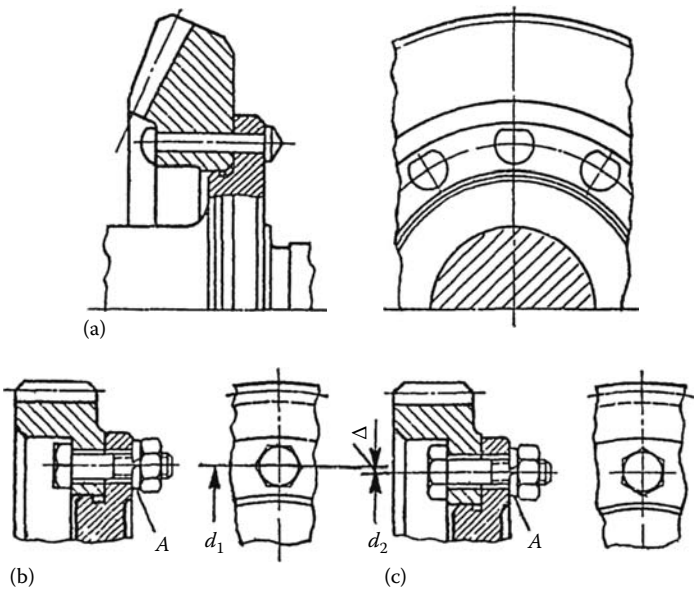


FIGURE 2.42
Methods of fastening the final drive wheel: (a) using rivets; (b) using bolts secured against unscrewing; (c) using bolts not secured against unscrewing; d_1 and d_2, bolt location circle diameters; Δ, difference between the diameters of the bolt circle in cases (b) and (c); *A*, spring washer.

bevel gear of the rear axle of a truck with gross mass of 3.9 ton by rivets, whose manufactured heads have a one-sided chamfer that allows placing them at a larger distance from the center of the gear's axis.

In similar bolted joints, it is recommended to use bolts with a reduced-size head, placed by its edge flush with the surface of the recess of the gear head (Figure 2.42b). A less suitable location of these bolts is shown in Figure 2.42c. Locating the heads as per Figure 2.42b has the additional convenience of preventing the bolts from turning when being tightened in the course of the component's assembly. The use of this version is effective when the bolt's location circle diameter is not too large. The amount Δ by which this diameter can be increased depends on the type of the head and on the bolt thread's diameter.

Consider another example of reinforcing bolt joints. Figure 2.43 shows the joining of crown 1 of a driven bevel gear to hub 4 by means of bolts 3. At very high loads on this transmission the connecting bolts are subjected to shear and crushing stresses. In order to fully relieve these stresses, the design being examined utilizes stiff rings 2. It can be easily seen that in this case the bolts are subjected to only one kind of load—tension, stemming from the force applied in tightening them. This makes it possible to reduce the number of bolts and use bolts with smaller diameter and, consequently, with smaller heads. The latter is very important when the components are packaged compactly.

It is important to prevent the bolts from loosening due to vibrations. Note that the slit spring washers *A* shown in Figure 2.42b and c cannot be used in closed transmissions because of their brittleness. They sometimes break when the nuts are tightened and their fragments may fall out from beneath the bolt heads or nuts, something that may have catastrophic consequences for the gear transmissions, should these fragments find their way into the spaces between the gear teeth.

Figure 2.43 shows a very old method of holding bolts in place by means of a wire 5 that is still used in certain vehicles.

The rule to be followed when using this method is that the tightening force of the wire should be in the direction of the turn of the bolts. This is seen from Figure 2.43: if it is imagined that the bolts are turned counterclockwise, the joint will not allow unscrewing of the bolts.

Most frequently the means for preventing bolted joints from unscrewing in rotating components, including differentials, consists in up to 2 mm thick stamped steel plate

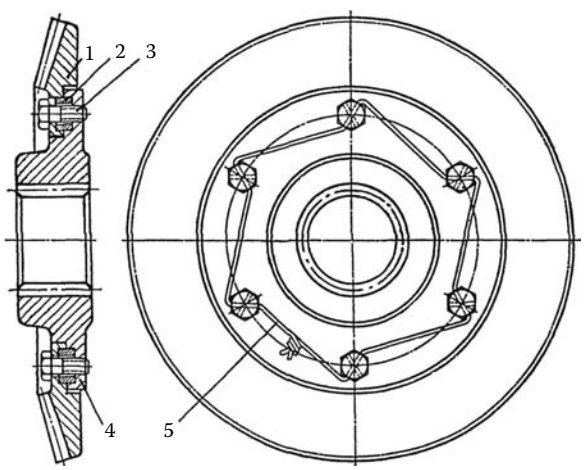


FIGURE 2.43
Method of using wire for retaining the driven-gear fastening bolts: 1, driven gear of the final-drive; 2, shear-loaded rings; 3, fastening bolts; 4, hub; 5, wire.

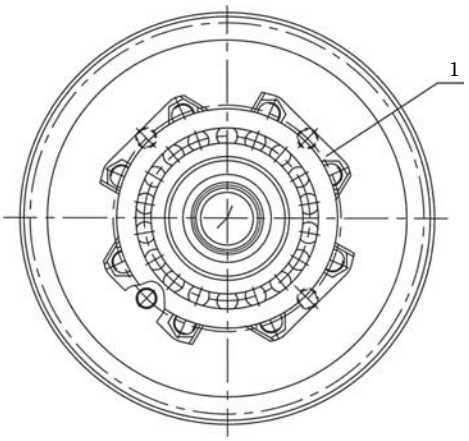


FIGURE 2.44
Retaining the driven final drive gear fastening nuts: 1, steel plate with turned up edges.

with edges somewhat turned up for the simplifying assembly. After the assembly of the component and tightening the joint, the edges of the plates 1 are bent over the faces of two adjoining bolts (or nuts), connected by the plate (see Figure 2.44).

Note that this method is quite reliable, but it should be utilized to allow using standard plates when the bolts are distributed uniformly over a circle. One of the shortcomings of this method consists in the need to orient the facets of the bolts, as a rule, in the direction of increasing their tightening moments, so that the upturned parts of the plate would be located directly at the side facets of the bolt heads. This causes the bolts to be tightened nonuniformly over the entire circumference of the contacting surface. At present bolts are usually locked by knurling the inner surfaces of the bolt heads and also by means of durable adhesive compositions. Nuts may also be prevented from unscrewing by making them with an internal oval (see Figure 2.45).

Some loads on fasteners are relieved in a more complex way. For example, reducing the forces on the rivets of the bracket that serves as the support of the free end of the leaf spring required replacing the stamped bracket (Figure 2.46a) by one that was cast (see Figure 2.46b). This made it possible to position the rivets in a manner that highly reduced the force on them.



FIGURE 2.45
Oval nut secured against unscrewing.

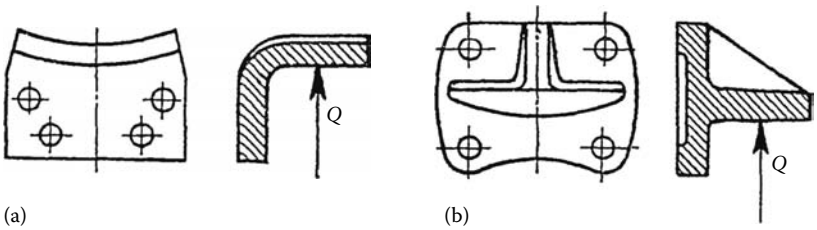


FIGURE 2.46
Design of the spring support bracket: (a) stamped; (b) cast; Q is the force that acts on the cantilevered flange of the bracket.

The simplest radial-thrust bearings should not be subjected to loads higher than they can handle. For this reason reduction gear should be designed so as to arrange the gears in the most rational manner so that the axial components of forces that arise in the meshing of their teeth should cancel one another. It will be shown how this can be achieved with reference to layouts shown in Figure 2.47. Two-stage speed reducers employ two sets of helical teeth.

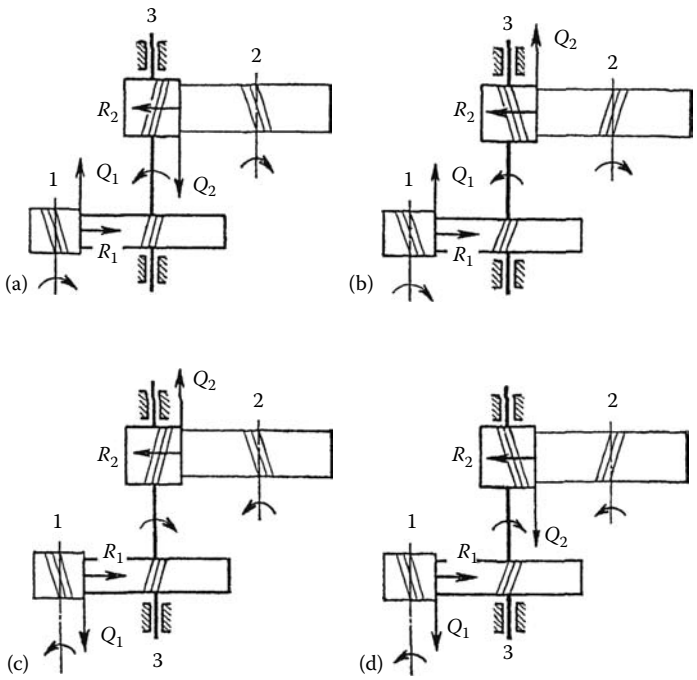


FIGURE 2.47
Designs of two-stage reducing gear employing helical gears: (a) version with the same slope of the teeth on the gears of the intermediate shaft and clockwise rotation of the drive gear; (b) version with oppositely directed slope of the teeth of the intermediate-shaft gears and clockwise rotation of the drive gear; (c) same as in (a), but with counterclockwise rotation of the drive gear; (d) same as in (b), but with counterclockwise rotation of the drive gear; 1, drive gear; 2, driven gear; 3, intermediate shaft; Q_1 and Q_2 are the axial components of resultant forces; R_1 and R_2 are the radial components of resultant forces.

The direction of the axial components Q_1 and Q_2 of forces in the gear meshing depends on the direction of the slope of the teeth, the direction of rotation of the shaft and also on the function of a given toothed wheel, whether driving or driven. The layouts shown in (a) through (d) show differences in the direction of axial components for the gears of the speed reducer's intermediate shaft 3. Wheel 2 serves as the driven element, whereas gear 1 serves as the driving element. The direction of radial components R_1 and R_2 does not change. When the intermediate shaft rotates counterclockwise (see Figure 2.47a) and with the teeth of the gears having the same slope, the axial force decreases, since vectors Q_1 and Q_2 act in opposite directions. When the slopes of the teeth are opposite (see Figure 2.47b), the axial force increases. Consequently, when the shaft rotates counterclockwise, the slopes of the teeth of the wheel and the gear should be the same. On the other hand, when intermediate shaft 3 rotates clockwise and the slopes of the teeth are the same (see Figure 2.47c) the axial force decreases. When the teeth have different slopes (see Figure 2.47d) the situation is opposite. The above analysis suggests the following. The best arrangements of these reducers from the point of view of lessening the forces on the intermediate shaft are those shown in (a) and (c), whereas arrangements (b) and (d) are highly undesirable.

Consider methods of adjusting tapered bearings and bevel tooth gearings. The pretensioning in the bearings of the shaft of the driven bevel gear is, as a rule, adjusted by means of two large end nuts 3 (see Figure 2.48).

Adjustment of the bearings is followed by adjusting the clearances in the gear meshing. For this purpose, one of the nuts 3 is screwed out, whereas the second is screwed in through the same angle. This causes the driven bevel gear together with the housing of the differential to move in the axial direction, while retaining the previously adjusted pretensioning in the bearings. The end nuts are immobilized by plates that are inserted into slots in nuts 3 and by bolts. Axial movement of the pinion in Figure 2.48 is obtained by changing thickness Δ of a stack of adjustment shims. As a result of these adjustments the pair of final drive gears should be positioned in a manner that the gears would mesh along the entire length of the tooth and the side clearance between the teeth would be 0.1–0.4 mm. Note that the size of the side clearance is governed by the module of the gears and by the degree

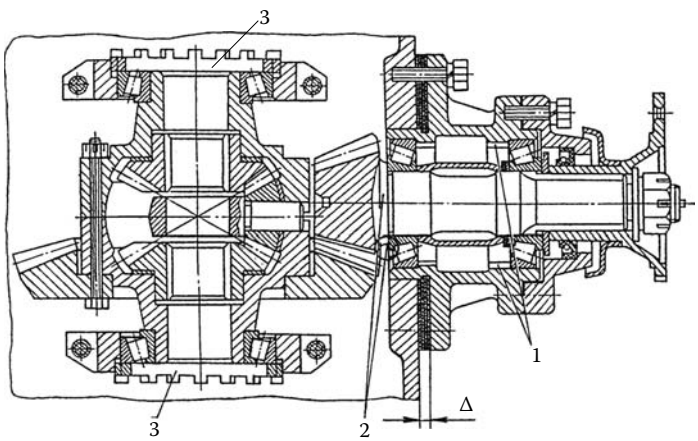


FIGURE 2.48
Central reduction gear of a vehicle's driving axle: 1, slots for pushing out (disassembly) of the bearing; 2, thrust collar of the final drive gear-shaft; 3, adjustment nuts.

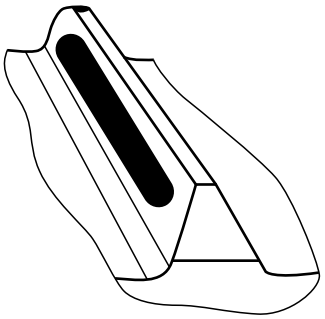


FIGURE 2.49
Location of the contact patch on the tooth of the axle driven bevel gear.

of precision of gear-tooth manufacture. The correctness of mutual location of the gear teeth is checked after adjusting their meshing by checking the location of the spot of contact on the driven gear. Figure 2.49 shows the proper location of the contact spot. Its area in precision-made gears may occupy up to 80% of the tooth's contact surface. Methods of fixing the contact spot by fine-tuning the locations of the gear wheels are usually given in the vehicle operation manuals.

The pretensioning of bearings can be adjusted in several ways. As a rule, mass-produced components come with a set of adjustment washers 2 (see Figure 2.41) of different thickness (up to 6–8 sets) that are then selected to conform to the actual element geometry. The number of sets depends on the precision of the component's elements. Batch produced components come with massive spacing bushings 1 (see Figure 2.41) without using washers. The bushings are filed down to the length needed for obtaining a normal pretension.

Very frequently, in particular in cars, thin-walled spring bushings are used instead of adjustment washers and massive spacing bushing (see 1 in Figure 2.50). These deform to the required length in the course of bearing adjustment. In this case a certain pretensioning is produced between the cones of the bearings. The pretensioning force still is not equal to the force taken up by the cone of the bearing. This stems from the existence of allowances in the manufacture of mating components (shafts, housing, bearings, etc.). For this reason the length of the spacing bushing is, as a rule, selected for providing the required pretensioning limits individually for each specific transmission.

Disassembly devices are a very important, although a little-mentioned element of bearing components of the final drive of a vehicle. Figure 2.51 shows one of the designs of a disassembly device to be used for removing body 2 with bearings that is snugly seated in sleeve 1 of the final drive.

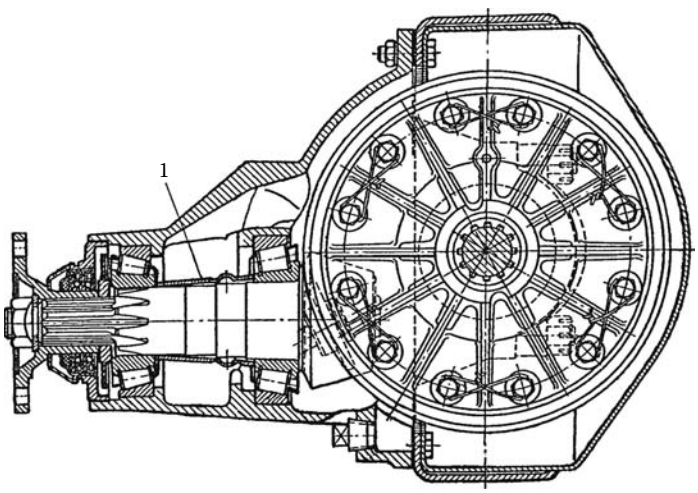


FIGURE 2.50
Design of hypoid final drive of a car drive axle: 1, thin-walled spring bushing.

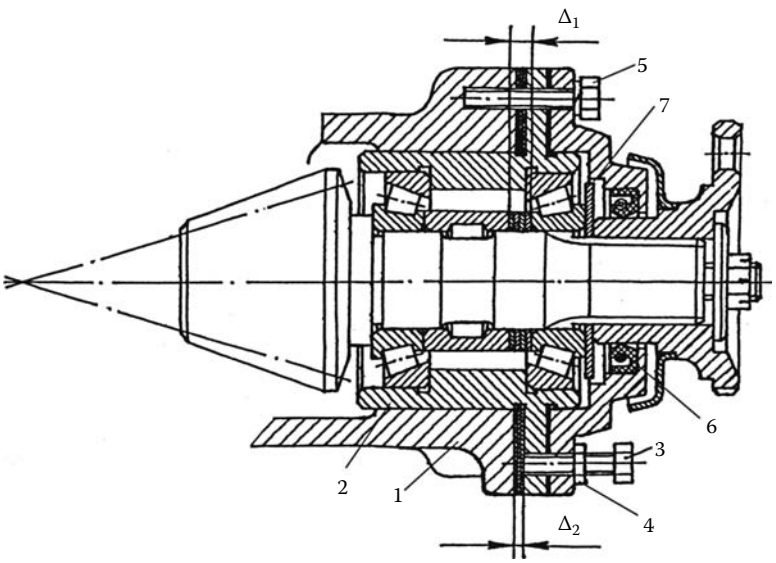


FIGURE 2.51
Drive-gear unit with bearings installed in a separate body: 1, sleeve; 2, bearing case; 3, disassembly bolts; 4, lock nut; 5, fastening bolts; 6, packing; 7, deflecting washer; Δ_1 is the size of the set of shims for bearing adjustment; Δ_2 is the size of the set of shims for adjusting the bevel-gear meshing.

It is usually comprised of two bolts 3, fastened to the roof of the bearing case by locknuts 4. Unscrewing the locknuts while uniformly screwing in disassembly bolts 3 that bear on the end of the sleeve of case 1, pushes bearing case 2 out. This, obviously, must be preceded by unscrewing bolts 5 of the bearing-body cover. In mass production, in order to improve the external appearance of the assembled product and simultaneously save components used for disassembly of bearing units, bodies and covers, use is made of the same bolts 5 (since they must in any case be removed before disassembly). Then bolts 3 and nuts 4 are not installed when assembling the unit and the holes remaining in it are protected from corrosion by special plastic plugs. The clearances in the bearings are adjusted by axially tensioning their cones and by sets of adjustment shims Δ_1, whereas the clearance in the gear meshing of the final drive is adjusted by means of packing shims Δ_2.

Still another example is shown in Figure 2.48. The ends of the cups of the bearings of the pinion shaft rest on the collars of the bearing body, whereas the end of the cone of one of them, on the pinion's side facet. To facilitate removal (disassembly) of the cups, two diametrically opposite slots 1 are produced at each side of the bearing body. They partially uncover the end of the cup to allow gripping it using the gripping device of the disassembly fixture. To remove the cone of the bearing from the gear shaft, access to its end facing the side facet of the pinion is left open. This is made possible by making the diameter of the side facet somewhat smaller than the outer diameter of the cone of the bearing (see 2 in Figure 2.48). If it is impossible to reduce the diameter of the side facet, then it is replaced by a spacer ring that is placed between the end of the pinion and the cone of the bearing (see Figure 2.41). This ring simultaneously serves for placing the final drive pinion at the distance required by assembly considerations.

Consider now the question of component durability. Durability is the ability of components to withstand all kinds of wear of the working surfaces and their potential subsequent

breakage. Improving the durability of the rubbing surfaces of components requires that they be designed with the following design and manufacturing considerations in mind:

- Keeping the pressures and contact stresses on component surfaces within permissible limits
- Ensuring optimal finish of rubbing surfaces
- Performing chemical and heat treatment of the surface layer (carburizing, carbonitriding, cyaniding, nitriding, induction hardening, etc.)
- Strengthening of surfaces, including rolling of fillets, sandblasting)

Surfaces subject to intensive wear are designed to be made of materials with high antifriction properties. Wear of working surfaces is reduced and their corrosion is minimized by specifying suitable lubricants and creating systems for supplying lubricants to them; arrangements are made for removal of heat from rubbing surfaces if the lubricants are incapable of sufficient heat removal. Corrosion is reduced by specifying protective metal coating and special paint applications.

A designer must constantly strive to make the shape of components simple and manufacturable. The last term applies to producing a design that can be manufactured in the most rational manner. Manufacturability is reflected in the cost. It must hence always be remembered that manufacturing processes capable of producing a component at the lowest cost should not do so at the penalty of the component's quality.

The concept of design manufacturability can be analyzed using the following example. Specifying a sunk key slot for the stepped shaft shown in Figure 2.52a is an example of poor manufacturability design, since the output rate of finger (end) mills that are used for milling such slots is very low.

This will manifest itself particularly under mass production conditions. As compared with this, specification of Woodruf (semicircular) key slots (see Figure 2.52b) is an example of manufacturable design because Woodruf key slots are milled by disk milling machines that have a much higher output rate than end mills. An even more manufacturable design is that with Woodruf key slots of the same size on both steps of the shaft (see Figure 2.52c). The manufacturability of this design is improved in the first place, since it dispenses with replacement of the milling cutter or with moving the shaft to another milling machine, and secondly because it allows using the same keys (reducing the nomenclature of the elements within the component), milling cutters (reducing the cutting-tool nomenclature) and reducing the nomenclature of measuring and inspection tools. It can be easily seen that the last shaft design is fully validated also from the point of view of the load on the keys. The same torque T is transmitted at the shaft lengths between the midpoints of lengths with diameters d_1 and d_2. If it is assumed that the torque is applied to the keys with an arm equal to the radius of the pertinent step, then the forces will come as $F_1 = 2T/d_1$ and $F_2 = 2T/d_2$. But $d_2 > d_1$ and hence $F_2 < F_1$. Calculations thus show that in this case there is no reason to use keys of a different size on the shaft.

Two general forms of specifying differential designing problems are possible:

- Designing a differential for a newly designed vehicle
- Designing a new differential for a vehicle already in production and on the market

In the first case there are no limitations on the design. On the other hand, when designing a new differential for an existing vehicle the product engineer faces many technical

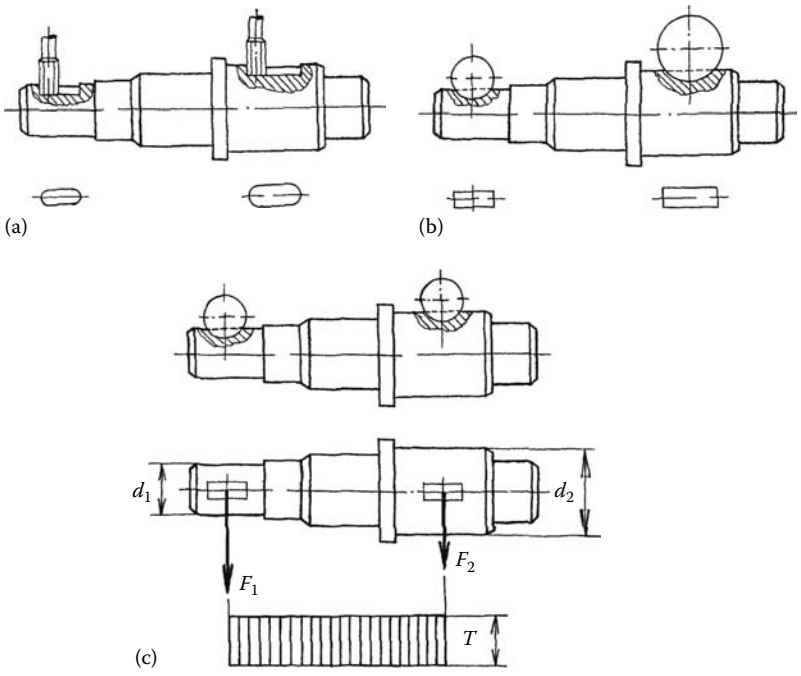


FIGURE 2.52
Design of shaft with key slots: (a) machined by finger (end) mill (poor manufacturability design); (b) and (c) machined by disk mills (manufacturable designs); d_1 and d_2 are the diameters of the necks of the shaft; F_1 and F_2 are the radial forces acting on the keys; T is the torque transmitted by the shaft.

problems. In the first place, the design should not require rebuilding the axle case and its elements. This requires leaving the base distance H (see Figure 2.53) between the bearings of the differential's housing as well as the bearings themselves unchanged.

To avoid redesigning the entire differential and changing the original gear ratio of the final drive, the location and number of teeth of the final-drive gear A (see Figure 2.53) must also be left unchanged. The location of the splined ends of the half axles also cannot be changed. In this case changes may be made only, to the extent that this is possible, in the space around the differential, the housing of the differential itself, the side gears, the pinions and the spider.

A design solution in which the bolts of the differential that connect the driven bevel gear of the final drive to the differential housing are subject to break should be avoided. Such a solution is shown in Figure 2.54a.

In this case, the bolts are subjected to break produced by force Q_a that is parallel to the principal axis of rotation of the differential and is a component of the force in the meshing of the final-drive gears. The design can be improved by using a two-stage final drive (see Figure 2.54b) with cylindrical gears in the second stage. It should, however, be remembered that two-stage final drives are preferable only when their gear ratio is 1:7. This is done, among others, in buses, where it is required to provide for the shortest distance between the passenger-space floor and the ground. Sometimes two-stage final drives are used at lower gear ratios, such as 1:5.5. This requires using small gears, a factor that also facilitates reducing the distance between the vehicle's floor and the ground. The floor of cars is caused to sit low by using hypoid final drives (see Figure 2.50) in which the axis of

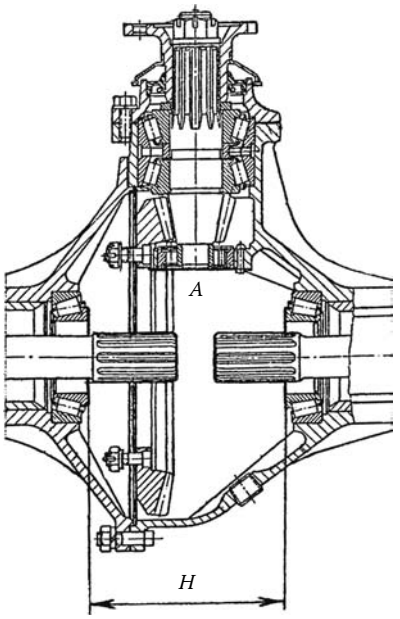


FIGURE 2.53
Examples of structural limitations in designing a new differential for a vehicle already being produced.

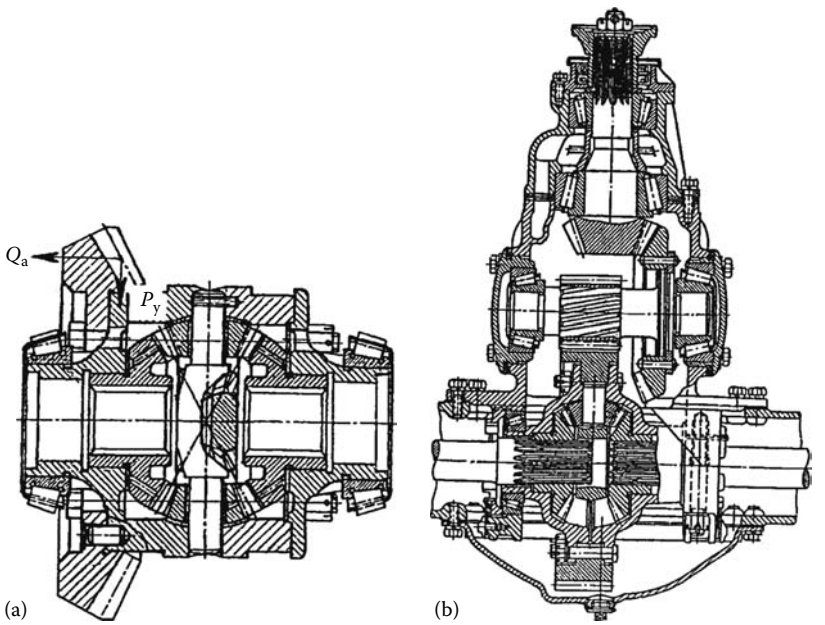


FIGURE 2.54
Design solutions for fastening the final-drive wheel: (a) irrational design; (b) rational design; Q_a and P_y are the axial and radial components acting in the meshing; the third force that is perpendicular to the sheet is not shown.

rotation of the pinion is located beneath the axis of rotation of the driven gear. Such drives have a low noise level, are well suited for heavy loads and allow obtaining a high gear ratio while using a final drive pinion with a small number of teeth. As a rule, such drives have a higher efficiency as compared with other types of teeth.

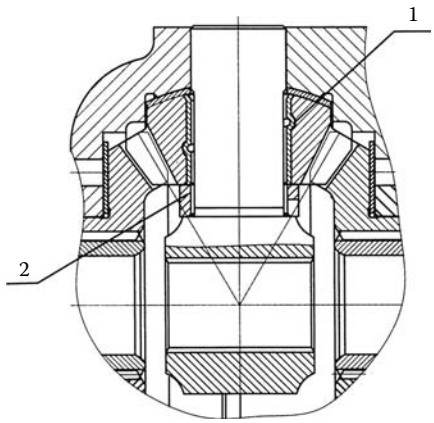


FIGURE 2.55
A version of axial securing of the rolled-up bronze bushing of the pinion: 1, rolled out part of the rolled-up bronze bushing; 2, thrust ring.

As mentioned before, differentials usually employ from two to four pinions. This makes it possible to avoid large bending forces on the journals of the pins and the spider and, most importantly, keep the differentials relatively small. Two pinions are usually used in the differentials of cars, even though cases when three pinions are used are also known. The pinions and the side gears should have a finely adjusted meshing with short teeth since, as a rule, they employ a small number of teeth. Pinions and side gears are manufactured from high-quality alloyed steels and are carburized. Pinion pins are made in the form of a complete spider (usually in heavier vehicles, Figures 2.48 and 2.54b). In lighter vehicles, the pinions are usually placed on two separately manufactured pins (see Figure 2.54a). The advantages and shortcomings of these designs were discussed in Section 2.4. Pinions are usually equipped with bronze bushings by means of which they rotate on the journals of the pins or spider. The bushings, made of tubular material, are pressed into the holes of pinions. Designs exist in which tubular bushings are pressed onto the spider pins. When rolled-up bushings (also called split bushings) are used, they are prevented from being pressed out from the pinions by rolling out 1 and thrust rings 2 (see Figure 2.55).

The most recent practice is not to use bronze bushings in differentials of heavy-duty vehicles that include, among others, high-power agriculture tractors, due to the particularly high pressures that arise in the spider-pinions contact. In such a case the pinions are installed on roller (pin) bearings 1 (see Figure 2.56).

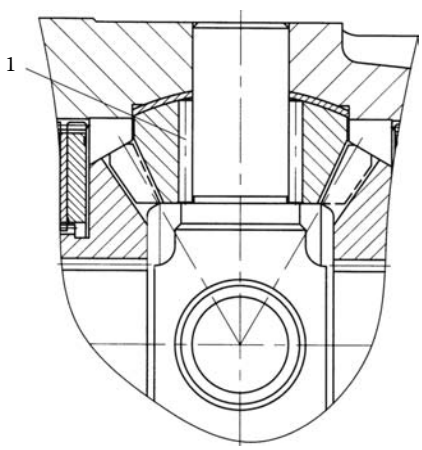


FIGURE 2.56
A method of placing a pinion on a roller bearing: 1, roller bearing.

Note that this design solution requires reducing somewhat the diameter of the spider pins while leaving the pinion teeth of the ordinary size. But, in spite of this, this still increases the service life of the pinion-spider coupling.

The axial forces exerted by the pinions and side gears are transmitted to the walls of the differential's housing through thrust washers. The pinions may use spherical (Figure 2.37a) or flat (Figure 2.37b) washers. As mentioned in Section 2.4, differentials with spherically shaped ends of pinions and similar thrust washers exhibit a somewhat higher robustness of the pinion–spider-pin rubbing pair than those employing flat-end pinions and flat thrust washers. Obviously, the spherical shape reduces somewhat the load on the pin, by taking up a part of the circumferential force. From this point of view, spherical pinion ends and spherical thrust washers of pinions are preferable.

The differential housing is manufactured either by casting from high-strength or malleable cast iron or by forging from high-quality steel. It is usually made demountable in the plane of the pinion axes, but may be open and not demountable when two pinions are used. Holes for supplying and removing the differential's lubricant are provided in the two parts of the differential's housing. The housing is supported on bearings that are most frequently single-row tapered roller bearings and less frequently radial-thrust ball bearings. All depends on the magnitude of the axial force exerted on the differential housing by the driven gear of the final drive. The interwheel differential is usually located in the middle of the axle.

Differentials of wheeled vehicles are, as a rule, designed according to a common concept. Still, some differentials exist that are an exception to this rule. The most original differential designs are examined below. Figure 2.57 shows the design of a cylindrical gear interwheel differential that is used in certain trucks.

Here the differential is placed ahead of the space between the half axles. The torque from the input shaft is transmitted to the differential housing and then, by pinions, to two gear shafts that drive the half axles. The right gear shaft is directly coupled to the final drive pinion of the bevel-gear pair of one of the half axles. The left gear shaft is coupled to the final drive pinion of the bevel-gear pair of the other half axle by a long hollow shaft. To ensure independent coupling of the two bevel-gear pairs, the half axles together with their bevel gears are shifted relative to one another in the longitudinal direction by approximately the size of the bevel-gear tooth. This arrangement of the differential drive of the half axles made it possible to solve a number of additional problems. In particular, it made it possible to make the axle the drive through axle without much difficulty. This, in its turn, makes it possible, by sequentially connecting such axles, to create a family of multiwheel drive vehicles with a different number of unified driving axles and also to put each driving wheel on an individual suspension. The wheel, together with its half axle, casing and final drive driven gear, may perform angular motion (rolling) about the central longitudinal axis of the axle. In this case, the driven gear that sits on the half axle rolls about the final drive bevel pinion.

Figure 2.58 is a schematic of the design of an open spur-gear differential.

Usually such differentials have imposing dimensions. This differential is made unique by the fact that it is much smaller than its usual counterparts. This was made possible by using pinions 6 connected rigidly by a single shaft that have the same number of teeth but a different module. This made it possible to bring the tooth wheels of the pinions close to one another, thus reducing the differential's dimensions.

This differential is constructed as follows. Side gears 4 and 7 are seated on half axles 3 and 8. The side gears have 21 teeth each, but the tooth module of gear 4 is 4.5 mm, whereas that of gear 7 is 5 mm, meaning the gear 7 has a larger diameter. A small clearance exists

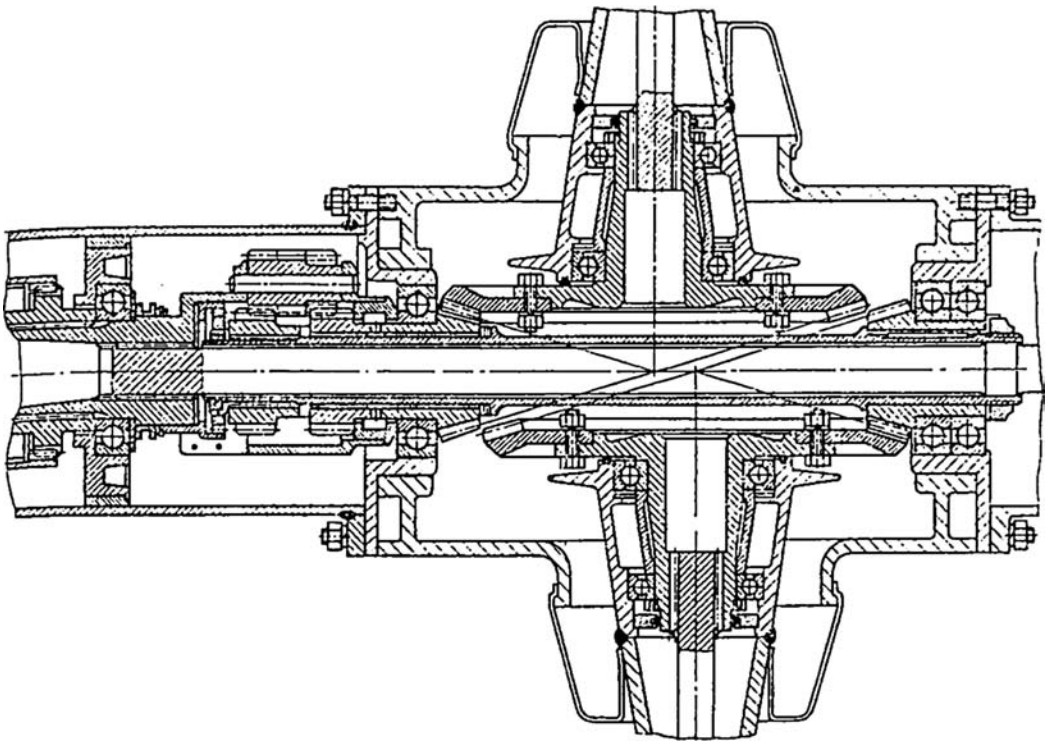


FIGURE 2.57
Spur-gear interwheel differential of a truck.

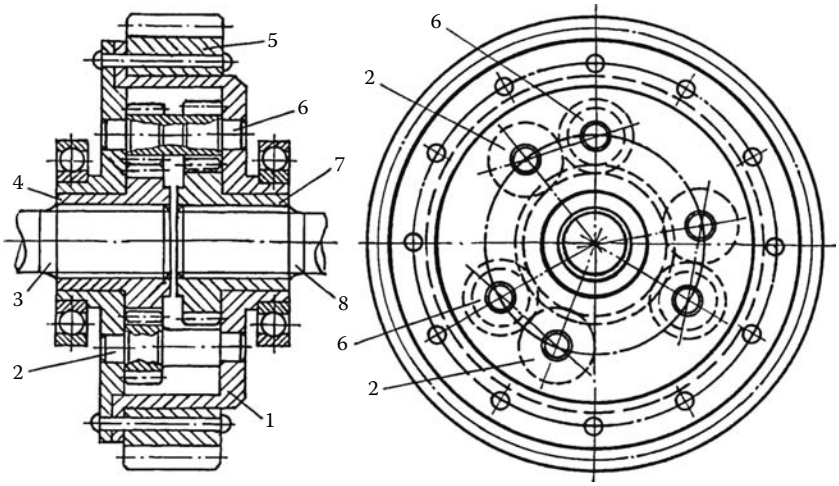


FIGURE 2.58
Differential with spur gears: 1, casing; 2, intermediate pinion; 3 and 8, half axles (output shafts); 4 and 7, side gears; 5, driven gear of the final drive; 6, pinion.

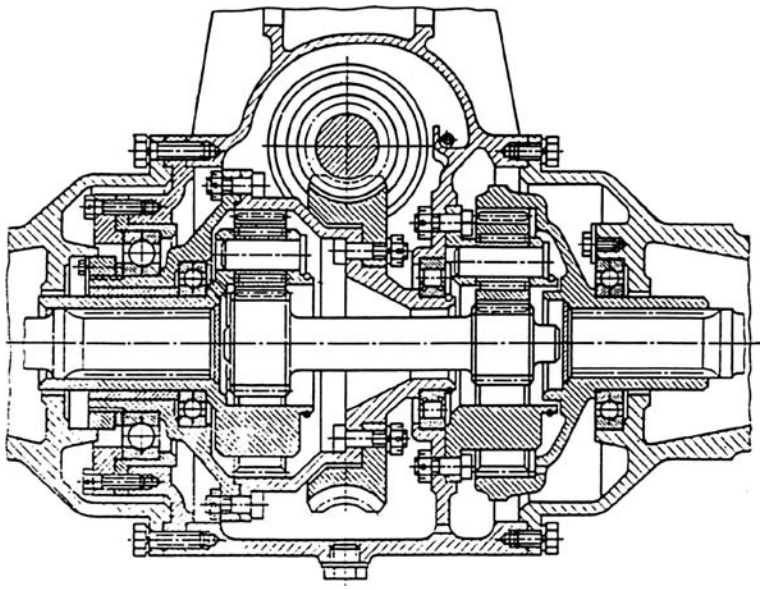


FIGURE 2.59
Interwheel differential with double planetary transmission.

between the ends of both these side gears. The transmission from one side gear to another is by means of three pinions 6. The left toothed wheel of the pinion, that has a somewhat smaller diameter, has 11 teeth with a module of 4.5 mm and meshes with gear 4 by means of intermediate pinion 2. There are three such intermediate pinions 2 in the differential and such a number of pinions 6. The right toothed wheel (having the larger diameter) of the pinion 6 also has 11 teeth, but with a module of 5 mm. It meshes directly with side gear 7. The mechanism is held in casing 1 with driven gear 5 of the final drive.

The differential shown in Figure 2.59 is also an original interwheel differential.

The mechanism consists of two planetary rows with spur gears. The torque in it is transmitted from the final worm drive to the epicyclical (ring) gear of the left row. The axles of the pinions and the carrier of this row are coupled to the left half axle that transmits torque to the left driving wheel. The sun gears of both rows are connected by a common shaft. The axles of the pinions of the right row do not rotate and are fastened to the speed reducer housing. The torque to the right half axle (to the right driving wheel) is transmitted from the epicyclical (ring) gear of the right row.

2.5.2 Design of Differential Geometry

As discussed in Section 2.4, improvement of differentials is still high on the engineering agenda. This is because the conditions of their operation become increasingly more complex. In the truck industry, the ever-increasing traction loads on axles caused by the rising carrying capacity of vehicles and the use of two-, three- and more driven units (trailers and semitrailers) has caused an increase in the loads to which components of differentials are subjected. With rising specific powers of the vehicles, their speeds and, in particular, with introduction of wheel-hub planetary gear drives, the velocity mode of differential performance has become increasingly more complicated. This caused increasing wear of the

differentials' components; their breakage and premature failures have become more frequent. All this is detrimental to the reliability and trouble-free performance of vehicles.

The wear of differential components basically stems from two operational factors: load forces and the rate of sliding of rubbing surfaces. Whereas the load forces on the differential's components can be determined to some extent, this does not apply to the velocity mode. There is virtually no relative motion of the differential's components when the vehicle travels in a straight path. This motion occurs only when the vehicle travels along a curved path and also under unfavorable road conditions, when the wheels have different skids. For this reason, it is very difficult to determine the velocity mode of the differential's components. This is responsible for the fact that engineering design of differentials is, as a rule, limited to analysis of load forces. This problem became particularly acute with the advent of vehicles with wheel-hub gear drives in their driving axles, since the dimensions of the differentials of these vehicles are smaller because they are subject to lesser load forces. However, this increases the importance of velocity factors, but these are left out of calculations.

The above made it necessary to develop, albeit a conditional, but sufficiently satisfactory method of design which could allow assessing the robustness of a given differential from the point of view of wear resistance and service life. A method was developed in the course of research that was based on comparing the results of calculating approximating criteria of differentials of different vehicles of similar class under identical operating conditions. This approach makes it possible to draw conclusions on the perfection level of the differential's geometry at the design stage as compared with existing designs.

A vexing and complicated problem remained in creating a design method: what are the criteria to be used in assessing and comparing the differentials of different vehicles? What criteria should be in the focal point when designing new mechanisms? Such criteria are current almost or entirely not available. For this reason, the creation of the method had to be started with developing criteria to be used in assessment. They are basically conditional or semiconditional, but it turned out that they quite satisfactorily characterize the operating processes of the mechanism and, what is of most substance, are convenient in comparison and comparative assessment of the differentials of a variety of vehicles.

The force and velocity factors taken together determine the energy load (energy loading) of the mechanism. It is obvious that this loading is associated not only with operating factors, but also with the geometric parameters of the differential. This made it necessary to introduce a conditional dimensional parameter of the differential—the conditional cross-sectional area of the mechanism (see Figure 2.60)

$$A_{\mathrm{d}} = z_{\mathrm{g}} z_{\mathrm{c}} m_{\mathrm{te}}^2 \tag{2.87}$$

where z_{g} and z_{c} are the numbers of teeth of the side gear and pinion, whereas m_{te} is the outer module.

The energy-loading factor K_{N}, kW/cm^2 of a differential, which is the result of dividing the power P_0 supplied to the differential, by the conditional area A_{d}

$$K_{\mathrm{N}} = \frac{P_0}{z_{\mathrm{g}} z_{\mathrm{c}} m_{\mathrm{te}}^2} \tag{2.88}$$

was suggested as the first assessment criterion.

Factor K_{N} is a rather conditional complex indicator of the intensity of the working process of the differential. A given differential can be assessed by comparing the values of K_{N} of differentials of different vehicles.

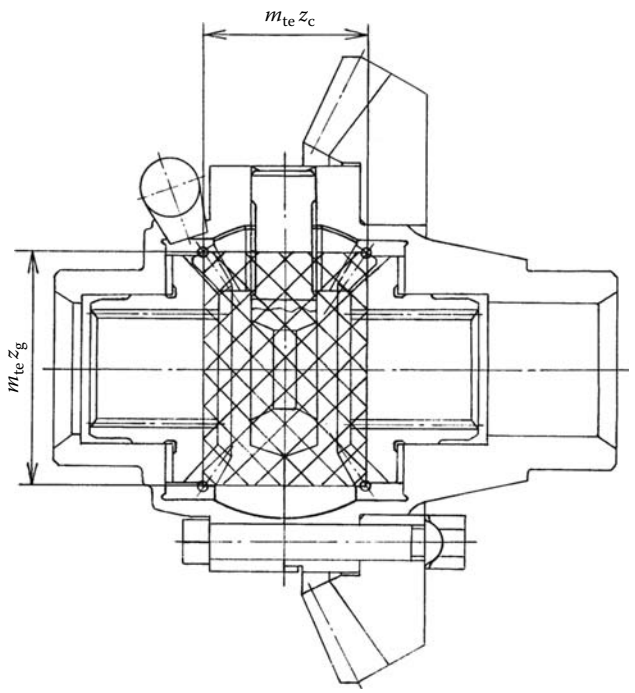


FIGURE 2.60
Conditional area of a differential.

Since power is work per unit time, it may be assumed that K_N reflects to some extent the theoretical level of wear of elements of differentials of the vehicles being compared over the same time of their operation. It is assumed here that the magnitude of wear is proportional to the friction work in the differential and with it, to the power.

For comparative assessment of the elements of differentials of different vehicles during the travel over their entire service life one also introduces the lifetime mileage wear factor. A certain amount of friction work is performed in each vehicular differential over the specified mileage:

$$W_0 = P_0(1 - \eta_n)t \tag{2.89}$$

where η_n is the efficiency of the differential, t is the time of operation of the vehicle over the lifetime mileage L_a. It is assumed that the magnitude of wear of the differential's elements is proportional to the friction work W_0. Dividing W_0 by A_d, yields the conditional specific friction work that shall be called the mileage wear factor K_u, or simply the wear factor:

$$K_u = \frac{W_0}{A_d} = \frac{P_0(1 - \eta_n)t}{A_d} \tag{2.90}$$

Setting $t = \dfrac{L_a}{V_a}$, formula (2.90) is written as

$$K_u = \frac{P_0(1 - \eta_n)L_a}{A_d V_a} \tag{2.91}$$

Vehicle velocity V_a shall be defined somewhat later in this section.

If it is assumed that the mileage L_a of the differentials of the different vehicles being compared is the same (in which case it can be eliminated from formula (2.91)), then the physical meaning of K_u consists in reflecting to some measure the theoretical degree of wear of the differential's elements over a given mileage.

The next criterion for differential assessment is an indicator that reflects the angular or linear velocity of a given element of a differential under the following conditions: one output shaft of the mechanism rotates whereas the other is stopped, in which case the work of the engine and transmission is that expended in the vehicle's rectilinear motion at velocity V_a. Thus, the angular and linear velocities of the pinion relative to the spider pin (on the friction surface) is given by the expressions (Figure 2.61)

$$\omega_c = \omega_0 \frac{z_g}{z_c} \tag{2.92}$$

$$V_c = \omega_c r_{sp} \tag{2.93}$$

Additional assessment criteria are also used. These are

- Torque T_0 on the differential's housing, calculated from the circumferential forces of the wheels $F'^{(\prime\prime)}_{xi}$, gear ratios of the wheel-hub planetary gear drives and radii of the wheels
- The differential's force loading factor

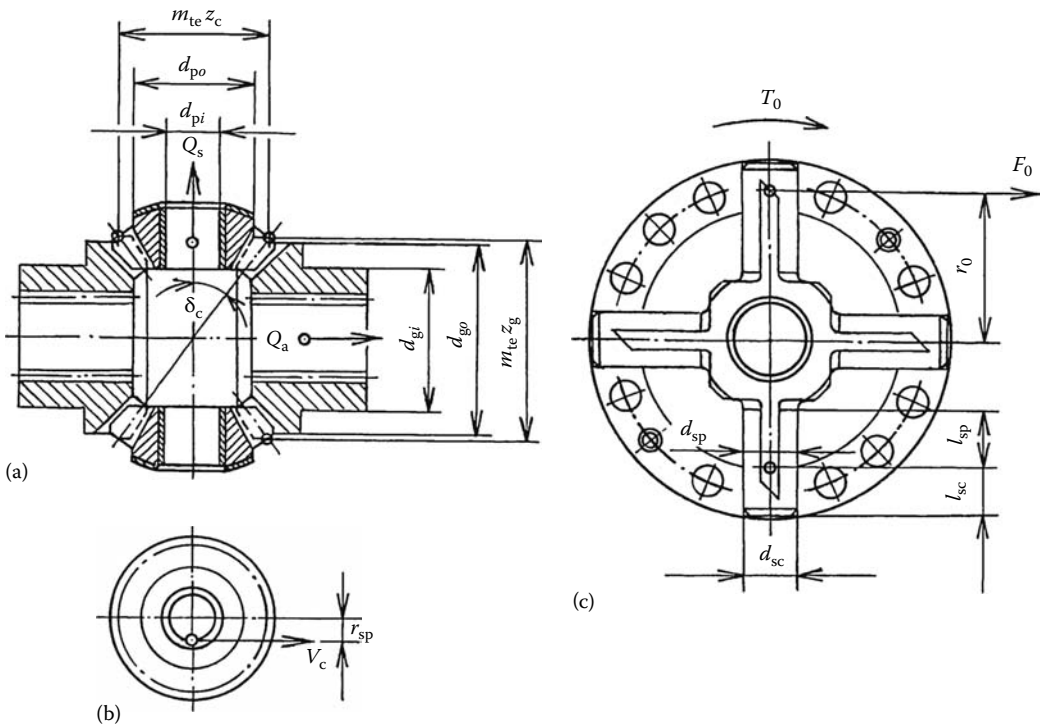


FIGURE 2.61
A differential: (a) longitudinal cross section; (b) top view of a pinion; (c) side cross section.

$$K_{\mathrm{M}} = \frac{T_0}{m_{\mathrm{te}}^2 z_{\mathrm{g}} z_{\mathrm{c}}} \tag{2.94}$$

- The circumferential force and pressure at the contact between the spider and the pinion (in four-pinion differentials)

$$F_{\mathrm{b}} = \frac{T_0}{2m_{\mathrm{te}} z_{\mathrm{g}}}, \quad p_{\mathrm{b}} = \frac{F_{\mathrm{b}}}{d_{\mathrm{sp}} l_{\mathrm{sp}}} \tag{2.95}$$

- The circumferential force and pressure in the contact between the spider and the housing (in four-pinion differentials)

$$F_0 = \frac{T_0}{4r_0}, \quad p_0 = \frac{F_0}{d_{\mathrm{sc}} l_{\mathrm{sc}}} \tag{2.96}$$

- Axial force and pressure in the thrust washer of the side gear

$$Q_{\mathrm{a}} = \frac{T_0 \tan \alpha_{\mathrm{w}} \cos \delta_{\mathrm{c}}}{m_{\mathrm{te}} z_{\mathrm{g}}} \tag{2.97}$$

$$p_{\mathrm{a}} = \frac{Q_{\mathrm{a}}}{0.25\pi\left(d_{go}^2 - d_{gi}^2\right)}$$

where α_{w} is the pressure angle and δ_{c} is the pitch angle of the pinion

- Axial force and pressure in the pinion washer

$$Q_{\mathrm{s}} = \frac{T_0 \tan \alpha_{\mathrm{w}} \sin \delta_{\mathrm{c}}}{2m_{\mathrm{te}} z_{\mathrm{g}}} \tag{2.98}$$

$$p_{\mathrm{c}} = \frac{Q_{\mathrm{s}}}{0.25\pi\left(d_{\mathrm{p}o}^2 - d_{\mathrm{p}i}^2\right)}$$

Formulae (2.87) through (2.98) were used for analytically investigating the assessment criteria of interwheel differentials of different vehicles, the results of which are presented below.

2.5.2.1 Highway Heavy-Duty Trucks

The method described above assumes that vehicles the differentials of which are being compared travel under similar conditions. The investigation was performed for the following conditions of all the trucks consisting of 4×2, 6×4, and 6×6 tractors and semitrailers. The calculations were performed for mass m_{a} of a fully loaded truck. The velocity assumed for calculating the velocity modes of the differential's elements was that measured in traveling over high-grade roads from the expression

$$V_{\mathrm{avg}} = 0.8 V_{\max} \tag{2.99}$$

Expression (2.99) was compiled on the basis of experimental data that show that the average operating speed of highway heavy-duty trucks is of the order of 80% of the maximum speed $V_{\max}$ if any limitations on the driving speed of the trucks are removed (Farobin and Shuplyakov). The average operating speed of off-road all-wheel drive vehicles traveling on paved roads also does not exceed 0.8 of the maximum. The hypothetical velocity mode of elements of differentials of trucks moving outside paved roads was calculated by analyzing the average velocities of timber-carrying trucks. It was established that for such vehicles moving under off-road conditions

$$V_{\text{avg}} = 0.48V_{\max} \tag{2.100}$$

The total circumferential force for uniform travel of a truck over a horizontal path was determined from the expression

$$F_{x\Sigma} = m_{\text{a}}gf + D_{\text{a}} \tag{2.101}$$

where D_{a} is the air drag; the rolling resistance coefficient f was taken to be a speed function of the trucks.

The power $P^{\text{in}}_{w\Sigma}$ that is developed by the wheels of the driving axle of a 4×2 tractor can be calculated from the formula (to simplify the computations, it was assumed that it is equal to power P_0 supplied to the interwheel differential)

$$P^{\text{in}}_{w\Sigma} = P_0 = F_{x\Sigma}V_{\text{avg}} \tag{2.102}$$

For 6×4 tractors with symmetrical interaxle differential in the tandem, the circumferential force F_x and the power P_0, referred to one axle, are

$$F_x = 0.5F_{x\Sigma}, \quad P_0 = 0.5F_{x\Sigma}V_{\text{avg}} = F_xV_{\text{avg}} \tag{2.103}$$

For 6×6 tractors with asymmetrical differential in the transfer case with a gear ratio of, let us say $u_{\text{d}} = 2$,

$$F_x = \frac{F_{x\Sigma}}{1 + u_{\text{d}}} = \frac{F_{x\Sigma}}{3}, \quad P_0 = F_xV_{\text{avg}} \tag{2.104}$$

The parameters computed from formulae (2.99) through (2.104) determine the operating mode of the drive axle's differential. Using these formulae, formula (2.91) for the mileage wear factor is written as

$$K_{\text{u}} = \frac{(m_{\text{a}}gf + D_{\text{a}})(1 - \eta_{\text{n}})L_{\text{a}}}{l_{\text{MK}}A_{\text{d}}} \tag{2.105}$$

where $l_{\text{MK}} = 1$, 2, and 3, respectively, for 4×2, 6×4 and 6×6 tractors.

Studies were performed on the assumption that the total mileage traveled was the same for all the vehicles, which allowed eliminating L_{a} from formula (2.105). The value of K_{u} is decisively affected by mass m_{a} of the truck and by the differential's cross-sectional area A_{d}. For this reason, when lacking certain data contained in formula (2.105), it is possible to use the simplified relationship

$$K'_{\text{u}} = \frac{m_{\text{a}}}{l_{\text{MK}}A_{\text{d}}} \tag{2.106}$$

Since the method suggested above is based on comparing differentials of different vehicles, it becomes necessary to analyze the greatest possible number of trucks. The values of power and mass and geometric parameters of trucks and their differentials were taken from advertisement catalogs and by direct measurements of parts of the differentials. The values of these parameters are given in Tables 2.9 and 2.10 (the notation of the principal geometric parameters is given in Figure 2.61).

The results of analytic investigation of assessment criteria of interwheel differentials are listed in Table 2.11.

As expected, factors K_N and K_u have higher values in vehicles with wheel-hub gear drives. This is seen from Table 2.11 and also from Figures 2.62 and 2.63.

The average values of K_N for vehicles with wheel-hub gear drives and without them are 0.67 and 0.30, respectively. The ratio of these two is 2.23. Here the values of K_N and K_u for 4×2 vehicles if greater than for 6×4 vehicles. The latter stems from the higher traction load on the axles of the 4×2 vehicles, which are seen from Figures 2.62 and 2.63.

The results of investigating the velocity modes of components of differentials are presented in Table 2.11 and Figure 2.64.

The linear velocity V_c of motion of the pinion over the pin of the spider of vehicles with wheel-hub gear drives is much higher. The average value of these velocities is 2.67 m/s, while being only 1.02 m/s for vehicles without wheel-hub gear drives. The ratio of these quantities is 2.62. The above applies also to other sliding elements of the differential's components.

On the other hand, the pressure in the contact between the pinion and the spider pin are almost the same in vehicles with and without wheel-hub gear drives (Table 2.11 and Figure 2.65).

The close values of p_b and the marked difference in V_c of these and other vehicles are in fact responsible for the higher energy loading of the differentials of vehicles with wheel-hub gear drives. Other data were also obtained in the course of the computations and these are listed in Table 2.11.

Figures 2.62 and 2.63 give the values of K_N and K_u as a function of the power load P_0 on the axles (for 6×4 vehicles—for one of the two axles). On the basis of this it becomes possible to compare and assess the loading and wear resistance of the differentials of axles of different vehicles. The graphs presented in Figures 2.64 and 2.65 were constructed on the same principle.

2.5.2.2 Articulated Timber Carriers

The above situation was observed also in investigating the interwheel differentials of 11 articulated timber carriers (tractor-semitrailer combinations), of which eight models had wheel-hub gear drives (see Table 2.12).

The values of the energy loading factor of the KrAZ carrier that does not have a wheel-hub gear drive is much lower than in timber carriers with such differentials (Figure 2.66).

The same applies to the Renault differential with low gear ratio of its wheel-hub gear drive. The differentials of Mercedes-Benz vehicles are subjected to a greater load both because of the smaller cross-sectional area, A_d and the presence of a wheel-hub gear drive.

The interwheel differentials of timber carriers with wheel-hub gear drives are subjected to larger working loads and hence have higher wear rates. However, it is known that the use of wheel-hub gear drives in heavy-duty vehicles caused improvement of a number of their design and operational indicators. The mass and dimensions of the central speed reducers became smaller, the energy load on the half axles was decreased, etc. This, in its

TABLE 2.9

Estimated Parameters of Highway Heavy-Duty Trucks

No.	Model	Full Mass m_a, t	Mass Taken by Drive Wheels m_{dr}, t	Engine Power P_e, kW / HP	Engine Speed rad/s / rpm	Speed m/s / km/h: Maximum V_{max}	Speed m/s / km/h: Average Operational V_{avg}	Gear Ratio: Driving Axle u_a	Gear Ratio: Final Drive u_f	Gear Ratio: Wheel-Hub Gear Drive u_k	Tire: Radius r, m
4 × 2											
1	ZIL 130 B1	18.53	7.9	110.3 / 150	334.9 / 3200	24.93 / 90	19.94 / 71.78	6.32	6.32	—	9–20 / 0.485
2	MAZ 200 B	23.06	10.2	95.7 / 130	209.3 / 2000	15.28 / 55	12.22 / 43.99	9.81	9.81	—	12–20 / 0.522
3	MAZ 504 B	32.35	10.0	176.5 / 240	219.8 / 2100	23.55 / 85	18.84 / 67.82	7.74	2.67	2.9	11R 20 / 0.505
4	MAZ 5432	34.00	10.0	206.0 / 280	219.8 / 2100	25.48 / 92	20.38 / 73.37	5.88	1.714	3.428	11R 20 / 0.505
6 × 4											
5	ZIL 133 ГЯ	29.34	13.4	154.4 / 210	272.1 / 2600	23.55 / 85	18.84 / 67.82	6.83	6.83	—	9–20 / 0.485
6	KamAZ 54112	33.33	14.0	154.4 / 210	272.1 / 2600	22.2 / 80	17.78 / 63.94	7.22	7.22	—	9–20 / 0.485
7	KamAZ 258 Б1	39.20	18.0	176.5 / 240	219.8 / 2100	18.84 / 68	15.07 / 54.25	8.21	8.21	—	12–20 / 0.522
8	MAZ 64227	38.00	18.0	236.5 / 320	219.8 / 2100	25.48 / 92	20.38 / 73.37	5.88	1.714	3.428	11R 20 / 0.505
9	Scania 142N	38.00	18.0	256.7 / 350	230.3 / 2200	27.70 / 100	22.16 / 79.78	3.89	3.89	—	11R 20 / 0.505
10	Volvo F 12	38.00	20.0	276 / 375	230.3 / 2200	29.17 / 105	23.34 / 84.02	4.88	2.44	2	11R 20 / 0.505
11	Mercedes Benz 2232	38.00	16.0	257.6 / 350	261.7 / 2500	27.15 / 98	21.72 / 78.19	5.27	1.33	3.96	11R 20 / 0.505
12	Renault R 310 T	34.28	16.0	225.2 / 306	219.8 / 2100	31.94 / 115	25.55 / 91.98	5.90	2.95	2	11R 20 / 0.505

TABLE 2.10

Estimated Parameters of Interwheel Differentials

		Side Gear					Pinion									Spider			
		Tooth Number	Outer Friction Diameter, mm	Inner Friction Diameter, mm	Average Friction Radius, mm	Average Gear Radius, mm	Tooth Number	Outer Friction Diameter, mm	Inner Friction Diameter, mm	Average Friction Radius, mm	Average Pinion Radius, mm	Pitch Angle, deg	Outer Module, mm	Pressure Angle, deg	Conditional Cross Section Area, cm^2	Spider Pin Diameter in Contact with Pinion, mm	Spider Pin Length in contact with Pinion, mm	Spider Pin Length in contact with Case, mm	Average Radius, mm
No.	Model	z_g	d_{go}	d_{gi}	r_{gf}	r_g	z_c	d_{po}	d_{pi}	r_{cf}	r_c	δ_c	m_{te}	α_w	A_d	d_{sp}	l_{sp}	l_{sc}	r_0
4 × 2																			
1	ZIL 130 B1	22	122	60	45.50	55	11	58	28	21.50	30	26°34′	6.35	22°30′	97.58	28	30	12	85
2	MAZ 200 B	22	140	82	55.50	75	11	70	30	25	37	26°34′	8	20°	154.88	30	32	20	108
3	MAZ 504 B	18	100	68	42	43	11	56	26	20.50	25	31°30′	6	22°30′	71.28	25	28	22	75
4	MAZ 5432	16	110	70.5	45.13	49	11	65	32	24.25	31	34°31′	7	22°30′	86.24	32	29.5	25	85
6 × 4																			
5	ZIL 133 ГЯ	22	122	60	45.50	55	11	58	28	21.50	30	26°34′	6.35	22°30′	97.58	28	30	12	85
6	KamAZ 54112	22	124	76	50	58	11	58	30	22	29	26°34′	6.35	22°30′	97.58	28	30	18	87
7	KamAZ 258 Б1	22	148	82	57.50	74	11	72	33	26.25	36	26°34′	8	20°	154.88	30	39	18	108
8	MAZ 64227	16	110	70.5	45.13	49	11	65	32	24.25	31	34°31′	7	22°30′	86.24	32	29.5	25	85
9	Scania 142N	18	124	80	51	68	11	76	34	27.20	37	31°26′	7.75	22°30′	118.92	32	34	26	95
10	Volvo F 12	16	122	72	48.5	57	9	65	30	23.75	33	29°22′	8.25	22°30′	98.01	30	29	22	88
11	Mercedes Benz 2232	16	82	62	36	48	10	48	22	17.50	23	32°	5.75	22°30′	52.90	22	24	18	65
12	Renault R 310 T	16	92	65	39.25	42	11	65	26	22.75	32	34°31′	7	22°30′	86.24	26	29	28	85

TABLE 2.11

Evaluation Criteria of Heavy-Duty Trucks' Interwheel Open Differentials

No.	Model	$F_{x\Sigma}$, kN	$P^{in}_{w\Sigma}$, kW	k_N, $\frac{kW}{cm^2}$	$k_u \times 10$, $\frac{kN}{cm^2}$ k'_u, $\frac{t}{cm^2}$	ω_0, rad/s ω_c, rad/s V_c, m/s	F_b, kN p_b, MPa	F_0, kN p_0, MPa	Q_a, kN p_a, MPa	Q_c, kN p_c, MPa
4 × 2										
1	ZIL 130 B1	2.68	53.52	0.55	0.27	41.12	4.66	3.83	3.45	0.86
					0.19	82.24	5.55	11.39	0.39	0.43
						1.15				
2	MAZ 200 B	1.89	23.05	0.15	0.12	23.42	2.80	2.28	1.82	0.45
					0.15	46.84	2.91	3.80	0.18	0.14
						0.70				
3	MAZ 504 B	3.31	62.38	0.88	0.46	108.19	2.67	1.92	1.88	0.58
					0.45	177.04	3.81	3.49	0.45	0.30
						2.21				
4	MAZ 5432	3.67	74.82	0.87	0.43	138.37	2.41	1.59	1.65	0.57
					0.39	201.26	2.51	1.99	0.29	0.23
						3.22				
6 × 4										
5	ZIL 133 ГЯ	3.14	59.07	0.30	0.16	38.85	2.72	2.23	2.01	0.50
					0.15	77.69	3.23	6.64	0.23	0.25
						1.09				
6	KamAZ 54112	3.20	56.76	0.29	0.16	36.82	2.77	2.23	2.05	0.51
					0.17	73.24	3.30	4.42	0.27	0.27
						1.03				
7	KrAZ 258 Б1	3.14	47.35	0.15	0.10	28.87	2.33	1.90	1.52	0.38
					0.13	57.75	1.99	3.51	0.13	0.12
						0.87				
8	MAZ 64227	3.91	79.63	0.46	0.23	138.37	1.28	0.85	0.88	0.30
					0.22	201.26	1.34	1.06	0.16	0.12
						3.22				
9	Scania 142N	3.67	81.29	0.34	0.15	43.88	3.32	2.44	2.35	0.72
					0.16	71.81	2.71	2.68	0.33	0.20
						1.26				
10	Volvo F 12	3.90	90.91	0.46	0.20	92.42	1.86	1.40	1.34	0.38
					0.19	164.30	2.14	2.12	0.18	0.14
						2.46				
11	Mercedes Benz 2232	3.59	77.89	0.74	0.34	170.32	1.24	0.87	0.87	0.27
					0.36	272.51	2.35	2.19	0.39	0.19
						3.00				
12	Renault R 310 T	4.18	106.91	0.62	0.24	101.20	2.36	1.55	1.61	0.55
					0.20	147.19	3.13	2.13	0.48	0.20
						1.91				

turn made it possible to increase the clearance (the distance to the ground), which is particularly important for terrain vehicles. Experience shows that it is possible to find ways of increasing the wear resistance of differentials also for vehicles with wheel-hub gear drives. These include, in the first place improved circulating lubrication systems (see material in Section 2.5.3).

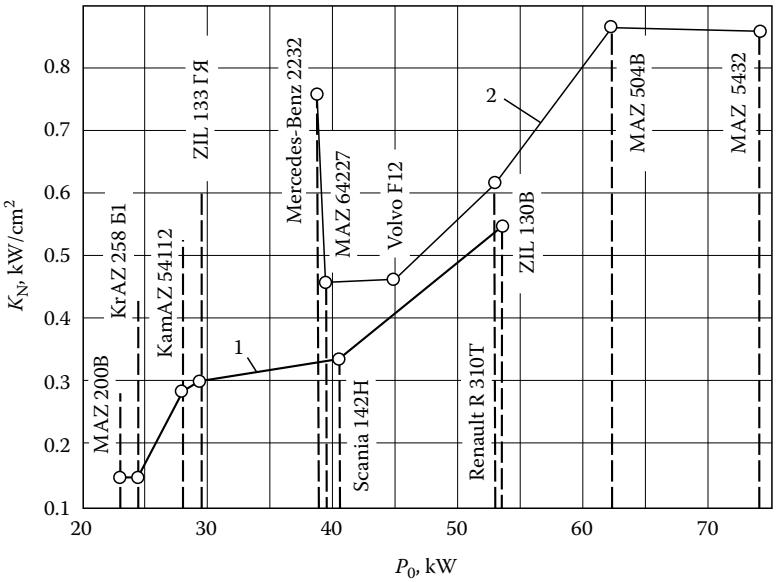


FIGURE 2.62
Energy loading factors K_N. 1, trucks without wheel-hub gear drives; 2, trucks with wheel-hub gear drives.

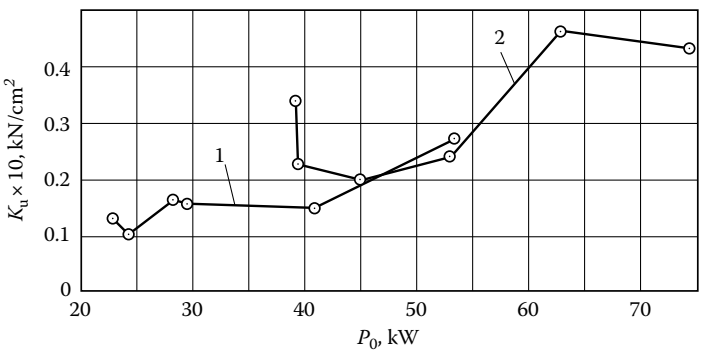


FIGURE 2.63
Mileage wear factors K_u. 1, trucks without wheel-hub gear drives; 2, trucks with wheel-hub gear drives.

2.5.2.3 Farm Tractors

The comparative assessment of performance of interwheel differentials was performed for road and field conditions, postulated to be the same for all the tractors under study. It was assumed that the tractors move uniformly in a straight line with the traction load consisting of grain-field stubble.

Drawbar pull (traction load) F_d of the tractors varies within wide limits depending on the farm implements and tools that the tractor operates. The calculations were based on the value of the most probable load F_d^m that is equal to the mathematical expectation of the tractor drawbar pull distribution density. Analysis of the distribution density of F_d—the

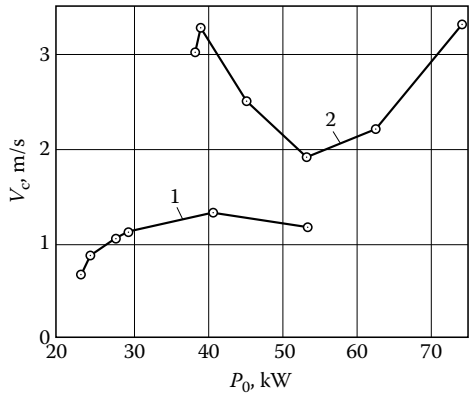


FIGURE 2.64
Linear sliding velocities V_c: 1, trucks without wheel-hub gear drives; 2, trucks with wheel-hub gear drives.

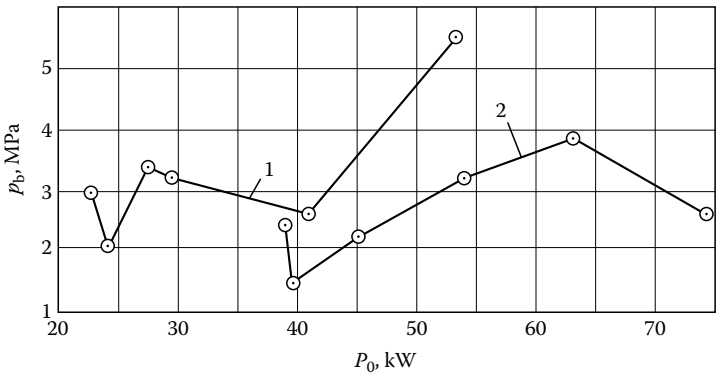


FIGURE 2.65
Pressure p_b in the contacts of pinions and spider pins: 1, trucks without wheel-hub gear drives; 2, trucks with wheel-hub gear drives.

drawbar pulls of tractors showed that the value of F_d^m can be determined with sufficient accuracy from the expression:

$$F_d^m = 0.6F_d^N \tag{2.107}$$

where F_d^N is the nominal drawbar pull that defines the traction class of the tractor.

For the conditions of motion under study the total circumferential force of the tractor's wheels is

$$F_{x\Sigma} = m_a g f + F_d^m \tag{2.108}$$

The rolling resistance factor f that represents the rolling resistance force on the wheels was taken to be the same for all the tractors and equal to 0.1.

Force $F_{x\Sigma}$ determines the loads on the elements of interwheel differentials of 4×2 tractors. In calculating the loads of these differentials of 4×4 tractors, this force should be distributed between the two driving axles with consideration of the specifics of interaxle power-dividing units.

TABLE 2.12

Estimated Parameters of Articulated Timber Carriers

No.	Model	Full Mass m_a, t	Mass Taken by Drive Wheels m_{dr}, t	Engine Power P_e, kW/HP	Speed m/s / km/h: Maximum V_{max}	Speed m/s / km/h: Average Operational V_{avg}	Gear Ratio: Driving Axle u_a	Gear Ratio: Final Drive u_f	Gear Ratio: Wheel-Hub Gear Drive u_k	Tire: Radius r, m
6 × 4										
1	Mercedes Benz 2232S-I				26/93	21/74	5.261	1.329		12 R 22.5/0.527
	Mercedes Benz 2232S-II	38	16	235.5/320	23/82	18/66	5.921	1.495	3.96	
	Mercedes Benz 2232S-III				20/72	16/58	6.734	1.701		
2	Mercedes Benz 2635	38	20	260.5/354	22/80	17.8/64	6.734	1.701	3.96	12 R 22.5/0.527
3	Renault GBH 340	40	21	247/336	22/80	17.8/64	5.9	2.95	2	12 R 22.5/0.527
4	KrAZ E6437	47	20.8	235/320	20.1/72.5	16/58	8.17	8.17	—	12.00-20/0.537
6 × 6										
5	KamAZ 43105	27.35	15.53	154.4/210	24/85	19/68	7.22	7.22	—	12.20 × 400-533/0.549
6	MAZ 6425	44	26	235.5/320	24/85	19/68	6.59	1.92	3.428	12.00-20/0.537
7	Mercedes Benz 2635 AK/35	44	27.5	260.5/354	22/80	17.8/64	6.734	1.701	3.96	12 R 22.5/0.527
8	KrAZ 6437	47	26.8	235/320	20.1/72.5	16/58	8.17	8.17	—	12.00-20/0.537
9	MoAZ 7411	88.61	48.76	368/500	19/68	15/54	15.06	2.69	5.6	16.00-25/0.712

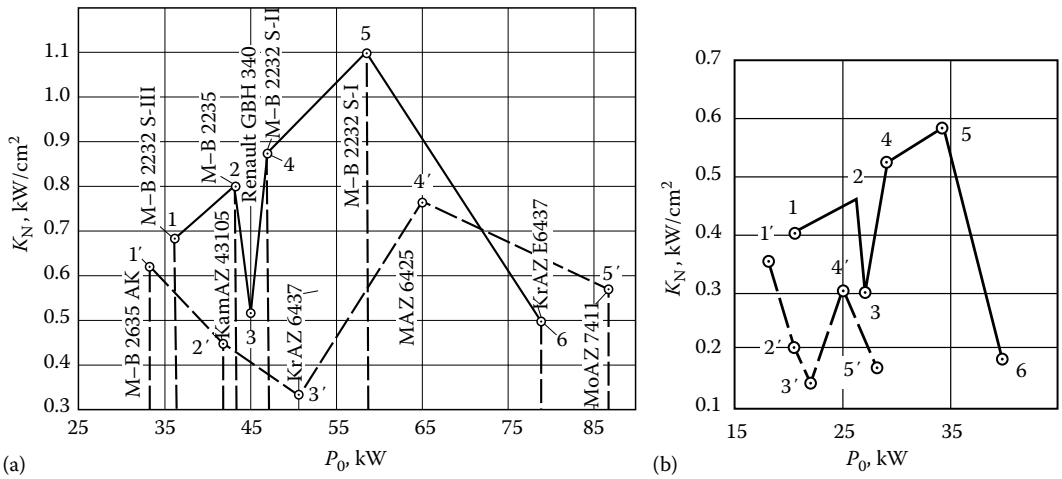


FIGURE 2.66
Energy loading factors K_N (a) dirt road; (b) concrete road; the solid curves are for 6 × 4 trucks; the dashed curves are for 6 × 6 trucks.

The velocity modes of the components of differentials were calculated on the assumption that all the tractors move at the same speed of 12 km/h (3.33 m/s). This approach stems from the virtually identical maximum design velocities of modern wheeled tractors (35–40 km/h) on which the average operational vehicle speed depends. In addition, the recommended tractor speed for performing agricultural work is usually 10–12 km/h.

Tables 2.13 and 2.14 list the parameters of wheeled tractors and their interwheel differentials. These data were used for calculating assessment criteria, the values of which are listed in Table 2.15. The low values of energy loading factors K_N of traction class 0.6 tractors T 16M and T 25A stem from the rather generous dimensions of their differential (here, 0.6 corresponds to $F_d^N = 6$ kN in Table 2.13).

The values of K_N of differentials of 4 × 2 tractors of class 1.4 are higher than those of differentials of the rear axles of 4 × 4 tractors of the same class. The fact that the MTZ 82 and 102 also have front driving axles reduces the energy loading of the differentials of its rear axle by approximately 1.6-fold as compared with MTZ 80 and 100 tractors. It should be noted here that this reduction was obtained by virtue of reduction of load forces, whereas the velocity modes V_c of all the differentials are approximately the same. Thus, the force loading factor K_M of the rear axles of the MTZ 82 and MTZ 102 is smaller than these factors for differentials of MTZ 80 and MT 100 1.64- and 1.59-fold respectively. The above is illustrated by the graphs in Figure 2.67 constructed from data of Table 2.15.

This figure shows by solid curves the assessment criteria of differentials of 4 × 2 tractors, by dashed curves—those of the differentials of rear axles of 4 × 4 tractors and by dash-dotted curves—of the front axles of these tractors.

On the whole, the coefficients of energy loading of the differentials of rear axles of 4 × 4 tractors are approximately the same and amount to 0.375 on the average. The values of energy loading of differentials of the front axles of 4 × 4 tractors are determined by the nature of variations in the force and velocity factors (see Figure 2.67).

The method suggested in this section made it possible to compare the operational indices of differentials of different vehicles and to thus assess the degree of perfection of these

TABLE 2.13

Estimated Parameters of Farm Tractors

No.	Model	Nominal Drawbar Pull F_d^N, kN	Average Operational Drawbar Pull F_d^m, kN	Full Mass m_a, t	Mass Taken by Drive Wheels m_{dr}, t	Engine Power P_e, kW / HP	Average Operational Speed V_{avg}, m/s / km/h	Wheel-Hub Gear Drive u_k	Tires of Drive Wheels	Tire Radius r, m
4 × 2										
1	T 16M	6	3.6	1.81	1.48	14.7 / 20	3.33 / 12	5.83	9.5–32	0.59
2	T 25A	6	3.6	2.02	1.32	18.4 / 25	3.33 / 12	4.75	9.5–32	0.59
3	MT3 80	14	8.4	3.52	2.20	55.2 / 75	3.33 / 12	5.31	15.5 R 38	0.73
4	MT3 100	14	8.4	3.85	2.48	77.2 / 105	3.33 / 12	5.31	16.9 R 38	0.75
4 × 4										
5	MT3 82	14	8.4	3.73	1.38[a] / 2.35	55.2 / 75	3.33 / 12	6.14[a] / 5.31	11.2–20[a] / 15.5 R 38	0.47[a] / 0.73
6	MT3 102	14	8.4	4.05	1.54[a] / 2.51	77.2 / 105	3.33 / 12	6.14[a] / 5.31	11.2–20[a] / 15.5 R 38	0.47[a] / 0.75
7	MT3 142	20	12	5.18	1.90[a] / 3.28	110.3 / 150	3.33 / 12	7.6[a] / 6.2	16–20[a] / 18.4 R 38	0.51[a] / 0.82
8	T 150 K	30	18	8.14	4.07[a] / 4.07	129.0 / 175	3.33 / 12	3.59[a] / 3.59	21.3 R 24[a] / 21.3 R 24	0.64[a] / 0.64

[a] Front axle parameter in numerator, rear axle parameter in denominator.

TABLE 2.14

Estimated Parameters of Interwheel Differentials

		Side Gear					Pinion									Spider			
No.	Model	Tooth Number z_g	Outer Friction Diameter, mm d_{go}	Inner Friction Diameter, mm d_{gi}	Average Friction Radius, mm r_{gf}	Average Gear Radius, mm r_g	Tooth Number z_c	Outer Friction Fiameter, mm d_{po}	Inner Friction Diameter, mm d_{pi}	Average Friction Radius, mm r_{cf}	Average Pinion Radius, mm r_c	Pitch Angle, deg δ_c	Outer Module, mm m_{te}	Pressure Angle, deg α_w	Conditional Cross-Section Area, cm^2 A_d	Spider Pin Diameter in Contact with Pinion, mm d_{sp}	Spider Pin Length in Contact with Pinion, mm l_{sp}	Spider Pin Length in Contact with Case, mm l_{sc}	Average Radius, mm r_0
4 × 2 and 4 × 4 (differentials of rear drive axles)																			
1	T 16M T 25A	27	94	55	37.25	54	18	55	28	20.75	36	33°42′	4	17°30′	77.76	28	30.5	16	78
2	MTZ 80/82 MTZ 100/102	22	102	62	41	55	12	48	25	18.28	30	28°37′	5	20°	66	25	27	23	78
3	MTZ 142	22	120	74	48.5	71.5	11	55	30	21.25	35.75	26°34′	6.5	20°	102.24	30	37	12	88
4	T 150K	26	132	65	49.25	71.5	14	64	32	24	38.5	28°18′	5.5	45°	110.11	30	37	20	96
4 × 4 (differentials of front drive axles)																			
5	MTZ 82 MTZ 102 MTZ 142	16	78	56	33.5	36	10	39.5	16	13.9	22.5	32°	4.5	20°	32.4	16	27	16	32

TABLE 2.15

Evaluation Criteria of Farm Tractors' Interwheel Open Differentials

No.	Model	$F_x\Sigma$, kN	P_0, kW	k_N, $\frac{kW}{cm^2}$	$k_u \times 10$, $\frac{kN}{cm^2}$ $\frac{k'_u}{t}$ $\frac{}{cm^2}$	ω_0, rad/s ω_c, rad/s V_c, m/s	F_b, kN p_b, MPa	F_0, kN p_0, MPa	Q_a, kN p_a, MPa	Q_c, kN p_c, MPa
4 × 2										
1	T 16M	5.38	17.90	0.23	0.70	32.90 49.36 0.69	2.52 2.95	1.74 3.89	1.32 0.29	0.44 0.25
2	T 25A	5.58	18.59	0.24	0.89	26.81 40.21 0.56	3.21 3.76	2.22 4.96	1.68 0.37	0.56 0.32
3	MTZ 80	11.85	39.47	0.60	2.47	24.22 44.41 0.56	7.41 10.97	5.22 9.08	4.73 0.92	1.29 0.98
4	MTZ 100	12.18	40.55	0.61	2.61	23.58 43.22 0.54	7.82 11.58	5.51 9.59	4.99 0.97	1.36 1.03
4 × 4 (differentials of rear drive axles)										
5	MTZ 82	12.06	24.42	0.37	1.51	24.22 44.41 0.56	4.53 6.70	3.19 5.55	2.89 0.56	0.79 0.60
6	MTZ 102	12.37	25.49	0.39	1.64	23.58 43.22 0.54	4.92 7.28	3.47 6.03	3.14 0.61	0.86 0.65
7	MTZ 142	17.08	36.02	0.35	1.40	25.21 50.42 0.76	5.00 4.50	4.06 11.28	3.25 0.46	0.81 0.49
8	T 150K	25.98	43.26	0.39	2.10	18.68 34.69 0.52	8.10 7.29	6.03 10.05	14.25 1.38	3.83 1.59
4 × 4 (differentials of front drive axles)										
9	MTZ 82	12.06	14.86	0.46	1.03	44.45 71.12 0.57	2.32 5.37	1.39 10.88	1.43 0.62	0.45 0.44
10	MTZ 102	12.37	15.71	0.48	1.11	43.50 69.60 0.56	2.51 5.80	1.50 11.75	1.55 0.67	0.48 0.47
11	MTZ 142	17.08	20.86	0.64	1.30	49.72 79.55 0.64	2.91 6.75	1.75 13.66	1.80 0.78	0.56 0.55

mechanisms from the point of view of loading and wear resistance. This problem is solved by using the suggested assessment criteria:

- Factor K_N of energy loading of the differential
- Accumulated mileage wear factor K_u

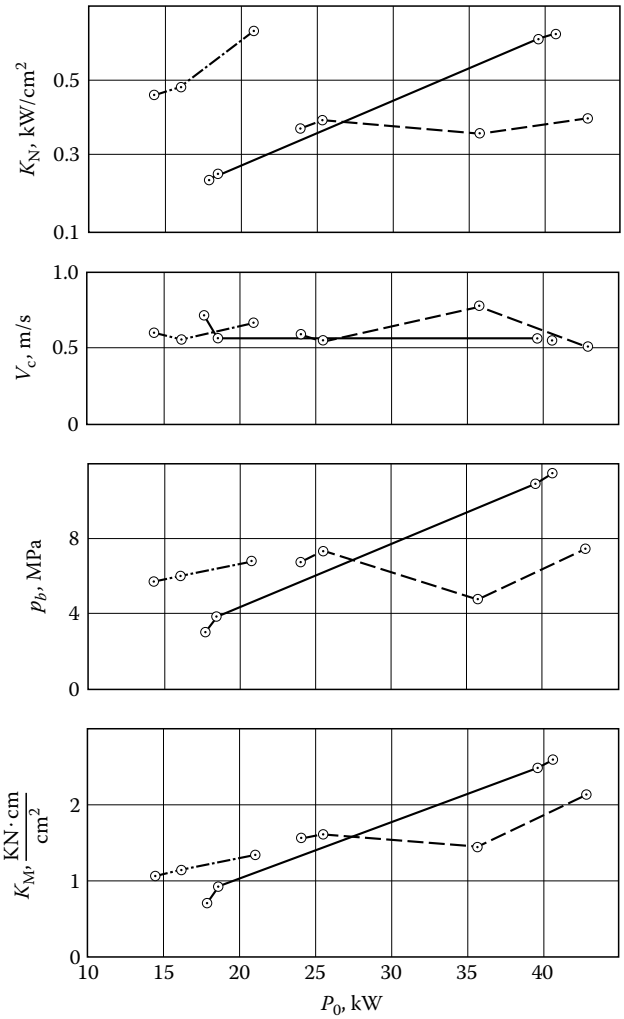


FIGURE 2.67
Criteria for evaluation of interwheel differentials: 4 × 2 farm tractors, 4 × 4 farm tractors (front axle differentials), 4 × 4 farm tractors (rear axle differentials).

and also by comparison and assessment of the velocity and force indicators. The use of the suggested conditional cross-sectional area A_d of the differential made it possible to not only compare the dimensions of different differentials, but also provided convenience for comparative assessment of the principal design and operational indicators of differentials.

This method is also useful in assessing the power and velocity modes and energy loading of the same differential in cases when it is used in different vehicles. In this case, it is always possible to predict negative and positive changes in the operation of the mechanism when put to use on new vehicle models.

2.5.3 Oil Lubrication Systems

The high-energy loading of differentials and the elevated wear of rubbing surfaces and premature failures associated with this were discussed above. One of the effective ways of increasing the operating life of differentials consists in improving their lubrication systems.

Whereas splash oiling of rubbing surface was sufficient in the not so distant past, at present this method was made obsolete by the previously mentioned factors. Current lubrication systems for differentials should provide for the following: taking the oil from the axle housing, cleaning the oil and feeding it into the differential, lubricating and cooling the rubbing surfaces, and removing the oil together with the products of wear from the mechanism. This means that lubrication systems must produce a stable flow of oil through the differential. The need for this was confirmed by examining differentials of vehicles without provision for through-flow of the oil. It was found that products of wear of components and other inclusions precipitated on the spherical surface of the housing of such differentials. This layer may be as thick as 3–4 mm in differentials of tractors of highway trucks with a full mass of 42 ton after accumulating 350,000 km of travel. This layer moves right up to the points of contact between the pinions and the housing. Its thickness exceeds that of the thrust washers of pinions, which interfere with the supply of oil to the washers and bushings of the pinions and also to the thrust washers of the side gears.

The lubrication systems of differentials of driving axles can be subdivided into three groups by their operating principle:

- Passive systems
- Active systems
- Forced circulation systems

The operating principle of passive systems consists in placing various oil-trapping pockets on segments with vortical flows of the oil being sprayed, from which the oil flows by gravity over special grooves to the friction areas. Active type systems provide for placing on the rotating components of additional elements, for example, in the form of disks, from which the oil is pushed off in the course of rotation by oil traps and is directed over appropriate grooves to the rubbing surfaces. Forced circulation systems are those in which oil is supplied to difficult-to-reach rubbing pairs by all kinds of pumps and other devices for which pumping oil through them is not a direct function. There also exist composite systems that combine within themselves elements of the above three types of lubricating system.

The device shown schematically in Figure 2.68 serves as a typical representative of the most extensively used lubricating system of the driving axle speed reducer.

It operates as follows. Oil vortices that are generated by driven bevel gear 1, move to oil trapping pocket 2, whence the oil is directed along a channel in the case casting to the space between the bearings, which lubricates bearing 3 and, what is most substantive, bearing 4. Bearing 4, being of the tapered kind, acts as a centrifugal pump and produces pressure in the forward part of the packing gland that causes the oil to flow through the packing glands and fouls the outer surfaces of the axle case. To prevent this from happening, the system has a channel 5 by means of which the oil is returned to the case space 6.

Supply of oil to rotating mechanisms, particularly into the housing of the differential for lubricating the rubbing surfaces of pinions and side gears, presents a special problem. Nevertheless, effective flow-through lubricating systems for differentials were developed and are used in current-production vehicles. Some of these are now examined in more detail.

Figure 2.69 shows one of the earlier designs of a driving-axle differential with improved lubrication system.

In it, disks 2 and 8 are fastened to the driven, bevel and spur gears. The rotating disks pick up oil by viscous friction and then this oil is pushed off by tubular oil traps 1 and 9

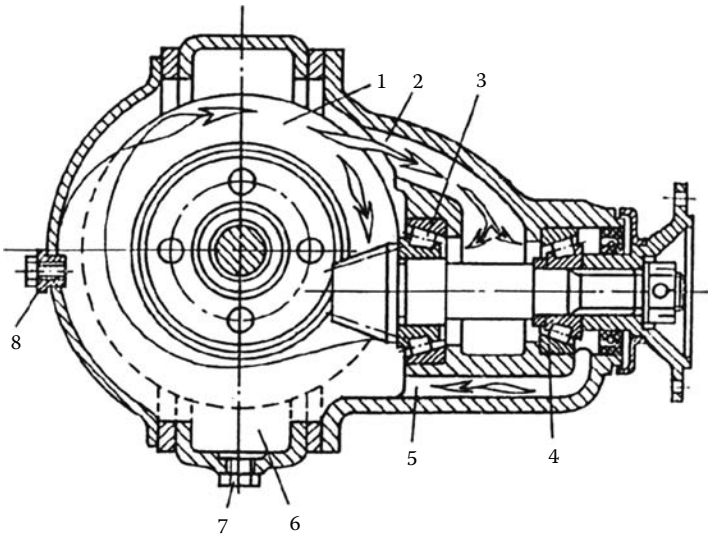


FIGURE 2.68
Final drive of automobile axle: 1, driven gear; 2, oil-trap pocket; 3, rear bearing; 4, front bearing; 5, draining channel; 6, oil bath; 7, drain port plug; 8, inlet port plug.

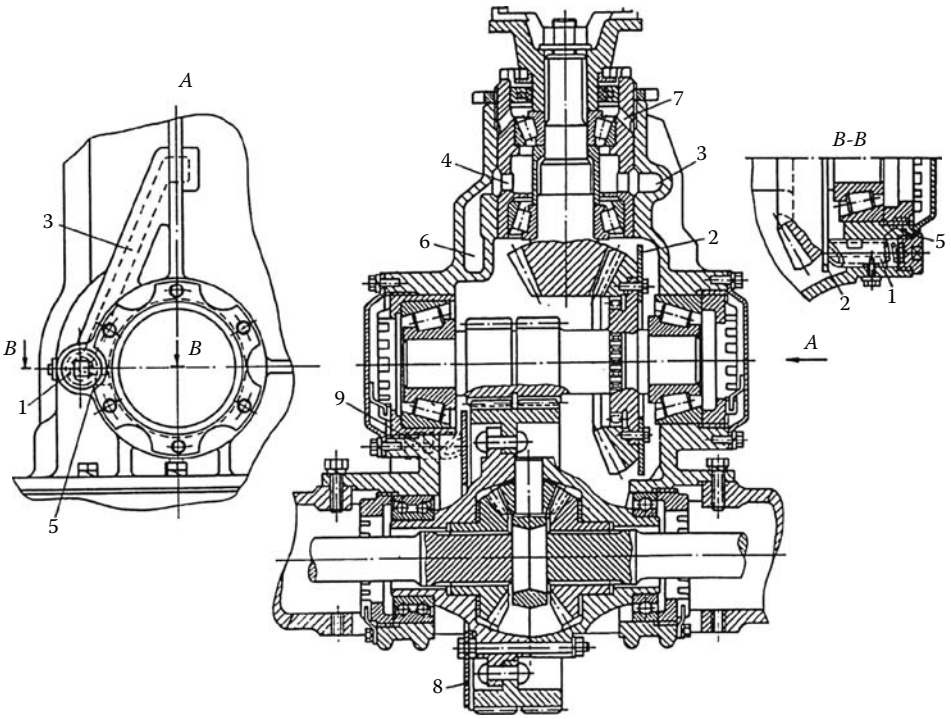


FIGURE 2.69
Final drive and differential of a truck: 1 and 9, tubular oil traps; 2 and 8, disks; 3, 5, and 6, oil channels; 4, inlet port; 7, drain port.

that are tightly pressed to the disks by springs. In oil trap 1 the oil flow is separated by the sidewall into two parts. One part is directed along channel 3 to the bearings of the bevel-driving pinion, whereas the other part, along channel 5 to the right bearing of the spur driving pinion. The left bearing of this pinion is lubricated by oil supplied from oil trap 9. In addition to these two oil traps, an oil-trapping pocket is located above the driving bevel pinion; oil to this trap is fed by ordinary splashing and then it is directed through channel 6 and port 4 to the bearings of the driving spur gear. This oil flow is redundant and serves for improving the reliability of the lubrication system.

Unlike the preceding, the reduction gear set shown in Figure 2.70 is a two stage (two velocities) device.

Its first stage consists of a pair of bevel gears, and the other, a planetary gear set that is installed into the same housing as the differential. As a result, the differential itself became encased in a double housing. This differential design makes it extremely difficult to access the inner rubbing surfaces of the differential and required additional design modifications to allow supply of oil to the differential housing. The design modification and its operation have the following form. Disk 5 with a T cross section is fastened on the driven bevel gear. Similar to the previous design, tubular oil trap 1 that collects the oil and divides the resultant oil stream into two parts is pressed by a spring to the cylindrical part of this disk. One part of the flow is directed along channel 2 to the tapered bearings of the final drive bevel pinion and the other, along channel 3, to the right tapered bearing of the differential. The closed adjustment nut of this bearing forms a chamber from which the oil is pumped by the bearing that serves as a pump to the housing of the planetary speed reducer and the housing of the differential through ports 7 and 6, respectively. The oil flowing from the housing of the planetary speed reducer lubricates the left tapered bearing of this mechanism through ports 4. The remaining rubbing surfaces of the elements of this device are splash lubricated.

Figure 2.71 shows the differential of the driving axle of a heavy-duty truck with flow-through lubrication system.

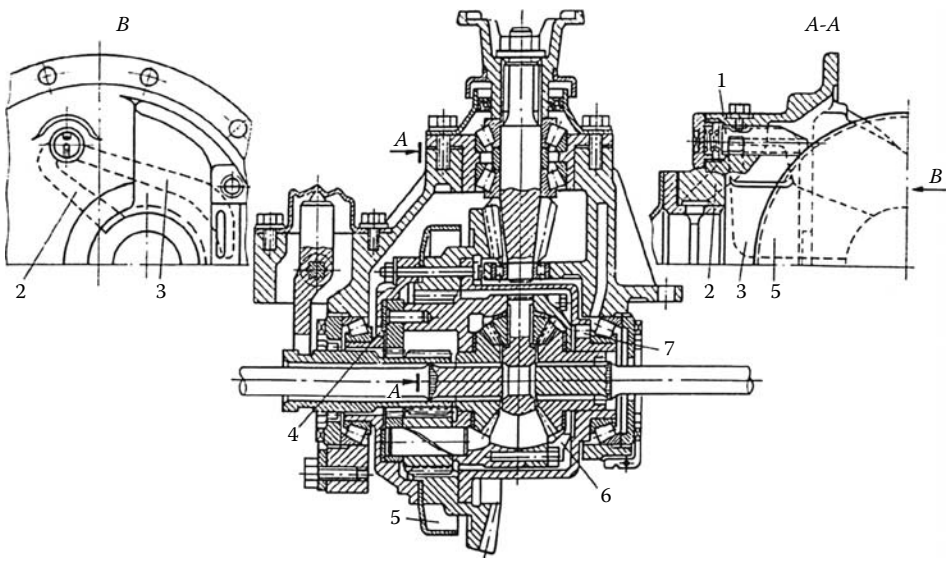


FIGURE 2.70
Final drive and differential of a truck: 1, tubular oil trap; 2 and 3, oil channels; 4, drain port; 5, disk; 6 and 7, inlet ports.

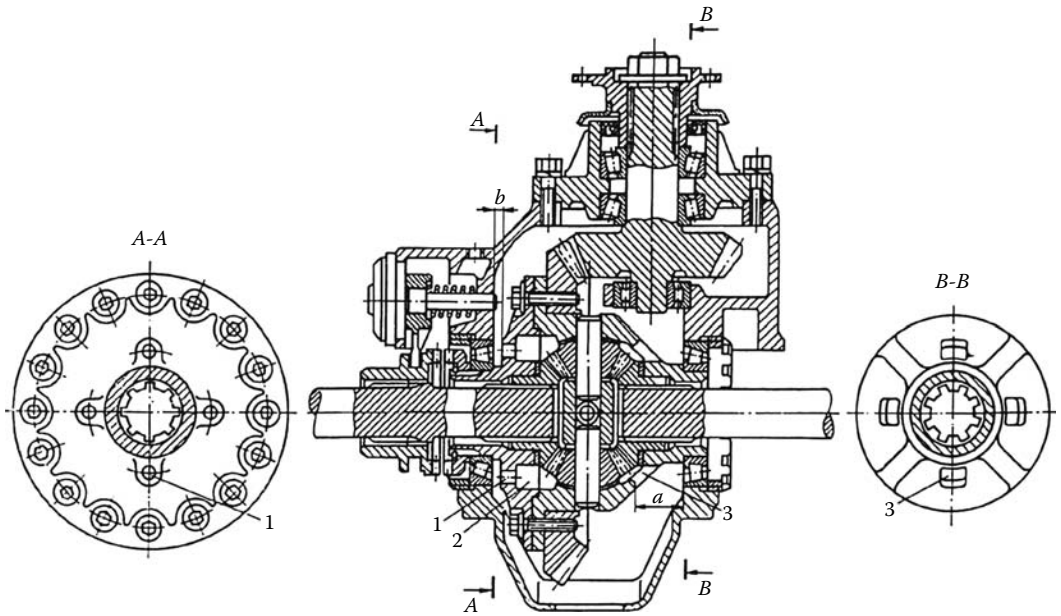


FIGURE 2.71
Final drive and differential of a heavy-duty truck: 1, inlet ports; 2, chamber; 3, drain ports.

The oil flowing down from the left wall of the axle's case is captured by the tapered pumping bearing and it is pumped by it through ports 1 into the differential's housing. First, the oil enters chamber 2 where it is partially purified by centrifugal action. Then the oil from which rough inclusions (products of element wear) were removed flows to the rubbing surfaces of pinions and side gears, their thrust washers and bushings. The oil leaves the differential's housing through ports of its right-hand part. These ports are located at distance *a* away from the right bearing. To allow satisfactory oil flow, the total cross-sectional area of the discharge ports was made threefold larger than that of the input ports. And to provide for continuous supply of oil to the pumping bearing and then to the differential's housing, the surface of the left half of this housing is placed as close as possible to the left wall of the axle's case (see dimension *b* in Figure 2.71). The latter promotes copious capture of oil onto the left wall of the axle's case and a similarly copious flow of oil to the pumping bearing.

The flow-through lubricating system shown in Figure 2.71, as other flow-through systems of other vehicles, is much more effective than the nonflow-through versions, since it not only lubricates the rubbing surfaces, but also rapidly cools them and removes products of rubbing-surface wear from the mechanism's housing.

Figure 2.72 shows the differential of the driving axle of a truck with a lubricating system similar to that previously examined in Figure 2.71, but having additional features.

The oil is pumped through ports 1 in the differential's housing. The oil centrifuging chamber 2 is somewhat larger and has four radially arranged fins that prevent the oil ring from rotating thus preventing washing off of products of wear from the chamber's wall. Another feature specific to this lubricating system is the fact that its output ports 3 are located very close to the second tapered bearing of the differential, whose pumping activity may prevent discharge of oil from the differential's housing. This is prevented by placing

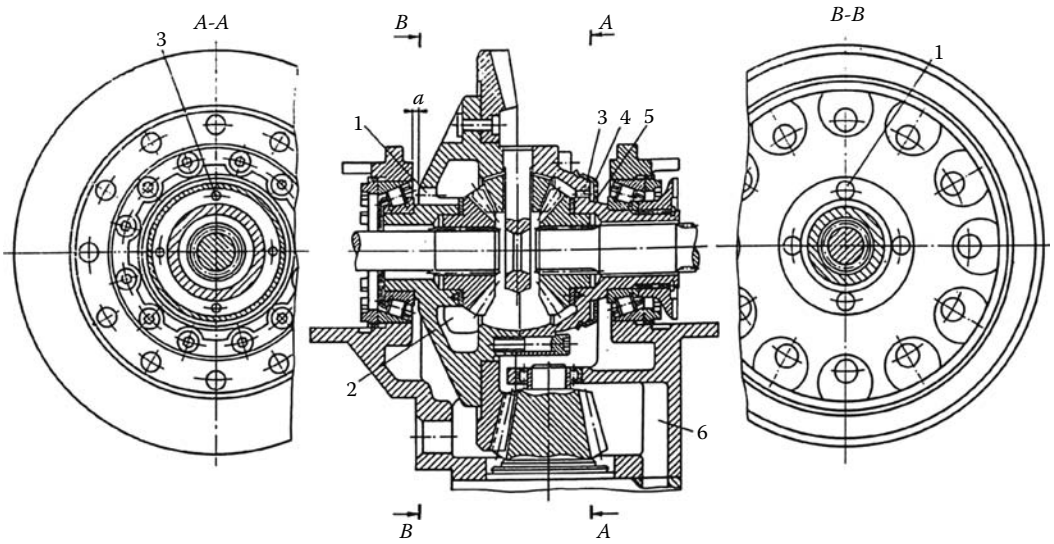


FIGURE 2.72
Final drive and differential of a heavy-duty truck: 1, inlet port; 2, chamber; 3, outlet port; 4, baffle; 5, annular slot; 6, oil pocket.

baffle 4, fixed to the housing, upstream of the discharge ports. The baffle not only eliminates the obstacle to the discharge of oil from the pumping bearing, but somewhat accelerates the discharge of oil from the differential's housing by the ejection action of the oil that is discharged by the right pumping bearing.

The heavy-duty truck the speed reducing system of which is shown in Figure 2.73 has an original flow-through lubricating system of the interwheel differential.

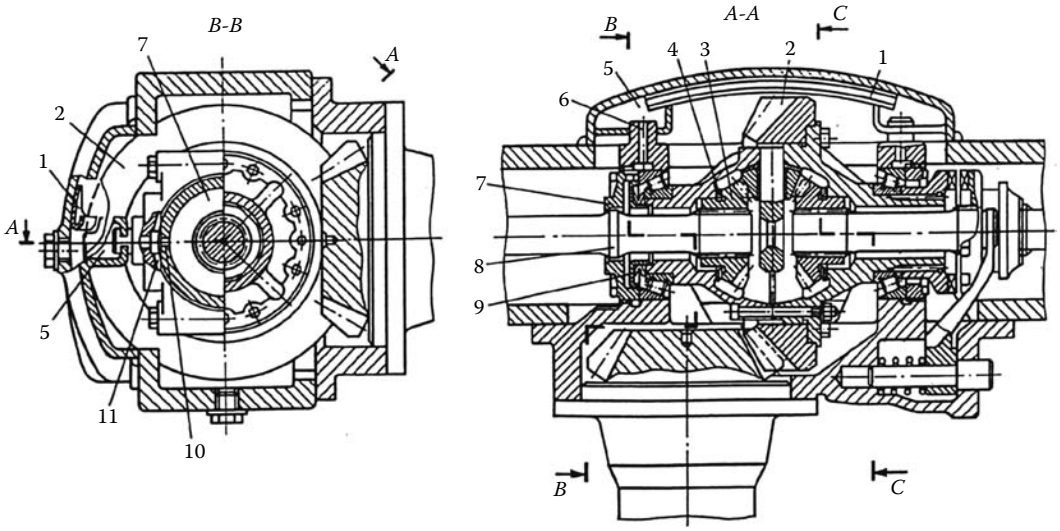


FIGURE 2.73
Final drive and differential of a heavy-duty truck: 1, trough; 2, driven gear; 3, side gear; 4, thrust washer; 5, oil pocket; 6, oil channel; 7, adjustment nut space; 8, half axle; 9, packing; 10, port; 11, annular groove.

It is constructed as follows. Trough 1, into which oil splashed by the final drive driven gear is welded along the rear wall of the axle's case. The oil from this trough flows to pocket 5, located across the differential's bearing, and then is directed along channel 6, located in the bearing's cover, into the space of adjustment nut 7. The space in the nut is formed by its wall and by a baffle adjoining the bearing. The baffle prevents pumping of the oil by the bearing from the space of the nut unit. This is also the duty of the V seal 9. The oil located in nut's space fills simultaneously the annular clearance between this space and the differential's housing half and the clearances between the flats on the cylindrical surface of the hub of side gear 3 and the half. Then the oil flows through slots in thrust washer 4, from which it moves into the differential's housing and to its rubbing surfaces. The slots of the thrust bearing are arranged radially and act as inter-blade passages in a centrifugal pump. Oil is sucked in through these passages by centrifugal force to the differential's housing from the adjustment-nut space. The shape and location of the slots of the thrust washer and of the flats on the hubs of the side wheel are shown in Figure 2.74.

The same slots and flats are provided on the thrust washer and hub of the side gear of the second half of the differential that, unlike the first, employs an ordinary annular adjustment nut. This allows draining the oil supplied to the differential's housing after lubricating all the elements of the mechanism to the axle's case. It should be noted that the flow-trough lubricating system of the interwheel differential shown in Figures 2.73 and 2.74 is quite effective. This is confirmed by the extended life of the vehicle and in particular of the differential.

In addition to the above-considered interwheel differential lubricating systems, other systems in which the oil is supplied directly to the differential may be employed. Special mention among these should be made of the system in which oil from the axle's case is drawn by special scoops (see Figure 2.75).

A lubricating system employing scoops requires special attention to the size and location of ports through which oil flows through the differential's housing. In one instance, the housing of a differential equipped with a lubricating system that uses scoops was made without outlet ports. This made it impossible for the oil supplied by the scoops to the housing to flow through it and the housing became a centrifuge. The oil supplied to it was centrifuged during the entire time of the vehicle's travel and the products of wear became

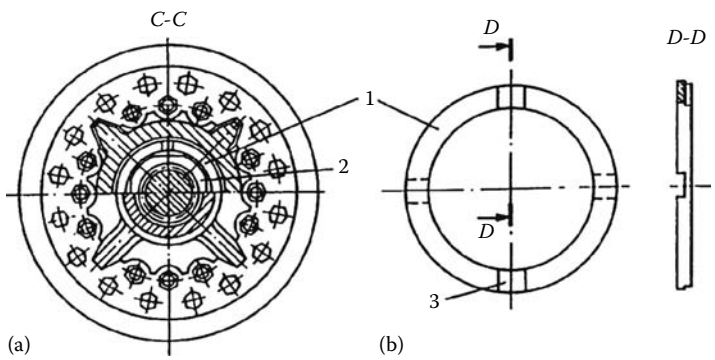


FIGURE 2.74
Elements of a differential: (a) section *C–C* (see Figure 2.73); (b) thrust washer of side gear; 1, thrust washer; 2, end of the side-gear hub with flats; 3, radial slot.

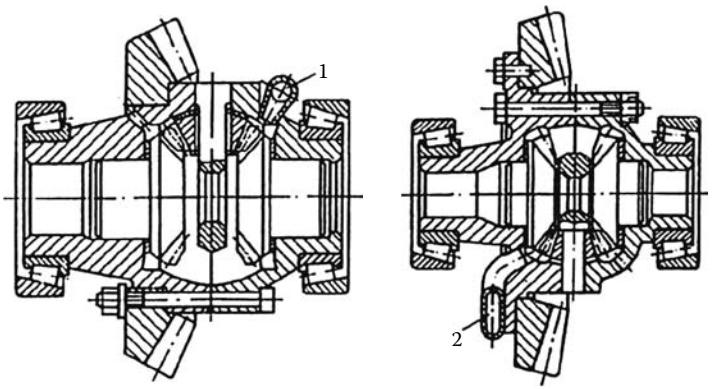


FIGURE 2.75
Differential with round, 1 and flat, 2 scoops.

continuously deposited at the ends of the thrust washers of the pinion. This happened from one trip to another with each newly supplied portion of oil. In the end the width of the deposited layer of the products of wear reached the width of the thrust washers of the pinions. The slots that served to lubricate the rubbing surfaces of the thrust washers of the pinions became plugged up and the washers failed very soon. Pits and other signs of intensive wear appeared on the bearing surfaces of the pinions.

Experience shows that, in order to provide for proper flow of oil in a scoop employing lubricant system, outlet ports should be placed on the casing, at least at the same level with the inlet ports of the scoops, as shown in Figure 2.75.

The above analysis of lubricating-system designs allows drawing the following conclusions:

- Lubricating systems of interwheel differentials and of final drives of driving axles underwent significant development as one of the means for increasing the service life of mechanism components and of the vehicles as a whole.
- Promise is held by designs of lubricating systems of interwheel differentials that ensure active flow of oil with washing out and removal of products of wear from the friction surfaces.
- A tendency was observed to use the housing of the interwheel differential as a centrifuge for removing products of wear and other inclusions from the driving-axle lubricating oil for which purpose a special space is provided in it.

2.6 Design of Interaxle Differentials and Transfer Cases

2.6.1 General Engineering Issues and Solutions

The first stage in designing an interaxle differential consists of selecting its conceptual design: whether the given vehicle needs a symmetrical or asymmetrical differential. This question is so important for providing the required operational properties that it will be discussed in a separate section (Section 2.9).

The interaxle differential should be designed together with other elements of the interaxle drive. Let us start with the most typical drive, all the elements of which (with the exception of drive shafts) are located in the transfer case. This case may be comprised of one, two or three housings. They, in addition to the interaxle differential, hold the reduction gears, clutches of all kinds, power takeoff transmissions, bearing units, lubricating systems and other devices. All these drive elements should be structurally interrelated with one another so as to make up a single unit.

Consider now the design features of transfer cases with interaxle differentials. Vehicles with two driving axles use single-housing transfer cases (in certain designs the interaxle differentials are built into the gearbox and there is no transfer case as such). The designs of transfer cases of three- and four-axle vehicles, and also in vehicles with a greater number of driving axles are much more complicated. In such vehicles they may be broken up into the main and auxiliary and even two auxiliary transfer cases. All depends on the number of reduction gears and other mechanisms, including the interaxle differential that should be placed in it. Breaking up a transfer case with a large set of mechanisms into smaller units allows using simpler transfer case designs holding a limited number of mechanisms within them. The design of such transfer cases is much simpler.

The design of transfer cases, irrespective of their complexity, should include lubrication systems with all their elements to allow for normal functioning and servicing. They may be self-contained and only very infrequently common to the entire set of components (elements) of the subdivided case. It must be remembered here that, the smaller the number of separate lubrication systems, the smaller the number of their accompanying elements (covers, plugs, filters, and similar). Nevertheless, it must not be forgotten that any design should always seek a compromise between potential alternatives.

In general, as pointed out previously, the transfer case may include principal design elements, control elements and additional mechanisms. The principal elements in transfer cases consist of reduction gears, interaxle differentials and adapter transmissions (one or several). The control elements may consist of tooth-type couplings, differential locking couplings, coupling shifting mechanisms, etc. The additional mechanisms may be power takeoff devices, parking brake, oil pump, fan, etc. On the other hand, it is convenient to classify transfer cases by attributes that characterize their general layout, i.e., by the mutual arrangement of the output shafts, by the type of the reduction gear installed in the case and certain other features. On the basis of this it is possible to list certain most typical kinematic layouts of transfer cases (see Figure 2.76).

The main attribute of layouts *a*, *b*, *c*, and *d* consists of the interaxle differential drive of the two output shafts 2 and 3 that are not co-axial with input shaft 1. Layouts *a* to *c* employ asymmetrical spur-gear differentials, whereas layouts *d* and *e* contain symmetrical and asymmetrical bevel-gear differentials, respectively. These layouts employ a clutch 4 that allows locking the interaxle differential in order to improve the traction properties and the mobility of the vehicle.

Figure 2.77 shows the design of a transfer case that follows layout *a* from Figure 2.76.

This design was the first to be designed in the former U.S.S.R. under the leadership of Dr. A. Kh. Lefarov for a 4×4 timber-carrier truck. The gear ratio of the interaxle differential was selected close to optimal to ensure minimal power loss in wheel slip.

One of the versions of a two-stage transfer case that follows layout b from Figure 2.76 is shown in Figure 2.78.

This transfer case has an asymmetrical interaxle spur-gear differential 1 in the continuously-engaged drive of the driving axles. On the input shaft of transfer case 3 is fastened drive gear 4, from which torque may be transmitted to the output shafts of front

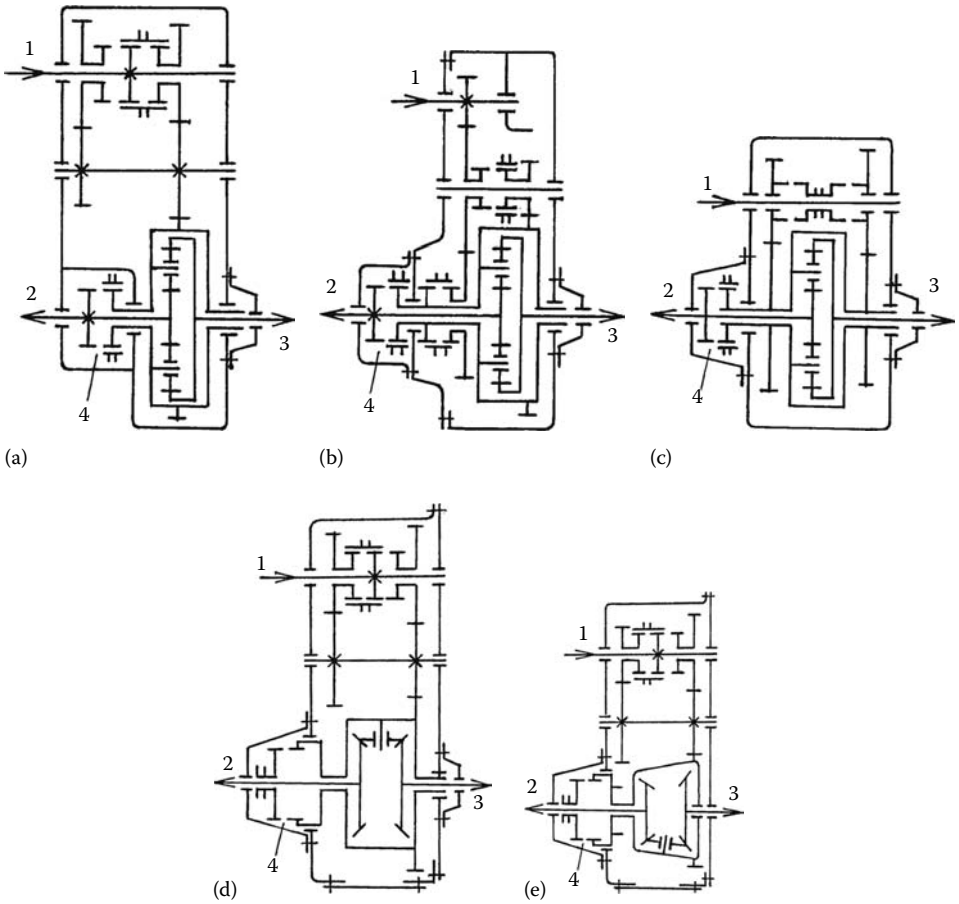


FIGURE 2.76
Transfer-case kinematic layouts: 1, input shaft; 2 and 3, output shafts; 4, tooth-type coupling.

axle 2 and of the rear tandem of axles 8 in two ways, depending on coupling clutches 6 and 7. When these clutches are in the position shown in the figure, the lower stage of the transfer case is engaged in which case the torque is transmitted to output shafts 2 and 8 additionally by means of gears 9 and 10. When the clutches are switched the higher stage of the transfer case is engaged and then the torque from the drive gear is transmitted to the output shafts by means of gear 5 bypassing gears 9 and 10. The ratio of torques transmitted to shafts 8 and 2 is equal to the gear ratio of spur-gear interaxle differential 1, which can be locked by clutch 11. In addition, a provision was made in this transfer case to take power off via gear 12 and shaft 13 by engaging clutch 14.

Figure 2.79 shows the design of a transfer case with a symmetrical interaxle differential.

This design differs from that in Figure 2.76d, which also employs a symmetrical differential by the fact that it has one, rather than two stages. It is seen by comparing Figures 2.76e and 2.79 that the transfer cases are of the two- and single-stage type; they also differ by the design of their spur-gear interaxle differentials: one is asymmetrical and the other is symmetrical.

Figure 2.80 shows layouts of transfer cases that may be called combined.

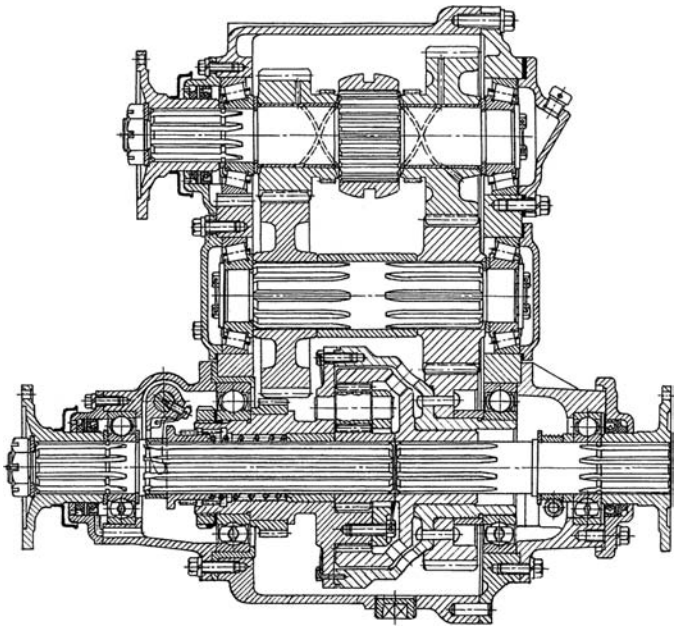


FIGURE 2.77
4 × 4 timber truck: transfer case.

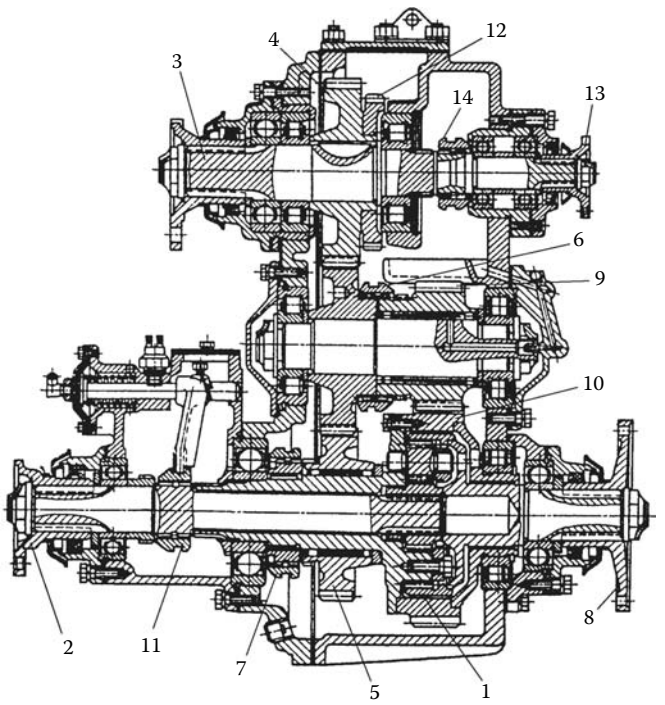


FIGURE 2.78
Transfer case design followed layout (b) from Figure 2.76.

Thus, the transfer case in Figure 2.80a is distinguished by the presence of one input (1) and three output shafts (2, 3, and 4). This layout has a differential drive between the middle and rear axles of the 3-axle vehicle and a positive engagement (i.e., a locked drive) to the front axle; the latter, driven by shaft 4, can be engaged under difficult

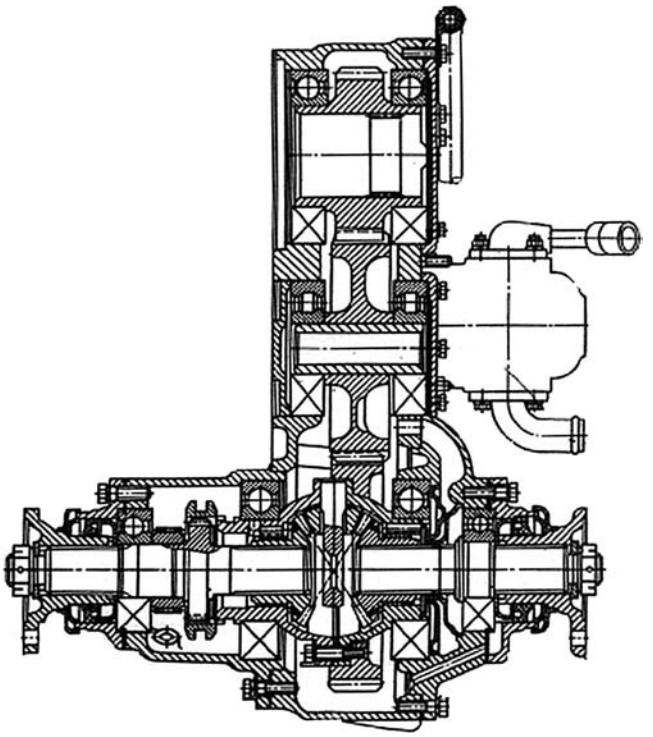


FIGURE 2.79
Design of transfer case with symmetrical interaxle differential.

driving conditions by clutch 5 and then disconnected when the vehicle travels on a paved road. Layouts *b* and *c* have in common separation of the power flow that passes through the gear meshes. Thus, layout *b* has a differential drive in which the power flow from inlet shaft 1 is divided between two identical gear transmissions 2 and 3 and is then combined in the housing of differential 4. In this arrangement, complete utilization of the capabilities of each of the transmissions requires that they be identical and precisely manufactured. Layout *c* has two identical two-stage reduction gears located behind interaxle differential 1. This design has the disadvantage that identical loading of the reduction gears was achieved by markedly complicating the design. Layout *d* is a combination of a locked drive of the two axles. The rear axle is driven by shaft 1 and the left and right front wheels are driven by shafts 2 and 3 linked by an interwheel differential. The use of engagement clutches 4 and 5 makes it possible to transmit the entire power flow only to the rear axle of the vehicle. Finally, layout e shows a transfer case with a planetary reduction gear. The three-link planetary mechanism 1 is used as a reduction gear at the higher stage, when the entire power is transmitted to the rear axle, driven by shaft 2. At the lower stage both vehicle axles are engaged and then the planetary mechanism acts as a interaxle differential that, if necessary, can be locked by clutch 3.

The selection of a preferable transfer-case conceptual design is a rather complicated matter and requires precise knowledge of the operating conditions of the vehicle, the required direction of shaft rotations and their placement conditions. In addition, this design must be selected with consideration of compatibility with models already in production, manufacturability of the design, convenience in servicing and repairs, profitability and similarity. New layouts and designs of transfer cases are continuously under development with an eye toward contributing to improvement of the driveline and operating properties of vehicles.

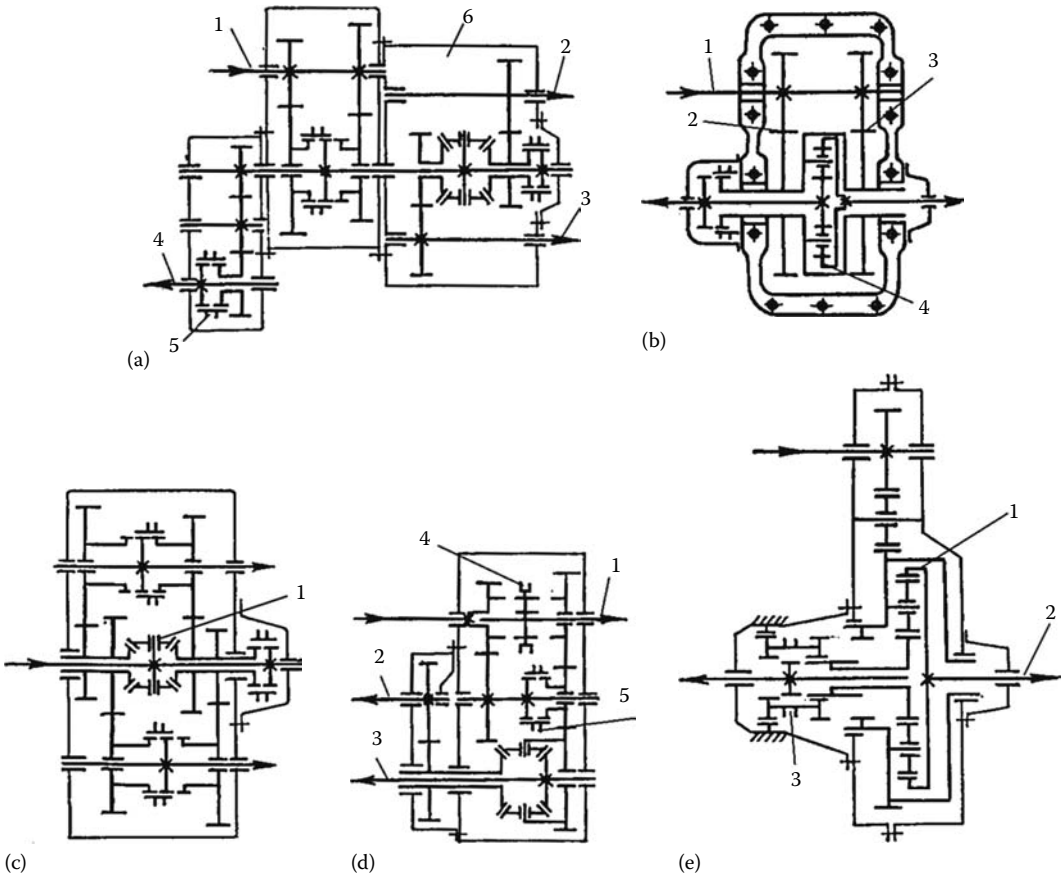


FIGURE 2.80
Kinematic layouts of transfer cases: 1, input shaft; 2, 3, and 4, output shafts; 5, clutch; 6, case.

Next to be considered are typical and more original designs and layouts of interaxle differentials. Figure 2.81a shows the arrangement of a symmetrical bevel-gear differential 1 and three-shaft transmission reduction gear 2, assembled together with the final drive of the forward rear axle of a 6 × 4 truck.

This arrangement uses an open differential. Torque from it is transmitted to both, equally loaded axles, through pinions 4 and spider 5, seated on the splines of the reduction gear's input shaft 6. The forward rear axle shown in Figure 2.81b uses a similar arrangement, but with some modification: its reduction gear is built into the housing of the axle's final drive. In the case of the arrangement shown in Figure 2.81a the transmission reduction gear has its own case 7 that is directly connected to forward rear axle housing 8. In both cases (Figure 2.81a and b) the interaxle differentials are of identical design and transmit identical torques to the axles.

The situation becomes somewhat different when the transmission reduction gear (1) is not built together with the housing of the vehicle's forward rear axle or (2) is replaced by the interaxle differential itself. In the case when it is separate, it acts either as an independent transfer case or as a transfer case connected directly to the gearbox. The situation when the interaxle differential itself acts as the transfer reduction gear is different and hence shall be

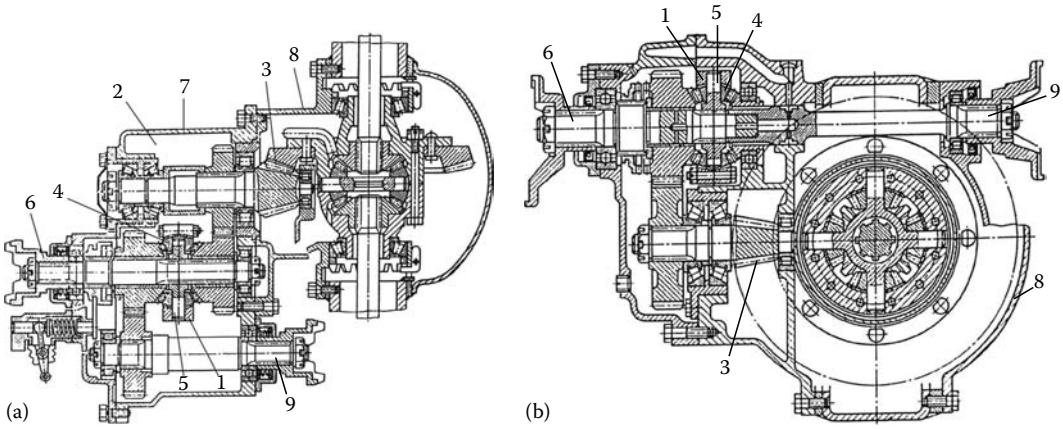


FIGURE 2.81
Design of interaxle, symmetrical open bevel-gear differential and a three-shaft transmission reduction gear, built as a single unit with the forward rear axle's final drive: 1, differential; 2, transmission reduction gear; 3, final drive; 4, pinion; 5, spider; 6, input shaft; 7, reduction gear case; 8, axle housing; 9, rear axle output shaft.

examined separately. Figure 2.82 shows a hypoid-gear final drive of the forward rear axle with built in bevel-gear differential 1.

This design is made different by the fact that the differential itself acts as the transfer reduction gear. It does not have additional shafts and gears as in the previously discussed designs. This, coupled with the use of a hypoid-gear transmission, made it possible to reduce the mass and dimensions of the vehicle's forward rear driving axle. Note that the differential in Figure 2.82 is locked by friction clutch 2.

This layout was also used in designing the bevel-gear interaxle differential with a two-stage final drive of the pass-through forward rear axle of a three-axle vehicle; this arrangement is shown in Figure 2.83.

The two-stage final drive of this axle consists of a pair of bevel and a pair of spur gears. The torque from input shaft 1 is transmitted to housing 2 of the interaxle differential and

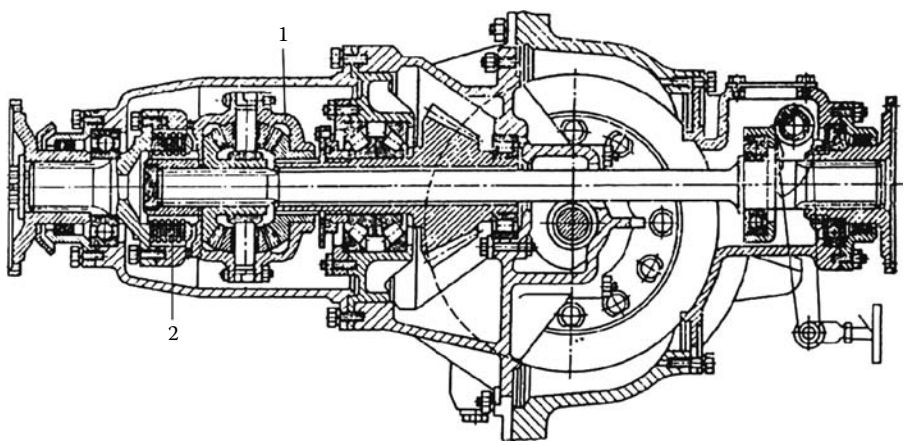


FIGURE 2.82
Hypoid-gear final drive of forward rear axle of a truck with built-in symmetrical interaxle bevel-gear differential.

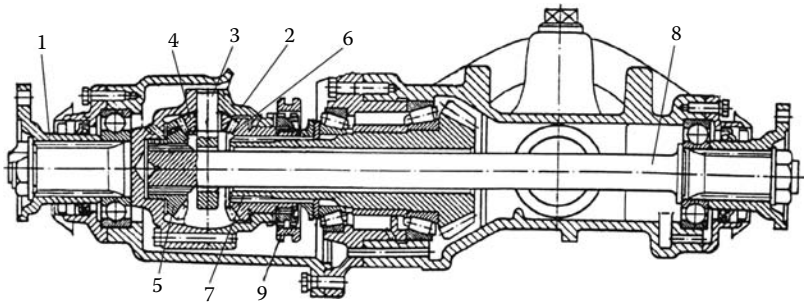


FIGURE 2.83
Bevel-gear interaxle differential with two-stage final drive of the pass-through forward rear axle of a three-axle vehicle: 1, input shaft; 2, differential housing; 3, spider; 4, pinion; 5, 6, left and right side gears; 7, tubular hub of the final drive driving gear; 8, intermediate shaft; 9, locking clutch.

from it through spider 3 and pinions 4 to two side gears 5 and 6. Right side gear 6 transmits the power to the forward rear axle through tubular hub 7 of the bevel driving gear of the first stage of its final drive. Simultaneously left side gear 5 transmits torque to the rear driving axle through intermediate shaft 8 that passes inside hollow hub 7 of the driving gear of the final drive of the forward rear axle. The differential is locked by locking clutch 9.

Less frequently, but still, symmetrical spur-gear differentials are used in forward rear axles of three-axle vehicles. One such design, together with the final drive of the forward rear axle, is shown in Figure 2.84.

The free-running mechanisms as interaxle differentials are mostly used in multiwheel trucks. One such arrangement is shown in Figure 2.85 (the free-running differential as such is examined in Chapter 5).

It should be noted that the pass-through shafts in pass-through driving axles should not be installed on rigid supports. Such shafts are, as a rule, long and slender and self-positioning supports are most suitable for them. When such supports are used, the

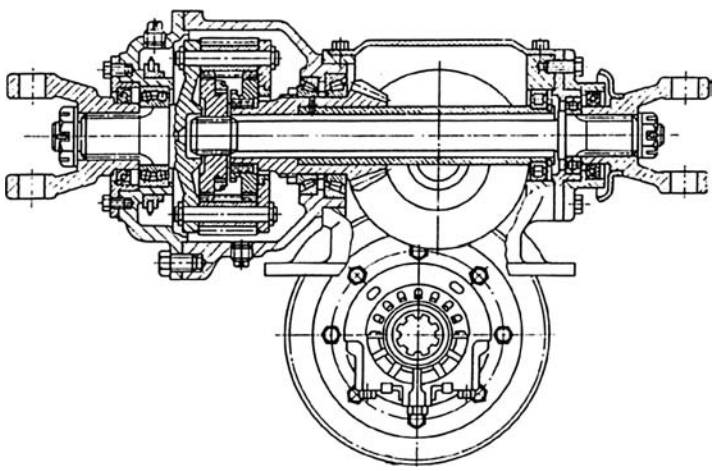


FIGURE 2.84
Symmetrical spur-gear interaxle differential with two-stage final drive of the pass-through forward rear axle of a three-axle vehicle.

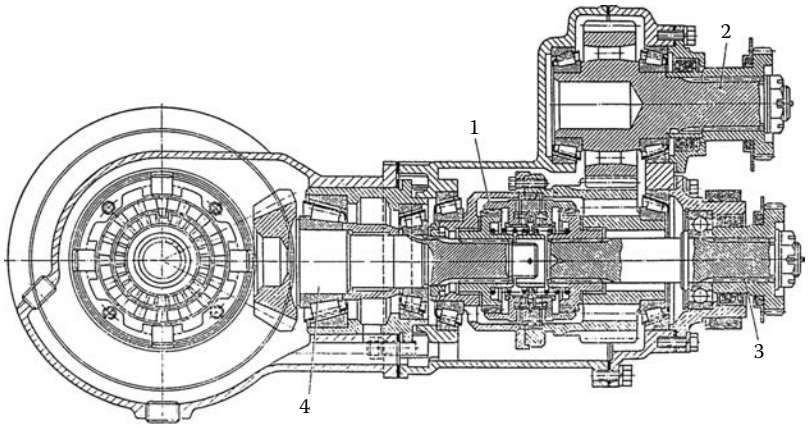


FIGURE 2.85
Free-running interaxle differential of a multiwheel drive terrain vehicle: 1, free-running differential; 2, input shaft; 3, 4, output shafts.

shafts are not subjected to large additional flexural forces that stem from noncoaxiality of distant bearing housings when they are constructed in one, and even more so in different cases. The forces that flex the shaft are transformed in the course of its rotation into an alternating-sign load that causes rapid failure of the shaft.

From the point of view of reliability and manufacturability, a two-support design of the shaft with the supports spaced apart is most preferable in any mechanism. Cantilevered and three-support shafts are the least desirable; of the latter, the most particularly undesirable arrangement is that of shafts on bearings, with bearing housings produced with more than one setting of the cutting tool. Bearing housings produced with two or more tool settings are very difficult to keep coaxial. The shortcomings of three-support shafts are well known: this gives rise to additional forces that overload both the shafts and their supports. This situation can be further aggravated by lower than necessary precision in component manufacture. For this reason, an effort should always be made to use two-support shafts, which ensures the most favorable loading of the components.

A large variety of driveline layouts was presented for all-wheel drive vehicles in Section 1.2. Vehicles with 8×8 wheel formula most frequently use a driveline system shown in Table 1.14 (item 7). In it, the front and rear driving tandems are relatively self-contained systems. They are interconnected by means of a symmetrical bevel-gear differential placed in a separate transfer case. Another arrangement, also shown in Table 1.14 (item 8) is used less frequently.

Currently interaxle differentials are used extensively also in 4×4 cars and sport utility vehicles. The drives of these cars are illustrated in Tables 1.15 and 1.16. An example of the simplest design is that of the interaxle drive of a SUV shown in Figure 2.86.

It consists of open bevel-gear differential 1, shafts 2 and 3 of the front and rear driving axle drives. The differential, which is locked by clutch 4, is located in a separate transfer case. Lately there appeared a large number of the so-called ''pure'' car drives, i.e., drives with a minimal number of components. One such drive and its design were already analyzed—this was the drive of the Audi-200 Turbo Quattro (see Figure 1.28).

Frequently, all-wheel drive models are designed on the basis of front-wheel drive models. As an example of the interaxle differential of such a 4×4 car consider the kinematic layout of the composite final drive of the front-steered driving axle with an

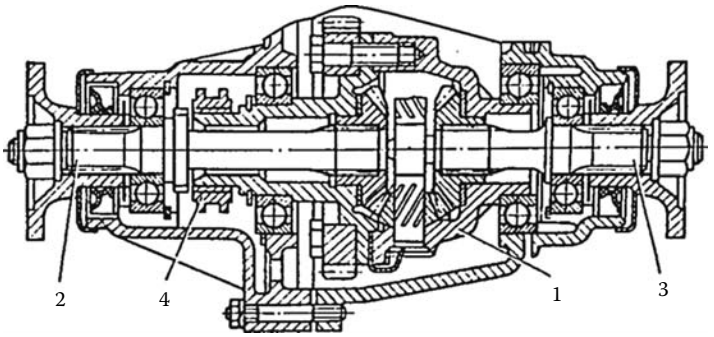


FIGURE 2.86
Example of the design of a symmetrical interaxle differential of a 4 × 4 car: 1, differential; 2, 3, output shafts; 4, locking clutch.

interaxle differential, in this case one using spur gears. This car has a transversely arranged engine and gearbox. The kinematic layout is shown in Figure 2.87.

The interaxle differential's gear 1 that is connected to the gearbox, transmits a part of the power through epicyclical gear 2, pinions 3, the differential's carrier 4, final drive wheel 5, and then through a driveshaft to the rear axle. In addition, the other part of the power, through pinions 3, sun gear 6 and bevel-gear interwheel differential 7 to the wheels of the front axle. The bevel-gear differential can be locked by means of expansion clutch 8. The torques on the links of this drive are now determined. The torque at the housing of the interwheel differential of the front axle is

$$T_{01} = T_0 \frac{r_1}{r_2} \tag{2.109}$$

where T_0 is the input torque, supplied to the interaxle differential. The torque at driven gear 5, connected to carrier 4 is given by the expression

$$T_2 = (2T_0/r_2)r_b = T_0(r_1 + r_2)/r_2 \tag{2.110}$$

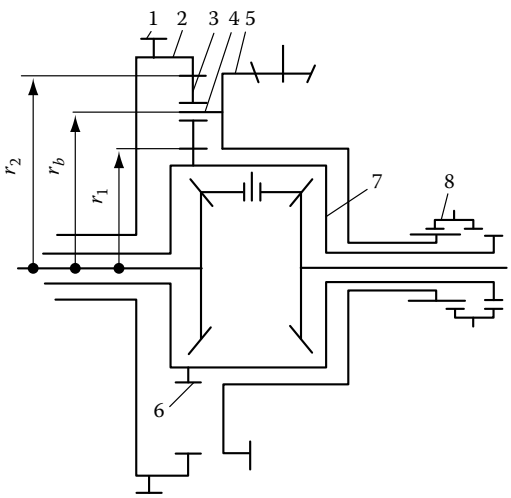


FIGURE 2.87
Kinematic layout of a final drive of the front drive axle combined with a spur-gear interaxle and bevel-gear interwheel differentials: 1, interaxle differential's gear; 2, epicyclical gear; 3, pinion; 4, differential's carrier; 5, final drive wheel; 6, sun gear; 7, interwheel differential; 8, locking clutch.

It is seen by comparing formulae (2.109) and (2.110) that when the final drives of the front and rear axles have the same gear ratios ($u_{f1} = u_{f2}$), the torques T_{01} and T_{02} at the housings of the interwheel differentials of both axles are not the same, i.e.,

$$T_{01} \neq T_{02} \tag{2.111}$$

where $T_{02} = T_2$. If it is required that these torques be equal, then the numerical values of u_{f1} and u_{f2} must be made different. The condition under which torques T_{01} and T_{02} will be equal is determined as

$$\frac{T_{02}}{T_{01}} = 1 = \frac{T_2 u_{f2}/u_{f1}}{T_0 r_1/r_2} = \frac{T_0(r_1 + r_2)u_{f2}/(u_{f1}r_2)}{T_0 r_1/r_2} = \frac{r_1 + r_2}{r_1}\frac{u_{f2}}{u_{f1}} \tag{2.112}$$

whence

$$\frac{u_{f1}}{u_{f2}} = \frac{r_1 + r_2}{r_1} = \frac{z_1 + z_2}{z_1} \tag{2.113}$$

i.e., the torques of both axles will be the same when the ratio of the gear ratios of the final drives of the axles would be equal to the ratio of the numbers of teeth z_1 and z_2 of the gears 2 and 6 of the interaxle differential.

2.6.2 Design of Differential Geometry

Results are presented of an investigation of interaxle differentials of driving tandems of 6×4 highway heavy-duty truck tractors and 6×4 and 6×6 timber-carrier tractors. The calculations were performed on the assumption that the tractors move as a part of fully loaded trucks, i.e., with fully loaded semitrailers and pole trailers.

The investigation was performed with highway trucks with 6×4 tractors from Table 2.9 and their similar MAZ trucks, with parameters listed in Table 2.16.

As compared with trucks employing a MAZ 64227 tractor and a semitrailer, the truck with the MAZ 64229 tractor has a full mass of 42 ton and a somewhat higher speed (the engine power is higher and the gear ratio of the final drive is smaller). Trucks with MAZ 64221 and MAZ 64226 tractors have an even higher gross weight and velocity. The MAZ E64221 tractor has no wheel-hub gear drives.

The parameters of timber-carrying vehicular trains together with 6×4, and 6×6 tractors, and pole trailers were given in Table 2.12.

The main geometric parameters of the interaxle differentials are listed in Table 2.17.

It was assumed that the parameters of differentials used on highway and timber-carrier tractors made by a given manufacturer are the same. It was assumed arbitrarily that the locked drive in the KamAZ 43105 tandem was replaced by the same interaxle differential as on the KamAZ 54112.

The average operating speed V_a of these trucks, as in the investigation of interwheel differentials, was calculated from expressions (2.99) and (2.100). The total circumferential force $F_{x\Sigma}$ of the trucks was calculated from formula 2.101 and the energy-loading factor of the differentials was obtained from the expression

$$K_N^{MO} = \frac{(m_a g f + D_a)V_a}{l_{MO}A_d} \tag{2.114}$$

TABLE 2.16

Estimated Parameters of Highway Heavy-Duty Trains MAZ (6 × 4 Tractors + Semitrailers)

No.	Model	Full Mass m_a, t	Mass Taken by Drive Wheels m_{dr}, t	Engine Power P_e, kW/HP	Speed m/s / km/h		Gear Ratio			Tire
					Maximum V_{max}	Average Operational V_{avg}	Drive Axle u_a	Final Drive u_f	Wheel-Hub Gear Drive u_k	Radius r, m
1	MAZ 64227	38	18	236.5/320	25.48/92	20.38/73.37	5.88	1.714	3.428	11R20/0.505
2	MAZ 64229	42	18	242.9/330	26.39/95	21.11/76	5.49	1.6	3.428	11R20/0.505
3	MAZ 64221	44	18	245/333	29.1/105	23.28/84	4.83	1.41	3.428	11R20/0.505
4	MAZ 64226	44	18	245/333	33.33/120	26.66/96	3.96	1.154	3.428	11R20/0.505
5	MAZ E64221	44	18	265/360	33.33/120	26.66/96	3.456	3.456	—	11R20/0.505

TABLE 2.17

Estimated Parameters of Interaxle Tandem Differentials

		Side Gear					Pinion									Spider			
No.	Model	Tooth Number z_g	Outer Friction Diameter, mm d_{go}	Inner Friction Diameter, mm d_{gi}	Average Friction Radius, mm r_{gf}	Average Gear Radius, mm r_g	Tooth Number z_c	Outer Friction Diameter, mm d_{po}	Inner Friction Diameter, mm d_{pi}	Average Friction Radius, mm r_{cf}	Average Pinion Radius, mm r_c	Pitch Angle δ_c	Outer Module m_{te}	Pressure Angle α_w	Conditional Cross Section Area, cm^2 A_d	Spider Pin Diameter in Contact with Pinion, mm d_{sp}	Spider Pin Length in Contact with Pinion, mm l_{sp}	Spider Pin Length in Contact with Case, mm l_{sc}	Average Radius, mm r_0
1	Mercedes Benz 2232, 2232S, 2635, 2635AK/35	18	118	86	51	49	10	52	30.2	20.55	27	29°	6.5	22°30′	76.05	27.1	25	17	75
2	Renault GBN 340, R310T	16	101	76	44.25	50.5	11	68	30	24.5	33	34°31′	7	22°30′	86.24	30	30	14	80
3	MAZ 64221, 64226, 64227, 64229, 6425	16	118	86	51	49	11	65	32	24.25	31	34°31′	7	22°30′	86.24	32	29.5	23	85
4	MAZ E64221	18	100	80	45	65	11	65	35	25	38.5	31°24′	8	22°30′	126.72	35	30	26	86
5	KamAZ 43105, 54112	20	103	85	47	45	11	45	23.5	17	25	28°49′	5	22°30′	55	22	18	18	68
6	KrAZ 6437, E6437	28	130	88 60	54.5 40	75	10	50	28	19.5	26	19°39′	6	22°30′	100.8	25	26	18	100
7	MoAZ 7411	22	138	92	57.5	65	11	66	34	25	33	26°34′	7	22°30′	118.58	30	34	22	102

whereas, the accumulated-mileage wear factor was found from the formula

$$K_{\mathrm{u}}^{\mathrm{MO}} = \frac{(m_{\mathrm{a}} g f + D_{\mathrm{a}})(1 - \eta_{\mathrm{n}}) L_{\mathrm{a}}}{l_{\mathrm{MO}} A_{\mathrm{d}}} \tag{2.115}$$

where l_{MO} is 1 and 1.5 respectively for the 6×4 and 6×6 tractors. The accumulated mileage L_{a} was assumed to be the same for all the trucks and hence was eliminated from formula (2.115).

The velocity modes of the tandem's interaxle differential may range within wide limits depending on the combinations of slip of the four wheels (see Table 2.1 and Figure 2.6). The angular velocity of the pinion ω_{c} and the sliding velocity V_{c} of the pinion on the pin of the spider were assumed to be as those given by formulae (2.92) and (2.93). The remaining assessment criteria of the interaxle differentials were calculated, as for their interwheel counterparts, from formulae (2.94) through (2.98).

The results of these theoretical studies of differentials of the previously mentioned 6×4 tractors of the highway trucks are listed in Table 2.18.

Analysis of these results shows that the values of the energy-loading factor $K_{\mathrm{N}}^{\mathrm{MO}}$ of the majority of differentials is of the order of 1 kW/cm^2. Only the Renault P310T, MAZ 64221 and MAZ 64226 have higher values of $K_{\mathrm{N}}^{\mathrm{MO}}$ amounting to respectively 1.24, 1.30, and 1.72.

TABLE 2.18

Evaluation Criteria of Heavy-Duty Trucks' Interaxle Tandem Open Differentials

No.	Model	$F_{x\Sigma}$, kN $P_{w\Sigma}^{in}$, kW	T_0, kN-m	$K_{\mathrm{N}}^{\mathrm{MO}}$, kW/cm^2	$K_{\mathrm{u}}^{\mathrm{MO}} \times 10$, kN/cm^2	ω_0, rad/s ω_c, rad/s V_c, m/s	F_b, kN p_b, MPa	Q_a, kN p_a, MPa	Q_c, kN p_c, MPa
1	KamAZ 54112	3.195 56.75	0.215	1.03	0.58	264.39 480.70 5.29	1.07 2.71	0.78 0.29	0.21 0.19
2	Renault R310	4.18 106.91	0.36	1.24	0.48	298.53 434.22 6.51	1.60 1.78	— —	0.37 0.13
3	Mercedes Benz 2232	3.59 77.89	0.34	1.02	0.47	229.93 413.88 5.61	1.45 2.14	1.05 0.20	0.29 0.21
4	MAZ 64227	3.90 79.53	0.34	0.92	0.45	237.16 334.97 5.52	1.50 1.59	1.02 0.20	0.35 0.14
5	MAZ 64229	4.82 90.27	0.36	1.05	0.50	245.63 357.29 5.72	1.64 1.74	1.12 0.22	0.38 0.15
6	MAZ 64221	4.82 112.14	0.50	1.30	0.56	222.82 324.10 5.19	2.25 2.38	1.53 0.30	0.53 0.21
7	MAZ 64226	5.55 148.05	0.71	1.72	0.64	208.87 303.81 4.86	3.16 3.35	2.16 0.42	0.74 0.30
8	MAZ E64221	5.55 148.05	0.81	1.05	0.44	182.48 298.60 5.23	2.82 2.68	— —	0.61 0.26

These higher than ordinary values of these factors of differentials of the above MAZ models is attributed to their higher loading capacities and velocities than the MAZ 64227 that served as the base model, for the same geometric parameters of the interaxle differential.

The following was found by comparing the assessment parameters of interaxle differentials with the corresponding values of parameters of interwheel differentials of the same vehicle (see Table 2.11).

The torque at the housing of the KamAZ interaxle differential is much lower than at its interwheel counterpart. At the same time the energy loading of the interaxle mechanism is approximately 3.5-fold higher, which stems from its markedly smaller (almost twofold) conditional cross-sectional area as compared with the interwheel differentials.

The values of K_N^{MO} of MAZ interaxle differentials are approximately twofold higher than those of their interwheel counterparts of the same vehicle models. The conditional cross-sectional areas of the interaxle and interwheel differentials of the MAZ vehicles are the same and their final-drive gear ratios are close to 2. These are indeed the factors that brought about the above relationship between their energy loading factors. The energy loading factor ratio of the interaxle and interwheel differentials of the Mercedes-Benz is smaller, being equal to 1.38. Evidently, a big difference in the values of factors K_N and K_N^{MO} of these two kinds of differentials makes it possible for them not to have the same service life.

Tables 2.19 and 2.20 list the results of theoretical investigations of assessment criteria of the interaxle differentials of the driving tandems of timber-carrier tractors when trucks move over dirt roads.

Data from these tables served for constructing Figures 2.88 and 2.89.

These data allow investigating the effect of geometric parameters of interaxle differentials on their energy loading, which, to some extent also represents their effect on the wear

TABLE 2.19

Evaluation Criteria of 6 × 4 Timber-Carrier Tractors' Interaxle Tandem Open Differentials

No.	Model	$F_{x\Sigma}$, kN $P_{w\Sigma}^{in}$, kW	T_0, kN-m	K_N^{MO}, $\frac{kW}{cm^2}$	$K_u^{MO} \times 10$, $\frac{kN}{cm^2}$	ω_0, rad/s ω_c, rad/s V_c, m/s	F_b, kN p_b, MPa	Q_a, kN p_a, MPa	Q_c, kN p_c, MPa
1	Mercedes Benz 2232S-I	9.34 226.63	0.93	1.53	1.23	124.63 224.33 3.04	4.00 5.90	2.89 0.56	0.80 0.57
2	Mercedes Benz 2232S-II	8.45 93.28	0.75	1.23	1.11	124.02 223.24 3.02	3.21 4.74	2.33 0.45	0.64 0.46
3	Mercedes Benz 2232S-III	7.58 72.76	0.59	0.96	1.00	122.70 220.87 2.99	2.53 3.74	1.84 0.36	0.51 0.36
4	Mercedes Benz 2635AK	8.16 86.14	0.64	1.13	1.07	134.90 242.81 3.29	2.73 4.03	1.98 0.39	0.55 0.39
5	Renault GBH-340	8.56 90.43	0.76	1.05	0.99	118.22 171.96 2.58	3.41 3.79	— —	0.80 0.27
6	KrAZ E6437	16.14 155.69	1.06	1.54	1.60	146.79 411.00 5.14	3.16 4.86	2.46 0.49	0.44 0.33

TABLE 2.20

Evaluation Criteria of 6 × 6 Timber-Carrier Tractors' Interaxle Tandem Open Differentials

No.	Model	$F_{x\Sigma}$, kN $P^{in}_{w\Sigma}$, kW	T_0, kN-m	k_N^{MO}, kW/cm²	$k_U^{MO} \times 10$, kN/cm²	ω_0, rad/s ω_c, rad/s V_c, m/s	F_b, kN p_b, MPa	Q_a, kN p_a, MPa	Q_c, kN p_c, MPa
1	KamAZ 43105	10.86 125.11	0.55	1.52	1.32	151.50 275.46 3.03	2.75 6.95	2.00 0.75	0.55 0.47
2	MAZ 6425	17.15 197.54	0.93	1.53	1.33	141.20 205.37 3.29	4.16 4.41	2.84 0.55	0.98 0.39
3	Mercedes Benz 2635AK/35	9.37 99.00	0.49	0.87	0.82	134.90 242.81 3.29	2.09 3.09	1.51 0.30	0.42 0.30
4	KrAZ 6437	16.14 155.69	0.71	1.03	1.07	146.79 411.00 5.14	2.10 3.24	1.64 0.33	0.29 0.22
5	MoAZ 7410	29.00 164.46	0.91	1.49	1.63	192.95 385.91 5.79	2.97 2.91	2.20 0.26	0.55 0.22

of these mechanisms. As expected, the energy loading of differentials of 6 × 4 tractors is higher than that of their counterparts of 6 × 6 tractors. For example, the value of K_N^{MO} of the 6 × 4 KrAZ E6437 timber carrier is 49.5% higher than that of the 6 × 6 KrAZ 6437. It is seen from Figure 2.88 that the higher values of K_N^{MO} stem either from higher force (Mercedes-Benz 22325S-I) or velocity (KrAZ E6437) modes. Here the energy loading of the interaxle differentials of the 6 × 4 timber carriers on dirt roads is virtually identical to the energy loading of interaxle differentials of 6 × 4 highway tractors (Figure 2.88 and Table 2.18).

It follows from Figure 2.89 that the high value of K_N^{MO} of the KamAZ differential are attributed to marked force loads on the mechanism that stem from its smaller size (the differential's cross-sectional area is smallest of all those listed in Table 2.17, whereas the value of K_N^{MO} from Table 2.20 and Figure 2.89 is one of the highest). Note that the velocity modes of this differential are not high, but this is insufficient for reducing the total energy loading of the mechanism. The above also applies to the interaxle differential of the MAZ 6425. Its high value of K_N^{MO} also stems from the higher force loading. On the other hand, the energy loading (wear) of the MoAZ 7411 differential is determined to a larger degree by velocity than force operating modes.

It follows from Figure 2.89 that interaxle differentials of driving tandems of two vehicles have lower values of K_N^{MO}. This is the Mercedes-Benz 2635AK and the KrAZ 6437. The pressures on the working surfaces of components of these two differentials are also approximately the same. At the same time, the velocity modes represented by velocity V_c of the two above differentials differ markedly. Analysis of computational data shows that the value of V_c of the KrAZ differential exceeds the value of this quantity of the Mercedes-Benz by 64%. This difference is attributable to the high value of the internal gear ratio of the KrAZ differential, which is $z_g/z_c = 2.8$.

Investigations based on the previously developed criteria provided insight into still another relationship. Figure 2.90 shows values of K_N^{MO} of interaxle differentials of tandems of MAZ and Mercedes-Benz highway and timber-carrier tractors.

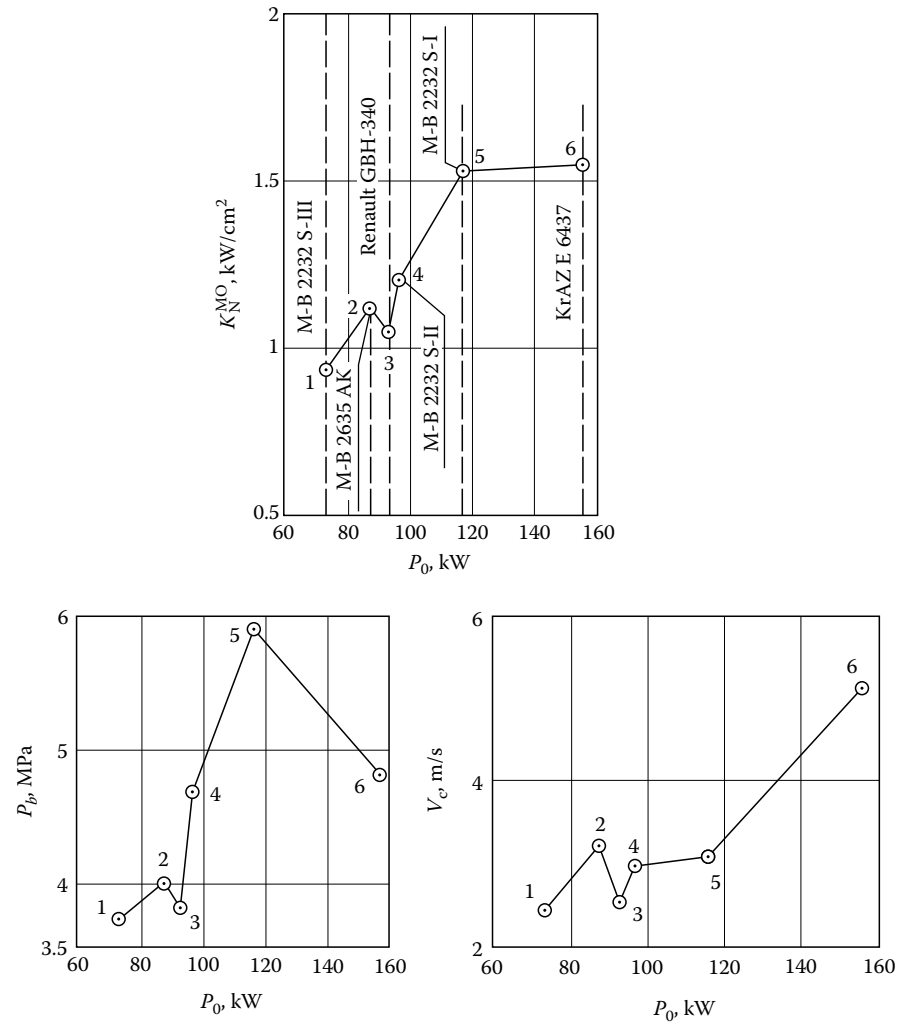


FIGURE 2.88
Evaluation criteria of 6 × 4 timber-carrier tractors' interaxle tandem open differentials (dirt road).

It is seen that the values of power fed to the differentials of these vehicles is approximately the same, with slightly higher lower and upper limits for the MAZ tractors. The power loading of Mercedes-Benz differentials is here higher for the same values of P_0 (steeper slope of the graph). The latter is attributed to smaller values of area A_d. It is quite reasonable to assume that the smaller size, together with the higher energy loading, and at the same time the higher operating life of the Mercedes-Benz differential, was attained by providing it with copious lubrication.

It is useful to compare the numerical values of the assessment criteria of the interwheel differentials of the 6 × 4 and 6 × 6 timber-carrier tractors (see Figure 2.66) with the corresponding criteria of the interaxle differentials of the driving tandems (see Tables 2.19 and 2.20). The same tendencies as for the differentials of highway trucks were found to exist here. At lower torques, the interaxle differentials have higher energy loading factors.

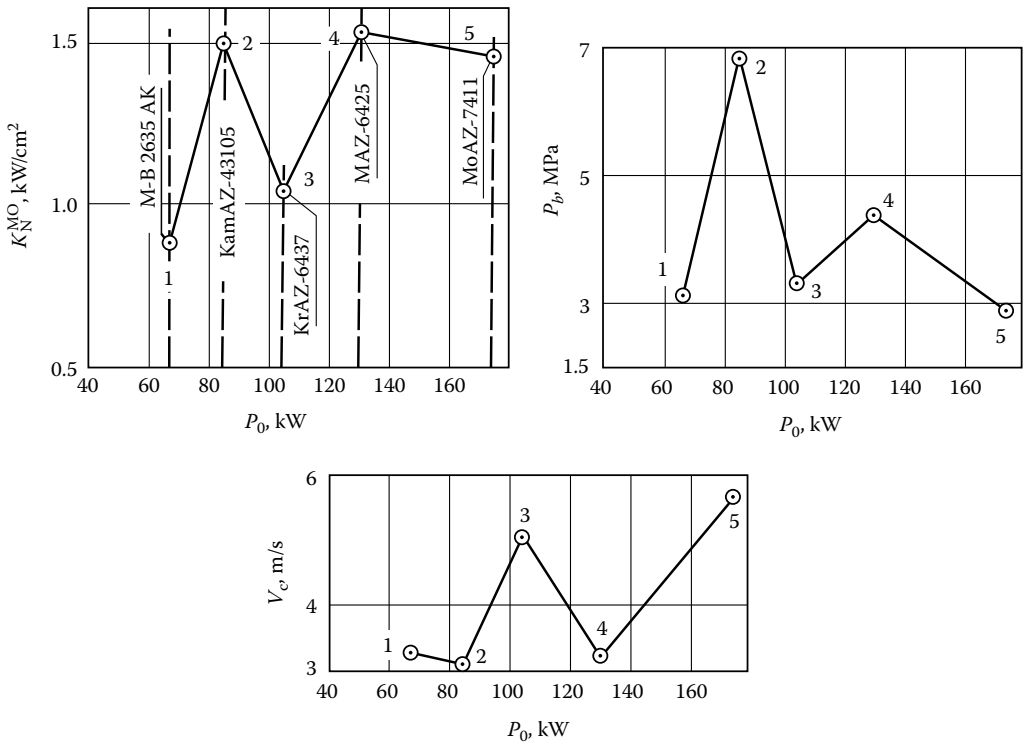


FIGURE 2.89
Evaluation criteria of 6 × 6 timber-carrier tractors' interaxle tandem open differentials (dirt road).

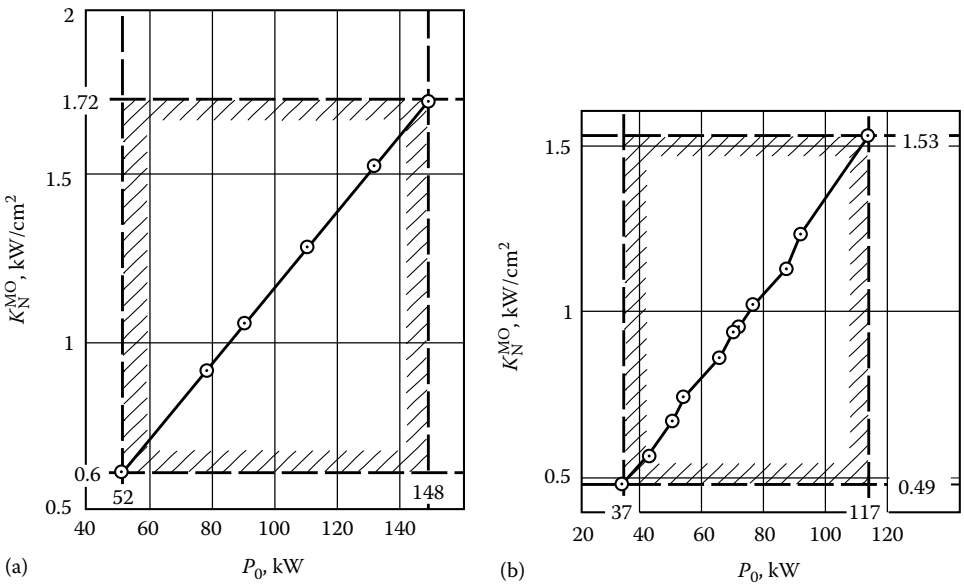


FIGURE 2.90
Energy loading factors of tandem interaxle differentials of highway and timber-carrier tractors: (a) MAZ; (b) Mercedes-Benz.

For example, the value of K_N^{MO} for the interaxle differential of the KrAZ 6437 is 3.12-fold higher than for the interwheel differential. This relationship between these coefficients is determined by the conditional cross-sectional areas of the differentials and by the gear ratios of the driving axles, i.e., by velocity modes. The ratio between these coefficients for interaxle and interwheel differentials of the 6×6 Mercedes-Benz is lower and amounts to 1.38.

It was thus shown that interaxle differentials transmit much higher power loads than their interwheel counterparts. The interaxle differentials operate under rather higher speed modes whereas they have almost the same force loads. This necessitates additional design measures to improve the operating life of interaxle differentials. One of the ways of achieving this is using improved lubrication systems. These must additionally be used because interaxle differentials are quite frequently located in their cases higher than the interwheel differentials in axles. Because of this, interaxle differentials appear to be quite frequently at a large distance from the oil level. At times, they are closely surrounded by components of other mechanisms, which interfere with designing a system of channels for supplying the lubricant to the housings of interaxle differentials and to the rubbing surfaces of their components. All this requires a radical approach to designing lubricating systems for interaxle differentials. The next section examines the designs of certain lubricating systems of interaxle differentials of driving tandems and also of transfer cases.

2.6.3 Oil Lubrication Systems

2.6.3.1 Lubrication Systems for Interaxle Differentials of Driving Tandems

The lubrication system of the forward rear pass-through axles and of the interaxle differential of the 6×4 highway tractor of a truck with a total mass of 38 ton (see Figure 2.91) is of great interest with respect to manufacture and operating efficiency.

The interaxle differential of this vehicle is located in a separate housing that directly adjoins the axle's case. This is not the case with the housing and the case of the axle that, conversely, are directly interconnected by the communicating-vessels principle by means of port 10 located at the level of oil-filling throats of the housing and the case and also of the oil drain channel 11. This mutual position provides for equalization of the oil level in both spaces as it is pumped from the case to bearings 14 and 15 by means of the final-drive wheel over the path: oil trapping pocket 8 with scrubber 6—sump 5—channel 9. From sump 5 the oil flows through channel 7 also to the rear bearing 3 of the interaxle differential. Front bearing 1 of this differential is lubricated by oil that accumulates in oil trapping pocket 2. The remaining rubbing elements of the interaxle differential are lubricated by oil supplied from the oil trapping pocket through port 13 in the hub of the side gear into the space between the input and output shafts of the mechanism.

The distribution of oil inside the interaxle differential and the distant bearing 12 from Figure 2.91 is most conveniently followed using the layout in Figure 2.92.

Oil flowing from oil trapping pocket 6 fills drill channels 4 and 7 in the input and pass-through shafts of the differential. Then its flow splits: through radial drill holes in the input shaft to bearings 3 and 5 of the side gears and through radial drill holes in the pass-through shaft to its rear distant bearing 9 (this is the bearing designated as 12 in Figure 2.91). Passing through grooves in the bearings of side gears, the oil fills the housing of the differential and lubricates the locations of gear meshing, thrust washers, and pinion bushings. Oil is drained from the housing of the differential into the housing of the transmission reduction gear through a slot between the housing of the differential and the distributing cylindrical gear. The oil is not drained from the space of the rear bearing

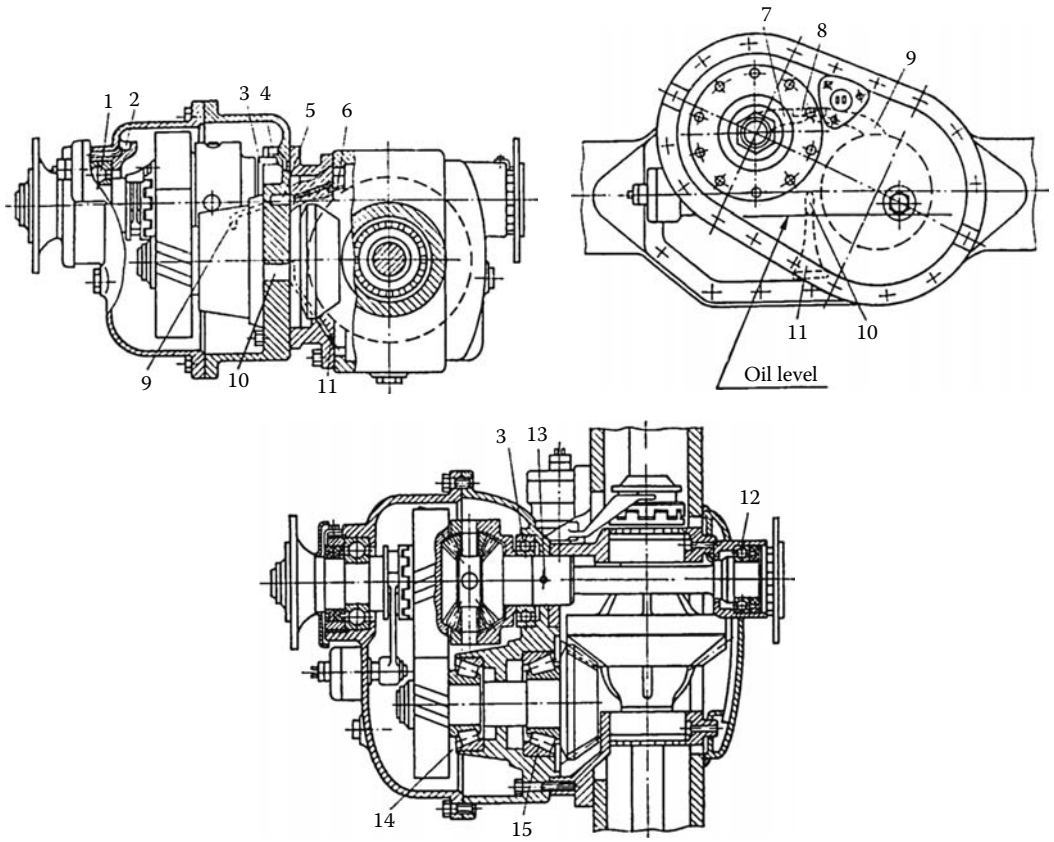


FIGURE 2.91
6 × 4 highway tractor: forward rear pass-through axle with interaxle differential: 1, front bearing; 2, 4, and 8, oil trapping pockets; 3, rear bearing; 5, oil sump; 6, scrubber; 7, 9, 11, oil channels; 10, port; 12, distant bearing; 13, through port; 14, 15, bearings of the final drive pinion.

support of the pass-through axle. Conversely, it is prevented from being drained by a slotted packing with oil circulation groove 8.

The lubrication system of the interaxle differential from Figure 2.92 operates under pressure determined by the potential energy of the oil that accumulates in oil trapping pockets. This arrangement is effective in locations when oil flows generated by rotating parts of the mechanism reach the highest point inside the case. If this is not the case or if vortical (splashing) flows in the highest point inside the case are not sufficiently copious, then a pump is added to the interaxle differential's lubrication system. Usually this is a gear pump, but a pump of another type may also be used.

A gear pump was used in the lubrication system of the interaxle differential of a 6 × 4 tractor (see Figure 2.93).

Rotation is transmitted from input flange 1 to input shaft 3 and then to spider 6. From it, motion is transmitted to pinions 5 and from them to the left and right side gears 5L and 5R. These gears set into motion flange 8 of the rear-axle drive and interwheel differential 10 of the forward rear axle. This lubrication system operates as follows. Pump 15 takes oil from the case and drives it under pressure into drill channel 9 of the axle of idle gear 2. Here products of wear and other possible inclusions are removed in preliminary filter 14 and then in fine

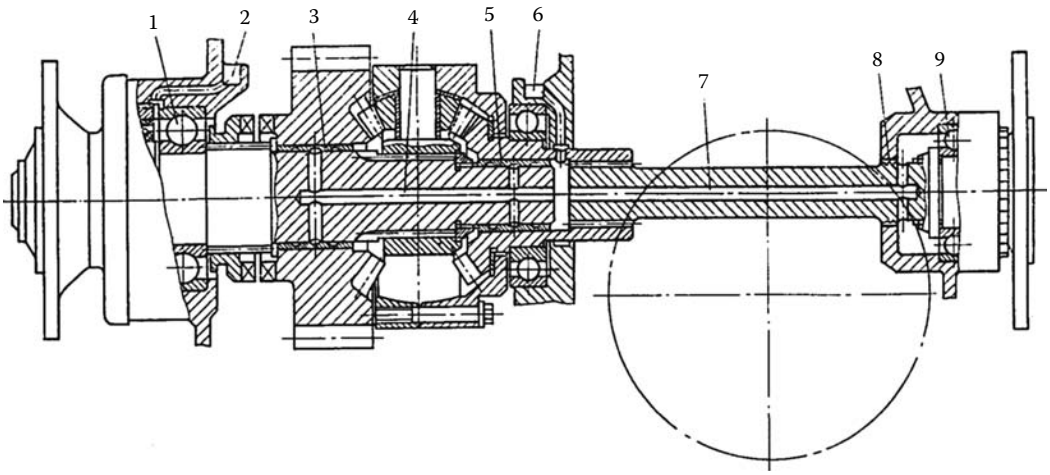


FIGURE 2.92
6 × 4 highway tractor: tandem interaxle differential: 1, front bearing; 2, 6, oil trapping pockets; 3, 5, side gear sliding bearings; 4, 7, oil channels; 8, slotted packing; 9, distant bearing.

filter 13. Drill channel 9 serves as a kind of distributing sump of the lubrication system, from which the oil is directed to the points of meshing of distribution gears 4 and 12 with idle gear 2, to the bearing of the latter gear and then along oil passages in the case walls, to bearings 11 of the axle's final drive and finally to sump 7 of the interaxle differential.

The arrangement shown in Figure 2.93 employs an interaxle differential without a housing. Hence only the bearings of side gears and pinions are force-lubricated from a pump. Lubrication of pinion bearings, more precisely, of the spider's pins, is a feature

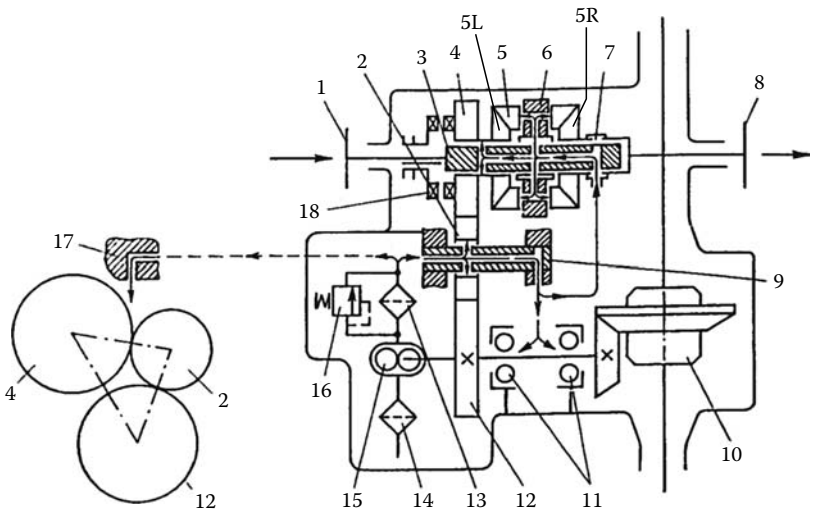


FIGURE 2.93
6 × 4 highway tractor: layout of tandem interaxle differential and lubrication system: 1, input flange; 2, idle gear; 3, input shaft; 4, 12, distribution gears; 5, pinion; 5L, 5R, left and right side gears; 6, spider; 7, oil sump; 8, flange of the rear-axle drive; 9, drill channel; 10, interwheel differential of the forward rear axle; 11, bearings; 13, fine filter; 14, preliminary filter; 15, gear pump.

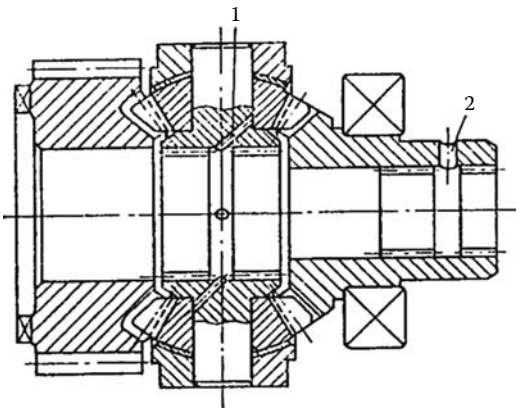


FIGURE 2.94
6 × 4 highway tractor: tandem interaxle differential design: 1, 2, oil channels.

specific to the lubrication system being considered. It is attained by means of special channels produced in the spider's fingers and in the right side gear. The shape and location of these channels (numbered 1 and 2) are shown in Figure 2.94.

Another feature specific to this lubrication system is the fact that it uses three methods for lubricating rubbing surfaces: jet splashing, directed jet, and contact lubrication under pressure. The first method is used for lubricating the locations of meshing between gears and pinions, since the differential does not have a housing. The second method is applied for lubricating the points of meshing of distribution gears 4 and 12 and idle gear 2, whereas the third method is used for lubricating all the remaining rubbing surfaces. Here, whereas oil jets are splached by rotating elements of the mechanism, directed jets are formed by a pump using a special tube or mouthpiece (see Figure 2.93) at the end of the oil channel, that is located over the rubbing location.

A gear-type oil pump is used in the lubrication system of an interaxle differential of still another 6 × 4 tractor intended for heavy-duty trucks. Figure 2.95 shows the layout of the forward rear and rear axles of the tractor.

In it oil pump 3 is rotated by a gear drive from the driving shaft of interaxle differential 1 and generates, according to some data, a flowrate of more than 11 L/min when the shaft

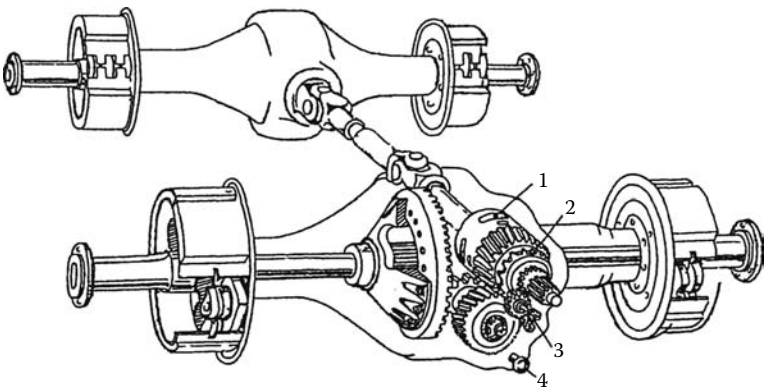


FIGURE 2.95
6 × 4 highway tractor: axle tandem: 1, interaxle differential; 2, locking clutch; 3, gear pump; 4, magnetic-type oil strainer.

rotates at 35 Hz. Item 2 shows the locking clutch of the differential, whereas item 4, a magnetic-type oil strainer.

The location of oil-supply channels within the interaxle differential housing and within the differential itself from Figure 2.95 was shown in Figure 2.81b. The main oil distributing channel of this lubrication system is located above the differential in the wall of the housing. Oil from it is supplied to the differential's rubbing locations through a sump and channels drilled in the pass-through and driving shafts of the mechanism. The journal of the driving shaft and the side-gear bearing are lubricated by the contact method inside the differential. The meshings between side gears and the differential's pinions are lubricated by the splash jet method.

Figure 2.96 shows still another pass-through axle with a unique interaxle differential lubrication system.

The uniqueness of this lubrication system consists in the fact that in it oil is supplied to the interaxle differential case through long annular channel 5 that requires overcoming a centrifugal force at the inlet to the channel. With reference to this feature, the system operates as follows. Oil that is supplied by being sprayed by driven wheel 6 to oil trapping pocket 7 is pushed by a centrifugal force from the inlet to the annular channel. But it encounters on its way the blades of configured washer 8. The blades are sloping in a

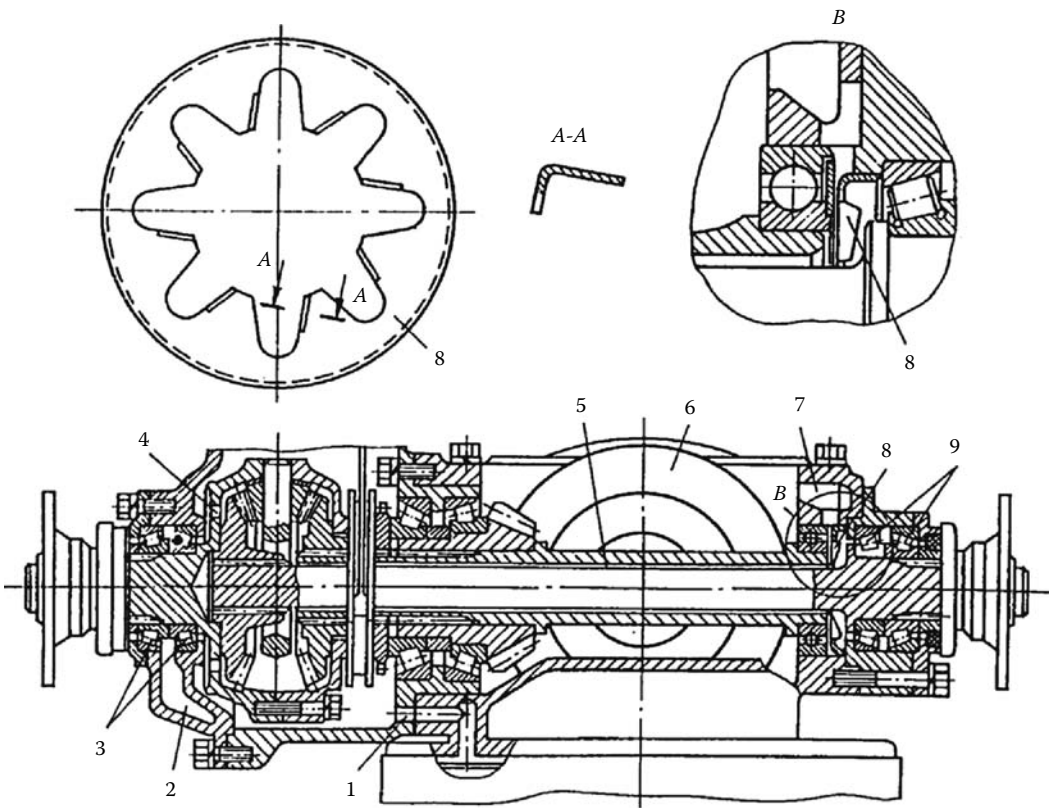


FIGURE 2.96
6 × 4 highway tractor: tandem interaxle differential design: 1, 2, oil draining channels; 3, bearings of the input shaft; 4, oil discharge ports; 5, annular channel; 6, driven gear of the final drive; 7, oil trapping pocket; 8, configured washer; 9, bearings of the pass-through shaft.

manner that forces the repelled oil flow to enter the annular channel under some pressure and then to enter the differential case. The oil then passes through oil discharge ports 4 in the differential housing, the forward bearings of the mechanism's input shaft, oil draining channels 2 and 1 and then to the axle's case.

In examining specific lubrication systems of differentials no mention was made of those of their component that do not directly participate in lubricating the rubbing surfaces, but without which not a single system can function. Some of the major requirements put to lubrication system and to the oil are considered now. First, the oil that is used to charge the system should be pure. Second, it should be purified in the course of operation to remove the products of wear of the components of mechanisms and their own. For this the system must include special filtration devices, settling volumes and magnetic traps for abrasives. Third, since the lubricating oil must not only lubricate the rubbing surfaces, but also to cool them, it should not become itself heated above the permissible temperature. When this temperature is exceeded the oil itself starts aging and the organic materials of seals start carbonizing. To prevent this from happening, lubrication systems must extensively use means for rejecting heat to the surroundings such as fins on the case walls. Additional fins markedly promote cooling of the lubricating oil. Reinforcement ribs of cases may also be used for this purpose. Quite precise results are obtained from heat-transfer calculations; however, in practice the volume and shape of cases are initially selected by analogy.

The case must be leakproof. All openings in it are closed by caps that are placed on 0.2–0.8 mm thick gaskets of cardboard or other packing material. The width of the gaskets and accordingly of the surfaces on which they are placed usually amounts to 12–20 mm. In order for the cover to apply uniform pressure to the gasket over the entire perimeter of the opening, holes for hold-down bolts are provided at 60–80 mm from one another. The quality of the packing here depends on the precision (flatness) of the underlying surfaces.

At the same time the lubrication system cannot be completely hermetically sealed, since when the unit becomes heated, the pressure within the case rises and oil may be pushed out through the packing, particularly through oil seals and packing rings. To prevent this from happening, a breather pipe, which is a device providing communication between the case and the atmosphere, is placed in the upper part of the case (most frequently in the filling-throat plug).

When designing high-mobility, including amphibious vehicles, breathing pipes must be provided in all the cases of the driveline and are lead out by means of tubes to the driver's cabin level. These measures are made necessary by the fact that cases, that heat up when operating in the air, cool down rapidly in water. This steeply reduces the pressure in their cavities and water starts sipping through the packing glands into the cases where it starts mixing with the oil. For this reason, in addition to placing a breather pipe, shaft openings in the cases of drive axles are sealed by two paired packing glands, turned through 180° relative to one another. One of them should prevent oil from leaking from the case and the other should prevent water from entering the case.

An effort should be made to provide a centralized lubrication system. This allows reducing the number of plugs and the nomenclature of oils. However, this cannot be always done. In such cases it is necessary to design individual systems using both liquid and solid lubricants. Individual lubrication is provided for individual bearings, for example, the bearings of hubs of the driving and driven wheels of a vehicle, bearings of cardan-transmission joints and similar. Solid lubricants are most frequently used in individual systems. These are supplied to the system by replacing filling ports by pressure lubricators that are installed in accessible locations on the pertinent housings.

2.6.3.2 Lubrication Systems for Transfer Cases

Not all the problems associated with wear of drive components and undesirable deterioration of certain operating factors can be solved by flow-through component lubrication systems. In many cases more active, forced lubrication systems with oil pumps, are needed. This applies particularly to transfer cases. Lubrication of rubbing surfaces under pressure in transfer cases is, as a rule, provided by externally coupled gear pumps. Lubrication systems with pumps are known as combined systems. Experiments show that the reliability of combined lubrication systems is problematic.

Gear pumps have a number of advantages. They are simple, in particular those with external coupling, are small and lightweight, may be operated at relative high rpm and short-term pressure overloads the magnitude and duration of which are limited only by the capacity of the bearings. However, in spite of these advantages, these pumps have a number of shortcomings that must be considered when put to use under a given set of conditions.

One of the major shortcomings of gear pumps is their inability to self-feed, i.e., the inability to operate when air is present in the intake cavity and in the pipe. They are only capable of working with an incompressible fluid—a liquid, if all the pipes of its intake part are filled with it. This is attained by placing the pump with the axis of its rotors at least at the level of the liquid surface within the transfer case. In cases when this was done, there are no or almost no problems with reliability of the operation of the pumped lubrication system. Problems arise, as a rule, when the lubrication system pumps are situated much above the oil-bath surface. The case of a transfer case lubricating gear pump used in a multiwheel drive vehicle shown in Figure 2.97 is most remarkable in this respect.

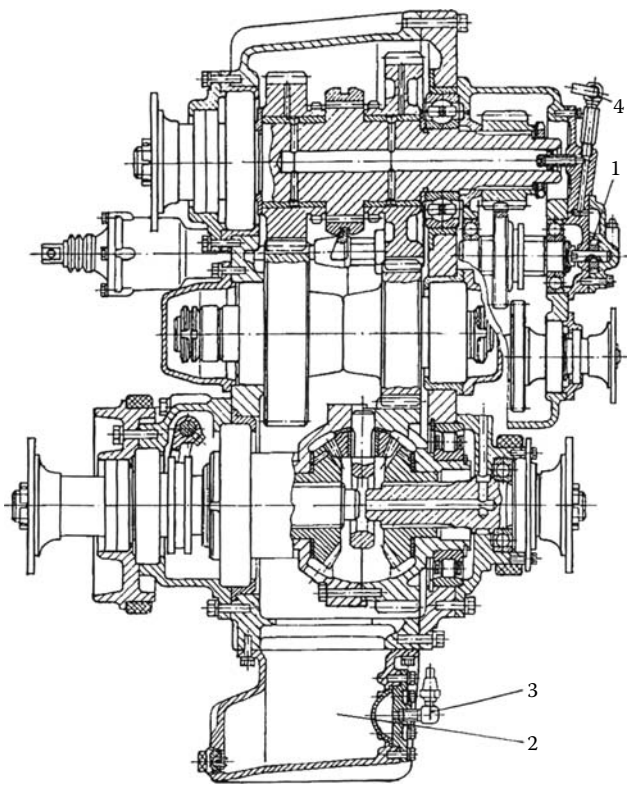


FIGURE 2.97
Transfer case of a multiwheel drive vehicle: 1, gear pump; 2, oil bath of the transfer case; 3, 4, ends of the intake pipe.

Initially the gear pump of the lubrication system of this transfer case was located on the same axis as that of the intermediate shaft of the power-takeoff case drive, which also operated the pump (see item 1 in Figure 2.97). It was intended that the pump should suck the oil from the oil bath 2 of the transfer case itself. The oil should go to the pump through the intake pipe shown by items 3 and 4. The distance between the axis of the pump's rotor and the oil-bath surface was about 0.5 m. Since the pump did not operate stably under these conditions, the operating instructions of the vehicle read that if no lubricant is supplied, in particular, after the vehicle was not operating for a long time, the pump must be filled with 200 g of MT-16P lubricant. This should be done after disconnecting the piping leading from the transfer case bottom to the pump. The piping should be reconnected after adding the oil. Following this instruction did not much improve the pump operation and, in addition, drivers were usually lax in following it. Then an internally coupled gear pump was designed. It was placed on the shaft of the transfer case's differential (see item 1 in Figure 2.98).

This partially solved the problem of lubrication-pump reliability. However, a full solution was achieved only after the pump was placed at the bottom of the oil bath that, however, was done at the penalty of increased complication of the pump's drive (see 1 and 2 in Figure 2.99).

The above shows that one of the criteria of stability of operation of gear pumps that should be known and definitely considered by the designer, consists in knowing the relationship between the level h_r of the axis of the pump's rotor and the liquid level (elevation of the oil-bath surface) h_s. This is expressed by the inequality

$$h_s - h_r \geq 0 \tag{2.116}$$

It must be remembered that gear pumps do not operate reliably with liquids containing large quantities of air (gas) for the same reason that they are incapable of self-intake. According to experimental data, the gear pump loses up to 6.5% of its pumping capacity when the fluid contains as little as 5% of air, whereas at 30% air content the pumping capacity loss is as high as 46%.

Intake losses of gear pumps are of significance. They are determined primarily by the extent to which the liquid fills the roots of the rotor teeth in the intake cavity. The centrifugal force developed by the rotor teeth is a serious hindrance to the penetration of

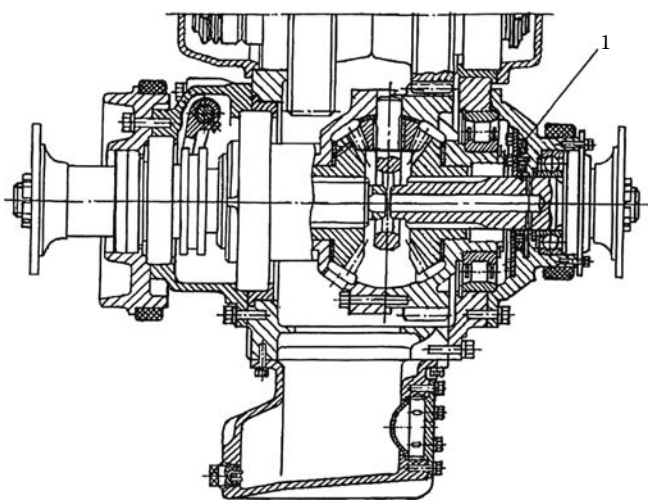


FIGURE 2.98
Transfer case of a multiwheel drive vehicle with internally coupled gear pump: 1, gear pump.

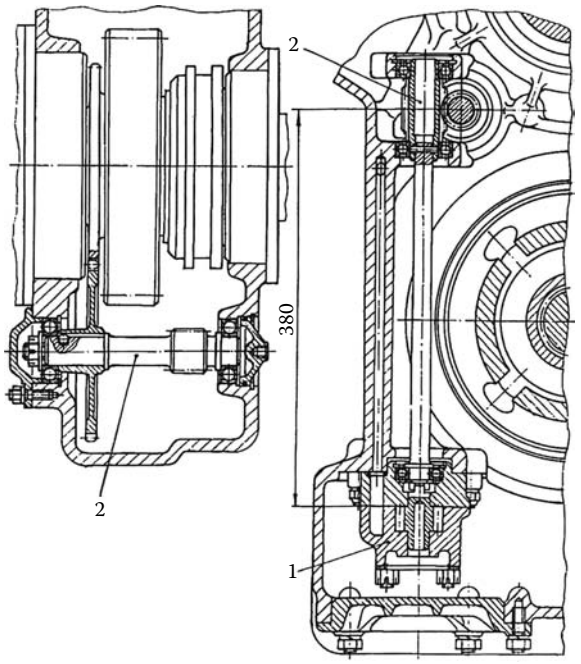


FIGURE 2.99
Transfer case of a multiwheel drive vehicle with improved gear pump: 1, gear pump; 2, pump drive.

oil to the rotor-teeth roots. This imposes a limitation on the rotating speed of the tooth crowns that should be coordinated with the viscosity of the fluid that is pumped within the operating temperature limits. The lower this viscosity, the higher the permissible speed of rotation of the rotor.

Still another criterion of properly designed forced lubrication system is the recommended velocity of the fluid in the intake pipe and in the intake cavity of the pump. For low-pressure and low-capacity pumps, it should be specified within the 1–2 m/s range. This range was established to achieve the lowest possible losses in the pump's intake zone.

A forced lubrication system with a gear oil pump is used for lubricating the components of the differential and other parts of the transfer case of a multifunction chassis (Figure 2.100).

The transfer case is installed on a vehicle chassis that is used with a variety of municipal vehicles, including garbage trucks in a manner that would not interfere with placement of working implements, for example, sweeping-machine brooms, beneath the frame. Both its output (driven) shafts with flanges 1 and 9 at their ends are arranged in the vertical plane. Here the shaft with flange 9 that leads to the rear axle is located at the level of the secondary shaft of the transmission. Because of this, lubrication of rubbing surfaces in this transfer case, particularly of components located on top, by simple spraying became a problem. Lubrication of hub-spider 7, pinions 8 with side gears 10, located in closed housing 6 of the interaxle differential became even more problematic. They are separated from the oil bath by a narrow passage between the walls of case 4. The narrow passage is in addition, partially blocked by driven gear 2 and intermediate gear 3. These gears provide lubrication only to the teeth of drive gear 5. For this reason, gear pump 11 is used for lubricating the components of the differential and its bearings. The pump is rotated by the front-axle drive shaft (see flange 1), takes in oil through a filter almost at the very bottom of the oil bath and feeds it under pressure along a tube into the differential cavity. The oil supplied to the differential's components is fed along branches from the main channel simultaneously to the bearings of the rear axle drive shaft.

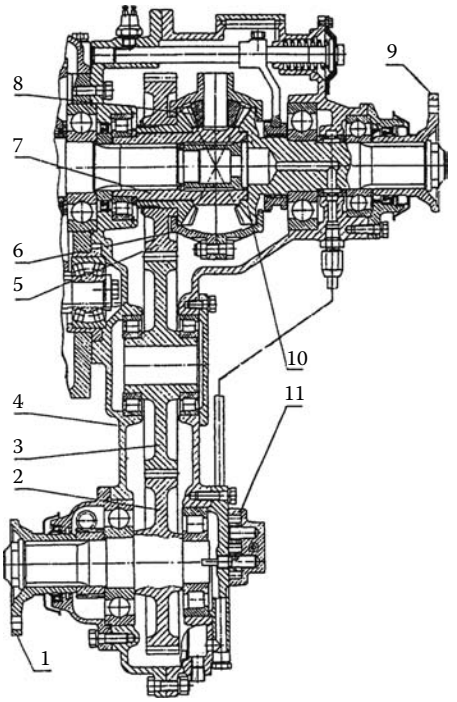


FIGURE 2.100
Transfer case of multifunction wheeled vehicle chassis: 1, 9, output flanges; 2, driven gear; 3, intermediate gear; 4, housing of the transfer case; 5, drive gear; 6, housing of the interaxle differential; 7, hub-spider; 8, pinion; 10, side gear; 11, gear pump.

A complex lubrication system is not needed in open-type reduction gear as, for example, in the reduction gear of the power takeoff from secondary shaft of the transmission 1 of the same vehicle chassis, shown in Figure 2.101.

The teeth of driving gear 7 of this power takeoff, of intermediate gear 2 and the teeth of driven gear 4 are lubricated by drawing oil from the case bath and transmitting it from one another. This oil also serves for direct lubrication of bearings 9 and 10 and the teeth of clutch 8. The bearings of shaft 6 and the teeth of clutch 5 are lubricated by oil sprayed by the reduction gearing. Only the needle bearing of driven gear 4 has to be force lubricated. As seen from the figure, oil is supplied to it from a pocket produced in the cap of the bearing seat of case 3. This pocket itself receives its oil as a spray produced by the teeth of gear 4.

Lubricating systems are not a noticeable part of a vehicle, but their role is major. Without these systems, not a single component of the vehicle, in particular, one operating at some speed is capable of reliably operating for a long time. For this reason, improvement of existing and development of new systems for lubricating parts of transportation and traction vehicles must be a continuous concern for designers.

Consider now certain specifics of designing and constructing driveshafts. When a vehicle with a relatively flexible frame moves, in particular under terrain and irregular road conditions, the components comprising the driveline are set into linear and angular motion relative to one another. In such cases, units that are installed on the vehicle's frame are connected by universal joints. The splined telescope joint of such a drive 2 (see Figure 2.102) compensates for linear motion, whereas the universal joints compensate for angular motion.

Since linear motion occurs while the driveshaft transmits torque, axial forces arise in the coupling. When they are large, the reduction gear supports may wear out prematurely, become damaged and even fail. In order to avoid this, the following rules be observed when designing universal joints. When the linearly moving and linearly nonmoving couplings of the universal driveshaft transmission are subject to the same load, the specific

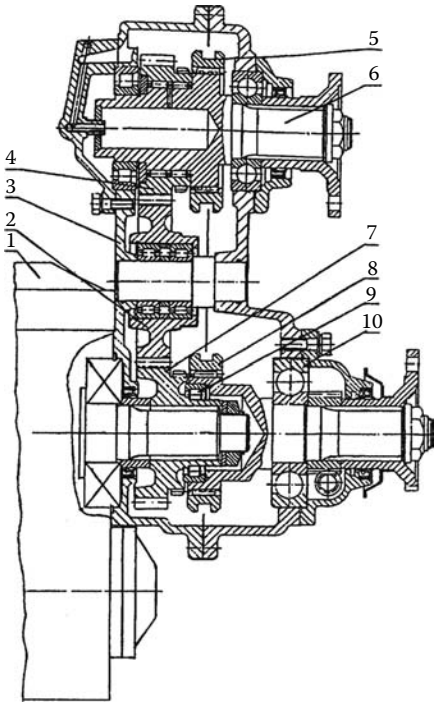


FIGURE 2.101
Power takeoff: 1, transmission; 2, intermediate gear; 3, case of the takeoff; 4, driven gear; 5, clutch; 6, shaft; 7, driving gear; 8, clutch; 9, 10, bearings.

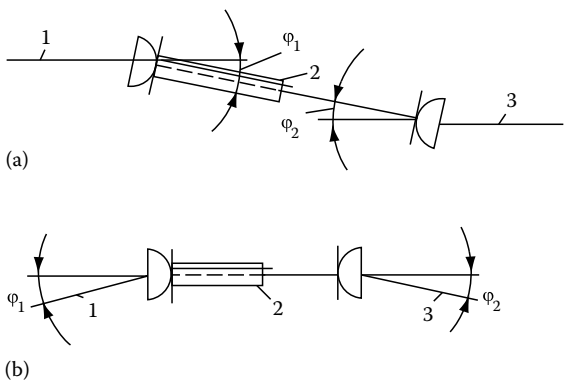


FIGURE 2.102
Splined telescope joint: (a), (b)—two configurations: 1, 3, input and output shafts; 2, splined telescope joint.

load on the splines of the former should be two- to threefold lower than on the latter. This prevents displacement of the lubricant from the spline joint. The linearly moving splined shaft of the driveshaft transmission should have a torsional resistance that is 1.5–2-fold higher than that of the nonmoving shaft. This is needed in order to avoid its angular deformation and seizing in the mating spline bushing of the nonmoving shaft. Seizing of a universal joint transmission may lead to its complete failure.

It is well known that the yokes at the ends of one driveshaft should be placed in the same plane, whereas the technical assembly instruction should make mention of the same factor, in order to prevent incorrect assembly of the driveshaft. If, for whatever reason, the yokes of one driveshaft became located in mutually perpendicular planes, then the

driven shaft of the transmission will rotate at variable speed, which is inadmissible. The universal joint drive elements should be located according to the layouts shown in Figure 2.102. An effort should be made to ensure that angles φ_1 and φ_2 should be equal. In this case, the velocities of the two shafts are full identical. When the driveshafts are designed to rotate at from 25 to 50 rad/s, angles φ_1 and φ_2 and should not be more than 3°–10°. It is not recommended to place the shafts at zero angle to one another in order to avoid brinelling—specific wear in the form of grooves that appear on the surfaces of the journal cross pins as a result of the vibration of the bearing needles. Brinelling of the journal cross pins also results from nonuniform distribution of load along the bearing needles when they are shifted relative to the axes of the working surfaces of the bearing cups. It manifests itself most frequently when the stiffness of the yokes or the surface hardness of the journal cross pins is insufficient.

Angles between driveshafts that are greater than 10° are also not permitted because of the great fluctuations in the driveshaft rotational speed that this causes. These angles may be increased for a brief period of time to 15° by way of relative shifting of the vehicle's units that are coupled by the driveshaft transmission. The highest permissible angles of universal joints located between the axles of tandems of multiwheel drive vehicles are 30°. This requires using specially designed longer than usual yokes. These limiting angles between the driveshafts are dictated by the potentiality of operating the multiwheel drive vehicle over surfaces cut up by ditches.

Even before developing complex mathematical models of the dynamics of driveshafts it is advisable to check their cross sections for the critical angular velocity (rpm) using the simple expression

$$n_{cr} = (12.4)10^6 \sqrt{\left(d_{out}^2 + d_{in}^2\right)/l^2} \tag{2.117}$$

where

d_{out} and d_{in}, are, respectively, the outer and inner diameters of the tube in cm
l is the distance between the centers of the universal joints in cm

Due to clearances that exist in universal joints and also of the possible wobbling of the flanges of the output shaft of the gearbox or of the transfer case and the axle drive bevel gear, the critical rpm are actually somewhat lower than those calculated. For this reason, the highest permissible rpm value of the driveshaft should not exceed $0.8n_{cr}$. Figure 2.103 shows cardan shafts that failed because the critical rpm was exceeded.

2.7 Designing Locking Devices

Two designs of locking arrangements for differentials, in which the locking clutch connects two (out of three) principal elements of the differentials, are in use. In the first arrangement (which is more common), one of the output shafts is connected to the housing of the differential (Figure 2.104a).

In the second arrangement, the two output shafts are coupled (Figure 2.104b). To be able to design and work out locking mechanisms, one must have available a technique for determining the torques that are applied to these mechanisms.

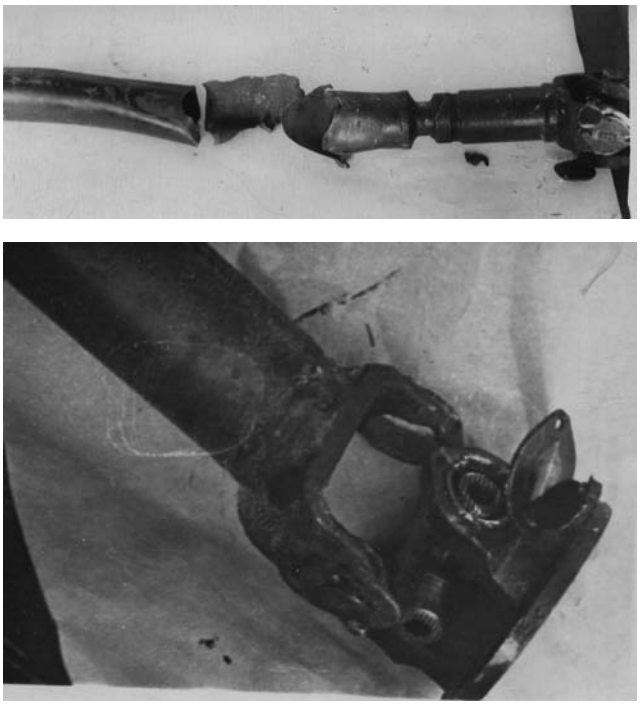


FIGURE 2.103
Driveshafts failed because of critical rpm.

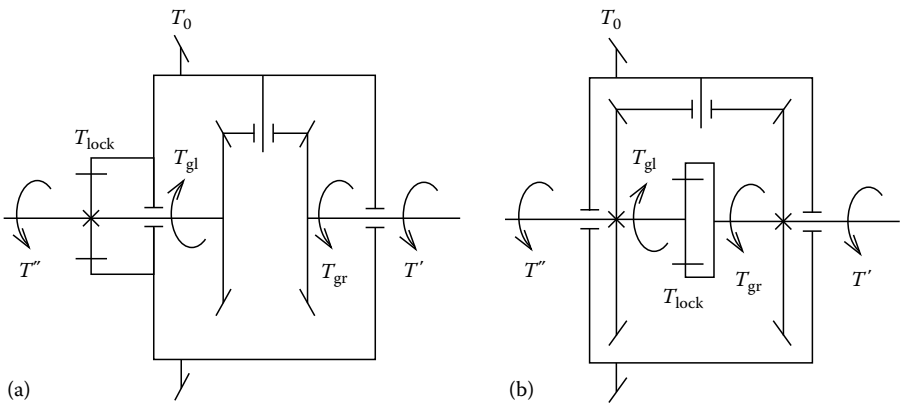


FIGURE 2.104
Layouts of locking differentials: arrangements (a) and (b).

Consider the first arrangement from Figure 2.104a. The right side gear is subjected to moment T_{gr} in the counterclockwise direction (viewing it from the right), equal to torque T' at the right output shaft. Moment T_{gl} at the left side gear, equal to moment T_{gr}, acts on the shaft of the locking clutch. This clutch is also subjected to counterclockwise torque T'' exerted by the left output shaft. Then the equation of torques acting on the locking clutch can be written as

$$T_{lock} = T'' - T' \tag{2.118}$$

It follows from this that under ordinary operating conditions the locking torque T_{lock} that is applied to elements of the locking clutch will always lie between T'' and T'. If the torque at one of the wheels is close to the limiting value dictated by conditions of coupling between the wheel and the surface of motion T_μ, i.e., $T'' \to T_\mu$, and $T' \to 0$, then the locking torque $T_{lock} \to T_\mu$. When T' is negative, which may occur with a vehicle with a locked differential taking a turn, $T_{lock} \to T_\mu$. When $T'' \to T_\mu$, whereas $T' \to (-T_\mu)$ then torque T_{lock} will have the maximum value of $T_{lock} = 2T_\mu$.

In the second arrangement, shown in Figure 2.104b, input torque T_0 is transmitted equally to the left and right side gears: $T_{gl} = T_{gr}$. These torques act on the locking clutch from two sides in opposing directions. Since $T'' > T'$ when the differential is locked, one may write the torque equation:

$$T_{gr} = T' + T_{lock}, \quad T_{gl} = T'' - T_{lock} \tag{2.119}$$

whence

$$T_{lock} = 0.5(T'' - T') \tag{2.220}$$

When $T'' \to T_\mu$ and $T' \to 0$, the locking torque is $T_{lock} = 0.5T_\mu$. When T' is negative, then $T_{lock} > 0.5T_\mu$. When $T'' \to T_\mu$ and $T' \to (-T_\mu)$, the locking torque attains its highest value of $T_{lock} = T_\mu$. It is seen from the above analysis that, under identical conditions of vehicle travel, in all cases the value of T_{lock} in the second arrangement will be one half of that under the first arrangement. However, the possibility of obtaining simpler design solutions causes the first arrangement to be more prevalent.

Locking devices of differentials may consist of jaw (cam), spline (expansion) and friction clutches, mechanisms with pin clutches are less frequently used. Figure 2.105 shows jaw (cam-type) locking clutches that connect the housing of the differential to one of its output shafts.

Similar designs are used in heavy-duty trucks such as Magirus, Mercedes-Benz, Scania and a number of others. Examples of the use of jaw-type clutches in the first arrangement consist, among others of the interwheel differentials shown in Figures 2.71 and 2.73. In Figures 2.81a and b and 2.92 the spline (tooth)-type and jaw-type clutches lock the interaxle differentials, connecting the input shafts, associated with the spiders and the left side bevel gears, manufactured together with the cylindrical gears of the interwheel differential's drive. In the interaxle differential from Figure 2.83 a spline clutch locks the housing to the right output shaft, and in the differential from Figure 2.82 a frictional plate clutch locks the housing to the left output shaft. Similar designs can be observed also in other figures of Section 2.6 (Figures 2.78; 2.79; 2.86; 2.100).

Figure 2.106 shows examples of designs of locking mechanisms of the second type, when the output shafts are connected (a) inside and (b) outside the differential.

An example of an earlier design of a pin-type differential locking clutch is shown in Figure 2.107.

Depressing pedal 1, the driver, by means of pull rod and level 2 with a helical spring, engages clutch 3 that locks the left side gear and housing 4, thus preventing pinions 5 from rotating relative to the spider. When pedal 1 is released the differential becomes unlocked by virtue of the potential energy of stretched spring 6 and the lever's helical spring 2.

Cam-type clutches are divided, on the basis of the shape of the cam as triangular, trapezoidal and rectangular. Triangular cams are not used in locking clutches of differentials because they cannot transmit high torques. Figure 2.108 shows rectangular and symmetrical trapezoidal cams with equal profile angles $\beta_p = \beta_0$.

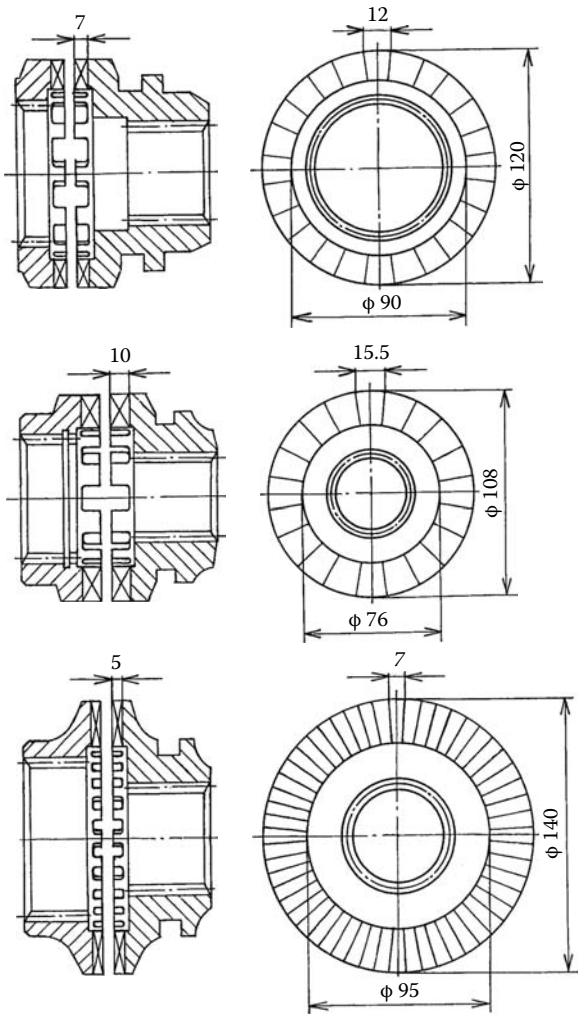


FIGURE 2.105
Jaw-type (cam-type) locking clutches.

The symmetrical profile is convenient for transmitting torque in both directions of clutch rotation. Symmetrically profiled trapezoidal cams are used in locking clutches of differentials. Rectangular cams are used less frequently because of difficulties in engaging such clutches, both when stopping and while driving and because it is impossible to obtain a clearance-less coupling of the cams. The inevitable lateral gap in rectangular cams that stems from manufacturing processes subjects the cams to impact loads when the direction of motion changes. In the case of trapezoidal cams, the lateral clearance is taken up as the cams move in axial direction.

It is convenient to have in both half-couplings trapezoidal cams of the same shape and height, which is indeed done in the differential-locking clutches. The number of cams is usually selected from 5 to 11. The slope of the lateral surface of the cams is selected to prevent self-disengagement of the half-coupling that is determined by the friction coefficient and by the normal force that acts on the lateral surface of the cam. In the majority of clutches, this angle ranges from 2° to 8°.

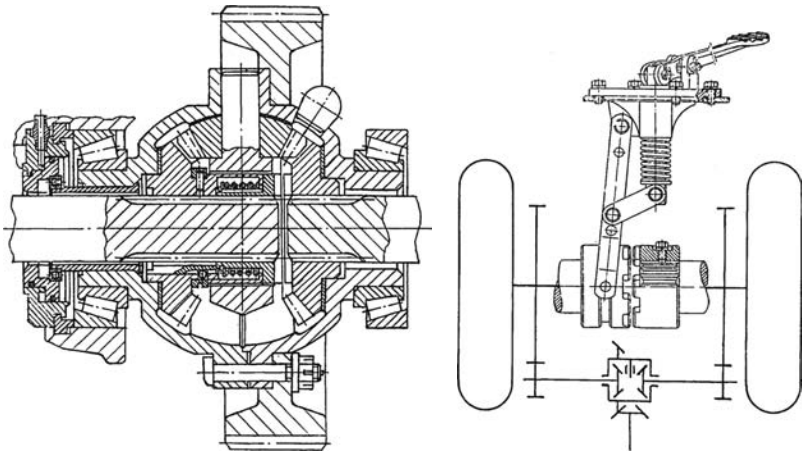


FIGURE 2.106
Locking differentials.

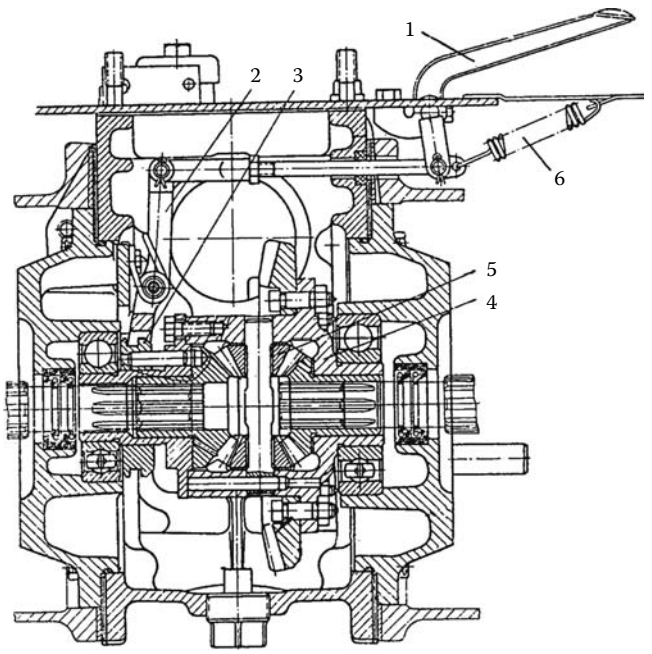


FIGURE 2.107
Locking differential with a pin clutch.

Differential locking clutches should be designed with consideration of capability of engagement and disengagement while the vehicle is in motion. Analytic and experimental studies show that the dangerous (destructive) load upon engagement of a cam-type clutch while the vehicle is in motion can be avoided if the strength and geometric parameters of the cams are properly selected. It is also important to ensure engagement of the clutch by adjusting the slope of the lateral surfaces of the cams and the axial engagement rate. In bearing stress analysis of the hardened steel cams and engagement of the clutch while

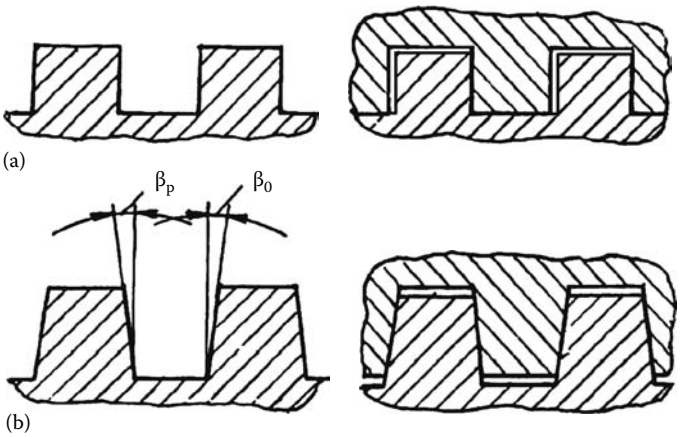


FIGURE 2.108
Rectangular and trapezoidal cams.

driving the bearing strength $[\sigma_{br}]$ is usually assumed to be 500–740 MPa. The actual stresses may be determined approximately from the expression

$$\sigma_{br} = T_{lock}/(r_{av}bhz) \leq [\sigma_{br}] \tag{2.221}$$

where
T_{lock} is the torque transmitted by the clutch, N-m
r_{av} is the average radius of the cams' location, m
b is the length of the cam, m
h is its height, m
z is the number of cams

To determine the rate of engagement of a cam-type clutch, one should know the time of alternation of the engagement positions at relative rotation of clutch-halves of n_{rel}, rpm. It is obtained from the expression

$$t = 60/(n_{rel}z_{eng}), \text{s} \tag{2.222}$$

where z_{eng} is the number of engagement positions, which is defined as the sum of possible engagements of the movable half-clutch during its single rotation. It is usually equal to the number of cams that the half-clutch has, that is, z.

Certain other parameters of the cam-type clutch are introduced and defined to examine the course of engagement of such a clutch. The angle between the engagement positions is known as the engagement angle. It is designated by the letter α and is obtained from the expression

$$\alpha = 360^\circ/z \tag{2.223}$$

Angle α for the case of clearance-less engagement is composed of the following angles (see Figure 2.109a): α_p, the central angle of the lateral work surface; α_o, the central angle of the opposite lateral surface; and α_b, the total central angle of the cam tips.

In clutches with equilateral trapeze profiled cams, $\alpha_p = \alpha_o$. Subsequently both designations of these central angles are used in order to retain the universal form of the following below expressions.

Consider now the course of engagement of a cam-type clutch. There are three cases, i.e., three modes, of engagement of a cam-type clutch while the vehicle is in motion: the

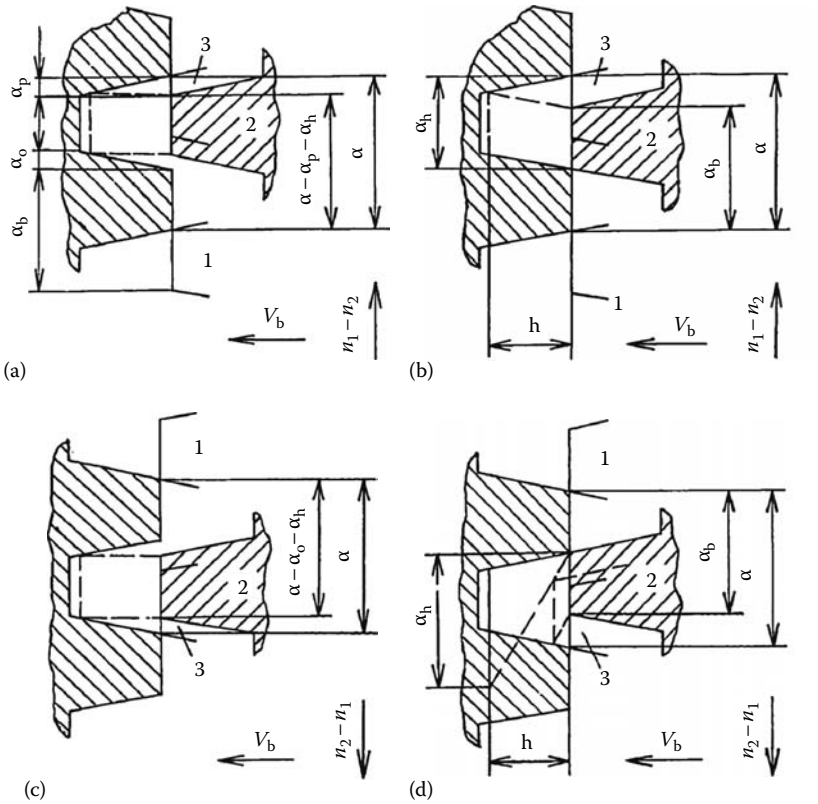


FIGURE 2.109
Layouts of clutches while the vehicle is in motion: (a), (b)—movable half-coupling is overrunning; (c), (d)—movable half-coupling is lagging.

case of synchronous rotation of the clutch halves ($n_1 = n_2$), the case when the driven half-clutch is lagging ($n_1 > n_2$) and the case when the driven half-clutch is overrunning ($n_1 < n_2$).

When the clutch halves rotate synchronously, the tips of the cams of one of the clutch halves may find themselves on the tips of the cam of the other half-clutch. The probability of this is $(100\alpha_b/\alpha)\%$. It is not difficult to guess that in this case the clutch will not become engaged. However, in the case of synchronous rotation of the clutch halves the opposite or working sides of the cams may come into contact. The probability of this case is $(100\alpha_o/\alpha)\%$ or $(100\alpha_p/\alpha)\%$. Here relative adjustment (after-engagement) of the clutch that is brought about by the engagement effort cannot be avoided. Fortunately, there is basically no reason for locking a differential by a clutch when its principal parts rotate synchronously and, if this happens, it is highly infrequent (the case of simultaneous spinning of the wheels connected by the differential, which is usually followed by separate slipping of the wheels).

A dangerous situation arises when the working sides of the cams are not engaged over their entire height. Here the probability is $(100\alpha_p/\alpha)\%$. The danger of this case consists of the fact that this may damage the cams. In addition, lack of agreement between the heights of the cams requires additional losses in the form of an additional force for after-engagement of the clutch. Such an engagement of the cam-type clutch may occur also in other operating modes.

When the driven half clutch lags, i.e., at $n_1 > n_2$, and $n_2 = 0$ in the case of complete tire slipping and stoppage of the vehicle, one can have (see Figure 2.109a)

$$n_1 - n_2 = n_{\text{rel}} < (1000\alpha_{\text{o}} V_{\text{b}})/(6h) \tag{2.224}$$

where

α_{o} is in degrees
V_{b} the speed of axial motion (engagement) of the moving half-clutch, m/s
h is in mm

This case is the most favorable for engaging the clutch. Then the cams most frequently are inserted over their total height h. The probability of this is the following: $100(\alpha - \alpha_{\text{p}} - \alpha_h)/\alpha$, %, where $\alpha_h = 6n_{\text{rel}}h/(1000V_{\text{b}})$. However, when the cams are not inserted over their entire height (see Figure 2.109b), one can have

$$n_{\text{rel}} > (1000\alpha_{\text{o}} V_{\text{b}})/(6h) \tag{2.225}$$

After-engagement of the half-clutch always requires additional effort. Hence, clutch parameters should be selected in a manner that would conform to the inequality 2.224 and there would be a sufficiently high probability that the cams are engaged over their entire height.

The case shown in Figure 2.109c is similar to the situation in Figure 2.109b. The difference consists in the fact that the overrunning shown in Figure 2.109c is carried out by half-clutch 2, i.e., $n_2 > n_1$.

In the case when the driven half clutch is overrunning ($n_1 < n_2$) (see Figure 2.109d), it is found that

$$n_2 - n_1 = n_{\text{rel}} \quad \text{and} \quad n_{\text{rel}} > (1000\alpha_{\text{p}} V_{\text{b}})/(6h) \tag{2.226}$$

This case is interesting because then the cams of the driving half-clutch always enter the cam space of the driven half-clutch freely, but not to the total height h. Then the clutch engaged under easier conditions than in the case of lagging, this means that at $n_1 > n_2$. In this case, free entry of the cams into the cam space of the overrunning half-clutch is less dangerous. After-engagement of the overrunning half-clutch in the direction opposite to that of rotation (slowing down) occurs easier.

When their parameters are properly selected, cam-type clutches may become engaged at relatively higher speeds. In one of the designs for an off-road heavy-duty vehicle engagement could be achieved at speeds of up to 30 rad/s.

The engagement and disengagement force can be calculated from the expression

$$F_{\text{b}} = T_{\text{lock}}[2\tan\varphi/d \pm \tan(\beta \pm \rho) r_{\text{av}}] \tag{2.227}$$

In this expression the plus signs apply to the engagement force, the minus signs to the disengagement force; T_{lock} is the torque transmitted by the clutch halves when they are engaged and disengaged under load; β is the angle of the working (β_{p}) or opposite (β_{o}) side of the cam profile, ρ is the friction angle ranging between 8° and 12° and d is the diameter of the half-clutch shaft.

Cases are frequent when designers of clutches with trapezoidally profiled cams follow the principle of design with rectangular cams. In the beginning the designer is simply unaware that such an analogy is entire impermissible. In the end, one becomes aware of the error, but

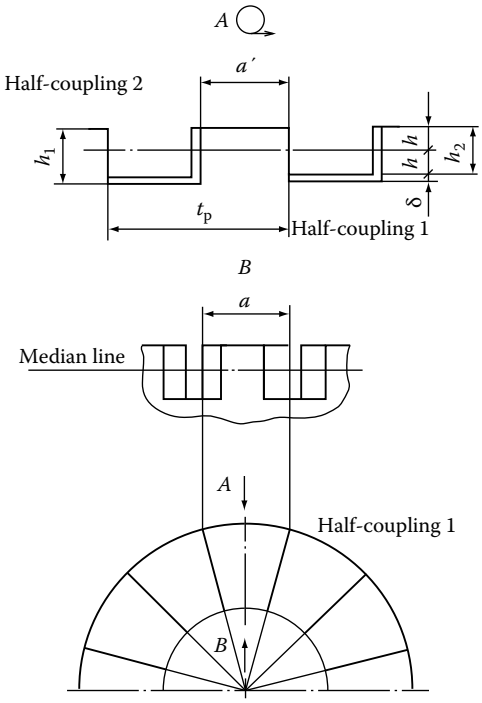


FIGURE 2.110
Geometry of rectangular cams.

the time has been wasted. The point here is that rectangularly profiled cams are designed by drawing rays from their common axial center in the main end view (see Figure 2.110).

This approach in this case is correct and does not cause any complications. The lateral surfaces of rectangular cams are found to be, as assumed, flat. Flat lateral surfaces of one half-clutch coincide with flat lateral surfaces of the other half-clutch that is indeed needed for the safe operation of the clutch and transmission of the torque.

The situation when trapezoidally shaped cams are designed in the same manner as rectangularly profiled cams is entirely different (see Figure 2.111).

In this case, the lateral surfaces of the trapezoidal cams are imparted, according to the law of descriptive geometry a skewed shape. They appear as nonequilateral trapezes on the main (end) view in direction *B* (Figure 2.111). And this at the time when ordinary (normal) planes in the case of identical height of cams over their entire length should be viewed as equilateral rectangles (see *B* in Figure 2.112).

The lateral skewed surfaces of two adjoining cams of different half-clutches cannot, in principle, contact over the entire surface, since their outer edges move apart when approaching the center from the periphery. This means that in the best case they may contact along a line and in the worst case, along individual points. However, this entirely impermissible, a clutch with such cams cannot operate.

The above means that in order to design operating clutches with trapezoidally shaped cams one must use some design method that *a priori* ensures insertion of the sloping surfaces of its cams in the form of normal planes. Such a method is shown graphically in Figure 2.112. Its description follows below.

Having specified, from strength considerations, the number z of cams, the outer circumference of the clutch on the main view is divided by $2z$. This yields central lines (see dash-dotted lines on the main view in Figure 2.112) that lie on a median plane that divides

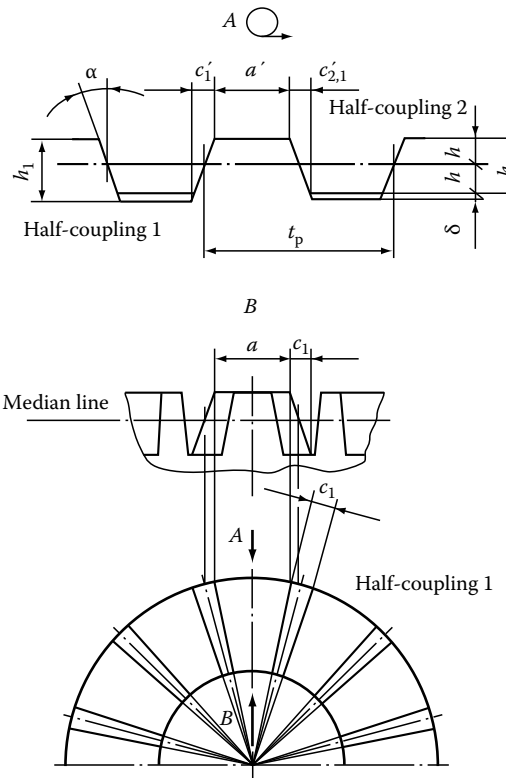


FIGURE 2.111
Incorrect geometry of trapezoidal cams.

the height of cams in halves. Then the view is developed onto the cams in direction *A*. The development is constructed relative to the median line (median plane) that is divided by the developed pitch t_p in such a manner as to obtain at least a single cam in each of the halves of the clutch under design. In order that the contact between the working surfaces of each clutch halves be full-fledged, the cams on one of the clutch halves are made higher ($h_1 > h_2$). The clearance δ thus obtained, together with the negative allowances for the cam widths ensure normal contact between the flat surfaces of the cams of booth clutch halves. After the development has been completely constructed, one returns to the main view. Now it serves for constructing a view on the working surfaces of cams of each of the clutch halves relative to the median lines. For this, depending on which of the half clutches (half clutch 1 or half clutch 2) over the height of the cam projections c_1 and $c_{2,1}$ of the sloping lines of the cam profile, obtained from developed projections c_1' and $c_{2,1}'$ are shown. Here, limiting the length of the cam by the inner diameter (closer to the center of the clutch), yields the working surfaces of the cams in the form of parallelograms provided that their short arcs are represented by their chords. It is possible to avoid constructing the view in the *B* direction if one is sure that the task was performed properly. View *B* is a control view. It is given in Figure 2.112 in order to show the cam from the point of view located in the center of the clutch. It is precisely in this view that the working surfaces of correctly designed cams look like parallelograms and conversely, when the cams were not properly designed, as nonequilateral trapezes (see view *B* in Figure 2.111).

Unlike cam-type locking clutches, spline clutches are designed as ordinary two- and three-link carriages of the vehicle's gearbox. Splined locking clutches are somewhat smaller than cam clutches.

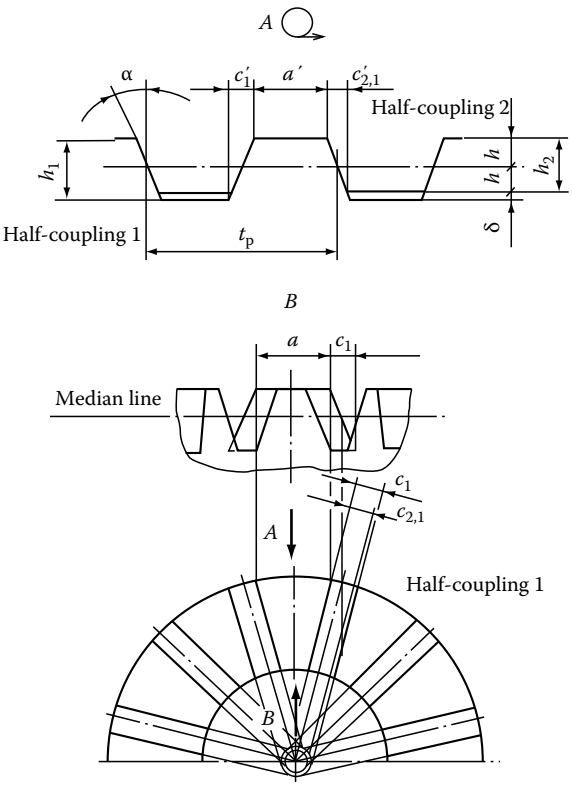


FIGURE 2.112
Correct geometry of trapezoidal cams.

Friction clutches for locking of differentials consist of multidisk hydraulic (oil) clutches. These clutches consist of stacks of disks comprised of several frictional pairs. Each frictional pair is made up of one small and one large disk. The small disks are usually connected to the hubs of side gears, most frequently by means of internal splines and the larger ones—by means of outside splines—to the housing of the differential. The teeth on the disks and the slots on the hubs and in the halves of the differential's housing can be made not involute, but rectangular. Such teeth and slots are not known to provide any design advantages. It is usually arranged in designing the disk stacks that when not under load the clearance between their disks would be 0.2–0.5 mm. The more frictional pairs in the stack, the smaller the clearance that should be specified between the disks in the free state. Depending on the material, the thickness of the disks ranges from 1.5–2 mm. Disks are made of steel, bronze, powder (composite) material and other currently available friction materials. Frictional pairs are arranged as steel–steel, steel–bronze, steel–composite material. Disks that are subject to chemical and thermal treatment (phosphating, copper coating, etc.) in order to increase their wear resistance and satisfactory mating; they should not be subject to warping. The nonflatness of their working surfaces should be reduced to the attainable minimum. The working surfaces of the disks must have oil grooves (radial, circular, and helical) to provide lubrication and to remove heat and friction products that form on them.

The drives of locking friction clutches are usually of the hydraulic or pneumatic type. One of the main problems in designing these clutches is ensuring low power losses in the drive and the required time interval for engaging/disengaging the clutch. Figure 2.113 presents a differential that is locked by a cam clutch 1.

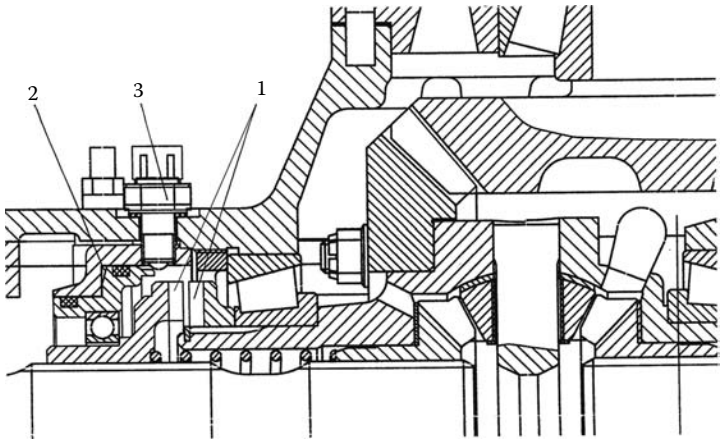


FIGURE 2.113
Differential with a hydraulic locking cam clutch.

The drive of the clutch is consists of a hydraulic system (cylinder 2 is shown in Figure 2.113) and electronic control system (sensor 3 of the system shows the state of the cam clutch—engaged or disengaged).

2.8 Wheel Power Distribution and Vehicle Performance

2.8.1 Generalized Vehicle Parameters and Energy/Fuel Efficiency

Wheel torques of vehicles with open-differential driveline systems are rather easily determined in accordance with the gear ratios of the differentials. However, the angular velocities and slippage of the wheels may take most different values. The latter complicate the calculation of the real velocity of the vehicle and its efficiency.

A method of design was developed in the literature that is suitable for multidrive vehicles that have identical wheels on all the axles and identical gear ratios in their drives. This applies to both symmetrical and asymmetrical differential drives, when a part of the driving axle is subjected to one torque value and the others to another. At the same time, multidrive transport and traction vehicles with different wheels on individual axles and different gear ratios in the drive are constantly under design. Such vehicles include many farm tractors and also certain multidrive vehicles, particularly heavy-duty trucks. For this reason, this section describes a method for calculating the torques of wheels, their slippage and wheel power with subsequent analysis of their energy efficiency. The method is based on generalized vehicle parameters.

To explain the substance of generalized parameters, first consider a driving axle with an open differential (Figure 2.114).

These results shall be applied to a 4×4 vehicle and then extended to a vehicle with n driving axles. Let the left and right wheels of the driving axle have different rolling radii in the driven mode $r_w^{0''} \neq r_w^{0'}$. This may occur because of different normal loads on the wheels, unequal pressures of air in the tires, different wear of the axle's tires and the existence of allowance in tire manufacture. When the wheels move in the driven mode (the wheel

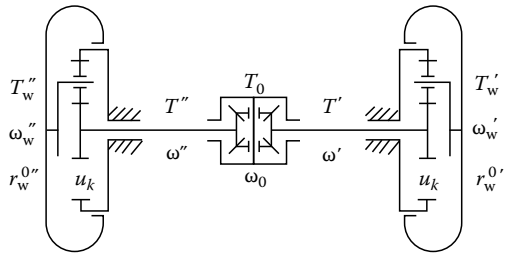


FIGURE 2.114
Driving axle with open differential.

torques are zero) the wheels will roll at different velocities ω_w' and ω_w'' while providing for equal linear velocities of both wheels V_t:

$$V_t = \omega_w'' r_w^{0''} = \omega_w' r_w^{0'} \tag{2.228}$$

In the case when the driving axle has a wheel-hub gear drive with gear ratio u_k, the theoretical velocity can be written as

$$V_t = \frac{\omega''}{u_k} r_w^{0''} = \frac{\omega'}{u_k} r_w^{0'} \tag{2.229}$$

where ω_w' and ω_w'' are the angular velocities of the output shafts of the differential.

The same velocity V_t can be written as

$$V_t = \omega_0 r_a^0 \tag{2.330}$$

where $\omega_0 = \dfrac{\omega'' + \omega'}{2}$ is the angular velocity of the axle's differential, whereas r_a^0 is the generalized rolling radius of the driving axles in the driven mode reduced to the differential's housing. The radius r_a^0 can be imagined as the rolling radius in the driven mode of a certain hypothetical wheel that rotates at angular velocity ω_0 and has the same linear velocity as axle, i.e., V_t.

The definition of r_a^0 is obtained from Figure 2.114 and force balance (1.35) of the wheel listed in Section 1.3.3 (for the sake of simplicity, the mechanical efficiency of the axle is not included):

$$\frac{T_w''}{r_w^{0''}} = \frac{T'' u_k}{r_w^{0''}} = F_x''; \quad \frac{T_w'}{r_w^{0'}} = \frac{T' u_k}{r_w^{0'}} = F_x' \tag{2.331}$$

where $T_{w''} = T_{w'}$ are the wheel torques and $T'' = T' = 0.5T_0$ are the torques at the output shafts of the axle's differential. The total circumferential force of the axle is

$$F_{x\Sigma} = F_x'' + F_x' = T_0 \frac{u_k \left(r_w^{0''} + r_w^{0'}\right)}{2 r_w^{0''} r_w^{0'}} \tag{2.332}$$

At the same time force $F_{x\Sigma}$ can be written as

$$F_{x\Sigma} = \frac{T_0}{r_a^0} \tag{2.333}$$

Equating (2.332) to (2.333), one can find the generalized rolling radius of the driving axle in the driven mode reduced to the housing of the interwheel differential:

$$r_{\mathrm{a}}^{0} = \frac{2r_{\mathrm{w}}^{0''}r_{\mathrm{w}}^{0'}}{\left(r_{\mathrm{w}}^{0''} + r_{\mathrm{w}}^{0'}\right)u_k} \tag{2.334}$$

For axles without wheel-hub gear drive r_{a}^{0} is determined from formula (2.334) at $u_k = 1$.

The slips of the left and right wheel of an axle in the driving mode may not be equal: $s_{\delta}'' \neq s_{\delta}'$. For this reason the actual linear velocity of the axle is better expressed in terms of the generalized axle slip factor $s_{\delta\mathrm{a}}$:

$$V_x = V_t(1 - s_{\delta\mathrm{a}}) = \omega_0 r_{\mathrm{a}}^{0}(1 - s_{\delta\mathrm{a}}) \tag{2.335}$$

To define $s_{\delta\mathrm{a}}$, the velocity V_x is written as

$$V_x = \omega_{\mathrm{w}}'' r_{\mathrm{w}}^{0''}\left(1 - s_{\delta}''\right) = \omega_{\mathrm{w}}' r_{\mathrm{w}}^{0'}\left(1 - s_{\delta}'\right) \tag{2.336}$$

or,

$$V_x = \frac{\omega''}{u_k} r_{\mathrm{w}}^{0''}\left(1 - s_{\delta}''\right) = \frac{\omega'}{u_k} r_{\mathrm{w}}^{0'}\left(1 - s_{\delta}'\right) \tag{2.337}$$

whence

$$\frac{\omega'}{\omega''} = \frac{r_{\mathrm{w}}^{0''}}{r_{\mathrm{w}}^{0'}} \frac{\left(1 - s_{\delta}''\right)}{\left(1 - s_{\delta}''\right)} \tag{2.338}$$

At the same time, angular velocities ω' and ω'' are related by expression (2.10) to angular velocity ω_0 of the differential's housing (see Section 2.1). Then, the angular velocity ω'' follows from (2.10) and (2.338) as

$$\omega'' = 2\omega_0 \frac{r_{\mathrm{w}}^{0'}\left(1 - s_{\delta}'\right)}{r_{\mathrm{w}}^{0'}\left(1 - s_{\delta}'\right) + r_{\mathrm{w}}^{0''}\left(1 - s_{\delta}''\right)} \tag{2.339}$$

Using expressions (2.335), (2.337), and (2.339), it is possible to derive a formula for calculating the generalized slippage of the axle that determines the actual velocity V_x of the axle in formula (2.335):

$$s_{\delta\mathrm{a}} = 1 - \frac{\left(r_{\mathrm{w}}^{0''} + r_{\mathrm{w}}^{0'}\right)\left(1 - s_{\delta}'\right)\left(1 - s_{\delta}''\right)}{r_{\mathrm{w}}^{0'}\left(1 - s_{\delta}'\right) + r_{\mathrm{w}}^{0''}\left(1 - s_{\delta}''\right)} \tag{2.340}$$

When the radii are equal $\left(r_{\mathrm{w}}^{0''} = r_{\mathrm{w}}^{0'} = r_{\mathrm{w}}^{0}\right)$ formula (2.340) becomes

$$s_{\delta\mathrm{a}} = 1 - \frac{2\left(1 - s_{\delta}'\right)\left(1 - s_{\delta}''\right)}{2 - s_{\delta}' - s_{\delta}''} \tag{2.341}$$

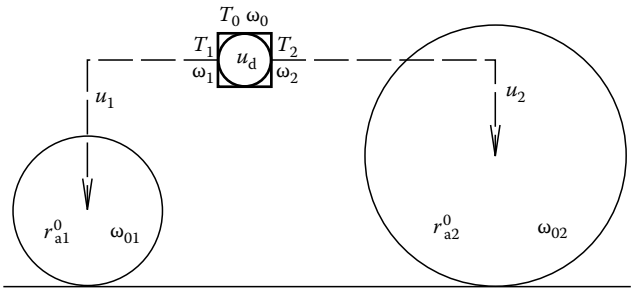


FIGURE 2.115
4×4 vehicle with asymmetrical interaxle differential.

If also the slips of both wheels are the same ($s'_\delta = s''_\delta = s_\delta$), then

$$s_{\delta a} = s'_\delta = s''_\delta = s_\delta \tag{2.342}$$

The generalized axle parameters consisting of axle radius r^0_a from formula (2.334) and slip $s_{\delta a}$ from formula (2.340) thus make it possible to calculate the actual axle velocity v_x from formula (2.335).

Consider now a 4×4 vehicle with asymmetrical interaxle differential with gear ratio u_d (Figure 2.115) and nonequal front and rear axle wheels that have generalized rolling radii r^0_{a1} and r^0_{a2}.

The gear ratios from the interaxle differential to the wheels of the front and rear axles are respectively u_1 and u_2. In the case when the driving axles have wheel-hub gear drives, u_1 and u_2 are determined by the gear ratios from the interaxle differential to the housings of the differentials of the front and rear axles.

The actual velocity of the vehicle can be written as

$$V_x = V_a(1 - s_{\delta a}) = \omega_0 r^0_a(1 - s_{\delta a}) \tag{2.343}$$

where V_a is the theoretical velocity of the vehicle, r^0_a is the generalized rolling radius of the vehicle in the driven mode reduced to the housing of the interaxle differential and $s_{\delta a}$ is the generalized slip of the vehicle.

To determine the vehicle's radius r^0_a,

$$\frac{T_1 u_1}{r^0_{a1}} = F_{x1} \quad \text{and} \quad \frac{T_2 u_2}{r^0_{a2}} = F_{x2} \tag{2.344}$$

Using formulae (2.28)

$$T_1 = T_0/(1 + u_d), \quad T_2 = T_0 u_d/(1 + u_d) \tag{2.345}$$

formulae (2.344) are transformed to

$$\begin{aligned} \frac{u_1}{r^0_{a1}} \frac{1}{1 + u_d} T_0 &= F_{x1} \\ \frac{u_2}{r^0_{a2}} \frac{u_d}{1 + u_d} T_0 &= F_{x2} \end{aligned} \tag{2.346}$$

Summing formulae (2.346) it is found

$$T_0 \frac{u_1 r_{a2}^0 + u_2 u_d r_{a1}^0}{r_{a1}^0 r_{a2}^0 (1 + u_d)} = F_{x\Sigma} \tag{2.347}$$

where $F_{x\Sigma} = F_{x1} + F_{x2}$.

At the same time, one may write

$$T_0 / r_a^0 = F_{x\Sigma} \tag{2.348}$$

Equating formulae (2.347) and (2.348) it is possible to find the generalized rolling radius of the vehicle in the driven mode reduced to the housing of the interaxle differential

$$r_a^0 = \frac{r_{a1}^0 r_{a2}^0 (1 + u_d)}{r_{a2}^0 u_1 + r_{a1}^0 u_2 u_d} \tag{2.349}$$

Radius r_a^0 is the rolling radius in the driven mode of a conditional (hypothetical) wheel that rotates at angular velocity ω_0 and has linear velocity V_a from formula (2.343).

In designing a vehicle with an interaxle differential agreement must be provided between the theoretical velocities ($V_{t1} = V_{t2}$), which is expressed by the equality

$$r_{a1}^0 u_2 = r_{a2}^0 u_1 \tag{2.350}$$

Hence, radius r_a^0 can be determined from the simpler expression

$$r_a^0 = \frac{r_{a1}^0}{u_2} = \frac{r_{a2}^0}{u_2} \tag{2.351}$$

The generalized slippage of the vehicle $s_{\delta a}$ is now found. For this, the actual velocity is written as

$$\begin{aligned} V_x &= \omega_{01} r_{a1}^0 (1 - s_{\delta a1}) = \frac{\omega_1}{u_1} r_{a1}^0 (1 - s_{\delta a1}) \\ V_x &= \frac{\omega_2}{u_2} r_{a2}^0 (1 - s_{\delta a2}) \end{aligned} \tag{2.352}$$

where ω_1 and ω_2 are the angular velocities of the output shafts of the interaxle differential (see Figure 2.115); $s_{\delta a1}$ and $s_{\delta a2}$ are the generalized slippages of the front and rear axles. It is found by equating the right-hand sides of expressions (2.352) and incorporating the condition of agreement of theoretical velocities (2.350) that

$$\frac{\omega_1}{\omega_2} = \frac{1 - s_{\delta a2}}{1 - s_{\delta a1}} \tag{2.353}$$

At the same time, ω_1 and ω_2 are interrelated by formula (2.9). Simultaneous solution of formulae (2.9) and (2.353) yields

$$\omega_2 = \omega_0 \frac{(1 + u_d)(1 - s_{\delta a1})}{1 - s_{\delta a2} + u_d (1 - s_{\delta a1})} \tag{2.354}$$

Using formulae (2.343), (2.352), and (2.354), the expression for the generalized slippage of the vehicle is written as

$$s_{\delta a} = 1 - \frac{(1 + u_d)(1 - s_{\delta a1})(1 - s_{\delta a2})}{1 - s_{\delta a2} + u_d(1 - s_{\delta a1})} \tag{2.355}$$

It follows from formula (2.355) that at different wheel slips the generalized slippage of the vehicle is equal neither to $s_{\delta a1}$ nor to $s_{\delta a2}$. If the axle slips are equal, i.e., $s_{\delta a1} = s_{\delta a2}$ then the generalized slippage of the vehicle is

$$s_{\delta a} = s_{\delta a1} = s_{\delta a2} \tag{2.356}$$

This means that once r_a^0 and $s_{\delta a}$ are calculated from formulae (2.349) and (2.355), it is possible to use expression (2.343) for finding the real velocity V_x of the vehicle.

A method is now examined for determining r_a^0 and $s_{\delta a}$ of a vehicle with n driving axles. All the multidrive vehicles with interaxle differential drives can be divided into two groups: with odd and even number of driving axles. Examples of such vehicles are shown in Table 2.21.

It is assumed that the gear ratios of the differentials are known. The method of their selection is examined in Section 2.9.

For a vehicle with even n the generalized slippage is first determined for each axle pair:

$$s_{\delta aj} = 1 - \frac{(1 + u_{dj})(1 - s_{\delta aj1})(1 - s_{\delta aj2})}{1 - s_{\delta aj2} + u_{dj}(1 - s_{\delta aj1})} \tag{2.357}$$

where j is the ordinal number of the axle pair interconnected by an interaxle differential whereas $s_{\delta aj1}$ and $s_{\delta aj2}$ are the generalized slips of the wheels of the jth pair of axles.

The number of factors $s_{\delta aj}$ depends on the number of the driving axles and may range from 1 to $0.5n$, i.e., $1 \leq j \leq 0.5n$. Thus, the value calculated from formula (2.357) for a vehicle with two driving axles will indeed be the generalized slippage $s_{\delta a}$ of the vehicle. For a vehicle with four axles (Table 2.21, variant *a*) this formula will yield values of $s_{\delta a1}$ and $s_{\delta a2}$, whereas for a vehicle with six axles (variant *a*), the values of $s_{\delta a1}$, $s_{\delta a2}$ and $s_{\delta a3}$.

This is followed by finding the generalized slippage of sets of axles coupled by differentials (or a set of axles and a single axle) and of the vehicle as a whole. The term set of axles shall apply to three or more axles coupled by differentials. With consideration of the slippages of axle pairs calculated from formula (2.357), the generalized slippage of the vth set of axles is

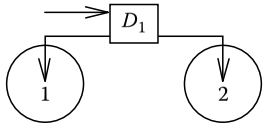
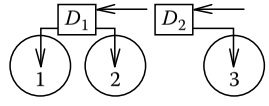
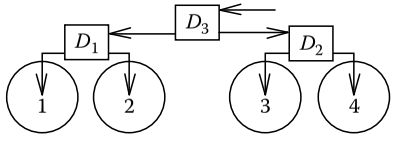
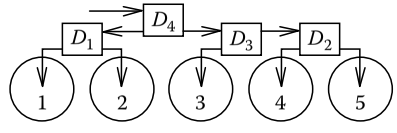
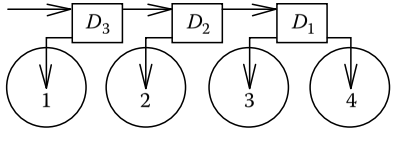
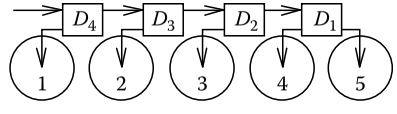
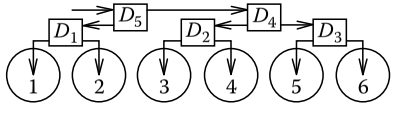
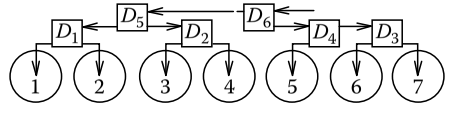
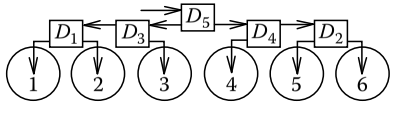
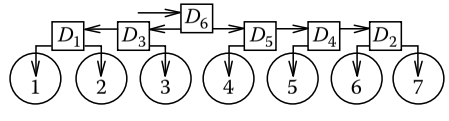
$$s_{\delta av} = 1 - \frac{(1 + u_{dv})(1 - s_{\delta aj})(1 - s_{\delta aj+1})}{1 - s_{\delta aj+1} + u_{dv}(1 - s_{\delta aj})} \tag{2.358}$$

where v is the ordinal number of the differential that couples a set of axles (or a set of axles to a single axle).

Parameter v for vehicles with even number of driving axles may range from $(0.5n - 1)$ to $(n - 2)$. Note that in determining slippage $s_{\delta av}$ of a set of axles and an individual axle, it is required to substitute the values of generalized slippage $s_{\delta aj}$ of the set of axles from formula

TABLE 2.21

Multiwheel Drive Vehicles with Interaxle Differentials

Group I			Group II		
Even Number of Drive Axles	**Variant**	**Driveline System Layout**	**Old Number of Drive Axles**	**Variant**	**Driveline System Layout**
2	*a*		3	*a*	
4	*a*		5	*a*	
	b			*b*	
6	*a*		7	*a*	
	b			*b*	

(2.357) and of an individual axle $s_{\delta i}$. The value of $s_{\delta a v}$ calculated from formula (2.358) at the highest value of v is indeed the generalized slippage of the vehicle $s_{\delta a}$.

In determining the generalized slippage $s_{\delta a}$ for vehicles of the second group (n is an odd number), parameter j in formula (2.357) may range from 1 to $0.5(n-1)$. The value of v in expression (2.358) may range from $0.5(n-1)$ to $(n-2)$.

Similarly, in the case of differentials coupling a set of axles (or a set of axles to a single axle), formula (2.349) can be used for calculating the generalized rolling radius r_a^0 reduced to the housing of the principal interaxle differential through which the entire engine power is transmitted to the wheels.

Calculations using the above relationships can be made only when the axle slippages $s_{\delta i}$ are known; these can be found by determining the wheel torques T_{wi} and the circumferential forces F_{xi}. To find these for both groups of vehicles, pertinent relationships, whose number should be equal to the number of driving axles, must be available. The algorithm for compiling these equations is now examined.

With reference to the gear ratios u_{dj} of the interaxle differentials, situated between each pair of axles, the expressions relating their circumferential forces are now compiled. For vehicles with an even n the number of such expressions may range from 1 to $0.5n$:

$$\frac{T_{j2}}{T_{j1}} = u_{dj}, \quad j = 1, 0.5n \tag{2.359}$$

where T_{j1} and T_{j2} are the torques at the output shafts of the differential located between the axles of the jth pair. Expressing these torques in terms of the circumferential forces of the axles, the following is obtained:

$$\frac{F_{xj2}}{F_{xj1}} = u_{dj}\frac{r^0_{aj1}u_{j2}}{r^0_{aj2}u_{j1}} \tag{2.360}$$

or with consideration of the condition of agreement of theoretical velocities of the axles,

$$\frac{F_{xj2}}{F_{xj1}} = u_{dj}, \quad j = 1, 0.5n \tag{2.361}$$

For vehicles with odd number n of driving axles the number of equations relating the circumferential forces of the sets of axles may comprise from 1 to $0.5(n-1)$:

$$\frac{F_{xj2}}{F_{xj1}} = u_{dj}\frac{r^0_{aj1}u_{j2}}{r^0_{aj2}u_{j1}} \quad \text{or} \quad \frac{F_{xj2}}{F_{xj1}} = u_{dj}, \quad j = 1, 0.5(n-1) \tag{2.362}$$

Now relationships between the circumferential forces of a set of axles (or a set of axles and a single axle), coupled by interaxle differentials are compiled. For vehicles with an even number of axles the number of such expressions may range from $(0.5n-1)$ to $(n-2)$:

$$\frac{\sum_{i=1}^{s} F_{xi}}{\sum_{i=1}^{t} F_{xi}} = u_{dv}, \quad v = (0.5n-1), (n-2) \tag{2.363}$$

where t and s is the number of axles in each of the groups of axles under consideration, coupled by a differential with gear ratio u_{dv}.

Note that the equation relating the circumferential forces of a set of axles and an individual axle coupled by a differential should be compiled by replacing $\sum_{i=1}^{t} F_{xi}$ in formula (2.363) by the value of F_{xi} of the given single axle.

For vehicles with odd n the number of the driving axles, the number of equations relating the circumferential forces of sets of axles may range from $0.5(n-1)$ to $(n-2)$:

$$\frac{\sum_{i=1}^{s} F_{xi}}{\sum_{i=1}^{t} F_{xi}} = u_{dv}, \quad v = 0.5(n-1), (n-2) \tag{2.364}$$

The total number of equations for vehicles of the first group (formulae (2.361) and (2.363)) and of the second group (formulae (2.362) and (2.364)) is equal to $(n-1)$. To obtain the missing equation use should be made of Equation (1.74) for the total circumferential force of the vehicle. Solving formula (1.74) simultaneously with formulae (2.361) and (2.262) or with formulae (2.362) and (2.364) makes possible calculating the circumferential forces of the axles of vehicles of respectively, the first and second groups at any placement of interaxle differentials between the individual axles and sets of axles.

Using the known values of F_{xi} of the axles it is possible to calculate the slip $s_{\delta i}$ using formulae from Section 1.3.2. The values of $s_{\delta i}$ and F_{xi} thus found allow calculating the generalized slippage of the vehicle $s_{\delta a}$ and its actual velocity of motion (formulae (2.335), (2.349), (2.357), and (2.358)) and to then assess the power losses in the running gear of transportation, traction, and transportation-traction vehicles. The next quantity to determine is the efficiency η_δ that assesses the power loss in slippage in the vehicle's wheel system. For a 4×4 vehicle, when using formula (2.361), the general formula (1.73) becomes

$$\eta_\delta = \frac{(1+u_d)(1-s_{\delta a1})(1-s_{\delta a2})}{1-s_{\delta a2}+u_d(1-s_{\delta a1})} \tag{2.365}$$

or, upon substitution of (2.355)

$$\eta_\delta = 1 - s_{\delta a} \tag{2.366}$$

Expression (2.366) is valid also for vehicles with n driving axles; slippage $s_{\delta a}$ and efficiency η_δ in this case are determined on the basis of slippages $s_{\delta i}$ of the axles, slippages $s_{\delta aj}$ of axle pairs and of axle sets $s_{\delta av}$ from formulae (2.357) and (2.358).

It follows from expression (2.366) and from equating it to formula (2.343) that for a differential interaxle drive with n driving axles the slippage $s_{\delta a}$ reflects both the loss of vehicle velocity and loss of power in slipping.

Expressions are now derived for determining the efficiency of the running gear of multiwheel drive vehicles when performing either transportation or traction work. Different versions of transportation-traction vehicles are described in Table 1.19.

Efficiency η_x^t of the running gear of a traction vehicle (Table 1.19, number 1) is determined by writing an expression for the power supplied to the driving wheels:

$$P_{w\Sigma}^{in} = V_a \sum_{i=1}^{n} F_{xi} \tag{2.367}$$

Then using formulae (1.67), (1.76), and (2.366) the expression for η_x^{t} becomes

$$\eta_x^{\mathrm{t}} = \frac{P_{\mathrm{d}}}{P_{\mathrm{w}\Sigma}^{\mathrm{in}}} = \frac{(1 - s_{\delta \mathrm{a}})F_{\mathrm{d}}}{\sum_{i=1}^{n} F_{xi}} = \eta_f \eta_\delta \tag{2.368}$$

The transportation efficiency of the running gear for a transportation vehicle (Table 1.19, number 2) is

$$\eta_x^{\mathrm{tr}} = \frac{(1 - s_{\delta \mathrm{a}}) \sum_{i=1}^{m} R_{xgi}}{\sum_{i=1}^{n} F_{xi}} \tag{2.369}$$

where m is the total number of axles; n is the number of driving axles and R_{xgi} is the rolling resistance of wheels of the ith axle stemming from the payload devolving upon that axle.

Formulae for determining the running gear efficiencies of the other versions of vehicles can be obtained similarly. These formulae are listed in Table 2.22; they can be used for assessing the power expended in the wheel system of various-purpose vehicles depending on the gear ratios of the differentials, dimensions (radii) of the wheels, the traction and weight loads of the vehicle, tire-surface characteristics, etc.

In addition, Table 2.22 lists formulae for determining the energy effectiveness of tractive, transportation, and transportation-tractive vehicles. These formulae were derived with consideration of the transmission efficiency η_{trm} and the efficiencies of each of the branches of the driveline system η_{mi} ($i = 1, n$, n is the number of driving axles). These criteria make it possible to assess the total effect of the differential drive system on the energy effectiveness of the vehicle with allowance for the effect of the driveline system both on the mechanical power losses in the wheel system and on the power losses in the drive as such.

As an illustration, consider the efficiency η_x^{t} of the running gear of a 4-ton farm tractor with differently sized wheels of the front and rear axles with an interaxle differential in its transfer case, moving over a field prepared for sowing. Figure 2.116 shows curves of η_x^{t} as a function of the drawbar load F_{d} at interaxle differential gear ratio of $u_{\mathrm{d}} = 2$; for comparison, the figure shows curves of η_x^{t} for cases of locked axle drive calculated from expressions that will be analyzed in Chapter 3.

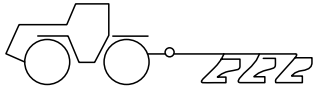
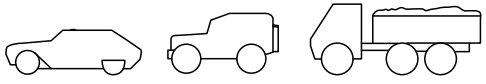
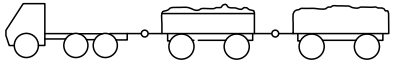
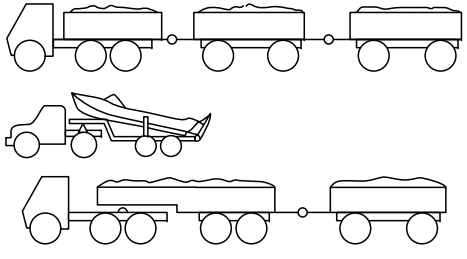
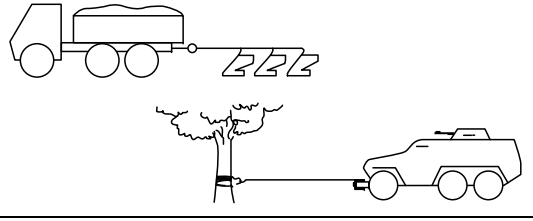
When a interaxle differential is used the values of η_x^{t} (curve 1) are virtually the same as in the case of synchronous locked up drive of the axles (curve 2) at tractive loads less than 10 kN. A locked up synchronous drive provides for equality of theoretical velocities of the front and rear axles, $V_{t1} = V_{t2}$. As F_{d} is increased further, the value of η_x^{t} when using a differential drive decreases because of the increased separate slippage of wheels. At $F_{\mathrm{d}} > 15$ kN the values of η_x^{t} are smaller than for a locked up drive for which $V_{t1} \neq V_{t2}$ (curve 3). In these cases then interaxle differential should be locked and then the values of η_x^{t} of the running gear will be the same as for a synchronous locked drive (curve 2).

The gear ratio of a differential has a marked effect on the energy effectiveness of a vehicle. Figure 2.117 shows curves of η_x^{t} of the same 4-ton tractor as a function of the gear ratio of the interaxle differential and of the drawbar loads F_{d}.

It is seen that at different tractive modes the maximum values of η_x^{t} correspond to different values of the differential's gear ratio that ranges from zero (the front axle is driving) to infinity (only one rear axle is driving). For convenience the quantity $\varepsilon = u_{\mathrm{d}}/(1 + u_{\mathrm{d}})$ that varies uniformly from zero to 1 when u_{d} goes from zero to infinity is plotted on the abscissa. It is clearly seen from Figure 2.117 that improving the energy/fuel effectiveness of the tractor requires a critical approach to selection of the gear ratio of the interaxle differential.

TABLE 2.22

Multiwheel Drive Vehicles with Differential Driveline Systems: Energy Efficiency

No.	Vehicle	Mode	Vehicle Efficiency
1		Tractive	$\eta_x^t = (1 - s_{\delta a})F_d \Big/ \sum_{i=1}^{n} F_{xi}$ $\eta_t = \eta_{trm}(1 - s_{\delta a})F_d \Big/ \left(\sum_{i=1}^{n} F_{xi}/\eta_{mi}\right)$
2		Transportational	$\eta_x^{tr} = \left[(1 - s_{\delta a})\sum_{i=1}^{m} R_{xgi}\right] \Big/ \sum_{i=1}^{n} F_{xi}$ $\eta_{tr} = \left[\eta_{trm}(1 - s_{\delta a})\sum_{i=1}^{m} R_{xgi}\right] \Big/ \left(\sum_{i=1}^{n} F_{xi}/\eta_{mi}\right)$
3		Transportational	$\eta_x^{tr} = \left[(1 - s_{\delta a})\sum_{i=1}^{c}\sum_{i=1}^{l} R_{xgi}\right] \Big/ \sum_{i=1}^{n} F_{xi}$ $\eta_{tr} = \left[\eta_{trm}(1 - s_{\delta a})\sum_{i=1}^{c}\sum_{i=1}^{l} R_{xgi}\right] \Big/ \left(\sum_{i=1}^{n} F_{xi}/\eta_{mi}\right)$
4		Transportational	$\eta_x^{tr} = (1 - s_{\delta a})\left(\sum_{i=1}^{m} R_{xgi} + \sum_{i=1}^{c}\sum_{i=1}^{l} R_{xgi}\right) \Big/ \sum_{i=1}^{n} F_{xi}$ $\eta_{tr} = \eta_{trm}(1 - s_{\delta a})\left(\sum_{i=1}^{m} R_{xgi} + \sum_{i=1}^{c}\sum_{i=1}^{l} R_{xgi}\right) \Big/ \left(\sum_{i=1}^{n} F_{xi}/\eta_{mi}\right)$
5		Combined	$\eta_{x\Sigma} = (1 - s_{\delta a})\left(\sum_{i=1}^{m} R_{xgi} + F_d\right) \Big/ \sum_{i=1}^{n} F_{xi}$ $\eta_{\Sigma} = \eta_{trm}(1 - s_{\delta a})\left(\sum_{i=1}^{m} R_{xgi} + F_d\right) \Big/ \left(\sum_{i=1}^{n} F_{xi}/\eta_{mi}\right)$

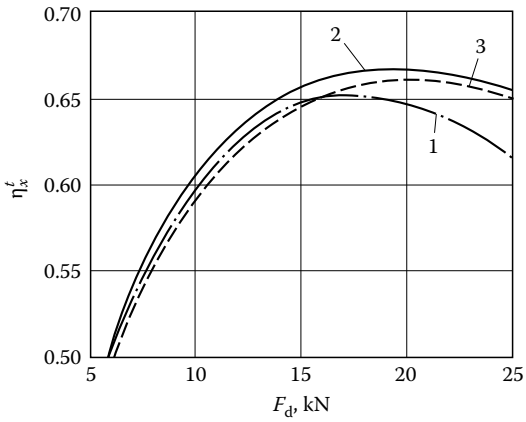


FIGURE 2.116
Running gear efficiency of a 4-ton farm tractor.

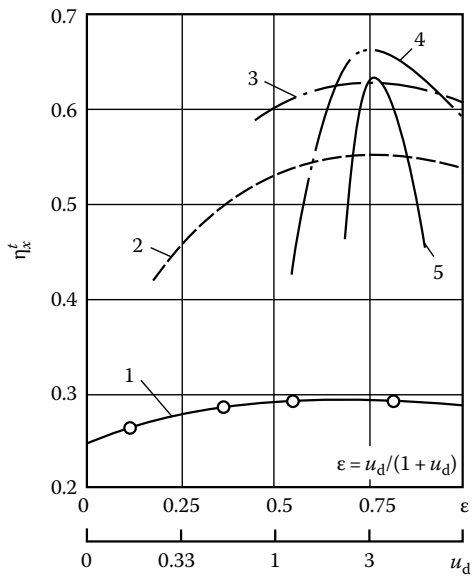


FIGURE 2.117
Running gear efficiency of a 4-ton farm tractor. 1, $F_d = 2.5$ kN; 2, $F_d = 8.5$ kN; 3, $F_d = 12.5$ kN; 4, $F_d = 16.5$ kN; 5, $F_d = 20.5$ kN.

Figure 2.118 shows the slip efficiency factor η_δ vs. factor $\varepsilon = \dfrac{u_d}{1+u_d}$ calculated for an 18-ton 4×4 truck with uniformly distributed gross weight between the axles.

Curve 1 corresponds to motion over an asphalt road, whereas curve 2, over packed soil. It is seen from this figure that the efficiency η_δ is at maximum when the torques are uniformly distributed between the axles ($u_d = 1$, $\varepsilon = 0.5$). The value of η_δ is smallest at $u_d = 0$ and $u_d = \infty$, i.e., when only one axle, the front or the rear, is the driving axle. In the case of two driving axles, but with nonuniformly distributed torques, η_δ takes intermediate values. The reduction in η_δ upon switching from two driving axles to one axle is particularly perceptible on deformable surfaces (curve 2, Figure 2.118).

Another illustration, Figure 2.119 shows the transportation efficiency η_x^{tr} of the running gear of 4×4 timber-carrier truck, whose maximum value corresponds to a gear ratio u_d close to 2.

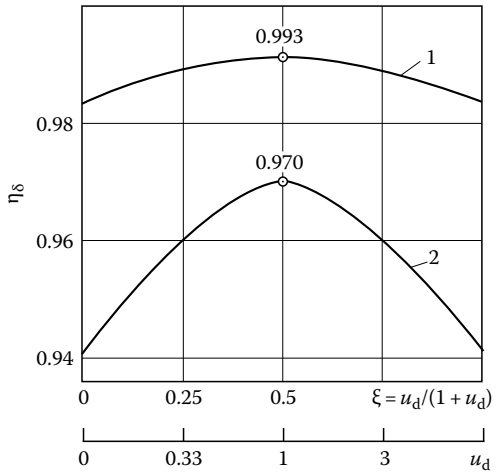


FIGURE 2.118
Slip efficiency of a 4 × 4 truck, full mass of 18 ton.

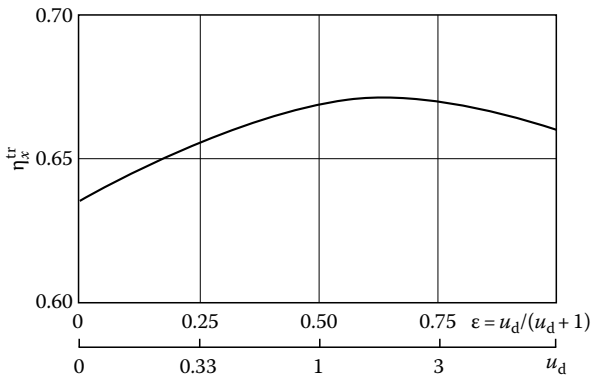


FIGURE 2.119
Transportation efficiency η_x^{tr} of the running gear of 4 × 4 timber-carrier truck.

The energy effectiveness of a vehicle with a differential drive moving along a curved path can be assessed employing formulae listed in Table 2.22. For this, the values of the generalized slippage $s_{\delta a}$ must be known. Examine now the manner of determining it, starting with a single driving axle taking a turn.

The angular velocity of the turn of the driving axle can be represented in terms of the linear velocities of the wheels and of the center of the axle. This is done using Figure 2.3:

$$\omega_a = \frac{\omega'_w r_w^{0'}(1 - s'_\delta)}{R'_t} = \frac{\omega''_w r_w^{0''}(1 - s''_\delta)}{R''_t} = \frac{\omega_0 r_a^0(1 - s_{\delta a})}{R_t} \tag{2.370}$$

where ω_a is the angular velocity of the vehicle about the vertical axis; R'_t and R''_t are the turning radii of the outer and inner wheels, whereas ω'_w and ω''_w are the angular velocities of the wheels; ω_0 is the angular velocity of the differential's housing. Formula (2.10) of the kinematics of an open differential together with formulae (2.370) yield an expression for the generalized slippage of the axle

$$s_{\delta a} = 1 - \frac{R_t\left(r_w^{0''} + r_w^{0'}\right)\left(1 - s''_\delta\right)\left(1 - s'_\delta\right)}{R''_t r_w^{0'}\left(1 - s'_\delta\right) + R'_t r_w^{0''}\left(1 - s''_\delta\right)} \tag{2.371}$$

Neglecting the difference in radii $r_w^{0'}$ and $r_w^{0''}$ of the left and right wheels, allows simplifying formula (2.371) to

$$s_{\delta a} = 1 - \frac{2R_t(1 - s''_\delta)(1 - s'_\delta)}{R''_t(1 - s'_\delta) + R'_t(1 - s''_\delta)} \tag{2.372}$$

When turning radii R_t, R''_t and R'_t tend to infinity (rectilinear motion), resolving the indefiniteness causes formula (2.372) to take the form of formula (2.341) that was obtained for rectilinear motion.

The next item to determine is the generalized slippage $s_{\delta a}$ of a tandem of two axles coupled by an open interaxle differential with gear ratio u_d. The wheels of the two axles have different dimensions and are steered (general case). The bicycle model of such a tandem is shown in Figure 2.120.

The actual axle velocities V_{x1} and V_{x2} have the same projections on the longitudinal axis, and are equal to the velocity represented by the generalized parameters

$$V_{x1}\cos\delta_1 = V_{x2}\cos\delta_2 = \omega_0 r_a^0(1 - s_{\delta a}) \tag{2.373}$$

or

$$\omega_{01} r_{a1}^0(1 - s_{\delta a1})\cos\delta_1 = \omega_{02} r_{a2}^0(1 - s_{\delta a2})\cos\delta_2 = \omega_0 r_a^0(1 - s_{\delta a})$$

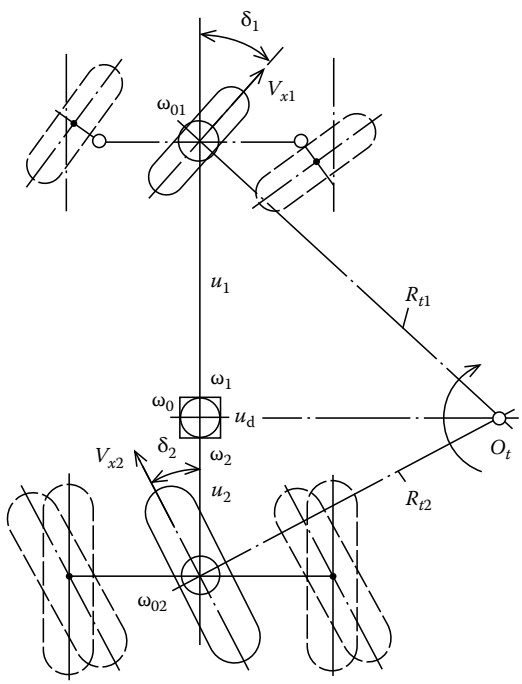


FIGURE 2.120
Two axles in turn.

where V_{x1} is determined from the first of formulae (2.352), whereas V_{x2} is obtained from the second of these formulae; ω_0 is the velocity of the interaxle differential; radius r_a^0 is calculated from formula (2.349). Substitution of formula (2.352) into (2.373), yields

$$\frac{\omega_{01} r_{a1}^0}{\omega_{02} r_{a2}^0} = \frac{\omega_1 r_{a1}^0 u_2}{u_1 \omega_2 r_{a2}^0} = \frac{(1 - s_{\delta a1}) \cos \delta_2}{(1 - s_{\delta a2}) \cos \delta_1} \tag{2.374}$$

In formula (2.374) the angular velocities ω_1 and ω_2 of the output shafts of the differential are related by formula (2.9) to the angular velocity of the housing of this differential which, using gear ratios u_1 and u_2 can be expressed as

$$\omega_0 = \frac{\omega_1 + \omega_2 u_d}{1 + u_d} = \frac{\omega_{01} u_1 + \omega_{02} u_2 u_d}{1 + u_d} \tag{2.375}$$

where ω_{01} and ω_{02} are the angular velocities of the housings of the differentials of the front and rear axles of the tandem from Figure 2.120.

Now ω_{01} is expressed using formula (2.374)

$$\omega_{01} = \frac{\omega_{02} r_{a2}^0}{r_{a1}^0} \frac{(1 - s_{\delta a1})}{(1 - s_{\delta a2})} \frac{\cos \delta_2}{\cos \delta_1} \tag{2.376}$$

and substituting formula (2.376) into (2.375), it is found that

$$\omega_{02} = \omega_0 (1 + u_d) \left[\frac{r_{a2}^0 u_1}{r_{a1}^0} \frac{(1 - s_{\delta 2})}{(1 - s_{\delta 1})} \frac{\cos \delta_2}{\cos \delta_1} + u_2 u_d \right]^{-1} \tag{2.377}$$

Upon substituting ω_{02} from formula (2.377) and r_a^0 from formula (2.349), into the second of formulae (2.373) and dividing by ω_0, the generalized slippage of the tandem is obtained by the expression

$$s_{\delta a} = 1 - \frac{(1 - s_{\delta a2})(r_{a2}^0 u_1 + r_{a1}^0 u_2 u_d)}{r_{a1}^0} \left[u_2 u_d + \frac{r_{a2}^0 u_1}{r_{a1}^0} \frac{(1 - s_{\delta a2})}{(1 - s_{\delta a1})} \frac{\cos \delta_2}{\cos \delta_1} \right]^{-1} \tag{2.378}$$

Formula (2.378) can be used for calculating the generalized slippage of a tandem taking a turn in the general case of $r_{a1}^0 \neq r_{a2}^0$ (different dimensions of the axles' tires or different normal loads and different tire air pressures), $u_1 \neq u_2$ and $u_d \neq 1$. The values of $s_{\delta a}$ thus calculated can be used for assessing the energy effectiveness of a tandem taking a turn using formulae from Table 2.22.

Consider now certain particular cases of the use of expression (2.378). In the case of identical radii ($r_{a1}^0 = r_{a2}^0$) and gear ratios ($u_1 = u_2$) formula (2.378) becomes

$$s_{\delta a} = 1 - \frac{(1 + u_d)(1 - s_{\delta a1})(1 - s_{\delta a2}) \cos \delta_1}{u_d (1 - s_{\delta a1}) \cos \delta_1 + (1 - s_{\delta a2}) \cos \delta_2} \tag{2.379}$$

When $\delta_2 = 0$ (a 4×4 vehicle with front-steered wheels)

$$s_{\delta a} = 1 - \frac{(1 + u_d)(1 - s_{\delta a1})(1 - s_{\delta a2}) \cos \delta_1}{u_d(1 - s_{\delta a1}) \cos \delta_1 + (1 - s_{\delta a2})} \tag{2.380}$$

For rectilinear motion ($\delta_1 = \delta_2 = 0$) formulae (2.379) and (2.380) take the form of formula (2.355). If the interaxle differential is symmetrical ($u_d = 1$), then formulae (2.379) and (2.380) become structurally identical to formula (2.341) in the case of rectilinear motion when $\delta_1 = \delta_2 = 0$.

It was thus shown that formulae (2.371) and (2.372) obtained above for determining the generalized slippage of an axle and formulae (2.378), (2.379), and (2.380) obtained for calculating the generalized slippage of a tandem of two driving axles make it possible to construct mathematical relationships for determining the generalized slippage of a vehicle with any number of driving axles (see Table 2.21), coupled by symmetrical and asymmetrical differentials. Note that any of these axles may be steered or nonsteered.

2.8.2 Vehicle Tractive and Velocity Properties

Consider a driving axle with an open differential. The maximum possible torque at one wheel, T_w^{max}, is determined by the maximum force of gripping between the wheel and the surface:

$$T_w^{max} = R_z(\mu_p + f)r_w^0 \tag{2.381}$$

where

R_z is the normal reaction of the wheel
μ_p is the peak friction coefficient
f is the rolling resistance coefficient
r_w^0 is the rolling radius of the tire in the driven mode

If the values of factors contained in the right-hand side of formula (2.381) are identical for both wheels, then the maximum torques of the wheels and their slippage will be attained simultaneously. If any given parameter of a wheel will turn out to be smaller, slippage will set in earlier for this wheel. Then the torques at both wheels will be reduced by the same amount.

In this case, the differential drive of two wheels does not allow to fully use the potential coupling traction force of the axle, for which reason the traction performance and the mobility of the vehicle become poorer. This may be observed upon redistribution of the load between the wheels, for example, when the vehicle travels on an incline or when it moves over a trench at an angle. In the first case the adhesive weight of two wheels of one side of the vehicle will decrease and in the second case that of two diagonally situated wheels.

The tractive performance of specimens of a model of a 4×4 earth-moving tractor with all its wheels rigidly fastened to the frame deteriorated steeply even at small road irregularities because of reduction of the adhesive weight on two diagonally situated wheels. The efficiency of this tractor improved markedly only after equipping its driving axles with locking differentials.

Redistribution of adhesive weight between wheels when moving over roads with irregular surfaces is encountered also in multiaxle vehicles and depends on the road irregularities and the properties of wheel suspensions. Redistribution of adhesive weight is also observed in high-speed vehicles traveling on horizontal road surfaces as a result of centrifugal forces that are generated when taking a turn. Significant weight redistribution between axles may also occur at high tractive loads and when moving uphill. When a differential is used as the interaxle power-dividing unit of such vehicles, their front wheels may slip.

Under ordinary operating conditions, tractive properties of vehicles with differential drives deteriorate because of slippage of individual wheels that find themselves on sections of the road with poor gripping properties. This happens when traveling over wet or snow-covered roads, etc. If the smaller peak friction coefficient of one wheel of the driving axle is designated by μ'_{p} and the greater such coefficient of the second wheel is designated by μ''_{p}, then the maximum traction torque of the axle is

$$T_{\text{w}}^{\max} = 2R_z(\mu'_{\text{p}} + f')r_{\text{w}}^0 \tag{2.382}$$

which is formulated as follows: the torque of the driving axle with differential drive of both the left and right wheels is always equal to twice the torque of the wheel that has the poorer gripping contact with the road.

At traction loads corresponding to ordinary operating conditions and when traveling over uniform soil, as a result of tangential deformation of the soil (and tires) the motion of the vehicle will be accompanied by equal slippage s_δ of both wheels. The total circumferential force of the driving axle is obtained from the expression (for example, for the case of linear relationship (1.25))

$$F_{x\Sigma} = 2K_x s_\delta \tag{2.383}$$

In certain cases, for example, when the tractor pulls a plow, its left and right wheels are subject to different gripping conditions ($K'_x \neq K''_x$) Earth-moving tractors and even vehicles traveling over roads may be subject to nonequal road gripping conditions. But since in the case of differential drive the wheel torques are identical, two wheels will slip in a nonequal manner, $s''_\delta \neq s'_\delta$. This is seen from the expressions

$$\begin{aligned} T'_{\text{w}} &= T''_{\text{w}} \\ F'_x r_{\text{w}}^{0'} &= F''_x r_{\text{w}}^{0''} \\ K'_x s'_\delta r_{\text{w}}^{0'} &= K''_x s''_\delta r_{\text{w}}^{0''} \end{aligned} \tag{2.384}$$

A similar situation ($s''_\delta \neq s'_\delta$) is possible also on a uniform surface of motion, but at nonequal weight loading of the wheels. In this case $K'_x \neq K''_x$ and $r_{\text{w}}^{0'} \neq r_{\text{w}}^{0''}$, which inevitably causes slips s'_δ and s''_δ in formulae (2.384) to be nonequal.

The next example to analyze is that of the tractive properties of a 6×6 tractor in which each of the axles have differently sized wheels. The driveline system is fully differential. Figure 2.121 shows: (a) the differential driveline system layout of the axle drives and (b) conceptual diagram of a device that ensures differential operating modes of the interaxle drives.

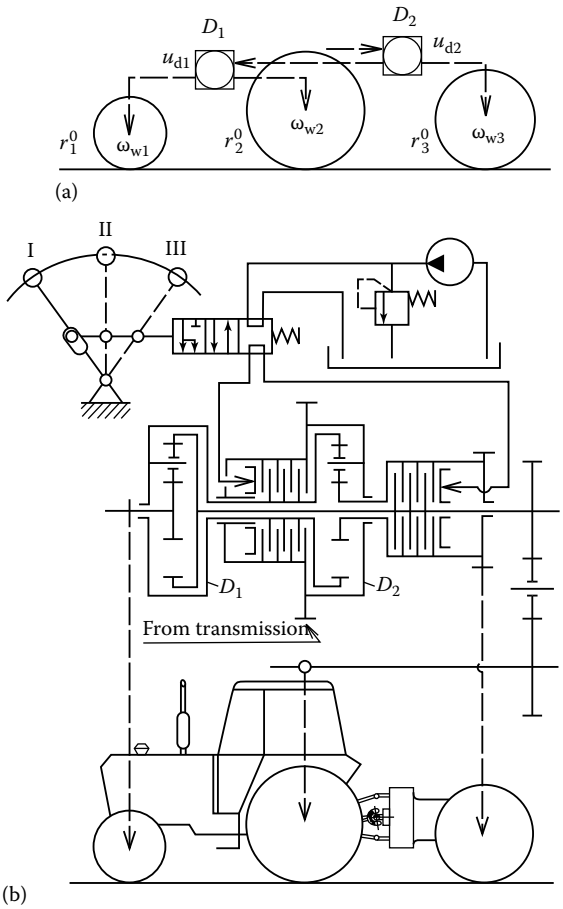


FIGURE 2.121
6×6 farm tractor.

In position I the drive of all the three axles is differential. In position II differential D_1 is locked. In position III both differentials (D_1 and D_2) are locked. Expressions are now compiled for the circumferential forces of the three axles in the case of a differential drive when moving at constant velocity:

$$\begin{aligned}
&\frac{F_{x2}r_{a2}^0}{F_{x1}r_{a1}^0} = u_{d1} \\
&\left(F_{x1}r_{a1}^0 + F_{x2}r_{a2}^0\right)/\left(F_{x3}r_{a3}^0\right) = u_{d2} \\
&F_{x\Sigma} = \sum_{i=1}^{3} F_{xi} = \sum_{i=1}^{3} R_{xi} + F_d
\end{aligned} \tag{2.385}$$

It should be reemphasized that the number of relationships for determining the circumferential forces of wheels, as is seen from formulae (2.385), is equal to the number of power-dividing units under consideration. In the present cases, there are two such equations. These are the first and second of formulae (2.385) that functionally relate the circumferential forces of the axles by the characteristics of the power-dividing units, i.e., by means of gear ratios u_{d1} and u_{d2} of the interaxle differentials. Supplementing these two equations by

the equation for the total circumferential force $F_{x\Sigma}$ makes it possible to determine forces F_{xi} ($i = 1, 3$), since the number of unknowns is the same as the number of equations in (2.385).

Using the values of F_{xi} found above and, for example, formula (1.26) for the case of nonlinear $F_x = f(s_\delta)$ it is possible to calculate the axle slips $s_{\delta i}$ ($i = 1, 3$) and to then determine the generalized slippage $s_{\delta a}$ of the tractor. For this use should first be made of formula (2.355) and the generalized slippage of the front and middle axles should be calculated:

$$s_{\delta a1} = 1 - \frac{(1 + u_{d1})(1 - s_{\delta 1})(1 - s_{\delta 2})}{1 - s_{\delta 2} + u_{d1}(1 - s_{\delta 1})} \tag{2.386}$$

Then formula (2.358) is used for finding the generalized slippage of the tractor as

$$s_{\delta a} = 1 - \frac{(1 + u_{d2})(1 - s_{\delta 3})(1 - s_{\delta a1})}{1 - s_{\delta a1} + u_{d2}(1 - s_{\delta 3})} \tag{2.387}$$

The value of $s_{\delta a}$ calculated from formula (2.387) can then be used for calculating the traction efficiency η_x^t of the running gear and the traction efficiency η_t of the tractor (see the formulae in Table 2.22). Figures 2.122 and 2.123 show some results of the calculations.

The circumferential forces of the axles vary in proportion to gear ratios u_{d1} and u_{d2}. At low values of drawbar load F_d variations in u_{d1} and u_{d2} have little effect on η_x^t (curves 1 and 2). At medium and high values of F_d the value of η_x^t depends more markedly on the values of

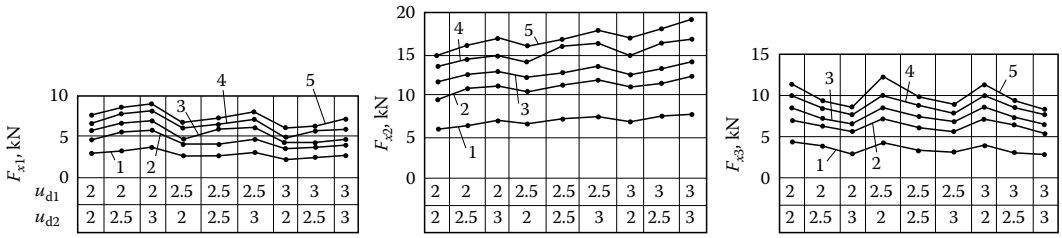


FIGURE 2.122
6 × 6 tractor: circumferential axle forces. 1, 2, 3, 4, and 5, F_d = 8; 16; 20; 24; and 28 kN.

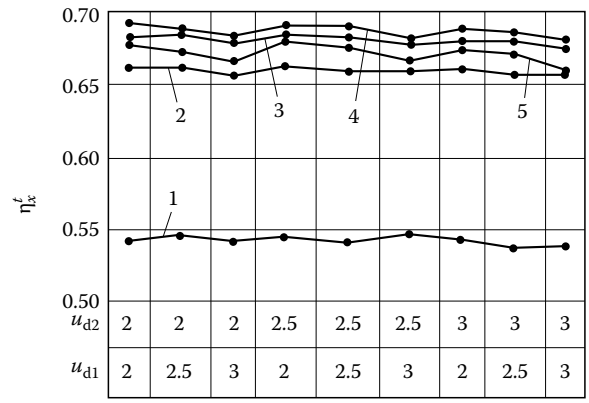


FIGURE 2.123
6 × 6 tractor: tractive running gear efficiency. 1, 2, 3, 4, and 5, F_d = 8; 16; 20; 24; and 28 kN.

u_{d1} and u_{d2} (curves 3–5). These data confirm the importance of selecting rational values of gear ratios of differentials, which is examined in Section 2.9, after analyzing in Section 2.8.3 the effect of the differential drive on the turnability and stability of vehicle motion.

2.8.3 Vehicle Turnability and Stability of Motion

To even more completely clarify the effect of the driveline system on the turnability and stability of vehicles, it is necessary to eliminate, to the extent possible, the effect of other factors. Hence, the first item considered is circular, steady-state low-velocity motion (there are no centrifugal forces) without the drawbar load F_d. For these conditions the effect of open differentials on the lateral force of wheels on which depend the wheel slip angles, meaning also the vehicle's turnability and stability, is determined.

When a driving axle with open differentials takes a turn, the wheel torques are equal to one another ($T'_w = T''_w$). It follows from this that

$$\begin{gathered} F'_x r_w^{0'} = F''_x r_w^{0''} \\ \text{or} \\ F''_x / F'_x = r_w^{0'} / r_w^{0''} \end{gathered} \tag{2.388}$$

i.e., the circumferential forces of the wheels are not equal if the rolling radii of wheels in the driven mode are not equal. Inequality of forces ($F''_x \neq F'_x$) produces a yaw moment in the plane of the road

$$M_B = 0.5\left(F''_x - F'_x\right) t_b \tag{2.389}$$

where t_b is the wheel tread. Moment M_B may assist the turn (Figure 2.124a, $F'_x > F''_x$) or interfere with it (Figure 2.124b, $F''_x > F'_x$). In accordance with this, M_B is known as assisting or resisting yaw moment.

Moment M_B, exerted on the driving wheel by the road, is overcome by lateral forces that arise in contacts of the front and rear wheels with the road. These forces F_{l1}^w and F_{l2}^w are now determined for a vehicle with a single rear driving axle (Figure 2.125a) and a single front driving axle (Figure 2.125b).

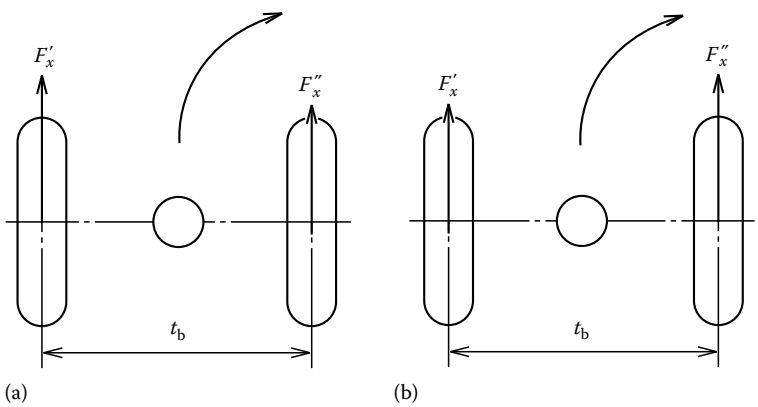


FIGURE 2.124
Driving axle in a right turn.

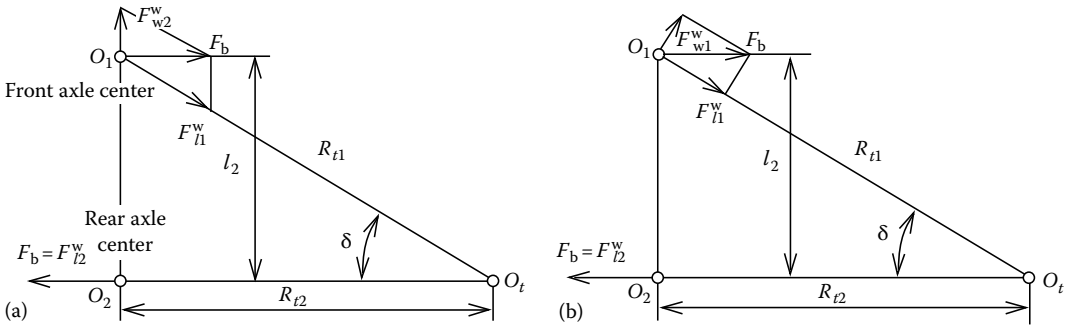


FIGURE 2.125
RWD vehicle (a) and FWD vehicle (b) in turn.

Resisting moment M_B is balanced by force couple F_B with arm equal to the vehicle wheelbase l_2. Force F_B in point O_2 is equal to the lateral force F^{w}_{l2} acting on the rear wheels. Force F_B should be resolved in point O_1 into two components. When it is the rear axle that is driving, the following forces are obtained (Figure 2.125a):

$$\begin{aligned} F_B &= F^{w}_{l2} = \frac{M_B}{l_2} \\ F^{w}_{l1} &= \frac{F_B}{\cos\delta} = \frac{M_B}{l_2 \cos\delta} \\ F^{w}_{w2} &= F_B \tan\delta = \frac{M_B}{l_2} \tan\delta \end{aligned} \tag{2.390}$$

And when the front axle is driving, the forces are (Figure 2.125b)

$$\begin{aligned} F_B &= F^{w}_{l2} = \frac{M_B}{l_2} \\ F^{w}_{l1} &= F_B \cos\delta = \frac{M_B}{l_2} \cos\delta \\ F^{w}_{w1} &= F_B \sin\delta = \frac{M_B}{l_2} \sin\delta \end{aligned} \tag{2.391}$$

In these formulae F^{w}_{w1} and F^{w}_{w2} are additional traction forces of the front and rear axles.

The ratio of lateral force F^{w}_{l1} when the front axle is the driving one from formula (2.391) to force F^{w}_{l1} in the case of a rear driving axle from formula (2.390) is $\cos^2\delta$. The ratio of force F^{w}_{w1} to force F^{w}_{w2} is equal to $\cos\delta$. This means that the lateral forces of the front wheels and the additional traction force are greater when the rear axle is driving. The sum of the moments of three forces from formulae (2.390) and (2.391) is equal to M_B. The forces and moments for the case of two and more driving axles are calculated similarly.

The question naturally arises as to the significance of moment M_B and forces, F^{w}_{l1} and F^{w}_{l2}, induced by inequality of circumferential forces, F''_x and F'_x, of the wheels of an axle with an open differential. It is seen from formula (2.388) that the inequality of the last two forces depends on the ratio of radii $r^{0''}_{w}$ and $r^{0'}_{w}$. It is obvious that the difference in radii under steady-state conditions is insignificant and accordingly the moment M_B and the additional

forces from Figure 2.125 can be neglected. Greater care is needed in these assessments when dealing with passenger cars and sports vehicles that take turns at high velocities. For example when a passenger car with a total mass of 2 ton with a 20% difference in radii $r_{\mathrm{w}}^{0''}$ and $r_{\mathrm{w}}^{0'}$ takes a turn, force F_{l1}^{w} may be as high as 200 N. For this reason, the decision concerning accounting for moment M_{B} induced by an open differential should be taken separately for each case of motion. It should be emphasized that formulae (2.389)–(2.391) above are general and can be used for assessing other power-dividing mechanisms, and not only open differentials (see Chapters 3 and 4).

The presence of torques at the axle's wheels has a marked effect on the axle's lateral slip resistance factor $K_{y\Sigma}$ (also known as the ''cornering stiffness''). The value of this factor may decrease even on roads with high wheel gripping properties, whereas under poor road conditions and in off-road travel, variations in the wheels' torques may exert a significant effect on the values of $K_{y\Sigma}$ and with it on the vehicle's stability of motion.

Usually the effect of torques T_{w} (or of circumferential forces F_x) of the wheels on the value of $K_{y\Sigma}$ is analyzed together with the distribution of weight between the left and right wheels of the axle. In the case when the wheels are subjected to high and identical gripping conditions, the values of $K_{y\Sigma}$ are close to the maximal, if the normal wheel reactions R''_{zi} and R'_{zi} are equal to one another. The lessening of the load on the inner wheel when the axle takes a turn (R''_{zi} decreases whereas R'_{zi} increases) may cause the value of $K_{y\Sigma}$ to decrease highly, and causes an increase in the lateral tire slip and deterioration in the stability of motion: the possibility of axle skid increases. The minimum values of $K_{y\Sigma}$ correspond to such a lessening of the normal load on the inner (relative to the turn) wheel at which this wheel attains complete slippage (the circumferential force of the wheel becomes equal to its value based on the conditions of gripping of the surface of motion). The presence of an open differential has a positive effect on the value of $K_{y\Sigma}$ when the axle takes a turn: the circumferential forces of the wheels are close to one another and do not additionally reduce the factor of lateral slip resistance (cornering stiffness) of the partially load-relieved inner wheel. Any increase in the circumferential forces of the inner wheel in this case will reduce its slip resistance factor, meaning also the value of $K_{y\Sigma}$, and decrease the vehicle's motion stability.

Consider now the effect of the interaxle drive on the lateral wheel forces. Let a 4×4 vehicle perform a steady-state turn at exceedingly small speed without a drawbar load. The interwheel differentials are open and do not cause yaw moment. The bicycle model of the vehicle is shown in Figure 2.126.

The lateral reactions, F_{l1}^{a} and F_{l2}^{a} for the above conditions of motion can be determined from equilibrium equations. It is found from equations of moments about point O_1 that

$$F_{l2}^{\mathrm{a}} = 0 \tag{2.392}$$

This shows that, in the absence of the drawbar pull and centrifugal forces, the lateral force of the rear wheels and their slip angle are independent of the type of the power-dividing unit installed between the driving axles. This is an important conclusion that must be taken into account when designing interaxle drives.

It is found from the equation of equilibrium of moments about point O_2 that the lateral force of front wheels induced by the interaxle drive is given by the expression

$$F_{l1}^{\mathrm{a}} = (R_{x1} - F_{x1}) \tan \delta \tag{2.393}$$

This expression shows that the magnitude and direction of the lateral force of the front wheels and consequently their slip angle are determined by the relationship between

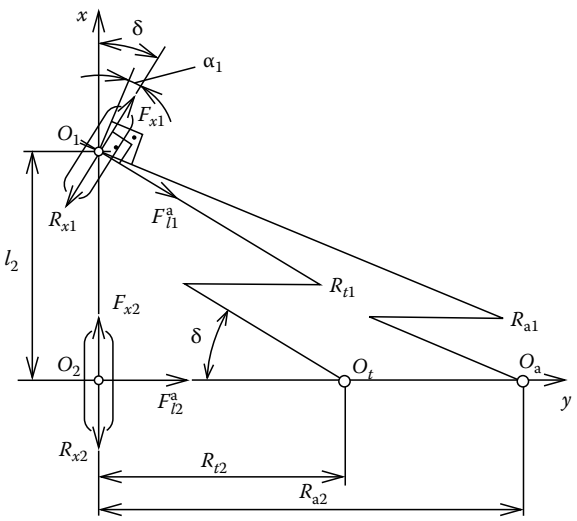


FIGURE 2.126
4 × 4 vehicle in turn.

resistance force R_{x1} and the circumferential force F_{x1}. The force F_{x1} here depends directly on the type of mechanism that divides the power between the vehicle's axles. For example, if the gear ratio of the interaxle differential provides a force F_{x1} equal to force R_{x1}, then the lateral force is $F^{a}_{l1} = 0$. If $R_{x1} > F_{x1}$ then $F^{a}_{l1} > 0$ and the slip of the front wheels will act toward increasing the turn radius (understeering). It is seen from Figure 2.126 that the appearance of force F^{a}_{l1} induces a slip angle α_1 and also increases the turn radius from R_{t1} to R_{a1} (R_{t2} increases to R_{a2}). If $R_{x1} < F_{x1}$, then force F^{a}_{l1} reverses its direction (oversteering). This is confirmed by computational and experimental data plotted in Figures 2.127 and 2.128.

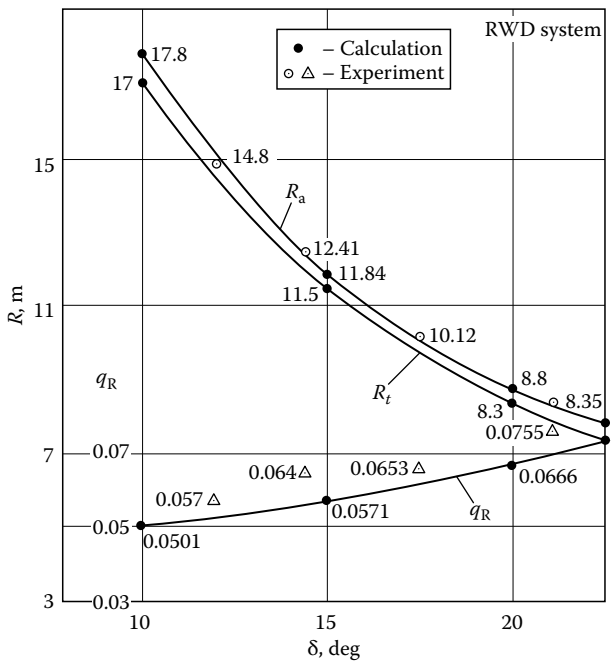


FIGURE 2.127
RWD truck in turn on soft soil at exceedingly small speed.

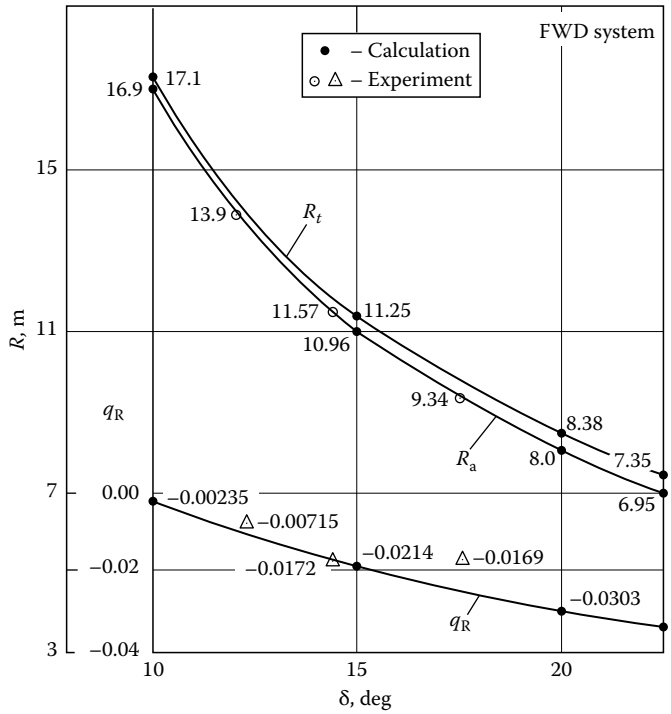


FIGURE 2.128
FWD truck in turn on soft soil at exceedingly small speed.

In fact, upon exceedingly slow turn of a truck with rear driving axle the actual turn radii R_a are somewhat larger than their theoretically determined value R_t (see Figure 2.127), that is, there is understeering, since $R_{x1} > F_{x1}$ (in this case $F_{x1} = 0$). The circumferential force F_{x1} of the front axle of a vehicle with front driving axle (see Figure 2.128) becomes higher than the rolling resistance force R_{x1}. As a result, force F_{l1} from formula (2.393) changes direction and causes a reduction in the actual turn radii R_a as compared with their computationally obtained values of R_t in Figure 2.128 (oversteering).

It should be emphasized that formulae (2.392) and (2.393) are general and hence also suitable for assessing other interaxle drive arrangements and are not the only ones using a differential.

The examination of a 4×4 vehicle with open interaxle differentials is now continued by compiling equilibrium of forces and moments referring to Figure 2.126:

$$\begin{aligned}
&\sum x = 0 : F_{x1}\cos\delta - F_{l1}^{a}\sin\delta - R_{x1}\cos\delta + F_{x2} - R_{x2} = 0\\
&\sum y = 0 : F_{x1}\sin\delta + F_{l1}^{a}\cos\delta - R_{x1}\sin\delta + F_{l2}^{a} = 0\\
&\sum M_{O_2} = 0 : F_{x1} l_2 \sin\delta + F_{l1}^{a}\cos\delta - R_{x1}\sin\delta = 0
\end{aligned} \tag{2.394}$$

The weight distribution factor is introduced in the form

$$u_w = \frac{W_2}{W_1} \tag{2.395}$$

whereas, the gear ratio of the interaxle differential is, as before, taken to

$$u_{\mathrm{d}} = \frac{T_{\mathrm{w2}}}{T_{\mathrm{w1}}} = \frac{F_{x2}}{F_{x1}} \frac{r^0_{\mathrm{a2}}}{r^0_{\mathrm{a1}}} \tag{2.396}$$

where r^0_{a1} and r^0_{a2} are the generalized rolling radii in the driven mode of the front and rear axles.

Simultaneous solution of the first and third of equations in (2.394) and Equations 2.395 and 2.396 followed by regrouping, yields

$$\begin{aligned} F_{x1} &= fW_{\mathrm{a}} \frac{1 + u_{\mathrm{w}} \cos\delta}{(1 + u_{\mathrm{w}})\left(1 + u_{\mathrm{d}} \dfrac{r^0_{\mathrm{a2}}}{r^0_{\mathrm{a1}}} \cos\delta\right)} \\ F_{x2} &= fW_{\mathrm{a}} u_{\mathrm{d}} \frac{1 + u_{\mathrm{w}} \cos\delta}{(1 + u_{\mathrm{w}})\left(1 + u_{\mathrm{d}} \dfrac{r^0_{\mathrm{a2}}}{r^0_{\mathrm{a1}}} \cos\delta\right)} \end{aligned} \tag{2.397}$$

where f is the wheel rolling resistance factor (taken to be the same for all the wheels) and W_{a} is the weight of the vehicle.

It follows from formulae (2.397) that in the case when $u_{\mathrm{d}} = u_{\mathrm{w}}$ and $r^0_{\mathrm{a2}} = r^0_{\mathrm{a1}}$ the following expressions apply:

$$\begin{aligned} &F_{x1} = fW_1 = R_{x1}; \quad F_{x2} = R_{x1} u_{\mathrm{d}} = fW_2 = R_{x2}; \\ &F^{\mathrm{a}}_{l1} = 0 \end{aligned} \tag{2.398}$$

If $u_{\mathrm{d}} \to \infty$ (RWD), then

$$\begin{aligned} &F_{x1} = 0; \quad F_{x2} = f\left(W_2 + \frac{W_1}{\cos\delta}\right) > fW_{\mathrm{a}} \\ &F^{\mathrm{a}}_{l1} = fW_{\mathrm{a}} \frac{1}{1 + u_{\mathrm{w}}} = R_{x1} \tan\delta, \end{aligned} \tag{2.399}$$

that corresponds to the slip of the front wheels in the direction of increasing turn radius.

If $u_{\mathrm{d}} \to 0$, (FWD), then

$$\begin{aligned} &F_{x2} = 0; \quad F_{x1} = f(W_1 + W_2 \cos\delta) < fW_{\mathrm{a}} \\ &F^{\mathrm{a}}_{l1} = -fW_{\mathrm{a}} \frac{u_{\mathrm{w}}}{1 + u_{\mathrm{w}}} \sin\delta = -R_{x2} \sin\delta, \end{aligned} \tag{2.400}$$

that corresponds to the slip of the front wheels in the direction of reduction of the turn radius.

The above analysis shows that there will be no lateral forces only in the particular case of $u_{\mathrm{d}} = u_{\mathrm{w}}$. If $u_{\mathrm{d}} \neq u_{\mathrm{w}}$ then there will also exist some lateral force on the front wheels, in spite of the fact that there is a differential in the interaxle drive. The expressions for forces F_{x1} and F_{x2} from formulae (2.399) and (2.400) show that circumferential force F_{x2} for an RWD vehicle increases when taking a turn (the rolling resistance force increases), whereas for an FWD vehicle the force F_{x1} decreases relative to the circumferential force developed when the vehicle travels in a straight path.

Expressions for F_{l1}^{a} from formulae (2.399) and (2.400) reflect the limiting values of this force (by sign and magnitude) for a given front-wheel turning angle δ.

The presence of an interaxle differential also affects the vehicle's stability of motion and handling. It should be expected, among others, that a passenger car with a symmetrical interaxle differential would react slower to the turning of the front-steered wheels than the same car, but with a rear-wheel drive system. This lag is almost imperceptible when starting the turn, but it becomes significant in motion with a constant wheel-turning angle and in particular when leaving the turn. For this reason a 4×4 car may avoid skid upon rapid return of the steering wheel to the zero angle, which turns out to be impossible for a similar car with a rear drive. Such a ''deceleration'' of a 4×4 car with interaxle differential manifests itself, as a rule, to a larger degree on roads with lower friction. If the interaxle differential is asymmetrical, then the lag in the vehicle's reaction to the turn of the steered wheels usually decreases. The reaction to a turn of the steered wheels of a 4×4 car with an asymmetrical interaxle differential approaches to that of one with a rear drive.

When the center of gravity of a 4×4 car with a symmetrical interaxle differential is shifted toward the rear axle the front axle slip resistance factor $K_{y\Sigma 1}$ decreases to a larger degree than $K_{y\Sigma 2}$ of the rear-axle wheels. This happens because normal loads on axles subjected to identical torques ($T_{w1} = T_{w2}$, symmetrical interaxle differential) are different, and causes different reductions in the values of $K_{y\Sigma 1}$ and $K_{y\Sigma 2}$ when both axles drive. Such a car can suffer from understeering that is more severe than that of a RWD vehicle.

2.9 Optimal and Reasonable Differential Gear Ratios: Control Principles

The gear ratio u_d of a differential was introduced in Section 2.1 for quantitative assessment of the distribution of the torque T_0 supplied to the housing of this mechanism between its two output shafts. If the interwheel differentials are symmetrical, i.e., the output torques are the same, $T' = T''$, then the interaxle differentials may even be asymmetrical, i.e., the torques T_1 and T_2 at their output shaft may not be the same:

$$T_1 \neq T_2, \quad u_d = \frac{T_2}{T_1} > 1 \tag{2.401}$$

It is rather obvious that the gear ratio u_d has a marked effect on the distribution of torques between the axles and, accordingly, on the slip power loss, i.e., the energy efficiency of the vehicle), the tractive capacity of the vehicle, its mobility, turnability and motion stability. For this reason, the determination of the values of u_d that improve the above properties of the vehicle (reasonable gear ratios) or ensure the top vehicle properties (the optimal gear ratios) are of definite practical interest.

Over many years the numerical values of u_d were selected based on the ratio of normal loads on the axles coupled by the differential. This approach is rather extensively used even at present. It is based on the need to simultaneously attain the gripping-based limiting values of circumferential forces of the wheels of these axles. The standard assumption was that the gripping conditions of the wheels of two axles are the same, i.e., $\mu_{px1} = \mu_{px2}$.

This condition for 4×4 vehicles with interaxle differentials having tires with different dimensions $r_{a1}^0 \neq r_{a2}^0$, and different normal loads $W_1 \neq W_2$ is written as

$$\frac{F_{x2}^{max}}{F_{x1}^{max}} = \frac{W_2 \mu_{px2}}{W_1 \mu_{px1}} = \frac{W_2}{W_1} = \frac{\lambda_2}{\lambda_1} = u_w \tag{2.402}$$

$u_w = \frac{W_2}{W_1}, \lambda_i = \frac{W_i}{W_a}$, $(i = 1, 2)$ is the normal loading factor of the ith axle and W_a is the gross weight of the vehicle. If condition (2.402) is satisfied, then the maximum torques at the output shafts of the interaxle differential of this vehicle are determined by the following relationships (the mechanical losses in the axle drives are assumed to be the same, $\eta_{M1} = \eta_{M2} = \eta_M$):

$$\begin{aligned} T_1^{max} &= \frac{F_{x1}^{max} r_{a1}^0}{u_1 \eta_M} = \frac{\mu_{px} W_1 r_{a1}^0}{u_1 \eta_M} \\ T_2^{max} &= \frac{F_{x2}^{max} r_{a2}^0}{u_2 \eta_M} = \frac{\mu_{px} W_2 r_{a2}^0}{u_2 \eta_M} \end{aligned} \tag{2.403}$$

The ratio of torques T_2^{max} and T_1^{max} equal, by definition, to u_d, is determined from (2.403) as

$$\frac{T_2^{max}}{T_1^{max}} = \frac{W_2}{W_1} \quad \text{or} \quad u_d = u_W \tag{2.404}$$

Note that formula (2.404) was derived on the assumption that $r_{a1}^0 u_2 = r_{a2}^0 u_1$. Conformance to this condition will ensure identical theoretical linear velocities of the centers of the front and rear axles in straight-line motion:

$$V_{t1} = V_{t2} = \frac{\omega_0}{u_1} r_{a1}^0 = \frac{\omega_0}{u_2} r_{a2}^0 \tag{2.405}$$

where ω_0 is the angular velocity of the housing of the interaxle differential.

All this means that the gear ratio of the differential should be equal to the ratio of the weights of the driving axles (including vehicles with different sizes of front and rear wheels). If the maximum circumferential force F_x^{max} of one of the axles decreases because of a reduction in the wheels-road gripping factor, or redistribution of loads between the axles, then the maximum circumferential force on the second axle also decreases. Consequently, the wheels of this axle will not slip and the maximum coupling force will not be obtained. As a result, the vehicle will lose mobility at high traction modes, the wheels of one of the axles will slip and those of the other will stop. If the front axle will be the one under unfavorable gripping conditions, then the circumferential force of the rear axle will be given by the expression

$$F_{x2} = F_{x1}^{max} u_d = \mu_{px1} W_1 u_d \tag{2.406}$$

Then the total circumferential force of the vehicle is

$$F_{x\Sigma} = F_{x1}^{max} + F_{x2} = \mu_{px1} W_1 (1 + u_d) \tag{2.407}$$

If the rear axle is the one under unfavorable gripping conditions, then the circumferential force of the front axle is found from the expression

$$F_{x1} = \frac{F_{x2}^{\max}}{u_{\mathrm{d}}} = \mu_{\mathrm{p}x2} W_2 / u_{\mathrm{d}} \tag{2.408}$$

In this case, the total circumferential force of the vehicle is (with taking into account formula (2.402))

$$F_{x\Sigma} = F_{x1} + F_{x2}^{\max} = \mu_{\mathrm{p}x2} W_2 \frac{1 + u_{\mathrm{d}}}{u_{\mathrm{d}}} = \mu_{\mathrm{p}x1} W_1 (1 + u_{\mathrm{d}}) \tag{2.409}$$

It follows from comparing formulae (2.407) and (2.409) that the loss of the total circumferential force $F_{x\Sigma}$ of a 4×4 vehicle with differential drive of the axles, including asymmetrical differentials and nonuniform distribution of weight between the axles occurs irrespective of which axle (rear or front) is on a slippery part of the road. This rule does not extend to cases when u_{d} is not equal to the ratio of adhesive weights u_{w}, i.e., when condition (2.402) is not satisfied.

If the above approach is extended to a vehicle with any even or odd number of driving axles (see Table 2.21), then the values of the gear ratios of interaxial differentials of such vehicles can be calculated from expressions given in Table 2.23.

In practice, the gear ratios of differentials are usually determined from the static loads of the axles of a vehicle with a payload. The values of u_{d} selected in such a manner may be termed reasonable. In fact, it is seen from the data in Section 2.8.3 that in this case no lateral forces arise on the wheels of a 4×4 vehicle that may affect its turnability or stability of motion. The positive effect of equality of u_{d} to the ratio u_{w} of normal loads on the load mode of a vehicle taking a turn was noted in Section 2.2. This method of selecting u_{d} was used for many years for highway vehicles in which circumferential forces of wheels are, under normal circumstances, far from their gripping-based values and, as a rule, are directly proportional to normal loads, and the gripping conditions of the wheels of the axles are the same.

At the same time, the normal loads on axles of many transportation and traction vehicles typically undergo substantial fluctuations. For example, in the case of farm tractors this is caused by changes in the drawbar pull F_{d} over a wide range. Transportation vehicles may move with higher accelerations and also over sloping surfaces, which markedly changes the normal loads as compared with their static values. As an illustration, consider a 6×6 timber-carrier truck. The gross mass of the truck is 47 ton. The truck's tractor has an interaxle differential with $u_{\mathrm{d}} = 2$ in the transfer case that distributes the torque between the front axle and the tandem that is comprised of the second and third axles. The static distribution of the gross weight between the tandem and the front axle is $u_{\mathrm{w}} = \dfrac{W_{2,3}}{W_1} = 3.24$. It is seen by comparing the numerical values of u_{d} and u_{w} that at the existing distribution of weight the front axle is clearly overloaded by the traction effort, since $u_{\mathrm{d}} < u_{\mathrm{w}}$. The front wheels of the truck frequently slip, particularly when starting from rest, when the load on the front wheels becomes additionally reduced. Investigation of the numerical values of u_{d} and u_{w} of trucks made by another manufacturer shows an opposite relationship between these parameters. Thus, for a 4×4 truck with gross weight of 128 kN the value of u_{d} at weight distribution $u_{\mathrm{w}} = 1.56$ is 2.5. Still another 4×4 truck of the same manufacturer with a gross weight of 187 kN and with the axle-load distribution factor of $u_{\mathrm{w}} = 1.79$, has a gear ratio of the interaxle differential of $u_{\mathrm{d}} = 3$.

TABLE 2.23

Differential Gear Ratio

Group One			Group Two		
Even Number of Drive Axles	**Variant**	**Gear Ratio**	**Odd Number of Drive Axles**	**Variant**	**Gear Ratio**
2	*a*	$u_{d1} = \lambda_2/\lambda_1$	3	*a*	$u_{d1} = \lambda_2/\lambda_1$; $u_{d2} = (\lambda_1 + \lambda_2)/\lambda_3$
4	*a*	$u_{d1} = \lambda_2/\lambda_1$; $u_{d2} = \lambda_4/\lambda_3$; $u_{d3} = (\lambda_3 + \lambda_4)/(\lambda_1/\lambda_2)$	5	*a*	$u_{d1} = \lambda_2/\lambda_1$; $u_{d2} = \lambda_5/\lambda_4$; $u_{d3} = (\lambda_4 + \lambda_5)/\lambda_3$; $u_{d4} = (\lambda_3 + \lambda_4 + \lambda_5)/(\lambda_1 + \lambda_2)$
	b	$u_{d1} = \lambda_4/\lambda_3$; $u_{d2} = (\lambda_3 + \lambda_4)/\lambda_2$; $u_{d3} = (\lambda_2 + \lambda_3 + \lambda_4)/\lambda_1$		*b*	$u_{d1} = \lambda_5/\lambda_4$; $u_{d2} = (\lambda_4/\lambda_5)/\lambda_3$; $u_{d3} = (\lambda_3 + \lambda_4/\lambda_5)/\lambda_2$; $u_{d4} = (\lambda_2 + \lambda_3 + \lambda_4 + \lambda_5)/\lambda_1$
6	*a*	$u_{d1} = \lambda_2/\lambda_1$; $u_{d2} = \lambda_4/\lambda_3$; $u_{d3} = \lambda_6/\lambda_5$; $u_{d4} = (\lambda_5 + \lambda_6)/(\lambda_3 + \lambda_4)$ $u_{d5} = (\lambda_3 + \lambda_4 + \lambda_5 + \lambda_6)/(\lambda_1 + \lambda_2)$	7	*a*	$u_{d1} = \lambda_2/\lambda_1$; $u_{d2} = \lambda_4/\lambda_3$; $u_{d3} = \lambda_7/\lambda_6$; $u_{d4} = (\lambda_6 + \lambda_7)/\lambda_5$; $u_{d5} = (\lambda_3 + \lambda_4)/(\lambda_1 + \lambda_2)$; $u_{d6} = (\lambda_1 + \lambda_2 + \lambda_3 + \lambda_4)/(\lambda_5 + \lambda_2 + \lambda_3)$
	b	$u_{d1} = \lambda_2/\lambda_1$; $u_{d2} = \lambda_6/\lambda_5$; $u_{d3} = (\lambda_1 + \lambda_2)/\lambda_3$; $u_{d4} = (\lambda_5 + \lambda_6)/\lambda_4$; $u_{d5} = (\lambda_4 + \lambda_5 + \lambda_6)/(\lambda_1 + \lambda_2 + \lambda_3)$		*b*	$u_{d1} = \lambda_2/\lambda_1$; $u_{d2} = \lambda_7/\lambda_6$; $u_{d3} = (\lambda_1 + \lambda_2)/\lambda_3$; $u_{d4} = (\lambda_6 + \lambda_7)/\lambda_5$; $u_{d5} = (\lambda_5 + \lambda_6 + \lambda_7)/\lambda_4$; $u_{d6} = (\lambda_4 + \lambda_5 + \lambda_6 + \lambda_7)/(\lambda_1 + \lambda_2 + \lambda_3)$

The above data point to the need to develop a method for determining the optimal values of gear ratios of interaxle differentials that would ensure the best operational properties of vehicles. Such a method is now examined for a 4×4 vehicle, each axle of which may have the same or different size wheels and the gripping conditions may be the same or different. It is required to determine the gear ratios for an interaxle differential of such a vehicle that would provide the maximum efficiency (minimum fuel consumption) and best tractive performance. The energy efficiency of the vehicle shall be described by the running gear efficiency, assuming equality of mechanical power losses of the front and rear axles, $\eta_{M1} = \eta_{M2}$. Formulae for calculating this efficiency are presented in Table 2.22 for different operational modes: traction, transportation, and combined (transportation and traction). If the 4×4 vehicle operates in the traction mode (for example, if it is a farm tractor) then one uses the formula for the tractive efficiency of the running gear from Table 2.22. If the vehicle under study operates in the transportation mode (a car, a pickup truck, etc.), then its efficiency should be assessed based on the transportation efficiency of the running gear system. For transportation-traction vehicles Table 2.22 also lists corresponding formulae for calculating the efficiency. It is obvious that any of these efficiencies

will be at maximum provided that the total slippage power losses $P_{\delta\Sigma} = \sum_{i=1}^{2} P_{\delta i}$ are at minimum. This shall be demonstrated using the transportation efficiency of the running gear from Table 2.22:

$$\eta_x^{\text{tr}} = \frac{\sum_{i=1}^{2} P_{\text{w}i}^{\text{in}} - \left(\sum_{i=1}^{2} P_{fci} + \sum_{i=1}^{2} P_{\delta i}\right)}{\sum_{i=1}^{2} P_{\text{w}i}^{\text{in}}} \tag{2.410}$$

where $\sum_{i=1}^{2} P_{\text{w}i}^{\text{in}}$ is the power supplied to the driving axles; whereas $\sum_{i=1}^{2} P_{fci}$ is the rolling resistance power needed for overcoming the rolling resistance forces of the axles' wheels, which stem from the curb weight of the vehicle.

Assuming that the circumferential force of the wheels F_x is a linear function of its slippage s_δ (see formula (1.25)), the slippage power losses $P_{\delta\Sigma}$ can be determined using their definition from Section 1.3.3 (see P_δ in formula (1.34)):

$$P_{\delta\Sigma} = \sum_{i=1}^{2} P_{\delta i} = \sum_{i=1}^{2} F_{xi} V_{ti} s_{\delta \text{a}i} = \sum_{i=1}^{2} K_{\text{a}i} V_{ti} s_{\delta \text{a}i}^2 \tag{2.411}$$

where V_{ti} are the theoretical velocities of the axles, $K_{\text{a}i}$ is the coefficient of tangential stiffness of the tires (tires and soil on deformable surfaces) of the axles. The numerical value of $K_{\text{a}i}$ is $2K_{xi}$, where K_{xi} is the tangential stiffness factor of one of the axle's tires. In formula (2.411) $s_{\delta \text{a}i}$ is the generalized slippage of driving axles:

$$s_{\delta \text{a}i} = \frac{F_{xi}}{K_{\text{a}i}}, \quad i = 1, 2 \tag{2.412}$$

Designating the total circumferential force of the vehicle as

$$F_{x\Sigma} = F_{x1} + F_{x2} \tag{2.413}$$

and introducing the gear ratio of the interaxle differential with taking into consideration formulae (2.344)

$$u_{\text{d}} = \frac{T_2}{T_1} = \frac{T_{\text{w}2}}{T_{\text{w}1}} \frac{u_1}{u_2} = \frac{F_{x2}}{F_{x1}} \frac{r_{\text{a}2}^0}{r_{\text{a}1}^0} \frac{u_1}{u_2}, \tag{2.414}$$

the slippages $s_{\delta \text{a}i}$ can be found as

$$s_{\delta \text{a}1} = \frac{F_{x\Sigma}}{K_{\text{a}1}(1 + u_{\text{d}})}; \quad s_{\delta \text{a}2} = \frac{F_{x\Sigma} u_{\text{d}}}{K_{\text{a}2}(1 + u_{\text{d}})} \tag{2.415}$$

Note that in formula (2.414) is supposed that $r_{\text{a}1}^0 u_2 = r_{\text{a}2}^0 u_1$ (see clarifications to formula (2.350)).

Now the relationship between the theoretical velocities of the axles is determined from the equality of the actual velocities of the centers of the driving axles:

$$V_x = V_{t1}(1 - s_{\delta \text{a}1}) = V_{t2}(1 - s_{\delta \text{a}2}) \tag{2.416}$$

Condition (2.9) can be written in terms of the linear velocities thus:

$$V_{\mathrm{a}} = \frac{V_{t1} + V_{t2}u_{\mathrm{d}}}{1 + u_{\mathrm{d}}} \tag{2.417}$$

where V_{a} is the theoretical velocity of the vehicle without slippage and $V_{t1} = V_{t2}$. Simultaneous solution of formulae (2.416) and (2.417) yields

$$\begin{aligned} V_{t1} &= V_{\mathrm{a}} \frac{(1 + u_{\mathrm{d}})(1 - s_{\delta \mathrm{a}2})}{u_{\mathrm{d}}(1 - s_{\delta \mathrm{a}1}) + (1 - s_{\delta \mathrm{a}2})} \\ V_{t2} &= V_{\mathrm{a}} \frac{(1 + u_{\mathrm{d}})(1 - s_{\delta \mathrm{a}1})}{u_{\mathrm{d}}(1 - s_{\delta \mathrm{a}1}) + (1 - s_{\delta \mathrm{a}2})} \end{aligned} \tag{2.418}$$

Substituting formulae (2.415) and (2.418) into formula (2.411) allows deriving the following expression for the slippage power:

$$P_{\delta\Sigma} = V_{\mathrm{a}} F_{x\Sigma}^2 \frac{K_{\mathrm{a}1}u_{\mathrm{d}}^2 + K_{\mathrm{a}2} - F_{x\Sigma}u_{\mathrm{d}}}{K_{\mathrm{a}1}K_{\mathrm{a}2}(1 + u_{\mathrm{d}})^2 - (K_{\mathrm{a}1} + K_{\mathrm{a}2})F_{x\Sigma}u_{\mathrm{d}}} \tag{2.419}$$

Formula (2.419) reflects the slippage power losses in the general case when the gripping conditions of the axles are different ($K_{\mathrm{a}1} \neq K_{\mathrm{a}2}$) and the interaxle differential is asymmetrical ($u_{\mathrm{d}} \neq 1$). If $u_{\mathrm{d}} = 1$, i.e., the interaxle differential is symmetrical, then formula (2.419) becomes

$$P_{\delta\Sigma} = V_{\mathrm{a}} F_{x\Sigma}^2 \frac{K_{\mathrm{a}1} + K_{\mathrm{a}2} - F_{x\Sigma}}{4K_{\mathrm{a}1}K_{\mathrm{a}2} - F_{x\Sigma}(K_{\mathrm{a}1} + K_{\mathrm{a}2})} \tag{2.420}$$

At identical gripping conditions ($K_{\mathrm{a}1} = K_{\mathrm{a}2} = K_{\mathrm{a}}$) and $u_{\mathrm{d}} = 1$,

$$P_{\delta\Sigma} = V_{\mathrm{a}} F_{x\Sigma}^2 \frac{2K_{\mathrm{a}} - F_{x\Sigma}}{4K_{\mathrm{a}}^2 - 2F_{x\Sigma}K_{\mathrm{a}}} = V_{\mathrm{a}} F_{x\Sigma}^2 \frac{1}{2K_{\mathrm{a}}} \tag{2.421}$$

If $K_{\mathrm{a}1} = K_{\mathrm{a}2} = K_{\mathrm{a}}$ but $u_{\mathrm{d}} \neq 1$, then

$$P_{\delta\Sigma} = V_{\mathrm{a}} F_{x\Sigma}^2 \frac{K_{\mathrm{a}}(1 + u_{\mathrm{d}}) - F_{x\Sigma}u_{\mathrm{d}}}{(1 + u_{\mathrm{d}})^2 K_{\mathrm{a}}^2 - 2F_{x\Sigma}u_{\mathrm{d}}K_{\mathrm{a}}} \tag{2.422}$$

It is of interest to subject general formula (2.419) to an extremum analysis in order to find the optimal value u_{d}^* at which the slippage power loss $P_{\delta\Sigma}$ is at minimum. For this, the derivative $\mathrm{d}P_{\delta\Sigma}/\mathrm{d}u_{\mathrm{d}}$ is determined and equated to zero:

$$\frac{\mathrm{d}P_{\delta\Sigma}}{\mathrm{d}u_{\mathrm{d}}} = \frac{\mathrm{d}}{\mathrm{d}u_{\mathrm{d}}} \frac{V_{\mathrm{a}} F_{x\Sigma}^2 (K_{\mathrm{a}1}u_{\mathrm{d}} + K_{\mathrm{a}2} - F_{x\Sigma}u_{\mathrm{d}})}{(1 + u_{\mathrm{d}})^2 K_{\mathrm{a}1}K_{\mathrm{a}2} - F_{x\Sigma}u_{\mathrm{d}}(K_{\mathrm{a}1} + K_{\mathrm{a}2})} = 0 \tag{2.423}$$

Formula (2.423) is solved for the differential's gear ratio and it is found that the optimal gear ratio u_{d}^* corresponding to $P_{\delta\Sigma} = \min$ is

$$u_{\mathrm{d}}^* = \frac{K_{\mathrm{a}2}}{K_{\mathrm{a}1}} \tag{2.424}$$

Using formula (2.414), the condition for agreement between the theoretical axle velocities $r_{a1}^0 u_2 = r_{a2}^0 u_1$ and the linear function (1.25), formula (2.424) is reduced to the form

$$u_d^* = \frac{K_{a2}}{K_{a1}} = \frac{F_{x2}}{F_{x1}} \tag{2.425}$$

This yields

$$\frac{F_{x2}}{K_{a2}} = \frac{F_{x1}}{K_{a1}} \quad \text{or} \quad s_{\delta a1} = s_{\delta a2} \tag{2.426}$$

It follows from this that in the case of a linear relationship between circumferential force F_x and slippage, the smallest power losses in the slippage of the wheel system will occur when the slippage of both axles will be the same, irrespective of the relationship between K_{a1} and K_{a2}. It can be concluded on this basis that the gear ratio of an interaxle differential should be regarded as optimal if it provides for equality of slippage of the front and rear wheels. For this, the optimal gear ratio of the differential should be equal to the ratio of K_{a2} and K_{a1} (see formula (2.424)).

Note that if under nonidentical gripping conditions of the axles (for example $K_{a1} < K_{a2}$), the gear ratio is made so that $u_d > \dfrac{K_{a2}}{K_{a1}}$, i.e., the circumferential force F_{x2} of the rear axle with good gripping conditions is increased even more by reducing the value of F_{x1} of the front axle. Then the slippage power losses increase just as in the case of $u_d < K_{a2}/K_{a1}$. The above is clearly illustrated in Figure 2.129.

Figure 2.129a shows the case when the interaxle differential distributes forces F_{x1} and F_{x2} in accordance with the gripping conditions represented by the values of K_{a1} and K_{a2} and provides for equality of the generalized slippages, $s_{\delta a1} = s_{\delta a2}$. In this case the gear ratio of the differential is optimal and equal to u_d^*. Figure 2.129b corresponds to $u_d = 1$: $F_{x1} = F_{x2}$ and $s_{\delta a1} \neq s_{\delta a2}$, since $K_{a1} \neq K_{a2}$. Finally Figure 2.129c shows the case when the front axle with good gripping conditions is loaded as so that $F_{x1} > F_{x2}$ and $s_{\delta a1} > s_{\delta a2}$. In all these three

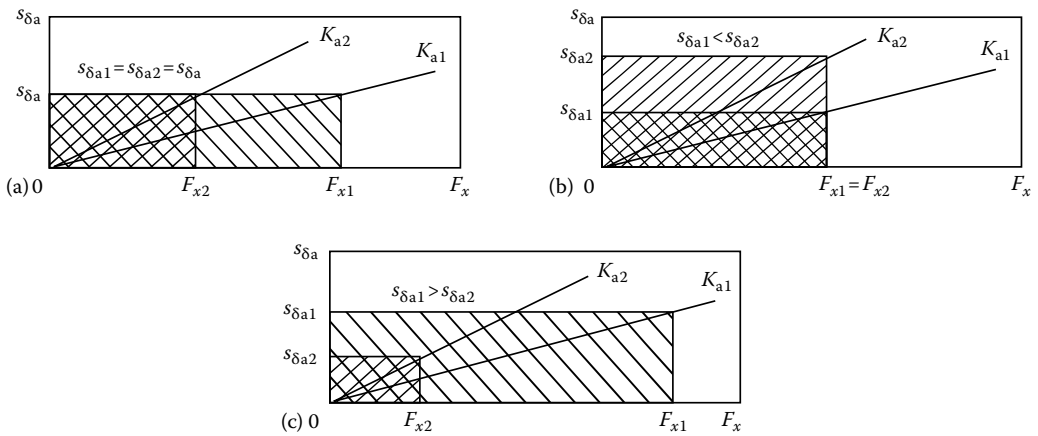


FIGURE 2.129
Slippage power analysis under different gripping conditions of the front and rear axles.

cases the shaded areas reflect at some scale the slippage power of the front and rear wheels (see shadings ▨ and ▨ for the front and rear axles, respectively). It can be easily seen that the sum of the two areas, $A = F_{x1}s_{\delta a1} + F_{x2}s_{\delta a2}$, i.e., the total slippage power $P_{\delta\Sigma}$ is at minimum in Figure 2.129a, which corresponds to equality of the generalized slippages of the front and rear axles, $s_{\delta a1}$ and $s_{\delta a2}$.

A quantitative assessment of the slippage power loss as a function of gripping conditions was obtained by calculations for a 4×4 tractor with a mass of 7.8 ton, identical wheels and symmetrical interaxle differential ($u_d = 1$). It was assumed that $F_{x2} = 30$ kN. The coefficient of longitudinal stiffness of the rear-axle tires was taken to be constant and equal to $K_{a2} = (5)10^2$ kN. The value of K_{a1} was assumed to decrease from $(5)10^2$ to $(1)10^2$ kN. The results of calculations are shown in Figure 2.130.

It is seen that the most economical mode corresponds to the case of

$$K_{a1} = K_{a2} = (5)10^2 \quad \text{and} \quad u_d^* = \frac{K_{a2}}{K_{a1}} = 1 \tag{2.427}$$

The tractive-velocity properties of the tractor in this case are also the best, since the slippage of the wheels of both axles is the same. When the numerical value of K_{a1} decreases (that is, when the gripping conditions of the front wheels become poorer), the circumferential forces of the axles remain equal to one another ($F_{x1} = F_{x2}$) as before (since the interaxle differential is symmetrical) and the slippage of the wheels of each of the axles is different. This mode is less economical; slippage power losses increase steeply with reduction in K_{a1}. There is no point to determine power $P_{\delta\Sigma}$ lost in slippage at $K_{a1} \to 0$ since in this case, the required circumferential force of $F_{x\Sigma} = 30$ kN will not be available and the tractor will stop. The theoretical minimal value of K_{a1} at which the force $F_{x\Sigma}$ is still available can be determined from expressions (2.415). At $u_d = 1$ and $s_{\delta a1} \to 1$ one can find

$$K_{a1} = \frac{F_{x\Sigma}}{2s_{\delta a1}} = \frac{F_{x\Sigma}}{2} \tag{2.428}$$

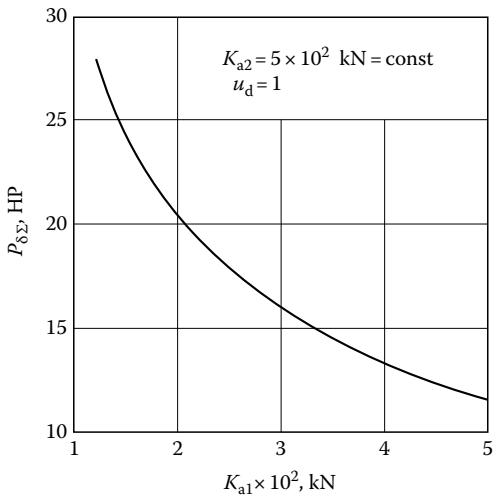


FIGURE 2.130
4×4 tractor: slippage power loss under different gripping conditions of the front and rear axles.

Since at low K_{a1} the generalized slippage, $s_{\delta a1} \to 1$, then the actual velocity of the tractor tends to zero, i.e.,

$$V_x = (V_{t1} - V_{\delta 1}) \to 0 \tag{2.429}$$

Still another important conclusion follows from formula (2.424) above: the optimum gear ratio of an interaxle differential is not equal to the reasonable gear ratio determined from the relationship of normal loads on the axles (see formula (2.404)). The method of determining u_d^* given above was implemented in mathematical models for determining the optimum distribution of power between the wheels of vehicles described in Section 6.6. These models incorporate probabilistic properties of roads: micro- and macro-profiles, rolling resistance factors, peak friction coefficients, and others. Consideration is also given to the distribution of the total mileage by kinds of roads and terrain. With consideration of these conditions and factors, the optimal gear ratios of interaxle differentials turn out to be higher than the values of reasonable gear ratios. As a study showed, a 4×4 SUV with a symmetrical interaxle differential and distribution of static normal loads between the axles under loaded conditions amounts to $u_w = 1.07$ should have an optimal gear ratio of $u_d^* = 1.30$ to 1.33. Some of the contemporary SUVs already have interaxle differential with gear ratios greater than the ratio of normal loads on the axles. As an example, one of them has a gear ratio of the interaxle differential equal to $u_d = \dfrac{T_2}{T_1} = 1.63$ and the ratio of the static normal loads of the axles $u_w = \dfrac{W_2}{W_1}$ is equal to unity (curb weight distribution) and 1.106 (gross weight distribution). The gear ratio of the interaxle differential of one of sports-type cars is $u_d = 1.86$.

The case of a truck is illustrated for a 4×4 vehicle with gross mass of 5.8 ton. The optimum gear ratio of its interaxle differential should be 1.5, whereas the distribution of weight on the axles is $u_w = \dfrac{W_2}{W_1} = 0.63$ (curb weight distribution) and $u_w = 1.13$ (gross weight distribution).

The use of differentials with optimal gear ratios makes it possible to improve the tractive performance of a vehicle by 20%–25% and to improve the energy efficiency, i.e., reduce the fuel consumption. Table 1.21 (see Section 1.4.3) has already presented data on the effect of the interaxle drive on the fuel consumption of a 4×4 timber-carrier truck. Here it can be additionally noted that similar results were obtained for a 4×4 truck with gross mass of 11.925 ton, made by the same company, in which the distribution of the curb and gross weight between the axles was respectively 0.88 and 1.67 for a gear ratio of the differential in the transfer case equal to 2.

It should be remembered in designing interaxle differentials with optimal gear ratios u_d^* that in this case the loads in the drive of the rear axle increase and that might have a negative effect on the service life of the driveline system components. Such a case was indeed encountered in our practice. The driveshafts and reduction gears of the front and rear axles were of a unified design in a 4×4 truck with a symmetrical interaxle differential. Then a higher-rating truck was designed based on this vehicle and the question arose of the need to use an asymmetrical differential with gear ratio of the order of two. The design work on the new differential, construction of experimental specimens and laboratory testing required a great deal of time. For this reason, the new machine with nonequal load on the different axles was designed with a symmetrical interaxle differential, the previously used driveshafts and reduction gears of the axles. This vehicle operated without

major problems since its operating conditions did not require a high tractive force. Only in individual cases, when the front wheel traveled on a slippery part of the road did they suffer from partial slippage. However, this shortcoming was eliminated by locking the interaxle differential.

Sometime later, a new differential specimen was manufactured and installed on this vehicle for operational testing. The splined end of the rear driveshaft broke down after the truck accumulated 13,500 km. The failure was fatigue induced. A new shaft was installed, but then the yoke of the joint of the new driveshaft broke after an additional 8,500 km of travel.

This situation was investigated and it was found that, whereas in the beginning the torques of the front and rear driveshafts were the same, the placement of the asymmetrical differential caused the operating moment of the rear-axle drive to increase by approximately 40% (because of a reduction in the moment of the front drive). This caused these fatigue failures. This example shows that the gear ratio of an interaxle differential should be selected not only upon consideration of the limiting traction force, but also with reference to the service-life conditions of the front and rear wheel drives.

It is rather obvious that the optimal gear ratio of a differential determined by averaging on the basis of modeling the behavior of a vehicle under different road and off-road conditions is only conditionally optimal, i.e., it is a trade-off kind of engineering solution, even though it is the best available. In fact, the optimum values of the gear ratios of interaxle differentials are different under different travel conditions. It is hence desirable to workout automatic systems for controlling these ratios. It will be demonstrated, as an illustration, how the gear ratio of an interaxle differential of a 4×4 tractor with a gross mass of 4.5 ton should vary. It is seen from Figure 2.117 that the maximum values of the efficiency η_x^t is provided by differentials with gear ratios that are different for different tractive loads, i.e., for different drawbar pulls F_d. If one selects from Figure 2.117 values of gear ratio of a differential corresponding to $\eta_x^t = \max$, then it is possible to construct the graph of $u_d^* = f(F_d)$ shown in Figure 2.131.

The curve in this figure shows how the differential gear ratio for the tractor should change with F_d. These data are fundamental for designing differentials with variable gear ratios and a system for controlling these ratios. Various approaches out to engineering implementation of this idea were worked. These approaches may or may not be related with the control of the driving-wheel torques. Two examples are now examined. Figure 2.132 shows a conceptual diagram of a 4×4 tractive vehicle with interaxle differential that allows smooth (step-less) automatic control of its gear ratio upon variation in F_d.

Housing 2 of planetary-type interaxle differential is connected to housing 1 of the transmission. This differential includes sun gear 3, connected by means of gears 4 and 5 to secondary shaft 6 of the transmission, connected to the final-drive pinion 8, and also crown gear 9, connected to shaft 10 of pump 11 of the hydraulic brake by means of gears 12 and 13. The third principal element of the differential consists of carrier 14, connected to the final drive pinion 15 of front axle 16 by means of shaft 17 and driveshaft 18. Hydraulic lift

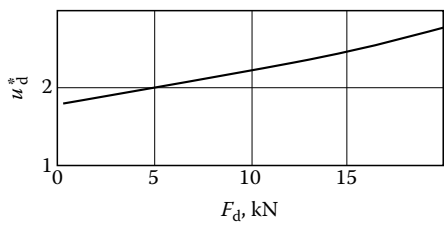


FIGURE 2.131
Optimal differential gear ratios.

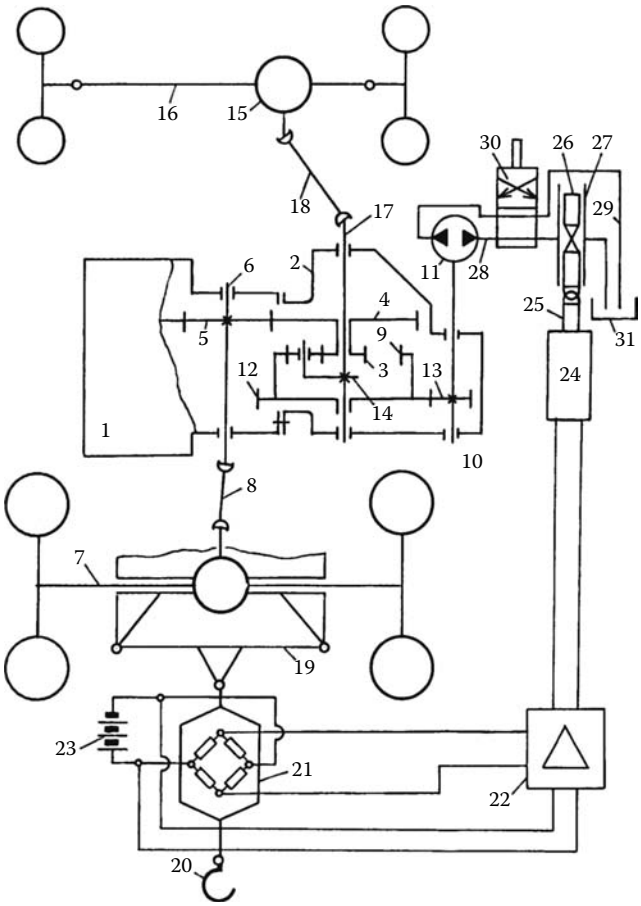


FIGURE 2.132
4 × 4 vehicle with a controlled interaxle differential.

linkage drawbar 19 is fastened to rear-axle housing 7. In this drawbar system 19 a drawbar load sensor 21 is placed ahead of hydraulic pick-up hitch 20. This sensor is electrically connected by means of amplifier 22 to power supply 23 and by way of electromagnet 24 that contains core 25 to slide valve 26 of the brake fluid control regulator 27. Hydraulic-brake pump 11 is connected by pressure 28 and suction 29 tubing through reversing slide valve 30 with hydraulic-fluid tank 31.

The drive operates as follows. Load on pick-up hitch 20 in the tractive mode ($F_d > 0$) causes redistribution of the weight between the driving axles in a manner that it increases on rear axle 7 and decreases on front axle 16. This decreases slippage $s_{\delta a2}$ of the rear wheels and increases slippage $s_{\delta a1}$ of the front wheels that increases the slippage power loss. In the case of deceleration ($F_d < 0$), conversely, $s_{\delta a2}$ increases while $s_{\delta a1}$ decreases. This drive controls the slippage of driving-axle wheels by utilizing the ability of the planetary-type interaxle differential to change its gear ratio in proportion to changes in the rotational frequency of crown gear 9, which is brought about by braking of the latter by hydraulic-brake pump 11. In this case, the torque is transmitted from the engine to gear 5 of secondary shaft 6 of the transmission and sun gear 3, where it is split into two flows. The first flow is directed to carrier 14 and then through driveshaft 18 and final drive 15 to front wheels 16. The second flow is directed through crown gear 9 to the drive of hydraulic-brake pump 11. This pump rotates, sucks in the working fluid from tank 31

and transmits it through reversing slide valve 30 along pressure tubing 28 to flow regulator 27, which, at a certain position of slide valve 26, produces a constant fluid-draining flow rate. Here pump 11 and gear 13 connected to its shaft rotate at constant speed that is determined by the flow rate preset by the flow regulator, and the ratio between the slippages of the two driving axles is determined by the position of slide valve 26. Simultaneously the load on drawbar 20 causes an electrical signal, proportional to the magnitude and direction of the force to appear on strain gage 21. The signal is amplified in electrical amplifier 22 and is transmitted to electromagnetic relay 24 with core 25 connected to slide valve 26 of the hydraulic brake flow regulator. At $F_d > 0$ (tractive mode) core 25 opens slide valve 26 and slows down the rotation of carrier 14 and driveshaft 18. At $F_d < 0$ (braking mode) core 25 covers slide valve 26 and slows down the rotation of crown gear 9 up to a complete stop. Then the rotational speed of carrier 14 and of driveshaft 18 connected to it increase. When driving in reverse, the change in direction of rotation of pump 11 requires switching its intake 29 and pressure 28 lines. This is accomplished by reversing slide valve 30 that causes hydraulic-brake flow regulator 27 to be continuously connected to pressure line 28. Calibrating strain gage pickup 21 as a function of the magnitude and direction of force F_d provides for automatic step less adjustment of the optimal ratio of slippage of both driving axles.

Another, ''indirect'' method for providing a ratio between the slippages of two driving axles corresponding to the minimum possible slippage power losses of a 4×4 vehicle is the possibility of adjusting (changing) the weight loads on the driving axles as a function of force F_d at constant interaxle differential gear ratio. Figure 2.133 shows a conceptual diagram of a 4×4 tractor with an interaxle differential.

Driving axles 1 and 2, connected by interaxle differential 4 are fastened on main frame 3. Frame 3 has guides 5 in which is installed additional frame 6 with power unit 7 that is coupled to main frame 3 by hydraulic cylinder 8. Power unit 7 is coupled to interaxle differential 4 by spline shaft 9. Hydraulic cylinder 8 is connected to pressure source 10 and

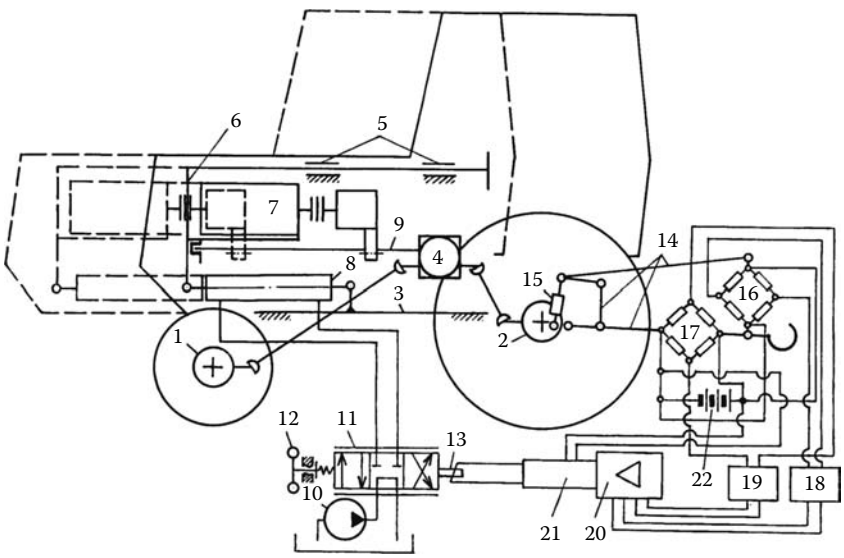


FIGURE 2.133
4×4 tractor with controlled weight distribution.

to the drain by means of a controllable slide valve 11 that is equipped with manual control 12 and electromagnet 13. Pull rods 14 of the lift linkage drawbar system, that are controlled by power cylinder 15 are fastened on main frame 3. Pickups 16 and 17 of the vertical and horizontal components of the drawbar pull are placed on pull rods 14. The outputs of these two pickups are connected through scaling resistors 18 and 19 to the input of summator 20, the outputs of which are connected through amplifier 21 to power supply 22. When the lift linkage drawbar system is not under load, additional frame 6 with power unit 7 is situated relative to main frame 3 in a manner that ensures equality of slippage of the front and rear wheels. When the lift linkage drawbar system is loaded by farm machinery that is being operated by the tractor, vertical and horizontal components of the drawbar pull arise in pull rods 14. These forces disturb the optimum distribution of weight over the driving axles of the 4×4 tractor and increase the total power lost in slippage. The effort exerted by the drawbar pull on sensors 16 and 17 causes the latter to generate electrical signals that are fed through scaling resistances 18 and 19 to summator 20. These resistances are needed because the vertical and horizontal components of the drawbar pull have a different effect on the redistribution of the weight loads over the driving axles of the 4×4 tractor. After summator 20 the signal is amplified in amplifier 21 and is fed to electromagnet 13 of slide valve 11. The latter produces a pressure in the pertinent cavity of hydraulic cylinder 8 that is proportional to the magnitude of the signal. The hydraulic cylinder then moves additional frame 6 over the distance needed for ensuring automatic, step-less redistribution of the weight loads on the driving axles of the 4×4 tractor that corresponds to the minimum possible slippage power losses. Manual control 12 is needed for correcting the initial position of additional frame 6, for example, when applying additional weights, when operating on different soil backgrounds or when the driving wheels of the tractor are not of the same size.

The data analyzed above on the optimum gear ratio u_{d}^{*} of the differential and controlling it are based on the theoretical principle of ensuring the minimum slippage power loss. Certain vehicles typically travel under conditions when it is necessary to ensure the maximum possible circumferential force $F_{x\Sigma}$ and not the minimum power losses. For example, to ensure mobility of terrain vehicles, including those used by the military, under extremum conditions, it is necessary to develop the maximum possible force $F_{x\Sigma}$ without regard for the higher fuel consumption. In accelerating of certain road vehicles, it is also necessary to exert a large force $F_{x\Sigma}$ in order to overcome the inertia of the translational and rotational masses of the vehicle (see formula (1.74)). It therefore makes sense to determine the extremum gear ratios $u_{\mathrm{d}}^{\mathrm{e}}$ of the interaxle differential that corresponds to the maximum circumferential force $F_{x\Sigma}^{\max}$ of a vehicle under road and terrain conditions. For all-wheel drive vehicles the numerical value of $F_{x\Sigma}^{\max}$ is determined not only by the tire-to-surface gripping factor, but also by the interaxle differential gear ratio. To illustrate this, consider the graphs in Figures 2.134 and 2.135 constructed for two 4×4 tractors with different front and rear wheels moving over a field in a straight line.

The graphs were constructed as a function of circumferential force $F_{x\Sigma}$ for three values of the interaxle differential gear ratio, 1, 2, and 5.

It is seen from Figures 2.134 and 2.135 that the circumferential forces F_{x1} and F_{x2} of the axles are determined both by the magnitude of force $F_{x\Sigma}$ and by the gear ratio u_{d} of the interaxle differential. Forces F_{x1} and F_{x2} naturally increase with increasing $F_{x\Sigma}$. Here at $u_{\mathrm{d}} = 1$, the traction load on the front axle increases more intensively, whereas at $u_{\mathrm{d}} > 1$ the traction load on the rear axle increases at a higher rate. Generalized slippages $s_{\delta a1}$ and $s_{\delta a2}$ increase with increasing $F_{x\Sigma}$ in accordance with exponential relationship (1.30). At elevated values of $F_{x\Sigma}$ that may be caused by increasing F_{d} (or inertia force F_{a}), generalized slippage

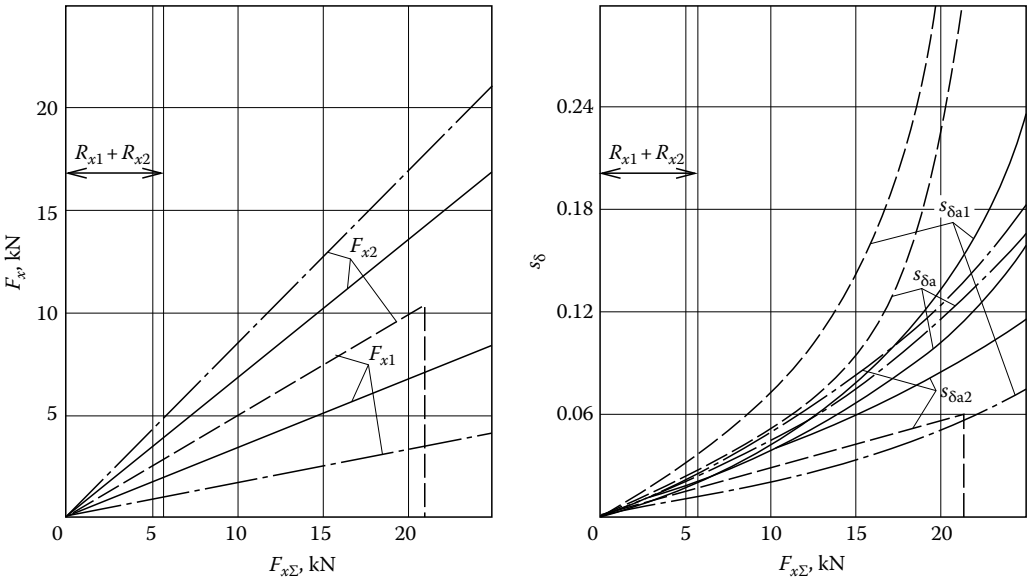


FIGURE 2.134
4 × 4 tractor of 5.6 ton: —— —— $u_d = 1$; ——— $u_d = 2$; —·— $u_d = 5$.

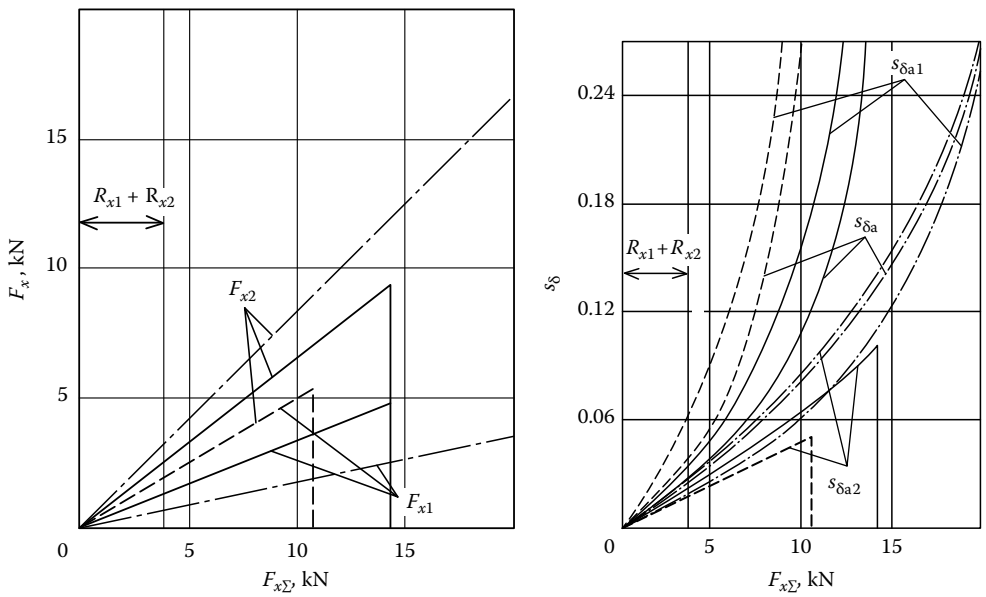


FIGURE 2.135
4 × 4 tractor of 3.7 ton: —— —— $u_d = 1$; ——— $u_d = 2$; —·— $u_d = 5$.

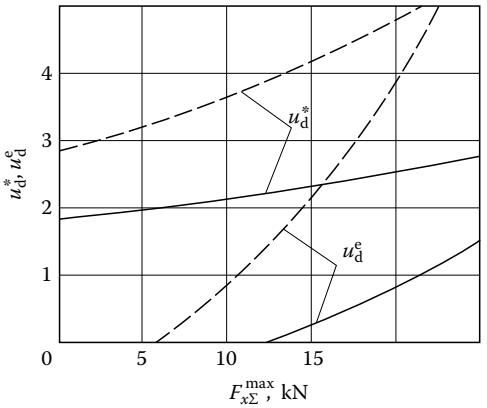


FIGURE 2.136
Characteristics of interaxle differentials: —— —— 4 × 4 tractor of 3.7 ton; ——— 4 × 4 tractor of 5.6 ton.

$s_{\delta a1}$ of front axle and generalized slippage $s_{\delta a}$ of the tractor as a whole increase markedly due to the removal of weight from the front wheels. At some value of $F_{x\Sigma}^{max}$ the front wheels slip completely and the rear wheels stop entirely ($s_{\delta a2} = 0$). Further travel becomes impossible. It may be said that under these conditions the vehicle reaches the limit of its mobility. For example, for a 5.6 ton 4 × 4 tractor from Figure 2.134 this takes place at $F_{x\Sigma}^{max} = 21.22$ kN, in the case when a symmetrical interaxle differential with $u_d^e = 1$ is used. For a 3.7 ton 4 × 4 tractor from Figure 2.135 the mobility limit is attained not only at $u_d^e = 1$, but also at $u_d^e = 2$. The limiting value of $F_{x\Sigma}^{max}$ at $u_d^e = 2$ is 14.37 kN.

Mobility limits of these tractors at u_d^e in the [0, ∞] range were established by similar calculations. The results of these calculations are plotted in Figure 2.136.

The extreme points of the graphs of $u_d^e = 0$ and $u_d^e = \infty$ represent modes when the front and rear axles, respectively, are the driving axles. The maximum possible force $F_{x\Sigma}^{max}$ increases with increasing u_d^e. These values of $F_{x\Sigma}^{max}$ are attained at values of u_d^e at which the distribution of $F_{x\Sigma}^{max}$ among the axles corresponds to such forces F_{x1} and F_{x2} that cause simultaneously the slippage of the wheels of both axles. Further increase in u_d reduces $F_{x\Sigma}^{max}$. In these cases the mobility limit is attained due to complete slippage of the rear wheels that become overloaded by high forces F_{x2} at elevated values of u_d^e.

The extremum values of ratios u_d^e as a function of $F_{x\Sigma}^{max}$ are plotted in Figure 2.136. The same figure also presents optimal values of u_d^* corresponding to maximum values of efficiency η_x^t of the running gears of the tractors (one of the curves of u_d^* is shown by a solid line, taken from Figure 2.131). It is seen from comparing the curves that the manner in which the gear ratios of interaxle differentials should be different upon changes in the total circumferential force of the vehicle. Selection of a given behavior of u_d depends on the goal to be achieved: providing maximum energy efficiency or the maximum possible circumferential force $F_{x\Sigma}^{max}$.

3

Automatic and Manual Positively Engaged Power-Dividing Units

3.1 Designs of Power-Dividing Units

Locked up power-dividing units, or positively engaged PDUs, provide for identical angular velocities of the wheels that they connect, or a constant ratio of angular velocities, independently of the conditions of the vehicle's motion. Automatic power-dividing units may control the ratio of angular velocities. A classification of positively locking drives of wheels and driving axles was provided in Figure 1.33. Consider now certain typical designs of such drives.

A classical example of an interwheel positive engagement may consist of the locked differential of the driving axle. Irrespective of whether the axle moves in a straight or a curved path, the angular velocities of the left and right wheels will always be the same. If a free-running differential was installed in the driving axle (for more detail on such differentials see Chapter 5), then the axle's wheels would rigidly be coupled to one another, that is, they would rotate at the same angular velocities. When the vehicle takes a turn, the free-running differential may disengage the overtaking wheel and the entire power will then be transmitted to the lagging wheel. Both examples pertain to a part-time locked drive. It should be emphasized that a full-time locked interwheel drive is not used in ordinary vehicles because the difference between the paths traveled by the wheels when making a turn is extremely different; this will cause the wheels to slip and skid relative to the road. As a rule, a locking positive interwheel drive is also not used on off-road vehicles. Even if the tires have a high tangential flexibility, their slip, particularly when taking a turn, may cause damage (break) of the grass layer, sinking of wheels into the soil, and loss of mobility.

The full-time locked drive is used in multiwheel drive vehicles as the interaxle drive of the driving tandems. Figure 1.40 shows the kinematic layout of a 12×12 vehicle with a full-time positive engagement of three axles of the rear tandem and full-time locked interaxle drive between the second and third axles. Figure 3.1 shows a design example of a full-time positive engagement of two tandem axles.

If a free-running differential is installed between two of the tandem's axles, then this results in a part-time positive engagement drive, since such a differential is capable of automatic disengagement of the overtaking axle (Figure 3.2).

The part-time positive engagement drive is extensively used in 4×4 vehicles in which one of the driving axles may be engaged and disengaged manually (see Table 1.10, items 1 and 2) and automatically (Table 1.10, items 3, 6, and 7). Several more examples are given in Tables 1.11, 1.12, and 1.14. Figure 3.3 shows kinematic layouts of transfer cases that

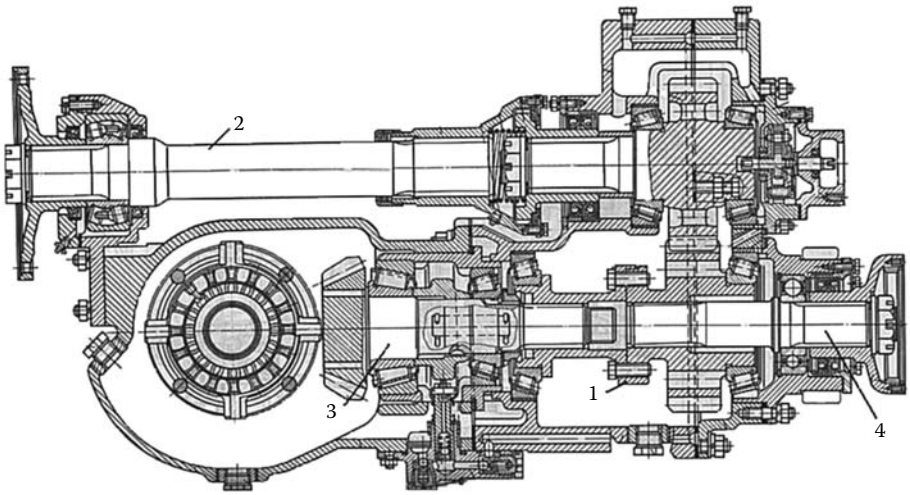


FIGURE 3.1
Interaxle drive of a tandem: 1, positively locked PDU; 2, input shaft; 3 and 4, output shafts.

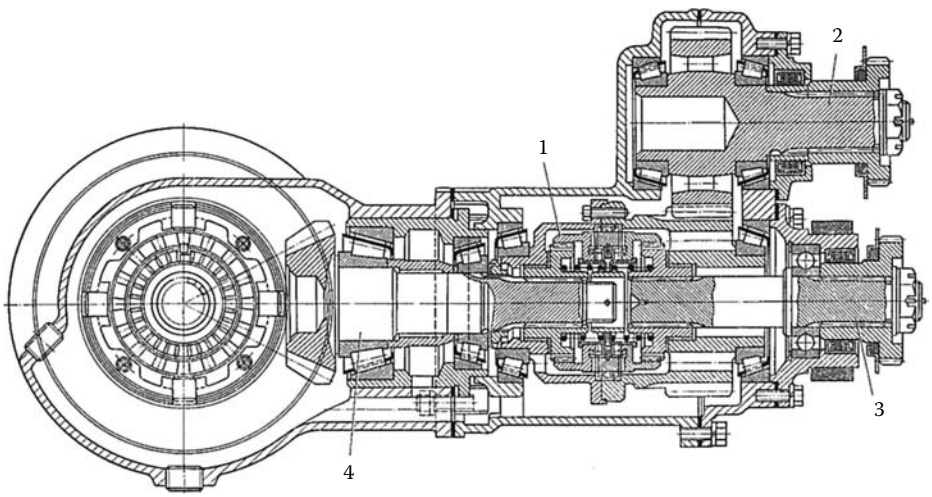


FIGURE 3.2
Interaxle drive of a tandem: 1, free-running differential; 2, input shaft; 3 and 4, output shafts.

provide for engagement/disengagement of the front axle while the power is supplied without interruption to the rear axle.

Rotation is continuously transmitted from input shaft 1 to shaft 2 of the rear axle drive. The output shafts of rear axle drive 2 and of the front axle drive 3 are not coaxial. The front axle is supplied with power from shaft 3, upon engagement of clutch 4. Figure 3.4 shows an example of a design of a transfer case, in which the front axle driven by shaft 1 is engaged simultaneously with the engagement of the lower stage by means of clutch 2.

Transfer cases designed as shown in Figure 3.5 differ from those shown in Figure 3.3 by the absence of direct transmission (the input shaft is not coaxial with any of the output shafts 2 and 3).

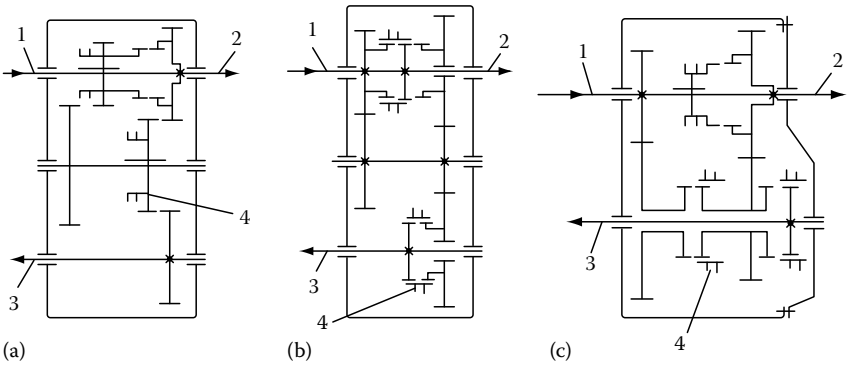


FIGURE 3.3
Kinematic layouts of transfer cases: 1, input shaft; 2, shaft of the rear axle drive; 3, shaft of the front axle drive; 4, clutch.

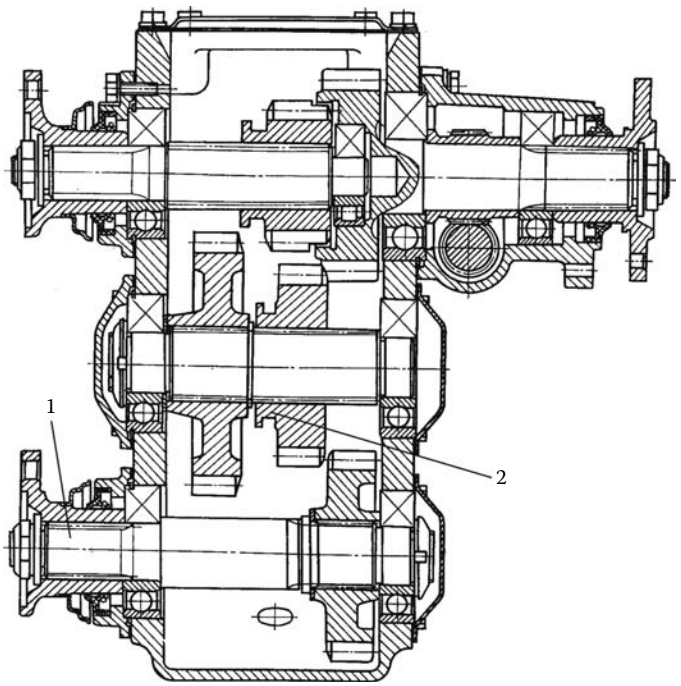


FIGURE 3.4
Transfer case: 1, shaft connected with the front axle drive; 2, clutch.

In layouts a and b, the front axle is engaged/disengaged by the driver by means of clutches 4. In layouts c and d, the front axle is engaged/disengaged automatically by means of free-wheel clutch 5 (which is also known as the free-running clutch) or free-running differential 5, respectively. The difference in principle between the transfer case designs shown in Figures 3.3 and 3.5 from the point of view of power consumption will be referred to in Section 3.3.1 when explaining the course of circulation of parasitic power in a positive engagement drive.

As a result of disengagement of one of the axles by means of the transfer case, the part of the driveline system that is disconnected from the power transmission remains connected to the wheels of the disengaged axle. These wheels are driven by the force applied to their

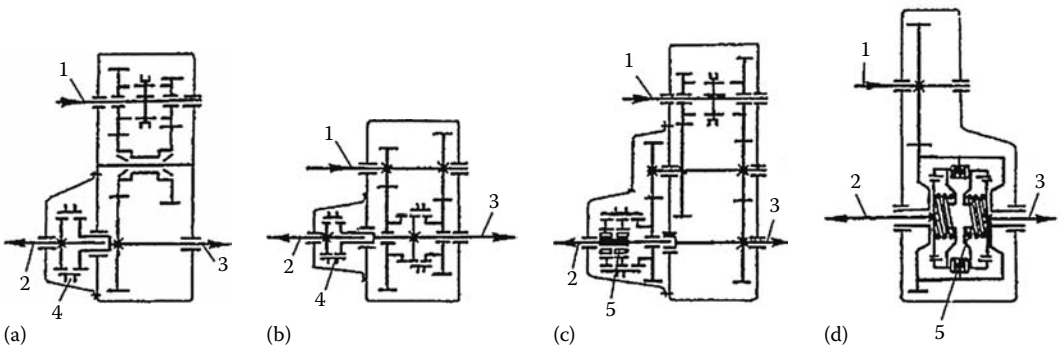


FIGURE 3.5
Kinematic layouts of transfer cases: 1, input shaft; 2, shaft of the front axle drive; 3, shaft of the rear axle drive; 4, clutch; 5, free-running clutch.

axle by the vehicle's body (in Figure 1.44 these wheels are those of the rear axle). The disconnected part of the drive increases, by virtue of its friction, the resistance to rolling of the wheels of the disengaged axle. This has given rise to the so-called disconnect devices and systems that are used: (i) either for disconnecting the half axles of the driving axle, or (ii) for disconnecting the wheels of the driving axle from the half axles (see Figure 3.6a and b).

The first such devices were mechanical and the wheels were disconnected manually with the vehicle stopped. Modern designs are capable of functioning, up to a certain vehicle velocity; they have remote control, for example, pneumatic, that disengages the gear-type clutch halves installed on wheel hubs of a given axle simultaneously upon disengagement of this axle in the transfer case (Figure 3.6c). Certain gear-type clutch halves of disengaging devices are used as locking devices of differentials (Section 2.7). Free-running clutches were mentioned in Section 1.1, whereas the kinematic layout of a 4×4 vehicle, in which the front axle is engaged by such a clutch, was shown as G in Figure 1.37. The use of free-running clutches as power transfer units in front-axle drives makes possible automatic engagement/disengagement of this axle in the following manner. When power is transmitted only to the rear wheels, ring 1 that is set into rotation by the front wheels, that are still not connected to the drive, but receive their rotation from the road, rotates at higher angular velocity than ring 2 that is set into rotation by the vehicle's engine (see Figure 3.7).

Differences in angular velocities are provided by introducing kinematic discrepancy (see Section 3.2). When the slip of the rear wheels is increased, the vehicle slows down and consequently, the speed of rotation of ring 1 decreases. At the instant when the speeds of rotation of rings 1 and 2 become identical, rollers 3 become wedged in between the rings and torque starts being transmitted to the front axle. Gear-type clutch 4 can be used for positively engaging the front axle bypassing the free-running clutch.

In order to attain the same front-axle operating modes when the vehicle is moving in reverse, use is made of two roller-type clutches 1 and 2 (Figure 3.8): one for forward and the other for reverse motion. Either of the clutches is engaged by means of a system of levers and links from the gearshift stick that switches from forward and reverse motion.

In order to provide for stable operation of free-running clutches, arrangements must be made to have rings 1 and 2 in Figure 3.7 rotate at different velocities under conditions of identical wheel gripping. For this the wheel drive is designed with design kinematic discrepancy (see Section 3.2), which reduces the fuel efficiency of the vehicle (see Section 3.4.1). To resolve this difficulty, an attempt was made to design a system of automatic

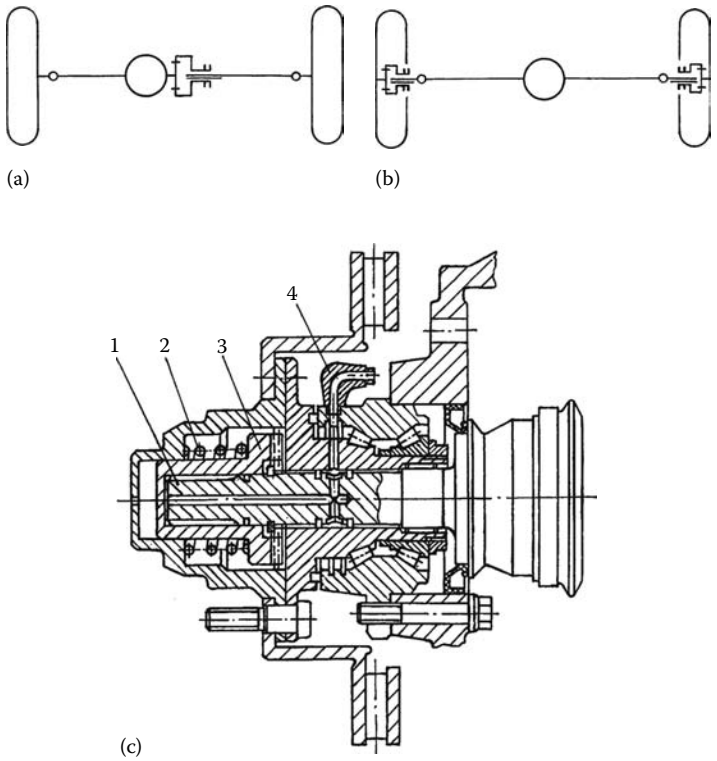


FIGURE 3.6
Layouts and design of disconnect devices: 1, half-axle; 2, spring; 3, half-coupling/cylinder; 4, pipe connection.

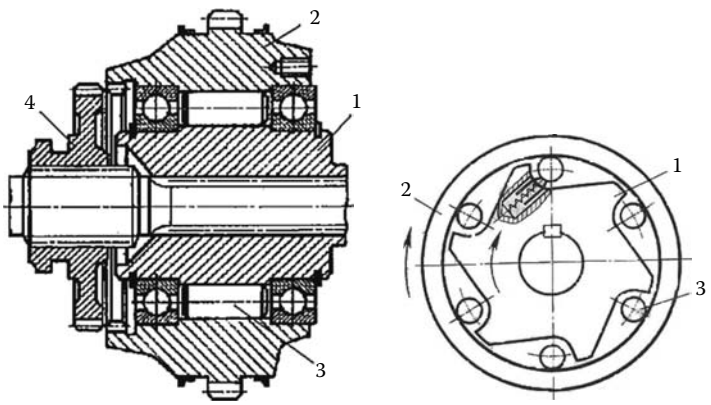


FIGURE 3.7
Free-running clutch.

engagement of the additional axle without introducing kinematic discrepancy. One such design is shown in Figure 3.9.

The vehicle's rear wheels are directly coupled to the engine, whereas the front axle is engaged by means of gear 1 that is rotated by the output shaft of the transmission, friction clutch 2 and shaft 3 of the front axle drive. Clutch 2 is loaded by spring 4, for which reason

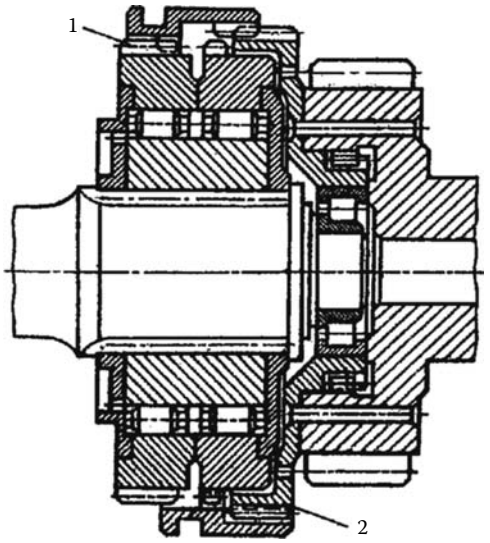


FIGURE 3.8
Double free-running clutch: 1 and 2, roller-type clutches.

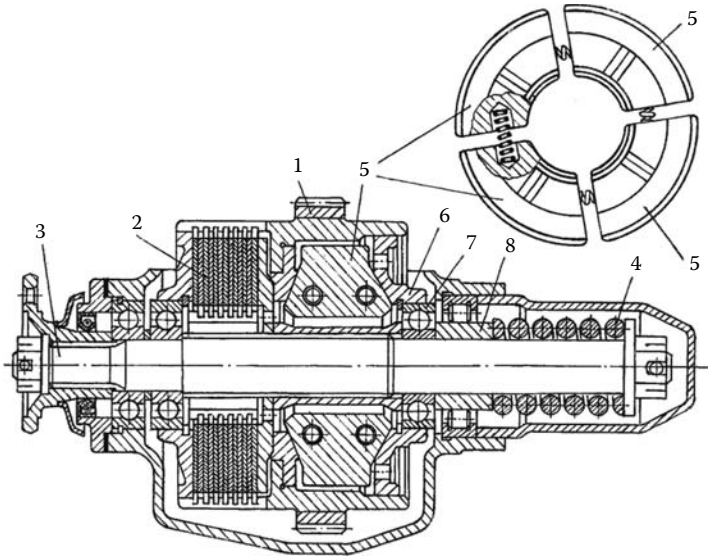


FIGURE 3.9
System of automatic engagement of the additional axle: 1, input shaft; 2, fruction clutch; 3, shaft connected with the front axle drive; 4, spring; 5, weight; 6, movable disk; 7, bearing; 8, bushing.

torque, known as drag torque that corresponds to the spring compression force, is transmitted to the front axle. When the slip of the rear wheels increases and with it the rotational speed of the housing of friction clutch 2, the centrifugal force of weights 5 increases. This force is taken up by movable disk 6 and is transmitted by means of bearings 7 to bushing 8. This causes additional compression of the disks of clutch 2 and the transmission of a greater torque to the front wheels. Note that the operation of the clutch does not require kinematic discrepancy. Preloading of clutch 2 by spring 4 will cause a constant small torque to be transmitted to the front axle. This smoothes the impact loads typical of certain designs at the instant of axle engagement.

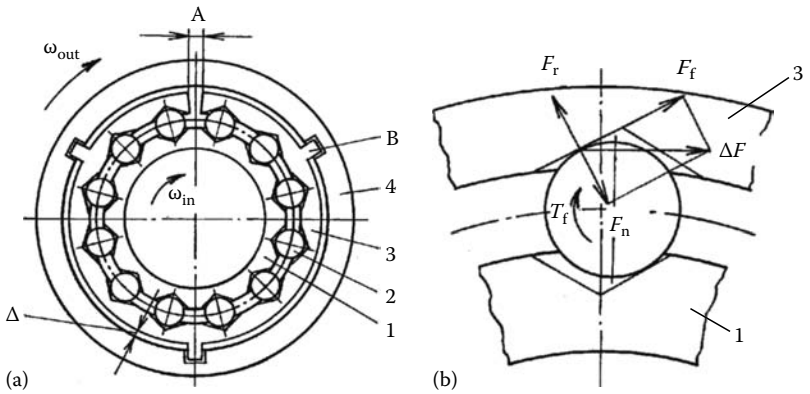


FIGURE 3.10
System of automatic engagement of the additional axle: 1, sprocket; 2, roller; 3, spring bushing; 4, ring; Δ, clearance; A, radial section; B, slit.

Figure 3.10 shows the layout of an automatic clutch for engaging an additional axle, which does not have a preliminary drag torque (similar to Bartus, 2006).

The clutch consists of sprocket 1 with V-shaped grooves and also slit spring bushing 3 with radial section A and grooves of the same shape as in the sprocket on its inner surface in order to receive rollers 2 and outer ring 4. Clearance Δ is provided between the outer surface of the slit spring bushing 3 and the inner surface of the ring 4. At the same time, the slit spring bushing is coupled to the ring by means of projections and slits B. Sprocket 1 is rigidly coupled to the drive (input) shaft, whereas ring 4 is rigidly coupled to the output shaft, which is further connected to the engaged wheel (or wheels) of the axle being engaged. The clutch operates as follows. The position of all the components in Figure 3.10a corresponds to $\omega_{out} = \omega_{in}$. When $\omega_{out} = \omega_{in}$ does not hold, that is, when there appears a difference ΔF between the circumferential forces acting on bushing 3 and on sprocket 1 and the relative motion between sprocket 1 and ring 4, rollers 2 take the position shown in Figure 3.10b. This figure shows normal forces F_n and F_r acting on the bushing 3 and the roller and also the friction force, F_f, of the roller. The friction torque, T_f, causes the roller to move. Slit spring bushing 3 then spreads and takes up the clearance Δ. There is some immediate friction between the inner surface of ring 4 and the outer surface of bushing 3. This friction causes the locking of the following elements: the input shaft, sprocket 1, rollers 2, slit spring bushing 3, ring 4, the output shaft.

All this causes the transmission of torque from the input shaft to the output shaft and from there to the wheel (or wheels) of the axle being engaged. Complete disengagement of the wheel (axle) occurs when the equality $\omega_{out} = \omega_{in}$ is restored, since no kinematic discrepancy was built into the design. The theoretical principles explaining the operation of such devices are provided in Sections 3.2 and 3.3.

Referring to the mechanical devices described earlier it is easy to understand the functional intent and operation of a wide class of electromechanical systems that are known as on-demand systems. Figure 3.11 shows an example of such a system described by Asgari and Hrovat (1997). The system ensures automatic engagement/disengagement of the front axle of a vehicle when its rear wheels are permanently coupled to the transmission.

This device, as those analyzed previously, couples the front axle when the rear wheels skid and actually when a difference arises between the velocities of driveshafts of the drive of the front and rear axles.

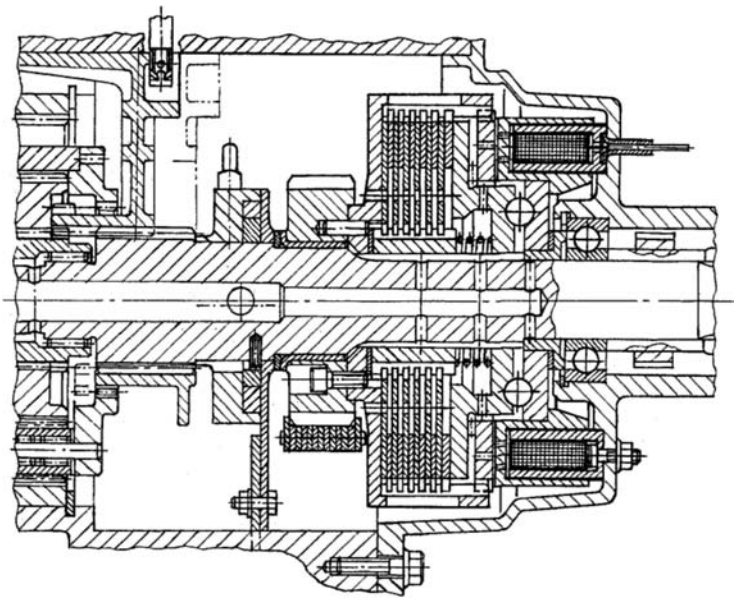


FIGURE 3.11
On-demand system.

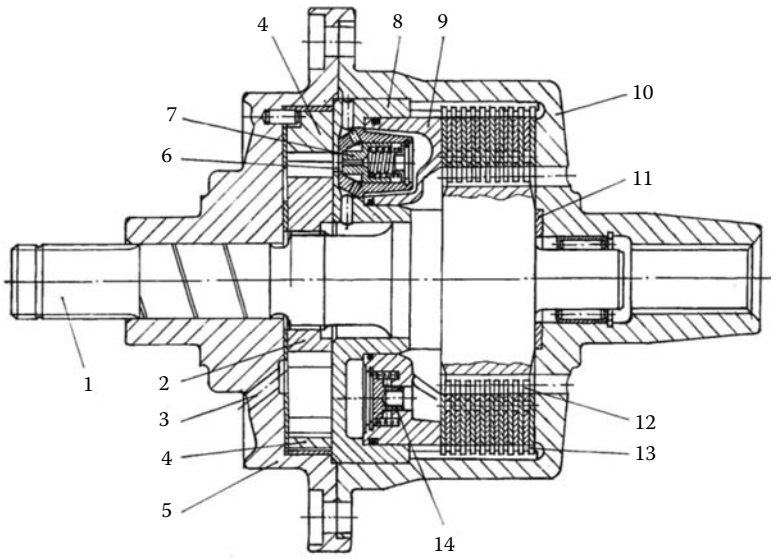


FIGURE 3.12
On-demand system, AutoRevyu (2006): 1, front axle drive; 2, pump rotor; 3, intake channel; 4, pump stator; 5, pump; 6, pressure channel; 7, reduction valve; 8, cylinder; 9, piston; 10, clutch housing; 11, thrust washer; 12, driven discs; 13, driving discs; 14, control valve.

Figure 3.12 shows a later design of an automatic clutch for engaging the front axle (the rear-driving axle is the primary moving mechanism).

In order to engage the front axle, that is, to transmit power to the front wheels, the drive's friction clutch must be locked. This is done using a gerotor pump. Rotor 2 of the pump is

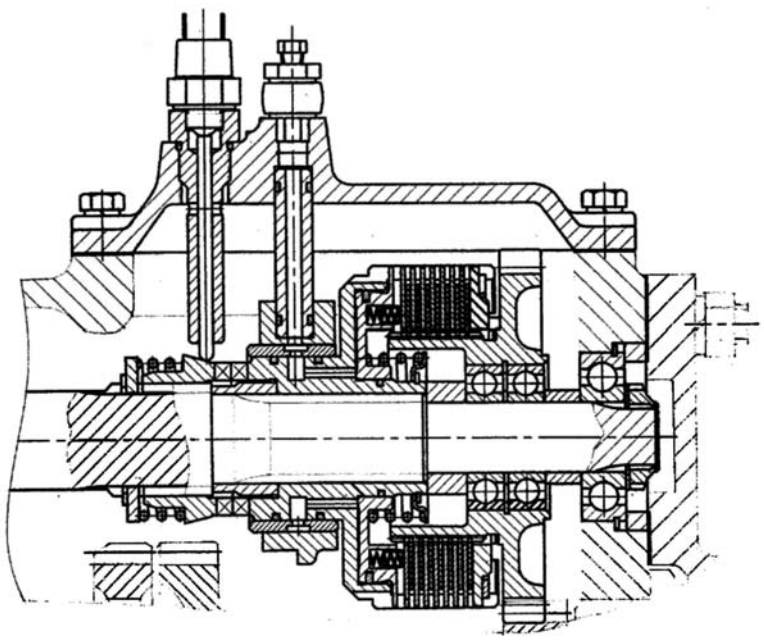


FIGURE 3.13
On-demand system.

connected to the front axle drive shaft 1, whereas stator 4 is connected to its housing, which is rotated by the transmission. When a difference arises between the rotations of the shaft and the housing of the clutch, the pump forces oil into cylinder 8 through channel 6. This produces in the cylinder a pressure that is controlled by reduction valve 7 and control valve 14. This pressure forces piston 9 to compress driving 13 and driven 12 disks, thus locking the shaft to the housing and then the clutch operates as a rigid link. All this engages the front axle.

Figure 3.13 shows the hydraulic clutch for engaging the additional axle. The clutch locks the front axle of a vehicle if there is a difference in the rotational speed of the input and output shafts. The difference in speeds is detected by an angular velocity sensor.

Work done to design all-wheel drive vehicles based on front-drive vehicle designs has resulted in the appearance of an entire class of power transfer units, meaning clutches for engaging the rear axle. However, conceptually they are based on the same design idea consisting of engaging the rear axle when the front wheel slip increases. Some manufacturing companies declare an improvement the in handling of vehicles when using such clutches for engaging the rear axle. The elevated slip of the front wheels is detected, as a rule, by measuring the difference in the angular velocities of the front and rear wheels. These systems usually make use of signals of other sensors: engine speed, longitudinal and lateral acceleration, vehicle speed, angle of the steering wheel, etc. The signals of the above sensors serve to control the torque transmitted to the rear wheels. One such design developed by Borg Warner is shown in Figure 3.14 (Alexander, 2005).

The presence in such systems of an electromagnetic solenoid, of elements that are movable in the axial direction, of a ball-ramp system and friction disks, points to the conceptual similarity of the systems. Their technical improvement consists in reducing internal power losses and power lost in driving the locking disks, including the reduction of the drag torque, and in developing advanced control algorithms.

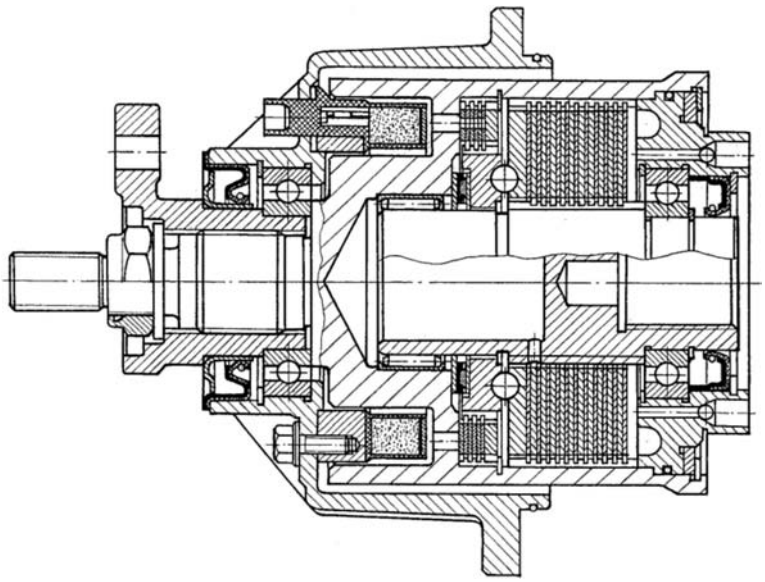


FIGURE 3.14
Power transfer unit.

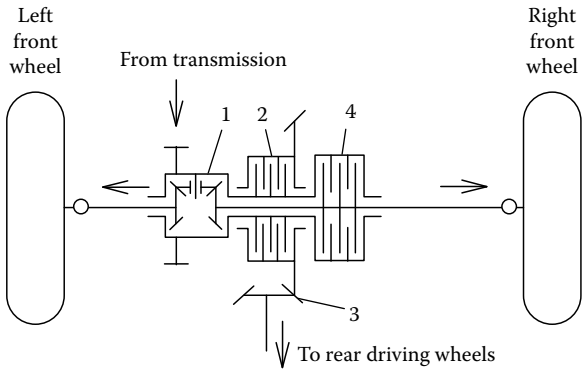


FIGURE 3.15
Layout of a 4 × 4 system: 1, front axle differential; 2 and 4, clutches; 3, final drive.

Controlled clutches that are not located in the transfer case, but in the case of the front axle started appearing relatively recently. Figure 3.15 shows the layout of one such drive.

Power is constantly supplied to differential 1 of the front axle from the transmission. When clutch 2, is partially or fully engaged, the power is transmitted through final drive 3 to the rear-axle wheels and clutch 4 can be used for locking differential 1.

In the layout of the drive shown in Figure 3.16 power is transmitted from the transmission to the rear wheels by final drive 1.

Clutches 2 and 3 can be used for distributing the power between the left and right wheels of the front, steered axle, of the vehicle: from complete disengagement of the front wheels to complete locking of the interwheel drive. However, it must be remembered here that this is accompanied by redistribution of power between the front and rear axles, since the interaxle drive is locked up.

It can be observed that many designs contain ball-ramp devices that are also used in friction safety clutches. It is of interest to analyze certain specifics of designing these

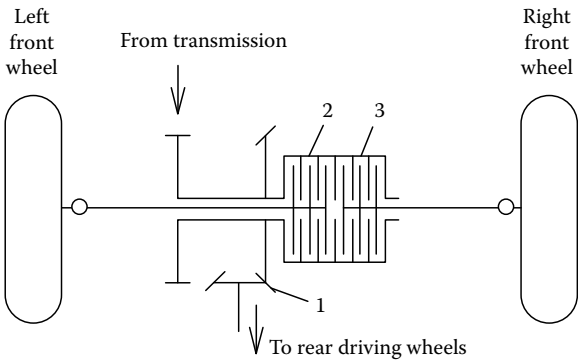


FIGURE 3.16
Layout of a 4 × 4 system: 1, final drive; 2, 3, clutches.

devices. The design shown in Figure 3.17a consists of driving disk clutch A and locking clutch B, pressure disks 1 and 2, and ball-type locking device 3 that is comprised of at least three angular grooves, that is, two sided ''tears'' 4 on both pressure disks with balls on them.

All these components are located in an oil-filled housing. The housing is rigidly coupled to shaft 1. Disk clutches A and B are connected to one of the ends of the housing by means of splines. Driving clutch A is connected to pressure disk 1, and locking clutch B to shaft II, also by splines, to its other end. The coupling of both pressure disks 1 and 2 to shaft II is free.

A control signal to engage an additional axle is the electromagnetic induction force F_i. When shaft I rotates without the control signal ($F_i = 0$), the disks of both clutches and both pressure disks are rotated by virtue of the circumferential forces of viscous friction. Since the pressure disks are free of other connections, they are acted upon only by viscous friction forces F_1 and F_2 (see Figure 3.17). These forces are equal to one another ($F_1 = F_2$)

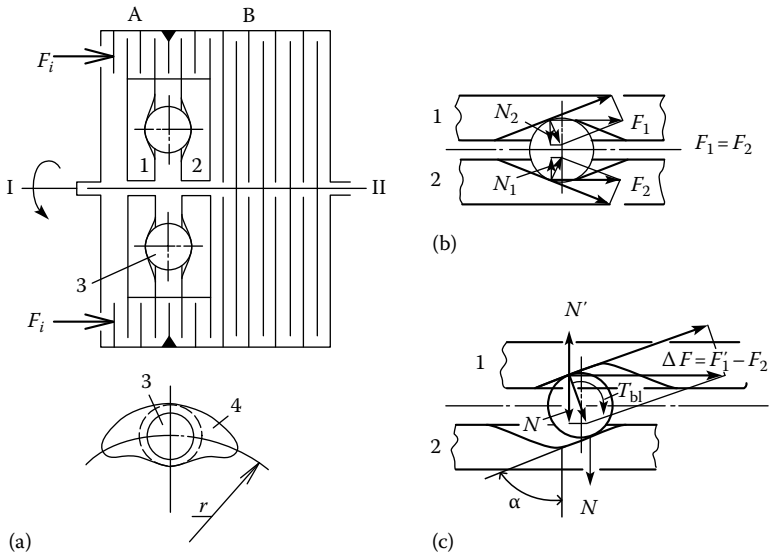


FIGURE 3.17
Coupling: 1, 2, pressure disks; 3, ball-type locking device; 4, angular groove; A, driving disk clutch; B, locking clutch.

and their components directed normal to the surface of balls are also equal. In view of this, the forces directed normal to the surfaces of the pressure disks are also equal, that is, $N_1 = N_2$. In this case, the latter are directed one against the other and this means that they press the pressure disks to the balls and the disks of the locking clutch do not operate under power. The situation is entirely different when the control signal, that is, the force F_i, appears. It activates control clutch A, which locks pressure disk 1 to the housing. Then the circumferential force of disk 1 becomes higher than F_1 and attains some value F_1'. This causes the appearance of a difference between the circumferential forces at the disks amounting to $\Delta F = F_1' - F_2$ (see Figure 3.17c). The component of this difference that is normal to the surface of pressure disks forms pressure force N normal to this surface and its reaction N'. After a plane-parallel transfer from disk 1 and application of force N to disk 2 there form forces that spread the pressure disks and the torque T_{bl}. The torque rotates the balls that roll over the surfaces of the ''tear'' grooves and spread pressure disks 1 and 2 by forces N' and N. In the course of being spread the pressure disks compress the disks of clutch B and thus lock the housing to shaft II, that is, shaft I to shaft II.

Note that the condition for the operation of a ball-type control device of a clutch is the adaptive property of the clutch that consists in self-regulation of the friction moment from its friction unit. The self-regulation property of the friction unit of this clutch depends on the load applied to it, the actual friction coefficient and the design parameter

$$C_V = r_M \tan\alpha / r \tag{3.1}$$

where

r_M is the average radius of the disks of the control clutch
r is the radius of location of the balls relative to the axis of rotation of the pressure disks
α is the angle of incline of the lateral surface of the ''tear-like'' groove

In designing a ball-type locking device, consideration must be given to the load on the control clutch, the actual coefficient of friction between the surfaces of the disks and the design parameter C_V. This parameter should conform to the condition:

$$C_V \leq 1/\mu_{max} \tag{3.2}$$

where, μ_{max} is the maximum friction coefficient of the material of the clutch disks.

Thus, despite their design differences, the drives considered above have a single common property: unlike the differential drive, the positive engagement drive provides for a constant ratio of angular velocities of the wheels (axles) which may be controlled in certain devices. This common property makes it possible to work out a general approach and theoretical fundamentals for resolving problems of distributing the power between the wheels of vehicles with positively engaged drives and assessing the operating properties of such vehicles. The subsequent sections of the present chapter are concerned with a single parameter that determines the distribution of power between wheels connected by a locking drive. The analytic description of this parameter, which is known as the kinematic discrepancy factor, serves for determining the slip ratios and circumferential forces of wheels, for assessing the power losses in locked up drives and in the wheel system of multiwheel drive vehicles, including presentation of

methods and approaches for assessing the energy efficiency and fuel economy of vehicles and analysis of the effect of the positive engagement drive on the operating properties of the vehicle.

3.2 Kinematic Discrepancy and Generalized Vehicle Parameters

The main feature specific to a positive engagement vehicle drive (i.e., locked drive) consists in kinematic discrepancy, that is, nonequality of the theoretical linear velocities of driving wheels and axles. Whereas the differential's gear ratio u_{d} is the principal parameter affecting the distribution of power among the wheels of vehicles with a differential drive, the kinematic discrepancy is the main factor in the distribution of power between the axles and the wheels coupled by the locked drive.

There are several reasons for the appearance of kinematic discrepancy. They can be understood by analyzing the formula for the theoretical velocity

$$V_{ti} = \omega_{\mathrm{w}i} r^0_{\mathrm{w}i}, \quad i = 1, n \tag{3.3}$$

that is, different values of velocities V_{ti} stem from differences in the values of angular velocities $\omega_{\mathrm{w}i}$ of the wheels and rolling radii in the driven mode $r^0_{\mathrm{w}i}$. Wheel radii $r^0_{\mathrm{w}i}$ may differ from one another because of differences in the normal loads on the wheels, unequal tire inflation pressure and differences in tire wear and due to manufacturing tolerance. In addition, wheels of different axles may be of different size. On the other hand, the angular velocities $\omega_{\mathrm{w}i}$ of the wheels are either the same (e.g., the angular velocities of wheels of an axle with locked interwheel differential), or the ratio of angular velocities is constant and independent of the conditions of motion (as was seen from data in Section 3.1, this takes place in systems of manual and automatic engagement/disengagement of one of the axles/set of axles). Methods of analytic assessment of kinematic discrepancy are now considered.

3.2.1 Vehicles with 4 × 4 Wheel Formula

The wheel travel paths, the angular velocities of the wheels and the linear velocities of wheel centers of a vehicle with wheels freely seated on shafts (e.g., a trailer), or an all-wheel drive car with differential driveline system of all of the wheels in the driven mode, including when taking a turn, are in natural concordance (see the equivalent layout of a vehicle in Figure 3.18).

Because of differences in the turning radii R_{t1} and R_{t2} the front and rear wheels travel through different paths O_1O_1' and O_2O_2'. For this reason the wheels will turn at different angular velocities if they are freely and independently seated on the shafts (the case of a trailer) or are coupled by an interaxle differential (a 4 × 4 vehicle).

If two axles are coupled by a positively locked drive, then kinematic consistency is also possible in rectilinear motion of the vehicle (Figure 3.19), and this is expressed by the formulae

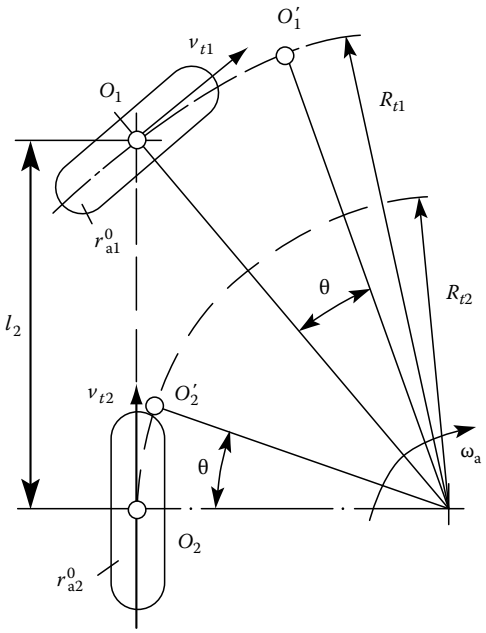


FIGURE 3.18
Equivalent layout of a 4 × 4 vehicle in turn.

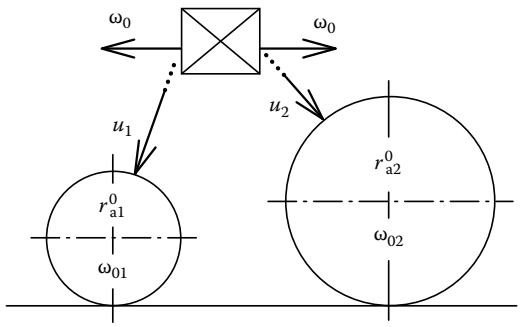


FIGURE 3.19
Equivalent layout of a 4 × 4 vehicle in straight line motion.

$$\begin{aligned} V_{t1} &= V_{t2} \\ \omega_{01} r_{a1}^0 &= \omega_{02} r_{a2}^0 \\ \frac{\omega_0}{u_1} r_{a1}^0 &= \frac{\omega_0}{u_2} r_{a2}^0 \end{aligned} \tag{3.4}$$

where,

r_{a1}^0 and r_{a2}^0 are the generalized rolling radii of the front and rear wheels, reduced to the interwheel differentials of the axles and calculated from formula (2.334)

ω_{01} and ω_{02} are the angular velocities of the interwheel differentials

u_1 and u_2 are the gear ratios from the shaft of the transfer case that rotates at angular velocity ω_0 to the housings of the interwheel differentials

Note, that if the vehicle does not use wheel-hub gear sets, then u_1 and u_2 are the gear ratios from the transfer case to the front and rear wheels, and the numerical values of the wheel-hub

gear set in formula (2.334) is set to unity ($u_k = 1$). If, however, the vehicle makes use of wheel-hub gear sets (in the general case $u_{k1} \neq u_{k2} \neq 1$), then u_1 and u_2 represent, as before the gear ratios from the transfer case to the housings of the interwheel differentials and the gear ratios u_{k1} and u_{k2} are included in calculating the generalized radii r^0_{a1} and r^0_{a2} from formula (2.334) in the course of reducing them to the interwheel differentials.

From formulae (3.4) the condition of kinematic agreement (the equality $V_{t1} = V_{t2}$) is written as

$$r^0_{a1} u_2 = r^0_{a2} u_1 \tag{3.5}$$

This means that the desired kinematic agreement may be attained even in the case of different dimensions (models of wheels), but of suitable gear ratios of the axles. If this equality is not satisfied, then there occurs kinematic discrepancy. To assess the extent of disagreement of the theoretical velocities v_{t1} and v_{t2} one introduces the kinematic discrepancy factor

$$m_{ru} = \frac{V_{t2} - V_{t1}}{V_{t2}} = \frac{r^0_{a2} u_1 - r^0_{a1} u_2}{r^0_{a2} u_1} \tag{3.6}$$

that incorporates the inequality of the rolling radii r^0_{a1} and r^0_{a2} and of the gear ratios u_1 and u_2.

At identical gear ratios one can have

$$m_r = \frac{r^0_{a2} - r^0_{a1}}{r^0_{a2}} \tag{3.7}$$

This case is encountered in vehicles with wheels of the same model, but with some difference in the rolling radii in the driven mode that stems from tolerances in wheel manufacture, differences in the wear of the tire tread, different tire inflation pressures, and unequal weight loads.

If the wheels are of rigorously equal size and the condition of $r^0_{a1} = r^0_{a2}$ is satisfied, but gear ratios u_1 and u_2 are different, then

$$m_u = \frac{u_1 - u_2}{u_1} \tag{3.8}$$

Kinematic discrepancy m_u is built into the drives of vehicle with identical wheels on all the axles that employ interaxle free-running clutches for automatically uncoupling one axle when moving on high-grade solid roads and for automatic locking of the interaxle drive in off-road travel.

Using formulae (3.3) through (3.8), it is possible to analyze:

1. *Design kinematic discrepancy* m^d_{ru} that stems from the very design of the vehicle (different gear ratios u_1 and u_2, different size of front and rear wheels, $r^0_{a1} \neq r^0_{a2}$)
2. *Operational-manufacturing kinematic discrepancy* m^o_r that arises from the inevitable difference in the dimensions of the tires due to manufacturing tolerances, unequal static and dynamic weight loads on the wheels, differences in tire air pressure, and in tire wear ($r^0_{a1} \neq r^0_{a2}$)

The selection of the numerical values of the design kinematic discrepancy and the ranges of variation in the operational-manufacturing kinematic discrepancy are analyzed in Section 3.6.

Condition 3.5 that assumes equality of the theoretical linear velocities of the axle centers holds in rectilinear motion and when taking a turn, provided that, both axles are steered and the rear wheels follow the path of the front wheels. When only one axle is steered and the centers of axles move over curves of different radii then, conversely, kinematic agreement of the traveled path and angular velocities of the front and rear wheels requires that the linear velocities of the axles' centers should not be equal. This is now expressed mathematically. The paths traversed by the front and rear wheels (Figure 3.18) can be expressed as:

$$D_1 = O_1O_1^{'} = V_{t1}t, \quad D_2 = O_2O_2^{'} = V_{t2}t \tag{3.9}$$

whence the time,

$$t = D_1/V_{t1} = D_2/V_{t2} \tag{3.10}$$

At the same time, D_1, D_2, V_{t1}, V_{t2} can be defined as (see Figures 3.18 and 3.19):

$$\begin{aligned} D_1 &= R_{t1}\theta, \quad D_2 = R_{t2}\theta \\ V_{t1} &= \frac{\omega_0}{u_1}r_{a1}^0, \quad V_{t2} = \frac{\omega_0}{u_2}r_{a2}^0 \end{aligned} \tag{3.11}$$

Substitution of formulae (3.11) into (3.10) yields the condition of agreement in curvilinear motion of the vehicle:

$$r_{a2}^0 u_1 R_{t1} = r_{a2}^0 u_2 R_{t2} \tag{3.12}$$

If this condition is not satisfied, then it will set on kinematic discrepancy that is assessed by a factor similar to that given by formula (3.6). This means that in the general case:

$$m_{ruR} = \frac{r_{a2}^0 u_1 R_{t1} - r_{a1}^0 u_2 R_{t2}}{r_{a2}^0 u_1 R_{t1}} \tag{3.13}$$

If radii r_{a1}^0 and r_{a2}^0 are equal to one another, then

$$m_{uR} = \frac{u_1 R_{t1} - u_2 R_{t2}}{u_1 R_{t1}} \tag{3.14}$$

If these radii are not equal, but the gear ratios u_1 and u_2 are equal, then

$$m_{rR} = \frac{r_{a2}^0 R_{t1} - r_{a1}^0 R_{t2}}{r_{a2}^0 R_{t1}} \tag{3.15}$$

At equal gear ratios and rolling radii

$$m_R = \frac{R_{t1} - R_{t2}}{R_{t1}} = 1 - \cos\delta \tag{3.16}$$

where, δ is the angle of the front steered wheels. It can be easily seen that kinematic discrepancy in a vehicle taking a turn with a minimal radius may amount to 25%–30% and even more than that.

Kinematic discrepancy may arise also because of irregularities of the road surface in the vertical plane (the front and rear wheels do not travel the same path when the vehicle moves in a straight line). However, even when the road is level, there are seven possible options when kinematic discrepancy may arise that is defined by formulae (3.6) through (3.8) and (3.13) through (3.16). It may turn out that not all the dimensional parameters needed for determining the kinematic discrepancy in the general cases defined by formulae (3.6), (3.13) through (3.15) are known. At the same time, particular values of kinematic discrepancy defined by formulae (3.7), (3.8), and (3.16) may turn out to be known. It is hence advisable to determine the relationship between the kinematic discrepancy factors for general and particular cases. This is done by transforming expression (3.13):

$$\begin{aligned} 1 - m_{ruR} &= \frac{r^0_{a1} u_2 R_{t2}}{r^0_{a2} u_1 R_{t1}} \\ &= \frac{r^0_{a2} - r^0_{a2} + r^0_{a1}}{r^0_{a2}} \cdot \frac{u_1 - u_1 + u_2}{u_1} \cdot \frac{R_{t1} - R_{t1} + R_{t2}}{R_{t1}} \\ &= (1 - m_r)(1 - m_u)(1 - m_R) \end{aligned}$$

This yields:

$$\begin{aligned} m_{ruR} &= 1 - (1 - m_r)(1 - m_u)(1 - m_R) \\ m_{ru} &= 1 - (1 - m_r)(1 - m_u) \\ m_{uR} &= 1 - (1 - m_u)(1 - m_R) \\ m_{rR} &= 1 - (1 - m_r)(1 - m_R) \end{aligned} \tag{3.17}$$

Formulae (3.17) define the exact values of the kinematic discrepancy factor in general cases in terms of the values of the particular factors. If the parentheses in any of these equations are opened and second- and higher-order infinitesimals are neglected (it is assumed that all the particular values of m are small), the approximate values of these factors can be expressed as:

$$\begin{aligned} m_{ruR} &= m_r + m_u + m_R \\ m_{ru} &= m_r + m_u \\ m_{uR} &= m_u + m_R \\ m_{rR} &= m_r + m_R \end{aligned} \tag{3.18}$$

This assumption is regarded as acceptable for practical calculations. The more precise formulae (3.17) may possibly be used only at minimum vehicle turning radius, when m_R significantly increases.

3.2.2 Vehicles with $2m \times 2n$ Wheel Formula

The kinematic discrepancy factor expressed by formula (3.13) assumed for assessing the positively engaged driveline system of a 4×4 vehicle is not suitable for vehicles with three and more driving axles. This, made it necessary to, work out a new method for assessing the locked drive of vehicles with any number of driving axles. The presentation of this method is started with examining a $2m \times 2n$ vehicle in rectilinear motion and will be followed by examining vehicles with steered wheels taking a turn and then articulated vehicles, and articulated vehicles with steered wheels taking a turn.

3.2.2.1 Vehicles with 2m × 2n Wheel Formula in Rectilinear Motion

Consider the rectilinear motion of a vehicle with positively locked up interaxle power-dividing units and free interwheel differentials of the driving axles on a hard, level road with negligible resistance to motion, that is, the case when the total circumferential force of the vehicle is close to zero, $F_{x\Sigma} \to 0$. Figure 3.20 shows the equivalent layout of such a vehicle, more precisely, of its driving axles, in which the left and right wheels were replaced by a single equivalent wheel with generalized rolling radius r^0_{ai} in the driven mode reduced to the housing of the interwheel differential using formula (2.334).

The velocity in this travel mode at given engine rpm and transmission setting will be termed the theoretical travel velocity V_a. In its turn, each driving axle separately has its own theoretical velocity V_{ti} defined as the product of the angular velocity ω_{0i} of the housing of the interwheel differential and the rolling radius in the driven mode, that is,

$$v_{ti} = \omega_{0i} r^0_{ai} = \frac{\omega_0}{u_i} r^0_{ai} \tag{3.19}$$

where, u_i is the gear ratio from the transfer case shaft to the housing of the differential of the ith axle (see Figure 3.20).

According to the method suggested here, the difference between the theoretical velocity V_{ti} of each axle and the theoretical velocity V_a of the vehicle is the kinematic discrepancy of the ith axle. And the ratio of this difference to velocity V_{ti} determines the kinematic discrepancy factor m_{Hi} of the given axle, that is,

$$m_{Hi} = \frac{V_{ti} - V_a}{V_{ti}} \tag{3.20}$$

It is obvious that this method of assessing the kinematic discrepancy of the velocities of the driving axles appears to be natural. The method immediately compares the two principal parameters of the axle: its velocity V_a as a part of the vehicle and the theoretical velocity V_{ti}, which it would have had, had it moved separately from the vehicle. The suggested approach is general since it obviates the need to compare the velocities V_{ti} of the different axles.

The physical meaning of the kinematic discrepancy factor m_{Hi} is now clarified. When the motion with a traction load is resisted ($F_{x\Sigma} > 0$), the actual velocity V_x of the vehicle is lower

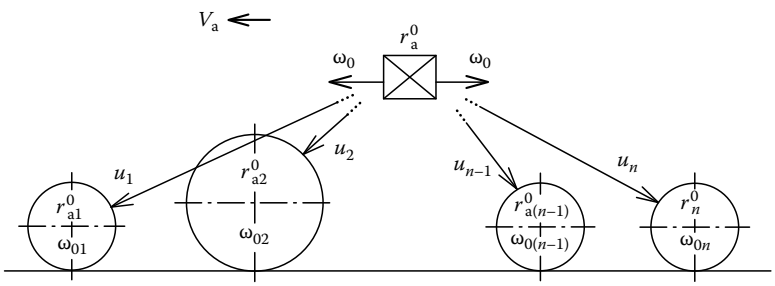


FIGURE 3.20
Equivalent layout of a $2m \times 2n$ vehicle in straight-line motion.

than the theoretical velocity V_a. This relative velocity loss is represented as the generalized slippage of the vehicle:

$$s_{\delta a} = \frac{V_a - V_x}{V_a} \tag{3.21}$$

whence,

$$V_x = V_a(1 - s_{\delta a}) \tag{3.22}$$

Since all of the vehicle's axles move at the same actual velocity V_x, one may write:

$$V_x = V_{ti}(1 - s_{\delta ai}) = V_a(1 - s_{\delta a}) \tag{3.23}$$

where, $s_{\delta ai}$ is the generalized slippage of the ith axle, determined based on slippages $s'_{\delta i}$ and $s''_{\delta i}$ of the left and right wheels from formulae (2.340) through (2.342). Transformation of equality (3.23) upon substitution of (3.20) yields:

$$s_{\delta ai} = m_{Hi} + (1 - m_{Hi})s_{\delta a} \tag{3.24}$$

The physical meaning of kinematic discrepancy m_{Hi} follows from expression (3.24) above. The kinematic discrepancy of the ith axle of a multiwheel drive vehicle is the generalized slippage $s_{\delta ai}$ (or the skid in the case of $m_{Hi} < 0$) of that axle in the absence of traction load, when $F_{x\Sigma} \to 0$ and $s_{\delta a} = 0$.

The above shows that, in the presence of kinematic discrepancy in the positive drive of axles of a vehicle moving over a road with negligible resistance without traction load, the wheels are subject to slippage, meaning also, to corresponding power losses in the wheel system.

When moving with a traction load, the slippage $s_{\delta ai}$ of axles is determined, both by the kinematic discrepancy factor m_{Hi} and the traction load of the vehicle, that is, by the value of $s_{\delta a}$.

A formula is now introduced for calculating m_{Hi}. The velocity V_a is determined from the expression:

$$V_a = \omega_0 r_a^0 \tag{3.25}$$

where

ω_0 is the angular velocity of the transfer case shaft (see Figure 3.20)

r_a^0 is the generalized rolling radius of the vehicle in the driven mode, reduced to this shaft

Upon substitution of formulae (3.19) and (3.25), formula (3.20) transforms to

$$m_{Hi} = 1 - r_a^0 \frac{u_i}{r_{ai}^0} \tag{3.26}$$

When $F_{x\Sigma} \to 0$ the relationship between circumferential force F_x and slippage s_δ is linear and is expressed by formula (1.25), in which the longitudinal stiffness factor K_{xi} of the tire

should be replaced by the same factor K_{ai} for the axle's tires (see formula (2.412)). With reference to the above,

$$F_{xi} = K_{ai} m_{Hi} = K_{ai}\left(1 - r_a^0 \frac{u_i}{r_{ai}^0}\right) \tag{3.27}$$

Since $F_{x\Sigma} \to 0$, the sum of the wheel torques T_{wi}, $i = 1, n$ reduced to the transfer case shaft is also equal to zero:

$$\sum_{i=1}^{n} F_{xi} r_{ai}^0 / u_i = 0 \tag{3.28}$$

Substitution of force F_{xi} from formula (3.27) into equality (3.28) and solving it for r_a^0 yields an expression for the generalized rolling radius of the vehicle in the driven mode, reduced to the transfer case shaft:

$$r_a^0 = \left(\sum_{i=1}^{n} K_{ai} r_{ai}^0 / u_i\right)\left(\sum_{i=1}^{n} K_{ai}\right)^{-1} \tag{3.29}$$

Using expression (3.29) above, formula (3.26) for the kinematic discrepancy of the ith axle of the vehicle is finally written as

$$m_{Hi} = 1 - \frac{u_1}{r_{ai}^0} \frac{\sum_{i=1}^{n} K_{ai} r_{ai}^0 / u_i}{\sum_{i=1}^{n} K_{ai}} \tag{3.30}$$

In the case when gear ratios u_i from the transfer case shaft to the driving axles of the vehicle are equal, formula (3.30) becomes

$$m_{Hi} = 1 - \frac{1}{r_{ai}^0} \frac{\sum_{i=1}^{n} K_{ai} r_{ai}^0}{\sum_{i=1}^{n} K_{ai}} \tag{3.31}$$

It is of interest to derive an expression relating the kinematic discrepancy factors m_{H1} and m_{H2} using formula (3.30) and the kinematic discrepancy factor m_{ru} from formula (3.6) for 4×4 vehicles. Simultaneous solution of these two equations yields:

$$m_{ru} = \frac{m_{H2} - m_{H1}}{1 - m_{H1}} \tag{3.32}$$

If, assuming m_{H1} to be small, the denominator of (3.32) is set to be equal to unity, one can write:

$$m_{ru} = m_{H2} - m_{H1} \tag{3.33}$$

The difference in results using formulae (3.32) and (3.33) for real values of m_{Hi} is not too great. For example, at $m_{H1} = -0.03$ and $m_{H2} = 0.07$, m_{ru} calculated from formula (3.32) is equal to 0.097 and that obtained from (3.33) is 0.1.

The following should be added to the analysis of formulae (3.33), (3.6), and (3.20). Zero value of m_{ru} has always corresponding to it zero values of m_{H1} and m_{H2}. The value of m_{ru} cannot be zero as a result of the zero equality of the difference $(m_{H2} - m_{H1})$, since in the case of kinematic discrepancy the factors m_{H1} and m_{H2} have different signs. This is shown in Section 3.6, in examining a case study of selecting rational values of kinematic discrepancy using formulae (3.6) and (3.30).

3.2.2.2 Vehicles with 2m × 2n Wheel Formula with Steered Wheels in Curvilinear Motion

When multiwheel drive vehicles travel over a curved course, the wheels of the individual axles traverse different paths during the same time and make it necessary to provide for kinematic consistency of the wheels: their angular velocities should be determined in accordance with the paths of motion. At the same time, the positive engagement of the interaxle drive provides a constant ratio of angular velocities of the wheels, irrespective of the curve of the course traveled. As a result, axles of vehicles moving in a curved path are subject to significant kinematic discrepancy.

A unified method of assessing the kinematic discrepancy both for rectilinear and curvilinear motion of multiwheel drive vehicles with any number of driving and steered axles, including those employing wheels of different size is presented in the following text.

First, the pertinent relationships are derived for the axles of a multiwheel drive frame-type vehicle with all steered wheels. These results, as shall be shown, can also be used for vehicles in which not all the wheels are steered. Consider the motion of a vehicle taking a turn on a solid road with a very low resistance, when the total circumferential force of the vehicle is close to zero. It is assumed, as before, that both wheels of each axle are replaced by a single conditional wheel, reduced to the housing of the interwheel differential. Under these conditions, the velocities V_{tai} of the conditional wheels are determined by the turning radii (or by the turning angles δ_i of the wheels). Here the projections of these velocities on the longitudinal axis of the vehicle are equal to one another. The velocity along the longitudinal axis, as in investigating rectilinear motion, shall be termed the vehicle's theoretical velocity V_a. Then velocity V_{tai} of the conditional wheel of the ith axle is

$$V_{tai} = V_a \sec \delta_i \tag{3.34}$$

At the same time, each of the axles has its own theoretical velocity V_{ti} that is equal to the product of the angular velocity ω_{0i} and the rolling radius r_{ai}^0 in the driven mode. The kinematic discrepancy of the ith axle shall be written as the difference between its velocities V_{ti} and V_{tai}, and the kinematic discrepancy factor shall be expressed as:

$$m_{Hi} = \frac{V_{ti} - V_{tai}}{V_{ti}} = \frac{V_{ti} - V_a \sec \delta_i}{V_{ti}} \tag{3.35}$$

The relative velocity loss of the ith axle is represented by the slippage factor:

$$s_{\delta ai} = \frac{V_{ti} - V_a(1 - s_{\delta a}) \sec \delta_a}{V_{ti}} \tag{3.36}$$

where, $s_{\delta a}$ is the generalized slippage of the vehicle that is caused by the resultant of the algebraic sum of projections onto the longitudinal axis of the vehicle of all forces that resist

the motion. Upon substitution of (3.36), formula (3.35) is transformed to a form similar to formula (3.24), that is,

$$s_{\delta ai} = m_{Hi} + (1 - m_{Hi}) s_{\delta a} \tag{3.37}$$

It follows from formula (3.37) that the kinematic discrepancy of the ith axles is equal to the slippage (skid at $m_{Hi} < 0$) of the wheels of this axle in curvilinear motion that occurs at very low resistance to motion ($F_{x\Sigma} \to 0$, $s_{\delta a} = 0$).

Formula (3.35) is now transformed to a form convenient for calculations. Velocity V_a is represented, as before, as the product of angular velocity ω_0 of the transfer case shaft and the generalized rolling radius of the vehicle r_a^0, reduced to the above shaft (see formula (3.25)). Then formula (3.35) becomes

$$m_{Hi} = 1 - r_a^0 \frac{u_i}{r_{ai}^0} \sec \delta_i \tag{3.38}$$

To be able to perform calculations using formula (3.38) one must know the radius r_a^0, which is now determined from equality to zero of the moment at the transfer case shaft:

$$\sum_{i=1}^{n} F_{xi} r_{ai}^0 / u_i = 0 \tag{3.39}$$

Assuming a linear relationship for the motion mode under study between the circumferential force F_{xi} of the wheel and its slippage $s_{\delta ai}$, formula (3.39) is written as:

$$\sum_{i=1}^{n} K_{ai} \left(1 - r_a^0 \frac{u_i}{r_{ai}^0} \sec \delta_i \right) r_{ai}^0 / u_i = 0 \tag{3.40}$$

whence, radius r_a^0 is equal to:

$$r_a^0 = \left(\sum_{i=1}^{n} K_{ai} r_{ai}^0 / u_i \right) \left(\sum_{i=1}^{n} K_{ai} \sec \delta_i \right)^{-1} \tag{3.41}$$

Upon substitution of formula (3.41), the expression for the kinematic discrepancy factor of the ith axle is finally written as:

$$m_{Hi} = 1 - \frac{u_i \sec \delta_i}{r_{ai}^0} \frac{\sum_{i=1}^{n} K_{ai} r_{ai}^0 / u_i}{\sum_{i=1}^{n} K_{ai} \sec \delta_i} \tag{3.42}$$

Analysis of formula (3.42) shows that the kinematic discrepancy of the ith axle when taking a turn is a function of coefficients K_{ai}, gear ratios u_i, radii r_{ai}^0 and wheel turn angles δ_i. It follows from this that formula (3.42) is unique for calculating m_{Hi} both when in curvilinear and in rectilinear motion. It makes it possible to determine the kinematic discrepancy of each axle in curvilinear motion with consideration of the kinematic discrepancy that occurs in rectilinear motion as a result of nonequality of r_{ai}^0, u_i and K_{ai}. On the other hand, when angles δ_i of all the axles are zero, formula (3.42) takes the form of (3.30) obtained for rectilinear motion. If not all the axles are steered, then $\delta_i = 0$ and sec $\delta_i = 1$ should be substituted when using formula (3.42).

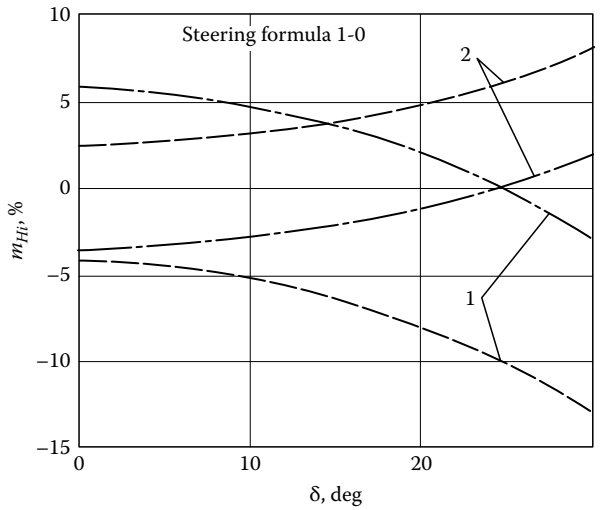


FIGURE 3.21
4 × 4 vehicle in turn: (1) m_{H1}; (2) m_{H2}.

Figure 3.21 shows as an illustration the values of factors m_{H1} and m_{H2} calculated from formula (3.42) for a 4×4 vehicle with locked interaxle differential as a function of angle of turn δ of the front wheels.

At $\delta = 0$ (rectilinear motion), $m_{H1} < m_{H2}$ (dashed lines) and $m_{H1} > m_{H2}$ (dash-dotted lines) are obtained, which stems from different combinations of radii r_{ai}^0 and gear ratios u_i, $i = 1, 2$. With increasing δ, the value of m_{H1} decreases and that of m_{H2} increases. As shall be shown, the circumferential forces of the front and rear axles will change accordingly.

Here is another example of utilizing formula (3.42). Consider the variation in kinematic discrepancy factors m_{Hi} when a 6×6 truck with full mass of 26 ton takes a turn as a function of the steering formula for three cases of axle locations on the base: the middle axle is shifted to the front, located in the middle of the base and shifted to the rear. Calculations were performed on the assumption that the interaxle drive is positively locked, and radii r_{ai}^0 of all the wheels and gear ratios u_i in their driveline system are the same. The calculations were performed for different front wheel turn angles δ_1, depending on which, the turn angle of the wheels of the another steered axle was determined based on the vehicle's steering formula. The results of these calculations are plotted in Figure 3.22a.

Factor m_{H1} takes negative values with increasing δ_1 and its absolute magnitude increases, that is, when turning under low traction loads the front wheels may exhibit negative slippage. Factor m_{H2} of the middle axle is positive at any steering formula and increases with increasing δ_1. However, this increase is minimal when the front and middle steered axles are located close to one another. The rear wheels have a negative m_{H3} only when the wheels are located uniformly over the base and when the front and rear wheels are steered. In the remaining cases $m_{H3} > 0$.

Figure 3.22b shows results of similar calculations performed for an 8×8 truck with full mass of 42 ton on the assumption that the interaxle drive is locked. It is seen that the steering formula exerts a marked effect on the values of factors m_{Hi}, meaning also on the distribution of circumferential forces F_{xi} between the axles when the vehicle takes a turn. The smallest difference in factors m_{Hi} in the examples considered above occurs when all the wheels are steered.

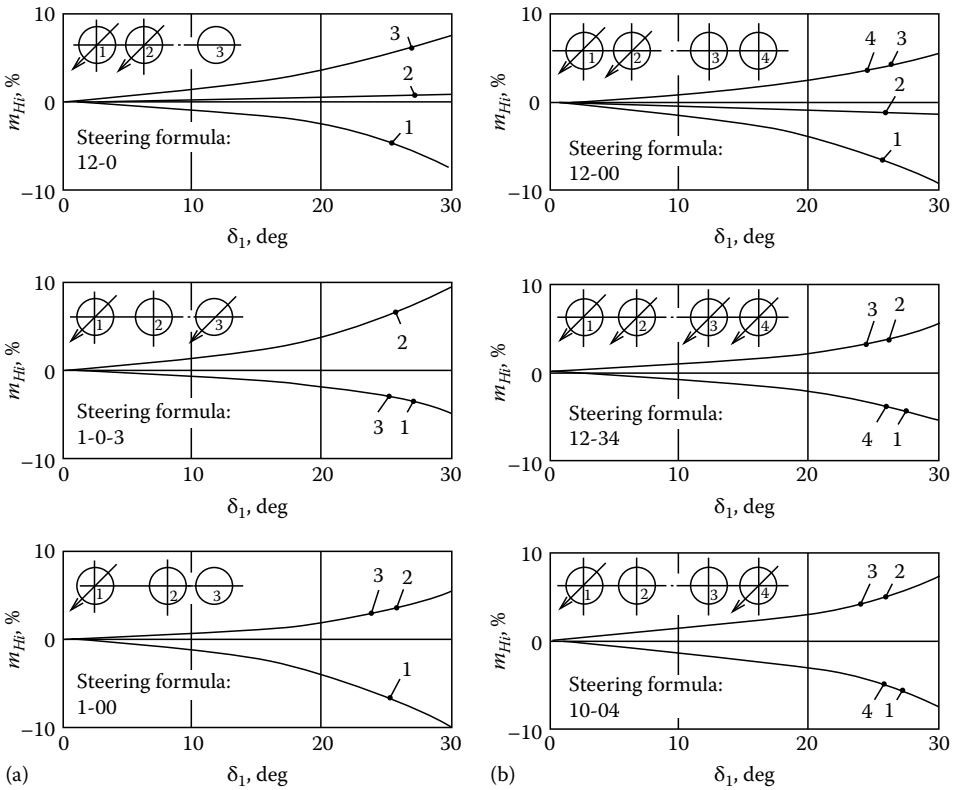


FIGURE 3.22
6 × 6 truck (a) and 8 × 8 truck (b) in turn: (1) m_{H1}; (2) m_{H2}; (3) m_{H3}; (4) m_{H4}.

3.2.2.3 Articulated 2m × 2n Vehicles with Steered Wheels

In addition to vehicles in which turning is implemented by steered wheels, extensive use is made of articulated vehicles, made up of several sections. Such an arrangement is extensively used with trucks and tractors. Experimental specimens of a farm tractor consisting of three sections connected by two hinges have also been manufactured by several companies. The use of articulated designs provides for good mobility of a vehicle with a smaller curb mass as compared with vehicular trains having the same cargo capacity. Some vehicles may use both articulated sections and sections with steered wheels. Examples of articulated vehicles and of articulated vehicles with steered wheels were described in Section 1.2 (see Tables 1.10 through 1.12). Formula shall now be derived for calculating kinematic discrepancy factors in a positive engagement drive of such vehicles moving in a curved path.

Figure 3.23 shows a computational layout of the turn of an articulated vehicle consisted of n sections.

Then in the case of motion with close to zero resistance forces, the velocities of the axles are interrelated as:

$$\omega_a = \frac{V_{ta1}}{R_{t1}} = \frac{V_{ta2}}{R_{t2}} = \frac{V_{ta3}}{R_{t3}} = \cdots = \frac{V_{tan}}{R_{tn}} \tag{3.43}$$

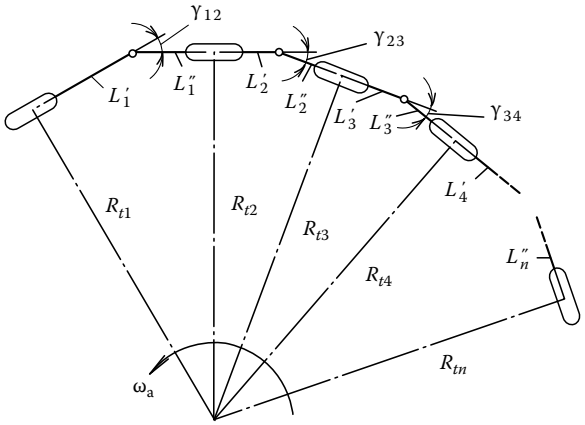


FIGURE 3.23
Equivalent layout of an articulated vehicle in turn.

The angular velocity ω_a of the vehicle's turn is written as:

$$\omega_a = \frac{V_a}{R_{ta}} = \frac{\omega_0 r_a^0}{R_{ta}} \tag{3.44}$$

where
V_a is the theoretical velocity of the vehicle
ω_0 is the angular velocity of the transfer case shaft
r_a^0 is the generalized rolling radius of the vehicle, reduced to the above shaft
R_{ta} is the turn radius of a conditional wheel with radius r_a^0

Using formulae (3.43) and (3.44), one can write

$$V_{tai} = \omega_0 r_a^0 \frac{R_{ti}}{R_{ta}}, \quad i = 1, n \tag{3.45}$$

Then the kinematic discrepancy factor of the ith axle of an articulated vehicle is determined from formulae (3.35) and (3.45) as:

$$m_{Hi} = 1 - \frac{u_i}{r_{ai}^0} r_a^0 \frac{R_{ti}}{R_{ta}} \tag{3.46}$$

The ratio r_a^0/R_{ta} is determined from equality to zero of the moment at the transfer-case shaft:

$$\sum_{i=1}^{n} F_{xi} r_{ai}^0 / u_i = \sum_{i=1}^{n} K_{ai} m_{Hi} r_{ai} / u_i = 0 \tag{3.47}$$

This, upon substitution of (3.46), yields

$$r_a^0 / R_{ta} = \left(\sum_{i=1}^{n} K_{ai} r_{ai}^0 / u_i \right) \left(\sum_{i=1}^{n} K_{ai} R_{ti} \right)^{-1} \tag{3.48}$$

Expression (3.46) then becomes

$$m_{Hi} = 1 - \frac{u_i R_{ti}}{r_{ai}^0} \frac{\sum_{i=1}^{n} K_{ai} r_{ai}^0 / u_i}{\sum_{i=1}^{n} K_{ai} R_{ti}} \tag{3.49}$$

Formula (3.49) makes it possible to calculate the kinematic discrepancy factor of axles of an articulated vehicle both in curvilinear motion with consideration of the inequality of turning radii R_{ti}, gear ratios u_i, wheel radii r_{ai}^0 and coefficients K_{ai} as in the case of rectilinear motion when $R_{ti} \to \infty$. The latter follows from analyzing expression (3.49) using the L'Hopital rule: in the limit of $R_{ti} \to \infty$ it takes the form of formula (3.30), obtained for rectilinear vehicle motion.

Formulae for determining the turning radii R_{ti} needed for performing calculations using (3.49) are easily obtained from examining the geometry of the vehicle's turn in Figure 3.23:

$$\begin{aligned} R_{ti} &= \frac{L_i' \cos \gamma_{i(i+1)} + L_i''}{\sin \gamma_{i(i+1)}}, \quad i = 1, \ (n-1); \\ R_{tn} &= \frac{L_n'' \cos \gamma_{(n-1)n} + L_n'}{\sin \gamma_{(n-1)n}} \end{aligned} \tag{3.50}$$

As an example consider now the variation in the kinematic discrepancy factors of a 4×4 articulated tractor with full mass of 5 ton making a turn as a function of the location of the articulation hinge and the articulation angle γ (Figure 3.24).

When the hinge is located in the middle of the base ($L' = L''$), factors m_{H1} and m_{H2} take zero values, which stems from absence of design kinematic discrepancy in the drives of the axles and equality of radii R_{t1} and R_{t2}. When the hinge is located closer to the front axle ($L' < L''$), factor m_{H1} of the front axle takes negative values, whereas second-axle factor m_{H2}

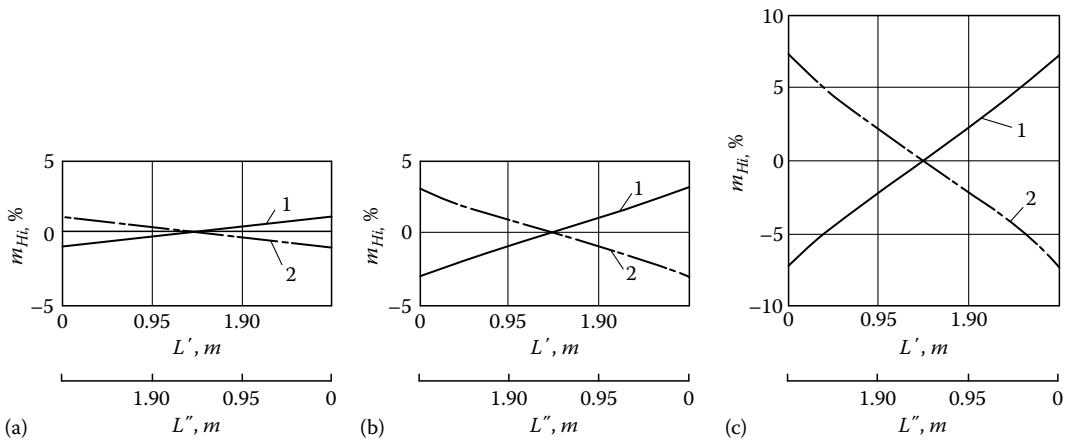


FIGURE 3.24
4×4 articulated tractor in turn: (a through c) $\gamma = 10$, 20, and 30°; 1, m_{H1}; 2, m_{H2}.

is positive. This reduces the circumferential traction force F_{x1} of the front axle and causes a corresponding rise in force F_{x2} of the rear axle as compared with their values when the hinge is located in the middle of the base.

In the case of $L' > L''$ when the hinge is located closer to the rear wheels, their factor m_{H2} is negative, whereas $m_{H1} > 0$. Then force F_{x2} decreases whereas F_{x1} increases. The highest values (both positive and negative) of factors m_{H1} and m_{H2} correspond to the case when the hinge is located at the axle of the front or rear wheels.

Thus, formula (3.49) can be used for calculating kinematic discrepancy factors m_{Hi} for articulated vehicles. Special studies showed that if the wheels of an articulated vehicle (see Figure 3.23) are also steered the form of formula (3.49) does not change. The effect of wheel turnability is incorporated by variation in turn radii R_{ti}.

As an illustration, calculate the kinematic discrepancy factors of a 6×6 power-module driven vehicular train with front steered wheels and an articulation hinge located between the second and third axles. Examples of using such a vehicle were described in Figure 1.38, whereas Table 1.12 (item 1) presents details on its chassis and driveline system. The second axle is the main driving link, whereas the first and third axles are automatically engaged/disengaged. It is assumed that all the axles of this vehicle are engaged, that is, coupled by a positive engagement drive without the disengagement option. The computational layout is shown in Figure 3.25, whereas the formulae for m_{Hi} have the form:

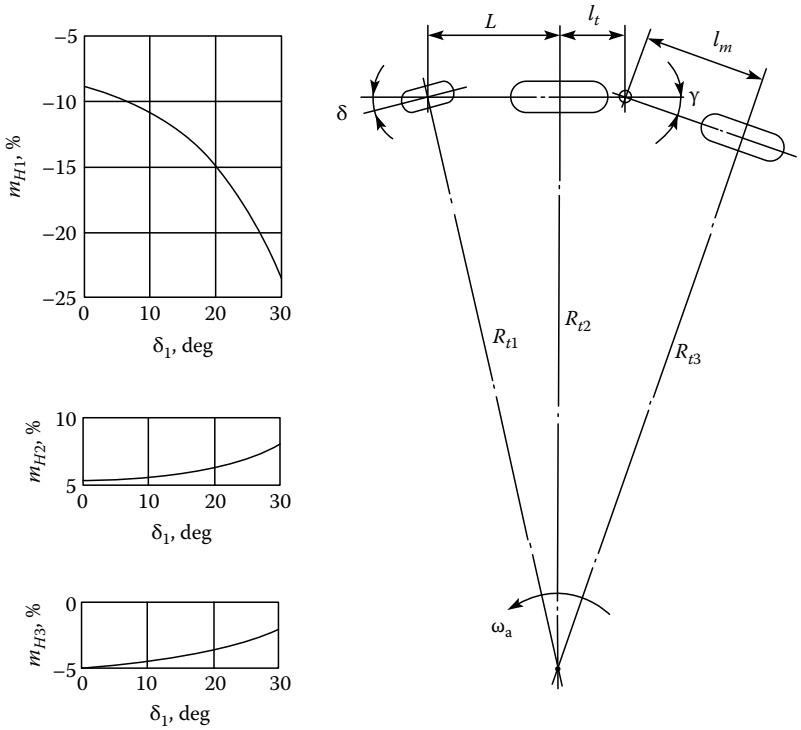


FIGURE 3.25
6×6 power-module driven vehicular train.

$$m_{H1} = 1 - \frac{u_1 L}{r^0_{a1} \sin\delta} D,$$

$$m_{H2} = 1 - \frac{u_2 L}{r^0_{a2} \tan\delta} D, \tag{3.51}$$

$$m_{H3} = 1 - \frac{u_3 (l_t + l_m \cos\gamma)}{r^0_{a3} \sin\delta} D,$$

where,

$$D = \frac{\sum_{i=1}^{3} K_{ai} r^0_{ai} / u_i}{K_{a1} L / \sin\delta + K_{a2} L / \tan\delta + K_{a3} (l_t + l_m \cos\gamma) / \sin\gamma}$$

and angles δ and γ are interrelated by the expression

$$\delta = \arctan\left(\frac{L \sin\gamma}{l_t \cos\gamma + l_m}\right) \tag{3.52}$$

Figure 3.25 shows the results of calculations using formulae (3.51) and (3.52) for the case when the articulation hinge is located in the middle between the second and third axles. Factor m_{H1} decreases perceptibly with increasing angle δ that also reduces the traction load on this axle. The values of the kinematic discrepancy factors and, accordingly the circumferential forces of the second and third axle increase when taking a turn.

It is obvious that the kinematic discrepancy of the axles, meaning also their traction loads, are affected not only by the distance $(l_t + l_m)$ between the second and third axles, but also by the relationship between these two distances (l_t and l_m), at constant value of their sum, that is, the values of m_{Hi} are also controlled by the location of the hinge of relative angular motion of its links.

Figure 3.26 shows calculated curves of m_{H3} of the third axle at front wheel turn angle of $\delta = 30°$ as a function of the relationship between l_t and l_m and of their sum.

Calculations show that upon an increase in l_t and corresponding reduction in l_m (when the hinge is moved from the second to the third axle) the value of m_{H3} decreases. This stems from increasing turning radius R_{t3} when the hinge is so shifted. When $(l_t + l_m)$ increases at $l_t =$ constant, the value of m_{H3} also increases.

The results plotted in Figures 3.25 and 3.26, allow assessing the distribution of circumferential forces between the three axles, which is of practical significance when installing free-running clutches in the front-axle and third-axle drives. Assume that both clutches

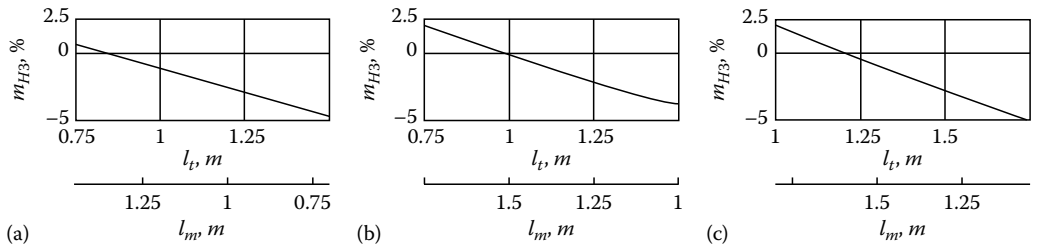


FIGURE 3.26
Kinematic discrepancy factors of the vehicle from Figure 3.25 when $\delta = 30°$: (a) $(l_t + l_m) = 2.2$ m; (b) $(l_t + l_m) = 2.5$ m; (c) $(l_t + l_m) = 2.8$ m.

coupled the axles in the traction mode in rectilinear motion. Then when starting the turn (δ increases) the circumferential force, F_{x1} of the front wheels will decrease and, when it will reach zero value, the free-running clutch will uncouple the front axle. Circumferential forces of the second F_{x2} and third F_{x3} axles will initially increase. After the front axle of the tractor is uncoupled, the relationship between forces F_{x2} and F_{x3} does not change upon further increase in δ and both axles will perform as driving axles in the turn, provided that $l_t = l_m$. If $l_t < l_m$, force F_{x2} will decrease, while force F_{x3} will increase. At $l_t > l_m$ force F_{x3} decreases while F_{x2} increases. In the last case, the wheels of the third axle may be uncoupled and only the wheels of the second axle will power the vehicle.

3.2.2.4 The Interwheel Positive Engagement

The data presented above pertain to a positive engagement of the interaxle driveline system. Interwheel positive engagements are also used in vehicles (e.g., when an interwheel differential is fully locked). It will be shown that the formulae derived above are also suitable for an interwheel positively locked drives. Based on the previously derived definition of kinematic discrepancy, expressions are written for kinematic discrepancy factors of the outer—relative to the turn center (single prime) and inter (double prime)—wheels of the *i*th axle of a vehicle (see Figure 3.27):

$$m'^{(\prime\prime)}_{Hi} = \frac{V'^{(\prime\prime)}_{ti} - V'^{(\prime\prime)}_{tai}}{V'^{(\prime\prime)}_{ti}} \tag{3.53}$$

From the ratio of wheel and axle-center velocities when taking a turn (similarly to formula (3.45)),

$$V'^{(\prime\prime)}_{tai} = \omega_{0i} r^0_{ai} \frac{R'^{(\prime\prime)}_{ti}}{R_{ti}} \tag{3.54}$$

where

r^0_{ai} is the generalized rolling radius of the axle in the driven mode, reduced to the housing of the interwheel power-dividing unit

R'_{ti}, R''_{ti}, and R_{ti} are the turning radii of the outer and inner wheels and of the center of the axle

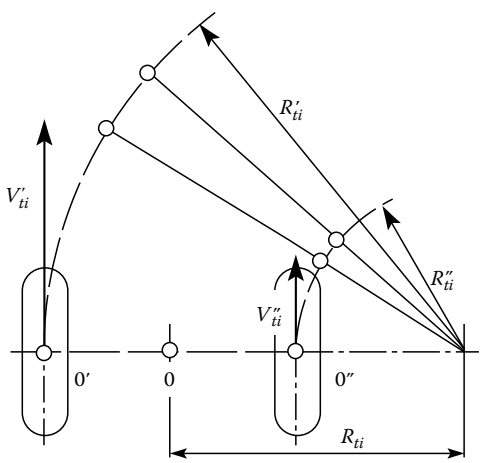


FIGURE 3.27
Driving axle with a locked up differential in turn.

Substitution of (3.54) into (3.53) yields:

$$m'^{(\prime\prime)}_{Hi} = 1 - \frac{u_{ki} r^{0}_{ai}}{r^{0'(\prime\prime)}_{wi}} \frac{R'^{(\prime\prime)}_{ti}}{R_{ti}} \tag{3.55}$$

where, u_{ki} are the gear ratio of the wheel-hub gear set.

It is found from zero equality of the total torque of the axle that:

$$r^{0}_{ai} = \frac{K'_{xi} r^{0'}_{wi} + K''_{xi} r^{0''}_{wi}}{K'_{xi} R'_{ti} + K''_{xi} R''_{ti}} \frac{R_{ti}}{u_{ki}} \tag{3.56}$$

If the vehicle does not have wheel-hub gear sets, then u_{ki} in formulae (3.55) and (3.56) should be set equal to unity. Upon substitution of (3.56), formula (3.55) takes the final form:

$$m'^{(\prime\prime)}_{Hi} = 1 - \frac{R'^{(\prime\prime)}_{ti}}{r^{0'(\prime\prime)}_{wi}} \frac{K'_{xi} r^{0'}_{wi} + K''_{xi} r^{0''}_{wi}}{K'_{xi} R'_{ti} + K'_{xi} R''_{ti}} \tag{3.57}$$

Formula (3.57) above, for an interwheel positively engaged drive has the same structure as formula (3.49) for the kinematic discrepancy factors of axles coupled by an interaxle positive engagement. Only the gear ratios u_i that are the same in the drives of the left and right wheels are missing. Gear ratios u_{ki} and turn radii R_{ti} canceled out in the course of regrouping of terms.

Slippages $s'^{(\prime\prime)}_{\delta i}$ of the wheels of the ith axle with a positive engagement of its two wheels are interrelated by an expression that follows from kinematic relationships between characteristic points of an axle in the course of a turn that has the same structure as formula (3.37)

$$s'^{(\prime\prime)}_{\delta i} = m'^{(\prime\prime)}_{Hi} + \left(1 - m'^{(\prime\prime)}_{Hi}\right) s_{\delta ai} \tag{3.58}$$

where, $s_{\delta ai}$ is the generalized slippage of the axle.

A method was thus developed for calculating the kinematic discrepancy factors of vehicles with positive engagement of axle and interwheel drives both in rectilinear and curvilinear motion when turning. These expressions can be used for vehicles with steered wheels, for articulated vehicles, and articulated vehicles with steered wheels including the case of differently sized wheels of individual axles and different gear ratios in their drives. The values of factors m_{Hi} thus calculated can be used for determining the circumferential forces of wheels and axles, their slippages and also power losses in the wheel system.

3.3 Wheel Slips and Circumferential Wheel Forces

The ratio of angular velocities of wheels in the case of a positive engagement drive is constant, irrespective of the conditions of motion. For this reason, under actual travel conditions, an inconsistency arises between the circumferential velocities of the individual wheels and the length of the path traveled by them. As a result of this, longitudinal forces arise in the contact between the wheels and the surface that cause corresponding

deformations of tires and the surface of travel, which induces redistribution of circumferential forces/torques between the wheels. This inconsistency was described in Section 3.2 by means of the kinematic discrepancy factor. In conjunction with this, it is advisable to establish analytically the effect of kinematic inconsistency on the circumferential forces and slippage of wheels. Let us start with 4×4 vehicles.

3.3.1 4×4 Vehicles

Consider the equivalent layout of a 4×4 vehicle with locked interaxle differentials in uniform rectilinear motion (see Figure 3.19). The torsional compliance of the axle drives is not taken into account, since its effect manifests only under transitional travel modes and does not affect the slippage of wheels after 1–1.5 wheel rotations when moving at constant velocity. The generalized slippage of the axles can be represented as follows:

$$s_{\delta a1} = \frac{V_{t1} - V_x}{V_{t1}}, \quad s_{\delta a2} = \frac{V_{t2} - V_x}{V_{t2}} \tag{3.59}$$

Since the actual velocity, V_x is the same for both axles, then

$$V_x = V_{t1} - V_{t1} s_{\delta a1} = V_{t2} - V_{t2} s_{\delta a2}$$

whence,

$$s_{\delta a2} = \frac{V_{t2} - V_{t1}}{V_{t2}} + \frac{V_{t1}}{V_{t2}} s_{\delta a1} = \frac{V_{t2} - V_{t1}}{V_{t2}} + \left(\frac{V_{t2}}{V_{t1}} - \frac{V_{t2} - V_{t1}}{V_{t2}} \right) s_{\delta a1} \tag{3.60}$$

Introduction of the kinematic discrepancy factor from formula (3.6) yields:

$$\begin{aligned} & s_{\delta a2} = m_{ru} + (1 - m_{ru}) s_{\delta a1} = m_{ru} + s_{\delta a1} - m_{ru} s_{\delta a1} \\ \text{or} \quad & s_{\delta a1} = \frac{s_{\delta a2} - m_{ru}}{1 - m_{ru}} \end{aligned} \tag{3.61}$$

The last term of the first formula can be neglected as a second-order infinitesimal. This assumption results in a lower-side error in calculating $s_{\delta a1}$ of $100 \dfrac{m_{ru}}{2}\%$. At $m_{ru} = 0.05$ this error amounts to 2.5%, whereas at $m_{ru} = 0.07$ it is 3.5%. The error in calculating $s_{\delta a2}$ is even smaller (on the higher side), since $s_{\delta a2} > s_{\delta a1}$. This assumption causes a change in the values of the slip efficiency η_δ in the third decimal point. If this assumption is allowed on the smallness of $m_{ru} s_{\delta a1}$, then formula (3.61) becomes:

$$s_{\delta a2} = s_{\delta a1} + m_{ru} \quad \text{or} \quad s_{\delta a1} = s_{\delta a2} - m_{ru} \tag{3.62}$$

Simplified formula (3.62) highly facilitates the further investigation of the traction dynamics of an all-wheel drive vehicle. The kinematic discrepancy m_{ru} may be caused by differences in the gear ratios of the axles, or by unequal rolling radii in the driven mode, or both of these together.

The relationship between $s_{\delta a1}$ and $s_{\delta a2}$ in curvilinear motion of the vehicle is now clarified. This is done with reference to Figure 3.18 on the assumption that the vehicle

does not move in the driven mode, but under the power of the engine's torque. The actual linear velocities of the axles are expressed in terms of their theoretical values:

$$\begin{aligned} V_{x1} &= V_{t1}(1 - s_{\delta a1}) = R_{t1}\omega_a \\ V_{x2} &= V_{t2}(1 - s_{\delta a2}) = R_{t2}\omega_a \end{aligned} \tag{3.63}$$

Dividing one of the above expressions by the other,

$$\frac{V_{t1}(1 - s_{\delta a1})}{V_{t2}(1 - s_{\delta a2})} = \frac{R_{t1}}{R_{t2}} \tag{3.64}$$

By taking into consideration formula (3.6) for the kinematic inconsistency m_{ru} and formulae (3.17), formula (3.64) can be transformed:

$$\begin{aligned} s_{\delta a2} &= 1 - \frac{R_{t2}}{R_{t1}}(1 - m_{ru})(1 - s_{\delta a1}) \\ &= 1 - \left(\frac{R_{t1}}{R_{t1}} - \frac{R_{t1} - R_{t2}}{R_{t1}}\right)(1 - m_{ru})(1 - s_{\delta a1}) \\ &= 1 - (1 - m_R)(1 - m_{ru})(1 - s_{\delta a1}) \\ &= 1 - (1 - m_{ruR})(1 - s_{\delta a1}) \end{aligned} \tag{3.65}$$

In the case of $V_{t1} = V_{t2}$, when $m_{ru} = 0$, expression (3.65) becomes:

$$s_{\delta a2} = m_R + s_{\delta a1} - m_R s_{\delta a1} \tag{3.66}$$

It was pointed out previously that in the case of rectilinear motion it is possible to neglect the term $m_{ru}s_{\delta a1}$ in formula (3.61) since m_{ru} usually does not exceed 0.08. Extending this assumption to formula (3.66), one can find, upon substitution of formula (3.16), that $m_{ru} = 0.08$ has corresponding to it the angle $\delta \approx 21°$. It follows from this that in the majority of turns, when angle δ does not exceed 21°, it is permissible to use the simplified relationship:

$$s_{\delta a2} = m_R + s_{\delta a1} \tag{3.67}$$

At higher values of δ the exact formula (3.66) should be used, since the error of using formula (3.67) increases at $\delta > 21°$. For example, at $\delta = 35°$ the kinematic discrepancy factor from formula (3.16) is $m_R = 0.18$, and the imprecision in determining the magnitude of slip may be as high as 9%.

The above imply that general formulae (3.61) and (3.65) and their simplifications (3.62) and (3.67) show that in the presence of kinematic inconsistency of theoretical velocities, the slippages of wheels of a vehicle with a positive engagement of the driving axles are not the same.

Analysis of a 4×4 vehicle moving at constant velocity in a straight path (Figure 3.19) is continued. It follows from formula (3.62) that can be used for investigating the slipping of the wheels of this vehicle, that the slippages, $s_{\delta a1}$ and $s_{\delta a2}$ may take both positive and negative values, depending on the magnitude and sign of m_{ru}. If $m_{ru} > 0$ (that is, in formula (3.6) $V_{t2} > V_{t1}$) and $m_{ru} > s_{\delta a2}$, then slip $s_{\delta a1}$ will be negative, $s_{\delta a1} < 0$. In the case of $m_{ru} < 0$ ($V_{t1} > V_{t2}$) and $|m_{ru}| > s_{\delta a1}$, then, as seen from formula (3.62), $s_{\delta a2} < 0$.

The negative slippages are in fact sliding or skidding. It is important to emphasize that both of the vehicle's axles are, as before, coupled by a positive engagement drive. For this reason the wheels of one axle move in the driving mode (their slippage is positive), whereas the wheels of the other axle operate in the braking mode (their slippage is negative). The same conclusion follows from analysis of the motion of a vehicle taking a turn using formula (3.67). Negative slippage means that the circumferential force of this axle is also negative. This is seen, among others, from formula (1.25) that relates the circumferential force F_x of the wheel and its slippage s_δ. It is now understood why under certain conditions the wheels of all-wheel drive vehicles are capable of rolling in the braking mode without uncoupling them from the driveline system and without applying a braking torque to the braking mechanism (see Figures 1.42e and 1.46).

The inception of negative circumferential force (negative torque) on a part of the wheels of a vehicle with positively locked axles is now analyzed in more detail. Figure 3.28 shows layouts of front and rear wheels coupled by a locked differential for the case when

$$m_{ru} > 0, \quad m_{ru} > s_{\delta a2}, \quad \text{and} \quad s_{\delta a1} < 0.$$

The solid-line arrows show the flow of power from the engine and the transmission to the transfer case and further to the rear wheels. The sliding front wheels with negative F_{x1} generate a torque that, when multiplied by the angular velocity of the front wheels, forms a power flow from the front wheels through the driveline system to the transfer case. This power flow is shown by the dash-line arrow. The two power flows combine in the driveline system from the transfer case to the rear wheels and produce on them a high positive torque T_{w2}. This torque, generates a significant circumferential force F_{x2} of the rear wheels, which is spent in overcoming the rolling resistance R_{x2} of these wheels and produces a significant propelling force $F_{\text{frame}.x}$ that is transmitted through the vehicle's frame to the front-wheels'

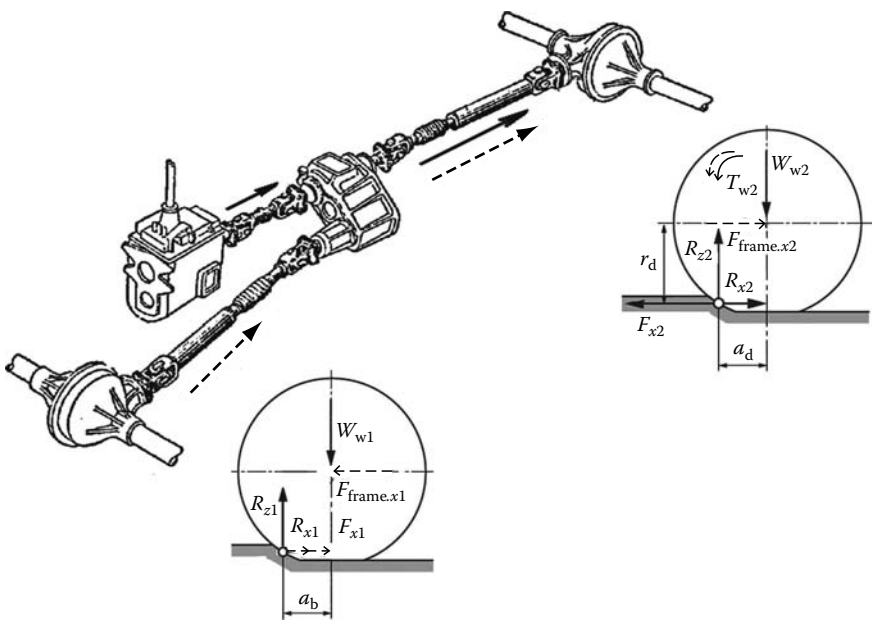


FIGURE 3.28
Parasitic power circulation in a 4 × 4 vehicle with positive engagement of two axles.

axle and overcomes the negative circumferential force F_{x1} and force R_{x1}. This generates a power flow that circulates in the closed loop consisting of: sliding front wheels—driveline system—driving rear wheels—vehicle's frame—sliding front wheels. It will be seen by inspecting the teeth of the final drive of the front axle of this vehicle that signs of wear appear on the rear side of the teeth, giving the impression that the vehicle traveled in reverse.

It follows from the above explanation of the processes that this circulating power is not an additional energy source, but solely puts an additional load on the driveline system and produces additional losses in it. For this reason, this circulating power is known as parasitic power.

Having explained the circulation of parasitic power, let us return to the diagrams of transfer cases from Figures 3.3 and 3.5. It is obvious that the layouts shown in Figures 3.3 and 3.5a and b permit parasitic power circulation under certain conditions. The principal difference between these layouts, however, consists in the fact that the gears of transfer cases from Figure 3.5a and b are not a part of the parasitic power circulation loop because the output shafts are coaxial. The noncoaxial arrangement of the transfer cases from Figure 3.3 is responsible for imposing an additional load on their gears under conditions of parasitic power circulation.

The mechanical power losses in the driveline system and wheel system are analyzed in Section 3.4. The present section continues the study of the effect of kinematic discrepancy on the circumferential forces on the wheels of axles of a 4×4 vehicle are now determined from Figure 3.19. The total circumferential force $F_{x\Sigma}$ of the vehicle is assumed to be known and equal to the applied resistance to motion. This force can be expressed upon substituting formula (2.412) in the following formula

$$F_{x\Sigma} = F_{x1} + F_{x2} = K_{a1} s_{\delta a1} + K_{a2} s_{\delta a2} \tag{3.68}$$

Simultaneous solution of formulae (3.62) and (3.68) yields the generalized slippages of the front and rear axles:

$$s_{\delta a1} = \frac{F_{x\Sigma} - K_{a2} m_{ru}}{K_{a1} + K_{a2}}, \quad s_{\delta a2} = \frac{F_{x\Sigma} + K_{a1} m_{ru}}{K_{a1} + K_{a2}} \tag{3.69}$$

then, using formula (2.412), the circumferential forces of the axles are expressed as:

$$\begin{aligned} F_{x1} &= K_{a1} \frac{F_{x\Sigma} - K_{a2} m_{ru}}{K_{a1} + K_{a2}} \\ F_{x2} &= K_{a2} \frac{F_{x\Sigma} + K_{a1} m_{ru}}{K_{a1} + K_{a2}} \end{aligned} \tag{3.70}$$

Equations 3.69 and 3.70 illustrate the dependence of the slippages and circumferential forces of the axles both on the total traction load of the vehicle, represented by force $F_{x\Sigma}$ and the kinematic discrepancy factor m_{ru}. If the wheels of both axles have equal longitudinal stiffness factors ($K_{a1} = K_{a2} = K_a$) (identical tires with equal normal loads and equal air pressure; the road conditions of axle travel are also the same), then

$$s_{\delta a1} = \frac{F_{x\Sigma}}{2K_a} - \frac{m_{ru}}{2}; \quad s_{\delta a2} = \frac{F_{x\Sigma}}{2K_a} + \frac{m_{ru}}{2} \tag{3.71}$$

If the kinematic discrepancy, is also equal to zero, then

$$s_{\delta a1} = s_{\delta a2} = \frac{F_{x\Sigma}}{2K_a} \tag{3.72}$$
$$F_{x1} = F_{x2} = 0.5F_{x\Sigma}$$

It is of interest to note that at very low total circumferential force of the vehicle, that is, at $F_{x\Sigma} \to 0$, one can have

$$s_{\delta a1} = -\frac{m_{ru}}{2}, \quad s_{\delta a2} = \frac{m_{ru}}{2}$$
$$F_{x1} = -K_a \frac{m_{ru}}{2}, \quad F_{x2} = K_a \frac{m_{ru}}{2} \tag{3.73}$$

Formulae (3.61), (3.62), (3.69), and (3.70) derived above allow gaining deeper insight into the operation of part-time driveline's that provide automatic engagement/disengagement of one or several axles of multiwheel drive vehicles. This shall be demonstrated for a 4×4 vehicle in which the front axle is engaged/disengaged using an overrunning clutch (see Figure 3.7). When the vehicle moves in a straight line over a well-paved road, the slippage $s_{\delta a2}$ is not too great and does not exceed the kinematic discrepancy m_{ru}. In this case, due to the design kinematic discrepancy m_{ru}, ring 2 is rotated by the engine at a lower speed than ring 1 that is rotated by the front wheels. For this reason, rollers 3 are not wedged in between rings 1 and 2 and no torque is transmitted to the front wheels. The front wheels are coupled to the driveline system only in the case when the rear-wheels slippage $s_{\delta a2}$ becomes equal to m_{ru}. In fact, it is seen from formula (3.62) that, when $s_{\delta a2} > m_{ru}$, $s_{\delta a1} > 0$ (and, accordingly, $F_{x1} > 0$). The linear velocity of the vehicle decreases when $s_{\delta a2}$ increases over the range $0 < s_{\delta a2} < m_{ru}$ and, as a result, the angular velocity of the front wheels, which are not yet connected to the driveline system and are rotated by the road, decreases. When m_{ru} attains the value of $s_{\delta a2}$, the angular velocities of rings 1 and 2 in Figure 3.7 equalize. As $s_{\delta a2}$ increases further, rollers 3 are wedged in and the torque from ring 1 starts being transmitted to the front wheels.

It is obvious that the slippage $s_{\delta a2}$ and with it the time when the front axle is engaged by means of the overrunning clutch, depends on the traction load $F_{x\Sigma}$. This shall be demonstrated for the case of $K_{a1} = K_{a2} = K_a$:

$$F_{x\Sigma} = F_{x1} + F_{x2} = K_a(s_{\delta a1} + s_{\delta a2}) \tag{3.74}$$

and, upon substitution of formula (3.62), this yields

$$F_{x\Sigma} = K_a(2s_{\delta a2} - m_{ru}) \tag{3.75}$$

Graphical interpretation of (3.75) is plotted in Figure 3.29 as the straight line $O_1A_1B_1$ for some value of m_{ru1} and straight line $O_2A_2B_2$ for another value $m_{ru2}(m_{ru2} > m_{ru1})$.

Points O_1 and O_2 serve as the origin of positive values of the total circumferential force $F_{x\Sigma}$. When the vehicle is moving forward, the front axle becomes engaged when the rear-axle wheels exceed the slippage $s_{\delta a2} = m_{ru1}$ (point A_1) and $s_{\delta a2} = m_{ru2}$ (point A_2). It is seen from Figure 3.29 that the abscissas of points A_1 and A_2 correspond to zero values of circumferential force F_{x1} of the front wheels. The ordinates of points A_1 and A_2 correspond

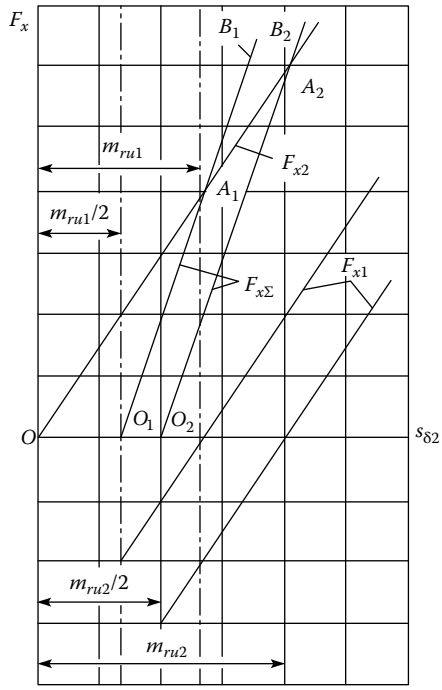


FIGURE 3.29
4 × 4 vehicle: circumferential wheel forces.

to the circumferential force of the rear wheels, $F_{x2} = F_{x\Sigma}$. This means that points A_1 and A_2 correspond to the borderline situation, when upon further increase in $F_{x\Sigma}$ and $s_{\delta a2}$, force F_{x1} becomes positive (the front axle becomes engaged) and $F_{x2} < F_{x\Sigma}$, that is,

$$F_{x\Sigma} = F_{x1} + F_{x2}$$

When the vehicle moves in reverse, the overrunning clutch becomes immediately engaged. In fact, rings 1 and 2 rotate in opposite direction and rollers 3 lock both rings (see Figure 3.7). In this case reducing force $F_{x\Sigma}$ to the ordinates of points A_1 and A_2 in Figure 3.29 will cause $s_{\delta a2}$ to be equal to kinematic inconsistency m_{ru1} (or m_{ru2}). At this instant, the front axle becomes disengaged and the vehicle will be propelled by force $F_{x2} = F_{x\Sigma}$.

It will be now shown that the distribution of circumferential forces and the generalized slippage of the axles depend on road conditions, that is, on the longitudinal stiffness coefficient K_a. At constant m_{ru}, when the vehicle travels over a solid road, the front driving axle will be engaged at a much higher traction load than the load transmitted by the principal, rear axle. This is seen from Figure 3.30.

Point A_1 on this figure corresponds to K_a^s, whereas point A_2 to $K_a^l \left(K_a^l > K_a^s\right)$. It follows from this that force F_{x1} of the front driving axle either decreases to a lesser extent than force F_{x2} of the principal driving axle, or becomes negative. In other words, the generalized slippage of the wheels of the front axle decreases slower than the generalized slippage of the wheels of the rear-driving axle. The overrunning clutch shown in Figure 3.8 provides identical engagement/disengagement of the front axle whether the vehicle moves forward or in reverse.

This demonstrates that kinematic inconsistency is necessary for ensuring automatic engagement/disengagement of the axle by means of the overrunning clutch. As was shown, the slippage and circumferential forces of the wheels are then not the same, but are

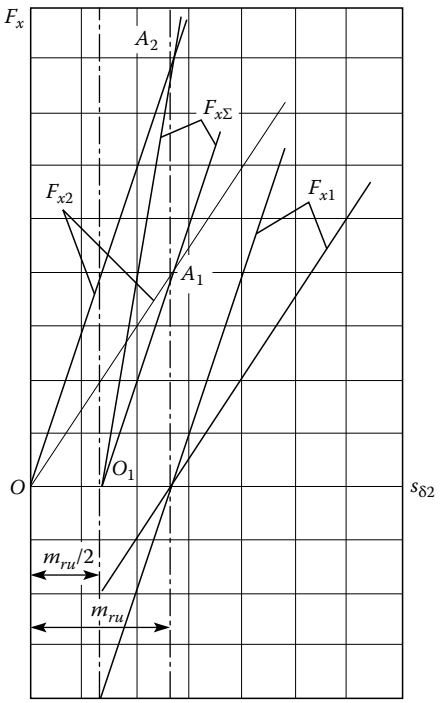


FIGURE 3.30
4×4 vehicle: circumferential wheel forces.

defined by formulae (3.69) and (3.70). If the value of the design kinematic discrepancy factor is specified based on recommendations in Section 3.6, then the overrunning clutch will provide reliable engagement/disengagement of the axle. Too low or negative values of the design kinematic discrepancy will cause the overrunning clutch to constantly operate in the ''engaged/disengaged'' mode or, at negative values of m_{ru}, the clutch will be continuously engaged, that is, the front axle will continuously operate under positive force F_{x1}. This is clearly seen from formulae (3.62), (3.69), and (3.70). The continuous engagement/disengagement of the overrunning clutch causes impact loads in the driveline system, whereas continuous engagement of the front axle obviates the need for placing the overrunning clutch. This must be remembered in designing driveline system with this type of clutch. The above also applies to some on-demand systems for engaging an additional axle. The absence of design kinematic discrepancy and the appearance of operational kinematic discrepancy may also cause similar phenomena in these driveline systems.

There is a necessity to directly determine engine torque split among the wheels in some engineering problems. Such torque distribution for a 4×4 vehicle with a positive engagement of the two driving axles can be described by the torque distribution factor u_p that is further determined using the expressions (3.70):

$$u_p = \frac{T_2}{T_1} = \frac{F_{x2} r^0_{a2}}{F_{x1} r^0_{a1}} \frac{u_1}{u_2} = \frac{F_{x\Sigma} + K_{a1} m_{ru}}{F_{x\Sigma} - K_{a2} m_{ru}} \frac{K_{a2}}{K_{a1}} \frac{r^0_{a2}}{r^0_{a1}} \frac{u_1}{u_2} \tag{3.76}$$

Note that the torque distribution factor u_p can also be defined as the gear ratio of an interaxle differential u_d that provides the same torque distribution between the two axles if $u_p = u_d$ ($F_{x1} > 0$; $F_{x2} > 0$). Hence, the expression (3.76) presents a mathematical link between the kinematic discrepancy m_{ru} of a 4×4 vehicle with a positively engaged

interaxle drive and the gear ratio u_d of an interaxle differential that, being employed on the vehicle, provides the same torque distribution between the front and rear axles as the kinematic discrepancy m_{ru}. Equation 3.76 is useful in vehicle complex models when the engine torque should be directly split between the axles.

The results obtained above shall be subsequently extended to vehicles with an arbitrary number of driving axles coupled by a positively engaged driveline system.

3.3.2 $2m \times 2n$ Vehicles

The case of n driving axles of a vehicle with total number m of driving and driven axles ($m \geq n$) was shown in Figure 3.20. The driving axles are coupled by a positively locked driveline system and the generalized slippage $s_{\delta ai}$ of the ith axle is determined by its kinematic discrepancy factor m_{Hi} and the generalized slippage $s_{\delta a}$ of the vehicle from formula (3.24). The kinematic discrepancy factors are calculated for all the axles from formula (3.30). Hence, in order to calculate slippage $s_{\delta ai}$, $i = 1, n$, it is first necessary to determine $s_{\delta a}$. For this, the relationship between the circumferential force F_{xi} of the axle and its generalized slippage $s_{\delta ai}$ is represented as $F_{xi} = f_i(s_{\delta ai})$. Examples of linear and nonlinear relationships were given in Section 1.3.2. Then the total circumferential force $F_{x\Sigma}$ of the vehicle that is assumed to be known and equal to the resistance to the vehicle's motion is defined as:

$$F_{x\Sigma} = \sum_{i=1}^{n} F_{xi} = \sum_{i=1}^{n} f_i(s_{\delta ai}) \tag{3.77}$$

or, upon substitution of formula (3.30)

$$\sum_{i=1}^{n} f_i(m_{Hi}, s_{\delta a}) = F_{x\Sigma} \tag{3.78}$$

When the values of m_{Hi}, $i = 1, n$ and $F_{x\Sigma}$ are known, generalized slippage $s_{\delta a}$ can be found from formula (3.78). In the case of exponential relationship (1.26), formula (3.78) becomes

$$\sum_{i=1}^{n} R_{zi}\mu_{pxi}(1 - \exp(-k_i(m_{Hi} + (1 - m_{Hi})s_{\delta a}))) = F_{x\Sigma} \tag{3.79}$$

whence, $s_{\delta a}$ can be determined by one of the iterative methods of solving algebraic equations. In the when $F_{xi} = K_{ai}s_{\delta ai}$ is linear, formula (3.78) simplifies highly and becomes:

$$s_{\delta a} = \frac{F_{x\Sigma} - \sum_{i=1}^{n} K_{ai}m_{Hi}}{\sum_{i=1}^{n} K_{ai}(1 - m_{Hi})} \tag{3.80}$$

Formulae (3.79) and (3.80) allow calculating the generalized slippage of the vehicle; this is followed by determining the generalized slippage of the axles $s_{\delta ai}$ from the expression (3.24) and then the circumferential forces F_{xi} from the assumed relationship $F_{xi} = f_i(s_{\delta ai})$. The value of $s_{\delta a}$ is also used for calculating the actual velocity of the vehicle using formula (3.23).

As an illustration, consider a 6×6 power-module driven vehicular train consisting of a 4×4 tractor and a technological (service) module, that is, an additional driving axle.

Examples of the use of such a vehicle were given in Section 1.2 (item 1 in Table 1.12 and Figure 1.39). The wheels of each of the three axles are of a different size and the interaxle driveline system is a positive engagement. It is proposed that the front axle of the tractor and the driving axle of the service module be engaged/disengaged automatically by means of overrunning clutches, for which reason design kinematic discrepancy should be introduced into the interaxle drive. This necessitates determining the order of engagement of the first and third axles in the traction mode and selecting the numerical values of kinematic discrepancy factors m_{Hi} $(i = 1, 3)$ to provide better energy efficiency of this vehicle. The question of the order of engagement boils down to deciding in what sequence should the first and the third axles be engaged when the traction load and the slippage of the wheels of the second, principal axle increase. Should it be the first, the third, or both simultaneously?

To solve this problem, it is first necessary to calculate the circumferential forces F_{xi} $(i = 1, 3)$ of the axles. This question is examined below using the exponential relationship (1.26). Force $F_{x\Sigma}$ contained in formula (3.78) is determined from the computational model of the power-module driven vehicular train shown in Figure 3.31.

Figure 3.32 shows the results of calculation of the circumferential forces of axles coupled rigidly by a positively locked driveline (without overrunning clutches in the axles' drives). The calculations were performed for different combination of design kinematic discrepancy factors m_{Hi} that are obtained by varying gear ratios u_i in the running gear of the axles (see formula (3.30)). The dashed lines correspond to the case of $F_{x\Sigma} \approx 0$, and the dash-dotted lines to travel without a load (idle) on a field prepared for sowing. Solid lines 1–4 reflect the circumferential forces of the axles for the case when the vehicle is loaded by different drawbar pull loads F_{d}.

The dashed lines graphically reflect the substance of phenomena associated with the inception of kinematic discrepancy in positive engagements of multiwheel drive vehicles. When the theoretical axle velocities are equal $(V_{t1} = V_{t2} = V_{t3})$, the circumferential forces F_{xi} are equal to zero (version a, Figure 3.32). Introduction of the design kinematic discrepancy into the axle drive causes, depending on the values and signs of factors m_{Hi}, the appearance of positive or negative circumferential forces at the axles (versions b–f in Figure 3.32). Even though the algebraic sum of these forces is equal zero, they cause slippage (sliding,

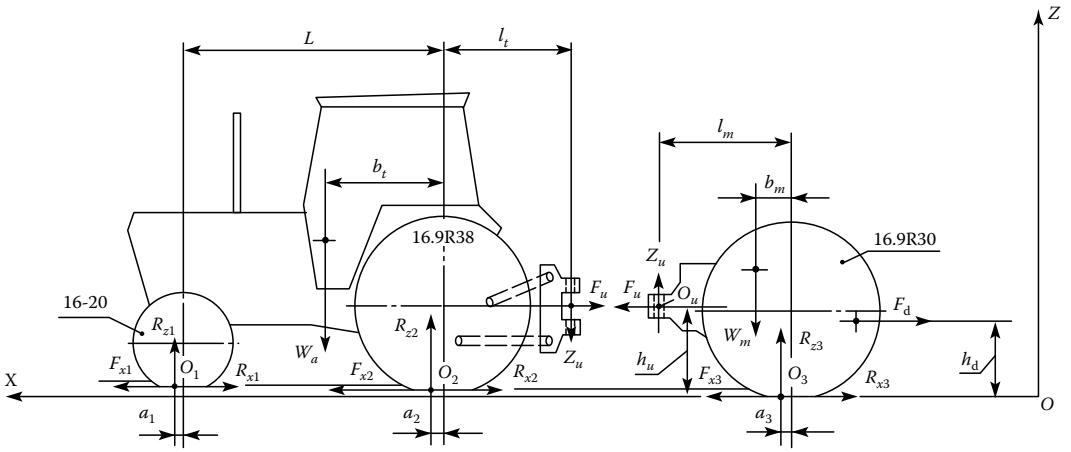


FIGURE 3.31
6 × 6 power-module driven vehicular train: free-body diagram.

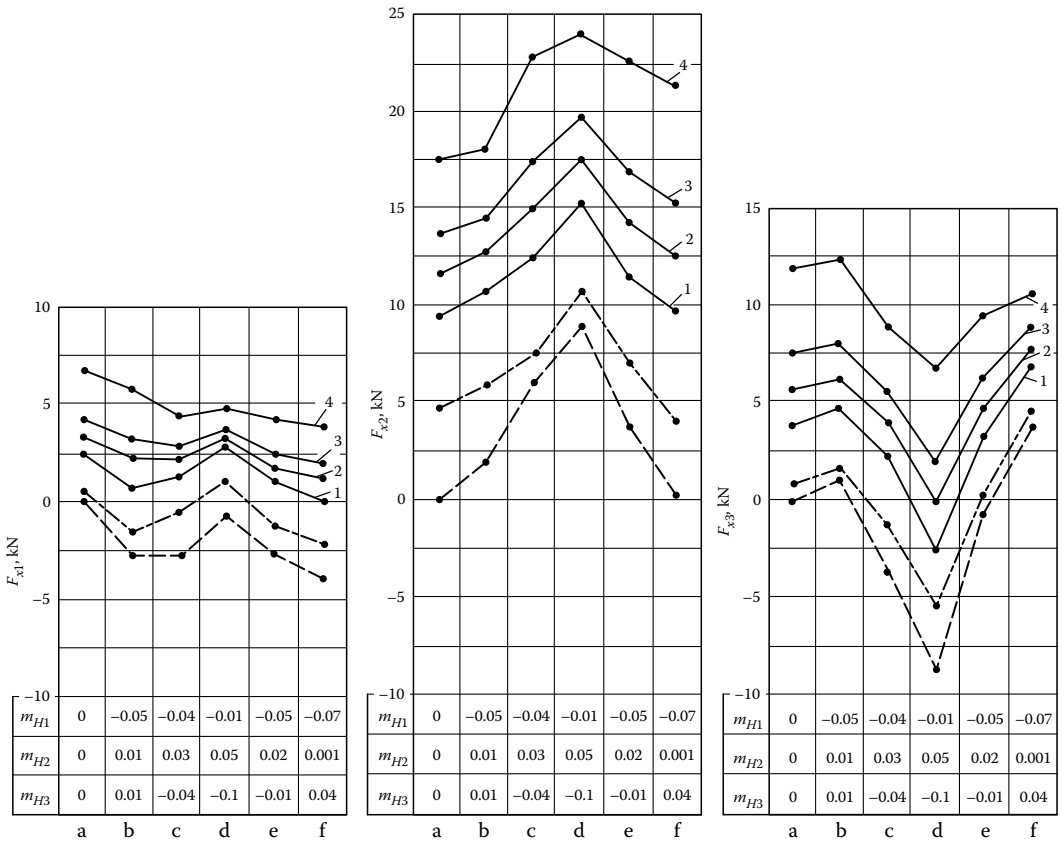


FIGURE 3.32
Circumferential force distributions among the axles of 6 × 6 power-module driven vehicular train. ---- $F_{x\Sigma} \approx 0$; —·— $F_d = 0; 1, 2, 3, 4, F_d = 10; 15; 20; 30$ kN; a, $V_{t1} = V_{t2} = V_{t3}$; b, $V_{t1} < V_{t2} = V_{t3}$; c, $V_{t2} < V_{t1} = V_{t3}$; d, $V_{t2} < V_{t1} < V_{t3}$; e, $V_{t2} > V_{t3} > V_{t1}$; f, $V_{t3} > V_{t2} > V_{t1}$.

i.e., negative slippage) of the axles' wheels, equal, as follows from formula (3.24) to the corresponding factors m_{Hi}.

As seen from Figure 3.32, the synchronous positive engagement of the drive axles that has corresponding to it zero values of m_{Hi} ensures positive circumferential forces of all the axles at all the values of traction load F_d (curves 1–4 version a).

When the theoretical velocities of the second and third axles are equal ($V_{t2} = V_{t3}$), their forces F_{x2} and F_{x3} are also equal and a certain specified lagging of the front axle ($V_{t1} < V_{t2} = V_{t3}$) may cause the force F_{x1} to become negative (version b). Calculations show that the latter occurs at traction loads smaller than 7.5 kN.

In the case of a positive engagement drive between the first and third axles and some lag of both of these behind the second axle, forces F_{x1} and F_{x3} are positive at traction loads higher than 3 kN (version c).

If the velocity V_{t3} of the third axle is even lower, compared with the second axle, than that of the first axle, then force F_{x3} is negative at $F_d < 16$ kN (version d).

In the case of $V_{t2} > V_{t3} > V_{t1}$ forces F_{x2} and F_{x3} are positive over the entire range of values of F_d, whereas force F_{x1} takes positive values at traction forces higher than 5 kN (version e).

If the kinematic discrepancy was selected in such a manner that $V_{t3} > V_{t2} > V_{t1}$, (version f), then force F_{x3} increases steeply, whereas F_{x1} is positive only at $F_d > 10$ kN.

The data presented above on the circumferential forces of axles are utilized in Section 3.4 in assessing the energy efficiency of this vehicle and are needed in designing overrunning clutches for engaging the first and third axle.

The examples examined above illustrate the distribution of circumferential forces between the driving axles, that is, no consideration was given to the distribution of forces between the left and right wheel of a given axle. Now an example is presented of compiling formulae for determining the circumferential forces and slippage of four wheels of a 4×4 vehicle in which all the three power-dividing units are positively locked. It is assumed that the relationship between circumferential force F_x and the slippage s_δ of the wheel is linear (see formula (1.25)). The principal equation consists of the sum of the circumferential forces of the wheels or of the sum of their projections on the longitudinal axles of the vehicle in the case of curvilinear motion, equal to the applied resistance:

$$\sum_{i=1}^{2} F_{xi}^{\prime(\prime\prime)} \cos \delta_i^{\prime(\prime\prime)} = F_{x\Sigma} \tag{3.81}$$

or, upon substitution of formula (1.25), one can have

$$\sum_{i=1}^{2} K_{xi}^{\prime(\prime\prime)} s_{\delta i}^{\prime(\prime\prime)} \cos \delta_i^{\prime(\prime\prime)} = F_{x\Sigma} \tag{3.82}$$

Formula (3.82) contains four unknown slippages $s_{\delta i}^{\prime(\prime\prime)}$, $i = 1, 2$. These are determined by compiling additional equations, using the relationships between the slippage of wheels, generalized slippage of the axles $s_{\delta ai}$, $i = 1, 2$, generalized slippage of the vehicle $s_{\delta a}$ and the kinematic discrepancy factors. The slippages $s_{\delta i}^{\prime(\prime\prime)}$, $i = 1, 2$ are related to the generalized slippages of the axles $s_{\delta ai}$, $i = 1, 2$ by formula (3.58), the application of which yields the following expressions

$$\begin{aligned} s_{\delta 1}^{\prime} &= m_{H1}^{\prime} + \left(1 - m_{H1}^{\prime}\right) s_{\delta a1} \\ s_{\delta 1}^{\prime\prime} &= m_{H1}^{\prime\prime} + \left(1 - m_{H1}^{\prime\prime}\right) s_{\delta a1} \\ s_{\delta 2}^{\prime} &= m_{H2}^{\prime} + \left(1 - m_{H2}^{\prime}\right) s_{\delta a2} \\ s_{\delta 2}^{\prime\prime} &= m_{H2}^{\prime\prime} + \left(1 - m_{H2}^{\prime\prime}\right) s_{\delta a2} \end{aligned} \tag{3.83}$$

where, the kinematic discrepancy factors $m_{Hi}^{\prime(\prime\prime)}$, $i = 1, 2$ are calculated from formula (3.57). In their turn, the generalized slippages $s_{\delta a1}$ and $s_{\delta a2}$ of the axles are related to the generalized slippage $s_{\delta a}$ of the vehicle by formula (3.24), on the basis of which are written two additional formulae:

$$\begin{aligned} s_{\delta a1} &= m_{H1} + (1 - m_{H1}) s_{\delta a} \\ s_{\delta a2} &= m_{H2} + (1 - m_{H2}) s_{\delta a} \end{aligned} \tag{3.84}$$

in which the kinematic discrepancy factors m_{H1} and m_{H2} are calculated from formula (3.30). The generalized rolling radii in the driven mode r_{a1}^0 and r_{a2}^0 contained in formula (3.30) are calculated using formula (3.56). The above means that the seven equations described by

formulae (3.82) through (3.84) contain seven unknowns: $s_{\delta i}^{\prime(\prime\prime)}$, $i = 1, 2$, $s_{\delta ai}$, $i = 1, 2$, and $s_{\delta a}$. After the wheel slippages $s_{\delta i}^{\prime(\prime\prime)}$, $i = 1, 2$ are determined from these equations, formula (1.25) can be used for calculating the circumferential wheel forces $F_{xi}^{\prime(\prime\prime)}$, $i = 1, 2$.

This means that the method developed in this section makes it possible to investigate the force intensity of a vehicle's axles that, as was shown, is determined by the numerical values and signs of the kinematic discrepancy factors $m_{Hi}^{\prime(\prime\prime)}$.

3.4 Wheel Power Distributions and Vehicle Energy/Fuel Efficiency

This section demonstrates the physical substance of changes in power losses in contact patches between the tires and the underlying surface and power losses in a positively engaged driveline system upon distribution of power among the driving axles. Analytic expressions are given for determining these losses as a function of the kinematic discrepancy, gripping conditions of the wheels and the total circumferential force of the vehicles. The methods and formulae that are presented are needed for assessing the energy and fuel efficiency of vehicles with positively locked driveline systems.

3.4.1 Mechanical Power Losses in Wheel Systems

In the presence of kinematic discrepancy, agreement between the travel, linear, and angular velocities of wheels is attained by additional longitudinal deformation of tires (of tires and soil on deformable surfaces). This is also because of possible relative motion of the patch of contact between the tire and the road and motion of the soil layers together with the tire on deforming surfaces. This changes the rolling radii of the wheels and causes redistribution of torques/circumferential forces between the wheels that affects power losses in the contact between wheels and the surface of motion. It should be emphasized that in this case reference is had to additional, positive or negative deformation relative to that determined by the tractive load of the vehicle in the absence of kinematic discrepancy. This discrepancy is thus seen to exert a direct effect on the relationship between the tire slippage factors and, consequently, on power losses in the wheel system and on the energy/fuel efficiency of vehicles. This shall be demonstrated analytically.

Start with examining an equivalent layout of a 4×4 vehicle with positive engagement of its axles in uniform rectilinear motion (see Figure 3.19). The slippage power losses of both axles for the case of the linear relationship (2.412):

$$\begin{aligned} P_{\delta 1} &= F_{x1} V_{\delta 1} = K_{\mathrm{a}1} s_{\delta \mathrm{a}1} V_{t1} s_{\delta \mathrm{a}1} = K_{\mathrm{a}1} V_{t1} s_{\delta \mathrm{a}1}^2 \\ P_{\delta 2} &= K_{\mathrm{a}2} V_{t2} s_{\delta \mathrm{a}2}^2 \\ P_{\delta \Sigma} &= \sum_{i=1}^{2} P_{\delta i} = \sum_{i=1}^{2} K_{\mathrm{a}i} V_{ti} s_{\delta \mathrm{a}i}^2 \end{aligned} \tag{3.85}$$

Analyze first the case of identical gripping conditions of both axles, that is, $K_{\mathrm{a}1} = K_{\mathrm{a}2} = K_{\mathrm{a}}$. With reference to formula (3.6) that relates the kinematic discrepancy factor m_{ru} with the theoretical velocities of the axles V_{t1} and V_{t2}, the formula for the slippage power losses become

$$P_{\delta \Sigma} = K_{\mathrm{a}} V_{t2} \left[s_{\delta \mathrm{a}1}^2 (1 - m_{ru}) + s_{\delta \mathrm{a}2} \right] \tag{3.86}$$

The generalized slippage $s_{\delta a}$ that is determined by the total circumferential force $F_{x\Sigma}$ is now introduced:

$$\begin{aligned} s_{\delta a} &= \frac{F_{x\Sigma}}{2K_a} \\ s_{\delta a} &= s_{\delta a1} + \frac{m_{ru}}{2} = s_{\delta a2} - \frac{m_{ru}}{2} \end{aligned} \tag{3.87}$$

Note that simplification of the second of expressions (3.87) yields formula (3.62) that relates the generalized slippages of the axles to the kinematic discrepancy m_{ru}. The factor $s_{\delta a}$ that is the same for both axles is determined by the traction load on the vehicle, which follows from the first of expressions (3.87).

Upon substitution of formulae (3.87), expression (3.86) becomes:

$$P_{\delta\Sigma} = K_a V_{t2}\left[(1 - m_{ru})\left(s_{\delta a} - \frac{m_{ru}}{2}\right)^2 + \left(s_{\delta a} + \frac{m_{ru}}{2}\right)^2\right] \tag{3.88}$$

Opening the parentheses and neglecting higher-order infinitesimals, yields:

$$P_{\delta\Sigma} = \frac{V_{t2}}{2K_a}\left(F_{x\Sigma}^2 + K_a^2 m_{ru}^2\right) \tag{3.89}$$

It follows from formula (3.89) that the power lost in slippage is a function of the square of the total circumferential force $F_{x\Sigma}$ on the vehicle and the square of the kinematic discrepancy factor m_{ru}. In the absence of kinematic discrepancy, $P_{\delta\Sigma}$ depends only on the traction load $F_{x\Sigma}$. In the absence of traction load and negligible resistance to motion ($F_{x\Sigma} \to 0$), for example, in the towing mode and the presence of kinematic discrepancy, $P_{\delta\Sigma}$ depends only on the value of m_{ru}:

$$P_{\delta\Sigma} = \frac{K_a V_{t2} m_{ru}^2}{2} \tag{3.90}$$

As an illustration, Figure 3.33 shows curves of $P_{\delta\Sigma}$ as a function of m_{ru} calculated from formula (3.89) for a 4×4 truck (tractor-semitrailer combination) moving with a loaded trailer over asphalt and on a dirt road.

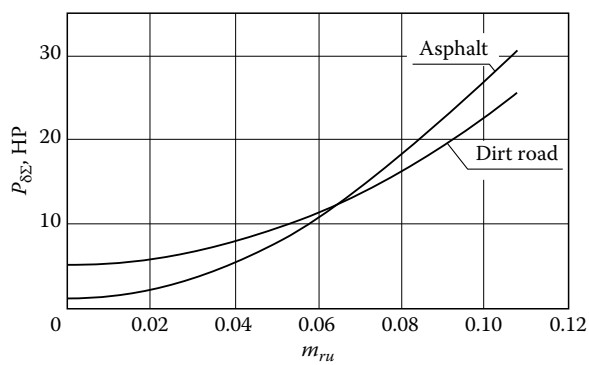


FIGURE 3.33
4×4 truck of total mass of 30 ton: slip power loss.

The locations of the origins of curves on the ordinate axis reflect the slippage power loss determined by the total load $F_{x\Sigma}$. It is seen that the greater m_{ru} the greater the power losses. When moving over soil (which is characterized by lower longitudinal stiffness K_a of the tires and the soil) the power losses that stem from load $F_{x\Sigma}$ are greater, but the rate of increase of these losses with increasing m_{ru} is smaller than on paved roads.

From formula (3.89) and Figure 3.33 follows an important result: an increase in $P_{\delta\Sigma}$ occurs not only upon power circulation (see Figure 3.28) but also in cases when slippage of front and rear wheels is not the same, that is, in the presence of kinematic discrepancy. For the case of identical gripping conditions of both axles under study here ($K_{a1} = K_{a2} = K_a$) the law of increase in power loss in the wheel system can be formulated thus: slippage power losses $P_{\delta\Sigma}$ at unchanged total load ($F_{x\Sigma} = F_{x1} + F_{x2} = \text{constant}$) increase with increasing difference between the circumferential forces of the axles (F_{x1} and F_{x2}), that is, upon increasing the redistribution of power between the axles.

The next item consists in clarifying what are the slippage power losses $P_{\delta\Sigma}$ of a 4×4 vehicle in the case of different gripping conditions of the front and rear axles, that is, when $K_{a1} \neq K_{a2}$. This is done using formula (3.85) that defines $P_{\delta\Sigma}$ in general form. This formula was transformed in Section 2.9 to a form that is represented by formula (2.419). It was shown in that section that the minimum value of $P_{\delta\Sigma}$ is attained at $s_{\delta a1} = s_{\delta a2}$. This equality is attained by a locked axle drive with zero kinematic discrepancy (see formula (3.61) at $m_{ru} = 0$). Hence, substitution of

$$s_{\delta a1} = s_{\delta a2} = \frac{F_{x1}}{K_{a1}} = \frac{F_{x2}}{K_{a2}} \tag{3.91}$$

into (2.419) yields the following expression for the slippage power loss with a locked drive of the axles with $m_{ru} = 0$:

$$P_{\delta\Sigma} = V_a F_{x\Sigma}^2 \frac{1}{K_{a1} + K_{a2}} \tag{3.92}$$

Figure 3.34 displays the results of calculations using formula (3.92), represented by curve 1 for a 7.8 ton 4×4 tractor with identical wheels and total circumferential force $F_{x\Sigma} = 30$ kN.

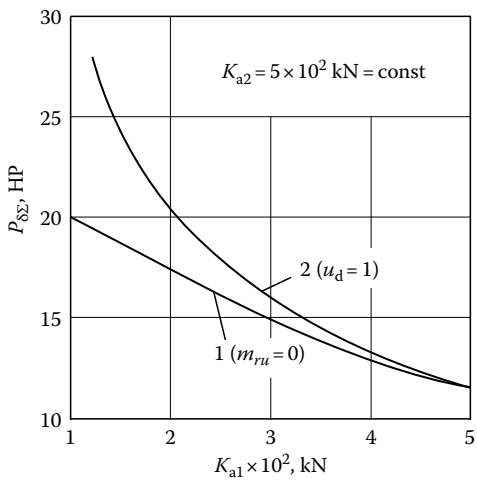


FIGURE 3.34
4×4 tractor: slip power losses. 1, $m_{ru} = 0$; $s_{\delta a1} = s_{\delta a2}$; 2, $u_d = 1$.

The longitudinal stiffness factor was taken to be constant and equal to $K_{a2} = 5 \times 10^2$ kN, whereas K_{a1} ranged from 5×10^2 to 1×10^2 kN. Curve 2 transferred to Figure 3.34 from Figure 2.130 corresponds to a interaxle differential with $u_d = 1$. It is seen that curve 1, corresponding to a positive engagement of the axles with zero kinematic discrepancy reflects the most efficient mode of the wheel system operation at variable K_{a1} when $s_{\delta a1} = s_{\delta a2}$ and $F_{x1} \neq F_{x2}$.

It should be emphasized in summing up the material presented above, that slippage power losses of a 4×4 vehicle at zero traction load ($F_{x\Sigma} \to 0$) increase in proportion to the square of the kinematic inconsistency. The slippage losses that stem from traction load $F_{x\Sigma}$ are of constant magnitude and are composed of losses caused by kinematic discrepancy over the entire range of values of m_{ru}. The harder the surface of motion, the lower the traction-load slippage losses. Conversely, the harder the surface, the more rapidly the kinematic discrepancy caused losses increase.

To obtain a relative assessment of slippage power losses it is convenient to use the slip efficiency η_δ (see formulae (1.72) and (1.73)) and the efficiencies of running gear, also presented in Section 1.4.2. Assuming that the circumferential force F_x is a linear function of the slippage, that is, $F_x = K_a s_{\delta a}$, expression (1.73) can be reduced to the following form (for 4×4 vehicles):

$$\eta_\delta = 1 - \frac{K_{a1} s_{\delta a1}^2 (1 - s_{\delta a2}) + K_{a2} s_{\delta a2}^2 (1 - s_{\delta a1})}{K_{a1} s_{\delta a1} (1 - s_{\delta a2}) + K_{a2} s_{\delta a2} (1 - s_{\delta a1})} \tag{3.93}$$

At identical gripping conditions, when $K_{a1} = K_{a2} = K_a$, formula (3.93) becomes:

$$\eta_\delta = 1 - \frac{s_{\delta a1}^2 (1 - s_{\delta a2}) + s_{\delta a2}^2 (1 - s_{\delta a1})}{s_{\delta a1} (1 - s_{\delta a2}) + s_{\delta a2} (1 - s_{\delta a1})} \tag{3.94}$$

To calculate efficiency η_δ of a 4×4 vehicle with a positive engagement of the driving axles, it is first necessary to determine the slippages $s_{\delta a1}$ and $s_{\delta a2}$. These slippages are determined from formulae (3.69) for the case when the relationship $F_x = K_a s_{\delta a}$ is linear. If $F_x = f(s_\delta)$ is nonlinear, then formulae (3.24) and (3.78) must be used. Consider the calculation of η_δ for the case of a 7.8 ton 4×4 tractor with positively locked axles. The gripping conditions are assumed to be the same ($K_{a1} = K_{a2} = K_a$) and the equation $F_x = f(s_\delta)$ is taken to be linear. Figure 3.35 presents a case of calculation for driving over stubble.

Straight line AB on this figure corresponds to motion with two driving axles at $m_{ru} = 0$. Straight line AC is for motion with solely the rear-driving axle. Curves 1 through 8 represent the efficiency η_δ of the tractor with both axles operating and in the presence of kinematic discrepancy. The location of curves 1 through 8 relative to straight line AB reemphasize the fact that introducing kinematic discrepancy causes inequality of generalized slippages of the axles and reduction in slippage efficiency η_δ. As the traction load increases, curves 1 through 8 approach asymptotically line AB. The points of interaction of these curves with straight line AC correspond to cases when circumferential force F_{x1} of the front axle becomes zero. The right-hand sides of curves 1–8 relative to line AC reflect cases when forces F_{x1} and F_{x2} and slippages $s_{\delta a1}$ and $s_{\delta a2}$ are positive. The left-hand side branches of these curves correspond to cases when F_{x1} and $s_{\delta a1}$ are negative, whereas the corresponding forces and slippages of the rear axle are positive, that is, when parasitic power circulation occurs. It is seen that in these cases the energy efficiency of a 4×4 tractor with

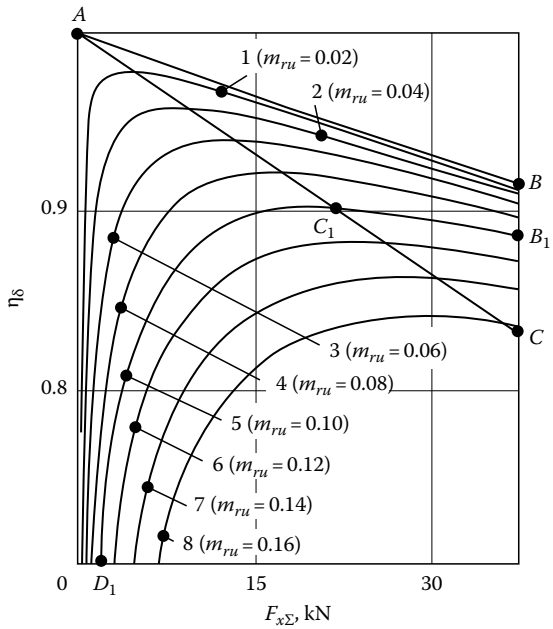


FIGURE 3.35
4 × 4 tractor with mass of 7.8 ton: slip efficiency vs. total circumferential force and kinematic discrepancy.

positively engaged axles is much lower than for the same tractor with the front axle disengaged.

Whereas, in the case of only the rear axle operating, or when two driving axles operate at $m_{ru} = 0$, the efficiency increases with decreasing $F_{x\Sigma}$ and tends to unity as $F_{x\Sigma} \to 0$, then in the presence of kinematic discrepancy the value of η_δ decreases at low $F_{x\Sigma}$ and $\eta_\delta \to 0$ as $F_{x\Sigma} \to 0$. In the last case the two axles slip in opposite directions, that is, slip power losses occur.

The energy efficiency of this tractor can be improved by installing an overrunning clutch in its interaxle drive. In fact, when $F_{x\Sigma}$ is reduced, the curve of η_δ will pass (for example, at $m_{ru} = 0.1$) along B_1C_1. The overrunning clutch will disengage the front axle in point C_1 and, instead of decreasing along curve C_1D_1, the curve of η_δ will vary along straight line C_1A. This behavior can be followed in Figure 3.35 also at other values of m_{ru}. This means that the existence of kinematic discrepancy, while reducing η_δ when both axles with positive circumferential forces F_{x1} and F_{x2} are engaged (segment C_1B_1 is located below AB) ensures reliable operation of the overrunning clutch and automatic disengagement of the front axle at $F_{x1} = 0$ (point C_1) upon a further increase in η_δ (segment AC_1 lies above C_1D_1). For this reason the design of an overrunning clutch amounts to finding a compromise between providing automatic engagement/disengagement of one axle and retaining a sufficiently satisfactory energy efficiency of the vehicle.

It must be remembered in practical application of the above analytic formulae that they are limited by the application of linear and nonlinear functional relationship that relate the circumferential force and the torque of the wheel to the wheel's rolling radius and slippage (reference were already made previously to the pertinent formulae from Section 1.3.2.). Under certain conditions, the use of linear relationships may cause significant quantitative errors. Such conditions include the motion of a vehicle with traction loads F_d that exceed the nominal. The higher values of F_d increase the total circumferential force $F_{x\Sigma}$ of the vehicle and, as a result, cause an increase in the circumferential forces of the

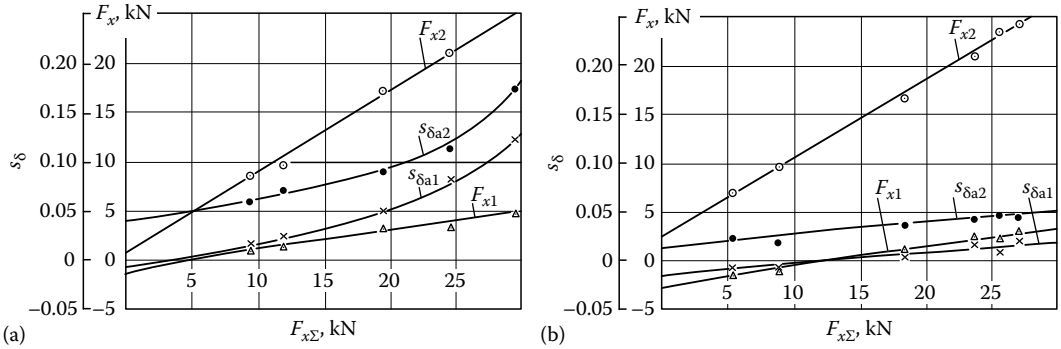


FIGURE 3.36
5.6-ton 4 × 4 tractor: (a) asphalt; (b) sowing-ready field.

wheels (recall that $F_{x\Sigma} = \sum_{i=1}^{n} F_{xi}$). An increase in forces F_{xi} increases the wheel slippages $s_{\delta i}$, that is, shifts the functional relationship $F_x = f(s_\delta)$ to the nonlinear range. As an illustration of the above, Figure 3.36 shows the computed and experimental values of the circumferential forces and slippages of the axles of a 5.6-ton 4×4 tractor with differently sized tires on the front and rear wheels. The tractor moves in straight line with a constant speed.

The interaxle drive is positively engaged and the kinematic discrepancy factor (m_{ru}) is 0.0372. It is seen that the use of linear relationships $F_x = f(s_\delta)$ for rear and front tires on an asphalt-paved road provides for satisfactory agreement between the predicted and experimental data in Figure 3.36a. At the same time the use of linear functions $F_x = f(s_\delta)$ instead of nonlinear ones when moving on deforming surfaces (sowing-ready field, Figure 3.36b) would have caused a significant difference between the computed and measured data. The satisfactory agreement of the results in Figure 3.36b is brought about by using nonlinear functions $F_x = f(s_\delta)$ in the calculations. It should be emphasized that $F_{x\Sigma}$ may increase also as a result of elevated inertia loads in the course of accelerating a vehicle, in heavy winds (air resistance) and on terrain.

In all-wheel drive vehicles with positive engagement of the driving axles an increase in the kinematic discrepancy may cause significant differences in slippage of wheels, that is, such large absolute values of slippage that are related nonlinearly to the circumferential forces of the wheels. The above is confirmed by data from Figure 3.37 that show the drawbar loads F_d that must be applied to a 4×4 tractor in order to bring about automatic engagement of its front axle by means of an overrunning clutch: the higher the numerical value of m_{ru}, the greater force F_d is needed for slippage $s_{\delta a2}$ to exceed this value of m_{ru} (see formula (3.62)) and to engage the front axle ($s_{\delta a1} > 0$).

Straight lines 1 were computed for a linear relationship $F_x = f(s_\delta)$, whereas curves 2 were computed from a nonlinear relationship between F_x and s_δ. The experimental results are in good agreement with curve 2 over the entire range of F_d and m_{ru}. At the same time, the relative errors of the analytic and experimental data for motion over asphalt (straight line 1) were 19% and 35% at $m_{ru} = 0.0917$ and $m_{ru} = -0.1054$, respectively. This discrepancy shows that the nonlinear relationship $F_x = f(s_\delta)$ should also be used for dense surfaces of motion when dealing with elevated wheel slippages. In the example under study (straight line 1 in Figure 3.37), the behavior of $F_x = f(s_\delta)$ for front wheels markedly deviates from linearity at $F_x \geq 7$ kN.

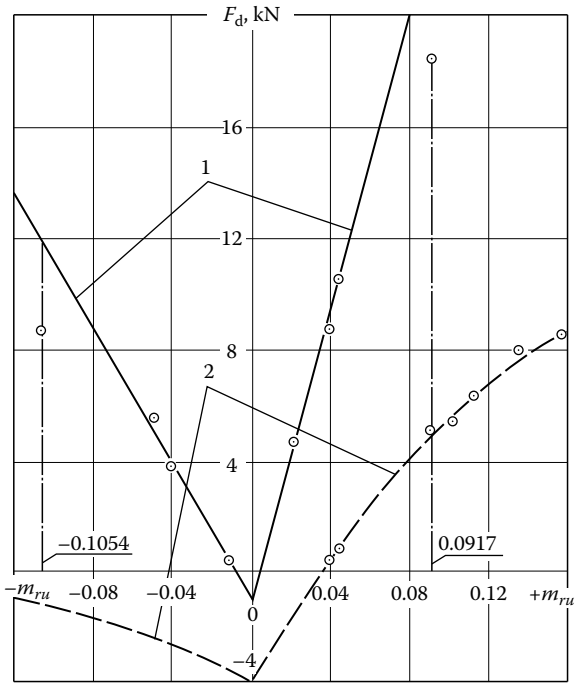


FIGURE 3.37
3.7-ton 4 × 4 tractor: drawbar pull vs. kinematic discrepancy: 1, asphalt; 2, terrain.

The examination of the energy efficiency of running gear of 4 × 4 vehicles with positive engagement of the drive axles is completed using the following example that graphically illustrates the feasibility of using the suggested method for modern drive designs. Consider a 15.2 kN SUV in which the rear axle is engaged by a friction clutch when the front-wheel slippage is increased. The drive of the axles is shown schematically in Figure 3.38 and the different clutch designs were examined in Section 3.1.

The vehicle accelerates in rectilinear motion. At the point in time under study the linear acceleration is $a_x = 2.6$ m/s^2. A significant redistribution of weight between the axles caused a difference in the rolling radii in the driven mode with the result that $r^0_{a1} = 0.286$ m and $r^0_{a2} = 0.278$ m. Because of this in the positively engaged axles (the clutch is fully locked), there arises a kinematic discrepancy of $m_r = (r^0_{a2} - r^0_{a1})/r^0_{a2} = -0.0288$.

Two cases of road conditions are examined: (i) all the wheels are on dry asphalt; (ii) the front wheels are on snow-covered asphalt, whereas the rear wheels are on still dry asphalt. Below are presented results of calculations for the following states of the rear-axle engagement clutch:

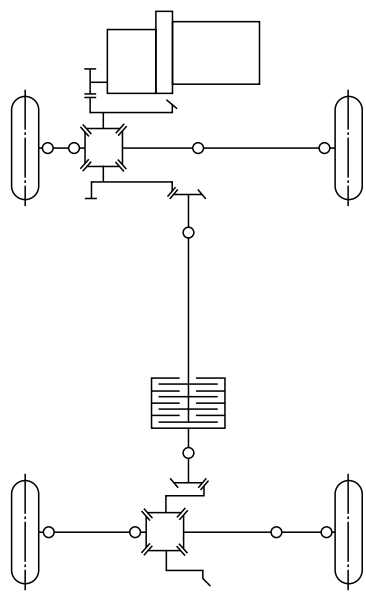


FIGURE 3.38
4 × 4 SUV: driveline system layout.

1. The clutch is disengaged, only the front axle is driving.
2. The clutch is fully engaged, both axles, coupled by a positively locked drive, are driving.
3. The clutch is partially engaged, that is, its disks have relative rotation. It is assumed that the clutch transmits a friction slippage torque T_{fr} equal to 50% of the torque corresponding to a fully-engaged clutch.

The results of numerical studies are listed in Table 3.1.

When the vehicle accelerates on an asphalt road, slippage efficiency η_δ is only slightly smaller than when using the 4×2 arrangement because of somewhat greater slippage of the front wheels as compared with slippage of the wheels of both axles in the case when the clutch is fully locked. Since a kinematic discrepancy m_r arose, the value of η_δ is somewhat lower than it would have been at $m_r = 0$. It is not advisable to control the friction torque of the clutch, that is, to unlock it partially, in this mode, since it reduces η_δ. Travel of the front wheels over a snow-covered part of the road causes a marked rise in their slippage and significant reduction in η_δ when the vehicle is driven by a single axle. Complete locking of the clutch, even in the case of $m_r = -0.0288$ significantly improves the energy efficiency: the value of η_δ increases from 0.921 to 0.9725. Partial unlocking of the clutch, that is, controlling the friction torque transmitted by it, in this driving mode is also inadvisable. It is seen from Table 3.1 that partial unlocking causes a drop in η_δ.

Formulae shall now be obtained for assessing the energy efficiency of the wheel system of multiwheel drive vehicles with any specified number n of driving axles, coupled by a positive locking engagement. The computational model was shown previously in Figure 3.20. The slippage power losses are:

$$P_{\delta\Sigma} = \sum_{i=1}^{n} P_{\delta i} = \sum_{i=1}^{n} F_{xi} V_{ti} s_{\delta ai} = \omega_0 r_{\text{a}}^0 (1 - s_{\delta \text{a}}) \sum_{i=1}^{n} F_{xi} \tag{3.95}$$

TABLE 3.1

4×4 SUV: Analytical Evaluation

Driveline System	**Asphalt/Asphalt**		**Snow Road/Asphalt**	
Circumferential forces and slip coefficients	F_{x1}/F_{x2}, kN	$s_{\delta a1}/s_{\delta a2}$	F_{x1}/F_{x2}, kN	$s_{\delta a1}/s_{\delta a2}$
4×2	4.181/0	0.031/0	4.261/0	0.079/0
4×4, clutch plates fully locked, $m_r = -0.0288$	3.99/0.18	0.0299/0.0011	2.2172/2.0436	0.04106/0.01226
4×4, clutch plates not fully locked, $T_{\text{fr}} = 0.5T_{\text{fr}}^{\max}$	4.09/0.092	0.0307/0.00055	3.2394/1.0216	0.05998/0.00613
Slip efficiency, η_δ				
4×2	0.969		0.921	
4×4, clutch plates fully locked $m_r = -0.0288$	0.971		0.9725	
4×4, clutch plates not fully locked, $T_{\text{fr}} = 0.5T_{\text{fr}}^{\max}$	0.970		0.952	

The power supplied to the driving wheels is defined as:

$$P_{w\Sigma} = \sum_{i=1}^{n} P_{wi}^{in} = \sum_{i=1}^{n} F_{xi} V_{ti} = \sum_{i=1}^{n} F_{xi} \omega_{0i} r_{ai}^{0} = \omega_0 \sum_{i=1}^{n} F_{xi} \frac{r_{ai}^{0}}{u_i} \tag{3.96}$$

Then, using formulae (3.95) and (3.96), the slippage efficiency is expressed as:

$$\eta_\delta = \frac{r_a^0 (1 - s_{\delta a}) \sum_{i=1}^{n} F_{xi}}{\sum_{i=1}^{n} F_{xi} \frac{r_{ai}^0}{u_i}} \tag{3.97}$$

Expression (3.97) above can be used for determining η_δ when the vehicle performs both traction and transportation operations. In the first case, the generalized slippage $s_{\delta a}$ of the vehicle will be obtained from formula (3.78) with consideration of drawbar load F_d that is a component of the total circumferential force $F_{x\Sigma}$, which is seen from formula (1.74). In the second case, $F_d = 0$ (transportation mode). For this reason the value of $F_{x\Sigma}$ is determined by the remaining components of formula (1.74). In the case of uniform motion at moderate velocity over a horizontal surface the value of $F_{x\Sigma}$ and, respectively, $s_{\delta a}$ is determined solely by the forces of rolling resistance of the wheels of the vehicle that transports a payload.

A formula is now obtained for determining the efficiency of running gear and of multi-wheel drive vehicles as a whole when performing traction or transportation work. This will be done for the versions of transportation-traction vehicles listed in Table 1.19. For the first version of such a vehicle from this table, the traction efficiency of the running gear, in accordance to formulae (1.67) and (3.96), will be:

$$\eta_x^t = \frac{r_a^0 (1 - s_{\delta a}) F_d}{\sum_{i=1}^{n} F_{xi} \frac{r_{ai}^0}{u_i}} \tag{3.98}$$

Formula (3.98) above has the same structure as formula (1.67). This can be demonstrated by multiplying the numerator and denominator of formula (3.98) by $\sum_{i=1}^{n} F_{xi}$ and comparing the results with formulae (3.97) and with the expression for η_f from formula (1.68).

For a payload, carrying vehicle (version 2, Table 1.19) the transportation efficiency of the running gear will be determined from formula (1.81) that for the case of the equivalent layout of a vehicle with locked differential from Figure 3.20, takes the form:

$$\eta_x^{tr} = \frac{\sum_{i=1}^{m} P_{fgi}}{\sum_{i=1}^{n} P_{wi}^{in}} = \frac{r_a^0 (1 - s_{\delta a}) \sum_{i=1}^{m} R_{xgi}}{\sum_{i=1}^{n} F_{xi} \frac{r_{ai}^0}{u_i}} \tag{3.99}$$

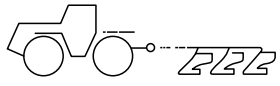
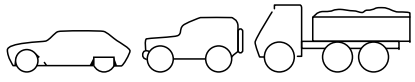
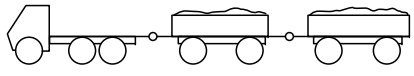
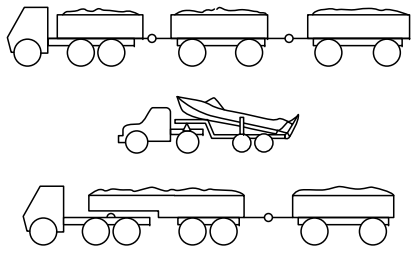
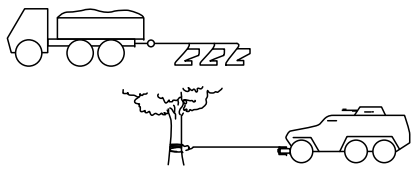
Formulae for determining the efficiency of running gear of the other versions of vehicles from Table 1.19 were obtained similarly on the condition that the interaxle drive is positively engaged. These expressions are listed in Table 3.2.

3.4.2 Mechanical Power Losses in Driveline Systems

General relationships for relative assessment of the power losses in a driveline system were presented in Section 1.4.1 without regard to the type of the power-dividing units. This section is concerned with power losses in a positively engaged drive and clarifies their

TABLE 3.2

Multiwheel Drive Vehicles with Positive Engagement of Drive Axles: Running Gear Efficiency

No.	Vehicle	Mode	Running Gear Efficiency
1		Tractive	$\eta_x^{\text{tr}} = r_{\text{a}}^0(1 - s_{\delta\text{a}})F_{\text{d}} \Big/ \left(\sum_{i=1}^{n} F_{xi} r_{\text{a}i}^0 / u_i\right)$
2		Transportational	$\eta_x^{\text{tr}} = \left[r_{\text{a}}^0(1 - s_{\delta\text{a}}) \sum_{i=1}^{m} R_{xgi}\right] \Big/ \left(\sum_{i=1}^{n} F_{xi} r_{\text{a}i}^0 / u_i\right)$
3		Transportational	$\eta_x^{\text{tr}} = \left[r_{\text{a}}^0(1 - s_{\delta\text{a}}) \sum_{i=1}^{c} \sum_{i=1}^{l} R_{xgi}\right] \Big/ \left(\sum_{i=1}^{n} F_{xi} r_{\text{a}i}^0 / u_i\right)$
4		Transportational	$\eta_x^{\text{tr}} = \left[r_{\text{a}}^0(1 - s_{\delta\text{a}}) \left(\sum_{i=1}^{m} R_{xgi} + \sum_{i=1}^{c} \sum_{i=1}^{l} R_{xgi}\right)\right] \Big/ \left(\sum_{i=1}^{n} F_{xi} r_{\text{a}i}^0 / u_i\right)$
5		Combined	$\eta_x^{\text{tr}} = \left[r_{\text{a}}^0(1 - s_{\delta\text{a}}) \left(\sum_{i=1}^{m} R_{xgi} + F_{\text{d}}\right)\right] \Big/ \left(\sum_{i=1}^{n} F_{xi} r_{\text{a}i}^0 / u_i\right)$

consistency with the general conclusions drawn in Section 1.4.1. Start with examining a 4×4 vehicle having a general layout of axles shown in Figure 3.19. It is assumed that the power is supplied from the transfer case to the wheels, that is, there is no parasitic power circulation.

The power lost in the driveline system of the front and rear axle can be written in the form:

$$\begin{aligned} P_{\text{drl1}} &= \frac{P_{\text{w1}}^{\text{in}}}{\eta_{\text{M1}}}(1-\eta_{\text{M1}}) \\ P_{\text{drl2}} &= \frac{P_{\text{w2}}^{\text{in}}}{\eta_{\text{M2}}}(1-\eta_{\text{M2}}) \end{aligned} \tag{3.100}$$

where

$P_{\text{w1}}^{\text{in}}$ and $P_{\text{w2}}^{\text{in}}$ are the powers supplied to the front and rear wheels

η_{M1} and η_{M2} are the mechanical efficiencies of the drives from the transfer case to the front and rear wheels

Assuming that the relationship between the circumferential force of the wheels F_x and the slippage is linear, power $P_{\text{w1}}^{\text{in}}$, $i = 1, 2$ is written as

$$\begin{aligned} P_{\text{w1}}^{\text{in}} &= F_{x1}V_{t1} = K_{\text{a1}}s_{\delta\text{a1}}V_{t1} \\ P_{\text{w2}}^{\text{in}} &= F_{x2}V_{t2} = K_{\text{a2}}s_{\delta\text{a2}}V_{t2} \end{aligned} \tag{3.101}$$

where, the theoretical axle velocities V_{t1} and V_{t2} are related to the kinematic discrepancy m_{ru} by formula (3.6). The generalized slippages $s_{\delta\text{a1}}$ and $s_{\delta\text{a2}}$ of the axles are related to the generalized slippage $s_{\delta\text{a}}$ of the vehicle by formula (3.87). Using formulae (3.6), (3.87), and (3.101), the power lost in the drives to both axles is given by the expression (second-order infinitesimals are neglected);

$$P_{\text{drl}} = P_{\text{drl1}} + P_{\text{drl2}} = V_{t2}\left[K_{\text{a1}}(2s_{\delta\text{a}} - m_{ru})\frac{1-\eta_{\text{M1}}}{\eta_{\text{M1}}} + K_{\text{a2}}(2s_{\delta\text{a}} + m_{ru})\frac{1-\eta_{\text{M2}}}{\eta_{\text{M2}}}\right] \tag{3.102}$$

It follows from formula (3.102) above that the power losses in a positively locked drive of axles of a 4×4 vehicle at a specified circumferential force $F_{x\Sigma}$ (i.e., at a specified generalized slippage $s_{\delta\text{a}}$) depends on the kinematic discrepancy m_{ru}, that is, on the distribution of power between the front and rear axles. This conclusion is general, since it was drawn for general conditions that are expressed in nonequal mechanical efficiencies in the drives of the axles ($\eta_{\text{M1}} \neq \eta_{\text{M2}}$), at different wheel sizes and gripping conditions of the wheels ($K_{\text{a1}} \neq K_{\text{a2}}$). If it is assumed that $\eta_{\text{M1}} = \eta_{\text{M2}} = \eta_{\text{M}}$ and $K_{\text{a1}} = K_{\text{a2}} = K_{\text{a}}$, then formula (3.102) reduces to the expression:

$$P_{\text{drl}} = 2K_{\text{a}}s_{\delta\text{a}}V_{t2}\frac{1-\eta_{\text{M}}}{\eta_{\text{M}}} = F_{x\Sigma}V_{t2}\frac{1-\eta_{\text{M}}}{\eta_{\text{M}}}, \tag{3.103}$$

from which it follows that, for a given traction load on the vehicle represented by force $F_{x\Sigma}$ and any of its distributions among the axles (within the limits of positive values of F_{x1} and F_{x2}, $F_{x1} + F_{x2} = F_{x\Sigma}$), the power losses in the driveline system are constant. Note that the conclusions drawn from analysis of formulae (3.102) and (3.103) are in complete agreement with conclusions from Section 1.4.1 pertaining to formulae (1.62) and (1.63).

Examine now the parasitic power circulation mode when, for example, the generalized slippage of the wheels of the front axle is negative, $s_{\delta a1} < 0$. The power losses in the drives are now determined by assuming $\eta_{M1} = \eta_{M2} = \eta_M$ and $K_{a1} = K_{a2} = K_a$:

$$\begin{aligned} P_{drl1} &= K_a V_{t1} s_{\delta a1}(1-\eta_M) = K_a V_{t2} s_{\delta a1}(1-\eta_M)(1-m_{ru}) \\ P_{drl2} &= K_a V_{t2} s_{\delta a2} \frac{1-\eta_M}{\eta_M} \end{aligned} \tag{3.104}$$

Substitution of the absolute values of $s_{\delta a1}$ and $s_{\delta a2}$ from formulae (3.87) into formulae (3.104) and dropping second-order infinitesimals, yields

$$P_{drl} = P_{drl1} + P_{drl2} = K_a V_{t2} \frac{1-\eta_M}{\eta_M} \left[s_{\delta a}(1-\eta_M) + \frac{m_{ru}}{2}(1+\eta_M) \right]$$

or

$$P_{drl} = K_a V_{t2} \left[s_{\delta a} \frac{(1-\eta_M)^2}{\eta_M} + \frac{1-\eta_M^2}{\eta_M} \frac{m_{ru}}{2} \right] \tag{3.105}$$

It should be emphasized that expression (3.105) is valid only in the case of $\frac{m_{ru}}{2} > s_{\delta a}$, that is, in the case of parasitic-power circulation, $s_{\delta a1} < 0$ (see formula (3.87)). If $F_{x\Sigma} \to 0$, that is, if it can be assumed that $s_{\delta a} = 0$, then expression (3.105) is valid for any values of the kinematic discrepancy m_{ru}. Under these conditions formula (3.105) becomes

$$P_{drl} = K_a V_{t2} m_{ru} \frac{1-\eta_M^2}{2\eta_M} \tag{3.106}$$

It follows from formula (3.106) above that in the absence of a traction load and in the presence of kinematic discrepancy (towing mode) the power losses that exist in the driveline system are a function of the factor m_{ru} and efficiency η_M. These losses are induced by parasitic power circulation.

Consider the case of utilizing formulae (3.103) and (3.106) for assessing the power losses in the driveline system of a 4×4 tractor moving uniformly in a straight line as a part of a truck with a total mass of $m_a = 30$ ton. The theoretical velocity is $V_{t2} = 36$ km/h. Two cases are considered: driving on an asphalt-paved road with rolling resistance factor f taken to be the same for all the wheels and equal to 0.02 and driving on a dirt road with $f = 0.05$. The longitudinal stiffness factors are taken to be $K_a = 4 \times 10^2$ kN on the asphalt and $K_a = 2.5 \times 10^2$ kN on the dirt road. The mechanical efficiency is $\eta_M = 0.9$. Figure 3.39 shows a graph of power lost in the driveline system as a function of the traction load, represented by $s_{\delta a}$ and of m_{ru}.

The graph was constructed as follows. Two slanting straight lines were constructed from formula (3.106) for the two assumed values of K_a. These lines reflect the power losses in the driveline system caused solely by the existence of m_{ru}. Then formula (3.103) was used for determining the power losses that depend only on the total circumferential force $F_{x\Sigma}$ at the same theoretical travel velocity. Note that under the conditions of motion considered here the total circumferential force is equal to the rolling resistance of the wheels, that is, $F_{x\Sigma} = m_a g f$. The values of P_{drl} calculated using formula (3.103) are laid off along the ordinate axis (see points A and B in Figure 3.39). Horizontal straight lines AA_1 and BB_1

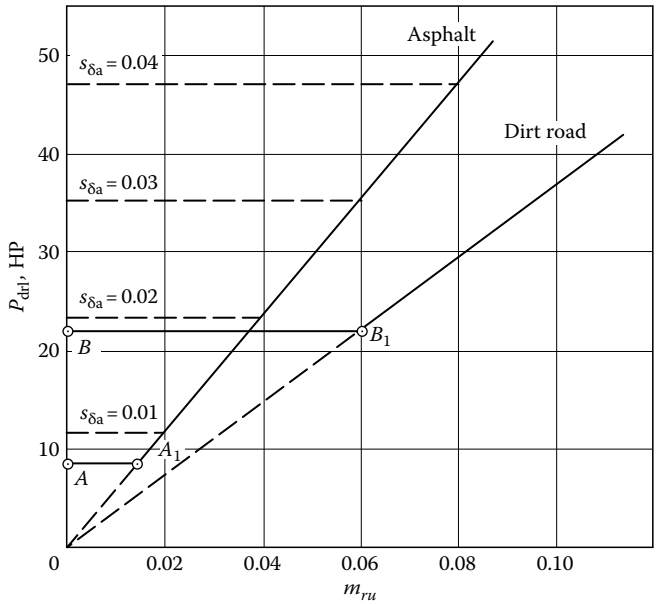


FIGURE 3.39
Mechanical power loss in the driveline system of a 4 × 4 tractor.

are drawn through points A and B up to the intersection with the slanting straight lines. The meaning of the resulting graph is as follows. The lengths of horizontal line segments AA_1 and BB_1 define the range values of m_{ru} at which the circumferential forces of both axles, F_{x1} and F_{x2}, are positive and the power losses in the drives to the front and rear axles are constant and calculated from formula (3.103). In this case $s_{\delta a} > m_{ru}/2$. At higher values of m_{ru}, lying on the axis of abscissa to the right of points A_1 and B_1 forces F_{x1} are negative and there exists circulation of parasitic power. The numerical values of P_{drl} in this case are determined by the slanting lines and increase with m_{ru}. In this case, $s_{\delta a} < \dfrac{m_{ru}}{2}$.

Analysis of Figure 3.39 shows that the higher the traction load, that is, the higher the values of $s_{\delta a}$ shown on the graph, the wider the range of values of m_{ru} at which the power losses remain constant. This means that, the higher the traction load, the lesser is the effect of the value of m_{ru} on the power losses in the driveline system. Elevated longitudinal stiffness of the tires and soil also reduces the effect of m_{ru} on power losses in the driveline system, but increases the traction-load losses. Any point on the graph located to the left of the slanting straight lines shows the possible power losses in the driveline system. These straight lines as such define the boundaries of these points.

It additionally follows from examining Figure 3.39 that vehicles with positively engaged driveline system traveling over hard-pavement roads suffer from perceptible increase in power losses, meaning also in forces resisting the motion, as a result of the inevitable presence of the operational and manufacture kinematic discrepancy. The above applies to vehicles with on-demand systems or with other systems that make no allowance for the design kinematic discrepancy. For example, at $m_{ru} = 0.04$ that is probable, considering tolerances in the manufacture of most tires, the power losses in the driveline system for a vehicle traveling on an asphalt-paved road are approximately threefold greater than those at $m_r = 0$, that is, than losses that would have occurred with a interaxle differential. It follows from this that, from the point of view of power losses in the driveline systems, the interaxle differential is or at least a system that ensures reliable disengagement of one of the axles, preferable for all-wheel drive vehicles that to a large

extent travel over well-paved roads. The elevated power losses may be transformed into an additional circumferential force F_{ad} of the wheels that is needed for motion of a vehicle with positively locked axles. Definition of force F_{ad} brings to light an important factor for understanding the physical meaning of the effect of a positive engagement in the driveline system as such and in the wheel system of an all-wheel drive vehicle and on the effect of these combined losses on the fuel consumption. These problems are examined in the next section.

3.4.3 Combined Power Losses in Driveline and Wheel Systems—Fuel Consumption

In determining the combined losses it is convenient to assume that all the forces that resist motion are equal to zero and to consider only forces that stem from the internal losses in the positively engaged driveline system and in the wheel system of the vehicle that depend on the kinematic discrepancy. Before examining the case of the 4×4 vehicle, consider isolated towing of the front axle in the braking mode and determine the power loss in slippage at negative circumferential force F_{x1} of the wheels and also the slippage efficiency η_δ of this axle. The equivalent computational model is shown in Figure 3.40, from which one can have

$$\begin{aligned} F_{ad} &= F_{x1} \\ T_{01} &= F_{ad} r_{a1}^0 \end{aligned} \tag{3.107}$$

where
F_{ad} is the force applied to the wheel to tow it
r_{a1}^0 is the reduced rolling radius of the axle's wheels in the driven mode
T_{01} is the braking torque of the axle

Had the axle's wheels been rigid and, accordingly, no power would have been lost in the longitudinal deflection of tires, then the braking power would have been given by the expression:

$$P_b = T_{01}\omega_{01} = F_{ad} r_{ai}^0 \omega_{01} = F_{ad} V_{t1} = P_{ad}^r \tag{3.108}$$

In the case of elastic tires and the same velocity V_{t1}, the longitudinal deflection of the tires causes some reduction in the rotational velocity because the rolling radius of the wheels increases to r_{a1}. To maintain the same angular velocity, that is, to ensure constancy of

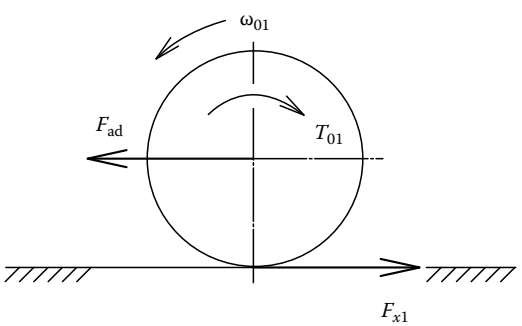


FIGURE 3.40
Longitudinal forces and torque of an axle in the braking mode.

power at wheel shafts P_b, the linear velocity must be increased somewhat. The value of this increment in fact determines the additional power needed for towing the axle with elastic tires that compensates the power lost in slippage. This new linear velocity is as follows:

$$V_x = \omega_{01} r_{a1} = \omega_{01}\left(r_{a1}^0 + \frac{T_{01}}{K_a}\right) = V_{t1} + F_{ad} V_{t1} \frac{1}{K_a}, \tag{3.109}$$

and the corresponding power can be calculated from the expression:

$$P_{ad} = F_{ad} V_x = F_{ad} V_{t1} + F_{ad}^2 V_{t1} \frac{1}{K_a} = P_{ad}^r + P_\delta \tag{3.110}$$

It follows from formula (3.110) above that the power P_{ad} spent for slippage of an axle with elastic tires is equal to the sum of two powers:

P_{ad}^r is the power spent for towing the axle with rigid wheels;
P_δ is the power spent for slippage of the elastic tires.

Then the slippage efficiency of an axle in the braking mode is obtained from the ratio of powers expended with rigid and elastic wheels:

$$\eta_{\delta 1} = \frac{P_{ad}^r}{P_{ad}} = \frac{F_{ad} V_{t1}}{F_{ad} V_x} = \frac{V_{t1}}{V_{t1} + V_{t1} \dfrac{F_{x1}}{K_a}} = \frac{1}{1 + s_{\delta a1}} \tag{3.111}$$

Using the above results for one axle, consider the motion of a 4×4 with a positively engaged driveline system in the presence of kinematic discrepancy in the towing mode (see Figure 3.41).

The tire sizes and the gripping conditions are assumed the same, that is, $K_{a1} = K_{a2} = K_a$. The force balance yields the expression

$$F_{x1} - F_{x2} = F_{ad} \tag{3.112}$$

Using formulae (3.70), determine the difference of forces F_{x2} and F_{x1} when their numerical values are positive:

$$F_{x2} - F_{x1} = \left(\frac{F_{x\Sigma}}{2K_a} + \frac{m_{ru}}{2}\right) K_a - \left(\frac{F_{x\Sigma}}{2K_a} - \frac{m_{ru}}{2}\right) K_a = K_a m_{ru} \tag{3.113}$$

In the case when F_{x1} is negative (this case is considered in Figure 3.41):

$$F_{x2} - (-F_{x1}) = F_{x2} + F_{x1} = K_a m_{ru} \tag{3.114}$$

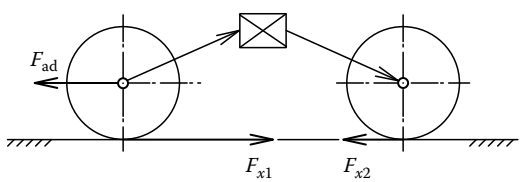


FIGURE 3.41
External forces of a 4×4 vehicle in towing mode.

The relationship between the absolute values of F_{x1} and F_{x2} can also be expressed in terms of the mechanical efficiency η_M and the gear ratios u_1 and u_2 in view of the fact that the power circulation proceeds from the front axle to the rear axle:

$$F_{x2} = F_{x1}\eta_M^2(1 - m_{ru}) \tag{3.115}$$

where, efficiency η_M of the driveline system from the transfer case to the wheels is taken to be the same for the front and the rear wheels, including both direct and reverse direction of the power flow.

Formulae (3.112), (3.114), and (3.115) derived above are now used for determining the forces F_{x1}, F_{x2} and F_{ad}:

$$\begin{aligned} F_{x1} &= \frac{K_a m_{ru} + F_{ad}}{2} \\ F_{x2} &= \frac{K_a m_{ru} - F_{ad}}{2} = F_{x1}\eta_M^2(1 - m_{ru}) \\ F_{ad} &= K_a m_{ru}\frac{1 - (1 - m_{ru})\eta_M^2}{1 + (1 - m_{ru})\eta_M^2} \end{aligned} \tag{3.116}$$

It follows from this that the additional force F_{ad} depends on the kinematic discrepancy m_{ru}, longitudinal stiffness K_a of the tires and driveline efficiency η_M. The power expended in slippage from Figure 3.41 is obtained by using the last of formulae (3.116):

$$P_{ad} = F_{ad}V_x = K_a m_{ru}V_x\frac{1-(1-m_{ru})\eta_M^2}{1 + (1-m_{ru})\eta_M^2} \tag{3.117}$$

It is of practical interest to compile mathematical expressions for the three forms of power loss:

$P_{\delta 1}$ is power lost in slippage of the front braking axle;
$P_{\delta 2}$ is power lost in slippage of the rear driving axle;
P_{drl} is power loss in the driveline system and

to check whether the sum of these three powers will be equal to power P_{ad} from formula (3.117). The slippage powers are equal to:

$$\begin{aligned} P_{\delta 1} &= F_{x1}V_{\delta 1} = F_{x1}(V_x - V_{t1}) \\ P_{\delta 2} &= F_{x2}V_{\delta 2} = F_{x1}(1-m_{ru})\eta_M^2(V_{t2} - V_x) \end{aligned} \tag{3.118}$$

In formulae (3.118) replace V_{t1} and V_{t2} by the actual velocity V_x:

$$\begin{aligned} V_x &= V_{t1}(1-s_{\delta a1}) = V_{t1}\left[1 - \left(s_{\delta a} - \frac{m_{ru}}{2}\right)\right] = V_{t1}\left(1 - s_{\delta a} + \frac{m_{ru}}{2}\right) \\ V_x &= V_{t2}(1-s_{\delta a2}) = V_{t2}\left[1 - \left(s_{\delta a} + \frac{m_{ru}}{2}\right)\right] = V_{t2}\left(1 - s_{\delta a} - \frac{m_{ru}}{2}\right) \end{aligned} \tag{3.119}$$

In the example in Figure 3.41 being analyzed there is no traction load (the vehicle is being towed), that is, $s_{\delta a} = 0$, then

$$V_{t1} = V_x\frac{2}{2 + m_{ru}}, \quad V_{t2} = V_x\frac{2}{2 - m_{ru}} \tag{3.120}$$

Note that it follows from expressions (3.120)

$$V_{t1} = V_{t2}\frac{2 - m_{ru}}{2 + m_{ru}} \tag{3.121}$$

and from expression (3.6)

$$V_{t1} = V_{t2}(1 - m_{ru}) \tag{3.122}$$

It is seen by comparing the coefficients of V_{t2} in formulae (3.121) and (3.122) that they differ by the amount m_{ru}^2. Neglecting this quantity as a second-order infinitesimal allows using both formulae (3.121) and (3.122). This difference stems from the fact that the relationship derived from formula (3.122) was obtained from the very definition of m_{ru}, which means it is an exact relationship, whereas the relationship obtained from expression (3.121) was obtained in terms of $s_{\delta a1}$ and $s_{\delta a2}$, the values of which are determined from the approximate formula (3.62).

Using formulae (3.120), it is found that:

$$\begin{aligned} P_{\delta 1} &= F_{x1}V_x\frac{m_{ru}}{2 + m_{ru}} \\ P_{\delta 2} &= F_{x1}(1 - m_{ru})\eta_{\mathrm{M}}^2 V_x\frac{m_{ru}}{2 - m_{ru}} \\ P_{\delta\Sigma} &= P_{\delta 1} + P_{\delta 2} = F_{x1}V_x\left[\frac{m_{ru}}{2 + m_{ru}} + \frac{m_{ru}(1 - m_{ru})\eta_{\mathrm{M}}^2}{2 - m_{ru}}\right] \end{aligned} \tag{3.123}$$

Now the losses in the driveline system are defined as the difference in the powers at the front and rear axles of the vehicle:

$$\begin{aligned} P_{\mathrm{drl}} &= F_{x1}V_{t1} - F_{x2}V_{t2} = F_{x1}V_x\frac{2}{2 + m_{ru}} - F_{x1}(1 - m_{ru})\eta_{\mathrm{M}}^2 V_x\frac{2}{2 - m_{ru}} \\ &= F_{x1}V_x\left[\frac{2}{2 + m_{ru}} - \frac{2(1 - m_{ru})\eta_{\mathrm{M}}^2}{2 - m_{ru}}\right] \end{aligned} \tag{3.124}$$

Adding powers $P_{\delta\Sigma}$ from formulae (3.123) and P_{drl} from formula (3.124), replacing forces F_{x1} and F_{ad} by their values from expressions (3.116) and regrouping, yields Equation 3.117. The above investigations thus confirm that in towing a 4×4 vehicle with positively engaged driveline system, which contains kinematic discrepancy, the driveline system itself and the wheel system expend a power P_{ad} in addition to the power used up in overcoming the resistance to motion exerted by the road. The value of P_{ad} depends on the value of m_{ru}, the longitudinal stiffness of the tires and soil K_{a} and the mechanical efficiency η_{M}.

In the theoretical case, corresponding to $\eta_{\mathrm{M}} = 1$ the expression for F_{ad} from (3.116) and P_{ad} from (3.117) become:

$$F_{\mathrm{ad}}^{\delta} = \frac{K_a m_{ru}^2}{2 - m_{ru}}, \quad P_{\mathrm{ad}}^{\delta} = \frac{K_a V_x m_{ru}^2}{2 - m_{ru}} \tag{3.125}$$

The expression for P_{ad}^{δ} in (3.125) reflects in this case the slippage power loss and becomes identical to formula (3.90) if V_{t2} in it is replaced by V_x from expression (3.120). Figure 3.42 graphically shows forces F_{ad} and F_{ad}^{δ} from formulae (3.116) and (3.125)

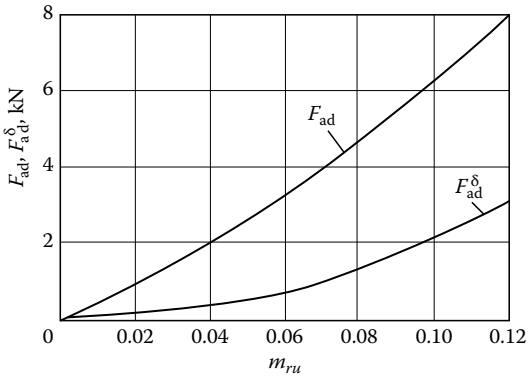


FIGURE 3.42
Additional forces of a 4 × 4 truck in towing mode

constructed for a 4×4 tractor with a trailer, the parameters and conditions of motion of which are given in Section 3.4.2.

Consider now a 4×4 vehicle, but not in the towing mode, but when being self-propelled. It will be shown that the additional power P_{ad} is not constant, but decreases with increasing traction load of the vehicle. The balance of power supplied to the transfer case of the vehicle in uniform rectilinear motion over a horizontal surface in the absence of air resistance is written as:

$$P_M = P_f + P_{drl} + P_\delta + P_{ad} \tag{3.126}$$

where

P_M is the power at the transfer-case input

P_f is the rolling resistance power

P_{drl} and P_δ are the powers lost in the driveline system and as a result of slippage of the wheels and depending only on the traction load of the vehicle

Power P_{ad} can be represented as the sum

$$P_{ad} = P_{drl}^{ad} + P_\delta^{ad} \tag{3.127}$$

where, P_{drl}^{ad} and P_δ^{ad} are also powers lost in the driveline system and in slippage of the wheels, but these are additional losses associated with positive engagement of the drive axles and appearance of kinematic discrepancy m_{ru}. Formulae (3.126) and (3.127) clearly show that in determining the power P_M that is needed for motion, consideration must be given to additional losses that stem from the kinematic discrepancy m_{ru}. Figure 3.43 shows graphs constructed from data of Figures 3.39 and 3.33 that reflect the dependence of the power losses in the driveline system and in slippage as a function of the generalized slippage $s_{\delta a}$ of the vehicle (that is proportional to force $F_{x\Sigma}$ and to the current gripping factor $\mu_x = F_{x\Sigma}/W_a$).

It should be emphasized that the graphs were constructed at a single constant value of the kinematic discrepancy factor $m_{ru} = 0.06$ for motion on asphalt. The horizontal line 1 shows the total power losses in the driveline system $\left(P_{drl} + P_{drl}^{ad}\right)$. Slanted straight line 2 shows the total power losses P_{drl}^{ad} in the driveline caused by the traction load. The segments of ordinates between horizontal line 1 and slanted line 2 reflect the power losses P_{drl}^{ad} caused by the kinematic discrepancy $m_{ru} = 0.06$. It is seen from the graph that, the

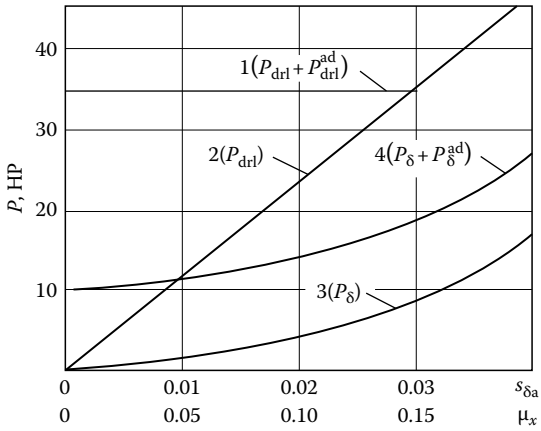


FIGURE 3.43
Poser losses vs. tractive load, i.e., current gripping factor (or generalized slippage) on asphalt; $m_{ru} = 0.06$.

higher the traction load, the lower the additional power losses $P_{\text{drl}}^{\text{ad}}$ in the driveline system. There are no additional losses at the segment $s_{\delta a} = 0.03 - 0.04$. Curve 3 in Figure 3.43 presents the slip power loss P_δ due to the tractive load, and curve 4 gives the total slip power losses $P_\delta + P_\delta^{\text{ad}}$. The segments of ordinates located between curves 3 and 4 reflect additional power loss P_δ^{ad} that is caused by kinematic discrepancy $m_{ru} = 0.06$.

Curve 1 in Figure 3.44 shows the total losses $\left(P_{\text{drl}} + P_\delta + P_{\text{drl}}^{\text{ad}} + P_\delta^{\text{ad}}\right)$ whereas curve 2 reflects only the additional power losses $\left(P_{\text{drl}}^{\text{ad}} + P_\delta^{\text{ad}}\right)$.

It is seen from the figure that the additional power losses decrease with increasing traction load.

The data presented above are now summed up. The kinematic discrepancy that is present in the course of towing mode of vehicles with positively engaged driveline system causes additional power losses in propelling the vehicle as compared with the case of motion without kinematic discrepancy.

This additionally consumed power is not a constant quantity for a given vehicle and for a given surface of motion. Having its highest value at zero traction load (towing mode), this additional power decreases with increasing traction load.

The additionally lost power is made up of two components: power lost in the driveline system and that lost in the wheel system. The first decreases with increasing traction

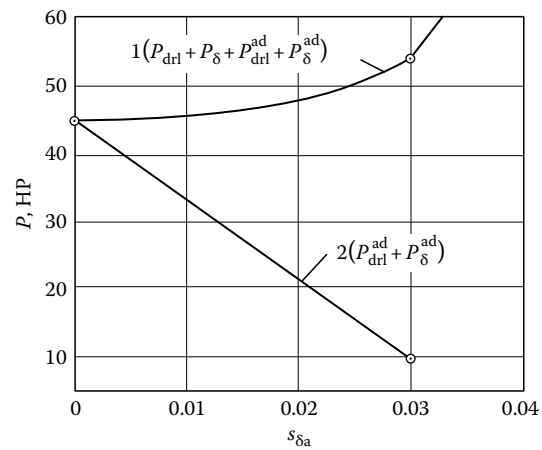


FIGURE 3.44
Poser losses vs. generalized slippage on asphalt; $m_{ru} = 0.06$.

load and may even be zero at some value of this load. The second is constant over the entire range of traction load.

This additionally lost power is particularly perceptible in driving over solid roads, when the longitudinal stiffness factor K_x is large. Even an inexperienced driver notes that the engine of a vehicle with positively engaged driveline system starts working harder when moving from a road-less stretch of soil onto a road. This is associated with the above additional power loss.

The studies described above were performed for the case of rectilinear motion of the vehicle when the non-equality of the rolling radii of the wheels in the driven mode and the difference in the gear ratios u_1 and u_2 in the axle drives cause the appearance of kinematic discrepancy m_{ru}. Even greater kinematic discrepancies m_{ruR} arise when the vehicle turns, which is the main reason for the marked increase of the resistance to motion of vehicles with positive engagement in the driveline system on curved segments of roads.

These additional power losses are reflected in the fuel consumption and reduce the fuel efficiency of any vehicle with a positively engaged driveline system. As an illustration, Figure 3.45 shows the results of investigating the fuel consumption of a 3.7-ton 4×4 tractor with different sizes of front and rear wheels with positively engaged power-dividing interaxle unit in which the kinematic discrepancy m_{ru} was modified by placing gears with different numbers of teeth in the front-axle drive.

The theoretical (curves 1 through 3) and experimental (symbols) data given in Figure 3.45 on the effect of the magnitude and sign of m_{ru} on the fuel consumption were determined for the tractor operating on two types of surfaces of motion. It follows from Figure 3.45 that when the tractor moves over a field ready for sowing without operating any machinery (solid curve 1) the fuel consumption is higher than when moving over a dry asphalt-paved road (dashed curve 1), which is caused by the higher losses for overcoming the resistance forces when moving over a ready for sowing field. In all cases, including that of a tractor with traction load, the lowest fuel consumption occurs in the absence of kinematic discrepancy ($m_{ru} = 0$). The presence in the tractor, of both negative and positive kinematic discrepancy, increases the fuel consumption as compared

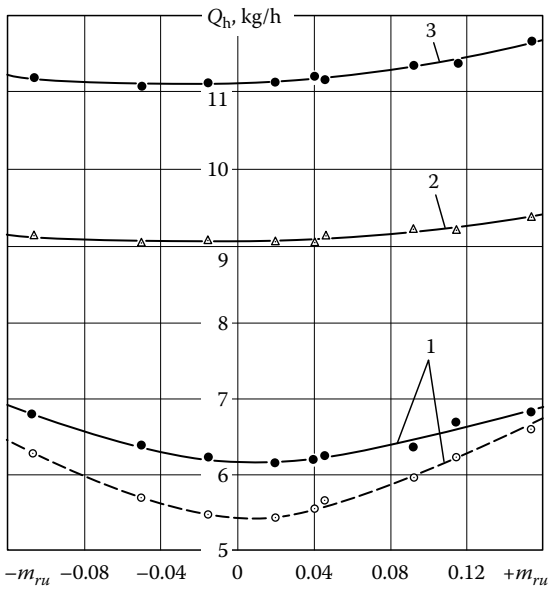


FIGURE 3.45
4×4 tractor: fuel consumption. 1, Idle motion; 2, with a trailer, 2PTS-6 ($F_d = 6.2$ kN); 3, $F_d = 10$ kN. — —, Asphalt; ———, ready for sowing field.

with the case of $m_{ru} = 0$; here at $m_{ru} > 0$ the fuel consumption increases somewhat more than at $m_{ru} < 0$. The effect of the absolute magnitude of kinematic discrepancy on the increase in fuel consumption as compared with operation at $m_{ru} = 0$ lessens upon increasing traction load. Thus, whereas in the case of a tractor moving over a sowing-ready field an increase in m_{ru} from 0.0394 to 0.1101 causes a 0.41 kg/h (6.6%) rise in fuel consumption, then in the case when working on the same field, but with a loaded trailer 2PTS-6 ($F_d = 6.2$ kN) the fuel consumption at the same values of m_{ru} increases by 0.18 kg/h (1.9%). It additionally follows from Figure 3.45 that the difference between the predicted and measured data on fuel consumption was within the limits of measurement error.

To obtain a comprehensive assessment of the fuel efficiency from results of field tests, a comparison of the fuel consumption was performed of tractors traveling over a sowing-ready field in the 4×4 mode (the two axles are positively engaged) and the 4×2 mode (the front axle is disengaged, the rear-axle differential is locked) as a function of the drawbar load F_d. This was done based on the fuel consumption variation factor:

$$\eta_h = \frac{Q_h^\circ}{Q_h} \tag{3.128}$$

where

Q_h° is the fuel consumption per hour when the vehicle moves in the 4×2 mode and an open differential without a load over a sowing-ready field

Q_h is the per hour fuel consumption at some specified load F_d of the same vehicle, but with modified wheel formula and/or changes in the working mode of the interwheel power-dividing unit

The dependence of the fuel consumption factors on the drawbar load for a 3.7-ton 4×4 tractor is shown in Figure 3.46, whereas the same data for a 5.6-ton tractor are shown in Figure 3.47.

It follows from these figures that the factor η_h decreases with increasing drawbar load F_d, that is, the fuel consumption increases for both tractors both in the 4×2 and 4×4 mode. However, the rate of these changes is not the same. At low drawbar loads the fuel consumption when operating in the 4×2 mode is smaller, and the factor η_h is higher (dashed curves in Figures 3.46 and 3.47) than when operating in the 4×4 that is caused by the existence of kinematic discrepancy and the elevated power losses associated with it. With increasing drawbar loads, the curves of factors η_h of both these drive modes come closer to one another and at some value of F_d the values η_h for tractors operating in both modes become equal. Analysis of the torques at the front wheels of the tractors in the 4×4 operating mode at this value of F_d shows that they are virtually zero. This means that at some value of F_d the parasitic power circulation mode (when the circumferential forces of the front wheels, is $F_{x1} < 0$) is replaced by modes with positive values of F_{x1}.

At even higher values of F_d the fuel consumption when operating in the 4×4 mode is lower and the value of η_h is higher than when operating in the 4×2 mode. For example, at $m_{ru} = 0.0917$ the fuel consumption of a 4×4 3.7-ton tractor on a sowing-ready field in the 4×4 mode becomes lower than when operating in the 4×2 mode at $F_d > 4.8$ kN.

The data presented above provided insight into the substance of power loss of the driveline system and wheel system of 4×4 vehicles with positively engaged drive in the presence/absence of kinematic discrepancy over a wide range of traction loads. Analytical

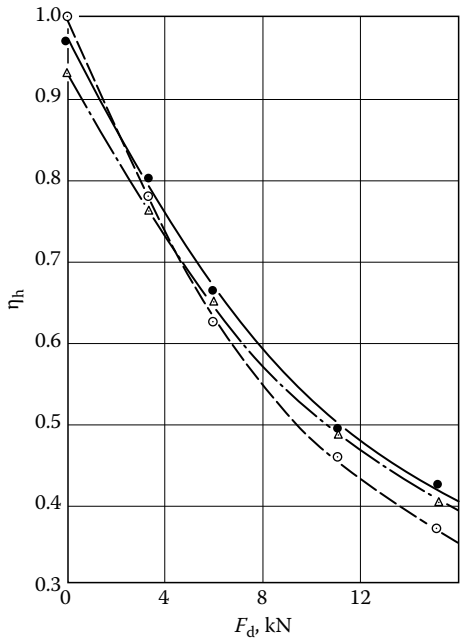


FIGURE 3.46
3.7-ton tractor: (•) 4×4, $m_{ru} = 0.0394$; (Δ) 4×4, $m_{ru} = 0.0917$; (°) 4×2.

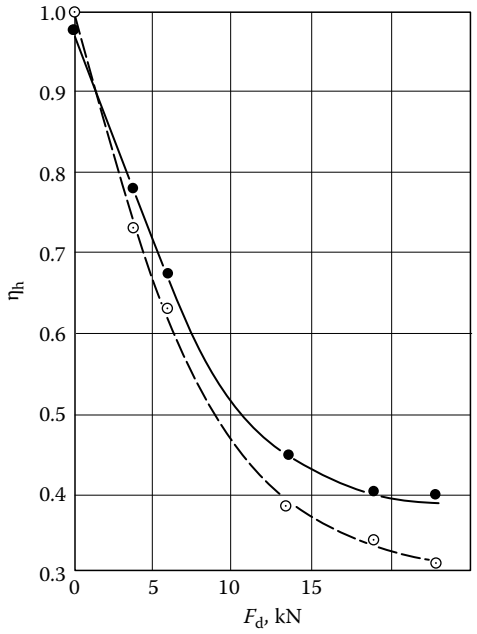


FIGURE 3.47
5.6-ton tractor: (•) 4×4, $m_{ru} = 0.0372$; (°) 4×2.

and experimental data on fuel consumption confirmed the theoretical results concerning the energy efficiency of the driveline system and wheel system of 4×4 vehicles. The methods developed here may be used for investigating various type of power-dividing units that provide positive engagement of the driving axles of 4×4 vehicles.

The present section is concluded by deriving analytic relationships for assessing the energy efficiency of vehicles with any specified number n of positively engaged driving axles. This will be done for all types of vehicles listed in Table 1.19. The computational model of the axles is given in Figure 3.20.

The power developed by the engine is represented by the expression

$$P_{\mathrm{e}} = \frac{\omega_0}{\eta_{\mathrm{trm}}} \sum_{i=1}^{n} \frac{F_{xi} r_{ai}^0}{u_i \eta_{\mathrm{M}i}^{\kappa}}, \quad \kappa = \operatorname{sign} F_{xi} \tag{3.129}$$

where

ω_0 is the angular velocity of the transfer case shaft

η_{trm} is the mechanical efficiency of the transmission

The traction power developed by a traction vehicle (see item 1 in Table 1.19) is:

$$P_{\mathrm{d}} = F_{\mathrm{d}} V_x = F_{\mathrm{d}} \omega_0 r_{\mathrm{a}}^0 (1 - s_{\delta \mathrm{a}}) \tag{3.130}$$

Then the traction efficiency of a vehicle operating at traction load F_{d} will be given by the expression:

$$\eta_{\mathrm{t}} = \frac{P_{\mathrm{d}}}{P_{\mathrm{e}}} = \frac{\eta_{\mathrm{trm}} r_{\mathrm{a}}^0 (1 - s_{\delta \mathrm{a}}) F_{\mathrm{d}}}{\sum_{i=1}^{n} \frac{F_{xi} r_{ai}^0}{u_i \eta_{\mathrm{M}i}^{\kappa}}} \tag{3.131}$$

Methods relating to determining the generalized slippage $s_{\delta \mathrm{a}}$ of the vehicle, of the circumferential forces F_{xi} of the axles when their sum $F_{x\Sigma} = \sum_{i=1}^{n} F_{xi}$ is known, and the generalized rolling radius in the vehicle's driven mode r_{a}^0 (reduced to the transfer case shaft, see Figure 3.20) were discussed in preceding sections.

The transportation efficiency for a payload-conveying vehicle (item 2 in Table 1.19) is determined from the expression:

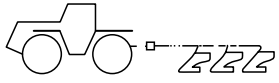
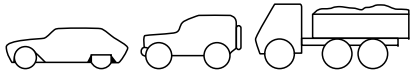
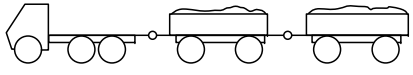
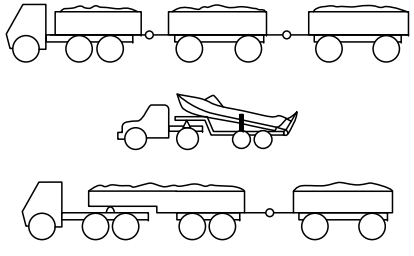
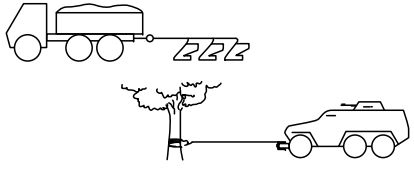
$$\eta_{\mathrm{tr}} = \frac{P_{fg\Sigma}}{P_{\mathrm{e}}} = \frac{\eta_{\mathrm{trm}} r_{\mathrm{a}}^0 (1 - s_{\delta \mathrm{a}}) \sum_{i=1}^{m} R_{xgi}}{\sum_{i=1}^{n} \frac{F_{xi} r_{ai}^0}{u_i \eta_{\mathrm{M}i}^{\kappa}}} \tag{3.132}$$

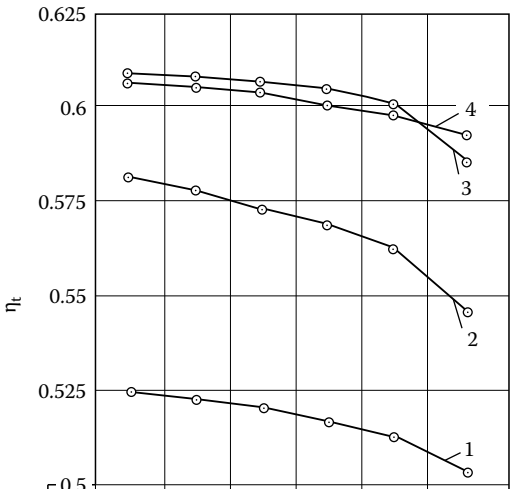
Note that parameters $P_{fg\Sigma}$ and R_{xgi}, $i = 1, m$ were examined in Section 1.4.2. Formulae for the efficiency of all the remaining types of vehicles from Table 1.19 can be determined similarly. These analytic relationships are listed in Table 3.3.

As an illustration of the application of formulae from Table 3.3, an energy assessment of the 6×6 power-module driven vehicular train was performed (see item 1 in Table 1.12 and Figures 1.39 and 3.31). The question of selecting the kinematic discrepancy factors in the axle drives for ensuring automatic engagement/disengagement of the first and third axles by means of overrunning clutches was formulated in Section 3.3.2. In that section were determined the circumferential forces F_{xi}, $i = 1, 3$ of axles, their generalized slippages and the generalized slippage $s_{\delta \mathrm{a}}$ of this vehicle. Figure 3.48 presents the values of traction efficiency η_{t} of this vehicle corresponding to the same traction loads F_{d} and the kinematic discrepancy factor m_{Hi} as the circumferential forces F_{xi}, $i = 1, 3$ of the axles from Figure 3.32 (curves 1–4).

TABLE 3.3

Multiwheel Drive Vehicles with Positive Engagement of Driving Axles: Energy Efficiency

No.	Vehicle	Mode	Vehicle Efficiency
1		Tractive	$\eta_{tr} = \left[\eta_{trm} r_a^0 (1 - s_{\delta a}) F_d\right] \Big/ \left[\sum_{i=1}^{n} F_{xi} r_{ai}^0 / \left(u_i \eta_{Mi}^x\right)\right]$
2		Transporiational	$\eta_{tr} = \left[\eta_{trm} r_a^0 (1 - s_{\delta a}) \sum_{i=1}^{m} R_{xgi}\right] \Big/ \left[\sum_{i=1}^{n} F_{xi} r_{ai}^0 / \left(u_i \eta_{Mi}^x\right)\right]$
3		Transportational	$\eta_{tr} = \left[\eta_{trm} r_a^0 (1 - s_{\delta a}) \sum_{i=1}^{c} \sum_{i=1}^{l} R_{xgi}\right] \Big/ \left[\sum_{i=1}^{n} F_{xi} r_{ai}^0 / \left(u_i \eta_{Mi}^x\right)\right]$
4		Transportational	$\eta_{tr} = \left[\eta_{trm} r_a^0 (1 - s_{\delta a}) \left(\sum_{i=1}^{m} R_{xgi} + \sum_{i=1}^{c} \sum_{i=1}^{l} R_{xgi}\right)\right] \Big/ \left[\sum_{i=1}^{n} F_{xi} r_{ai}^0 / \left(u_i \eta_{Mi}^x\right)\right]$
5		Combined	$\eta_{tr} = \left[\eta_{trm} r_a^0 (1 - s_{\delta a}) \left(\sum_{i=1}^{m} R_{xgi} + F_d\right)\right] \Big/ \left[\sum_{i=1}^{n} F_{xi} r_{ai}^0 / \left(u_i \eta_{Mi}^x\right)\right]$



m_{H1}	0	−0.05	−0.04	−0.01	−0.05	0.07
m_{H2}	0	0.01	0.03	0.05	0.02	0.001
m_{H3}	0	0.01	−0.04	−0.1	−0.01	0.04
	a	b	c	d	e	f

FIGURE 3.48
Tractive efficiency of a 6 × 6 power-module driven vehicular train 1–4—see in Figure 3.32.

As seen from Figure 3.48, modifying gear ratios u_i brings about the appearance of kinematic discrepancy and reduction in the traction efficiency of the vehicle. From the cases under study, when the theoretical velocities of the axles are not the same, the maximum values of η_t correspond to the case of $V_{t1} < V_{t2} = V_{t3}$ (version b). Employing

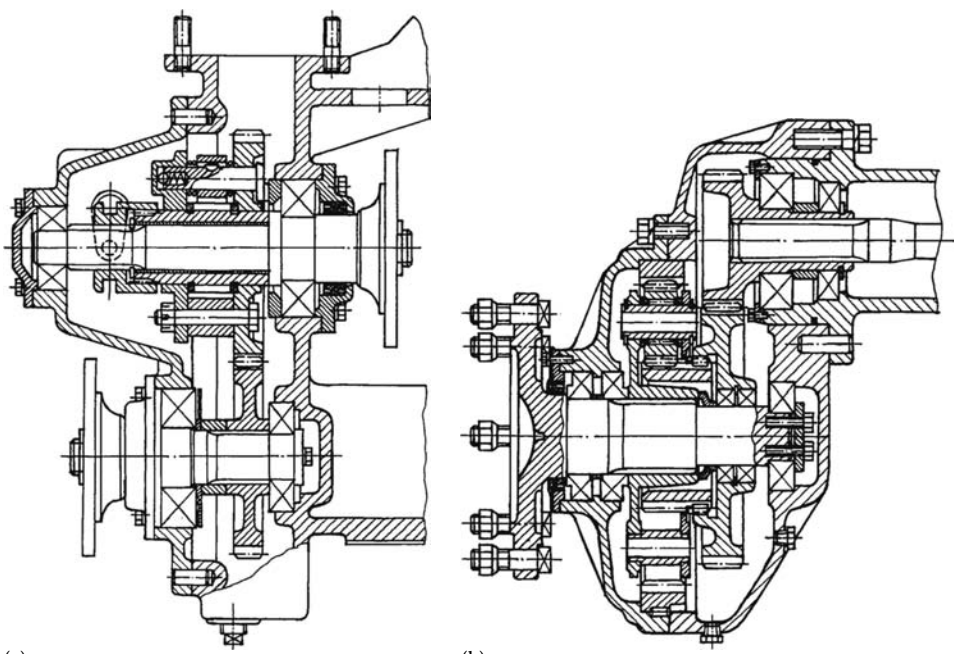


FIGURE 3.49
Transfer case with overrunning clutch (a) and wheel-hub gear drive (b) of the third-axle drive.

an overrunning clutch in the drive of the front wheels will make it possible to engage/disengage them automatically.

If an overrunning clutch was installed in the drive of the third axle, then it is necessary to ensure that $V_{t1} < V_{t3} < V_{t2}$. When the velocities V_{ti} are related as follows, the third axle will be engaged first upon increase in traction load and this will follow by engagement of the front wheels. Even though efficiency η_t (version c) will decrease somewhat as compared with versions a and b, it will still be higher than at other relationships between V_{ti} (versions d–f). The efficiency of this vehicle will be lowest at $V_{t2} > V_{t1} > V_{t3}$, when the front wheels are engaged first and only then the third-axle wheels. At other combinations of V_{ti} the traction efficiency takes intermediate values. Figure 3.49 shows the design of the transfer case with an overrunning clutch (a) and wheel-hub gear drive (b) in the drive of the third axle that ensures the required relationship $V_{t1} < V_{t3} < V_{t2}$ between the theoretical velocities by appropriate combinations of the tooth numbers of the gears in mesh and by the axles' rolling radii in the driven mode.

3.5 Wheel Power Distribution and Vehicle Performance

This section is concerned with certain features in the effect of a positively engaged driveline system on the performance of a vehicle. These are questions concerning the tractive and velocity operational properties of vehicles, effect of certain features of the suspension on the redistribution of forces in positively engaged driveline and specific questions of the effect of a positive engagement on the turnability and stability of vehicles.

3.5.1 Vehicle Tractive and Velocity Operational Properties

Expression 1.68 introduced the slippage efficiency η_δ that represents both the energy and velocity efficiency of a 4×2 vehicle, that is, factor η_δ can be used for assessing both power losses and losses of velocity in a 4×2 vehicle that are caused by slippage of the driving wheels (reference is made to an equivalent layout in which two wheels of each axle are replaced by an equivalent wheel).

The matter of assessing power losses and losses in velocity of multiwheel drive vehicles with a positively engaged driveline system is much more complex. This is now demonstrated. Formula (3.97) was obtained in Section 3.4.1 for the slippage efficiency η_δ of a vehicle with any specified number n of driving axles in the presence of kinematic discrepancy m_{Hi}, $i = 1, n$ in the driveline system. Analysis of expression (3.97) and its comparison with formula (3.20) for calculating the actual velocity V_x of the vehicle show the following: whereas the generalized slippage $s_{\delta a}$ reflects the loss of velocity due to the longitudinal deformation of the tires and the soil, η_δ reflects the power loss that arises due to these deformations. This means that in the presence of kinematic discrepancy the generalized slippage $s_{\delta a}$ cannot be used for assessing the slippage power loss in multiwheel drive vehicles, as this can be done in 4×2 vehicles (see formula (1.68)).

When there is no kinematic discrepancy (complete consistency of the theoretical velocities of axles expressed, for example, for 4×4 vehicles by formula (3.5)), formula (3.97) becomes

$$\eta_\delta = 1 - s_{\delta a}, \tag{3.133}$$

that is, in this case the generalized slippage of the vehicle reflects both loss of velocity and power loss caused by tire slippage.

To describe the difference in the power and velocity losses it is advisable to introduce still another criterion, known as the vehicle velocity variation factor in the presence of kinematic discrepancy in the running gear:

$$\eta_v = 1 - s_{\delta a} \tag{3.134}$$

It is seen from formulae (3.97), (3.133), and (3.134) that η_v is identical to η_δ only when there is no kinematic discrepancy. Figure 3.50 shows analytic curves of η_v and η_δ for a 5.6-ton 4×4 tractor with differently sized front and rear wheels as a function of the total circumferential force $F_{x\Sigma}$ of the wheels when moving over a sowing-ready field.

Note that force $F_{x\Sigma}$ was changed in the calculations by changing one of its components—the drawbar load F_d. It is seen that η_v is numerically identical with η_δ only at $m_{ru} = 0$. The curves of η_v monotonically and nonlinearly decrease with increasing $F_{x\Sigma}$. Here when m_{ru} is positive and equal to 0.08, $\eta_\delta < \eta_v$ over the entire range of variation in F_d. At negative kinematic discrepancy of $m_{ru} = -0.08$ one can see that $\eta_\delta < \eta_v$ only at $F_{x\Sigma} < 12.2$ kN. Comparison of curves in Figure 3.50 graphically demonstrates the necessity of using different criteria for assessing the power loss in slippage and the velocity loss of 4×4 vehicles with a positively engaged driveline system. Still another practical advice for experimental and analytical research follows from Figure 3.50. Slippage power losses cannot be assessed experimentally from the change in the actual velocity of a multiwheel drive vehicle. However, this can be done analytically or experimentally using formula (3.97). On the other hand, variation in the actual velocity can be determined analytically or experimentally using formulae (3.78) and (3.134).

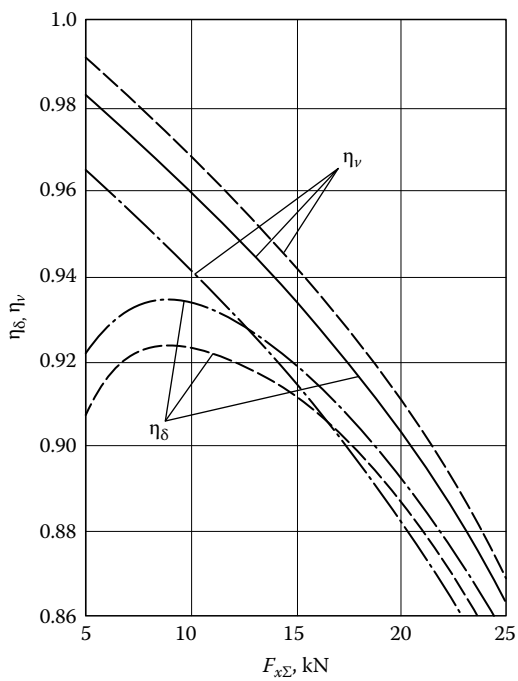


FIGURE 3.50
5.6-ton 4×4 tractor: slippage efficiency η_δ and velocity variation factor η_v: ———, $m_{ru} = 0$; — —, $m_{ru} = 0.08$; —·—, $m_{ru} = -0.08$.

The kinematic discrepancy has a marked effect also on the vehicles' traction. Figure 3.37 has already previously shown the value of drawbar load F_{d} at which the front axle of the tractor is shifted into the traction mode by means of an overrunning clutch. It is seen from this figure that, when the kinematic discrepancy m_{ru} becomes larger, higher values of F_{d} are needed for engaging the front axle and improving the traction performance of the tractor.

Kinematic discrepancy exerts a different effect on the traction of vehicles depending on the kind of surface over which they travel. An overrunning clutch was installed in one specimen of a 4×4 timber-carrier truck in order to engage both axles in translational motion and to disengage the front axle when taking a turn. First, a design kinematic discrepancy $m_u = 0.08$ was administered into the driveline system. In the course of operation of the truck during which traction loads were rather significant, the front axle was engaged at a very high, almost maximum, traction torque on the rear axle. This was observed over relatively hard roads and caused supercharging of the rear axle and under-loading of the front axle. This value of m_u had a negative effect on the traction performance of the vehicle and affected the dynamic loading of the components of the truck's driveline systems. For vehicles that operate on soft soil (earth moving machines, farm tractors, other terrain vehicles) the kinematic discrepancy has a lesser effect on the loading of the driveline components. The value of m_{ru} in these vehicles is usually selected from considerations of energy efficiency. Details on selecting m_{ru} are given in Section 3.6.

The properties of a positively engaged driveline system must be taken into account in designing vehicle suspension. Here is an example. A 6×6 truck rated at 5 ton with all the three axles positively engaged was tested on an asphalt-paved road. The axles of the tandem axles were subjected to identical conditions: dimensions of wheels, the tire inflation pressures and the weight load were the same. In uniform rectilinear motion, the torque of the forward rear axle turned out to be approximately 1.5-fold greater than the torque of the reward rear axle, that is, $T_{\mathrm{w2}}/T_{\mathrm{w3}} = 1.5$. Under steady turning conditions the torque turned out to be higher at the rear axle and the ratio of torques $T_{\mathrm{w2}}/T_{\mathrm{w3}}$ was approximately 0.5. The difference in traction load on the second and third axle was the result of kinematic discrepancy that arose in the course of travel. This discrepancy appeared because of redistribution of weight in the course of travel: the load on the reward rear axle increases whereas that on the forward rear axle decreases. The weight redistribution is caused by the sloping arrangement of the reaction arms of the suspension that was provided in order to ensure the required angles of driveshaft arrangement. Placing the arms horizontally would have prevented this weight redistribution. This weight redistribution reduced the rolling radius of the wheels of the third axle in the driven mode and increased the rolling radius in the driven mode of the second axle wheels. This has produced kinematic discrepancy between the second and third axle determined by formula (3.7) upon replacing subscripts 1 and 2 by 2 and 3:

$$m_r = \frac{r^0_{\mathrm{a3}} - r^0_{\mathrm{a2}}}{r^0_{\mathrm{a3}}} \tag{3.135}$$

It is seen from formula (3.135) that $m_r < 0$ since $r^0_{\mathrm{a2}} > r^0_{\mathrm{a3}}$. At negative kinematic discrepancy the second relationship between slippages in formulae (3.62) as applied to the second and third axles is:

$$s_{\delta \mathrm{a2}} = s_{\delta \mathrm{a3}} - (-m_r) = s_{\delta \mathrm{a3}} + m_r \tag{3.136}$$

Relationship $s_{\delta a2} > s_{\delta a3}$ between the slippages from formula (3.136) defines the higher traction load on the forward rear axle: $F_{x2} > F_{x3}$ or $T_{w2} > T_{w3}$.

3.5.2 Vehicle Turnability and Stability of Motion

The examination of the effect of a positively engaged driveline system on the turnability is started with the *i*th driving axle of a vehicle having *n* driving axles. It will be assumed for simplicity that the normal loads, dimensions of tires and their air pressures are the same and the total circumferential force $F_{x\Sigma i}$ of the axle is known and constant when taking a turn. Situations that are more complicated shall be examined later on. The computational model is shown in Figure 3.51a.

Determine the circumferential forces F''_{xi} and F'_{xi} of the wheels as a function of turning radius R_{ti}. For this, the following force balance can be written down:

$$F''_{xi} + F'_{xi} = F_{x\Sigma i} \tag{3.137}$$

and for the tire slippages:

$$\frac{V''_{xi}}{V'_{xi}} = \frac{\omega_{wi} r^0_{wi}(1 - s''_{\delta i})}{\omega_{wi} r^0_{wi}(1 - s'_{\delta i})} = \frac{1 - s''_{\delta i}}{1 - s'_{\delta i}} = \frac{R_{ti} - 0.5t_{Bi}}{R_{ti} + 0.5t_{Bi}} \tag{3.138}$$

The missing equations are compiled as follows:

$$F''_{xi} = f''_i(s''_{\delta i}) \quad \text{and} \quad F'_{xi} = f'_i(s'_{\delta i}) \tag{3.139}$$

which, as previously stated in Section 1.3.2, may be both linear and nonlinear. Figures 3.52 through 3.55 show the results of calculations in the form of the current gripping factors $\mu''_{xi} = F''_{xi}/W_w$ and $\mu'_{xi} = F'_{xi}/W_w$ for the case when $F_x = f(s_\delta)$ is an exponential relationship (1.26).

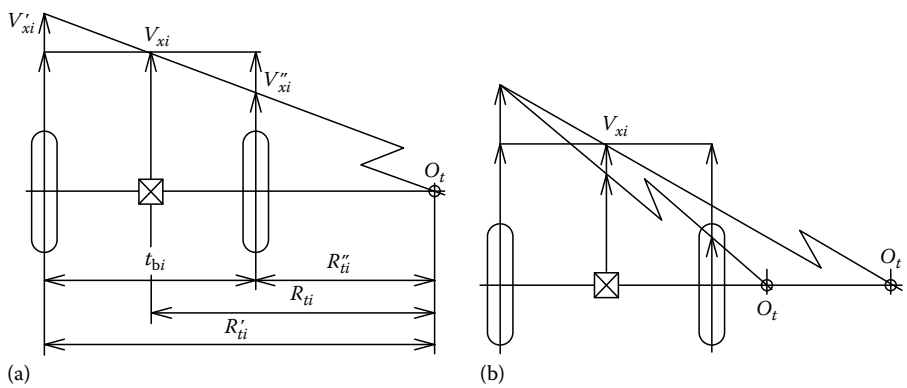


FIGURE 3.51
Driving axle with positive engagement of the wheels in turn: (a), $\mu''_{xi} < \mu''_{pxi}$; (b), $\mu''_{xi} = \mu''_{pxi}$.

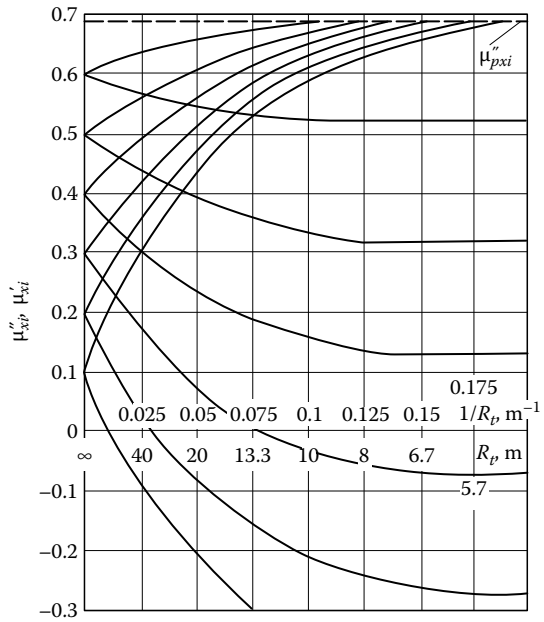


FIGURE 3.52
Driving axle with positive engagement of the wheels taking a turn on a sow-ready field: current gripping factors; $W''_w = W'_w = 15$ kN; $t_b = 2$m; tire model of 465-868P; $p_w = 0.16$ MPa.

Even preliminary analysis of the components of the formulae shows that the slippage $s''_{\delta i}$ of the inner wheel increases while that of the outer wheel ($s'_{\delta i}$) decreases with reduction in the turning radius R_{ti}, that is, with increasing kinematic discrepancy. Circumferential forces F''_{xi} and F'_{xi} of the wheels, and with them, the factors μ''_{xi} and μ'_{xi} will change accordingly. Once factor μ''_{xi} has attained its peak value μ''_{pxi}, a further reduction in R_{ti}

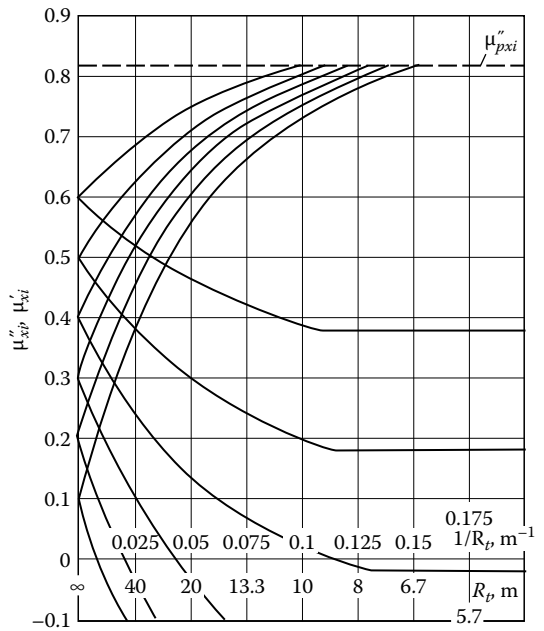


FIGURE 3.53
Driving axle with positive engagement of the wheels taking a turn on a stubble field: current gripping factors; $W''_w = W'_w = 15$ kN; $t_b = 2$m; tire model of 465-868P; $p_w = 0.16$ MPa.

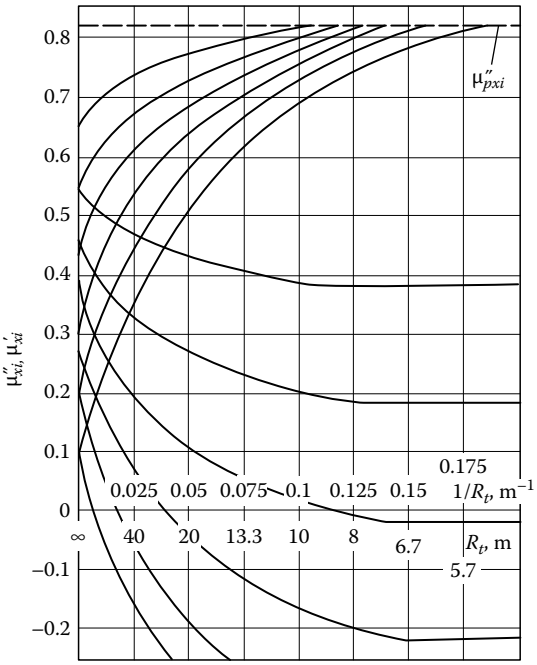


FIGURE 3.54
Driving axle with positive engagement of the wheels taking a turn when the inner wheel is on stubble and the outer wheel is on sow-ready ground: current gripping factors; $W''_w = W'_w = 15$ kN; $t_b = 2$m; tire model of 465-868P; $p_w = 0.16$ MPa.

will not cause redistribution of the circumferential forces. As R_{ti} will subsequently decrease, the linear velocity of the center of the outer wheel will remain constant, whereas the linear velocities of the center of the axle and of the inner wheel will decrease (see this in Figure 3.51b). This means that slippage of the outer wheel attains its minimum value of

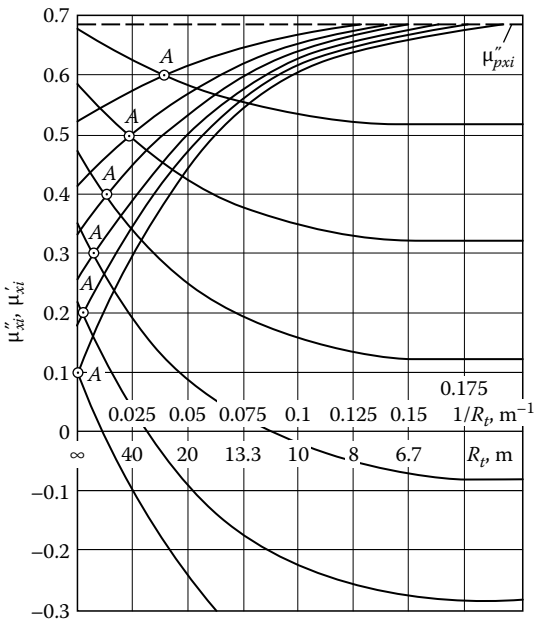


FIGURE 3.55
Driving axle with positive engagement of the wheels taking a turn when the inner wheel is on sow-ready ground and the outer wheel is on stubble: current gripping factors; $W''_w = W'_w = 15$ kN; $t_b = 2$m; tire model of 465-868P; $p_w = 0.16$ MPa.

$s'_{\delta i\,\min}$, whereas the inner wheel reaches its complete slippage $s''_{\delta i\,\max}$ that corresponds to the highest circumferential force $F''_{xi\,\max} = \mu''_{pxi} W_{wi}$.

As seen from Figures 3.52 and 3.53, the variation in μ''_{xi} and μ'_{xi} occurs at a lower pace with increasing $F_{x\Sigma}$. At the same force $F_{x\Sigma i}$ the variation in F''_{xi} and F'_{xi} takes place at a higher rate on dense (stubble in the case under study) then on soft soils.

If the gripping conditions of the left and right wheels are different, then the redistribution of circumferential forces between the wheels of the axle occurs more rapidly over the entire range of values of $F_{x\Sigma i}$ when the inner wheel moves over dense ground and the outer wheel over soft soil (see Figure 3.54) than in cases when the gripping conditions of the wheels are the same (Figures 3.52 and 3.53) or when the inner wheel moves over softer soil (Figure 3.55).

If the inner wheel moves over soil that is softer than that under the outer wheel (Figure 3.55), then at large values of R_{ti} (at low turn angles of the front steered wheels) the circumferential force of the outer wheel (μ'_x) is greater than that of the inner wheel (μ''_x). The value of μ'_{xi} decreases with decreasing R_{ti} whereas that of μ''_{xi} increases and, at some value of R_{ti}, these two become equal ($\mu''_{xi} = \mu'_{xi}$, points A in Figure 3.55). Here, the greater the total circumferential force $F_{x\Sigma i}$, the lower the value of R_{ti} at which this equality is attained. The horizontal segments of μ''_{xi} and μ'_{xi} in Figures 3.52 through 3.55 correspond to the case when circumferential force F''_{xi} of the inner wheel attains the highest gripping possible and a further reduction in R_{ti} does not cause redistribution of force $F_{x\Sigma i}$ between the left and right wheels.

The lack of equality of forces F''_{xi} and F'_{xi} of an axle taking a turn generates in the plane of the road the moment M_{Bi} (see formula (2.389)). Figure 3.56 reflects results of calculation of the moment M_{Bi} that were calculated using the data from Figures 3.52 to 3.55.

Positive engagement of the wheels results in most cases in a situation when $F''_{xi} > F'_{xi}$ and this means that moment M_{Bi} interferes with making the turn. The value of M_{Bi} increases with decreasing R_{ti}. The higher the value of $F_{x\Sigma i}$ at the same value of R_{ti}, the smaller M_{Bi}. The highest values of M_{Bi} (at the same values of $F_{x\Sigma i}$) correspond to the case when the inner wheel moves over denser ground than the outer wheel. When the inner wheel moves over ground that is softer than that under the outer wheel, at large turning radii a moment that facilitates the turn acts in the plane of motion (curve 3, negative values of M_{Bi} at $1/R_t < 0.025$ in Figure 3.56).

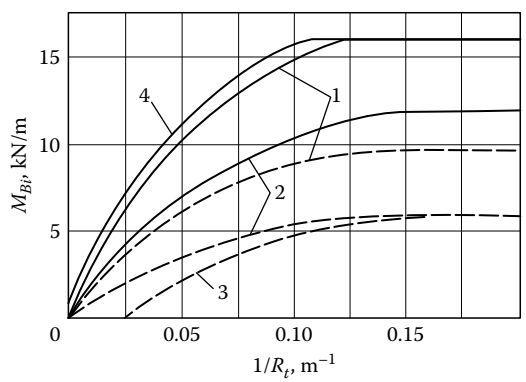


FIGURE 3.56
Moment M_{Bi} in various gripping conditions: 1, on stubble; 2, sow-ready field; 3, inner wheel on sow-ready soil and outer wheel on stubble; 4, inner wheel on stubble and outer wheel on sow-ready soil; ———, $(\mu''_{xi} + \mu'_{xi})/2 = 0.3$; — —, $(\mu''_{xi} + \mu'_{xi})/2 = 0.5$.

A simple and very clear analytic relationship for the moment of resistance to turning can be derived from formula (2.389) for the case when the relationship $F_x = K_x s_\delta$ is linear. Having determined the tire slippage from the geometry of Figure 3.51a in terms of the generalized slippage $s_{\delta ai}$ of the axle:

$$\begin{aligned} s'_{\delta i} &= s_{\delta ai} - \frac{0.5 t_{Bi}}{R_{ti}} \\ s''_{\delta i} &= s_{\delta ai} + \frac{0.5 t_{Bi}}{R_{ti}} \end{aligned} \tag{3.140}$$

the moment of resistance of the turn can be found from formula (2.389):

$$M_{Bi} = \frac{t_{Bi}^2 K_{xi}}{2R_{ti}}(1 - s_{\delta ai}) \tag{3.141}$$

Analysis of formula (3.141) also shows that the moment resisting the turn of the driving axle increases with decreasing R_{ti} and decreases with increasing traction load represented by the value of $s_{\delta ai}$. On denser soil and on hard roads the value of M_{Bi} increases since the longitudinal stiffness factor K_{xi} is higher. Moment M_{Bi} is sensitive to variations in the wheel track t_{Bi} (square term).

It is obvious that the total moment of resistance to a vehicle's turn exerted by positive engagements of all its interwheel power-dividing units is given by the algebraic sum of resistances to turn of the individual axles:

$$M_{B\Sigma} = \sum_{i=1}^{n} M_{Bi} \tag{3.142}$$

Moment M_{Bi} exerted on the axle by the road (or the sum $M_{B\Sigma}$ of moments in the case of several driving axles) is overcome by wheel side reactions that arise in the contacts between the tires and the road. For example, formulae (2.390) and (2.391) to calculate F_{l1}^{w} and F_{l2}^{w} were obtained in Section 2.8.3 for the case of 4×2 rear and front drive vehicles, respectively. Simultaneous application of these formulae allows calculating the lateral reactions of the wheels of 4×4 vehicles. As an illustration Figure 3.57 shows the values of lateral forces F_{l1}^{w} of the front wheels of an 18-ton 4×4 truck with an open interaxle differential and positively engaged interwheel power-dividing units.

These significant lateral forces give rise to large tire slip angles. As result, the actual turning radius markedly exceeds the value of the theoretical turning radius calculated without allowance for the slip angles. The above is illustrated by graphs of the turning radius variation factor q_R calculated from formula (1.117) and plotted in Figure 3.58.

The above means that positive engagement of the interwheel power-dividing units generates, in the majority of cases a moment of resistance to the vehicle's turning, an increase in the lateral forces and in the tire slip angles. This increases the turning radius, that is, the vehicle starts manifesting understeering behavior. In the case of negative turn resistance moments (i.e., a moment that facilitates turning arises in the plane of the road), the vehicle exhibits oversteering behavior. At least two conclusions can be drawn from the above: (i) the turnability of a vehicle can be controlled by controlling the circumferential forces (torques) of the axle's wheels, and (ii) in controlling the torques consideration should be given to the properties of the surface over which the left and right wheels travel; they

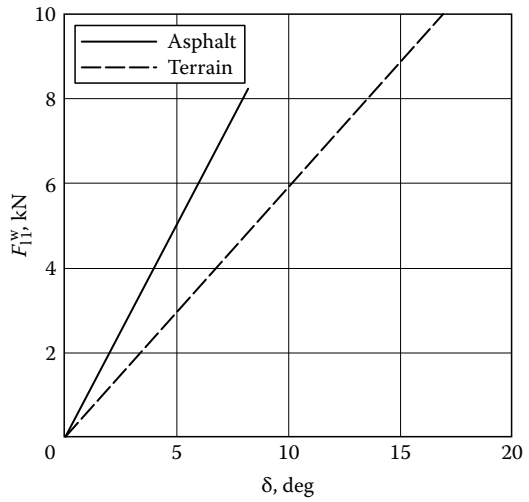


FIGURE 3.57
Lateral forces of the front wheels exerted by the positively engaged interwheel power-dividing units.

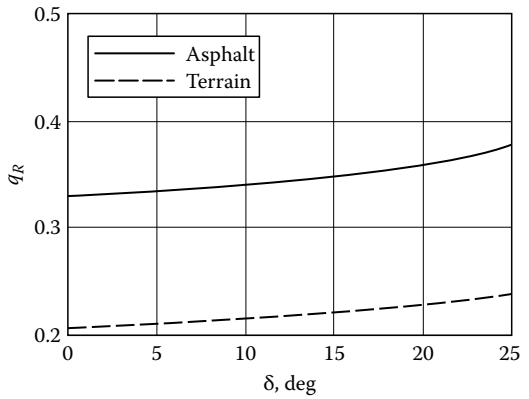


FIGURE 3.58
Turning radius variation factor.

may cause the appearance of a moment that interferes with turning as well as one that facilitates turning.

When a vehicle takes a turn, particularly at high velocities, the weight becomes redistributed between the left and right wheels; this changes the rolling radii of wheels in the driven mode and the behavior of the tires and the soil. Consider now the specifics of calculating moment M_{Bi} under these conditions.

The turning of an axle with positively locked interwheel unit causes kinematic discrepancy that is represented by the two factors m''_{Hi} and m'_{Hi}. Their numerical values can be calculated from formula (3.57) as a function of the rolling radii of the left and right wheels in the driven mode, turning radii of the wheels and the tangential stiffness of the tires. Now, using these values of m''_{Hi} and m'_{Hi}, one determines the slippages $s''_{\delta i}$ and $s'_{\delta i}$ of the left and right wheels of the axle using formula (3.58) and the known value of the generalized slippage of the axle $s_{\delta ai}$. The next stage of calculations consists in determining the circumferential forces F''_{xi} and F'_{xi} of the axle using slippages $s''_{\delta i}$ and $s'_{\delta i}$ and the functional relationships $F_x = f(s_\delta)$ (some linear and some nonlinear relationships were given in Section 1.3.2). The last stage of computations involves finding moment M_{Bi} from formula (2.389).

For the case governed by the linear relationship (1.25), following the above algorithm allows finding the following expression for M_{Bi}:

$$\begin{aligned} M_{Bi} &= 0.5t_{Bi}\left(F''_{xi} - F'_{xi}\right) = 0.5t_{Bi}\left(K''_{xi}s''_{\delta i} - K'_{xi}s'_{\delta i}\right) \\ &= 0.5t_{Bi}\left\{K''_{xi}\left[m''_{Hi} + \left(1 - m''_{Hi}\right)s_{\delta ai}\right] - K'_{xi}\left[m'_{Hi} + \left(1 - m'_{Hi}\right)s_{\delta ai}\right]\right\} \\ &= 0.5t_{Bi}\left\{\left(K''_{xi}m''_{Hi} - K'_{xi}m'_{Hi}\right) + \left[K''_{xi}\left(1 - m''_{Hi}\right) - K'_{xi}\left(1 - m'_{Hi}\right)\right]s_{\delta ai}\right\} \end{aligned} \tag{3.143}$$

and finally it is found that:

$$M_{Bi} = 0.5t_{Bi}\left[\left(K''_{xi} - K'_{xi}\right)s_{\delta ai} + \left(K''_{xi}m''_{Hi} - K'_{xi}m'_{Hi}\right)\left(1 - s_{\delta ai}\right)\right] \tag{3.144}$$

It must be remembered when using formula (3.144) that the double prime pertains to the lagging (inner) wheel and the single prime to the advancing (outer) wheel (see Figure 3.51). Expression (3.144) is convenient because it allows determining the conditions of the inception of the turning resistance moment and the moment that facilitates the turning. If the generalized slippage $s_{\delta ai}$ of the axle is positive (i.e., the given axle moves in the driving mode), then for the turning resistance moment to arise it is necessary that the numerical value of M_{Bi} be positive. If $M_{Bi} < 0$, then a moment that facilitates the running arises. The reasons for the appearance of positive and negative M_{Bi} stem from combinations of parameters contained in formula (3.144). At identical gripping conditions of the wheels the first term in the square brackets is negative, since when the weight is redistributed while turning in a manner that increases the load on the outer wheel, the longitudinal elasticity of its tire decreases and accordingly the longitudinal stiffness factor K'_{xi} increases, that is, $K'_{xi} > K''_{xi}$. Under these conditions the magnitude and sign of M_{Bi} will depend on the magnitude and sign of the second term in the square brackets, that is, on the ratio of the kinematic discrepancy factors m''_{Hi} and m'_{Hi}. Such an analysis is important in conceptual design of systems of control of kinematic discrepancy (some examples are analyzed in Section 3.6).

The next item to examine is the effect of a positively engaged interaxle drive on the turnability of 4×4 vehicles. Formulae (2.392) and (2.393) that establish the effect of the circumferential forces of the axles on the lateral forces of the front and rear wheels were obtained previously. It follows from formula (2.392) that the type of the interaxle power-dividing unit does not affect the lateral force of the rear wheels and $F^{\mathrm{a}}_{l2} = 0$. The numerical value and sign of F^{a}_{l1} depend perceptibly on circumferential forces of the front wheels, meaning also on the type of the interaxle PDU. Using general formula (2.393) determine the force F^{a}_{l1} for the case of a positively engaged interaxle power-dividing unit. In this case, circumferential force F_{x1} of the front wheels can be determined from expression (3.71) (on the condition that the wheels are of the same size, $K_{a1} = K_{a2} = K_a$, and that the relationship $F_x = K_{\mathrm{a}}s_{\delta\mathrm{a}}$ is linear). For this, the value of m_R from formula (3.16) should be substituted into (3.71):

$$F_{x1} = K_{\mathrm{a}1}s_{\delta\mathrm{a}1} = K_{\mathrm{a}}\left(\frac{F_{x\Sigma}}{2K_{\mathrm{a}}} - \frac{m_R}{2}\right) = R_{x1} - \frac{m_R K_{\mathrm{a}}}{2} = R_{x1} - \frac{K_{\mathrm{a}}(1 - \cos\delta)}{2} \tag{3.145}$$

where, it was assumed that $R_{x1} = R_{x2} = 0.5F_{x\Sigma}$ and δ is the turning angle of the steered wheels. Then the lateral force of the front wheels that is caused by the positively engaged

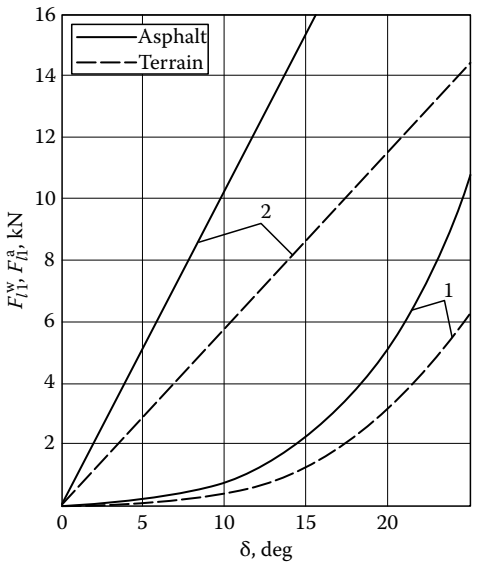


FIGURE 3.59
18-ton 4×4 truck: lateral forces of the front wheels. 1, F_{l1}^{a}; 2, F_{l1}^{w}.

interaxle power-dividing unit will be determined from expression (2.393) that is transformed to:

$$F_{l1}^{a} = 0.5K_{a}(1 - \cos\delta)\tan\delta \tag{3.146}$$

An important conclusion can be drawn from formula (3.146): lateral force F_{l1}^{a} that arises when the interaxle power-dividing unit is positively engaged is independent of the geometric parameters of the vehicle and is determined solely by the longitudinal stiffness of the front tires and by the wheel turning angle δ (on the assumptions made). Figure 3.59 shows curves of F_{l1}^{a} of an 18-ton 4×4 truck with positively engaged interaxle unit and open interwheel differentials (curves 1).

For comparison this figure also shows the lateral forces F_{l1}^{w} of the front wheels (curves 2) that stem from locking of the interwheel differentials (in this case the interaxle differential here is of the open kind). Curves 2 were transferred to Figure 3.59 from Figure 3.57. It follows from comparing curves 1 and 2 that positive engagement of the interwheel power-dividing unit increases vehicle understeering to a much greater extent than when locking the interaxle unit. In fact, the lateral force F_{l1}^{w} causes a much greater increase in the actual turning radius as compared with its theoretical value than in the case of the force F_{l1}^{a}. The above is confirmed by the values of factor q_R from Figure 3.60 that compares curves 1 taken from Figure 3.58 with curves 2 corresponding to a positive engagement in the interaxle drive.

Positive engagement of the interaxle driveline on passenger cars that frequently perform turns at high velocities may cause a marked increase in the turning radius, particularly on wet roads, that is, surfaces with poor gripping properties. This must be remembered in designing all kinds of devices that serve for engaging an axle when a difference appears in the angular velocities of the front and rear wheels. It was found in testing a minivan on a steep turn on a wet road that the front axle was automatically positively engaged by the device that received a signal concerning differences in the angular velocities of the front and rear wheels. The negative circumferential force F_{x1} that arose due to engaging the

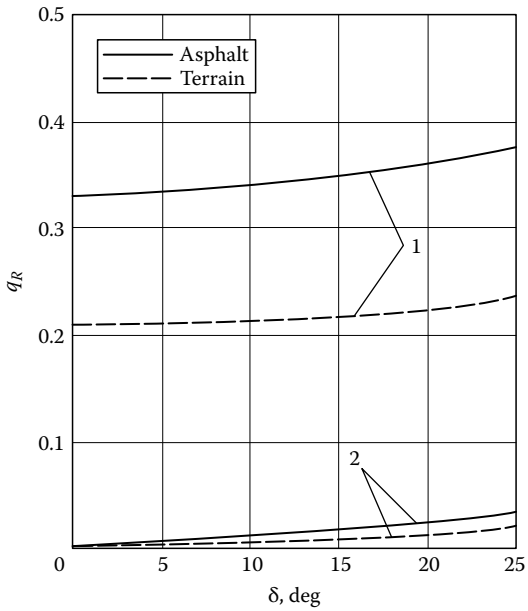


FIGURE 3.60
18-ton 4 × 4 truck: turning radius variation factor with positive engagement in (1) interwheel drives of the front and rear axles; (2) interaxle drive.

interaxle unit increased the lateral force of the front wheels. This caused a marked increase in the slip angles of the front wheels (the turn was performed on a wet road) and in the turn radius that almost ended in an accident.

The negative effect of a locked interaxle power-dividing unit on the turnability of a vehicle that manifests itself in increasing the turning radius increases if the driveline system contains a design kinematic discrepancy. Figure 3.61 shows the circumferential forces F_{x1} and F_{x2} of the axles, the lateral force F_{l1}^{a} and the turning radius variation factor q_R calculated for the turning of a 3.7-ton 4 × 4 tractor with different-size wheels on the rear and front axles moving without performing any work on asphalt (a) and stubble (b).

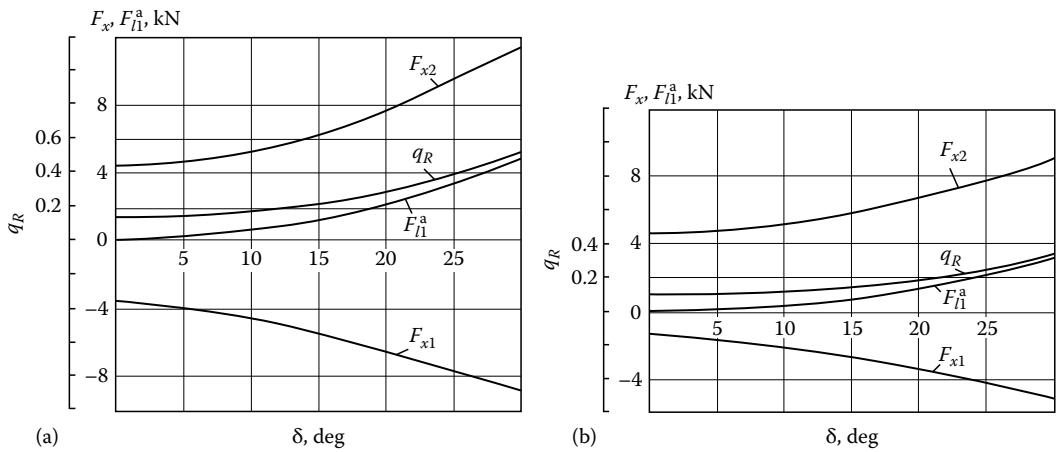


FIGURE 3.61
3.7-ton 4 × 4 tractor making a turn on (a) asphalt; (b) stubble.

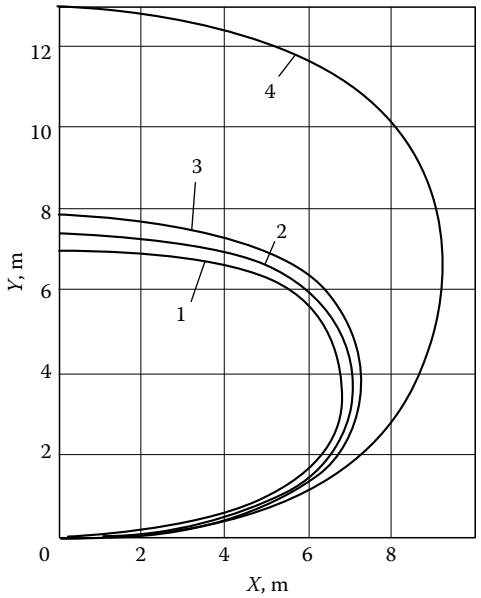


FIGURE 3.62
5.6-ton tractor in loop-less turn (1) with no wheel slip angles (theoretical curve); (2) 4 × 4 with open interaxle differential and gear ratio $u_d = 2$; (3) 4 × 2 with rear drive axle; (4) 4 × 4 with positively engaged driveline and with $m_{H1} = -0.02$ and $m_{H1} = 0.025$.

The presence of the design kinematic discrepancy $m_{ru} = 0.053$ and it increase by means of the emerging component m_R highly increases the turning radius. Note that F_{x1} is negative in both cases and this means that also force F_{l1}^{a} increases markedly with increasing δ.

The effect of different types of interaxle drivelines on the turn path can be compared using data in Figure 3.62.

This figure shows the analytically computed paths of loop-less turn under no-load conditions of a 5.6-ton tractor with different-size rear and front wheels. The computations were performed for the following wheel formulae: 4 × 2 with rear drive axle, 4 × 4 with positively engaged driveline and with $m_{H1} = -0.02$ and $m_{H1} = 0.025$; 4 × 4 with open interaxle differential and gear ratio $u_d = 2$. The interwheel differentials were regarded as open and symmetrical. A linear variation in time of turn angle δ of the front wheels was specified for the start of the turn (first segment) and then the motion continued with the maximum value δ_{max} (second segment). At the third segment that corresponded to getting out of the turn, angle δ was varied in such a manner that the plane of the front wheel be parallel to the *X*-axis when the rectilinear motion commenced. The paths can be compared by means of factors introduced by formulae (1.118), the numerical values of which are shown in Table 3.4. It is seen from this table that the tractor with the interaxle differential exhibits the best turnability.

TABLE 3.4
Characteristics of Turnability

Driveline Configuration	K_A	K_X	K_Y
4 × 2	1.18	1.05	1.11
4 × 4 with interaxle differential	1.07	1.02	1.02
4 × 4 with positively engaged interaxle unit	2.48	1.33	1.81

Positive engagement of the interaxle and interwheel power-dividing units has a perceptible effect on vehicle's stability of motion. The physical substance of this effect consists in the fact that the redistribution of circumferential forces between the vehicle's wheels may markedly reduce the ability of certain wheels to take up an applied lateral force. This reduces the stability of motion. The most typical example of the effect of the driveline system on stability is the motion of a vehicle in an off-road track, when the vehicle is subject to clearly seen lateral displacement.

Automobiles with positively engaged driveline systems that have understeering typically respond slowly to the turn of the steering wheel. The delay in reaction of an automobile to the driver's action becomes increasingly greater with increasing turn angle of the steered wheels.

The stability of a vehicle with positively engaged drive traveling on hard-surfaced roads may deteriorate, particularly at high speeds. The effect of the driveline system on the turnability and stability of motion should be investigated using mathematical multi-body models of vehicles with consideration of the specifics of the suspension and of the steering system. Some results are discussed in Chapter 6.

3.6 Optimal and Reasonable Kinematic Discrepancy: Control Principles

It was previously shown that in order to minimize the slippage power and improve the fuel efficiency, the kinematic discrepancy factor in a positively engaged driveline system of a 4×4 vehicle should be equal to zero: $m_{ru} = 0$ (note that this was proved in case of linear function of $F_x = K_x s_\delta$). The zero value may be regarded as optimal from the point of view fuel efficiency. However, to ensure automatic engagement/disengagement of one of the axles it is necessary to introduce some kinematic discrepancy ($m_{ru} \neq 0$) into the drive, the value of which may be termed *reasonable*. This value of m_{ru} should ensure stable engagement and disengagement of the axle and the reduction in the vehicle's efficiency should not be perceptible. Consider the principles of selecting such a reasonable value of the kinematic discrepancy factor. Recall (see Section 3.2) that irrespective of the design discrepancy factor (that is here designated by m_{ru}^{d}) there always exists an operational-manufacturing kinematic discrepancy factor (that is designated by m_r^{o}). If these two factors are of equal magnitude but of opposite sign, then a zero (or close to zero) kinematic discrepancy is formed in the drive and the additional axle will constantly operate in the ''engaged/disengaged'' mode. The automatic engagement device of this axle does not then function properly, that is, it does not provide reliable engagement and thereafter also reliable disengagement.

However, if these factors (m_{ru}^{d} and m_r^{o}) are of the same sign, then the total kinematic discrepancy may turn out to be rather high. The wheels of the principal axle should be subject to significant slippage before the additional axle is engaged. This reduces the traction and velocity performance of the vehicle and its mobility. It is clear from the above that before specifying a reasonable design kinematic discrepancy it is necessary to assess the limits of variation of the operational-manufacturing discrepancy m_r^{o}.

The ranges of variation in m_r^{o} were investigated for 3.7 and 5.6-ton 4×4 tractors. The values of u_1 and u_2 conformed to the specifications. The effect of tire-manufacturing tolerances and the tire inflation pressure on variation in the kinematic discrepancy relative

TABLE 3.5

Tractor 4 × 4, Mass of 5.6 ton: Kinematic Discrepancy

	Kinematic Discrepancy		
Parameters in Change	$m_{\min}$	m_{ru}	$m_{\max}$
Inflation pressure	−0.0071	0.0372	0.0729
Tire tolerance	−0.0234	0.0372	0.0840
Weight load	0.0282	0.0372	0.0501

to its value at nominal radii and nominal air pressure was investigated at constant nominal axle loads. The limits of variation in the pressure in the front tires were 0.06−0.25 MPa and of that in the rear tires 0.06–0.22 MPa. The effect of weight loads of the axles on variation of the factor m_r° under the above conditions was investigated over a range of 7.5–20 kN for the front axles and 22.9–31 kN for the rear axles. The minimum kinematic discrepancy $m_{\min}$ (at the highest value of r_{a1}^0 and lowest value of r_{a2}^0) and the maximum kinematic discrepancy $m_{\max}$ (at the lowest value of r_{a1}^0 and highest value of r_{a2}^0) were calculated.

The different values of m_{ru}^{d} in the drive of the 3.7 ton 4 × 4 tractor were obtained by using different tires sizes and also by varying the number z of teeth of one of the transfer-case gears: $z = 37$, 39, and 41 (the resultant changes in the axis-to-axis distance were compensated by means of a set of shims). Table 3.5 lists data of computations for a 5.6-ton 4 × 4 tractor, whereas Tables 3.6 through 3.8 present these data for a 3.7-ton 4 × 4 tractor.

Analysis of data in the above-mentioned tables shows that a change in the weight loads on the axles has the least effect on the kinematic discrepancy as compared with manufacturing tolerance and tire pressure. Thus, when weight W_1 is increased upon a simultaneous reduction in weight W_2, the kinematic discrepancy of the 5.6-ton tractor increases from 0.0282 to 0.0501 or by 0.0219 (see Table 3.5). The kinematic discrepancy of the 3.7-ton tractor in this case does not change by more than 0.0377 (Table 3.6).

The tire pressure has a marked effect on the kinematic discrepancy varying for the 5.6-ton tractor from −0.0071 to 0.0729 (Table 3.5). For the 3.7-ton tractor, when equipped by batch produced 11.2-20 and 15.5R38 tires the kinematic discrepancy ranges from

TABLE 3.6

Tractor 4 × 4, Mass of 3.70 ton: Kinematic Discrepancy due to Change in Axle Weight Loads

		Rear Tires			
		15.5R38		16.9R38	
Front Tires	z	$m_{\min}$	$m_{\max}$	$m_{\min}$	$m_{\max}$
8.3-20	37	0.0142	0.0452	0.0785	0.1125
11.2-20	37	−0.0107	0.0270	0.0545	0.0962
16.0-20	37	−0.1176	−0.0989	−0.0448	−0.0214
8.3-20	39	0.0640	0.0934	0.1250	0.1573
11.2-20	39	0.0394	0.0771	0.1020	0.1422
16.0-20	39	−0.0612	−0.0434	0.0079	0.0302
8.3-20	41	0.1102	0.1382	0.1682	0.1990
11.2-20	41	0.0868	0.1226	0.1463	0.1845
16.0-20	41	−0.0088	0.0081	0.5569	0.0781

TABLE 3.7

Tractor 4 × 4, Mass of 3.70 ton: Kinematic Discrepancy due to Change in the Inflation Pressure

		Rear Tires					
		15.5R38			16.9R38		
Front Tires	z	$m_{\min}$	m_{ru}	$m_{\max}$	$m_{\min}$	m_{ru}	$m_{\max}$
8.3-20	37	−0.0158	0.0434	0.0802	0.0542	0.1101	0.1420
11.2-20	37	−0.0527	−0.0117	0.0305	0.0199	0.0588	0.0957
11.0-20	37	−0.1386	−0.1054	0.0540	−0.0509	−0.0095	0.0355
16.0-20	37	−0.1503	−0.1176	−0.0742	−0.0711	−0.0397	−0.0020
8.3-20	39	0.0356	0.0917	0.1266	0.1020	0.1551	0.1854
11.2-20	39	0.0005	0.0394	0.0795	0.0694	0.1015	0.1413
11.0-20	39	−0.0816	−0.0496	0.0082	0.0022	0.0415	0.0842
16.0-20	39	0.0922	−0.0612	−0.0199	−0.0110	−0.0128	0.0486
8.3-20	41	0.0832	0.1365	0.1697	0.1463	0.1968	0.2256
11.2-20	41	0.0499	0.0868	0.1249	0.1153	0.1505	0.1837
11.0-20	41	−0.0187	0.0204	0.0667	0.0515	0.0888	0.1294
16.0-20	41	−0.0383	−0.0088	0.0304	0.0332	0.0616	0.0956

0.0005 to 0.0795 (Table 3.7). For tires of other sizes the difference between $m_{\max}$ and $m_{\min}$ may be as high as 0.0898 (Table 3.7).

The difference in the value of the rolling radii of wheels, r^0_{a1} and r^0_{a2}, within the limits of manufacturing tolerance causes an even more significant variation in kinematic discrepancy. The range of kinematic discrepancy for the 5.6-ton tractor ranges from −0.0234 to 0.0834 (Table 3.5). For the 3.7-ton tractor this quantity ranges from −0.0188 to 0.0972 for the standard tire set (Table 3.8).

It can be concluded as a whole on the basis of data in Tables 3.5 through 3.8 that the variation in vertical loads on the axles changes the kinematic discrepancy by 3.8%, the difference in tire pressures of rear and front wheels changes the discrepancy by 9% and the tire manufacturing tolerances result in a variation of 13.5%. The simultaneous effect of all the above factors may modify the kinematic discrepancy by 21%.

Under actual operating conditions, real combinations of normal weight loads, air pressures in the rear and front wheels and deviation of radii from the nominal are rather far from their extreme values. Thus, the operating-manufacturing kinematic discrepancy factor of all-wheel drive trucks caused by tire-manufacturing tolerances amounts to 1.5%–2%, because of differences in tire pressure −1%–1.5%, the same being true concerning differences in the normal static load on the tires. The dynamic redistribution of the weight load between the vehicle axles may cause the kinematic discrepancy to amount to 4%–5%.

For this reason, the design kinematic discrepancy factor m^{d}_{ru} in presently manufactured vehicles usually ranges between 0.05 and 0.08. It allows providing for reliable automatic engagement and disengagement of one of the axles upon the inevitable operational-manufacturing discrepancy in axle theoretical velocities V_{t1} and V_{t2}.

The methods developed in the preceding sections can be used for predicting the effect of certain factors on the operational-manufacturing kinematic discrepancy and the energy efficiency of the vehicles and, on the basis of such analysis, recommendations for industrial processes can be worked out. As an illustrative example consider the technical problem of specifying the tolerance for manufacturing the outer diameter of a 1500 × 600–635 tire of

TABLE 3.8

Tractor 4 × 4, Mass of 3.70 ton: Kinematic Discrepancy due to Tolerance in Manufacturing

		Rear Tires			
		15.5R38		16.9R38	
Front Tires	z	$m_{\min}$	$m_{\max}$	$m_{\min}$	$m_{\max}$
8.3-20	37	−0.0358	0.0984	0.0302	0.1634
11.2-20	37	−0.0730	0.0492	−0.0047	0.1178
11.0-20	37	−0.1698	−0.0347	−0.0765	0.0585
16.0-20	37	−0.1794	−0.0472	−0.1042	0.0284
8.3-20	39	0.0165	0.1439	0.0782	0.2051
11.2-20	39	−0.0188	0.0972	0.0460	0.1623
11.0-20	39	−0.1047	0.0166	−0.0221	0.1061
16.0-20	39	−0.1198	0.0057	−0.0484	0.0775
8.3-20	41	0.0651	0.1862	0.1247	0.2449
11.2-20	41	0.0314	0.1418	0.0932	0.1031
11.0-20	41	−0.0378	0.0841	0.0283	0.1502
16.0-20	41	−0.0645	0.0548	0.0033	0.1230

an all-wheel drive 8 × 8 truck with a positive engagement of its interaxle power-dividing units. The calculations were made on the assumption that the wheels can be manufactured as ideally identical conforming to the nominal value of the outer diameter, as well as different caused by tolerances of the outer diameter. In the latter case, the wheel radii can be regarded as random quantities. The random rolling radii of the wheels in the driven mode were determined by assuming a normal distribution of random quantities and setting the outer-diameter tolerance of the wheels equal to $\pm 3\sigma$ (where σ is the rms deviation of the random quantity). Outer-diameter tolerance Δ of the tire under study is ±15 mm. Calculations were also performed on the assumption of $\Delta = \pm 10$ mm and $\Delta = \pm 5$ mm.

The radii determined in this manner served for determining the kinematic discrepancy factors m_{Hi} and then the circumferential forces of the axles F_{xi} ($i = 1, 4$) when the truck moves on asphalt (see Figure 3.63).

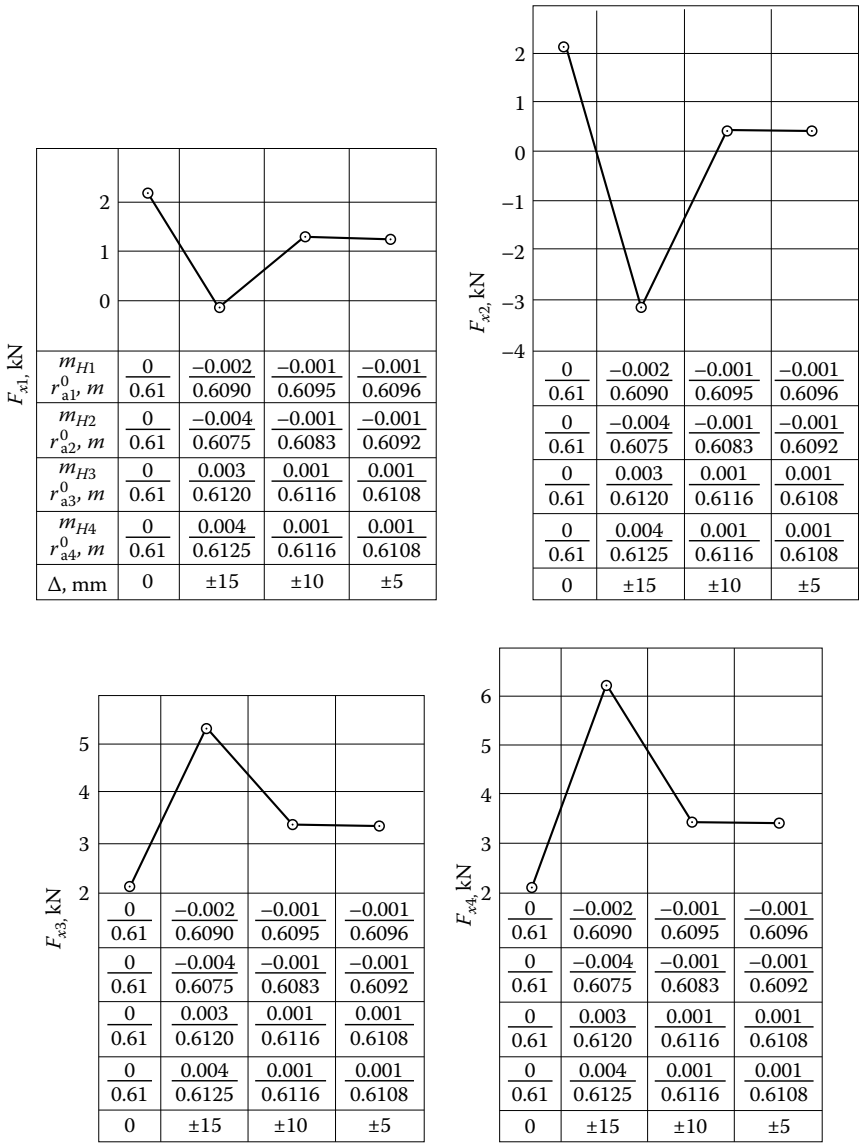
It is seen that at zero kinematic discrepancy the circumferential forces of the axles are the same (the ideal, theoretical case).

The difference in tire radii at Δ ±15 mm caused a perceptibly nonuniform traction load of the axles. This non-uniformity decreases at $\Delta = \pm 10$ mm, whereas in the case of $\Delta = \pm 5$ mm the traction forces on the axles virtually do not differ from the case of $\Delta = \pm 10$ mm. The pertinent values of the efficiencies η_x^{tr} and η_{tr} are given in Figure 3.64.

For this reason, some toughening of the requirements to the precision in manufacturing the tire diameter is sensible also from the point of view of the truck's traction dynamics and energy efficiency.

Consider still another example that illustrates how reasonable values of the kinematic discrepancy factor are introduced into the design of the driveline system that ensure automatic engagement and disengagement of the front axle of a 3.7-ton 4 × 4 tractor using an overrunning clutch. Note also that this design has a provision for forced engagement of the front axle by the tractor driver.

Normal operation of the overrunning clutch on the tractor modifications that are equipped with different tires requires establishing the appropriate gear ratios in the

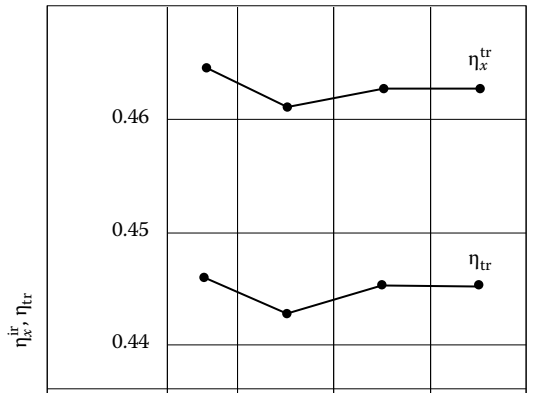


m_{H1} r^0_{a1}, m	0 0.61	−0.002 0.6090	−0.001 0.6095	−0.001 0.6096
m_{H2} r^0_{a2}, m	0 0.61	−0.004 0.6075	−0.001 0.6083	−0.001 0.6092
m_{H3} r^0_{a3}, m	0 0.61	0.003 0.6120	0.001 0.6116	0.001 0.6108
m_{H4} r^0_{a4}, m	0 0.61	0.004 0.6125	0.001 0.6116	0.001 0.6108
Δ, mm	0	±15	±10	±5

FIGURE 3.63
8 × 8 truck: circumferential forces.

axles' drives that would provide the reasonable kinematic discrepancy between the axles of the different tractor modifications. It was established that the minimum design modifications of the driveline system are attained by changing the gear ratio u_1 in the drive of the front axle by proper selection of the number z_{a2} of the transfer case gear while retaining the number z_{a1} of teeth of the gearbox gear connected to it. The results of studies are listed in Table 3.9 (see ''Automatic mode'').

It follows from these data that in virtually all versions of the given tractor providing for normal operation of the overrunning clutch requires using a transfer case gear with number of teeth $z_{a2} = 41$ ($z_{a2} = 42$ for tractors used in rice cultivation) instead of $z_{a2} = 39$



$\frac{m_{H1}}{r^0_{a1},\ m}$	0 0.61	−0.002 0.6090	−0.001 0.6095	−0.001 0.6096
$\frac{m_{H2}}{r^0_{a2},\ m}$	0 0.61	−0.004 0.6075	−0.001 0.6083	−0.001 0.6092
$\frac{m_{H3}}{r^0_{a3},\ m}$	0 0.61	0.003 0.6120	0.001 0.6116	0.001 0.6108
$\frac{m_{H4}}{r^0_{a4},\ m}$	0 0.61	0.004 0.6125	0.001 0.6116	0.001 0.6108
Δ, mm	0	±15	±10	±5

FIGURE 3.64
8 × 8 truck: energy efficiencies.

in the standard-production tractor. The kinematic discrepancy factors of the axles for the recommended values of z_{a2} have different signs and are numerically equal to: $m_{H1} = -0.029$ to -0.058 and $m_{H2} = 0.007$–0.030. These values of m_{Hi} have corresponding to them the kinematic discrepancy factor from formula (3.6) of $m_{ru} = 0.05$–0.08. In the case of $z_{a2} = 39$, $m_{ru} \approx 0.02$, which is clearly insufficient for normal operation of the clutch.

Whereas automatic engagement/disengagement of the front axle requires a certain kinematic discrepancy, this is not needed when the front axle is engaged manually. The kinematic discrepancy of the axles in the last case may again be eliminated by changing the gear ratio u_1 in the front axle drive. This can be done by using a reduction gear that is engaged instead of the overrunning clutch only when the axles are engaged manually. This is the principle underlying the design of the transfer case shown in Figure 3.65.

This design combines automatic engagement of the front axle by means of the overrunning clutch and manual engagement of this axle with simultaneous reduction to zero of the kinematic discrepancy when employing manual engagement. The arrangement of parts in Figure 3.65a corresponds to automatic operation of the transfer case. For manual engagement of the front axle the geared clutch half 2 should be moved to the right limiting position. This disengages it from ring 3 and engages it to clutch half 7. As a result, the torque from the gear box bypasses the overrunning clutch and is transmitted to shaft 1 by the gear pair 8 and 6 (z_{n1} and z_{n2}), the gear ratio of which differs from the gear ratio of gear 8 and the outer ring 5 (teeth z_{a1} and z_{a2}). The general view of the transfer case is shown in Figure 3.65b.

Table 3.9 (see ''Manual mode'') gives values of u_1 calculated on the basis of teeth numbers z_{n1} and z_{n2} of gears 6 and 8. It is seen that the kinematic discrepancy m_{ru} of the axles at these values of u_1 in the manual front-axle engagement mode is quite close to zero. Factors m_{H1} and m_{H2} are here also small by absolute magnitude and differ by signs.

Experience in using this new transfer case showed that it has a positive effect on the tractor's operation. Figure 3.65c shows the rate of fuel consumption per hour Q_h of the

TABLE 3.9

4 × 4 Tractor: Automatic and Manual Modes in Transfer Case

	Mode							
	Automatic				Manual			
Front Tires / Rear Tires	$\frac{z_{a2}}{z_{a1}}$	u_1	m_{ru}	$\frac{m_{H1}}{m_{H2}}$	$\frac{z_{n2}}{z_{n1}}$	u_1	m_{ru}	$\frac{m_{H1}}{m_{H2}}$
11.2-20 / 15.5R38	41/22	12.229	0.07	−0.045/0.028	40/23	11.495	0.01	−0.0062/0.0039
11.2-20 / 13.6R38	41/22	12.229	0.05	−0.045/0.007	40/23	11.495	−0.01	0.0051/−0.0049
11.2-20 / 15.5-38	41/22	12.229	0.08	−0.054/0.030	40/23	11.495	0.02	−0.0141/0.0063
9.5/9-20 / 15.5R38	41/22	12.229	0.08	−0.055/0.029	40/23	11.495	0.02	−0.0152/0.0052
9.5/9-20 / 13.6R38	41/22	12.229	0.07	−0.043/0.030	40/23	11.495	0.006	−0.0039/0.0021
9.5/9-20 / 15.5-38	41/22	12.229	0.08	−0.054/0.030	40/23	11.495	0.02	−0.0180/0.0055
11.2-20 / 18.4/15-30	41/22	12.229	0.05	−0.029/0.022	40/23	11.495	−0.01	0.0091/−0.0009
10.0-16 / 16.9R30	41/22	12.229	0.08	−0.058/0.027	40/23	11.495	0.02	−0.0179/0.0025
11.2-20 / 15.5R38	41/22	12.229	0.07	−0.045/0.028	40/23	11.495	0.01	−0.0062/0.0039
16.0-20 (Φ-76) / 18.4R34 (Φ-44)	42/22	12.527	0.07	−0.052/0.022	41/23	11.775	−0.005	0.0028/−0.0018
16.0-20 (Φ-64) / 18.4R34 (Φ-11)	42/22	12.527	0.05	−0.035/0.017	41/23	11.775	−0.01	0.0038/−0.0062

tractor with a standard and the new transfer case when engaging the second gear in transmission and in experiments on a field after the potatoes were harvested. When the front axle of the tractor with the new transfer case was manually engaged the fuel consumption dropped by 8% as compared with the case of engagement using the overrunning clutch. This reduction was attained due to the new design of the clutch that makes it possible to virtually eliminate the design kinematic discrepancy of the axles when they are manually engaged. The fuel consumption per hour of the tractor with the standard transfer case is virtually identical irrespective of the front axle engagement mode, whether automatic or manual. An analysis of oscillograms of the torques taken with the new design clutch ensures clear engagement/disengagement of the front axle by means of the kinematic discrepancy. Because of the low value of m_{ru}^{d} of the tractor with the standard transfer case, undesirable periodic engagement/disengagement of the front axle is observed even when operating at no load (idle motion).

Reduction of the design kinematic discrepancy to zero upon manual engagement of the front axle can be treated as control of the kinematic discrepancy. This example gives rise to the thought of the need to control the numerical value and sign of the kinematic discrepancy factor upon changes in the conditions of the vehicle's motion, for example, when taking a turn. Values of the kinematic discrepancy under a certain control can be termed optimal.

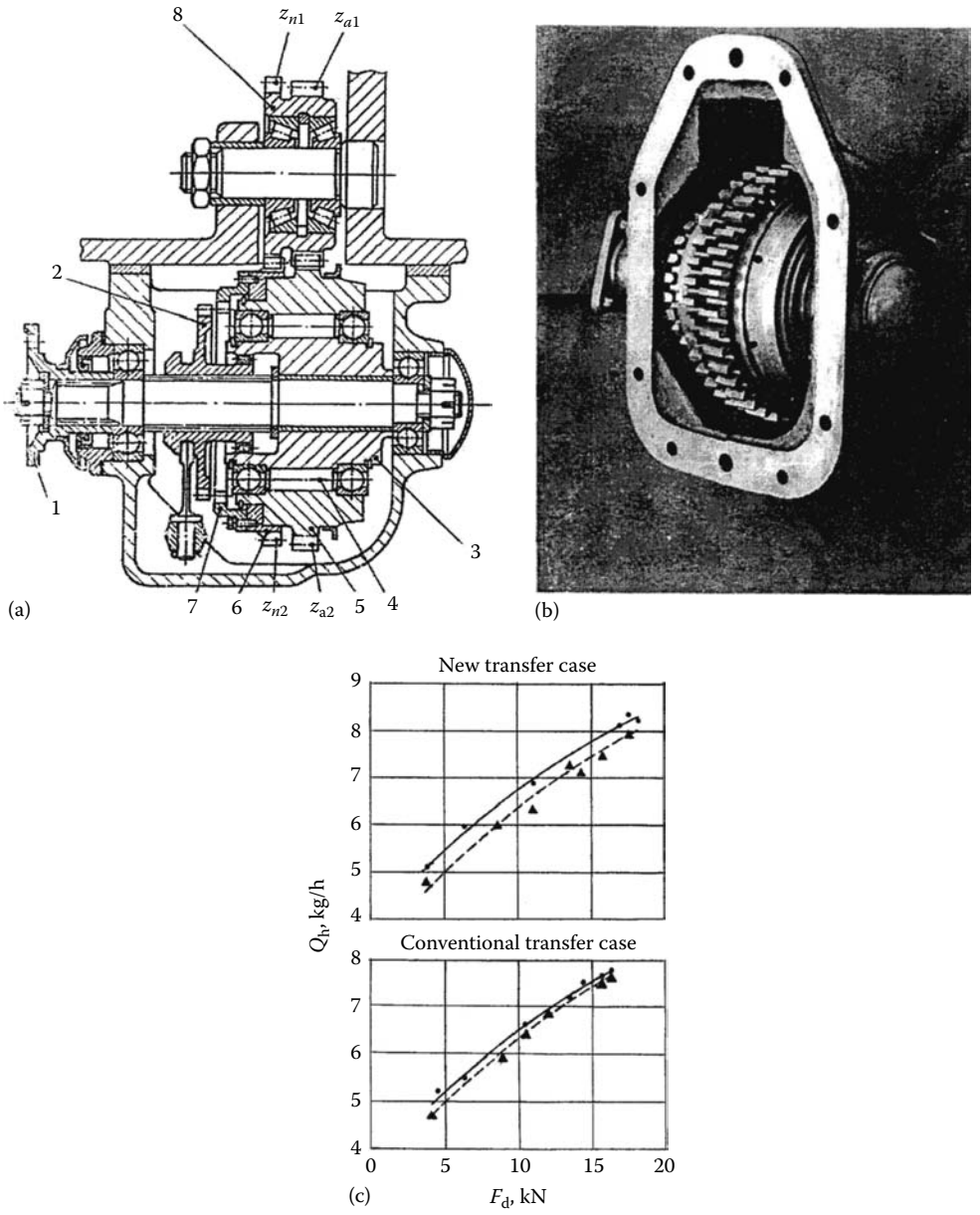


FIGURE 3.65
New design of transfer case: 1, output shaft connected with the front axle drive; 2, geared clutch half; 3, ring; 4, roller; 5, ring; 6, 8, gear pair; 7, clutch half; —— automatic mode; - - - manual mode.

Consider a 4×4 vehicle with front steered wheels and positively engaged interaxle power-dividing unit, which does not have a design kinematic discrepancy, that is, the kinematic discrepancy factor from formula (3.6) is equal to zero ($m_{ru} = 0$). Assume that the operational-manufacturing discrepancy is also zero. When this vehicle takes a turn the kinematic discrepancy m_R that is caused by differences in the turning radii of the front

and rear axles, $R_{t1} \neq R_{t2}$, and calculated from formula (3.16) arises. The numerical value of m_R is positive and increases with the angle of turn δ of the front wheels. The increase in m_R brings about an increase in the circumferential force F_{x2} of the rear wheels and reduction in circumferential force F_{x1} of the front wheels. This is seen from formulae (3.70) into which m_R should be substituted instead of the zero-valued m_{ru}. At large δ, m_R attains substantial values that may cause parasitic power circulation, that is, negative values of F_{x1}. This changes the direction and increases the numerical value of the lateral reaction F_{l1} from formula (2.343) and simultaneously increases vehicle understeering. If the gear ratios u_1 or u_2 in the drives of the axles are changed in the course of the turn, then the kinematic discrepancy m_{uR} may be reduced to zero and the increase in understeering of the vehicle can be avoided. This shall be shown using the expression for m_{uR} from formulae (3.17):

$$m_{uR} = 1 - (1 - m_u)(1 - m_R) = 0 \tag{3.147}$$

whence, using formulae (3.8) and (3.16), is obtained:

$$u_2 = u_1/\cos\delta \tag{3.148}$$

or

$$u_1 = u_2 \cos\delta \tag{3.149}$$

Formula (3.148) shows the manner of variation in the gear ratio u_2 of the rear-axle drive at constant gear ratio u_1 of the front axle drive and varying wheel-turning angle δ. It is seen that in this case $u_2 > u_1$ with increasing δ and $m_u < 0$ (see formula (3.8)). At positive m_R and negative m_u the kinematic discrepancy factor m_{uR} remains equal to zero (see formula (3.147)). Formula (3.149) shows the manner of variation in gear ratio u_1 at $u_2 =$ constant. In this case $u_1 < u_2$.

Gear ratios u_1 and u_2 are in general determined by the gear ratios u_{f1} and u_{f2} of the final drives and the gear ratios of the wheel-hub reduction gears u_{k1} and u_{k2}:

$$u_1 = u_{f1}u_{k1} \quad \text{and} \quad u_2 = u_{f2}u_{k2} \tag{3.150}$$

To implement formulae (3.148) and (3.149) in practice, power-transmitting units with variable gear ratios u_{PTU1} and u_{PTU2} should be installed in the axle drives. Thus, when implementing formula (3.148) upon substitution of formulae (3.150) one can have

$$u_{PTU1}u_{f2}u_{k2} = u_{f1}u_{k1}/\cos\delta \tag{3.151}$$

or

$$u_{PTU2} = u_{f1}u_{k1}/(u_{f2}u_{k2}\cos\delta) \tag{3.152}$$

When implementing formula (3.149) the necessary expression for u_{PTU1} is obtained in the following form:

$$u_{PTU1} = u_{f2}u_{k2}\cos\delta/(u_{f1}u_{k1}) \tag{3.153}$$

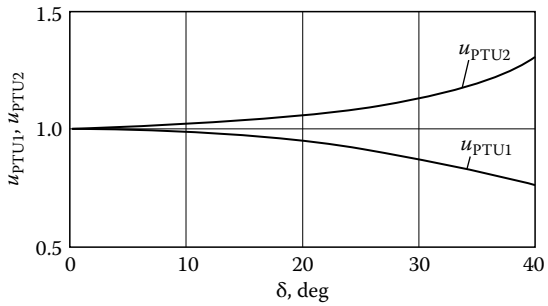


FIGURE 3.66
PTU gear ratios.

If the vehicle has no wheel-hub reduction gears then gear ratios u_1 and u_2 are determined only by the gear ratios of the final drives u_{f1} and u_{f2}. Here usually $u_{f1} = u_{f2}$. In this case, formulae (3.152) and (3.153) simplify and become:

$$u_{PTU2} = 1/\cos\delta \tag{3.154}$$

$$u_{PTU1} = \cos\delta \tag{3.155}$$

Formulae (3.154) and (3.155) are plotted in Figure 3.66.

The use of the additional power-transmitting unit in the drive of either the rear axle (for implementing formula (3.154)) or of the front axle (for implementing formula (3.155)) will cause differences in the mechanical power loss in the drives, that is, $\eta_{M1} \neq \eta_{M2}$ (see Section 1.4.1). To provide for equality of these two efficiencies it is necessary to install a power-transmitting unit in each of the drives of the axles, that is, to simultaneously control the values of u_1 and u_2. The control formula is obtained from (3.14) thus:

$$(u_1 R_{t1} - u_2 R_{t2})/u_1 R_{t1} = 0 \tag{3.156}$$

whence,

$$u_1/u_2 = R_{t2}/R_{t1} \tag{3.157}$$

It follows from the geometry of a vehicle in turn

$$R_{t2}/R_{t1} = \cos\delta \tag{3.158}$$

and finally,

$$u_1/u_2 = \cos\delta, \tag{3.159}$$

that is, when simultaneously controlling the values of u_1 and u_2 their ratio must be maintained equal to cos δ. To achieve this, u_1 should decrease when the vehicle turns and u_2 should increase. Note that formula (3.159) corresponds to the particular cases expressed by formulae (3.148) and (3.149) when either u_1 or u_2 are assumed to be constant.

Conformance to formulae (3.148), (3.149), and (3.159) ensures zero kinematic discrepancy in the turning of a 4×4 vehicle. Laws for controlling the values of u_1 and u_2 that would ensure negative values of m_{uR}, that would promote oversteering of the vehicle, can be obtained similarly.

4

Limited Slip Differentials

As noted in Chapter 1, limited slip differentials have been used in a large variety of vehicles for many decades. The invention of the concept of such mechanisms many years ago can be regarded as the first step toward developing an automatic drive that exhibits the positive properties of the differential and positively engaged driveline systems and which, to a large extent, is free of the shortcomings of these drives. Limited slip differentials, while retaining the differential effect, ensure the redistribution of the torque between the axle's wheels, increasing the torque at the wheel with better gripping of the surface of motion upon a reduction of the torque at the wheel that is subjected to poorer gripping conditions. This also applies to the use of the mechanisms as interaxle power-dividing units: the driving axles with better gripping conditions develop a larger torque, whereas those with poorer gripping conditions develop a smaller torque. Over the last 50–70 years, many successful designs of these mechanisms have appeared and their refinement and upgradation continue to the present day.

Usually, the redistribution of torques between output shafts in limited slip differentials is based on the use of elevated internal friction. A prolonged investigation of these mechanisms showed that, in spite of design differences, they could be investigated and designed from a common point of view. This led to the formulation of general relationships in the operation of limited slip differentials and analytic relationships of similar structures were developed for this purpose. These and other results are described in this chapter.

4.1 Torque Biasing and Locking Performance

Consider the operating principle of the limited slip differential. Assume that there exists a certain reduction gear with a stationary casing, consisting of a set of gear meshings (Figure 4.1a).

Let the gear ratio of this reduction gear be -1, meaning that ω_{rel}, the angular velocities of the shafts, are the same by absolute magnitude and of opposite direction. A braking device that develops braking torque, T', is placed on one of the shafts (output) of the reduction gear, whereas torque, T'', is applied to the other (input) shaft. With allowance for frictional losses in the reduction gear, it may be written as

$$T' = T''\eta_d \tag{4.1}$$

It is seen from condition (4.1) that $T'' > T'$. The differences between these two torques can be increased by reducing the reduction gear efficiency η_d, that is, by increasing the internal friction in this device. Note that the driving (input) shaft has the attribute of coincidence of the direction of motion of the torque and of the angular velocity, whereas the attribute of the driven (output) shaft consists of their opposite rotation directions. It can be easily

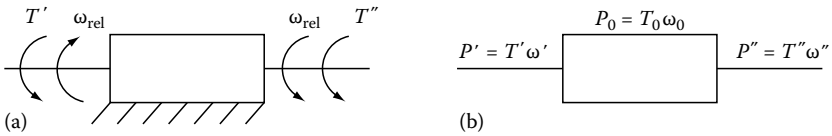


FIGURE 4.1
Reduction gear with (a) stationary and (b) rotating case.

shown that the driving shaft may become the driven one and vice versa. Such a reduction gear is symmetrical with respect to its force properties.

If the reduction gear considered here is rotated at an angular velocity, ω_0, then the force relationships do not change, that is, this device can perform the functions of an open symmetrical differential. If one of the wheels in the driving axle with an open differential finds itself under poor road conditions and its slippage starts increasing, then torque T' and the relative angular velocity of the shaft (i.e., the velocity of the wheel with the higher slippage) are of opposite directions, whereas at the other shaft (i.e., the wheel) the torque T'' and the relative angular velocity are in the same direction; here $T'' > T'$. This means that, as a result of the increased friction in the mechanism, a higher torque is generated on the wheel with better gripping conditions, while the torque at the other wheel, with poorer gripping conditions decreases accordingly.

This gives rise to the obvious question: whether the use of limited slip differentials with intentionally augmented friction is not detrimental to the mechanical efficiency of the vehicle. Designate the power supplied to the case of the limited slip differential by P_0 and the powers at its output by P'' and P' (see Figure 4.1b). Then the efficiency that reflects the power losses is written as

$$\eta_n = \frac{P'' + P'}{P_0} \tag{4.2}$$

where

$$P'' = T''\omega'' = T''(\omega_0 - \omega_{rel})$$
$$P' = T'\omega' = T'(\omega_0 + \omega_{rel})$$
$$P_0 = T_0\omega_0 = (T'' + T')\omega_0 = T'(1 + 1/\eta_d)\omega_0$$

where ω_{rel} is the relative angular velocity of the case with each of the output shafts. Estimate the value of η_n when the axle makes a turn. Upon substitution of formula (2.15), expression (4.2) takes the form:

$$\eta_n = 1 - \frac{t_B}{2R_t}\frac{1 - \eta_d}{1 + \eta_d} \tag{4.3}$$

This shows that efficiency η_n that reflects the loss of power as it is transmitted from the input to the output links is, unlike η_d, a variable quantity and a function of turning radius R_t. The analysis of formula (4.3) shows that η_n is rather high even at low η_d. This means that power losses in the limited slip differential are negligible. This is so because, in spite of

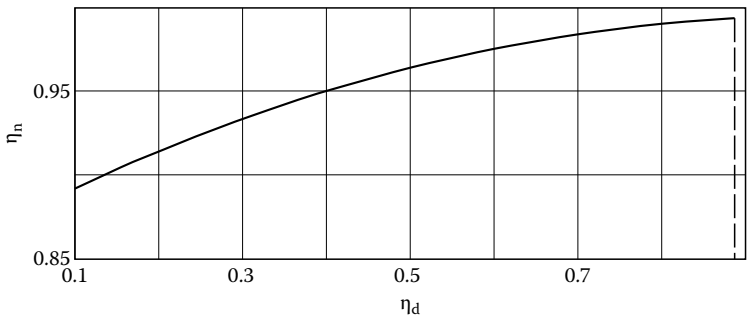


FIGURE 4.2
Efficiency η_n as a function of efficiency η_d of the differential.

the significant internal friction in the differential, the velocities of the relative motions of its components are small. It is quite obvious that low values of η_d need not be an obstacle to the use of limited slip differentials. Figure 4.2 is a plot of formula (4.3) for the driving axle with a wheel track $t_B = 1.9$ m when moving in a circle with radius $R_t = 7.5$ m.

The effect of internal friction torque T_r on the locking properties of the differential that manifest in the redistribution of torques between the out shafts is now clarified. The balance of torques acting on the differential as on a three-link mechanism is written as

$$T'' + T' = T_0; \quad T'' - T' = T_r \tag{4.4}$$

whence the torques at the output shafts are

$$\begin{aligned} T'' &= 0.5(T_0 + T_r) \\ T' &= 0.5(T_0 - T_r) \end{aligned} \tag{4.5}$$

The ratio of torques (of the higher to the lower) at the output shafts of limited slip differentials in their relative rotation is known as the locking coefficient or the torque bias:

$$K_d = \frac{T''}{T'} = \frac{T_0 + T_r}{T_0 - T_r} \tag{4.6}$$

Torques T', T'', and T_r are not only interrelated but each one separately is a function of the tractive load and of the efficiency of the differential:

$$\begin{aligned} T_r &= T'(1 - \eta_d)/\eta_d \\ T_0 &= T'(1 + \eta_d)/\eta_d \end{aligned} \tag{4.7}$$

The elimination of torque T' from formulae (4.7) results in the expression:

$$T_r = T_0(1 - \eta_d)/(1 + \eta_d) \tag{4.8}$$

The substitution of (4.8) into Equations 4.5 yields

$$\begin{aligned} T'' &= T_0/(1+\eta_d) \\ T' &= T_0\eta_d/(1+\eta_d) \end{aligned} \tag{4.9}$$

and, upon substitution of (4.1) and (4.6), torques T'' and T' can be expressed in terms of the torque bias K_d:

$$\begin{aligned} T'' &= T_0K_d/(1+K_d) \\ T' &= T_0/(1+K_d) \end{aligned} \tag{4.10}$$

The assessment of the locking performance of the mechanism by means of the factor K_d is rather obvious for use in computational studies and is convenient in experimental studies both under laboratory and proving ground conditions.

In certain cases (see Chapter 5), it is convenient to assess the locking properties of mechanisms using another indicator—the relative friction torque:

$$K_r = \frac{T_r}{T_0} = \frac{T'' - T'}{T_0} \tag{4.11}$$

The factors K_d and K_r are interrelated as

$$\begin{aligned} K_r &= \frac{K_d - 1}{K_d + 1} \\ K_d &= \frac{1 + K_r}{1 - K_r} \end{aligned} \tag{4.12}$$

As shall be shown later in this chapter, in the majority of cases the relative friction torque, K_r, can be represented to a sufficient approximation as the product of some generalized sliding (dynamic) friction coefficient, μ, that represents friction between all the components of the differential and the geometric parameter, P, that reflects the specifics of the mechanism's design, that is,

$$K_r = \mu P \tag{4.13}$$

Upon substitution of formula (4.13) the torque bias is expressed as

$$K_d = \frac{1 + \mu P}{1 - \mu P} \tag{4.14}$$

Parameter P is also a singular indicator of the locking properties of the differential. Formula (4.14) is plotted in Figure 4.3.

Consider certain features of the operation of limited slip differentials. Many mechanisms are initially locked when subjected to torque T_0. When such an axle moves in a straight line, the angular velocities of the output shafts as well as the torques are the same (see point 1 in Figure 4.4, the gripping conditions of the wheels are assumed to be the same).

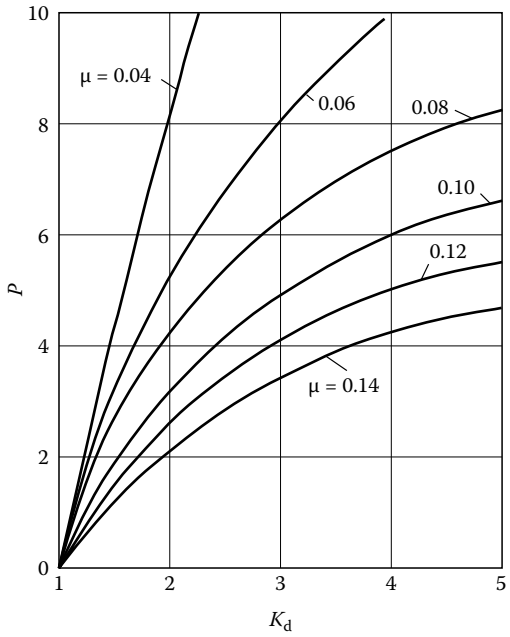


FIGURE 4.3
Plot of K_d as a function of P and μ.

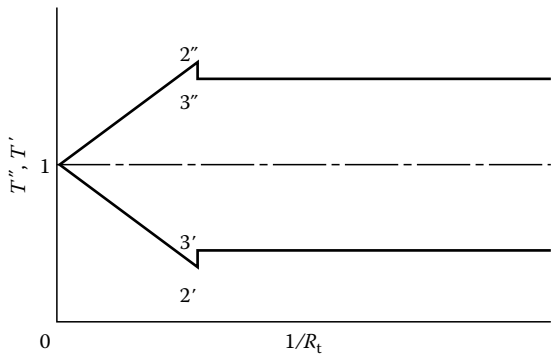


FIGURE 4.4
Torques at the output shaft of a limited slip differential when the axle makes a turn.

When starting a turn, when turning radius R_t decreases and the path curvature $1/R_t$ increases, torque T'' at the inner output shaft increases and at the outer T' decreases. During this period the differential is still locked, which causes the appearance of kinematic discrepancy (see Chapter 3) between the theoretical velocities of the axle's wheels. This changes the wheel slippage, $s''_\delta > s'_\delta$, and the torques, $T'' > T'$. This is observed up to values of R_t corresponding to points 2″ and 2′ in Figure 4.4. The ordinates of these two points give the values of torques T'' and T' at the instant of actuation of the differential, that is, at the instant of the appearance of relative rotation of the output shafts. The ratio of these torques is represented by the so-called static locking coefficient, K_{dp}, determined by the static friction torque, T_{rs}, and static friction coefficient, μ_s:

$$K_{dp} = \frac{T''_{(2)}}{T'_{(2)}} = \frac{T_0 + T_{rs}}{T_0 - T_{rs}} = \frac{1 + \mu_s P}{1 - \mu_s P} \tag{4.15}$$

Since the sliding (dynamic) friction coefficient, μ, is somewhat smaller than μ_s, after the differential is actuated, torques T'' and T' (points 3″ and 3′ in Figure 4.4) change. The ratio of torques in these points is equal to the value of the torque bias K_d from formulae (4.6) and (4.14) that is determined at relative rotations of the differential's output shafts. Further increase in R_t does not affect the relative rotation of the differential's output shaft (i.e., the differential effect is retained; torques T'' and T' do not change if the tractive load does not change, see Figure 4.4). The actual curves are oscillatory because of the unstable value of the friction factor. When the tractive load changes, that is, at a different value of torque T_0, point 1 on the ordinate axis will take another position, which will also cause a change in the positions of points 2′ and 2″, 3′ and 3″.

One of the major questions in developing a new design of a limited slip differential is that of selecting the values of torque bias. It can be easily shown that increasing K_d improves the utilization of the adhesive weight of the driving axle and the vehicle's mobility. However, this causes the properties of the interwheel limited slip differential to come close to those of a positively engaged drive, which is detrimental to the vehicle's turnability. The methodology of selecting optimum locking coefficients is analyzed in Chapter 6. Here only certain principles needed for understanding the problem are presented.

The conditions of a vehicle's motion are defined by combinations of potentially possible gripping factors of the left, μ'_{px}, and right, μ''_{px}, wheels of the driving axle. Assume that the gripping factor of each of the wheels can range from 0.1 (ice) to 0.7 (dry asphalt). In the orthogonal coordinate system (see Figure 4.5), the domain ABCD of possible values is limited by the straight lines $\mu'_{px} = 0.1$ and $\mu''_{px} = 0.7$, $\mu''_{px} = 0.1$ and $\mu'_{px} = 0.7$. At $K_d = 7$ the wheel can develop its circumferential force at all the possible combinations of its gripping conditions with the surface.

At lower values of K_d, the domain within which the gripping of the wheel can be fully utilized decreases. Consider the case of $K_d = 4$. Draw lines $\mu''_{px} = 4\mu'_{px}$ and $\mu''_{px} = \mu'_{px}/4$. The resulting figure AEFCGH reflects the domain of conditions within which complete utilizing of gripping is possible. The area of the above figure comprises 93.8% of the area of the square ABCD. This means that, at equally probable combination of gripping conditions of the wheels with the surface and $K_d = 4$, the probability PB that the wheels will utilize the gripping is 93.8%:

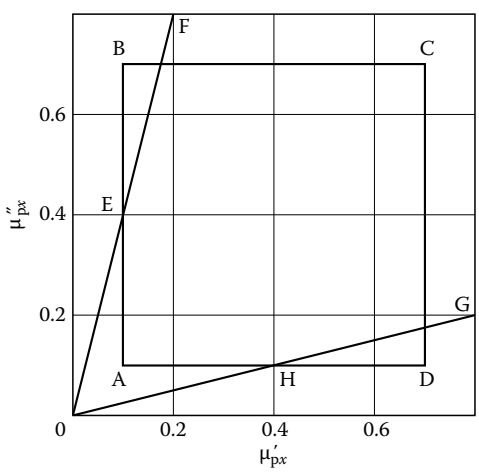


FIGURE 4.5
Diagram for determining the probability of utilization of gripping by an axle's wheels.

$$\mathrm{PB}_{K_\mathrm{d}=4} = \frac{A_{\mathrm{AEFCGH}}}{A_{\mathrm{ABCD}}} = 1 - \frac{1}{K_\mathrm{d}} \left(\frac{\mu_{px}^{\max} - K_\mathrm{d}\mu_{px}^{\min}}{\mu_{px}^{\max} - \mu_{px}^{\min}} \right)^2$$
$$= 1 - \frac{1}{4} \left(\frac{0.7 - (4)(0.1)}{0.7 - 0.1} \right)^2 = 0.938 \tag{4.16}$$

In 6.2% of combinations of gripping conditions, having $K_\mathrm{d} = 4$ is insufficient for both wheels of the axle to develop circumferential forces sufficient for ensuring mobility of the vehicle under these conditions. It can be shown similarly that at $K_\mathrm{d} = 3$, the probability of complete utilization of the gripping conditions is 85%:

$$\mathrm{PB}_{K_\mathrm{d}=3} = 1 - \frac{1}{3} \left(\frac{0.7 - (3)(0.1)}{0.7 - 0.1} \right)^2 = 0.85 \tag{4.17}$$

Based on the above data and experience in designing and operating limited slip differentials, it may be assumed that the sensible values of K_d lie in the range of 2.5–4. Usually these values of K_d provide sufficient mobility and satisfactory turnability of vehicles.

Limited slip differentials can be subdivided by their design versions and operating principles into mechanisms:

1. With constant locking coefficient (torque bias)
2. With variable locking coefficient (e.g., sensitive either to the input torque, T_0, or to the relative velocity of the output shafts)

The first group includes the largest number of mechanisms. These are differentials with disk-type friction clutches, worm-gear, and cam mechanisms. The second group includes mechanisms with a locking performance provided by disk-type friction clutches and also differentials with hydraulic resistance to the relative rotation of components. Typical layouts and designs are analyzed in the subsequent sections.

4.2 Disk Differentials without Additional Lockers

An essential feature of the different designs of limited slip differentials with disk friction clutches consists in the method of producing forces that compress the clutch. Figure 4.6a shows a differential in which the disk clutches are compressed solely by axial forces that arise in the meshings of the side gears and pinions when a torque is applied to the mechanism.

The driving disks are splined to the differential's case, whereas the driven disks are similarly linked to the side gears. The friction torque in the clutches, produced by the axial forces in the meshings of bevel gears, causes a partial locking of the case and the side gears that are connected to the output shafts and then to the vehicle's wheels. This differential does not have any additional locking devices that would compress the disk clutches.

To determine the locking coefficient (torque bias) of such a differential, consider free-body diagrams of its principal elements; case 1 with the carrier, one pinion 3 (equivalent to all the pinions of the differential) and two side gears 2. These elements are shown in

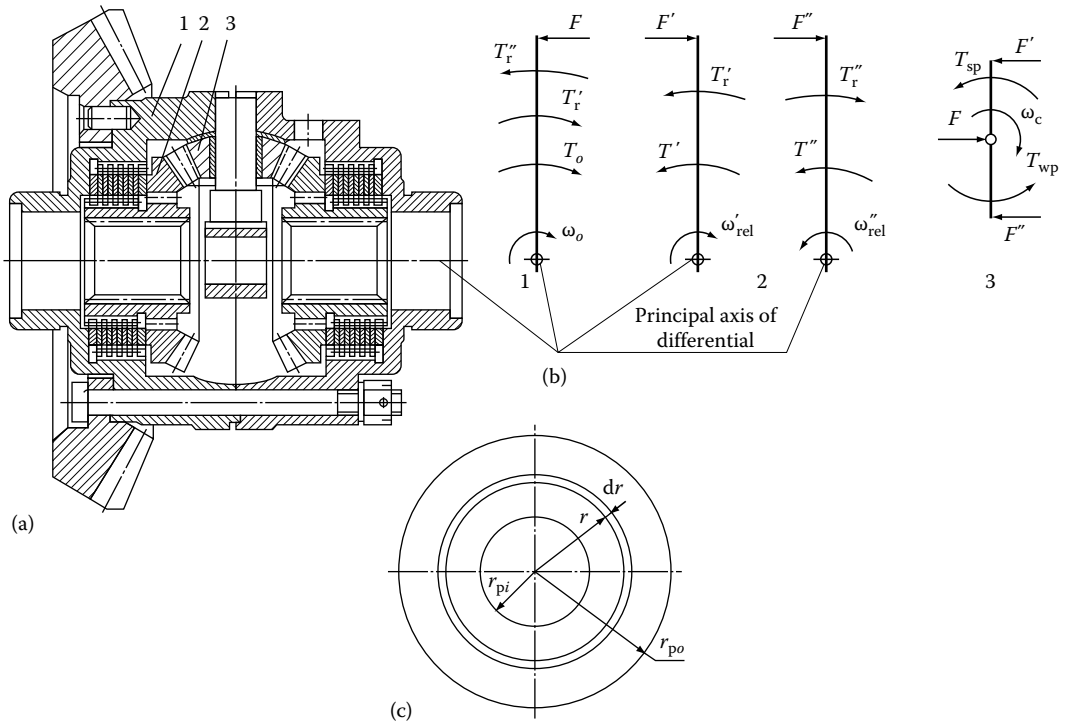


FIGURE 4.6
Design and free-body diagrams of a limited slip differential without additional lockers.

Figure 4.6b in the form of rotating rods. The notation used in this figure is as follows: F is the total circumferential force exerted by the pinions on the differential's carrier; F'' and F' are the total circumferential forces in the pinion meshings, respectively with the lagging and advancing side gears; T_0 is the torque fed to the mechanism's case; T'' and T' are the torques at the respective side gears; T''_r and T'_r are the friction torques in the disk clutches located respectively on the side of the lagging and advancing side gears; T_{wp} and T_{sp} are the friction torques, respectively of the pinions at the differential's case and of pinions at the carrier-pins; ω_0 is the angular velocity of the differential's case; ω''_{rel} and ω'_{rel} are the relative angular velocities of the lagging and advancing side gears and the case ($\omega''_{rel} = \omega'_{rel}$); ω_c is the relative angular velocity of the pinions and of the carrier pins.

Forces F'' and F' are found from the equilibrium of pinions 3 from Figure 4.6 in the following manner:

$$F' = \frac{F}{2} - \frac{T_{wp} + T_{sp}}{2r_c}$$
$$F'' = \frac{F}{2} + \frac{T_{wp} + T_{sp}}{2r_c} \tag{4.18}$$

where

$r_c = \dfrac{mz_c}{2}$ is the medium pitch radius of the pinion

m is the midsection module

z_c is the pinion's tooth number

Torques T_{wp} and T_{sp} are proportional to circumferential force F. Define these friction torques. The elementary friction torque dT_{wp} is (see Figure 4.6c)

$$dT_{wp} = 2\pi\mu p r^2 dr \tag{4.19}$$

where p is the pressure at the contact between the pinion and the case (it is assumed that p is constant):

$$p = \frac{Q_s}{\pi\left(r_{po}^2 - r_{pi}^2\right)} \tag{4.20}$$

$Q_s = F\tan\alpha_w \sin\delta_c$ is the axial force exerted by the side gears on the pinions; α_w is the pressure angle and δ_c is the pinion pitch angle. Integration of (4.19) yields:

$$\begin{aligned} T_{wp} &= \frac{2}{3}\pi\mu p\left(r_{po}^3 - r_{pi}^3\right) \\ &= \frac{2}{3}\pi Q_s \frac{r_{po}^3 - r_{pi}^3}{r_{po}^2 - r_{pi}^2} = \pi Q_s r_{wp} \end{aligned} \tag{4.21}$$

where $r_{wp} = \frac{2}{3}\frac{r_{po}^3 - r_{pi}^3}{r_{po}^2 - r_{pi}^2}$ is the friction radius of the pinion at the case (or the friction radius of the thrust washer if such is placed between the pinion and the case). Note that at $r_{po}/r_{pi} \geq 0.6$ the radius r_{wp} can be determined from the expression

$$r_{wp} = 0.5(r_{po} + r_{pi}) \tag{4.22}$$

The error of this approximation does not exceed 2%.

The friction torque between the pinions and the carrier pins is obtained from the formula

$$T_{sp} = \mu F r_{sp} \tag{4.23}$$

where $r_{sp} = 0.5d_{pi}$ is the radius of the carrier's pin. The geometric parameters from formulae (4.21) and (4.23) are shown graphically in Figures 2.61 and 4.6c. Note that it is permissible to assume in calculating the torque bias that the inner diameter of the pinion's washer and its bushing are the same and are given by diameter d_{pi} in Figure 2.61 (Figure 4.6c shows the radius r_{pi}). This assumption was made above in defining radii r_{wp} and r_{sp}.

Using expressions for T_{wp} and T_{sp} obtained above, the circumferential forces from (4.18) are represented as:

$$\begin{aligned} F' &= 0.5F(1 - \mu B) \\ F'' &= 0.5F(1 + \mu B) \end{aligned} \tag{4.24}$$

where B, the dimensionless geometric parameter of the differential, is given by the formula:

$$B = \frac{r_{wp}\tan\alpha_w \sin\delta_c + r_{sp}}{r_c} \tag{4.25}$$

Torques T'' and T' are determined from the equilibrium of side gears 2 from Figure 4.6:

$$\begin{aligned} T' &= F' r_g - T'_r \\ T'' &= F'' r_g + T''_r \end{aligned} \tag{4.26}$$

where

$r_g = \dfrac{m z_g}{2}$ is the medium pitch radius of the side gear
m is the midsection module
z_g is the number of gear teeth

Friction torques T'_r and T''_r at the disk clutches are equal to:

$$\begin{aligned} T'_r &= \mu Q'_a r_M i_M = \mu F' \tan\alpha_w \cos\delta_c r_M i_M \\ T''_r &= \mu Q''_a r_M i_M = \mu F'' \tan\alpha_w \cos\delta_c r_M i_M \end{aligned} \tag{4.27}$$

where

Q'_a and Q''_a are axial forces exerted by the pinions on the side gears (see Figure 2.61)
r_M is the friction radius of the driving and driven disks determined from the outer and inner diameters of the disks from Figure 4.6a
i_M is the number of friction pairs in one disk clutch

The number of friction pairs in one of the clutches in Figure 4.6a is $i_M = 11$. Note that the number of friction pairs is not equal to the number of disks (10), and the number i_M of friction pairs was calculated by including couples such as the side gear—driving disk and driven disk—differential case.

Introduce still another dimensionless parameter of the differential

$$A = \frac{r_M i_M \tan\alpha_w \cos\delta_c}{r_g} \tag{4.28}$$

Then friction torques from formula (4.27) take the form:

$$\begin{aligned} T'_r &= \mu F' r_g A \\ T''_r &= \mu F'' r_g A \end{aligned} \tag{4.29}$$

Upon substitution of formulae (4.24) and (4.29), the torques T' and T'' at the side gears from formula (4.26) will take the final form:

$$\begin{aligned} T' &= \frac{F}{2} r_g (1 - \mu A)(1 - \mu B) \\ T'' &= \frac{F}{2} r_g (1 + \mu A)(1 + \mu B) \end{aligned} \tag{4.30}$$

Based on the definition of the locking factor expressed by formula (4.6) it is possible, upon substitution of formula (4.30), to compile a mathematical expression for calculating the torque bias of the differential from Figure 4.6:

$$K_d = \frac{(1 + \mu A)(1 + \mu B)}{(1 - \mu A)(1 - \mu B)} \tag{4.31}$$

The first cofactor here reflects the effect on the value of K_d of the friction in the disk clutches, whereas the second cofactor represents the friction between the pinions and the carrier and the pinions with the thrust washers (case). The structure of formula (4.31) is identical to that of (4.14).

It is seen from formula (4.31) that the torque bias factor is independent of the load on the differential and is constant for a given value of μ. In fact, friction coefficient μ is not constant, which causes some variation in the numerical values of K_d. These questions are discussed in Chapter 8 in which are presented methods and results of experimental studies of limited slip differentials.

Note that substitution of the static friction factor μ_s instead of the dynamic factor μ into formula (4.31) allows obtaining an expression for determining the static locking coefficient K_{dp} defined by formula (4.15).

Formula (4.31) is convenient because it allows to ensure, the required value of the locking coefficient already at the design stage, by modifying the differential's geometric parameters contained in formulae (4.25) and (4.28) for dimensionless parameters A and B. For example, locking coefficient K_d of the differential shown in Figure 4.7 was increased from 1.43 to 2.32 by changing the pressure angle α_w from 20° to 45° while holding the remaining parameters contained in formulae (4.25) and (4.28) unchanged (the calculations were performed at $\mu = 0.1$).

It is of interest to note that expression (4.31) can be used for calculating the locking factors of open bevel-gear differentials by assuming that $i_M = 1$. As an illustration, Table 4.1 lists the values of A and B and the computed values of K_d of open bevel-gear interwheel differentials of four trucks.

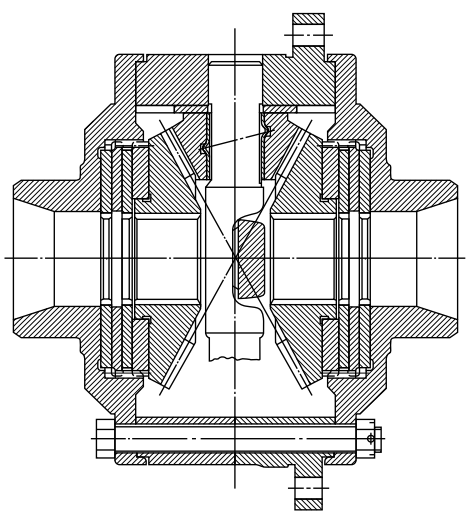


FIGURE 4.7
A limited slip differential. (From Smirnov, V. I. et al., *Vestnik XPI*, 3, 55, 1976.)

TABLE 4.1

Open Differentials: Parameters and Torque Bias

Vehicle	Parameter A	Parameter B	Torque Bias K_d
GAZ-53A	0.630	0.300	1.20
ZIL-130	0.780	0.320	1.25
KrAZ-219	0.506	0.245	1.16
MAZ-500	0.720	0.340	1.24

It is seen that open differentials exhibit certain locking properties ensuring a 16%–25% redistribution of torques between their output shafts. It should be emphasized at the same time that as the vehicle accumulates more mileage and the friction surfaces become worn, the value of friction factor μ decreases, and K_d tends to 1.

It is possible to assume for practical calculations that $P_1 = A + B$ and use the approximate expression that follows from (4.31):

$$K_d = \frac{1 + \mu P_1}{1 - \mu P_1} \tag{4.32}$$

Consider still another method of calculating K_d that does not require compiling equilibrium equations for the differential's components and yields results with satisfactory accuracy. The entire friction in the limited slip differential is divided into two groups: the primary and the secondary. Primary friction consists of friction in the clutches and the secondary friction, between the pinions at the carrier pins and the case. It is quite evident that the primary friction in the clutches exerts the primary effect on the numerical values of K_d. The method suggested here consists of a computational formula for the locking factor in the form:

$$K_d = K_p \frac{T_0 + T_{rp}}{T_0 - T_{rp}} \tag{4.33}$$

where

T_{rp} is the torque of the primary friction in the differential's clutches

K_p is a correction factor accounting for the secondary friction in the differential and calculated from the expression

$$K_p = \frac{1 + \mu B}{1 - \mu B}, \tag{4.34}$$

where torque T_{rp} of primary friction in the two clutches is:

$$T_{rp} = 2\,\mu Q_a\, r_M i_M \tag{4.35}$$

Formulae (4.33) through (4.35) were used for calculating K_p for open interwheel differentials of three trucks of different type and load rating. The results are listed in Table 4.2

TABLE 4.2

Correction Factor

Friction Coefficient, μ	Correction Factor K_p for Vehicle Differentials			Single Correction Factor, K_{pu}
	MTZ-100	MoAZ-542	ZIL-130	
0.06	1.09	1.11	1.10	1.10
0.08	1.13	1.15	1.14	1.14
0.10	1.16	1.19	1.17	1.17
0.12	1.19	1.23	1.20	1.20

whence it can be seen that the numerical values of K_p do not differ much from one another.

This allows assuming a single correction factor K_{pu} for a given value of μ that can be used for calculating K_d of the differentials of all vehicles. With reference to the above, formula (4.33) will take the form:

$$K_d = K_{pu}\frac{T_0 + T_{rp}}{T_0 - T_{rp}} \tag{4.36}$$

Calculations show that the values of locking factors from formulae (4.31) and (4.36) are virtually identical.

Formulae (4.35) and (4.36) will be suitable also for other types of differentials that are discussed in this chapter. It must be remembered that in this case T_{rp} is determined not only by the forces of the bevel gears, but also by additional devices that generate axial forces in the differentials. Consider details in the coming section.

4.3 Disk Differentials with Cam Lockers

Differentials with cam lockers employ cam clutches that transmit torque from the side gears to the output shafts. The axial forces arising when transmitting torque to the sloping edges of the cams are used for compressing the friction clutches. Consider the following three design layouts of a differential with a cam locker. Layouts I and II differ by the location of the cams at the faces of the side gears (see Figures 4.8 and 4.10a).

In both these layouts, the case elements (spider and differential's halves) take up axial forces arising in the meshings of the cam clutches. As opposed to these, in layout III (see Figure 4.11a) the axial forces arising in the cam clutches are not applied to elements of the differential's casing.

Consider a differential designed according to layout I (Figure 4.8a). The torques of side gears 3 are transmitted to thrust bushings 4 through trapezoidal end cams. The axial forces of the cams applied to the pressure disks compress the friction clutches.

The formula for determining the locking coefficient is derived by analyzing the diagram of forces and torques acting on the mechanism's links (Figure 4.9).

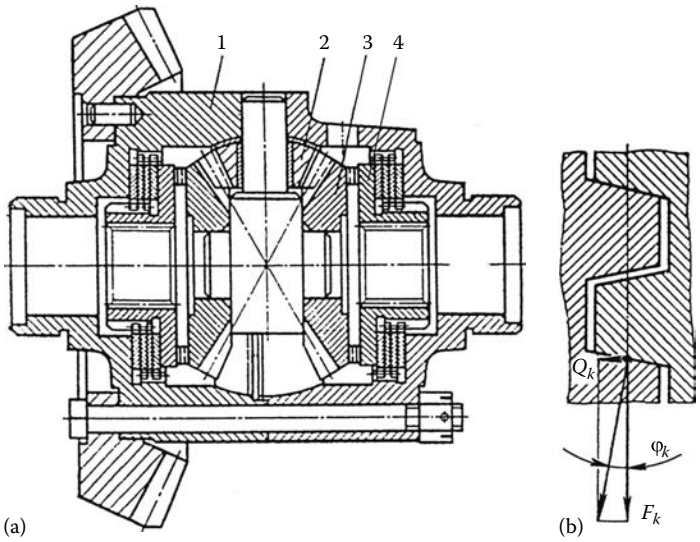


FIGURE 4.8
Differential with cam locker (layout I): (a) longitudinal section through the differential; (b) diagram of forces in the cams.

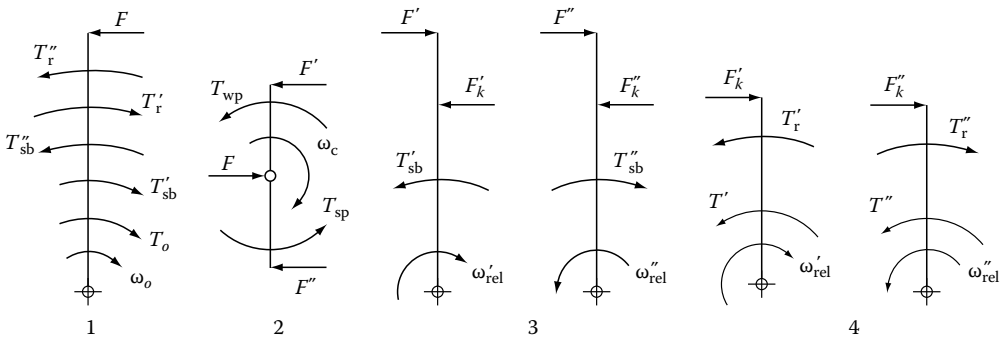


FIGURE 4.9
Free-body diagram of the principal elements of the differential from Figure 4.8: 1, case; 2, pinions; 3, side gears; 4, thrust bushings.

The value of the axial forces Q_k is determined by the angle φ_k of the slope of the working edges of the cams (see Figure 4.8b). The axial forces of the cams applied to the side gears are opposite to the axial forces of the gear meshing and exceed the latter. For this reason, the resultant axial forces press the side gears to the limiting ends of the spider.

The free-body diagrams in Figure 4.9 can be used for compiling the equilibrium equations of the side gears:

$$\begin{aligned} F' r_g - F'_k r_k - T'_{sb} &= 0 \\ F'' r_g - F''_k r_k - T''_{sb} &= 0 \end{aligned} \tag{4.37}$$

where

F'_k and F''_k are the circumferential forces of the cams of the advancing and lagging gears (see also Figure 4.8b)

T'_{sb} and T''_{sb} are the torques of friction at the spider of the inner edges, respectively, of the advancing and lagging side gears

r_k is the medium radius of the end cams

r_g is the radius given by formula (4.26)

Torques T'_{sb} and T''_{sb} determined by the difference between the axial forces of the cams and the axial forces in the meshings of side gears with pinions, can be represented as:

$$\begin{aligned} T'_{sb} &= \mu r_{kp}\left(F'_k \tan\varphi_k - F' \tan\alpha_w \cos\delta_c\right) \\ T''_{sb} &= \mu r_{kp}\left(F''_k \tan\varphi_k - F'' \tan\alpha_w \cos\delta_c\right) \end{aligned} \tag{4.38}$$

where r_{kp} is the radius of friction between the inner end of the side gear and the spider.

Substitution of (4.37) into (4.38) yields the circumferential forces at the cams:

$$\begin{aligned} F'_k &= F' \frac{r_g(1+\mu D)}{r_k(1+\mu C)} \\ F''_k &= F'' \frac{r_g(1-\mu D)}{r_k(1-\mu C)} \end{aligned} \tag{4.39}$$

where $C = r_{kp}\tan\varphi_k/r_k$ and $D = r_{kp}\tan\alpha_w\cos\delta_c/r_g$ are dimensionless geometric parameters.

The diagram of forces and torques acting on the pinions of the differential under consideration (see item 2 in Figure 4.9) is the same as in the previously analyzed mechanism (see Figure 4.6b). Hence, expressions (4.24) are valid also for the differential considered here from Figure 4.8. Substitution of (4.24) allows transforming formula (4.39) to the form:

$$\begin{aligned} F'_k &= \frac{F r_g(1-\mu B)(1+\mu D)}{2r_k(1+\mu C)} \\ F''_k &= \frac{F r_g(1+\mu B)(1-\mu D)}{2r_k(1-\mu C)} \end{aligned} \tag{4.40}$$

The equilibrium equation of thrust bushings 4 from Figure 4.9 can be used for finding the torques at the output shafts of the differential:

$$\begin{aligned} T' &= F'_k r_k - T'_{sb} = F'_k r_k(1-\mu E) \\ T'' &= F''_k r_k - T''_{sb} = F''_k r_k(1+\mu E) \end{aligned} \tag{4.41}$$

where $E = r_M i_M \tan\varphi_k/r_k$.

Substitution of forces F'_k and F''_k from (4.40) into formulae (4.41) yields

$$\begin{aligned} T' &= \frac{Fr_g(1-\mu B)(1-\mu E)(1+\mu D)}{2(1+\mu C)} \\ T'' &= \frac{Fr_g(1+\mu B)(1+\mu E)(1-\mu D)}{2(1-\mu C)} \end{aligned} \tag{4.42}$$

The locking coefficient is obtained by dividing T'' by T':

$$K_d = \frac{1+\mu B}{1-\mu B}\frac{1+\mu E}{1-\mu E}\frac{1+\mu C}{1-\mu C}\frac{1-\mu D}{1+\mu D} \tag{4.43}$$

The first cofactor reflects the effect on K_d of friction in the pinions, the second in the clutches, and the third in the friction of the faces of side gears at the spider. The fourth cofactor represents the reduction in the force of friction of the faces of side gears as a result of axial forces in the gear meshing. If the third and fourth cofactors are neglected, and if terms containing μ^2 in the numerator and denominator of the fraction obtained by multiplying the first cofactor by the second are also dropped, then an expression sufficiently accurate for practical calculations becomes

$$K_d = \frac{1+\mu P_2}{1-\mu P_2} \tag{4.44}$$

where $P_2 = B + E$. The error of using formula (4.44) instead of the more exact formula (4.43) is less than 5% if $K_d \leq 7$.

In this differential, the specified locking coefficient can be obtained by adjusting the angle φ_k. It, however, has the disadvantage of a highly complicated design. The resultant of axial forces acting on side gears is directed to the pinions, which reduces the clearances in the tooth meshing when the rubbing surfaces of the spider and the faces of the hubs of the side gears wear out. The reduction of clearances in the meshings of the differential's gears has a detrimental effect on their performance.

Consider another design of a cam-type compression device of a differential the design of which follows layout II (Figure 4.10).

As in the first version, this design employs two disk clutches. Disks with external teeth are linked to the case, whereas those with inner teeth to the hubs of side gears. The disks are compressed by axial forces in the meshing of trapezoidal expansion cams of side gears 3 and intermediate bushings 4, located on the half-axle splines. The axial forces of the expansions cams and of gear meshings that act on the side gears add up; unlike the previous design version, they are directed toward the disk clutches. This means that in this case, the clearances in the mechanism's gear meshings are not decreased and there is no danger of deterioration of their performance.

Circumferential forces F'_k and F''_k in the meshings of expansion cams, shown in the free-body diagrams in Figure 4.10b, are found from the equilibrium equations of the side gears:

$$\begin{aligned} F'r_g - F'_k r_k - T'_r &= 0 \\ F''r_g - F''_k r_k + T''_r &= 0 \end{aligned} \tag{4.45}$$

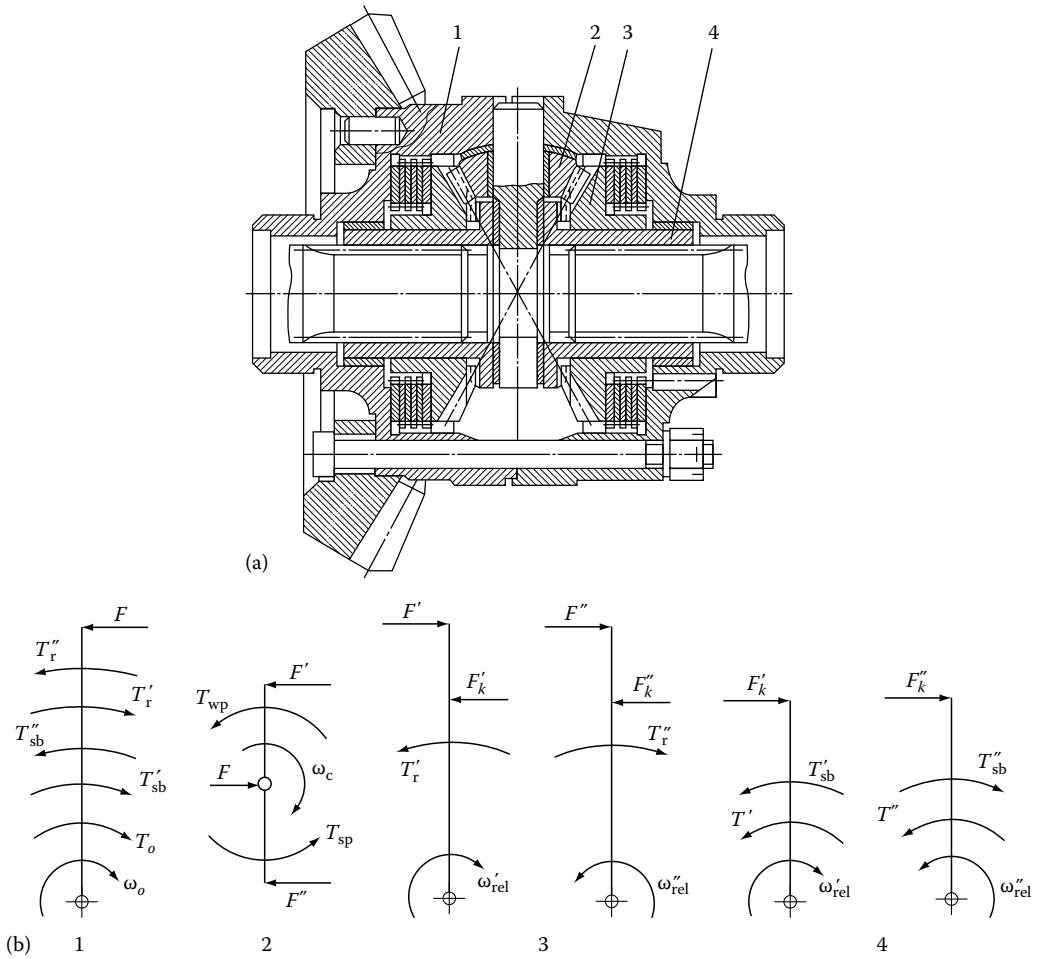


FIGURE 4.10
Differential with cam locker (layout II): (a) longitudinal section through the differential; (b) free-body diagrams of principal elements.

In Equations 4.45 the friction torques T'_r and T''_r in the disk clutches are determined by the axial forces of the cams and the axial forces in the meshings between the pinions and the side gears:

$$\begin{aligned} T'_r &= \mu r_M i_M \left(F'_k \tan\varphi_k + F' \tan\alpha_w \cos\delta_c\right) \\ T''_r &= \mu r_M i_M (F''_k \tan\varphi_k + F'' \tan\alpha_w \cos\,\delta_c) \end{aligned} \tag{4.46}$$

Substitution of formulae (4.46) and (4.24) into Equations 4.45 yields the following expressions for circumferential forces F'_k and F''_k:

$$\begin{aligned} F'_k &= \frac{F r_g (1-\mu A)(1-\mu B)}{2 r_k (1+\mu E)} \\ F''_k &= \frac{F r_g (1+\mu A)(1+\mu B)}{2 r_k (1-\mu E)} \end{aligned} \tag{4.47}$$

From the equilibrium of intermediate bushing 4 (see Figure 4.10a and b) the torques T' and T'' of the output shafts of the differential are obtained:

$$\begin{aligned} T' &= F'_k r_k - T'_{sb} = F'_k r_k (1 - \mu r_{kp} \tan \varphi_k / r_k) \\ T'' &= F''_k r_k + T''_{sb} = F''_k r_k (1 + \mu r_{kp} \tan \varphi_k / r_k) \end{aligned} \tag{4.48}$$

where T'_{sb} and T''_{sb} are the friction torques of intermediate bushings 4 and the spider. Substitution of expression (4.48) for forces F'_k and F''_k into Equation 4.47 yields:

$$\begin{aligned} T' &= \frac{F r_g (1 - \mu A)(1 - \mu B)(1 - \mu C)}{2(1 + \mu E)} \\ T'' &= \frac{F r_g (1 + \mu A)(1 + \mu B)(1 + \mu C)}{2(1 - \mu E)} \end{aligned} \tag{4.49}$$

Then the locking coefficient will be given by the expression:

$$K_d = \frac{1 + \mu A}{1 - \mu A} \frac{1 + \mu B}{1 - \mu B} \frac{1 + \mu C}{1 - \mu C} \frac{1 + \mu E}{1 - \mu E} \tag{4.50}$$

If the first and second cofactors in formula (4.50) are multiplied in pairs and terms containing μ^2 in the resulting fractions are neglected, then the expression for K_d will become:

$$K_d = \frac{1 + \mu P_1}{1 - \mu P_1} \frac{1 + \mu P_3}{1 - \mu P_3} \tag{4.51}$$

where $P_1 = A + B$ was introduced in Section 4.2, whereas $P_3 = C + E$. Formula (4.51) yields values of K_d that are on the high side as compared with the more rigorous formula (4.50). This difference increases with the locking coefficient (for $K_d \leq 7$ it does not exceed 5%).

The shortcomings of the differential designed along layout II consist of certain technical difficulties in manufacturing trapezoidal end cams. The smallness of the mechanism makes its assembly difficult. The small bearing surface of the intermediate bushing in the bushing-spider friction couple may in such cases cause excessive pressure.

In differentials with cam lockers that follow design III (Figure 4.11a) there is no friction between components and the face of the spider.

The computational diagram of forces and torques acting on the components of this differential is shown in Figure 4.11b. Circumferential forces F' and F'' in the gear meshings are given by Equations 4.24. From the equilibrium of thrust bushings 4 linked to the output shafts of the differential, one can have

$$\begin{aligned} T' &= F'_k r_k - T'_r - T'_{sb} \\ T'' &= F''_k r_k + T''_r + T''_{sb} \end{aligned} \tag{4.52}$$

where T'_{sb} and T''_{sb} are the friction torque of the thrust flanges of bushings 4 and the differential's case.

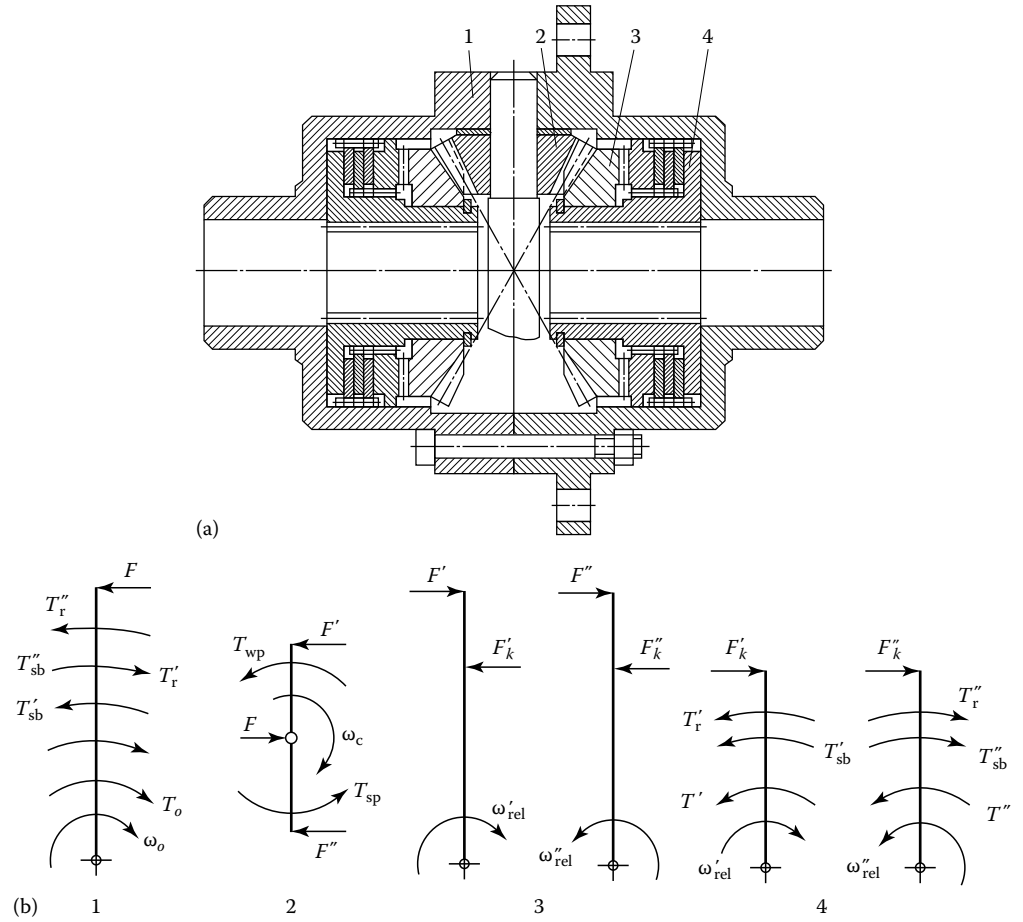


FIGURE 4.11
Differential with cam locker (layout III): (a) longitudinal section through the differential; (b) free-body diagrams of principal elements.

The friction clutches in this differential are compressed solely by axial forces that arise in the cams of side gears 3 and pressure disks. Hence the friction torques in these clutches are:

$$\begin{aligned} T'_r &= \mu F'_k r_M i_M \tan\varphi_k \\ T''_r &= \mu F''_k r_M i_M \tan\varphi_k \end{aligned} \tag{4.53}$$

Circumferential forces F'_k and F''_k of the cams can be expressed in terms of circumferential forces F' and F'' exerted on the side gears by the pinions, using diagrams 3 from Figure 4.11b. Then the friction torques from (4.53) will be written as:

$$\begin{aligned} T'_r &= \mu F'_k r_g r_M i_M \tan\varphi_k / r_k \\ T''_r &= \mu F''_k r_g r_M i_M \tan\varphi_k / r_k \end{aligned} \tag{4.54}$$

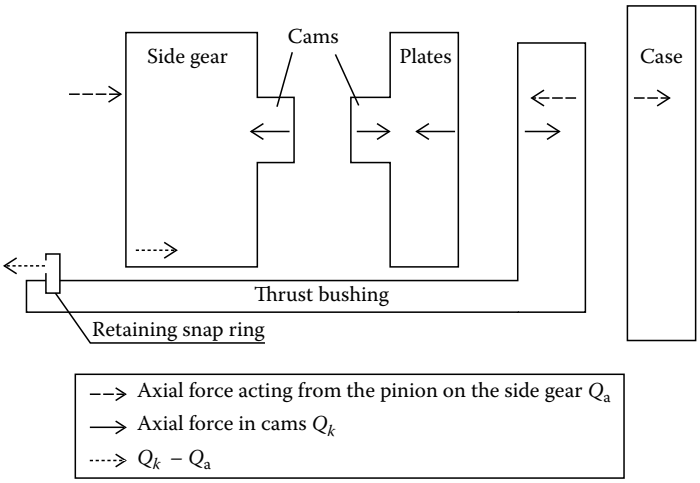


FIGURE 4.12
Schematic diagram of axial forces.

Thrust bushings 4 are pressed to the differential case by axial forces arising in the meshings between the pinions and side gears 3. This is seen from Figure 4.12.

Then friction torques T'_{sb} and T''_{sb} from formulae (4.52) will be written as:

$$\begin{aligned} T'_{sb} &= \mu F' r_{kp} \tan\alpha_w \cos\delta_c \\ T''_{sb} &= \mu F'' r_{kp} \tan\alpha_w \cos\ \delta_c \end{aligned} \tag{4.55}$$

where r_{kp} is the mean radius of friction between the thrust flange of bushings 4 and the case. Substitution of expressions (4.54) and (4.55) into (4.52) while also employing the previously introduced notation B, D, and E, allows defining the torques at the output shafts of the differential:

$$\begin{aligned} T' &= 0.5 F r_g [1 - \mu(D + E)](1 - \mu B) \\ T'' &= 0.5 F r_g [1 + \mu(D + E)](1 + \mu B) \end{aligned} \tag{4.56}$$

whence, the torque bias factor of the differential is obtained by dividing T'' by T':

$$K_d = \frac{1 + \mu(D + E)}{1 - \mu(D + E)} \frac{1 + \mu B}{1 - \mu B} \tag{4.57}$$

Note that K_d of this differential can be calculated with sufficient accuracy also from formula (4.44). If the values of the calculated locking coefficient lie within the range of from 3 to 7, then the values of K_d calculated from formula (4.44) deviate from those obtained from formula (4.57) by 4.5%–1%.

4.4 Disk Differentials with V-Lockers

Differentials with lockers consisting of V-shaped grooves that serve as the location of the pinion pins in the case are in extensive use. There are two design versions of such a differential. In version I the axial forces compress disk clutches by way of pressure cups located on the splines of the side-gear hubs. In version II the axial forces compress the disk clutches by means of pressure cups that are parts of the carrier, that is, are linked to the differential's case. Figure 4.13 shows a limited slip differential constructed according to version I.

Separate floating pinion pins enter V-shaped grooves in the differential's case. Two flats that form an obtuse angle $2\varphi_k$ are provided at the ends of the pins. The surfaces of grooves in the case form the same angle (here the vertices of the angles in adjoining grooves in the case are directed in opposite directions). Torque from the differential's case is transmitted to the two pinion pins. This produces circumferential forces F_0 and axial forces Q_0 on the inclined surfaces of the grooves. The axial forces are transmitted by the cylindrical shoulders of the pinions to the ends of pressure cups and compress the disk clutches (see force Q_{gb} in Figure 4.13). In addition, the pressure cups are subjected to axial forces arising in gear meshings (force Q_a). An expression for calculating the locking coefficient of this differential can be derived using free-body diagrams of its principal elements.

At the same time, a very large number of tests performed with version I differentials provided an insight into a very specific feature of this conceptual design. It turned out the locking coefficient takes different values upon left and right turns of the driving axle with such a differential (i.e., upon lagging of the left or right output shaft). Additional analytic studies were needed for determining the reasons for this kind of behavior and for eliminating it.

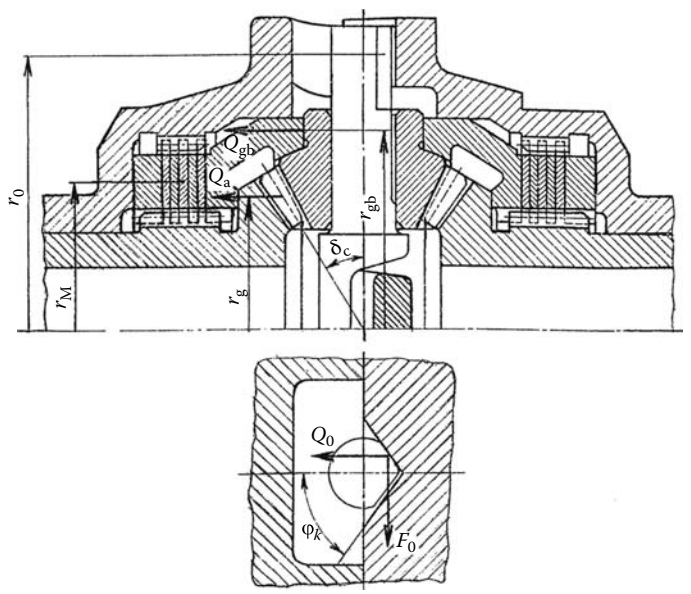


FIGURE 4.13
Limited slip differential (version I).

It was proved that this differential has symmetrical locking performance (i.e., same values of the locking coefficient upon lagging of the left or right shaft) only when the circumferential force of the differential's case is distributed equally to the two pinion pins. If, however, one pin in this mechanism is subjected to a circumferential force that is larger than the other then the friction torque of one clutch is greater than that of the other and the locking coefficient takes different values upon lagging of the left or right shafts. Unequal loading of the pinion pins is a specific feature of this mechanism and stems from the fact that it impossible to manufacture ''perfectly identical'' components. Virtually all the version I mechanisms exhibit asymmetricity of locking performance. Consider a general case when unequal circumferential forces are transmitted to each pinion pair from their pins. Then the circumferential forces applied to the pins that induce the axial forces that compress the friction clutches of the advancing and lagging half axles, respectively, are:

$$F_1 = \xi F; \quad F_2 = (1 - \xi)F \tag{4.58}$$

where

ξ is the factor of distribution of load between the pinion pins
F is the total circumferential force exerted by the pinions on the pins at arm r_g

The equation of equilibrium of the pinions relative to their pins yields

$$F_1' \approx F_1'' = 0.5F; \quad F_2' \approx F_2'' = 0.5F \tag{4.59}$$

where F_1' and F_1'', F_2' and F_2'' are the circumferential forces at the teeth of each pinion pair. These expressions were obtained without considering the friction forces in the pinions (friction at the pins, over the spheres and ends of the cups). The error of this assumption is less than 2%.

The total circumferential forces F' and F'' at the teeth of each side gear exerted by the meshing with the pinions

$$F' = F_1' + F_2' = 0.5F; \quad F'' = F_1'' + F_2'' = 0.5F \tag{4.60}$$

The torques at the half axles are determined from the equation of equilibrium of the side gears:

$$T' = 0.5Fr_g - T_r' - T_b'; \quad T'' = 0.5Fr_g + T_r'' + T_b'' \tag{4.61}$$

where T_r' and T_r'' are the friction torques in the disk clutches, whereas T_b' and T_b'' are friction torques in the pressure cups arising between the shoulders of the pinions and the ends of these cups. The friction torques in disk clutches arise as a result of the application of axial forces Q' and Q'', each of which adds to the axial force Q_a arising in the meshing of the differential's gears and to axial force Q_{gb} that arises on the sloping grooves of the differential's case and is transmitted to the pressure cup by way of the pinion shoulder, that is,

$$Q' = Q_a' + Q_{gb}'; \quad Q'' = Q_a'' + Q_{gb}'' \tag{4.62}$$

Axial forces Q'_a and Q''_a are determined from familiar expressions of bevel gears:

$$Q'_a = Q''_a = Q_a = 0.5F \tan \alpha_w \cos \delta_c \tag{4.63}$$

and the axial forces Q'_{gb} and Q''_{gb} are obtained from the expressions

$$\begin{aligned} Q'_{gb} &= F_1 r_g \tan \varphi_k / r_0 = \xi F r_g \tan \varphi_k / r_0 \\ Q''_{gb} &= F_2 r_g \tan \varphi_k / r_0 = (1 - \xi) F r_g \tan \varphi_k / r_0 \end{aligned} \tag{4.64}$$

where φ_k is the slope of the working surface of the V-shaped groove in the differential's case, whereas r_0 is the arm of the circumferential forces on this groove. Then the friction torques in the disk clutches and at the pressure cups are as follows

$$\begin{aligned} T'_r &= \mu Q' r_M i_M; \quad T''_r = \mu Q'' r_M i_M \\ T'_{gb} &= \mu Q'_{gb} r_{gb}; \quad T''_{gb} = \mu Q''_{gb} r_{gb} \end{aligned} \tag{4.65}$$

where r_{gb} is the friction radius of the end of the pressure cup at the pinion's shoulder. Substitution into Equation 4.61 of the values of components obtained above and regrouping yields

$$\begin{aligned} T' &= 0.5 F r_g [1 - \mu(2\xi E' + A)] \\ T'' &= 0.5 F r_g \{1 + \mu[2(1 - \xi)E' + A]\} \end{aligned} \tag{4.66}$$

where

$$\begin{aligned} E' &= (r_M i_M + r_{gb}) \tan \varphi_k / r_0 \\ A &= r_M i_M \tan \alpha_w \cos \delta_c / r_g \end{aligned}$$

For the mechanism under consideration and $E' =$ constant and $A =$ constant. It is found by dividing T'' by T' that the torque bias factor is

$$K_d = \frac{1 + \mu[2(1 - \xi)E' + A]}{1 - \mu(2\xi E' + A)} \tag{4.67}$$

It is seen from formula (4.67) that K_d is a function of the extent ξ of redistribution of the circumferential force F between the pinion pins (Figure 4.14).

Curves 1 and 2 correspond to mechanisms with three and five friction pairs i_M in each disk clutch.

The distribution of total force F into forces F_1 and F_2 that are in general not equal in magnitude may take only one value. The force corresponding to the advancing output shaft is designated by F_1 whereas that corresponding to the lagging output shaft by F_2. Note that any of the two output shafts may be advancing or lagging. Hence in one case F_1 will designate a larger and F_2 a smaller force, whereas in another case, conversely, F_1 will designate the smaller and F_2 the larger force. Consequently each of the factors ξ and K_d may have two values depending on which output shaft is advancing. Let, for example, when making a left turn $\xi = 0.8$. Then for a differential with some specified parameters A and E' it is found from formula (4.67) that $K_d = 6.5$. Upon a right turn $\xi = 0.2$ and $K_d = 2.8$.

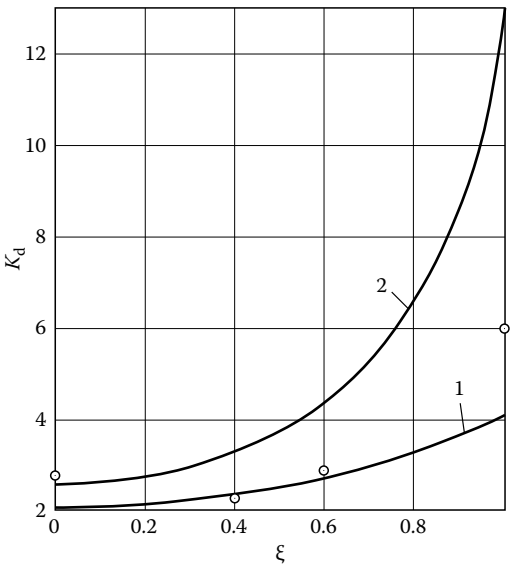


FIGURE 4.14
Plot of K_d vs. ξ at $\varphi_k = 45°$, i_M: (1) 3; (2) 5.

At $\xi = 0.5$ formula (4.67) is transformed into an expression corresponding to a differential with symmetrical locking properties.

A major difficulty in experimental determination of K_d consists in obtaining a specific value of ξ (with the exception of $\xi = 0$ and $\xi = 1$). For this in the first case ($\xi = 0$) it suffices to remove the pin with two pinions on the advancing-shaft side, and in the second case ($\xi = 1$) to remove the pin with pinions on the side of the lagging shaft. For a mechanism with three friction pairs at $\xi = 0$ the experimental value of K_d is 1.8, whereas the analytically obtained value is 2.02. At $\xi = 1$ because of the large friction in the clutch and certain instability of the friction coefficient, the experimental value of K_d ranges between 6 and 10. The analytically obtained value of K_d for $\xi = 1$ is 4.41. For a mechanism with five friction pairs at $\xi = 0$, $K_d = 2.75$, the analytically obtained value being 2.50. At $\xi = 1$ the differential is jammed and the analytic value was $K_d = 17.5$.

For the purpose obtaining intermediate values of ξ and K_d, a mechanism with three friction pairs was assembled using high-precision manufactured components and tested. The torque bias factor of one advancing half axle was 2.35, being 2.90 for the other advancing half axle, which corresponds to $\xi = 0.4$ and $\xi = 0.6$. The experimental results as well as a number of other data are in agreement with analytic studies and results. Note that the experimental methods of determining K_d are given in Chapter 8.

These studies provided a more comprehensive insight into the properties of limited slip differentials with separate floating pinion pins and showed that symmetrical locking is possible only when two pinion pins are subjected to the same load. In the opposite case, the locking performance depends on the direction of relative rotation of the output shafts and the locking factor is determined from formula (4.67).

Nonuniformity of the load applied to the pins stems from component dimensions, mutual perpendicularity of the axes of the pinion pins, inequality of the disk stacks of the two clutches, etc. Consequently, individual components of the mechanism must be manufactured very precisely. Nevertheless, such differentials are in extensive use.

Total circumferential force F at the pinion pins does not depend on the friction torques of the clutches, provided that these torques are equal. Equality of torques is attained at

$\xi = 0.5$. In the differential under study force F is a function not only of torque T_0 supplied to the differential's case, but also of ξ, which results from the following. The equation of torques applied to the mechanism is written as:

$$T' + T'' = T_0$$

Substitution of the values of torques T' and T'' at the half axles from formula (4.66) into this formula yields:

$$T_0 = Fr_g[1 + \mu(1 - 2\xi)E'] \tag{4.68}$$

whence,

$$F = \frac{T_0}{[1 + \mu(1 - 2\xi)E']r_g} = \delta\frac{T_0}{r_g} \tag{4.69}$$

Factor $\delta = [1 + \mu(1 - 2\xi)E']^{-1}$ is the ratio of circumferential force F obtained from formula (4.69) in the case when the friction torques of the clutches are not equal ($\xi \neq 0.5$) to the circumferential force $F = T_0/r_g$ obtained when the friction torques of the clutches are equal ($\xi = 0.5$). For example, at $\xi = 0$ and $\xi = 1$ for one of the differentials under study ($\varphi_k = 55^\circ$, $i_M = 3$) the computed values of δ are respectively 0.75 and 1.50.

Investigations show that if the axial force of the heavier-loaded pin compresses the clutch of the advancing shaft, then the locking coefficient increases steeply. If the axial force of this pin compresses the clutch of the lagging shaft, then the locking coefficient is smaller than that calculated on the assumption of $\xi = 0.5$. Hence, measures must be taken to develop the designs and processes for manufacturing and assembling the mechanisms that would provide for a close-to-uniform loading of both the pinion pins. Such measures include in the first place providing for mutual perpendicularity of the pinion pins and equality of the total thickness of the two stacks of the differential's disks. A quantitative assessment of the effect of nonperpendicularity of pinion pins and inequality of the thickness of clutch disk stacks on the symmetrical nature of the locking performance can be obtained from the asymmetry factor introduced by P. N. Stepaniuk and L. S. Izrailevich

$$j = K'_d/K''_d \tag{4.70}$$

where K'_d and K''_d are respectively the larger and smaller values of locking coefficients that were determined in stand experiments when braking one and the other of the output shafts. Figure 4.15 shows the asymmetry factor j of a differential with three friction pairs as a function of nonperpendicularity Δg of the surfaces of the V-shaped grooves in the differential's halves and difference Δl in the thickness of clutch disk stacks.

The greater the nonperpendicularity and the difference in the thickness of clutch disk stacks the higher is the asymmetry factor j. An acceptable asymmetry ($j = 1.2$) is that which occurs when the thickness difference Δl is 0.3 mm, something that is attainable in mass production and at a nonperpendicularity of $\Delta g = 0.15$ mm.

Obtaining mutual perpendicularity of the V-shaped grooves in assembled differential cases involves certain manufacturing difficulties. The grooves are machined (pull broached) not when assembled, as is the case of openings for pinion pins in the cases of open differentials, but are produced in each half of the case followed by centering based on

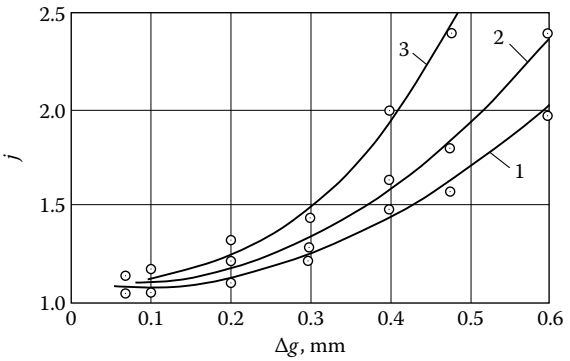


FIGURE 4.15
Asymmetry factor j as a function of mutual nonperpendicularity of the grooves Δg, Δl, mm: (1) 0.05; (2) 0.15; (3) 0.32.

one of the drill holes for clamping bolts. It was found experimentally that the symmetry of the locking performance of differentials with nonperpendicularity of the V-shaped grooves in an assembled case of 0.6 mm is unsatisfactory. In certain cases the mechanism seized, the parts broke, and the tires of the affected axle wore excessively. The precision of mutual perpendicularity of the grooves can be improved by means of special devices that modify the technology of producing the grooves in the case.

The limited slip differential shown in Figure 4.16 follows design version II and represents the further development of differentials designed according to version I.

The design of the locker shown in Figure 4.16 ensures that the differential's locking performance will be symmetrical. The projections of pressure cups 1 enter axial grooves 2 of the case. The torque is transmitted to the pins of pinions 3 by symmetrical V-shaped grooves produced at the ends of cups 1. Each such cup is subjected to the axial force

$$Q_{\text{gb}} = 0.5Fr_{\text{g}} \tan \varphi_k / r_{\text{gb}} \tag{4.70}$$

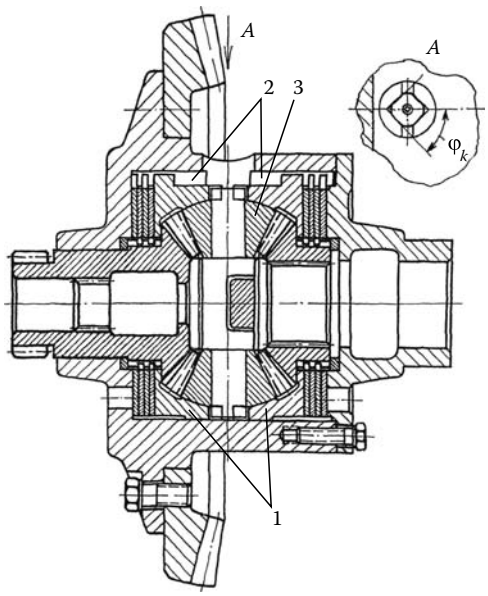


FIGURE 4.16
Limited slip differential (version II). (Based on Jaskiewicz, Z., *Driving Axles*, Mashinostroenie Publishing House, Moscow, 1985.)

The pressure cups are also subjected to forces arising in the meshings between the pinions and the side gears:

$$\begin{aligned} Q'_{\mathrm{a}} &= F' \tan \alpha_{\mathrm{w}} \cos \delta_{\mathrm{c}} \\ Q''_{\mathrm{a}} &= F'' \tan \alpha_{\mathrm{w}} \cos \delta_{\mathrm{c}} \end{aligned} \tag{4.71}$$

Circumferential forces F' and F'' at the advancing and lagging side gears are determined from the conditions of equilibrium of the pinions that correspond to expression (4.18). Consequently, forces F' and F'' are given by formulae (4.24).

The balance equations of the side gears can be used for formulating the expressions

$$\begin{aligned} T' &= F' r_{\mathrm{g}} - T'_{\mathrm{r}} - T'_{\mathrm{gb}} \\ T'' &= F'' r_{\mathrm{g}} + T''_{\mathrm{r}} + T''_{\mathrm{gb}} \end{aligned} \tag{4.72}$$

where T'_{gb} and T''_{gb} are friction torques of the advancing and lagging gears at the pressure cups. Substitution into Equations 4.72 expressions for their terms and collecting terms yields:

$$\begin{aligned} T' &= 0.5 F r_{\mathrm{g}} [1 - \mu(A' + B + E'' + \mu A' B)] \\ T'' &= 0.5 F r_{\mathrm{g}} [1 + \mu(A' + B + E'' + \mu A' B)] \\ A' &= (r_{\mathrm{M}} i_{\mathrm{M}} + r_0) \tan \alpha_{\mathrm{w}} \cos \delta_{\mathrm{c}} / r_{\mathrm{g}} \\ E'' &= r_{\mathrm{M}} i_{\mathrm{M}} \tan \varphi_k / r_0 \end{aligned} \tag{4.73}$$

Then the formula for the locking coefficient becomes:

$$K_{\mathrm{d}} = \frac{1 + \mu(A' + B + E'' + \mu A' B)}{1 - \mu(A' + B + E'' + \mu A' B)} \tag{4.74}$$

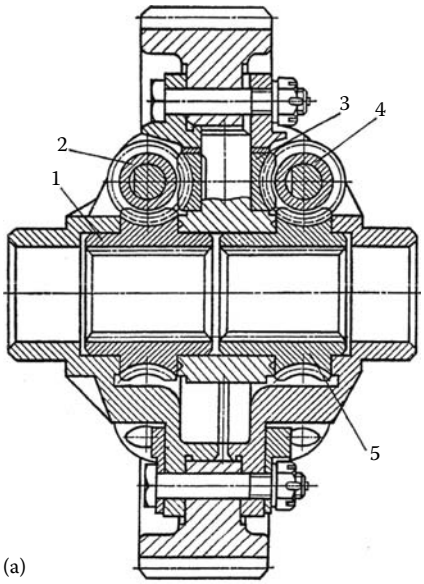
Neglecting the last term in the sum in the parentheses as being negligible, expression (4.74) can be simplified to

$$K_{\mathrm{d}} = \frac{1 + \mu P_4}{1 - \mu P_4} \tag{4.75}$$

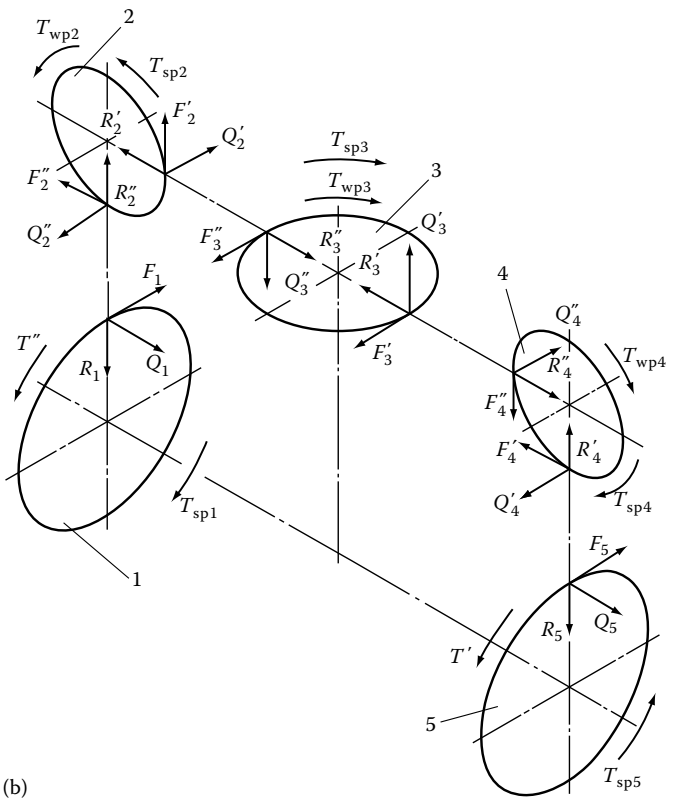
where $P_4 = A' + B + E''$.

4.5 Worm-Gear Differentials

The term ''worm-gear differentials'' applies to mechanisms in which the kinematic linkage between the half axles is implemented by means of two kinds of gear transmissions—worm gear and helical gear. Worm-gear differentials (Figure 4.17) may have high locking coefficients because of the elevated friction in the worm couples.

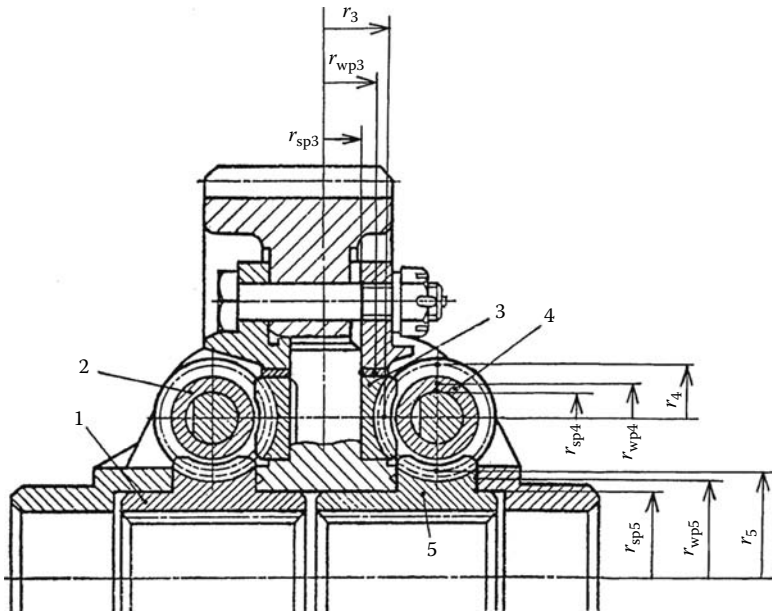


(a)



(b)

FIGURE 4.17
Worm-gear differential: (a) design; (b) schematic diagram of forces and torques.



(c)

FIGURE 4.17 (continued)
(c) radii.

The differential's case holds side worm-gear wheels 1 and 5 that mesh with worms 2 and 4. The latter serve as pinions. Worms 2 and 4 are coupled by worm-gear wheels 3. Under this arrangement, this mechanism utilizes three rows of pinions 2–4. Each row contains four and sometimes three pinions. Such differentials were tested, among others, on 6×6 trucks. Locking coefficient K_d ranged between 6 and 10 for different operating modes. The forces acting on the meshing of the worm-gear transmission are determined with consideration of friction forces on the active surfaces of the worm threads and teeth of the worm gear. The circumferential F, axial Q, and radial R forces that act on the worm are designated by the subscript w and those acting on the worm gear by the subscript wg.

These forces are interrelated as

$$\begin{aligned} F_{wg} &= Q_w = F_w/\tan(\gamma \pm \rho) \\ R_w &= R_{wg} = F_{wg} \tan \alpha_w = F_w \tan \alpha_w/\tan(\gamma \pm \rho) \end{aligned} \tag{4.76}$$

where

γ is the lead angle of the worm thread
ρ is the friction angle
α_w is the pressure angle of the worm thread in normal cross section

The plus sign is assigned to the driving worm and the minus sign to the driven worm.

It follows from comparing formulae (4.1) and (4.6) that the locking coefficient K_d can be determined from the known efficiency η_d:

$$K_d = 1/\eta_d \tag{4.77}$$

If the friction of the ends of the worms and worm gears at the case and the friction in the journals of the three rows of pinions are neglected, then it is rather easy to find η_d that reflects only the friction in the meshing of the worm couples. For a driving worm and a driven worm gear

$$\eta_{dr} = \tan\gamma/\tan(\gamma + \rho);$$

and for a driven worm and driving worm gear

$$\eta_{dg} = \tan(\gamma - \rho)/\tan\gamma.$$

Then for the worm-gear differential

$$K_d = \frac{1}{(\eta_{dr}\eta_{dg})^2} = \left[\frac{\tan(\gamma + \rho)}{\tan(\gamma - \rho)}\right]^2 \tag{4.78}$$

This shows that the locking coefficient of a worm-gear differential is a function of angle γ. A more exact expression for K_d that would also include friction in all the elements of the transmission can be obtained by analyzing the conditions of equilibrium of each worm gear and worm of the mechanism. Figure 4.17b presents the diagram of forces acting in the meshings and of friction torques arising in the supports of the worm gears and worms (the figure does not show the reaction forces). An efficiency is introduced that represents the losses in the supports of each individual worm gear and worm. Additional notation is used for each ith element thus:

r_i, pitch radius
r_{wpi}, friction radius of the thrust end
r_{spi}, radius of journal

These radii are shown for elements 4 and 5 of the differential in Figure 4.17c. The equilibrium equation of worm gear 1 from Figure 4.17a is:

$$T'' - F_1 r_1 - T_{wp1} = 0 \tag{4.79}$$

where $T_{wp1} = \mu r_{wp1} F_1 \tan(\gamma - \rho)$ is the friction torque of the end of worm gear 1 at the differential's case. Upon substitution of formula (4.79) the efficiency that includes friction losses in the supports of the lagging worm gear is given by the expression:

$$\eta_1 = \frac{F_1 r_1}{T''} = \left[1 + \mu r_{wp1} \tan(\gamma - \rho)/r_1\right]^{-1} \tag{4.80}$$

The equilibrium equation of worm 2

$$F_2'' r_2 - F_2' r_2 - T_{sp2} - T_{wp2} = 0 \tag{4.81}$$

where T_{wp2} is the friction torque of the end of worm 2, whereas T_{sp2} is the friction torque in the journal of worm 2. These torques are given by the formulae:

$$T_{wp2} = \mu r_{wp2}(Q_2'' - Q_2') = \mu r_{wp2}\left[\frac{F_2''}{\tan(\gamma - \rho)} - \frac{F_2'}{\tan(\gamma + \rho)}\right], \tag{4.82}$$

where r_{wp2} is the friction radius of the end of worm 2.

$$\begin{aligned} T_{sp2} &= \mu r_{sp2}\sqrt{(F_2'' + R_2')^2 + (F_2' + R_2'')^2} \\ &= \mu r_2 F_2' \frac{r_{sp2}}{r_2}\sqrt{\left(\frac{1}{\eta_2} + \frac{\tan\alpha_w}{\tan(\gamma + \rho)}\right)^2 + \left(1 + \frac{\tan\alpha_w}{\eta_2 \tan(\gamma - \rho)}\right)^2} \end{aligned} \tag{4.83}$$

Designating

$$B_{sp2} = \frac{r_{wp2}}{r_2}\sqrt{\left(\frac{1}{\eta_2} + \frac{\tan\alpha_w}{\tan(\gamma + \rho)}\right)^2 + \left(1 + \frac{\tan\alpha_w}{\eta_2 \tan(\gamma - \rho)}\right)^2}$$

reduces formula (4.83) to the form:

$$T_{sp2} = \mu r_2 F_2' B_{sp2} \tag{4.84}$$

where

r_{sp2} is the radius of the axis (journal) of worm 2

η_2 is the efficiency that accounts for friction losses of worm 2 in the end and in the journal, $\eta_2 = F_2'/F_2''$

Substitution of the expressions for T_{sp2} and T_{wp2} into formula (4.81) yields

$$F_2'' r_2\left(1 - \mu\frac{r_{wp2}}{r_2 \tan(\gamma - \rho)}\right) = F_2' r_2\left(1 - \mu\frac{r_{wp2}}{r_2 \tan(\gamma + \rho)} + \mu B_{sp2}\right) \tag{4.85}$$

whence,

$$\eta_2 = \frac{F_2'}{F_2''} = \frac{1 - \mu r_{wp2}/[r_2 \tan(\gamma - \rho)]}{1 - \mu r_{wp2}/[r_2 \tan(\gamma + \rho)] + \mu B_{sp2}} \tag{4.86}$$

Equation 4.86 should be solved by one of the numerical methods.

The equilibrium equation of worm gear 3 has the form

$$F_3'' r_3 - F_3' r_3 - \mu r_{wp3}(Q_3'' - Q_3') - \mu r_{sp3}(F_3'' - F_3') = 0 \tag{4.87}$$

Here $T_{wp3} = \mu r_{wp3}(Q_3'' - Q_3')$ is the friction torque of the end, whereas, $T_{sp3} = \mu r_{sp3}(F_3'' - F_3')$ is the friction torque of gear 3 at the axis.

It follows from Equation 4.87 that

$$F_3''r_3\left\{1-\mu\left[r_{wp3}\tan(\gamma+\rho)+r_{sp3}\right]/r_3\right\} = F_3'r_3\left\{1-\mu\left[r_{wp3}\tan(\gamma-\rho)-r_{sp3}\right]/r_3\right\} \tag{4.88}$$

Then the efficiency that accounts for losses in the supports of the pinions of the middle row (Figure 4.17b) is:

$$\eta_3=\frac{1-\mu[r_{wp3}\tan(\gamma+\rho)+r_{sp3}]/r_3}{1-\mu[r_{wp3}\tan(\gamma-\rho)-r_{sp3}]/r_3} \tag{4.89}$$

Expression (4.89) was derived on the assumption that the force that loads of the journal is determined solely by the sum of circumferential forces $\left(F_3''+F_3'\right)$; this assumption has virtually no effect on the computational results.

The equilibrium equation of worm 4

$$F_4''r_4-F_4'r_4-T_{sp4}-T_{wp4}=0 \tag{4.90}$$

where T_{wp4} is the friction torque of the end of worm 4, whereas T_{sp4} is the friction torque in the journal of worm 4. These torques are given by the expression:

$$T_{wp4}=\mu r_{wp4}\left(Q_4''-Q_4'\right)=\mu r_{wp4}\left[\frac{F_4''}{\tan(\gamma-\rho)}-\frac{F_4'}{\tan(\gamma+\rho)}\right] \tag{4.91}$$

$$T_{sp4}=\mu r_4F_4'\frac{r_{sp4}}{r_4}\sqrt{\left(\frac{1}{\eta_4}-\frac{\tan\alpha_w}{\tan(\gamma+\rho)}\right)^2-\left(1-\frac{\tan\alpha_w}{\eta_4\tan(\gamma-\rho)}\right)^2} = \mu r_4F_4'B_{sp4}$$

where

$$B_{sp4}=\frac{r_{sp4}}{r_4}\sqrt{\left(\frac{1}{\eta_4}-\frac{\tan\alpha_w}{\tan(\gamma+\rho)}\right)^2+\left(1-\frac{\tan\alpha_w}{\eta_4\tan(\gamma-\rho)}\right)^2}$$

Then the efficiency that accounts for losses in the supports of the worms that mesh with the lagging side gear is:

$$\eta_4=\frac{F_4'}{F_4''}=\frac{1-\mu r_{wp4}/[r_4\tan(\gamma-\rho)]}{1-\mu r_{wp4}/[r_4\tan(\gamma+\rho)]+\mu B_{sp4}} \tag{4.92}$$

Equation 4.92 should be solved by one of the numerical methods.

The equilibrium equation of worm gear 5 is:

$$T'-F_5r_5+T_{wp5}=0 \tag{4.93}$$

where $T_{wp5}=\mu r_{wp5}F_5\tan(\gamma+\rho)$ is the friction torque of the end of worm gear 5.

Upon substitution of (4.93), the efficiency that accounts for friction losses of the end of side worm gear 5 is given by the expression:

$$\eta_5 = \frac{T'}{F_5 r_5} = 1 - \mu r_{wp5} \tan(\gamma + \rho)/r_5 \tag{4.94}$$

The total efficiency that accounts for friction losses in the supports of all the gears and worms is equal to the product of the individual efficiencies.

$$\eta_0 = \eta_1\ \eta_2\ \eta_3\ \eta_4\ \eta_5 \tag{4.95}$$

From this, the formula for calculating K_d of a worm-gear differential is written as:

$$K_d = \frac{1}{\eta_0}\left[\frac{\tan(\gamma + \rho)}{\tan(\gamma - \rho)}\right]^2 \tag{4.96}$$

Calculations performed for the differential from Figure 4.17a at $\gamma = 21.8°$, $\rho = 5.71°$, and $\mu = 0.1$ yielded the following results: $K_d = 3.3$ from formula (4.78), $K_d = 6.5$ from formula (4.96). It is seen that the disagreement between the computed values of K_d is significant. For this reason, approximate formula (4.78) is not recommended for calculating the locking factors of worm-gear differentials. Smaller values of the torque bias (from 1.8 to 3) are usually subjects to interwheel differentials of passenger cars.

Figure 4.18 shows the design schematic of a helical-gear differential that is used on 4×4 off-road trucks.

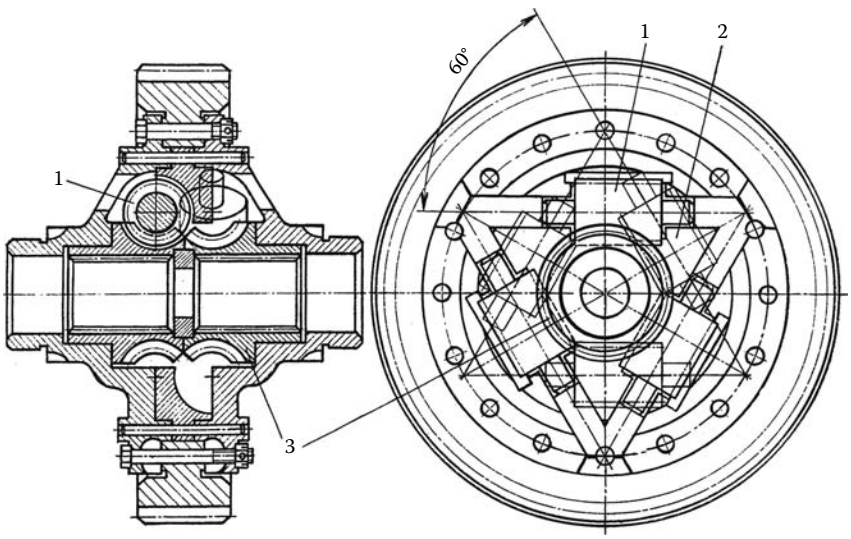


FIGURE 4.18
Helical-gear differential. (Based on Jaskiewicz, Z., *Driving Axles*, Mashinostroenie Publishing House, Moscow, 1985.)

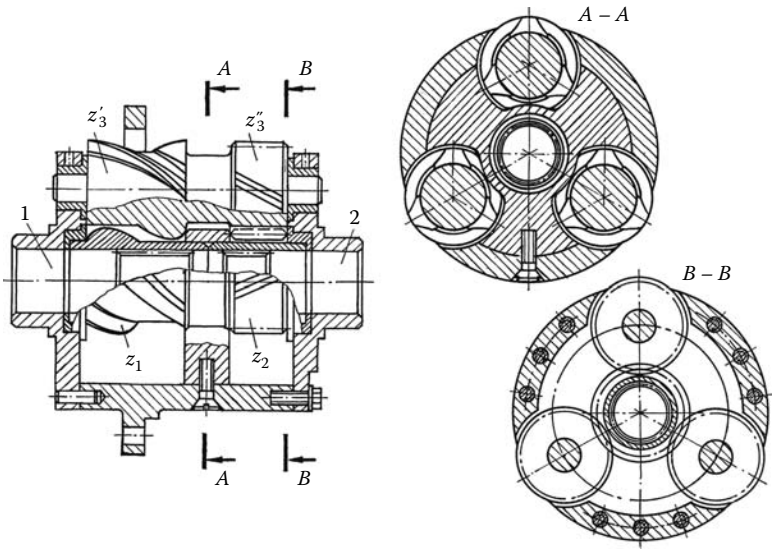


FIGURE 4.19
Differential with helical gears of the same direction. (Based on Mudrov, A.G., *Vestnik Mashinistroenia* (*News of Machinebuilding*), 2, 73, 2002.)

This differential is different from most such mechanisms by the fact that it does not have the middle row of pinions and that pinions 1 and 2 of the right and left row mesh directly with one another. To provide for mutually oppositely directed rotation of the output shafts of the differential the pinions of both rows have the same direction of the tooth's slope. The lead angle is 30°, whereas the assembly angle between the pinion axes is 60°. Pinions 1 and 2 mesh by the middle part of their teeth with the teeth of side gears 3, and by the ends of the teeth, with the adjoining pinions. The design of some helical-gear differentials is simplified by introducing straight-tooth rings, provided on both ends of each pinion. Those toothed rings link pinions of the two rows.

Figure 4.19 shows still another differential design. It differs from similar mechanisms by a pair of gears (z_1 and z'_3) with parallel axes of rotation and helical teeth that have special noninvolute end profiles.

Helical gears z_2 and z''_3 have involute profiles. The gear ratio of the first pair of gears is positive and equal to $+1$, whereas that of the second pair of gears is negative and equal to -1. Gears z_1 and z_2 are splined to the output shafts that are installed in the differential through openings 1 and 2 in the mechanism's case. Gears z'_3 and z''_3, manufactured integrally with their shaft, are linked by means of the journals of this shaft to the differential's case and function as pinions. This couple of gears 3 is shown separately in Figure 4.20.

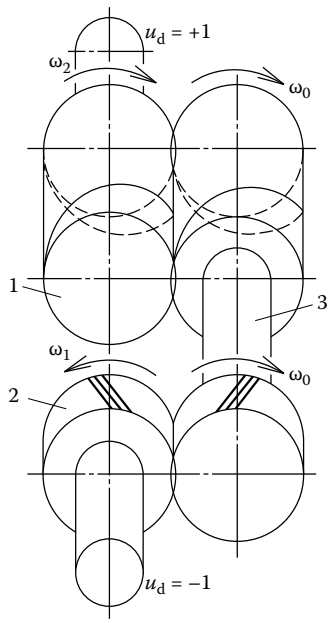


FIGURE 4.20
Pinion of the differential from Figure 4.20.

Number 1 in this figure shows a pair of helical gears. The teeth of both gears of this couple are machined in the direction of the right-hand slope, for which reason both gears rotate in the same direction (see ω_0 and ω_2). The gear ratio of this couple is $+1$. Number 2 designates a pair of helical gears rotating in opposite directions (see ω_0 and ω_1). The gear ratio of this couple is -1. The differential uses a total of three pinions (see Figure 4.20). The locking coefficient of the differential may be as high as 8 because of friction that arises in the gear couple with positive gear ratio. At the same efficiencies, the temperature to which a reduction mechanism with gears of this profile is heated up is markedly lower than in its worm-gear counterparts.

4.6 Cam-Plunger Differentials

The cam-plunger differential is a cam-plunger mechanism that obeys the principal equation of the differential's kinematics (see formula (2.10)). The function of the carrier in this differential is performed by a cage with plungers (pushers) and the two output links of the differential consist of cam sprockets. The friction torque that causes redistribution of the torques between the output links stems from the sliding of the plungers over the cage and at the cam surfaces at the sprockets.

Figure 4.21 shows a schematic of a cam-plunger differential that is usually used in off-road trucks.

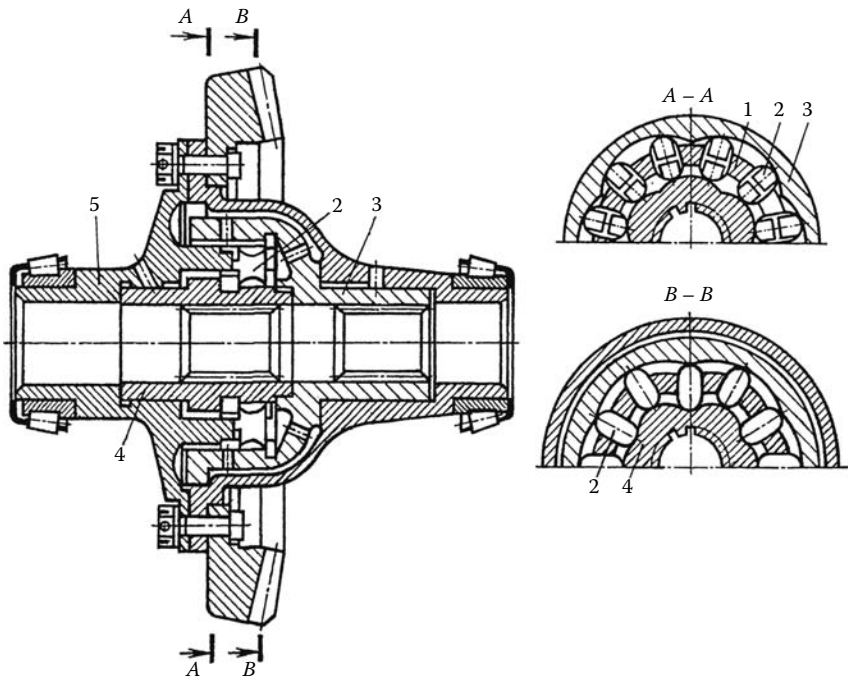


FIGURE 4.21
Cam-plunger differential.

The differential consists of inner 4 and outer 3 sprockets and 24 plungers 2 located in radial apertures of cage 1 in two rows spaced at half-steps over the circumference (see sections *A* and *B* in Figure 4.21). Cage 1 is constructed as a single entity with the left half 5 of the differential's case. Plungers 2 mate with the outer cams of inner sprocket 4 and with inner cams of outer sprocket 3. The sprockets are splined to the output shafts (the shafts are not shown in Figure 4.21). Six cams that mate with plungers 2 of both rows are arranged uniformly over the circumference of outer sprocket 3. Inner sprocket 4 has two independent rows of cams; each row has six cams uniformly distributed over the circumference. The cams of one row are shifted over the circumference by half a step relative to the cams of the other row. Plungers 2 in this differential serve as pinions. If the angular velocities of the output shafts are the same, then the plungers remain stationary relative to the cage and the sprockets. In the opposite case, for example, when the vehicle makes a turn, one sprocket advances relative to the driving cage, whereas the other lags behind it. Here the cage, while advancing relative to the lagging sprocket, forces the plungers to move in a radial direction to the extent that they move over the cam surfaces. The opposite ends of the plungers act in the same manner on the surfaces of the second sprocket, causing it to move at an angular velocity higher than that of the cage.

Six plungers of each row transmit torque, whereas the other six remain on the nonworking surfaces of the cams. The array of plungers in a given row alternates its operation with those of the other row. This being so, twelve plungers are involved in transmitting the torque. Only at the time when all the 12 plungers of a given row find themselves in extreme locations (in the depressions and at the vertices of the cams) is the entire load transmitted by 6 plungers of the second row.

To simplify the manufacturing technology, the working surfaces of the cams and of the plungers of cam differentials are constructed along the arcs of circles. The shapes of cams comprised of circle arcs, are shown in Figure 4.22.

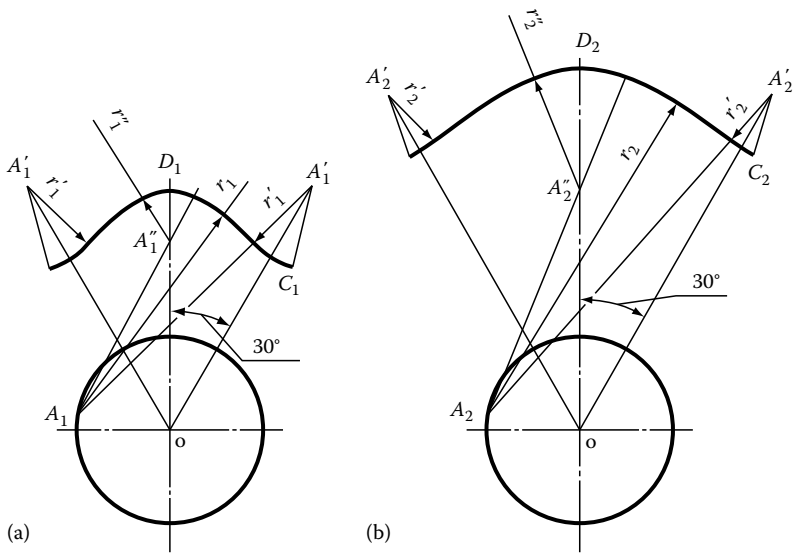


FIGURE 4.22
Shapes of sprocket cams: (a) inner sprocket; (b) outer sprocket.

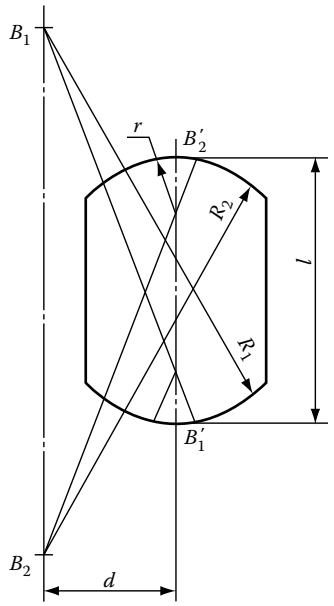


FIGURE 4.23
Shape of plunger.

Both profiles (or shapes) are symmetrical relative to straight lines OD_1 and OD_2. The shape of the cam of the inner sprocket is formed by circle arcs with centers in points A_1, A_1', and A_1'', corresponding to radii r_1, r_1', and r_1''. The shape of the cam of the outer sprocket is formed by circle arcs with centers in points A_2, A_2', and A_2'', corresponding to radii r_2, r_2', and r_2''. Figure 4.23 shows the shape of a plunger.

This shape is symmetrical about the centerline and is formed by circle arcs with centers in points B_1 and B_2 that correspond to radii R_1 and R_2 (that are equal to one another) and radius r.

Figure 4.24a and b shows a cam mechanism in a position when the sprocket shape segments that operate are those formed by arcs of circles r_1 and r_2, and the plungers formed by arcs of circles R_1 and R_2.

The position of centers A_1 and A_2 of circle arcs with radii r_1 and r_2 is determined by angles β_1 and β_2 between the plunger axis and the radii $|OA_1|$ and $|OA_2|$, respectively.

It was found that the gear ratio of a cam differential when the cage is stationary is virtually constant and equal to minus one (-1). This means that when one sprocket rotates about the cage through angle $\Delta\beta$, the other sprocket will rotate through the same angle in the opposite direction. Find the pressure angles

$$\psi_1 = \arcsin\left(\frac{|OA_1|\sin\beta_1 + d}{r_1 + R_1}\right);$$
$$\psi_2 = \arcsin\left(\frac{|OA_2|\sin\beta_2 - d}{r_2 - R_2}\right) \tag{4.97}$$

It will be assumed in determining the reactions in the couples of the cam differential that the wheel of the vehicle connected to the inner sprocket rotates slower than the wheel connected to the outer sprocket. The triangle of forces (Figure 4.24c) acting on the plunger yields, according to the law of sines

$$\frac{N_1}{\cos(\psi_2 - 2\rho)} = \frac{N_2}{\cos(\psi_1 + 2\rho)} = \frac{N_3}{\sin(\psi_1 + \psi_2)}, \tag{4.98}$$

where ρ is the friction angle.

Torques T_1 and T_2 transmitted by the outer and inner sprockets are

$$T_1 = N_1 h_1 z; \quad T_2 = N_2 h_2 z \tag{4.99}$$

where z is the number of working cams in each sprocket. Arm h_1 in formula (4.99) is obtained from the triangle ΔOE_1M_1

$$h_1 = r_{M1}\sin(\gamma_1 + \rho), \tag{4.100}$$

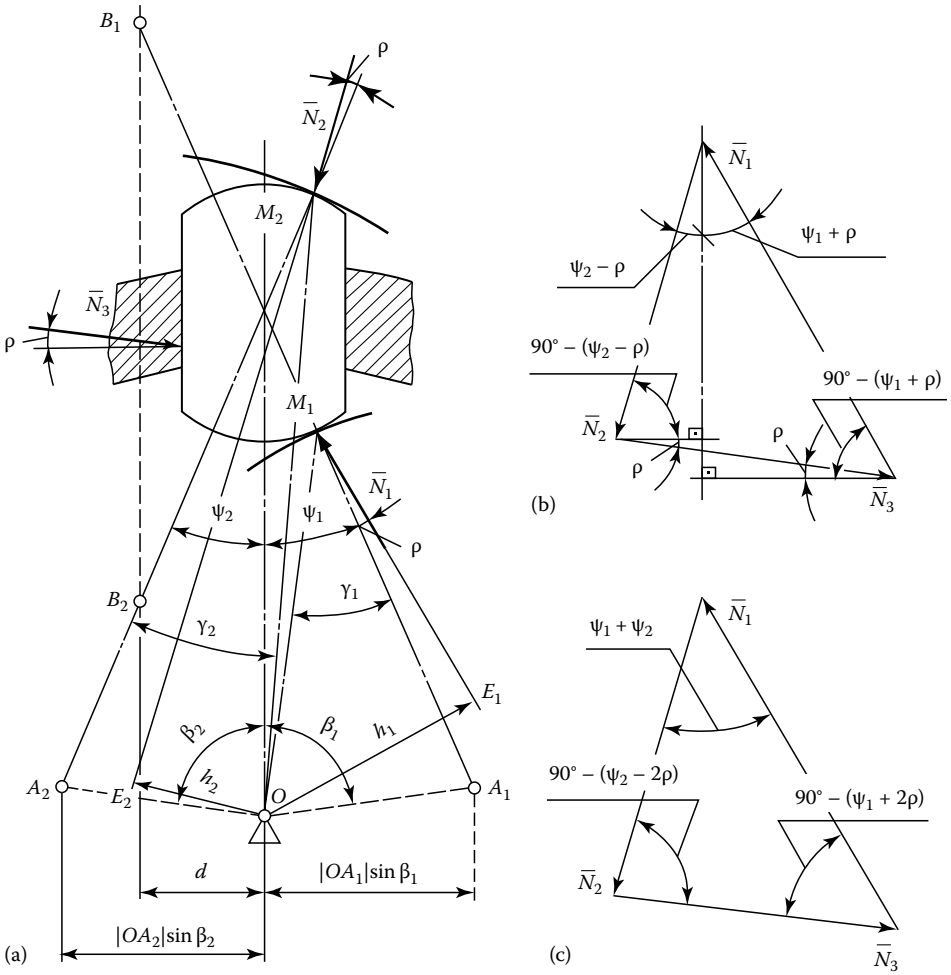


FIGURE 4.24
Cam-plunger mechanism of a differential: (a) cam-plunger mechanism; (b) angles and force triangle reduction diagram; (c) reduced diagram of forces acting on the plunger when the inner sprocket is lagging.

where from triangle ΔOA_1M_1 according to the law of cosines

$$r_{M1} = |OM_1| = \sqrt{|OA_1|^2 + r_1^2 - 2|OA_1|r_1 \cos[180^0 - (\beta_1 + \psi_1)]}$$
$$= \sqrt{|OA_1|^2 + r_1^2 + 2|OA_1|r_1 \cos(\beta_1 + \psi_1)}$$

Angle γ_1 is found from the same triangle ΔOA_1M_1

$$\gamma_1 = \arcsin\left[|OA_1| \sin[180^0 - (\beta_1 + \psi_1)]/r_{M1}\right]$$
$$= \arcsin[|OA_1| \sin(\beta_1 + \psi_1)/r_{M1}]$$

Arm h_2 in formula (4.99) is determined from triangle ΔOM_2E_2

$$h_2 = r_{M2}\sin(\gamma_2 - \rho), \tag{4.101}$$

where r_{M2} is determined from ΔOM_2A_2

$$\begin{aligned} r_{M2} = |OM_2| &= \sqrt{|OA_2|^2 + r_2^2 - 2|OA_2|r_2\cos[180^0 - (\beta_2 + \psi_2)]} \\ &= \sqrt{|OA_2|^2 + r_2^2 + 2|OA_2|r_2\cos(\beta_2 + \psi_2)} \end{aligned}$$

Angle γ_2 is found from triangle ΔOM_2A_2

$$\begin{aligned} \gamma_2 &= \arcsin\left[|OA_2|\sin[180^0 - (\beta_2 + \psi_2)]/r_{M2}\right] \\ &= \arcsin[|OA_2|\sin(\beta_2 + \psi_2)/r_{M2}] \end{aligned}$$

The ratio of the larger torque T_1 to the smaller T_2 is, by definition, the locking coefficient K_{d1}. Transformation of ratio T_1/T_2 yields

$$K_{d1} = \frac{r_{M1}\cos(\psi_2 - 2\rho)\sin(\gamma_1 + \rho)}{r_{M2}\cos(\psi_1 + 2\rho)\sin(\gamma_2 - \rho)} \tag{4.102}$$

Similarly, for the case when the outer sprocket is advancing ($\omega_2 < \omega_1$),

$$K_{d2} = \frac{r_{M2}\cos(\psi_1 - 2\rho)\sin(\gamma_2 + \rho)}{r_{M1}\cos(\psi_2 + 2\rho)\sin(\gamma_1 - \rho)} \tag{4.103}$$

It is seen from the analysis of formulae (4.102) and (4.103), that in order to avoid complete seizing of the differential's cam mechanism, when the output shafts cannot rotate relative to one another, it is required to conform to the conditions

$$\psi_1 + 2\rho < \pi/2; \quad \gamma_2 - \rho > 0; \quad \psi_2 + 2\rho < \pi/2; \quad \gamma_1 - \rho > 0 \tag{4.104}$$

Note that $K_{d1} > K_{d2}$. The difference in the locking coefficients increases in direct proportion to the length of the plunger and to the magnitude of the friction factor represented by friction angle ρ. For the differential shown in Figure 4.21, in the case when only six plungers operate, the torque biases are $K_{d1} = 3.1$ and $K_{d2} = 2.1$ at $\rho = 3.43°$. Since it is, the right driving wheel of the vehicle that usually slips when driving over the road shoulders, the inner sprocket of the differential should be connected to the left driving wheel, similar to the manner provided in Figure 4.21.

Some companies use this differential design in three-axle trucks as interwheel as well as interaxle differentials. There exist cam-plunger differentials with only a single row of plungers with nonidentical number of cams on the sprockets. Thus, the number of cams of the outer and inner sprockets of one of such differentials is respectively 13 and 11 and the number of plungers is 8; theoretically the largest possible number of plungers is equal to the sum of the number of cams on both sprockets. A small number of plungers in this differential (three fold smaller than in the differential shown in Figure 4.21) have a detrimental effect on the service life of the mechanism, because of the higher pressure in the contact between the plungers and the sprocket cams.

4.7 Torque Sensitive Differentials

The locking properties in the previously analyzed limited slip differentials come into play only when torque T_0 is applied to the case. The locking coefficient as such of these differentials does not depend on T_0 and is determined solely by the geometries of the mechanisms (if it is assumed that friction factor μ is constant, independent of the pressure at the rubbing surfaces and consequently, of T_0).

A large number of differentials exist in which the locking coefficient depends explicitly on the torque applied to them. In one class of differentials of this type the internal friction torque and accordingly the locking coefficient decrease with increasing T_0. From this also stems the designation of these mechanisms—differentials with decreasing friction torque.

Early designs of differentials with decreasing friction torque had two cone friction clutches. The clutches were compressed by plate springs. The highest friction torque in the mechanisms is observed when no torque T_0 is applied to the case. With rising T_0 the axial forces of the bevel gear meshing counteract the spring forces and thus reduce the friction torque in the cone clutches. At some value of T_0, the forces of the disk springs are balanced by the axial forces in the meshing between gears and pinions and the primary friction in the cone clutches becomes zero. In this case, the mechanism functions as an open bevel-gear differential.

The sliding of the plate springs over the support surfaces (the case and the cone of the friction clutch) in the course of the differential's operation may cause elevated wear of components, reduction in the compression force of the springs, and in the locking properties of the differential. The degree of spring compression also depends on changes in the dimensions of the differential's components. As analysis shows, a 0.1 mm reduction in the diameter of the cone clutch at angle $\gamma = 15^\circ$ may cause it to move axially 0.2 mm toward the side gear with an up to 35% reduction of the spring's compression force as compared with the initial value.

Figure 4.25 shows a schematic diagram of a recent differential with disk-type friction clutches in which the friction torque also decreases with increasing T_0.

The case of the differential is comprised of two halves, each of which consists of two interconnected parts 1 and 2; friction clutches 3 compressed by the plate springs are located between these two parts. The halves assembled in this manner are subassemblies of one assembly—the differential. After the halves are assembled, the mechanism is assembled in the same manner as an open bevel-gear differential. In this differential design, it is possible to more precisely specify the disk compression forces that depend primarily on the precision with which four linear dimensions of the differential's halves and the friction clutches are made. This makes it possible to check the spring compression in the course of assembly of the mechanism that allows using adjustment shims to compensate for manufacturing inaccuracies and to ensure the required stability of the differential's locking performance.

The extreme disks of the friction clutches on which the plate springs bear have a smaller internal diameter than the remaining disks. The hubs of the side gears bear on these disks. Splining the differential's case to the extreme disks of the clutch eliminates sliding of the springs relative to these components, something that reduces their wear.

The primary friction in the disk clutches of the differential in Figure 4.25 when torque T_0 is not applied is represented by the initial friction torque:

$$T_{\text{rp}}^{\text{s}} = 2\mu Q_{\text{sp}} r_{\text{M}} i_{\text{M}} \tag{4.105}$$

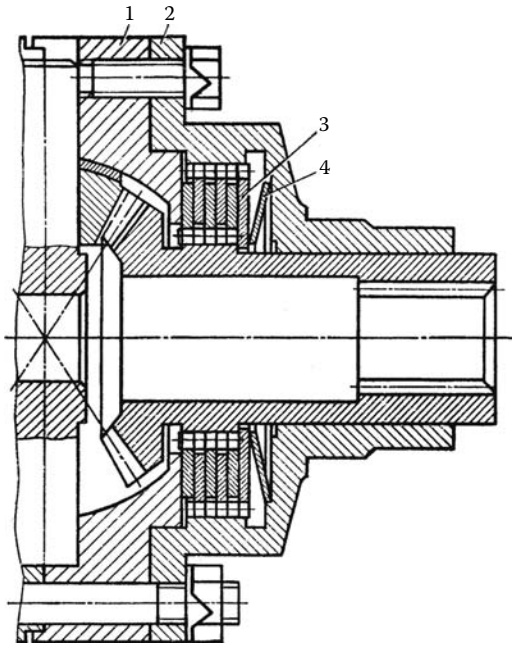


FIGURE 4.25
Differential with disk clutches.

where Q_{sp} is the precompression of the spring of one of the clutches. Designating $H = 2Q_{sp}r_M i_M$ one can have:

$$T_{rp}^{s} = \mu H \tag{4.106}$$

Application of torque T_0 to the case of the mechanism, gives rise to forces Q_a in the gear meshing that counteract the spring forces Q_{sp}. This reduces the degree of clutch compression and causes the disks of each clutch to become compressed by a force equal to the difference $(Q_{sp} - Q_a)$. The primary friction torque in the two clutches under current conditions is:

$$T_{rp} = 2(Q_{sp} - Q_a)\mu r_M i_M \tag{4.107}$$

Expressing force Q_a in terms of the differential's geometric parameters and of the torque T_0 (see formula (2.84)) and substituting (4.106), transforms formula (4.107) to:

$$T_{rp} = \mu H - \mu A T_0 \tag{4.108}$$

where $A = r_M i_M \tan\alpha_w \cos\delta_c / r_g$. Formula (4.108) is plotted in Figure 4.26.

Even though the maximum friction torque is given by formula (4.106), a situation in which the friction torque is at a maximum never occurs. This means that the output shafts of the mechanism cannot have relative motion when the torques at both of them are positive ($T' > 0$ and $T'' > 0$). The maximum friction torque T_{rp}^{sn} at which the above relative rotation of the output shafts is positive (the differential is actuated) can be determined from the condition that the torque at the advancing shaft is $T' = 0$. Consequently, $T_r^{sn} = T'' = T_0$. Then expression (4.108) yields

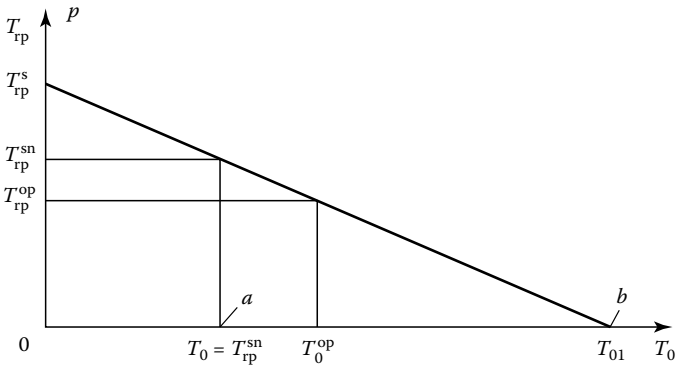


FIGURE 4.26
Primary friction torque vs. input torque.

$$T^{sn}_{rp} = T^{s}_{rp}/(1 + \mu A) = \mu H/(1 + \mu A) \tag{4.109}$$

Thus, the range within which the differential effect is possible lies to the right of point *a* that corresponds to $T_0 = T^{sn}_{rp}$ (see Figure 4.26). The differential may become actuated to the left of point *a* only when a negative torque appears on the advancing output shaft.

By equating the right-hand side of formula (4.108) to zero, it is possible to determine the value of torque $T_0 = T_{01}$ at which this differential with decreasing friction torque will start working as an open differential (point *b* in Figure 4.26):

$$T_{01} = H/A \tag{4.110}$$

Formulae (4.106) and (4.108) through (4.110) point to a relationship between the geometric parameters of the differential and its operating properties, primary internal friction torque T_{rp} and the torque T_0 at the case.

Compile an expression for calculating the locking coefficient of the differential from Figure 4.26. Substitution of (4.108) into formula (4.36) and regrouping yields:

$$K_d = K_{pu}\frac{(1 - \mu A)T_0 + \mu H}{(1 + \mu A)T_0 - \mu H} \tag{4.111}$$

Formula (4.111) relates the locking properties of the differential assessed by K_d with its geometric parameters A and H and the torque T_0. Formula (4.111) is plotted in Figure 4.27.

The location of the asymptote and the graph depends on parameters A and H, varying which allows changing the location of the asymptotes and accordingly of the locking coefficient. For example, moving the vertical asymptote to the left reduces the range of tractive loads that lie to the left of point *a* (see Figure 4.26), and corresponding to the activation of the differential only upon application of a negative torque to the output shaft.

The locking coefficient of a differential with a decreasing friction torque is a variable quantity and is hence somewhat inconvenient in calculations, even though it clearly illustrates the redistribution of torques between the differential's output shafts. In designing a differential with specific locking properties, it is possible to use an indicator that shall be termed as the specific initial primary friction torque:

$$K^{s}_{r} = T^{s}_{rp}/T_{01} = \mu A \tag{4.112}$$

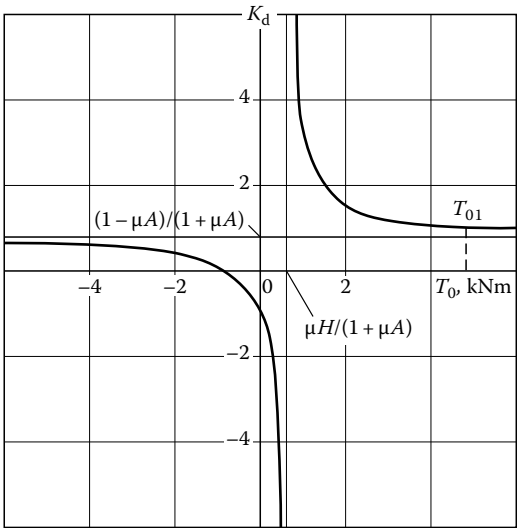


FIGURE 4.27
Locking coefficient of differential with decreasing friction torque.

The linearity of $T_{rp} = f(T_0)$ allows writing from similitude of the triangles in Figure 4.26:

$$K_r^s = T_{rp}^s / \left(T_{01} - T_0^{op}\right) \tag{4.113}$$

where T_0^{op} is torque at the differential's case in the principal operation mode of the vehicle's travel whereas T_{rp}^{op} is the primary friction torque that corresponds to this mode of motion.

Dividing the numerator and denominator of expression (4.113) by T_r^{op}, yields:

$$K_r^s = \left(T_{rp}^{op} / T_0^{op}\right) / \left(T_{01} / T_0^{op} - 1\right) \tag{4.114}$$

where, the ratio

$$K_r^{op} = T_{rp}^{op} / T_0^{op} \tag{4.115}$$

shall be termed the specific primary friction torque at the principal mode of motion.

If it is assumed that, the vertical load on the axle's wheels is constant and the rolling radii of the wheels in the driven mode are equal, then

$$T_{01} / T_0^{op} = \mu_{x1} / \mu_x^{op} \tag{4.116}$$

and finally,

$$K_r^s = K_r^{op} / \left(\mu_{x1} / \mu_x^{op} - 1\right) \tag{4.117}$$

where μ_{x1} and μ_x^{op} are the current friction factors corresponding to torques T_{01} and T_0^{op} (see Section 1.3.2) the values of which are selected from the intended operating conditions of the vehicle being designed.

The specific friction torque K_r^{op} in formula (4.117) determines the locking properties of the differential at the principal operational mode of the vehicle. Its value should be specified based on the design specifics of the vehicle, its intended use and operating conditions. Thus, if it is assumed $K_r^{op} = 0.5 - 0.6$ then these values have corresponding to them $K_d = 3 - 4$ at the principal operational mode (see formulae (4.12) that relate K_r and K_d). The numerical values $K_d = 3 - 4$ are sufficiently high for ensuring high tractive and velocity properties of off-road vehicles (this was discussed in Section 4.1). The values of K_d that decrease from 2.6 to 1.5 when torque T_0 at the case of the differential of a medium-class rear-wheel drive car increases, improve the stability of its rectilinear motion. These values of K_d have corresponding to them $K_r^{op} = 0.44 - 0.2$, which can be used in calculations from formula (4.117) in the course of the differential's design.

If values of K_r^{op}, μ_{x1}, and μ_x^{op} are specified, then formula (4.117) can be used for determining K_r^s and then it becomes possible to calculate all the features of the locking performance of the differential discussed above, including determining design parameters A and H that ensure these properties.

It was thus shown that the principal criterion of the locking properties of a differential with decreasing friction torque, in addition to the locking coefficient, should be the specific initial primary friction torque K_r^s that represents the degree of reduction in the friction torque, and is obtained from formula (4.117). The use of this parameter allows providing the required locking properties of the differential already at the design stage.

Nevertheless, the decision on the need of using such a differential should be taken after a comprehensive analysis of its effect on the vehicle's properties. Tests of the previously mentioned medium-class RWD car showed that such a differential improves the tractive and velocity properties of the vehicle, which was able to start moving with one of the wheels hanging out. The car moved at high speeds when making a turn while moving uphill, since the tractive load on the driving wheel that increases in this case reduced the locking performance of the differential and accordingly also the turn resistance moment (the latter is discussed in Section 4.11). The use of such differentials in the driving axles of farm tractors is not always advisable, since such tractors usually operate with high tractive loads and the locking properties of the differential are needed precisely under these circumstances. For example, while plowing, when the wheels at one side of the tractor travel in the furrow and the gripping conditions of the axle's wheels are different. A differential with decreasing friction torque will not provide the necessary tractive properties under these conditions. However, in certain cases the use of such differentials on tractive vehicles can be justified. For example, in Section 6.4 a characteristic of this kind was synthesized for the differential of the rear axle of a 4×4 loader.

Still another class of differentials in which the locking coefficient depends on the applied torque T_0 is formed by mechanisms with constant primary friction torque. The friction clutches of these differentials are compressed by a constant force of precompressed springs or a hydraulic (pneumatic) cylinder with constant working-fluid (air) pressure. Figure 4.28 shows schematic diagrams of such mechanisms.

The clutches provide frictional coupling between the differential's case and the output shafts or between the output shafts.

When friction torque in one of the clutches of the differential from Figure 4.28a is T_{rp}, the primary friction torque in the two clutches is $2T_{rp}$:

$$2T_r = 2\mu Q_{sp} r_M i_M = \text{const} \tag{4.118}$$

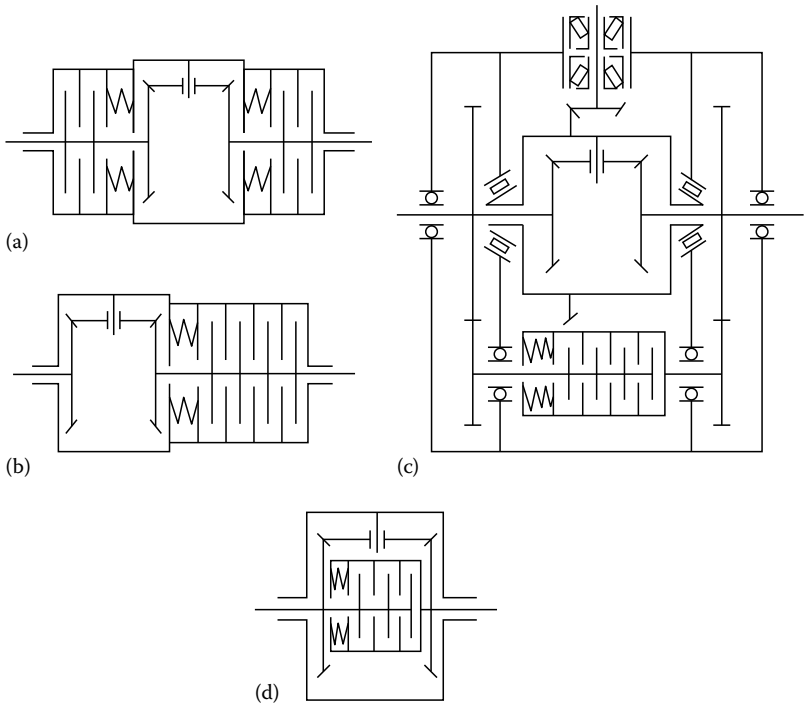


FIGURE 4.28
Schematic diagrams of differentials with constant friction torque.

where Q_{sp} is the clutch compression force. Then the locking coefficient of this differential is determined from expression (4.36):

$$K_d = K_{pu}\frac{T_0 + 2T_r}{T_0 - 2T_r} \tag{4.119}$$

Since T_{rp} is constant, whereas torque T_0 is variable, the locking coefficient K_d from (4.119) is a variable quantity and a function of T_0. As T_0 increases K_d decreases. The torque T_0 is a function of the tractive load of the vehicle and of the road-gripping conditions.

Figure 4.28b presents a schematic diagram of a differential one of the output shafts of which is linked to the casing of a multidisk clutch. The disks are subjected to a constant force. In spite of the fact that the differential has a single clutch, its primary friction torque T_{rp} is independent of which output shaft is the advancing one. Thus, if the shaft on the side of the clutch is the lagging one (see Figure 4.28b) and torque T' is transmitted to the advancing output shaft of the differential by the side gear, then the same torque is transmitted to the lagging output shaft by the second side gear in addition to torque T_{rp} from the clutch, that is,

$$T'' = T' + T_{rp}$$

whence,

$$T_{rp} = T'' - T' \tag{4.120}$$

If the lagging shaft is the one located at the side opposite of that of the friction clutch, then torque T'' at the lagging output shaft is caused by the torque applied by the side gear. The same torque is also transmitted to the advancing output shaft, but the friction torque T_{rp} is subtracted from that torque. For this reason the torque at the advancing output shaft is

$$T' = T'' - T_{rp}$$

whence again,

$$T_{rp} = T'' - T' \tag{4.121}$$

It is seen by comparing formulae (4.120) and (4.121) that the friction torque T_{rp} is always constant irrespective of which of the two output shafts advances. With reference to this, the locking coefficient is defined as

$$K_d = K_{pu}\frac{T_0 + T_{rp}}{T_0 - T_{rp}} \tag{4.122}$$

Figure 4.28c shows a schematic diagram of a differential in which the disk clutch with constant friction torque ($T_{rp} = \text{const}$) is connected between the output shafts by an external coupling. The primary friction torque for such a differential, with reference to the gear ratio u_r of the spur-gear couple is equal to $T_{rp}u_r$ and the torques at its output shafts when the differential is activated are:

$$\begin{aligned} T'' &= 0.5T_0 + T_{rp}u_r \\ T' &= 0.5T_0 - T_{rp}u_r \end{aligned} \tag{4.123}$$

The locking coefficient, accordingly, is

$$K_d = K_{pu}\frac{T_0 + 2T_r u_r}{T_0 - 2T_r u_r} \tag{4.124}$$

It is seen by comparing formulae (4.122) and (4.124) that, in order to provide for the same values of K_d, the friction torque of the clutch of the differential from Figure 4.28c can be $2u_r$-fold smaller than the friction torque of the clutch of the differential from Figure 4.28b.

A clutch may be placed between the output shafts of a differential by means of an internal coupling (Figure 4.28d). In this case, the primary friction torque is equal to torque T_{rp} at the clutch, and the locking coefficient:

$$K_d = K_{pu}\frac{T_0 + 2T_{rp}}{T_0 - 2T_{rp}} \tag{4.125}$$

Expression (4.125) is similar to (4.124). The difference consists in the absence of the term representing the effect of the external gear transmission (u_r).

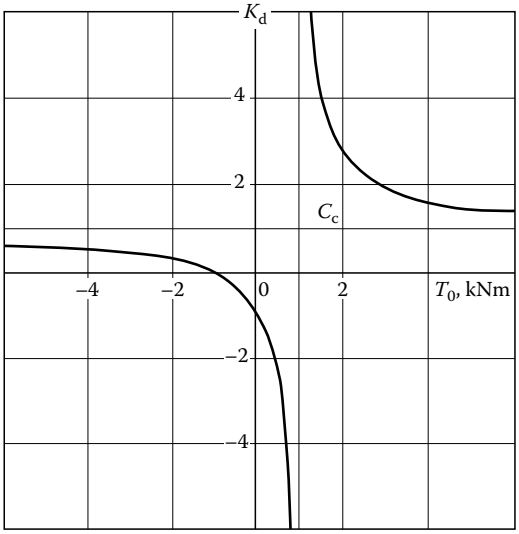


FIGURE 4.29
Locking factor of differential with constant friction torque.

Comparing formulae (4.119), (4.122), (4.124) and (4.125) makes it possible to compile a general formula for the locking coefficient of differentials with constant friction torque clutches

$$K_d = K_{pu}\frac{T_0 + C_c}{T_0 - C_c} \tag{4.126}$$

where C_c is a constant specific to the given mechanism. Formula (4.126) is plotted in Figure 4.29 from which it is seen that K_d decreases when torque T_0 increases.

This causes the locking performance of differentials with constant primary friction torque and of differential with decreasing primary friction torque to be similar (see Figure 4.27). In spite of this external similitude, these differentials exert a principally different effect on the axle's resistance to turn and on the vehicle's turnability (see Section 4.11).

Differentials with locking coefficient dependent on the input torque T_0 include mixed-type mechanisms that combine locking elements with properties specific to differentials with constant design K_d, with increasing and constant primary friction torques. Consider the schematic of one such differential (Figure 4.30).

Friction clutches 1 are compressed by springs 2 and are held in the differential's case 4 by means of snap ring 3. As long as the axial forces in the gear meshing, the values of which are a function of T_0, are smaller than the compression forces of the springs, the friction clutches transmit constant torques produced solely by the spring forces. Here the mechanism performs as a differential with constant primary friction clutches. When torque T_0 attains some value T_1, and upon a further rise in T_0, axial forces Q_a in the meshing exceed forces Q_{sp} and compress the friction clutches. In this case, the mechanism operates as a differential with constant design locking coefficient. Hence the formulae for the locking coefficient are:

at $T_0 \le T_1$,

$$K_d = K_{pu}\frac{T_1 + C_c}{T_0 - C_c}, \quad C_c = 2\mu Q_{sp} r_M i_M \tag{4.127}$$

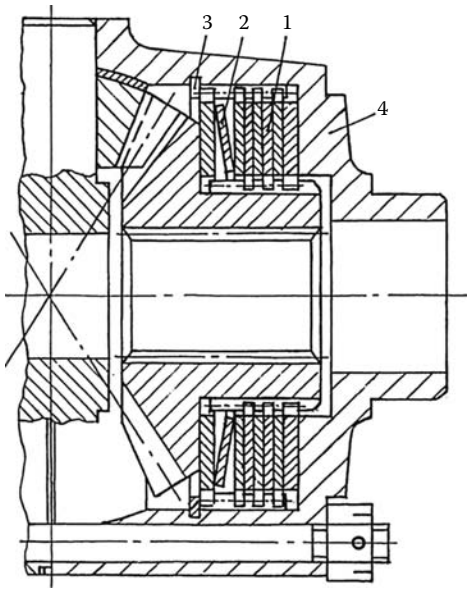


FIGURE 4.30
Mixed-type differential.

at $T_0 > T_1$,

$$K_d = K_{pu}\frac{(1+\mu A)}{(1-\mu A)}, \quad A = r_M i_M \tan\alpha_w \cos\delta_c / r_g \tag{4.128}$$

The results of calculations using formulae (4.127) and (4.128) are represented by curve 1 in Figure 4.31.

If the primary friction torque T_{rp} is a linearly increasing function of T_0 and $T_{rp} \neq 0$ at $T_0 = 0$, then the locking factor is equal to (see curve 2 in Figure 4.31):

$$K_d = K_{pu}\frac{(1+\mu A)T_0 + \mu C_c}{(1-\mu A)T_0 - \mu C_c} \tag{4.129}$$

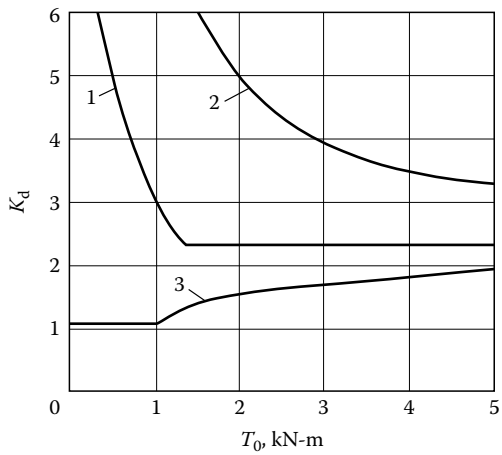


FIGURE 4.31
Properties of mixed-type differentials.

In the case when the locking properties of the differential do not come into play at $T_0 \leq T_2$, whereas at $T_0 > T_2$ the primary friction torque T_{rp} is a linearly increasing function of T_0, the locking coefficient of such a differential is given by the expressions:

$$K_d = \begin{cases} K_{pu} & \text{at } T_0 \leq T_2 \\ \dfrac{(1+\mu A)T_0 - \mu C_c}{(1-\mu A)T_0 + \mu C_c} & \text{at } T_0 > T_2 \end{cases} \tag{4.130}$$

In formulae (4.129) and (4.130) the parameters C_c and A are determined in the same manner as in formulae (4.127) and (4.128). Formulae (4.130) are represented by curve 3 in Figure 4.31.

In addition to the specifics of the locking properties shown in Figure 4.31 it is possible to compile also different formulae for calculating the locking coefficient by proceeding similarly. The large variety of designs of mixed-type differential stems from the intended purpose and specific operational conditions of the vehicles in which these mechanisms are to be used.

Studies carried out over a large number of years in power-dividing units of the same vehicle show that at times it is necessary to use limited slip differentials with different locking properties. In conjunction with this, the design of these differentials should be unified based on the use of design elements of the same type. Actually, however, differentials are produced by different companies and are used on different vehicles, for which reason they are comprised of different types of elements. Figure 4.32 shows design schematics of unified limited slip differentials that exhibit different locking properties depending on the placement and interaction of typical elements of only slightly modified design.

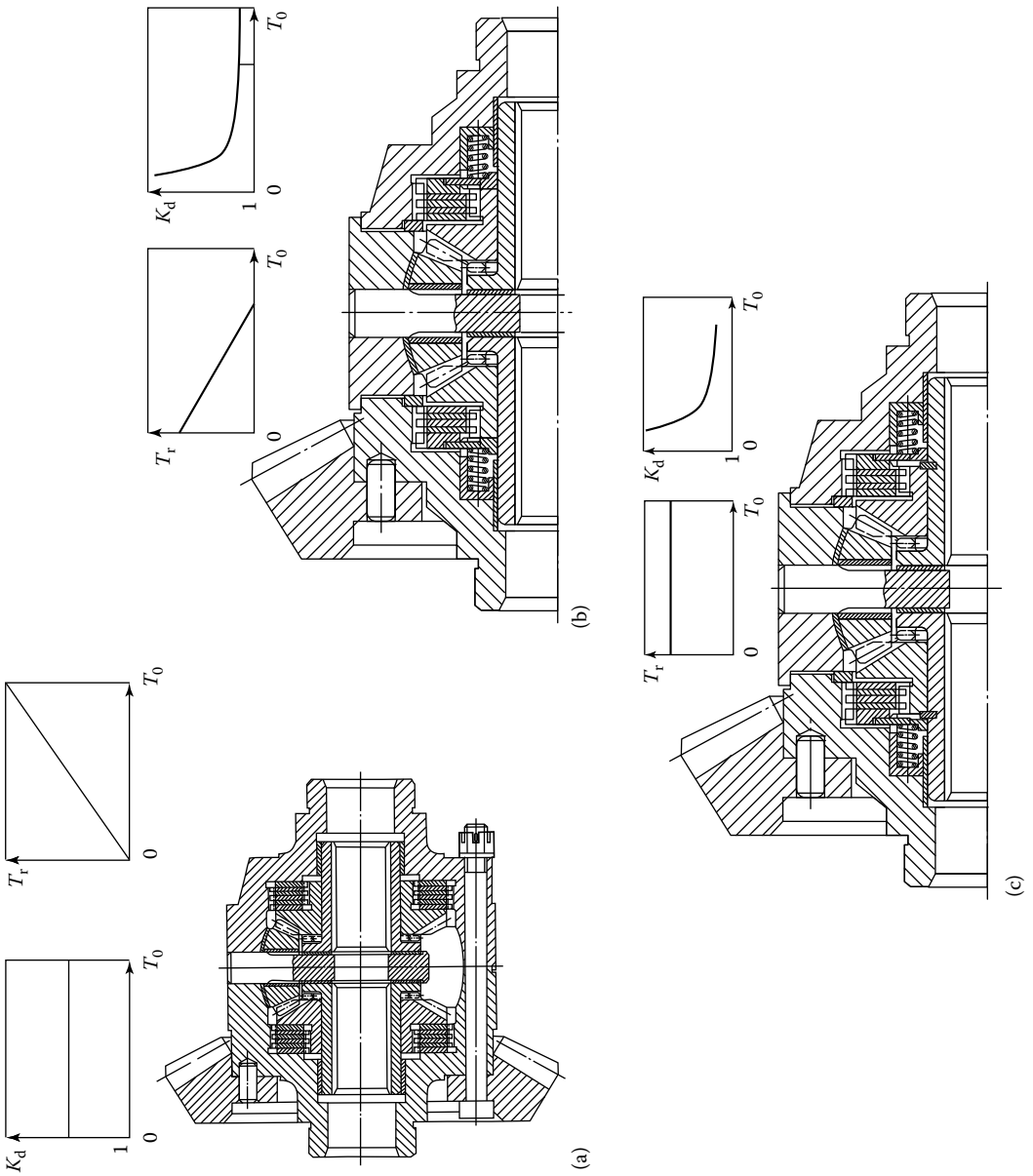
The differentials employ cylindrical springs that are inserted into separately assembled elastic stacks. The locking coefficient of the differential from Figure 4.32a can be calculated from formulae (4.50). Formulae for calculating K_d of differentials from Figure 4.32b and c can be obtained using the data in the present section and formulae (4.111) and (4.126). Formulae (4.127) and (4.128), (4.129) and (4.130) can be used for deriving new formulae for calculating K_d of differentials from Figure 4.32d through f. It is suggested that the reader derive these formulae.

Some of the layouts shown in Figure 4.32 were used for designing limited slip differentials. In Chapter 6, for example, in Figure 6.17 the unified limited slip differentials for the front and rear axles of a 4×4 single-bucket loader and the design and experimental performance curves of the differentials are shown. These differentials used plate-type springs instead of cylindrical springs. The locking properties of the differentials were proved using a methodology described in Section 6.4, whereas the geometric parameters were selected based on formulae for the locking factors analyzed in the present section.

Figure 4.33 shows an interwheel limited slip differential for the front axles of 186–300 kW 4×4 farm tractors, for the rear axles of 110 and 135 kW 6×6 articulated tractors with front steered wheels and for the rear axles of 60 kW 4×4 articulated tractors.

This is a limited slip differential, the locking properties of which come into play in tractors with traction loads (plowing, cultivating, etc.). The mechanism functions as an open differential when the tractor moves over high-grade roads. The performance curve of the locking properties of the differential is shown in Figure 4.34.

The values of the locking coefficient were selected on the basis of optimum distribution of power between the wheels of the tractors that would ensure high-traction performance when working with farm machinery that require traction torques T_0 shown in Figure 4.34 for the case of 6×6 tractors.


K_d
1
0
T_0
T_r
0
T_0
(a)
K_d
1
0
T_0
T_r
0
T_0
(b)
K_d
1
0
T_0
T_r
0
T_0
(c)

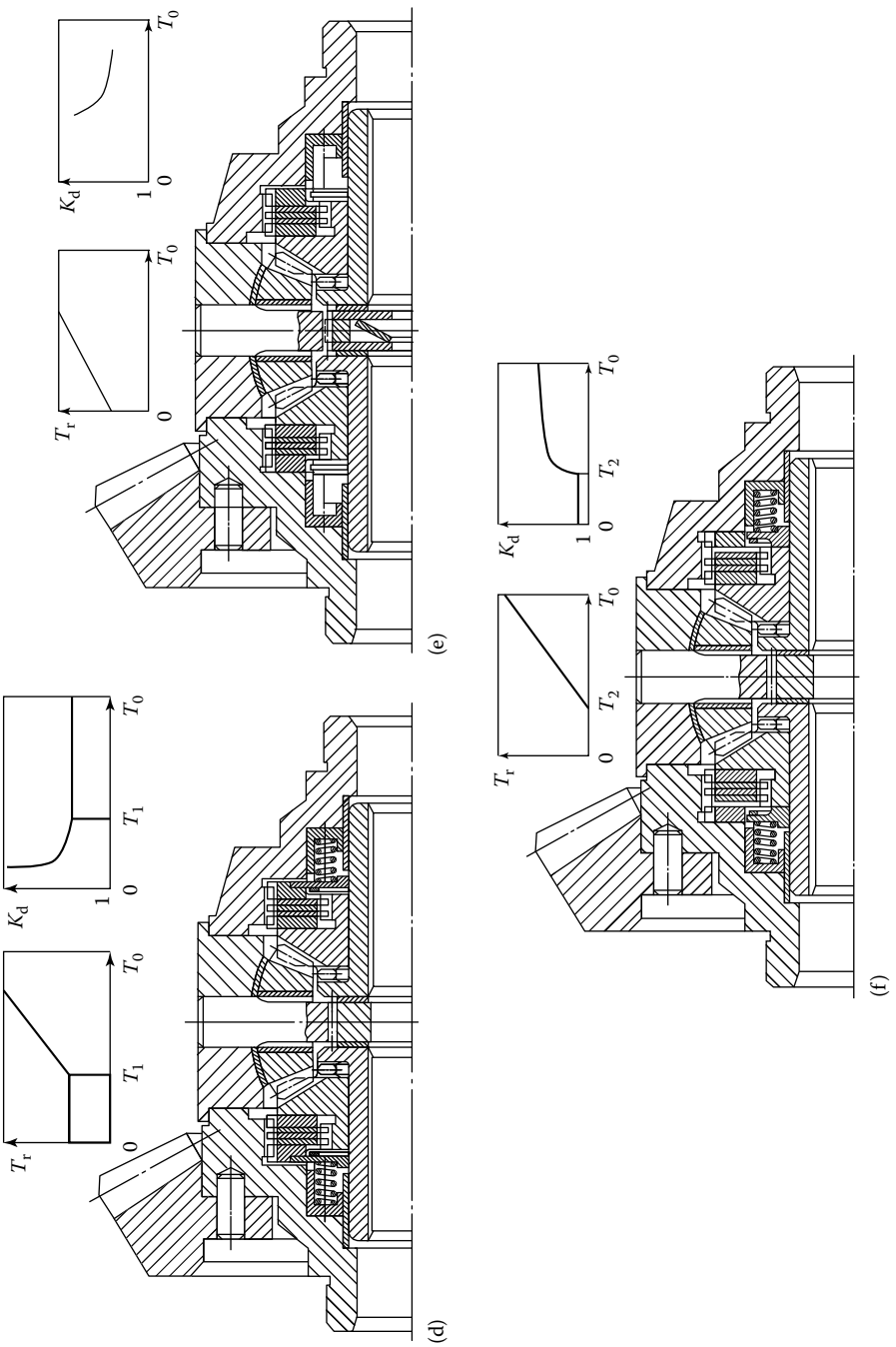


FIGURE 4.32
Unified limited slip differentials.

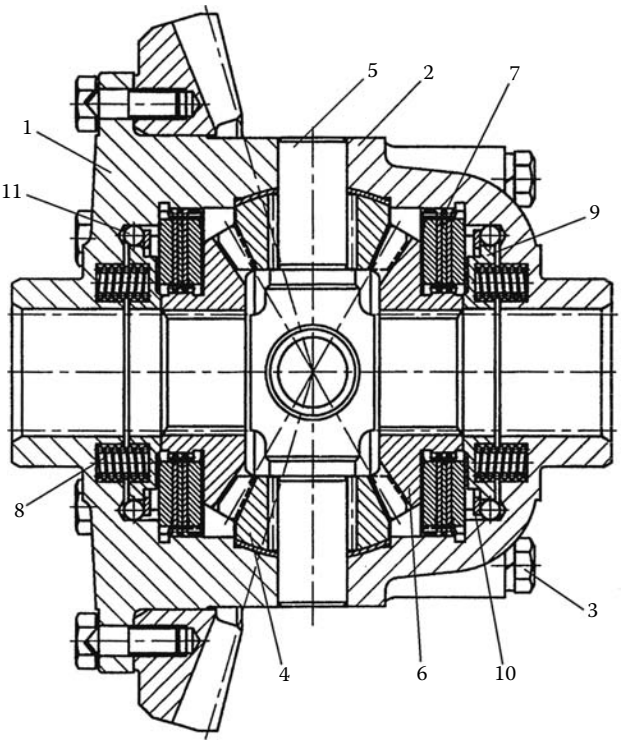


FIGURE 4.33
Limited slip differential.

Four bevel gear pinions 4 on spider 5 and side gears 6 capable of axial movement are held in case 1 and cover 2 of the differential (see Figure 4.33) bolted together by bolts 3. Disk clutches 7, the drive disks of which are splined to case 1 and cover 2 and the driven disks of which are connected to side gears 6, are located between case elements 1 and 2 and side gears 6. Case elements 1 and 2 have recesses machined into them. Precompressed elastic elements (springs) 8 bear on these recesses by one of their ends, whereas the other end of these elements bears against recesses in disks 9 placed in the case elements. These disks are capable of axial movement that is limited by retaining rings 10. Disks 9 are secured against turning by means of retaining balls 11.

The differential operates as follows. When no torque T_0 is applied to case elements 1 and 2, there is clearance between the ends of side gears 6 and their closest disks 7 of the friction clutches, and between the disks of the friction clutches. This provides free rotation in the friction clutches and absence of friction between them.

When torque starts being applied to the differential's case elements and keeps on increasing, the axial components of the forces of the bevel-gear meshing of pinions 4 and side gears 6 start acting through their small ends on disks 9, forcing elastic elements 8 to compress. Here the friction-disk clutches, because of insufficient forces in the meshing between the pinions and the side gears are not compressed to take the entire clearances in the clutches and they are not subjected to friction torque. This occurs until the total axial components of the bevel gear meshing become equal to the forces exerted by the compressed elastic elements.

As the torque T_0 is increased further, the exceeding axial components of the forces of the bevel gear meshing of pinions 4 and side gears 6 will compress elastic elements 8 by the amount of the above clearances. Here the disks closer to the case elements will push against them. As the torque is increased even further, the components of these forces will press,

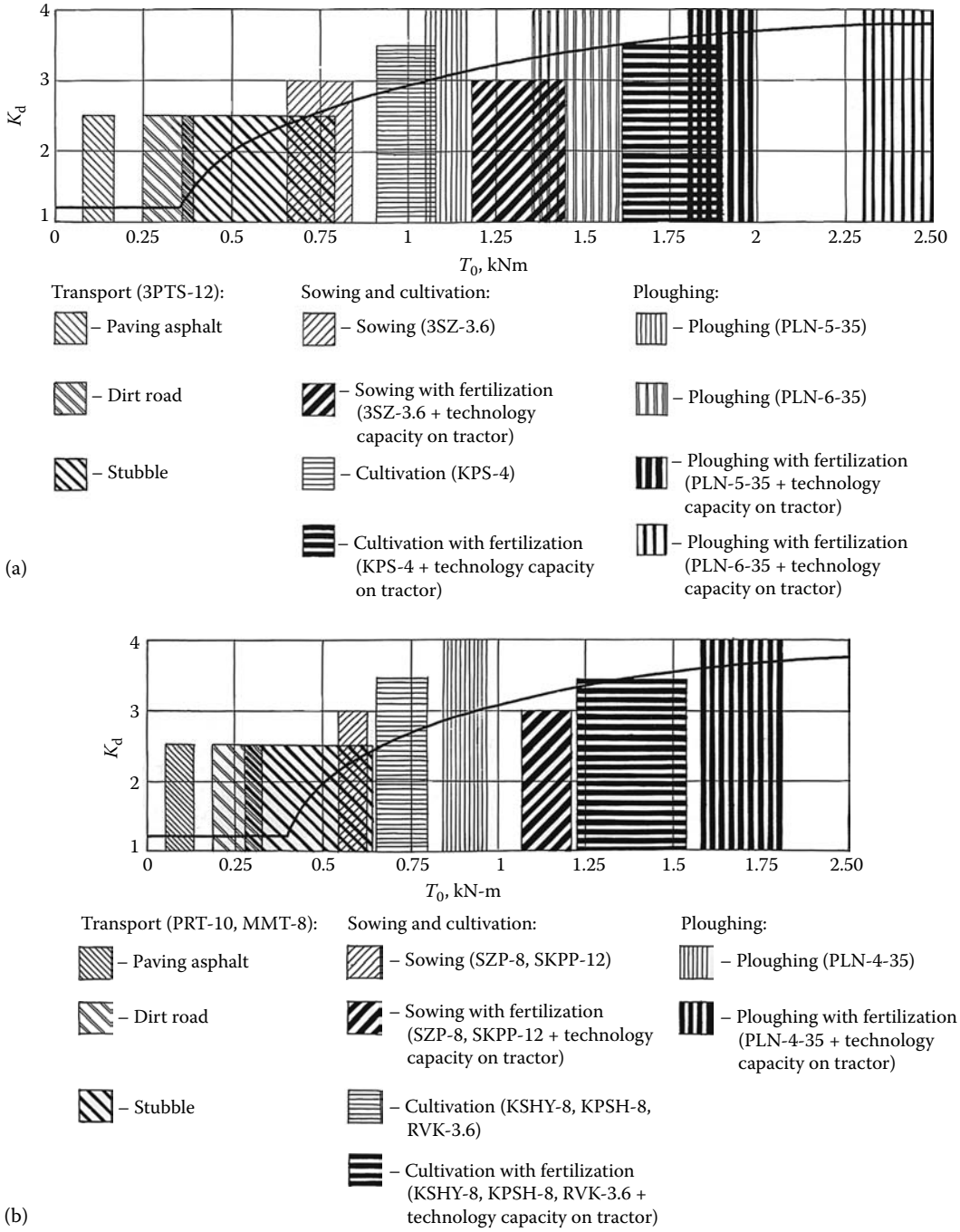


FIGURE 4.34
Locking properties of the differential from Figure 4.33.

though the large ends of side gears 6, the friction-clutch disks to one another. As a result, a friction torque will appear in the friction clutches and will increase with the torque at case elements 1 and 2 and induce the required locking action. The locking properties of such a differential are brought into play within the range of traction loads of a tractor that operates farming equipment.

4.8 Speed Sensitive Differentials

The term ''speed sensitive differentials'' is applied in the engineering literature and in industrial practice to a class of limited slip differentials the locking properties of which depend on the difference in angular velocities of their principal components: the case and the output shafts. These mechanisms include differentials with hydraulic resistance. The principal device that provides the differential with locking properties is a hydraulic pump.

The design and operating principle of these differentials consists in the following. An oil pump (gear-type, gerotor-type, plunger-type, impeller or other) is installed between two links of the mechanism. The driving shaft is linked to one of the mechanism's links whereas the pump's casing is connected to the other. When the links of the differential rotate relative to one another, the shaft and the casing of the pump also perform relative rotation. The pump pumps oil through small-diameter calibrated apertures. The resistance of these apertures to the flow of oil produces a load torque at the pump shaft and a reactive torque of the same magnitude on the pump casing. These torques bring about redistribution of torques between the output shafts of the differential mechanism.

Figure 4.35 shows a schematic of a speed sensitive differential with a hydraulic resistance in which a plunger-type rotary pump is built in between one of the output shafts and the case.

One of cups 4 of this differential is made in the form of a cylinder block and has radial openings A in which is located plungers 3. Cam sprocket 1 is seated on the splines of

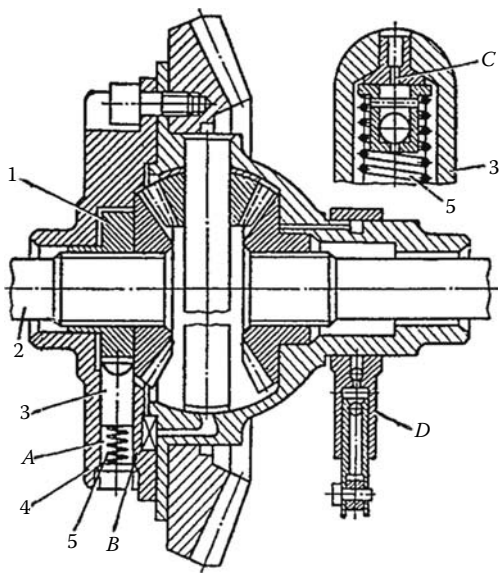


FIGURE 4.35
Differential with hydraulic resistance.

output shaft 2. The plungers are pressed to the cams by springs 5. Each plunger 3 is provided with a valve device with calibrated aperture *C*, intended for discharging the oil. The cylinder block has discharge ports *B* with valves through which the oil from the differential's case flows into the cylinders. Special device *D* provides for continuous supply of oil inside the differential's case.

When the vehicle motion is rectilinear and there is no separate slippage of wheels, the plunger pump does not operate. However, when the wheels rotate at different angular velocities (separate wheel slippage, making a turn) the cams move in sequence onto the plungers which, moving in the radial direction, push the oil through calibrated ports *C* and produce a pressure in the system. The elevated oil pressure in its turn increases the circumferential forces in the points of interaction between the cams and the plungers, and this produces additional torques at the output shaft and the differential's case that are equal in magnitude and of opposite sign.

Determining the locking coefficient of the differential. It is known that the resistance to flow of a fluid through a port is proportional to the square of the fluid flow, which is proportional to the relative velocity of the shaft and the pump's casing. In this case, it is convenient to express the resistance to fluid flow in terms of the torque T_{rp} at the shaft and at the pump casing.

The pressure difference produced by the pump is calculated from the formula

$$\Delta p = \zeta \frac{\rho_o}{2} \left(\frac{Q}{z A_o} \right) \tag{4.131}$$

where

ζ is the drag coefficient of the throttling aperture
ρ_o is the density of the working fluid
Q is the pump capacity
z is the number of throttling apertures
A_o is the net cross sectional area of the throttling aperture

The pump capacity is given by the expression

$$Q = \eta_v V_o n_{\text{rel}} = \frac{\eta_v V_o}{2\pi} \omega_{\text{rel}} \tag{4.132}$$

where

η_v is the volumetric efficiency of the pump
V_o is the working volume of the pump
n_{rel} is the pump shaft (output shaft of the differential) rpm relative to the casing
ω_{rel} is the relative angular velocity of the output shaft

Substitution of expression (4.131) into (4.132) yields

$$\Delta p = \zeta \frac{\rho_o}{8\pi^2} \left(\frac{\eta_v V_o}{z A_o} \right)^2 \omega_{\text{rel}}^2 \tag{4.133}$$

The pump's resistance torque T_{rp}

$$T_{\text{rp}} = \frac{\eta_v}{\eta}\frac{\Delta p V_o}{2\pi} \tag{4.134}$$

where η is the total efficiency of the pump.

Substitution of Δp from expression (4.133) into formula (4.134) yields

$$T_{\text{rp}} = \frac{\zeta \rho_o (\eta_v V_o)^3}{16\pi^3 \eta (zA_o)^2}\omega_{\text{rel}}^2 = c_\omega \omega_{\text{rel}}^2 \tag{4.135}$$

here, $c_\omega = \dfrac{\zeta \rho_o (\eta_v V_o)^3}{16\pi^3 \eta (zA_o)^2}$.

Since the pump is installed between the case and one of the output shafts, the relative angular velocity is

$$\omega_{\text{rel}} = \omega' - \omega_0 = 0.5(\omega' - \omega'') \tag{4.136}$$

Upon substitution of expressions (4.135) and (4.136), formula (4.36) for calculating the locking coefficient of a differential with a hydraulic resistance can be written as:

$$\begin{aligned} K_{\text{d}} &= K_{\text{pu}}\frac{T_0 + T_{\text{rp}}}{T_0 - T_{\text{rp}}} = K_{\text{pu}}\frac{T_0 + c_\omega \omega_{\text{rel}}^2}{T_0 - c_\omega \omega_{\text{rel}}^2} \\ &= K_{\text{pu}}\frac{T_0 + 0.25 c_\omega (\omega' - \omega'')^2}{T_0 - 0.25 c_\omega (\omega' - \omega'')^2} \end{aligned} \tag{4.137}$$

Figure 4.36 is a plot of expression (4.137) at variable ω_{rel}.

It is seen that low values of ω_{rel} of links during the vehicle's turn do not produce extensive locking in a differential with a hydraulic resistance. For this reason, virtually no moment from the redistribution of circumferential forces between the wheels of the axle that would interfere with the turn arises in the plane of the road (for more details see Section 4.11). At the same time, the elevated values of ω_{rel} when individual wheels slips create the redistribution of torques between the wheels, which provides for improved mobility of wheeled vehicles under off-road conditions. It is seen from formula (4.137) that the locking coefficient of the differential depends also on torque T_0 at the mechanism's case.

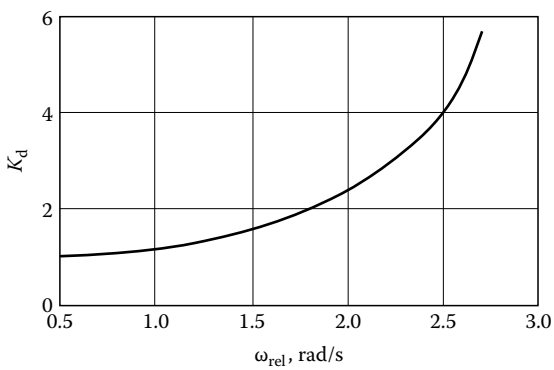


FIGURE 4.36
Locking coefficient of a differential with hydraulic resistance.

Whereas the use of differential with hydraulic resistance on high-speed cars is justified, their use on heavy-duty, high-mobility vehicles is far from being advisable, because the numerical values of ω_{rel} upon separate slippage of wheels in low gear do not differ much from ω_{rel} of a vehicle making a turn at high speed.

It is rather obvious that differentials with a hydraulic resistance are not suitable for tractors and excavation vehicles. It was found that their wheels rotate at different angular velocities as a result of unequal slippage for prolonged periods of time when working in soft soils; here the values of ω_{rel} are rather low. This happens, among others, when plowing when the wheels of one side move in the furrow and those of the other side on stubble. In addition, the example presented below manifests the technical difficulties of making such mechanisms for off-road vehicles. For example, for a 4×2 vehicle with gross weight of $W_a = 100$ kN, rolling radius in the driven mode of $r_w^0 = 0.465$ m and resistance to motion of $\psi = 0.2$ (includes resistance to the rolling of the vehicle's wheels and resistance to uphill motion) requires the following torque at the differential's case

$$T_0 = \psi W_a r_w^0 = (0.2)(100)(0.465) = 9.3 \text{ kN-m}$$

The pump torque T_{rp} needed for attaining a locking coefficient of $K_d = 3$ is obtained from formula (4.137) at $K_{pu} = 1.17$ (see Table 4.2):

$$T_{rp} = \frac{K_d/K_{pu} - 1}{K_d/K_{pu} + 1} T_0 = \frac{3/1.17 - 1}{3/1.17 + 1} 9.3 = 4.1 \text{ kN-m}$$

At maximum pressure $\Delta p = 40$ MPa of the working fluid at the pump discharge, the pump's working volume V_0 is given by formula (4.134) (not corrected for the efficiency) as:

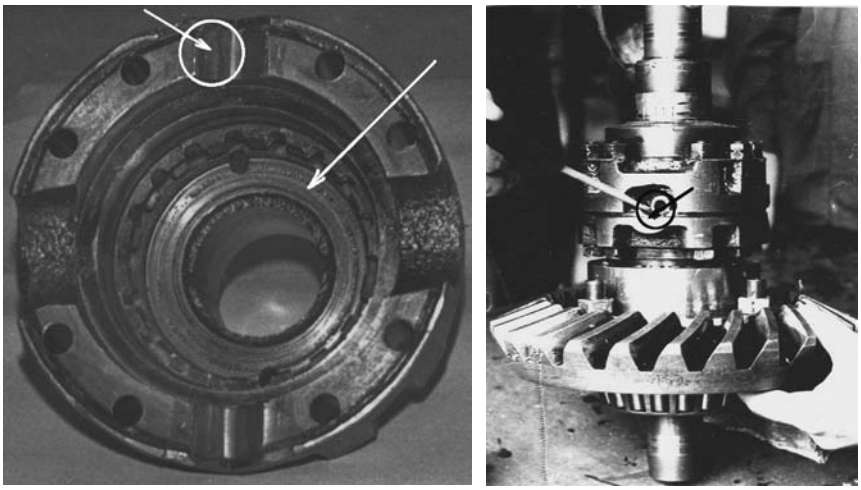
$$V_0 = \frac{2\pi T_{rp}}{\Delta p} = \frac{(2)(3.14)(4100)}{40} = 644 \text{ cm}^3$$

In certain existing differentials the peak values of torque T_{rp} are approximately 2.7 kNm when ω_{rel} attains values of $5.5 - 6$ rad/s.

4.9 Force Fluctuations in Disk Differentials

Experience in the use of limited slip differentials shows that premature wear and scuffing in the points of contact between the case and the clutch disks (see the right-hand arrow in Figure 4.37a), wear of pins beneath the pinions and scuffing of the disk surfaces are observed in certain cases.

Excessive wear was detected in the V-shaped grooves in the case at the contact with the pinion pins (left arrow in Figure 4.37a). The wear of grooves of the differential's case in some mechanisms was as much as 0.5–1.3 mm after 6000–7000 h of operation. This increases the travel of the floating pins with pinions (see Figure 4.37b), something that has a negative effect on the meshing of the pinions with the differential's side gears. Fluctuation of torques at the output shafts of differentials and, with this, instability of the locking coefficient K_d and a reduction in this factor upon extended operation of the vehicle were also observed.



(a) (b)

FIGURE 4.37
Differential showing places of wear.

One of the principal reasons for the above is the oscillatory nature of the total axial forces of meshings and of the side gears, which was discussed in Section 2.3. Since the manner of variation in the axial forces is determined by the ratio of z_c, the number of teeth of the pinions and the side gears z_g, the variation in K_d also depends on these ratios. Determine K_d of limited slip differentials in which the friction clutches are compressed by forces of bevel gear meshing of the pinions and side gears with different combinations of the number of teeth. The torques of the friction clutches are:

$$T_r'' = \mu Q_{al} r_M i_M, \quad T_r' = \mu Q_{ar} r_M i_M \tag{4.138}$$

or

$$T_r'' = \mu r_M i_M \frac{T_0}{8r_g} Y_l, \quad T_r' = \mu r_M i_M \frac{T_0}{8r_g} Y_r \tag{4.139}$$

where Y_l and Y_r are the ordinates of the total specific axial forces $(8r_g/T_0)Q_{al}$ and $(8r_g/T_0)Q_{ar}$ from Figures 2.20, 2.22, 2.26, and 2.29 that were constructed for four possible combinations of z_c and z_g. Substitution of formulae (4.36) and (4.139) allows obtaining the following expression for the locking coefficient:

$$K_d = K_{pu} \frac{1 + (8r_g/T_0)(Y_l + Y_r) r_M i_M \mu}{1 - (8r_g/T_0)(Y_l + Y_r) r_M i_M \mu} \tag{4.140}$$

Figure 4.38 is a plot of values of K_d given by formula (4.140) for four differentials with different combinations of z_c and z_g that cause variation in axial forces on the previously mentioned figures.

Parameters (r_g, r_M, i_M) of the differentials were selected in such a manner that the mechanisms would have approximately the same values of K_d calculated at

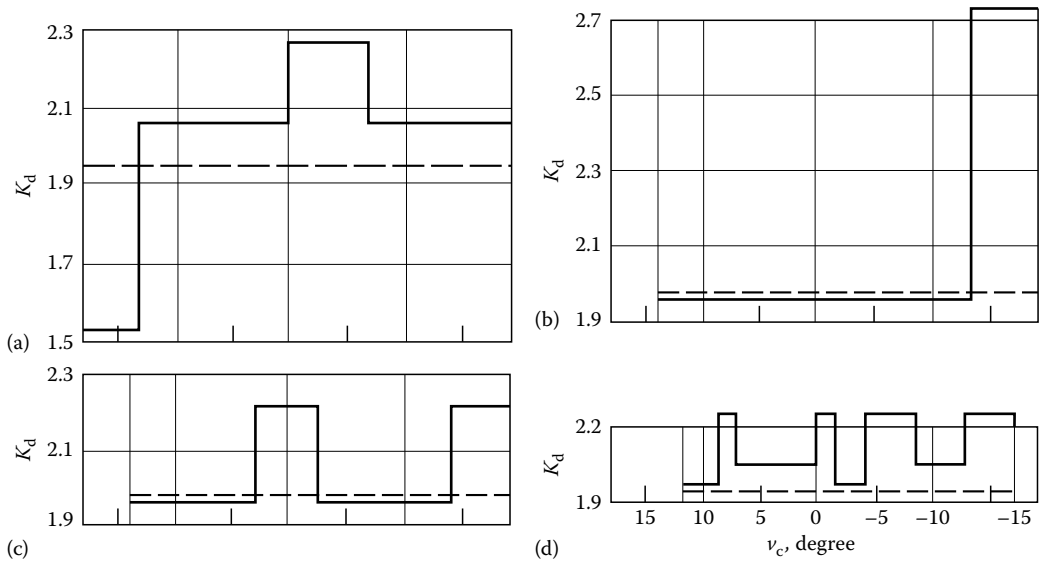


FIGURE 4.38
Locking factor of differentials of four groups with different combinations of z_c and z_g, group: (a) I; (b) II; (c) III; (d) IV.

$\alpha_k = \alpha_w = \text{const}$. The variations in axial forces in the meshings between the pinions and the side gears bring about the step-wise behavior of the locking coefficient in Figure 4.38. The variation in this factor is represented by the ratios:

$$K_{\max} = K_d^{\max}/K_d, \quad K_{\text{ext}} = K_d^{\max}/K_d^{\min} \tag{4.141}$$

where $K_d^{\max}$ and $K_d^{\min}$ are the limiting values of K_d from Figure 4.38, whereas K_d is the value of the locking coefficient calculated without allowance for the fluctuations (see dash lines in Figure 4.38). The values of coefficients from formulae (4.141) determined based on Figure 4.38 are listed in Table 4.3.

Now consider the reasons for the wear of the grooves in the differential's case in the contact with the floating pinion pins (see Figure 4.37). Usually axial forces Q_0 in these grooves are calculated with reference to Figure 4.13, which yields

$$Q_0 = F \tan \varphi_k = \frac{T_0}{4r_0} \tan \varphi_k \tag{4.142}$$

TABLE 4.3
Change in Torque Biases

Group	r_g, mm	r_M, mm	i_M	K_d	$K_{\max}$	K_{ext}
I	29.6	33.5	7	1.94	1.170	1.500
II	44.5	51.4	7	1.96	1.382	1.383
III	44.0	50.0	7	1.98	1.130	1.150
IV	59.0	43.5	10	1.97	1.185	1.180

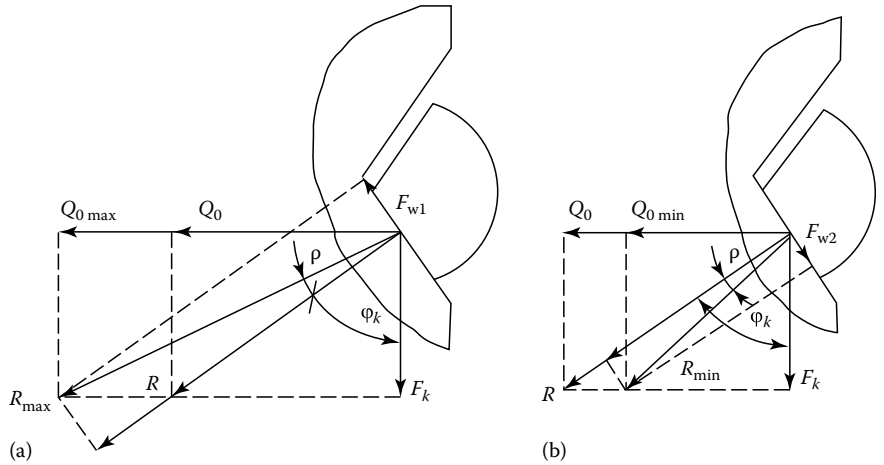


FIGURE 4.39
Forces applied to the groove in the case by the pinion pins.

However, it was noted in the course of testing these differentials that the axial forces Q_0 fluctuate. It was established as a result of a large number of experiments that this happens because of the unstable, variable thickness of the disk's stacks of the friction clutches. When the disks slide relative to one another, the thickness of the stack varies from some minimum to some maximum value. This stems from certain out of flatness of the disks. This fluctuation in the thickness of the disk stacks causes cyclical sliding of the pinion pins over the surface of the grooves in the case. The latter, with consideration of friction, produces a cyclical variation in the axial forces in the contacts between the pinion pins and the case. When the stack thickness increases, the axial force Q_0 rises to the value $Q_{0\,max}$ (Figure 4.39a) at which the resultant force deviates through friction angle ρ from the normal to the working surface of the groove and force F_{w1} becomes equal to the static friction force in the contact between the pinion pin and the groove in the case.

The axial forces vary similarly upon a reduction in thickness of the disk stack (Figure 4.39b). The minimum and maximum values of the axial forces brought about by the relative sliding of the disks must be calculated from the expressions:

$$\begin{aligned} Q_{0\,max} &= \frac{T_0}{4r_0}\tan(\varphi_k + \rho) \\ Q_{0\,min} &= \frac{T_0}{4r_0}\tan(\varphi_k - \rho) \end{aligned} \tag{4.143}$$

The fluctuations in axial forces caused by the out of flatness of the clutch disks can be assessed by means of factors representing the extent of variation in these forces:

$$K_{k1} = Q_{0\,max}/Q_0, \quad K_{k2} = Q_{0\,max}/Q_{0\,min} \tag{4.144}$$

where Q_0 is calculated from formula (4.142). Substitution of (4.143) yields

$$K_{k1} = \tan(\varphi_k + \rho)/\tan\varphi_k, \quad K_{k2} = \tan(\varphi_k + \rho)/\tan(\varphi_k - \rho) \tag{4.145}$$

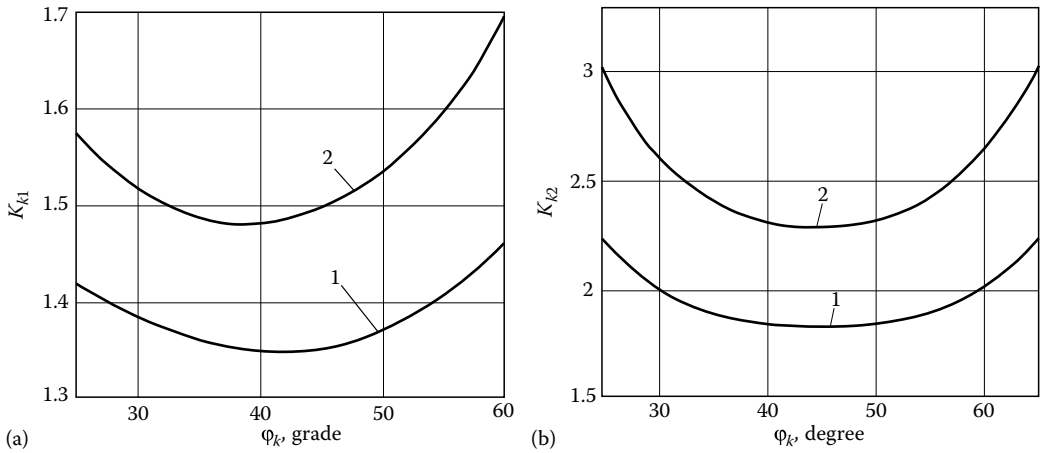


FIGURE 4.40
Factor of variation in axial forces in the contact between the pinion pins and the grooves in the case, μ_s: (1) 0.15; (2) 0.20.

Formula (4.145) is plotted in Figure 4.40 for different values of static friction factor μ_s corresponding to different values of friction angle ρ.

It follows from formulae (4.145) that the extent of variation in the axial forces depends not only on the conditions of friction between the pinion pins and the case, but also of angle φ_k—the design parameter of the differential. Thus, at $\mu_s = 0.15$ and $\varphi_k = 55^\circ$ the maximum axial forces $Q_{0\max}$ exceed the calculated Q_0 by a factor of 1.42 and at $\varphi_k = 45^\circ$, by a factor of 1.35.

The variation in the axial forces changes projections $R_{\max}$ and $R_{\min}$ on the normal to the plane of the groove, that causes a change in pressure q_k in the contact between the pinion pins and the groove. The maximum pressure is determined from Figure 4.39a as

$$q_{k\max} = R_{\max} \cos \rho / A \tag{4.146}$$

where A is the area of contact of one groove with a pinion pin. It follows from Figures 4.39a and 4.13 that

$$R_{\max} = T_0 / [4r_0 \cos (\varphi_k + \rho)] \tag{4.147}$$

Then

$$q_{k\max} = T_0 \cos \rho / [4r_0 A \cos (\varphi_k + \rho)] \tag{4.148}$$

By analogy with Figure 4.39b the minimum pressure is

$$q_{k\min} = T_0 \cos \rho / [4r_0 A \cos (\varphi_k - \rho)] \tag{4.149}$$

Figure 4.41a is a plot of the calculated pressure in the contact between the pinion pins and the groove in the case of the differential of the front axle of a 3.7-ton tractor at variable angle φ_k.

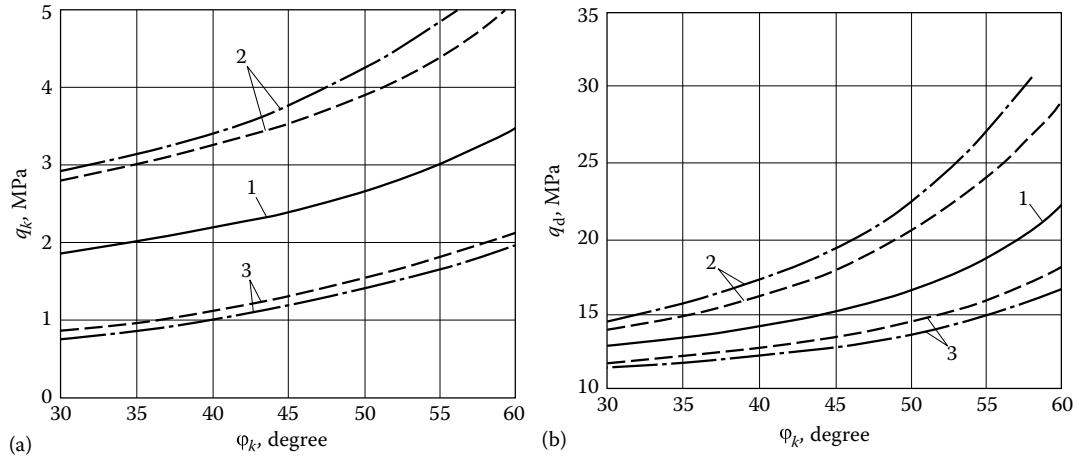


FIGURE 4.41
Pressure at the elements of the differential as a function of angle φ_k at $T_0 = 0.4$ kN-m. (a) Pressure at the grooves; (b) pressure at the disks; μ_s: ———, 0; — —, 0.15; —·—, 0.20.

Curve 1 corresponds to pressure q_k, without correction for friction between the pinion pin and the groove in the case, whereas curves 2 and 3, to pressures $q_{k\max}$ and $q_{k\min}$ corrected for this friction. At $\varphi_k = 55^\circ$ $q_{k\max}$ exceeds q_k by a factor of 1.28. Reducing φ_k to 45° reduces $q_{k\max}$ by a factor of 1.4 as compared with its value at $\varphi_k = 55^\circ$.

The fluctuations in axial forces in the grooves of the differential's case caused by a variation in the thickness of the disk stacks in the course of their relative sliding cause pressure changes at the disks themselves.

The variable axial forces of additional lockers and of the axial forces of bevel-gear meshings of the limited slip differential bring about a marked variation in the total internal axial forces.

To determine the extremal pressure on disks caused by these forces:

$$\begin{aligned} q_{d\max} &= q_{da\max} + q_{dk\max} \\ q_{d\min} &= q_{da\min} + q_{dk\min} \end{aligned} \tag{4.150}$$

where

$q_{da\max}$ and $q_{da\min}$ are the maximum and minimum pressure at the disks caused by extremal axial forces of the meshings between the pinions and side gears

$q_{dk\max}$ and $q_{dk\min}$ are the same and caused by axial forces in the contact between the pinion pins and the case

Other possible combinations of axial forces of the meshing and of additional locking devices correspond to pressure at the disks within the range $[q_{d\max}; q_{d\min}]$. The calculated pressures of the differential's disks are plotted in Figure 4.41b. Curve 1 shows the variation in the total pressure q_a at the disks produced by forces Q_a and Q_{gb} calculated from formulae (2.84) and (4.70). Curves 2 and 3 reflect the total pressures $q_{d\max}$ and $q_{d\min}$ from formulae (4.150). It is seen that pressure $q_{d\max}$ at $\varphi_k = 55^\circ$ exceeds q_d by a factor of 1.45.

Fluctuations of pressure at the disks between $q_{\mathrm{d\,max}}$ and $q_{\mathrm{d\,min}}$ change the friction torques in the clutches and, accordingly, the coefficient K_{d}. The maximum and minimum possible values of this coefficient for the differential from Figure 4.13 are determined from the corresponding friction torques in the two disk clutches:

$$\left(T''_{\mathrm{rp}} + T'_{\mathrm{rp}}\right)_{\max} = \left[\frac{T_0}{8r_{\mathrm{g}}} Y_{\mathrm{l\,max}} + \frac{T_0}{2r_{\mathrm{gb}}} \tan\left(\varphi_k + \rho\right)\right] \mu r_{\mathrm{M}} i_{\mathrm{M}} + \left[\frac{T_0}{8r_{\mathrm{g}}} Y_{\mathrm{r\,max}} + \frac{T_0}{2r_{\mathrm{gb}}} \tan\left(\varphi_k + \rho\right)\right] \mu r_{\mathrm{M}} i_{\mathrm{M}} \tag{4.151}$$

where $Y_{\mathrm{l\,max}}$ and $Y_{\mathrm{r\,max}}$ are the ordinates of the total specific axial forces $(8r_{\mathrm{g}}/T_0)Q_{\mathrm{al}}$ and $(8r_{\mathrm{g}}/T_0)Q_{\mathrm{ar}}$ from Figure 2.20 that correspond to the maximum of K_{d} in Figure 4.38a;

$$\left(T''_{\mathrm{rp}} + T'_{\mathrm{rp}}\right)_{\min} = \left[\frac{T_0}{8r_{\mathrm{g}}} Y_{\mathrm{l\,min}} + \frac{T_0}{2r_{\mathrm{gb}}} \tan\left(\varphi_k - \rho\right)\right] \mu r_{\mathrm{M}} i_{\mathrm{M}} + \left[\frac{T_0}{8r_{\mathrm{g}}} Y_{\mathrm{r\,min}} + \frac{T_0}{2r_{\mathrm{gb}}} \tan\left(\varphi_k - \rho\right)\right] \mu r_{\mathrm{M}} i_{\mathrm{M}} \tag{4.152}$$

where $Y_{\mathrm{l\,min}}$ and $Y_{\mathrm{r\,min}}$ are the ordinates of forces $(8r_{\mathrm{g}}/T_0)Q_{\mathrm{al}}$ and $(8r_{\mathrm{g}}/T_0)Q_{\mathrm{ar}}$ from Figure 2.20 that correspond to the minimum of K_{d} in Figure 4.38a. The results of calculations performed using formulae (4.36), (4.151) and (4.152) are shown in Figure 4.42 curves 2 and 3.

Curves 1 reflect the values of K_{d} determined without correction for fluctuations in the friction torques of the clutch.

Note that the fluctuations in the values of K_{d} improve the vehicle's mobility. Moreover, differentials exist that induce periodic fluctuations in the power gear ratio using teeth with a special profile or elliptically shaped pinions. These fluctuations in the locking coefficient (see Figure 4.42) stem from variation in the axial forces of bevel-gear meshings and

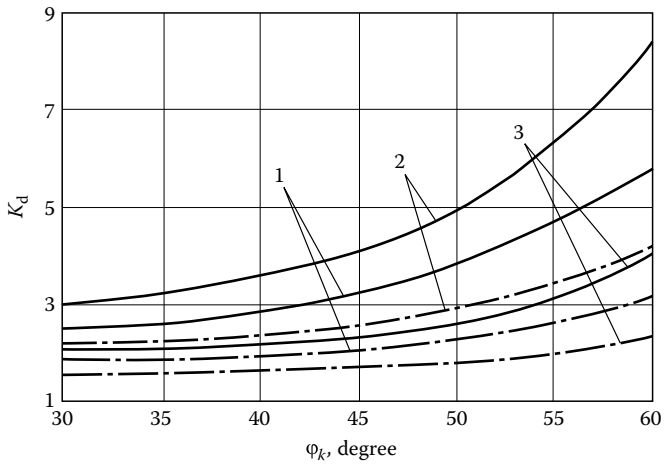


FIGURE 4.42
Locking coefficient K_{d} as a function of angle φ_k. i_{M}: —·—, 3; ———, 5.

additional lockers, the maximum values of which are not incorporated in the current computational methods. An increase in the axial forces in the course of their fluctuations causes pressure rises at the clutch disks and other components and an elevated wear of the latter. It hence becomes necessary to find a way for eliminating or at least limiting this occurrence (e.g., reducing the pressure at the friction pairs, improving their lubrication, increasing the precision of component manufacture, etc.).

It is very important to properly select the optimum value of angle φ_k that controls the axial forces, including their maximum value. From the point of view of fluctuations in the internal forces of differentials the values of φ_k should be reduced. The resulting reduction in K_d can be compensated by increasing the number of disks in the friction clutches. However, a substantial reduction in φ_k is undesirable because this would excessively reduce the axial forces and the locking properties of the differential. Thus, at $\varphi_k = 35^\circ$ the axial forces of the additional lockers are reduced to values of these forces in the meshing between the side gears and the pinions. It was found that 45° is the optimal value of φ_k. At this value the extent of fluctuations of the axial forces (ratio of $Q_{0\max}$ to $Q_{0\min}$) is at the minimum (see Figure 4.40b).

Other means of reducing the extent of fluctuations of Q_k also exist (e.g., by placing damping devices in the disk clutches of the differentials). These devices may be of a variety of designs. Figure 4.43 shows two versions of such devices.

Nonprecompressed plate springs 1 are installed in each friction clutch of the differential shown in Figure 4.43a. This ensures that there will be no friction in the clutches at $T_0 = 0$. The springs rest on disks 2 linked to the case, for which reason there is no slipping in the points of contact between the disks and the springs when the differential's components rotate relative to one another. A differential with dampers operates as follows. When the output shafts start rotating relative to one another, the change in the thickness of the disk stacks produces an additional deformation Δh of the plate springs. This causes the axial forces in the contact between the case and the pinion pins to increase above the value of Q_0 calculated from formula (4.142) only by the amount ΔQ_0 in proportion to deformation Δh from the load curve of the spring.

Note that significant deformations of the springs caused by insufficient stiffness and high loads T_0 (overloading) may bring about an increase in the gaps in the bevel meshings of the

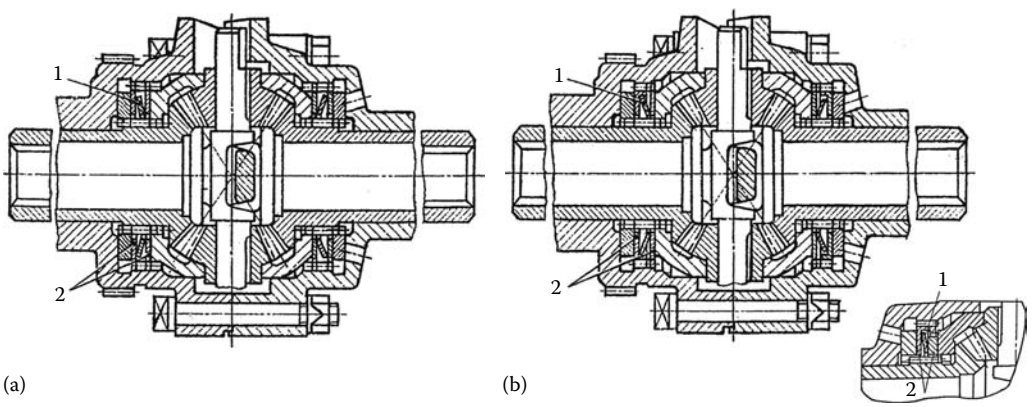


FIGURE 4.43
Differential with dampers. (a) Version I; (b) version II.

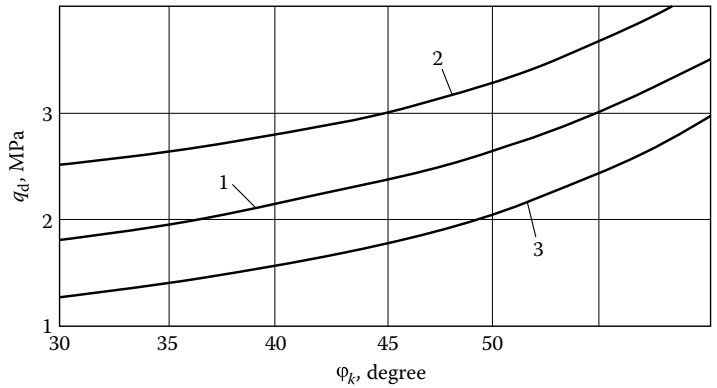


FIGURE 4.44
Pressure at the disks of the differential with dampers as a function of angle φ_k at $T_0 = 0.4$ kN-m and $\mu_s = 0.2$.

differential and cause them to malfunction. In order to provide for normal operation of the bevel-gear mesh, the axial movement of the disks of the differential in Figure 4.43b in which the springs are located is limited as follows. At substantial tractive loads both parts of the disks in which the springs are installed contact one another and thus limit further deformation of the springs. This prevents the side gears to slide out of the meshing with the pinions.

When dampers are used the pressure at the disks changes virtually only because of fluctuations of the axial forces of the bevel gears of the differential, that is, formulae (4.150) become:

$$\begin{aligned} q_{\mathrm{d\,max}} &= q_{\mathrm{da\,max}} + q_{\mathrm{d}k} \\ q_{\mathrm{d\,min}} &= q_{\mathrm{da\,min}} + q_{\mathrm{d}k} \end{aligned} \tag{4.153}$$

The results of calculations using formulae (4.153) are plotted in Figure 4.44 (curves 2 and 3).

Curve 1 corresponds to the pressure at the disks, without correction for fluctuations in the axial forces. It follows from comparing Figures 4.44 and 4.41b that the use of dampers provides an 1.33-fold reduction in $q_{\mathrm{d\,max}}$. Chapter 8 presents results of experimental studies that confirm the effectiveness of dampers.

4.10 Tractive Performance and Yaw Moment of a Drive Axle

A limited slip differential can be regarded as a compromise engineering solution that to some extent includes positive properties and eliminates shortcomings of two driveline systems—the differential and the positive engagement. The above shall be demonstrated for the case of a single drive axle in uniform rectilinear motion. An open bevel-gear differential used in driving axles has the positive property of transmitting equal torques to wheels that can roll with different angular velocities. The magnitude of these torques may

be any, up to the complete utilization of the adhesive weight. However, it is inevitable that when the gripping conditions at one of the driving wheels under off-road situations deteriorate, the traction force at the other wheel also decrease. As a result, this wheel does not fully utilize the potential gripping tractive force. This reduces the overall tractive force and decreases the mobility of the vehicle as a whole. When using a positively engaged drive, conversely, the wheel rpm becomes identical, but the tractive forces of the wheels are then not equal and depend on the gripping conditions of each wheel.

The maximum circumferential force of both of the axle's wheels when using an open differential is (it is assumed that the rolling radii $r_{\mathrm{w}}^{0\prime}$ and $r_{\mathrm{w}}^{0\prime\prime}$ of the wheels are the same):

$$\begin{aligned} F_{x\Sigma}^{\max} &= F_x' + F_x'' \\ &= 2F_x' = 2W_{\mathrm{w}}'\mu_{\mathrm{p}x}' \end{aligned} \tag{4.154}$$

where $\mu_{\mathrm{p}x}'$ is the gripping factor of the wheel under the poorer gripping conditions.

When using a positively engaged wheel drive (i.e., when the differential is locked):

$$F_{x\Sigma}^{\max} = F_x' + F_x'' = W_{\mathrm{w}}'\mu_{\mathrm{p}x}' + W_{\mathrm{w}}''\mu_{\mathrm{p}x}'' \tag{4.155}$$

where $\mu_{\mathrm{p}x}''$ is the gripping factor of the wheel under the better gripping conditions, $\mu_{\mathrm{p}x}'' > \mu_{\mathrm{p}x}'$.

When the axle is equipped with a limited slip differential, its maximum circumferential force takes an intermediate value that is close to the values of $F_{x\Sigma}$ with a locked or differential drive depending on the value of the locking coefficient K_{d}:

$$\begin{aligned} F_{x\Sigma}^{\max} &= F_x' + F_x'' = W_{\mathrm{w}}'\mu_{\mathrm{p}x}' + W_{\mathrm{w}}'\mu_{\mathrm{p}x}'K_{\mathrm{d}} \\ &= W_{\mathrm{w}}'\mu_{\mathrm{p}x}'(1 + K_{\mathrm{d}}) \end{aligned} \tag{4.156}$$

Let $\mu_{\mathrm{p}x}' = 0.2$, $\mu_{\mathrm{p}x}'' = 0.8$ and $K_{\mathrm{d}} = 2.5$; the normal wheel loads are the same, $W_{\mathrm{w}}'' = W_{\mathrm{w}}' = W_{\mathrm{w}}$. Then the maximum circumferential forces of the axle with positive and differential drives and when using a limited slip differential, will be in the ratio 1.0:0.4:0.7. These ratios determine the mobility of a vehicle with a single driving axle as a function of the three previously discussed types of interwheel drives.

The design of the interwheel drive affects not only the maximum circumferential force $F_{x\Sigma}^{\max}$ of the axle, but also the energy efficiency (the fuel economy) and the productivity of the vehicle at any intermediate value of $F_{x\Sigma}$.

Most of the time, limited slip differentials lock the output shafts while transmitting the torque T_0. If then the gripping conditions of the wheels start changing, the differential starts redistributing the torques between the wheels in such a manner that a higher torque will be fed to the wheel with better gripping conditions and a lower torque to the one with poorer gripping conditions. This redistribution of the torques stems from the laws controlling the operation of a positive drive, analyzed in Chapter 3. When the ratio of the higher torque T'' to that of the lower T' attains the value of K_{dp} (see formula (4.15)), the differential is ''triggered'' (actuated), that is, the output shafts start rotating at different velocities. The ratio T''/T' then does not become one as in an open differential, and only decreases somewhat to the value of the locking coefficient K_{d} from formula (4.6). The value of K_{d} determines the extent of redistribution (inequality) of torques T'' and T' at relative rotation of the differential's output shafts. This follows from formulae (4.10).

With reference to the above, consider the effect of the locking properties of a limited slip differential, that is, of its locking coefficient K_d, on the power lost in slipping of the wheels of a drive axle in rectilinear motion. It will be assumed that the rolling radii of the wheels in the driven mode are equal ($r_w^{0\prime} = r_w^{0\prime\prime} = r_w^0$) and the relationship between the wheel's circumferential force F_x and the wheel slip s_δ is expressed by formula (1.25). The gripping conditions of the wheels are taken to be different, which can be expressed mathematically by different values of the longitudinal stiffness factors K_x' and K_x'' of the tires of the left and right wheels (see formula (1.25)). With the differential actuated, the circumferential forces of the wheels are obtained from formulae (1.25) and (4.10):

$$\begin{aligned} F_x'' &= K_x'' s_\delta'' = F_{x\Sigma} K_d/(1 + K_d) \\ F_x' &= K_x' s_\delta' = F_{x\Sigma}/(1 + K_d) \end{aligned} \tag{4.157}$$

where $F_{x\Sigma} = F_x'' + F_x'$ is the total circumferential force of the axle, assumed to be known and equal to the algebraic sum of resistance to the axle's motion. If forces F_x'' and F_x' and slippages s_δ'' and s_δ' from formula (4.157) are substituted into (1.72), then it is possible to obtain the following expression for the slippage efficiency of the driving axle with an actuated limited slip differential:

$$\eta_\delta = 1 - \frac{F_{x\Sigma}\left(K_d^2 K_x' + K_x''\right) - F_{x\Sigma}^2 K_d}{K_x'' K_x' (1 + K_d)^2 - F_{x\Sigma} K_d \left(K_x' + K_x''\right)} \tag{4.158}$$

The results of calculations using formula (4.158) are plotted in Figure 4.45.

This figure also shows the results of calculating η_δ of the same axle with an open differential and with locked wheel drive. These calculations were performed using

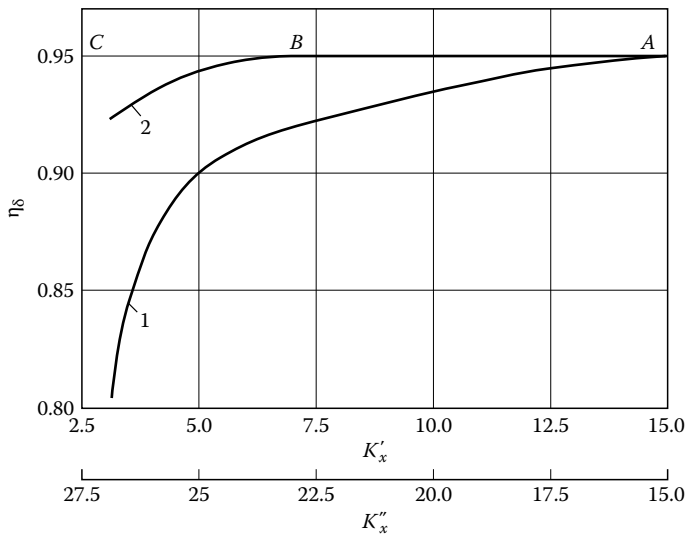


FIGURE 4.45
Efficiency η_δ as a function of K_x'' and K_x'.

formula (1.72) in which, for the case of an open differential, are substituted the following parameters:

$$s''_\delta = F''_x/K''_x; \quad s'_\delta = F'_x/K'_x$$
$$F''_x = F'_x = 0.5F_{x\Sigma} \tag{4.159}$$

whereas, for a positive engagement of the wheels:

$$s''_\delta = s'_\delta = s_\delta = F_{x\Sigma}/\left(K''_x + K'_x\right)$$
$$F''_x = K''_x s'_\delta; \quad F'_x = K'_x s_\delta \tag{4.160}$$

Point A in Figure 4.45 corresponds to the case of $K'_x = K''_x$ and efficiency η_δ is the same for all the three drives. For a locked drive η_δ is the same over the entire range of variation in K'_x and K''_x (straight line AC) at equal wheel slippages. In the case of an open differential, the efficiency decreases upon increasing difference between K'_x and K''_x (curve 1) while the difference in wheel slippage increases. In the case of a limited slip differential the drive acts over segment AB as a positive drive for which reason the efficiency remains constant. When the ratio F''_x/F'_x (or, which is the same thing as the ratio K''_x/K'_x) attains the value of K_d (see point B), the differential is actuated. The difference in wheel slippages increases with K''_x/K'_x and the efficiency decreases (curve 2).

It follows from the above that the smallest slippage power losses in the case of different wheel gripping conditions are observed with a positive drive. The power losses when using limited slip differentials are rather low. When using a differential drive the power losses are on the high side. Chapter 8 discusses the results of testing of vehicles within the context of the material above.

Consider now the performance of the driving axle when traveling in a curved path using a positive drive, an open differential and a limited slip differential. The main question of the effect of the driveline system on the features of curvilinear travel is that of calculating M_B—the yaw moment (the moment, which resists or assists the driving axle to turn). When the axle has an open differential, the circumferential wheel forces F''_x and F'_x under ordinary operating conditions do not differ to the extent that the value of M_B from formula (2.389) would attain values that would have a marked effect on the actual turning radius R_a.

The effect of a positively engaged drive of the axle's wheels on the turn yaw moment M_B was discussed in detail in Section 3.5.2. The values of this moment calculated from formula (3.141), may be quite high. This shall be validated by the following example. The contact between the tire and the road generates a stabilizing moment caused by shifting of the longitudinal force of the wheel F_w relative to the wheel's axis (see point B in Figure 1.61). This moment, which is usually included in calculating the stability and handling of vehicles, is approximately 30–35-fold smaller than moment M_B.

When a limited slip differential is used in the axle, the value of M_B during the first period of its operation (positively locked-drive mode) is determined by the difference between torques T'' and T' (see lines 12″ and 12′ in Figure 4.4). When $T''/T' = K_d$ (see horizontal lines in Figure 4.4) the output shafts of the differential rotate relative to one another and there are no subsequent changes in T'' and T'. The value of M_B also stops increasing. Moment M_{Bd} of resistance to the turning of the axle with the limited slip differential actuated can be determined by substituting F''_x and F'_x from (4.157) into formula (2.389):

$$M_{\mathrm{Bd}} = 0.5t_{\mathrm{B}}F_{x\Sigma}(K_{\mathrm{d}} - 1)/(K_{\mathrm{d}} + 1)$$
$$= 0.5t_{\mathrm{B}}F_{x\Sigma}K_{\mathrm{r}} \tag{4.161}$$

where $F_{x\Sigma}$ is the total circumferential force of the axle, $F_{x\Sigma} = F''_x + F'_x$.

Equating the right-hand sides of formulae (3.141) and (4.161) allows finding the turn radius R_{td} at which the differential is actuated and the turn resistance moment stops increasing:

$$R_{\mathrm{td}} = 0.5t_{\mathrm{B}}\frac{K_{\mathrm{d}} + 1}{K_{\mathrm{d}} - 1}\frac{1 - s_{\delta\mathrm{a}}}{s_{\delta\mathrm{a}}}$$
$$= 0.5t_{\mathrm{B}}\frac{1 - s_{\delta\mathrm{a}}}{K_{\mathrm{r}}s_{\delta\mathrm{a}}} \tag{4.162}$$

For this reason, the use of limited slip differentials makes it possible to limit the highest value of the turn resistance moment and thus control the vehicle's handling. Under standard operating conditions at $s_{\delta\mathrm{a}} \approx 0.015 - 0.025$ the value of M_{Bd} of the driving axle is much smaller than that of M_{B} with a fully locked differential. Thus a limited slip differential with $K_{\mathrm{d}} = 3$ that provides rather high tractive properties induces, at $s_{\delta\mathrm{a}} = 0.025$, a moment M_{Bd} that is approximately sixfold smaller than the maximum value of M_{B} with a fully locked differential.

If it is remembered that in many cases vehicles make a turn at low tractive load and at times at zero load (making a turn by inertia), it becomes obvious that the negative effect of the limited slip differential in the course of a turn is insignificant.

Analysis of formula (4.162) additionally shows that when moving over deforming soil and in the presence of a tractive load, it is possible to perform a turn even when the differential is not actuated. The above may occur because radius R_{td} depends not only on K_{d}, but also on the tractive load of the axle and on the density of the soil, that is, on $s_{\delta\mathrm{a}}$. An increase in the tractive load reduces the value of R_{td} at which the differential is actuated. For example, if the design value of R_{td} is only 8 m, and the turn occurs at $R_{\mathrm{t}} > 8$ m, then the differential is not actuated.

Formulae (4.161) and (4.162) are convenient because they allow estimating M_{Bd} and R_{td} based on the locking indicators K_{d} and K_{r} of the differential under design. This shall be demonstrated for the case of mechanisms with decreasing and constant friction moments from Figures 4.25 and 4.28. In spite of the similarity of their performance curves (Figures 4.27 and 4.29) and of the effect on the tractive properties of the vehicles, these differentials exert a different effect on M_{Bd}, the turn resisting moment. Substituting the locking coefficients K_{d} from formulae (4.111) and (4.126) into expression (4.161), it is possible (neglecting K_{pu}) to obtain:

for differentials with decreasing friction moment

$$M^{\mathrm{r}}_{\mathrm{Bd}} = \frac{0.5t_{\mathrm{B}}}{r^0_{\mathrm{w}}}(\mu H - 0.5\mu A T_0) \tag{4.163}$$

and for differentials with constant friction moment

$$M^{\mathrm{c}}_{\mathrm{Bd}} = 0.5t_{\mathrm{B}}C_{\mathrm{c}}/r^0_{\mathrm{w}} \tag{4.164}$$

It is seen from formulae (4.163) and (4.164) that M_{Bd}^{c} is constant and independent of the tractive load of the axle, that is, of T_0. At the same time, M_{Bd}^{r} decreases with increasing T_0. The difference in the manner of variation in the axle turn resistance moments causes differences in the lateral forces of the wheels and in the effect on the vehicle's handling.

4.11 Asymmetrical Interaxle Differentials

The use of open differential mechanisms in interaxle drives reduces the mobility of the vehicle under off-road conditions. This is the reason for employing standby locking in vehicles equipped with a differential interaxle drive. Another approach to improve the mobility of all-wheel drive vehicles consists of using interaxle limited slip differentials.

In principle, any of the previously discussed limited slip differentials can be used as an interaxle drive. However, the conditions and tasks of the interaxle drive are somewhat different from those of the interwheel drive. Thus, in the interaxle drive of a 4×4 vehicle with front steered wheels the shaft that advances relative to the case of the differential in the course of a turn will be the one that transmits the torque to the steered axle that stems from the kinematics of the vehicle's turn. On the other hand, the use of a limited slip differential somewhat affects the handling. For this reason, it is desirable that, when the drive shaft of the steered front axle advances, the locking coefficient should be moderate, but be somewhat higher upon advancing (slipping) of the nonsteered rear axle. For this reason, for example, a 4×4 vehicle traveling over roads with a hard pavement with weight uniformly distributed between the axles should be provided with a kinematically symmetrical differential with asymmetrical locking properties. This problem is solved to some extent in the mechanism shown in Figure 4.46.

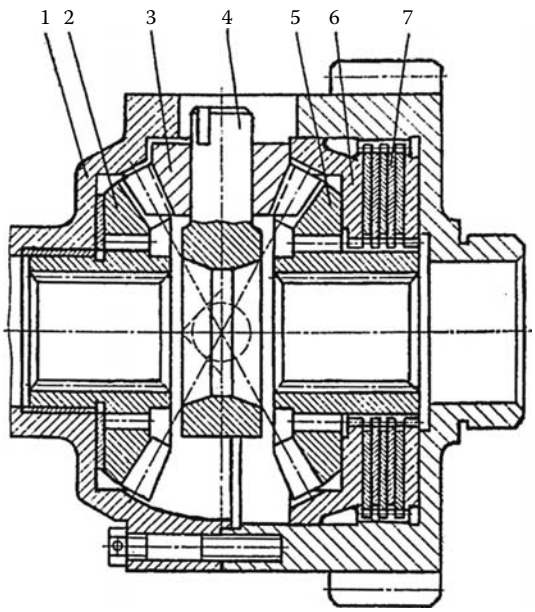


FIGURE 4.46
Bevel-gear interaxle differential with asymmetrical locking properties.

The mechanism operates as follows. Torque from case 1 is transmitted to spider 4 by means of the sloping surfaces of V-shaped grooves in the front half of the differential's case and corresponding flats on the spider's pins. This imposes axial forces on the spider and these compress the disks of clutch 7, located in the rear half of the case by way of shoulders of pinions 3 and pressure cup 6.

When the rear, relative to the case, output shaft with bevel gear 5 advances, the friction torque of the clutch is transmitted to the case. This torque is added to torque T_0 that is transmitted to the case by the engine, which increases the axial forces that compress the clutch. All this increases the locking coefficient (torque bias).

When the front output shaft advances, a part of the torque is transmitted through the clutch to the hub of gear 5. This causes the torque taken up by the spider and with it the force that compresses the clutch to decrease with simultaneous reduction in the torque bias factor. The torque bias factor is thus expressed as

$$K_{d1} = T_1''/T_2'; \quad K_{d2} = T_2''/T_1' \tag{4.165}$$

where T_1'' and T_2' are the respective torques at the front lagging and the rear advancing shafts, whereas T_2'' and T_1' are the torques at the rear lagging and front advancing shafts.

The design of the differential from Figure 4.46 was prompted by discovery of the existence of asymmetricity of the locking properties of the differential shown in Figure 4.13 (this asymmetricity of the locking properties is described in detail in Section 4.4). This asymmetricity is even greater in the differential from Figure 4.46 because of its use of one disk clutch instead of two and a unidirectional locker, that is, a spider with V-flats directed toward the clutch.

To obtain expressions for calculating K_{d1} and K_{d2} from formula (4.67). The formula for K_{d1} is derived by substituting $\xi = 0$ into formula (4.67) and by replacing in the numerator of this formula, the parameter A by the parameter

$$D = (r_{kp}/r_g)\tan\alpha_w \cos\delta_c \tag{4.166}$$

where r_{kp} is the radius of friction of the side gear at the differential's case.

The expression for K_{d2} is obtained by substituting $\xi = 1$ into formula (4.67) and by replacing in the denominator of this formula the parameter A by the parameter D from (4.166).

This means that when the front output shaft advances relative to the differential's case, which occurs when the front wheels slip or in the turn of a vehicle with front steered axle, the locking coefficient is

$$K_{d2} = \frac{1 + \mu(2E' + A)}{1 - \mu D} \tag{4.167}$$

When the rear output shaft advances and the front shaft lags (slippage of rear wheels),

$$K_{d1} = \frac{1 + \mu D}{1 - \mu(2E' + A)} \tag{4.168}$$

The parameters A and E' should be calculated from formulae (4.66).

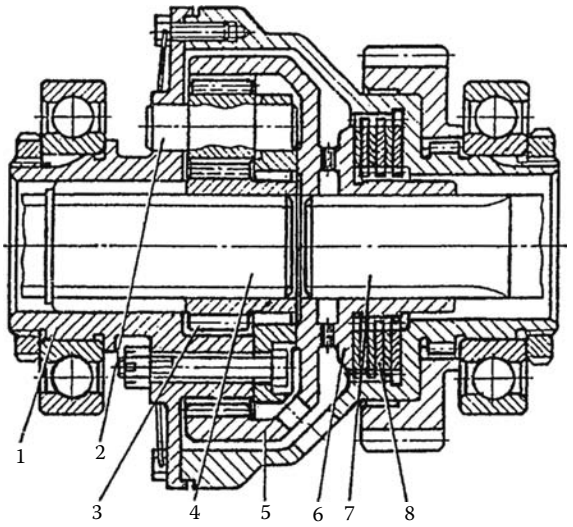


FIGURE 4.47
Asymmetrical interaxle limited slip differential.

Vehicles with nonuniform normal load traveling over hard-pavement roads and deformable soils are equipped with kinematically asymmetrical differentials with asymmetrical locking properties. One of such differentials is shown in Figure 4.47.

The torque is transmitted from case by pinions 2 to sun gear 3 of the drive shaft of the front axle 4 and the epicyclic gear 5. Then the torque from gear 5 is transmitted by means of bushing 6 to shaft 7 by way of trapezoidal cams located at the end of gear 5 and by splines of bushing 6. When the cams transmit the circumferential force F_k the axial force Q_k arises on their sloping working surfaces. This force compresses the disk stack of friction clutch 8 by means of the flange of bushing 6. The value of force Q_k is determined in the manner shown in Figure 4.8b. The reactive force equal to it is taken up by the case through the end of the epicyclical gear. The friction torque of the disk clutch prevents relative motion of output shafts 1 and 7.

If the front output shaft advances, then the torques at the output shafts are

$$T_1' = Fr_1; \quad T_2'' = Fr_2 + T_r \tag{4.169}$$

where

F is the circumferential force in the meshing between the pinions and the sun and epicyclical gears
T_1' and T_2'' are the torques at the front and rear shafts
r_1 and r_2 are the radii of the pitch circles of the sun and epicyclical gears

Substitution of the expression

$$T_\mathrm{r} = \mu F r_2 (r_\mathrm{M} i_\mathrm{M}/r_k) \tan \varphi_k \tag{4.170}$$

into the equation for T_2'' from (4.169) yields

$$T_2'' = Fr_2[1 + \mu(r_\mathrm{M} i_\mathrm{M}/r_k) \tan \varphi_k] \tag{4.171}$$

When the rear output shaft advances:

$$T_1'' = Fr_1; \quad T_2' = Fr_2[1 - \mu(r_M i_M / r_k) \tan \varphi_k] \tag{4.172}$$

The locking coefficient are found from the ratios of the torques thus:

$$\begin{aligned} K_{d1} &= T_1''/T_2' = \frac{1}{u_d[1 - \mu(r_M i_M / r_k) \tan \varphi_k]} \\ K_{d2} &= T_2''/T_1' = u_d[1 + \mu(r_M i_M / r_k) \tan \varphi_k] \end{aligned} \tag{4.173}$$

where $u_d = r_2/r_1$ is the gear ratio of the differential. In the differential designed for a 4×4 timber-carrier truck $K_{d1} = 1$ and $K_{d2} = 3$ at $u_d = 2$.

Further development of the design of the differential from Figure 4.47 has yielded a mechanism shown in Figure 4.48.

The differential was designed for a 5700 kg 4×4 tractor with different-size front and rear wheels and with different axle loads. At low and medium drawbar pull loads F_d and stable gripping conditions of the wheels, the axial force of trapezoidal cams 1 is balanced by the compression force of plate spring 2. The disks friction clutch I are not compressed and the differential operates as an open asymmetrical differential with a gear ratio u_d (Figure 4.49a).

Clutch I is locked only at low drawbar loads, when the wheels of one of the axles finds itself in poor gripping conditions or in the case when a significant part of the normal load is removed from the given axles when the farming implements are hitched to the tractor. Locking of clutch I in these cases improves the tractive performance of the tractor.

At elevated tractive loads F_d the axial force of cams 1 increases, spring 2 is compressed further and the gap Δ is eliminated. As a result, bushing 3 compresses the disks of friction clutch II, increasing the friction torque in the differential. The mechanism starts operating as a limited slip differential with locking coefficient K_d (Figure 4.49a). The value of K_d of the differential at tractive loads with advancing front wheels (the tractor makes a turn, elevated slipping of the front wheels as compared with the rear wheels) can be calculated from the expression:

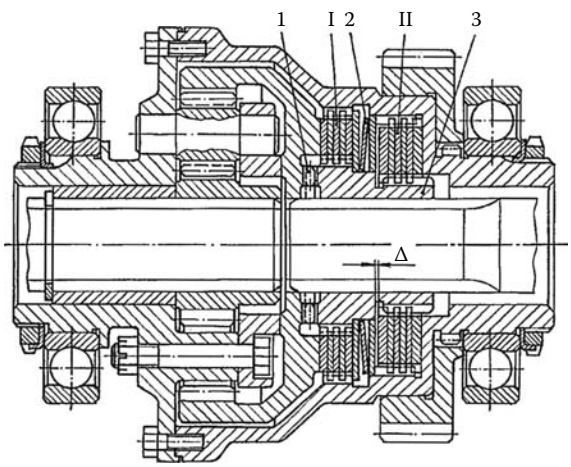


FIGURE 4.48
Interaxle asymmetrical limited slip differential with stepped performance curve.

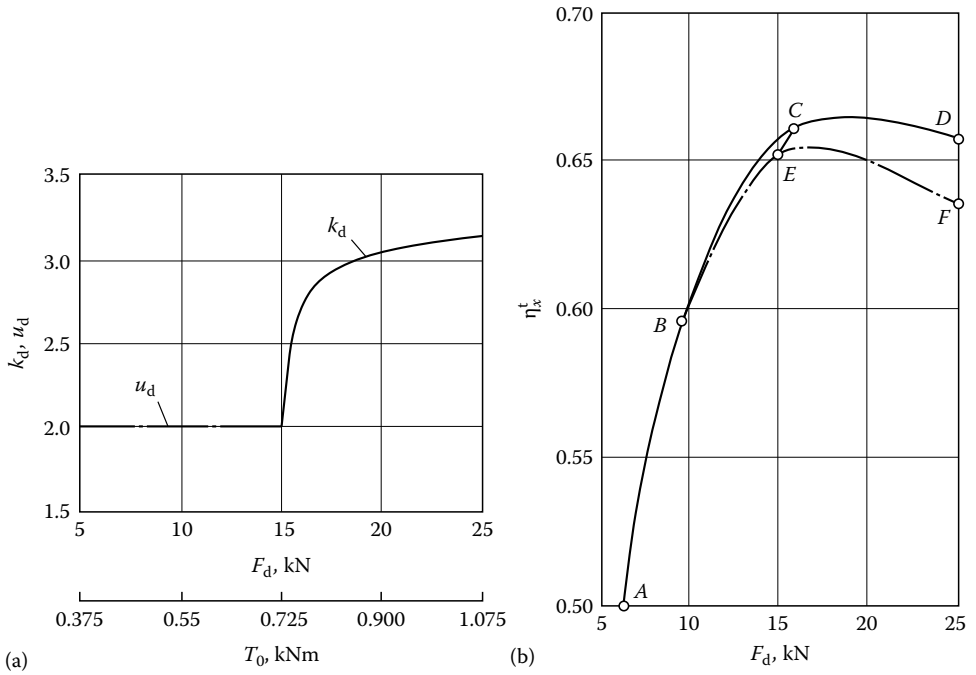


FIGURE 4.49
(a) Locking performance curve and (b) tractive efficiency of running gear.

$$K_d = u_d\left[1 + \mu(r_M i_M / r_k)\tan\varphi_k - \mu\frac{Q_{sp}}{T_0}\frac{u_d + 1}{u_d} r_M i_M\right] \tag{4.174}$$

where Q_{sp} is the preliminary compression force of the spring.

Figure 4.49a is a plot of locking coefficient K_d as a function of torque T_0 and tractive load F_d of a tractor. The parameters of the differential, of its friction clutches, spring and trapezoidal cams were selected in such a manner that the differential would operate at tractive loads of up to 15 kN as an open asymmetrical differential with gear ratio $u_d = 2$ (dash-dotted line in Figure 4.49a). At this tractive mode the tractive efficiency η_x^t of the running gear of the tractor with an open interaxle differential and with synchronous locked drive of axles, differ little from one another. The difference becomes perceptible at higher F_d. This is reflected in Figure 4.49b, on which curve *ABCD* corresponds to a locked drive of the axles with zero design kinematic discrepancy, whereas curve *ABEF* to a differential drive with $u_d = 2$.

Using a limited slip differential in the interaxle drive prevents reduction in efficiency at high F_d that occurs with an open differential drive. The locking properties of the differential start manifesting themselves at $F_d > 15$ kN thus the friction torque in clutch II and with it the locking coefficient K_d, start increasing (solid curve in Figure 4.49a). This reduces the difference in the axle slippages and increases the efficiency (segment *EC* in Figure 4.49b). In point *C*, the friction torque of clutch II is sufficient for locking the differential, and as F_d increases further the values of η_x^t, are the same as in the positively locked drive (segment *CD*).

5

Free-Running Differentials and Viscous Clutches

5.1 Design and Operating Principles of Free-Running Differentials

By virtue of circumstances, the term ''free-running differential'' came into use in the automotive terminology of the countries of the former Soviet Union as a designation of mechanisms that were known in the United States as the ''NoSPIN Differential'' and later on as the ''Detroit Locker.'' There are several design concepts of free-running differentials. Most often, these mechanisms consist of two-sided free-running geared clutches. They are capable of operation in automotive drives and are frequently used instead of other differentials. These mechanisms, similar to the positively engaged drive, rigidly lock the wheels of the vehicle on straight segments of the road, ensuring that the wheels grip the surface in a satisfactory manner, and consequently ensuring the high mobility of the vehicle. In the case when the vehicle takes a turn at a high traction load, the torques are continuously redistributed by decreasing the torque at the advancing wheel (at the advancing axles in the case when free-running differential is used in the interaxle drive) and increasing the torque at the lagging wheel (axle). Here the free-running differential will not be actuated, that is, the wheels will remain rigidly coupled until the torque at the advancing wheel (axle) will not drop to zero. When zero torque is attained, the free-running differential will definitely disengage this wheel (axle), thus eliminating the circulation of parasitic power and the appearance of negative circumferential forces on the leading wheels. The wheels (axles) are disengaged, as a rule, in turns with good gripping of the road and moderate traction load on the vehicle. The automatically disengaged advancing wheels move in the driven mode. This means that the power coupling between the left and the right wheels of the driving axle (or between the axles) is lost. The free-running differential in this case maintains only a kinematic coupling between the disengaged advancing wheel (axle) and with the driving wheel of the axle (axles) that has not been disengaged from the driveline system.

The property of this mechanism to disengage the advancing wheel (axle) and thus to ensure the needed difference in the rpm of the wheels when taking a turn is implemented when the vehicle moves both forward and in reverse, in turning in either direction, and in deceleration and coasting modes. Consider a design of the free-running differential, as shown in Figure 5.1.

In this differential, the final drive driven gear 1 and housing 2 of the differential itself comprise together with driving clutch 7, the driving link of the mechanism. Four pins to the differential's housing rigidly fasten the driving clutch. Radial rectangular teeth are arranged rigorously one opposite the other at both ends of the clutch. Mechanisms with 12 and 18 teeth at each end of the clutch are most extensively used. Two teeth (each at one side) are longer and form key-like tooth 8 on the inner cylindrical surface of the clutch.

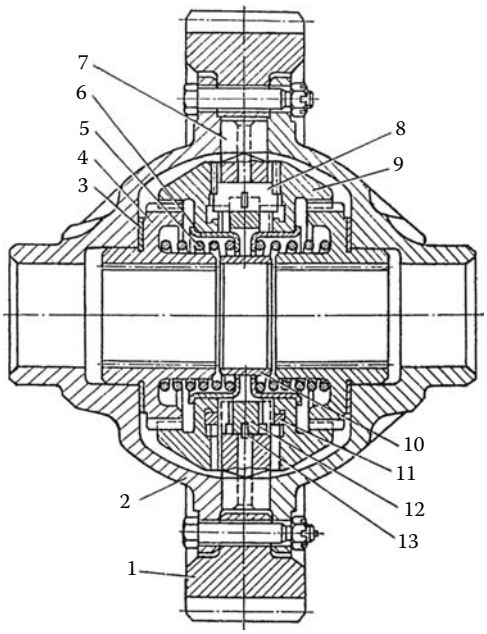


FIGURE 5.1
A free-running differential: 1, final drive driven gear; 2, housing of the differential; 3, washer; 4, side spur gear; 5, axial spring; 6, spring mount; 7, driving clutch; 8, key-like tooth; 9, driven half clutch; 10, spacing sleeve; 11, slit-spring lock ring; 12, central ring; 13, spring retaining ring.

Two driven half clutches 9 that have similar teeth are in engagement with the teeth of the driving clutch. The width of the tooth space of the gear rings of the driving clutch and of the driven half clutches is much greater than the thickness of the teeth. This is made in order that the driven half clutches should be able to rotate relative to the driving clutch by some angle. In specimens of differentials with 18 teeth, the angular pitch of the tooth is 7°20″ and the angular pitch of the tooth space is 12°40″, whereas the relative turning angle is 5°20″.

Spaces between the teeth of the driving clutch and the driven clutch halves are needed in order to facilitate the withdrawal (disengagement) of these same teeth when one of the clutch halves is uncoupled. Moving in the axial direction upon disengagement, the clutch half slides over the teeth of the side spur gear 4 that is rigidly splined to the half axle, as in an ordinary bevel-gear differential, and bears by its end through washer 3 on the wall of the differential's housing 2.

Each clutch half has, in addition the previously mentioned straight teeth, another inner gear ring with trapezoidal end teeth (these are also known as cams). These teeth are arranged coaxially with the straight teeth, due to which their number is the same as the number of the straight teeth. The slit-spring lock ring 11 with trapezoidal teeth similar to those of the gear ring is seated with some interference on the gear ring. In this arrangement, each tooth of this ring serves as a continuation of the tooth of the clutch half. The slit in ring 11 allows seating this ring with interference and facilitates the placing of elongated teeth or the key of the driving clutch.

Central ring 12 in Figure 5.1 and 2 in Figure 5.2 is located inside the driving clutch.

This ring is held in the middle position by a spring retaining ring (items 13 and 3 in Figures 5.1 and 5.2, respectively). Radial apertures are provided in journals over the circumference of the driving clutch to allow the disassembly of the retaining ring. The central ring has at both of its ends teeth that mesh with the teeth of both half clutches and both retaining rings. The length of each tooth of the central ring is equal to the sum of the lengths of the teeth of the clutch half and of the retaining ring.

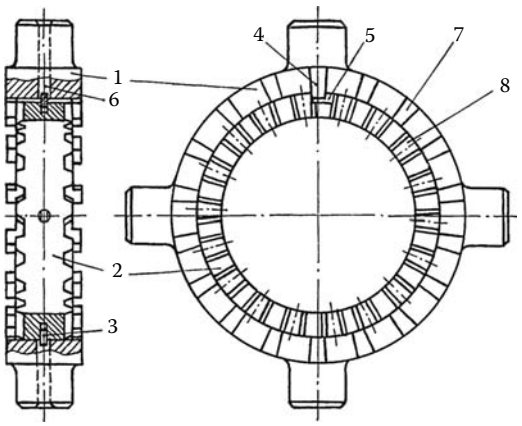


FIGURE 5.2
Assembled driving clutch of a free-running differential: 1, the driving clutch proper; 2, central ring; 3, spring retaining ring; 4, elongated key-like tooth; 5, circular slot; 6, disassembly aperture; 7, straight power-transmitting teeth (cams); 8, trapezoidal teeth (cams).

The outer cylindrical surface of the central ring has a wide circumferential slot 5 (Figure 5.2) in which the elongated key-like tooth 4 of the driving clutch is situated. The key-like tooth limits the angular displacement of the central ring relative to the driving clutch within the limits of the slot. Two compressed springs 5 (Figure 5.1) and their mounts 6 prevent the clutch half from self-disengaging. Each spring is additionally compressed when the clutch half is disengaged when taking a turn and returns the clutch half to the previous position when the turn is completed. Spacing sleeve 10 prevents the side spur gears from moving inside when the axle halves are placed in the course of assembly and disassembly of the differential. For safety reasons, a special clamping bolt is used when assembling and disassembling the differential; it is removed after the compressed mechanism is installed in the differential's housing.

As noted in Section 1.1, the ''Multi-Pull'' differential (see Figure 1.30a) was one of the first free-running differentials in the evolution process. It was far from being perfect. It was as noisy as a rattle. However, this was not its greatest shortcoming. Its greatest shortcoming was that its service life was very short. This was caused by point contacts between the spheres and the lateral surfaces of the teeth of the clutch halves. The spheres served to engage and disengage the half clutches of the leading wheels when the vehicle started and completed the turns. These same spheres were unable—as this is done in modern free-running differentials by spring-loaded gears—to ensure the noiseless sliding of the ends of the clutch-half cams upon their disengagement over the faces of the driving-clutch cams.

The ''Thornton-Tandem'' (Detroit) free-running differential appeared on the market in 1937. Its operating principle was the same as that of the Multi-Pull. However, it was much more advanced than the first free-running differential. The design of the engagement of the driving clutch and the driven half clutches allowed the elimination of the spheres. The Thornton-Tandem free-running differential was much more reliable and had a longer service life than the Multi-Pull.

The present level of perfection was attained by free-running differentials with the arrival of the NoSPIN Differential, made by the Automotive Products Company (Detroit). The NoSPIN Differential not only had a much longer service life than its Thornton-Tandem forerunner, but it was also noiseless. Quiet operation was attained by separating the teeth of the clutch halves into two rings—a moving ring and a stationary one—and the driving clutch acquired an elongated tooth and a circular slot at the central ring. It is precisely, the moving ring that became the spring-type gear ring that together with the tooth and the slot

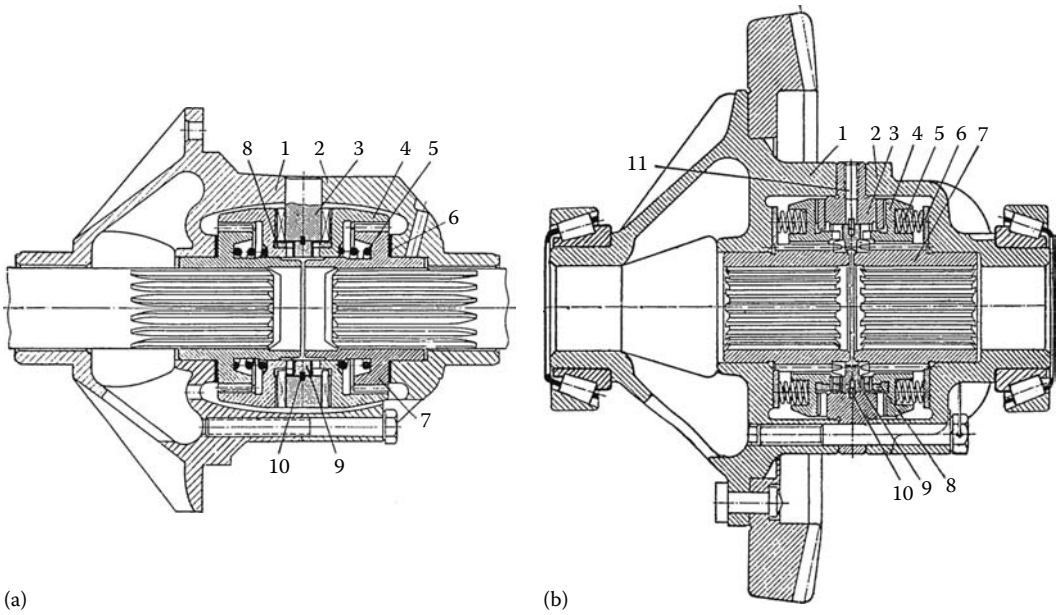


FIGURE 5.3
Designs of free-running differentials of (a) 4 × 2 truck; (b) 6×6 truck: 1, left half of the differential's housing; 2, right half of the differential's housing; 3, driving clutch; 4, driven clutch half; 5, spring; 6, thrust washer; 7, hub of driven clutch half; 8, slit spring retaining ring; 9, central ring; 10, lock ring; 11, disassembly aperture.

provided the ensured smooth and consequently noiseless sliding of the faces of the clutch-half teeth at the time of their disengagement over the faces of the driving clutch. The noiseless and long-lived NoSPIN Differential has come into extensive use for both road and off-road vehicles. Another example is the free-running differential of a 12-ton 4 × 2 truck, shown in Figures 1.30b and 5.1, and the free-running differentials designed for a 4 × 2 truck of 5.15 ton gross mass and of a 6 × 6 truck of 8.7 ton of gross mass. Their design concepts are shown in Figure 5.3.

Consider the operating principles of modern free-running differentials for different motion modes of a vehicle. When the vehicle moves forward in the traction mode along a straight path (item 1 in Figure 5.4a), the free-running differential acts as a single rigidly locked unit.

In this case, there is no relative motion of the components. The same occurs when the vehicle moves in reverse in the traction mode (item 2 in Figure 5.4a). However, during the period when the vehicle switches from forward to reverse in the traction mode, the differential breaks up into two links: link *A* and link *B*. Link *A* is made up of the driving clutch and the differential's housing and link *B*, of two driven clutch halves, combined with one another by means of a spring through the central ring; link *B* also includes two slit-spring lock rings and two half-axle gears. Hence, when the direction of motion of the vehicle changes (from forward to reverse motion) link *B* turns about link *A* through an angle corresponding to the clearance between the straight teeth of the driving clutch and the half clutches. The turning of the central ring and of spring lock rings of link *B* is made possible in this case by wide slot 5 (see Figure 5.2) in the central ring and wide slits of the spring lock rings. The same happens to the free-running differential when a vehicle moving forward (1) or in reverse (2) along a straight path comes to a stop (see Figure 5.4b).

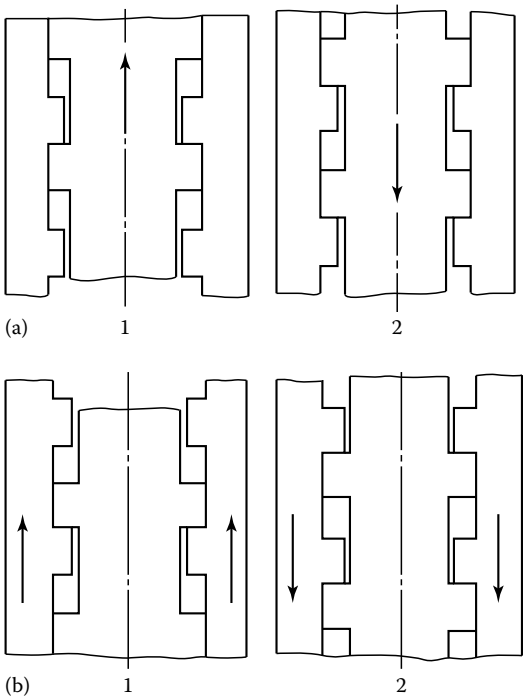


FIGURE 5.4
Schematic diagram of the force interaction between the driving clutch of the free-running differential and the driven clutch halves with (a) the vehicle moving in the traction mode; (b) the vehicle moving in the braking mode: 1, forward travel along a straight line; 2, reverse travel along a straight line.

Consider the start of a vehicle's turn and its motion during the turn. When the vehicle starts turning, the free-running differential decomposes into two kinematic links, A' and B'. Here one of them (let it be link A') is connected to the inner and the other (B') to the outer, relative to the vehicle's center of turn, wheel of the driving axle. Link A' continues to ensure the forward motion of the vehicle. At the same time, link B' starts disengaging the outer (advancing) wheel from the driving link. Link A' is composed of the driving clutch with the remaining components (differential's housing, central ring clutch half of the inner wheel of the vehicle with toothed spring slit lock ring, and the half-axle gear), whereas link B' is comprised of the clutch half of the outer wheel of the vehicle with its toothed spring lock ring and second half-axle gear. When the vehicle starts entering the turn, the outer clutch half of link B' together with the toothed spring lock ring frees itself of the load in the meshing of the rectangular teeth and starts rotating faster than the driving clutch by virtue of the accelerated rotation of the outer wheel of the vehicle. At the same time, link A' (the driving clutch and other elements) retains the previous angular velocity together with the inner wheel of the vehicle. On the other hand, the driven clutch half of the outer wheel together with its spring lock ring performs both rotary, overtaking the driving clutch, and axial translations simultaneously relative to the driving clutch until it is completely disengaged from it. The axial travels of the advancing clutch half and the spring lock ring are made possible by their trapezoidal teeth that mesh with similar teeth of the central ring of the driving clutch. At the instant when lock ring 3 (see Figure 5.5a) of the advancing clutch half will start bearing by its end onto the elongated key-like tooth 1 of the driving clutch, it will move to become a part of the driving link A'.

At the same time, the clutch half itself continues rotating at the same angular velocity as the outer wheel of the vehicle. It cannot become reengaged (coupled to the driving clutch, or link A'), since it is prevented from axial translation by the slit-spring lock ring that

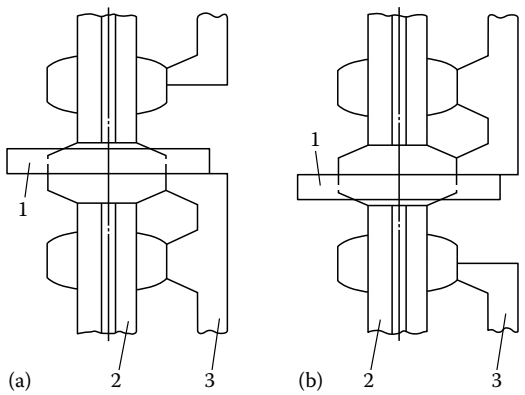


FIGURE 5.5
Schematic diagram of the disengagement of lock ring 3 of the free-running differential (a) moving forward; (b) moving in reverse: 1, key-like tooth of the driving clutch; 2, central ring.

becomes coupled to the driving clutch in such a manner that the end of its trapezoidal teeth bear on the ends of the teeth of central wheel 2. The disengaged advancing clutch slides over the rear smooth surface of the lock ring, bearing on it by its shoulder. Such a design eliminates constant disengagement/engagement of the outer wheel that was observed in the early designs of free-running differentials and thus further reduces the noise level and increases the service life of the differential. During the entire turn link A' remains the only active link of the free-running differential. At the completion of the turn, when the vehicle returns to rectilinear motion, the angular velocity of the clutch half of the outer advancing wheel becomes equal to the angular velocity of link A' and it again, coupling first to the slit lock ring that belonged before to link B', combines with link A' into a single kinematic link, that is, into a locked free-running differential. The operation of the free-running differential of a vehicle turning in reverse (see Figure 5.5b) is identical to that when taking a turn while moving forward.

The operation of the free-running differential when the vehicle turns while being decelerated by the engine is somewhat different. In this case the links A' and B' are replaced by the familiar links B and A at the very start of deceleration. Here the leading link of the mechanism is link B, that is, the clutch halves of the differential with the side gears and link A becomes the driven link. The following occurs simultaneously with the switch of the links. Link A turns relative to link B, backward through an angle determined by the clearance between straight teeth of the driving clutch and the driven clutch halves (see Figure 5.4b). Here the teeth of the clutch halves (of link B) start exerting pressure on the teeth of link A by their other side. This means that, as the vehicle starts being decelerated by the engine, clutch half 1 that is external relative to the vehicle's center of turn (see Figure 5.6) is not able to turn forward and disengage.

That is, the angular velocities of the outer clutch half 1 and of driving clutch 2 that are of opposite sign become equal in magnitude and neutralize one another in absolute motion. At the same time, clutch half 3 that is internal relative to the center of turn of

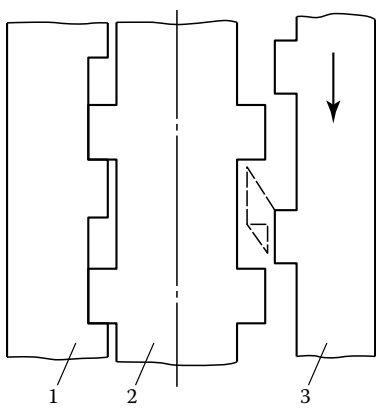


FIGURE 5.6
Schematic diagram of disengagement of the inner clutch half of a free-running differential of a vehicle turning while being decelerated by the engine.

the vehicle starts decelerating together with the inner wheel of the driving axle at a higher angular velocity than outer driven clutch half 1 and driving clutch 2 that have become combined into the new kinematic link A'. Having become, by virtue of slowing down rotation, the kinematic link B', the internal driven clutch half is disengaged in the final analysis and remains in the state of a driven link until the vehicle starts the completion of the turn. This means that, when a vehicle takes a turn while being decelerated by the engine, it is the inner (relative to the center of the vehicle's turn) clutch in the free-running differential that is disengaged, rather than the outer driven clutch half.

The most work-consuming problem in designing a free-running differential is ensuring its proper operation when the vehicle takes a turn while coasting. In this case, no circumferential forces are there that would press the teeth of the adjoining elements of the mechanism to one another between the rectilinear power-transmitting teeth of the driven clutch halves and the driving clutch. This results from the fact that the position of both toothed rings of the driven clutch halves relative to the teeth of the driving clutch and the central ring may be any within the limits of their lateral clearance. This requires analyzing what may happen in such a case and what should be done to prevent the potential malfunction of the mechanism.

When the vehicle starts turning while coasting, a force P_n appears in the meshing of the teeth of driving clutch half 3 that is external relative to the center of turn of the vehicle and central ring 2 of driving clutch that is induced by the advancing wheel (see Figure 5.7a).

This force consists of circumferential force F_n and axial force Q_n that are interrelated by the expression $Q_n = F_n \tan \varphi_\kappa$, where φ_κ is the slope of the working surfaces of the teeth of the clutch half and of the central ring. Reactive forces F_p and Q_p of the same magnitude simultaneously appear in the meshing of the inner clutch half 1 and the central ring 2. They start increasing, overcoming the compression force of the springs. As a result, also inner clutch half 1 will start disengaging, and its spring will accordingly be compressed. Moving simultaneously in opposite directions, clutch halves 1 and 3 do not manage to disengage completely. The ends of their straight teeth move earlier right up to the ends of the teeth of driving clutch 2 (see Figure 5.8).

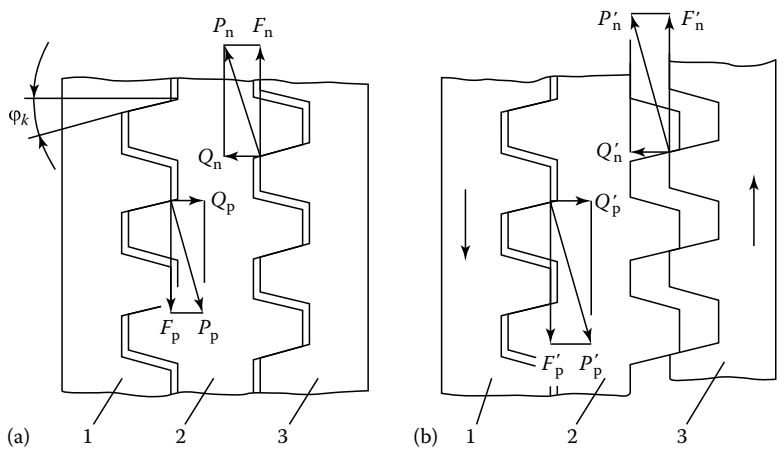


FIGURE 5.7
Schematic diagram of force interaction between the driven clutch halves and the central ring of the free-running differential when the vehicle turns while coasting at (a) the start of the turn; (b) the end of the turn.

Here continuation of disengagement of the driven clutch halves becomes impossible and they take some intermediate position (see Figure 5.7b). This means that the differential is locked. Obviously, the wheels of the driving axle are at that time prevented from rotating at different angular velocities. This, in its turn, interferes with the proper turning of the vehicle. The straight teeth of the differential's mechanism start being subject to extreme loads and that at times cause them to break.

Note that in the traction mode the driven clutch halves do not simultaneously perform axial translation, even though in this case the reactive axial force Q_p increases in the same manner as in the preceding case. This is so because, in this case an axial friction force acts at the ends of the straight meshing teeth in addition to the axial force of the spring that prevents self-disengagement of the inner driven clutch half. There is no such friction in the meshing of straight power teeth of the mechanism when the vehicle takes a turn while coasting.

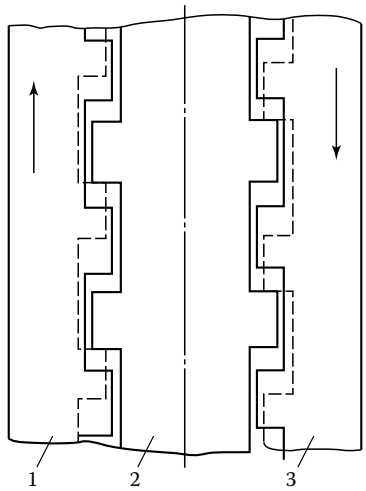


FIGURE 5.8
Schematic diagram of disengagement of the driven clutch halves of a free-running differential when the vehicle turns while coasting.

Departure from kinematic processes in the mechanism of the free-running differential when the vehicle turned while coasting required at its time new design solutions. This brought about the appearance of central ring 2 with convex lateral tooth surfaces shaped along a circular arc (see Figure 5.9).

When the teeth were so shaped, as outer clutch half 3 was disengaging, circumferential force F'_n did not increase as this occurred with flat lateral tooth surfaces, but conversely decreased in spite of the fact that the axial force Q'_n increased. It follows from the condition of equilibrium of the center ring ($F'_n = F'_p$) that circumferential force F'_p of inner driven clutch half 1 also decreases. Consequently, the axial force that acts on the inner clutch half also does not increase. The clutch half additionally too does not self-disengage since the difference in axial forces of both driven clutch halves is taken up by the lock ring. Nevertheless, the outer driven clutch half becomes completely disengaged.

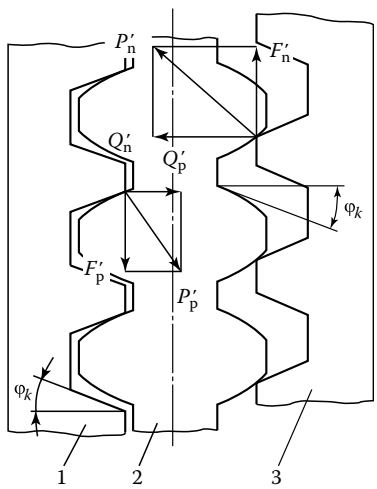


FIGURE 5.9
Schematic diagram of force interaction between the driven clutch halves and the central ring of a free-running differential that has central-ring teeth with convex lateral surfaces.

Note that the functions of driven half clutches in the course of turning of a coasting vehicle may shift. It may turn out that it is the driven clutch half that is internal—relative to the center of turn of the vehicle—that will be disengaged, whereas the outer driven half clutch remains engaged. This depends to some degree on maintaining equality of the forces exerted by the differential's springs.

It should be additionally noted that the force exerted by the compressed spring of free-running differentials should be selected with consideration of the torque that is

transmitted. Thus, it is recommended that in free-running differentials of driving axles with maximum load of $T_0 \cong 15.0$ kN-m the springs should have a force of 400–450 N. At the same time, the spring force in the free-running differential of a most heavy-duty scraper with $T_0 \cong 70.0$ kN-m should be about 600 N.

It must be remembered when springs are selected for a differential based on its power rating that both springs in a given mechanism must have forces equal to one another as close as possible. Since the spring forces depend highly on the difference in their length in the free state, it is recommended that springs for a given mechanism should be selected in pairs with close lengths in the free state.

Certain shortcomings in the design of individual elements of free-running differential were discovered in the course of investigation of their functioning principles. This made it possible to introduce corrections into the design of different differentials and also to the overall differential design. The use of the slit-spring lock ring with trapezoidally shaped teeth that prevents noisy operation of the clutch halves when the vehicle takes turn was noted previously. This was a very important refinement of the design of the free-running differential as a whole. Refining the shortcomings of the different components of the differential that were discovered in different vehicle travel modes played an important role in ensuring its satisfactory operation. Thus, arc-shaped working surfaces of the teeth of the central gear instead of flat surfaces were introduced in order to ensure disengagement of the half-clutch when the vehicle took a turn when coasting. For teeth 6–7 mm high, the radius of curvature of the concave surfaces should be 23 mm. Here the tangent at the tooth root should deviate from the normal by 20° and that at the tip of the tooth by 40°.

It is obvious that the height of the teeth of the central ring determines the axial movement of the clutch half in the course of disengagement. It should hence be the same as the height of the straight teeth of the driving clutch and of both clutch halves. It is precisely under these conditions that the straight teeth of the clutch halves are able to become uncoupled from the teeth of the driving clutch. Nevertheless, there were a number of cases when the driven clutch half did not fully disengage at this relationship between the heights of teeth. For this reason, it is recommended that in order to ensure reliable disengagement of clutch halves the heights of the teeth of the central ring should be higher than the heights of the straight teeth and clutch halves with tolerances of 0.2–0.3 mm. This clearance between the tips of the power-transmitting straight teeth of the clutch and clutch halves ensures that each of the clutch halves will be able to rotate freely in the disengaged situation.

The teeth of the spring lock ring are a continuation of the trapezoidal teeth of the clutch halves. For this reason, the teeth of the ring and of the clutch half should be the same. However, from the practical point of view, because the teeth of the lock ring are produced with some tolerance, these teeth turn out in some cases to be slightly, but still higher than the teeth of the half clutch. For this reason, the lock ring is not capable of completely disengaging from the central ring and to take the position shown in Figure 5.5. For the same reason also the clutch half may not be able to precisely take up its fully disengaged location. It continuously approaches the point of disengagement and then immediately reengages. This occurs as it turns through each tooth. This is accompanied by rattle-like noise of the mechanism. This occurred in free-running differentials that were not provided with a slit lock ring. To eliminate this, it is recommended that the teeth of the lock ring be made 0.15–0.20 mm shorter than the height of the trapezoidal teeth of the clutch half. This ensures normal disengagement of the clutch half and noise-less operation of the differential.

Making the teeth of lock ring 1 as a continuation of the trapezoidal teeth of clutch half 3 also means that the lateral surface of the teeth would be situated in the same plane (see Figure 5.10a).

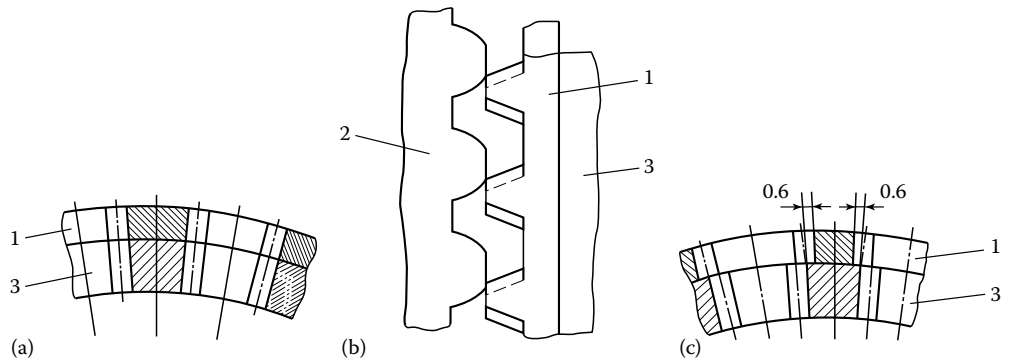


FIGURE 5.10
Schematic diagram of the interaction between the slit lock ring and the driven clutch half of a free-running differential.

However, in certain cases this caused the clutch half that rotated backward as a part of disengagement, to move off the tips of teeth of central ring 2 earlier than the lock ring. During that time, the lock ring continued bearing with the edges of its teeth on the teeth of the central ring, taking up the entire pressure of the springs (see Figure 5.10b). Under these conditions, one of the wheels of the driving axle of the vehicle became disconnected from the driving link of the mechanism and the vehicle was forced to move under the power of only the second wheel. To eliminate this situation, the teeth of the lock ring should be made 1.2–1.3 mm thinner than those of the clutch half. In a free-running differential (see Figure 5.10c), the thickness of the lock ring teeth was reduced by 1.2 mm.

The slit-spring lock ring is installed between the outer and inner gear ring of the driven clutch half with pretension. The specific magnitude of pretension referred to 1 mm of the seating diameter of the shoulder on which the ring bears by its outer cylindrical surface should be about 0.03–0.05 mm. It should be said that in the initial specimens of free-running differentials the lock ring was seated on the outer diameter of the ring of trapezoidal teeth of the clutch half. However, it was established in the course of testing that the centrifugal force that is applied to the slit-spring lock ring that rotates at a high velocity, causes its pretension and friction at the bearing surface to decrease. This is one of the reasons for the malfunction of the early mechanism. This shortcoming of the earlier mechanisms is taken into account in currently produced free-running differentials and the slit lock ring is placed in the clutch half with pretension in such a manner that it is pressed to its shoulder not by the inner, but outer lateral surface. In this case, the centrifugal forces not only do not reduce but even increase the friction force, thus improving the mechanism's operation.

The selection of the width of the slit of the lock ring at both the design and manufacturing stages is not a simple matter. In the assembled mechanism of the free-running differential the width of the slit should be equal (see dimension *a* in Figure 5.11) to the distance between two adjoining tips of the teeth of the tooth ring of the lock ring. Only in this case, it is possible to ensure normal engagement in the required instant of the driven clutch half of the wheel that advances in the course of the turn and noiseless operation of the mechanism's links.

It was additionally found in the course of testing of free-running differentials that certain of its components could be modified. For example, the single-piece elongated key-like

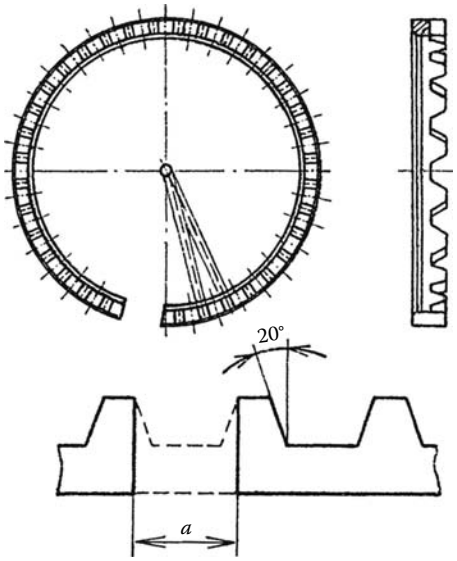


FIGURE 5.11
Slit-spring lock ring of a free-running differential.

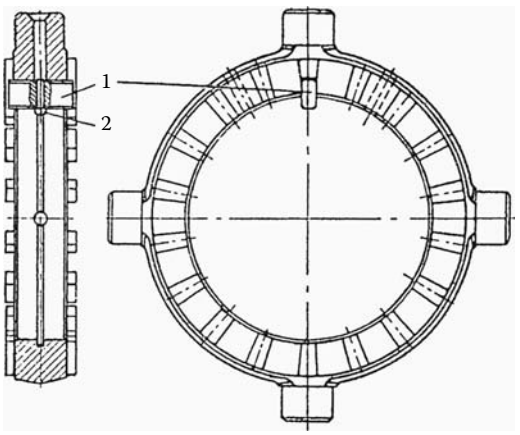


FIGURE 5.12
Driving clutch of free-running differential: 1, key that replaces the elongated key-like tooth; 2, key-fixing dowel.

tooth in the driving clutch can be replaced by an actual key 1 (see Figure 5.12) fastened to the clutch by dowel 2.

This method of increasing the length of the driving-clutch tooth is used in the free-running differential shown in Figure 5.1. Certain free-running differentials use several springs in the driven clutch (see Figure 5.3b) arranged over the periphery relative to the central axis of the mechanism, rather than two central springs. Note that no matter what modifications are introduced in the free-running differentials, their principal design remains unchanged.

5.2 Applications of Free-Running Differentials

Operating experience shows that currently produced free-running differentials are quite reliable, for which reason they have come into extensive use. They are utilized on various emergency and fire-fighting vehicles, dumpsters, petroleum tank trucks, farmers'

automobiles, timber carriers, school buses, snow-removal vehicles, road-service and road-construction vehicles, military, and other vehicles. Approximately 3–4 decades ago, these differentials came into use in certain types of heavy-duty wheeled farm tractors.

Initially free-running differentials were used only as interwheel power dividing units of terrain trucks (Figures 1.22 and 1.23) and then in both axles of articulated farm tractors (see Figure 1.35). A conceptual design of an interwheel free-running differential is shown in Figure 5.13.

Then their use was extended to interaxle drives. Figure 5.14 shows a conceptual design of a free-running differential in the transfer case between the steered and nonsteered driving

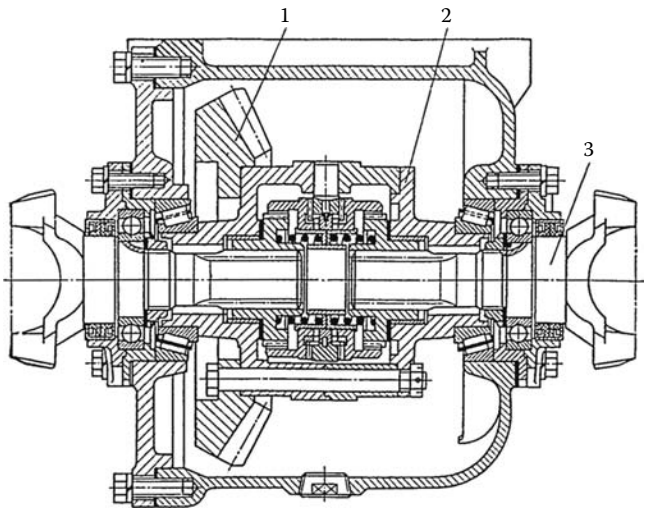


FIGURE 5.13
Final drive of the driving axle of an off-road vehicle with a free-running differential: 1, final-drive bevel gear; 2, differential; 3, half axle.

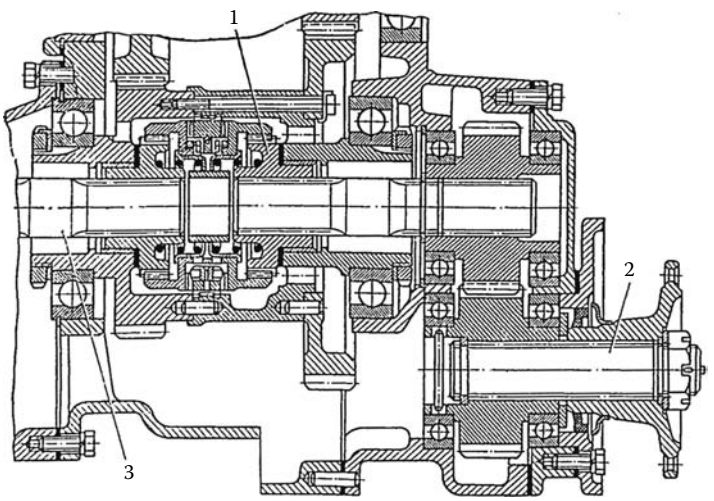


FIGURE 5.14
Free-running differential in the interaxle drive of a 4 × 4 vehicle: 1, differential; 2 and 3, drive shafts respectively of the front and rear axles.

axles of a 4×4 vehicle, whereas in Figure 1.40 (position 2) in the drive between the first and second axles with steered wheels of a 12×12 vehicle.

The free-running differentials are often employed in the interaxle drive of the front tandem with steered wheels of 8×8 vehicles.

Beyond any doubt, free-running differentials are rather complicated mechanisms. This has frequently caused design mistakes and, as a result, unsatisfactory operation of such differentials. However, experience shows that properly designed free-running differentials are extremely reliable in operation. Note that these mechanisms have virtually no sliding friction when subject to tractive loads and hence do not wear out early. With current production methods, the labor input needed for manufacturing free-running differentials is comparable and may even be lower than that of manufacturing interaxle bevel-gear differentials with locking devices. The manufacturing precision required by these differentials is not any higher than that of producing other modern-vehicle transmission components.

It follows from experience of operating free-running differentials that the conditions of work of this mechanism in the interaxle drive of front tandems with steered wheels of an 8×8 vehicle are more favorable than in the rear tandem with nonsteered wheels.

The advancing axle in the front tandem when making a turn is always the first one. For this reason, the corresponding half clutch of the front axle that became uncoupled at the start of the turn remains in this state until the turn is completed. At the same time, both half clutches of the rear tandem are alternately uncoupled and coupled depending on the road irregularities. This indeed makes for unfavorable conditions for the operation of the free-running differential in the rear tandem of vehicles. The majority of the rather few failures, of the free-running differentials as a whole, occurs in the interaxle drive of the rear tandem. Note that all these phenomena manifest themselves to a greater degree when moving on roads with hard pavements and to a lesser extent in terrain travel. The unstable disengagement and engagement of the half clutches of the interaxle free-running differential of the driving tandem with nonsteered axles, that is, rather minor and short-period advancing of one or another axle, allows the conclusion that the free-running differentials in the rear tandem can be replaced by a positive engagement between the tandem's axles (for certain suspension systems).

Experience in using free-running differentials, in the interaxle drive between the steered and nonsteered driving axles of 4×4 vehicles, shows that the mechanism operates more reliably with less number of engagements/disengagements of the half clutches. To prevent frequent engagements/disengagements, which is caused by vertical irregularities when moving over roads with hard pavements, the drive is designed with a kinematic discrepancy between the theoretical linear velocities of both axles. It is small, of the order of 4%–5%, but entirely sufficient to ensure that when the vehicle moves over high-grade roads, one axle (as a rule, the front steered axle) would be stably disengaged. Only when the vehicle moves under off-road conditions, when the rear-axle wheels are subject to partial slippage, is the front axle reengaged.

Observations and experience show that the most important condition for preventing self-disengagement of the half clutches of free-running differentials operating under heavy loads consists in strict perpendicularity of the lateral surfaces of their straight teeth and of the straight teeth of the driving clutch relative to the pitch plane. However, at times after the teeth are cut, in particular, with a poorly sharpened cutting tool, there occurs an insignificant, but detectable by measuring instruments, narrowing down of the teeth toward their tooth tips. Certain companies have instituted a procedure of undercutting the tooth roots, that is, they impart the tooth a trapezoidal instead of the straight shape at its root, in order to eliminate this shortcoming. Undercutting of straight teeth of the

free-running differentials, among others, in 6×6 8.7 ton trucks, amounts to 0.45 ± 0.03 mm for a 4 mm high tooth (see Figure 5.15).

The first differentials in the former U.S.S.R. were design for the MAZ and ZIL automobiles, and in the Central Research Institute of Automotive Vehicles and Engines (NAMI). These mechanisms were used on MAZ-502 4×4 trucks, 8×8 and 12×12 terrain vehicles designed and manufactured at the Minsk Company of Wheeled Trucks (MZKT), on ZIL-164 and ZIL-157 trucks and also on KrAZ-210, GAZ-51 and GAZ-63 trucks. Some of the test results of free-running differentials are presented in Chapter 8.

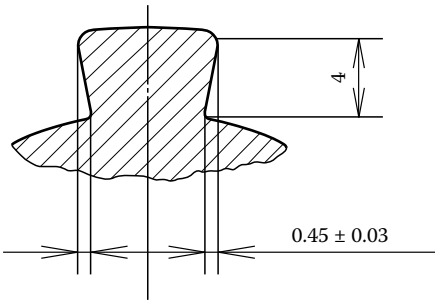


FIGURE 5.15
Cross section of an undercut tooth.

5.3 Viscous Clutches: Operation and Design Aspects

Multidisk viscous clutches are still another device that have come into extensive use for locking of differentials and for automatic engagement of the additional driving axle. They have received the name viscous clutch (viscodrive) because of the unusual fluid that they use. Viscous clutches use unique fluids (oils) that are known as non-Newtonian, that is, unlike Newtonian fluids, these are compressible. These are organosilicon—polymethylsiloxane or simply siloxane fluids with nominal viscosity from 5000 to 100,000 centistokes at temperatures above +20°C. Siloxane fluids are transparent, have no smell and are nontoxic. They are polymers consisting of peculiar chains (spiral macromolecules).

Fluids and oils usually employed in engineering start flowing when subjected to small shear strains. They exhibit a constant strain rate at a constant stress. This means that their properties are close to those of a perfect incompressible fluid, for which reason they have been termed incompressible or Newtonian. They strictly obey the laws of classical fluid dynamics. Unlike Newtonian, non-Newtonian fluids, that is, siloxanes are perceptibly compressible. Their strain behavior is composed of truly elastic, viscoelastic and viscous-fluid components. The first component of the strain of siloxanes—the elastic component, is usually small and can be neglected. The other two components are significant compared with the first and are those responsible for the viscous-clutch operation.

The viscosity of siloxanes changes as a function of the strain intensity or of the velocity gradient between the fluid layers. The viscosity that changes as a function of the strain intensity or of the strain rate is known as effective or structural viscosity of the fluid and the phenomenon as such of variation in the viscosity of siloxanes is known as the viscosity anomaly.

The study of the viscous flow of siloxanes is the concern of the science of rheology. It focuses on the effect of forces on the fluid layers. At very small strains, the equilibrium in siloxane systems is shifted toward restoration of deformed structures to the point that the structural changes in this case do not have a marked effect on the viscosity of these fluids. Hence, the flow of siloxanes at low strain rate virtually does not differ from Newtonian (incompressible) fluids. At the initial strain segment, the flow of siloxanes has the highest viscosity, which is known as the initial non-Newtonian or the highest Newtonian viscosity.

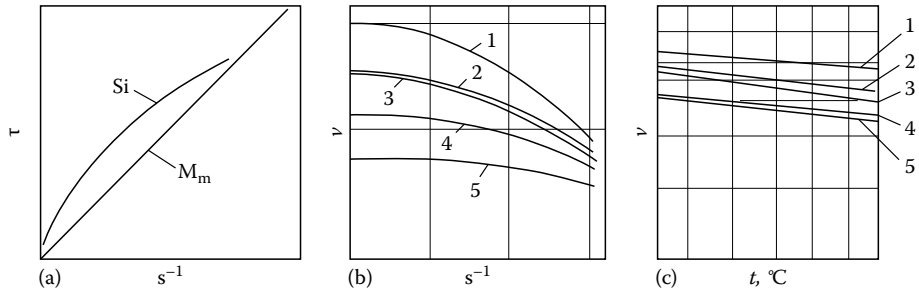


FIGURE 5.16
Properties of siloxanes: (a) shear stresses as a function of the shear strain rate (Si for siloxane fluids, M_m for machine oils); (b) effective viscosity of siloxane as a function of the shear strain rate PV (principal viscosity): $(PV)_1 > (PV)_2 > (PV)_3 > (PV)_4 > (PV)_5$; (c) effective viscosity as a function of temperature, $(PV)_1 > (PV)_2 > (PV)_3 > (PV)_4 > (PV)_5$.

Frequently the viscosity of siloxanes at low shear strain rates is termed the lower limiting or basic viscosity.

As the shear strain rate starts increasing, shear stress τ starts building up rapidly between the siloxane layers (see Figure 5.16a).

This stems from the activation of the viscoelastic strain. Having attained a certain magnitude, the shear strain rate continues rising, but somewhat slower. This means that the viscous-fluid strain has been triggered. This is accompanied by the breakup of molecular linkages between the different fluid layers and the efficiency of the momentum of transfer from one layer to another starts decreasing. This, in its turn reduces the shear stress at the given strain rate gradient (see Figure 5.16b).

Unlike ordinary engineering fluids, the viscoelastic component in siloxanes subjected to shear strains causes the appearance of normal (bursting) stresses. This stems from the fact that the macromolecular formations of non-Newtonian fluids become stretched in the direction of the force. They simultaneously tend to return to the location they had in their previous state. However, since this cannot be attained, they start swelling in the transverse direction. That is, the macromolecules that tend to contract in the direction opposite to that of the applied force expand in a direction perpendicular to the direction of the force that stretches them. This important tendency and activity of siloxane molecules has been termed the Weisenberg effect.

Siloxanes have another specific property known as thixotropy. Thixotropy is the ability of a fluid to self-restore its structure that has been disturbed by some mechanical effect. This property allows siloxanes to recuperate immediately after the viscous-fluid strain has been removed. It is of importance to the functioning of viscous clutches that the thixotropic restoration of the fluid's structure is a mechanically reversible process that is capable of multiple repetitions. This process is reversible to the point that both the structure of the siloxanes and their effective viscosity is fully restored.

Figure 5.16c shows the effect of temperature on the viscosity of siloxanes. As seen from the figure, when the temperature rises from, the effective viscosity of siloxane fluids drops, but not as rapidly as the viscosity of an ordinary engineering fluid.

Siloxanes exhibit a very large expansion coefficient. At positive temperatures from 25 to 175°C their expansion coefficient is $(9.5–10) \cdot 10^{-4}/°C$. This is approximately 40-fold greater than that of aluminum alloys. The above properties of siloxanes manifest themselves fully when they are used in viscous clutches.

As mentioned in Section 1.1 (see Figure 1.29), the viscous clutch consists of a device comprised of an airtight casing and separate shaft. The casing holds a set of disks that are alternately connected by means of splines to the shaft and to the casing proper. In addition, the casing is filled by 90%–93% with siloxane, corresponding to volume filling factors of $K_V = 0.90–0.93$. The disks are free to move in the axial direction. Usually slots are provided in disks connected to the shaft and openings in disks connected to the casing. The slots and openings facilitate the flow of fluid between the disks in the course of operation of the clutch.

All the force processes occurring in the viscous clutch are a function of the kinematics of its links—the disks of the shaft and casing and the working fluid—siloxane (Figure 5.17).

The viscous clutch starts operating when the casing and shaft start rotating relative to one another ($n' > n''$). Here the appearance of shear stresses produced by strain forces in thin layers of the viscous siloxane generates forces that push the adjoining disks apart and thus link them one to another, since the axial motion of the disks is highly limited. By linking the disks of the shaft and of the casing with one another the swollen (Weisenberg effect) siloxane that fills the clutch casing links, that is, locks the casing and shaft together. This is precisely what is required from a locking clutch.

In designing viscous clutches, special emphasis is paid on experimental studies that allow determining the effect of the design on the course of the internal working processes, meaning also on the overall functioning of these devices. Experimental studies established the following typical periods in the operation of the clutch. When the angular velocity of the driving and driven elements differ only slightly from one another, that is, at low relative velocity $\Delta n = n' - n''$, the torsional stiffness of the clutch and the torque T transmitted by it are determined solely by the friction torque of the moving packings of the shaft (see Figure 5.18).

This corresponds to the case when the flow of siloxane does not differ from that of a Newtonian fluid. Then the viscosity of the siloxane is at a maximum and is known as the lower limiting or basic viscosity.

When Δn increases, the torsional stiffness of the clutch becomes higher. From this time, the torque T is transmitted by the clutch by virtue of viscous friction in layers of the working fluid between the disks. This corresponds to the case of swelling of siloxane and filling of the clutch casing.

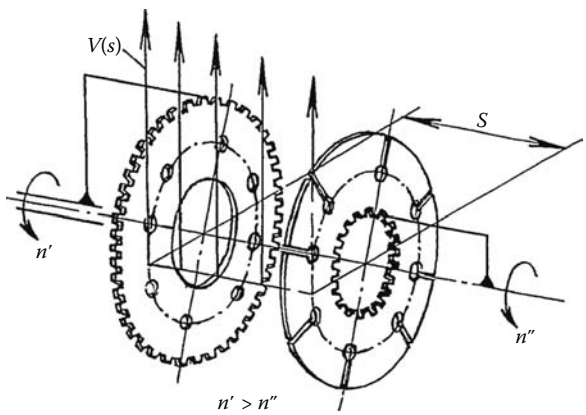


FIGURE 5.17
Distribution of strain rate $V(s)$ of siloxane between disks at casing rpm n' and shaft rpm n'' ($n' > n''$); s is the distance between the disks.

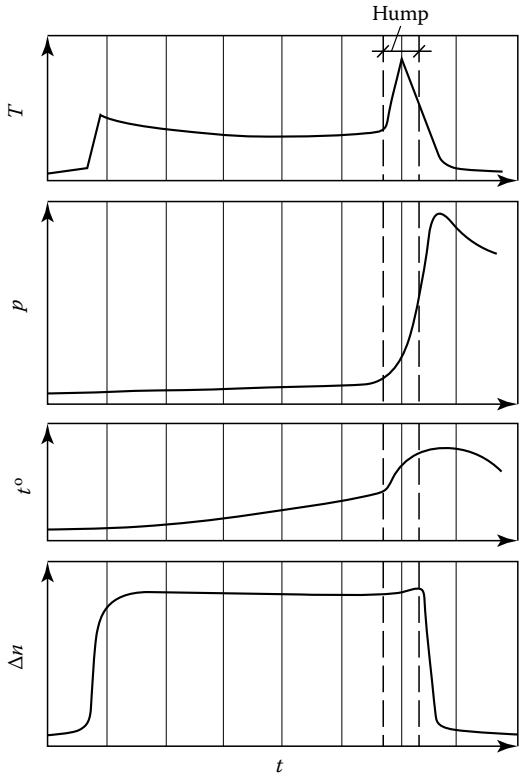


FIGURE 5.18
Test-stand curve of viscous clutch operation: T is the torque transmitted by the clutch, p is the system pressure of the siloxane within the clutch casing; t° is the temperature of the siloxane; Δn is the relative rpm of the shaft and clutch casing; t is the time.

Starting with some value of Δn the torque transmitted by the clutch continues increasing at a decreasing rate. The pressure p inside the casing continues to rise, but not too significantly, whereas the siloxane's temperature increases at a more rapid pace (see Figure 5.18). This period of clutch operation corresponds to the initial stage of breakdown of molecular links in the siloxane layers between the disks.

At some point in time, the value of Δn stabilizes. At the same time, the working-fluid temperature starts increasing perceptibly and the torque transmitted by the clutch decreases smoothly. This mode is known as ''viscous,'' since both the viscoelastic and viscous-fluid strains act simultaneously and actively in the fluid, with the latter being predominant.

After some period of operation of the clutch in the viscous mode with constant Δn, the temperature starts rising abruptly at some point in time (see Figure 5.18), pressure p inside the casing increases steeply with the simultaneous rise in the torque T transmitted by the clutch. These abrupt changes in viscous clutches were given the name ''hump.''

It was established that if the value of Δn is maintained at the previous level when the hump is reached, the clutch might fail due to excess pressure in the casing. Conversely, if the increase in torsional stiffness will allow the clutch to equalize the shaft and casing rpm, then after some time the temperature and pressure in it will drop, thixotropy will set in and after some time, it will again become possible to apply loads to the clutch.

It was additionally found out in the course of experiments that the value of Δn is a function of the initial viscosity of the siloxane. As Δn appears and increases to some value, shear stress is first induced and then appears in the siloxane and the clutch starts transmitting torque, that is, its shaft and casing starts locking one another. It was further noticed

that, the smaller the distance between the disks the greater, at the level of the same disk radii, the gradients of linear velocities and hence the larger the shear stresses. These stresses force the siloxane to flow between the disks. This causes the formation of concentric zones of siloxane mass transfer parallel to the longitudinal axis of the clutch. The higher the basic viscosity of the siloxane the clearer are the concentric zones delineated between them. The pressure p_s of the siloxane along the disk radii virtually does not change in the narrow spaces between the disks that are smaller than the spaces separating the concentric mass transfer zones from one another. The pressure p_s is not equal to the system pressure p, but is much higher. This indicates that friction forces in the narrow spaces between the disks in this case highly exceed the inertia forces of the siloxane macromolecules. The latter can be neglected provided that the basic viscosity of the siloxane used in the clutch is greater than 1000 centistokes. Pressures p_s and p tend to equalize in the course of clutch operation.

Two forces ensure the continuity of the siloxane layer in the spaces between disks, the size of which does not exceed the permissible limits (the magnitude of these limits is discussed further in this section), that wets and pushes apart the disks in the axial direction. The first force is the continuously increasing force of the system pressure that builds up by virtue of expansion of the siloxane when the temperature in the clutch increases. The second force comes from the normal stresses induced in the siloxane layer that stem from the viscoelastic strain of the fluid upon changes in the rpm values of the shaft and casing. The normal stresses (forces) in viscous clutches change along the disk radii.

Further away along the radius from the axis of rotation is the smaller normal stress σ_n (Figure 5.19).

This stems from the fact that the shear strain rate at the larger radius is higher and the viscosity of the siloxane is less effective. It should be noted that the effect of viscoelastic strain on the magnitude of axial forces is approximately by an order of magnitude smaller than the system pressure in the clutch. The viscoelastic pressure decreases with increasing spaces between the disks, starting with a minimum value that ensures retention of a continuous siloxane layer. The shear stresses and consequently the torque transmitted by the pair of disks that form the clearance decrease simultaneously.

Differences in spaces between the clutch disks are thus seen to be the cause of different pressures between them and of the appearance of axial forces that tend to increase wide spaces and reduce narrow ones. This means that in this case the system tends toward equalization of pressure in the adjoining gaps. This equalization is hindered by friction forces within the siloxane, or by the throttling effect. In spite of this effect, the pressure between the disks equalizes (levels out) in the end. For this reason, because of the reduction in the size of small spaces between the disks there arises limiting or virtually dry mechanical friction. This abruptly increases the torque transmitted by the clutch. The system pressure compresses the disks, the temperature of the siloxane undergoes an abrupt rise and the clutch starts operating in the hump mode. Then, about 50% of the total number of disk pairs participates in torque transfer. The value of Δn goes to zero at high torque and heat release stops immediately. The clutch cools down and after some time returns to the viscous operating mode. Note that the hump mode is not operational. It

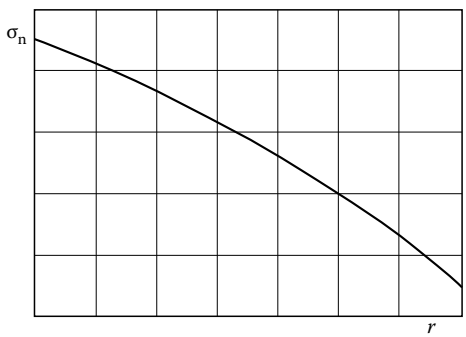


FIGURE 5.19
Variation in normal stress σ_n along disk radii r.

becomes unsafe if the siloxane fills up the clutch before Δn reaches zero. If this happens, the pressure and temperature in the clutch will increase steeply and may cause the clutch to fail.

All the known factors that affect the viscous clutch performance in one or another way may be subdivided into two groups. One of them is comprised of factors that depend on the clutch design and the other on factors that depend on its operating conditions. The first group includes:

1. Geometric parameters that determine the dimensions and shape of the disks
2. Number of disks
3. Average size of gaps between the disks
4. Presence or absence of spacing rings between the disks
5. Basic viscosity of the siloxane at the specified temperature (usually at $t = 25°C$)
6. The extent to which the clutch is filled or the relative volume of air (inert gas) that remains in the casing after it was filled at $t = 25°C$
7. Friction torque produced by the moving packings of the shaft
8. Maximum working pressures and temperatures at which the moving packings do not fail

The second group is comprised of the following factors:

1. Absolute and relative shaft and casing rpm
2. Gradient of variation in the relative rpm of the shaft and casing and, consequently, of the siloxane layers
3. Temperature within the clutch casing
4. Time of operation of the clutch at relative shaft and casing rotations

Consider the effect of certain factors on the nature of operation of the clutch in the viscous mode. It is seen from Figure 5.20a that the use of siloxane with higher basic viscosity increases the torsional stiffness of the clutch.

Its relative torque T/T_0 increases steeply (here T is the torque developed by the clutch in the viscous operating mode, whereas T_0 is the input torque). However, siloxanes with high initial (basic) viscosity create difficulties when filled into the clutch and in clutches that were somehow or other filled their viscosity increases irreversibly upon prolonged

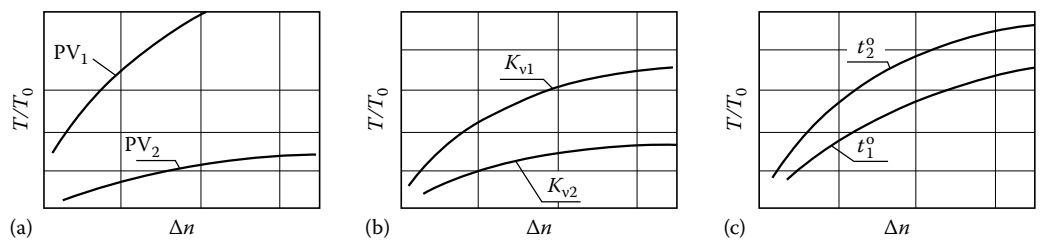


FIGURE 5.20
Effect of various factors on the transmission of torque by a viscous clutch in the viscous mode of (a) the principal viscosity of siloxane, $(PV)_1 > (PV)_2$; (b) the clutch filling factor, $K_{V1} > K_{V2}$; (c) the siloxane temperature $t_1^\circ > t_2^\circ$.

application of shear loads. For this reason, prevalent viscous clutches employ siloxanes with initial viscosity not exceeding 100,000 centistokes.

An inert gas is used for filling viscous clutches with siloxane. It facilitates the filling of the clutch and subsequently increases the viscosity of the siloxane in it. Figure 5.20b shows the effect of the degree of filling of the clutch by siloxane on its relative torque. It is seen that the more siloxane in the clutch the higher is the torque developed by it at the same Δn.

As noted previously, temperature variations within the clutch also affect the torque transmission by it. Initially, as the temperature in the clutch rises up to the appearance of the hump, the torque transmitted by it also increases with Δn. The same happens when the hump appears but at a much lower rate (see Figure 5.20c).

The spaces between disks in the viscous clutch are usually specified at $s = 0.1–0.2$ mm. In order to prevent the disks from physically pressing on one another upon application of axial forces, some clutches use spacing rings between the shaft and casing disks, whereas others use them only between similar disks. These disks ensure stable distribution of gaps along the axis of the clutch, but this reduces the torque transmitted by it. When the size of the gap goes up, the torque transmitted by the clutch reduces.

The performance of a viscous clutch depends to a large degree on the selected disk shapes, the presence in them of openings, cutouts, and slits of different configurations. Smooth disk surfaces interfere with the transverse flow of siloxane from the spaces between them, whereas a nonuniform distribution of pressure over the disk radius produces a flexing moment that subjects the disks to flexural strain. This perceptibly degrades the clutch performance. Correct selection of the configuration of opening and slots in the shaft and casing disks steeply increases the torque transmitted by the clutch. This effect may be twofold. The openings and slots promote the flow of siloxane between the disks and uniform distribution of temperature, both over the disk surfaces and the entire volume of the clutch's casing.

It was found that the rate of rise of the torque transmitted by the clutch depends not only on Δn, but also on the rate of increase in this difference. This stems from the thixotropic properties of siloxane. The dependence of torque T on Δn in this case is as a hysteresis loop, which depends on the initial viscosity of the siloxane.

To ensure trouble-free operation of the viscous clutch even in the extreme hump mode, the following recommendations should be considered at the design stage:

1. The clutch components must be able to withstand high temperature and pressure without being damaged.
2. The axial travel of disks must be unhindered, that is, spacing rings should be eliminated.
3. Disk perforations should allow siloxane to flow from spaces between the disks with allowing the disks to come into contact.
4. Providing the disk surfaces with wear-resistance coatings, which will allow them to operate in the mixed or dry-friction mode.
5. Providing for ability to withstand high specific loads on the clutch and for sufficient duration of their application.

Prolonged operation of the viscous clutch in the viscous mode when some of the above conditions are met causes it to switch to the hump mode. For this contingency, the clutch should have 7%–10% of air or an inert gas as a protective surge damper that would prevent a steep rise in the system pressure under hump operation. In addition, the presence of air

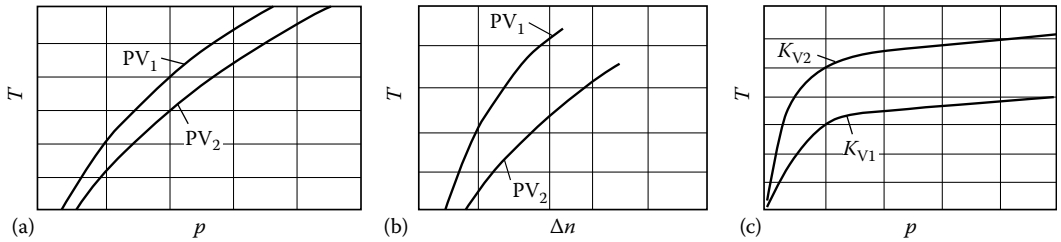


FIGURE 5.21
Effect of various factors on the shift of viscous-clutch operation to the hump mode: (a) principal viscosity of siloxanes upon change in system pressure p in the clutch, $(PV)_1 > (PV)_2$; (b) principal viscosity of siloxanes upon change Δn in the rpm of the shaft and casing of the viscous clutch, $(PV)_1 > (PV)_2$; (c) extent of filling the clutch with siloxane upon change in system pressure p, $K_{V1} > K_{V2}$.

(inert gas) in the clutch limits the maximum temperature in it and prolongs the time needed to attain the hump mode. The maximum values of system pressure and temperature in the clutch are limited respectively to 10–12.5 MPa and 100°C–125°C. Accordingly, air or some other inert gas serving as a surge damper may protect the clutch from failure, for example, upon prolonged slippage of one of the wheels of the driving axle of a vehicle when it is used as locking device in the differential. In this case, the clutch locks the differential's half axles; Δn becomes equal to zero and the system pressure in clutch drops. The effect of various factors on the shift of clutch operation to the hump mode is shown in Figure 5.21. Under the same system pressure, the clutch locks tighter when the viscosity of siloxanes is higher; thus, a high viscosity will promote full lock of the clutch and this will prevent the hump mode frome occurring (Figure 5.21a). The same trend takes place under Δn variation (Figure 5.21b). Torque function in Figure 5.21c shows that the hump mode is more probable under lower clutch filling factor.

The comparative properties of viscous clutches can be compared using certain analytic relationships. The torque transmitted by a pair of disks in the viscous mode can be calculated from the expression

$$T_i = (\pi^2 \Delta n \nu \rho_m r_o^4 / 2s)(1 - r_i/r_o)^4 \tag{5.1}$$

where

Δn is the relative rpm of the shaft and casing of the viscous clutch, Hz
ν is the basic viscosity of the siloxane, centistokes
ρ_m is the density of the siloxane, kg/m^3
s is the size of the space between the disks, mm
r_i is the inside radius of the disks
r_o is their outside radius, mm

This formula may be simplified to the form

$$T_i = \pi^2 \Delta n \nu \rho_m (r_o^4 - r_i^4) \tag{5.2}$$

As a whole, the torque transmitted by viscous clutch can be represented by the formula

$$T = [T_i(z - 1)/2]k_\varphi + T_y \tag{5.3}$$

where

z is the total number of disks

k_φ is an empirical factor that represents the shape of the disks and the degree to which the siloxane fills the clutch

T_y is the friction torque produced by the moving packings of the shaft of the clutch

It follows from formulae (5.1) and (5.3) that the radius of the disks of the clutch is a fourth power quantity in these expressions, whereas the number of disks is only a first-power quantity. This is a factor of importance in viscous clutch design.

The torque transmitted by the viscous clutch when switching to the hump mode is calculated from the expression

$$T = 2(\pi\mu\Delta p)(r_o^3 - r_i^3)/3 \tag{5.4}$$

where μ is the friction coefficient of the disks, whereas, $\Delta p = p_s - p$ is the pressure difference of the pressure between the disks and the system pressure in the clutch casing.

It should be noted in conclusion that, since siloxanes do not obey the laws of classical fluid dynamics and the theory does not yet provide a sufficiently complete and accurate quantitative description of the processes occurring in it, in actual designs of such clutches many parameters are selected experimentally. It can, nevertheless be definitely stated that viscous-clutch disks should be manufactured from soft, 0.25–1 mm thick, sheet steel. The disk surfaces must be polished and provided with 5–50 μm thick antiscuff coating. For example, certain manufacturers coat the surfaces of the disks of their viscous clutches by nickel. The disks in other viscous clutches are nitrated. As yet, there are no clear recommendations on the configuration of disk perforations. For example, radial slots are made on the casing disks of certain clutches, with round openings on shaft disks.

Viscous clutches have come into use in the interwheel and interaxle drives of cars and minivans as locking devices of differentials and of mechanisms for automatic engagement/disengagement of the additional axle. This axle maybe both the front and the rear one. It is known that rigid locking of the steered wheels in front-wheel drive cars is not desirable. For this reason, viscous clutches should not be recommended for these vehicles.

6

Combined Automated Mechanical Driveline Systems

6.1 Vehicle Operational Properties

In the previous chapters, simple driveline systems were analyzed, that is either differential or positively engaged or other single-type wheel drive systems. Combined driveline systems are combinations that are comprised of simple systems (see Figure 1.34). If the mechanisms and systems in the power-dividing units of a vehicle with combined driveline systems function automatically, then such systems are additionally known as automated. Precisely such drives are used in the majority of vehicles. This section presents the methods of compiling the equations for determining the distribution of power between the wheels and assessing the operational properties of these vehicles. These methods incorporate the effect of the principal design solutions of the vehicles: drive formulae, axle formulae, and steering formulae (see Section 1.2).

6.1.1 Vehicles with Steered Wheels

Consider a frame-type vehicle with a total number m of axles of which n are driving axles, $n \leq m$. Assume that all the axles are steered. The particular cases when not all the axles steer the vehicle's motion are obtained by setting the corresponding wheel turn angles equal to zero. The planar motion of such a multiwheel drive vehicle takes place in a plane with a system of fixed coordinates XOY (see Figure 6.1).

A moving frame of reference xoy is associated with the vehicle's center of mass. The motion of the vehicle is described mathematically using Appel's equations:

$$\frac{\partial S}{\partial \ddot{\pi}_i} = Q_i, \quad i = 1, k \tag{6.1}$$

where

S is the acceleration energy
$\ddot{\pi}_i$ is the quasi-acceleration
Q_i is a generalized force corresponding to the ith quasi-coordinate
k is the number of quasi-coordinates

The motion of the vehicle is described by three generalized coordinates of the center of mass: X_a, Y_a, and β_a—the angle between the longitudinal axis of the vehicle and the OX

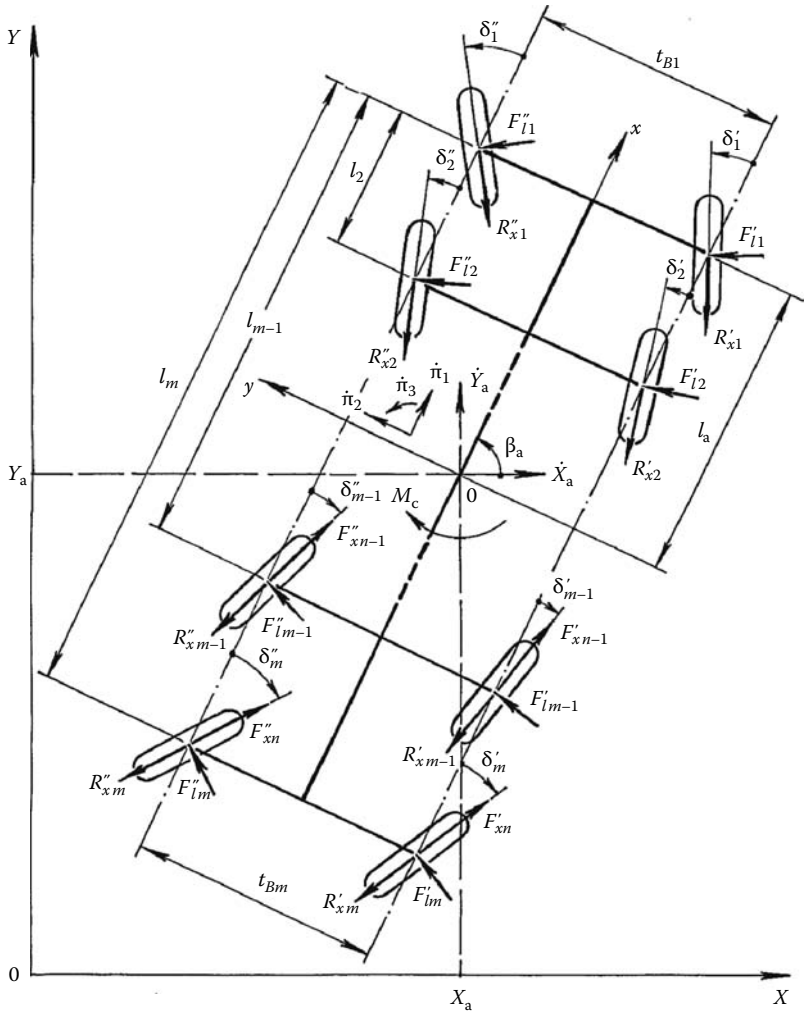


FIGURE 6.1
Vehicle free-body diagram.

axis. Equations in the form of Equations 6.1 are compiled by introducing three quasi-velocities $\dot{\pi}_1$, $\dot{\pi}_2$, and $\dot{\pi}_3$ related to X_a, Y_a, and β_a by the expressions

$$\begin{aligned} \dot{X}_a &= \dot{\pi}_1 \cos\beta_a - \dot{\pi}_2 \sin\beta_a \\ \dot{Y}_a &= \dot{\pi}_1 \sin\beta_a + \dot{\pi}_2 \cos\beta_a \\ \dot{\beta}_a &= \dot{\pi}_3 \end{aligned} \tag{6.2}$$

The acceleration energy, S, of the vehicle that is comprised of the energy of acceleration of the translational motion of the center of mass and the energy of rotational motion about this center is determined on the basis of (6.2), retaining terms containing the quasi-accelerations:

$$S = \frac{m_a}{2}\left(\ddot{X}_a^2 + \ddot{Y}_a^2 + \rho_a^2\ddot{\beta}_a^2\right)$$
$$= \frac{m_a}{2}\left(\ddot{\pi}_1^2 - 2\ddot{\pi}_1\dot{\pi}_2\dot{\pi}_3 + \ddot{\pi}_2^2 + 2\ddot{\pi}_2\dot{\pi}_1\dot{\pi}_3 + \rho_a^2\ddot{\pi}_3^2\right) \tag{6.3}$$

where m_a and ρ_a are the mass of the vehicle and its radius of inertia.

The generalized forces, Q_i, that correspond to the above quasi-coordinates, are determined from the expression of the virtual work:

$$\delta A_1 = Q_1\delta\pi_i, \quad i = 1,3 \tag{6.4}$$

Making use of Equations 6.1, 6.3, and 6.4, the equations of motion of the vehicle become

$$m_a(\ddot{\pi}_1 - \dot{\pi}_2\dot{\pi}_3) = \sum_{i=1}^{n} F_{xi}'^{(\prime\prime)}\cos\delta_i'^{(\prime\prime)} - \sum_{i=1}^{m} R_{xi}'^{(\prime\prime)}\cos\delta_i'^{(\prime\prime)} - \sum_{i=1}^{m} F_{li}'^{(\prime\prime)}\sin\delta_i'^{(\prime\prime)}$$

$$m_a(\ddot{\pi}_2 + \dot{\pi}_1\dot{\pi}_3) = \sum_{i=1}^{n} F_{xi}'^{(\prime\prime)}\sin\delta_i'^{(\prime\prime)} - \sum_{i=1}^{m} R_{xi}'^{(\prime\prime)}\sin\delta_i'^{(\prime\prime)} + \sum_{i=1}^{m} F_{li}'^{(\prime\prime)}\cos\delta_i'^{(\prime\prime)}$$

$$m_a\rho_a^2\ddot{\pi}_3 = 0.5\sum_{i=1}^{n}\left(F_{xi}'\cos\delta_i' - F_{xi}''\cos\delta_i''\right)t_{Bi} + \sum_{i=1}^{n}\left(F_{xi}'\sin\delta_i' + F_{xi}''\sin\delta_i''\right)(l_a - l_i)$$
$$- 0.5\sum_{i=1}^{m}\left(R_{xi}'\cos\delta_i' - R_{xi}''\cos\delta_i''\right)t_{Bi}$$
$$- \sum_{i=1}^{m}\left(R_x'\sin\delta_i' + R_x''\sin\delta_i''\right)(l_a - l_i) - 0.5\sum_{i=1}^{m}\left(F_{li}'\sin\delta_i' - F_{li}''\sin\delta_i''\right)t_{Bi}$$
$$+ \sum_{i=1}^{m}\left(F_{li}'\cos\delta_i' + F_{li}''\cos\delta_i''\right)(l_a - l_i) - M_c \tag{6.5}$$

where M_c is the moment resisting the turn that arises in the contact between the wheels and the surface of motion. The nature of the appearance of moment M_c is explained by the location of the resultant reactions exerted on the wheel by the surface (see Figure 1.61). A great deal of experience has been accumulated in engineering literature on the analytic and experimental determination of M_c.

The law governing the variation in the angles $\delta_i'^{(\prime\prime)}, i = 1, m$ of the turn of the wheels in time is specified from the consideration of the situation to be investigated: start of turn, change of the lane of motion, overtaking with return to the lane of motion, etc. In Equations 6.5, the angles of the wheel turning in a counterclockwise direction are positive, and those turning in a clockwise direction are negative. If the angles for a group of axles are set equal to zero $\delta_i'^{(\prime\prime)} = 0$, then these axles become nonsteered.

The manner in which the normal loads on the wheels change, on which tangential and lateral reactions depend to a high extent, in the course of the turn, is assumed to be known. The pertinent equations for determining it are compiled using a three-dimensional computational model of an actual vehicle with allowance for the stiffness of the suspensions, tires, and soil. These equations are not given in this section in order not to divert attention from the main topic under study.

Solving Equations 6.5 requires eliminating redundant unknowns from it. The lateral wheel reactions $F_{li}^{\prime(\prime\prime)}, i = 1, m$ can be expressed in terms of the lateral slip angles $\alpha_i^{\prime(\prime\prime)}$ employing the nonlinear theory of lateral slip (see formula (1.45)). At the same time, the slip angles shall be represented by projections $V_{xi}^{\prime(\prime\prime)}$ and $V_{yi}^{\prime(\prime\prime)}$ of the velocities of the wheels on the longitudinal and lateral axes of the vehicle:

$$\alpha_i^{\prime(\prime\prime)} = \delta_i^{\prime(\prime\prime)} - \arctan\left(V_{yi}^{\prime(\prime\prime)} \Big/ V_{xi}^{\prime(\prime\prime)}\right) \tag{6.6}$$

where $V_{xi}^{\prime(\prime\prime)} = \dot{\pi}_1 \pm 0.5 t_{\mathrm{B}i}\dot{\pi}_3$

$$V_{yi}^{\prime(\prime\prime)} = \dot{\pi}_2 + (l_{\mathrm{a}} - l_i)\dot{\pi}_3$$

This means that, after the wheel slip angles are expressed in terms of quasivelocities, there remain in Equations 6.5 redundant unknown circumferential forces of the wheels $F_{xi}^{\prime(\prime\prime)}, i = 1, n$. The number of the unknowns can be reduced by compiling equations relating the circumferential forces, the wheel slippage, and the generalized slippage of the axles, of sets of axles, and of the vehicle.

In differential driveline systems, the relationships between slippages and circumferential forces were presented in Chapter 2. In the case of a positively engaged drive, the distribution of power between the wheels depend largely on the magnitude of kinematic discrepancy (see Chapter 3).

When limited slip differentials and other self-locking differentials are used in the drives of axles and wheels, consideration must be given to two possible states of the mechanisms: locked/engaged (there is no differential effect) or activated (the differential effect exists with possible distribution of torques between the output shafts of the mechanisms). In the first case, the circumferential forces of the wheels (torques) are determined as with the positively engaged drive, in the second, the ratio of torques at the output shafts of the differentials are equal to the locking coefficient (torque bias) K_{d}. The latter may be either constant or variable, which depends on the operational factors, for example, on the torque T_0 on the housing of the differential. In certain cases, it is preferable to use the specific friction moment K_{r} (see formula (4.12)). Thus, for the free-running differentials, after disengaging one of the output shafts $K_{\mathrm{r}} = 1$, whereas the value of the locking coefficient K_{d} is equal to infinity, which is not always convenient to use in calculations.

This means that the analytic relationships from Chapters 2 through 5 should be used for mathematically describing the force-type (circumferential force and torque) and velocity-type (velocities and slippages) parameters of wheels and axles that are connected by the different power-dividing units. Actually, these relationships describe the locking properties of the power-dividing units and serve as equations of constraints that are imposed by the power-dividing units on the force and kinematic parameters of the driving wheels, that is, on the distribution of power between the axles. The number and type of the mechanisms in the power-dividing units determine the number of these constraint equations. As a result of adding these constraint equations that are determined by the driveline system, to the set (6.5) of equations of motion, the only unknown remaining in it, in addition to the three unknown coordinates X_{a}, Y_{a}, and β_{a}, is the vehicle's generalized slippage $s_{\delta\mathrm{a}}$. This means that one equation is still required for solving Equations 6.5. Under these circumstances it is possible to assume that the velocity of motion along the longitudinal axis of the vehicle is constant and given, which will ensure the equality of the number of equations and of the unknowns contained in them. Another approach is based on

simultaneously solving Equations 6.5 and equations describing the engine-transmission-driveline-wheels dynamic-torque system.

In cases when it is not necessary to consider the torsional oscillation of the transmission and driveline system, it is possible to use the following relationships between the engine torque T_e and the circumferential forces of the wheels F''_{xi} and F'_{xi}:

$$T_e u_{trm} \eta_{trm} = \sum_{i=1}^{n} \frac{T_{0i}}{u_i \eta_{Mi}} \tag{6.7}$$

$$T_{0i} = \left(F''_{xi} r^{0''}_{wi} + F'_{xi} r^{0'}_{wi}\right)/(u_k \eta_k)$$

If the vehicle does not have wheel-hub gear sets, then $u_k = 1$ and $\eta_k = 1$. The engine torque in Equation 6.7 can be represented as a function of the angular velocity ω_e of the crankshaft according to one of the available relationships. In its turn, ω_e is expressed in terms of the gear ratios of the transmission, the radii and slippage of wheels, and geometric parameters of the vehicle, by the quasi-velocity of the center of mass. After these transformations, Equation 6.7 can be used for a simultaneous solution with equations of motions compiled for vehicles with any turning layout. For vehicles with steered wheels, the motion of which is described by Equations 6.5, the final form of Equation 6.7 simplifies highly and becomes:

$$\dot{\pi}_1 = \omega_0 r^0_a (1 - s_{\delta a}) = \frac{\omega_e}{u_{trm}} r^0_a (1 - s_{\delta a})$$

or,

$$\dot{\pi}_1 = \frac{f(T_e)}{u_{trm}} r^0_a (1 - s_{\delta a}) \tag{6.8}$$

where T_e is defined by Equation 6.7.

This means that, after the transformations of the above, Equations 6.5 and 6.8 contain only four unknowns. The solution of these equations yields the numerical values of the wheel forces $F'^{(\prime\prime)}_{xi}$ and wheel slippages $s'^{(\prime\prime)}_{\delta i}$ for different driveline systems, different wheel arrangements on the wheelbase, and different arrangements for steering systems. These values of forces and slippages and the calculated coordinates X_a, Y_a, and β_a are used for assessing the energy efficiency and other operational properties of vehicles and for constructing the actual path of motion (the general criteria were discussed in Sections 1.4 and 1.5 and written out in detail in the subsequent chapters).

A particular difficulty in compiling a general algorithm of the computational study of curvilinear motion of multiaxle drive vehicles using the above equations consists in determining the circumferential forces of the wheels. For an example, this question is examined in more detail for the case of a vehicle with a positively engaged interaxle drive whose driving axles are equipped with self-locking (or open) differentials. The initial conditions (at $t = 0$) in integrating Equations 6.5 consist of data obtained for a uniform rectilinear motion of the vehicle.

Figure 6.2 shows a block diagram of the algorithm for determining the circumferential forces and slippages of the wheels that serves as a basis for the pertinent subroutine of the computer investigation.

To provide for logical transitions in this subroutine, it is necessary to specify, in the main program of the study of the curvilinear motion of the vehicle, a database known as *KL* the

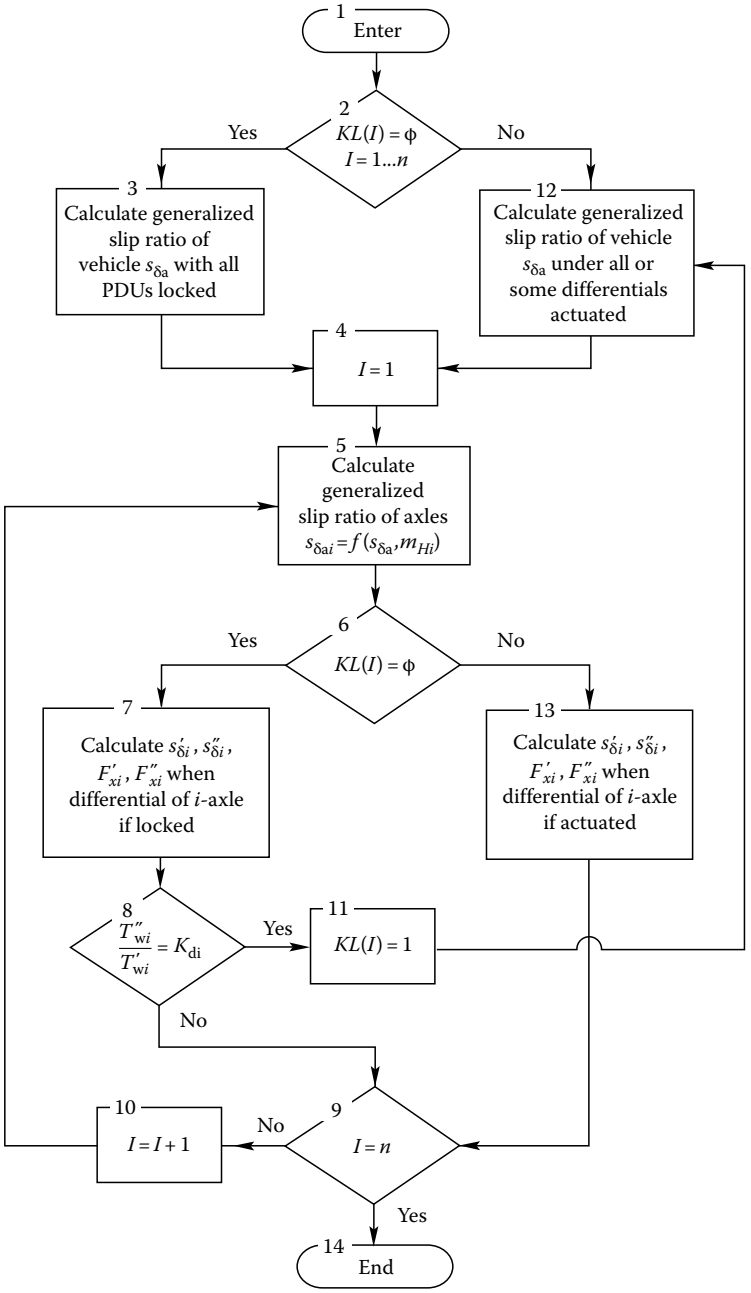


FIGURE 6.2
Block diagram.

dimensionality of which is equal to the number of the driving axles and all the elements are equal to zero.

The first approach to the subroutine for calculating the circumferential forces consists in determining the slippage $s_{\delta a}$ of the vehicle from Equation 6.8 on the condition that the interwheel differentials are locked (see item 3 in Figure 6.2). Then the generalized slippage

factors $s_{\delta ai}$, forces $F_{xi}^{\prime(\prime\prime)}$ and wheel slippages $s_{\delta i}^{\prime(\prime\prime)}$ are determined sequentially for all the n axles (items 5 and 7). Then the execution of the subroutine is stopped.

As soon as the check condition shown in item 8 is satisfied (i.e., the differential of at least one axle is actuated), the calculations are shifted to new formulae for calculating the generalized slippage $s_{\delta a}$ of the vehicle (item 12). At the same time, the element of the database *KL*, the number of which is equal to the number of the axle with the actuated differential, takes the value 1. This allows shifting to position 13 for calculating the circumferential forces and generalized slippages of the wheels of axles the differentials of which were actuated.

In turning to the subroutine at the next computational step, the generalized slippage $s_{\delta a}$ of the vehicle is determined either on the basis of position 3 or 12, depending on whether or not a differential of even one of the axles was actuated at the preceding computational step. Note that to determine the circumferential forces of the wheels of vehicles with open differentials in the axles, the input data must be fed by nonzero elements of the database *KL*.

Figure 6.3 illustrates the effect of different driveline systems on the turnability and stability of motion of a 24.465 ton 6×6 off-road truck.

The motion becomes unstable at the steered wheel angle $\delta = 11°$ and $R'_{a1} = 25.8$ m when the truck employs open interwheel differentials in its tandem (Figure 6.3a). At this steered angle the gripping force utilization factors are close to unity and the truck cannot make the turn (the truck is said to lose its turnability). The same truck with free-running interwheel differentials in the tandem becomes unstable at $R'_{a1} \geq 31$ m and $\delta \geq 11°$. In this case, the gripping force utilization factor of the front steered axle is $K_{\mu 1} = 1$ (see Figure 6.3b). The truck with free-running differentials should have its speed of 7 m/s and less to make a turn with the turn radius of $R'_{a1} = 30$ m. Table 6.1 presents additional results on the turnability and stability of the truck with three more different driveline systems (the gear ratio of the interaxle differential is $u_d = 2$ for the driveline systems shown by positions 3 and 4).

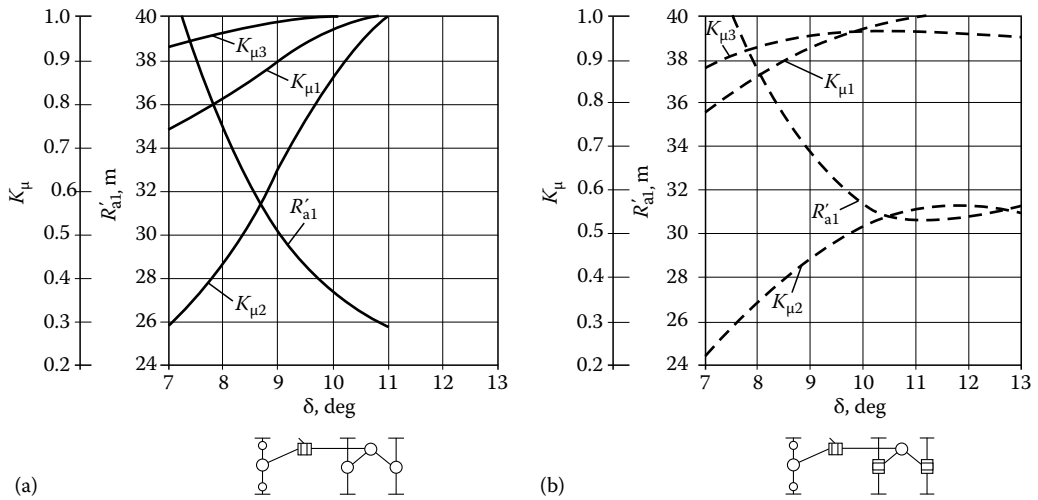
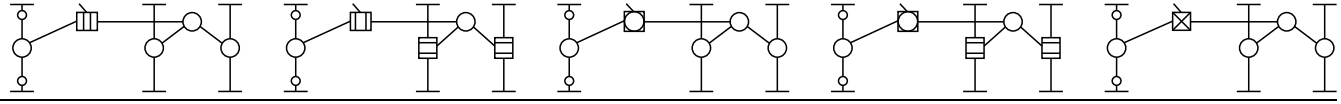


FIGURE 6.3
24.465 ton 6×6 off-road truck: actual turn radius of the front outer wheel R'_{a1} and the gripping force utilization factor K_μ on a slippery road ($V_x = 7$ m/s; $\mu_{px} = 0.2$); (a) and (b) – different driveline systems.

TABLE 6.1

Critical Speeds of 24.465 ton 6 × 6 Off-Road Truck

		Critical Speed, m/s				
		1	2	3	4	5
Friction Factor, μ_{px}	**Actual Turn Radius, R'_{a1}, m**					
0.8	30	14.3	13.9	14.5	14.4	14.2
	60	19.7	19.9	20.4	20.5	20.2
0.6	30	12.5	12.1	12.8	12.5	14.2
	60	17.4	17.4	18.0	17.9	17.8
0.4	30	10.1	9.9	10.6	10.2	10.6
	60	14.5	14.3	14.9	14.6	14.8
0.2	30	7.3	6.9	7.6	7.1	8.0
	60	10.2	10.0	10.5	10.2	10.5

It is seen from the table, the critical speed reduces when the surface conditions get worse (the friction coefficient decreases). The use of free-running interwheel differentials does not dramatically impact the critical speed of the truck comparing with open differentials in the tandem axles in good road conditions (positions 1 and 2, 3 and 4 in Table 6.1). The same can be noticed on the use of an interaxle free-running differential, an open asymmetrical differential, and positively locked transfer case (positions 2, 3, and 5). The impact becomes more visible in poor gripping conditions (lower values of the friction factor).

Figures 6.4 through 6.7 show the results of studies on the circumferential forces, energy efficiency, turnability, and stability of motion of an 8×8 terrain vehicle with a gross mass of about 40 ton with different driveline systems in curvilinear motion.

It is seen by comparing Figures 6.4 and 6.5 that locking of the interaxle differential of the front tandem or the central differential in the transfer case (or their simultaneous locking) highly increases the nonuniformity in the distribution of circumferential forces F_{xi} when taking a turn, causes parasitic power circulation, and reduces the transportation efficiency of the running gear. This also causes changes in the wheel slip angles and increases the actual turning radius R_a (the shortest distance from the turning center to the vehicle's longitudinal axis) of the vehicle (Figure 6.6). The change in R_a as compared with the theoretical turning radius R_t (without lateral slip) is illustrated by curves of variation in the turning radius variation factor q_R from formula (1.117) on this figure. The greatest increase in R_a and, consequently, in q_R, occurs with the central differential in the transfer case (Figure 6.6c) locked and at the same time positively engaged with the interaxle differential of the front tandem (see Figure 6.6d).

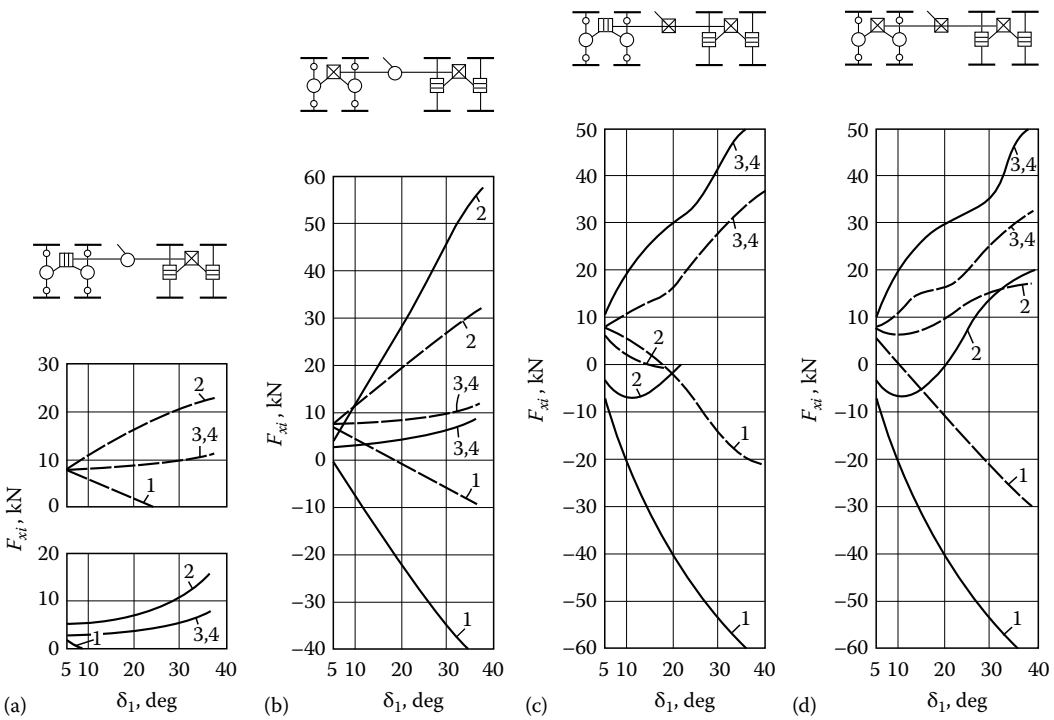


FIGURE 6.4
8×8 terrain vehicle: circumferential wheel forces in turn; $\bar{\pi} = 10$ km/h. ———, asphalt; — —, soil; axle numbers: 1, 2, 3, and 4.

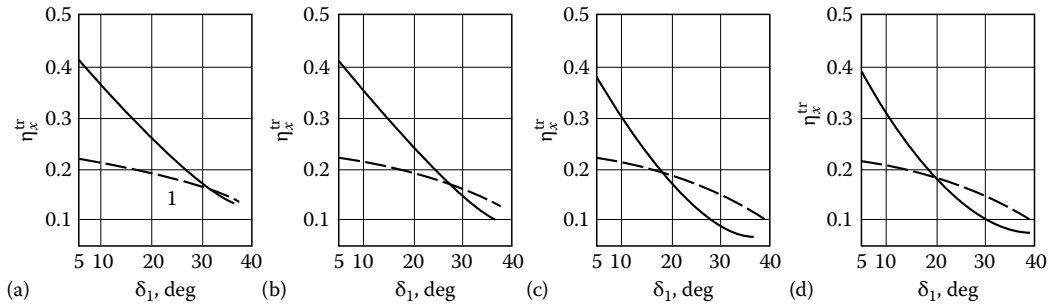


FIGURE 6.5
8 × 8 terrain vehicle: transportation running gear efficiency in turn; $\dot{\pi} = 10$ km/h. ———, asphalt; — —, soil.

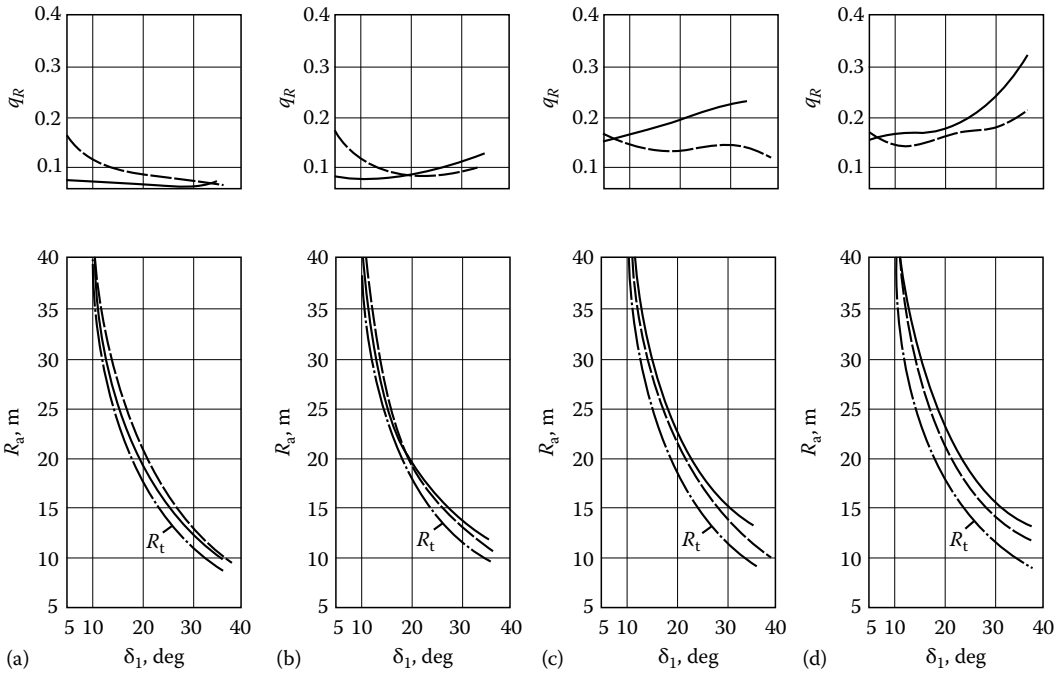


FIGURE 6.6
8 × 8 terrain vehicle: theoretical and actual radii of turn and turning radius variation factor; $\dot{\pi} = 10$ km/h. ———, asphalt; — —, soil.

The nonuniformity in the distribution of forces F_{xi}, caused by locking of the interaxle differentials reduces the available gripping force of the wheels and the stability of the vehicle's motion. This is illustrated by analytic curves of the gripping force utilization factor $K_{\mu i}$ from formula (1.119), shown in Figure 6.7. The three-driveline systems (Figure 6.7b through d) have close values of $K_{\mu i}$, which points to a high level of utilization of the gripping by wheels of all the axles simultaneously. Usually, the partial lateral slip of wheels sets on at $K_{\mu i} > 0.5$. This phenomenon for vehicles with the driveline systems

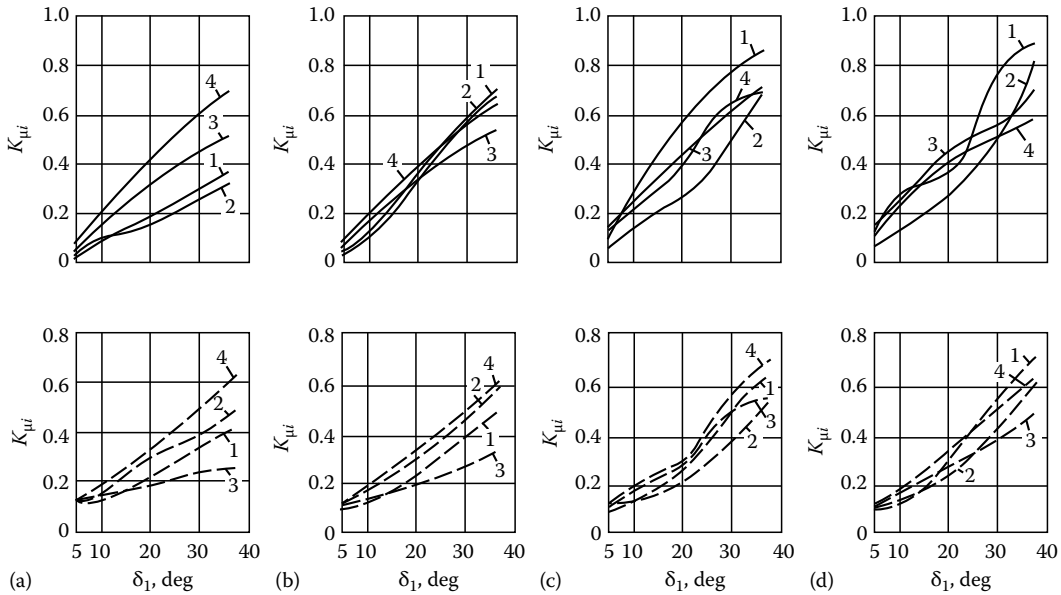


FIGURE 6.7
8×8 terrain vehicle: gripping force utilization factors; $\dot{\pi} = 10$ km/h. ———, asphalt; — —, soil; axle numbers: 1, 2, 3, and 4.

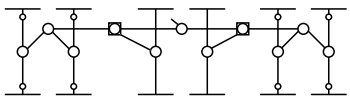
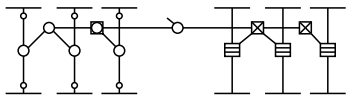
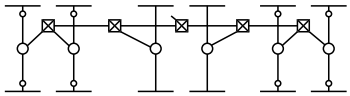
under study is observed at the front-wheel turning angle δ_1 from 27° to 30°. Comparison of the values of $K_{\mu i}$ shows that the vehicle with the driveline system shown in Figure 6.7a exhibits better stability.

Table 6.2 shows three layouts of the chassis and driveline system of a 12×12 vehicle with a gross mass of the order of 80 ton.

A computational study of a vehicle with these chassis designs and driveline systems has shown the following. Version 1 exhibits the best turnability. The minimum actual turning

TABLE 6.2

12×12 Vehicles

No.	Chassis and Driveline System Layout	Wheel Formula	Drive Formula	Axle Formula	Steering Formula
1		12 × 12	123456	2-2-2	12-00-56
2		12 × 12	123456	3-3	123-000
3		12 × 12	123456	2-2-2	12-00-56

radius of a vehicle as per version 1 is 7 m smaller than version 2. In circular motion with a radius of 25 m on a solid road, turning angle δ_1 of the front wheels is 1.73-fold smaller and the energy indicator is 1.64-fold smaller as compared with version 2. The vehicle of version 3 with a positively engaged interaxle differential has turnability parameters close to that of version 1 with a differential drive only at small δ_1. When the latter is increased, the turnability and stability of motion indicators of the vehicle of version 3 become perceptibly poorer.

In the turning of a vehicle with steering formula 12-00-56 the actual center of turn O_a shifts forward. As a result, the radius of the turn over the trace of the rear outer wheel is larger than the turn radius over the trace of the front outer wheel.

The above method of calculating the circumferential forces and slippages of the wheels of vehicles with different driveline systems can be also used in investigating the unsteady curvilinear motion. Consider the results of investigating the initiation of a turn of a 3.7 ton 4×4 tractor in the second gear over stubble (the front wheels are smaller than the rear wheels). The tractor turns under no load condition with a triple furrow plow suspended in the transportation position. The calculations were performed on the assumption that the interaxle drive is positively locked and that the axles have open symmetrical differentials. At the turn initiation segment, the turning rate of the steered wheels was 10°/s, and after 30° were reached, the steered wheels were no longer turned. Figure 6.8a shows the distribution of circumferential forces F_{x1} and F_{x2} between the axles under the above conditions of motion. Introducing the design kinematic discrepancy by changing the gear ratios in the drive of the tractor's axles reduces F_{x1} and increases F_{x2}.

The suspending of the plow exerts a greater effect on F_{x2} than on F_{x1}. Figure 6.7b shows the computed paths of the motion of the tractor under no load conditions over stubble under the same front-wheel turning conditions. For comparison, the figure shows the path of motion of the tractor in the absence of lateral wheel slip (curve 1). It is seen by comparing curve 1 with curves 2 and 3 obtained in the presence of lateral slip that locking the interaxle drive has a marked effect on the path of motion and on the actual turning radius R_a. The variation in the latter is illustrated in Figure 6.8b by the curves of factor q_R.

Introducing the design kinematic discrepancy $m_{H1} = -0.043$ and $m_{H2} = 0.024$ does not have a marked effect on the path of the tractor's motion (curves 2 and 3 in Figure 6.8b). The kinematic discrepancy has a greater effect on the wheel slippage power loss (Figure 6.8c). This result is in agreement with data from Sections 2.8, 3.4, and 3.5.

6.1.2 Articulated Vehicles with Steered Wheels

The steering arrangement under which segments of a vehicle are made to move relatively to one another combined with the use of steered wheels is in rather extensive use. Tractors and power-module driven vehicular trains (see Table 1.12), articulated trucks, tactical military vehicles, and some of planetary rover prototypes are types of vehicles that frequently utilize such steering arrangements.

It appears advisable to compile the equations of motion of articulated vehicles on the basis of a multimass computational model compiled by the number of segments. Unlike the single-mass model, such an approach allows incorporating the variation in the vehicle's moment of inertia about a vertical axis, because the segments fold together in the course of the turn.

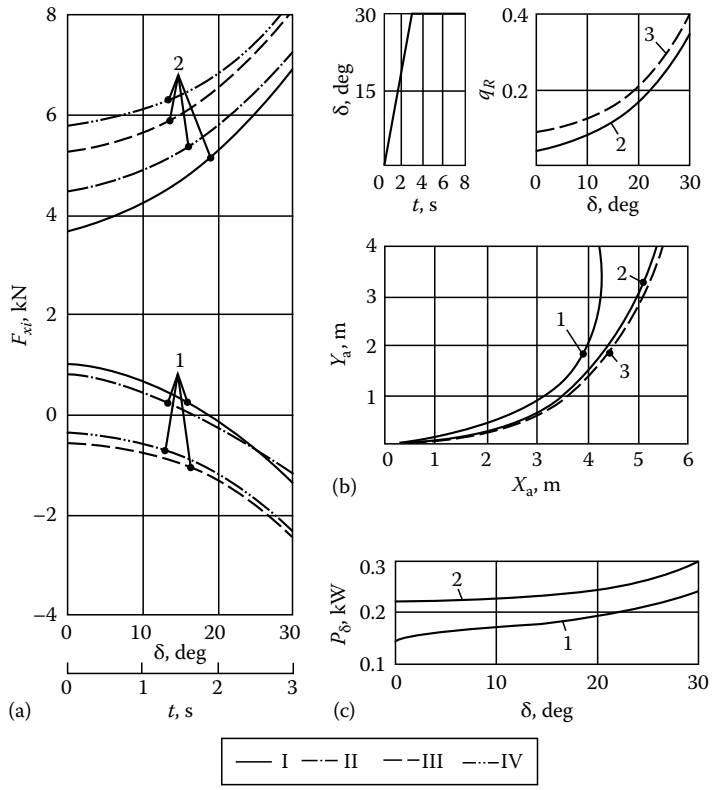


FIGURE 6.8
3.7 ton 4 × 4 tractor entering a turn with no traction load; (a) circumferential forces F_{x1} (1) and F_{x2} (2): I and II with no plow and with a plow at zero design kinematic discrepancy; III and IV with no plow and with a plow at $m_{H1} = -0.043$; $m_{H2} = 0.024$; (b) trajectory path (X_a and Y_a) and the turning radius variation factor q_R: 1, with no lateral slip; 2, at zero design kinematic discrepancy; 3, at $m_{H1} = -0.043$; $m_{H2} = 0.024$; (c) slippage power losses P_δ: 1 and 2, at zero design kinematic discrepancy and at $m_{H1} = -0.043$; $m_{H2} = 0.024$.

Consider a method for investigating the effect of the driveline systems on the force loads on the wheels for the case of an articulated vehicle. The computational two-mass model of the motion is shown in Figure 6.9.

Such a model can be used, for example, in investigating the turning of power-module driven vehicular trains (Figures 1.38 and 3.31) and, after some refinements—of vehicular timber carriers. After the method is examined for the above vehicles, it can be extended to other layouts of articulated vehicles.

The vehicle moves over a straight horizontal surface in the fixed $X0Y$ coordinate system. Moving coordinate systems $x_1 0_1 y_1$ and $x_2 0_2 y_2$ are associated with the centers of mass of the links (segments). The location of the vehicle in the $X0Y$ coordinate system is determined by the coordinates of the centers of mass X_a, Y_a and X_M, Y_M and also by the angles β_a and β_M between their longitudinal axes and the $0X$ coordinate axis.

To compile equations in the Appel form (6.1), six quasi-coordinates are introduced that are related to the coordinates of the links in the fixed $X0Y$ coordinate system by the equations (Figure 6.9):

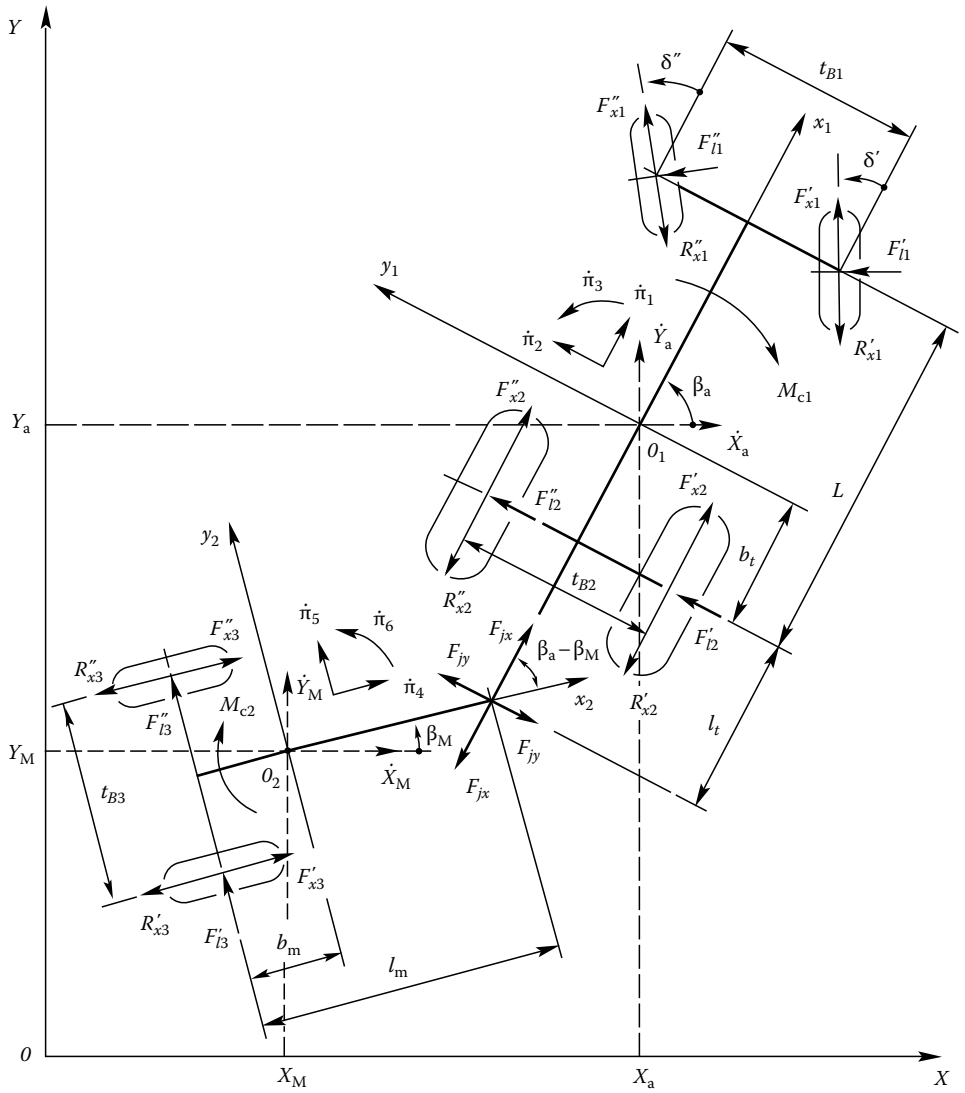


FIGURE 6.9
6 × 6 power-module driven vehicular train: free-body diagram.

$$
\begin{aligned}
\dot{X}_a &= \dot{\pi}_1 \cos\beta_a - \dot{\pi}_2 \sin\beta_a,\\
\dot{Y}_a &= \dot{\pi}_1 \sin\beta_a + \dot{\pi}_2 \cos\beta_a,\\
\dot{\beta}_a &= \dot{\pi}_3\\
\dot{X}_M &= \dot{\pi}_4 \cos\beta_M - \dot{\pi}_5 \sin\beta_M,\\
\dot{Y}_M &= \dot{\pi}_4 \sin\beta_M + \dot{\pi}_5 \cos\beta_M,\\
\dot{\beta}_M &= \dot{\pi}_6
\end{aligned}
\tag{6.9}
$$

The acceleration energy is determined as the sum of the acceleration energies of the links:

$$S = S_{\mathrm{a}} + S_{\mathrm{M}} = \frac{1}{2} m_{\mathrm{a}} \left(\ddot{X}_{\mathrm{a}}^2 + \ddot{Y}_{\mathrm{a}}^2 + \rho_{\mathrm{a}}^2 \ddot{\beta}_{\mathrm{a}}^2 \right) + \frac{1}{2} m_{\mathrm{M}} \left(\ddot{X}_{\mathrm{M}}^2 + \ddot{Y}_{\mathrm{M}}^2 + \rho_{\mathrm{M}}^2 \ddot{\beta}_{\mathrm{M}}^2 \right), \tag{6.10}$$

where m_{a} and m_{M} are the masses of the links and ρ_{a} and ρ_{M} are the radii of inertia of the links.

Making use of Equations 6.9 and 6.10 and the expressions for the generalized forces Q_i obtained from the virtual works from formula (6.4), the equations of motion of the articulated vehicle become

$$\begin{aligned}
m_{\mathrm{a}}(\ddot{\pi}_1 - \dot{\pi}_2 \dot{\pi}_3) &= \left(F''_{x1} - R''_{x1}\right) \cos \delta''_1 + \left(F'_{x1} - R'_{x1}\right) \cos \delta'_1 \\
&\quad - F''_{l1} \sin \delta''_1 - F'_{l1} \sin \delta'_1 + F''_{x2} + F'_{x2} - R''_{x2} - R'_{x1} - F_{jx}; \\
m_{\mathrm{a}}(\ddot{\pi}_2 + \dot{\pi}_1 \dot{\pi}_3) &= \left(F''_{x1} - R''_{x1}\right) \sin \delta''_1 + \left(F'_{x1} - R'_{x1}\right) \sin \delta'_1 \\
&\quad + F''_{l1} \cos \delta''_1 + F'_{l1} \cos \delta'_1 + F''_{l2} + F'_{l2} + F_{jy}; \\
m_{\mathrm{a}} \rho_{\mathrm{a}}^2 \ddot{\pi}_3 &= 0.5 t_{\mathrm{B1}} \left[-\left(F''_{x1} - R''_{x1}\right) \cos \delta''_1 + F''_{l1} \sin \delta''_1 \right] \\
&\quad + 0.5 t_{\mathrm{B1}} \left[\left(F'_{x1} - R'_{x1}\right) \cos \delta'_1 - F'_{l1} \sin \delta'_1 \right] \\
&\quad + (L - b_t) \left[\left(F''_{x1} - R''_{x1}\right) \sin \delta''_1 + F''_{l1} \cos \delta''_1 \right] \\
&\quad + (L - b_t) \left[\left(F'_{x1} - R'_{x1}\right) \sin \delta'_1 + F'_{l1} \cos \delta''_1 \right] \\
&\quad - 0.5 t_{\mathrm{B2}} \left(F''_{x2} - R''_{x2}\right) + 0.5 t_{\mathrm{B2}} \left(F'_{x2} - R'_{x2}\right) \\
&\quad - \left(F''_{l2} + F'_{l2}\right) b_t - F_{jy}(b_t + l_t) - M_{\mathrm{c1}}; \\
m_{\mathrm{M}}(\ddot{\pi}_4 - \dot{\pi}_5 \dot{\pi}_6) &= F''_{x3} - R''_{x3} + F'_{x3} - R'_{x3} + F_{jx} \cos(\beta_{\mathrm{a}} - \beta_{\mathrm{M}}) \\
&\quad + F_{jy} \sin(\beta_{\mathrm{a}} - \beta_{\mathrm{M}}); \\
m_{\mathrm{M}}(\ddot{\pi}_4 + \dot{\pi}_5 \dot{\pi}_6) &= F''_{l3} + F'_{l3} + F_{jx} \sin(\beta_{\mathrm{a}} - \beta_{\mathrm{M}}) \\
&\quad - F_{jy} \cos(\beta_{\mathrm{a}} - \beta_{\mathrm{M}}) \\
m_{\mathrm{M}} \rho_{\mathrm{M}}^2 \ddot{\pi}_6 &= -0.5 t_{\mathrm{B3}} \left(F''_{x3} - R''_{x3}\right) + 0.5 t_{\mathrm{B3}} \left(F'_{x3} - R'_{x3}\right) \\
&\quad - \left(F''_{l3} + F'_{l3}\right) b_{\mathrm{m}} + F_{jx} \sin(\beta_{\mathrm{a}} - \beta_{\mathrm{M}})(l_{\mathrm{m}} - b_{\mathrm{m}}) \\
&\quad - F_{jy} \cos(\beta_{\mathrm{a}} - \beta_{\mathrm{M}})(l_{\mathrm{m}} - b_{\mathrm{m}}) - M_{\mathrm{c2}}.
\end{aligned} \tag{6.11}$$

where M_{c1} and M_{c2} are the moments of resistance to the turn in the contact between the tires of the links and the support surface.

The lateral reactions of the wheels are, as before, represented as the product of the lateral slip resistance factors and the slip angles (see formula (1.45)). The slip angles, in their turn are expressed in terms of the angles of turn of the wheels and the projection of the velocities

of the wheels on the longitudinal and transverse axes of the links. For the front, steered wheels,

$$\alpha_1^{\prime(\prime\prime)} = \delta_1^{\prime(\prime\prime)} - \arctan\frac{V_{y1}^{\prime(\prime\prime)}}{V_{x1}^{\prime(\prime\prime)}}, \tag{6.12}$$

for the wheels of the second and third axles:

$$\alpha_2^{\prime(\prime\prime)} = \arctan\frac{V_{y2}^{\prime(\prime\prime)}}{V_{x2}^{\prime(\prime\prime)}}, \quad \alpha_3^{\prime(\prime\prime)} = \arctan\frac{V_{y3}^{\prime(\prime\prime)}}{V_{x3}^{\prime(\prime\prime)}}, \tag{6.13}$$

where $V_{xi}^{\prime(\prime\prime)}$ and $V_{yi}^{\prime(\prime\prime)}$, as in formula (6.6), can be expressed in terms of the corresponding quasi-velocities and geometric parameters of the vehicle.

The presence of the hinge makes it possible to compile equations relating the velocities of the vehicle's links that are needed for solving differential equations (6.11) in order to eliminate the redundant unknowns from them. These relationships are derived from postulating equality of the velocities of both links at their hinge connection and are

$$\begin{aligned}
&\dot{\pi}_1 - \dot{\pi}_4\cos(\beta_a - \beta_M) - [\dot{\pi}_5 + \dot{\pi}_6(l_m - b_m)]\sin(\beta_a - \beta_m) = 0,\\
&\dot{\pi}_2 - \dot{\pi}_3(b_t + l_t) + \dot{\pi}_4\sin(\beta_a - \beta_M) - [\dot{\pi}_5 + \dot{\pi}_6(l_m - b_m)]\cos(\beta_a - \beta_M) = 0
\end{aligned} \tag{6.14}$$

If now components F_{jx} and F_{jy} of the force at the hinge are determined from the first two of Equations 6.11 and their value is substituted into the third equation, expressing the quasi-velocities and quasi-accelerations with subscripts 1 and 2 from equations of constraints (6.14), then only the circumferential forces of the wheels will remain redundant in the four resulting equations. This requires establishing additional relationships between forces $F_{xi}^{\prime(\prime\prime)}$ in order that the number of equations is equal to the number of the unknowns contained in them. The form of these equations depends on the driveline system of the wheels and can be compiled for any of them on the basis of the relationships presented in Chapters 2 through 5. A method of calculating circumferential forces of the 6×6 power-module driven vehicular train is shown in Figure 6.9. The interaxle driveline is a positive engagement, the first and third axles employ limited slip differentials, whereas the second has an automatically locking differential that disengages when the front wheels turn through an angle $\delta = 8^\circ$. The relationships between the circumferential forces and the wheel slippage are now established. At the initial part of the turn, at low values of δ, all the interwheel differentials are locked and the relationships between generalized slippages $s_{\delta ai}$ of the axles and the generalized slippage $s_{\delta a}$ of the vehicle are determined by formula (3.37). The axle generalized slippages, in their turn, are related to the slippages $s'_{\delta i}$ and $s''_{\delta i}$ of the wheels by formula (3.58).

If one of the limited slip differentials has been actuated or if the automatically locking differential of the second axle has been unlocked, then the relationships between the generalized slippage $s_{\delta ai}$ of this axle and the slippages $s'_{\delta i}$ and $s''_{\delta i}$ of its wheels is given by formula (6.17), and the ratio of the circumferential forces of the wheels is equal to the locking coefficient K_{di}. Then for the second axle one must set $K_{d2} = 1$. The above-established

sequence of computations using these relationships in the course of simultaneous solution of equations of motion (6.11) and Equation 6.7 comprise the algorithm of calculating the circumferential forces and wheel slippages when taking a turn. A block diagram of this algorithm is given in Figure 6.2.

Consider now the method of compiling relationships between the circumferential forces of the wheels for the case of a timber carrier consisting of a 4×4 tractor and a pole trailer with driven wheels. The driving axles of the tractor are equipped with open symmetrical differentials and the transfer case with an asymmetrical differential with a gear ratio $u_{\mathrm{d}} = 2$. The following relationships exist between the circumferential forces of the wheels (for better clarity the wheel radii are assumed to be the same);

$$F''_{x1} = F'_{x1}; \quad F''_{x2} = F'_{x2}; \quad \frac{F''_{x2} + F'_{x2}}{F''_{x1} + F'_{x1}} = u_{\mathrm{d}} \tag{6.15}$$

If it is assumed that $F_x = K_x s_\delta$, then relationships (6.15) become

$$K''_{x1} s''_{\delta 1} = K'_{x1} s'_{\delta 1}; \quad K''_{x2} s''_{\delta 2} = K'_{x2} s'_{\delta 2}; \quad \frac{K''_{x2} s''_{\delta 2} + K'_{x2} s'_{\delta 2}}{K''_{x1} s''_{\delta 1} + K'_{x1} s'_{\delta 1}} = u_{\mathrm{d}} \tag{6.16}$$

Using the assumptions made in Chapter 2, the relationships between wheel slippages $s^{\prime(\prime\prime)}_{\delta i}$, generalized slippages $s_{\delta \mathrm{a}i}$ of the axles, and the generalized slippage $s_{\delta \mathrm{a}}$ of the vehicle are written as

$$s_{\delta \mathrm{a}i} = 1 - \frac{2R_{\mathrm{t}i}(1 - s'_{\delta i})(1 - s''_{\delta i})}{R'_{ti}(1 - s''_{\delta i}) + R''_{ti}(1 - s'_{\delta i})}, \quad i = 1, 2 \tag{6.17}$$

$$s_{\delta \mathrm{a}} = 1 - \frac{R_{\mathrm{ta}}(1 + u_{\mathrm{d}})(1 - s_{\delta \mathrm{a}1})(1 - s_{\delta \mathrm{a}2})}{R_{\mathrm{t}1}(1 - s_{\delta \mathrm{a}2}) + R_{\mathrm{t}2} u_{\mathrm{d}}(1 - s_{\delta \mathrm{a}1})}$$

where the turning radii $R_{\mathrm{t}1}$, $R_{\mathrm{t}2}$, R_{ta}, R'_{ti}, and R''_{ti} are expressed in terms of the geometric parameters of the tractor and the turning angles of the wheels.

This means that expressions (6.16) and (6.17) make it possible to represent the circumferential forces as a function of the generalized slippage $s_{\delta \mathrm{a}}$ of the vehicle that is determined in the course of the solution of the equations of motion together with Equation 6.8. The proper equations of motion (6.11) must be modified to account for the placement of two nondriving axles with dual tires in the second (pole) link of the timber carrier vehicular train.

Figure 6.10 shows the computed curves that reflect the characteristics of the timber carrier in circular motion on an asphalt-paved road with different values of the turn angle δ of the front wheels.

The circumferential forces of the axles increase with δ and the difference in their slippage also increases but insignificantly. Here the ratio F_{x2}/F_{x1} is constant and equal to $u_{\mathrm{d}} = 2$. The transportation running gear efficiency η_x^{tr} decreases, which is primarily caused by the increase in the resistance to motion. The difference between the theoretical and actual turn radii (with allowance for wheel slip) represented by the factor q_R from formula (1.117) amounts to 12.5%.

6.2 A Method of Synthesizing Driveline Systems with Optimal Properties

Section 1.5 was concerned with a vehicle's operational properties. The criteria for assessing these properties depend on the properties of the vehicle driveline systems. Based on these data the main principles of design of the driveline system were formulated in Section 1.6. These principles are used in this section for developing a method of search of optimal distributions of power among the wheels of multiwheel drive vehicles.

The previously mentioned analysis of the operational properties of transportation-traction vehicles and the criteria for their assessment indicates that the determination of the optimal distribution of power between the wheels is a multicriteria problem. The search for such relationships on the basis of criteria of various operational properties may yield contradictory results, for example, locking the interwheel differential improves the mobility of the vehicle, but its turnability deteriorates. For this reason, one of the methods of solution of multicriteria problems should solve the problem of finding optimal distributions of power to the wheels. Consider a method and a general algorithm of optimizing the power supplied to the wheels and synthesis of the properties of the mechanisms for power-dividing units of multiwheel drive transportation-traction vehicles.

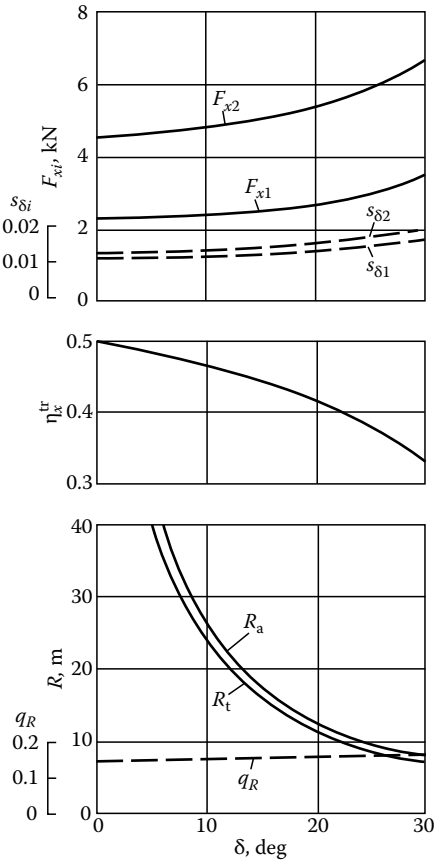


FIGURE 6.10
Force, kinematic, and energy characteristics of a timber carrier.

The principal optimization criteria (that are also called quality functionals) in investigating highway and off-road automobiles and tractors shall consist of the criteria of traction and velocity properties. These consist of the efficiencies of the running gear: the transportation efficiency η_x^{tr}, the traction efficiency η_x^{t}, and the total efficiency $\eta_{x\Sigma}$. This approach is based on the fact that these criteria, as previously mentioned in Section 1.5, are directly related to the productivity of automobile and tractor engineering. Pertinent constraints shall be imposed on the indicators of other operational properties.

In keeping with the above, the general form of the objective function for highway and off-road trucks and vehicular trains is

$$\eta_x^{tr} \rightarrow \max \tag{6.18}$$

upon the following constraints on the parameters being optimized

$$\sum_{i=1}^{n} F_{xi}^{\prime(\prime\prime)*} = F_{x\Sigma},$$

$$0 < F_{xi}^{\prime(\prime\prime)*} < R_{zi}^{\prime(\prime\prime)} \mu_{pxi}^{\prime(\prime\prime)} \tag{6.19}$$

$$F_{xi}^{\prime(\prime\prime)*} = f_i^{\prime(\prime\prime)}\left(s_{\delta i}^{\prime(\prime\prime)*}\right), \quad i = 1, n$$

The total circumferential force $F_{x\Sigma}$ of the driving wheels is calculated from formula (1.74), whose form is refined to accommodate the type of vehicle under study and of the work that it performs. As noted in Section 1.6, the problem of finding the optimum distribution of power between the wheels is solved as the inverse problem of dynamics. This specifies the required functional relationship between the vehicle's velocity V_x and its acceleration a_x. Such a relationship was compiled from the analysis of statistical data:

$$a_x = a_x^{\max}\left[\frac{1}{\alpha_1 + (V_{xc}/V_x)^{\alpha_2}} - \alpha_1\right]^{1/\alpha_2} \tag{6.20}$$

where $a_x^{\max}$ is the maximum acceleration that corresponds to the onset of the increase in velocity and V_{xc} is the steady velocity attained in the course of acceleration. The values of $a_x^{\max}$ and V_{xc} should be specified with consideration of their desired values depending on the type of the vehicle. The approximation factors are, $\alpha_1 = 0.618$ and $\alpha_2 = 0.830$.

The specific form of the objective function is determined from formulae presented in Section 1.4.2 depending, for an example, on the presence and combination of semitrailer and trailer links of the vehicular train and the relationship between the driving and driven axles.

In investigating tractors (traction vehicles), it is necessary to compile the objective function for finding optimal values of $F_{xi}^{\prime(\prime\prime)*}$ and $s_{\delta i}^{\prime(\prime\prime)*}$, which is as follows:

$$\eta_x^t \rightarrow \max \tag{6.21}$$

This function makes it possible to optimize the distribution of wheel power in traction work with farm and working equipment at constraints (6.19). The form of the latter is modified, somewhat, for farm tractors because of the need to limit the level of wheel slippage to preserve the soil layer of the fields:

$$\sum_{i=1}^{n} F_{xi}^{\prime(\prime\prime)*} = F_{x\Sigma}$$
$$0 < F_{xi}^{\prime(\prime\prime)*} \le F_{x\Delta i}^{\prime(\prime\prime)} \tag{6.22}$$

where $F_{x\Delta i}^{\prime(\prime\prime)}$ corresponds to the maximum permissible slippage $s_{\delta\Delta i}^{\prime(\prime\prime)}$. For all-wheel drive tractors at nominal drawbar pull usually $s_{\delta\Delta i}^{\prime(\prime\prime)} = 0.14$.

The circumferential forces of the wheels and their slippages found from formulae (6.18) through (6.22) correspond to optimal distributions of power among the wheels, that is, the best traction and velocity properties and energy efficiency of the vehicle's running gear.

The algorithm for finding the optimal distribution of power between the wheels on the basis of previously presented objective functions is shown in Figure 6.11.

The first stage consists of compiling mathematical models of rectilinear motion of the vehicle under the principal operational conditions and these serve for determining the total circumferential force $F_{x\Sigma}$ equal to the sum of forces resisting the motion that is needed for this motion. For highway vehicles, this means moving over horizontal roads with up and

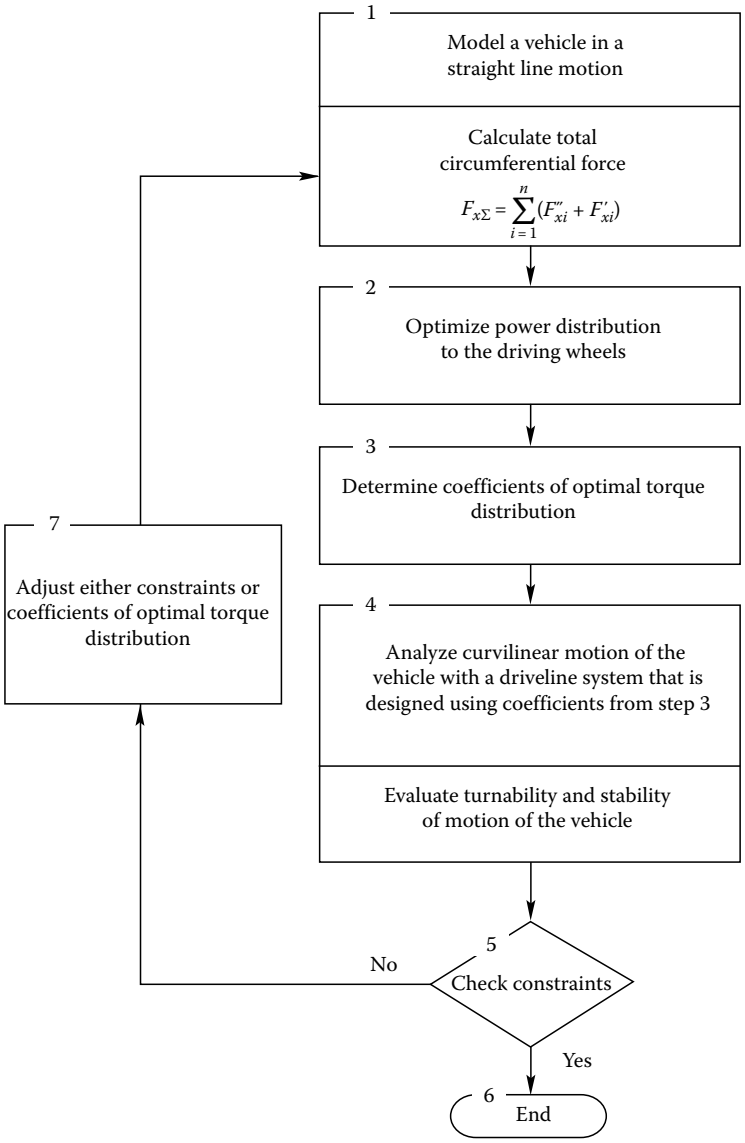


FIGURE 6.11
Algorithm for determining optimal wheel power distribution.

down slopes. The mathematical models for off-road vehicles should be compiled for conditions of motion over deformable soil. However, provisions must be made to make possible modeling of motion over high-grade roads. Mathematical models of tractors that are usually compiled for conditions of motion over soil should incorporate specifics of its operational conditions (for example, the fact that the tractor moves at a slant when plowing, when the wheels of one side roll in the furrow and those of the other side on the stubble; probability of work with different drawbar forces). In all cases, the possibility of the onset of different gripping conditions beneath individual wheels must be considered for all the transportation-traction vehicles.

After the values of the total circumferential force of the vehicle $F_{x\Sigma}$ needed for motion have been calculated from mathematical models, a search is made for optimal distributions of forces $F_{xi}^{\prime(\prime\prime)*}$ on the basis of previously compiled objective functions and constraints (Figure 6.11, item 2).

Then optimal wheel torques $T_{\mathrm{w}i}^{\prime(\prime\prime)*}$ are calculated on the basis of the optimal values of the circumferential forces of the wheels $F_{xi}^{\prime(\prime\prime)*}$ and rolling radii in the driven mode $r_{\mathrm{w}i}^{0\prime(\prime\prime)}$. This is followed by computing the factors of the optimal distribution of torques among the driving wheels:

$$K_{\mathrm{m}ki} = \frac{T_{\mathrm{w}i}^{\prime\prime *}}{T_{\mathrm{w}i}^{\prime *}}; \quad K_{\mathrm{m}ki}^{\prime\prime} = \frac{T_{\mathrm{w}i}^{\prime\prime *}}{T_{\mathrm{w}i}^{\prime\prime *} + T_{\mathrm{w}i}^{\prime *}}; \quad K_{\mathrm{m}ki}^{\prime} = \frac{T_{\mathrm{w}i}^{\prime *}}{T_{\mathrm{w}i}^{\prime\prime *} + T_{\mathrm{w}i}^{\prime *}}; \quad i = 1, n \tag{6.23}$$

and between the axles

$$K_{\mathrm{m}oi} = \frac{T_{\mathrm{w}i}^{\prime\prime *} + T_{\mathrm{w}i}^{\prime *}}{\sum_{i=1}^{n} T_{\mathrm{w}i}^{\prime(\prime\prime)*}}; \quad K_{\mathrm{m}oi}^{k,\ldots kk-l,\ldots ll} = \frac{\sum_{i=l}^{ll} T_{\mathrm{w}i}^{\prime(\prime\prime)*}}{\sum_{i=k}^{kk} T_{\mathrm{w}i}^{\prime(\prime\prime)*}}; \tag{6.24}$$

where *l*, *ll*, *k*, and *kk* are the numbers of the driving axles, between which the distribution of optimal traction forces is investigated. These factors are investigated at the next stage (Figure 6.11, item 3). The values of the distribution factors found in this manner make it possible to synthesize the optimal properties of mechanisms for interaxle and interwheel power-dividing units. In fact, having designed driveline systems that provide a torque distribution as indicated by factors $K_{\mathrm{m}ki}$ and $K_{\mathrm{m}oi}$ obtained above, it can be claimed that the efficiencies of the running gear of the transportation-traction vehicles under discussion will, under actual operating conditions, be close to the optimal, that is, the distribution of power among the wheels will be close to optimal. Thus, for example, in designing the limited slip interwheel differentials their locking coefficients $K_{\mathrm{d}i} = T_{\mathrm{w}i}^{\prime\prime}/T_{\mathrm{w}i}^{\prime}$ should correspond to the relationships governing the variation in the distribution of $K_{\mathrm{m}ki}$ from formulae (6.23).

Then the problem of the effect of the optimal power distributions and properties of mechanisms in power-dividing units that bring about conformance to these laws on other operating properties of the transportation-traction vehicles, such as their turnability and stability of motion arises. As previously noted, constraints must be imposed on the assessment criteria of these properties. Hence, further investigations include calculation of the criteria of turnability and stability followed by a check on the conformance to the constraints (Figure 6.11, items 4 and 5). For this, one compiles mathematical models of the vehicle's motion that incorporate the optimal power distributions that were found and the properties of the mechanisms that implement these laws. Section 6.1 was concerned with methods for compiling equations and examples for vehicles with different mechanisms in the power-dividing units. The solutions of these equations of motion serve for determining turnability and stability criteria that are compared with the constraints:

$$q_R = \frac{R_{\mathrm{a}} - R_{\mathrm{t}}}{R_{\mathrm{t}}} \le \varepsilon_R; \quad E \le \varepsilon_E$$

$$K_{\mu i} = \frac{\sqrt{F_{xi}^2 + F_{li}^2}}{\mu_{\mathrm{p}xi} R_{zi}} \le \varepsilon_\mu; \quad V_{\mathrm{cr}} > V_x \tag{6.25}$$

where ε_R, ε_E and ε_μ are the constraints, V_x is the actual velocity of the vehicle along its longitudinal axis and V_{cr} is the critical velocity. The energy expended in curvilinear motion of the vehicles can be assessed by the applicable efficiencies of the running gear and by the efficiency of the vehicles in the traction, transportation, and traction-transportation (combined) modes.

If constraints (6.25) are satisfied, then the problem is regarded as solved and the power distributions and properties of mechanisms that satisfy these laws are regarded as optimal. If any of the constraints (6.25) is not satisfied and are not regarded as satisfactory by the investigator, they are corrected. In individual cases, when constraints (6.25) cannot be changed from safety considerations, it may become necessary to constrain the distribution factors from formulae (6.23) and (6.24). This is reflected by item 7 in Figure 6.11. Then the researcher returns to item 1 and the solution is reiterated.

Section 6.3 presents a mathematical analysis of the objective functions, the results of which are needed for practical design of mechanisms and systems for dividing the power between the driving wheels. The algorithm thus worked out is applied in Sections 6.4 through 6.6 for particular and general problems of synthesis of properties of mechanisms for vehicular power-dividing systems.

6.3 Objective Function Analysis

A mathematical analysis of the criteria of vehicle operational properties (which are considered objective functions) is carried out for finding their extrema values and determining the boundary conditions that allow the extremes of the objective functions to occur. This analysis must precede the optimization of power at each of the driving wheels and development of algorithms for optimizing the properties of driveline systems and further controlling vehicle performance.

The purpose of this section is to carry out such a mathematical analysis of one of the objective functions and to present some mathematical fundamentals and principles for controlling power distributions to the driving wheels that follow from that analysis. The developments reported in this section include a mathematical model of a multiwheel drive vehicle with any arbitrary given number m of axles and number n of driving axles and an objective function to optimize vehicle energy efficiency and tractive and velocity operational properties. In addition, the mathematical model-based analysis is followed by some principles and recommendations for design practice.

The mathematical analysis is preceded by analysis of the results of investigations performed previously by various investigators that have a bearing on the problem of optimizing the power distribution between the driving wheels. The first analysis of wheel slips and wheel longitudinal forces was given in the 1905 publication of Zhukovsky.

It was subsequently found that the wheel torque/circumferential wheel force is functionally linked to the effective tire rolling radius/tire slip. This function can be either linear or nonlinear depending on the specifics of the interaction between the tire and the surface of motion. Conditions at which the power loss in the tire-surface contact patches of a vehicle is at a minimum have been discussed for decades based on some function or the other.

Chudakov (1946) and Korotonoshko (1948) proved that a difference in the effective rolling radii could lead to the inequality of wheel torques and to parasitic power generation that

imposes a load on the vehicle's driveline and increases fuel consumption. Dr. Chudakov's analysis was done for an experimentally proven linear function relating the wheel torque and the effective rolling radius given by formula (1.20).

It was found by a rigorous theoretical analysis and confirmed in experiments by Lefarov and his research group in the 1960s and 1970s that the power expended in wheel slippage by a 4×4 vehicle, is at a minimum at equal slippages of the front and rear wheels (see Sections 1.4.3, 2.9, and 3.4):

$$s_{\delta 1} = s_{\delta 2} \tag{6.26}$$

This was proved based on the formula (1.25) derived by Dr. Lefarov for tires rolling on firm and dense surfaces. The result presented by formula (6.26) holds irrespective of whether or not the longitudinal stiffness factors of the front and rear tires (or tires and soil) are equal to one another. It is totally independent of the road conditions. Dr. Lefarov proved this through an analysis of the first derivative of the total power expended on wheel slippage with respect to the degree of the distribution of the circumferential wheel forces between the driving axles of a 4×4 vehicle.

Chudakov showed in 1972 that the best tractive performance of a 4×4 tractor with positive engagement of the driving axles is attained at equal theoretical velocities of the front and rear wheels assuming the same tire slip.

The above results are in use for designing locking differentials and on-demand systems for decades. Indeed, when an interwheel differential is fully locked, the slip factors of the left and right wheels of vehicle in rectilinear motion are virtually the same.

For numerous deformable surfaces, the function relating tire slip s_δ and circumferential force F_x becomes nonlinear due to the soil structure and its moisture. Such nonlinear functions are either derived mathematically using a tire-soil model of deflections or found experimentally from statistical analysis of experimental data.

Guskov and Buimov concluded in the late 1960s that the tractive efficiency of a 4×4 tractor with positively engaged front and rear axles is highest when the slip factors of the front and rear wheels are not equal. This was derived using function (1.26) on assumption of the same factors μ_{px} and k for both the front and rear wheels; as stated in that paper, efficiency also depends on the shifting of weight between the front and rear wheels.

J. Wong proved analytically in his seminal study published in 1970 that the slip efficiency is at maximum when the slip of the front wheels equals that of the rear wheels. This was done for a 4×4 vehicle subjected to a drawbar load under normal operating conditions; the study was based on a tire–soil interaction research carried out by Reece (1964).

Wong et al. (1998, 2000) proved experimentally that the slip efficiency attains its maximum at a theoretical speed ratio equal or close to 1. Simply stated, the slip efficiency reaches its peak when the theoretical velocities of the front and rear wheels are equal to one another. The equality in these theoretical speeds causes the slips of the front and rear wheels to be equal. This conclusion was extended to the vehicle tractive efficiency with reference to the fact that the slip efficiency is a major component of this efficiency.

Steinkamf showed in 1972, using test data obtained for a 4×4 tractor with different front and rear wheels, that higher running gear efficiencies are attained at equal slip factors for all the wheels in the vast majority of road conditions.

In the late of 1970s, an experimental research by Murillo-Soto and Smith for a physical model of a 4×4 tractor with identical front and rear wheels showed that the relationship between the model tractive efficiency and the angular velocity ratio of the front and rear

wheels ω_{w1}/ω_{w2} is ambiguous. The behavior of this relationship is strongly influenced by the hitch height h_d and the weight shift factors $\lambda_1 = W_1/W_a$ and $\lambda_2 = W_2/W_a$. For example, at $\omega_{w1} = \omega_{w2}$, the efficiency is at maximum if $\lambda_1 = 0.62$, $\lambda_2 = 0.38$ and the hitch height is at maximum. In the case of the minimum and average values of h_d, the efficiency drops to its minimum if $\omega_{w1}/\omega_{w2} = 1.1$.

Skoibeda recommended in 1979 that unequal slips of front and rear wheels cause a vehicle to operate at maximum efficiency if it is assumed that the relationship between the circumferential wheel force and tire slip is represented by a nonlinear function.

An analysis carried out by Katsigin et al. in 1982 with the nonlinear function (1.26) and experimental data showed that a 4×4 vehicle with synchronous positive engagement of the drive axles, $V_{t1} = V_{t2}$, had higher values of the running gear efficiency at nominal design operational values of the drawbar pull. The kinematic discrepancy, $V_{t1} \neq V_{t2}$, enables to increase the efficiency under the very high traction loads.

Furthermore, investigators report different results on the influence of tire slips and power distributions between the driving wheels on the vehicle efficiency and its components. These are the vehicle running gear efficiency and the slip efficiency. However, the majority agrees with the necessity to provide equal slippages for the front and rear wheels to improve the vehicle's efficiency. The studies referred to were performed for vehicles in steady motion and a majority of them was concerned about vehicles loaded by the drawbar pull without a payload. Thus, additional analytical research is required to define the conditions in which the efficiency of a multiwheel drive vehicle, with any arbitrary given number of driving axles, attains its maximum, and to determine the optimum power distributions between the driving wheels that would provide the vehicle with the maximum running gear efficiency. An example of a research pertaining to a vehicle, with a payload in both steady and nonsteady motion, on a nonflat surface is presented below. The reader who is interested solely in the results of the analysis and not in the mathematical operations may refer immediately to the conclusions placed at the end of this section.

The transportation running gear efficiency of a vehicle with an arbitrary number of axles was given by formulae (1.80) and (1.81) for steady motion and by formula (1.89) for nonsteady motion. The advantage of these formulae is that they reflect the influence of both the total power $P^{in}_{w\Sigma}$ applied to the driving wheels (see formula (1.77)) and of the distribution of this power between these wheels (see the denominator of formula (1.80)) on the vehicle running gear efficiency. Indeed, different values of power $P^{in}_{w\Sigma}$ yield different values of efficiency η^{tr}_x. In addition, when the total power $P^{in}_{w\Sigma}$, that is constant for a particular given moment of time, is then distributed between the driving wheels in various proportions, this causes the circumferential forces $F'^{(\prime\prime)}_{xi}$ and slip coefficients $s'^{(\prime\prime)}_{\delta i}$ of the driving wheels to differ from one another, at this moment of time. Hence, different combinations of $\{F'^{(\prime\prime)}_{xi}, s'^{(\prime\prime)}_{\delta i}\}$, $i = 1, n$ yield different values of efficiency η^{tr}_x as seen from formula (1.80).

The transportation running gear efficiency η^{tr}_x from the above formula (1.80), taken together with the mechanical efficiencies η_{trm} and η_M, which represent the power loss in the course of transmission of the flow of power from the engine to the driving wheels, yields the vehicle efficiency in the transportation mode

$$\eta_{tr} = \eta_{trm}\eta_M\eta^{tr}_x \tag{6.27}$$

The structure of formula (6.27) is similar to that of the formula of the tractive efficiency η_t of a vehicle in the tractive mode obtained from formula (1.66).

Once formulae (1.80), (1.81), and (1.89) have been derived, the objective function for finding the optimum power distributions to each of the drive wheels can be expressed as

$$\eta_x^{\text{tr}} \rightarrow \max \tag{6.28}$$

The maximum of the transportation gear efficiency shall comply with the best energy efficiency of the vehicles' wheel system and the best vehicle tractive and velocity operational properties.

As seen from formulae (1.80), (1.81), and (1.89), the optimum power distributions to the driving wheels $\{P'^*_{\text{w}1}, P''^*_{\text{w}1}, P'^*_{\text{w}2}, P''^*_{\text{w}2} \ldots P'^*_{\text{wn}}, P''^*_{\text{wn}}\}$ that minimize power loss $P_{\delta\Sigma}$ and cause efficiency η_x^{tr} to attain its maximum value, are provided by specific combinations of the optimum circumferential forces, $F'^{(\prime\prime)*}_{xi}$, and optimum slip coefficients, $s'^{(\prime\prime)*}_{\delta i}$, $i = 1, n$.

Consider boundary constraints for the optimization parameters, forces $F'^{(\prime\prime)*}_{xi}$ and slip coefficients $s'^{(\prime\prime)*}_{\delta i}$, $i = 1, n$. The number of the optimization parameters $F'^{(\prime\prime)*}_{xi}$ and $s'^{(\prime\prime)*}_{\delta i}$ is determined by the given number n of drive axles. The values of forces $F'^{(\prime\prime)*}_{xi}$ should be positive but limited by the road/off-road conditions:

$$0 \langle F'^{(\prime\prime)*}_{xi} \langle \mu'^{(\prime\prime)}_{\text{p}xi} R'^{(\prime\prime)}_{zi}, i = 1, n \tag{6.29}$$

here, $\mu'^{(\prime\prime)}_{\text{p}xi}$ is the peak friction coefficient of a tire. Accordingly, the optimum slip coefficients are

$$0 \langle s'^{(\prime\prime)*}_{\delta i} \langle 1, i = 1, n \tag{6.30}$$

At the same time, the summation of the optimum forces $F'^{(\prime\prime)*}_{xi}$ equal to the total circumferential force $F_{x\Sigma}$ is predetermined by the total resistance to vehicle motion. Hence, values of the force $F_{x\Sigma}$ are calculated using the equation of motion that is obtained from the vehicle's free-body diagram. For a vehicle with n driving axles and m driving and driven axles ($m \geq n$) the expression for the total circumferential force becomes:

$$F_{x\Sigma} = \sum_{i=1}^{n} F'^{(\prime\prime)*}_{xi} = \text{W}_\text{a} a_x \delta_\text{r} / g \pm \text{W}_\text{a} \sin\, \theta_\text{n} + \sum_{i=1}^{m} R'^{(\prime\prime)}_{xi} + D_\text{a} \tag{6.31}$$

where δ_r is the mass factor that accounts for the rotating masses of the vehicle. This factor and the air drag D_a can be computed based on well-known recommendations from engineering vehicle dynamics literature.

One more condition for optimizing the power distribution between the wheels should be defined by a function that relates the wheel circumferential force and the slip coefficient. The optimum values of forces $F'^{(\prime\prime)*}_{xi}$ and slip coefficients $s'^{(\prime\prime)*}_{\delta i}$ should correlate with one another in accordance with the function:

$$F'^{(\prime\prime)}_{xi} = f'^{(\prime\prime)}_i \left(s'^{(\prime\prime)}_{\delta i} \right), \quad i = 1, n \tag{6.32}$$

Summing up, the objective function given by formula (6.28) serves to optimize the vehicle running gear efficiency and, accordingly, the vehicle tractive and velocity operational properties.

This is to be implemented by determining the optimum wheel circumferential forces $F'^{(\prime\prime)*}_{xi}$ and optimum slip factors $s'^{(\prime\prime)*}_{\delta i}$, $i = 1, n$ that are consistent with the optimization constraints given by formulae (6.29) through (6.32). The optimum values of parameters

$F'^{(\prime\prime)*}_{xi}$ and $s'^{(\prime\prime)*}_{\delta i}$ should then be used to determine the optimum input power for each and all the drive wheels, $P'^{(\prime\prime)*}_{wi}$, $i = 1, n$ and $P^{in*}_{w\Sigma}$. This may be done using the formulae from Sections 1.3.3 and 1.4.2.

The substitution of the nonlinear relationship between the circumferential force and tire slip from formula (1.26) into expression (1.89) yields:

$$\eta^{tr}_x = \frac{\sum_{i=1}^{m}\left(R'_{xgi} + R''_{xgi}\right) \pm W_g \sin\theta_n \pm \frac{W_g}{g} a_x}{\sum_{i=1}^{n}\left(\frac{R'_{zi}\mu'_{pxi}\left(1-\exp\left(-k'_i s'_{\delta i}\right)\right)}{1-s'_{\delta i}} + \frac{R''_{zi}\mu''_{pxi}\left(1-\exp\left(-k''_i s''_{\delta i}\right)\right)}{1-s''_{\delta i}}\right)} \tag{6.33}$$

The process of maximizing function (6.33) can be replaced by the minimization of the following function that stems from the denominator of function (6.33)

$$\sum_{i=1}^{n} b'^{(\prime\prime)}_i \left(1 - \exp\left(-k'^{(\prime\prime)}_i s'^{(\prime\prime)}_{\delta i}\right)\right) / \left(1 - s'^{(\prime\prime)}_{\delta i}\right) \to \min \tag{6.34}$$

where $b'^{(\prime\prime)}_i = R'^{(\prime\prime)}_{zi}\mu'^{(\prime\prime)}_{pxi}$.

The following notation is introduced for the purpose of analyzing formula (6.34):

$$\overrightarrow{s_\delta} = \left(s'_{\delta 1}, s''_{\delta 1}, \ldots, s'_{\delta n}, s''_{\delta n}\right), \quad \overrightarrow{b} = \left(b'_1, b''_1, \ldots, b'_n, b''_n\right), \quad \overrightarrow{k} = \left(k'_1, k''_1, \ldots, k'_n, k''_n\right) \tag{6.35}$$

Here, $\overrightarrow{s_\delta}$, $\vec{b}$, and $\vec{k}$ are vectors of space R^{2n}; $\vec{b}$ and $\vec{k}$ are fixed vectors with positive coordinates. This notation was used for compiling the two following functions:

$$F\left(\overrightarrow{s_\delta}, \overrightarrow{b}, \overrightarrow{k}\right) = \sum_{i=1}^{n} b'^{(\prime\prime)}_i \left(1 - \exp\left(-k'^{(\prime\prime)}_i s'^{(\prime\prime)}_{\delta i}\right)\right) / \left(1 - s'^{(\prime\prime)}_{\delta i}\right) \tag{6.36}$$

$$G\left(\overrightarrow{s_\delta}, \overrightarrow{b}, \overrightarrow{k}\right) = \sum_{i=1}^{n} b'^{(\prime\prime)}_i \left(1 - \exp\left(-k'^{(\prime\prime)}_i s'^{(\prime\prime)}_{\delta i}\right)\right) - A \tag{6.37}$$

where A is a positive constant. Parameter B, defined by vectors $\vec{b}$ and $\vec{k}$, has been additionally included for the purpose of this analysis

$$B = \sum_{i=1}^{n} b'^{(\prime\prime)}_i \left(1 - \exp\left(-k'^{(\prime\prime)}_i s'^{(\prime\prime)}_{\delta i}\right)\right) \tag{6.38}$$

Finally, utilizing formulae (6.34) through (6.37), the minimization problem (6.34) can be expressed as

$$F\left(\overrightarrow{s_\delta}, \overrightarrow{b}, \overrightarrow{k}\right) \to \min \tag{6.39}$$

at the conditions,

$$G\left(\overrightarrow{s_\delta}, \overrightarrow{b}, \overrightarrow{k}\right) = 0 \tag{6.40}$$

$$s'^{(\prime\prime)}_{\delta i} \in [0; 1], \quad i = 1, n$$

The second boundary condition in (6.40) was modified to allow analyzing the problem expressed by formulae (6.39) and (6.40); the conditions now are

$$G(\overrightarrow{s_\delta}, \overrightarrow{b}, \overrightarrow{k}) = 0 \tag{6.41}$$
$$s_{\delta i}^{\prime(\prime\prime)} \langle 1, i = 1, n$$

Such a substitution does not significantly affect the mathematical description of the tire slip process. However, it should be noted that conditions (6.40) should be considered somewhat later on.

Compose Lagrange function for problem (6.39) and (6.41)

$$L(\overrightarrow{s_\delta}, \lambda) = F(\overrightarrow{s_\delta}, \overrightarrow{b}, \overrightarrow{k}) + \lambda G(\overrightarrow{s_\delta}, \overrightarrow{b}, \overrightarrow{k}) \tag{6.42}$$

where λ is the Lagrange factor.

The necessary conditions of an extremum of the function follow from the equations

$$\frac{\partial L}{\partial s_{\delta i}^{\prime(\prime\prime)}} = 0, \quad i = 1, n \tag{6.43}$$
$$G \equiv 0$$

whence,

$$\begin{aligned} &b_i^{\prime(\prime\prime)} k_i^{\prime(\prime\prime)} \exp\left(-k_i^{\prime(\prime\prime)} s_{\delta i}^{\prime(\prime\prime)}\right) / \left(1 - s_{\delta i}^{\prime(\prime\prime)}\right) + b_i^{\prime(\prime\prime)} \left(1 - \exp\left(-k_i^{\prime(\prime\prime)} s_{\delta i}^{\prime(\prime\prime)}\right)\right) / \left(1 - s_{\delta i}^{\prime(\prime\prime)}\right)^2 \\ &\quad + b_i^{\prime(\prime\prime)} k_i^{\prime(\prime\prime)} \exp\left(-k_i^{\prime(\prime\prime)} s_{\delta i}^{\prime(\prime\prime)}\right) \lambda = 0 \end{aligned} \tag{6.44}$$
$$i = 1, n$$
$$G \equiv 0$$

Equation 6.44 for finding the necessary conditions for the extremum of function (6.39) can be rewritten as follows:

$$\begin{cases} 1/\left(1 - s_{\delta i}^{\prime(\prime\prime)}\right) + \left(\exp\left(k_i^{\prime(\prime\prime)} s_{\delta i}^{\prime(\prime\prime)}\right) - 1\right) / \left(k_i^{\prime(\prime\prime)} \left(1 - s_{\delta i}^{\prime(\prime\prime)}\right)^2\right) = -\lambda \\ \sum\limits_{i=1}^{n} b_i^{\prime(\prime\prime)} \left(1 - \exp\left(-k_i^{\prime(\prime\prime)} s_{\delta i}^{\prime(\prime\prime)}\right)\right) = A \end{cases} \tag{6.45}$$
$$i = 1, n.$$

Examine the function that follows from the Equation 6.45

$$\alpha(x) = 1/(1 - x) + (\exp(kx) - 1)/(k(1 - x)^2) \tag{6.46}$$

at $k > 0$ and with the argument of x over the interval $(-\infty, 1)$.

Lemma 6.1: Prove that function $\alpha(x)$ increases monotonically from 0 to $+\infty$ when the argument x belongs to the interval $(-\infty, 1)$.

The limits of function (6.46) are found to be

$$\lim_{x\to-\infty}\alpha(x)=0 \quad \text{and} \quad \lim_{x\to1-0}\alpha(x)=+\infty. \tag{6.47}$$

The first derivative of function $\alpha(x)$ is

$$\frac{d\alpha}{dx}=\frac{k(1-x)+k(1-x)\exp(kx)+2(\exp(kx)-1)}{k(1-x)^3} \tag{6.48}$$

Designating the numerator of expression (6.48) as

$$\beta(x)=k(1-x)+k(1-x)\exp(kx)+2(\exp(kx)-1), \tag{6.49}$$

becomes obvious that Lemma 6.1 could be regarded as proven if the expression

$$\min_{x\in(-\infty;\,1)}\beta(x)>0 \tag{6.50}$$

could be proven. For this purpose, find the derivatives

$$\frac{d\beta}{dx}=-k+k^2(1-x)\exp(kx)+k\exp(kx), \tag{6.51}$$

$$\frac{d^2\beta}{dx^2}=k^3(1-x)\exp(kx)$$

Since

$$\frac{d^2\beta}{dx^2}>0 \quad \text{when } x\in(-\infty;\,1) \quad \text{and} \quad \frac{d\beta}{dx}>0 \quad \text{when } x=0,$$

the following limits take place:

$$\lim_{x\to-\infty}\frac{d\beta}{dx}=-k; \quad \lim_{x\to1}\frac{d\beta}{dx}=k(\exp(k)-1)>0.$$

It should be noted here that the minimum of function $\beta(x)$ over interval $(-\infty, 1)$ of the argument x is located at a point in $x_0\langle 0$. This point x_0 is the only solution of the equation $\frac{d\beta}{dx}=0$ when $x=x_0$, e.g.

$$k(1-x_0)\exp(kx_0)+\exp(kx_0)=1 \quad \text{or} \quad \exp(kx_0)-1=-k(1-x_0)\exp(kx_0). \tag{6.52}$$

Using formulae (6.49), (6.50), and (6.52), it is found that

$$\begin{aligned}\min_{x\in(-\infty;\,1)}\beta(x)&=\beta(x_0)=k(1-x_0)+k(1-x_0)\exp(kx_0)+\exp(kx_0)+\exp(kx_0)-2\\&=k(1-x_0)+\exp(kx_0)-1=k(1-x_0)(1-\exp(kx_0))>0\end{aligned}$$

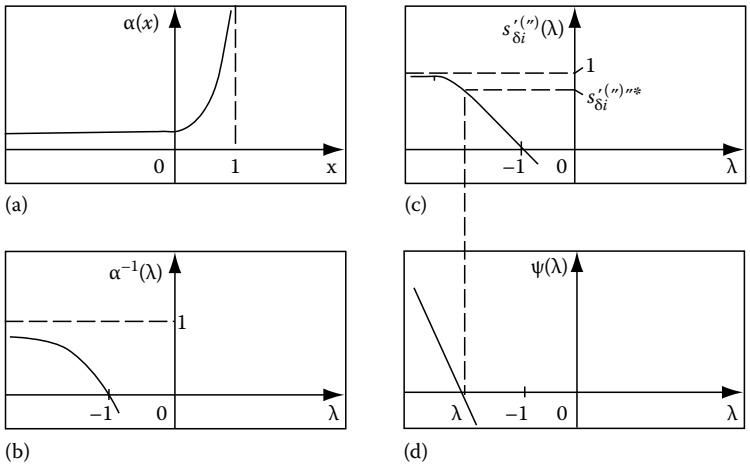


FIGURE 6.12
Objective function analysis. (a) Function given by formula (6.46). (b) Graphical presentation of Corollary 6.1. (c) Function given by formula (6.53). (d) Function given by formula (6.54).

This means that $\alpha(x)$ increases monotonically from 0 to $+\infty$ over the interval $(-\infty, 1)$ of argument x.

Q.E.D.

A graphic interpretation of function $\alpha(x)$ is presented in Figure 6.12a.

Lemma 6.1 has a corollary.

Corollary 6.1

(a) For any $\lambda > 0$, equation $\alpha(x) = \lambda$ has the only solution over the interval $(-\infty, 1)$ of argument x

(b) The inverse function $\alpha^{-1}(\lambda)$ is defined, continuous, and increases monotonically from $-\infty$ to 1 over the interval $(0, +\infty)$

(c) $\alpha^{-1}(-1) = 0$

The corollary is shown in Figure 6.12b.

Based on previously proven Lemma 6.1 and Corollary 6.1, prove Theorem 6.1 that establishes the existence of a solution of Equations 6.45 that is the optimum plan for the optimization problem (6.39) and (6.41).

Theorem 6.1: Set of Equations 6.45 has a solution if, and only if, $B > A$; this solution $\left(s'^{*}_{\delta 1}, s''^{*}_{\delta 1}, \ldots, s'^{*}_{\delta n}, s''^{*}_{\delta n}, \lambda^{*}\right)$ is unique with $\lambda^{*} \in (-\infty; 1)$ and $s'^{(\prime\prime)*}_{\delta i} \in (0; 1)$, $i = 1, n$.

Proof of Theorem 6.1. When $B \leq A$, the parameters $s'^{(\prime\prime)}_{\delta i}$, $i = 1, n$ do not belong to the interval, $(-\infty, 1)$, which is not in agreement with problem (6.39) and (6.41). Hence, set of Equations 6.45 can have a solution if, and only if, $B > A$.

Thus, it is necessary to prove that the solution $\left(s'^{*}_{\delta 1}, s''^{*}_{\delta 1}, \ldots, s'^{*}_{\delta n}, s''^{*}_{\delta n}, \lambda^{*}\right)$ has the indicated properties, e.g., $\lambda^{*} \in (-\infty; 1)$ and $s'^{(\prime\prime)*}_{\delta i} \in (0; 1)$, $i = 1, n$.

Consider functions $s'^{(\prime\prime)}_{\delta i}(\lambda), i = 1, n$. The values of these functions are the roots of the following equations from the set of Equations 6.45:

$$1/\left(1 - s'^{(\prime\prime)}_{\delta i}\right) + \left(\exp\left(k'^{(\prime\prime)}_{i} s'^{(\prime\prime)}_{\delta i}\right) - 1\right)/\left(k'^{(\prime\prime)}_{i}\left(1 - s'^{(\prime\prime)}_{\delta i}\right)^{2}\right) = -\lambda \qquad (6.53)$$

$$i = 1, n.$$

According to Corollary 6.1, these functions $s'^{(\prime\prime)}_{\delta i}(\lambda)$ are defined, continuous, and monotonically decreasing over the interval $(-\infty; 0)$ of λ. Also, $s'^{(\prime\prime)}_{\delta i}(-1) = 0$ and $\lim_{\lambda \to -\infty} s'^{(\prime\prime)}_{\delta i}(\lambda) = 1$ for all numbers i: $i = 1, n$. Functions $s'^{(\prime\prime)}_{\delta i}(\lambda)$ are plotted in Figure 6.12c. Then, the two following statements are correct for the continuous function:

$$\Psi(\lambda) = \sum_{i=1}^{n} b'^{(\prime\prime)}_{i}\left(1 - \exp\left(-k'^{(\prime\prime)}_{i} s'^{(\prime\prime)}_{\delta i}(\lambda)\right)\right) - A \qquad (6.54)$$

(1) this function decreases monotonically and (2) the following expressions apply:

$$\lim_{\lambda \to -\infty} \Psi(\lambda) = B - A, \quad \Psi(-1) = -A < 0. \qquad (6.55)$$

here, A is a positive constant in formula (6.37); B is defined by formula (6.38).

Therefore, equation $\Psi(\lambda) = 0$ has only one root λ^{*} and $\lambda^{*} < -1$ (see Figure 6.12d). Hence, the range of $\left(s'^{*}_{\delta 1}, s''^{*}_{\delta 1}, \ldots, s'^{*}_{\delta n}, s''^{*}_{\delta n}, \lambda^{*}\right)$, over which, $s'^{(\prime\prime)*}_{\delta i} = s'^{(\prime\prime)}_{\delta i}(\lambda^{*})$, is the unique solution of the set of equations (6.45).

It can be seen by comparing Figures 6.12c and 6.12d, that $s'^{(\prime\prime)*}_{\delta i} \in (0; 1)$.

Q.E.D.

Theorem 6.1 that was proven as above has another corollary.

Corollary 6.2

If $B > A$ and if all the coordinates of the vector $\overrightarrow{k} = \left(k'_1, k''_1, \ldots, k'_n, k''_n\right)$ from formula (6.35) are equal to one another, that is, if $k'^{(\prime\prime)}_{i} = k$ for $i = 1, n$, the solution $\left(s'^{*}_{\delta 1}, s''^{*}_{\delta 1}, \ldots, s'^{*}_{\delta n}, s''^{*}_{\delta n}, \lambda^{*}\right)$ of the set of Equations 6.45 is such that all numbers $s'^{(\prime\prime)*}_{\delta i}$ are equal to one another, that is, $s'^{(\prime\prime)*}_{\delta i} = s^{*}_{\delta}$, $i = 1, n$. In this case, the optimal parameter s^{*}_{δ} can be determined from the last of Equations 6.45 as follows

$$s^{*}_{\delta} = -\frac{1}{k} \ln\left(1 - \frac{A}{\sum_{i=1}^{n} b'^{(\prime\prime)}_{i}}\right) \qquad (6.56)$$

The above analysis for the minimizing function (6.39) under one-sided boundary conditions (6.41) has thus yielded the conditions of existence of the optimal value of the slip coefficients $s'^{(\prime\prime)*}_{\delta i}$, $i = 1, n$ exist. The objective function (6.39) attains its minimum value at the same values of the slip coefficients $s'^{(\prime\prime)*}_{\delta i} = s^{*}_{\delta}$, $i = 1, n$ if, and only if, the coordinates $k'^{(\prime\prime)}_{i}$, $i = 1, n$

of vector $\vec{k}$ are equal to one another. It must be remembered that coordinates $k_i^{\prime(\prime\prime)}$ represent the tire/soil interaction (see formula (1.26)). It should be noted that the friction factors $\mu_{pxi}^{\prime(\prime\prime)}$, $i = 1, n$ and the normal reactions $R_{zi}^{\prime(\prime\prime)}$ in formula (1.26) above do not affect the above conclusion.

Hence, the efficiency η_x^{tr} in formula (6.33) is at a maximum when the vehicle driveline provides the driving wheels with the same slips irrespective of whether the friction factors $\mu_{pxi}^{\prime(\prime\prime)}$ are the same or not. However, this is true only, if components $k_i^{(\prime\prime)}$ have the same value for all the tires of the vehicle.

Based on the analysis above, consider the optimization problem (6.39) with its actual two-sided boundary conditions (6.40).

Lemma 6.2: If $B > A$ and if the plan of $\left(s_{\delta 1}^{\prime *}, s_{\delta 1}^{\prime\prime *}, \ldots, s_{\delta n}^{\prime *}, s_{\delta n}^{\prime\prime *}, \lambda^*\right)$ is the solution of a set of Equations 6.45, there exist the following relationships that stem from the Lagrange function (6.42)

$$\frac{\partial^2 L}{\partial\left(s_{\delta i}^{\prime(\prime\prime)}\right)^2}\left(s_{\delta 1}^{\prime *}, s_{\delta 1}^{\prime\prime *}, \ldots, s_{\delta n}^{\prime *}, s_{\delta n}^{\prime\prime *}, \lambda^*\right) > 0, \quad i = 1, n. \tag{6.57}$$

Proof Find derivative $\frac{\partial^2 L}{\partial\left(s_{\delta i}^{\prime(\prime\prime)}\right)^2}$ of Lagrange function (6.42):

$$\begin{aligned}\frac{\partial^2 L}{\partial\left(s_{\delta i}^{\prime(\prime\prime)}\right)^2} &= -\frac{\left(k_i^{\prime(\prime\prime)}\right)^2 b_i^{\prime(\prime\prime)} \exp\left(-k_i^{\prime(\prime\prime)} s_{\delta i}^{\prime(\prime\prime)}\right)}{1 - s_{\delta i}^{\prime(\prime\prime)}} + \frac{2k_i^{\prime(\prime\prime)} b_i^{\prime(\prime\prime)} \exp\left(-k_i^{\prime(\prime\prime)} s_{\delta i}^{\prime(\prime\prime)}\right)}{\left(1 - s_{\delta i}^{\prime(\prime\prime)}\right)^2} \\ &+ \frac{2b_i^{\prime(\prime\prime)}\left(1 - \exp\left(-k_i^{\prime(\prime\prime)} s_{\delta i}^{\prime(\prime\prime)}\right)\right)}{\left(1 - s_{\delta i}^{\prime(\prime\prime)}\right)^3} - \left(k_i^{\prime(\prime\prime)}\right)^2 b_i^{\prime(\prime\prime)} \exp\left(-k_i^{\prime(\prime\prime)} s_{\delta i}^{\prime(\prime\prime)}\right)\lambda\end{aligned} \tag{6.58}$$

Assuming that λ^* is functionally related to parameters $s_{\delta 1}^{\prime *}, s_{\delta 1}^{\prime\prime *}, \ldots, s_{\delta n}^{\prime *}, s_{\delta n}^{\prime\prime *}$ by Equations 6.45, the derivative (6.58) can be only positive, e.g.,

$$\begin{aligned}\frac{\partial^2 L}{\partial\left(s_{\delta i}^{\prime(\prime\prime)}\right)^2}\left(s_{\delta 1}^{\prime *}, s_{\delta 1}^{\prime\prime *}, \ldots, s_{\delta n}^{\prime *}, s_{\delta n}^{\prime\prime *}, \lambda^*\right) &= -\frac{\left(k_i^{\prime(\prime\prime)}\right)^2 b_i^{\prime(\prime\prime)} \exp\left(-k_i^{\prime(\prime\prime)} s_{\delta i}^{\prime(\prime\prime)*}\right)}{1 - s_{\delta i}^{\prime(\prime\prime)*}} \\ &+ \frac{2k_i^{\prime(\prime\prime)} b_i^{\prime(\prime\prime)} \exp\left(-k_i^{\prime(\prime\prime)} s_{\delta i}^{\prime(\prime\prime)*}\right)}{\left(1 - s_{\delta i}^{\prime(\prime\prime)*}\right)^2} + \frac{2b_i^{\prime(\prime\prime)}\left(1 - \exp\left(k_i^{\prime(\prime\prime)} s_{\delta i}^{\prime(\prime\prime)*}\right)\right)}{\left(1 - s_{\delta i}^{\prime(\prime\prime)*}\right)^3} \\ &+ \frac{\left(k_i^{\prime(\prime\prime)}\right)^2 b_i^{\prime(\prime\prime)} \exp\left(-k_i^{\prime(\prime\prime)} s_{\delta i}^{\prime(\prime\prime)*}\right)}{1 - s_{\delta i}^{\prime(\prime\prime)*}} + \frac{k_i^{\prime(\prime\prime)} b_i^{\prime(\prime\prime)} \exp\left(-k_i^{\prime(\prime\prime)} s_{\delta i}^{\prime(\prime\prime)*}\right)\left(\exp\left(k_i^{\prime(\prime\prime)} s_{\delta i}^{\prime(\prime\prime)*}\right) - 1\right)}{\left(1 - s_{\delta i}^{\prime(\prime\prime)*}\right)^2} \\ &= \frac{k_i^{\prime(\prime\prime)} b_i^{\prime(\prime\prime)}\left(\exp\left(-k_i^{\prime(\prime\prime)} s_{\delta i}^{\prime(\prime\prime)*}\right) + 1\right)}{\left(1 - s_{\delta i}^{\prime(\prime\prime)*}\right)^2} + \frac{2b_i^{\prime(\prime\prime)}\left(1 - \exp\left(-k_i^{\prime(\prime\prime)} s_{\delta i}^{\prime(\prime\prime)*}\right)\right)}{\left(1 - s_{\delta i}^{\prime(\prime\prime)*}\right)^3} > 0\end{aligned} \tag{6.59}$$

Formula (6.59) is true because all parameters $s_{\delta i}^{\prime(\prime\prime)*}$ are positive by virtue of theorem 6.1.

Q.E.D.

A corollary follows from Lemma 6.2 and from the fact that $\frac{\partial^2 L}{\partial s_{\delta i}^{\prime(\prime\prime)} \partial s_{\delta j}^{\prime(\prime\prime)}} \equiv 0$, $i \neq j$.

Corollary 6.3: For any $ds'_{\delta 1}, ds''_{\delta 1}, \ldots, ds'_{\delta n}, ds''_{\delta n}$ not simultaneously equal to zero, the following condition is satisfied

$$d^2L\left(s'^*_{\delta 1}, s''^*_{\delta 1}, \ldots \delta'^*_{\delta n}, s''^*_{\delta n}, \lambda^*, ds'_{\delta 1}, ds''_{\delta 1}, \ldots ds'_{\delta n}, ds''_{\delta n}\right) > 0 \tag{6.60}$$

Hence, the plan of $\left(s'^*_{\delta 1}, s''^*_{\delta 1}, \ldots, s'^*_{\delta n}, s''^*_{\delta n}, \lambda^*\right)$ is the local minimum.

Theorem 6.2: If $B > A$, the problem defined by formulae (6.39) and (6.40) has the unique solution of $\left(s'^*_{\delta 1}, s''^*_{\delta 1}, \ldots, s'^*_{\delta n}, s''^*_{\delta n}\right)$ that can be determined from Equations 6.45. Additionally, if $k_i^{\prime(\prime\prime)} = k$, $i = 1, n$, the solution has the same components, that is, $s_{\delta i}^{\prime(\prime\prime)*} = s_\delta{}^*$, where $s_\delta{}^*$ is given by the formula (6.56).

The problem defined by formulae (6.39) and (6.40) does not have a solution if $B \leq A$.

Proof of Theorem 6.2 If $B \leq A$, the conditions given by formulae (6.37), (6.38), and (6.40) are not compatible and hence the problem has no solution.

Let $B > A$. As shown by Lemma 6.2 and Corollary 6.3, the minimization problem defined by formulae (6.39) and (6.40) has a unique solution that is $\left(s'^*_{\delta 1}, s''^*_{\delta 1}, \ldots, s'^*_{\delta n}, s''^*_{\delta n}\right)$; and all parameters $s_{\delta i}^{\prime(\prime\prime)*} \in (0; 1)$. Hence, the solution $\left(s'^*_{\delta 1}, s''^*_{\delta 1}, \ldots, s'^*_{\delta n}, s''^*_{\delta n}\right)$ is the unique solution of the minimization problem.

Additionally, if all the parameters of vector $\vec{k}$ are the same, that is, if $k_i^{\prime(\prime\prime)} = k$, $i = 1, n$, then all the parameters $s_{\delta i}^{\prime(\prime\prime)*}$ are equal to one another and obtainable from formula (6.56).

Q.E.D.

Formally, Theorem 6.2 and Corollary 6.3 guarantee the uniqueness of the local minimum. At the same time, this minimum is also the global minimum for two reasons. First, condition $G \equiv 0$ given in formula (6.43) cannot be satisfied if only any of the parameters $s_{\delta i}^{\prime(\prime\prime)} \to -\infty$. Second, $F \to +\infty$ (see formula (6.39)) if only any parameter $s_{\delta i}^{\prime(\prime\prime)} \to 1$. Consequently, the minimum cannot be located on the boundaries of $s_{\delta i}^{\prime(\prime\prime)}$-domain.

As shown by the mathematical analysis above, the maximum of efficiency η_x^{tr} could be attained under unequal slip coefficients $s_{\delta i}^{\prime(\prime\prime)*}$ if and only if factors $k_i^{\prime(\prime\prime)}$ in function (1.26) differ from one another. Factors $k_i^{\prime(\prime\prime)}$ are different when (1) a vehicle moving on a firm road has different tire inflations, and the tires are of the same size; (2) a vehicle moving on a firm road has tires of different models on different drive axles, or (3) a vehicle with identical/different tires is moving on a damp deformable surface when the wheels of one of the sides of the vehicle are on the same track, but have a different grip on the soil due to the differences in the degree of soil compression and, accordingly, different gripping properties.

Within the context of the above results, it is necessary to estimate the difference between the wheel slip coefficients $s_{\delta i}^{\prime(\prime\prime)*}$, $i = 1, n$ at the maximum values of efficiency η_x^{tr}.

To do this, the set of Equations 6.45 can be written as follows:

$$\text{Function}\,(s_\delta, k) \equiv -\lambda \tag{6.61}$$

where

$$\text{Function}\,(s_\delta, k) = \frac{1}{1 - s_\delta} + \frac{\exp(ks_\delta) - 1}{k(1 - s_\delta)^2} \tag{6.62}$$

Equation 6.62 is an implicit function such that

$$s_\delta(k) = F(k, \lambda) \tag{6.63}$$

for which the following may be written:

$$s_\delta(k + \Delta) - s_\delta(k) = \dot{s}_{\delta k}(\xi)\Delta \tag{6.64}$$

here, $\xi \in [k, k + \Delta]$, $\dot{s}_{\delta k}$ is the derivative of function (6.63) with respect to argument k.

The derivative $\dot{s}_{\delta k}$ of implicit function (6.63) is determined using formula (6.62)

$$\dot{s}_{\delta k} = -\frac{\partial \text{Function}/\partial k}{\partial \text{Function}/\partial s_\delta}$$

where

$$\partial \text{Function}/\partial k = \frac{s_\delta \exp(k s_\delta)}{k(1 - s_\delta)^2} - \frac{\exp(k s_\delta) - 1}{k^2(1 - s_\delta)^2} \tag{6.65}$$

$$\partial \text{Function}/\partial s_\delta = \frac{1}{(1 - s_\delta)^2} + \frac{\exp(k s_\delta)}{(1 - s_\delta)^2} + \frac{2(\exp(k s_\delta) - 1)}{k(1 - s_\delta)^3}$$

Expressions (6.64) and (6.65) can be used for estimating the degree of difference between the optimal values of the slip coefficients $s_{\delta i}^{\prime(\prime\prime)*}$ when factors $k_i^{\prime(\prime\prime)}$, $i = 1, n$ differ from one another. That could be done ''from the top,'' e.g., the maximal differences between the slip coefficients could be estimated. This is done using the derivative $\dot{s}_{\delta k}$ (see Figure 6.13).

In Figure 6.13, the difference between factors $\dot{s}_{\delta i}^{\prime(\prime\prime)*}$ is not constant, but changes depending on the vehicle's total circumferential force $F_{x\Sigma}$ and grip conditions between the vehicle's tires and the soil.

As shown in Figure 6.13, the values of $|\dot{s}_{\delta k}|$ are very small within the operational range of the total circumferential force $F_{x\Sigma}$ when $s_\delta < 0.20 - 0.25$ for both, the firm surfaces with higher values of k and deformable soils with lower values of k. Hence, the differences between the coefficients $s_{\delta i}^{\prime(\prime\prime)*}$ at maximum efficiency η_x^{tr} are very small. For example, the values of factor $s_\delta(k + \Delta) - s_\delta(k)$ from formula (6.64) do not exceed 0.032 for a 5.7 ton vehicle with different-size front and rear tires on a ready-to-plant field ($k_1 = 4.095$ and $k_2 = 7.107$). For 4×4 vehicles with the same tire models on the front and rear axles, the factor $s_\delta(k + \Delta) - s_\delta(k)$ takes even lower values.

The difference between slip factors $s_{\delta i}^{\prime(\prime\prime)*}$ increases when the vehicle is subjected to very high traction loads; under such conditions, the total circumferential force $F_{x\Sigma}$ attains higher values than in typical operational modes and the tires may start spinning. Indeed, as follows from Figure 6.13, factor $s_\delta(k + \Delta) - s_\delta(k)$ increases by $0.10 - 0.12$ when $s_\delta = 0.65 - 0.75$. These results are important for designing power-dividing units. As follows from Figure 6.13, such units can provide equal slip ratios for driving wheels within the operational range of traction loads when tire slip ratios do not exceed 0.25. This will not negatively affect the vehicle energy efficiency and fuel consumption.

The above results were also proven by analysis of an 8×8 vehicle. Table 6.3 complements those results by computational results of the 8×8 vehicle moving on flat virgin soil at a constant speed of 10 km/h.

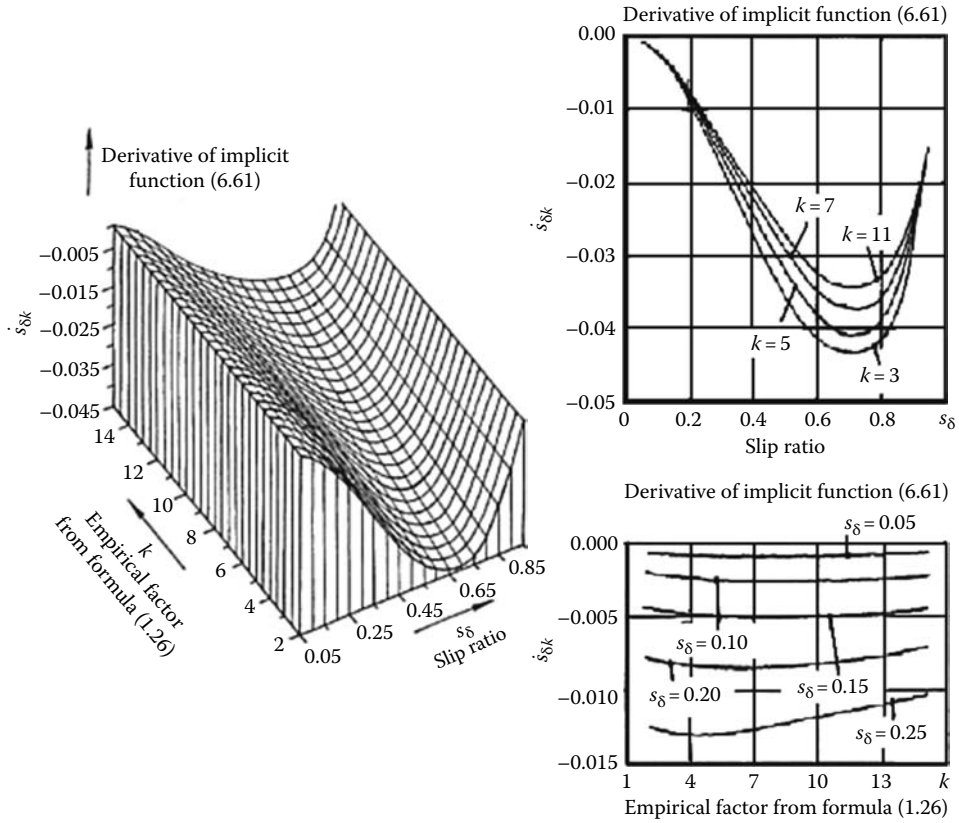


FIGURE 6.13
For analyzing tire slips under maximal efficiency: 3D (a) and 2D (b) graphs.

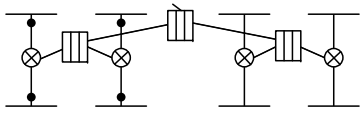
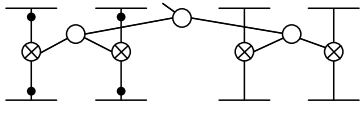
The total weight of the vehicle was of 314 kN. The computations were performed for different driveline systems that have open symmetrical differentials, limited slip differentials, and free-running differentials. It was assumed that the limited slip differentials have a constant torque bias of 3; the effective rolling radii of the wheels in the driven mode (no torque applied) are not the same due to the manufacturing tolerances and their values follow a normal distribution.

The driveline systems considered above provide different distributions of power to the driving wheels. This results in different values of the transportation running gear efficiency of the vehicle, η_x^{tr}. The vehicle with a driveline system that guarantees equal tire slips has a better efficiency than the same vehicle with driveline systems that have different tire slips. The differences between these slippages under real operating conditions are greater than the difference between the tires' slips at maximum efficiency that follow from the above analysis and from Figure 6.13.

Mathematical analysis has thus proven that the maximum running gear efficiency of a multiwheel drive vehicle can be achieved in actual practice if the vehicle driveline system provides the same slip factors for all the drive wheels. This is true whether the vehicle accelerates or moves at a constant speed on a flat or hilly surface within the range of the operational circumferential forces when tire slippages do not exceed 0.2–0.25.

TABLE 6.3

8× 8 Vehicle with Different Driveline Systems: Slip Ratios and Running Gear Efficiency

No.	Driveline System	$s'_{\delta 1}$	$s''_{\delta 1}$	$s'_{\delta 2}$	$s''_{\delta 2}$	$s'_{\delta 3}$	$s''_{\delta 3}$	$s'_{\delta 4}$	$s''_{\delta 4}$	η_x^{tr}
1	Hypothetical driveline system that provides the vehicle with identical slips at all the driving wheels	0.0205	0.0205	0.0205	0.0205	0.0205	0.0205	0.0205	0.0205	0.3285
2		0.0161	0.0196	0.0220	0.0171	0.0245	0.0253	0.0163	0.0222	0.3216
3		0.0187	0.0221	0.0228	0.0179	0.0199	0.0207	0.0175	0.0233	0.3217

The results of the above analysis are applicable to vehicles under any off-/on-road conditions, when the exponential functions (1.26) relating the circumferential wheel force and slip coefficient hold; factors $k_i^{\prime(\prime\prime)}$, $i = 1, n$ for the vehicle's tires in these functions may be the same or different depending on the tire/soil (road) interactions.

As a part of designing a driveline system for a multiwheel drive vehicle, design engineers should incorporate power dividing units that provide the vehicles with equal tire slip coefficients to guarantee maximum vehicle running gear efficiency and, accordingly, minimum fuel consumption.

6.4 Synthesis of the Properties of Interwheel Power-Dividing Units

Consider the practical application of the method of synthesis of driveline systems for determining the optimal properties of interwheel power-dividing units on the condition that the properties of the interaxle drive of the vehicle are known. Such a formulation of the problem is applicable when it is necessary to improve the operating properties of a vehicle with satisfactorily performing interaxle driveline system by refining the interwheel drives. For example, in order to improve the traction-gripping properties and output of 4×4 single-bucket loading tractors with positive engagement in the interaxle drive by using interwheel limited slip differentials instead of open differentials. Here, certain designs of articulated loaders employ limited slip differentials with constant design locking coefficients (torque biases) in both the driving axles. Other loader models use limited slip differentials in the front axles and free-running differentials in the rear axles.

The advantages of using these mechanisms in loaders stem from the fact that limited slip differentials with properly selected locking properties improve the traction performance of the vehicles and do not markedly affect their turnability. In addition, these automatic devices do not require driver input for controlling their operation. The latter is particularly important for loaders in which the driver is called upon to operate the controls more than 3000 times during an hour of continuous operation.

The example of a 10.5 ton operational mass, 4×4 single-bucket articulated loader with positively engaged interaxle driveline is used below to investigate the determination of the optimal distribution of power between the left and right wheels of the axles and for the synthesis of the optimal properties of mechanisms for interwheel power-dividing units. These results subsequently are used to validate the optimal locking properties of limited slip differentials for the front and rear axles of the loader and to work out their design.

The mathematical model of the loader under principal operating conditions is now compiled. The most energy intensive of all the components of the working cycle of a loader that requires elevated traction-gripping properties is scooping of the material into the bucket. The most progressive method of gathering the material is the composite method when, while the loader is moving, the loader arm is lifted and the bucket is rotated at the same time. For this reason, the problem above is being solved by mathematical modeling of the scooping up of the material by the composite method.

Figure 6.14 shows the generalized three-dimensional computational model representing the motion of a loader moving downhill while being tilted to the side, from which it is possible to derive typical cases of motion: over a horizontal surface, moving downhill and while being tilted to a side.

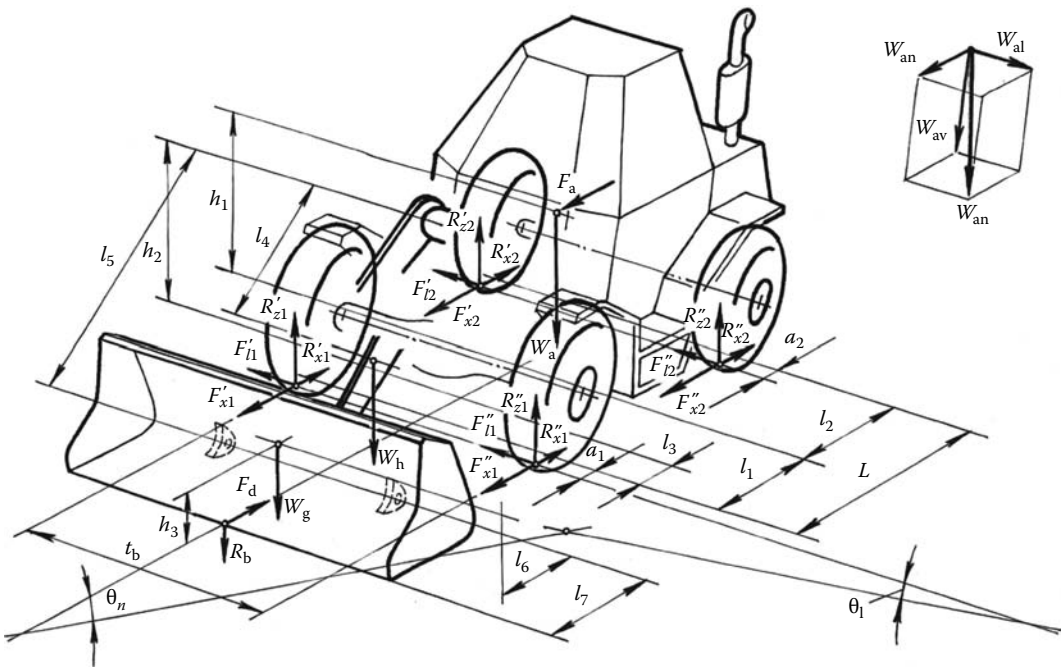


FIGURE 6.14
4 × 4 loader: a fee-body diagram.

The pressure force F_d and the digging force R_b change markedly in the course of scooping up of the material. Analysis of the results of testing of loaders yielded relationships that can be used for determining F_d and R_b in the first approximation:

$$F_d = 3.33\frac{F_d^{max}}{t_{max}}t \quad \text{at } t \le 0.3t_{max};$$

$$F_d = 1.60F_d^{max} - 2\frac{F_d^{max}}{t_{max}}t \quad \text{at } 0.3t_{max} < t \le 0.45t_{max};$$

$$F_d = 0.90F_d^{max} - 0.60\frac{F_d^{max}}{t_{max}}t \quad \text{at } 0.45t_{max} < t \le t_{max}; \tag{6.66}$$

$$R_b = \frac{F_d^{max}}{t_{max}}t \quad \text{at } t \le 0.5t_{max};$$

$$R_b = 0.90F_d^{max} - 0.80\frac{F_d^{max}}{t_{max}}t \quad \text{at } 0.5t_{max} < t \le t_{max}$$

where

t is the current time of scooping up the material
F_d^{max} is the maximum value of the pressure force

The objective function here consists of the traction efficiency of the running gear from formula (1.67):

$$\eta_x^t \to \max \tag{6.67}$$

upon the following constraints on the circumferential forces $F_{xi}^{\prime(\prime\prime)*}$ of wheel slippage $s_{\delta i}^{\prime(\prime\prime)*}$ being optimized:

$$\begin{gathered}\sum_{i=1}^{2} F_{xi}^{\prime(\prime\prime)*} = F_{x\Sigma}, \\ s_{\delta ai} = m_{\mathrm{H}i} + (1 - m_{\mathrm{H}i}) s_{\delta a} \\ F_{xi}^{\prime(\prime\prime)*} = R_{zi}^{\prime(\prime\prime)} \mu_{\mathrm{p}xi}^{\prime(\prime\prime)} \left(1 - \exp\left(-k_i^{\prime(\prime\prime)} s_{\delta i}^{\prime(\prime\prime)*}\right)\right) \\ 0 < F_{xi}^{\prime(\prime\prime)*} \le \mu_{\mathrm{p}xi}^{\prime(\prime\prime)} R_{zi}^{\prime(\prime\prime)}, \quad i = 1, 2\end{gathered} \tag{6.68}$$

where the total circumferential forces $F_{x\Sigma}$ needed to affect motion is determined from the equation, compiled on the basis of Figure 6.14:

$$F_{x\Sigma} = \sum_{i=1}^{2} R_{xi}^{\prime(\prime\prime)*} + F_{\mathrm{d}} - F_{\mathrm{a}} - W_{\mathrm{an}} - W_{\mathrm{hn}} - W_{\mathrm{gn}} \tag{6.69}$$

where W_{an}, W_{hn}, and W_{gn} are the longitudinal components of the weight of the loader, working implements and the weight of the soil in the bucket, whereas F_{a} is the inertia force.

To ensure high traction-gripping performance of the loader over the range of the operational traction loads, it is required to ensure the equality of slippages of the left and right wheels of each axle, that is $s_{\delta i}^{\prime *} = s_{\delta i}^{\prime\prime *} = s_{\delta ai}$, $i = 1, 2$. Hence, in this case the optimal distribution of circumferential forces between the wheels can be determined by reducing Equations 6.68 and 6.69 to an equation that is solved for the generalized slippage of the loader $s_{\delta a}$. After $s_{\delta a}$ and the optimal slippages of the wheels $s_{\delta i}^{\prime(\prime\prime)*}$ are determined, the optimal forces $F_{xi}^{\prime(\prime\prime)*}$ are calculated from the formulae (6.68).

If it becomes necessary to directly asses the fuel consumption in the course of the investigations, this can be done using expressions given below. First, the torque at torque converter turbine (for a loader with hydro-mechanical transmission) is determined from the previously found optimal values of the circumferential forces:

$$T_t = \frac{\sum_{i=1}^{2} F_{xi}^{\prime(\prime\prime)*} r_{\mathrm{w}i}^{0\prime(\prime\prime)} / (u_i \eta_{\mathrm{M}i})}{u_{\mathrm{trm}} \eta_{\mathrm{trm}}} \tag{6.70}$$

where u_{trm} and η_{trm} are the gear ratio and the mechanical efficiency of the transmission. Then the angular velocity ω_t of the turbine wheel is determined from the output curve of the torque converter. Parameters T_t and ω_t make it possible, with consideration of the performance parameters of the torque converter and the engine, to calculate the angular

velocity ω_e and the torque T_e of the crankshaft, and from them the consumption Q_h of fuel per hour from one of the available relationships and the specific fuel consumption

$$g_d = Q_h/P_d \tag{6.71}$$

The modeling was concerned with the scooping up of material under the principal work conditions: at the same and different gripping conditions of the wheels, on a horizontal surface and with a side slant. The theoretically possible case of moving at an incline with a side slant was also investigated.

Figure 6.15a and b gives the values of the normal reactions and optimal circumferential forces of the wheels for the case when the loader scoops up material while situated at a slant on a hard soil surface.

The angle of slant θ_l is 5°, which is usually the maximum slant angle of the work area. As seen from the graphs, the normal loads on the front wheels increase during the first half of the scooping operation and then decrease. The normal reactions of the rear wheels first decrease and then increase. The optimal values of circumferential forces of the loader's wheels change accordingly. Here, the circumferential forces of the wheels on the side located lower along the slant are greater than of the wheels located at the higher part of the slant. These variations in reactions $R_{zi}^{\prime(\prime\prime)}$ and optimal forces $F_{xi}^{\prime(\prime\prime)*}$ are caused by the effect of the pressure F_d and digging R_b forces, inertia force F_a, and the slope of the surface of motion.

The data presented in Figure 6.15a and b were used for calculating the torques T_{01} and T_{02} reduced to the housings of the mechanisms in the interwheel power-dividing units, where formula (6.23) was used for calculating the optimal torques distribution factors K_{mk1} and K_{mk2}. The results of these calculations are shown in Figure 6.15c and d whence it follows that when working with a side slant K_{mk1} is more stable, whereas K_{mk2} varies markedly. Data from Figure 6.15c and d serve as input information for determining/synthesizing the optimal properties of the limited slip differentials for the driving

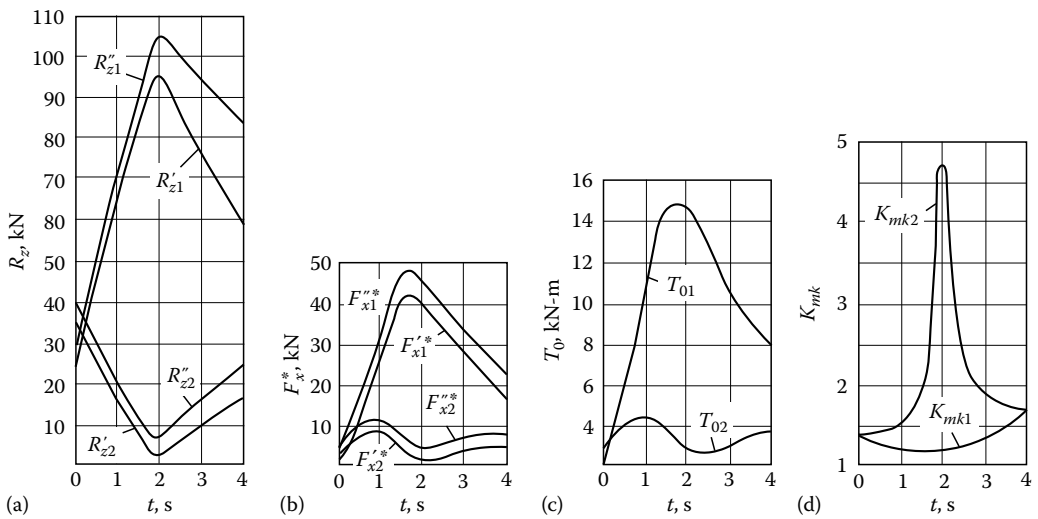


FIGURE 6.15
4×4 loader parameters on a hard soil surface, $\theta_l = 5°$; $\theta_n = 0$.

axles of the loader that correspond to the maximum values of efficiency from the objective function (6.67). These properties are now determined for the case of limited slip differentials, the locking coefficient of which is functionally related to torque T_0 at the housing. For this, the relationships from Figure 6.15c and d are reconstructed into functions such as $K_{mki} = f_i(T_{0i}), i = 1, 2$ by eliminating the time t. These functions are shown graphically in Figure 6.16a.

The arrows show the directions of the variation in factors K_{mk1} and K_{mk2} upon changes in torques T_{01} and T_{02}. Similar relationships were obtained for scooping up of material when the loader was on a 5° transverse incline and on a horizontal surface, but at different gripping conditions of the left and right wheels (see Figure 6.16b through d). Figure 6.16e and f shows the behavior of K_{mk1} and K_{mk2} when the material is scooped up in the bucket with the loader inclined in the longitudinal and lateral direction at the same and different wheel gripping conditions. The shape of the curves is similar to those in Figure 6.16a through d.

It is seen from the data above that the distribution of torques between the wheels of the front axle is more stable. The values of K_{mk2} vary markedly with variation in T_{02}; in all cases there are typical segments of reduction in K_{mk2} with increasing T_{02}.

Analysis of the curves of $K_{mki} = f_i(T_{0i})$, as obtained above shows that, in order to ensure the maximum traction-gripping properties of the loader for its principal operating conditions at different and same properties of the soil beneath the wheels, on a horizontal surface and when moving at an incline (longitudinal, transverse, and combined) the driving axles should be equipped with limited slip differentials having the following properties of the locking devices. The front axle should be provided with a limited slip differential with constant design locking coefficient K_{d1}, or a differential the torque bias of which increases with T_{01} (see Figure 4.32f). The rear axle differential should have a decreasing

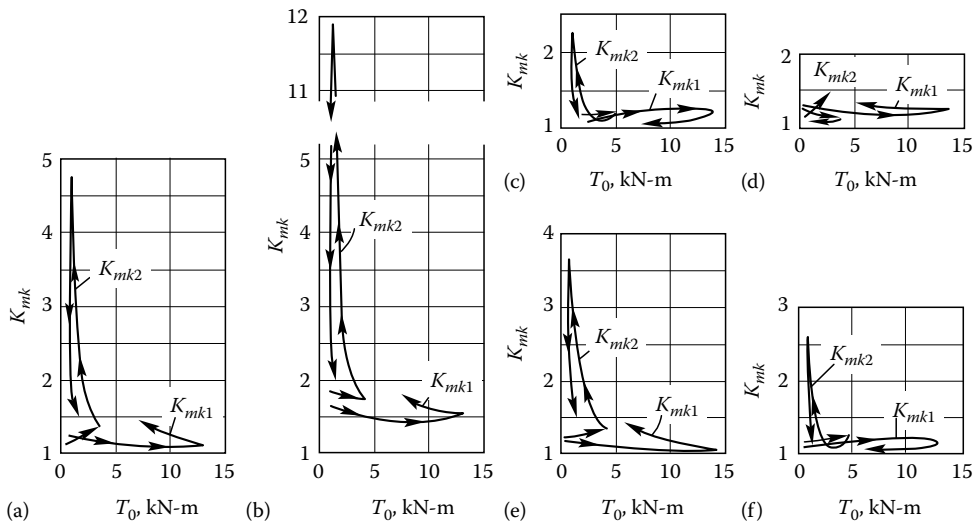


FIGURE 6.16
Optimal torque distribution factors: (a) all wheels on a hard soil surface, $\theta_l = 5°$; $\theta_n = 0$; (b) upper wheels on a hard soil surface, lower wheels on an over damped surface, $\theta_l = 5°$; $\theta_n = 0$; (c) upper wheels on an over damped surface, lower wheels on a hard soil surface, $\theta_l = 5°$; $\theta_n = 0$; (d) right side wheels on an over damped surface, left side wheels on a hard soil surface, $\theta_l = 5°$; $\theta_n = 0$; (e) all wheel on a hard soul surface $\theta_l = 5°$; $\theta_n = 0$; (f) upper wheels on a hard soil surface, lower wheels on an over damped surface, $\theta_l = 5°$; $\theta_n = 5°$.

friction torque, whose locking coefficient K_{d2} decreases with increasing torque T_{02} at the mechanism's housing.

The values of K_{d1} and K_{d2} should exceed the predicted values of K_{mk1} and K_{mk2} (Figure 6.16) in order that the limited slip differentials should not become actuated under real operating conditions and to thus ensure equality of the slippages ($s'^{*}_{\delta i} = s''^{*}_{\delta i}$). Consider a method of determining the numerical values of K_{d1} and K_{d2}.

Under actual travel conditions, the wheel torques fluctuate about average values. Experimental data show that the variation factors V_B of the torques of tractor wheels when working with traction load and locked interwheel differentials may be as high as 25%–35%. For this reason, the practical limits of the scatter of torques about the mean value $\bar{x}$ may be determined from the familiar statistical formulae:

$$\begin{aligned} \text{upper limit } u_u &= \bar{x} + k\sigma \\ \text{lower limit } u_l &= \bar{x} - k\sigma \end{aligned} \tag{6.72}$$

where $\sigma = \bar{x}V_B$ is the rms deviation and k is a factor selected from statistical tables on the condition that at least 90% sample elements belong with a probability of at least 0.9–0.95 to the interval $[u_u; u_l]$.

Making use of formula (6.72) the required value of the locking coefficient can be determined from the expression:

$$K_{di} = \frac{u_u}{u_l} = \frac{\bar{x}''(1 + kV_B)}{\bar{x}'(1 - kV_B)} \tag{6.73}$$

where $\bar{x}''/\bar{x}'$ is the torque bias determined from the mean values of the optimum torques, that is, upon incorporation of factors K_{mki} from Figure 6.16. Making use of formula (6.73), techniques for calculating the locking properties from Chapter 4 and results of the investigations described above, the unified designs of limited slip differentials were worked out for both of the loader's axles. The exploded views of these differentials and the predicted and experimental properties of their locking performance are shown in Figure 6.17.

Consider now the traction properties of a loader that correspond to the optimum distribution of power between the loader's wheels. Figure 6.18a shows the energy performance of the loader.

The manner of variation in η_x^t in the course of scooping up the material that was obtained is determined by the corresponding total circumferential force $F_{x\Sigma}$ and its distribution between the wheels, the rolling resistance $R_{x\Sigma} = \sum_{i=1}^{2} R_{xi}^{\prime(\prime\prime)}$ (see Figure 6.18b) that depend on the pressure and digging forces, the inertia force, and the mass of material in the bucket. It should be emphasized that these values of η_x^t are the maximum possible under the given operating conditions, since they correspond to the optimum distribution of power between the wheels and, accordingly, torques, and circumferential forces shown in Figure 6.15b. Any other power distribution will have lower running gear efficiency.

The maximum values of η_x^t in Figure 6.18a together with the efficiencies η_M of the mechanical part of the driveline system, of the transmission η_{trm} and of the torque converter η_{gt} define the maximum possible values of the traction efficiency η_t of the loader. The corresponding computed curves are shown in Figure 6.18c. This figure also shows a graph of the minimum possible specific fuel consumption g_d when moving in the first gear, the manner of variation in which in the course of scooping is opposite to that of the maximum possible traction efficiency.

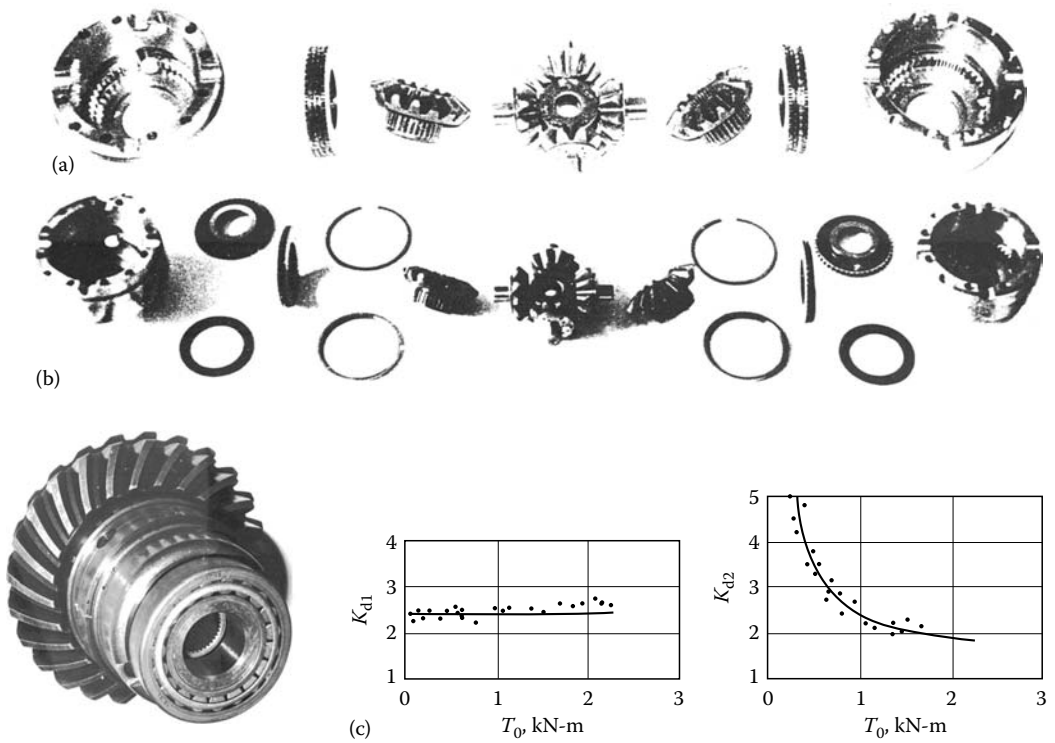


FIGURE 6.17
Designs and torque biases of unified limited slip differentials for the front and rear axles.

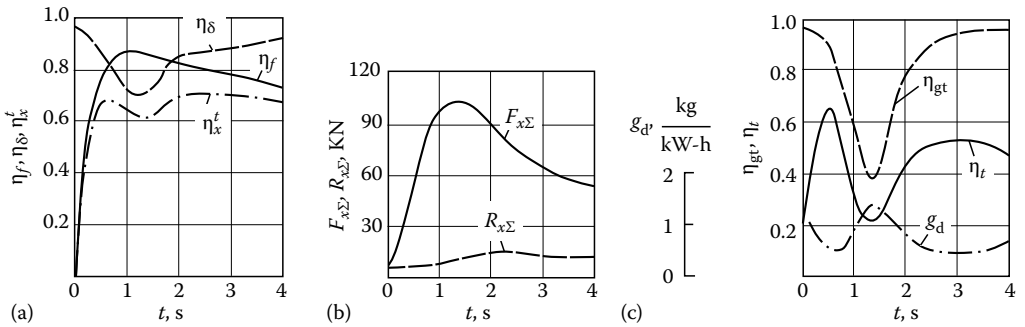


FIGURE 6.18
Optimal energy and force characteristics on a hard soil surface, $\theta_l = 5°$; $\theta_n = 0$.

Figure 6.19 shows the maximum possible values of η_x^t of the loader's running gear efficiency under different operating conditions, the optimal traction power distribution that is represented by torque distribution factors K_{mki} from Figure 6.16a through d.

Further, in keeping with the algorithm of searching the optimum distribution of power between the wheels and of synthesis of the properties of the driveline system shown in Figure 6.11, it is necessary to assess the effect of the factors K_{mk1} and K_{mk2} (torque biases K_{d1} and K_{d2}) thus found on the turnability and stability of the loader's motion.

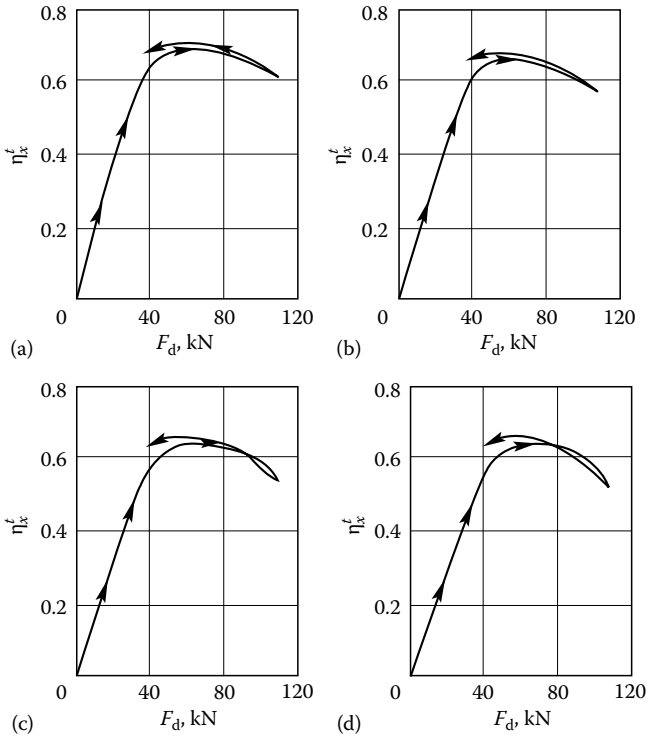


FIGURE 6.19
Maximum traction running gear efficiency: a, b, c, and d correspond to a, b, c, and d on Figure 6.16.

In the case when a limited slip differential is installed in the *i*th driving axle, a moment of resistance to turning appears in the plane of the road to the vehicle's taking a turn and this moment is determined, after the differential is actuated from the general formula (4.161)

$$M_{\mathrm{Bd}i} = 0.5 t_{\mathrm{B}i} \frac{K_{\mathrm{d}i} - 1}{K_{\mathrm{d}i} + 1} F_{x\Sigma i} \tag{6.74}$$

where $F_{x\Sigma i}$ is the circumferential force of the *i*th axle, $F_{x\Sigma i} = F''_{xi} + F'_{xi}$.

To ensure the required turnability of a loader with limited slip interwheel differentials (while retaining high traction properties) there is a need to keep the total moment of turning resistance under control

$$M_{\mathrm{Bd}\Sigma} = \sum_{i=1}^{2} M_{\mathrm{Bd}i} \tag{6.75}$$

It appears that regulation of this moment is best implemented by installing limited slip differentials with different properties in the corresponding driving axles.

Consider now the relationships for determining the moment of resistance to the turning of the axle using limited slip differential with different properties. The turning resistance moment that is induced by installing differentials with decreasing friction is calculated from formula (4.163). It is seen from this formula that, this moment decreases if the torque

T_0 at the differential's housing increases. It follows from formula (6.74) that when a limited slip differential with a constant design locking coefficient K_d is installed this moment increases with the traction load on that axle $F_{x\Sigma i}$ (i.e., with the increase in torque T_0 supplied to this differential).

The above analysis of turning resistance moments allows the conclusion that the optimal characteristics of the limited slip interwheel differentials determined previously based on the traction properties and energy efficiency of the loader are successful also from the point of view of turnability. When the loader turns with increasing segment angularity, γ, kinematic discrepancy appears between the axles that are coupled by the positively engaged drive. Here the location of the hinge between the segments toward the front axle causes its kinematic discrepancy factor m_{H1} to become negative and to decrease with increasing γ while factor m_{H2} of the rear axle is positive and increases. The above will become clearer by reference to Figure 3.24. This reduces the circumferential force F_{x1} of the front wheels and increases force F_{x2} of the rear wheels. For this reason moment M_{Bd1} of resistance to turn of the front axle with a differential having a constant K_{d1} decreases and moment M_{Bd2} of resistance to turn of the rear axle, in which the differential with decreasing friction is installed, also decreases. As a result, the total moment of resistance to turning of the loader from formula (6.75) decreases. This is shown by solid curves in Figure 6.20a.

The reduction in turning resistance moment $M_{Bd\Sigma}$ has a positive effect on the variation of the actual turning radius R_{a2} (the shortest distance from the center of turn to the longitudinal axis of the second segment of the loader): its increase as compared with the theoretical radius R_{t2} by the factor q_R does not exceed 14% (see Figure 6.20b, solid curves). This manner of variation in R_{a2}, as shown by the comparative analysis with data for other vehicles appears to be acceptable.

It is noted for comparison that if the same differential with constant locking coefficient as installed in the front axle is used in the rear axle, then the turnability of the loader deteriorates (see Figure 6.20a and b, dashed curves). In this case $M_{Bd\Sigma}$ does not decrease, but remains virtually constant independently of the angle γ between the segments. The turning radius increases accordingly.

The use of limited slip differentials developed above improves the stability of motion of the loader. The redistribution of circumferential forces between the wheels and their resulting lateral reactions do not markedly increase the factors $K'^{(n)}_{\mu i}$ of utilization of the gripping forces of the wheels (see formula 1.119) in the course of the loader's turning. As seen from Figure 6.20c, the values of these factors are much smaller than 0.5. This provides for side skid-less rolling of the wheels.

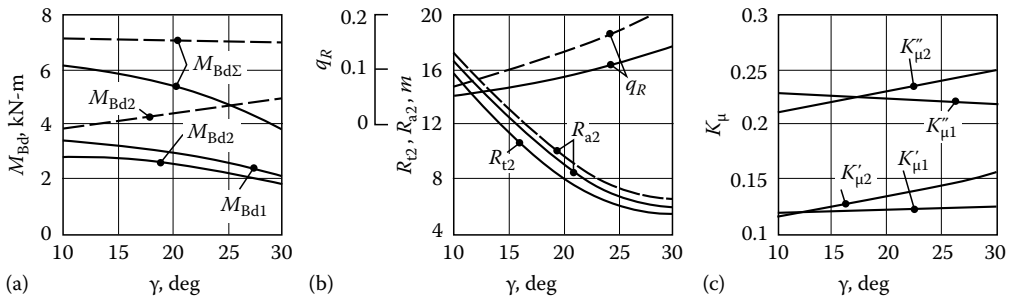


FIGURE 6.20
Characteristics of turnability and stability of motion on a hard soil surface, $\theta_l = 0$; $\theta_n = 0$.

It was thus demonstrated that the use of the method suggested in this section is capable of validating the optimal properties of limited slip differentials for both axles of articulated 4×4 loaders that ensure the maximum possible traction properties and energy efficiency of loaders under principal operating conditions while retaining stability of motion and not being detrimental to the turnability.

6.5 Synthesis of Properties of Interaxle Power-Dividing Units

The search for relationships that describe the optimum power distribution among the driving axles and the synthesis of the properties of interaxle drives of transportation-traction vehicles is carried out in the same sequence as for the previously analyzed interwheel drives.

This section goes into more detail on the determination of the optimum distributions of power to the driving axles and optimum torques of the axles in conjunction with the geometric parameters of multiwheel drive vehicles—the location of the center of gravity and the arrangement of the wheels on the wheelbase. Usually these geometric parameters are selected to ensure the ability of the vehicle to move over irregular terrain and the reduction of normal dynamic loads on the running gear of the vehicle. Less attention is paid to their effect on the traction properties and the ability of the vehicle to travel over unpaved, boggy, and snow-covered roads.

Figure 6.21 shows a computational model of uniform travel of a 6×6 traction vehicle (tractor) with individual wheel suspension over deforming soil.

The mathematical model of optimization of the distribution of power among the axles for these travel conditions is written as:

$$\eta_x^{\mathrm{t}} = \frac{F_{\mathrm{d}}}{\sum_{i=1}^{3} F_{xi} + \sum_{i=1}^{3} \frac{F_{xi} s_{\delta ai}}{1 - s_{\delta ai}}} \rightarrow \max \tag{6.76}$$

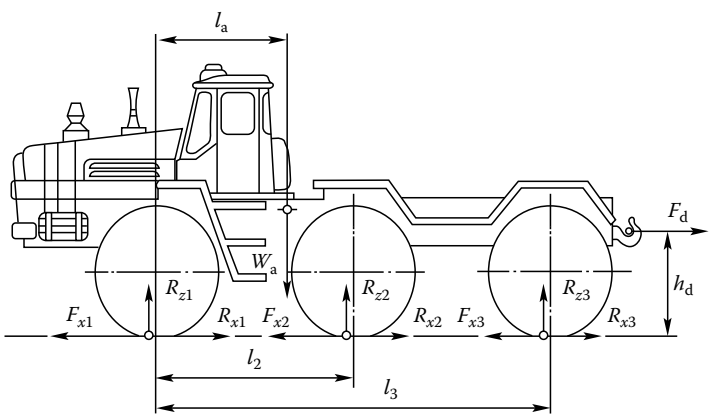


FIGURE 6.21
6×6 traction vehicle: free-body diagram.

$$\sum_{i=1}^{3} F_{xi} = F_{x\Sigma} = \sum_{i=1}^{3} R_{xi} + F_{\mathrm{d}}$$

$$0 < F_{xi}^{*} < \mu_{\mathrm{p}xi} R_{zi}$$

$$F_{xi}^{*} = R_{zi}\mu_{\mathrm{p}xi}(1 - \exp(-k_i s_{\delta ai}^{*}))$$

The results of the investigations on the above mentioned 9 ton 6×6 vehicle with 16.9R30 tires when moving over a plowed field with caked soil are presented below. Figure 6.22

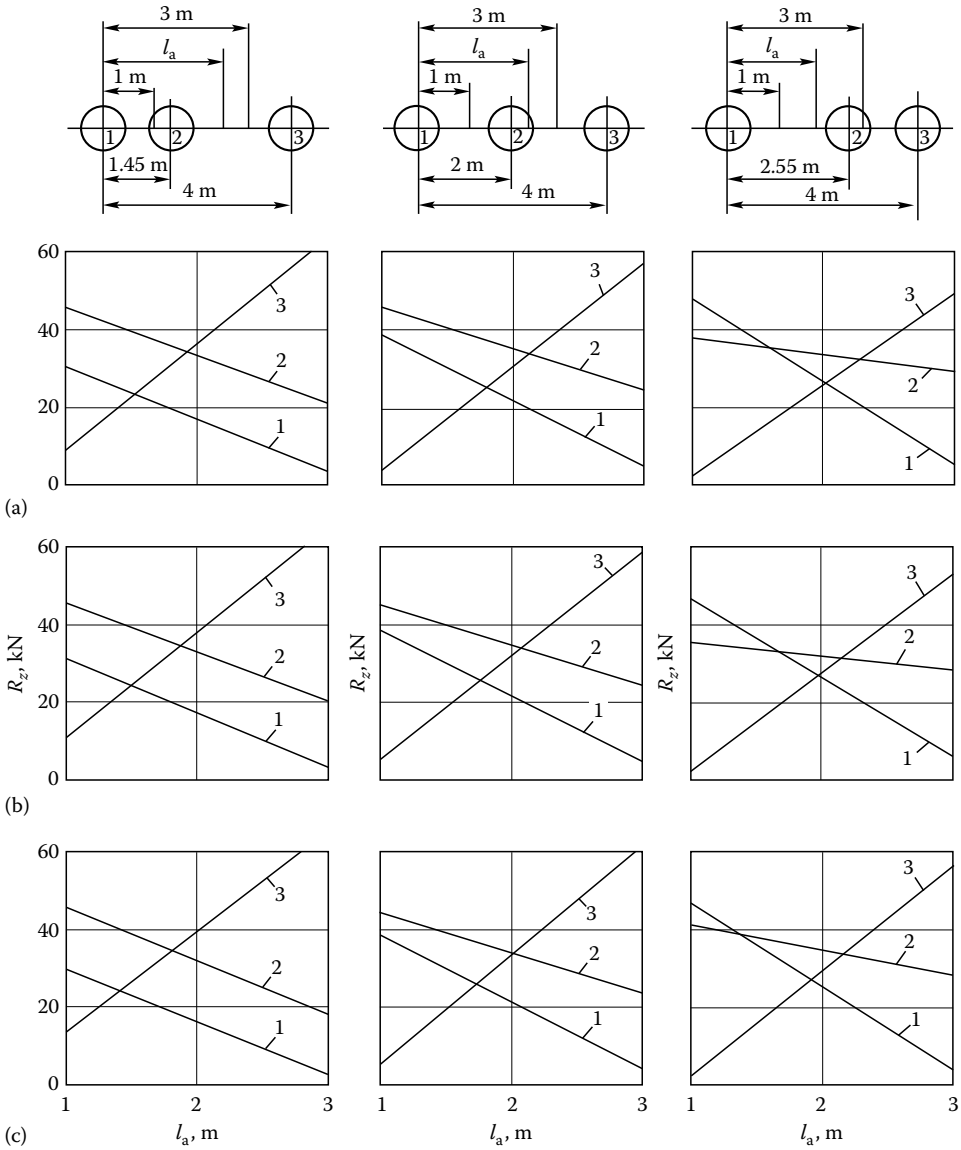


FIGURE 6.22
Normal reactions of the axles: (a), (b), (c)—$F_{\mathrm{d}} = 20, 30,$ and 40 kN.

shows the distribution of the normal reactions between the axles as a function of the location of center of gravity l_a and traction load F_d for three forms of second axle arrangement: as close as possible to the front wheels, in the middle of the wheelbase and as close as possible to the rear wheels.

The curves of the total resistance to the rolling of the wheels, $R_{x\Sigma} = \sum_{i=1}^{3} R_{xi}$, for these three arrangements are plotted in Figure 6.23.

The distribution of normal loads between the axles has a marked effect on the rolling resistance $R_{x\Sigma}$. In all the wheel arrangements the value of $R_{x\Sigma}$ is at a minimum in regions with more uniform distribution of normal reaction R_{zi}. Hence the value of $R_{x\Sigma}$ is at a minimum with increasing F_d at lower values of l_a.

Figure 6.24 presents the maximum possible, under the travel conditions being considered here, efficiencies of the running gear of the vehicle that are provided by the pertinent distribution of power among the axles.

The optimal distributions of circumferential forces F_{xi}^* that correspond to the optimal distribution of power, defined by factors K_{moi} from the first of formulae (6.24) are plotted in Figure 6.25.

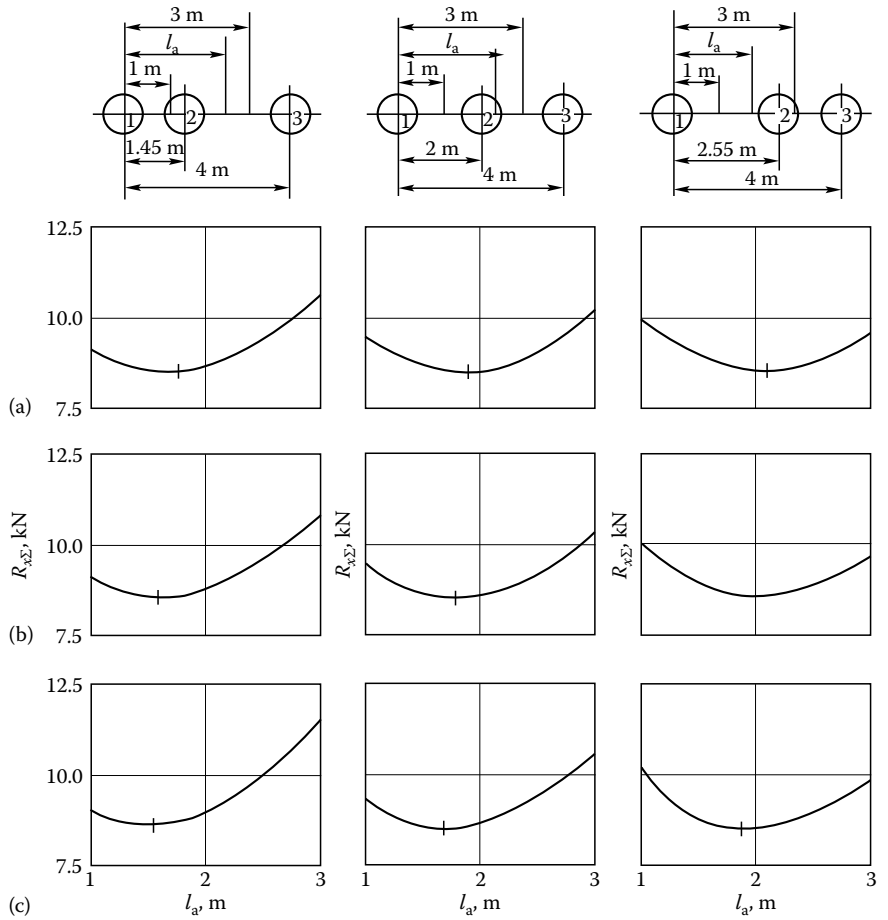


FIGURE 6.23
Total rolling resistance $R_{x\Sigma}$: (a), (b), (c)—$F_d = 20, 30,$ and 40 kN.

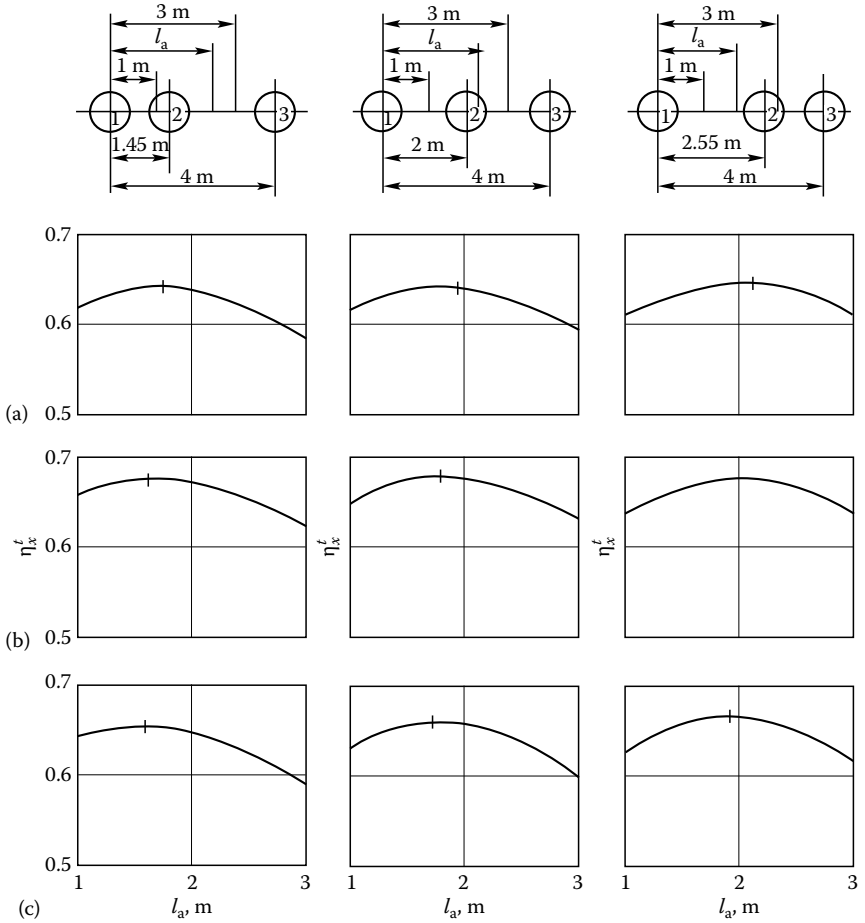


FIGURE 6.24
Maximum traction running gear efficiency: (a), (b), (c)—$F_d = 20, 30,$ and 40 kN.

At any other relationships between the circumferential forces of the axles, the efficiency η_x^t has values lower than those shown in Figure 6.24.

The above graphs show the manner in which the optimum relationship of the torques of the axles in the overall traction balance of the vehicle should change upon a change in the location of the center of gravity and traction load for the three different arrangements of the middle wheels. For example, when the wheels are arranged uniformly over the wheelbase and l_a is increased (the center of gravity is moved to the rear) it is necessary to increase torque T_{a3}^* while decreasing torques T_{a1}^* and T_{a2}^* at the front and middle axles.

It was found that the optimum distribution of axle torques is attained when the generalized slippages of the axles are virtually the same (the dashed curve in Figure 6.25). The differences between the slippages start only in the 4th–5th decimal points under standard loading conditions and with the 3rd decimal point at high traction loads. These results confirm the data of mathematical analysis presented in Section 6.3 on the virtual equality of slippage of wheels that correspond to the maximum efficiency under standard loading conditions.

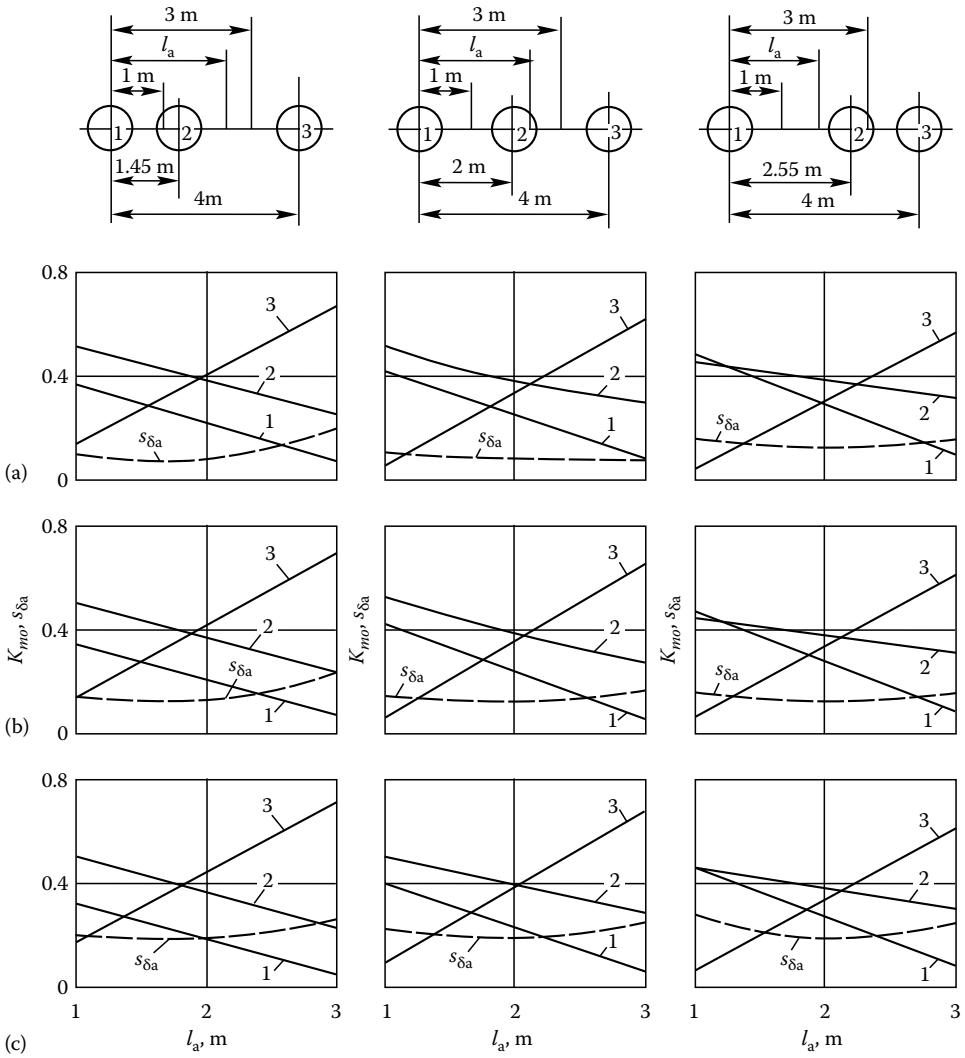


FIGURE 6.25
Factors of the optimal distribution of torques among the driving axles: (a), (b), (c)—$F_d = 20, 30,$ and 40 kN.

It follows from Figure 6.24 that the middle-wheel location arrangements discussed here have, under different traction loads, such locations of the center of gravity l_a at which η_x^t takes the maximum value of the maximum possible values. When F_d increases, the values of l_a decrease for all the three arrangements of the middle wheels. The maximum value of the maximum possible values of η_x^t correspond to the minimum of rolling resistance $R_{x\Sigma}$ (see Figure 6.23) and more uniform distribution of the loads between the axles (see Figure 6.22).

When the middle wheels are shifted from the front wheels to the rear wheels, the maximum efficiency of the maximum possible changes somewhat (see Figure 6.24). It is hence of interest to investigate in more detail the effect of parameter l_2 on the traction performance of the vehicle. The results of these studies are shown in Figures 6.26 through

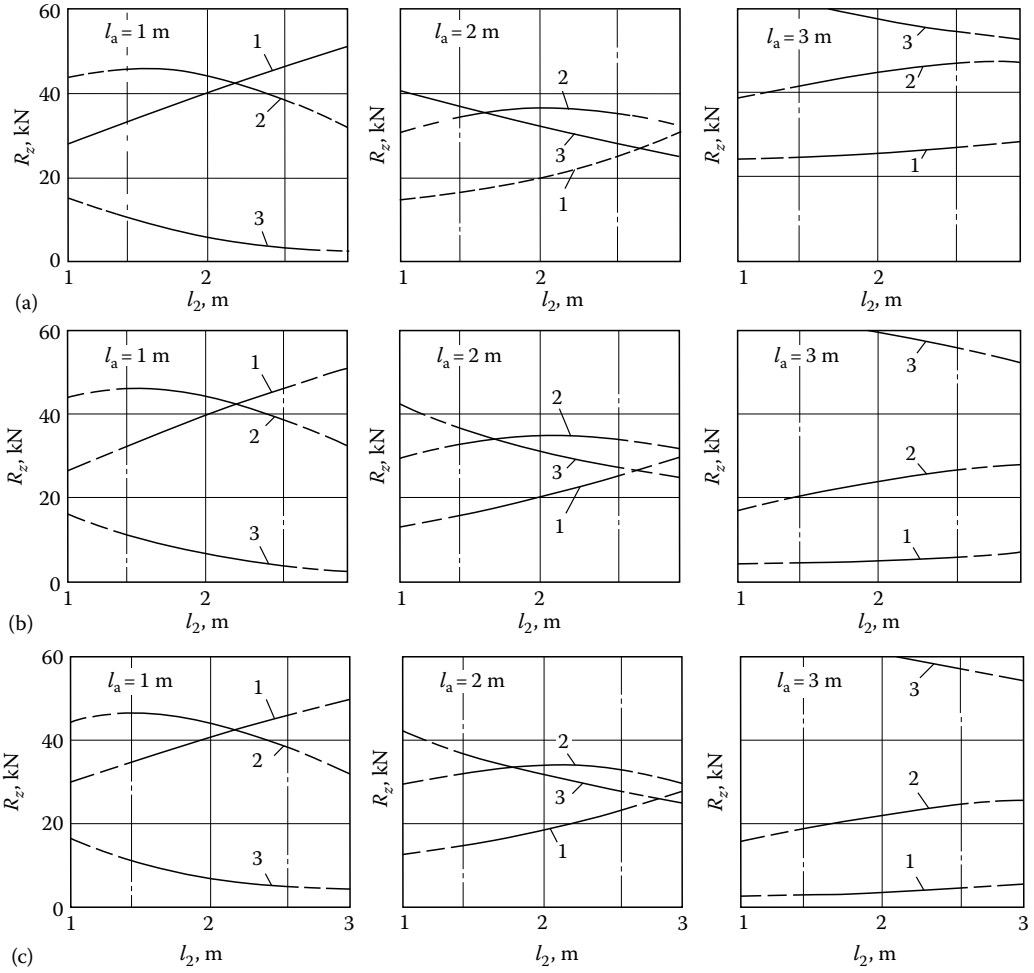


FIGURE 6.26
Normal reactions of the axles: (a), (b), (c)—$F_d = 20, 30,$ and 40 kN.

6.29 for different traction forces F_d and three values of l_a. In these figures, the dash-dotted vertical lines delimit the practically possible extremal values of l_2.

When the middle wheels are shifted from the front to the rear wheels the nonuniformity in the distribution of normal reactions increases at $l_a = 1$ m and decreases at $l_a = 2$ and 3 m (Figure 6.26). The total rolling resistance force $R_{x\Sigma}$ of the wheels increases or decreases in accordance with this, and this causes the same changes in the maximum efficiency of the vehicle running gear that is possible under these conditions of motion (Figures 6.27 and 6.28). These maximum efficiencies are attained by the corresponding optimum distributions of the axle torques of the wheels which, as seen from Figure 6.29, should to a certain degree vary in accordance with the variation in normal reactions R_{zi}.

It follows from Figure 6.28 that for the same traction loads higher maximum efficiencies correspond to the case when the center of gravity is close to the middle of the wheelbase. Then the location of the middle axle has effect on the efficiency. For example, at $F_d = 40$ kN and $l_a = 2$ m, η_x^t increases from 0.65 to 0.665 when l_2 is changed from 1.45 to 2.55 m.

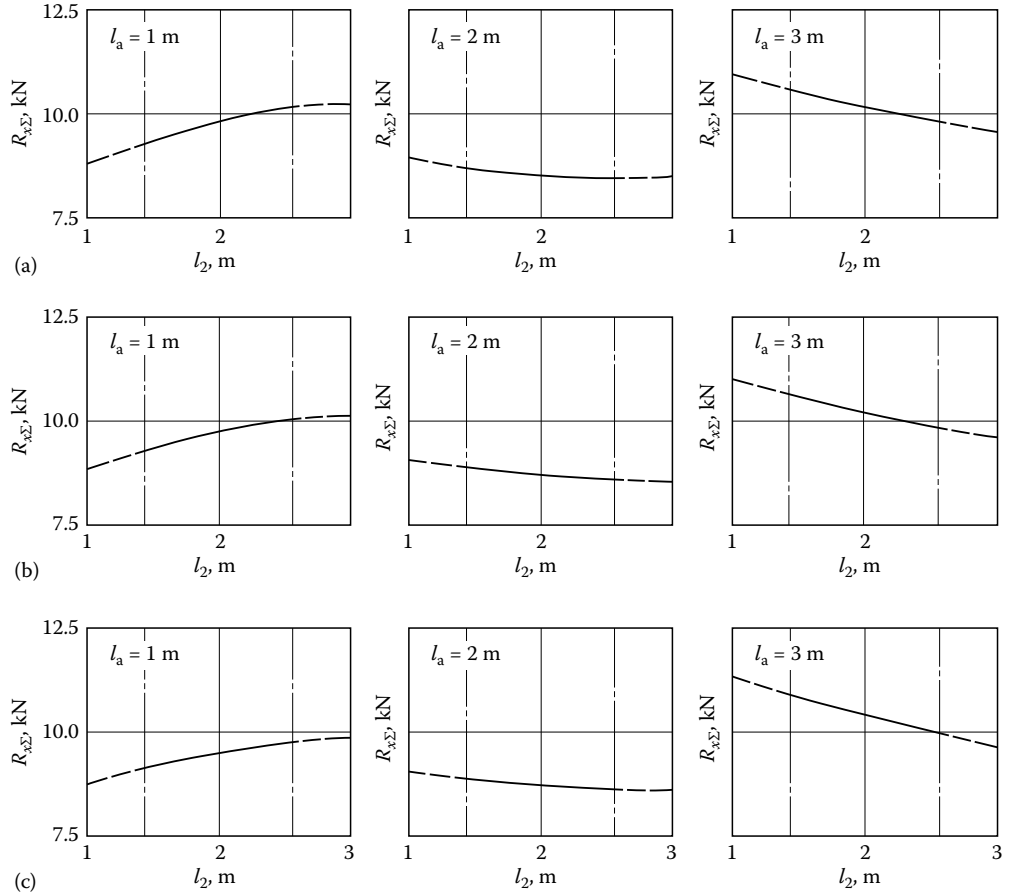


FIGURE 6.27
Total rolling resistance $R_{x\Sigma}$: (a), (b), (c)—$F_d = 20, 30,$ and 40 kN.

When the center of gravity is shifted to the front or rear wheels, then the location of the middle axle exerts a somewhat greater effect on the efficiency. However, varying l_2 does not allow attaining the same efficiencies as at $l_a = 2$ m. For example, at $F_d = 40$ kN and $l_a = 3$ m the efficiency increases from 0.58 to 0.62, when l_2 is varied from 1.45 to 2.55 m.

It was found by examining the theoretically determined values of efficiency (see Figures 6.24 and 6.28) that it is possible to determine such optimal values of parameters l_a^* and l_2^* at which η_x^t can take the highest value of the maximum possible. For this purpose, level lines corresponding to constant values of η_x^t at different combinations of l_a and l_2 were constructed based on Figures 6.23 and 6.28. These constructions are shown in Figure 6.30 from which it is seen that the levels are not continuous and converge in a point on the dash-dotted straight line that corresponds to $l_2 = 2.55$ m.

This means that the optimum value of l_2^* is limited by the actually possible shift of the middle to the rear wheels, that is $l_2^* = 2.55$ m.

The optimum value of l_a^* decreases with increasing traction load: point * on the dash-dotted curve in Figure 6.30 delimited by the curve of the 5th level that is shifted to the left. The variation in the optimum l_a^* as a function of F_d is shown in Figure 6.31.

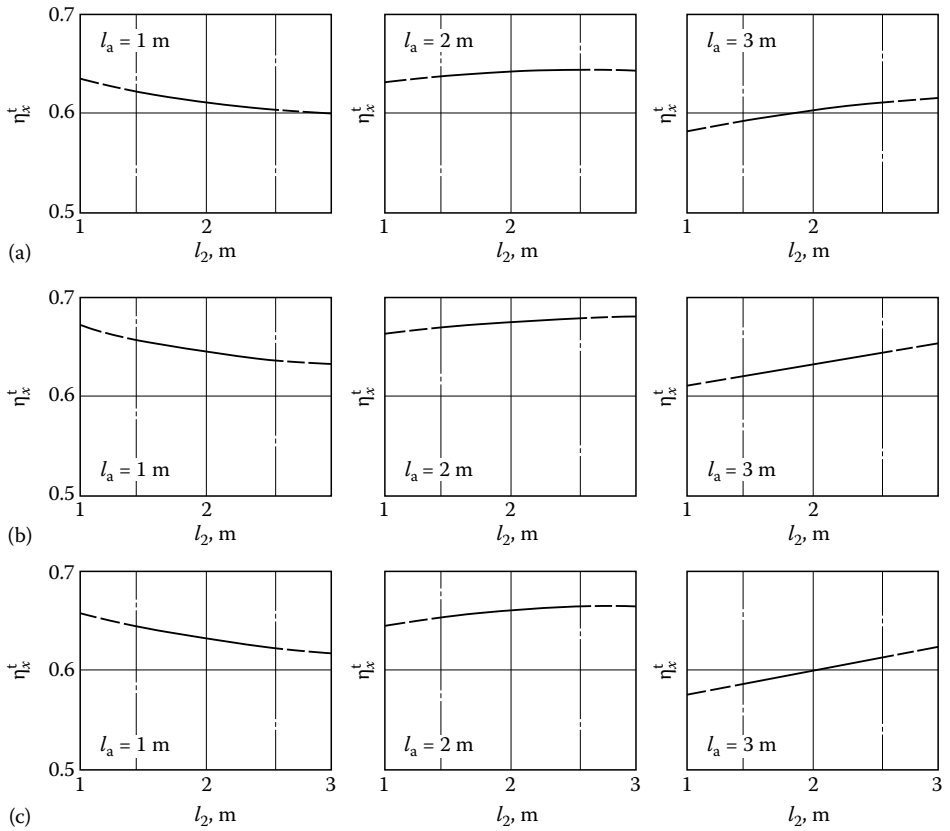


FIGURE 6.28
Maximum traction running gear efficiency: (a), (b), (c)—$F_d = 20, 30,$ and 40 kN.

At operating loads of F_d up to 40 kN, to which the drawbar coefficient $\mu_d = F_d/W_a = 0.44$ corresponds, the value of l_a^*, decreases from 2.15 to 1.9. Accordingly, the dimensionless ratio l_a^*/l_3 decreases from 0.52 to 0.46. The above studies thus show that, in order to attain the maximum possible traction properties, the middle and rear wheels should be located as close to one another as possible. The center of gravity then should be so located that the ratio l_a/l_3 lies between 0.46 and 0.52.

If the vehicle layout requires that the wheels be distributed uniformly over the base, this will be least detrimental to η_x^t only at l_a/l_3 between 0.43 and 0.503. To provide for high running gear efficiency of the traction vehicle when the middle wheels are located close to the front wheels it is necessary to ensure that l_a/l_3 lies between 0.39 and 0.46 (Figure 6.31). Note that lately various devices have been invented that allow changing the center of gravity of a vehicle upon change in the traction load.

To attain the highest of the maximum values of the running gear efficiency over the range of recommended values of l_a/l_3 it is necessary to provide for an optimum distribution of torques among the axles. Figure 6.32 shows curves of the ratios K_{moi} as a function of traction force F_d constructed from data in Figure 6.25 and 6.29 that represent the percentile ratio of the optimum torques of the axles in the total traction torque balance of the vehicle.

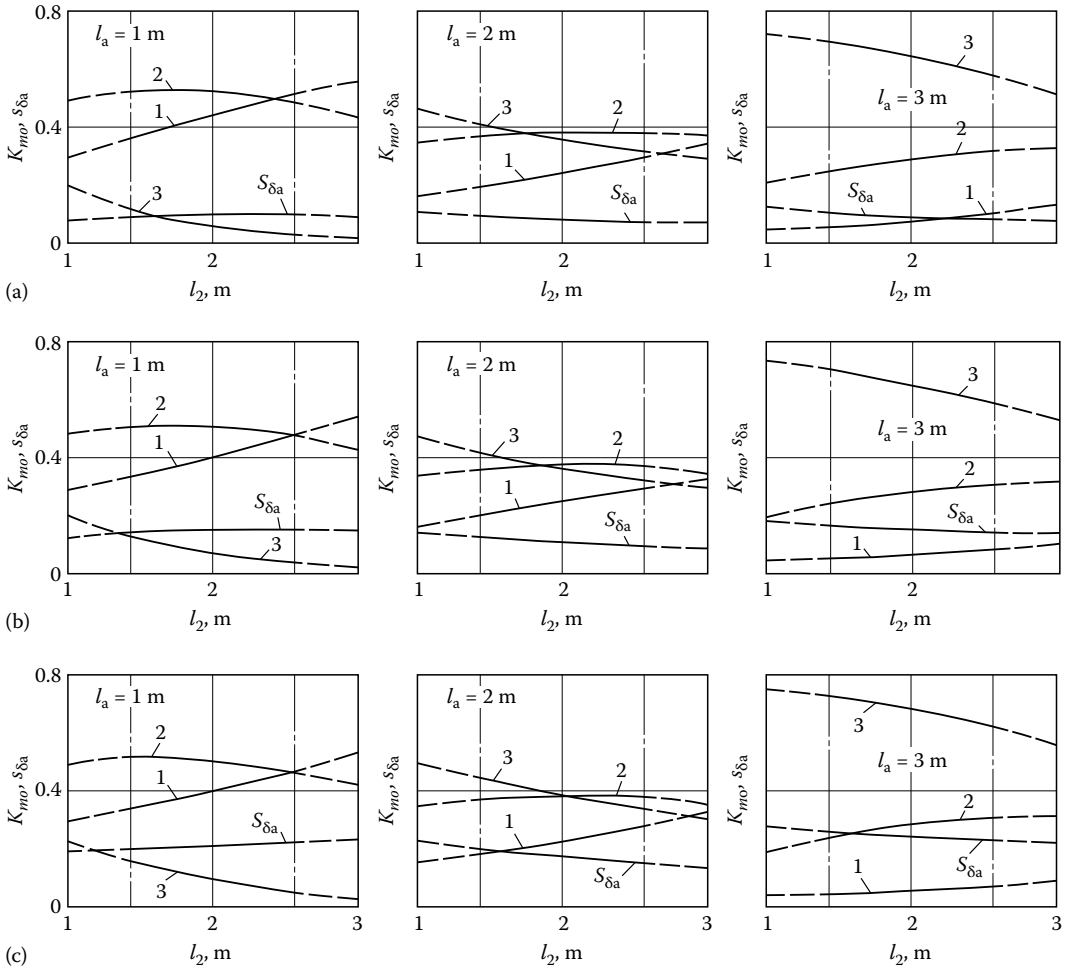


FIGURE 6.29
Factors of the optimal distribution of torques among the driving axles: (a), (b), (c)—$F_d = 20, 30,$ and 40 kN.

In all the three locations of the middle axle under discussion here, the optimum torques of the first and second axles decrease and the optimum torque of the third axle increases with increasing F_d.

The above results relating K_{moi} and F_d can be used in working out the algorithm of automatic control of the distribution of axle torques of vehicles, for example, with an individual electrical drive of the wheels.

The properties of the mechanical and mechatronic driveline systems with mechanisms located in power-dividing units of axles, transfer cases, and of reduction gears, should also account for changes in the ratios between the optimal torques (Figure 6.32). Thus, for example, the fact that the factors K_{mo1} and K_{mo2} vary in the same manner points to the advisability of placing two mechanisms: one between the first and second axles and another between the first and second axles on the one side and third axle on the other. This recommendation, evidently does not apply when the middle wheels are located close

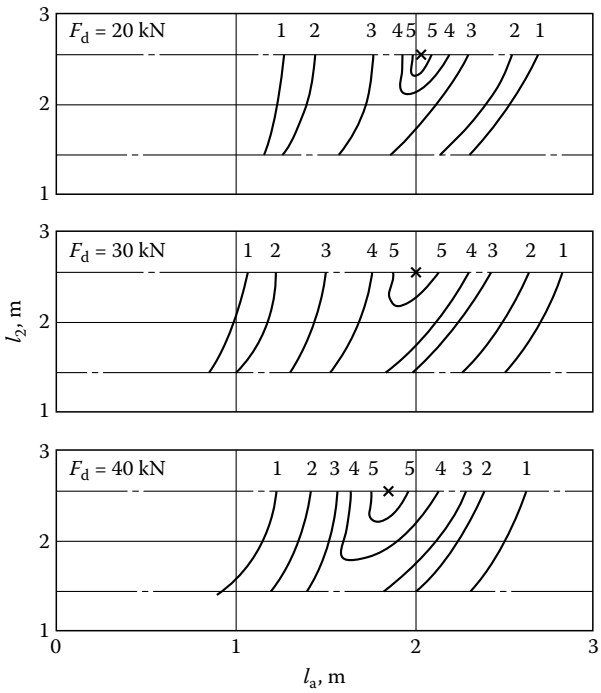


FIGURE 6.30
Level lines of η_x^t at different combinations of l_a and l_2.

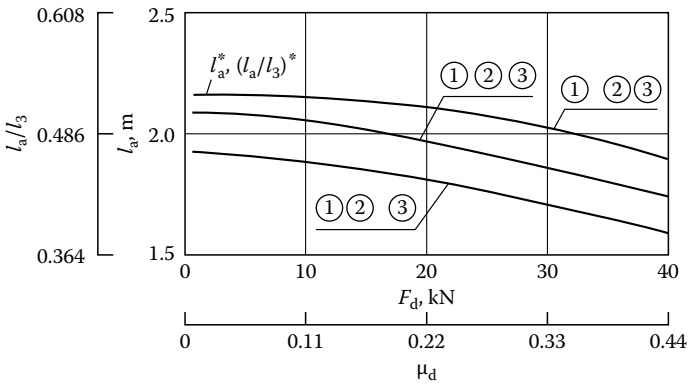


FIGURE 6.31
Recommended values of $l_a^*(l_a^*/l_3)$.

to the rear wheels when layout conditions make it preferable to place one mechanism in the power-dividing unit between the second and third axles and another mechanism between the first axle, on the one side, and second and third axle on the other.

For greater clarity it is more convenient for illustration purposes to use the factors $K_{moi}^{k,\ldots kk\text{-}l,\ldots ll}$ from the second of formulae (6.24) that describe the optimum distribution of torques among axles and clusters of axles. The relationships between these factors and the traction load F_d obtained based on the graphs from Figure 6.32 are shown in Figure 6.33 for different relative locations of wheels on the basis and the minimum and maximum values of l_a/l_3 recommended for them.

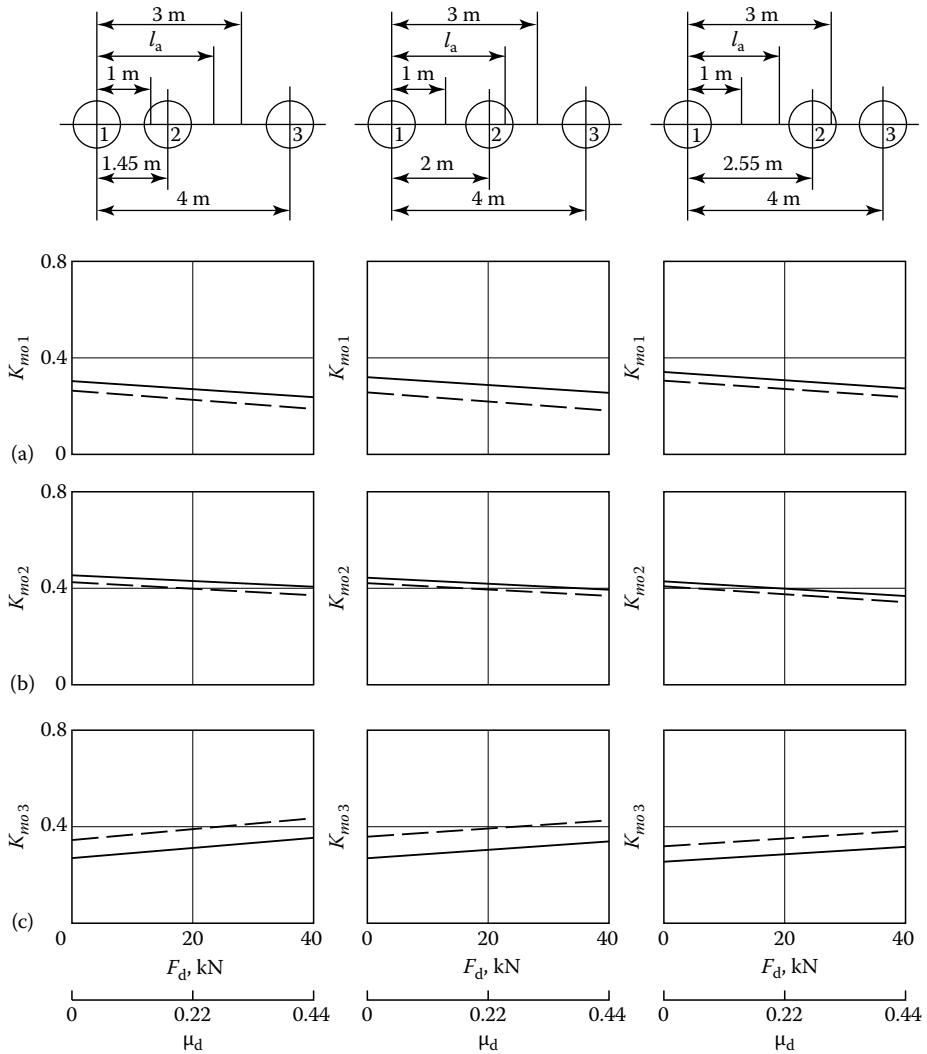


FIGURE 6.32
Factors K_{moi} of the optimal distribution of torques between the driving axles. ———, minimum recommended l_a/l_3; — —, maximum recommended l_a/l_3.

It is seen that for driveline systems (Figure 6.33a and b) the ratio of the torques of the first and second axles represented by the factor K_{mo}^{1-2} remains virtually constant over the entire range of standard operating values of F_d. This points to the possibility of placing an asymmetric differential with standby locking device or a limited slip differential with constant design locking coefficient. The course of variation in the factor $K_{mo}^{1,2-3}$ makes it possible to place in the second power-dividing unit a limited slip differential with variable torque bias that decreases with an increase of the torque at its housing (with the increasing traction force F_d).

The above advantages of the driveline system arrangement of a vehicle with the middle wheels close to the rear ones, shown in Figure 6.33c brought about changes in factors K_{mo}^{2-3}

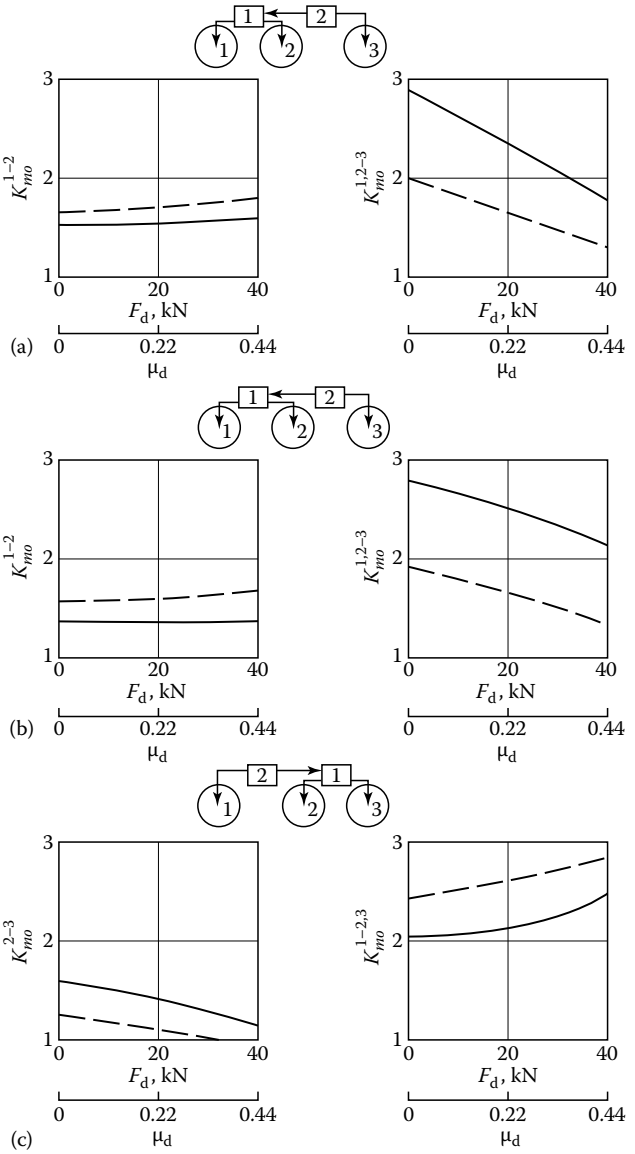


FIGURE 6.33
Factors $K_{moi}^{k,\ldots kk-l,\ldots ll}$ of the optimal distribution of torques between the driving axles. ———, minimum recommended l_a/l_3; — —, maximum recommended l_a/l_3.

and $K_{mo}^{1,2-3}$ with increasing F_d. For this reason, the interaxle power-dividing units of such a vehicle should be equipped with mechanisms with behavior corresponding to variation in these factors of the distribution of optimal torques that also ensure equality of wheel slippage. These, among others, may be limited slip differentials. Their locking coefficients should then be taken constant or they may increase and decrease in accordance with the manner of variation in factors K_{mo}^{2-3} and $K_{mo}^{1,2-3}$. The properties of the limited slip differentials should be adjusted finally with reference to the algorithm of synthesis of the properties of driveline systems (see Figure 6.11), that is by investigating the turnability and stability of the motion of a vehicle with the potential mechanisms in the interaxle drive.

6.6 Synthesis of Properties of Interwheel and Interaxle Power-Dividing Units

This section is concerned with problems of theory and of practical synthesis of properties of driveline systems in the general case when it is necessary to determine the optimal properties both for interwheel and interaxle drives.

6.6.1 The Mathematical Model of a Vehicle

The first stage, in keeping with the algorithm from Figure 6.11, involves working out the mathematical model of the vehicle. Figure 6.34 shows a computational model of an 8×8 vehicle with a payload in its body, individual wheel suspension, and moving over a surface with macro- and micro-irregularities.

For vehicles with different number of driving wheels, the method and algorithm of the studies will be the same; only the quantitative aspect of the calculations, that is, the number of equations of oscillation of the unsprung masses, equations for finding the optimal distributions of power between the wheels will be different. Compilation of the computational model requires making certain assumptions concerning the linearity/nonlinearity of the properties of the elastic elements of the suspension and of the shock absorbers, consideration of dry friction in the suspensions (for example, by adding the dry friction

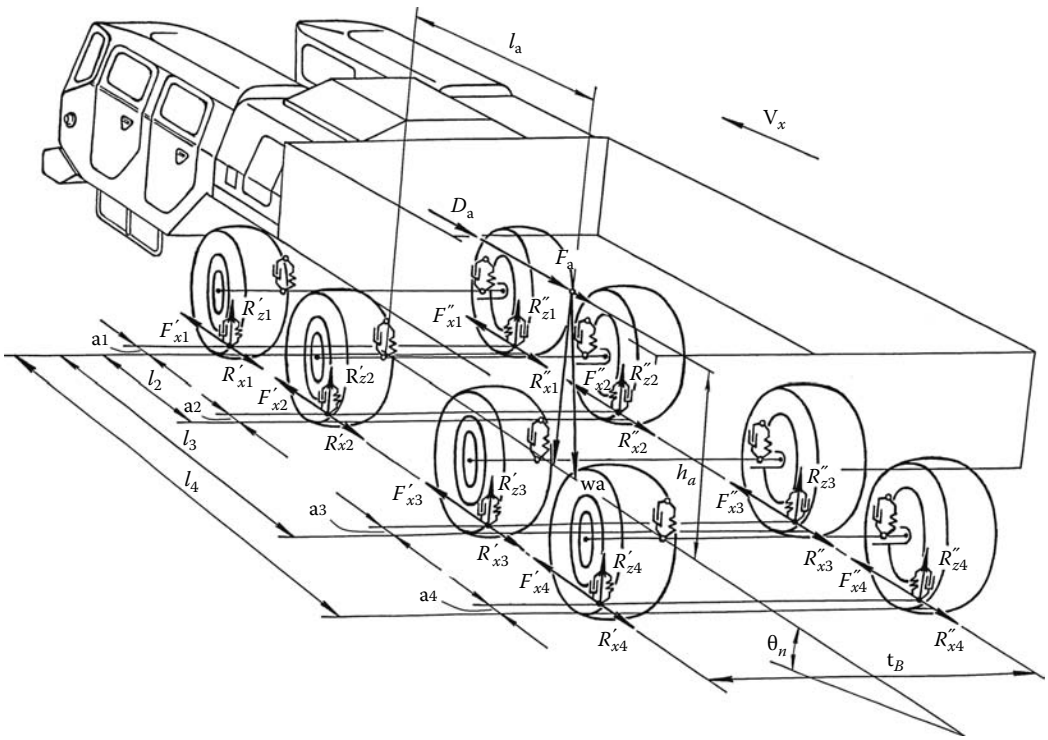


FIGURE 6.34
8×8 terrain vehicle: a free-body diagram.

to the resistance factors of the shock absorbers), etc. It is usually assumed in this study that the engine and the transmission provide the required power for an accelerated and steady state motion of the vehicle with the specified velocity. This allows simplifying the mathematical model without detriment to the accuracy of the results, and to focus primarily on the optimization of the distribution of power among the wheels, and determining the optimal properties of the power-dividing units.

After the determination of the above, the investigations of the powertrain (engine + transmission + driveline system) can be continued by compiling another model of the vehicle, with a consideration of the properties of its transmission and engine, in which the input wheel power was determined from the first model that is described below.

With reference to the free-body diagram in Figure 6.34, the equation of motion with the longitudinal acceleration a_x of the vehicle that is needed for determining the total circumferential force $F_{x\Sigma}$ is:

$$F_{x\Sigma} = \sum_{i=1}^{4} F_{xi}^{\prime(\prime\prime)*} = W_{\mathrm{a}} a_x \delta_r / g \pm W_{\mathrm{a}} \sin\theta_n + \sum_{i=1}^{4} R_{xi}^{\prime(\prime\prime)} + D_{\mathrm{a}} \tag{6.77}$$

where δ_r is the mass factor that makes allowance for the rotating masses of the vehicle. This factor, the wheel resistance forces $R_{xi}^{\prime(\prime\prime)}$, and the air drag D_{a} can be computed on the basis of well-known recommendations from the engineering literature on vehicle dynamics. Figure 6.34 clarifies the physical meaning of the remaining components of Equation 6.77.

The numerical values of acceleration a_x should be specified from the required velocities V_x that the vehicle should have while accelerating. This approach of synthesizing the properties of driveline systems based on inverse vehicle dynamics that are as per the required kinematic parameters to determine the circumferential forces should be applied to the vehicle wheels. The reference to inverse vehicle dynamics was made in Section 1.6 while discussing the principles of the design of driveline systems. In the first approximation, it is possible to use the hyperbolic relationship (6.20). The values of the maximum acceleration are taken from the range of 0.4 to 2.6 m/s^2 depending on the type of surface of motion and the specified steady-state motion velocity $V_{x\mathrm{c}}$. For the vehicle from Figure 6.34 the values of $V_{x\mathrm{c}}$ range from 5 to 35 km/h and are limited by the gripping properties of the support surface, the macro-topography, and if contact between some of the wheels and the surface of motion is lost. Figure 6.35 shows examples of kinematic parameters calculated from (6.20) at different values of $a_x^{\max}$ and $V_{x\mathrm{c}}$.

From the value of V_x thus found and from the specified value of $V_{x\mathrm{c}}$ it becomes possible to calculate the air drag D_{a} at the acceleration and steady-state motion stages.

Rolling resistance forces $R_{xi}^{\prime(\prime\prime)}$ can be calculated only when the values of the normal wheel reactions $R_{zi}^{\prime(\prime\prime)}$ are known. These were determined from reactions $R_{zi}^{s\prime(\prime\prime)}$ obtained for the cases of motion over a straight inclined/horizontal support surface (suspension's action included) with allowance for dynamic components induced by the tires and micro-topography:

$$R_{zi}^{\prime(\prime\prime)} = R_{zi}^{s\prime(\prime\prime)} + C_{ti}^{\prime(\prime\prime)}\left(\xi_i^{\prime(\prime\prime)} - q_i^{\prime(\prime\prime)}\right) + K_t^{\prime(\prime\prime)}\left(\dot{\xi}_i^{\prime(\prime\prime)} - \dot{q}_i^{\prime(\prime\prime)}\right) \tag{6.78}$$

where $C_{ti}^{\prime(\prime\prime)}$ is the normal stiffness of the tire (or the reduced stiffness of the tire and the soil when moving over a deforming surface), $K_t^{\prime(\prime\prime)}$ is the tire's damping factor (or the reduced damping factor of the tire and the soil), $q_i^{\prime(\prime\prime)}$ is the height of the surface micro-profile,

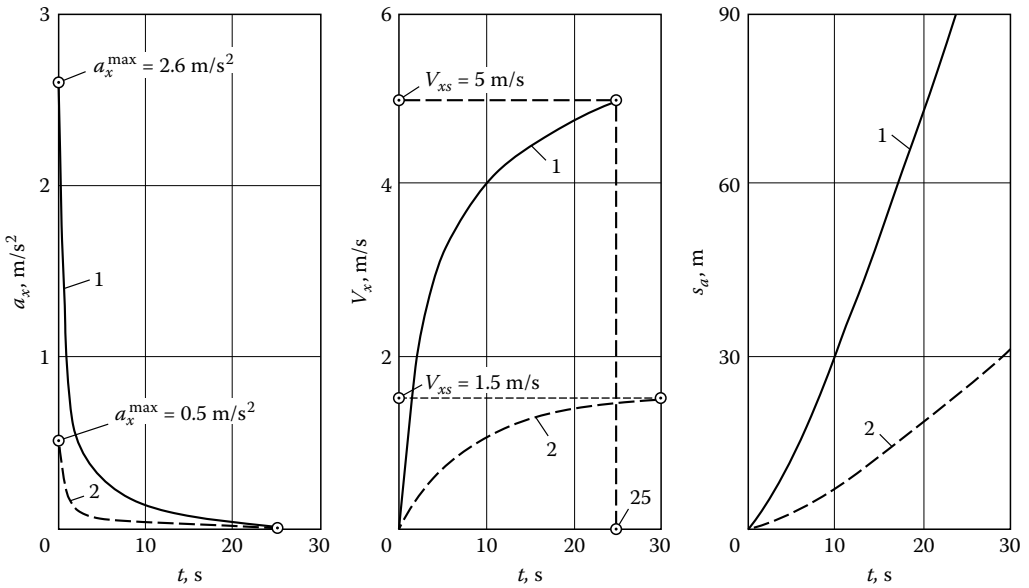


FIGURE 6.35
Specified kinematic parameters (program of motion): 1, $a_x^{max} = 2.6$ m/s^2; $V_{xc} = 5$ m/s; 2, $a_x^{max} = 0.5$ m/s^2; $V_{xc} = 1.53$ m/s.

and $\xi_i'^{(\prime\prime)}$ is the translational displacement of the unsprung mass normal to the surface of motion, $m_i'^{(\prime\prime)}, i = 1,4$.

The values of $\xi_i'^{(\prime\prime)}$ and $q_i'^{(\prime\prime)}$ and their derivatives needed for performing the calculations from formula (6.78) were found by compiling equations of oscillations of the sprung and unsprung masses of the vehicle using second-order Lagrange equations. The generalized coordinates for describing the oscillations of the sprung mass were the following: translation z of the center of the sprung mass normal to the support surface and α_x and α_y, the angles of rotation about the vehicle's longitudinal and transverse axes. The generalized coordinates for the unsprung masses $m_i'^{(\prime\prime)}$ consisted of their motions normal to the surface $\xi_i'^{(\prime\prime)}$. To simplify the calculations of potential energy, the deformations of the elastic elements of the suspension and the tires were reckoned from the static equilibrium position. Considering the above, the equations of oscillations are written as

$$\left(\frac{W_a}{g} - \sum_{i=1}^{4} m_i'^{(\prime\prime)}\right)\ddot{z} + \sum_{i=1}^{4} C'_{pi}\left(z + \alpha_y(l_a - l_i) - \xi'_i - 0.5t_B\alpha_x\right)$$
$$+ \sum_{i=1}^{4} C''_{pi}\left(z + \alpha_y(l_a - l_i) - \xi''_i + 0.5t_B\alpha_x\right)$$
$$+ \sum_{i=1}^{4} K'_{pi}\left(\dot{z} + \dot{\alpha}_y(l_a - l_i) - \dot{\xi}'_i - 0.5t_B\dot{\alpha}_x\right)$$
$$+ \sum_{i=1}^{4} K''_{pi}\left(\dot{z} + \dot{\alpha}_y(l_a - l_i) - \dot{\xi}''_i + 0.5t_B\dot{\alpha}_x\right) = 0; \qquad (6.79)$$

$$I_y\ddot{\alpha}_y + \sum_{i=1}^{4} C'_{pi}\left(z + \alpha_y(l_a - l_i) - \xi'_i - 0.5t_B\alpha_x\right)(l_a - l_i)$$
$$+ \sum_{i=1}^{4} C''_{pi}\left(z + \alpha_y(l_a - l_i) - \xi'_i + 0.5t_B\alpha_x\right)(l_a - l_i)$$
$$+ \sum_{i=1}^{4} K'_{pi}\left(\dot{z} + \dot{\alpha}_y(l_a - l_i) - \dot{\xi}'_i - 0.5t_B\dot{\alpha}_x\right)(l_a - l_i)$$
$$+ \sum_{i=1}^{4} K''_{pi}\left(\dot{z} + \dot{\alpha}_y(l_a - l_i) - \dot{\xi}''_i + 0.5t_B\dot{\alpha}_x\right)(l_a - l_i) = 0;$$

$$I_x\ddot{\alpha}_x - \sum_{i=1}^{4} C'_{pi}\left(z + \alpha_y(l_a - l_i) - \xi'_i - 0.5t_B\alpha_x\right)0.5t_B$$
$$+ \sum_{i=1}^{4} C''_{pi}\left(z + \alpha_y(l_a - l_i) - \xi'_i + 0.5t_B\alpha_x\right)0.5t_B$$
$$- \sum_{i=1}^{4} K'_{pi}\left(\dot{z} + \dot{\alpha}_y(l_a - l_i) - \dot{\xi}'_i - 0.5t_B\dot{\alpha}_x\right)0.5t_B$$
$$+ \sum_{i=1}^{4} K''_{pi}\left(\dot{z} + \dot{\alpha}_y(l_a - l_i) - \dot{\xi}''_i + 0.5t_B\dot{\alpha}_x\right)0.5t_B = 0;$$

$$m'_i\ddot{\xi}'_i - C'_{pi}\left(z + \alpha_y(l_a - l_i) - \xi'_i - 0.5t_B\alpha_x\right)$$
$$+ C'_{ti}\left(\xi'_i - q'_i\right) - K'_{pi}\left(\dot{z} + \dot{\alpha}_y(l_a - l_i) - \dot{\xi}'_i - 0.5t_B\dot{\alpha}_x\right)$$
$$+ K'_{ti}\left(\dot{\xi}'_i - \dot{q}'_i\right) = 0;$$

$$m''_i\ddot{\xi}''_i - C''_{pi}\left(z + \alpha_y(l_a - l_i) - \xi''_i + 0.5t_B\alpha_x\right)$$
$$+ C''_{ti}\left(\xi''_i - q''_i\right) - K''_{pi}\left(\dot{z} + \dot{\alpha}_y(l_a - l_i) - \dot{\xi}''_i + 0.5t_B\dot{\alpha}_x\right)$$
$$+ K''_{ti}\left(\dot{\xi}''_i - \dot{q}''_i\right) = 0; \quad i = 1, 4$$

Where I_x and I_y are the moments of inertia of the sprung mass; $C'^{(\prime)}_{pi}$ is the stiffness of the suspension at a wheel and $K'^{(\prime)}_{pi}$ is the shock-absorber resistance factor reduced to a wheel.

The micro- and macro-topographic features needed for solving Equations 6.77 through 6.79 were modeled using correlation functions and statistical data on the sloping of the roads and off-road surfaces of motion. The set of ordinates Q_i of the macro-topographic irregularities corresponding to coordinates x_i in the direction of the vehicle's motion were determined with modeling step h; the features of the sloping of the surface of motion on the segments $[x_{i-1}, x_i)$ were calculated as:

$$\cos\,\theta_{ni} = \frac{h}{\sqrt{h^2 + (Q_i - Q_{i-1})^2}}; \quad \sin\,\theta_{ni} = \frac{Q_i - Q_{i-1}}{\sqrt{h^2 + (Q_i - Q_{i-1})^2}} \tag{6.80}$$

The heights of the micro-profiles (assumed independently for the left and right sides of the vehicle) were transformed into a continuous function on the basis of points (x_i, q_i) by means of a spline interpolation using a third-order polynomial of $F(x)$ such that:

$$F(x_i) = q_i, \quad x \in [x_{i-1}, x_i] \tag{6.81}$$
$$F(x) = a_i x^3 + b_i x^2 + c_i x + d_i$$
$$\ddot{F}(x_0) = \ddot{F}(x_N) = 0$$

where x_0 and x_N are the abscissae of the first and last points. The use of spline interpolation allowed to model both the height $q_i^{\prime(\prime\prime)}$ for wheels of different clusters of axles and to determine analytically the derivatives $\dot{q}_i^{\prime(\prime\prime)}$ needed for solving Equations 6.79.

Analytical investigations must be based on properly selected and validated probability of motion over different roads and terrain. Thus for any conditions of motion, the state of the surface of motion, including the specific seasons need to be incorporated. For example, a concrete highway may be dry, snow-covered, worn out, etc. The studies described in Section 6.6 were performed on the assumption of equally probable states of the pavement for each form of road. As a result, the most typical road conditions were compiled on the basis of comparative analysis and these conditions served to formulate the different cases under study (Tables 6.4 and 6.5).

The micro-profile modeling step was selected with due consideration of a typical micro-profile used in road surveying. The modeling step and the sample standard deviations of the macro-profile were selected with the consideration of the greatest principal longitudinal slopes of the roads.

The gripping conditions of the wheels were also modeled as random quantities. It was assumed that the distribution of the rolling resistance factors $f_0^{\prime(\prime\prime)}$ at the creeper speed is normal and that the gripping factors $\mu_{pxi}^{\prime(\prime\prime)}$ obey the truncated normal distribution. The same distribution was assumed for modeling the characteristic factor k from the exponential relationship

TABLE 6.4

Characteristics of Roads and Terrain: Micro-Profiles

		Micro-Profile	
Road/Terrain	**Condition/State**	**Sample Standard Deviation, m**	**Increment Size, m**
Cement concrete road, $P_f = 0.2$	Dry	0.0082	0.5…1.5
	Worn-out	0.0249	
	Winter time	0.0150	
Belgian paved road, $P_f = 0.1$	Even	0.0200	0.5…1
	Large cobble stone	0.0355	
	Worn-out	0.0380	
Gravel and broken–stone road, $P_f = 0.2$	Public dry	0.0337	0.5…1
	Wood dry	0.0432	
Dirt road, $P_f = 0.4$	Dry, improved	0.0407	0.5…1
	Dry, worn-out	0.0528	
	Poor wet	0.0400	
Terrain, $P_f = 0.1$	Turf-covered	0.0477	0.5…1
	Snow-covered	0.0136	

TABLE 6.5

Characteristics of Roads and Terrain: Macro-Profiles

		Macro-Profile				
Road/Terrain	**Country**	**Sample Standard Deviation, m**	**Increment Size, m**	**Maximal Slope, %/deg**	**Sample Standard Deviation of Slope, deg**	**Road Class**
Cement concrete road	Flat	0.995	160	3%/1.72°	0.57°	I
	Broken	0.999	75	4%/2.29°	0.76°	II
	Mountain	0.916	55	5%/2.86°	0.95°	III
Belgian paved road	Flat	0.916	55	5%/2.86°	0.95°	III
	Broken	0.799	40	6%/3.43°	1.15°	IV
	Mountain	0.698	30	7%/4°	1.33°	V
Gravel and broken-stone road	Flat	1.104	55	6%/3.43°	1.15°	IV
	Broken	0.803	40	6%/3.43°	1.15°	IV
	Mountain	0.693	30	7%/4°	1.33°	V
Dirt road	Flat	0.929	40	7%/4°	1.33°	V
	Broken	0.698	30	7%/4°	1.33°	V
	Mountain	0.464	20	7%/4°	1.33°	V
Terrain	Flat	0.698	30	7%/4°	1.33°	—
	Rugged	0.597	20	9%/5.14°	1.71°	—

(1.26), for which pertinent experimental data were used. The values of $\mu_{pxi}^{\prime(\prime\prime)}$ were corrected with allowance of the number of passes of wheels over one track. Consideration was also given to the effect of the number of passes of wheels over the track and of the vehicle velocity in the rolling resistance, as defined by Farobin and Shuplyakov (1983), and Shalyagin (1986):

$$f_i^{\prime(\prime\prime)} = f_{0i}^{\prime(\prime\prime)} + k_c V_x, \tag{6.82}$$

$$f_{0i}^{\prime(\prime\prime)} = f_{01}^{\prime(\prime\prime)}(1 - 0.85 \log_{10} i), \quad i = 1, 4$$

here, $f_0^{\prime(\prime\prime)}$ is the rolling resistance coefficient at the creeper speed; k_c is the velocity factor.

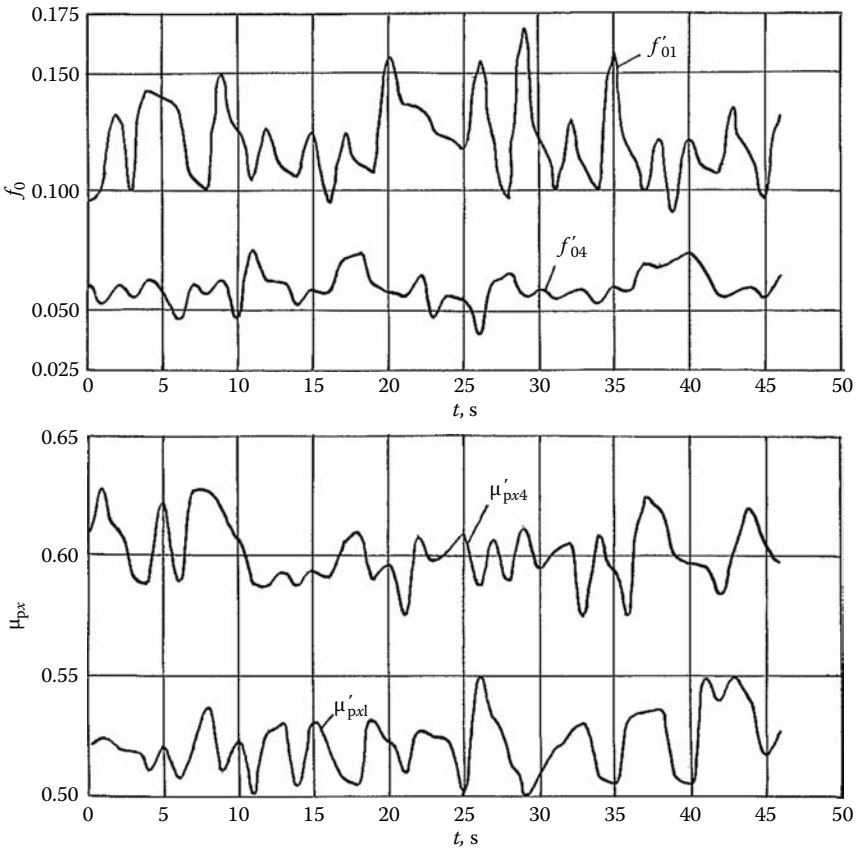


FIGURE 6.36
Probabilistic rolling resistance factor and friction coefficient on meadow.

The vehicle model simulated 33 random quantities. Figure 6.36 shows examples of random implementation of the rolling resistance factors and gripping factors of the front and rear wheels of one side of an 8×8 vehicle obtained by the modeling method described above.

Equations 6.77 through 6.82 above make it possible to calculate the total circumferential forces $F_{x\Sigma} = \sum_{i=1}^{4} F_{xi}^{\prime(\prime\prime)*}$ needed for motion and then to determine the optimal distributions of circumferential forces $F_{xi}^{\prime(\prime\prime)*}$ of the wheels that correspond to the optimum distribution of power among the wheels. Equation 6.45 are now used for finding optimal slippages $s_{\delta i}^{\prime(\prime\prime)*}$ for the 8×8 vehicle:

$$\frac{1}{1 - s_{\delta i}^{\prime(\prime\prime)*}} + \frac{e^{k_i^{\prime(\prime\prime)} s_{\delta i}^{\prime(\prime\prime)*}} - 1}{k_i^{\prime(\prime\prime)} \left(1 - s_{\delta i}^{\prime(\prime\prime)*}\right)^2} = -\lambda, \quad i = 1, 4 \tag{6.83}$$

$$\sum_{i=1}^{4} R_{zi}^{\prime(\prime\prime)} \mu_{pxi}^{\prime(\prime\prime)} \left(1 - e^{-k_i^{\prime(\prime\prime)} s_{\delta i}^{\prime(\prime\prime)*}}\right) = \sum_{i=1}^{4} F_{xi}^{\prime(\prime\prime)*}$$

The optimal values of the circumferential forces $F_{xi}^{\prime(\prime\prime)*}$ can be determined from formula (1.26) and then utilized for determining the factors of the optimal distribution of wheel torques. Using formulae (6.23) and (6.24) these distributions are expressed as:

$$K_{mki} = \frac{F_{xi}^{\prime\prime *} r_{\mathrm{w}i}^{0\prime\prime}}{F_{xi}^{\prime *} r_{\mathrm{w}i}^{0\prime}}, \quad F_{xi}^{\prime\prime *} r_{\mathrm{w}i}^{0\prime\prime} > F_{xi}^{\prime *} r_{\mathrm{w}i}^{0\prime}, \quad i = 1,4$$

$$K_{mo}^{1\text{-}2} = \frac{F_{xi}^{\prime\prime *} r_{\mathrm{w}i}^{0\prime\prime} + F_{xi}^{\prime *} r_{\mathrm{w}i}^{0\prime}}{F_{xj}^{\prime\prime *} r_{\mathrm{w}j}^{0\prime\prime} + F_{xj}^{\prime *} r_{\mathrm{w}j}^{0\prime}}, \quad F_{xi}^{\prime\prime *} r_{\mathrm{w}i}^{0\prime\prime} + F_{xi}^{\prime *} r_{\mathrm{w}i}^{0\prime} > F_{xj}^{\prime\prime *} r_{\mathrm{w}j}^{0\prime\prime} + F_{xj}^{\prime *} r_{\mathrm{w}j}^{0\prime}$$

$$i = 1 \text{ or } 2$$
$$j = 2 \text{ or } 1 \tag{6.84}$$

$$K_{mo}^{3\text{-}4} = \frac{F_{xi}^{\prime\prime *} r_{\mathrm{w}i}^{0\prime\prime} + F_{xi}^{\prime *} r_{\mathrm{w}i}^{0\prime}}{F_{xj}^{\prime\prime *} r_{\mathrm{w}j}^{0\prime\prime} + F_{xj}^{\prime *} r_{\mathrm{w}j}^{0\prime}}, \quad F_{xi}^{\prime\prime *} r_{\mathrm{w}i}^{0\prime\prime} + F_{xi}^{\prime *} r_{\mathrm{w}i}^{0\prime} > F_{xj}^{\prime\prime *} r_{\mathrm{w}j}^{0\prime\prime} + F_{xj}^{\prime *} r_{\mathrm{w}j}^{0\prime}$$

$$i = 3 \text{ or } 4$$
$$j = 4 \text{ or } 3$$

$$K_{mo}^{1,2\text{-}3,4} = \frac{\sum_{i=l}^{ll} \left(F_{xi}^{\prime\prime *} r_{\mathrm{w}i}^{0\prime\prime} + F_{xi}^{\prime *} r_{\mathrm{w}i}^{0\prime}\right)}{\sum_{i=k}^{kk} \left(F_{xi}^{\prime\prime *} r_{\mathrm{w}i}^{0\prime\prime} + F_{xi}^{\prime *} r_{\mathrm{w}i}^{0\prime}\right)},$$

$$\sum_{i=l}^{ll} \left(F_{xi}^{\prime\prime *} r_{\mathrm{w}i}^{0\prime\prime} + F_{xi}^{\prime *} r_{\mathrm{w}i}^{0\prime}\right) > \sum_{i=k}^{kk} \left(F_{xi}^{\prime\prime *} r_{\mathrm{w}i}^{0\prime\prime} + F_{xi}^{\prime *} r_{\mathrm{w}i}^{0\prime}\right)$$

$$l = 1 \text{ or } 3; \quad ll = 2 \text{ or } 4; \quad k = 3 \text{ or } 1; \quad kk = 4 \text{ or } 2$$

Figure 6.37 shows the interwheel and interaxle power dividing units of the 8×8 vehicle, the factors for their mechanisms were calculated using (6.84).

It should be noted that the results obtained in the course of modeling vary continuously in time. In fact, because of the motion with acceleration, the presence of macro- and micro-profiles of the road or terrain and random gripping conditions, the normal reactions, rolling resistance and the desired optimal circumferential forces of the wheels are random functions since their specific form at each point in time is not *a priori* known. Here these random functions tend to develop in time, that is, they are transient. For this reason, the results obtained in this manner are not final for selecting the optimal properties of interwheel and interaxle drives, since it still remains unclear which values of factors from formulae (6.84)

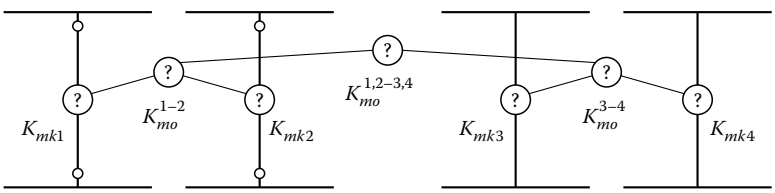


FIGURE 6.37
8×8 vehicle: Power-dividing units under optimization.

should be preferred in designing. This necessitated the development of statistical assessment methods of the results of modeling and the selection of the most acceptable solution that is to be regarded as optimal. To ensure reliability of results in determining the properties of these random functions, the motion of the vehicle was modeled 20 times for each surface (20 trips for each surface) and the probability of the confidence intervals of the statistical properties was 0.9. The results of these studies are presented in Section 6.6.2.

6.6.2 Optimal Properties

One of the first questions of interest to the investigator is the extent to which the real distribution of power among the wheels provided by the existing driveline systems corresponds to their optimal values and whether it is necessary to improve it. This question is resolved by mathematical modeling of the motion of a vehicle with the same mass and geometric parameters and the same velocity modes and under the same road/terrain conditions, but with a standard-production driveline system used on the vehicle and shown in Figure 6.34 simultaneously with seeking the optimal forces $F_{xi}^{\prime(\prime\prime)*}$ of the vehicle's wheels. The distribution of the total circumferential force among the wheels of such a vehicle was determined using methods presented in Chapters 2 through 5 and Section 6.1. The efficiency of the running gear was calculated from formulae in Section 1.4.2.

Figure 6.38 presents the predicted curves of the maximum efficiency η_{x*}^{tr} of the running gear (curves 1) that correspond to the optimum distribution of the circumferential

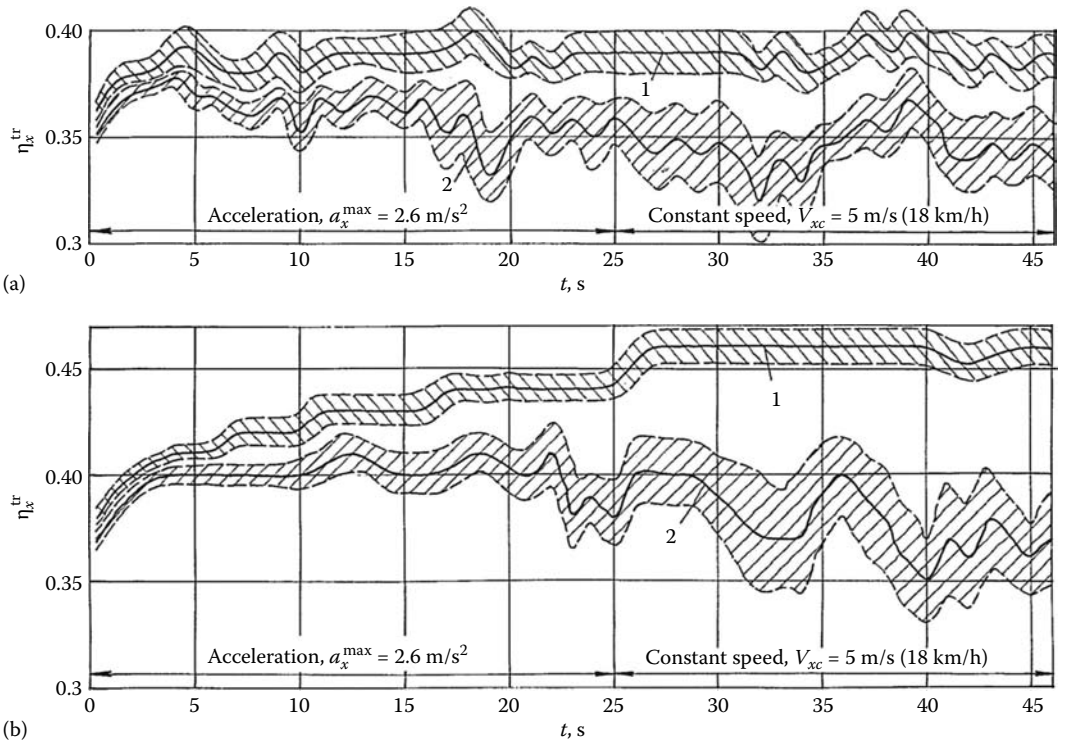


FIGURE 6.38
8 × 8 vehicle: the running gear efficiency. 1, under optimum wheel power distribution; 2, with the standard-production driveline system. (a) meadow; (b) concrete highway on level terrain.

forces $F_{xi}^{\prime(\prime\prime)*}$ and of the efficiency η_{xc}^{tr} of the running gear of a vehicle with the existing driveline system (curves 2) that correspond to motion over a meadow (a) and over a concrete highway (b) on level terrain.

In this and subsequent figures the dashed curve shows the boundaries of confidence intervals. It is seen by comparing the curves that the ratio $\eta_{x*}^{tr}/\eta_{xc}^{tr}$ is 1.03–1.15 when moving over meadowland and 1.09–1.31 for the case of a concrete highway. These results show that there is space and a possibility for improvement. For this purpose an analysis is presented here of the relationships governing the distribution of power among the axles and the left and right wheels of each axle.

Figures 6.39 through 6.41 show the computational curves of the statistical assessments of factor K_{mk1} of the distribution of the optimal torques $T_{w1}^{\prime\prime*}$ and $T_{w1}^{\prime*}$ among the wheels of the

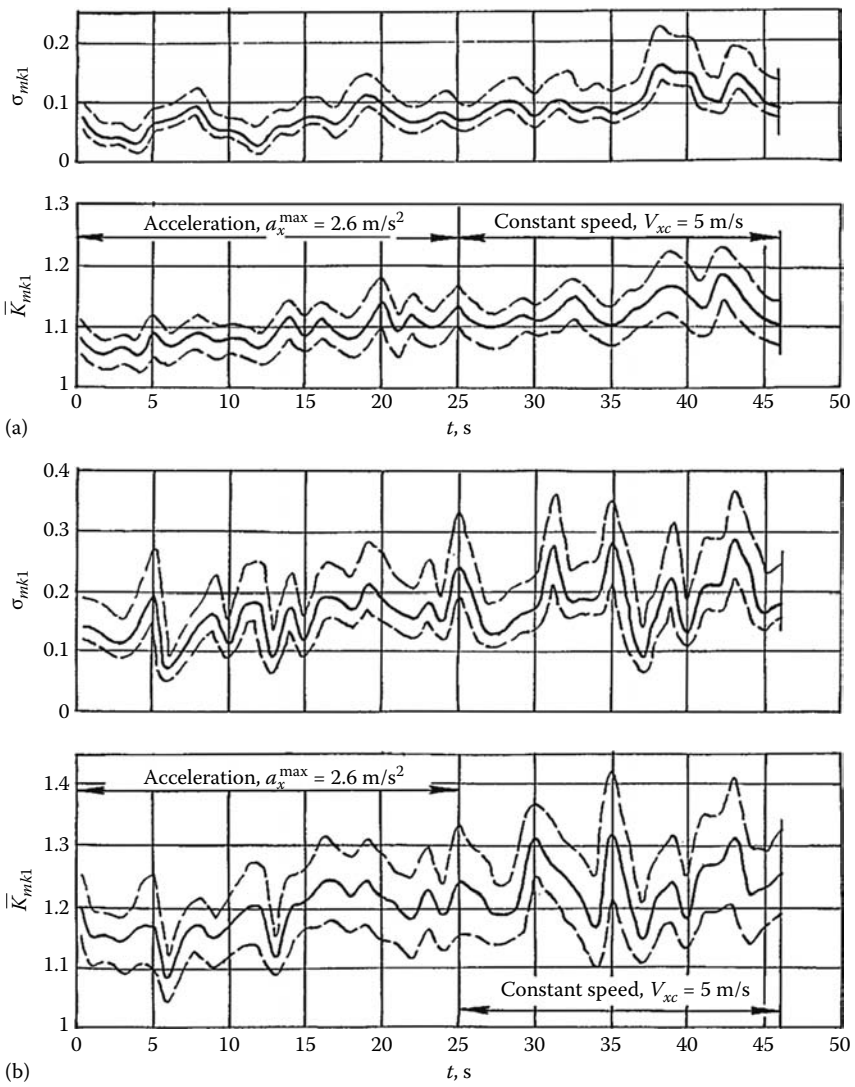


FIGURE 6.39
Statistical assessments of factor K_{mk1}: (a) concrete highway on level terrain; (b) Belgian paved road.

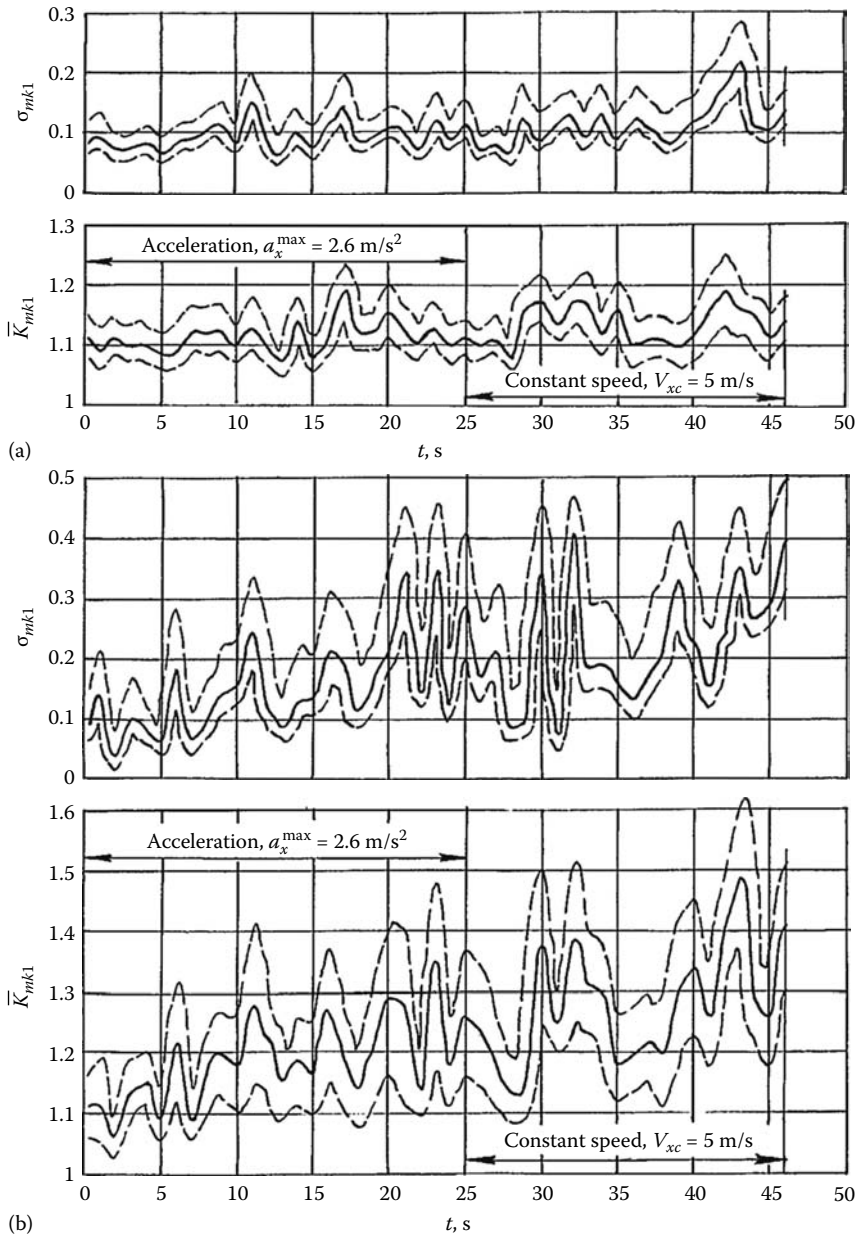


FIGURE 6.40
Statistical assessments of factor K_{mk1}: (a) flat dry dirt road in satisfactory condition; (b) flat poor dry dirt road.

forward axle which correspond to the optimal wheel power distribution (i.e., maximum of η_x^{tr}) under the required program of motion given by the expression (6.20). The figures present results for six different road conditions: these are the mean values $\bar{K}_{mk1}$ and the rms deviations σ_{mk1}.

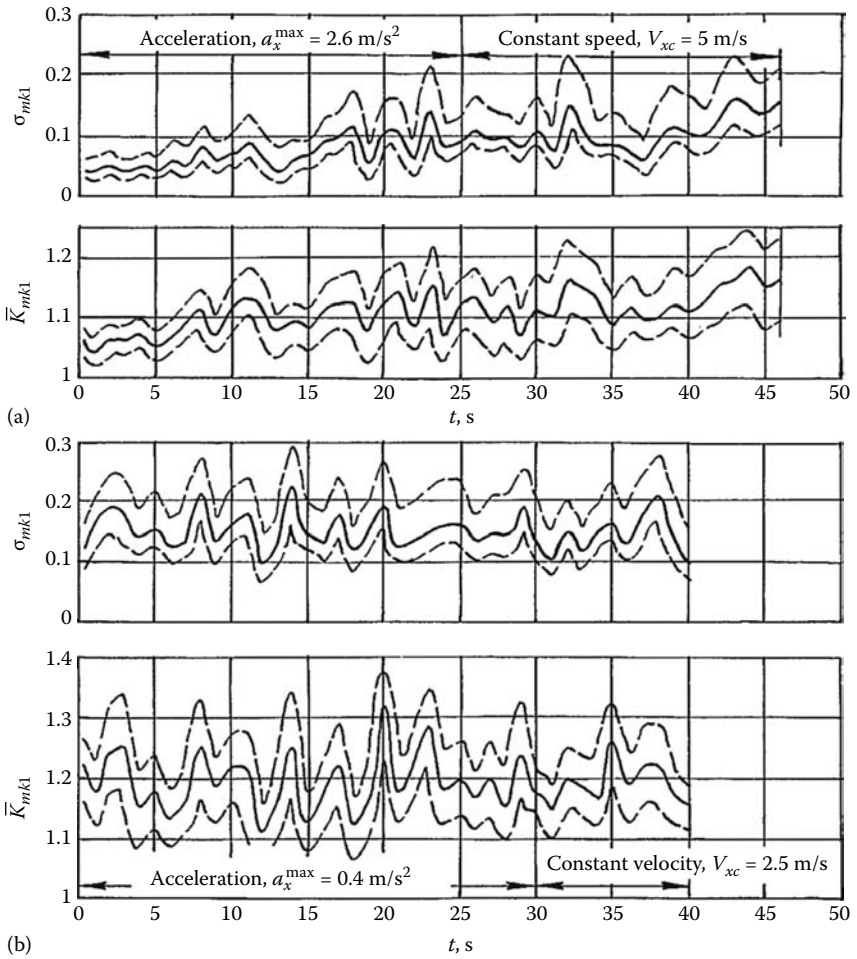


FIGURE 6.41
Statistical assessments of factor K_{mk1}: (a) meadow on level terrain; (b) snow-covered terrain.

Comparative analysis of these and other results showed that the numerical values of K_{mk1} are highly affected by changes in gripping conditions ($\mu_{pxi}^{\prime(\prime\prime)}$ and $f_{0i}^{\prime(\prime\prime)}$) and by the presence of a micro-profile that exerts, depending on the vehicle velocity, a greater or lesser effect on the normal reaction of the wheels and, accordingly on $T_{wi}^{\prime(\prime\prime)*}$. Here on nondeforming surfaces with relative slight variations in μ_{px} and f_0 it is the second factor (the micro-profile) that predominates. This is indicated by the variation factors V_{B1} that describe the scatter of the random values of K_{mk1} relative to their mean values $\bar{K}_{mk1}$ and amounting on the average to 14.4% on a concrete-paved highway and 21.2% on cobblestones. The values of K_{mk1} on deforming surfaces are determined by combinations of the above two factors. Thus, when moving from a dirt road in satisfactory condition to a bumpy dirt road, the average values of V_{B1} increase from 17.7% to 27.5%. At the same time, when moving over meadowland or over snow-covered soil, on which the rms deviations of the micro-profile are lesser than on a dirt road, the variation factors of V_{B1} of K_{mk1} are,

respectively, 13.6% and 16.8%. Similar processes are typical also for factors K_{mk2}, K_{mk3} and K_{mk4} of the distribution of the optimal torques between the left and the right wheels of the remaining axles. Thus, when the vehicle moves over snow-covered ground with irregular topography the mean value of factor V_{B4} of variation factor K_{mk4} is 13%, being 16% on meadowland and as high as 37% on a bumpy dirt road.

The effect of local topography on the values of K_{mki} manifests itself in the vehicle's velocity. Thus, the lower velocities under mountainous conditions as compared with level terrain are the cause of lesser fluctuations of normal reactions, meaning also in $T_{wi}^{\prime(\prime\prime)*}$ and in K_{mki}. For example, the average value of factor V_{B1} of variation in factor K_{mk1} on a dry bumpy/poor dirt road is 27.5%, in a level location at $V_{xc} = 20$ km/h and 8.2% under mountainous conditions at $V_{xc} = 5.5$ km/h.

It was found that substantial quantitative differences between factors K_{mki} of the first and subsequent axles are typical of certain underlying surfaces. This is typical of deforming driving surfaces such as meadowland and dirt roads (see Figures 6.40, 6.41a and 6.42, and 6.43) on which the stiffness behavior of the tire-soil were observed to vary when the wheels rolled on one track.

It is known that the normal stiffness of the tires decreases somewhat and the normal stiffness of the soil increases markedly for each sequential pass of the wheel. Investigations show that this increases the deviation of the normal reactions of the wheels of the last axle from their mean values. When moving over meadowland on a flat terrain, the ratio of the greater normal reaction to the smaller normal reaction of the wheels of the first axle amount on the average to 1.1, whereas for the wheels of the fourth axle it is 1.18. This increases the fluctuations of forces $F_{x4}^{\prime(\prime\prime)*}$ and, as a result, also the value of K_{mk4}. Even greater differences are observed between K_{mki} when moving over a bumpy dirt road on which this phenomenon is supplemented by the strong effect of the micro-profile. At the

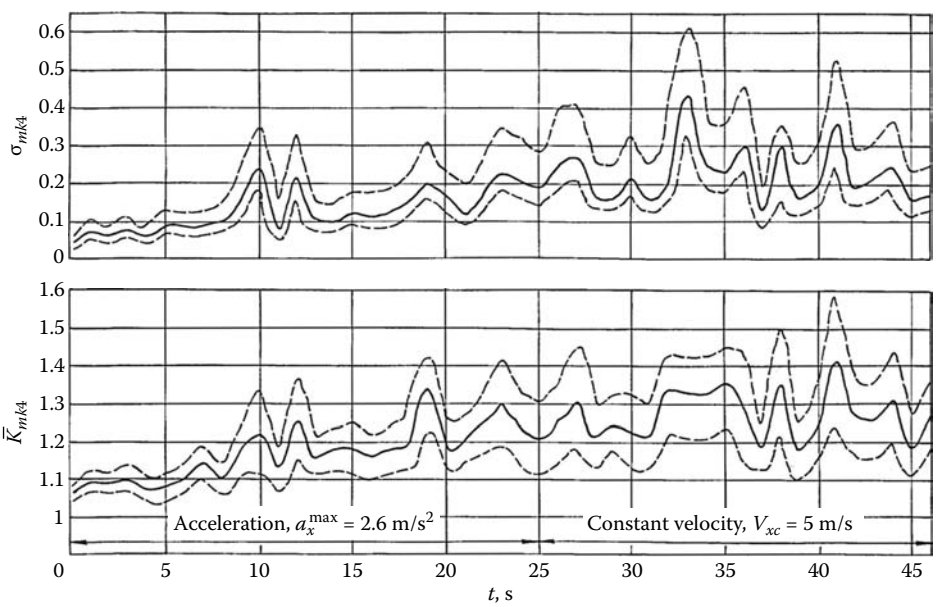


FIGURE 6.42
Statistical assessments of factor K_{mk4} on a meadow on level terrain.

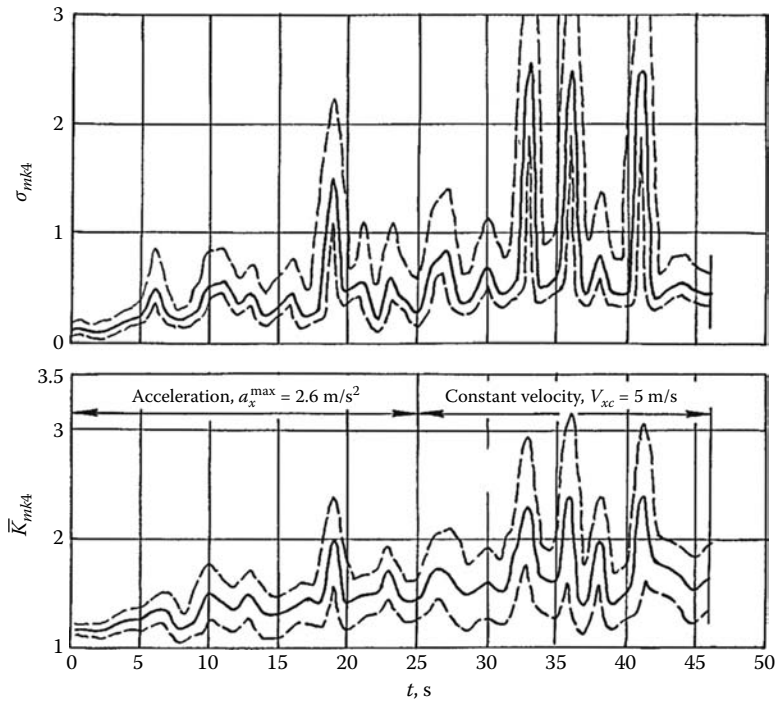


FIGURE 6.43
Statistical assessments of factor K_{mk4} on a poor dirt road on level terrain.

same time, on snow-covered ground, where the compaction of snow does not markedly affect the stiffness of the solid base, the values of K_{mk1} and K_{mk4} are approximately the same (Figures 6.41b and 6.44).

In addition to the calculations the results of which are plotted in Figures 6.39 through 6.44 computational studies of the motion of a vehicle were carried out for eleven road conditions. This has yielded sets (families) of results on $\bar{K}^{tl}_{mki}$ and σ^{tl}_{mki}, where $i = 1, 4$ is the number of the axle, $l = 1, 17$ is the number of the surface of motion used in computations and $t = 1, t_{\max}$ is the time instant. These results serve as the input data for selecting the final solution. There exist various criteria for taking a decision. Preliminary analysis of available criteria shows that those most suitable for our problem of synthesis of features of mechanisms of interwheel and interaxle power-dividing units are the limiting optimality criterion *LO* and the Bayes–Laplace criterion *BL*. In addition to the above, other criteria shall be examined that shall be termed as the modified optimality criterion *LOM* and the modified Bayes–Laplace criterion *BLM*. The need of using this approach shall be demonstrated below. Now an algorithm of utilizing each of these criteria for the synthesis problem under study shall be compiled.

First the set of mean values $\bar{K}^{tl}_{mki}$ and of the rms deviations σ^{tl}_{mki} are replaced by pairs of optimal values $\bar{K}^{rl}_{mki}$ and σ^{rl}_{mki} using the *BL* and *BLM* criteria and by pairs of optimal $\bar{K}^{pl}_{mki}$ and σ^{pl}_{mki} using the *LO* and *LOM* criteria. The parameters $\bar{K}^{pl}_{mki}$ and σ^{pl}_{mki} shall be taken to be equal to the highest of the values of $\bar{K}^{tl}_{mki}$ and σ^{tl}_{mki}:

$$\bar{K}^{pl}_{mki} = \max_t \bar{K}^{tl}_{mki}, \quad \sigma^{pl}_{mki} = \max_t \sigma^{tl}_{mki} \tag{6.85}$$

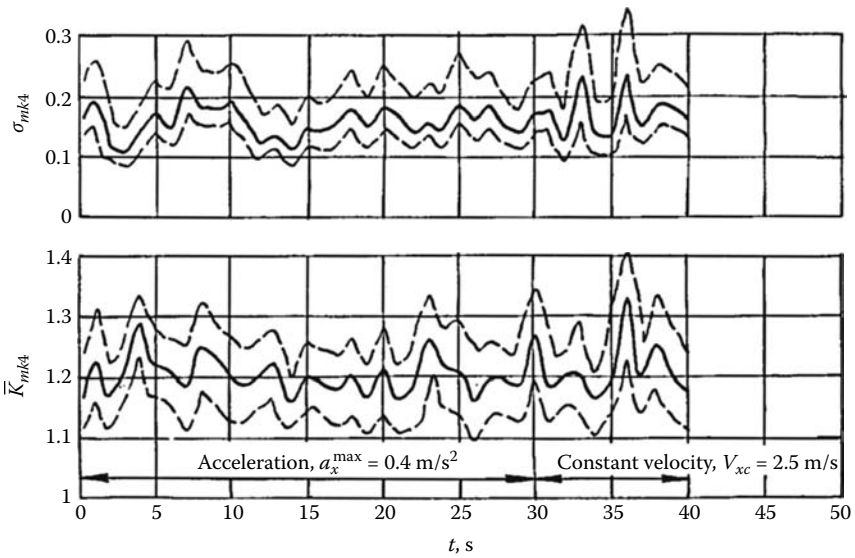


FIGURE 6.44
Statistical assessments of factor K_{mk4} on a snow-covered terrain.

and the parameters $\bar{K}^{rl}_{mki}$ and σ^{rl}_{mki} shall be defined by the expressions

$$\bar{K}^{rl}_{mki} = \sum_{t=1}^{t_{\max}} \bar{K}^{tl}_{mki} p_t, \quad \sigma^{rl}_{mki} = \sum_{t=1}^{t_{\max}} \sigma^{tl}_{mki} p_t \tag{6.86}$$

where p_t is the probability of appearance of tth parameters $\bar{K}^{tl}_{mki}$ and σ^{tl}_{mki}. Formulae (6.85) and (6.86) were applied for working up the results of studies of the distributions coefficients of optimal torques between the wheels of each of the four axles. The numerical results are listed in Table 6.6.

This means that for all the 17 road conditions by each criterion for each factor K_{mki} $(i = 1, 4)$ were obtained pairs of optimal parameters $\bar{K}^{pl}_{mki}$ and σ^{pl}_{mki} ($\bar{K}^{rl}_{mki}$ and σ^{rl}_{mki}) on the basis of which the locking coefficients of the interwheel differentials of the 8×8 vehicle shall be determined.

It is known that the value of a random quantity only rarely goes past the limits of the interval $(m_x \pm 3\sigma)$ and in the majority of cases it is contained within this interval. In addition, the hypothesis of normal distribution of random values of K_{mki} taken at the same points in time from 20 trips of the vehicle was confirmed at the 0.1–0.05 significance level. Assuming this three-sigma range of scattering of random values of K_{mki}, the optimum locking coefficients for each lth road conditions are determined as follows:

$$K^{LO}_{\mathrm{d}li} = K^{LOM}_{\mathrm{d}li} = \bar{K}^{pl}_{mki} + 3\sigma^{pl}_{mki} \tag{6.87}$$

when using data based on the *LO* and *LOM* criteria and

$$K^{BL}_{\mathrm{d}li} = K^{BLM}_{\mathrm{d}li} = \bar{K}^{rl}_{mki} + 3\sigma^{rl}_{mki} \tag{6.88}$$

TABLE 6.6

Statistical Assessment of Optimum Torque Distribution Factors

		Optimal Parameters $\bar{K}_{mk}^{pl}$ and σ_{mk}^{pl} ($\bar{K}_{mk}^{rl}$ and σ_{mk}^{rl})																
		Cement-Concrete Road				Belgian Paved Road		Gravel and Broken-Stone Road		Dirt Road				Terrain				
Coefficients K_{mki} $i = 1, 4$	Criteria	Flat	Flat, Winter Time	Mountain	Flat, Worn-Out	Flat	Flat, Large Cobble Stone	Flat, Public	Mountain, Wood	Flat, Dry	Flat-Dry Worn-Out	Mountain, Dry	Mountain, Dry Worn-Out	Flat, Poor Wet Worn-Out	Flat, Meadow	Broken, Meadow	Flat, Snow	Broken, Snow
K_{mk1}	LO,	1.18V	1.24	1.12	1.36	1.32	1.95	1.84	1.89	1.19	1.49	1.11	1.10	1.12	1.18	1.16	1.30	1 31
	LOM	0.17Λ	0.21	0.10	0.40	0.28	0.98	0.89	0.92	0.21	0.41	0.09	0.09	0.09	0.16	0.16	0.22	0.22
	BL,	1.11V	1.14	1.07	1.23	1.21	1.42	1.39	1.48	1.11	1.23	1.07	1.07	1.09	1.11	1.11	1.17	1.19
	BLM	0.09Λ	0.11	0.05	0.20	0.17	0.43	0.41	0.53	0.11	0.18	0.05	0.06	0.07	0.10	0.10	0.14	0.14
K_{mk2}	LO,	1.16	1.20	1.10	1.37	1.30	1.72	1.70	1.84	1.24	1.51	1.14	1.14	1.14	1.31	1.26	1.31	1.31
	LOM	0.14	0.16	0.09	0.34	0.26	0.83	0.79	0.77	0.21	0.69	0.13	0.12	0.11	0.26	0.24	0.20	0.21
	BL,	1.10	1.14	1.06	1.23	1.22	1.46	1.42	1.41	1.15	1.32	1.08	1.10	1.10	1.15	1.15	1.20	1.21
	BLM	0.08	0.11	0.04	0.19	0.18	0.42	0.39	0.44	0.13	0.28	0.05	0.07	0.07	0.12	0.13	0.15	0.15
K_{mk3}	LO,	1.15	1.20	1.08	1.31	1.31	1.85	1.83	1.77	1.28	2.28	1.17	0.16	1.15	1.35	1.30	1.26	1.25
	LOM	0.15	0.16	0.07	0.38	0.28	0.84	0.80	0.64	0.25	2.07	0.16	0.12	0.15	0.31	0.30	0.23	0.23
	BL,	1.09	1.12	1.05	1.20	1.19	1.41	1.39	1.39	1.17	1.41	1.12	1.11	1.11	1.17	1.17	1.20	1.20
	BLM	0.08	0.10	0.04	0.17	0.15	0.41	0.37	0.35	0.14	0.44	0.10	0.08	0.07	0.16	0.15	0.16	0.16
K_{mk4}	LO,	1.16	1 16	1.11	1.31	1.31	0.79	1.75	1.80	1.31	2.40	1.18	1.21	1.17	1.41	1.34	1.29	1.33
	LOM	0.13	0.17	0.06	0.31	0.25	0.98	0.90	0.68	0.30	2.51	0.19	0.20	0.16	0.43	0.36	0.23	0.24
	BL,	1.09	1.13	1.05	1.20	1.19	1.42	1.40	1.42	1.20	1.60	1.13	1.12	1.11	1.21	1.22	1.20	1.21
	BLM	0.11	0.12	0.04	0.17	0.16	0.42	0.39	0.49	0.17	0.59	0.12	0.09	0.09	0.19	0.18	0.16	0.16

Notes: V—sample mean K_{mk}^{pl} (K_{mk}^{rl}), Λ—sample standard deviation σ_{mk}^{pl}(σ_{mk}^{rl}).

when using data based on the *BL* and *BLM* criteria. Figures 6.45 and 6.46 show the results of calculations using formulae (6.87) and (6.88) and the data of Table 6.6.

Different degrees of locking properties of interwheel differentials of all the four axles are needed under different road conditions and for different states of the pavement of the same type of roads. The mode of variation in the locking coefficients on different motion surfaces is attributable to the same factors as those governing the variation in the distribution of the factors of optimum torque distribution that were analyzed previously (Figures 6.39 through 6.44). Note that the optimum values of $K_{\text{d}li}^{LO}$ and $K_{\text{d}li}^{LOM}$ exceed the values of locking factors $K_{\text{d}li}^{BL}$ and $K_{\text{d}li}^{BLM}$. This is caused by the different approaches to the definition of the components of formulae (6.87) and (6.88) calculated from expressions (6.85) and (6.86) and the data from Table 6.6.

The results presented above are needed for the final selection of the optimum locking coefficients when it is required to find the most suitable result from the set of results in Figures 6.45 and 6.46. For this it is necessary to obtain from the 17 pairs of values of $\bar{K}_{mki}^{pl}$ and σ_{mki}^{pl} ($\bar{K}_{mki}^{rl}$ and σ_{mki}^{rl}) in Table 6.6 one pair that should serve as the target in calculating the locking coefficients and in working out the design of the mechanisms. The following versions are made possible by the assumed criteria. Based on the Limiting Optimality criterion *LO* and the Bayes–Laplace criterion *BL* the highest value from those calculated from formulae (6.85) and (6.86) are taken:

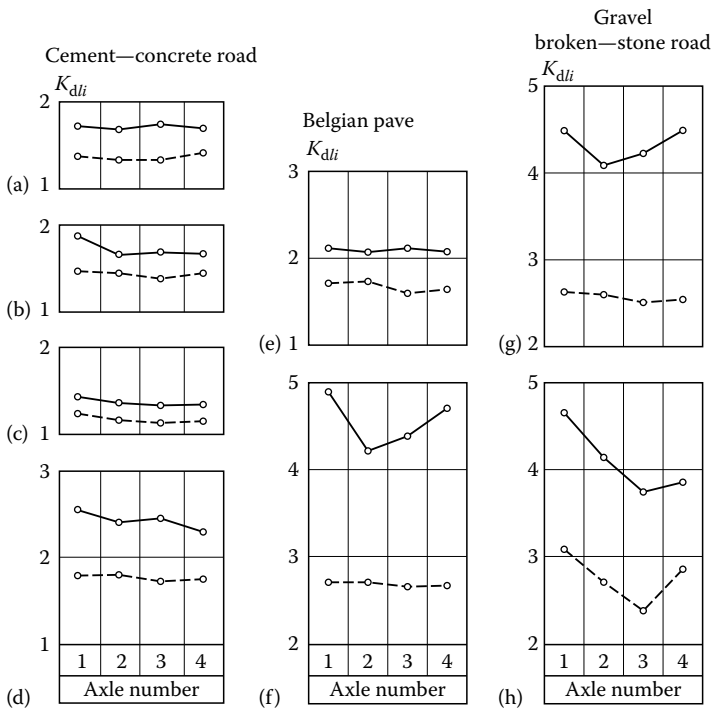


FIGURE 6.45
Optimal torque biases of the interwheel differentials: (a) level terrain; (b) snow-covered on level terrain; (c) in mountains; (d) level terrain, worn out; (e) level terrain; (f) large cobblestone on level terrain; (g) level terrain; (h) wood road in mountains. ———, LO and LOM criteria; — —, BL and BLM criteria.

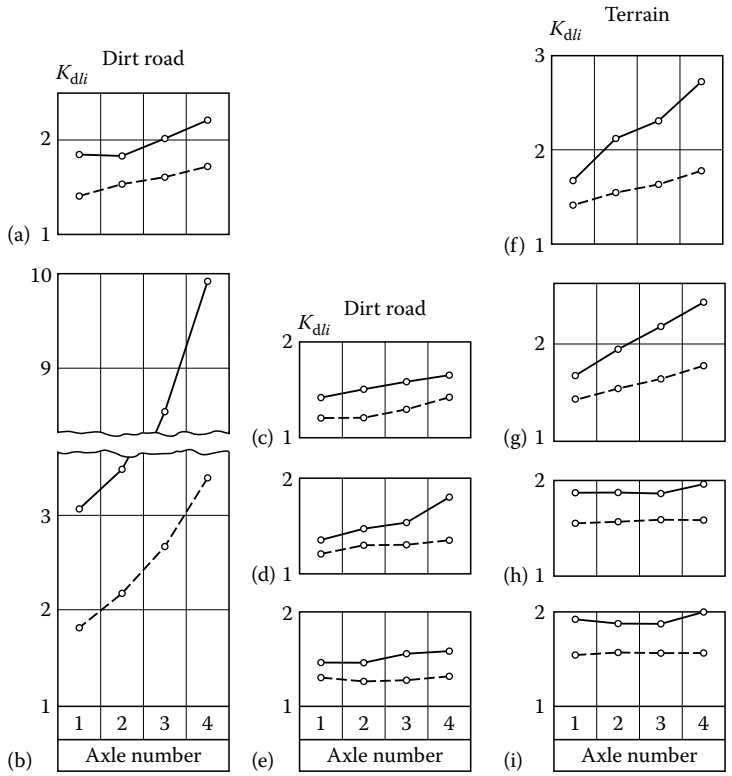


FIGURE 6.46
Optimal torque biases of the interwheel differentials: (a) dry on level terrain; (b) dry worn out on level terrain; (c) in mountains; (d) dry worn out in mountain; (e) poor wet worn out level terrain; (f) meadow on level terrain; (g) meadow in broken terrain; (h) snow field on level terrain; (i) snow field on broken terrain. ———, LO and LOM criteria; — —, BL and BLM criteria.

$$\bar{K}_{mki}^{LO*} = \max_{l} \bar{K}_{mki}^{pl} = \max_{l} \left(\max_{t} \bar{K}_{mki}^{tl} \right), \tag{6.89}$$

$$\sigma_{mki}^{LO*} = \max_{l} \sigma_{mki}^{pl} = \max_{l} \left(\max_{t} \sigma_{mki}^{tl} \right),$$

$$\bar{K}_{mki}^{BL*} = \max_{l} \bar{K}_{mki}^{rl} = \max_{l} \left(\sum_{t=1}^{t_{\max}} \bar{K}_{mki}^{tl} p_t \right), \tag{6.90}$$

$$\sigma_{mki}^{BL*} = \max_{l} \sigma_{mki}^{rl} = \max_{l} \left(\sum_{t=1}^{t_{\max}} \sigma_{mki}^{tl} p_t \right)$$

When using the modified criteria introduced above allowance is made for the probability p_f that the vehicle will travel on roads of different types:

$$\bar{K}_{mki}^{LOM*} = \sum_{f=1}^{d} \left(\max_{s_f} \bar{K}_{mki}^{pl} \right) p_f, \tag{6.91}$$

$$\sigma_{mki}^{LOM*} = \sum_{f=1}^{d} \left(\max_{s_f} \sigma_{mki}^{pl} \right) p_f,$$

$$\bar{K}_{mki}^{BLM*} = \sum_{f=1}^{d} \frac{\sum_{l=1}^{s_f} \bar{K}_{mki}^{rl}}{s_f} p_f, \tag{6.92}$$

$$\sigma_{mki}^{BLM*} = \sum_{f=1}^{d} \frac{\sum_{l=1}^{s_f} \sigma_{mki}^{rl}}{s_f} p_f,$$

where s_f is the number of states of each type of road (for example, $s_f = 4$ for a concrete road, see Table 6.6) and $d = 5$ is the number of types of roads assumed in the investigation.

The desired optimal locking coefficients of the interwheel differentials of the 8×8 vehicle is determined from the expressions

$$K_{\mathrm{d}i}^{LO} = \bar{K}_{mki}^{LO*} + 3\sigma_{mki}^{LO*},$$

$$K_{\mathrm{d}i}^{LOM} = \bar{K}_{mki}^{LOM*} + 3\sigma_{mki}^{LOM*}, \tag{6.93}$$

$$K_{\mathrm{d}i}^{BL} = \bar{K}_{mki}^{BL*} + 3\sigma_{mki}^{BL*},$$

$$K_{\mathrm{d}i}^{BLM} = \bar{K}_{mki}^{BLM*} + 3\sigma_{mki}^{BLM*}, \quad i = 1, 4$$

The results of calculations using formulae (6.93) are presented as broken lines in Figure 6.47.

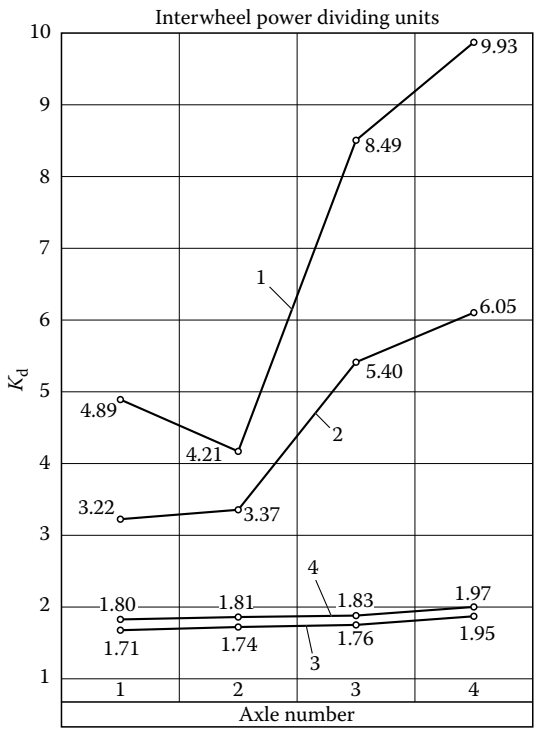


FIGURE 6.47
Optimal locking factors of the interwheel differentials. Criteria: 1, LO; 2, LOM; 3, BL; 4, BLM.

If now the designs are based on values of K_{di}^{LO} (broken line 1), this allows obtaining optimal torques of wheels in full accordance with all the combinations of the gripping conditions. However, this requires quite superior locking properties of the interwheel differentials of the first and second axles and virtually complete locking of the differentials of the third and fourth axles. However, superior locking properties of differentials are not needed under most road conditions as this is seen from Figures 6.45 and 6.46.

Conversely, the use of *BL* and *BLM* criteria will result in selecting values of K_{di}^{BL} (Figure 6.47, broken line 3) and K_{di}^{BLM} (broken line 4) at which, in the majority of cases, the optimal torques of the wheels are not achieved, which reduces the traction properties of the vehicle.

The most acceptable results are obtained when using the previously introduced Modified Limiting Optimality criterion *LOM*, which on the one hand, is oriented to the maximum values of $\bar{K}_{mki}^{pl}$ and σ_{mki}^{pl}, and on the other takes into account the probabilities of operating the vehicle under different road conditions. If the interwheel differentials are manufactured with locking coefficients K_{di}^{LOM}, (Figure 6.47, broken line 2), this will ensure full utilization of the optimum torques under 77% of road conditions. The latter follows from the comparison of Figure 6.47 with Figures 6.45 and 6.46. The higher values of K_{d3}^{LOM} and K_{d4}^{LOM} indicate that it is possible to use free-running differentials here, and that will increase the number of road conditions with full utilization of the optimum wheel torques, to 82%.

The knowledge of optimum properties of the interwheel differentials alone is insufficient for ensuring that the optimum distribution of the torques between the left and right wheels of each axle would be normal. It is additionally necessary to have the optimum properties of the interaxle power-dividing units, on which the axle torques depend. Consider the results of these studies (Figure 6.48).

It was established that under all the road/terrain conditions under study the torque of the second axle is greater than that of the first. This stems from the existing distribution of weight between the vehicle's axles and changes in the normal reactions and gripping properties of the wheels in the course of travel. This requires placing an asymmetrical differential between these axles, whereas the standard-production vehicle uses a symmetrical mechanism. In keeping with the above, the average value of factor K_{mo}^{1-2} from formulae (6.84) should

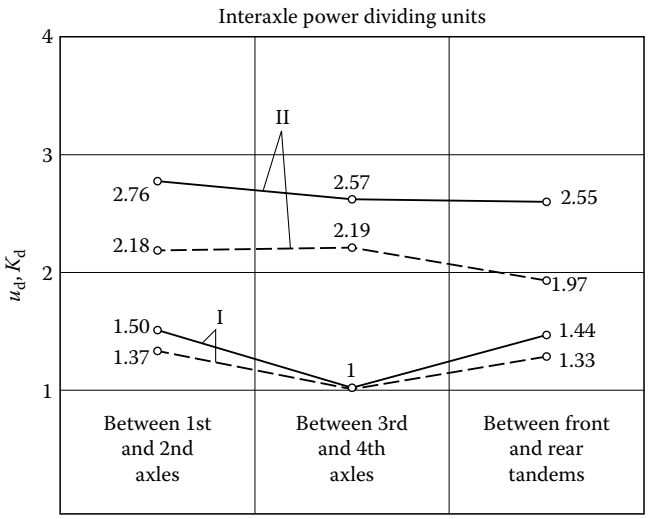


FIGURE 6.48
Optimal locking coefficients of the interaxle power-dividing units: I, u_d; II, K_d. Criteria: ———, LO; — —, LOM.

be regarded as the gear ratio u_{d1} of an open asymmetrical differential between these axles. Further closeness between the real values of T_{w1} and T_{w2} and the optimal values T^*_{w1} and T^*_{w2} and, accordingly improvement of the traction performance of the vehicle, can be attained by designing a self-locking asymmetrical differential whose locking performance should be calculated with allowance for the values of $\bar{K}^{1\text{-}2}_{mo}$ and $\sigma^{1\text{-}2}_{mo}$.

The interaxle differential of the rear tandem should be an open symmetrical differential with $u_{d2}=1$ or a limited slip differential based on the latter. This is indicated by the relationship between the values of optimal torques T^*_{w3} and T^*_{w4} (Figure 6.48).

It was shown that the symmetrical differential ordinarily used in the transfer case should be replaced by an asymmetrical differential, since the optimal torque of the rear tandem is higher, under all road/terrain conditions, than that of the front tandem. The corresponding points on broken lines in Figure 6.48 reflect the above and their numerical values must be used in designing the interaxle differential for the transfer case.

It was thus demonstrated that it is advisable to use limited slip differentials in all the axles of the vehicle under study (free-running differentials may be used in the third and fourth axles), asymmetrical differentials in the transfer case and in the interaxle drive of the front tandem and a symmetrical interaxle differential in the rear tandem (see Figure 6.49).

Here the interaxle differential of the front tandem can be of the limited slip-type, whereas the transfer case differential should have reserve-locking capacity. Such an arrangement of these mechanisms in the power-dividing units improves the mobility, traction and velocity properties and fuel economy of the vehicle, if the power-dividing units are designed with consideration of the above data on their optimum properties. It shall be demonstrated, as an illustration, how these data should be utilized in designing limited slip differentials for the first and second axles.

Each combination of probable conditions of motion from Tables 6.4 and 6.5 has corresponding to it certain ranges of variation in the wheel torques $T^{\prime(n)*}_{wi}$, $(i=1, 2)$ from Table 6.6 and, accordingly of torques T_{01} and T_{02} at the cases of differentials of the first and second axles. From this it follows that: the axle torque T_{0i} $(i=1, 2)$ can be used as the input

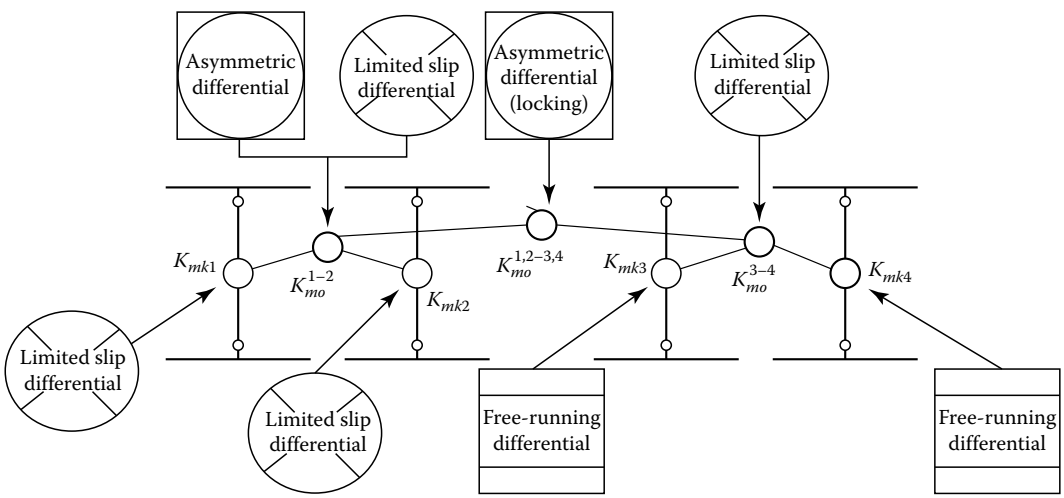


FIGURE 6.49
Optimal power-dividing units.

parameter for automatic control of its own distribution between the right and left wheels according to the relationships:

$$T_{0i} = \left(T''^{*}_{wi} + T'^{*}_{wi}\right)/u_k, \quad i = 1,2 \tag{6.94}$$

Analysis shows that when the 8×8 vehicle under study moves over general-purpose roads the actual torques at the cases of the differentials vary within the range of 240–2200 N-m. In rapid acceleration and travel over bumpy dirt roads, including the time of the year when the roads are impassable, and also under off-road conditions, snow-covered surface and marshland, the values of T_{0i}, $i = 1,2$ are always greater than 2200 N-m. In other words, the conditions of motion clearly delimit the values of T_{0i}: under poor traveling conditions the torque is higher than 2200 N-m. This increase in T_{0i} should be accompanied by an increase in the optimum locking coefficient of the limited slip differential K^{*}_{di}, $i = 1,2$. The optimum values of K^{*}_{di} were already determined based on data from Table 6.6. In keeping with the above, Figure 6.50a shows two segments of the curve of $K^{*}_{di} = f_i(T_{0i})$ that must be taken into account in designing differentials.

Further, this vehicle may travel under conditions when one of the axle's wheels would lose touch with the road, something that sharply reduces the torque T_0 at the case of the differential. In such cases, it is advisable to have high values of the locking coefficient (see Figure 6.50b). Overall, the form of the desired curve of the locking properties of the limited slip differential for the first and second axles compiled from Figure 6.50a and b is shown in Figure 6.50c. Use of this latter figure and data from Table 6.6 with formulae from Section 4.7 that relate the locking coefficient K_d to the geometric parameters of the differential mathematically, indeed served for designing an actual differential.

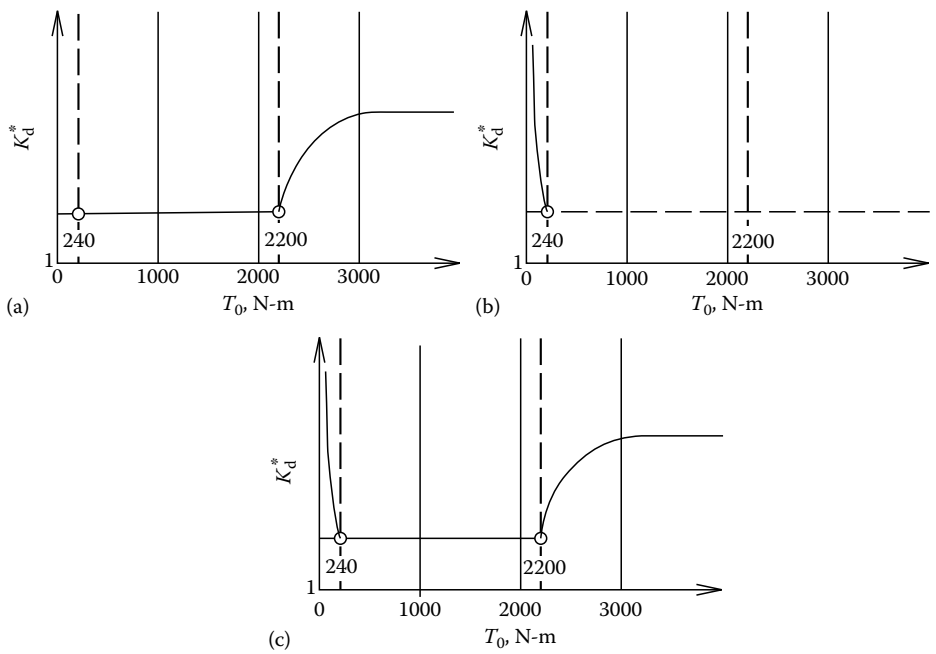


FIGURE 6.50
Optimum locking coefficient.

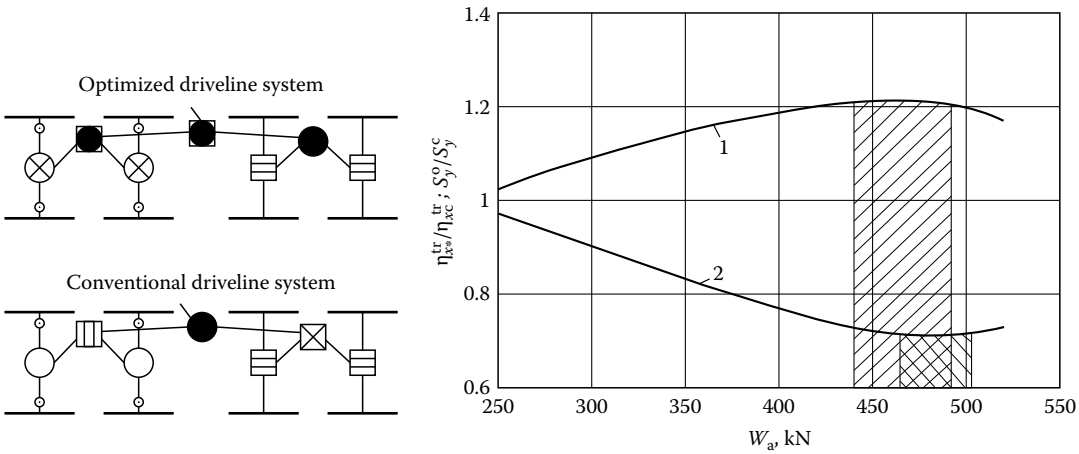


FIGURE 6.51
Technical and economic evaluation of the 8 × 8 vehicle.

Subsequent analytic studies of curvilinear motion of a vehicle with optimal power-dividing units from Figure 6.49 showed that this vehicle has satisfactory turnability and stability of motion. The indicators of these properties of the vehicle approximately correspond to the indicators of the vehicle with a driveline system from Figure 6.4a and are better than the indicators of vehicles that use driveline systems shown in Figure 6.4b through d.

It is advantageous to analyze the above results on optimization of the driveline system of the 8 × 8 vehicle, also from the point of the engineering-economy criteria. The principal criterion of engineering-economy efficiency of using a vehicle usually consists of the specific net cost

$$S_y = \frac{S_{\text{pr}} + S_{\text{ec}}}{T_{\text{h}}} \tag{6.95}$$

where S_{pr} is the net cost of manufacturing (producing) the vehicle, referred to an hour of its standard operation, S_{ec} is the net cost of an hour of transportation work of the vehicle and T_{h} is the theoretical output per hour. Formula (6.95) was used for investigating the 8 × 8 vehicle from the current production and with optimized driveline systems moving in first gear over a bumpy dirt road during the time of the year when roads are impassable. It was assumed that the torque converter is locked and that the engine operates at the full fuel feed. The net cost of production and the prices of the differentials were assumed based on the price list of the company that manufactures the given 8 × 8 vehicle. The results of computations using formula (6.95) are reflected by curve 1 in Figure 6.51 that shows the ratio of the specific net cost S^{o}_y of the vehicle with optimal driveline system to the specific cost S^c_y of the vehicle employing a standard production driveline system.

Curve 2 in Figure 6.51 shows the ratio $\eta^{\text{tr}}_{x*}/\eta^{\text{tr}}_{xc}$ of efficiencies of the running gear of a vehicle with optimal and a standard driveline system. As seen from this figure, the ranges of extreme values of these two indicators overlap. It can be concluded from this that the efficiency of the running gear can be used to a sufficiently accurate approximation for assessing the engineering-economy level of a vehicle.

7

Mechatronic Driveline Systems

7.1 Simple, Combined, and Integrated Driveline Systems—A Brief Overview

The definitions of simple, combined, and integrated driveline systems were given in Section 1.2 (see Figure 1.34). Power-dividing units (PDUs) and driveline systems as a whole that are purely mechanical systems were analyzed in the previous chapters. Mechatronic driveline systems are a new direction in the application of mechatronics to the development of automotive systems. Several examples of mechatronic systems were given in Table 1.17. This chapter examines the sources and causes for the appearance of mechatronic systems and the principal directions of their development. This will clarify the need for the separate consideration of mechatronic systems and the structure and content of the subsequent sections of this chapter.

It is commonly assumed that the beginning of the era of electronics and electronic control systems that started making their way into all domains of economic activity, including the automotive industry, was in the 1950s. The most active application of electromechanical and electronic devices for controlling work processes of individual units and systems of ground vehicles, including cars, trucks, and buses started in the second half of the 1980s. As the different electromechanical (hydraulic and pneumatic) systems started developing, it became obvious that (i) the development of mechanical and electrical/electronic subsystems must be based on new principles that would lead to the creation of designs in which each of the subsystems would ensure conformance to the functioning requirements of the other subsystems, and (ii) different vehicular systems cannot ensure better vehicle performance if they do not interact with one another.

Item (i) can be clarified by reference to the requirement of zero-lateral-gap meshing of gears (no backlash) that are used in systems with electronic control. Another example may consist of magneto-rheological and electro-rheological fluids that are only recently coming into use in vehicular systems but give rise to a long series of new requirements to the design of mechanical subsystems. The appearance of these requirements and their actual implementation brought about continually new engineering solutions of mechanical subsystems that ensure the mechanical isolation of such fluids, the prevention of chemical interaction with the surfaces of the surrounding parts while at the same time retaining the properties of the fluids, and ensuring the functional properties of the entire system.

It may be stated with sufficient justification that the mutual entry and the combination of the principles of the design of mechanical, electrical, and electronic units and systems has resulted in the appearance of mechatronics, a science that integrates the above scientific disciplines and further develops each one in combination with the others.

This was facilitated by the development of computer science, and information and electronic technologies.

In explaining item (ii), various protocols (e.g., the CAN Protocol) that were developed in order to ensure and coordinate the functioning of the vehicle's systems can be pointed out.

Electronic differential locking devices started appearing during the 1970s and 1980s. Locking in these designs was usually triggered by detecting differences in the angular velocities of the wheels and unlocking—after some time had elapsed. Gradually, the control of a single differential was replaced by the control of interaxial and interwheel coupling units. Table 7.1 presents examples of driveline systems of 4×2 and 4×4 vehicles and the designations of these systems given by their manufacturers.

These systems came to be known in the engineering literature as ''torque vectoring'' and ''torque management.'' As an illustration, consider one of the designs of the 4MATIC system by A. Zomotor et al. (1986) that has been in use since the 1980s. The schematic diagram of this system is shown in Figure 7.1.

It is comprised of a transfer case with asymmetrical spur gear interaxle differential 3 (the gear ratio of the mechanism is $65/35 \approx 1.86$). Its crown gear is coupled to engine 1, its carrier to rear-axle differential 8, and its sun gear to front-axle differential 2. The interaxle differential is equipped with a normally engaged locking friction clutch that couples the differential's carrier to the hollow shaft of its sun gear. This friction clutch is locked and unlocked by hydraulic power cylinder 4. The interaxle differential is also equipped with a front-axle drive friction clutch. It is locked and unlocked by hydraulic power cylinder 5. The rear-axle differential includes two multidisk friction clutches that are compressed, under certain conditions, by hydraulic cylinders 6 and 7. The operation of hydraulic cylinders 4 through 7 is controlled by an electronic system consisting of a microprocessor 13 with an additional memory device. The microprocessor, with induction sensors 9 and 10 of the rear-wheel rpm and induction sensors 11 and 12 of the front-wheel rpm and

TABLE 7.1

Simple and Combined Mechatronic Drivelines

Wheel Formula	PDUs Being Controlled	System Designation
4×2	Interwheel	Antislip differential (ASD)
		Active torque transfer system (ATTS)
		Direct yaw control (DYC)
		TracRite
4×4, part time	Interaxle	AutoTrack
		Control-Track
		Active torque split system
		Active torque control 4×4
4×4, part time	Interaxle and one or two interwheel	Quadra-Track Vari-lock progressive differentials
4×4, full time	Interaxle	Variable torque distribution
4×4, full time	Interaxle and one or two interwheel	4MATIC Active yaw control (AYC) $4 \times$ MOTION

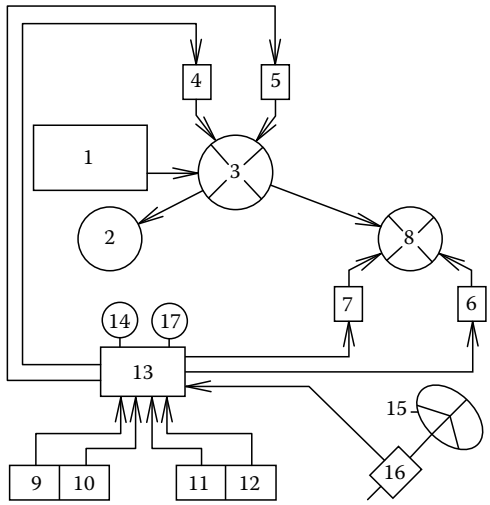


FIGURE 7.1
Schematic diagram of the 4MATIC system.

with induction sensor 16 of the turn of steering wheel 15, comprises the electronic control system. The system processes the sensor signals and generates a control signal as required by the situation. The control signal operates an electronically actuated valve through which oil flows to the specific hydraulic cylinder that locks or unlocks the pertinent clutch. Indicator 14 informs the driver about all the potentially dangerous road conditions and indicator 17 signalizes the system malfunctions.

The 4MATIC system operates as follows. Under ordinary conditions, only the rear axle provides traction with the differential unlocked. This is the zero-operating level of the automatic system. If, for some reason, the gripping conditions of the rear wheels turn out to be insufficient and the stability of motion is lost, the front-wheel drive is actuated, that is, both of the vehicle's axles become fully driven by the interaxle differential. As opposed to the previous, this is the first operating level of the 4MATIC system. If supplying power to the front axle is insufficient for restoring the vehicle's stability of motion, the system switches to operating level 2. This involves locking the interaxle differential. And in cases when even this is insufficient, the system switches to operating level 3 that additionally locks the rear driving axle differential.

The operation of the 4MATIC systems ensures smooth switching between the working levels without abrupt changes in the torque. The switching occurs as a function of the behavior of the following parameters: wheel slippage, front-wheel-turning angle, velocity, and acceleration of the vehicle.

Slippage is determined by the comparison of the rpm of the left and right wheels of the rear-driving axle. This involves the correction by the turning angle. If the slippage exceeds the limiting value for the given vehicle velocity, the system is switched to the next level of operation. When slippage does not drop to the permissible level within some specified time, the system switches to operation at the next level. If slippage decreases, the system remains at the current operating level for some specified time and then returns to the previous operating level. The cyclicity when moving under boundary conditions between levels is eliminated by including a ''teaching'' algorithm that will be discussed later in this chapter. If, however, after switching to a higher level and returning to the current level the system returns to the higher level within less than 2 s, then the level-setting period

will gradually increase. Three stages—0.7, 2.5, and 7.5 s—are provided for this case. The rear-axle differential clutch cannot be actuated at vehicle velocities in excess of 38 km/h and if the rpm of the front-axle wheels is lower than that of the rear wheels.

The wheel-turning angle sensors make it possible for the system to determine whether the vehicle travels in a straight path or makes a turn. If the threshold value of the turning angle is exceeded, the system switches immediately to operating level 1 even if there is no wheel slippage. A return to the zero level occurs when the vehicle is sensed to move in a straight path, unless the limiting values of other parameters have been attained. When the vehicle decelerates, the system immediately switches to the zero-operating level.

The vehicle's velocity may also trigger switching to another operating level. When the speed drops to 5 km/h, the system switches to level 1 and remains in it as long as the velocity does not reach 20 km/h. Then it returns to the zero level, unless the limiting values of other parameters are attained. This makes it possible to start moving only with both axles engaged. Level 3 is switched off in any case at velocities in excess of 38 km/h. If the vehicle velocity is less than 20 km/h, then rear-wheel slippage immediately causes switching to the third level, bypassing the lower levels.

The threshold acceleration in the 4MATIC system is 0.5 m/s^2. If the actual acceleration exceeds this threshold value, then the system switches to level 1 that permits an engaged total drive of both axles at higher-than-threshold accelerations.

A case is possible, when moving on, for example, a slippery, ice-covered road, where the switching on of the total differential drive turns out to be insufficient for getting the vehicle to move. Even locking both differentials in a sequence does not help because the rapidly slipping wheels smooth out the underlying surface and reduce its gripping properties to the limit. This situation can be avoided by providing the system with a ''teaching'' algorithm. If, after starting to attempt to move for 0.5 s after both the differentials are locked the linear velocity of at least one of the wheels does not exceed 5 km/h, the system switches to operating level 3 and maintains it for 7.5 s. The third operating level is disabled by depressing the brake pedal. Another feature of this system consists in the ability of the driver to control the driveline system manually.

Obviously, it may be assumed that the appearance of the integrated driveline systems stems from the development of systems that are known as traction control (TC) systems and acceleration-slip-regulation (ASR). These systems brake the slipping wheel and reduce the engine crank rpm. Such systems are used for improving the stability of motion and maintaining the acceleration and for improving the traction performance by reducing the wheel slippage. In addition to these systems, other systems such as stability traction (StabiliTrak), electronic traction system (ETS), automatic stability control (ASC), electronic stability program (ESP), dynamic stability control (DSC), vehicle stability control (VSC), vehicle stability assist (VSA), and vehicle dynamic control (VDC) are also used extensively.

During the last several years, there has been some information about design developments in which the control of PDUs was integrated with the control of other systems, in particular, those of suspension and steering system controls. The term ''active suspension'' was joined by terms such as ''active steering'' and ''active anti-roll system.'' The integration of the control of these mechatronic systems and mechatronic driveline systems has, as its purpose, to optimize the longitudinal, lateral, and vertical vehicle dynamics.

It should be particularly emphasized that mechatronic driveline systems (simple, combined, and integrated) are currently intensively developed for a variety of vehicle types: highway and terrain vehicles, trucks with different capacities, and for special-purpose

vehicles (military, farm, and industrial tractors), various passenger cars, sports cars, and sport-utility vehicles (SUVs).

The integrated approach to the design of vehicular mechatronic systems makes it possible to significantly improve their dynamics and operational performance. Cars equipped with mechatronic systems are capable of prolonged curvilinear motion at steering-wheel-turning angles of 65°–100° with lateral acceleration exceeding the lateral accelerations by 14%–32% of similar cars with mechanical drives of the four wheels. The use of mechatronic driveline systems allows the significant control of the vehicle's yaw moment. As a result, cars with mechatronic driveline systems require 20%–60% smaller angles of turn of the steering wheel when switching lane than similar cars with systems based on braking of the wheels. At the same time, the time of performing this maneuver decreases by approximately 30%–35%. The yaw rate (the angular velocity of the turning of the vehicle about the vertical axis) is 5%–15% smaller. The actuation time of mechatronic systems (also known as reaction time) is usually 100 ms or more. Some companies even claim a reaction time of the order of 80 ms. The significant ''flexibility'' of mechatronic systems in controlling the wheel torques makes it possible to effectively control the dynamic behavior of vehicles. For example, when performing a 90° turn, a vehicle with control of the torque distribution between the front and rear axles may perform in the same manner as a rear-wheel drive vehicle when starting the turn, whereas when completing the turn, a large fraction of the torque is transmitted to the front wheels. The redistribution of torques between the front and rear, left and right wheels may markedly improve the traction performance of the vehicle and increase the rate of acceleration.

Currently there is practically no manufacturer of driveline systems and their components that is not involved in the development of mechatronic systems. Analysis shows that attention in designing mechatronic systems is focused on the following problems. The system concept selection is usually based on the desire to improve vehicle dynamics and in the first place by improving the stability and by increasing the velocity of motion by controlling the wheel torques. The handling of the vehicle that was referred to in Section 1.5 is not always investigated and analyzed. This approach is justified in the case of multi-drive vehicles (see Section 1.5), but it is not advisable to ignore the handling aspects of high-speed vehicles. Focusing their attention on vehicle dynamics and control of wheel torques, investigators disregard the energy and fuel efficiency of vehicles. This void is filled in Sections 7.5 and 7.6: the properties of mechatronic systems are synthesized based on the optimal distribution of power among the wheels, and the control algorithms of PDUs of high-speed vehicles are worked out with consideration of the handling performance.

Many new, previously unexplored problems of driveline systems design arise in the course of the design of mechatronic systems. Thus, the reduction of the actuation time of mechatronic systems depends to a large extent on the quality of the algorithm of control of the force and kinematic parameters of the wheel and on the feasibility of effective real time assessment of road conditions. These two problems are analyzed in Sections 7.2 and 7.3. These studies allowed working out a strategy of controlling the force and kinematic wheel parameters. The algorithm of control of the angular velocity of a wheel based on the above strategy that dispenses with the torque sensor and ensures control within the limits of the actuation time of mechatronic PDUs is analyzed in Section 7.2. Section 7.3 that deals with the assessment of road conditions, analyzes the principles of control of the wheel's rolling radius, which is a component of the previously mentioned strategy of control of the force and kinematic parameters of the wheel. Finally, Section 7.7 is concerned with certain aspects of hybrid drives that are important in providing an optimum distribution of power

between the wheels of hybrid vehicles, and their dynamics and performance control. Hybrid drives are the way to individual control of the power supplied to each of the vehicle's wheels. It should be noted in conclusion that mechatronic driveline systems are in the very beginning of their development and the number of problems associated with their design and effect on the vehicle performance increases constantly and may serve as the topic of another book.

7.2 Inverse Wheel Dynamics and Control

In the final analysis, mechatronic driveline systems are intended for controlling the force and kinematic parameters of a vehicle's wheels. The power is transmitted from the PDUs to the wheels through a system of drive elements that include gears, shafts, clutches, packing, and other possible elements. It is hence important, when designing such systems for high-speed vehicles, to make allowance for the stiffness and inertia properties of the transmission from the PDUs to the wheels, since they affect the torques and angular velocities of the wheels in real time. In addition, it is important to have available algorithms for control of the torques and angular velocities of the wheels proper. Such algorithms should be worked out before designing the PDUs of the mechatronic systems. In fact, refined algorithms of control of the parameters of wheels that ensure the required kinematics and dynamics of the wheels and their performance, determine the requirements put to the design of PDUs. The consideration of the features of the transmission of power from the wheels to the PDUs serves as the basis for developing algorithms for the control of these units.

This section presents an innovative method of studying wheel dynamics and wheel performance control based on the inverse dynamics formulation of the problem. Such an approach opens up a new way to the optimization and control of both vehicle dynamics and performance by optimizing and controlling power distribution to the drive wheels.

The equation of motion of a wheel is initially derived from the wheel power balance equation that makes the former equation more general. This equation of motion serves as the basis for studying both direct and inverse wheel dynamics. Development of a control strategy based on the inverse wheel dynamics approach includes wheel torque control that provides a wheel with both the specified angular velocity and rolling radius and with the required functionals of quality, consisting of the slippage power loss and the wheel's cycloid area. The first part in implementing the presently developed strategy of inverse wheel dynamics and performance control consists of an algorithm for angular velocity control.

Let us begin by examining the control strategy. Let the linear velocity of the wheel center be controlled by changing the wheel torque transmitted to the wheel from the vehicle's driveline system: some function $V_{xs}(t)$ represents required (specified) values of the velocity as a function of time t. Multiplication of the specified angular velocity ω_{ws} by the rolling radius r_{ws} yields the required velocity V_{xs} (a reminder: see formula (1.7)).

Using the definition of the effective rolling radius given in Section 1.3.2 (see also Figure 1.50) it is possible to introduce the cycloid that is described by the peripheral points of an assumed stiff wheel with radius r_{ws}. This cycloid is shown in Figure 7.2. The distance traveled by the wheel during one complete revolution is

$$A_1A_2 = 2\pi r_{ws} \tag{7.1}$$

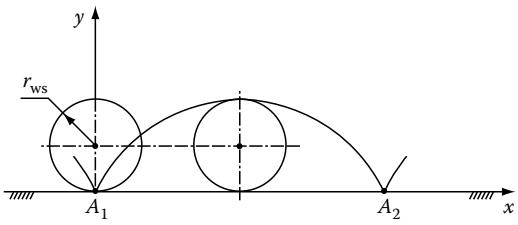


FIGURE 7.2
Cycloid of a rigid wheel with radius r_{ws}.

The concept presented by formula (7.1) is convenient for relating the wheel radius r_{ws} to the distance S_w traveled by the wheel during n_w revolutions:

$$r_{ws} = S_w/(2\pi n_w) \tag{7.2}$$

Several more formulae that are needed for further mathematical treatment are hereby defined. The current coordinates of a point on the wheel circumference are:

$$\begin{aligned} x &= r_{ws}(\theta - \sin\,\theta) \\ y &= r_{ws}(1 - \cos\,\theta) \end{aligned} \tag{7.3}$$

where θ is the wheel's turning angle, $0 \le \theta \le 360^\circ$. After eliminating angle θ from Equations 7.3, the equation of the cycloid takes the form:

$$x = r_{ws}\arccos\left(\frac{r_{ws} - y}{r_{ws}}\right) - \sqrt{2r_{ws}y - y^2} \tag{7.4}$$

The area constrained by the arc $\overset{\frown}{A_1A_2}$ and the line segment A_1A_2 in Figure 7.2 is:

$$A_c = 3\pi r_{ws}^2 \tag{7.5}$$

Consider a procedure of assigning values of ω_{ws} and r_{ws}. Start by solving the following inverse dynamics problem: determine the wheel torque T_w in Equation 1.42 assuming that the payload $F_{frame.x}$ and a rolling resistance force R_x are given, and that additional two components are predetermined by the required kinematic parameters of the wheel (this is because velocities and accelerations are specified in inverse dynamics). Designate the torque that should be applied to the wheel to overcome the resistance to its motion as $T_w = T_{ws}$. Second, using a linear or nonlinear (depending on the surface–tire interaction conditions, see Figure 7.3a and b) function $r_w = f(T_w)$, determine the required rolling radius r_{ws}. Finally, calculate the required angular velocity of the wheel ω_{ws} using formula (1.7) based on known V_{xs} and r_{ws}. Thus, to provide the required velocity V_{xs}, the wheel should be supplied with torque T_{ws}. If this is so, the wheel will rotate at ω_{ws} and have a radius of r_{ws}.

Let the coordinates of point A on line/curve 1 in Figure 7.3 be $T_{w1} = T_{ws}$ and r_{ws}, and let cycloid 1 in Figure 7.4 be computed using formulae (7.3) and the radius r_{ws}, $0 \le \theta \le 360^\circ$. The area under cycloid 1 is obtained from formula (7.1) as A_{cs}.

Should the rolling conditions deteriorate (line/curve 2), the rolling radius will become smaller (the slippage will become greater). This is shown by the arrow between points A and B at constant torque $T_{w1} = T_{ws}$ in Figure 7.3. This lower value of r_w results in a different cycloid (2 in Figure 7.4).

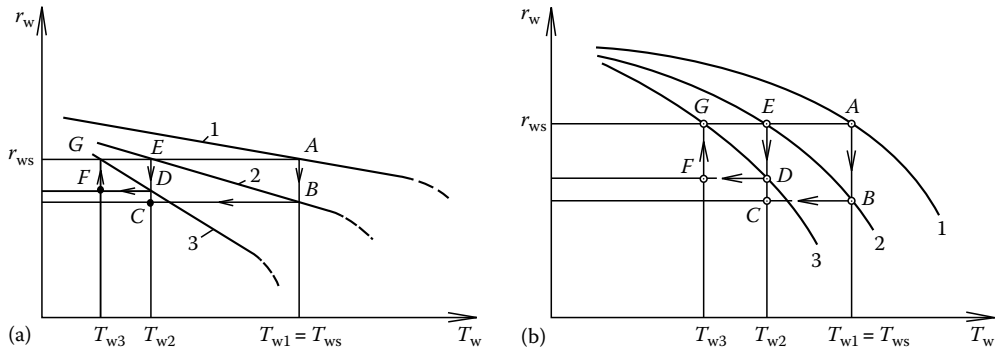


FIGURE 7.3
Torque vs. rolling radius diagram under various road/terrain conditions.

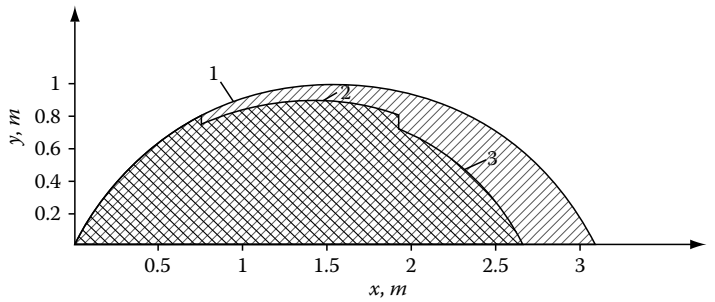


FIGURE 7.4
Cycloids under various road conditions: area A_{cs} ▨, area A_{sh} ▩.

If the energy supplied to the wheel is sufficient for maintaining the angular velocity ω_{ws} and reducing the torque from $T_{w1} = T_{ws}$ to T_{w2}, the linear velocity will be restored to the required value of V_{xs}. Then the rolling radius will revert to its required value of r_{ws} (see points E and A in Figure 7.3).

If the road conditions deteriorate further (line/curve 3), the rolling radius will attain the value given by the ordinate of point D in Figure 7.3 and this radius will generate cycloid 3 as in Figure 7.4. It is now necessary to further reduce the wheel torque to restore the radius r_w to its required value of r_{ws} (see point G in Figure 7.3). The described approach can be used to control the linear velocity V_{xs} at constant angular velocity ω_{ws} if the wheel torque drop from $T_{w1} = T_{ws}$ to T_{w3} is sufficient for overcoming the resistance to motion under these poor conditions. This is seen from formula (1.42).

If the rolling resistance force R_x under poor road conditions requires a greater wheel torque given by formula (1.42) than the value of T_{w1} needed to restore the radius $r_w \rightarrow r_{ws}$, a different approach should be used for controlling the velocity V_{xs}. In this case the angular velocity should be changed to a value that, upon being multiplied by some value of r_w, would again maintain the required velocity V_{xs}. The question is how to determine that value of the angular velocity. Current control methods link angular velocity ω_w and torque T_w by a certain function $\omega_w = f(T_w)$ that is specified in the energy source of the wheel, for example, an internal combustion engine, an electric motor, etc.

This section suggests an alternate method that does not involve finding the required value of ω_w from its mathematical link to the wheel torque. The approach suggested here opens new vistas for synthesizing previously unknown functions relating torque T_w to angular velocity ω_w, which should be used in designing energy supplies to the drive wheels.

The search for the appropriate value of ω_w should be correlated with the minimization of the slip power P_δ in formula (1.41), which is a function of both the angular velocity ω_w and the rolling radius r_w. Wheel dynamics is linked to wheel performance optimization in this manner. The search for the value of radius r_w can be replaced by maximization of the shaded area A_{sh} under the cycloids in Figure 7.4. The decision of whether P_δ or A_{sh} should be used as the criterion is based on which of them is more convenient in implementing the control algorithm. The power slip and the shaded area under cycloids are the quality functionals that characterize wheel performance. The above can be formulated as follows:

$$\begin{aligned} &P_\delta = F_x\omega_w\left(r_w^0 - r_w\right) \rightarrow \min \quad \text{or} \quad A_{sh} \rightarrow A_{cs} \\ &0 < r_w \leq r_{ws} \\ &A_{cs} = 3\pi r_{ws}^2 \\ &\omega_w r_w = V_{xs}. \end{aligned} \tag{7.6}$$

The control strategy is thus based on two parallel processes: (i) control of angular velocity ω_w and (ii) control of linear velocity V_x, e.g., of the rolling radius r_w. This section presents an algorithm for controlling the wheel angular velocity as the first part in the implementation of this newly developed strategy.

The algorithm for controlling the wheel's angular velocity is now analyzed. Rewrite Equation 1.42 to the form

$$\dot{\omega}_w = \frac{T_w}{I_w} - f_w \tag{7.7}$$

where $f_w = (R_x + F_{frame.x} + F_a)r_w^0/I_w$ is a nonlinear function, since the rolling resistance force R_x can change randomly when road conditions change, and the acceleration a_x in the formula for the force F_a is not necessarily constant. Equation 7.7 is a basic equation for forming the control torque that should provide a programmable motion of the wheel with the required kinematic parameters. The biggest problem in using Equation 7.7 is that of determining function f_w that requires sophisticated sensors and additional computation. However, a possibility exists to construct control laws that do not require full information about the function presented here. Such control laws are known as control-by-acceleration algorithms that are used in some robotic applications. To apply control-by-acceleration principles to inverse wheel dynamics and performance control, Equation 7.7 can be written as

$$\dot{\omega}_w = \varepsilon_w(\omega_w, T_w) \tag{7.8}$$

where the wheel's angular acceleration ε_w is a function made nonlinear by the nonlinearity of function f_w in formula (7.7).

Formulate the control problem as follows. Let the initial angular velocity of the wheel at time $t = 0$ be $\omega_w(0) = \omega_{w0}$. It is required to develop a control algorithm to determine the

wheel torque T_{ws} for which the angular velocity $\omega_w = \omega_{ws}$. It is also required that the process $\omega_w \to \omega_{ws}$ be governed by the following relationships:

$$\begin{aligned} \omega_w(t) &= \omega_{w*}(t) \\ \omega_{ws} - \omega_{w*}(t) &= C_w e^{-\rho_w t} \end{aligned} \tag{7.9}$$

where

$\omega_{w*}(t)$ is a given (required) variation of the angular velocity ω_w to its required value of ω_{ws}

$C_w = \omega_{ws} - \omega_{w0}$ is a constant

$\rho_w > 0$ is a constant that determines the rate of decay of the deviation $\delta(t) = \omega_{ws} - \omega_w(t)$

As seen from formulae (7.9), the deviation δ that measures the difference between the required and current values of the angular velocity should be obtained from a differential equation:

$$\begin{aligned} \frac{d\delta(t)}{dt} + \rho_w \delta(t) &= 0 \\ \delta(0) &= C_w \end{aligned} \tag{7.10}$$

Formulae (7.9) and (7.10) determine the kinematic law of variation in the angular velocity since this law does not consider forces and torques applied to the wheel. The actual (dynamic) law describing the variation of ω_w from $\omega_{w0} = \omega_w|_{t=0}$ to $\omega_w = \omega_{ws}$ should be constructed upon considering the wheel's differential equation of motion. Construct the dynamic law by solving the inverse dynamics problem.

First, find the acceleration $\varepsilon_w(t) = \varepsilon_{w*}(t)$ that corresponds to the required angular velocity of the wheel, $\omega_w(t) = \omega_{w*}(t)$. Acceleration $\varepsilon_{w*}(t)$ can be computed by differentiating $\omega_{w*}(t)$ from formula (7.9) and then substituting the result of the differentiation in formula (7.8):

$$\begin{aligned} \omega_{w*}(t) &= \omega_{ws} - C_w e^{-\rho_w t} \\ \varepsilon_{w*}(t) &= \dot{\omega}_{w*}(t) = \rho_w C_w e^{-\rho_w t} \end{aligned} \tag{7.11}$$

The second formula of (7.11) determines the program for controlling the angular acceleration $\varepsilon_w(t)$ that will ensure conformance to the expression for the angular velocity $\omega_w(t) = \omega_{w*}(t)$. An important note: this equation conforms to the concept of inverse dynamics.

Now compile an expression for $C_w e^{-\rho_w t}$ as a function of the angular velocity ω_w. Substitution of $C_w e^{-\rho_w t}$ from the kinematic law given by formula (7.9) into the second formula of (7.11) yields

$$\varepsilon_{w*} = \rho_w(\omega_{ws} - \omega_w) \tag{7.12}$$

Formula (7.12) presents the required values of the angular acceleration that is compatible with the discrepancy (deviation) $\delta = \omega_{ws} - \omega_w$. Acceleration ε_{w*} is generated by torque T_{w*} that can be found from the equation:

$$\varepsilon_w(\omega_w, T_{w*}) = \rho_w(\omega_{ws} - \omega_w), \quad t \geq 0 \tag{7.13}$$

Suppose now that it is possible to measure the angular acceleration $\dot{\omega}_w(t)$ of the wheel in motion. If this is so, then the numerical value of function $\varepsilon_w(\omega_w, T_w)$ in formula (7.8) is

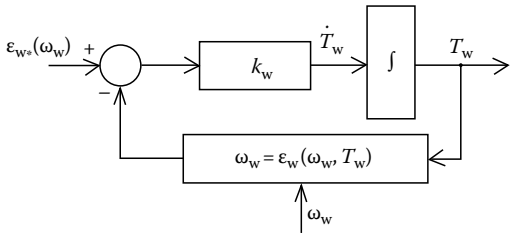


FIGURE 7.5
Acceleration loop diagram.

known at any given moment of time. This information on the angular acceleration can be used to solve Equation 7.13 under the uncertain mathematical analytical function ε_w. Torque T_w should take on values such that the equality below holds at any time $t > 0$:

$$\dot{\omega}_w(t) = \varepsilon_{w*}(\omega_w) \tag{7.14}$$

Two situations are possible:

1. If $T_w = T_{w*}$, then $\varepsilon_{w*}(\omega_w) - \dot{\omega}_w = 0$
2. If $T_w = T_{w*} \pm \Delta T_w$, then $\varepsilon_{w*}(\omega_w) - \dot{\omega}_w \neq 0$ (7.15)

When dealing with the second situation, the wheel torque should be adjusted so as to provide $\Delta T_w \to 0$ that immediately leads to $(\varepsilon_{w*}(\omega_w) - \dot{\omega}_w) \to 0$. It means that torque T_w should be controlled by a discrepancy $(\varepsilon_{w*}(\omega_w) - \dot{\omega}_w)$ in the acceleration. This type of control can be implemented based on a tracking control loop for acceleration shown in Figure 7.5.

The input consists of the required acceleration $\varepsilon_{w*}(\omega_w)$ computed from formula (7.12). This acceleration is compared with the actual acceleration $\dot{\omega}_w(t)$, and then the time rate change of the wheel torque, $\dot{T}_w$, is determined using the discrepancy $(\varepsilon_{w*}(\omega_w) - \dot{\omega}_w)$. The wheel torque appears as an integral of

$$\dot{T}_w = k_w(\varepsilon_{w*} - \dot{\omega}_w) \tag{7.16}$$

where k_w is a proportionality factor (gain factor) representing the gain in the acceleration control loop. Obviously, the torque obtained from integrating formula (7.16) is not equal to some given required torque T_{w*} that could be found from the equation of motion (7.7) in which all the terms are retained. However, at certain values of factor k_w the difference $(T_{w*} - T_w)$ can be neglected (as shown further in this section).

Finally, there are two loops in the block diagram (Figure 7.6): (i) an internal loop to control the acceleration $\dot{\omega}_w$, and (ii) an external loop to control the angular velocity ω_w.

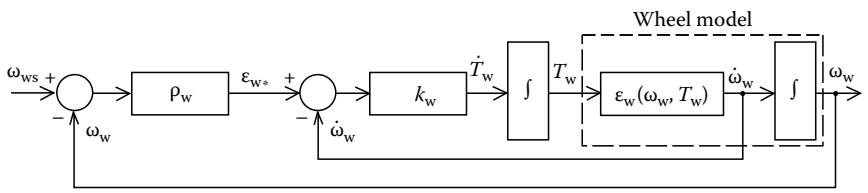


FIGURE 7.6
Control block diagram.

These two control loops comprise a feature of the control algorithm presented by formulae (7.8), (7.12), and (7.16). This feature consists in the fact that there is no need to determine the nonlinear function f_w and its components in formula (7.7) when implementing the control algorithm. This feature is rooted in the fact that the actual acceleration $\dot{\omega}_w$, which is the numerical value of function $\varepsilon_w(\omega_w, T_w)$ and is measured by a sensor, is used to compute the wheel torque, T_w. This numerical value of $\dot{\omega}_w$ already includes the nonlinear function f_w since it is measured rather than computed. Therefore, the control algorithm given by formulae (7.8), (7.12), and (7.16) determines the programmable motion of the wheel at the required angular velocity.

Implementation of the control algorithm described above requires addressing the problem of accuracy and stability of angular velocity control. This problem arises since there are two control loops in the block diagram shown in Figure 7.6. The degree of approximation of the wheel torque T_w of the required value T_{w*} depends on the time rate of change of the angular velocity $\omega_w(t)$. The lower the rate of angular velocity change, the smaller is the difference $(T_w - T_{w*})$. At the same time, as seen from Figure 7.6, the time rate of change of the torque T_w conforms to the rate of the process $\dot{\omega}_w(t) \rightarrow \varepsilon_w$, which is needed to implement the kinematic law $\omega_{w*}(t) \rightarrow \omega_{ws}$ given by formulae (7.9) and (7.10).

Accuracy in implementing the kinematic law can be provided by a higher acceleration-loop gain, for example by a larger gain factor k_w in formula (7.16). It is of essence to note that algorithms based on control-by-acceleration principle are stable under higher values of k_w. This can be demonstrated by deriving a differential equation of the closed-loop system. Differentiating Equation 7.7 yields

$$\ddot{\omega}_w = \frac{\dot{T}_w}{I_w} \tag{7.17}$$

Substituting now (7.12) and (7.16) into formula (7.17), it is found:

$$\ddot{\omega}_w + \frac{k_w}{I_w}\dot{\omega}_w + \rho_\omega \frac{k_w}{I_w}\omega_w = \rho_\omega \frac{k_w}{I_w}\omega_{ws} \tag{7.18}$$

It is seen by analyzing Equation 7.18 that an appropriate value of the coefficient k_w can be assigned, and at which the algorithm presented by (7.12) and (7.16) provides the required wheel torque $T_w \approx T_{w*}$. This will lead to an appropriate approximation of the actual process $\omega_w(t) \rightarrow \omega_{ws}$ to the desired one, which is $\omega_{w*}(t) \rightarrow \omega_{ws}$. In addition, the rate of response of the acceleration loop will be rather higher than the speed of the angular velocity loop (see the loops in Figure 7.6). Therefore, the control process in the closed-loop system will be determined by the parameters of the external loop only.

The system is stable under marked parametric variations. As shown in Figure 7.7 damping transients still occur at one-order increase in the moment of inertia I_w of the wheel. The transient response can be improved by changing the gain factor k_w.

The transient response ranges from 0.1 to 0.035 s when the factor k_w increases from 200 to 500 as illustrated in Figure 7.8.

It should be noted that modern wheel torque management systems have response times of 0.080 to 0.100 s and higher. Hence, a sufficient transient response can also be obtained when the moment of inertia of a wheel is rather large. This can be done by further increasing the gain factor (Figure 7.9).

It should be emphasized in conclusion that the above method of wheel dynamics and performance control is based on the inverse dynamics formulation. The strategy described

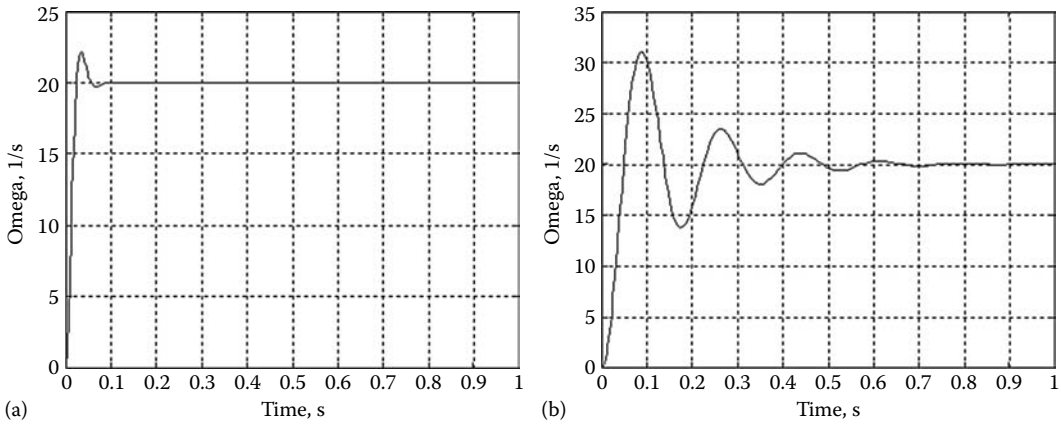


FIGURE 7.7
Transient processes, $\rho_w = 100$; $k_w = 200$; when moment of inertia is (a) 1.5 kg m^2 and (b) 15 kg m^2.

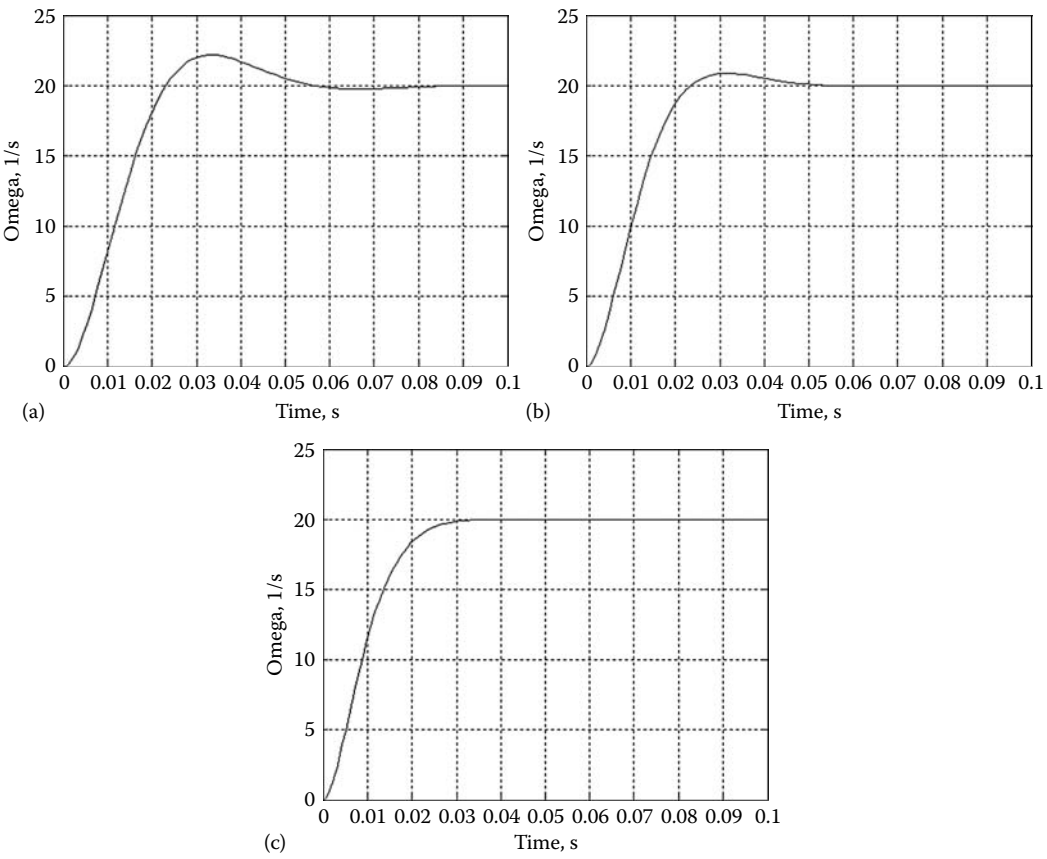


FIGURE 7.8
Transient processes, $\rho_w = 100$; moment of inertia $I_w = 1.5\,\text{kg m}^2$. k_w: (a) 200; (b) 300; (c) 500.

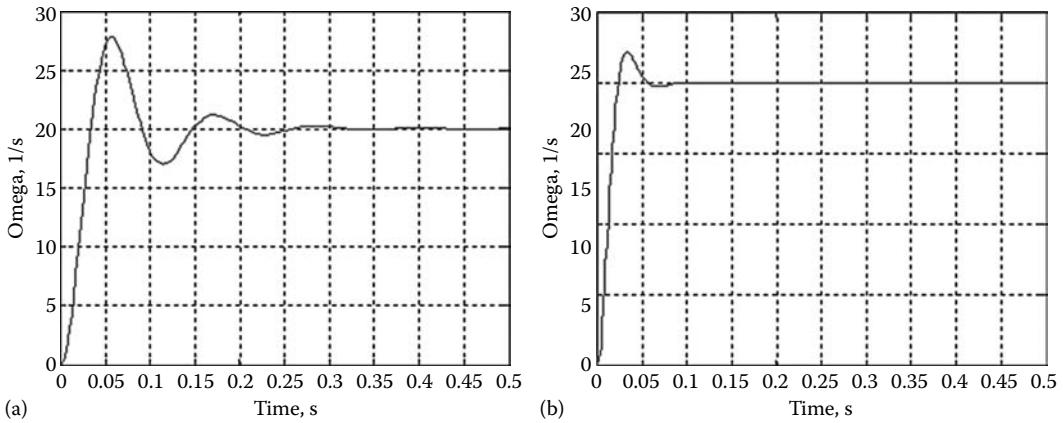


FIGURE 7.9
Transient processes, $\rho_w = 100$; moment of inertia $I_w = 15\,\text{kg}\,\text{m}^2$, k_w: (a) 500; (b) 2000.

above differs from currently used control strategies since it invokes the idea of controlling both the angular velocity and the rolling radius of a wheel so as to obtain the required quality functionals. The above strategy of wheel angular velocity control algorithm that consists in varying the wheel torque is based on the inverse wheel dynamics and the control-by-acceleration principle. The implementation of the algorithm does not require complete information on wheel forces, including the rolling resistance force, the inertia force, and the wheel frame force. The control algorithm is distinguished by its adaptability and very slight sensitivity to changes in parametric and external disturbances. The study of the inverse wheel dynamics and control described above is a key to further advances in vehicle performance control by distributing optimal power to the drive wheels. The reason for this is that the inverse wheel dynamics is in essence rooted in the power balance equation of a wheel.

The above algorithm of control of the angular velocity of a wheel implements one part of the control strategy developed in this section. The next section analyzes the principles of controlling the rolling radius within the context of assessment of the gripping conditions between the wheel and the surface of motion.

7.3 Proactive Assessment of Terrain Conditions

This section addresses several problems of design of algorithms and devices for proactive determination of the properties of the support surface that affect the interaction between the tires and the surface. The formulation as such of this engineering problem is not actually new and it was investigated apparently for the first time during the 1960s and its results were used in the first designs of planetary landing vehicles. The mobility of these vehicles was assessed by comparing the measured slippage s_δ and the rolling resistance factor f with the specified critical values. This made it possible to determine impassable areas without measuring the physical and mechanical properties of the soil to formulate local travel paths of the vehicle and to optimize the operating mode of the traction motors when moving in these paths.

Subsequently, studies in this field became more active, something that stems in the first place from the explosive development of antilock brake systems and then of the traction control systems. Two principal engineering problems were solved and are still being improved upon today by different methods:

1. Determination of the peak friction (gripping) coefficient: μ_{px} and μ_p (see formulae (1.27) and (1.28)).
2. Determination of the slope of the tractive/brake force—slip ratio functions that are frequently termed the ''slippage curves.''

Both problems are illustrated in Figure 7.10 for the case of a wheel in the driving mode.

The results of the solution of these problems are used for controlling the wheel slippage (slip ratio) to ensure maximum acceleration (deceleration) of the vehicle for which it is required to develop the maximum tractive (braking) force. Knowledge of the slope of the slippage curve makes it possible to assess the gripping properties of the support surface: for a given tractive force of a wheel its slippage will be greater on surfaces with poorer gripping conditions (see Figure 7.10). In investigating the longitudinal and lateral dynamics of the vehicle the problem of assessing μ_{px} and μ_p is complicated by the effect of the wheel's lateral slip angle on the slope of the graphs in Figure 7.10. In this case, there arises the additional problem of determining a reasonable relationship between the current friction coefficients in the longitudinal and lateral directions of the wheel.

Various approaches and methods were developed for solving the above problem. One set of method consists in investigating the state of the surface of motion by means of optical tools. For example, a TV camera is used for assessing the road's pavement: dry or wet, is there a film of water on the road, snow, or ice. Different road states are determined based on differences in the rate of reflection of light from the different surfaces. This property is used for determining the friction coefficient. Another set of methods is based on analytic determination of the functional relationships between the deformations of the tire and the peak friction factor followed by utilizing this in control logarithms. A significant part of studies is performed in a third direction, based on the study of curves plotted in Figure 7.10 and introducing additional parameters that allow assessing the slope of the curves and the peak friction coefficients. Other approaches to solving the two problems mentioned above also exist. Commonly, they are based on indirect assessment of road conditions. Apparently, it makes no sense to express preference for a given approach of those listed above, since the methods under development have not come into sufficient practical use under real conditions. In addition, these methods are frequently worked out for a specific kind of vehicle. For example, modern methods of traction control

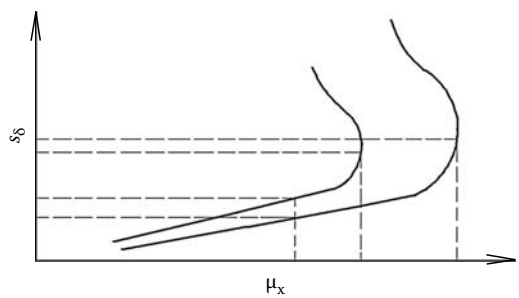


FIGURE 7.10
Current friction factors—slip ratios curves.

that are developed for planetary landing vehicles incorporate the feasibility of measuring the wheel torques, which is far from being justified for cars (unless less expensive, simple, and reliable torque sensors can be developed).

It should be particularly emphasized that the methods discussed above were developed with reference to the control of the wheel torque and its angular velocity using the vehicle's braking system and its fuel supply system. Such systems reduce the wheel slippage by reducing its angular velocity. The control of the wheel's input power by means of mechatronic driveline systems have fundamental specifics that are analyzed in this section within the context of the assessment of gripping conditions. These specifics shall be formulated as a set of technical specifications that mechatronic driveline systems should satisfy.

The first specification to be met in designing mechatronic driveline systems that have the capability of assessing road conditions, consists in the fact that these conditions must be assessed over a time interval that is smaller than or at least commensurate with the time of reaction of the wheel to changes in road conditions. Note that the wheel reacts to changes in these conditions by changes in the angular velocity and deformation of the tires caused by variation in reactions by the surface of motion. Satisfaction of this specification will allow accelerating the transmission of signals to the control of mechatronic PDUs by reducing the time difference between the control response and the reaction of the wheel to changes in road conditions. The above becomes the source of a second requirement: the time of actuation of the mechatronic PDU should also be as close as possible to the time of the wheel's reaction to changes in road conditions. A combined satisfaction of the first and second requirements will significantly improve the control of mechatronic PDUs by bringing its actuation time closer to the course of changes in road conditions that occur in real time.

A third specification is now formulated. The problem of assessing the peak friction coefficient and determining the slope of functions that relate the tractive force of the wheel (or the current friction coefficient) to slippage is usually solved using information on this slippage that, as a rule, is assessed based on its angular velocity. It shall be shown now that this is insufficient for working out effective mechatronic PDUs. The wheel slip ratio is determined using formula (1.19), from which it is seen that slippage s_δ is a function of both the wheel's angular velocity ω_w and of the rolling radius r_w. It is hence expedient to assess the road conditions not on the basis of the slip factor s_δ, but of its components ω_w and r_w. To clarify the above, consider, for example, an ith driving axle in the course of a turn when both wheels are rigidly connected to one another. In this case the angular velocities of both wheels are the same, but the slippage is different—$s'_{\delta i} \neq s'_{\delta i}$. This stems from the fact that the turning of an axle with positively locked wheels is accompanied by kinematic discrepancy that is represented by factors $m'^{(\prime\prime)}_{Hi}$ from formula (3.57). The difference in turning radii R'_{ti} and R''_{ti} and also nonequality of the rolling radii $r^{0\prime}_{wi}$ and $r^{0\prime\prime}_{wi}$ in the driven mode and in the longitudinal tire stiffness factors K'_{xi} and K''_{xi} caused by redistribution of weight between the wheels while taking a turn causes the appearance of kinematic discrepancy and accordingly of differences in wheel slip (see formula (3.58)). It follows from formula (1.19) that the wheel rolling radii in the driving mode r'_{wi} and r''_{wi} are not the same. Physically the difference in these two radii at identical angular wheel velocities ω'_{wi} and ω''_{wi} ($\omega'_{wi} = \omega''_{wi}$) are caused by different longitudinal deformations of the tires, soil, and different relative travels of the tires with regards to the surface. If the axle's wheels are allowed some relative rotation, when its PDU is not fully locked, then one has $\omega'_{wi} \neq \omega''_{wi}$ and $r'_{wi} \neq r''_{wi}$. By virtue of the above, it is advisable to break up the determination and assessment of wheel slippage into two parts: determining the angular velocity and the rolling radius in the driving mode (it is precisely such a strategy of wheel control that was suggested in Section 7.2). This in fact is the third requirement put to the design of

mechatronic systems for assessing road conditions and controlling the PDUs. The above make the timeliness of the studies for designing tire deformation measuring systems important.

It is also possible to use another path for the combined assessment of the wheel's angular velocity ω_w and the rolling radius r_w in the driving mode that is analyzed below. It is assumed for simplicity that the relationship between the wheel's torque T_w and the radius r_w can be described by Dr. E. Chudakov's linear Equation 1.20. If the relationship $r_w = f(T_w)$ is nonlinear under certain conditions, then it can be linearized using a piece-wise-linear approximation. Solving formula (1.20) for the tire (tire and soil on deforming surfaces) longitudinal elasticity factor λ_w and differentiating it, yields:

$$\dot{\lambda}_w = -\frac{(r_w^0 - r_w)\dot{T}_w}{T_w^2} - \frac{\dot{r}_w}{T_w} \tag{7.19}$$

Formula (7.19) is convenient both for the analysis of variation in the wheel's gripping conditions and for controlling the mechatronic PDUs. To clarify the above, return to the problem of stabilizing the linear wheel velocity $V_{xs} = \omega_{xs} r_{xs}$ that served as the basis of the wheel control strategy (see Section 7.2) and consider the control of the rolling radius in the driving mode.

Analysis of formula (7.19) shows that it is necessary to analyze the following three states:

1. $\dot{\lambda}_w = 0$
2. $\dot{\lambda}_w < 0$
3. $\dot{\lambda}_w > 0$

In the case, when $\dot{\lambda}_w = 0$ the longitudinal elasticity factor λ_w is constant, that is, the slope of $r_w = f(T_w)$ in Figure 7.3 and accordingly the gripping conditions do not change. Wheel torque T_w should be controlled in a manner such that the value of the rolling radius be r_{ws}.

If $\dot{\lambda}_w < 0$, that is, the value of λ_w decreases and the wheel's gripping conditions are improved, then again T_w should be controlled in a manner intended to restore the equality $r_w = r_{ws}$.

The most unfavorable situation occurs at $\dot{\lambda}_w > 0$, when λ_w increases and the wheel's gripping conditions become poorer. In this case, as was previously shown in Figure 7.3, the rolling radius can be maintained at the level of the value of r_{ws} only by reducing T_w. If, however, it becomes necessary to reduce the value of T_w to the point that it will not suffice to overcome the resistance to motion under the poor gripping conditions, then it becomes impossible to restore radius r_w to the value of r_{ws}. In improving the energy efficiency of the wheel, functionals from formulae (7.6) should be used to control the rolling radius r_w and angular velocity ω_w.

Formula (7.19) may be used for indirect assessment of the degree to which the wheel utilizes its gripping of the surface for producing the circumferential force F_x (or traction force F_w). In other words, formula (7.19) allows assessing the extent to which the current gripping coefficient $\mu_x = F_x/R_z$ is close to its maximum value $\mu_{px} = F_x^{max}/R_z$ (see formulae (1.26) and (1.27)). The situation when $\mu_x \to \mu_{px}$ is dangerous because the entire gripping of the wheel is utilized in producing the longitudinal force and the wheel is unable to take up lateral forces, which causes skidding. This was discussed in Section 1.3.4. The assessment of the extent to which μ_x approaches μ_{px} replaces the direct determination of the numerical values of the peak friction coefficient μ_{px} that was discussed at the start of this section

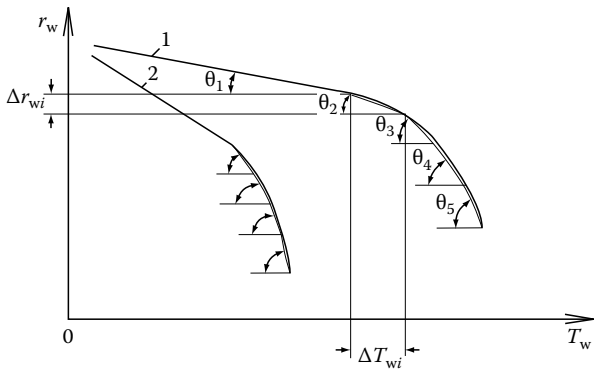


FIGURE 7.11
Piecewise-linear approximation of $r_w = f(T_w)$.

(first problem). This approach highly simplifies the control algorithm. Factor μ_x tends to its peak value μ_{px} upon a marked increase in torque T_w under good wheel gripping conditions and relatively low values of T_w in the case when the gripping conditions become poorer. This corresponds to the nonlinear segments in Figure 7.11.

Piecewise-linear approximation of these nonlinear graphs shows that the angle $\theta \to 90°$. The physical meaning of tan θ that represents the slope of the individual segments consists in the fact that it is equal to the longitudinal elasticity factor λ_w. In fact, using Dr. Chudakov's equation (see Equation 1.20) and Figure 7.11,

$$\tan \theta_i = \lambda_{wi} = \frac{\Delta r_{wi}}{\Delta T_{wi}} \tag{7.20}$$

It is seen from Figure 7.11 that $\Delta T_{wi} \to 0$ and $\lambda_{wi} = \tan \theta_i \to \infty$ upon deterioration of gripping conditions, whereas $\mu_x \to \mu_{px}$. This property may be used for indirect assessment of the closeness of μ_x to μ_{px} that can be judged from the rate of variation in $\dot{\lambda}_w$ from Equation 7.19. The above is important not only under poor road conditions but also when the conditions of gripping between the wheel and the surface are quite satisfactory. For example, when a vehicle turns with the axle differential locked, the circumferential force F_x of the inner wheel may quite rapidly attain a value close to F_x^{max} from formula (1.26). This process may also be monitored on the basis of the behavior of $\dot{\lambda}_w$.

There are several remarks on modeling $\dot{\lambda}_w$ using formula (7.19). The direct use of data on torque T_w and its derivative $\dot{T}_w$ is possible, for example, on vehicles with individual electrical wheel drive, when the mechanical parameters can be replaced by their electrical analogs. If vehicles with mechatronic driveline systems are equipped with torque sensors, then they should be definitely used in the system for assessing $\dot{\lambda}_w$. As an illustration, Figure 7.12 presents an experimental curve of T_w obtained in testing a 4×4 SUV on a 4×4 chassis dynamometer that is described in Chapter 8.

This figure also shows the derivatives $\dot{T}_w$ obtained from value of T_w for each 50 ms time interval.

When no torque sensors are available on conventional vehicles, it is possible to use an algorithm that does not require data on T_w, but utilizes data on the angular velocity (acceleration) for determining the wheel's T_w. Such an algorithm, constructed on the principles of inverse dynamics of the wheel was analyzed in Section 7.2 for the case control of the angular velocity of the wheel.

There exists still another interesting aspect in assessing road conditions for the design of mechatronic driveline systems. If the front wheels of a vehicle propelled in a straight line by two driving axles find themselves in poor gripping conditions with the surface of

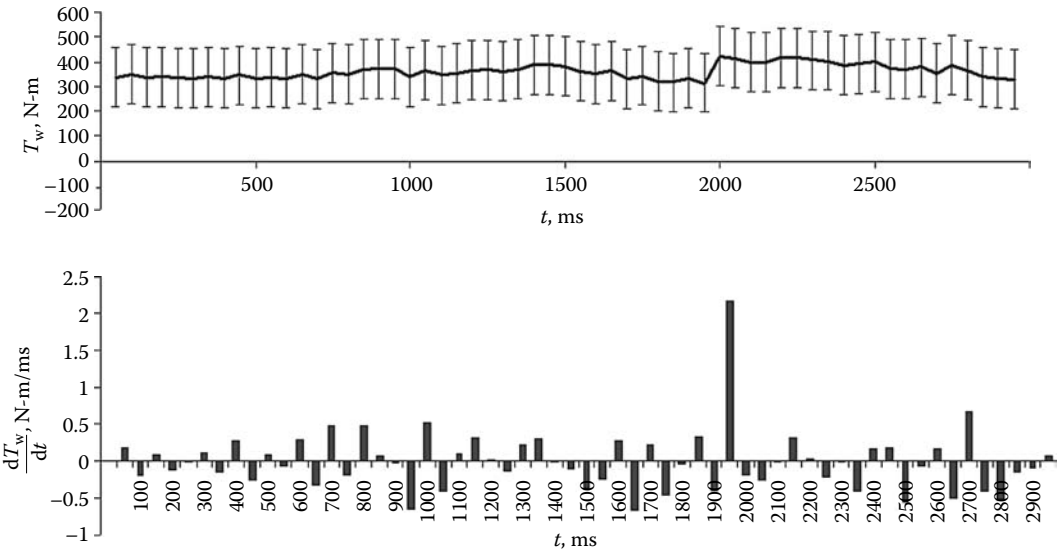


FIGURE 7.12
The torque and its derivative with respect to time for a P265/70R17 tire.

motion, then the rear wheels will also be subject to the same conditions after a time segment t that depends on the vehicle velocity V_x and the length l_2 of the wheelbase. If it is assumed that $V_x = \text{const}$, then the time that t should be used for such control of the mechatronic system that would improve the vehicle's performance up to deterioration of the gripping conditions of the rear wheels is:

$$t = l_2/V_x \tag{7.21}$$

Figure 7.13 shows the time t (a ''time delay'' of a kind) as a function of V_x and l_2 for vehicles of different classes and purposes: passenger cars, trucks, and military vehicles.

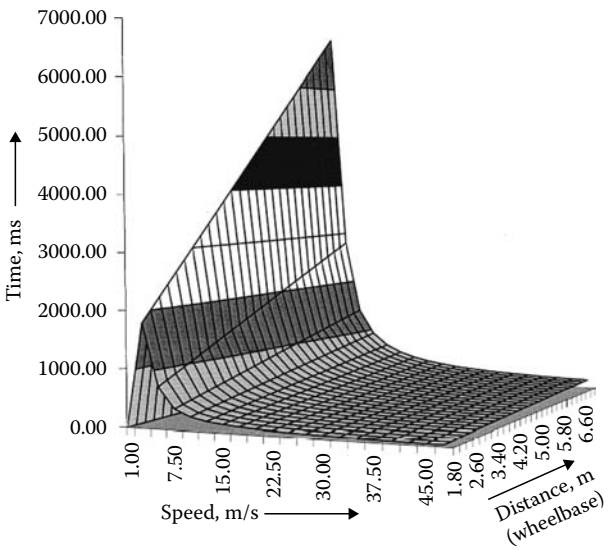


FIGURE 7.13
''Time delay'' between front and rear wheels.

Thus, the requirements of the systems of assessment of wheel gripping conditions formulated above should be used in working out algorithms for the control of PDUs of mechatronic driveline systems. The details needed for this were discussed in this section.

7.4 Kinematics and Dynamics of Mechanical Subsystems

Mechanical subsystems of contemporary mechatronic systems for dividing power among the driving axles and the left and right wheels of these axles consist of planetary transmissions with limited friction clutches. Work in this direction started as early as the 1980s for terrain all-wheel drive vehicles, but did not go past test specimens. The idea as such of designing planetary transmissions with controlled friction elements has been rooted in work on planetary gearboxes and differential turning mechanisms of tracked vehicles that started as early as the beginning of the twentieth century. Various systems were actively used in tanks and other tracked vehicles already during World War II.

Some of the differential turning mechanisms have an advantage, as they do not put a significant additional load on the engine when the vehicle turns. Here the power in the friction clutches is not expended only in friction but may be transmitted as recuperation power to the outer track. Figure 7.14 proves that differential turning mechanisms require lower torque as compared with side friction clutches for executing a turn of a given tank.

A feature specific to differential turning mechanisms is the fact that in the turning of a tracked vehicle the velocity of the inner track decreases and that of the outer track increases as compared with the velocity of both tracks when moving in a straight line. This property made it possible to use such a system in wheeled vehicles, but then as a part of mechatronic systems, this is used for distributing the power among the wheels. The relative flexibility of differential turning mechanisms in distributing power between their output shafts combined with electronic controls make them attractive for advanced engineering developments.

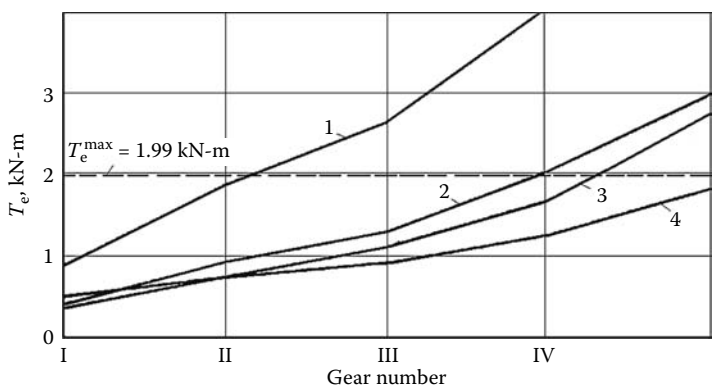


FIGURE 7.14
Engine torque T_e needed by a tank to perform a turn: 1, side friction clutches; 2, double differential; 3, two-stage planetary turning mechanism; 4, German Panther-type turning mechanism.

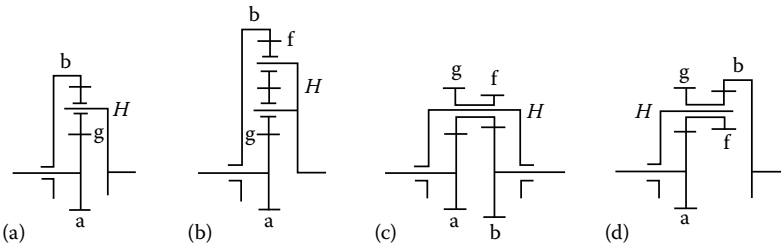


FIGURE 7.15
Planetary gear drives.

It is useful to precede the consideration of specific systems by recalling general information on kinematic and power features of three-link planetary transmissions. These data were given partially in Section 2.1 for open differential mechanisms. For any of the planetary transmissions in Figure 7.15 the angular velocities ω_a and ω_b of elements a and b with carrier H assumed to be stationary are interrelated as:

$$(\omega_a - \omega_H)/(\omega_b - \omega_H) = i_{ab}^H \tag{7.22}$$

whence follows that

$$\left(1 - i_{ab}^H\right)\omega_H = \omega_a - i_{ab}^H \omega_b \tag{7.23}$$

where, the constant i_{ab}^H is known as the internal gear ratio u_d.

Planetary transmission design parameter K introduced in Section 2.1 for open differentials is usually defined as the absolute numerical value of the ratio of angular velocity ω_a to angular velocity ω_b ($\omega_a > \omega_b$, see Figure 7.15) with the carrier stationary ($\omega_H = 0$). Design parameter K for transmissions with single-ring planetary pinions (Figure 7.15a) or pair planetary pinions (Figure 7.15b) is determined as the ratio of the number of teeth:

$$K = \frac{z_b}{z_a} \tag{7.24}$$

For transmissions with two-ring planetary pinions (Figure 7.15c and d)

$$K = \frac{z_b}{z_a}\frac{z_g}{z_f} \tag{7.25}$$

The design parameter is always positive ($K \geq 1$). Recall that K is equal to the differential's gear ratio u_d introduced in Section 2.1.

Referring to formulae (7.22) through (7.25), consider the relationships between torques T_a, T_b, and T_H at the three elements of the planetary gear sets. It is assumed that all the links rotate at constant angular velocities and that there are no power losses within the transmissions. Then from considerations of balance and of conservation of energy,

$$\begin{aligned} T_a + T_b + T_H &= 0 \\ T_a\omega_a + T_b\omega_b + T_H\omega_H &= 0 \end{aligned} \tag{7.26}$$

It is found from formulae (7.26) that

$$T_{\mathrm{a}}(\omega_{\mathrm{a}} - \omega_H) + T_{\mathrm{b}}(\omega_{\mathrm{b}} - \omega_H) = 0 \tag{7.27}$$

Upon substitution of (7.22), formula (7.27) becomes:

$$i_{\mathrm{ab}}^H T_{\mathrm{a}} + T_{\mathrm{b}} = 0 \tag{7.28}$$

Substitution of the expression for T_{b} from formula (7.28) into the first formula of (7.26) yields

$$\left(1 - i_{\mathrm{ab}}^H\right) T_{\mathrm{a}} + T_H = 0 \tag{7.29}$$

Formulae (7.28) and (7.29) relate the torques acting on elements of the planetary transmissions.

The general nature of formulae (7.22), (7.23), (7.28), and (7.29) is now demonstrated for the case of automotive differentials for which i_{ab}^H is negative (i.e., elements a and b rotate in opposite directions when carrier H is does not rotate);

$$i_{\mathrm{ab}}^H = -K \tag{7.30}$$

where, K is determined from formulae (7.24) and (7.25). For symmetrical differentials ($K = 1$) formula (7.22) yields:

$$2\omega_H = \omega_{\mathrm{a}} + \omega_{\mathrm{b}} \tag{7.31}$$

or reverting to the notation in Section 2.1

$$\omega_0 = \frac{\omega' + \omega''}{2} \tag{7.32}$$

Formula (7.32) is identical to formula (2.10). From formula (7.28) for symmetrical differentials follows:

$$T_{\mathrm{a}} = T_{\mathrm{b}} \tag{7.33}$$

that is, $T' = T''$, as was shown in Section 2.1.

For asymmetrical differentials, formula (7.22), upon substitution of formula (7.30) and the notation $\omega_H = \omega_0, \omega_{\mathrm{a}} = \omega', \text{and } \omega_{\mathrm{b}} = \omega''$, becomes:

$$\omega_0 = \frac{\omega' + K\omega''}{(1 + K)} \tag{7.34}$$

With reference to the fact that $K = u_{\mathrm{d}}$ (u_{d} is the gear ratio of the differential) formula (7.34) takes the form of formula (2.9):

$$\omega_0 = \frac{\omega' + u_{\mathrm{d}}\omega''}{(1 + u_{\mathrm{d}})} \tag{7.35}$$

In accordance with formulae (7.28) and (7.30), the torques at the shafts of the asymmetrical differential are related as

$$T_b/T_a = K \tag{7.36}$$

or, designating $T_a = T'$ and $T_b = T''$ and substituting formula (7.24) yields formula (2.27):

$$\frac{T''}{T'} = K = u_d \tag{7.37}$$

7.4.1 The Open Differential

The open differential was used in early tank designs as the turning mechanism. However, cases were observed during WWII that turning caused tank engines to stall. This stems from the fact that open differentials put a rather heavy load on the engines. Open differentials are not currently used on tanks.

For many decades now, certain farm wheeled tractors are equipped with two brake pedals. This is done to markedly decrease the turning radius of tractors: turning is implemented in the ''tank manner,'' that is, about a stopped wheel. When a tractor operates across a slope the use of separate braking of wheels makes it possible to brake the upper, slipping wheel that bears a lower normal load. It is most likely that the concept of separate braking of the wheels of tractors became the basis for the evolvement of current traction control systems and stability control systems.

In many mechatronic systems braking of the slipping wheel and locking of differentials occur after the differences in the angular velocities of the wheels exceeds a certain threshold value. This section demonstrates the shortcomings of this method and suggests a more effective concept for designing control algorithms.

Formulae (2.15) were obtained in Section 2.1 for determining the angular velocities ω' and ω'' of the output shafts of an open differential in a 4×2 rear-wheel drive vehicle. Figure 7.16a shows a schematic diagram of a rear-driving axle with an open differential that allows illustrating formulae (2.15).

Note that in Figure 7.16a the angular velocities of the output shafts ω' and ω'' are equal to the angular velocities of the wheels ω'_w and ω''_w. It is obvious that the difference $|\omega' - \omega''|$ depends on the angular velocity ω_0 of the differential's case. This leads to the non-uniqueness of a threshold value of $\Delta_{|\omega'-\omega''|}$, exceeding which the slipping wheel should slow down or the axle's differential should lock. In other words, the value of $\Delta_{|\omega'-\omega''|}$ should be different at different values of ω_0.

It may be noted that the ratio ω'/ω'' is independent of the differential's velocity ω_0. For this reason, it is advisable to lock the differential and brake the slipping wheel when ratio ω'/ω'' exceeds the threshold value of $\Delta_{\omega'/\omega''}$. This threshold value is related only to geometric parameters: the tread t_B and the theoretical turning radius R_t. If the turning radius is expressed in terms of the vehicle's base length l_2 and the turning angle δ

$$R_t = l_2/\tan\delta \tag{7.38}$$

then the threshold value $\Delta_{\omega'/\omega''}$ will be found from formulae (2.15) and (7.38):

$$\begin{aligned}\Delta_{\omega'/\omega''} &= \frac{1+\frac{t_B}{2R_t}}{1-\frac{t_B}{2R_t}} = \frac{2l_2/\tan\delta + t_B}{2(l_2/\tan\delta)} \frac{2(l_2/\tan\delta)}{2(l_2/\tan\delta) - t_B} \\ &= \frac{2l_2 + t_B\tan\delta}{\tan\delta} \frac{\tan\delta}{2l_2 - t_B\tan\delta} = \frac{2l_2 + t_B\tan\delta}{2l_2 - t_B\tan\delta}\end{aligned} \tag{7.39}$$

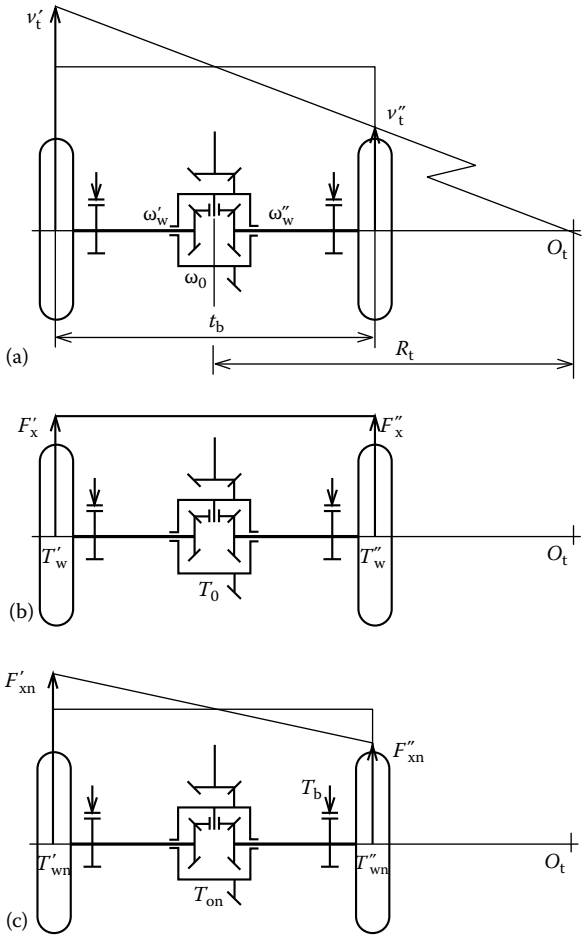


FIGURE 7.16
Drive axle with open differential: (a) kinematics; (b) torque/force analysis in turn; (c) torque/force analysis with a brake engaged.

Formula (7.39) is convenient because, for known l_2 and t_B, $\Delta_{\omega'/\omega''}$ is determined solely by the uniqueness of the relationship $\Delta_{\omega'/\omega''} = f(l_2, t_B, \delta)$ from this formula. In view of the above, it is advisable to replace $\Delta_{|\omega'-\omega''|}$ in the differential's locking and slipping wheel braking algorithm by the quantity $\Delta_{\omega'/\omega''}$ that is determined from formula (7.39), in which angle δ can be easily defined in terms of the turning angle of the steering wheel.

The axle's turning radius R_t can be expressed from the axle's velocity diagram (Figure 7.16a) with allowance for the fact that $\omega_0 = 0.5(\omega' + \omega'')$:

$$R_t = 0.5 t_B \frac{V'_t + V''_t}{V'_t - V''_t} = 0.5 t_B \frac{\omega' + \omega''}{\omega' - \omega''} = t_B \frac{\omega_0}{\omega' - \omega''} \tag{7.40}$$

If the right-wheel brake is actuated ($\omega'' = 0, \omega' = 2\omega_0$), then the minimum turning radius is equal to one-half of the axle's tread:

$$R_{t\,min} = 0.5 t_B \tag{7.41}$$

The next step consists of force analysis of an open differential. It was shown in Section 2.1 that if internal friction losses in the bearings and in the gear meshing are neglected, then the torque T_0 transmitted to the differential's case is divided in equal halves between the side gears in the direction from these gears to the axle halves and the wheels:

$$\begin{aligned} T'_{\mathrm{w}} &= T''_{\mathrm{w}} \\ T_0 &= T'_{\mathrm{w}} + T''_{\mathrm{w}} \end{aligned} \tag{7.42}$$

If it is assumed that the rolling radii of the right and left wheels are the same $r_{\mathrm{w}}^{0\prime} = r_{\mathrm{w}}^{0\prime\prime} = r_{\mathrm{w}}^{0}$, then the circumferential forces of the wheels in steady motion are the same (Figure 7.16b):

$$F'_{\mathrm{x}} = F''_{\mathrm{x}} = \frac{T'_{\mathrm{w}}}{r_{\mathrm{w}}^{0}} = \frac{T''_{\mathrm{w}}}{r_{\mathrm{w}}^{0}} = \frac{T_0}{2r_{\mathrm{w}}^{0}} \tag{7.43}$$

The actuation of one of the brakes (see Figure 7.16c) brings about the appearance of braking torque T_{b} that presents additional resistance to motion. The torque needed to cause the axle to move with one of the wheels immobilized is greater than the torque given by formula (7.42). The new value of T_0 is:

$$T_{0n} = T_0 + T_{\mathrm{b}} = T'_{\mathrm{w}} + T''_{\mathrm{w}} + T_{\mathrm{b}} \tag{7.44}$$

Torque T_{0n} is distributed between the axle's wheels as follows:

$$\begin{aligned} T'_{\mathrm{w}n} &= 0.5T_{0n} \\ T''_{\mathrm{w}n} &= 0.5T_{0n} - T_{\mathrm{b}} \end{aligned} \tag{7.45}$$

From this the circumferential forces of the wheels (see Figure 7.16c) are:

$$\begin{aligned} F'_{\mathrm{x}n} &= \frac{T_{0n}}{2r_{\mathrm{w}}^{0}} \\ F''_{\mathrm{x}n} &= \frac{T_{0n}}{2r_{\mathrm{w}}^{0}} - \frac{T_{\mathrm{b}}}{r_{\mathrm{w}}^{0}} \end{aligned} \tag{7.46}$$

It is seen that $F'_{\mathrm{x}n} \neq F''_{\mathrm{x}n}$. This effect is utilized in traction control systems in which the slipping wheel is slowed down and a smaller torque $T''_{\mathrm{w}n}$ is transmitted, whereas the other wheel that finds itself in better gripping conditions transmits a larger torque $T'_{\mathrm{w}n}$.

The difference $(F'_{\mathrm{x}n} - F''_{\mathrm{x}n})$ induces an assisting yaw moment in the plane of the road that is determined from formulae (2.389) and Figure 7.16c:

$$M_{\mathrm{B}} = 0.5t_{\mathrm{B}}(F'_{\mathrm{x}n} - F''_{\mathrm{x}n}) \tag{7.47}$$

Upon substitution of formulae (7.46), this yaw moment becomes:

$$M_{\mathrm{B}} = \frac{T_{\mathrm{b}}t_{\mathrm{B}}}{2r_{\mathrm{w}}^{0}} \tag{7.48}$$

Yaw moment M_B is used in stability control systems for improving the stability of the vehicle's motion by decelerating the wheels, i.e. generating assisting or resisting yaw moments. The brake torque T_b and the power absorbed by the brake are of substantial magnitude, something that puts a large additional load on the engine.

7.4.2 Double Differentials

Tracked vehicles, in particular turning mechanisms of tanks, make use of double differentials. These, relatively simple mechanisms, provide quite satisfactory tracked-vehicle turning dynamics.

Interest in double differentials has appeared during the past several years as in mechanisms that can be utilized also in wheeled vehicles for redistributing power among the driving wheels. This section presents an analysis of kinematic and power relationships that describe the operation of the double differential in its use both in wheeled and tracked vehicles.

Figure 7.17a and b shows the kinematic diagrams of double differentials.

The double differential consists of an outer and inner differential. The gears of the outer differential with radius r_{go} are connected to braking mechanisms by means of hollow shafts. The pinions of the outer and inner differentials with radii r_{co} and r_{ci} are rigidly

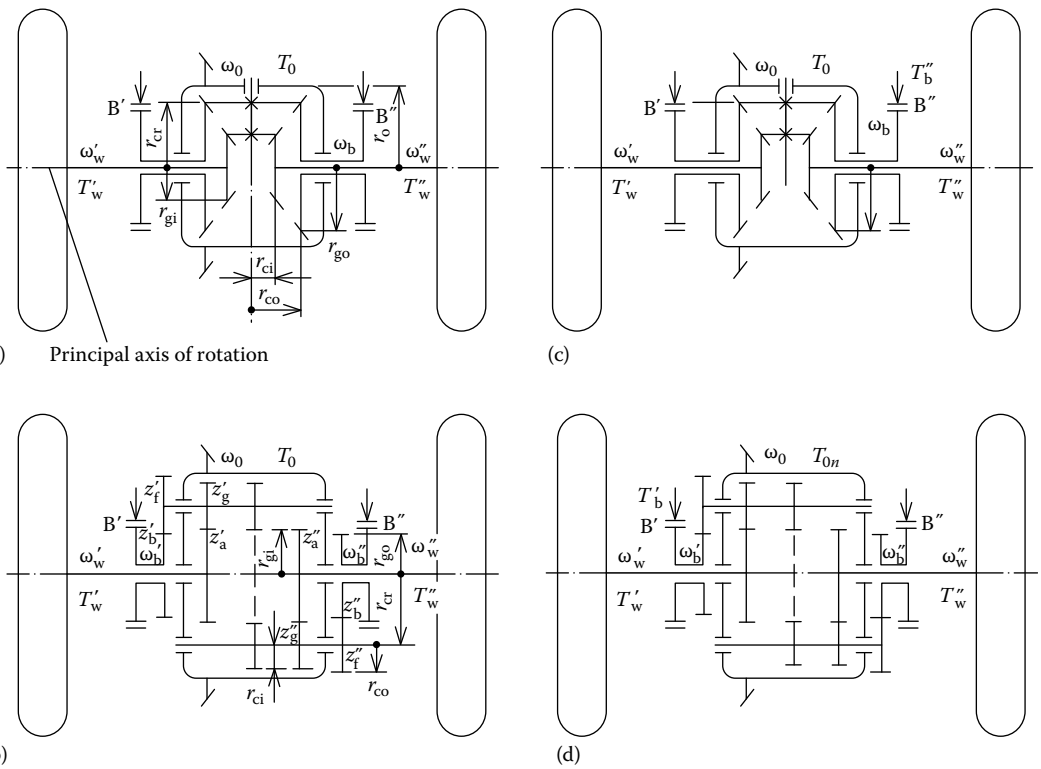


FIGURE 7.17
Bevel-gear and spur-gear double differentials: (a) and (b) rectilinear motion; (c) and (d) making a turn.

connected to one another by means of a common axis. The half axles are interconnected by means of gears with radii r_{gi} and the inner pinions are interconnected in the same manner as in an open symmetrical differential. If the outer differential and the braking mechanisms are removed, then the double differential becomes the simple (open) differential that was analyzed above.

In rectilinear motion of a vehicle, all the elements of the double differential have the same angular velocity ω_0 relative to the principal axis of rotation. Both brakes are disabled and hence the outer differential does not affect the operational functions of the double differential. The latter then operates as an open differential.

A tracked vehicle is made to turn by applying one of the brakes. For example, when making a right turn when the right brake is subjected to torque T_b'' (see Figure 7.17c) the angular velocity ω_w' of the shaft coupled to the outer track, increases, whereas the angular velocity ω_w'' of the shaft that drives the inner track decreases. Figure 7.17d corresponds to a left turn.

Turning of wheeled vehicles with steering systems and double differentials in the driving axles may be brought about by turning the steered wheels, and in principle, there is no need to operate the brakes of the double differential. However, if one of the axle's wheels finds itself under poor road conditions and starts spinning, then actuating the brake of the double differential that is located on the side of the slipping wheel will increase the torque at the second of the axle's wheels and thus improve the tractive and velocity properties of the vehicle. In addition, controlling the brakes of the double differential causes unequal torques and circumferential forces of the wheels that induce a yawing moment in the plane of the road, which may be used for controlling the stability of motion and turnability of the vehicle. Details of this are now considered.

The kinematic relationships are determined by constructing a diagram of the velocities of the outer pinion, both for the bevel-gear (Figure 7.18a) and spur-gear (Figure 7.18b) differentials.

The linear velocity of the center of the outer pinion in its rotation relative to the principal axis of the differential is $\omega_0 r_{cr}$. The linear velocity of the point of meshing between the pinion and the brake-side gear with angular velocity ω_b when it is located on the side of the center of turn of the vehicle is $\omega_b r_{go}$ (for a bevel-gear differential $r_{go} = r_{cr}$). These

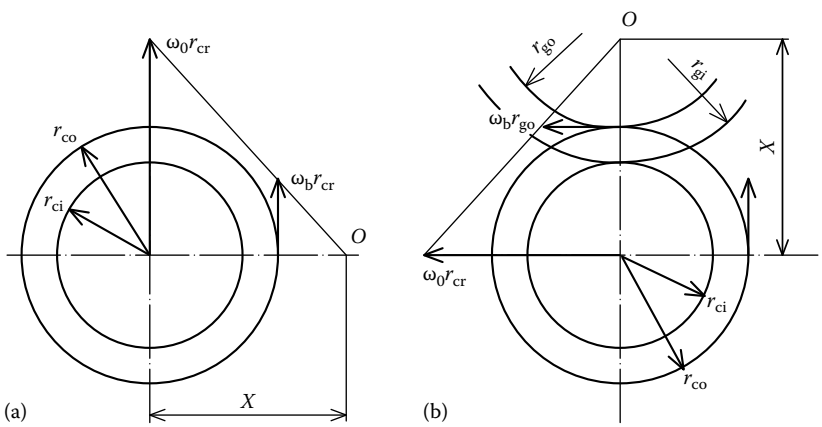


FIGURE 7.18
Velocity polygons of the outer pinions: (a) bevel-gear double differential; (b) spur-gear double differential.

vectors define the velocity diagram of the outer pinion in the plane of its rotation and its instantaneous center of rotation O.

Designating the angular velocity of the pinion as ω_c allows wiring the linear velocity of the center of the pinion as $\omega_c x$. Since $\omega_0 r_{go} = \omega_c x$, then

$$\omega_c = \omega_0 r_{cr}/x \tag{7.49}$$

The equality of linear velocities of the points of meshing of the side gear and the inner pinion in relative motion makes it possible to write that $\omega_{rel} r_{gi} = \omega_c r_{ci} i$. This yields

$$\omega_{rel} = \omega_c r_{ci}/r_{gi} = \omega_0 r_{cr} r_{ci}/(x r_{gi}) \tag{7.50}$$

where ω_{rel} is the angular velocity of the output shaft relative to the differential's case.

The absolute velocities of the output shaft connected to the wheels are

$$\begin{aligned} \omega' &= \omega_0 + r_{rel} = \omega_0\left(1 + \frac{r_{cr} r_{ci}}{x r_{gi}}\right) \\ \omega'' &= \omega_0 - r_{rel} = \omega_0\left(1 - \frac{r_{cr} r_{ci}}{x r_{gi}}\right) \end{aligned} \tag{7.51}$$

When the brake side gear does not rotate (fully stopped) and the vehicle turns with minimum radius $R_{t\,min}$, one can have $x = r_{co}$. Then

$$\begin{aligned} \omega'_{w\,max} &= \omega_0\left(1 + \frac{r_{cr} r_{ci}}{r_{co} r_{gi}}\right) = \omega_0\left(1 + u_{dd}^{-1}\right) \\ \omega'_{w\,min} &= \omega_0\left(1 - \frac{r_{cr} r_{ci}}{r_{co} r_{gi}}\right) = \omega_0\left(1 - u_{dd}^{-1}\right) \end{aligned} \tag{7.52}$$

where $u_{dd} = \dfrac{r_{co} r_{gi}}{r_{cr} r_{ci}}$ is the gear ratio of the double differential. For bevel-gear double differentials $r_{cr} = r_{go}$ and hence $u_{dd} = \dfrac{r_{co} r_{gi}}{r_{go} r_{ci}}$. Usually, u_{dd} ranges between 2 and 2.5. Note that gear ratio u_{dd} may also be expressed in terms of the number of teeth of the gears, for example, by compiling a gear ratio from gear b′ coupled to brake B′ to gear a′ coupled to the left wheel (see Figure 7.17b):

$$i^H_{b'a'} = \frac{\omega_{b'} - \omega_0}{\omega'_w - \omega_0} = \frac{z_{f'}}{z_{b'}} \frac{z_{a'}}{z_{g'}} = K = u_{dd} \tag{7.53}$$

where

$\omega_{b'}$ is the velocity of gear b′ coupled to brake B′

ω_0 is the angular velocity of the differential's case (this case is the same as link H in planetary transmissions in Figure 7.15)

ω'_w is the angular velocity of the left wheel coupled to gear a′, $\omega'_w = \omega_{a'}$

K is the design parameter

Gear ratio $i^H_{b'a''}$ from brake B′ to gear a″ is

$$i^H_{b'a''} = \frac{\omega_{b'} - \omega_0}{\omega''_w - \omega_0} = -\frac{z_{f'} z_{g''} z_{a''}}{z_{b'} z_{g'} z_{g''}} = -K = -u_{dd} \tag{7.54}$$

since $z_{a''} = z_{a'}$.

The analysis of formulae (7.52) is continued here. Dividing them term by term it is possible to obtain the ratio of angular velocities with a fully engaged brake that corresponds to turning of the vehicle with minimum turning radius $R_{t\,min}$:

$$\omega'_{w\,max}/\omega''_{w\,min} = \left(1 + u_{dd}^{-1}\right)/\left(1 - u_{dd}^{-1}\right) \tag{7.55}$$

On the other hand, it follows from the velocity diagram in the course of the vehicle's turn (see formulae (2.15)):

$$\omega'_{w\,max}/\omega'_{w\,min} = (R_{t\,min} + 0.5t_B)/(R_{t\,min} - 0.5t_B) \tag{7.56}$$

Simultaneous solution of formulae (7.55) and (7.56) yields:

$$R_{t\,min} = 0.5t_B u_{dd} \tag{7.57}$$

When the turning radius of the vehicle changes from infinity (in rectilinear motion) to $R_{t\,min}$, the angular velocity of gear b coupled to the brake goes from ω_0 to zero, whereas the angular velocity of the output shaft of the double differential, coupled to the inner wheel, goes from ω_0 to $\omega''_{w\,min}$. This means that, unlike an open differential, complete stopping of the side gear of the outer differential by means of a brake does not bring the inner wheel of the vehicle to a complete stop. For this reason, the minimum turning radii of a vehicle with a double differential will also be different from those when an open differential is used (see formulae (7.57) and (7.41)).

From Figure 7.18b yields

$$\omega_b r_{go}/(\omega_0 r_{cr}) = (x - r_{co})/x$$

whence,

$$\omega_b = \omega_0[(x - r_{co})/x](r_{cr}/r_{go}) \tag{7.58}$$

For a bevel-gear double differential from Figure 7.17a the last fraction r_{cr}/r_{go} in formula (7.58) cancels out since $r_{cr} = r_{go}$.

It follows from expression (7.58) that the angular velocity ω_b is (i) positive when $x > r_{co}$ (vehicle turning with incompletely stopped lagging brake gear), (ii) is equal to zero when $x = r_{c0}$ (turning with the brake gear fully stopped), and (iii) may take a negative value when x lies between r_{co} and r_{ci}. Here ω_b has the highest negative value when the inner half axle is stopped. Such a case is possible if outside forces are applied to cause the vehicle to perform a sharp turn such that the inner half axle stops.

Consider the torque balance in double differentials. When the vehicle travels in a straight line the torque T_0 at the differential's case is divided equally between the output shafts coupled to the wheels (the brakes of the double differential are not actuated, see Figure 7.17a and b):

$$T_0 = T'_w + T''_w$$
$$T'_w = T''_w \tag{7.59}$$

When the vehicle turns a brake torque T'_b or T''_b is applied to brake B′ or brake B″. Figure 7.17c shows the actuation of the right brake B″, which corresponds to a right turn of the vehicle. The torque balance about the principal axis of rotation of the double differential is written as (without allowance for internal friction in the elements)

$$T_0 = T'_w + T''_w + T_b \tag{7.60}$$

To determine the torques T'_w and T''_w, consider the equilibrium of a double pinion about the axis of its rotation. This analysis shall be performed for a double bevel-gear pinion consisting of an outer and an inner pinion shown in Figures 7.17a,c and 7.19.

The torque equilibrium equation about point O in Figure 7.19 is:

$$\frac{T'_w}{r_{gi}} r_{ci} = \frac{T''_w}{r_{gi}} r_{ci} + \frac{T''_b}{r_{go}} r_{co} \tag{7.61}$$

where

$\frac{T'_w}{r_{gi}}$ and $\frac{T''_w}{r_{gi}}$ are the tangential forces in the meshing between the inner pinion and the left and right side gears of the inner differential

$\frac{T''_w}{r_{go}}$ is the circumferential force in the meshing between the outer pinion and the outer side gear when the braking torque T_b is applied

$\frac{T_0}{r_o}$ is the circumferential force exerted on the axis of the double pinion by the differential's case

It can be noticed that both parts of Equation 7.61 should, in principle, be divided by the number of the double pinions in the double differential. This was not done because it does not affect the course of the discussion or the results obtained using formula (7.61). Indeed,

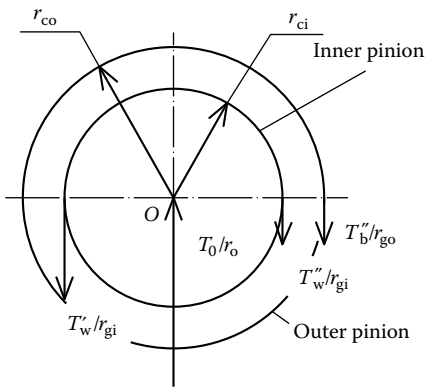


FIGURE 7.19
Double pinion equilibrium.

the number of double pinions can be cancelled out from the left and right hand sides of Equation 7.61.

Since $r_{cr} = r_{go}$ (see Figure 7.17a), formulae (7.60) and (7.61) are solved relative to the torques at the half axles of the bevel-gear double differential:

$$\begin{aligned} T'_w &= 0.5T_0 + 0.5T''_b(u_{dd} - 1) \\ T''_w &= 0.5T_0 - 0.5T''_b(u_{dd} + 1) \end{aligned} \tag{7.62}$$

Formulae for calculating torques T'_w and T''_{wn} can also be derived for spur-gear double differentials. This shall be done by a somewhat different method by examining a left turn, when brake B′ is actuated (Figure 7.17d).

It can be found from formulae (7.53) and (7.54) that:

$$\begin{aligned} (1 - K)\omega_0 &= \omega_{b'} - K\omega'_w \\ (1 + K)\omega_0 &= \omega_{b'} + K\omega''_w \end{aligned} \tag{7.63}$$

Solution of formulae (7.63) for ω_0 and $\omega_{b'}$ yields

$$\begin{aligned} \omega_0 &= \frac{1}{2}(\omega'_w + \omega''_w) \\ \omega_{b'} &= \frac{1}{2}(K + 1)\omega'_w - \frac{1}{2}(K - 1)\omega''_w \end{aligned} \tag{7.64}$$

The power balance in a turn (left turn, brake B′ is actuated) is now compiled neglecting power losses in the transmission links of the double differential and having reference to the fact that the braking power is always negative:

$$T'_w\omega'_w + T''_w\omega''_w = T_0\omega_0 - T'_b\omega_{b'} \tag{7.65}$$

Substitution of ω_0 and $\omega_{b'}$ from (7.64) into (7.65) yields:

$$T'_w\omega'_w + T''_w\omega''_w = \frac{1}{2}\left[T_0 - T'_b(K + 1)\right]\omega'_w + \frac{1}{2}\left[T_0 + T'_b(K - 1)\right]\omega''_w \tag{7.66}$$

Equating the coefficients of ω'_w and ω''_w from both parts of formula (7.66), finally yields:

$$\begin{aligned} T'_w &= 0.5T_0 - 0.5T'_b(K + 1) \\ T''_w &= 0.5T_0 + 0.5T'_b(K - 1) \end{aligned} \tag{7.67}$$

The outer wheel in formulae (7.67) is the right wheel (since a left turn is dealt with) and the torque T''_w at this wheel is greater than the torque T'_w at the left inner wheel. Formulae (7.62) reflect the torque for a right turn (brake B″ is actuated), that is, $T'_w > T''_w$.

It is seen from formula (7.62) that torque T''_w at the inner wheel (track) may take positive, zero, and negative values depending on the braking level provided by braking torque T''_b and the relationships between the terms in the right hand of the formula for T''_w. A similar analysis can be done for formula (7.67).

It can be seen from formula (7.62) that at $T''_w < 0$, then the circumferential force of the lagging wheel (track) is smaller than zero, $F''_x < 0$, the flow of power from this wheel (track) is not dissipated in the brake, but it is transmitted to the outer wheel (track). This became possible because of the existence of a kinematic coupling between the wheels (tracks) by means of the inner differential, whereas the connection between the engine and the brake is by means of the outer differential. This gives rise to power circulation along the loop: inner wheel (track)—inner differential—outer wheel (track)—road—inner wheel (track). This power recuperation markedly reduces the load on the engine. Here the power absorbed by the brake is smaller than when using an open differential and this indeed is the advantage of the double differential over an open one. The power flows and the course of recuperation are shown in Figure 7.20.

Now, the difference in torques T'_w and T''_w from formulae (7.62) causes a difference in the circumferential forces

$$F'_x = \frac{T'_w}{r^0_w}, \quad F''_x = \frac{T''_w}{r^0_w} \tag{7.68}$$

which is needed for implementing the turning of tracked and special wheeled vehicles in turn control mechanisms that employ double differentials. The force difference $\left(F'_x - F''_x\right)$ can also be used for controlling the dynamics of wheeled vehicles with steered wheels. Indeed if the force difference $\left(F'_x - F''_x\right)$ is expressed in terms of torques T'_w and T''_w, using formulae (7.68) and (7.62), then the yawing moment in the plane of the road will be given by formula (2.389):

$$M_B = \frac{T_b t_b}{2r^0_w} u_{dd} \tag{7.69}$$

It can be observed by comparing formulae (7.69) and (7.48) that in order to obtain the required value of M_B, the brake torque will be smaller by a factor of u_{dd} with the double differential than with an open differential. From this, it follows that the size of the brake that provides torque T_b will be smaller when using the double differential.

The power losses in a double differential are now estimated. The power supplied to its case is

$$P_0 = T_0 \omega_0 \tag{7.70}$$

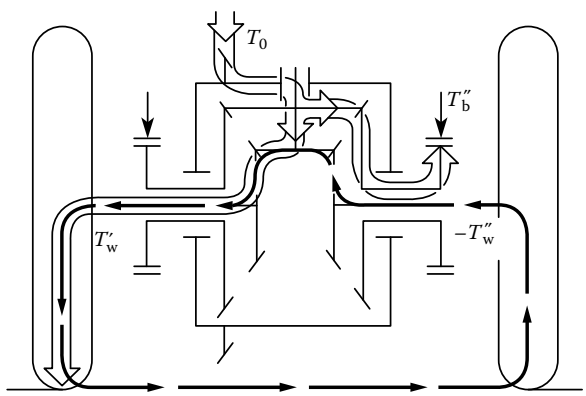


FIGURE 7.20
Recuperation of power in a double differential at $T''_w < 0$.

whereas, the power supplied by this mechanism to the wheels is expressed as

$$P_{in\Sigma} = T'_w\omega'_w + T''_w\omega''_w \tag{7.71}$$

When making a left turn, which involves actuating brake B′, the wheel torques are given by formulae (7.67). Substitution of expressions for T'_w and T''_w from (7.67) into (7.71) yields:

$$P_{in\Sigma} = T_0\omega_0 - T'_b(K+1)\omega_0 + T'_bK\omega''_w \tag{7.72}$$

When making a left turn the angular velocity ω''_w is the velocity of the right, outer wheel that, upon substitution of formulae (2.15), is obtained from the expression (it should be remembered that formulae (2.15) were derived for a right turn):

$$\omega''_w = \omega_0\left(1 + \frac{t_B}{2R_t}\right) = \omega_0\left(1 + \frac{1}{\rho}\right) \tag{7.73}$$

Formula (7.73) introduces the relative turning radius $\rho = 2R_t/t_B$ of the center of the driving axle. Substitution of (7.73) into Equation 7.73 yields

$$P_{in\Sigma} = \left[T_0 - T'_b\left(1 - \frac{K}{\rho}\right)\right]\omega_0 \tag{7.74}$$

Then, neglecting internal power losses in the gearings and bearings of the double differential, its efficiency when the axle makes a left turn by actuating the brake is determined from the expression

$$\eta = \frac{P_{in\Sigma}}{P_0} = 1 - \frac{T'_b}{T_0}\left(1 - \frac{K}{\rho}\right) \tag{7.75}$$

Similarly, upon a right turn of the axle, when brake B″ with braking torque T''_b is actuated, the efficiency is:

$$\eta = 1 - \frac{T''_b}{T_0}\left(1 - \frac{K}{\rho}\right) \tag{7.76}$$

It is seen from formulae (7.75) and (7.76) that if design parameter K, calculated from formula (7.53) is selected to be as given by the expression

$$K = \frac{z_{f'}}{z_{b'}}\frac{z_{a'}}{z_{g'}} = \frac{2R_{t\,min}}{t_B} = \rho_r \tag{7.77}$$

then, when making a turn with a minimum radius $R_{t\,min}$ it is possible to attain $\eta = 1$ (if internal losses within the differential are neglected).

7.4.3 The Open Differential with Three-Link Planetary Rows

This PDU includes a symmetrical bevel-gear differential *abH*, two additional three-link planetary mechanisms (TPM) a′b′H' and a″b″H'' and two brakes B′ and B″ (Figure 7.21).

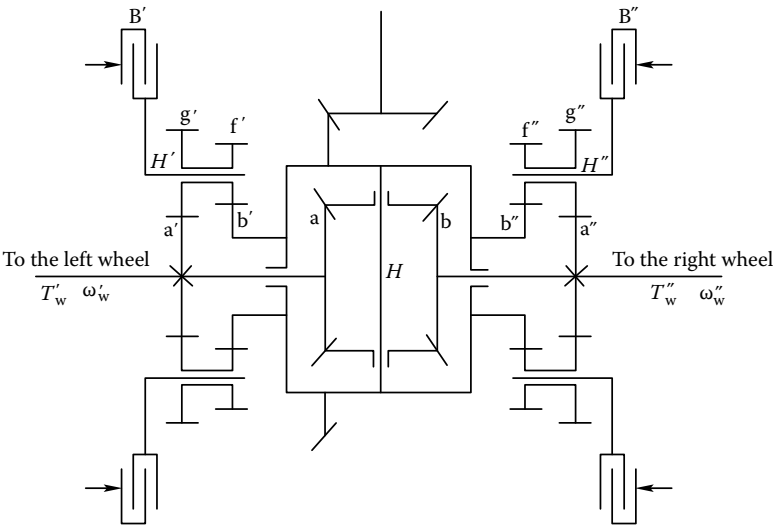


FIGURE 7.21
Open differential with two three-link planetary mechanisms.

The kinematic coupling equations for a symmetrical differential with internal gear ratio $i^H_{ab} = -1$ is

$$2\omega_H = \omega_a + \omega_b \tag{7.78}$$

Links a and b are rigidly linked to the wheels for which reason $\omega_a = \omega'_w$ and $\omega_b = \omega''_w$. Link H is rigidly linked to the differential's case that rotates at angular velocity $\omega_0 = \omega_H$. Formula (7.78) can be rewritten in the form:

$$2\omega_0 = \omega'_w + \omega''_w \tag{7.79}$$

The kinematic coupling equation of additional TPM with the same positive internal gear ratio ($i_{a'b'} = i_{a''b''} = K$) is

$$(1 - K)\omega_{H'} = \omega_{a'} - K\omega_{b'} \tag{7.80}$$

$$(1 - K)\omega_{H''} = \omega_{a''} - K\omega_{b''} \tag{7.81}$$

It follows from the diagram in Figure 7.21 that $\omega'_a = \omega'_w$ and $\omega''_a = \omega''_w$. Transforming formulae (7.80) and (7.81) yields

$$(K - 1)\omega_{H'} = K\omega_0 - \omega'_w \tag{7.82}$$

$$(K - 1)\omega_{H''} = K\omega_0 - \omega''_w \tag{7.83}$$

The angular velocities $\omega_{H'}$ and $\omega_{H''}$ are equal to the angular velocities of slip of friction elements of brakes B′ and B″, respectively

$$\omega_{H'} = \frac{K\omega_0 - \omega'_w}{K - 1} \tag{7.84}$$

$$\omega_{H''} = \frac{K\omega_0 - \omega''_w}{K - 1} \tag{7.85}$$

Substitution of ω'_w and ω''_w from formulae (2.15) into formulae (7.84) and (7.85) yields

$$\omega_{H''} = \frac{K - 1 + t_B/(2R_t)}{K - 1}\omega_0 = \left[1 + \frac{t_B}{2R_t(K-1)}\right]\omega_0 \tag{7.86}$$

$$\omega_{H'} = \left[1 - \frac{t_B}{2R_t(K-1)}\right]\omega_0$$

It follows from the last expression that when a vehicle turns with the radius $R_t = R_{t\ min}$ the sliding velocity of friction elements of the actuated brake B′ is $\omega_{H'} = 0$, if

$$K = 1 + \frac{t_B}{2R_{t\ min}} \tag{7.87}$$

Reduction of irreversible sliding losses in brakes requires selecting the design parameter of each additional TPM from formula (7.87), rounded off to the next highest number. Then when making a turn with radius $R_t > R_{t\,min}$ the torque exerted on the brake by the carrier of the additional TPM is equal in magnitude to the friction torque of the brake and is directed in the same direction as torque T_0 acting on the differential's case.

Then for the case of a right turn, the balance equations of the torques of the left additional TPM are:

$$\begin{aligned} (1 - K)T_{a'} + T_{H'} &= 0 \\ KT_{a'} + T_{b'} &= 0 \end{aligned} \tag{7.88}$$

Solution of Equations 7.88 yields

$$T_{a'} = \frac{1}{K-1}T_{H'} \tag{7.89}$$

$$T_{b'} = -\frac{K}{K-1}T_{H'} \tag{7.90}$$

The balance equations of the differential

$$\begin{aligned} (1 + K)T_a + T_H &= 0 \\ -KT_a + T_b &= 0 \end{aligned} \tag{7.91}$$

Since, the design parameter K for a symmetrical differential is equal to 1, solution of formula (7.91) yields

$$T_a = T_b \tag{7.92}$$

$$T_H = -2T_a \tag{7.93}$$

It follows from the equilibrium of the differential's case that

$$T_0 + T_H + T_{b'} = 0 \tag{7.94}$$

Substitution of formulae (7.90), (7.92), and (7.93) yields

$$T_{\mathrm{a}} = T_{\mathrm{b}} = 0.5\left(T_0 - \frac{K}{K-1}T_{H'}\right) \tag{7.95}$$

Torque T'_{w} applied to the left, advancing half axle by the PDU

$$T'_{\mathrm{w}} = T_{\mathrm{b}} + T_{\mathrm{a}'} = 0.5\left(T_0 - \frac{K}{K-1}T_{H'}\right) + \frac{1}{K-1}T_{H'} \tag{7.96}$$

Torque T''_{w} applied to the right, lagging half axle by the PDU

$$T''_{\mathrm{w}} = T_{\mathrm{a}} + T_{\mathrm{a}'} = 0.5\left(T_0 - \frac{K}{K-1}T_{H'}\right) \tag{7.97}$$

Here $T_{\mathrm{a}'} = 0$ since brake B″ is disengaged.

It is seen that $T'_{\mathrm{w}} > T''_{\mathrm{w}}$, that is, the torque at the left, advancing wheel is higher than at the lagging right wheel. Such a relationship between torques and, accordingly, between the circumferential forces of the wheels increases vehicle oversteering.

The difference in the torques at the axle halves in the course of a turn is

$$\Delta T_{\mathrm{w}} = T'_{\mathrm{w}} - T''_{\mathrm{w}} = \frac{1}{K-1}T_{H'} \tag{7.98}$$

The total torque at the axle halves in the course of a turn is

$$T_{\mathrm{w}\Sigma} = T'_{\mathrm{w}} + T''_{\mathrm{w}} = T_0 - T_{H'} \tag{7.99}$$

whence, the torque supplied to the differential's case is

$$T_0 = T_{\mathrm{w}\Sigma} + T_{H'} \tag{7.100}$$

Now consider a situation when brake B′ is locked only partially, but not fully, that is, the friction elements of brake B′ are sliding relative to one another. In this case, the braking power is dissipated as heat to the surroundings. This reduces the efficiency of the PDU. Power P_0 supplied to the PDU is

$$P_0 = T_0\omega_0 = (T_{\mathrm{w}\Sigma} + T_{H'})\omega_0 \tag{7.101}$$

The power removed from the PDU neglecting the losses in the gear meshings and in the bearing is actually the power that is supplied to the axle's wheels:

$$\begin{aligned} P^{\mathrm{in}}_{\mathrm{w}\Sigma} &= T''_{\mathrm{w}}\omega''_{\mathrm{w}} + T'_{\mathrm{w}}\omega'_{\mathrm{w}} = \left(T''_{\mathrm{w}} + T'_{\mathrm{w}}\right)\omega_0 + T'_{\mathrm{w}} - T''_{\mathrm{w}}\left(\omega'_{\mathrm{w}} - \omega''_{\mathrm{w}}\right) \\ &= T_{\mathrm{w}\Sigma}\omega_0 + T_{H'}\left(\omega'_{\mathrm{w}} - \omega''_{\mathrm{w}}\right)/(K-1) \end{aligned} \tag{7.102}$$

Then the efficiency of the PDU, corrected for energy losses only, in the actuated brake is:

$$\eta_{\mathrm{PDU}} = \frac{P^{\mathrm{in}}_{\mathrm{w}\Sigma}}{P_0} = \frac{T_{\mathrm{w}\Sigma} + T_{H'}\left(\omega'_{\mathrm{w}} - \omega''_{\mathrm{w}}\right)/(\omega_0(K-1))}{T_{\mathrm{w}\Sigma} + T_{H'}} \tag{7.103}$$

It may be assumed that, when turning at radius R_t on a dry asphalt road, the difference in the angular velocities of the wheels is given by formula (2.15):

$$\omega'_w - \omega''_w = \frac{t_B}{R_t}\omega_0 \tag{7.104}$$

If it is assumed that $K = 1 + \frac{t_B}{2R_{t\min}}$, then

$$\eta_{PDU} = \frac{T_{w\Sigma} + 2T_{H'}R_{t\min}/R_t}{T_{w\Sigma} + T_{H'}} \tag{7.105}$$

Note that in the case of $R_t = R_{t\min}$ and fully activated brake B′($T_{H'} = 0$), $\eta_{PDU} = 1$.

If the advancing wheel (the left wheel in the case under consideration) finds itself in the course of the turn on a slippery part of the road, then its angular velocity may become $\omega'_w > K\omega_0$ because of slippage. Then, according to formula (7.84), the sliding velocity $\omega_{H'}$ of the friction elements of brake B′ changes sign. The direction of friction torque $T_{H'}$ at the brake shaft changes accordingly. In this case, torque T''_w at the lagging wheel becomes greater than torque T'_w at the advancing wheel:

$$T''_w = 0.5\left(T_0 + \frac{K}{K-1}T_{H'}\right) \tag{7.106}$$

$$T'_w = 0.5\left(T_0 + \frac{K}{K-1}T_{H'}\right) - \frac{1}{K-1}T_{H'}$$

The total torque at the wheels

$$T_{w\Sigma} = T'_w + T''_w = T_0 + T_{H'} \tag{7.107}$$

The torque at the differential's case

$$T_0 = T_{w\Sigma} - T_{H'} \tag{7.108}$$

7.4.4 Single-Row Planetary Mechanism with Mating Pinions

This PDU with single-row planetary mechanism ab$H$ and mating pinions (see Figure 7.22) has a positive internal gear ratio

$$i^H_{ab} = K = \frac{z_b}{z_a} \tag{7.109}$$

where, z_a and z_b are the number of teeth of gears a and b, respectively.

The left wheel of an axle with this PDU is coupled through the half axle to gear a, and the right wheel, whereas the right wheel is also coupled through the half axle and to the carrier H. Epicyclical gear b is rigidly fastened to the case of the three-link planetary mechanism that shall be termed the differential's case. This case, rotating at angular velocity ω_0, is connected to the right half axle through additional gear transmissions—a step-up and a step-down transmission. These transmissions are activated by means of couplings c2 and c3.

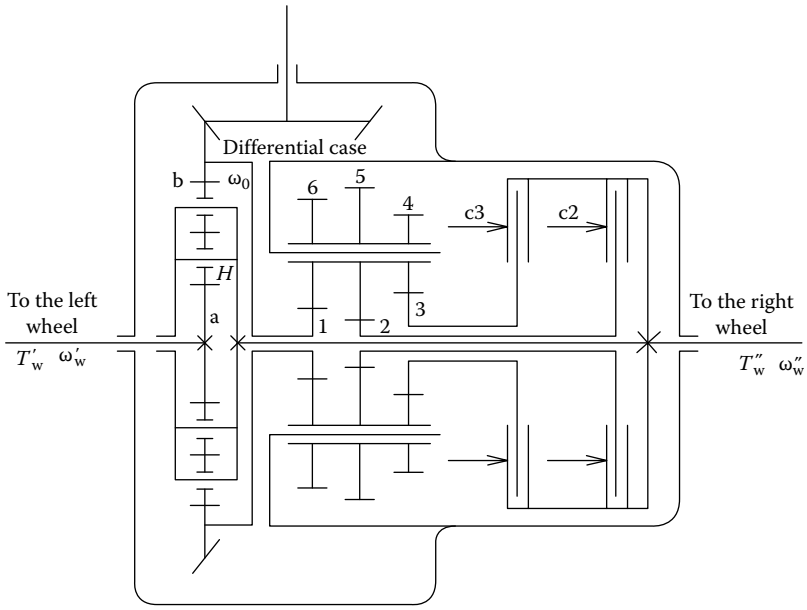


FIGURE 7.22
Single-row planetary mechanism with mating pinions.

The kinematic coupling equation of the PDU under consideration is:

$$(1 - K)\omega_H = \omega_a - K\omega_b \tag{7.110}$$

In the case of $K = 2$ formula (7.110) takes the same form as the kinematic coupling Equation 7.78 of a symmetrical differential.

The torque balance of such a PDU at $K = 2$ is given by the expressions:

$$T_a = T_H \tag{7.111}$$

$$T_b = -2T_a \tag{7.112}$$

Consider the operation of this PDU when the axle moves in the course of a turn.

Left turn. In this case step-up coupling c2 (with i_{21}) is actuated:

$$i_{21} = \frac{\omega_2}{\omega_1} = \frac{z_1}{z_6}\frac{z_5}{z_2} \tag{7.113}$$

where $\omega_1 = \omega_0$.

It is advisable to assume in designing such mechanisms (the fact that this is obvious shall be demonstrated further down in this section) that:

$$i_{21} = 1 + \frac{t_B}{2R_{t\min}} = 1 + \frac{1}{\rho_r} \tag{7.114}$$

where ρ_r is the dimensionless turning radius corresponding to the turning of the axle with a minimum radius $R_{\mathrm{t\,min}}$:

$$\rho_{\mathrm{r}} = \frac{2R_{\mathrm{t\,min}}}{t_{\mathrm{B}}} \tag{7.115}$$

Then

$$\omega_2 = \omega_0 i_{21} = \left(1 + \frac{1}{\rho_r}\right)\omega_0 \tag{7.116}$$

In a left turn, the wheel that advances is the right wheel and it rotates at angular velocity

$$\omega''_{\mathrm{w}} = \left(1 + \frac{1}{\rho}\right)\omega_0 \tag{7.117}$$

where, ρ is the dimensionless turning radius that corresponds to the turning of the axle with some radius $R_{\mathrm{t}} > R_{\mathrm{t\,min}}$, that is,

$$\rho = \frac{2R_{\mathrm{t}}}{t_{\mathrm{B}}} > \rho_r \tag{7.118}$$

It can be seen by comparing formulae (7.115) through (7.118) that $\omega_2 > \omega''_{\mathrm{w}}$. For this reason, the right advancing half shaft, coupled to the right wheel is subjected to friction torque T_{c2} of coupling c2 directed in the direction of rotation of ω''_{w} that adds up to the torque T_H. As a result the torque exerted by the PDU on the right wheel is:

$$T''_{\mathrm{w}} = T_{\mathrm{c2}} + T_H = T_{\mathrm{c2}} + T'_{\mathrm{w}} \tag{7.119}$$

Formula (7.119) was obtained by assuming that the gear ratio is such as given by formula (7.114).

The torque supplied to the left wheel by the PDU is obtained from the expression

$$T'_{\mathrm{w}} = T_{\mathrm{a}} \tag{7.120}$$

The torque exerted on gear z_1 that is rigidly fastened to the differential's case is:

$$T_1 = -i_{21} T_{\mathrm{c2}} \tag{7.121}$$

If the equation of equilibrium of the differential's case is written as

$$T_0 + T_1 + T_{\mathrm{b}} = 0 \tag{7.122}$$

and formulae (7.112) and (7.121) are substituted into it, then the torque at the differential's case is found to be

$$T_0 = 2T_{\mathrm{a}} + i_{21} T_{\mathrm{c2}} \tag{7.123}$$

If T_a is expressed by formula (7.123) and this expression is substituted into formulae (7.120) and (7.119), then it becomes possible to determine the wheel torques as a function of the input torque T_0 in the differential and of the friction torque T_{c2}:

$$T'_w = (T_0 - i_{21}T_{c2})/2 \tag{7.124}$$
$$T''_w = (T_0 - i_{21}T_{c2})/2 + T_{c2}$$

The total torque of the driving axle is

$$T_{w\Sigma} = T'_w + T''_w = T_0 - T_{c2}(i_{21} - 1) = T_0 - T_{c2}\frac{1}{\rho_r} \tag{7.125}$$

whence:

$$T_0 = T_{w\Sigma} + T_{c2}\frac{1}{\rho_r} \tag{7.126}$$

Formula (7.126) is convenient for determining torque T_0 (i.e., the load on the engine) from a known torque $T_{w\Sigma}$ determined from the resistance to motion and known T_{c2} and ρ_r.

The difference in the torques at the wheels is determined by the magnitude of the friction torque T_{c2}, which is seen from formula (7.124)

$$T_{c2} = T''_w - T'_w \tag{7.127}$$

Then it follows from formulae (7.125) and (7.127) that:

$$T''_w = (T_{w\Sigma} + T_{c2})/2$$
$$T'_w = (T_{w\Sigma} - T_{c2})/2 \tag{7.128}$$

As seen from formula (7.128), the wheel torques are determined by the total resistance to motion, represented by $T_{w\Sigma}$ and by T_{c2}—the friction torque in coupling c2.

The power supplied to the axle's wheels is

$$\begin{aligned} P^{in}_{w\Sigma} &= T''_w\omega''_w + T'_w\omega'_w \\ &= T_{w\Sigma}\frac{\omega''_w + \omega'_w}{2} + T_{c2}\frac{\omega''_w - \omega'_w}{2} \\ &= \left(T_{w\Sigma} + T_{c2}\frac{1}{\rho}\right)\omega_0 \end{aligned} \tag{7.129}$$

whereas, the power supplied to the PDU is given by the expression

$$P_0 = T_0\omega_0 = \left(T_{w\Sigma} + T_{c2}\frac{1}{\rho_r}\right)\omega_0 \tag{7.130}$$

Upon substitution of formulae (7.129) and (7.130) the efficiency of the PDU, neglecting the losses in couplings and bearings and taking into account only the losses of the sliding of friction elements in coupling c2, is:

$$\eta = \frac{P_{w\Sigma}^{in}}{P_0} = \frac{T_{w\Sigma} + T_{c2}\frac{1}{\rho}}{T_{w\Sigma} + T_{c2}\frac{1}{\rho_r}} \tag{7.131}$$

When making a turn with radius $R_{t\,min}$ when $\rho = \rho_r, \eta = 1$.

If, when making a left turn, the right, advancing wheel finds itself on slippery part of the road and its slippage increases, then T_{c2} changes sign at $\omega_2 < \omega''_w$. Then

$$\begin{aligned} T'_w &= \frac{T_{w\Sigma} + T_{c2}}{2} \\ T''_w &= \frac{T_{w\Sigma} - T_{c2}}{2} \end{aligned} \tag{7.132}$$

that is, the PDU operates as a limited-slip differential: the larger torque T'_w, is transmitted to the left wheel, which is under better road-gripping conditions.

Right turn. Now it is the left wheel that advances $(\omega'_w > \omega''_w)$. Step-down transmission coupling c3 is actuated

$$i_{31} = \frac{\omega_3}{\omega_0} = \frac{z_4}{z_3}\frac{z_1}{z_6} \tag{7.133}$$

It is advisable (for the same consideration as before) to assume that

$$i_{31} = 1 - \frac{1}{\rho_r} \tag{7.134}$$

Then

$$\omega_3 = i_{31}\omega_0 = \left(1 - \frac{1}{\rho_r}\right)\omega_0 \tag{7.135}$$

The right, lagging wheel rotates at an angular velocity

$$\omega''_w = \left(1 - \frac{1}{\rho}\right)\omega_0 \tag{7.136}$$

Because $\rho_r < \rho, \omega_3 < \omega''_w$ and the torque at the lagging wheel is

$$T''_w = T_H - T_{c3} \tag{7.137}$$

the torque at the left, advancing wheel:

$$T'_w = T_a = T_H \tag{7.138}$$

As in the case of the left turn, one can find

$$\begin{aligned} T'_w &= (T_{w\Sigma} + T_{c3})/2; \\ T''_w &= (T_{w\Sigma} - T_{c3})/2; \\ T_0 &= T_{w\Sigma} + T_{c3}\frac{1}{\rho_r} \end{aligned} \tag{7.139}$$

The efficiency of the PDU corrected only for losses in the sliding of the actuated coupling c3 is

$$\eta = \frac{P_{in\Sigma}}{P_0} = \frac{T_{w\Sigma} + T_{c3}/\rho}{T_{w\Sigma} + T_{c3}/\rho_r} \tag{7.140}$$

and becomes equal to 1 at $\rho = \rho_r$.

If the left wheel finds itself on a slippery part of the road and starts slipping, then at $\omega_3 > \omega''_w$ the coupling torque T_{c3} applied to the lagging wheel changes sign. Then

$$\begin{aligned} T'_w &= \frac{(T_{w\Sigma} - T_{c3})}{2}; \\ T''_w &= \frac{(T_{w\Sigma} + T_{c3})}{2} \end{aligned} \tag{7.141}$$

The larger torque is transmitted to the right wheel that is in better road gripping conditions.

7.5 Design of Simple and Combined Driveline Systems

This section is concerned with a method for synthesizing the characteristics of mechatronic systems for controlling the distribution of power among the driving wheels and with working out a control algorithm that can then be implemented in a programmable logic device. These problems are solved for the case of an 8×8 transportation vehicle—but the synthesis method presented here for compiling mathematical models should still be emphasized—the stages in the development and implementation of algorithms are general in nature and can be used also for other types of vehicles (traction, transportation-traction, see Table 1.19) and with other wheel formulae.

The objects of concern here are the simple and combined driveline systems. The simple system is represented by a fully differential drive system of the wheels of an 8×8 vehicle, the seven differentials of which (see formula (1.4)) may be automatically locked and unlocked. A vehicle with unlocked differentials has sufficient turnability and stability of motion under satisfactory gripping conditions. The currently employed locking of some or all differentials improves the mobility and tractive and velocity properties of the vehicle. The problem consists in determining those interwheel and interaxle differentials of the vehicle that should be locked or unlocked at a given point in time.

The combined driveline system under study here is explained by means of Figure 6.49, which represents the optimal mechanical driveline system and its PDUs. The combined mechatronic driveline system was compiled based on the above mechanical system in the following manner. The interaxle drive and the interwheel drives of the rear tandem remain mechanical, that is, such as they are shown in Figure 6.49. The remaining PDUs are taken to be mechatronic systems that lock and unlock the differentials installed in these units. Both systems—the simple and the combined, are shown in Figure 7.23.

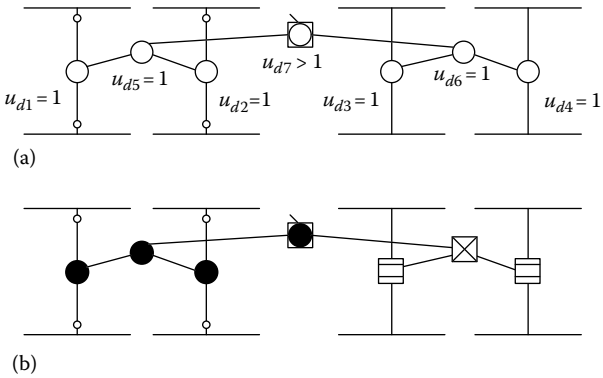


FIGURE 7.23
Simple (a) and combined (b) driveline systems of an 8×8 vehicle.

The principal stages of the studies, known as rapid prototyping of mechatronic systems, include:

1. Developing a method and synthesizing the characteristics of mechatronic systems for locking differentials on the basis of the solution of the problem of search of optimum power distributions among the wheels. This problem was solved in Section 6.6 and its results are used in the present section;
2. Development, verification, and optimizing of an algorithm for parallel control of locking/unlocking of differentials;
3. Hardware implementation of the parallel control algorithm in the form of a working prototype, using one of the existing Field Programmable Circuit technologies.

The optimum distribution of power among the wheels of the 8×8 vehicle under study should be determined by using the mathematical model described in Section 6.6.1. The results of these studies in the form of the statistical estimates of the optimal torque distribution factors (see formulae (6.23) and (6.24)) were analyzed in Section 6.6.2. These optimal torque distribution factors can be represented by some probabilistic functions such as:

$$\begin{aligned} K_{\text{mk}i} &= f_i(t), \quad i = 1,4 \\ K_{\text{mo}}^{1\text{-}2} &= f_{1\text{-}2}(t) \\ K_{\text{mo}}^{3\text{-}4} &= f_{3\text{-}4}(t) \\ K_{\text{mo}}^{1,2\text{-}3,4} &= f_{1,2\text{-}3,4}(t) \end{aligned} \tag{7.142}$$

The physical meaning of expressions (7.142) consists in the fact that, at any point in time t, there exist certain values of the factors of torque distribution between the wheels that correspond to optimum power distribution. Had the driveline system ensured a distribution of torques in accordance with functions (7.142) at any point in time, then the transportation efficiency η_x^{tr} of the running gear system of the vehicle would have been at a maximum, that is, the distribution of power among the wheels should be optimal.

Optimization of the distribution of power to the wheels should be supplemented by mathematical simulation of the motion of still another vehicle that has the same mass and

geometry and system features as the vehicle with optimum power distribution between the wheels. The second vehicle differs only by having a fully differential driveline system. The motion of both vehicles should be modeled under precisely identical on-road/off-road conditions. Both vehicles should have the same velocities of rectilinear motion at each point of time.

The efficiency of the running gear system of the second vehicle (with the differential driveline system) can be determined from formula (1.89), for which purpose the circumferential forces $F_{xi}^{\prime(\prime\prime)\mathrm{d}}, i = 1,4$ and their slippages $s_{\delta i}^{\prime(\prime\prime)\mathrm{d}}$ must be first calculated. Formulae for calculating the circumferential forces of wheels can be compiled using methods from Section 2.8 and with reference to Figure 7.23a:

$$\begin{aligned}
F_{xi}^{\prime\mathrm{d}} r_{wi}^{0\prime} &= F_{xi}^{\prime\prime\mathrm{d}} r_{wi}^{0\prime\prime}, \quad i = 1,4 \\
F_{x1}^{\prime\mathrm{d}} r_{w1}^{0\prime} + F_{x1}^{\prime\prime\mathrm{d}} r_{w1}^{0\prime\prime} &= F_{x2}^{\prime\mathrm{d}} r_{w2}^{0\prime} + F_{x2}^{\prime\prime\mathrm{d}} r_{w2}^{0\prime\prime} \\
F_{x3}^{\prime\mathrm{d}} r_{w3}^{0\prime} + F_{x3}^{\prime\prime\mathrm{d}} r_{w3}^{0\prime\prime} &= F_{x4}^{\prime\mathrm{d}} r_{w4}^{0\prime} + F_{x4}^{\prime\prime\mathrm{d}} r_{w4}^{0\prime\prime} \\
u_{\mathrm{d}7} &= \frac{F_{x3}^{\prime\mathrm{d}} r_{w3}^{0\prime} + F_{x3}^{\prime\prime\mathrm{d}} r_{w3}^{0\prime\prime} + F_{x4}^{\prime\mathrm{d}} r_{w4}^{0\prime} + F_{x4}^{\prime\prime\mathrm{d}} r_{w4}^{0\prime\prime}}{F_{x1}^{\prime\mathrm{d}} r_{w1}^{0\prime} + F_{x1}^{\prime\prime\mathrm{d}} r_{w1}^{0\prime\prime} + F_{x2}^{\prime\mathrm{d}} r_{w2}^{0\prime} + F_{x2}^{\prime\prime\mathrm{d}} r_{w2}^{0\prime\prime}} \\
F_{x\Sigma} &= \sum_{i=1}^{4} F_{xi}^{\prime(\prime\prime)}
\end{aligned} \tag{7.143}$$

In formulae (7.143) the total circumferential force $F_{x\Sigma}$ of the vehicle is assumed to be known, since it can be computed from formula (1.74).

The next step consists in calculating the slippage of all the eight wheels using the known functions $F_x = f(s_\delta)$. For example, the wheel slippage can be found from formula (1.26):

$$s_{\delta i}^{\prime(\prime\prime)} = -\frac{1}{k_i^{\prime(\prime\prime)}} \ln\left(1 - \frac{F_{xi}^{\prime(\prime\prime)}}{\mu_{pxi}^{\prime(\prime\prime)} R_{zi}^{\prime(\prime\prime)}}\right), \quad i = 1,4 \tag{7.144}$$

and then the probability functions

$$\begin{aligned}
&s_{\delta i}^{\prime\prime}/s_{\delta i}^{\prime} = f(t) \\
&i = 1,4
\end{aligned} \tag{7.145}$$

in which the ratio of slippages is determined by dividing the larger value by the smaller one, that is, $s_{\delta i}^{\prime\prime}/s_{\delta i}^{\prime}. > 1$, should be calculated.

Then the generalized slippages of the driving axles, the generalized slippages of the front and rear tandems, and the generalized slippage of the vehicle are calculated using the values of $s_\delta^{\prime(\prime\prime)}$ ($i = 1, 4$) and formulae from Section 2.8:

generalized slippages of axles

$$s_{\delta \mathrm{a}i} = \frac{(1 + u_{\mathrm{d}i})\left(1 - s_{\delta i}^{\prime}\right)\left(1 - s_{\delta i}^{\prime\prime}\right)}{1 - s_{\delta i}^{\prime\prime} + u_{\mathrm{d}i}\left(1 - s_{\delta i}^{\prime}\right)}, \quad i = 1,4 \tag{7.146}$$

generalized slippages of the front and rear tandems:

$$s_{\delta a1,2} = \frac{(1+u_{d5})(1-s_{\delta a1})(1-s_{\delta a2})}{1-s_{\delta a2}+u_{d5}(1-s_{\delta a1})}$$
$$s_{\delta a3,4} = \frac{(1+u_{d6})(1-s_{\delta a3})(1-s_{\delta a4})}{1-s_{\delta a4}+u_{d6}(1-s_{\delta a3})} \tag{7.147}$$

generalized slippage of the vehicle

$$s_{\delta a} = \frac{(1+u_{d7})(1-s_{\delta a1,2})(1-s_{\delta a3,4})}{1-s_{\delta a3,4}+u_{d7}(1-s_{\delta a1,2})} \tag{7.148}$$

The values of generalized slippages of axles calculated from formula (7.146) are then used for compiling probability functions such as

$$s_{\delta a2(1)}/s_{\delta a1(2)} = f_{1\text{-}2}(t) \tag{7.149}$$

$$s_{\delta a4(3)}/s_{\delta a3(4)} = f_{3\text{-}4}(t) \tag{7.150}$$

The ratio of the generalized slippages in formulae (7.149) and (7.150) is always greater than unity. This is reflected in the symbols of these formulae in the following manner. If at a given point of time $s_{\delta a2} > s_{\delta a1}$, then the ratio of the generalized slippages in formula (7.149) is defined as $s_{\delta a2}/s_{\delta a1}$. However, if $s_{\delta a1} > s_{\delta a2}$ then the ratio of the slippages is calculated as $s_{\delta a1}/s_{\delta a2}$. The above also applies to the generalized slippages in formula (7.150).

The ratio of the generalized slippages $s_{\delta a1,2}$ of the front and $s_{\delta a3,4}$ of the rear tandems is determined similarly:

$$s_{\delta a3,4(1,2)}/s_{\delta a1,2(3,4)} = f_{1,2\text{-}3,4}(t) \tag{7.151}$$

The ratio of the generalized slippages in formula (7.151) is greater than unity, since the ratio is calculated as $s_{\delta a1,2}/s_{\delta a3,4}$ at $s_{\delta a1,2} > s_{\delta a3,4}$ and as $s_{\delta a3,4}/s_{\delta a1,2}$ at $s_{\delta a3,4} > s_{\delta a1,2}$.

It is seen by comparing formulae (7.145) and (7.149) through (7.151) with formulae (7.142) that all of them consist of probability functions of time t. Replacement of variables in all these formulae by eliminating t, yields the following relationships:

$$\begin{aligned} K_{mki} &= f_i\left(s''_{\delta i}/s'_{\delta i}\right), \quad i = 1,4 \\ K_{mo}^{1\text{-}2} &= f_{1\text{-}2}(s_{\delta a2(1)}/s_{\delta a1(2)}) \\ K_{mo}^{3\text{-}4} &= f_{3\text{-}4}(s_{\delta a4(3)}/s_{\delta a3(4)}) \\ K_{mo}^{1,2\text{-}3,4} &= f_{1,2\text{-}3,4}(s_{\delta a3,4(1,2)}/s_{\delta a1,2(3,4)}) \end{aligned} \tag{7.152}$$

The physical meaning of relationships (7.152) is now clarified. If the input signal in the differentials locking control system consists of the ratios of wheel slippages and the ratios of the generalized slippages of axles and tandems, then the optimum locking degrees (or the optimum values of torque bias) of each of the seven differentials, are precisely defined by the values of factors $K_{mki}, (i = 1,4)$, $K_{mo}^{1\text{-}2}$, $K_{mo}^{3\text{-}4}$, and $K_{mo}^{1,2\text{-}3,4}$ from formulae (7.152).

Consider the practical application of data obtained from formulae (7.152). The range of variation of the ratios of the slippage of axles and of the generalized slippages of the axles and tandems of the vehicle with a differential driveline system is subdivided into intervals with some step Δ. For example, the intervals that are obtained for $\Delta = 0.05$ are $[1 \ldots 1.05), [1.05 \ldots 1.10), [1.10 \ldots 1.15)$ and so on. The values of factors $K_{\text{mk}i}, (i = 1, 4)$, $K_{\text{mo}}^{1\text{-}2}$, $K_{\text{mo}}^{3\text{-}4}$, and $K_{\text{mo}}^{1,2\text{-}3,4}$ are averaged within each interval. As an illustration, Figure 7.24 shows plots of the mean values of factor $\bar{K}_{\text{mk1}}$ for 4 of the 17 on-road/off-road motion conditions under study.

Initially such graphs were constructed separately for acceleration and for steady-state motion, but it turned out that they are virtually identical. The rms-corrected values of $\bar{K}_{\text{mk1}}$ make it possible to determined the degree of locking of the front-axle differential, which, as seen from Figure 7.24, should increase, with the ratio $s''_{\delta 1}/s'_{\delta 1}$ of slippages of the wheels of this axle.

The next item to explore is the frequency at which the ratios of wheel slippages and the ratios of generalized slippages of the axles attain values from each of the intervals $[1 \ldots 1.05), [1.05 \ldots 1.10), [1.10 \ldots 1.15)$ and so on. Figure 7.25 shows histograms of the distribution of values of $s''_{\delta 1}/s'_{\delta 1}$.

On a dry dirt road the highest frequency occurs at $s''_{\delta 1}/s'_{\delta 1} = 1 - 1.2$, whereas values of $s''_{\delta 1}/s'_{\delta 1} = 1.4 - 1.6$ are encountered quite infrequently. The distribution of $s''_{\delta 1}/s'_{\delta 1}$ on

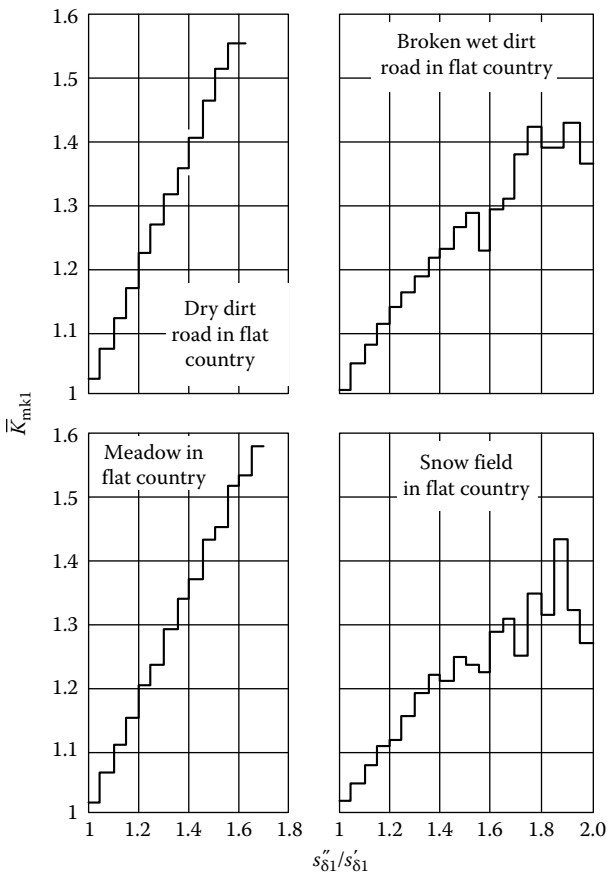


FIGURE 7.24
Factor of the distribution of optimal torques T''^{*}_{w1} and T'^{*}_{w1}.

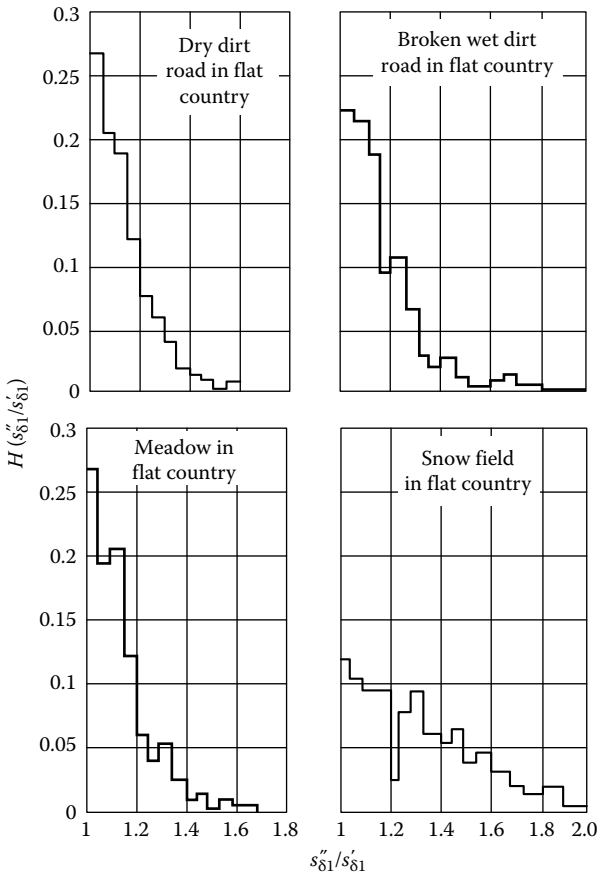


FIGURE 7.25
Histograms of the distribution of $s''_{\delta 1}/s'_{\delta 1}$.

meadowland is approximately the same. When moving over surfaces with poor gripping conditions (particularly on snow-covered ground), the frequencies of ratio $s''_{\delta 1}/s'_{\delta 1}$ are some close to one another. These data on the frequencies of slippage ratios are needed for deciding the need of locking for the given differentials of a vehicle. It was established that in the majority of cases there is no need to lock the differentials on dense surfaces of motion. This follows from Figure 7.26, which shows the average values of efficiency $\bar{\eta}^{tr}_{xd}$ of the running gear system of the 8×8 vehicle with differential driveline system and the average values of the maximum efficiency $\bar{\eta}^{tr}_{x*}$ of the running gear system of the same vehicle that corresponds to the optimum distribution of power between the wheels.

On a dry dirt road both these efficiency are virtually identical up to values of $s''_{\delta 1}/s'_{\delta 1} = 1.30$. Starting with $s''_{\delta 1}/s'_{\delta 1} = 1.35$ and higher the ratio $\bar{\eta}^{tr}_{x*}/\bar{\eta}^{tr}_{xd}$ is 1.02–1.09. Under motion conditions of which 6.5% takes place on a dirt road (see Figure 7.25), it is necessary to lock the differential of the front axle. Ratio $\bar{\eta}^{tr}_{x*}/\bar{\eta}^{tr}_{xd}$ on snow covered ground amounts to 1.05–1.25 at $s''_{\delta 1}/s'_{\delta 1} = 1 - 2$. The frequencies of all the wheel slippage conditions are considerable (see Figure 7.25), which points to the need of frequently locking the differential. The curves of the optimal degree of locking the remaining differentials of the vehicle in Figure 7.23a may be obtained in similar way.

A question common to all the differentials is the moment at which the differential should be unlocked. There are several possible approaches for this problem. For example, the

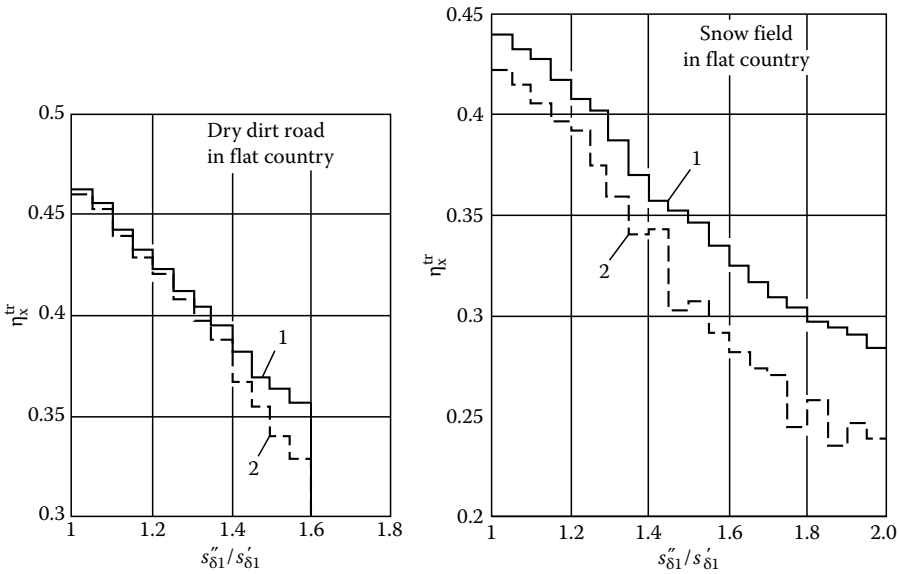


FIGURE 7.26
Running gear system efficiency of an 8 × 8 vehicle: 1, with optimum power distribution between the wheels, $\bar{\eta}^{tr}_{x*}$; 2, with a differential driveline system, $\bar{\eta}^{tr}_{xd}$.

differential, which was fully locked, should be unlocked if the ratio of its output torques becomes lower than a given threshold. This might require torque sensors. An easier approach is that the differential is unlocked after staying locked for a certain while. Consider this second approach and determine the duration of the interval during which the differential should remain locked before it gets unlocked.

A study of the results of modeling the 8 × 8 vehicle with open differentials (Figure 7.23a) shows that the time intervals Δt of the separate slippages of the left and right wheels, and of the axles are not the same. The higher values of Δt correspond to a separate slippage of left and right wheels, whereas the lower values to a separate slippage of the axles. In addition, the values of Δt depend to a large extent on the gripping properties of the support surface. It was established that Δt ranges between 5 and 15 s. These values may be assumed for specifying the duration of the time intervals during which the differentials should not be unlocked after they were locked.

The principal results obtained from the mathematical modeling of rectilinear motion of two identical 8 × 8 vehicles that differ solely by the design of their driveline systems are as follows. In one vehicle the power is distributed among the wheels in a manner such that the running gear system efficiency would be at the maximum, whereas in the other vehicle it is in accordance with the features of the differential driveline from Figure 7.23a.

In keeping with the general algorithm shown in Figure 6.11, the next step should consist in investigating the vehicle's curvilinear motion. The procedure to be followed in this case is delineated in Section 6.1. The turnability and stability of motion of the vehicle under study can be assessed to some extent by using data presented in Figures 6.4 through 6.6. The main result of such an assessment may consist of compiling the condition for conservation of sufficient handling of the vehicle. This condition is compiled from formula (1.120) for the sensitivity of the vehicle to the driver's control input and from Figure 1.81.

Assuming the turnability of the vehicle with the differential driveline system to be close to neutral, the condition is written as

$$|(r/\delta_1)_N - (r/\delta_1)_c| < \Delta_h \tag{7.153}$$

where

r is the yaw rate, that is, the angular velocity of the vehicle about the vertical axis

δ_1 is the turning angle of the front wheels (it is easily determined from the turning geometry of the vehicle and from the angles δ_1'' and δ_1' of the left and right wheels of the front axle)

N is a symbol that indicates that the value of r/δ_1 corresponds to the turnability of a vehicle with a differential driveline system which is close to neutralsteering (straight line 1 in Figure 1.81)

c is a symbol that shows that the value of r/δ_1 is determined from the readings of sensors at the current time, when a part or all of the vehicle's differentials may be locked

Δ_h is some specified threshold value

Upon departure from condition (7.153) and $(r/\delta_1)_c > (r/\delta_1)_N$, the vehicle exhibits oversteering (curve 2 on Figure 1.81). Differentials locked at this point in time may remain locked provided that the vehicle's motion does not exceed some specified value $[V_x]$:

$$V_x \leq [V_x] \tag{7.154}$$

and the lateral acceleration a_y of the vehicle does not exceed the specified value $[a_y]$:

$$a_y \leq [a_y] \tag{7.155}$$

If at least one of the above conditions ((7.154) or (7.155)) is not satisfied, then all the differentials are unlocked. Differentials must be unlocked at $V_x > [V_x]$, for example, when moving at high velocities over high-quality roads. If, however, condition (7.154) is not satisfied, this means that the vehicle is close to sideslip, which may be followed by rollover. Hence the differentials should be unlocked. In the opposite case, the values of factors K_μ from formula (1.119) may exceed critical values and the sideslip may occur earlier.

If, however, conditions (7.154) and (7.155) are satisfied, but condition (7.153) at $(r/\delta_1)_c > (r/\delta_1)_N$ is not satisfied, then differential 7 (see Figure 7.23a) should be locked. If that differential is already locked, then differentials 5 and 6 should be locked. Locking of these differentials will aid in the transition from oversteering to neutral steering.

If departure from condition (7.153) occurred at $(r/\delta_1)_c < (r/\delta_1)_N$, then all the differentials should be unlocked and should not be locked until formula (7.153) is satisfied again. At this departure from condition (7.153) the vehicle suffers from understeering (see curve 3 in Figure 1.81) and locking the differentials will only aggravate the situation, by additionally increasing the turning radius. This means that condition (7.153) becomes a substantive element of the algorithm of the mechatronic system of control of the locking/unlocking modes of differentials.

Additional elements of the algorithm to be considered are the following. If any of the vehicle's tires is damaged, then simultaneously by actuating the centralized tire inflation system, the interwheel differential of the axle with the damaged tire should be locked. This will cause the vehicle to retain its mobility. As a rule, this differential should not be unlocked in order to conform to condition (7.153). Tires are usually damaged under extreme traveling conditions when mobility is of greater significance than the magnitude of the vehicle's

turning radius. The differentials should be unlocked if the brake pedal has been operated (this does not apply to the case of the damaged tire) or if the transmission is in neutral.

In addition, if the slippage of both wheels of any axle exceeds the permissible value, then the interaxle differentials must be unlocked. Leaving them locked would cause redistribution of the circumferential forces between the axles, increasing these forces on the wheels of individual axles and the slippage of these axles. The higher than ordinary circumferential forces of these axles make it more difficult for their wheels to take up lateral forces, something that may infringe upon the stability of motion.

Other useful elements that exist may be included in the algorithm of controlling the locking/unlocking of differentials. In our example, the elements already discussed are considered.

The previously discussed elements of the algorithm can be formally described in the form of logical Boolean variables that take the values of their set {0, 1}:

1. a—the brake pedal was not depressed. If it was depressed then all the differentials should be unlocked;
2. b—the transmission is not in neutral. If it is neutral then all the differentials will become unlocked;
3. c_1 to c_4—the centralized tire inflation system was actuated and at least one tire is damaged. The differential of the axle with the damaged tire is locked and will no longer be unlocked if the driver will not disable the entire differential blocking control system. The numbers 1–4 correspond to the numbers of the four axles of the vehicle from 7.23a;
4. d_1 to d_7—the locking mechanisms of all of the vehicle's seven differentials are in operating conditions (the numbering of the differentials is shown in Figure 7.23a); if they are not in operating conditions (not in order), then the differentials with the corresponding numbers are not locked;
5. e_1 to e_7—imbalances of slippages (i.e., the ratios of the slippages) exceed the permissible values: imbalance of left and right wheels of the four axles (e_1 to e_4), imbalance of the generalized slippages of the first and second axles (e_5), imbalance of the generalized slippages of the third and fourth axles (e_6), imbalance of the generalized slippages of the front and rear tandem (e_7). The differentials with corresponding numbers in Figure 7.23a are locked upon the appearance of any of these imbalances;
6. t_1 to t_7—threshold values of times during which the corresponding differentials remain locked; if the time interval during which the differential was locked did not exceed t_i, then this differential remains locked. This is true if there are no signals for unlocking the differentials specified in the items below;
7. m_1 to m_4—slippages of both wheels of one of the four axles do not exceed the permissible value. If the slippages of both wheels of one of the axles 1–4, the differential of which was locked, exceed the permissible value, then differentials 5–7 will unlock;
8. f—handling condition (7.153) is satisfied. If departure from condition (7.153) occurs in such a manner that $(r/\delta_1)_c > (r/\delta_1)_N$, then differential 7 is locked and if it was already locked, then differentials 5 and 6 are locked. If, however, departure from condition (7.153) occurs at $(r/\delta_1)_c < (r/\delta_1)_N$, then all the differentials are unlocked;

9. v—the velocity is sufficiently low, meaning that condition (7.153) is satisfied and the differentials locked at that time may remain locked; if condition (7.153) is not satisfied, then all the differentials will become unlocked;
10. g—the lateral acceleration of the vehicle does not exceed the permissible value (see formula (7.155)); if it exceeds that value, then all the differentials should be unlocked;
11. k—the logic control device is activated (by the driver).

The values of parameters in items 1 through 11 are determined by sensors and fed to the input of the logical control system. The activation of the system and the appearance of signals of locking or unlocking of differentials are determined in the additional manual control mode. This means that the driver disables the logical control system and takes over the task of locking/unlocking of the differentials.

7.6 Design of Integrated Driveline Systems

The traction control system, one of the most popular systems, is extensively used in recent times for improving the traction and velocity properties of vehicles. Traction control is used in many types of vehicles—from passenger cars to heavy-duty trucks. The feasibility of using this system on planetary exploration vehicles is under consideration. The idea underlying this control system consists in braking the wheel (wheels) of a vehicle that finds itself under poor surface gripping conditions and in controlling the engine fuel-supply system. It has been published in literature dealing with developments in traction control that these systems are compatible with differentials of different types used in vehicles. Hence the analysis of traction control systems and further improvement of the traction, velocity, and other operational properties of vehicles and their fuel efficiency can be approached—in a different way—by examining the control by the braking system and the engine's fuel supply system (i.e., traction control) together with the control of the vehicle's PDUs. Such a combination of systems can be treated as an integrated driveline system (Figure 1.34). The advantages of this approach shall be demonstrated for the case of a 12-wheel heavy-duty highway vehicular train (truck), consisting of a 4×2 tractor and a three-axle semitrailer with a total mass of 42 ton (Figure 7.27).

In this section, the following principal problems associated with development of the integrated system are solved:

1. Mathematical models of motion of the vehicular train under probabilistic road conditions are worked out;
2. These mathematical models are used to determine the optimum distributions of power between the driving wheels and the power distributions corresponding to the existing driveline system of the tractor employing an open differential in the rear driving axle;
3. Advanced characteristics for the system of brake control of the slipping wheel and for the system controlling the locking differential of the driving axle are synthesized on the basis of the solution of problems (1) and (2);



FIGURE 7.27
12-wheel heavy-duty highway vehicular train.

4. A parallel control algorithm of the integrated driveline system, including differential locking control, control of the slipping wheel brake, and control of the engine fuel supply system is developed, verified, and optimized;
5. Hardware implementation of the parallel control algorithm in the form of a working prototype is carried out using one of the available Field Programmable Circuit technologies.

Actually, problems 1 through 5 encompass the principal stages of a process known as rapid prototyping of mechatronic systems.

7.6.1 Optimal Power Distribution and Features of the System

Figure 7.28 shows the computational model of rectilinear accelerated motion of the vehicular train on a support surface that can be modeled both as one that is deformable or nondeformable.

The surface has macro- and micro-topographic features that affect the dynamic normal wheel reactions. It is assumed that the surface of motion does not have a lateral slant; however, the micro-topography is modeled as being different for the left and right wheels of the vehicular train. The gripping conditions of the wheels are modeled in a probabilistic manner, which manifests itself in modeling probable values of the rolling resistance coefficients of all the wheels $f_i^{\prime(\prime\prime)}, (i = 1, 5)$ and the gripping coefficients of the driving wheels $\mu_{px2}^{\prime(\prime\prime)}$. It is assumed that the engine and the transmission provide the required power for acceleration and steady-state motion of the vehicle at the specified speed. The approaches to modeling the above parameters were analyzed in Section 6.6.

The problem of optimizing the distribution of power between the driving wheels of the rear axle is formulated as the inverse dynamics problem. This means that, for the specified probabilistic conditions of motion, one seeks such distributions of power between the wheels that correspond to the maximum of some quality functional while simultaneously ensuring the specified kinematic parameters of the vehicular train, that is, the required

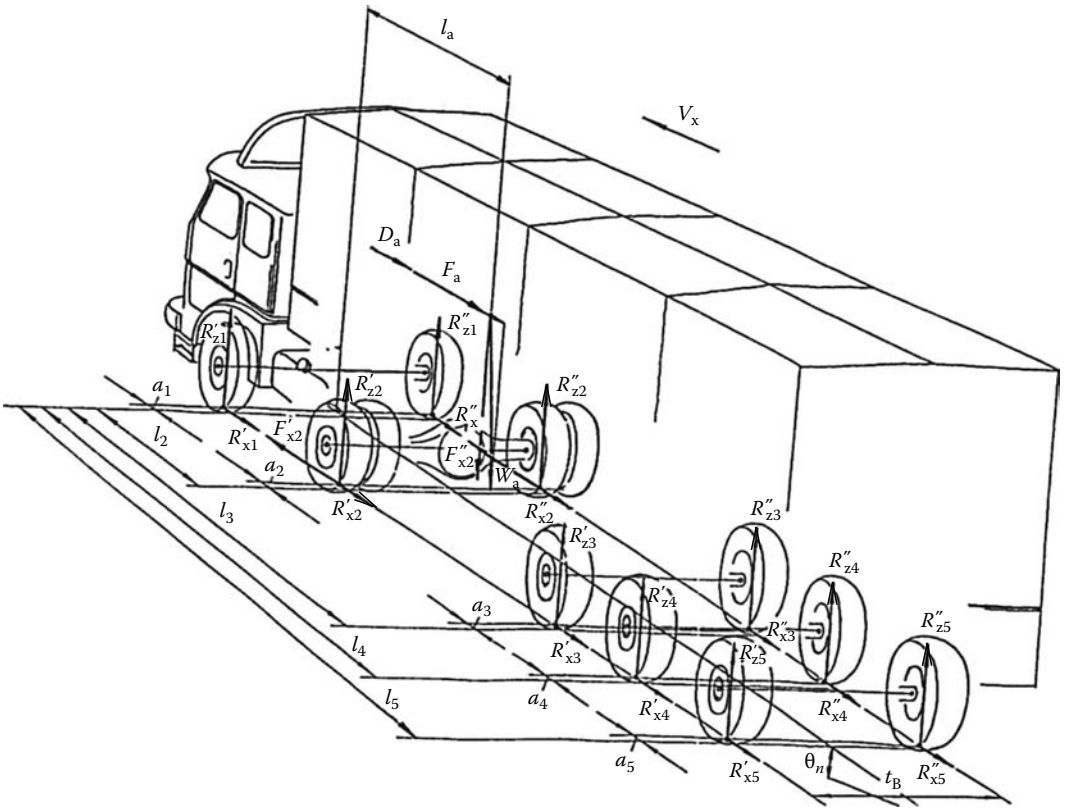


FIGURE 7.28
Free-body diagram of the vehicular train.

course of acceleration. In connection with this, the functional relationship between the velocity and acceleration of the vehicular train is taken to be the same as in Section 6.6.1. The quality functional is represented by the running gear efficiency η_x^{tr} (see formula (6.33)). Using the above assumptions and approaches to modeling the motion of a vehicular train on the basis of the inverse dynamics problem, the formulae for optimal slippage of the driving wheels $s''^*_{\delta 2}$ and $s'^*_{\delta 2}$ are written in the same way as in Section 6.6.1:

$$\begin{gathered}
\frac{\frac{1}{1-s'^*_{\delta 2}} + e^{k'_2 s'^*_{\delta 2}} - 1}{k'_2\left(1 - s'^*_{\delta 2}\right) = -\lambda} \\
\frac{1}{1 - s''^*_{\delta 2}} + \frac{e^{k''_2 s''^*_2} - 1}{k''_2\left(1 - s''^*_{\delta 2}\right)} = -\lambda \\
R''_{z2}\mu''_{px2}\left(1 - e^{-k''_2 s''_{\delta 2}}\right) + R'_{z2}\mu'_{px2}\left(1 - e^{-k'_2 s'^*_{\delta 2}}\right) = F_{x\Sigma}
\end{gathered} \tag{7.156}$$

where, λ is the Lagrange multiplier, whereas the total wheel force $F_{x\Sigma}$ is calculated using the computational model in Figure 7.28:

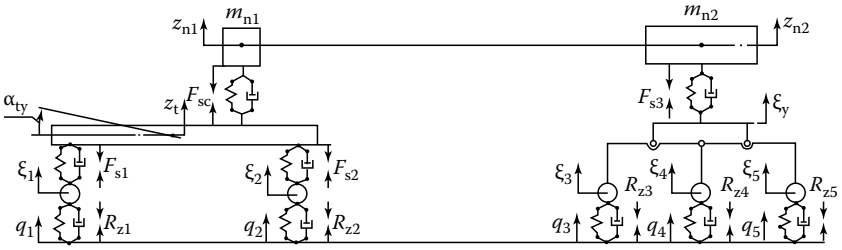


FIGURE 7.29
Computational layout of the sprung and unsprung masses in the longitudinal plane.

$$F_{x\Sigma} = F'^{*}_{x2} + F''^{*}_{x2} = W_a a_x \delta_r / g \pm W_a \sin\,\theta_n + \sum_{i=1}^{5} R'^{(\prime\prime)}_{xi} + D_a \tag{7.157}$$

where, δ_r is a mass factor that accounts for the rotating masses of the vehicle.

Equations 7.156 and 7.157 are solved as follows. The normal dynamic reactions of the wheels $R'^{(\prime\prime)}_{zi}, (i = 1, 5)$ are calculated with consideration of the macro and micro-irregularities of the road. For this purpose, computation models of the oscillations of the sprung and unsprung masses in the longitudinal and transverse planes shown in Figures 7.29 and 7.30 are compiled.

With the consideration of the probabilistic values of the rolling resistance factors $f'^{(\prime\prime)}_i, (i = 1, 5)$ and normal reactions $R'^{(\prime\prime)}_{zi}, (i = 1, 5)$, the wheel rolling resistance forces $R'^{(\prime\prime)}_{xi}$

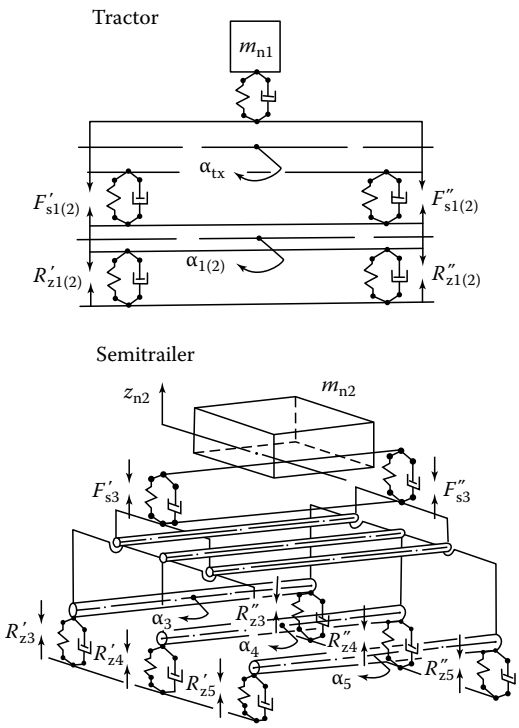


FIGURE 7.30
Computational layout of the sprung and unsprung masses in the transverse plane.

and their sum $\sum_{i=1}^{5} R_{xi}^{\prime(\prime\prime)}$ needed for the formula (7.157) are calculated. Then the values of angle θ_n (see Figure 7.28) are found from a model of the road's macro-topography and the quantity $\pm W_a \sin \theta_n$ needed for solving Equation 7.157 is calculated. The air drag D_a and the quantity $W_a a_x \delta_r / g$ are calculated from data on the velocity and acceleration of the vehicular train. In this manner all the components of formula (7.157) become known and this makes it possible to determine the force $F_{x\Sigma}$. Its value is substituted into Equations 7.156, from which the optimum slippages of driving wheels $s_{\delta 2}^{\prime\prime *}$ and $s_{\delta 2}^{\prime *}$ are determined. Then the optimal circumferential forces of the wheels $F_{x2}^{\prime\prime *}$ and $F_{x2}^{\prime *}$ are calculated using formula (1.26) from which the optimal wheel torques $T_{w2}^{\prime\prime *}$ and $T_{w2}^{\prime *}$ are determined. These torques should be applied to the wheels in order to provide for maximum possible efficiency η_{x*}^{tr} when the vehicular train moves at a velocity V_x and an acceleration a_x. Torques $T_{w2}^{\prime\prime *}$ and $T_{w2}^{\prime *}$ can be used for determining the coefficient of optimum distribution of the torques from formula (6.84):

$$K_{mk2} = \frac{F_{x2}^{\prime\prime *} r_{w2}^{0\prime\prime}}{F_{x2}^{\prime *} r_{w2}^{0\prime}} = \frac{T_{w2}^{\prime\prime *}}{T_{w2}^{\prime *}} \tag{7.158}$$

The higher torque is substituted into the numerator of formula (7.158), whereas the lower torque into the denominator. This means that K_{mk2} is always greater than 1. It corresponds to the optimum redistribution of the torque between the wheels and may be used for synthesizing the laws of control of the interwheel PDU (e.g., for developing algorithms of control of the driving axle's differential locking).

The above procedure for solving Equations 7.156 and determining K_{mk2} is implemented within the time domain, that is, $K_{mk2} = f(t)$ is treated as a probabilistic function. To find its statistical features, it is necessary to model a sufficiently large number of vehicular-train runs under the specified probabilistic travel conditions. In the investigations the results of which are presented in this section, the number of runs (trips) was 20 for each of the road conditions under study.

The same vehicular train, but with an open differential in the driving axle moving under the same road conditions and with the same velocity and acceleration, was modeled simultaneously by modeling the optimum distribution of power between the driving wheels and the determination of K_{mk2}. This means that computer modeling was performed of two vehicular trains that differed from one another only by the fact that in one of them the power was distributed among the wheels in the optimal manner, whereas in the other, with allowance for the features of the open differential. The probabilistic features of the roads, the velocities, and accelerations were the same for both vehicular trains.

Consider a method for determining the circumferential forces $F_{x2}^{\prime\prime d}$ and $F_{x2}^{\prime d}$ and slippages $s_{\delta 2}^{\prime\prime d}$ and $s_{\delta 2}^{\prime d}$ of the wheels of the rear axle of the vehicular-train tractor (Figure 7.27), connected by open differentials. The circumferential forces are determined from the equality of the wheel torques and on the basis of the previously calculated value of $F_{x\Sigma}$ (see formula (7.157)):

$$\begin{aligned} F_{x2}^{\prime\prime d} r_{w2}^{0\prime\prime} &= F_{x2}^{\prime d} r_{w2}^{0\prime} \\ F_{x2}^{\prime\prime d} + F_{x2}^{\prime d} &= F_{x\Sigma} \end{aligned} \tag{7.159}$$

Then the wheel slippages are calculated using formula (1.26) from Section (1.3.2):

$$\begin{aligned} s_{\delta 2}^{\prime\prime \mathrm{d}} &= -\frac{1}{k_2^{\prime\prime}} \ln\left(1 - \frac{F_{\mathrm{x}2}^{\prime\prime \mathrm{d}}}{\mu_{\mathrm{px}2}^{\prime\prime} R_{\mathrm{z}2}^{\prime\prime}}\right) \\ s_{\delta 2}^{\prime \mathrm{d}} &= -\frac{1}{k_2^{\prime}} \ln\left(1 - \frac{F_{\mathrm{x}2}^{\prime \mathrm{d}}}{\mu_{\mathrm{px}2}^{\prime} R_{\mathrm{z}2}^{\prime}}\right) \end{aligned} \tag{7.160}$$

Using the previously found values of $s_{\delta 2}^{\mathrm{d}\prime\prime}$ and $s_{\delta 2}^{\mathrm{d}\prime}$ and formula (2.340) it is possible to calculate the generalized slippage of the axle

$$s_{\delta \mathrm{a}2} = 1 - \frac{\left(r_{\mathrm{w}2}^{0\prime\prime} + r_{\mathrm{w}2}^{0\prime}\right)\left(1 - s_{\delta 2}^{\prime \mathrm{d}}\right)\left(1 - s_{\delta 2}^{\prime\prime \mathrm{d}}\right)}{r_{\mathrm{w}2}^{0\prime}\left(1 - s_{\delta 2}^{\prime \mathrm{d}}\right) + r_{\mathrm{w}2}^{0\prime\prime}\left(1 - s_{\delta 2}^{\prime\prime \mathrm{d}}\right)} \tag{7.161}$$

Equations 7.159 through 7.161 define the power and kinematic parameters of the driving wheels and this means the transportation efficiency $\eta_{\mathrm{x}}^{\mathrm{tr}}$ of the vehicular train's running gear as well.

The specified velocity of translational motion V_{x} and wheel slippages $s_{\delta 2}^{\prime\prime \mathrm{d}}$ and $s_{\delta 2}^{\prime \mathrm{d}}$ are now used for calculating the angular velocities of the wheels:

$$\begin{aligned} \omega_{\mathrm{w}2}^{\prime\prime} &= V_{\mathrm{x}} / \left(r_{\mathrm{w}2}^{0\prime\prime}\left(1 - s_{\delta 2}^{\prime\prime \mathrm{d}}\right)\right) \\ \omega_{\mathrm{w}2}^{\prime} &= V_{\mathrm{x}} / \left(r_{\mathrm{w}2}^{0\prime}\left(1 - s_{\delta 2}^{\prime \mathrm{d}}\right)\right) \end{aligned} \tag{7.162}$$

Another vehicular train is now added to these two trucks, one with optimum power distribution and the other, with an open differential. Modeling for this third vehicular train includes determining the circumferential forces of the wheels upon activating the traction control system, when the wheel with the highest slippage is braked. Obviously, the system should provide the best approximation of circumferential forces $F_{\mathrm{x}2}^{\prime\prime}$ and $F_{\mathrm{x}2}^{\prime}$ of their optimal values $F_{\mathrm{x}2}^{\prime\prime *}$ and $F_{\mathrm{x}2}^{\prime *}$ and, respectively, the best approximation of $\eta_{\mathrm{x}}^{\mathrm{tr}}$ of its maximum value $\eta_{\mathrm{x}*}^{\mathrm{tr}}$. For this purpose, as shown by investigations, the best results are obtained if activating the traction control system ensures equality of the wheel's circumferential force $F_{\mathrm{x}2}^{\prime\prime \mathrm{tc}}$ to its optimal value $F_{\mathrm{x}2}^{\prime\prime *}$ determined under the same gripping conditions. The subscript tc indicates that traction control has been activated. The above is now illustrated graphically. Figure 7.31 shows two curves of slipping of the wheels of the driving axle of a vehicular train traveling under different gripping conditions.

If wheel forces $F_{\mathrm{x}2}^{\prime\prime}$ and $F_{\mathrm{x}2}^{\prime}$ in the case when the axle is equipped with an open differential (the rolling radii of the wheels in the driven mode are assumed to be equal, that is, $r_{\mathrm{w}2}^{0\prime\prime} = r_{\mathrm{w}2}^{0\prime}$) are assumed to be equal, then the wheel slippages are not the same, that is, $s_{\delta 2}^{\prime\prime \mathrm{d}} \neq s_{\delta 2}^{\prime \mathrm{d}}$. To obtain the optimal force $F_{x2}^{\prime\prime *}$ on the wheel operating under better gripping conditions, some braking torque T_{b} must be applied to the other wheel operating under poorer gripping conditions. In fact, when T_{b} is applied to the slipping wheel, the torque at the other wheel, operating under better conditions, increases. This is caused by virtue of the symmetrical properties of the open differential: the torques at its output shafts are

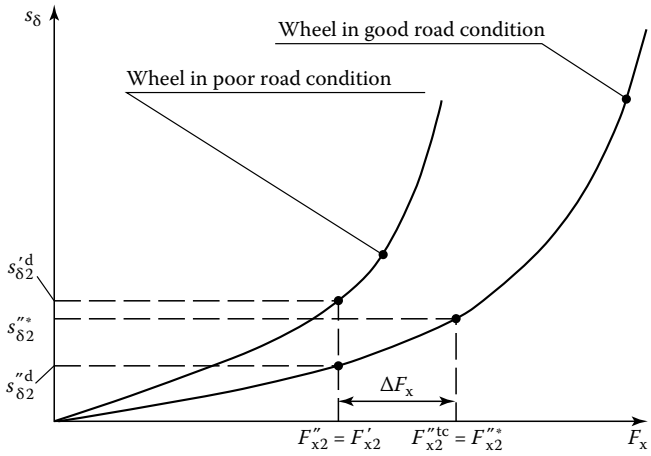


FIGURE 7.31
Slip–circumferential force curves.

always the same. Torque T_b should be such that an increase in T''_{w2} should bring about the desired increase in F''^{tc}_{x2} to F''^{*}_{x2}:

$$F''^{tc}_{x2} = F''^{*}_{x2} = F''_{x2} + \Delta F_x \tag{7.163}$$

where, ΔF_x is some addition to force F''^{tc}_{x2}. When traction control is activated, force F''^{tc}_{x2} of the wheel operating under better conditions increases to F''^{*}_{x2}, slippage $s''^{tc}_{\delta 2}$ of this wheel becomes:

$$s''^{tc}_{\delta 2} = s''^{*}_{\delta 2} \tag{7.164}$$

Now ΔF_x is determined. The torque T'^{tc}_{w2} of the wheel with poorer gripping conditions is spent for producing a circumferential force in the contact between the wheel and the road that is equal to F'_{x2} and for overcoming the braking torque T_b that is supplied to the brake. With reference to this, the conditional circumferential force F'^{tc}_{x2} determined by torque T'^{tc}_{w2} is represented as the sum of forces:

$$F'^{tc}_{x2} = F'_{x2} + \Delta F_x \tag{7.165}$$

where, ΔF_x is given by the expression:

$$\Delta F_x = \frac{T_b u_k}{r^{0\prime}_{w2}} \tag{7.166}$$

In the above formula u_k is the gear ratio of the wheel-hub gear drive ($u_k = 1$ when there is no wheel-hub gear drive). Term ΔF_x in formula (7.166) is a conditional addition to the circumferential force of the wheel with the poorer gripping properties that stems from the application of the torque T_b. This additional force ΔF_x does not arise in the contact between this wheel and the road, for which reason, force F'^{tc}_{x2} in formula (7.165) has been termed conditional. Additional force ΔF_x increases the actual circumferential force F''^{tc}_{x2} of the wheel with the better gripping conditions, which is seen from formula (7.163).

Several parameters describing the processes occurring in brake mechanisms are now introduced. The friction power in the braking mechanism is

$$P_b = T_b\omega_w = T_b V_x / \left(r_{w2}^{0\prime}\left(1 - s_{\delta 2}^{\prime tc}\right)\right) \tag{7.167}$$

To assess the energy load on the braking mechanism, the energy intensity factor is considered:

$$K_f = P_b/(2A_s) \tag{7.168}$$

where

$A_s = b_s l_s$ is the area of a single brake shoe

b_s and l_s are the width and length of the bearing surface of the shoe

Even though, factor K_f is a conditional indicator, it makes it possible to provide a comparative assessment of braking mechanisms with different b_s and l_s. The temperature rise of the braking drum when traction control is activated is assessed by the following expression that is frequently used in investigating brakes:

$$t^\circ = \frac{\Delta F_x}{A_b K_{ht}}\left(1 - \exp\left(-\frac{s_t A_b K_{ht}}{m_b C_b}\right)\right) \tag{7.169}$$

where

A_b is the area of the brake drum cooling surface

m_b is the mass of the drum and of the components associated with it

C_b is the specific heat of the drum

K_{ht} is the coefficient of heat transfer between the drum and the air

s_t is the run of the vehicular train over which force ΔF_x, related to the brake torque T_b by formula (7.166), acts

Summing up, from the values of t° obtained for the different ΔF_x, it is possible to find the total temperature rise in the left and right braking mechanisms of the driving axle when the vehicular train accelerates.

It was assumed in this study that the traction control system reacts to any (even very small) difference in the slippages of the driving axles of the tractor and that braking occurs instantaneously without rise in the air pressure in the brake chambers. This operating mode and, accordingly, features of the traction control system shall be termed theoretical. Such an approach will enable determining and analyzing all the possible values of the efficiencies of the vehicular-train running gear and to validly select the differences between the slippages of the wheel at which the drop in efficiency is not so perceptible. These threshold values of wheel slippage are needed in developing an algorithm of the operation of a real traction control system. At the same time, the approach suggested here, allows estimating the maximum possible energy intensities and temperature modes of braking mechanisms.

Consider the results of modeling the travel of three vehicular trains over a concrete-paved road on level terrain in winter (compacted-snow road). The maximum acceleration is $a_x^{max} = 0.55$ m/s^2. The fully loaded vehicular train is accelerated to the steady-state velocity of $V_{xc} = 16.67$ m/s (60 km/h).

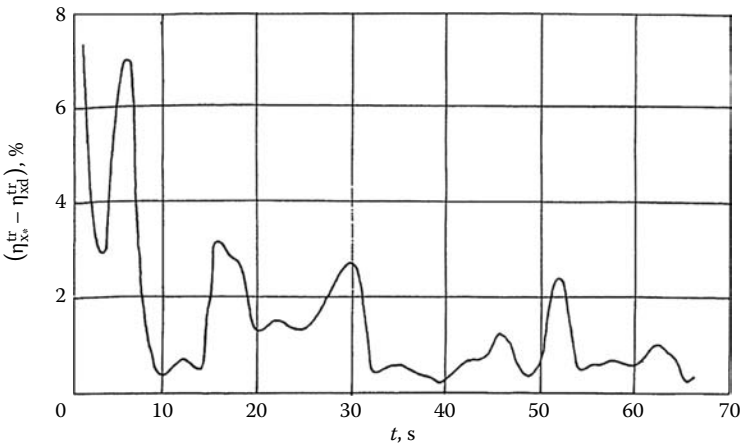


FIGURE 7.32
Relation between the efficiencies η^{tr}_{x*} and η^{tr}_{xd}.

Figure 7.32 shows a graph that illustrates the difference between the maximum possible efficiency η^{tr}_{x*} and the efficiency η^{tr}_{xd} corresponding to open-differential drive of the driving wheels of the tractor.

This difference is as high as 7.5% at the high first-stage vehicular-train acceleration rates, when the travel time goes from 0 to 8 s. This difference in efficiencies stems from the large difference between the slippages of the driving wheels of the tractor with an open differential in the course of accelerating on a snow-covered highway (Figure 7.33).

Wheel slippages can be equalized and accordingly the traction-velocity performance of the vehicular train can be increased to the maximum possible under the given road conditions by controlling the wheel torques. Figure 7.34 shows curve 1 of factor K_{mk2} representing the optimum distribution of the wheel torques in the course of acceleration.

If the system controlling the wheel torques, causes their values to conform to the values of K_{mk2}, then the running gear efficiency, as an indicator of the traction and velocity

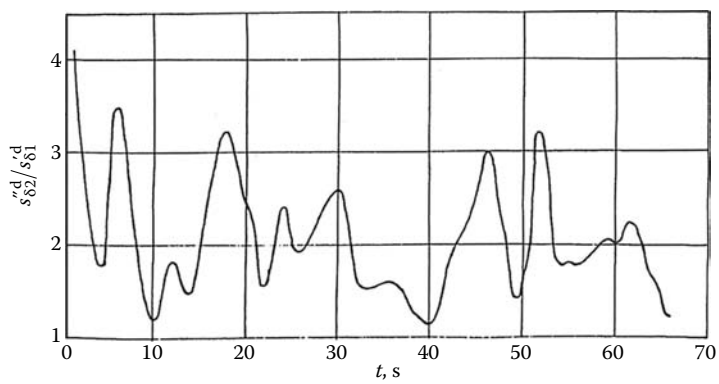


FIGURE 7.33
Ratio of the wheel slippages of the tractor with the open differential on a snow-covered highway.

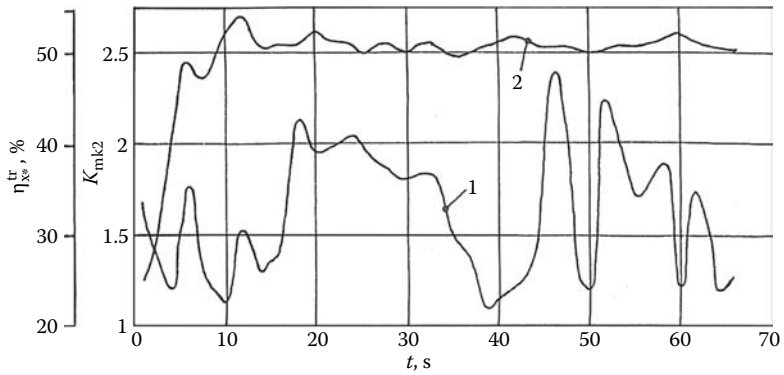


FIGURE 7.34
Maximum efficiency and optimum wheel torque distribution factor.

properties will be at maximum. The values of K_{mk2} in Figure 7.34 and their corresponding values of optimal wheel torques T''^{*}_{w2} and T'^{*}_{w2} may be attained, for example, by controlling the operation of the locking mechanism of the driving axle differential. Timely activation of the locking mechanism will ensure that the wheel slippages are equal and that the efficiency will increase to the maximum possible values of η_{x*}^{tr} for the given travel conditions (Figure 7.34, curve 2).

Before considering in detail the question of the operating modes of the differential's locking, the effect of the previously described method of the functioning of the traction control system on the traction and velocity property of the vehicular train is analyzed. Studies show that braking the wheel with the higher slippage increases the total circumferential force of the vehicular train (Figure 7.35).

Its rise during the entire course of acceleration with traction control is from 0.8 to 5.9 kN as compared with the same vehicular train with an open interwheel differential, and is particularly perceptible during the first 16 to 20 s of travel.

The use of traction control highly reduces the difference between the wheel slippages. Figure 7.36 shows computed values of the ratios of the greater to the smaller slippage.

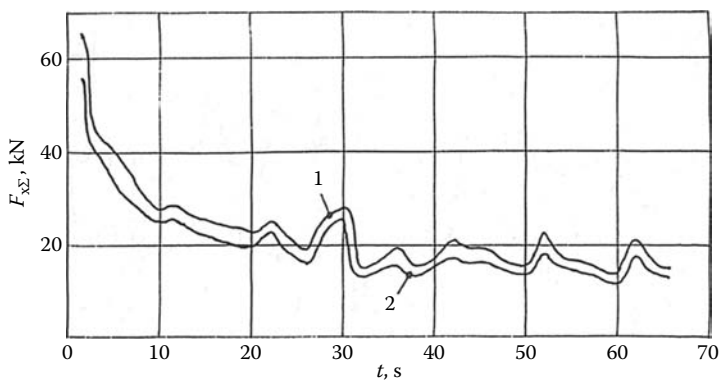


FIGURE 7.35
Total circumferential force.

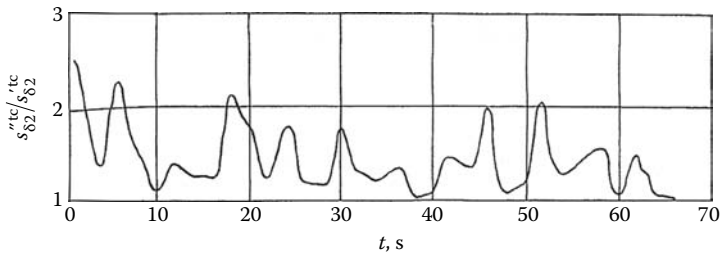


FIGURE 7.36
Ratio of the wheel slippages of the tractor with traction control.

It is seen by comparing Figures 7.33 and 7.36 that the suggested method of traction control operation (see Figure 7.31) makes it possible to reduce the mean wheel slippage ratio to 1.38 (for comparison: when using an open interwheel differential the mean value of this ratio is 2.16).

It is important to note that only after 6–8 s of travel do the values of η^{tr}_{xtc} of the running gear of a vehicular train with traction control come close to the maximum possible values η^{tr}_{x*} attained based on the optimal distribution of power between the wheels. This confirms the effectiveness of the method suggested above for controlling the wheel circumferential forces using traction control at this acceleration stage (see Figure 7.31). At the same time, during the first 8 s of the vehicular-train travel the ratio $\eta^{tr}_{x*}/\eta^{tr}_{xtc}$ ranges from 1 to 1.15. This indicates that even a method of traction control functioning intended for providing an optimum power distribution between the wheels is not capable of providing maximum values of efficiency. In connection with this, at the initial acceleration stage, when the travel velocity is low, the traction-velocity performance of the vehicular train should be improved using the system that controls the differential locking mechanism.

The above described studies thus show that in order to improve the traction and velocity properties of a vehicular train it is advisable to use a traction control system (control of the brakes of the driving wheels) and a system for distributing the power between the wheels, based on controlling the locking-unlocking of the interwheel differential. This process of combined control can be provided by designing an integrated system that ensures parallel control of the above systems.

Consider the results of numerical investigations needed for designing such an integrated system. Analysis shows (Figure 7.36) that the threshold value Δ_δ, the ratio of slippage of driving axle wheels at which braking of the wheel with the greater slippage should be started, can be taken to be 1.35–1.40. This will provide for high traction and velocity properties of the vehicular train. In fact, under acceleration conditions when ratio Δ_δ of the slippages of driving wheels is smaller than the threshold value of 1.35–1.40 and the traction control is not activated, the difference between the maximum efficiency η^{tr}_{x*} and the efficiency η^{tr}_{xd} of the running gear of the vehicular train with open interwheel differential is insignificant, amounting to 0.40%–0.45% (see Figures 7.32 and 7.33). It is not advisable to increase Δ_δ, since at wheel slippage ratio of 1.5 the difference between η^{tr}_{x*} and η^{tr}_{xd} amounts to 0.5–1.2. On the other hand, the suggested value of Δ_δ, covers the mean value of this ratio, equal to 1.38 provided by traction control (see Figure 7.36). As previously noted, at this value of Δ_δ the traction control system will ensure virtually the maximum possible efficiency of the running gear after the first 6–8 s of the vehicular-train travel.

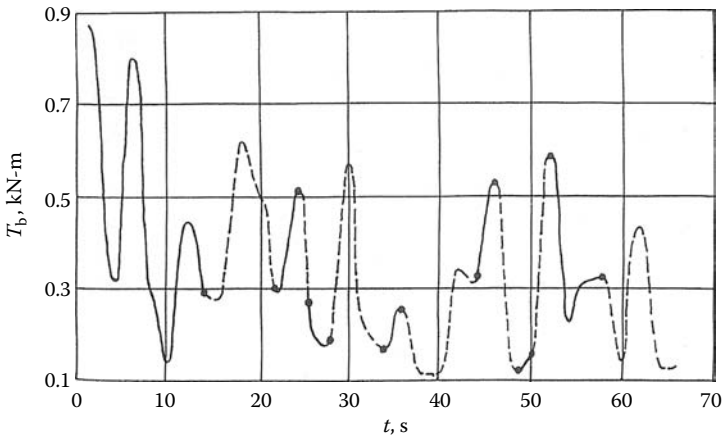


FIGURE 7.37
Brake torque in traction control.

The same threshold value of Δ_δ can be taken also as the threshold value for actuating the locking of the interwheel differential at the initial acceleration stage. Then at lower values of Δ_δ, when the differential's locking will not be activated, the difference $\left(\eta_{x*}^{tr} - \eta_{xd}^{tr}\right)$ between the efficiencies will again be negligible.

Consider certain technical aspects needed for implementing the above recommendations. Figure 7.37 is a graphical representation of the values of brake torque T_b that should be produced by means of the brake of the slipping wheel (alternately the right or the left) in the course of vehicular-train acceleration.

Note that the node points —•— in Figure 7.37 do not belong to the graph, since they correspond to the change in the wheel to be braked. The value of torque T_b during the first 8 s of acceleration will amount to 0.30–0.85 kN-m with the mean value of 0.36 kN-m over the entire course of acceleration. These values approximately correspond to the braking moment of a 6×4 truck with a gross mass of 24.2 ton when it is decelerated at the rate of 0.981 m/s^2. The mean value of the friction power P_b in the braking mechanism of the slipping wheel amounts to 8.29 kW, with a maximum of 22 kW. Accordingly the mean value of the load intensity factor K_t of the braking mechanism during the entire course of vehicular-train acceleration is 47.91 kW/m^2 with a maximum value of 127.6 kW/m^2. If the specific friction work U_f is calculated on the basis of the mean value of K_t with consideration of the mean time of operation of a single braking mechanism, then the latter will amount to 0.20 kJ/cm^2, which is significantly less than the value of 0.6–0.8 kJ/cm^2 usually permitted for trucks and buses:

$$U_f = P_b t / A_s \tag{7.170}$$

where, t is the mean time of operation of one of the brakes of the driving wheels when the vehicular train accelerates to the specified velocity.

Temperature gain t° of the brake drums during the entire course of vehicular-train acceleration will amount to approximately 23°C–25°C. Even if traction control is treated as continuous braking of the slipping wheel during the entire acceleration (and the modeling was performed on the assumption that traction control reacts to any differences

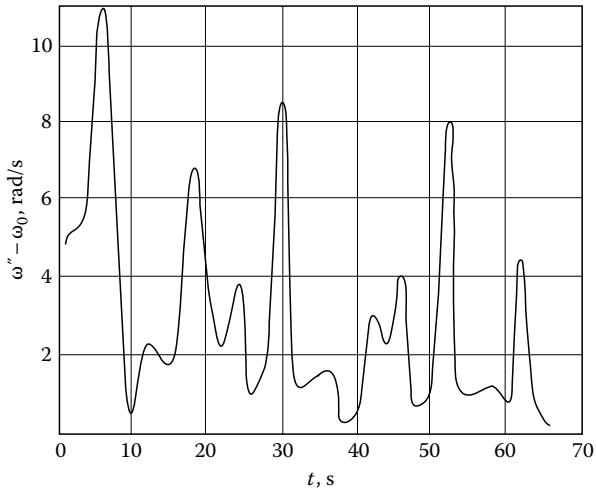


FIGURE 7.38
Difference between ω'' and ω_0.

between the wheel slippages), then this value of t° does not markedly exceed the permissible temperature gain of the drum during a single braking act that is usually 20°C. The value of t° can be reduced by introducing into the traction control operation algorithm the previously suggested value of ratio Δ_δ of wheel slippage at which this system is activated and also by designing an integrated system involving integrated use of traction control and locking the interwheel differential.

Differential locking mechanisms usually consist of gear, cam or other type of clutches. Their serviceability depends to a large measure on the relative velocity of rotation of the elements being coupled. To assess the feasibility of the use of a given differential locking clutch when the vehicular train is accelerated, analyze the relation between the angular velocity ω_0 of the differential's housing and the angular velocity ω'' of one of its output shafts in the case when neither the differential locking nor traction control have been activated. Figure 7.38 is a graphical representations of the values of $(\omega'' - \omega_0)$ for the case of $\omega'' > \omega_0$.

The mean value of $(\omega'' - \omega_0)$ during acceleration is 2.93 rad/s, whereas the maximum difference in the angular velocity of the driven and driving links of the differential is approximately 11 rad/s. These values can be used as a first approximation in designing the differential locking mechanism. They do not exceed the values of 10–15 rad/s of the relative rotational velocity of the half clutches that are usually recommended. Designs of cam clutches are in existence that are capable of coupling and uncoupling at relative angular velocity of the links being joined in the order of 30 rad/s (this was mentioned in Section 2.7).

After the threshold value of Δ_δ at which locking starts, is determined, consider the question of the time when it goes into operation. The higher slippage occurring in the course of the vehicular train acceleration alternates between each of the driving wheels (this is seen from Figure 7.37). Here the time segment Δt during which one wheel has a slippage greater than the other differs for different acceleration stages. During the first 20 s of vehicular-train motion, Δt ranges from 8 to 12 s, whereas during the subsequent stage the range is 4–8 s. These values of Δt should be taken into account when working out the differential locking control algorithm in determining the time during which the locking mechanism should not be disconnected after it was activated.

Consider the results of numerical studies for the case of operating a vehicular train on class IV and V roads. Class IV roads have pavements such as bituminous concrete, crushed stone, gravel, sand, soil, and low-strength stone materials held together by binding substances. Class V roads have a poor coating of soil, fastened or improved by additives.

As an example of the travel of a vehicular train on a class IV road, consider travel over a cobblestone road over a flat terrain in winter (compacted-snow road). The maximum acceleration that the vehicular train can develop under these road conditions is $a_x^{max} = 0.55\ m/s^2$. As an example of travel of the vehicular train over a class V road consider travel over a dirt road of satisfactory state over a level terrain after a rain. In this case the maximum acceleration is $a_x^{max} = 0.44\ m/s^2$. The maximum steady velocity was taken to be the same for both examples and equal to $V_{xc} = 30$ km/h. The principal results of these investigations are listed in Table 7.2, where they are compared with results obtained for a snow-covered concrete-paved road.

It is seen that the difference between the maximum possible efficiency η_{x*}^{tr} and efficiency η_{xd}^{tr} of the running gear of a vehicular train with an open differential increases as compared with data obtained for the case of a snow-covered concrete-paved road (Table 7.2, column 2). This stems both from the large difference between the slippages of the axle's wheels (see column 3) and the increasing wheel rolling resistance on such roads.

To obtain the optimum circumferential force $F_{x2}''^{*}$ on the wheel with better gripping conditions by means of a traction control system, the mean value of increase ΔF_x of the vehicular train should be 1.43-fold greater on the cobblestone road and 3.77-fold greater on the dirt road as compared with the concrete-paved road (column 4). It should be emphasized that an increase of $\Delta F_x = 7.77$ kN on a dirt road is quite large and amounts to 24.3% of the total circumferential force $F_{x\Sigma}$ needed for travel under these conditions.

The increase in the total circumferential force of the vehicular train provided by the traction control system reduces the difference between the wheel slippages (column 5). However, ratios $\left(\eta_{x*}^{tr}/\eta_{xtc}^{tr}\right)$ are rather high for all the aforementioned types of roads during the first 8 s of motion, that is, at the most rapid stage of acceleration, when acceleration rates lie in the region of maximum values (see column 6). This confirms the previously made statement on the need to lock the differential at this acceleration stage.

Loads on braking mechanisms (column 7) are higher on cobblestone and dirt roads as compared with the concrete-paved road. This is particularly typical of the dirt road with the high rolling resistance, when the energy intensity factor K_t of the braking mechanism is 1.17-fold higher than K_t on the concrete-paved roads at a two-fold smaller steady travel velocity (columns 8 and 1). This causes higher heating of the brakes on the dirt road (column 9). Note that the lower values of K_t and of t° on the cobblestone road as compared with a concrete-paved road (columns 1, 8, and 9) stem from the lower steady travel velocity to which the vehicular train is accelerated.

The values of Δ_δ (Table 7.2, column 10) were taken to be the same for all the roads, since they are lower than their values for the vehicular train with an open differential (column 3) and the slippage ratio from column 5 provided by the theoretical features of the traction control system. Such an approach will ensure that the real traction control system will be more effective.

Data in column 11 give the relative angular velocities of the links of the interwheel open differential that should be used as target values in designing the locking clutch. Note that the values of 1.35–1.40 assumed as the threshold values of Δ_δ for activating the differential locking mechanism correspond to such values of $(\omega'' - \omega_0)$ that in the majority of cases are smaller and in certain cases somewhat exceed the mean values of $(\omega'' - \omega_0)$ from Table 7.2.

TABLE 7.2

Analytical Results

	Tractive and Velocity Properties					Brake Mechanism Parameters			Recommendations for Design		
Road Conditions	$\left(\eta_{x*}^{tr}-\eta_{xd}^{tr}\right)_{max}$, % **Accelerating 0 through 8 s**	$\left(\frac{s_{\delta 2}^{''d}}{s_{\delta 2}^{'d}}\right)_{mid}$	ΔF_x, kN	$\left(\frac{s_{\delta 2}^{''tc}}{s_{\delta 2}^{'tc}}\right)_{mid}$	$\left(\frac{\eta_{x*}^{tr}}{\eta_{xtc}^{tr}}\right)_{max}$ **Accelerating 0 through 8 s**	T_b, kN-m	K_f, kW/m^2	$t°$, °C	Δ_δ	$(\omega'' - \omega_o)$, rad/s	Δt, s
1	**2**	**3**	**4**	**5**	**6**	**7**	**8**	**9**	**10**	**11**	**12**
Cement-concrete road covered with snow $V_{xc} = 60$ km/h	7.5	2.16	$\frac{2.06^a}{5.89}$	1.38	1.15	$\frac{0.36^a}{0.85}$	47.91	25	1.35–1.40	$\frac{2.93^a}{11.00}$	8–12 for $t = 0$–20 s; 4–8 when $t > 20$ s
Cobblestone road covered with snow $V_{xc} = 30$ km/h	9.8	1.96	$\frac{2.94}{8.80}$	1.42	1.11	$\frac{0.51}{1.43}$	23.71	11	1.35–1.40	$\frac{2.44}{15.57}$	4–12 for $t = 0$–20 s; 4–8 when $t > 20$ s
Dirt road after rain $V_{xc} = 30$ km/h	11.8	1.95	$\frac{7.77}{16.63}$	1.48	1.15	$\frac{1.00}{2.70}$	55.80	30	1.35–1.40	$\frac{4.08}{16.45}$	2–4 for $t = 0$–20 s; 2–8 when $t > 20$ s

[a] Mean in numerator; maximum in denominator.

It is seen from column 12 that on a deforming surface the time segment Δt during which one wheel will have a greater slippage than the other is much smaller than the values of Δt on nondeforming surfaces (particularly during the first 20 s of acceleration). This means that the need for alternating braking of wheels arises more frequently on a deforming road, which causes more intensive work of the traction control system and of the braking mechanisms. Under these travel conditions, it is more effective to resort to locking the differential. Data in column 12 shows that one may assume Δt of 10–15 s, during which the locking will not be disabled after it was activated in order to provide the maximum possible traction and velocity properties of the vehicular train.

The results of investigations presented in this section demonstrate the effectiveness of the suggested method for improving the traction and velocity properties of a highway vehicular train under all the travel conditions under study. In essence, the method is based on controlling the distribution of power between the wheels of the tractor by controlling the locking of the differential and the brakes of the driving wheels when traveling under poor road gripping conditions.

The use of the traction control system significantly improves the traction and velocity properties while retaining the high efficiency of the vehicular train as compared with one that employs a differential drive arrangement under poor gripping conditions when traction control is activated when the wheel slippage ratio Δ_δ attains a value of 1.35–1.4. At this threshold value of this ratio the temperature level of the braking mechanisms lies within permissible limits, even if it is assumed that traction control reacts to any difference in wheel slippages. The thermal load can be reduced further by locking the differential for the first 8–15 s of acceleration prior to controlling the braking of the driving wheel, and by keeping the differential locked at moderate travel velocities. This will ensure high traction and velocity properties of the vehicular train under all the travel conditions. The above results allow developing an algorithm for control of an integrated system of distributing the power among the tractor wheels.

7.6.2 Synthesis and Implementation of a Parallel Control Algorithm

7.6.2.1 Logical Control Languages

Note that control algorithms differ markedly from the classical computational algorithms. The latter process input data that, in principle, already contain the desired result: all that needs be done is to compute it from the input data. As opposed to this, control algorithms describe a method of correlating the control system under design with the object of control. This correlation amounts to a continuous exchange of information between the system and the object of control. The concept of input data loses its meaning as the data processed by the algorithm may be supplied to it continuously. The purpose of the algorithm is no longer obtaining some specific result in a concentrated form, but generating a sequence of control signals that control the behavior of the object of control.

Logical control algorithms are a particular case of the wider class of control algorithms. They process information represented by Boolean variables that select values from the set {0, 1}. The majority of logical control algorithms have typical features known as parallelism and asynchronicity.

An algorithm is called parallel if it allows and provides for the possibility of simultaneously performing several operations. Asynchronicity manifests itself in some indefiniteness in the time needed for performing the operations contained in the algorithm. Sequential algorithms are not critical to such uncertainty, as it does not exert any influence on the algorithm execution, except for the influence on the run-time. However, the

situation becomes radically different in the case of parallel algorithms, since this indefiniteness may cause races between simultaneously performed operations and in many cases, these races may turn out to be a hazard, interfering with the algorithm's performance. In these cases, the algorithm is termed incorrect (ill-posed).

A number of languages were suggested for describing logical control algorithms, including the PRALU—prime algorithms of logical control. A simplified and slightly modified version of this language, which is sufficient for the problem under study, is presented in the following text.

7.6.2.1.1 A Version of the PRALU Language

The algorithm is represented by a set of numbered propositions: the propositions are assigned marks μ_i, the role of which is played by natural numbers.

Each proposition consists of a sequence of chains in the form

$$-k'_j \rightarrow k''_j \rightarrow \nu_j,$$

where, k'_j and k''_j are elementary conjunctions of logical variables contained in the algorithm, whereas ν_j is a chain mark, that is also specified by some natural number.

The elementary conjunctions are interpreted as certain events that occur when the conjunction takes the value 1. Event k'_j represents a condition that is a part of the waiting operation $-k'_j$, event k''_j is a part of the action operation $\rightarrow k''_j$. A pair of these operations forms a condition-action type configuration: if event k'_j took place, then event k''_j should occur. In other words, satisfaction of the fragment of the algorithm consists in the following: if conjunction k'_j has taken on the value 1, then also conjunction k''_j becomes unity by assigning values of 1 to all its co-factors. This is followed by the jump operation $\rightarrow \nu_j$: the control is transferred to the proposition whose mark is the same as mark ν_j of the just implemented chain. Here all the conjunctions k'_j that belong to the same proposition should be orthogonal, not simultaneously acquiring the value of 1. For this reason, the satisfaction of a proposition reduces each time to satisfying only one chain (for which $k'_j = 1$).

7.6.2.2 The Logical Control Algorithm

The PRALU language makes it possible to formalize and automate the synthesis of a logic circuit that implements the logical control algorithm that is described in the language. This shall be demonstrated for the case of a logical control algorithm for imbalance of slippages, developed based on investigations, the results of which are presented in Section 7.6.1. This section defined the limits of the values of physical variables, which made it possible to use the logical model of the control process by introducing the pertinent logical variables—Boolean variables that take values from set {0, 1}.

These logical variables and the events represented by them (by the value 1) are listed below. They were described in more detail before in this chapter, and the meaning of expressions ''low velocity,'' ''moderate velocity,'' etc. were refined there:

v_1—low velocity,
v_2—moderate velocity,
v_3—high velocity,
b—the brake pedal is not depressed,
c—the gearshift level is not in neutral (the truck's transmission is manual),
d—the main clutch is engaged,
n—the engine crankshaft rpm is higher than the minimal permissible,

r—the wheel slippage imbalance exceeds the permissible level;
m—the slippages of both wheels exceed the permissible level,
f—the condition (7.153) is satisfied,
e—the differential's locking mechanism is operational,
i—the braking system is operational,
h—the fuel-pump rack control mechanism is operational,
g—the brake temperatures are within permissible limits,
k—the logical control device is actuated (by the driver).

These values are picked up from pertinent sensors installed in the vehicle and are fed to the input of the logical control system. Control signals that lead to events enumerated below should appear at the output poles of the loop:

L—the drive axle differential is locked,
B—the wheel with the highest slippage is braked,
F—the fuel-pump rack moves in a direction that reduces the fuel supply.

These signals are generated at certain control modes or states of the control system:

S(*L*)—differential locking mode,
S(B)—braking mode,
S(F)—fuel-feed reduction mode.

Their sequencing order is determined in the additional mode:

S(M)—manual control and sensor signal processing mode.

In the formal description of the control algorithm, these modes are represented, respectively, by propositions 1, 2, 3, and 4.

1:	- v_1 $\bar{\text{e}} \rightarrow \bar{\text{L}} \rightarrow 4$	Differential locking mode *S*(L)
	- v_1 $\bar{\text{f}} \rightarrow \bar{L} \rightarrow 4$	
	- v_1 b c d r e f $\bar{\text{m}} \rightarrow L \rightarrow 4$	
	- v_1 e f m $\rightarrow \bar{L} \rightarrow 4$	
	- $\bar{v}_1 \rightarrow \bar{L} \rightarrow 4$	
2:	- v_2 $\bar{\text{i}} \rightarrow \overline{\text{B}} \rightarrow 4$	Braking mode *S*(B)
	- v_2 $\bar{\text{f}} \rightarrow \overline{\text{B}} \rightarrow 4$	
	- v_2 b c d r g f i $\rightarrow$ B $\rightarrow 4$	
	- v_2 $\bar{\text{g}}$ f i $\rightarrow \overline{\text{B}} \rightarrow 4$	
	- $\bar{v}_2 \rightarrow \overline{\text{B}} \rightarrow 4$	
3:	- v_3 $\bar{\text{h}} \rightarrow \bar{\text{F}} \rightarrow 4$	Fuel supply reduction mode *S*(F)
	- v_3 $\bar{\text{n}} \rightarrow \bar{\text{F}} \rightarrow 4$	
	- v_3 $\bar{\text{m}}$ b c d h n r $\rightarrow$ F $\rightarrow 4$	
	- v_3 h m n $\rightarrow \bar{\text{F}} \rightarrow 4$	
	- $\bar{v}_3 \rightarrow \bar{\text{F}} \rightarrow 4$	
4:	- k $v_1 \rightarrow 1$	Manual control and sensor signal
	- k $v_2 \rightarrow 2$	Processing mode *S*(M)
	- k $v_3 \rightarrow 3$	

The algorithm is cyclical. Assume that the system is in the manual control mode. Look at proposition 4. It is seen that when variable k acquires the value 1 (the driver actuated the automated system) the control will shift to the differential blocking mode if the velocity is low, to the braking mode if the velocity is moderate and to the S(F) mode at high velocity.

Assume that the system has shifted to the differential locking mode. When condition v_1 b c d r e f $\bar{\text{m}} = 1$ is satisfied, the third chain in proposition 1 will be actuated and this will bring about the generation of the locking signal L and the control will revert to proposition 4. Should another chain be actuated, the differential will become unlocked and the control will be again shifted to proposition 4.

In the braking mode one deals with the condition v_2 b c d r g f i $= 1$ and, when it is satisfied (the third chain in the proposition is actuated) the braking signal B is generated. When other chains are actuated, the braking signal will be annulled. In any case, after this the control will revert to proposition 4.

The same applies to proposition 3 that pertains to the fuel supply reduction mode. The condition that is analyzed in it is v_3 $\bar{\text{m}}$ b c d h n r $= 1$, the satisfaction of which generates signal F that causes the fuel pump rack to move to lower fuel supply location. This signal will not be generated when other chains are actuated. Again, after any chain is actuated, the control reverts to proposition 4.

7.6.2.2.1 Representing the Control Algorithm by a System of Sequents

There exist two methods of implementing automatic control.

The first consists of using a computer aboard the vehicle. In this case the control is implemented by a program in which the control algorithm is usually represented in the language of algorithmic graphs.

The second method consists in constructing a logic circuit on some elemental basis. For example, that logic circuit can be constructed based on AND-OR-NOT elements or, on the more recent basis of a programmable logic device (PLD). An example of using a programmable logic array (PLA) is given in the following text. To synthesize such a circuit, it is advisable to shift from describing the algorithm in the PRALU language to its representation in the language of sequents, as shall be shown later.

To begin with, four triggers, the states of which shall be represented by the pertinent Boolean variables (1—the trigger is actuated—SET, 0—the trigger is not actuated—RESET) shown in Table 7.3, are introduced into the logical circuit.

Unity values of these variables will indicate that the control device is in the pertinent mode.

Supplementing the previously introduced variables by them allows shifting from the chains of the algorithm in the PRALU language to their equivalent condition-action type prime sequents.

TABLE 7.3

Triggers and Their Boolean Variables

Control Mode	Trigger	Variable
Differential locking mode	p_1	s_1
Braking mode	p_2	s_2
Fuel supply reduction mode	p_3	s_3
Manual control and sensor signal processing mode	p_4	s_4

The term *prime sequent* is applied to an expression in the form $k_i' \vdash k_i''$ with elementary conjunctions k_i' and k_i'', that is interpreted as follows: if at any point in time the conjunction k_i' is equal to 1, then immediately thereafter conjunction k_i'' also takes the value 1.

For example, the first chain in the algorithm will have corresponding to it the prime sequent

$$s_1 v_1 \bar{e} | - \bar{L} \bar{s}_1 s_4$$

It is interpreted as follows. If at any point of time, the differential is in the locked mode ($s_1 = 1$), the vehicle velocity is low ($v_1 = 1$) and the locking mechanism is not operational ($e = 0$), then the differential should be unlocked (by assigning the value of 0 to variable L) and manual control should be initiated (assigning the value of 0 to variable s_1 and the value of 1 to variable s_4).

All the chains of the algorithm are subjected to a similar transformation. The result is represented by the following Table 7.4.

7.6.2.2.2 Control Algorithm Implementation Circuit

The prime-sequents system shown in Table 7.4 can be used for synthesizing a programmable logical matrix (PLM) that implements the logical control algorithm upon slippage imbalance. Since the algorithm is rather simple, it is possible to manage with one PLM with feedback, as shown in Figure 7.39.

The PLM consists of two matrix logic circuits connected in parallel and produced on a single crystal. Each of them consists of two families of conducting lines situated in two parallel planes. Any pair of lines from different planes may be connected by a transistor

TABLE 7.4

The Control Algorithm in Prime Sequents

Chains of the Algorithm	Their Equivalent Prime Sequents
1: - v_1 $\bar{e} \rightarrow \bar{L} \rightarrow 4$	$s_1\ v_1\ \bar{e} \mid - \bar{L}\ \bar{s}_1\ s_4$
- v_1 $\bar{f} \rightarrow \bar{L} \rightarrow 4$	$s_1\ v_1\ \bar{f} \mid - \bar{L}\ \bar{s}_1\ s_4$
- v_1 b c d r e f $\bar{m} \rightarrow L \rightarrow 4$	$s_1\ v_1$ b c d r e f $\bar{m} \mid - L\ \bar{s}_1\ s_4$
- v_1 e f m $\rightarrow \bar{L} \rightarrow 4$	$s_1\ v_1$ e f m $\mid - \bar{L}\ \bar{s}_1\ s_4$
- $\bar{v}_1 \rightarrow \bar{L} \rightarrow 4$	$s_1\ \bar{v}_1 \mid - \bar{L}\ \bar{s}_1\ s_4$
2: - v_2 $\bar{i} \rightarrow \overline{B} \rightarrow 4$	$s_2\ v_2\ \bar{i} \mid - \overline{B}\ \bar{s}_2\ s_4$
- v_2 $\bar{f} \rightarrow \overline{B} \rightarrow 4$	$s_2\ v_2\ \bar{f} \mid - \overline{B}\ \bar{s}_2\ s_4$
- v_2 b c d r g f i $\rightarrow B \rightarrow 4$	$s_2\ v_2$ b c d r g f i $\mid - B\ \bar{s}_2\ s_4$
- v_2 $\bar{g}$ f i $\rightarrow \overline{B} \rightarrow 4$	$s_2\ v_2\ \bar{g}$ f i $\mid - \overline{B}\ \bar{s}_2\ s_4$
- $\bar{v}_2 \rightarrow \overline{B} \rightarrow 4$	$s_2\ \bar{v}_2 \mid - \overline{B}\ \bar{s}_2\ s_4$
3: - v_3 $\bar{h} \rightarrow \bar{F} \rightarrow 4$	$s_3\ v_3\ \bar{h} \mid - \bar{F}\ \bar{s}_3\ s_4$
- v_3 $\bar{n} \rightarrow \bar{F} \rightarrow 4$	$s_3\ v_3\ \bar{n} \mid - \bar{F}\ \bar{s}_3\ s_4$
- v_3 $\bar{m}$ b c d h n r $\rightarrow F \rightarrow 4$	$s_3\ v_3\ \bar{m}$ b c d h n r $\mid - F\ \bar{s}_3\ s_4$
- v_3 h m n $\rightarrow \bar{F} \rightarrow 4$	$s_3\ v_3$ h m n $\mid - \bar{F}\ \bar{s}_3\ s_4$
- $\bar{v}_3 \rightarrow \bar{F} \rightarrow 4$	$s_3\ \bar{v}_3 \mid - \bar{F}\ \bar{s}_3\ s_4$
4: - k $v_1 \rightarrow 1$	$s_4\ \bar{k}\ v_1 \mid - \bar{s}_4\ s_1$
- k $v_2 \rightarrow 2$	$s_4\ \bar{k}\ v_2 \mid - \bar{s}_4\ s_2$
- k $v_3 \rightarrow 3$	$s_4\ \bar{k}\ v_3 \mid - \bar{s}_4\ s_3$

and the set of such connections is most conveniently represented by a corresponding Boolean matrix (1—a connection exists, 0—there is no connection). The first matrix is known as the conjunction matrix, and the second as the disjunction matrix.

The structure of these matrices can be obtained directly from the sequents system. Variables from the left sides of the sequents, as well as their negations obtained by inverters are fed to the input poles of the first matrix; the values of conjunctions represented by the left parts of the sequents are picked up from the output poles. These values are fed to the corresponding input poles of the second matrix, the output poles of which control the states of seven triggers causing them to be in the actuated (set) or passive (reset) state. The outputs of three of these triggers supply values of the output variables for the control system as a whole. These are the differential locking signal (L), braking signal (B), and fuel supply reduction signal (F).

The four remaining triggers put out the current state of the system and they provide the feedback in the PLM, determining the signs of variables s_1, s_2, s_3, and s_4, used as the input in the first matrix.

The structure of the PLM obtained in this manner, defined by the array of transistors that are employed, is shown in Figure 7.39. The transistor locations are given by bold dots. It is represented by a matrix pair with 18 columns corresponding to prime sequents. The columns of the first (top) matrix define the conjunctions that represent the left parts of the sequents, whereas the columns of the second (bottom) matrix define conjunctions representing the right parts of the sequents. The rows of the second matrix are interpreted as disjunctions of the conjunctions noted in it that were implemented in the first matrix.

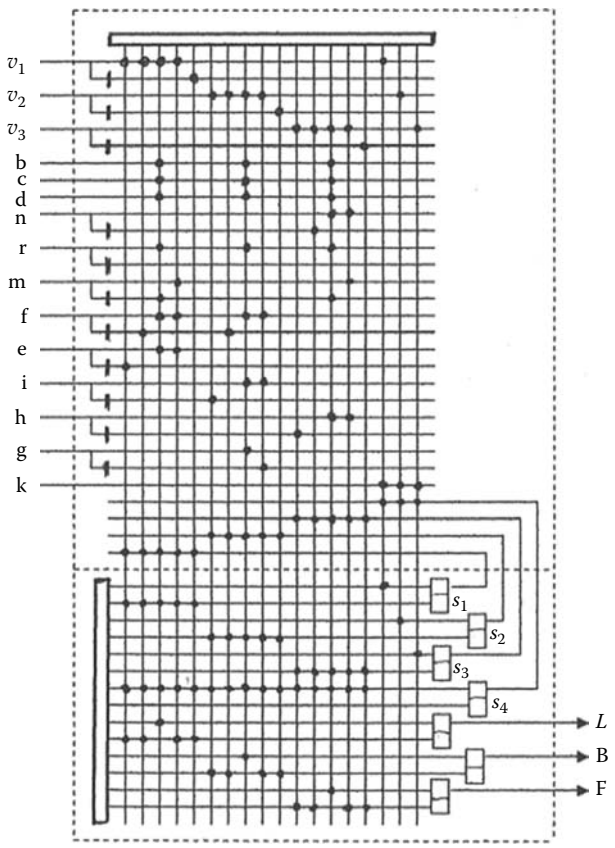


FIGURE 7.39
PLM implementation.

For example, the conjunction $s_1\ v_1\ \bar{e}$ is implemented in the left column of the first matrix, whereas the bottom row of the second matrix, representing the shifting of the trigger to *reset*, implements the disjunction

$$s_3\, v_3\ \bar{h} \vee s_3\, v_3\ \bar{n} \vee s_3\, v_3\ h\ m\ n \vee s_3\ \bar{v}_3.$$

7.7 Hybrid Driveline Systems

For many decades now, work is being done to design hybrid drivelines, of alternate mechanical and mechatronic systems, the design of which is based on that of mechanical systems (see Sections 7.1 through 7.6). These hybrid driveline systems include hybrid-hydraulic and electrical wheel drives. The principal merit and advantage of such drivelines consists of their ability for the stepless transmission of power to the drive wheels and the feasibility of control of power flows to axles and individual wheels within a wide range. These driveline systems are known as hybrid, that is, systems that combine principles of hydraulic, electrical, and mechanical power transmission. It should also be emphasized that these systems are intentionally analyzed in this book in the chapter concerned with mechatronic systems. Hybrid-electro and hybrid-hydraulic systems contain combined control systems and the synthesis of such systems is increasingly based on principles of mechatronic systems design. Obviously, the number of engineering problems involved in designing hybrid driveline systems suffices to fill a number of books. For this reason, this book is concerned only with those design aspects that pertain to the distribution of power between drive wheels and with the effect on vehicle dynamics and performance.

7.7.1 Advanced Hybrid-Hydraulic Driveline Systems

Hybrid-hydraulic drives are technically more complex, high-tech, more labor intensive in production, and costly as compared with mechanical power transmissions. They have come into use on vehicles in which the specific requirements are transmission of power from the engine to the drive wheels and the working elements of the vehicle, and the control of power flows. These vehicles include forest-engineering and road-construction equipment and some military vehicles. In addition, hybrid hydraulic driveline systems are used in grain and fodder harvesting combines, farm, and industrial tractors. The smooth application of torques to the wheels of tractors, without a break in the power flow, promotes the preservation of the structure and properties of the soil.

Hybrid-hydraulic drives, in general, are subdivided into (i) hydrostatic full-flow drives (HD), in which the engine power is transmitted hydraulically to the wheels, and (ii) two-flow hydraulic-mechanical driveline systems (HMD) with differentials at the input and output, in which, the lesser part of the power (20%–40%) is transmitted hydraulically, whereas, the major part (60%–80%) is transmitted mechanically. Figure 7.40 illustrates the concepts of these systems.

One of the main advantages of full-flow driveline systems is the possibility of supplying each wheel individually by a separately controlled power flow, irrespective of its distance from the supply unit (Figure 7.40a). In the hydraulic-mechanical driveline system (HMD) (Figure 7.40b and c) the hydraulic part of the drive performs the functions of the regulator of the rotational velocity and torque at the output shaft, with the power supply to the drive

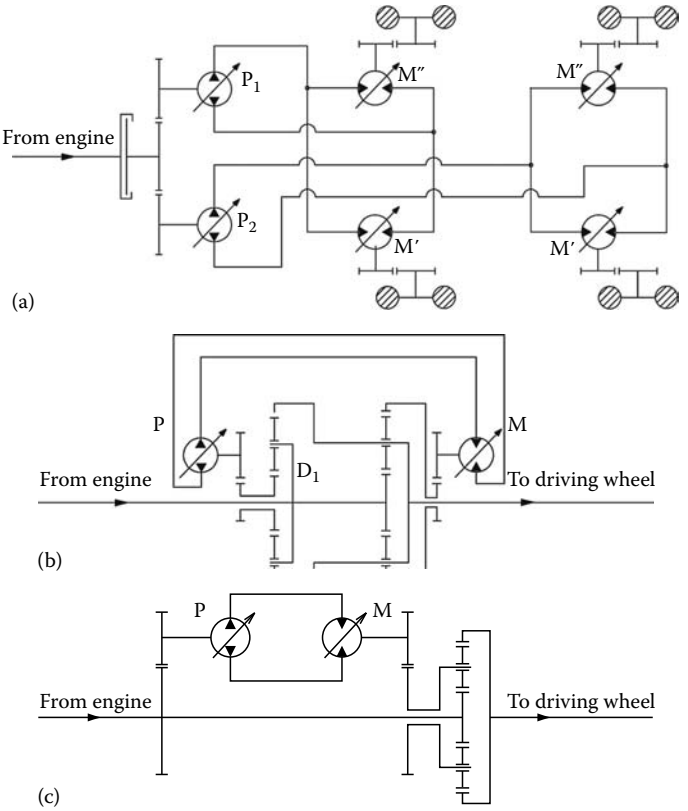


FIGURE 7.40
Schematic diagrams of hybrid-hydraulic driveline systems: (a) a full-flow system; (b) a hydraulic-mechanical driveline with two differentials; (c) a hydraulic-mechanical driveline with a differential at the output.

shaft of the HMD remaining constant. The overall efficiency of HMD is higher than the overall efficiency of the full-flow driveline systems and may be as high as 0.9–0.93. The HMD is constructed as a single unit with a common case and common output shaft, that is, it is capable of driving only a set of vehicle wheels interconnected by mechanical PDUs (see Figure 7.41). It should be noted in conjunction with this that HMDs do not require additional stepped gear transmissions.

HMDs have a much smaller power adjustment range than HDs (not more than 4.5), have no symmetrical reverse, exhibit power circulation in a number of modes, and present difficulties in automating the control by means of a control algorithm.

Since HMDs cannot provide controlled individual supply of power of each of the wheels of an all-wheel drive vehicle, which is very important when moving over deforming soil, consideration is hence limited to full-flow driveline systems, that is, HDs.

The advantages provided by hydraulic drivelines in wheeled vehicles can be divided into two groups. The first is made of advantages that follow from the use of hydrostatic powertrain as being one form of a step-less, wide-range wheel drive. The second group includes additional advantages that are inherent only to HD.

The first group presents the following principal advantages.

1. Step-less, without discontinuities in the power flow variation in the torque supplied to the wheels; this improves the average operating velocities when moving under off-road conditions by better utilizing the engine power, reducing the extent of damage to the soil and to the vegetable cover, and facilitating the steering of the vehicle.

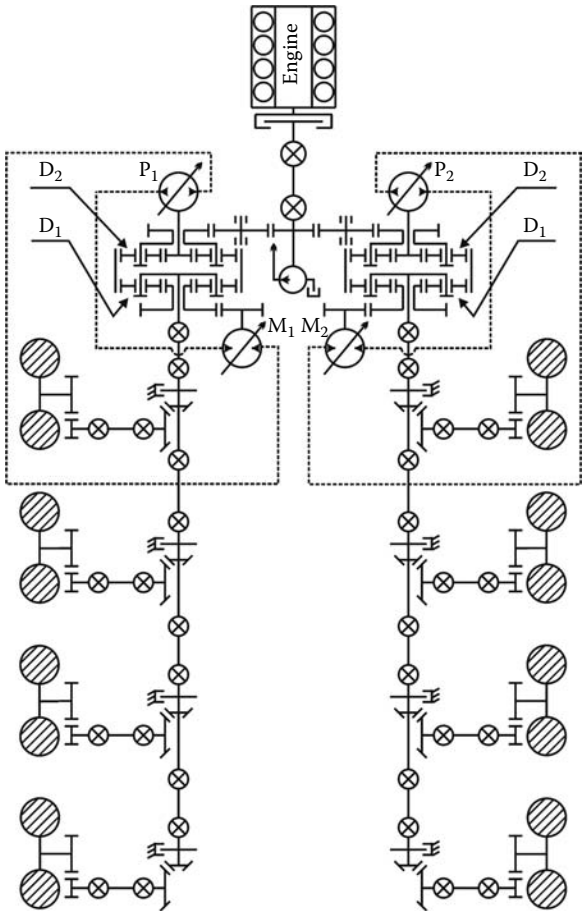


FIGURE 7.41
Schematic diagram of a two-flow hydraulic-mechanical driveline for a high-mobility wheeled vehicle with powered side-wheels.

2. Feasibility of having the powertrain operating in the optimal mode, that is, in a mode that is a compromise of requirements such as minimum fuel consumption, minimal toxicity of exhaust gases, optimal heat conditions, etc. This, in particular, makes it possible to use power plants with minor torque variation, including high-speed power plants (such as single-shaft turbines).
3. Feasibility to individually control the drive of each wheel. Here control can be implemented, among others, in accordance with the current gripping capabilities of the soil by each of the wheels, which improves the mobility and the traction and velocity properties of the vehicle. In addition, in this case it becomes possible to improve the turnability under off-road conditions by being able to perform a side/tight turn, up to a ''turn on the spot.''

The second group is comprised of the following principal advantages:

1. Functionally, the rigid kinematic and power performance curve of the HD approaches the performance curve of a mechanical step-less transmission and the short response time of the drive, which steeply reduces dynamic loads in the drive under varying operating conditions. From this stems the feasibility of precisely controlling the gear ratio by means of any preset algorithm.

2. The feasibility of installing an HD on a vehicle, with less consideration of the mutual location of units and components.
3. The feasibility of prolonged operation at low ''creeping'' velocity, which, for high-mobility vehicles amounts to 0.14–0.21 m/s and also upon a sudden stop (e.g., upon impacting an obstacle) without overheating the HD. Here the maximum torque is produced at the wheels at close to zero rpm and the power consumption may be negligible, that is, the drive engine may operate virtually at no-load rpm (the pump output is utilized only for replenishing leaks and parasitic flows).
4. Ease of obtaining a rapid (about 0.12 s) and, torque and kinematic-symmetrical reverse, something that allows to an energy ''swing out'' of a vehicle that got stuck without discontinuity of the power flow.
5. Moderate size and mass of the units and of the HD as a whole, particularly on vehicles with wheel formula 8×8 and above.
6. Reliability of the hydraulic-drive operation, relative independence of its performance on external factors (good dust and moisture protection), and feasibility of submerged operation.
7. Less maintenance in the course of the HD's operation (except for the replacement of filter elements every 200–300 h and of the working fluid every 2000–2500 h) and of lubrication and adjustment.
8. Safety of HD operations (the jet of the fluid that may be discharged in an accident contains only small quantity of energy and does not expand).
9. Convenience in power takeoff.
10. Availability of reliable means for protecting from overloads, dynamic impact (''water hammer''), jolts, etc.

At the same time, hydraulic driveline systems have certain inherent shortcomings that are either difficult or impossible to eliminate:

1. The transmission of power from the engine to the wheels involves double energy transformation: mechanical energy is converted into hydraulic energy and the latter is then transformed into mechanical energy. This reduces the overall efficiency of the vehicle as compared with a mechanical drive.
2. The complexity of HD design and its labor-intensive manufacture, including that of precision couples results in a very high unit cost of production. (The cost nowadays exhibits a tendency of decreasing).
3. The need for using matched reduction gear units between the engine and the pumps, and the hydraulic motors and wheels.
4. Elevated noise when operating at high pressure and high rpm (high-frequency oscillations of working fluid).
5. The high (much higher than average) proficiency and expertise of designers and manufacturing workers needed to ensure high-quality design, manufacture, assembly, adjustment, and mass production of HD components.
6. The fact that it cannot be used for braking, that is, in the throttling mode because throttling causes rapid overheating of the working fluid.

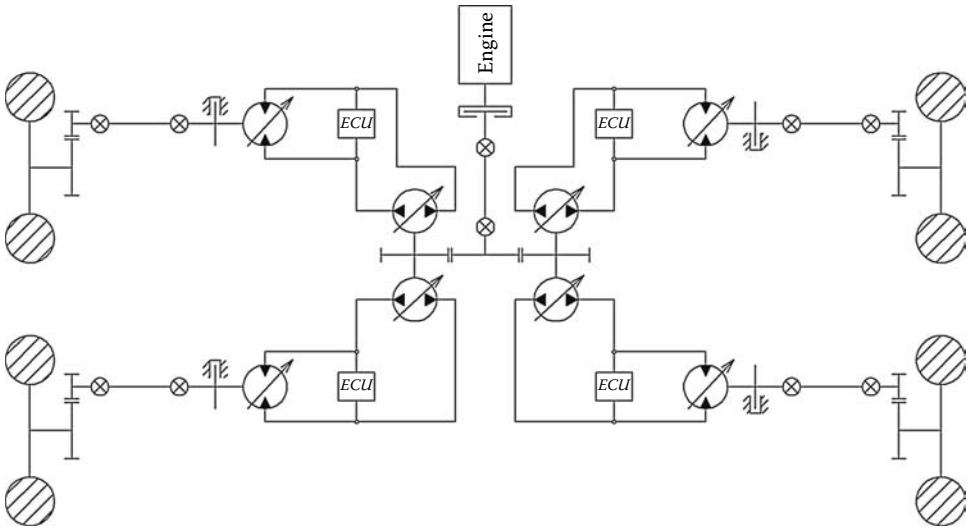


FIGURE 7.42
Version I. Schematic diagram of a vehicular HD with individual transmission for each wheel.

Our many years of experience in testing and designing hybrid hydraulic driveline systems points to the existence of seven promising design versions that can serve as the basis for synthesizing actual devices.

Version I. HD of a vehicle with an individual drive for each of its wheels (hydraulic-motor-pump drive) with self-contained control and independent power supply. This version is shown in Figure 7.42 for a 4×4 vehicle.

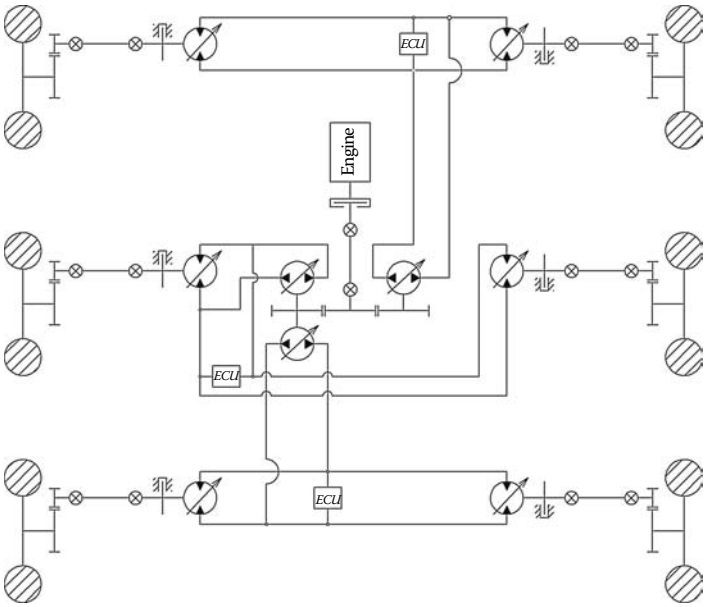
Version I is ideal for individual, flexible controlled distribution of power between all the drive wheels that ensures optimal vehicle dynamics and performance. Nevertheless, the large number of pumps and control loops, equal to the number of drive wheels, relatively complicates the design and causes manufacturing difficulties and it is hence not recommended for use on vehicles with a wheel formula higher than 4×4.

Version II. This hydraulic driveline system is made up of modular units consisting of a hydraulic pump and two hydraulic motors. Such modules are used for each wheel pair of one conditional axle with controlled hydraulic-differential coupling between the hydraulic motors that drive the wheels.

Figure 7.43 shows a schematic diagram of such a HD and the 6×6 ''Gidrohod-49061'' vehicle in which this design version is used.

Version II makes use of individual, flexibly adjustable supply of power to each conditional axle (pair of wheels) independent of other wheels that are able to operate independently. The coupling between the power modules is locked, but with optimal control of hydraulic units contained in the module, thus eliminating interaxle power circulation. In this version the number of drive pumps is one-half that of drive wheels, which makes for a sensible design. Nevertheless, there is a hydro-differential coupling between the wheels of one conditional axle. Separate control of the hydraulic motors of these wheels makes it possible to attain a value of the interwheel locking coefficient (torque bias) of the conditional axle of $K_d = 4.85$.

When moving over solid-pavement roads, all the power units of the HD can combine into a single hydraulic system. In this case, there comes about complete hydro-differential coupling between all the drive wheels and there is no power circulation between them. The



(a)



(b)

FIGURE 7.43
Version II. 6 × 6 ''Gidrokhod-49061'' vehicle with HD of version II: (a) HD schematic diagram; (b) the vehicle.

hydraulic motor of a wheel that becomes fully detached from the surface of motion may be switched in 0.12 s to the hydraulic ''zero,'' which corresponds to zero working volume of this hydraulic motor ($q_m = 0$). As a result, the hydraulic conduit of this wheel is shut off, which prevents the wheel from spinning and the general fluid line from a drop in the working fluid pressure. At the same time, the wheel is still capable of rotating, which is important in the case when it renews its contact with the ground. Investigations show that Version II is most advisable for use on vehicles with wheel formula 6×6, 10×10, and 12×12. In a number of cases, it is advisable to use an articulated chassis for the 12×12 wheel formula vehicle, made up of two 6×6 sections. Each section may have an independent unified power unit (engine with control systems, pump station, hydraulic motors,

power reducing gears, etc.). The power unit of the rear section is electrically remote controlled from the common control system of the articulated vehicle.

The kinematic and power coupling of the hydraulic motors of the wheels of a single conditional axle is defined as:

$$\frac{\omega'_{\mathrm{m}} q'_{\mathrm{m}}}{\eta_{v\mathrm{m}}} + \frac{\omega''_{\mathrm{m}} q''_{\mathrm{m}}}{\eta_{v\mathrm{m}}} = \omega_{\mathrm{p}} q_{\mathrm{p}} \eta_{v\mathrm{p}} \tag{7.171}$$

where ω_{m}, q_{m}, and $\eta_{v\mathrm{m}}$ are the angular velocity, working volume, and volumetric efficiency of the hydraulic motor, respectively (the symbols ′ and ″ pertain to the left and right wheel of the same conditional axle); ω_{p}, q_{p}, and $\eta_{v\mathrm{p}}$ are the angular velocity, working volume, and volumetric efficiency of the pump, respectively.

It follows from formula (7.171) that the angular velocities ω'_{m} and ω''_{m} of the hydraulic motors (respective velocities $\omega'_{\mathrm{w}}, \omega''_{\mathrm{w}}$ of the wheels) of each of the modular units can be changed by intentionally varying the working volumes q_{p} of the pump and q'_{m} and q''_{m} of the motors independently of the two other units of the 6×6 vehicle (Figure 7.43a). Thus, for example, increasing the rpm of two wheels of a single modular block may be attained by increasing q_{p} while retaining constant pressure in the hydraulic motors (i.e., of the torque at the wheels). The wheel rpm can also be increased by reducing the size of q'_{m} and q''_{m}, which will increase the pressure in the hydraulic system in order to maintain the wheel torques constant. This means that Version II fully allows individual control of the angular velocities of the wheels.

The torque at the hydraulic motor shaft is defined by the formula:

$$T_{\mathrm{m}} = \frac{1}{2\pi} \Delta p_{\mathrm{m}} q_{\mathrm{m}} \eta_{\mathrm{mm}} \tag{7.172}$$

where

Δp_{m} is the pressure difference along the hydraulic system main
η_{mm} is the mechanical efficiency of the hydraulic motor

When the hydraulic motors of the wheels of one conditional axle are connected in parallel (i.e., $\Delta p'_{\mathrm{m}} = \Delta p''_{\mathrm{m}}$) the ratio of the wheel torques is obtained from formula (7.172)

$$\frac{T''_{\mathrm{w}}}{T'_{\mathrm{w}}} = \frac{q''_{\mathrm{m}} \eta''_{\mathrm{mm}}}{q'_{\mathrm{m}} \eta'_{\mathrm{mm}}} \tag{7.173}$$

Formula (7.173) is the basic relationship for designing a system for controlling the torques of the wheels of the conditional axle.

The hydraulic power of the pump of each modular unit is:

$$P_{\mathrm{hp}} = k_1 \omega_{\mathrm{p}} q_{\mathrm{p}} \Delta p_{\mathrm{p}} \eta_{\mathrm{vp}} \eta_{\mathrm{mp}} \tag{7.174}$$

where

ω_{p} is the angular velocity of the pump
q_{p} is the working volume of the pump
Δp_{p} is the pressure difference in the supply line
η_{vp} is the volumetric efficiency of the pump
η_{mp} is its mechanical efficiency

The power supplied to two wheels of a single conditional axle is

$$P_{\mathrm{w}}^{\mathrm{in}} = k_2 \eta_{\mathrm{mr}} \left(T'_{\mathrm{w}} \omega'_{\mathrm{w}} \eta'_{\mathrm{vm}} + T''_{\mathrm{w}} \omega''_{\mathrm{w}} \eta''_{\mathrm{vm}} \right) \tag{7.175}$$

where, k_1 and k_2 are proportionality factors that represent the dimensionalities of the quantities contained in the formula and are specified as constant values for the given hydraulic units; η_{vm} is the volumetric efficiency of the hydraulic motor and η_{mr} is the mechanical efficiency of the output reduction gear.

Using formulae (7.174) and (7.175) one may write:

$$P_{\mathrm{w}}^{\mathrm{in}} = P_{\mathrm{hp}} \eta_{\mathrm{hp}\Sigma} \tag{7.176}$$

where, the overall efficiency of the hydraulic drive is:

$$\eta_{\mathrm{hp}\Sigma} = \eta_{\mathrm{pr}} \eta_{\mathrm{vp}} \eta_{\mathrm{mp}} \eta_{\mathrm{vm}} \eta_{\mathrm{mm}} \eta_{\mathrm{n}} \eta_{\mathrm{mr}} \tag{7.177}$$

where

η_{n} is the efficiency of the fluid supply mains

η_{pr} is the mechanical efficiency of the pump station

It can be concluded from formulae (1.171) through (7.177) that the power $P_{\mathrm{w}}^{\mathrm{in}}$, supplied to the wheels of each module can be controlled individually and independently of the two other modules in the 6×6 vehicle (Figure 7.43a) by varying the parameters T'_{m}, T''_{m} and ω'_{m}, ω''_{m}. The differences in the value of power $P_{\mathrm{w}}^{\mathrm{in}}$ supplied to the wheels of the different modules may be as much as 2–2.5-fold. The power between modular units (actually between the vehicle's axles) can be redistributed while maintaining the overall power supplied by the engine to all the three modules constant in this manner.

Version III. It provides for fully hydro-differential drive of all the wheels, that is, with respect to distribution of power between the wheels this version is fully analogous to the differential scheme of the mechanical drive of wheels (Figure 7.44).

Version III should be preferably used on heavy-duty, multiwheel drive chassis (up to 150 and more tons), on which special equipment (e.g., cranes) is to be installed. These, as a rule, move over routes when it is impossible for wheels to independently slip and lose contact with the road. Any difference in the gripping conditions of the drive wheels can be compensated for by adjusting the working volumes of the corresponding hydraulic motors, while retaining the complete hydro-differential drive as a whole. Should it happen that one of the wheels would lose touch with the ground, its spinning can be prevented by setting the corresponding hydraulic motor to ''zero.'' The pump station must include several controlled, reversing, and convertible pumps connected in parallel with the main fluid supply line. The use of several small pumps (instead of one large one) is more advisable from the point of view of improving their specific masses and dimensions and their energy performance. The presence of several pumps in the pumping station also improves the reliability of the hydraulic driveline operation, which is important for such chassis, since a malfunctioning (not mechanically broken down) pump can be disconnected from the hydraulic drivelines by setting it to the zero position without disconnecting it hydraulically.

This version suffers from a difficulty in synchronous control of the large number of hydraulic units and other components and also from the need of using more complex and

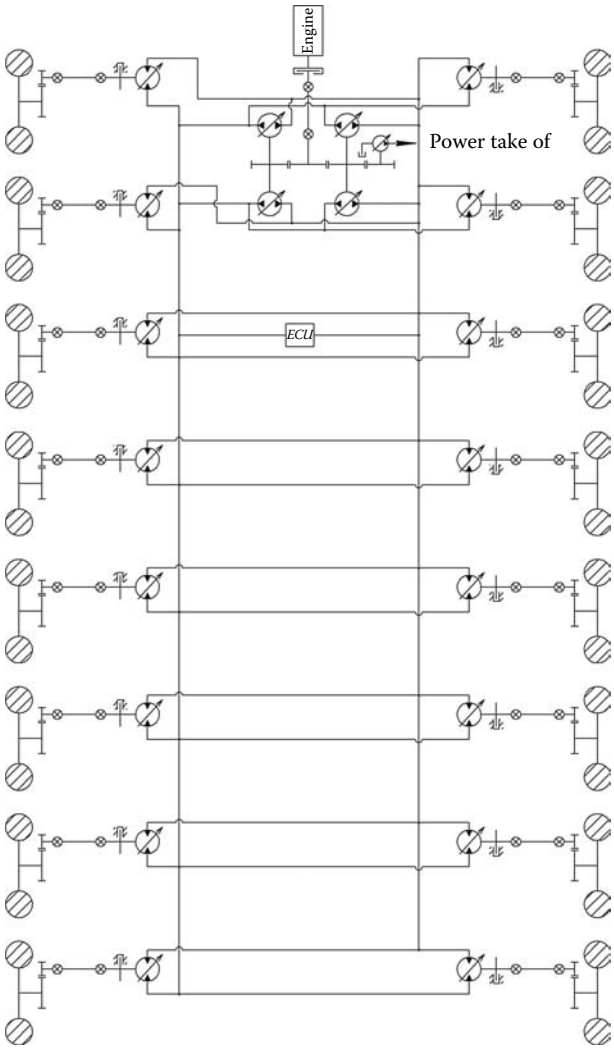


FIGURE 7.44
Version III. Schematic diagram of a vehicular HD with fully hydro-differential drive.

expensive hydraulic motors with zero nominal working volume (to prevent the disconnection of wheels that lose contact with the ground).

Version IV. An example of a vehicle with such a driveline system is shown in Figure 7.45. The wheels of each side have a positively locked mechanical drive and its hydraulic pump station. Both pump stations are driven together by the vehicle's engine.

When a vehicle with this driveline system moves under off-road conditions, both side hydraulic stations should be controlled synchronously (have their velocity ratio changed) by means of an on-board computer that prevents side-to-side power circulation. When the vehicle turns the velocity ratios of the side HDs change in a specific manner in accordance with the turn angles of the steered wheels, which provides for strictly specified turning radii. Motion under these conditions occurs at the fully locked drives of all the wheels, which provides for a maximum mobility of the vehicle on soft ground. The turnability of the vehicle can be improved by controlling HDs of both sides up to turning on one spot by means of mutually reversing the side HDs.

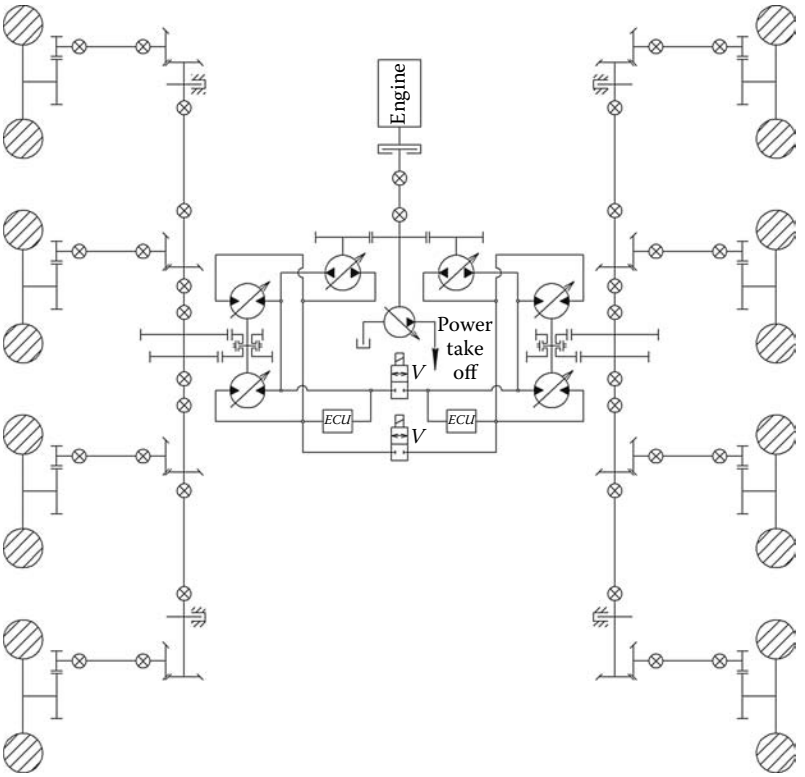


FIGURE 7.45
Version IV. Schematic diagram of a vehicular HD with separate side power supply.

When moving over roads with hard pavements both side HDs are hydraulically combined into a common hydraulic system by means of V-ring valves that prevent side-to-side power circulation. The vehicle is turned only by means of steered wheels with differential coupling between the sides. In this case, wheel-to-wheel circulation of power of each side is possible. The separate supply of power and torque to each individual wheel with individual ''flexible'' adjustment of these parameters according to specifications also becomes impossible. Version IV is recommended for high-mobility maneuverable vehicles operating under extreme road conditions (e.g., an armored personnel carrier with 8×8 wheel formula), where wheel-to-wheel power circulation is not taken into consideration and it is required that the drive as a whole is highly reliable in spite of possible damage to individual wheels, and the matter of primary concern is not fuel economy.

Version V. An example of an 8×8 articulated vehicle with this version is shown in Figure 7.46.

All the wheels (usually 4) of a single tandem have a common locked drive from its hydraulic transmission. The coupling between the axles within the tandem is locked (in view of the probability that one of the axles will lose contact with the ground). The coupling between the tandems is hydraulically positively locked (separate drive of the pumps serving the tandems) or hydro-differential (the circuits of both pumps are connected together by means of V-ring valves). The wheels of each axle are interconnected by means of mechanical differentials that are either of the open or limited slip type. The

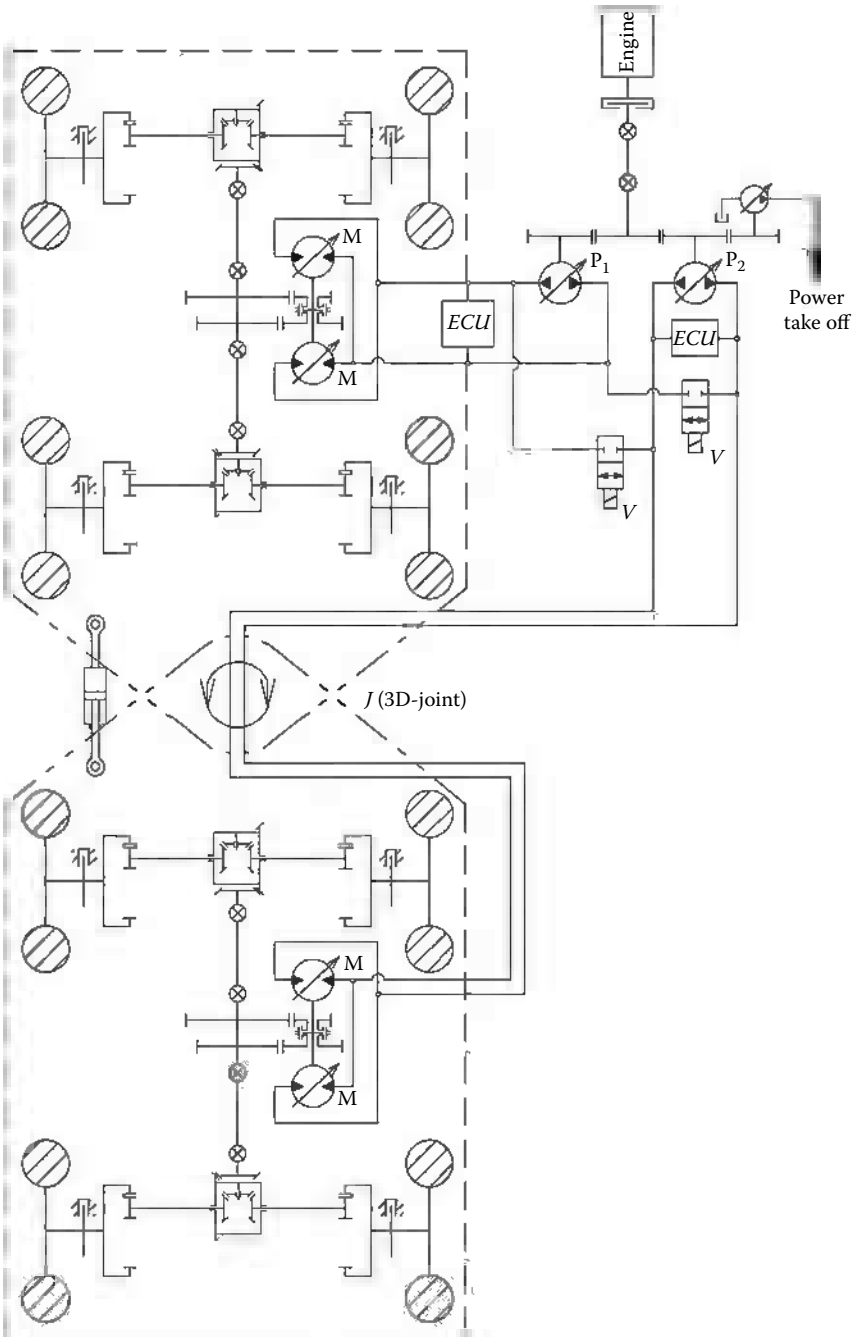


FIGURE 7.46
Version V. Schematic diagram of a vehicular HD with tandem drive system.

hydraulic coupling of the rear section pump to the rear hydraulic motors occurs by means of a rotary-hinge joint J (with 3 degrees of freedom).

Version V considered here does not provide for separate power and torque supply to each individual wheel. The mobility of a vehicle with this driveline system is assisted by locking the inter-tandem and intra-tandem drives, interwheel limited slip differentials, and articulation of sections (this reduces the power loss at the wheel that occurs in turning). The course stability is improved and the stability of motion in a turn increases. Upon jamming, the sections may fold relative to one another—''side swingout.'' In addition, the hydraulic system is simplified (less pumps, hydraulic motors, and electronic control units).

This version is recommended for use on multiwheel articulated vehicles with an axle arrangement that employ standard axles with locking interwheel differentials. This allows to easily attain complete (rigid) interaxle locking.

Version VI. An example of the vehicle is shown in Figure 7.47. In this and similar vehicles with such a hydraulic driveline system the wheels do not turn (side turn system). The significant power losses in turning (friction at the soil, its deformation, etc.) are compensated by rigid locked drive of all the wheels that prevent their separate slip, which improves the vehicle's mobility. The hydraulic driveline systems are controlled in such a manner when the vehicle turns as to ensure kinematic discrepancy of the sides

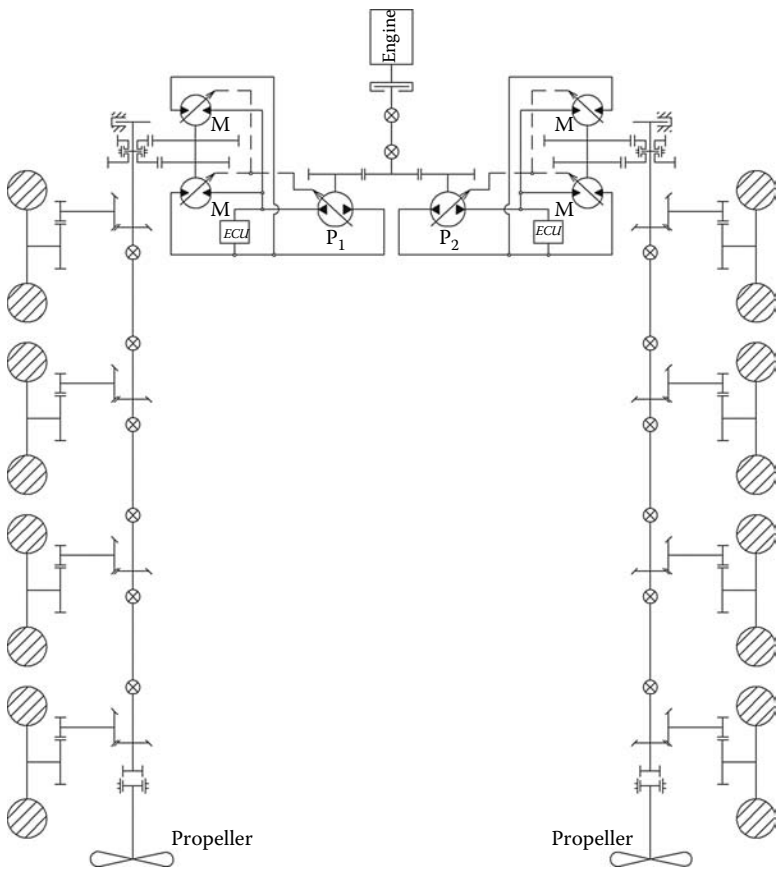


FIGURE 7.47
Version VI. Schematic diagram of a vehicular HD with side drive and turn systems.

that corresponds to their turn radius. This driveline layout is used on both wheeled and tracked vehicles.

Version VII. This version is illustrated in Figure 7.48 by an articulated vehicle with 12 driving wheels.

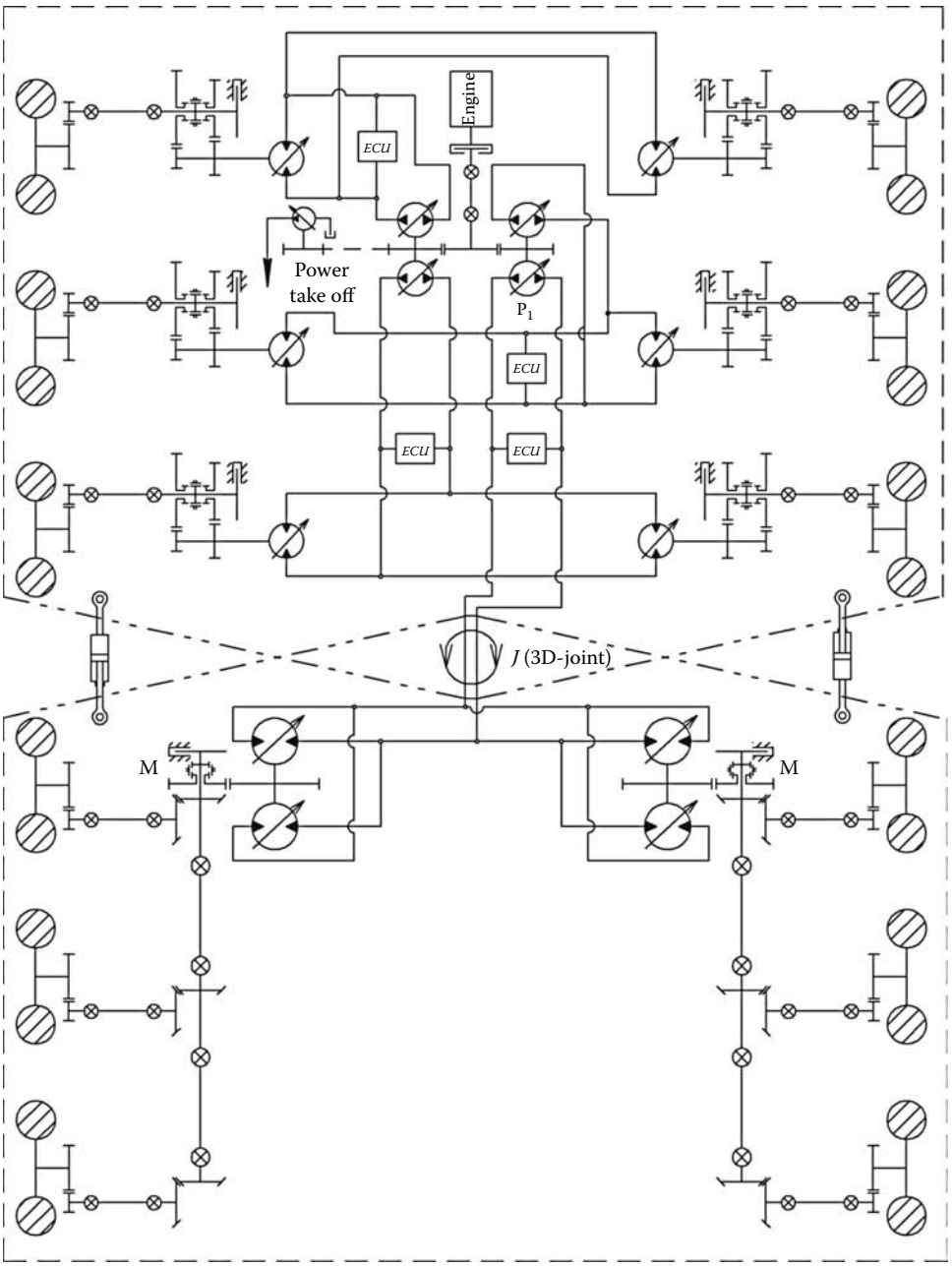


FIGURE 7.48
Version VII. Schematic diagram of a vehicular HD of an articulated (or with semitrailer) vehicle with active drive of all the wheels.

The design shown in Figure 7.48 illustrates the transmission of power to the drive wheels of a 12×12 articulated vehicle or 6×6 vehicle with steered wheels and hydraulic power supply to the semitrailer wheels. The pump station has a separate one (or two) adjustable reversing and convertible pump with its electronic control unit (ECU) that serves the controllable traction hydraulic motors of the rear section (or of the semitrailer) by way of a J turning hinge joint (with 3 degrees of freedom) that simultaneously serves as a draw bar device. By virtue of its design (Cardan joint with end hydraulic seals in the journals of its spider), this turning joint allows passing through it only two high-pressure hydraulic mains, the rear-wheel hydraulic motors may be interconnected only hydro-differentially, in parallel. In this case, it is advisable to block the wheels of each side into a single unit that is rotated by one or two hydraulic motors. Then the side-to-side coupling of the drive wheels will be hydro-differentially controlled with a maximum locking factor of the order of 4.85. The drive of the rear-section (semitrailer) wheels does not require anything additional. The tractor (front section) retains its individual flexible supply of power and torque to each wheel (or to a pair of wheels of a single conditional axle) with optimal control.

To reduce the hydraulic power that has to be supplied to the rear section (and accordingly, the number of hydraulic pumps and motors with corresponding reduction of their total mass) it is advisable to limit the use of active drive of the rear section (semitrailer) to a velocity range from $V_{\min}$ ($\sim$0.2 m/s) to approximately $0.5V_{\max}$. The hydraulic power of these machines is selected accordingly and preset at a factor of 2–2.5-fold smaller than for driving the tractor's wheels. When this velocity is attained, the rear drive is disconnected by switching off the ''M'' clutches of the hydraulic motors' reduction gear and by placing pump ''P_1'' that serves them to zero. When the driveline system of the tractor's driving wheels employs 2-step hydraulic-motor reduction gear it is advisable to disconnect the rear section (semitrailer) simultaneously with switching the hydraulic motors' reduction gear from level I (traction) to II (transportation). When the rear section (semitrailer) is in the driving mode, control of the pump ''P_1'' and of the rear hydraulic motors is performed by the on-board computer in a manner that ensures the additional traction force produced by their driving wheels and proportional to their gripping capabilities, and to eliminate power circulation when the sections operate in the braking mode.

One of the shortcomings of this design is its complex, insufficiently reliable and poorly dirt-protected two-stream intersection hydraulic J-type joint and the difficulties with remote control of the hydraulic motors of the rear section.

7.7.2 Design Selection of the Kind and Standard Dimension of Hydraulic Units

One of the first questions to be resolved in designing a full-flow hydrostatic driveline (HD) consists in selecting the kind of the hydraulic unit (high- or low-torque) and its standard dimension.

In the current-production of vehicular HD, the principal hydraulic units are exclusively axial-plunger pumps with sloping disk and sloping block, with end distribution, controllable, reversible, and convertible. They are used because virtually only pumps that follow this structural-power design are capable of ensuring stable and continuous supply of the working fluid.

The overall efficiency of these machines at full power is as high as 0.85–0.93 (the volumetric efficiency at nominal working-fluid viscosity is 0.95–0.985 and the mechanical efficiency ranges between 0.93 and 0.97) over a significant range of variation in its energy parameters. The working volumes range from 1.9×10^{-6} to 39.8×10^{-6} m^3/rad,

the maximum rotational speed ω_{max} goes from 300 to 625 rad/s, and the operating life is 6000–8000 h. The specific power per unit volume ranges between 22×10^3 and 37×10^3 kW/m^3, the specific power is up to 2.5×10^6 kW/m^3. The specific mass of noncontrolled hydraulic machines goes from 0.11 to 0.15 kg/kW, and of controlled machines is 0.12–0.2 kg/kW. The time of change of the operating volume from zero to maximum (and back) is not more than 0.1–0.12 s. The velocity range of the hydraulic motor adjustment ($D_c = \omega_{max}/\omega_{min}$) is as high as 200. At the present time only such parameters of principal hydraulic machines (pumps and hydraulic motors) are capable of ensuring the design of HDs with fully acceptable output indicators, in a number of competitive cases, on the basis of the total mass (the specific mass as a whole may not exceed 2.7–3.4 kg/kW), and dimensions with stepped mechanical transmissions. Based on the overall efficiency such HDs are comparable with branched out mechanical drives of the multi-wheel drive vehicle, being more convenient and effective to control. The above hydraulic machines are capable of normal operation at kinematic viscosity of the working fluid from 6×10^{-6} to 15×10^{-4} m^2/s, which makes it possible to use in these HD all-weather mineral hydraulic oils with an operating life of 2000 h at ambient temperatures of ±50°C.

Axial-plunger pumps with a sloping disk and rod connection between the piston and the flange of the drive shaft were previously extensively used in hydraulic drives of transportation vehicles and retain their place in certain hydraulic systems (see Figure 7.49).

Further development of these machines led to forming a specific design image of an axial-plunger hydraulic machine with a sloping disk and sliding-valve distribution (see Figure 7.50) that is capable of more effective performance in drives of wheeled vehicles.

The improved designs make extensive use of spherical distributors that are resistant to vibration, jolt, and impact that are usually encountered in the operation of the transportation vehicle. The sloping arrangement of supply ducts at the end of the cylinder block reduces their arrangement radius and thus decreases the sliding rate in the distributor. These hydraulic machines do not use a Cardan drive for the cylinder block. This allows reducing the diameter of cylinder-axis distribution and to decrease the number of cylinders to 7 and place the cylinders at 3–5 mm from one another. The cylinder blocks are usually

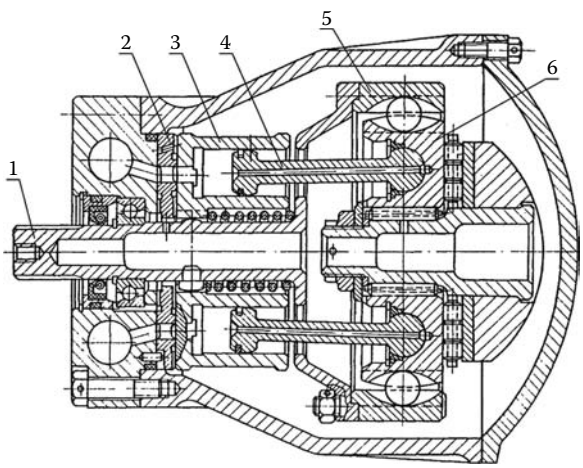


FIGURE 7.49
Axial-plunger hydraulic machine with sloping disk and power joint: 1, drive shaft; 2, distributor; 3, cylinder block; 4, connecting rod with piston; 5, synchronous power joint; 6, sloping disk.

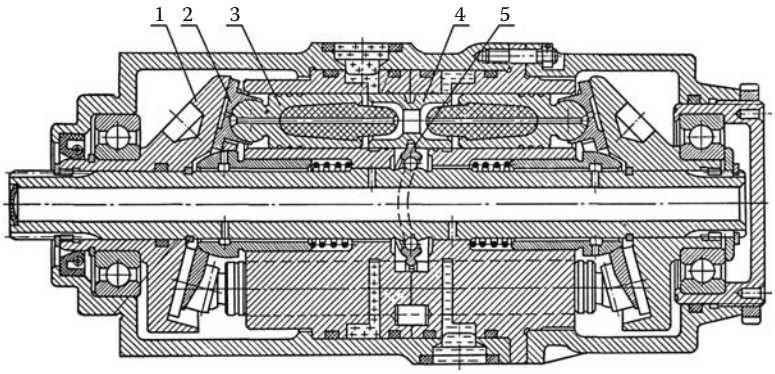


FIGURE 7.50
Duplex axial-plunger hydraulic machine with sloping disk and sliding-valve distribution: 1, Sloping disk; 2, hydrostatic shoe; 3, plunger; 4, distribution slide valve; 5, slide valve control.

constructed from a bimetal with an inverse friction couple (steel piston in bronze sleeve and bronze end of cylinder block with a steel distributor).

Axial-plunger pumps with a sloping disk and hydrostatic plunger shoe have been lately extensively refined and are as of present highly developed (Figure 7.51).

They have a rigid structure, relatively small dimensions and sensible outer shapes, moderate mass, convenience of drive and installation, ability of extended operation at high pressure, significant service life that is limited (when the working fluid is properly purified) only by the rolling bearings, simplicity and high manufacturability, and moderate cost. Axial-plunger pumps with a sloping disk are in a way inferior to such pumps with a sloping block. Nevertheless, they currently are dominant in HD with the cost being a major factor. In certain hydraulic systems, for example—aviation—axial plunger hydraulic machines with sloping disks have virtually displaced all other kinds of pumps, excluding gear pumps (for working pressures to 20 MPa).

The kinematic, force and energy parameters and characteristics of HDs can be calculated in the quasi-static mode, that is, without allowance for transients in the drive. For simplification of calculations, all the pumps of the HD can be treated as a single, hypothetical

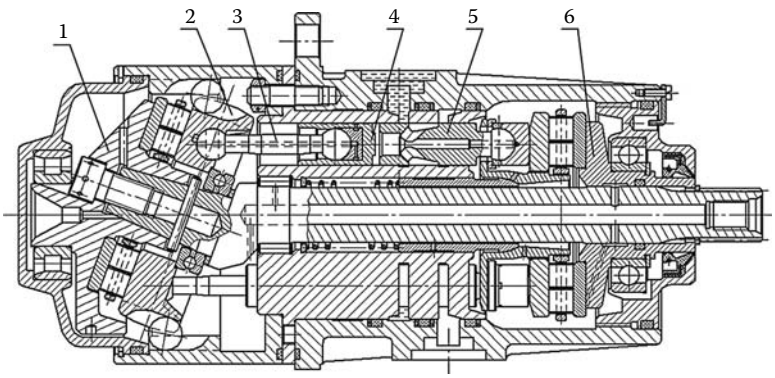


FIGURE 7.51
Axial-plunger hydraulic machine with sloping disk, with power joint, and slide valve distribution: 1, Impeller wheel; 2, synchronous power joint; 3, connecting rod; 4, piston; 5, distribution slide valve; 6, sloping slide valve control washer.

pump with a working volume equal to that of the sum of all working volumes of actual pumps. A single hypothetical motor with total working volume can replace all the hydraulic motors. If necessary, it is possible to then analyze the operation of each of the hydraulic circuits separately, but this is not needed in most cases.

To select the hydraulic machine from those available, it is necessary to formulate based on the specified parameters of the vehicle, the hydraulic machine parameters needed for implementing them. The first item to be selected is the maximum pressure level in the supply lines. Usually the maximum design pressure in HD amounts to 92%–95% of the maximum level specified by the hydraulic-machine manufacturer. This improves the reliability of hydraulic-machine operation at the maximum traction loads that are usually encountered in transportation vehicles, and generates a certain safety capacity should an off-design situation occur. Since the maximum pressure p_{max} usually employed in current-production hydraulic machines is 45 MPa, the specified pressure should not be lower than 35 MPa as otherwise it is difficult and at times impossible to obtain an HD with the required adjustment range and acceptable mass and dimensions.

The maximum design torque at one of the vehicle's wheels is calculated from:

$$T_w^{max} = k_{wd} \frac{D_{max} W_a r_a^0}{2n} \tag{7.178}$$

where

n is the number of drive axles
r_a^0 is the generalized rolling radius of the vehicle in the driven mode
W_a is the total weight of the vehicle
D_{max} is the maximum dynamic factor

whereas k_{wd} is a factor accounting for the dynamic redistribution of weight between the vehicle's wheels.

For 6×6 vehicles it is usually recommended to specify $k_{wd} = 2.3$–2.5, whereas for vehicles with a larger number of axles, $k_{wd} = 1.5$–2.0. For wheeled vehicles with a side drive of axles $k_{wd} = 1.6$–1.8. The increase in the design torque T_w^{max}, caused by introducing factor k_{wd} into formula (7.178) makes it necessary to use a larger hydraulic machine, which inevitably means one with a higher mass. If the dynamic redistribution of weight cannot be neglected in view of the operating conditions of the vehicle, then it suffices to use a two-stage reduction gear between the hydro motor and the wheel with a ratio of its lower and upper stages of the order of 1.5–1.8. This allows reducing the mass of the hydraulic machines.

The term dynamic factor applies to the ratio of the net tractive force of the vehicle F_w to its weight W_a

$$D = F_w / W_a \tag{7.179}$$

As in designing mechanical drives, it is assumed that the dynamic factor D_{min} at the maximum velocity is 0.04–0.045, that is, approximately the power adjustment range of the HD should be at least:

$$D_{HD} = \frac{D_{max}}{(0.04 \ldots 0.045)}, \tag{7.180}$$

where D_{max} usually ranges between 0.65 and 0.85. For high-mobility vehicles it is usually assumed that $D_{max} \geq 0.65$ and $D_{HD} = 17 - 22$.

The value of $T_{\mathrm{w}}^{\max}$ found from formula (7.178) is then used for determining the maximum working volume of a single hydraulic motor.

If each wheel of the vehicle has its own hydraulic motor (Figure 7.44), then its maximum working volume is found from the expression:

$$q_{\mathrm{m}}^{\max} = \frac{2\pi T_{\mathrm{w}}^{\max}}{z(p_{\max} - p_n)\eta_{\mathrm{mm}} u_{\mathrm{mr}} \eta_{\mathrm{mr}}} \tag{7.181}$$

In the case of side drive (Figure 7.45) the maximum working volume of the hydraulic motor is determined from the formula

$$q_{\mathrm{m}}^{\max} = \frac{2\pi T_{\mathrm{w}}^{\max} n}{z(p_{\max} - p_n)\eta_{\mathrm{mm}} u_{\mathrm{mr}} \eta_{\mathrm{mr}}} \tag{7.182}$$

In formulae (7.181) and (7.182), η_{mm} is the mechanical efficiency of the hydraulic motor at the maximum pressure of $p_{\max}$ (at the preliminary design stage it is possible to assume $\eta_{\mathrm{mm}} = 0.94$ for axial-plunger hydraulic motors); η_{mr} and u_{mr} are the efficiency and gear ratio of a gear transmission between the hydraulic motor and the vehicle's wheel (usually $u_{\mathrm{mr}} = 13 - 16$ and $\eta_{\mathrm{mr}} \geq 0.91$), z is the number of hydraulic motors that are driving one of the vehicle's wheel and p_n is the makeup pressure. When using a two-stage reduction gear for the hydraulic motor, u_{mr} includes the gear ratio of its lower stage.

The value of $q_{\mathrm{m}}^{\max}$ found from formulae (7.181) and (7.182) is used for selecting a hydraulic motor with a somewhat larger maximum working volume. To ensure that the design and the selected values of $q_{\mathrm{m}}^{\max}$ are in agreement, the gear ratio u_{mr} of the reduction gear (see formulae (7.181) and (7.182)) is changed.

When the vehicle employs an individual drive of each wheel, use is usually made of a single, high-rpm controllable hydraulic motor, but in a number of cases, particularly when the weight load per wheel is higher than 45 kN, it is advisable to use two hydraulic motors each, connected in parallel, while rigidly coupled mechanically with its common output reduction gear which increases the specific power of the hydraulic machines.

After the preliminary selection of a given kind and standard size of a hydraulic motor it is necessary to ensure that its maximum angular velocity $\omega_{\mathrm{m}}^{\max}$ when the vehicle moves at the maximum velocity $V_{\max}$ does not exceed the value specified by the manufacturer for operation of the hydraulic motor with a minimum working volume:

$$\omega_{\mathrm{m}}^{\max} = \frac{V_{\max} u_{\mathrm{mr}}}{r_{\mathrm{a}}^0} \tag{7.183}$$

The permissible deviation from the above is usually not more than 5% toward the larger value (employing the safety factor on the maximum angular velocity for which the hydraulic motor was designed).

For hydraulic motors, exceeding the maximum rpm causes a steep drop in the mechanical efficiency, overheating, and scratching of the cylinder block-distributor friction couple, excessive bearing wear, etc. In this context exceeding the maximum pressure, particularly if only for a short time (not exceeding 5 min) is less damaging. The majority of the currently produced hydraulic motors are capable of withstanding quite prolonged pressure overloads that are not limited so much by possible deformations and mechanical breakage as

by overheating of the friction couples (elevated throttling of leakages and parasitic flows) and marked reduction of the volumetric efficiency. In the case of HD, the specified maximum pressure may be exceeded, but by not more than 10%.

If ω_m^{max} from formula (7.183) differs from the value listed in the hydraulic-motor specifications, then the values of u_{mr} must be changed to attain agreement between the design value and the value given by the hydraulic-motor specifications. Here, it should be checked whether the maximum torque T_w^{max} at each wheel did not markedly change (more than 5%–8%).

The power adjustment range of a hydraulic motor is calculated from the expression:

$$D_{HD} = \frac{q_m^{max}\eta_{mm}}{q_m^{min}\eta_{mm}^{min}} \tag{7.184}$$

where, q_m^{min} is the minimum working volume (specified from the catalog). In axial-plunger hydraulic motors, this corresponds to a 5° slope of the cylinder block; η_{mm}^{min} is the mechanical efficiency of the hydraulic motor when operating at a minimum volume. It is determined from the general performance curve of the hydraulic motor.

All the pumps of the HDs are connected to a common pump station. The maximum output of each pump is determined from the conditions of the vehicle's motion at the maximum velocity. Here the working volumes of the hydraulic motors are at a minimum. The maximum flow rate of each pump that serves its cluster of hydraulic motors:

$$Q_{pj} = \frac{2\pi V_{max} u_{mr} \sum_{K=1}^{M} q_m^{min\,K}}{r_a^0 \eta_{vm}^{P\,min}} \left[\frac{m^3}{s}\right] \tag{7.185}$$

where

V_{max} is the vehicle's maximum speed
u_{mr} is the gear ratio of a hydro-motor's reduction gear
K is the ordinal number of the hydraulic motor
M is the number of hydraulic motors driven by the given pump
$\eta_{vm}^{P\,min}$ is the volumetric efficiency of the hydraulic motor at minimum supply-line pressure

Usually $\eta_{vm}^{P\,min} = 0.965 - 0.975$. Pumps are selected from catalogs of hydraulic products manufactured by leading companies.

As in selecting hydraulic motors, in certain cases it is advisable to replace a large pump by two small ones, connected hydraulically in parallel and rigidly coupled mechanically, which increases the specific power of the pumps. The design maximum out of a pump station:

$$\sum Q_p^{max} = \frac{2\pi V_{max} u_{mr} Z_M q_m^{min}}{r_a^0 \eta_{vm}} \left[\frac{m^3}{s}\right] \tag{7.186}$$

where, Z_M is the number of hydraulic motors.

Pumps selected from catalogs should satisfy the following requirements:

$$\sum Q_{\mathrm{p}}^{\max} = q_{\mathrm{p}}^{\max} Z_{\mathrm{p}} \omega_{\mathrm{p}}^{\max} \eta_{\mathrm{vp}} \tag{7.187}$$

where

$q_{\mathrm{p}}^{\max}$ is the maximum working volume of one pump

Z_{p} is the number of pumps

$\omega_{\mathrm{p}}^{\max}$ is the maximum pump rpm (usually 90%–92% of the limiting rpm)

η_{vp} is the volumetric efficiency of a pump at maximum rpm and at pressure of 8–10 MPa, which corresponds to motion at maximum velocity is taken to be 0.97

The actual pump output should exceed its design value by 5%–10%.

Example Problem

Calculation of traction and HD characteristics of the 6×6 ''Gidrokhod-49061'' vehicle (see Figure 7.43).

Input data:

Total mass $M_{\mathrm{a}} = 12{,}000$ kg;

Maximum linear velocity $V_{\max} = 25.5$ m/s;

Maximum dynamic factor $D_{\max} \geq 0.85$;

Dynamic factor when moving at maximum speed: $D_{\min} \geq 0.04$;

Vehicle generalized rolling radius in the driven mode $r_{\mathrm{a}}^{0} = 0.632$ M;

Maximum power of ZIL-4104 engine $P_{\mathrm{e}} = 231.6$ kW at angular velocity of $\omega_{\mathrm{e}} = 460.5$ rad/s;

Maximum free power of the engine (usually 88%–92% of P_{e}), $P_{\mathrm{e}}^{\mathrm{lib}} = 205.9$ kW at the same angular velocity;

Tire rolling resistance factor when moving at maximum velocity: $f^{\mathrm{V\,max}} = 0.022$;

Front area of vehicle: $A = 4.75$ m^2;

Air drag factor: $k_{\mathrm{a}} = 0.06$;

The hydraulic motors that were selected (made by ''Bosch Rexroth AG''):

Pumps: A4VG125EP2, $Z_{\mathrm{p}} = 3$; $q_{\mathrm{p}}^{\max} = 19.9 \times 10^{-6}$ m^3/rad; $p_{\max} = 43$ MPa; $p_n = 2$ MPa; $\Delta p_{\max} = 41$ MPa.

Hydraulic motors: A6VM160EP2, $Z_{\mathrm{m}} = 6$ (one hydraulic motor per wheel); $q_{\mathrm{m}}^{\max} = 25.48 \times 10^{-6}$ m^3/rad; $q_{\mathrm{m}}^{\min} = 5.25 \times 10^{-6}$ m^3/rad; $\omega_{\mathrm{m}}^{\max} = 523.3$ rad/s; $\omega_{\mathrm{m}}^{\min} = 4.186$ rad/s

The overall reduction gear ratio:

$$\sum u_{\mathrm{mr}} = \frac{D_{\max} M_{\mathrm{a}} g r_{\mathrm{a}}^{0}}{Z_{\mathrm{m}} q_{\mathrm{m}}^{\max} \Delta p_{\max} \eta_{\mathrm{mm}} \eta_{\mathrm{mr}}} = \frac{(0.9)(12{,}000)(9.81)(0.632)}{(6)(25.48)(41)(0.94)(0.91)} = 12.73$$

With reference to wheel reduction gear already installed on the ZIL chassis and the additional reduction gear of the hydraulic motor with a gear ratio $u_{\mathrm{mr}} = 1.423$ the real overall gear ratio is $\Sigma u_{\mathrm{mr}} = 12.713$.

The maximum angular velocity of the hydraulic motors when moving at the maximum linear velocity:

$$\omega_{\mathrm{m}}^{\max} = \frac{V_{\max}\Sigma u_{\mathrm{mr}}}{r_{\mathrm{a}}^{0}} = \frac{(25.5)(12,713)}{0.632} = 512.9 \text{ rad/s},$$

which is permissible (the limit is $\omega_{\mathrm{m}}^{\mathrm{lim}} = 523.3$ rad/s).

The required maximum output of the pump station:

$$\sum Q_{\mathrm{p}}^{\max} = \frac{\omega_{\mathrm{m}}^{\max} q_{\mathrm{m}}^{\min} Z_{\mathrm{m}}}{\eta_{\mathrm{vm}}} = \frac{(512.9)(5.25)(10^{-6})(6)}{(0.97)} = 0.0167 \text{ m}^3/\text{s};$$

The maximum angular velocity of each pump:

$$\omega_{\mathrm{p}}^{\max} = \frac{\sum Q_{\mathrm{p}}^{\max}}{Z_{\mathrm{p}} q_{\mathrm{p}}^{\max} \eta_{\mathrm{vp}}} = \frac{0.0167 \times 10^{6}}{(3)(19.9)(0.95)} = 294.4 \text{ rad/s},$$

which is permissible (the limit is $\omega_{\mathrm{p}}^{\mathrm{lim}} = 340.1$ rad/s).

Then the gear ratio of the distribution reduction gear of the pump station:

$$u_{\mathrm{pr}} = \frac{\omega_{\mathrm{e}}}{\omega_{\mathrm{p}}^{\max}} = \frac{460.5}{294.4} = 1.564;$$

The maximum total circumferential force at the wheels (in the ''stop'' mode):

$$F_{\mathrm{x}\Sigma}^{\max} = \frac{q_{\mathrm{m}}^{\max} \Delta p_{\max} Z_{\mathrm{m}} \eta_{\mathrm{mm}} \Sigma u_{\mathrm{mr}} \eta_{\mathrm{mr}}}{r_{\mathrm{a}}^{0}} = \frac{(25.48)(41)(6)(0.94)(12.713)(0.91)}{(0.632)}$$
$$= 105.8 \text{ kN}$$

which corresponds to the maximum dynamic factor:

$$D_{\max} = \frac{F_{\mathrm{x}\Sigma}^{\max}(10^3)}{M_{\mathrm{a}}(9.81)} = \frac{(105.8)(10^3)}{(12{,}000)(9.81)} = 0.899;$$

When moving at maximum linear velocity the total circumferential force at the wheels:

$$F_{\mathrm{x}\Sigma}^{V_{\max}} = \frac{P_{\mathrm{e}}^{\mathrm{lib}} \eta_{\mathrm{pr}} \eta_{\mathrm{vp}} \eta_{\mathrm{mp}} Z_{\mathrm{m}} q_{\mathrm{m}}^{\min} \eta_{\mathrm{mm}} u_{\mathrm{mr}} \eta_{\mathrm{mr}}}{Z_{\mathrm{p}} q_{\mathrm{p}}^{\max} \omega_{\mathrm{p}}^{\max} r_{\mathrm{a}}^{0}}$$
$$= \frac{(205,900)(0.96)(0.97)(0.925)(6)(5.25)(0.95)(12.713)(0.91)}{(3)(19.9)(294.4)(0.632)} = 5.422 \text{ kN}$$

which corresponds to the dynamic factor:

$$D_{\max} = \frac{F_{\mathrm{x}\Sigma}^{V_{\max}}}{M_{\mathrm{a}} g} = \frac{(5.422)10^3}{(12{,}000)(9.81)} = 0.046$$

The air drag when moving at maximum linear velocity:

$$D_{\mathrm{a}} = k_{\mathrm{a}} A V_{\max}^2 = (0.06)(4.75)(25.5^2) = 1818 \text{ N} = 1.818 \text{ kN}$$

The rolling resistance when moving at maximum velocity over a road with solid pavement:

$$R_{x\Sigma} = M_a g f^{V\max} = (12,000)(9.81)(0.022) = 2.59\,\text{kN}$$

The force that remains for overcoming the resistance to rise on a road with a solid pavement:

$$F_w = F_{x\Sigma}^{V_{\max}} - D_a - R_{x\Sigma} = 5.422 - 1.818 - 2.59 = 1.014\,\text{kN}.$$

From this, the possible angle θ_n of rise on a road with a solid pavement when moving at maximum velocity:

$$\theta_n = \arcsin\frac{F_w}{W_a} = \arcsin\frac{(1.014)10^3}{(12,000)(9.18)} = (8.61)10^{-3}\,\text{rad}$$

The minimum-stable linear velocity of the vehicle:

$$V_{\min} = \frac{\omega_m^{\min} r_a^0}{\sum u_{mr}} = \frac{(4.186)(0.632)}{12.713} = 0.208\,\text{m/s}.$$

When moving at maximum velocity and utilizing the free power of the engine, the pressure-drop in the working fluid in the supply lines:

$$\Delta p_{\min} = \frac{P_e^{\text{lib}}\eta_{pr}\eta_{vp}\eta_{mp}}{r_p q_p^{\max}\omega_p^{\max}} = \frac{(205,900)(0.96)(0.97)(0.925)}{(3)(19.9)(294.4)} = 9.9\,\text{MPa}$$

r_p is the number of pumps in the pump station (it is assumed here that all the pumps are the same).

The range of pump-station power regulation:

$$D_p = \frac{(p_{\max} - p_n)\eta_{mp}^{p_{\max}}}{\Delta p_{\min}\eta_{mp}^{p_{\min}}} = \frac{(43-2)(0.94)}{(9.9)(0.925)} = 4.208.$$

The range of hydraulic motor power regulation:

$$D_m = \frac{q_m^{\max}\eta_{mm}^{p_{\max}}}{q_m^{\min}\eta_{mm}^{p_{\min}}} = \frac{(25.48)(0.94)}{(5.25)(0.95)} = 4.8;$$

The total power range of regulating the HD of a vehicle at maximum power mode

$$\sum D_{HD} = D_p D_m = (4.208)(4.8) = 20.2;$$

The velocity range of HD regulation:

$$D_s = \frac{\omega_m^{\max}}{\omega_m^{\min}} = \frac{512.9}{4.186} = 122.5;$$

The total efficiency of the HD at the segment ''engine flywheel–tire rim'' for a vehicle moving at maximum traction and utilizing the maximum free power of the engine (see formula (7.177)):

$$\eta_{ph\Sigma}^{F_{max}} = \eta_{pr}\eta_{vp}^{P_{max}}\eta_{mp}^{P_{max}}\eta_{n}\eta_{vm}^{P_{max}}\eta_{mm}^{P_{max}}\eta_{mr}$$
$$= (0.96)(0.905)(0.94)(0.996)(0.92)(0.94)(0.91) = 0.64;$$

The total efficiency of HD under the same conditions when moving at $0.5V_{max}$:

$$\eta_{ph\Sigma}^{0.5V_{max}} = \eta_{pr}\eta_{vp}^{P_{mid}}\eta_{mp}^{P_{mid}}\eta_{n}\eta_{vm}^{P_{mid}}\eta_{mm}^{P_{mid}}\eta_{mr}$$
$$= (0.96)(0.94)(0.935)(0.994)(0.95)(0.95)(0.91) = 0.683;$$

The total efficiency of HD under the same conditions when moving at maximum velocity:

$$\eta_{ph\Sigma}^{V_{max}} = \eta_{pr}\eta_{vp}^{P_{min}}\eta_{mp}^{P_{min}}\eta_{n}\eta_{vm}^{P_{min}}\eta_{mm}^{P_{min}}\eta_{mr}$$
$$= (0.96)(0.97)(0.925)(0.992)(0.97)(0.95)(0.91) = 0.716$$

The 6×6 Gidrokhod-49061 vehicle with HD calculated by the suggested technique exhibited in test results that were close to those predicted.

8

Testing of Driveline Systems and Multiwheel Drive Vehicles

8.1 Laboratory Studies of the Locking Performance of Differentials

The analysis of problems arising during the course of design and manufacture of differentials makes it possible to validate the need to test the mechanisms from among the number of batch-produced units directly at the plant, and the need for experimental testing of newly designed and upgraded mechanisms.

The testing of differentials batch produced at the plant includes monitoring the stability of the manufacturing technology, which consists in checking the serviceability of the fully assembled mechanisms, plotting their performance curves, and partial running-in to provide for preliminary breaking-in of the rubbing surfaces. This is done by means of test rigs, frequently located directly in the manufacturing area. In addition, batch-produced differentials are checked out in the course of delivery and periodical field-tests of the vehicles on which they are installed.

Experimental investigations of new and upgraded differentials are performed on special test stands and on vehicles directly under open-road conditions. Depending on the aspects of interest and on the test stands that are used, stand testing of newly designed differentials can be subdivided into certain methods. In the first place, these are investigations for determining the internal forces of the differentials that work on determining their performance and checking for conformance of their actual locking properties to those underlying the design. The main purpose of these tests consists in verifying analytic studies and calculations of the differentials. Experimental checking is carried out, in the first place, of the predicted performance of the lockers, for example, the locking coefficient (torque bias) in limited slip differentials. For this reason, after a newly designed differential is constructed, it is necessary to check the similitude of the actual locking coefficient to that assumed in the design. This is done on a special stand or directly on the vehicle where the differential will be used. It must be remembered here that a more precise performance curve of a differential can be obtained only after preliminary running-in of the mechanism.

The relative motion of the three principal elements (the case and the two output shafts) of a differential under load and experimental determination of its locking coefficient are usually implemented on an open-type multipurpose stand. Figure 8.1 provides a general view of such a stand while Figure 8.2 illustrates the design of its balancing–braking device.

The rotation is transmitted from an electric motor through a gearbox, a Cardan shaft, and a worm-gear speed reducer to the differential being tested, installed in the housing of the central reduction gear. The rotation from the output shafts of the differential is then

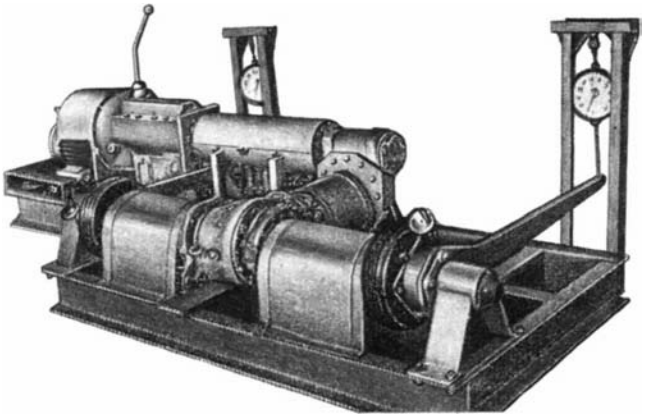


FIGURE 8.1
Multipurpose stand for testing limited slip differentials.

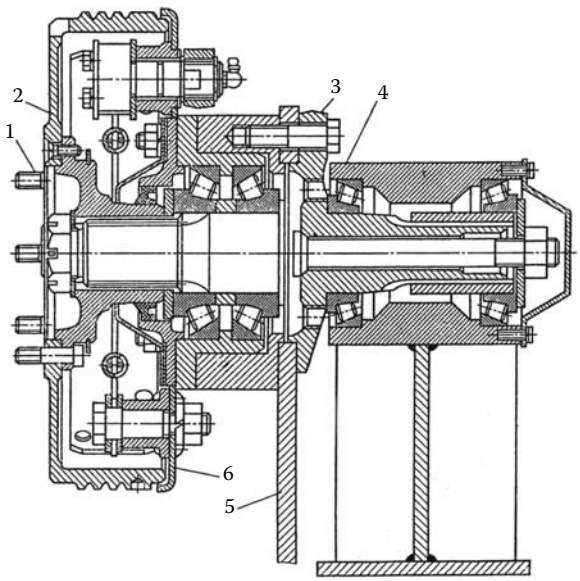


FIGURE 8.2
Balancing–braking device.

transmitted by means of Cardan shafts to two balancing–braking devices. Each of the Cardan shafts is pinned to braking drum 2, the shaft of which is held in tapered bearings of the moving hub of balancing lever 5. The support 6 of the braking mechanism is rigidly connected to the hub. For this reason, the friction torque that appears between the brake drum and the brake shoes is transmitted to the hub of the lever only after the brake is actuated by means of a loading device located on the support of the braking device (not shown in Figure 8.2). To reduce losses in rolling of the balancing lever, its shaft 3 rests on the tapered roller bearing installed in stationary frame 4 of the balancing–braking device. The balancing levers are connected to strain-gage dynamometers that provide a readout of the magnitude of torques at the output shafts of the differential being tested. The gearbox of the stand allows operating the stand at a variety of speed modes, including relative rotational velocities of the principal elements of the differential within the range of 0.65–2.24 rad/s. The use of adapters allows placing and testing differentials of different sizes.

Stands similar to that described above usually serve to check the relative rotation of the output shafts of open differentials in the course of their manufacture. This is done by braking of the output shafts alternately. This allows detecting the presence or absence of jamming of the components.

The locking performance of the differentials and their internal force working processes are also checked by stopping the output shafts separately and experiencing the relative rotation under load. Now the methods and results of testing limited slip differentials are considered.

The differential's shafts are set into relative rotation by loading them with braking torques employing the balancing–braking devices of the test stand for this purpose. These torques imitate the resistance exerted by the surfaces with different gripping properties on the motion of the vehicle's wheels.

The locking coefficient, K_d, of a limited slip differential, equal to the ratio of torques T'' and T' at the output shafts in their relative rotation and represented by formula (4.6), is determined as follows. Both balancing–braking devices are set to the no-load state before testing is started; the gearbox is then set to the required velocity and the electric motor is switched on. Its rotation is then transmitted to the differential and its three principal elements (the case and the two output shafts) rotate as a single entity without a load, since the balancing–braking devices were set to no load.

Then one of the differential's output shafts is stopped by means of the brake in one of the balancing–braking devices. While this shaft is stopped, the second shaft continues to rotate without a load and at twice the speed of the case (which is seen from formula (2.10)). This simulates an axle with one of its wheels out of contact with the surface.

Then the braking torque, T', is applied to the second shaft by means of the second balancing–braking device. This shaft continues rotating, whereas the initially stopped first shaft remains stationary but the torque T'' at it increases because of the differential's lockers. This simulates the motion of the axle operating under gripping conditions (as it is well known that the wheel in poorer conditions receives a lower torque T' and that in better conditions, the higher torque T''). As increasing braking force is applied stepwise to the second, rotating shaft, the torques T' and T'' at both output shafts of the differential increase; the sum of these forces determines the torque T_0 at the differential's case (see formula (4.4)). The numerical values of ratio T''/T' determined from the statistical characteristics of the measured torques T' and T'' determine the real values of the locking coefficient, K_d, at different force modes, represented by torque T_0, and at the specified speed setting determined by the stand's gearbox setting.

Consider now the technique of experimental determination of static locking coefficient introduced by formula (4.15). As in determining K_d, both balancing–braking devices are set to the no-load state before testing is started; the gearbox is then set to the required velocity and then the electric motor is switched on. The differential and its three principal elements rotate without a load at identical angular velocities. Starting with this point, the technique for determining K_{dp} starts differing from that of determining K_d. In this case, both output shafts are subjected to the same braking torques, that is, the arrangement simulates the motion of an axle with identical gripping conditions of both wheels. The limited slip differential then remains locked, but its locking properties do not come into play, since $T'' = T'$ and the angular velocities of the output shafts remain the same. Then the brake torque at one of the output shafts is increased by one of the balancing–braking devices, whereas the load on the second shaft remains unchanged. This changes the torques at the output shafts (see torques T' and T'' at segment AB in Figure 8.3).

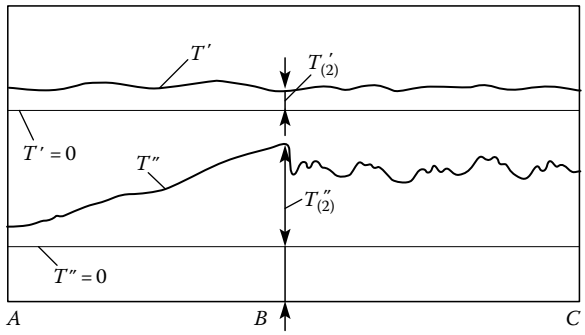


FIGURE 8.3
Torques at the output shafts of a limited slip differential.

The output shafts continue to rotate at the same angular velocities. The ratio of instantaneous values of torques in point B becomes equal to $T''_{(2)}/T'_{(2)}$, which in fact determines the value of K_{dp} (see formula (4.15)). The sum of torques $T''_{(2)}$ and $T'_{(2)}$ is equal to torque T_0 at the differential's case at the instant it is actuated, that is, when the output shaft subjected to the higher torque $T''_{(2)}$, stops and the relative motion of the three links of the mechanism starts. As seen from Figure 8.3, torque T'' at segment BC is lower than torque $T''_{(2)}$ in point B, which is caused by the fact that the friction surfaces of the differential switch from the static to the sliding friction. Note that the ratio of the average values of torques T'' and T' at segment BC is equal to locking coefficient K_d from formula (4.6).

The stand shown in Figure 8.1 is suitable for testing limited slip differentials both with constant and variable design locking coefficients, which are a function of torque T_0 at the case. The dependence of factors K_{dp} and K_d on T_0 is determined by increasing the initial torques at the output shafts, which increases the value of T_0. Differentials with locking coefficient dependent on the relative velocity of their elements can also be tested on this stand. This requires different gear settings in the gearbox.

Consider the results of testing of certain limited slip differentials. The four-pinion differential shown in Figure 4.6a was designed for a maximum load of $T_0^{max} = 6000$ N-m at its case. The number of friction pairs in one of the differential's clutches is $i_M = 11$; the number of side-gear teeth is $z_g = 16$ and of the pinion $z_c = 10$ (first group, see Table 2.2). The tests were performed at loads between 600 and 2300 N-m, which corresponds to a specific pressure at the friction surfaces of 50–180 N/cm^2. The initial specimens of the differential used steel disks with 0.45% carbon content, without heat treatment. Scratches appeared on the disks already at medium loads and testing was terminated.

Two sets of disks of alloy steel with 0.65% C and about 1% Mn were then prepared. These were heat treated to improve hardness. Disks in one of the sets were phosphate coated, whereas the others were electrolytically copper coated. In addition, lubricating grooves were provided on the friction surfaces of the same kind of both sets. Differentials with these sets of disks operated during the tests stably over the entire range of test loads. This time there were no scratches on the disk surfaces. Multiple experiments performed with these differentials also showed that the friction and locking coefficients vary with the torque T_0. Both the friction coefficient μ and the locking coefficient K_d increase with increasing T_0. Varying the load from 600 to 2300 N-m caused a variation of K_d from 1.6 to 2.3. The design value of this factor was 2.1 at $\mu = 0.1$. Similar variations in K_d with increasing load were observed when testing on this stand of disk-type limited slip differentials with additional lockers previously analyzed in Sections 4.3 and 4.4.

The course of internal working processes within limited slip differentials with additional lockers depends on their geometric parameters. In the differential shown in Figure 4.13 the angle φ_k of grooves in the case serves as such a parameter. Increasing this angle increases the axial force that compresses the disks and accordingly also the value of K_d. However, excessive increase of the disk compression forces and with it excess rise in pressure on their surfaces are detrimental to the lubrication of the rubbing components and have a negative effect on the mechanism's operation. If it is additionally remembered that the clutches in the differential in Figure 4.13 may be subjected to asymmetrical compression because of differences in the loads on the pinion pins (which was analyzed in Section 4.4), then the pressure at the working surfaces of disks of one of the clutches may turn out to be much higher than its design value. The testing of certain initially produced specimens of this differential was accompanied by screeching in the clutches, jerks in all parts of the mechanism, deep scratches, and ''temper color'' (of the type that forms when welding metal). For this reason, proper selection of angle φ_k is an important engineering problem. Some companies set this angle at 45°, which was previously confirmed by graphs in Figure 4.40.

The axial forces in the rotating gears of limited slip differentials that rotate at different velocities are subject to variations in their meshings and within each tooth pitch. These depend on the combination of the number of teeth of the side gear z_g and of the pinion z_c (see Section 2.3). The variation in axial forces arising in the contact between the slopes of the pinion pins and the V-grooves of the case are caused by fluctuations in the thickness of the disk stack (see Section 4.9). These phenomena were checked experimentally on the stand shown in Figure 8.1 by investigating five different designs of limited slip differentials based on the mechanism shown in Figure 4.13. The principal parameters of these differentials are listed in Table 8.1.

Table 8.2 lists the materials from which the disks tested in differentials given in Table 8.1 were made.

The bulk of the tests were performed with friction disks of set 1, of case hardened steel. The total nonperpendicularity of the axes of the pinions in these differentials was not more than 0.1 mm and the difference in the thickness of the friction disk stack was not more than 0.3 mm; this means that these differentials exhibited satisfactory symmetrical locking performance. The stand tests were performed with relative rotation of the differentials' elements under load. The axial forces exerted on the clutch disks by the grooves in the case were measured by cementing a strain-gage sensor, connected into a bridge system with three strain-gage sensors, placed on a separate metal plate (see Figure 8.4).

TABLE 8.1

Parameters of the Tested Differentials

Differential Number	Tooth Number of Side-Gear, z_g	Tooth Number of Pinion, z_c	Angle of Grooves in the Case, deg, φ_k	Number of Friction Pairs in One Clutch, i_M
1	16	10	55	3
2[a]	16	10	55	3
3	16	10	45	5
4	16	10	55	5

[a] Differential № 2 was equipped with dampers (see Figure 4.43).

TABLE 8.2

Friction Disk Sets

Part from Figure 4.13	Disk Set				
	1	2	3	4	5
Pressure cup	Casehardened steel, 0.25% C with traces of Cr, Mn, and Ti				Electrolytically copper-coated steel
Drive disk splined to the case	Hardened steel, 0.45% C with traces of Cr	Metal-ceramic powder coating	Bronze	Electrolytically copper-coated steel	
Driven disk splined to output shaft	Casehardened steel, 0.65% C with traces of Mn				Electrolytically copper-coated steel
Differential's case	Gray cast iron				
Presence of lubricating grooves	Annular, on both sides of drive disk	None	None	None	None

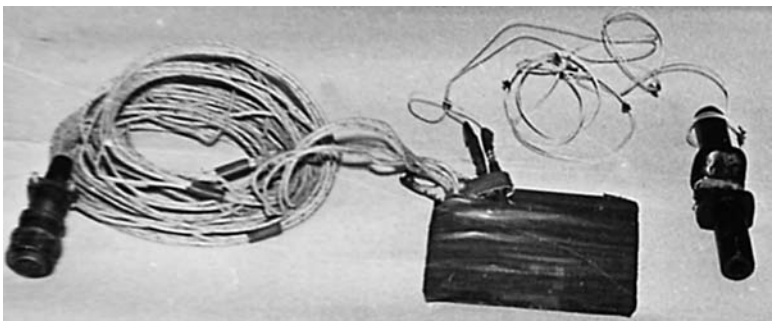


FIGURE 8.4
Sensor-equipped pinion pin.

Figure 8.5 shows specimens of recordings of typical segments of torques T'' and T' and the axial force Q_0 of the grooves in the case of differentials № 1 and № 2 with disks of set 1, from which it is seen that damping plate springs smooth out the fluctuations in the forces of the grooves and in the torque T''.

Note that two recordings of these parameters during a single relative rotation of the disks placed on one another confirmed satisfactory agreement of experimental curves. That is, the effect of out-of-flatness of the disks on force Q_0 does not change from one rotation to the other. The results of the statistical workup of the test data of differentials № 1 and № 2 are listed in Tables 8.3 and 8.4.

It is seen that when damping springs are used the variation in the forces of grooves of differential № 2 is 1.5- to 3.3-fold lesser as compared with that of differential № 1 that was not equipped with dampers. The reduction in the fluctuations of the axial forces of the grooves is demonstrated also by the experimental values of factor K_{k1} from formula (4.144). Thus, the maximum axial forces in differential № 1 exceed their average values by about a factor of 1.4, whereas in differential № 2 it is only 1.12- to 1.25-fold. The experimental value of $K_{k1} = 1.4$, corresponds to the same design value from formula (4.144) at a static friction coefficient between the grooves in the case and the pinion pin of 0.148.

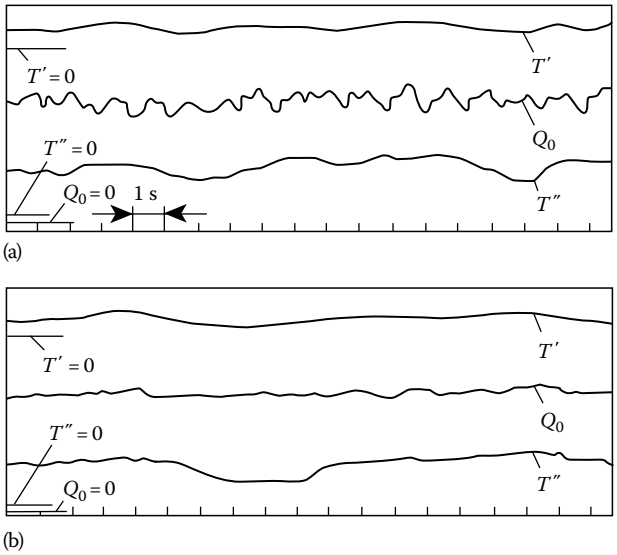


FIGURE 8.5
Torques and axial force of the grooves in the differential's case: (a) without dampers; (b) with dampers.

The variations in the axial forces of the grooves affect the magnitude of torque T'' of the stopped output shaft of the differential. Experiments showed (Tables 8.3 and 8.4) that the factors v''_B of variation in torque T'' of differential № 2 are smaller than the factor of variation of this torque of differential № 1. The range of variation in the locking-factor ratio K_d^{max}/K_d decreased accordingly from 1.73–1.78 to 1.21–1.30.

The results of testing of differential № 3 with disks from set 1 are listed in Table 8.5.

It is seen by comparing Table 8.5 with Table 8.3 that the fluctuations in the axial force of the groove in this differential are lesser than in differential № 1. The variations in T'' and K_d of differential № 3 are somewhat greater, which stems from the different numbers of friction couples in these differentials.

Table 8.6 lists test data on a differential designed as shown in Figure 4.6a with number of friction pairs $i_M = 11$ and of side-gear teeth $z_g = 16$ and of pinion teeth $z_c = 10$, with disks compressed solely by the axial forces of the bevel-tooth meshings.

It is seen that variations in the axial forces cause changes in torque T'' of the stopped output shaft and accordingly in the locking coefficient K_d. Comparison of these experimental data with results that follow from formulae (4.141) validated the analytic results obtained in Sections 2.3 and 4.9.

It follows from experience in operating limited slip differentials that their locking performance depends not only on the design concept specifics. A significant effect is exerted by the materials of which they are made and by certain operating factors. The results of the experimental studies of limited slip differentials with disks made of materials listed in Table 8.2 are considered in the following text.

Figure 8.6 shows experimental curves of locking coefficients K_{dp} and K_d as a function of torque T_0 of differential № 1 with design value of $K_d = 2.6$ at friction coefficient $\mu = 0.1$, angle of V-shaped grooves in the case $\varphi_k = 55°$ and number of friction pairs $i_M = 3$ and of differential № 3 with design $K_d = 3.14$, $\varphi_k = 45°$, and $i_M = 5$.

Both differentials used disks from set 1 in Table 8.2. It is seen from the figure that the locking coefficients K_{dp} and K_d in both differentials increase with increasing T_0. However, the locking performance of the differential with $\varphi_k = 45°$ is better than that of the

TABLE 8.3

Limited Slip Differential № 1

T'	T''					Q_0					K_{k1}	K_{k2}	K_d	K_d^{max}	K_d^{min}
$\bar{x}'$, kN-m	$\bar{x}''$, kN-m	σ'', kN-m	v'', %	u_u'', kN-m	u_l'', kN-m	$\bar{x}_0$, kN	σ_0, kN	v_0, %	u_{u0}, kN	u_{l0}, kN	$\frac{u_{u0}}{\bar{x}_0}$	$\frac{u_{u0}}{u_{l0}}$	$\frac{\bar{x}''}{\bar{x}'}$	$\frac{u_u''}{\bar{x}'}$	$\frac{u_l''}{\bar{x}'}$
0.09	0.25	0.031	12.4	0.32	0.18	4.28	0.75	17.5	6.0	2.56	1.40	2.34	2.78	3.56	2.0
0.15	0.43	0.06	14	0.55	0.31	7.0	0.98	14	9.81	4.19	1.41	2.35	2.9	3.67	2.07

$\bar{x}$, Mean; σ, standard deviation; v, coefficient of variation; u_u and u_l, upper and lower board values.

TABLE 8.4

Limited Slip Differential № 2

T'	T''					Q_0					K_{k1}	K_{k2}	K_d	K_d^{max}	K_d^{min}
$\bar{x}'$, kN-m	$\bar{x}''$, kN-m	σ'', kN-m	v'', %	u_u'', kN-m	u_l'', kN-m	$\bar{x}_0$, kN	σ_0, kN	v_0, %	u_{u0}, kN	u_{l0}, kN	$\frac{u_{u0}}{\bar{x}_0}$	$\frac{u_{u0}}{u_{l0}}$	$\frac{\bar{x}''}{\bar{x}'}$	$\frac{u_u''}{\bar{x}'}$	$\frac{u_l''}{\bar{x}'}$
0.08	0.21	0.013	6.2	0.23	0.19	3.33	0.35	10.6	4.08	2.58	1.22	1.57	2.63	2.88	2.38
0.10	0.28	0.021	7.6	0.32	0.24	4.33	0.28	6.5	5.11	3.55	1.18	1.43	2.8	3.2	2.4
0.14	0.42	0.027	6.4	0.48	0.36	6.66	0.35	5.3	7.48	5.84	1.12	1.28	3	3.4	2.6

$\bar{x}$, Mean; σ, standard deviation; v, coefficient of variation; u_u and u_l, upper and lower board values.

TABLE 8.5

Limited Slip Differential № 3

T'	T''					Q_0					K_{k1}	K_{k2}	K_d	K_d^{max}	K_d^{min}
$\bar{x}'$, kN-m	$\bar{x}''$, kN-m	σ'', kN-m	v'', %	u_u'', kN-m	u_l'', kN-m	$\bar{x}_0$, kN	σ_0, kN	v_0, %	u_{u0}, kN	u_{l0}, kN	$\frac{u_{u0}}{\bar{x}_0}$	$\frac{u_u}{u_{l0}}$	$\frac{\bar{x}''}{\bar{x}'}$	$\frac{u_u''}{\bar{x}'}$	$\frac{u_l''}{\bar{x}'}$
0.12	0.4	0.06	15	0.51	0.29	4.4	0.48	10.9	5.72	3.08	1.3	1.85	3.33	4.25	2.42
0.19	0.68	0.11	16.2	0.88	0.48	7.11	0.70	9.85	9.1	5.12	1.28	1.78	3.8	4.63	2.52

$\bar{x}$, Mean; σ, standard deviation; v, coefficient of variation; u_u and u_l, upper and lower board values.

TABLE 8.6

Limited Slip Differential (from Figure 4.6a)

T'	T''					K_d	K_d^{max}	K_d^{min}
$\bar{x}'$, kN-m	$\bar{x}''$, kN-m	σ'', kN-m	v'', %	u_u'', kN-m	u_l'', kN-m	$\frac{\bar{x}''}{\bar{x}'}$	$\frac{u_u''}{\bar{x}'}$	$\frac{u_e''}{\bar{x}'}$
0.06	0.13	0.014	10.8	0.16	0.10	2.17	2.61	1.67
0.13	0.30	0.032	10.6	0.36	0.24	2.31	2.77	1.85

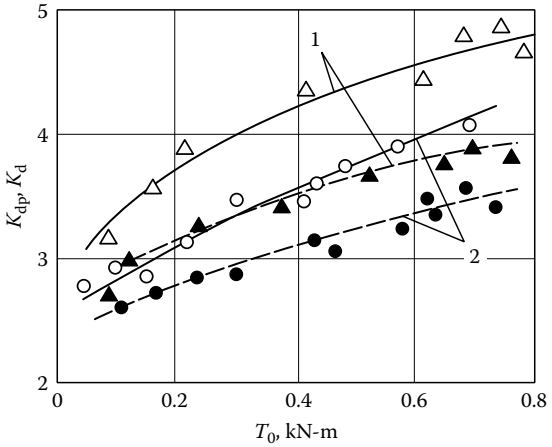


FIGURE 8.6
Locking coefficients K_{dp} (curves 1) and K_d (curves 2 at relative velocities of the disks of 0.65 rad/s): — —, differential № 1; ———, differential № 3.

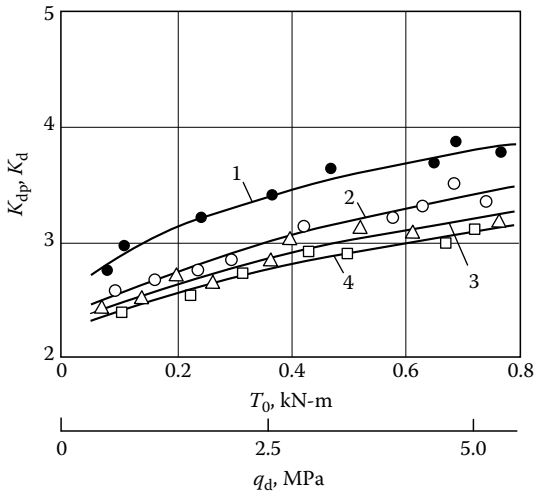


FIGURE 8.7
Locking coefficients K_{dp} (curve 1) and K_d (curves 2, 3, and 4 at relative disk velocities of 0.65, 1.21, and 2.24 rad/s) of differential № 1 with disk set 1.

differential with $\varphi_k = 55°$. This stems from the fact that differential № 3, in spite of the smaller angle of the grooves, has two more friction pairs in its clutches.

Figure 8.7 shows experimental curves obtained in testing differential № 1 with the first set of disks at three relative sliding rates of the disks.

It is seen from the figure (and was confirmed by statistical workup of experimental data) that coefficient K_d is relatively constant over the range of sliding rates from 0.65 to

2.24 rad/s, that is, the friction coefficient μ does not change (see formula (4.67) that relates K_d and μ). Note that constancy of μ for a number of friction materials at sliding velocities of less than 4 m/s is confirmed by many published sources. This linear sliding velocity approximately corresponds to an angular sliding velocity of the disks of 750 rad/s, which markedly exceeds the real values in differentials.

The results of investigations of differential № 1 with disk set 2 that employs steel-metal-ceramic-powder material friction pairs with angle $\varphi_k = 55^\circ$ and number of friction pairs $i_M = 3$ are represented by curves shown in Figure 8.8.

Comparison of the curves in Figure 8.8 with those from Figure 8.6 obtained for the same differential, but with disk set 1, suggests the following conclusion. The use of steel-metal-ceramics friction pairs instead of steel-steel pairs improves the locking performance of the limited slip differential. In addition, the performance of differential with disk set 2 with increasing T_0 is more stable.

Analytic assessment of the locking performance of new differentials in the course of design, in particular, calculation of locking coefficient K_{dp} is impossible without data on the static friction coefficient μ_s. The values of this factor were obtained from experimental data given in Figures 8.6 through 8.8. The experimental values of K_{dp} plotted in these figures were substituted into formula (4.67) from which the values of μ_s as a function of the applied torque T_0 were obtained for known geometric parameters of the differentials and $\xi = 0.5$, that is, $\mu_s = f(T_0)$. At the same time these values of T_0 were used for calculating pressures q_d at the disks, which yielded curves of $\mu_s = f(q_d)$ shown in Figure 8.9.

The static friction coefficient increases with the torque and accordingly with increase in pressure at the disks. Statistical workup of these data showed that they are best approximated by the following functions. For differential № 1 with steel disk set 1

$$\mu_s = 0.140T_0^{0.13}, \quad \mu_s = 0.108q_d^{0.13} \tag{8.1}$$

For differential № 3 with steel disk set 1

$$\mu_s = 0.130T_0^{0.10}, \quad \mu_s = 0.109q_d^{0.10} \tag{8.2}$$

For differential № 1 with disk set 2, that contains steel-metal-ceramics friction pairs

$$\mu_s = 0.150T_0^{0.095}, \quad \mu_s = 0.124q_d^{0.095} \tag{8.3}$$

Torque T_0 in formulae (8.1) through (8.3) is measured in kN-m, and the pressures q_d at the disks in MPa. The dynamic friction coefficient μ in differentials is discussed in Section 8.2.

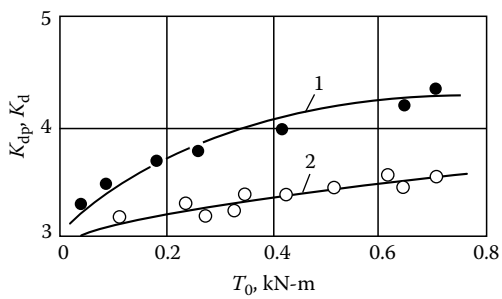


FIGURE 8.8
Locking coefficients K_{dp} (curve 1) and K_d (curve 2 at relative disk velocities of 0.65 rad/s) of differential № 1 with disk set 2.

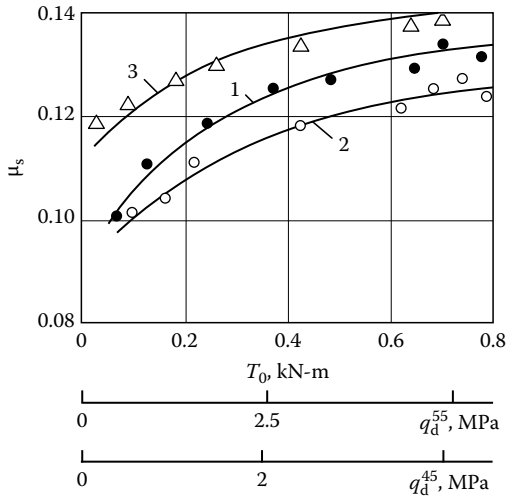


FIGURE 8.9
The static friction coefficient: 1, differential № 1, disk set 1 (scale q_d^{55}); 2, differential № 3, disk set 1 (scale q_d^{45}); 3, differential № 1, disk set 2 (scale q_d^{55}).

As the mileage accumulated by the vehicle increases, ensuring the stability of locking properties of limited slip differentials and in particular of their locking coefficients acquires increasingly greater significance. Satisfaction of this condition will promote retention of the operational properties of the vehicles over their service lifetime. The stability of the locking performance of the differentials was investigated by testing the three differentials the layouts of which are shown in Figure 4.13. The parameters of the differentials conformed to those of mechanism № 1 from Table 8.1, whereas the disks were those of set 1 from Table 8.2. The differentials operated for 5800, 6200, and 7100 h in the front axles of 4 × 4 farm tractors that had a nominal draw bar force rating of 14 kN. The differentials were tested on a stand (Figure 8.1) without preliminary disassembling without disturbing the completeness of the worked-in components.

It is seen by comparing the results of test plotted in Figures 8.10 through 8.12 with data of testing the new differential № 1 from Figure 8.6 that both the locking coefficient K_d and the static locking coefficient K_{dp} decrease with increasing operating time.

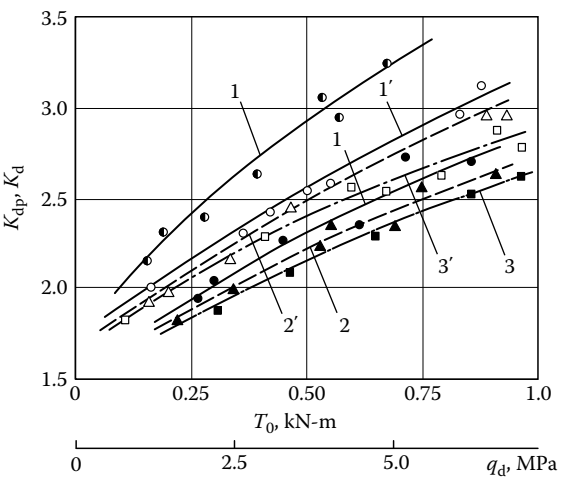


FIGURE 8.10
Differential with accumulated operating time of 5800 h: 1, K_{dp}; K_d: 2 and 2′, 3 and 3′, 4 and 4′ with the right and left shafts stopped and at relative disk sliding velocities of 0.65, 1.21, and 2.24 rad/s.

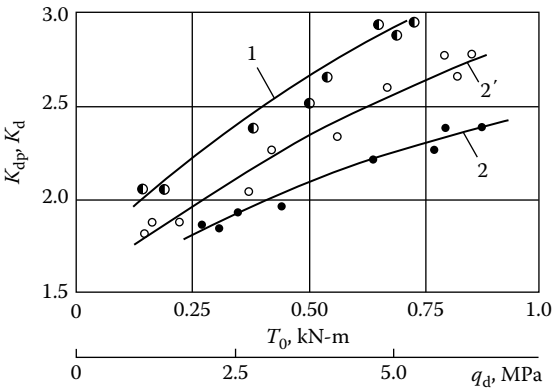


FIGURE 8.11
Differential with accumulated operating time of 6200 h: 1, K_{dP}, K_d: 2 and 2′ with the right and left output shafts stopped and at relative disk sliding velocity of 0.65 rad/s.

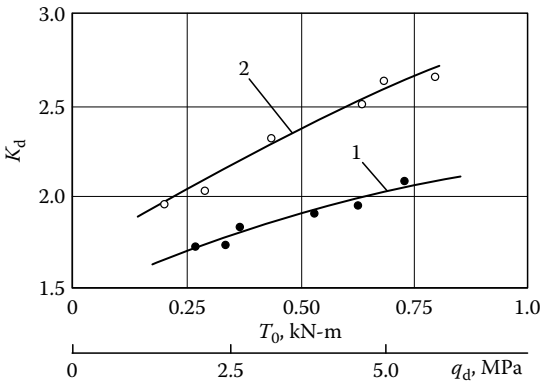


FIGURE 8.12
Differential with accumulated operating time of 7100 h. 1 and 2, K_d with the right and left output shafts stopped and at relative disk sliding velocity of 0.65 rad/s.

Differentials with accumulated operating time of 5800 and 6200 h exhibited satisfactory symmetry of locking performance. The asymmetry factor calculated from formula (4.70) and data in Figures 8.10 and 8.11 did not exceed 1.25. It is seen from Figure 8.12 that the differential with 7100 h of operation has acutely asymmetrical locking properties. This stems from the fact that this mechanism was manufactured before the nature of asymmetricity was investigated (this was discussed in Section 4.4) and before the differential's manufacturing process was modified. Note that, in spite of the large operating time of this differential, its locking properties did not become symmetrical, as is usually assumed in such cases. When this differential was disassembled, it was found that the working surfaces of the grooves in the case had up to 0.5 mm deep furrows, and the friction surface of the inner end of the case had up to 1 mm deep concentric flutes (see Figure 4.37a). Accordingly, the side of the disk that rubs against the case has tacked onto it lumps of metal that were formed from the transfer of material from the case to the disk. The remaining components of the differentials under study were in good shape. They showed no scratches, worn spots of bulges of metal on the inner and outer cylindrical necks of the pressure cups, spherical ends of the pinions, on the pins in the region of contact with the pinion, and on the sloping flat surfaces of the pins that contact with the grooves in the differential's case.

Figure 8.13 shows the results of still another investigation of the stability of the locking properties of differential № 1 with three different disk sets.

Three differentials № 1 were installed on three tractors that operated under similar standard operating conditions. The differentials were removed from the tractors after

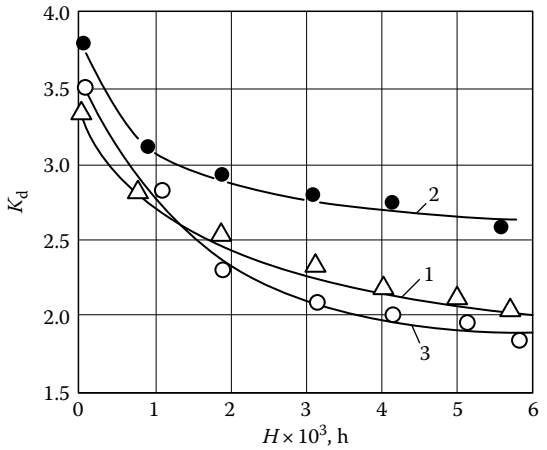


FIGURE 8.13
Locking coefficient K_d as a function of the service lifetime of differential № 1. Disk set number: 1, 1st set; 2, 2nd set; 3, 3rd set.

about 1000 h of operation and their locking coefficients were measured on the stand. The differentials themselves were not disassembled. It is seen that the value of K_d drops. The first experimental points of the three curves in Figure 8.13 correspond to values of K_d determined after 60 h running-in of the differentials after being installed on the tractors. The reduction in the locking coefficient stems from working-in of the disks and from the following: the rubbing surfaces of the disks wear out in the course of work, with a part of the products of wear remaining in the friction zone. Their presence reduces the friction coefficient, introducing an element of rolling into the relative sliding of the disks. After all the tests when the differentials were disassembled and inspected a large quantity of products of wear was detected . After the differentials were washed, their K_d and friction coefficient μ increased. The above is also confirmed by results of tests presented in Section 8.2.

It follows from Figure 8.13 that the most stable value of K_d is that of the differential whose disks contain steel-metal ceramics rubbing pairs (set 2). The locking coefficient of this differential decreased after 5750 h of operation by a factor of 1.45 as compared with its initial value, whereas K_d of differentials with sets 1 (steel-steel) and 3 (steel-bronze) decreased 1.7- and 1.84-fold, respectively. In addition, extrapolation of curves in Figure 8.13 shows that the rate of reduction in K_d with increasing operating time is smaller in the differential in which metal-ceramic disks are used.

The stand in Figure 8.1 can be used for testing other designs of limited slip differentials (for example, see Figure 6.17) and differentials of other types, using the same technique as employed for determining the locking coefficient.

In certain cases, it becomes necessary to determine the locking coefficients to retain the operating conditions to which the differentials are subjected during actual operation. This is done by constructing original test stands, the design of which incorporates the elements of the pertinent vehicles. As an illustration, Figure 8.14 shows such a stand constructed for determining K_d of the interaxle cam-plunger differential of a three-axle truck rated at 10 ton (mechanisms of this type were analyzed in Section 4.6).

This stand incorporates almost completely unit *A* of the vehicle, consisting of the interaxle differential together with the housing, bearings of the drive gear and of the run-through shaft of the tandem's second axle. This was done in order to obtain more precise test results. The only component that was replaced was one drive gear that was replaced by a specially made shaft 4 and this was done in order to allow connecting it to stand brakes 2.

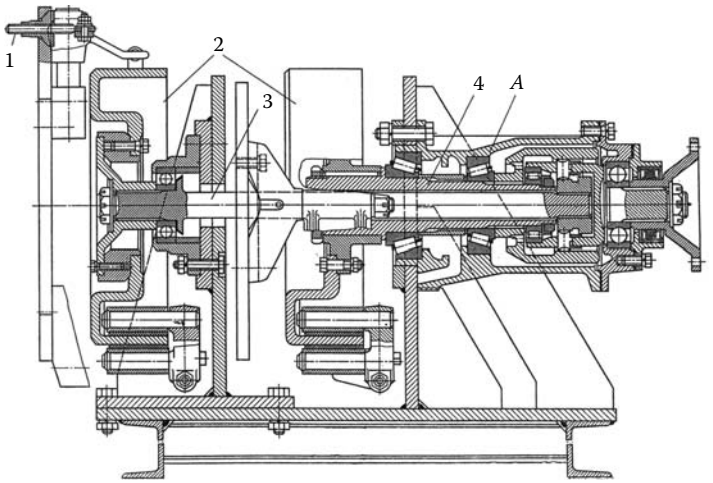


FIGURE 8.14
Design of stand for testing an interaxle cam-plunger differential.

The mechanism with the cam-plunger differential was fastened to the frame of the stand. In an actual vehicle power from the engine is supplied by means of a propeller shaft to the input flange of unit *A*, and then through a cage and the differential's plungers by means of shafts 3 and 4 to the forward rear and rearward rear axles. By analogy, on this test stand the input flange of unit *A* was connected by means of a drive shaft to the drive reduction gear, whereas shafts 3 and 4 were connected to the stand's brakes 2. Screws 1 adjusted the actuation (tightening) of the brakes. The differential that was tested accumulated 10,000 h of operation. Its components were in good shape. It was found that its locking coefficient was 2.5.

A separate class of test stands are used for investigating the reliability and service life, and to detect the appearance of wear damage in the newly designed differentials. Tests performed for this purpose bring about in many cases the need to construct unique stands. Such stands are constructed not only for prolonged testing of the differential as a whole, but also for testing and obtaining certain data on its components. Differentials may also be investigated directly together with the vehicle, both under laboratory conditions and on special test grounds. These matters are further analyzed in this chapter.

8.2 Laboratory Testing of Friction Clutches of Differentials

In the course of investigating and designing differentials with locking clutches, it is frequently necessary to make use of data that can be obtained only experimentally on special stands. These data include, among others, the real values of the sliding friction coefficients and their dependence on certain operating factors and on the material of disks of the locking clutches. In fact, the course of friction in disk clutches of differentials as friction pairs differs highly from conditions of testing on material specimens on friction testing machines. These clutches have several friction pairs that differ from one another by materials, real pressures in different friction plates, lubricating conditions of rubbing surfaces, and removal of heat from the friction zone. In this respect experimental

determination of the sliding friction coefficient μ, which would incorporate in its values the above specifics of friction in clutches is of definite interest. The numerical values of such a friction coefficient may be used, among others, in designing limited slip differentials and in calculating their locking coefficients (see Chapter 4).

It is impossible to experimentally determine μ and its dependence on the axial forces acting on the friction clutches using the stand shown in Figure 8.1. These axial forces depend on a large number of the differential's elements: meshings of pinions and side gears, cams, chamfers, collars, etc. It is hence extremely difficult to measure the total axial force that acts on friction disks. For this reason, a stand was designed for testing friction clutches of differentials that allows precisely presetting the axial force of disk compression and record the friction torque that arises in the clutch when this force is applied (see Figure 8.15).

The stand is driven by electric motor 1, the rotation from which is transmitted by two sets of speed reducers 2 to a side gear 3 of unit 4 that is tested. Test unit 4 that is balanced on a rolling and sliding bearing in the frame of the stand, consists of one-half of a limited slip differential assembled together with a friction clutch. The unit is lubricated with the same oil as the differential itself. Disk stack compression force Q is produced by screw couple 5 and is transmitted to the disks by compression strain-gage ring 6, rod 7, sphere 8, and insert 9, pressed into side gear 3. Force Q produces friction torque T_r between disks in the clutch that are connected to rotating gear 3, and nonrotating disks connected to the half-case of the differential. This friction torque is transmitted to unit 4 and is taken up by the frame of the stand by way of lever 10 fastened rigidly to the test unit and tension dynamometer 11. The friction torque is equal to

$$T_r = (F + G)L = \mu Q r_M i_M = \mu q_d A_M r_M i_M \tag{8.4}$$

where

F is the reading of dynamometer 11 determined from signals from its strain-gages cemented at its power rings

L is the arm of lever 10

GL is the resistance torque from the weight of lever 10 and dynamometer 11 determined by scales

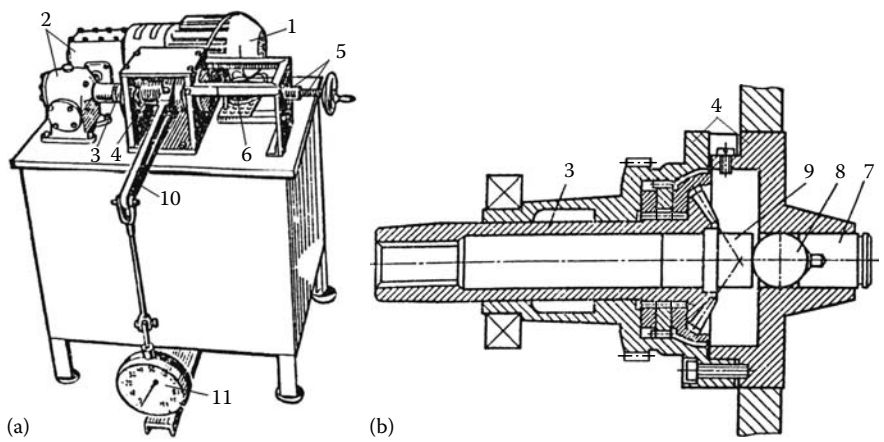


FIGURE 8.15
Stand for testing clutches of differentials: (a) general view; (b) unit being tested.

q_d is the design pressure in the contact of one friction pair
A_M is the area of one friction pair
r_M is the friction radius of the disks
i_M is the number of friction pairs ($i_M = 3$ in Figure 8.15b)

Using the measured values of T_r and Q at known values of r_M and i_M, friction coefficient μ is determined from expression (8.4) and its dependence on q_d. Studies can be performed at different relative sliding velocities of the disks, ω_{rel}, for different materials that are lubricated by different lubricants and for different numbers i_M of friction couples in one of the differential's clutches.

The limits of variation in pressures q_d on the disks and of their sliding velocities ω_{rel} should be determined before the tests start. For a limited slip differential of the front axle of a farm tractor, the results of testing of which are given further in this section, the maximum input torque at the case of this mechanism is $T_0^{max} = 0.6$ kN-m. This value of T_0^{max} corresponds to a maximum design pressure at the disks of $q_d^{max} = 3.0$ MPa. The speed at which this tractor moves when performing basic agricultural work does not exceed 2.8–3.3 m/s (10–12 km/h). When doing transportation work with a trailer the velocity of the tractor at turns does not exceed 2.5 m/s (9 km/h). These values of tractor speeds have disk slip velocities of $\omega_{rel} < 4$ rad/s corresponding to them. It follows from this that there is no point in investigating the effect of the sliding velocity on the friction coefficient μ for most of the friction materials, since the friction coefficient is constant within this range of sliding velocities (this was also mentioned in Section 8.1.)

Consider now the results of the test performed with $i_M = 3$ friction couples for the disk sets listed in Table 8.2. The results are plotted in Figures 8.16 through 8.19.

An analysis of all the figures allows the conclusion that the most stable values of the sliding friction coefficient is obtained with steel-steel (set № 1), steel-powder material (set № 2) and steel-bronze (set № 3) friction pairs. The friction coefficients with disk sets № 4

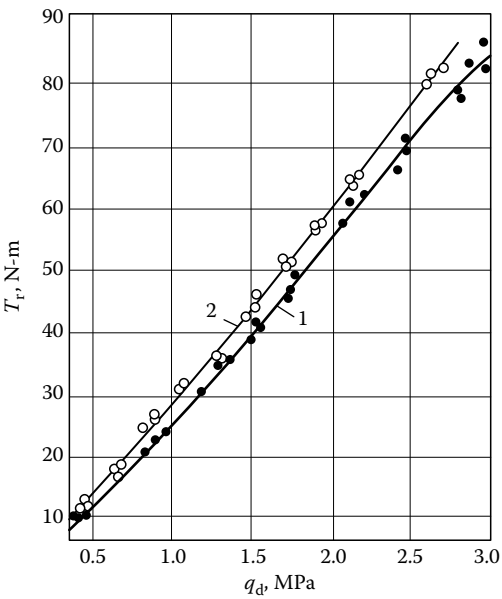


FIGURE 8.16
Friction torque T_r as a function of pressure q_d on the disks of clutches that contain friction pairs: 1, steel-steel (set № 1); 2, steel-bronze (set № 3).

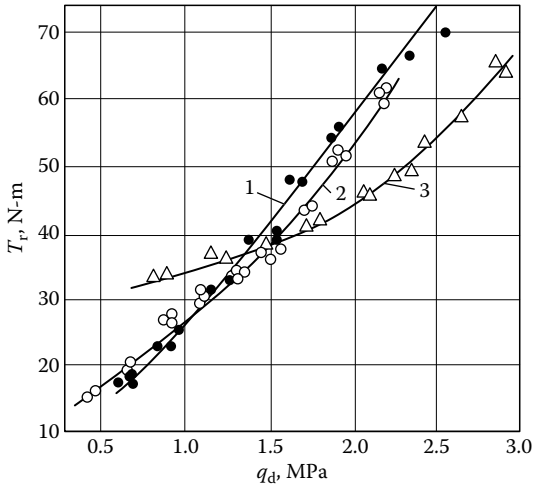


FIGURE 8.17
Friction torque T_r as a function of pressure q_d on the disks of clutches that contain friction pairs: 1, steel-powder metal (set № 2); 2, steel-copper coated disk (set № 4); 3, copper-coated disks (set № 5).

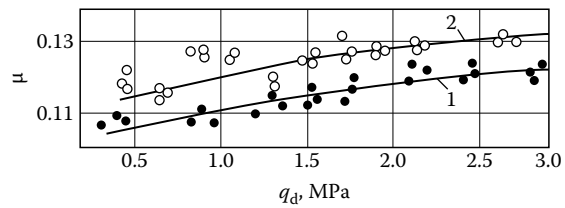


FIGURE 8.18
Sliding friction coefficient μ as a function of pressure q_d on the disks of clutches that contain friction pairs: 1, steel-steel (set № 1); 2, steel-bronze (set № 3).

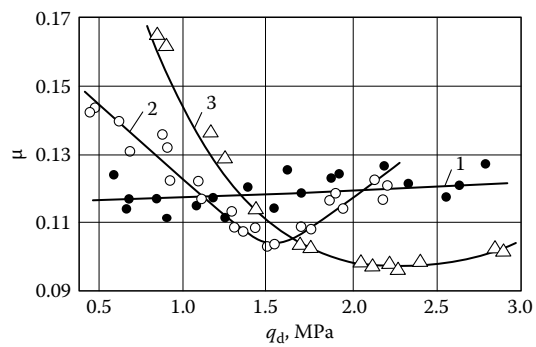


FIGURE 8.19
Sliding friction coefficient μ as a function of pressure q_d on the disks of clutches that contain friction pairs: 1, steel-powder metal (set № 2); 2, steel-copper-coated disk (set № 4); 3, copper-coated disks (set № 5).

and № 5 change perceptibly with increasing pressure q_d. The difference that was detected in the points of minimum of functions $\mu = f(q_d)$ of sets № 4 and № 5 stems from differences in the mechanical properties of the materials. For the softer materials, for set № 5 μ decreases at a higher rate than for set № 4. It is not desirable to use disks from materials of sets 4 and 5 in limited slip differentials because the friction coefficient varies within wide limits. This may highly change the locking coefficient, among others, and may bring about a rapid rise in it, causing the differential to seize (see Figure 4.3).

TABLE 8.7

Values of Coefficients in Formula (8.5)

Disk Set	a_0	a_1	a_2
1	0.09201	0.01608	−0.00257
2	0.11400	0.00388	−0.00057
3	0.10599	0.01608	−0.00257

Based on the results of testing of the clutches with sets № 1 through № 3 regression equations were obtained in the form of a second-power polynomial for calculating the friction coefficient

$$\mu = a_0 + a_1 q_d + a_2 q_d^2 \tag{8.5}$$

where, pressure q_d is in MPa. The values of the coefficients are listed in Table 8.7.

Calculations using formula (8.5) show that when q_d in disks of set № 1 vary within the range of 0.5–3.0 MPa the value of μ goes from 0.099 to 0.117. Accordingly, the minimum and maximum values of locking coefficient K_d of the differential of the tractor under study are 2.58 and 3.17. Formula (8.5) and the numerical values of the coefficients from Table 8.7 can be used for calculating the locking coefficients of similar limited slip differentials and for investing their effect on the vehicle's performance.

As mentioned in Section 8.1, the locking coefficient of limited slip differentials decreases with the operating times of these mechanisms. This is also confirmed by data of the following tests. Figure 8.20 shows test results obtained with a clutch, using disk set № 1.

The experiments were performed as follows. First curves of $\mu = f(q_d)$ of entirely new disks that were not worked-in were determined (curve 1). Then the disks were worked-in on that stand under a load of $q_d = 0.85$ MPa and, after 15 and 27 h of working-in, curves of $\mu = f(q_d)$ were determined anew. As seen from Figure 8.20, friction coefficient μ, and this

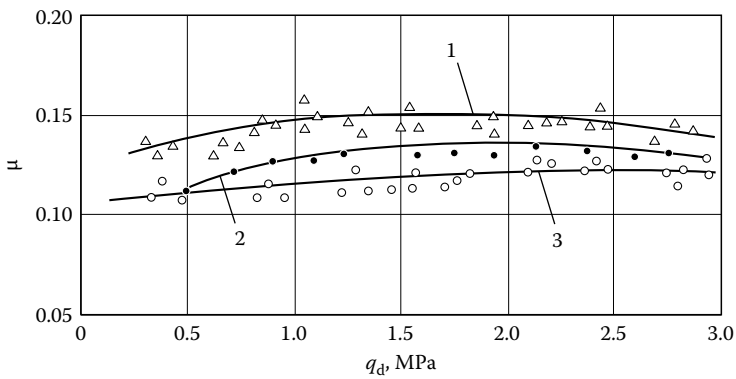


FIGURE 8.20

Sliding friction coefficient μ as a function of pressure q_d at disks from set № 1 with accumulated operating time, h: 1, 0; 2, 15; 3, 27; $\omega_{rel} = 0.15$ rad/s.

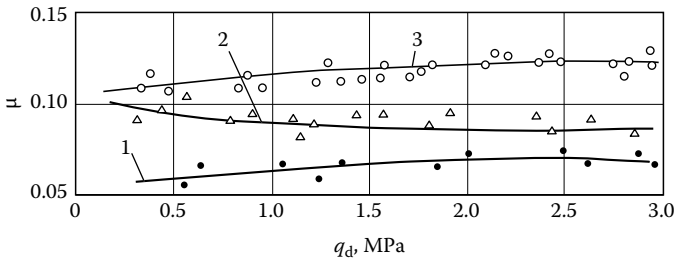


FIGURE 8.21
Sliding friction coefficient μ as a function of pressure q_d at the disks of clutches with accumulated operating time, h: 1, 6200 before washing down the disks; 2, 6200 after washing down the disks; 3, 27.

means that the locking coefficient K_d, tends to decrease. This drop in μ is caused by the working-in of the disks, which is particularly rapid during the first (initial) period of disk operation. During the working-in of the disks, wear products accumulate between them and they cause μ to decrease. To confirm this assertion directly (it was confirmed indirectly in Section 8.1) tests were performed with a clutch of a limited slip differentials with an accumulated operating time of 6200 h (the results of testing of the differential as such were discussed in Section 8.1).

In the beginning the tests were performed without disassembling the clutch, that is, a half of the differential's case together with the clutch was placed on the stand (Figure 8.15) and tested. Then the clutch was disassembled and the products of wear that stuck to the rubbing surfaces were washed off. Then the disks were relubricated by the same brand of lubricant, the clutch was assembled and retested on the stand. The results of the test are plotted in Figure 8.21.

The curve 1, represents the friction coefficient before washing down the disks, whereas curve 2, the friction coefficient after they were washed down. It is seen that washing the disks and removing the products of wear increases the friction coefficient by approximately 30%. However, the friction coefficient remains lower than for a disk stack of the same material that was worked-in for only 27 h (curve 3). This indicates that in order to stabilize the friction coefficient, meaning also the locking coefficient of limited slip differentials, it is necessary to reduce the wear of the rubbing surfaces by reducing the pressure on them and by using more wear-resistant materials. In addition, it is advisable to step up the circulation of lubricants between the disks in order to remove the products of wear from the rubbing zones. This is attained by producing oil grooves (radial, circular, and helical) on the disks and by using lubricating systems that provide for induced supply of oil to the differential, lubrication of its components and removal of oil from the differential. This is the topic of Section 8.3.

8.3 Laboratory Tests of Differential Lubrication Systems

A detailed analysis of the state of the components of differentials of vehicles with large accumulated mileage confirmed the need to work out and utilize effective lubrication systems. Thus, a study of interwheel differentials with oil-trapping scoops (such as

shown in Figure 2.75), used in the driveline systems of heavy-duty highway vehicular trains with 6 × 4 tractors showed the following (this is also mentioned in Section 2.5.3). The products of component wear and other impurities settle on the spherical surface of the differential's case. The thickness of these deposits is as high as 3–4 mm for an accumulated mileage of 350,000 km. The layer moves right up to the points of contact between the pinions and the case, which interferes with the flow of oil to the thrust washer and bushing of the pinions and to the thrust washer of the side gear. This causes significant wear of the pins of the spider beneath the pinions and abrasion of thrust washers of pinions and side gears. This brings about unmeshing of the pinions and side gears followed by breaking of the teeth.

The following cause the formation of a layer with products of wear. When the differential rotates, the oil that is captured by the scoops flows into the case and is pressed to its inner surface by centrifugal forces. This means that the oil inside the case starts being centrifuged and the products of wear and other impurities contained in it settle at the case walls precisely at the pinion thrust washers. This process is repeated periodically in the course of the vehicle's operation and causes a continuous thickening of the layer of wear products.

It is precisely such processes that occur in the bevel gear interwheel differentials of 6 × 4 trucks. For this reason, such drives need such lubricants that would ensure flow of oil through the differential and not only washing out of the wear products from the mechanism but their deposition in places specially allocated for this purpose.

In spite of the need to use flow-through lubricating systems for differentials, there is virtually no published data on the quantitative assessment of flowage of oil through the differential. There is no data on stands for use in such tests, on oil-measuring devices, and testing methods. However, data of such tests are needed for designing new and improved existing lubrication systems of differential mechanisms and of vehicle driveline systems as a whole. This section presents data from studies in this field performed by the authors.

Four different versions of flowage lubricating systems were designed and constructed for interwheel differentials of highway vehicle trains with a total mass of 42 ton driven by 6 × 4 tractors.

The oil supply to the differential in lubrication system № 1 (Figure 8.22) occurs as follows. The oil that is sprayed by the final drive driven gear flows to intake trough 4, located on the rear cover of the axle's housing and flows over it to pocket 5 of the cover of the right thrust bearing of the differential. Through a special port in the bearing's cover, it flows into groove 6 and then through opening 7 to the inner space of adjustment nut 10 that is insulated from the thrust bearing by cover 8 and seal 9. From there the oil flows to the differential through flattened spots and openings in its right side gear. The oil is removed from the axle's housing through similar ports 2 and flattened spots 3 in the left side gear.

Lubrication system № 2 (see Figure 8.23) differs from system № 1 by having the intake trough for oil intake to the differential in a higher position. Here trough 1 is placed above the final drive pinion. From it the oil flows into pocket 2 and then to the inner cavity of the adjustment nut. Otherwise, both systems are identical.

In lubrication system № 3 (Figure 8.24a) the oil enters the differential through two oil scoops 6, located on the right half of the case, whereas the oil is removed through four apertures 7 in the left half. The axes of these apertures are at an angle to the axis of rotation of the mechanism.

In lubrication system № 4, the oil enters the differential as in system № 2, and leaves it as in system № 3.

Differentials with flow-through lubrication systems were tested on a special stand shown schematically in Figure 8.24b and c. Axle 8 with the differential being tested is driven

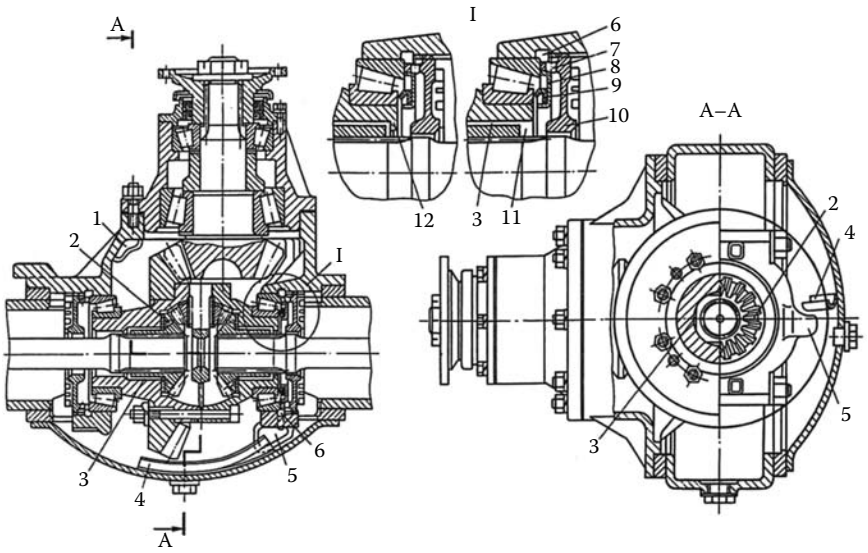


FIGURE 8.22
Interwheel differential with lubrication system № 1: 1 and 5, oil-sump pocket; 2, oil passage; 3, segmented oil passage; 4, trough; 6, annular groove; 7, inlet port; 8, adjustment nut cover; 9, L-shaped packing; 10, adjustment nut; 11, free space; 12, differential half's hub-collar.

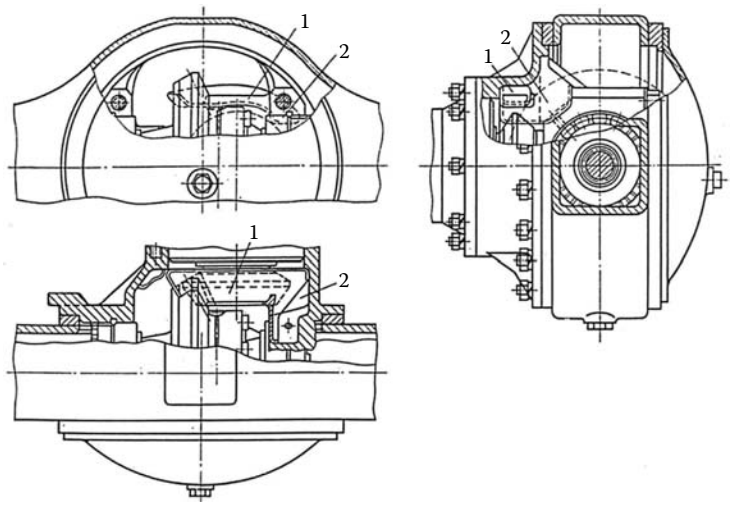


FIGURE 8.23
Interwheel differential with lubrication system № 2: 1, trough; 2, oil collecting pocket.

through driveshaft 9 by electric motor 10. The rpm of the electric motor shaft during the tests was set by instrument 11. During each experimental run, the temperature of the oil in the axle was maintained constant and monitored from readings of a sensor placed on the drain plug. Visual study of the oil flows was by means of observation ports in the housing that were covered by Plexiglas.

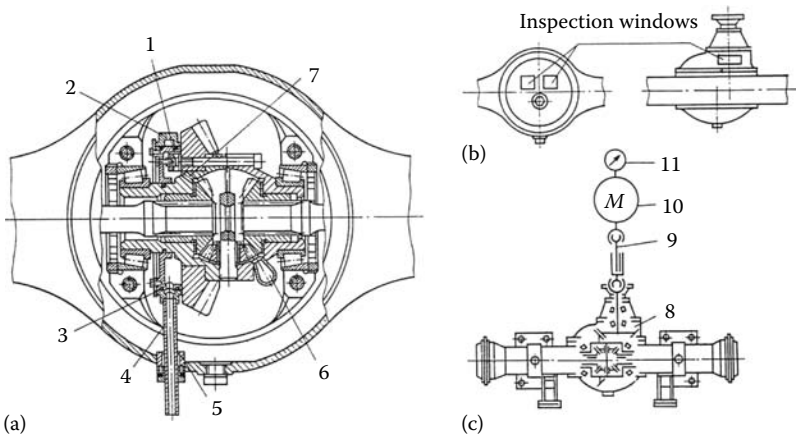


FIGURE 8.24
Interwheel differential with lubrication system № 3 (a) and schematic of test stand (b and c): 1, oil sump; 2, oil collecting ring; 3, collar-like ring; 4, oil-removal tube; 5, seal; 6, scoop; 7, oil-removal port; 8, test axle; 9, driveshaft; 10, electric motor; 11, tachometer.

The tests were performed without relative rotation of the mechanism's components, which corresponds to motion in a straight line, and with relative rotation of the side gears of the differential, when one of them was stopped while the other rotated at twice the velocity relative to the differential's case.

The flowage of the oil was assessed by its flow rate Q_m, that is, the quantity of oil that was discharged from the differential per unit time. The oil flow rate was measured using specially constructed oil meters. When oil from the testing systems № 1 and № 2 was removed from the differential by installing a pipe in the left half of the differential's case, the oil traveled over this pipe to a measuring device and was then returned to the axle's housing.

The oil flow rate in differentials with lubrication systems № 3 and № 4 was measured by a specially constructed oil meter shown in Figure 8.24a. It consists of a rotating ring (oil sump) 1 fastened to the differential's case and a stationary ring 2. Ring 2 is prevented from moving axially by washer 3 and from rotating by the oil-removal tube 4 installed in bushing 5 of the axle's housing and by a special locking bolt, screwed into ring and bearing on the axle's crankcase (the bolt is not shown in the drawing). Packing rings are installed between rings 1 and 2 and between ring 1 and the left half of the differential's case. The oil that leaves the differential through ports 7 flows to the oil meter and from it along tube 4 to a measuring device (not shown in the figure). The oil that flows to the measuring device was immediately returned to the axle's housing. For this reason, the quantity of oil located outside the axle did not exceed 0.5 L at any point of time.

The investigations were carried out at different velocities of the differentials, using different oil brands, and the volume and temperature of the oil in the reduction gear of the axle was varied. A certain value of rpm ω_0 of the differential was preset at the start of an experimental run and after 2–3 min, during which the flow of the oil within the case of the mechanism was established, the required data were taken. Then the experiments were repeated at other values of ω_0.

Here the experimental results on testing the lubricating systems described above are analyzed in sequence. The first to be investigated was the operation of lubricating system № 1 both visually through viewing ports in the housing of the axle with the inner part of the

housing electrically illuminated and by performing pertinent measurements. Observations of the flow of oil in the case of the axle showed that MT-16P oil (10 L) heated to 40°C–45°C gets sprayed into trough 4 (see Figure 8.22) by the final drive driven gear when the differential's case is rotating at $\omega_0 = 9.15$ rad/s (87.5 rpm) corresponding to a vehicular train velocity of 5 km/h. When the amount of the same oil in the housing is increased to 11 L, it starts being sprayed into the trough as early as at $\omega_0 = 6.1$ rad/s, or at a vehicle velocity of 3.3 km/h. If the angular velocity is lower than these values, the oil does not go into the trough.

Then the oil from trough 4 flows into pocket 5. The rate of flow of the oil through the trough is about 1 cm/s. This amount of oil does not cause the pocket to overflow. It remains full to $\frac{3}{4}$ of its volume. However, when the differential's rpm rises to 12.2 rad/s (vehicular train velocity of 6.6 km/h) and more the oil does not succeed in passing aperture 7 into the space of nut 10, pocket 5 becomes overfilled and the oil starts flowing from it into the housing.

At $\omega_0 = 24$–28 rad/s (230–262 rpm) and more, an oil column forms above pocket 5 and it is restrained between the back cover of the housing and the cover of the right bearing of the differential. Simultaneously the oil contained in the trough starts churning.

Observations of the discharge of oil from the space of nut 10 to the differential showed that its flow is not uniform. Oil that accumulated in nut 10 to some level would then spill over into the right bowl of the differential through collar 12. This repeated itself for an approximate period of 1.5 min, and after 15 min of the stand's operation at $\omega_0 = 12.2$ rad/s the oil flowing into the differential formed a stable oil film on its components.

The oil was observed to flow from the space within nut 10 to the mechanism only up to values of ω_0 about 28 rad/s. When the rate of rotation of the differential was increased further in steps of 5.24–122.2 rad/s (1167.2 rpm, i.e., with the driveshaft rotating at 2000 rpm) it was found that oil virtually does not enter the differential. This was confirmed by the fact that after the stand was operated over the above range of ω_0 for an hour and then stopped, virtually no oil was discharged from the left half of the differential.

The oil was discharged from the left half of a stopped differential only in the case when its rpm before it was stopped did not exceed 28 rad/s. The MT-16P oil started discharging from a stopped differential after 30 min of the stand's operation at $\omega_0 = 12.2$ rad/s. The lower viscosity AU oil (10 L) started discharging from the differential after 5 min of the stand's operation at $\omega_0 = 9.15$ rad/s.

It hence follows from the data that when system № 1 operates at ω_0 that does not exceed 28 rad/s, the oil fills the inner space of the differential, but this does not provide for flowage, that is, it does not leave the rotating mechanism. Oil starts to flow from the differential only after it is stopped. At $\omega_0 > 28$ rad/s oil virtually does not flow in to the differential.

These shortcomings of system № 1 made it necessary to seek ways of improving it. Thus, to facilitate the discharge of oil from the inner space of nut 10 collar 12 on the right half of the differential was removed (see item 11 in Figure 8.22). At the same time, the four radial ports in nut 10 were supplemented by four additional ports having a diameter of 8 mm. The width of trough 5 was also increased to 15 mm and the discharge port from pocket 5 into it was drilled out to a diameter of 12 mm (instead of the previous 8 mm).

The above steps eliminated the nonuniformity of flow of oil from the inner space of nut 10 into the differential's elements. Oil started flowing into the differential without interruption. For example, at $\omega_0 = 9.15$ rad/s the MT-16P oil started flowing to the differential as soon as 1–2 min of the stand's operation and after 5 min its flows became mixed with one another inside the differential's case. It was captured by the walls of the case, rose, and then fell, since at $\omega_0 = 9.15$ rad/s the centrifugal forces are still small and insufficient for pressing the oil flows to the inner surface of the differential.

This implies that the means undertaken for improving system № 1 yielded the desired result. The oil not only started flowing stably into the differential, but also to stably leave it through ports in the left half when the mechanism rotated.

In addition to testing the lubrication system № 1 with the MT-16P oil the system was tested with the lower-viscosity AU oil. Here, the flowage of the system was determined by flow rate Q_m of the oil as a function of the differential's rpm ω_0 and the design velocity of the vehicular train. The test results are plotted in Figure 8.25.

The oil flow rate Q_m, first increases with increasing ω_0 and then drops. It attains its maximum value of 88 cm^3/min at $\omega_0 = 12.2$ rad/s. The flowage of oil through the differential stops at $\omega_0 > 28$ rad/s, that is, at vehicular train velocity of 15 km/h. This may be explained as follows. As the angular velocity of the differential increases, the centrifugal forces press the oil to the inner surface of the mechanism's case and the oil ring that forms as a result prevents the oil from flowing from the space within nut 10. The pressure of the oil leaving the nut was insufficient for pushing the oil that fills the differential along the principal axis of the mechanism. To increase the pressure of the oil leaving the case, trough 4 was deepened and a deflector was placed above pocket 5. However, these design modifications did not yield the desired result.

Some increase in the pressure of the oil leaving the nut was attained by placing the trough higher, as was done in system № 2. In this system (see Figure 8.23), the oil flows into trough 1 when it is separated from the total layer of oil that forms on the final drive driven gear. In addition, some part of the oil enters the trough from the stream that forms in the course of rotation of the differential's case and of the heads of the bolts that hold the halves of the case together.

Tests of lubrication system № 2 showed that at $\omega_0 \leq 30$ rad/s the oil flows irrotationally along trough 1 (see Figure 8.23) into pocket 2 and then into the space of the nut. If $\omega_0 > 30$ rad/s, then the final drive driven gear, the differential's case and the heads of the bolts spray most of the oil above the trough. After being deflected by the axle housing, the oil

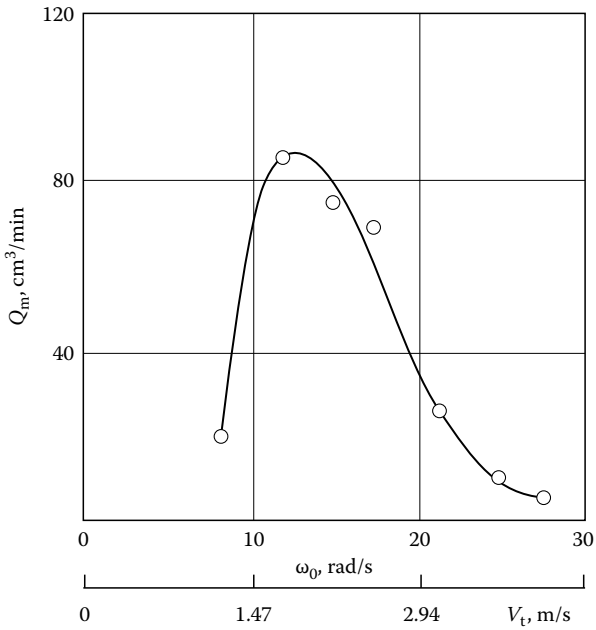


FIGURE 8.25
Flow rate of AU oil (10 L) in a differential with lubrication system № 1 as a function of rpm ω_0 of the case and the design velocity of the vehicular train at $t = 40°C \ldots 45°C$.

flows to the trough, whence one part of it is directed in the form of churning flows into the pocket whereas the other part returns to the housing. Flowage of oil through the differential in this case occurred at $\omega_0 < 40$ rad/s. At a higher rpm flowage stops because of the rising forces of resistance to the flow entering the differential. The results of measurements of the flow rates of AU and MT-16P oil through a differential with lubrication system № 2 are shown in Figure 8.26.

It can be concluded from the analyses of curves 1 and 2 and comparing them with the curve in Figure 8.25 that system № 2 has approximately the same maximum value Q_m^{max} of the flow rate as system № 1. However, the flowage of oil through the differential with system № 2 is retained over a somewhat wider range of velocities than in the differential with system № 1.

Testing a differential with lubrication system № 3 showed that it ensures a more complete filling of the differential by the lubricating oil. The oil flows from the differential through the oil meter in a continuous stream, which attests to a higher flowage of oil when using system № 3. The results of testing the flowage of the system of differential № 3 are plotted in Figures 8.27 and 8.28.

It is seen from the figures that the shape of all the curves is almost the same. Their complex shape stems from the form of oil flows in the axle's housing and these depend on the configuration of the inner space of the housing, on the design specifics of the final drive, and of the differential itself and also on the rpm of the latter.

When the oil volume is increased from 10 to 13 L, the maximum value Q_m^{max} of its flow rate increases approximately 3–4-fold. Thus, for example, for 10 L of oil and temperature between 40°C and 45°C the maximum flow rate is 550 cm^3/min, whereas in the case of 13 L oil in the axle housing and the same temperature $Q_m^{max} = 2200$ cm^3/min.

Flowage of oil through the differential is higher at medium and low differential rpm and decreases at high rpm. This behavior should be regarded as successful for a wheeled vehicle, since medium and low differential rpm values correspond to its motion while

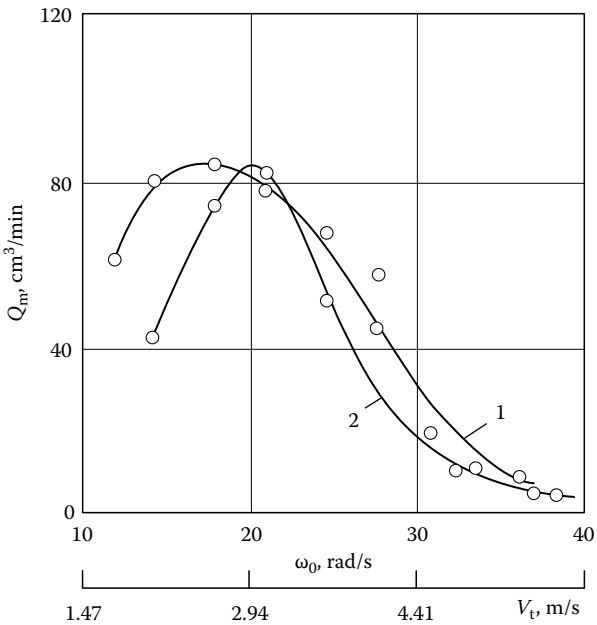


FIGURE 8.26
Flow rate of MT-16P oil (curve 1) and AU oil (curve 2) in a differential with lubrication system № 2 as a function of the case rpm ω_0 and the design vehicular train velocity at $t = 40°C \ldots 45°C$ with 10 L of oil in the housing.

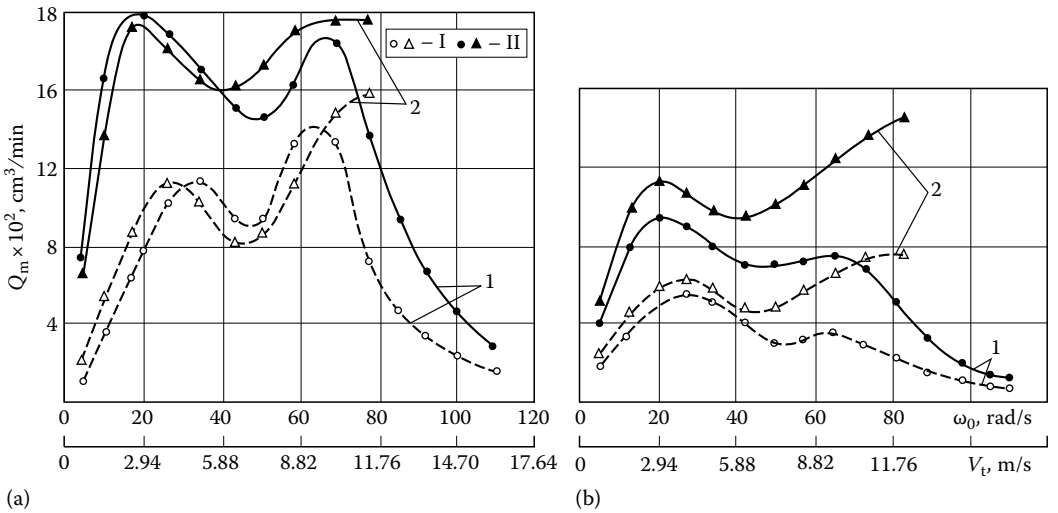


FIGURE 8.27
Flow rate of oil TSp-15K in a differential with system № 3 as a function of the case rpm ω_0 and of the design velocity of the vehicular train at 11.5 L (a) and 10 L (b) of oil in the axle housing: 1 and 2, respectively without relative motion of the differential's parts and with the right side gear stopped; *t*, °C: I, 40–45; II, 50–55.

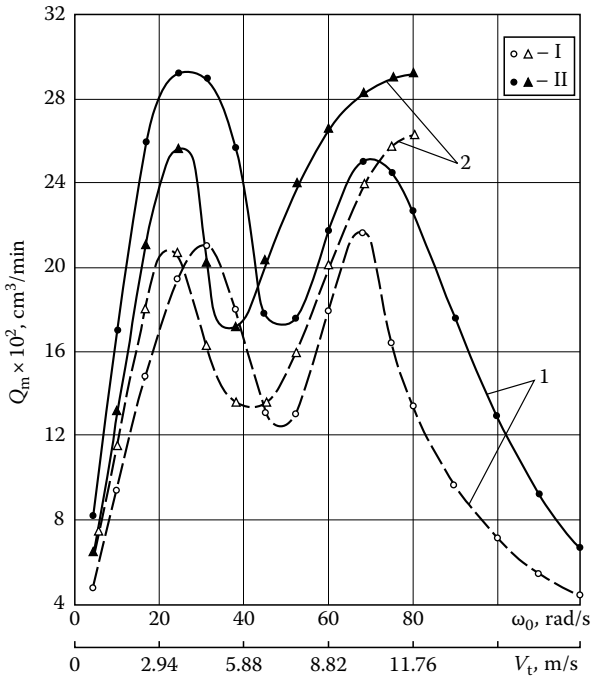


FIGURE 8.28
Flow rate of oil TSp-15K in a differential with system № 3 as a function of the case rpm ω_0 and of the design velocity of the vehicular train at 13 L of oil in the axle housing: 1 and 2, respectively without relative motion of the differential's parts and with the right side gear stopped; *t*, °C: I, 40–45; II, 50–55.

taking a turn or traveling over roads with low gripping properties, when the gears of the differential mechanism operate most strenuously. The differential's rpm is high when the vehicle moves in a straight line. At this time the differential's gears either do not rotate at all or almost do not rotate one relative another.

The flowage of oil in a differential with lubrication system № 3 increases with the temperature. Thus, when the temperature increases from 40°C–45°C to 50°C–55°C its flow rate increases by 50%–80%.

Tests of lubrication system № 4 showed that its flowage is also characterized by high values of oil flow rate over a rather wide range of ω_0 (see Figure 8.29).

The maximum value of $Q_m^{max} = 750\ cm^3/min$ is attained at oil temperature t of 50°C to 55°C and with 13 L of oil in the axle housing. Flowage of oil is retained up to a differential rpm of $\omega_0 = 131$ rad/s, which corresponds to a vehicular train velocity of 65 km/h) both without relative motion of the differential's components and with the right side gear stopped.

The effect of oil flowage on the discharge of products of wear was determined by comparative testing of a differential with system № 3 and another differential with the same system, but with plugged-up discharge ports 7 (see Figure 8.24a). Both differentials were tested on the stand shown in Figure 8.24b and c. The oil-metering device was removed for the tests that were performed with 13 L of MT-16P oil. Abrasive powder (remaining after machining components by an emery wheel) was added to the oil to simulate the products of wear. Approximately such wear products are contained in the oil after extended vehicular train operation. Two series of experiments were carried out; for the first series, 350 g of powder was added to the oil and for the second, 150 g. Each differential was tested for 5.5 h. In the course of the tests, the differential rpm was reset every 0.5 h in steps of 20.93 rad/s (200 rpm). After testing, the differentials were taken apart and inspected visually. Then, the abrasive mass that accumulated on the inner surfaces of the differentials' cases was collected and weighed. The flowage of the lubrication systems was assessed based on this weight.

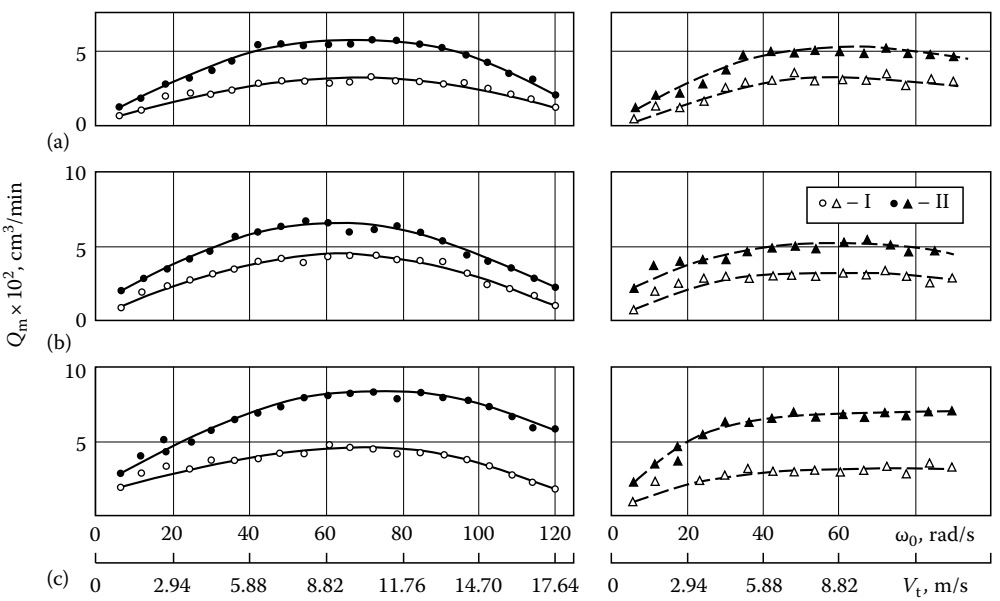


FIGURE 8.29
Flow rate of oil TSp-15K in a differential with system № 4 as a function of the case rpm ω_0 and of the design velocity of the vehicular train at 10 L (a), 11.5 L (b), and 13 L (c) of oil in the axle housing: Solid curves—without relative motion of the differential's components; dash-curves—with the right half axis (gear) stopped; t, °C: I, 40–45; II, 50–55.

TABLE 8.8

Results of Stand Testing of Differentials

Mass of Abrasive Powder Added to the Oil (g)	Mass of Abrasive Parts Precipitated on the Spherical Part of the Inner Space of the Differential's Case (g)	
	System № 3	System № 3 with Plugged-Up Discharge Ports
350	66	126
150	34	68

Inspection of the differential with plugged-up discharge ports (there is no flowage of oil through the differential) showed that the abrasive mass precipitates as a uniform layer over the entire inner surface of the differential's case, snugly approaching the points of contact between the pinions and the case. The thickness of the layer on the spherical surfaces of the case's halves between the pinions was 4–5 mm when 350 g of abrasive powder was added to the oil and 2–3 mm when 150 g of abrasive powder was used.

In the differential with flowage lubrication system № 3 the thickness of the abrasive on the spherical surface of the case was 2–3 mm when 350 g of abrasive was added and 1–1.5 mm when 150 g was used. The abrasive parts here precipitated only on the spherical part of the inner space of the differential's case and this was in the form of individual splotches. There were no deposits on the cylindrical parts of the case. The results of the measurement of the amount of abrasive mass are listed in Table 8.8.

It is seen from this table that the deposits of abrasives on the inner surface of the case of the differential with flowage system № 3 are approximately twofold less than in the differential with the plugged-up discharge ports.

Subsequent studies were directed toward developing effective flowage lubrication systems for the interaxle differentials of the drive tandem of the same vehicular trains with a overall mass of 42 ton driven by 6×4 tractors. This problem was divided into two tasks. The first consisted in searching in the reduction gear, a segment of active vortical flows near the interaxle differential and creating an oil trap of sufficient capacity there. The second task consisted in producing oil conduits both in the nonmoving part of the reduction gear and in the moving parts (shafts) and the pertinent connection of these conduits. The oil flow through them should reach the interaxle differential and lubricate it. The resulting design, in which the problem was solved, is shown in Figures 8.30 and 8.31.

The flowage of oil through the system was monitored based on its discharge from port 6 with all other radial ports that open into the plugged-up axial passage 5. The tests verified that shaping oil trap 1 as a turbine blade was a proper choice: the dynamic pressure that is generated within it is sufficient for filling the oil-collecting bushing with oil and for feeding oil to the axial channel 5 to port 6. Visual observations of the inner space of oil-collecting bushing 2 performed through a special port (it is closed by plug 7 in the photograph in Figure 8.30) showed that it is filled with oil when the differential rotates. At angular velocities of $\omega_0 = 42-49$ rad/s a stable discharge of oil in the form of individual droplets was observed from monitoring port 6.

Further studies were directed at refining the system to increase the oil flow through axial channel 5. This was done by designing a system for increasing the pressure of oil at the inlet to ports 3 (Figure 8.31a and b). It consisted of a screw pump with a square-thread, with parameters shown in Figure 8.31c. Tests of the system with the screw pump showed that stable discharge of oil occurs from reference port 6 in the form of a 2–3 mm diameter continuous jet over the range of $\omega_0 = 40-125$ rad/s.

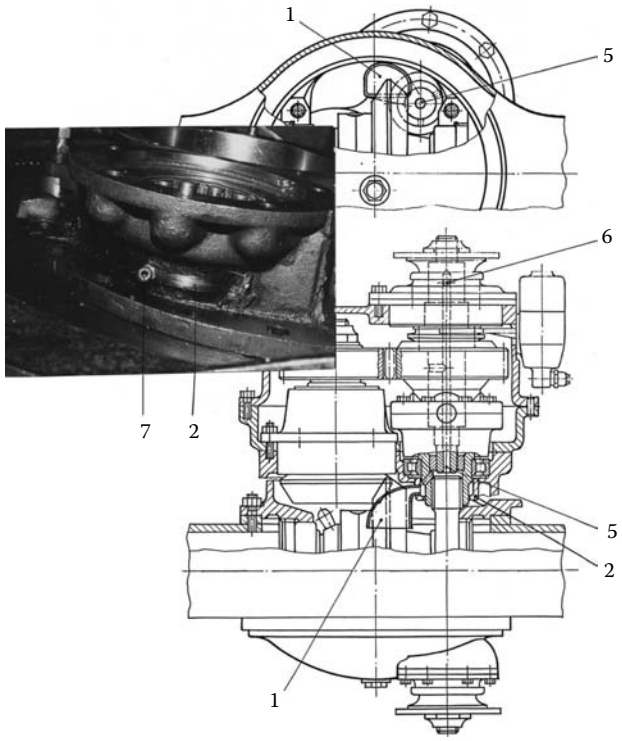


FIGURE 8.30
A general view of oil trap and oil collecting bushing of the lubrication system of the interaxle differential of a 6 × 4 tractor.

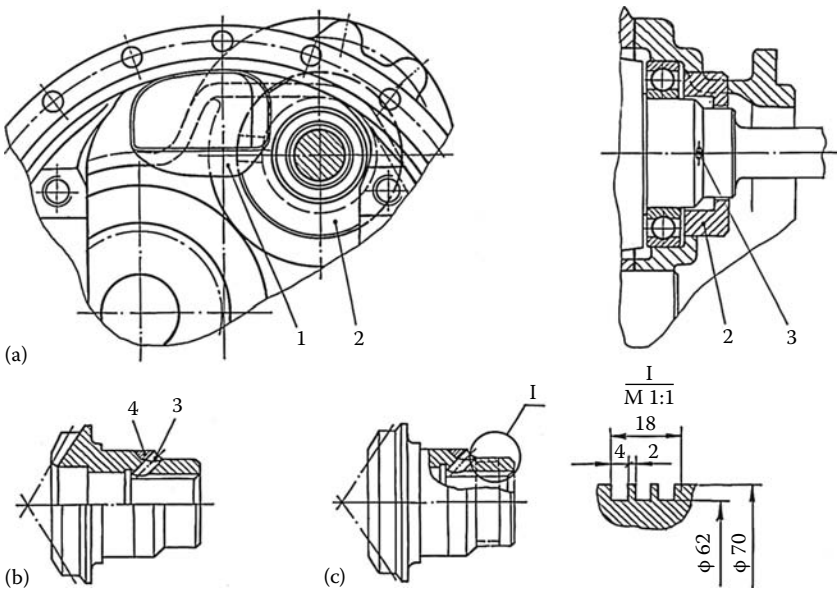


FIGURE 8.31
Elements of the lubrication system of the interaxle differential of a 6 × 4 tractor.

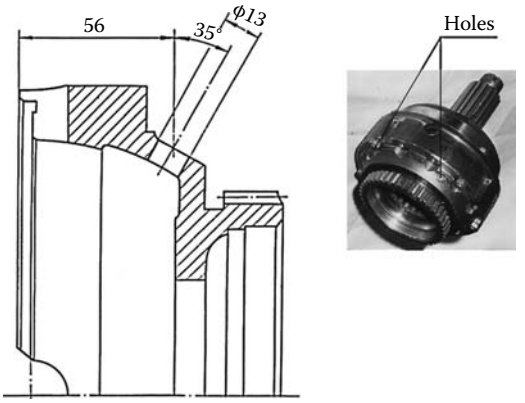


FIGURE 8.32
Interaxle differential of the drive tandem of a 6×4 tractor of a timber carrier with a total mass of 47 ton.

The investigation also included a study of the effect of the diameter and location of output ports on the discharge of oil from these mechanisms. The number of ports, their diameter and their location on the differential's case were selected with a consideration of the capacity of the channels over which oil is fed to the differential and the relationships between the diameters and location of the oil inlet and discharge ports previously investigated with interwheel differentials. In the interaxle differential specimen shown in Figure 8.32 the oil was discharged through four ports.

TABLE 8.9

Capacity of Oil Flow at the Inlet to the Interaxle Differential

Differential's Case (rpm)	Oil Flow Rate (cm^3/min)
300	Onset of oil feed
500	100
1000	280
1500	400
2000	740
2500	1080

The experiments were performed using 12 L of TSp-15K oil. Two drive tandems with interaxle differentials were tested: one of the differentials is shown in Figure 8.32, whereas the second was the same, but without discharge ports. It was found that oil enters both differentials (see Table 8.9).

Then, 350 g of abrasive powder was added to the oil. Each differential was tested with each cycle repeated seven times. During each cycle the differential was rotated at $\omega_0 = 84$ rad/s (800 rpm) for 15 min followed by a 10 min pause. The experiments showed that in the differential without discharge ports, a uniform continuous layer of abrasive particles was observed on the inner surface of the case; this layer approached flush to the points of contact between the pinions and the case and fully covered the pinion washers along their height. This layer was 6–8 mm thick. The mass of the moist-abrasive that precipitated inside the differential without discharge ports was 275 g. In the differential with discharge ports, the entire surface of the case half with discharge ports (see Figure 8.32) was clean without traces of the abrasive. On the inner surface of the second part of the case, abrasive particles precipitated in the form of individual 2–4 mm thick splotches. The total mass of abrasive that precipitated inside the differential with the ports was 127 g, that is, 2.17-fold less than in the differential without the ports.

The experiments described above thus demonstrated the capability and effectiveness of flowage lubrication systems of differentials, which confirms the need to use them in vehicles. The quantitative estimates of the flowage of various lubrication systems obtained in these experiments can be used in upgrading the existing, as well as designing new differential mechanisms.

8.4 4 × 4 Vehicle Chassis Dynamometer with Individual Roll Control

Sections 8.1 through 8.3 were concerned with methods, experimental stands, and results of investigating certain power dividing units and their subsystems. The logical next step in experimental studies of driveline systems and PDUs consists of an experimental check of their effect on the operational and consumer properties of vehicles. Such tests are needed for a number of basic reasons. In the first place, because testing of vehicles with newly developed driveline systems make it possible to obtain a comprehensive assessment of the effectiveness of new designs in their interactions with the other systems and mechanisms of vehicles. For example, the effect of a given driveline system on the traction properties of vehicles may change somewhat depending on the properties of tires, the stiffness of the driveline system itself, etc.

It is advisable to start the testing of vehicular driveline systems under laboratory conditions. This allows eliminating the effect of many random factors present when vehicles are tested on proving grounds such as changes in weather conditions and properties of the surfaces of motion; changes in the psychomotor behavior of the test driver, etc. These and other factors, imposed on the results of measurements may make it difficult to understand how the driveline system affects the dynamics and operational properties of the vehicles. Laboratory testing provide for multiple repeatability of the same test conditions and make it possible to not only assess in ''pure form'' the effect of the driveline system on the properties of vehicles, but also to determine certain characteristics and parameters of driveline systems that are needed for an analytic simulation. For this reason, vehicles are tested under road/terrain conditions after they were tested on special experimental stands.

There exist a large number of designs of vehicle chassis dynamometers for testing vehicles under laboratory conditions. Usually, the effect of the powertrain on the dynamics, operating properties, fuel economy, and emissions is investigated using vehicle chassis dynamometers with rolls. In addition, recently developed flat-belt road dynamometers provide the longitudinal and normal inputs on the wheels.

In conventional dynamometers for testing 4 × 2 vehicles the left and right rolls are rigidly fastened to one another, that is, rotate as a single unit. The same also applies to dynamometers for testing 4 × 4 vehicles. In such units usually all the rolls (left and right, front and rear) rotate at the same speed since they are mechanically coupled to one another. This rigid coupling makes it impossible to imitate various gripping conditions of the vehicle's wheels, or rotation of wheels at different speeds, which is typical when moving along a curve. For this reason, such test units do not allow investigating to a full extent the effect of the wheel driveline systems on the vehicle's properties. Designs of stands for experimental study of driveline systems and power dividing units should provide various modes of separate control of the front and rear, left and right rolls. Certain designs of test dynamometers are considered here.

Figure 8.33 is a schematic diagram of a stand for testing 4 × 2 vehicles.

A 4 × 2 vehicle 1 is placed by its front, drive, and steered wheels on freely rolling rolls 2 with braking devices (or electric motors) 3, and by its rear wheels on platform 4 that is capable of translation in the direction perpendicular to the longitudinal axis of the vehicle. Here the rear axle of the vehicle is fastened in the middle of the axis (see point 5) on the platform in such a manner that the moment of resistance to turning the vehicle would move it and, consequently, the vehicle proper in the transverse direction together with the platform. A free motion of the platform in the transverse direction is made possible by

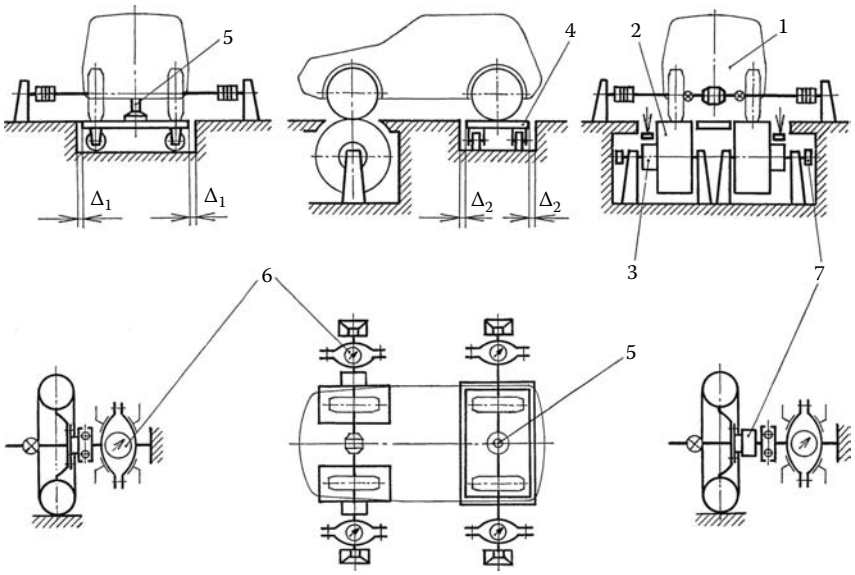


FIGURE 8.33
Chassis dynamometer for testing 4×2 vehicles.

sufficient gaps, Δ_1 and, as small as possible gaps, Δ_2. The surfaces of the platform in gap Δ_2 should be smooth and lubricated. They serve as guides. Spaces Δ_1 are used for measuring purposes. The platform's gap system should not permit the vehicle to ''run away'' past the permitted limits of the stand in the course of experiments. Lateral forces acting along the front and rear axles are measured by sensors 6. The torques and angular velocities of the vehicle's wheels and of the rolls are determined from readings of sensors 7. Curvilinear motion of the vehicle under a variety of gripping conditions is simulated by making possible separate control of the left and right rolls over which the front wheels run. The ratios of the angular velocities of the left and right wheels of the axle in curvilinear motion can be determined based on analytic expressions (2.15).

Figure 8.34 shows a general view of a dynamometer for testing 4×4 vehicles.

Table 8.10 presents the specifications of the dynamometer.

These data show the range of vehicles that can be tested on this dynamometer. The wheels of the vehicle being tested from its engine rotate four double rolls. Four power-absorbing units connected to the rolls produce the load. All or a part of the rolls may be connected mechanically provided a rigid coupling between all or a part of the rolls. When all the rolls are interconnected, the dynamometer is suitable for all forms of tests that are performed on contemporary conventional test units. These forms of tests are provided in the operating mode known as Control Mode 1 in Table 8.10. The reader may familiarize himself with these forms of tests by examining, among others, series MD-7000 units produced by Mustang Dynamometer.

The uniqueness of the vehicle chassis dynamometer from Figure 8.34 consists precisely in the fact that when all the rolls are disconnected from one another each one of them can be controlled individually, that is, independently of the remaining three rolls. Testing of vehicles when the rolls are controlled independently of one another is made possible in Control Mode 2. The stand with individual control of rolls provides extensive capabilities for testing of 4×2 and 4×4 vehicles. This applies in the first place to investigating the

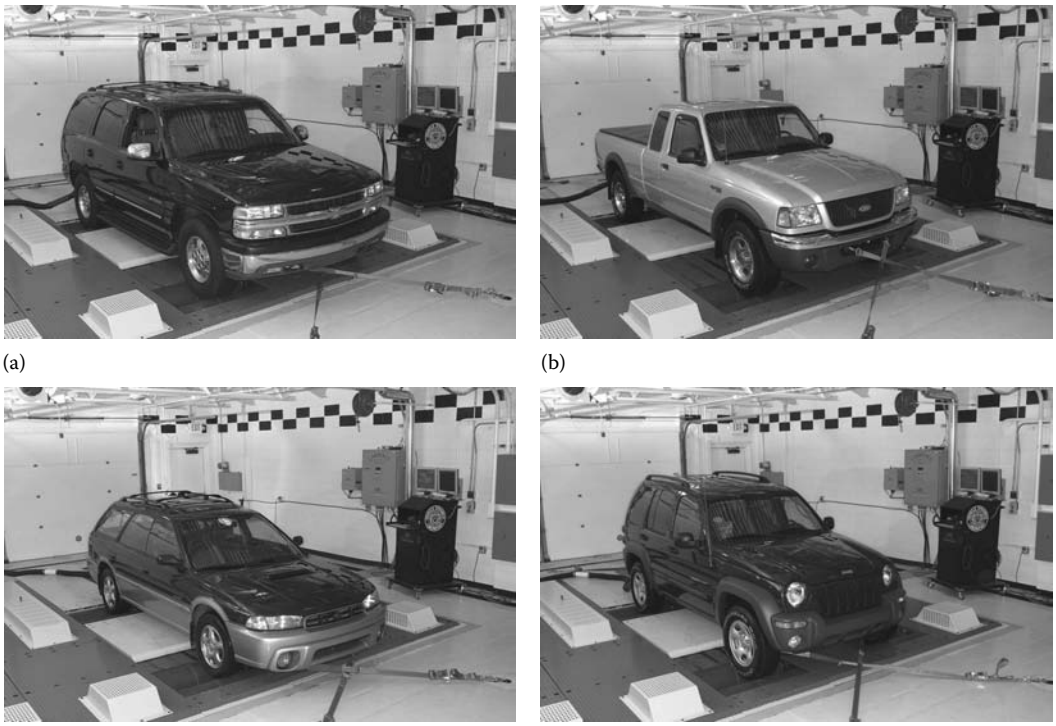


FIGURE 8.34
4×4 vehicle chassis dynamometer with individual roll control: testing vehicles.

vehicle traction and velocity operational properties and the energy/fuel efficiency by experimenting with power distribution between the drive wheels.

In fact, experiments with a given vehicle with different types of driveline systems and different combinations of mechanisms in the interaxle and interwheel power dividing units makes possible determining the ''best'' layout and PDUs from a given set of layouts and mechanisms. The ''best'' used here is in the sense of the positive effect on the previously mentioned vehicle properties.

The effectiveness of the dynamometer is clearly demonstrated when it is necessary to compare experimentally certain different vehicles of the same class but with different driveline systems. By testing vehicles under the same ''road'' or ''off-road'' conditions, it is possible to determine when one's development differs positively from the developments of others.

There is still another aspect of experimental investigations that is quite important in the course of developing a driveline system. The testing of a vehicle with a new driveline system developed based on the analytic methods from Chapters 6 or 7 by simulation of the power distribution between the wheels allows resolving the question of the extent to which the real power distribution provided by the new design is close to the theoretically optimal. In addition, it is possible to determine in the course of tests some parameters that are needed for developing specifications put to the newly developed driveline system and comparing their values with those obtained on analytic models. Such parameters include, among others, time delays between road conditions of the front and rear wheels,

TABLE 8.10

4×4 Vehicle Chassis Dynamometer Specification

The chassis dynamometer is for testing wheeled vehicles under electronically controlled conditions for each of the wheels to accommodate different driveline systems

General specification:	
Dynamometer type	Eddy current
Cooling type	Self air-cooled
Peak speed	100 mph
Power adsorption	175 hp/wheel—continuous; up to 350 hp/wheel—intermittent
Wheelbase	89–175 in.
Axle weight capacity	6000 1b/axle
Outer track	100 in.
Inner track	30 in.
Torque measurement	Load cell four sensors
Torque transfer	Power chain belt
Speed measurement	Hall-effect pick-up (60 rpm) four sensors
Controller type (Mode 1)	Computer based, embedded
Controller type (Mode 2)	DAQ based with RS2 32 communications to PC
Installation	Flush floor
Envelope dimensions	240 in. × 200 in.
Power (dynamometer)	240 V AC, three phase
Power (instrumentation)	1l5 V AC single phase

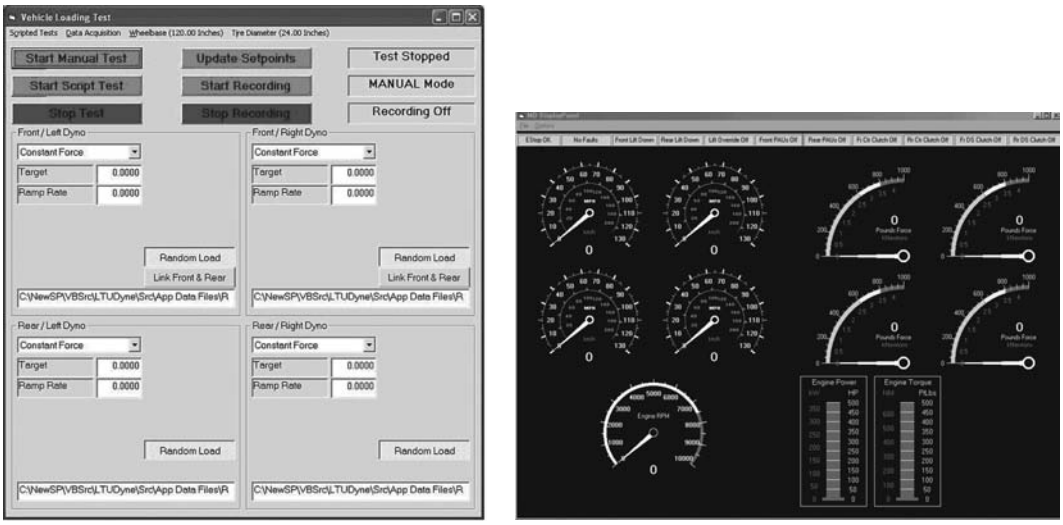
Notes: Control Mode 1—This control mode shall allow the operator to test a vehicle under loading conditions, whereby all or a part of the rolls shall be mechanically connected prior to commencement of any test exercise of this type. Control Mode 2—This control mode shall allow the operator to test a vehicle under operating conditions, whereby load to the vehicle driveline system is controlled separately at each wheel.

correlation between time thresholds and wheel torque and wheel angular velocity variations, time derivatives of wheel torques, and kinematic parameters such as angular accelerations and jerks. As an illustration refer to Figure 7.12, which was obtained in the course of tests using the dynamometer from Figure 8.34.

The vehicle chassis dynamometer shown in Figure 8.34 makes it possible to indirectly assess the effect of the driveline system on the turnability and stability of motion. For this, it is necessary to determine the lateral forces of the wheels and the yaw rate, when the circumferential forces of the left and right wheels, of the front and rear wheels are different.

Other types of tests in Control Mode 2 are also possible. These include durability tests, diagnostic tests, experimental studies of structural noise, and vibrations in driveline systems; testing of active safety systems (electronic stability programs) and emission tests.

Consider certain specific features of the control of the vehicle chassis dynamometer in Control Mode 2. Figure 8.35 shows the main and auxiliary screens that are used in this control mode. The auxiliary screen is used for visualizing the parameters being recorded. The main screen is divided into four corners—according to the number of control rolls. The user may specify a loading mode and parameters for each roll individually. Each roll may be controlled in the following modes: Force (Torque) Control, Speed Control, Power Control, and Vehicle Simulation Control. These modes are preset by clicking the desired mode (see Figure 8.36). Note that the word ''constant'' does not designate constancy of



(a) (b)

FIGURE 8.35
(a) The main and (b) auxiliary screens.

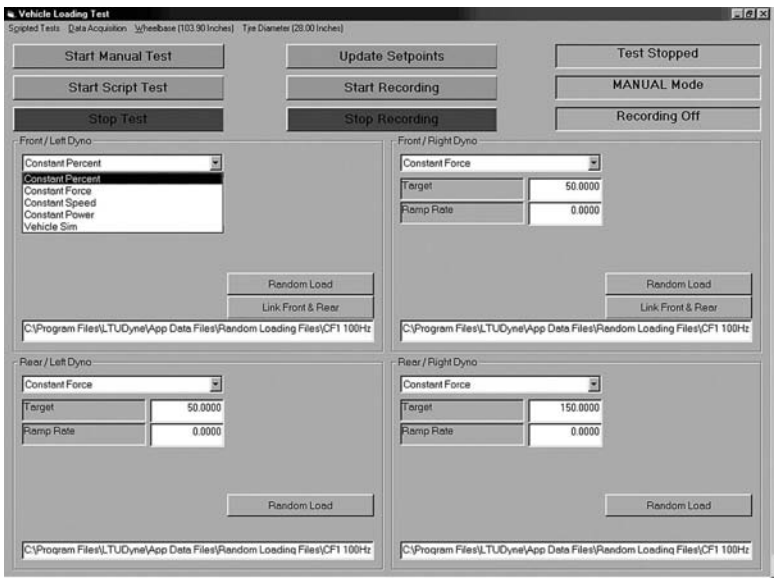


FIGURE 8.36
Test modes.

force, velocity, or power in the course of tests, but constancy of the specified profiles of these parameters. These profiles may be arranged as script files and then used for multiple testing of the same vehicle or different vehicles of similar class.

Specifying different profiles for different rolls allows simulating different gripping conditions of wheels, motion while turning, going uphill, etc.

The ''Random Load'' checkboxes make it possible to generate random loading values of the force (torque) that are then used for loading the rolls in tests in the Force (Torque) Control and Vehicle Simulation Control modes. Actually, these random loads represent probabilistic rolling resistance forces (torques) and may be formulated for different road/offroad conditions. Obviously, after a certain time interval of travel on nondeforming surfaces the rear wheels are subject to the same travel conditions as the front wheels. The magnitude of this time interval depends on the vehicle's wheelbase and on its speed. The ''Link Front & Rear'' checkboxes make it possible to provide the above time delay between the conditions of motion of the front and rear wheels.

In addition to the above test modes that are usually implemented using prepared script files, the user may also perform manually controlled tests. For this, the user should put in the pertinent numbers in each of the four corners (see Figure 8.35a) and click on the ''Start Manual Test.'' The dyno-controller will begin loading the vehicle with the specified load.

The ''Stop Test'' box should be clicked in case the user wants to stop loading the vehicle. The ''Update Setpoints'' will send the currently displayed set points to the dyno-controller. It means that the user can enter various values of them and then send all of them to the controller at one time. There are more features in the dynamometer that take into consideration the inertia properties of the rolls and their drive, parasitic power loss in the roll drives, etc.

Using the data-acquisition system allows defining channels that can be used for recording kinematic, force, and other parameters of the stand facility in the course of tests, for representing them graphically and for further work with them. The signals of the sensors of the vehicle being tested may also be recorded by the dynamometer's data-acquisition system or by a separate data-acquisition system. Both these systems should be synchronized. Parallel measurement of the parameters of the vehicle under test and of the dynamometer allow a real-time study of the effect of the driveline system and its power dividing units on the operational properties of the vehicle and on its dynamics upon changes in road conditions specified by the dynamometer.

Figure 8.37 shows the results of measurements of torques produced on the stand's rolls and of the linear velocities of the points of the periphery of the rolls (calculated from the

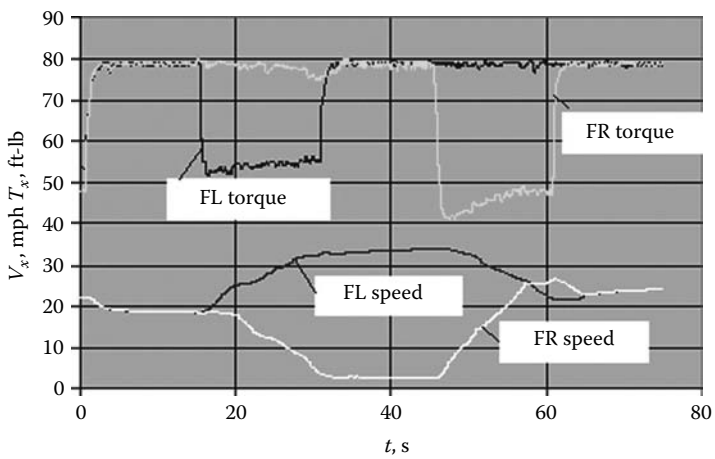


FIGURE 8.37
Resistance torque and velocities of rolls when testing a front-wheel-drive sedan.

measurement of angular velocities of the rolls and their radii) when testing a medium-class front-wheel drive sedan with an open differential in the drive axle.

As seen from this figure, the speeds of rolls (and of the vehicle's wheels) are the same during the first 18 s. This corresponds to the straight-line motion of wheels under identical gripping conditions—the resistance torques at left and right rolls (FL torque and FR torque) are the same. Then, the gripping conditions of the left wheel were changed abruptly—the resistance torque at the left roll (FL torque) decreased abruptly to its value that approximately corresponds to an ice-covered road. It is seen that, then the speed of the left roll (FL speed) increases and that of the right roll (FR speed) decreases to almost zero.

The left wheel of the car starts spinning and the right one virtually stops in view of the properties of the open differential that connects both the wheels. Curves in Figure 8.37 that correspond to the time interval from the 16th to the 30th second, demonstrate the effect of the inertia properties of the driveline system on the changes in speed of the rolls (wheels)—the manner of their variation does not correspond to changes in the torque, that is, changes in the gripping conditions. Similar situations occur after the 45th second, when the gripping conditions change abruptly beneath the right wheel of the car. The above results not only give an idea about the dynamics and kinematics of wheels coupled by an open differential, but they are additionally interesting by the fact that they make it possible to determine the threshold values of parameters and their derivatives needed for developing mechatronic systems for controlling the locking/unlocking of the differential. Among such parameters are, for example, the angular velocities of the wheels and their derivatives or the derivatives of torques.

Figure 8.38 shows certain results of testing a medium-class SUV in which the interaxle drive is positively locked and both axles are equipped with open differentials.

During the first 30 s the resistance to motion of the front and rear wheels is simulated as being different, but the speeds remain the same, since both axles are rigidly connected by a

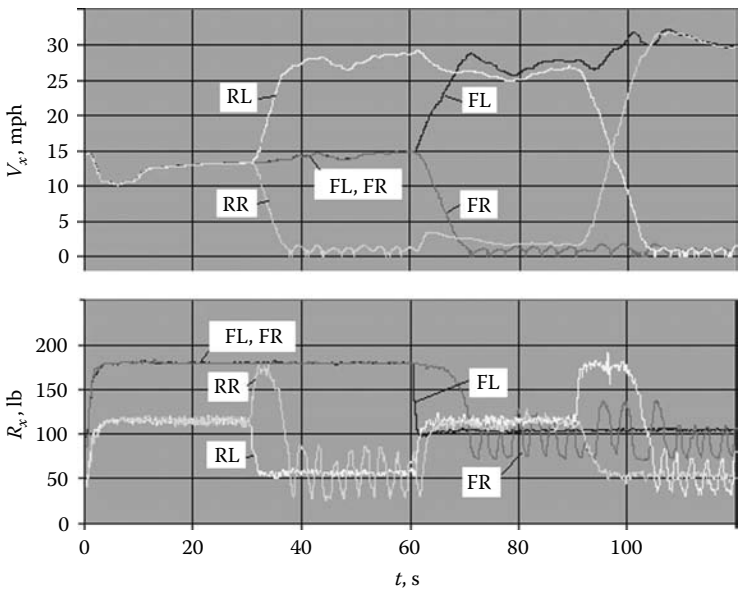


FIGURE 8.38
Resistance forces and velocities of rolls in testing a 4 × 4 SUV.

positively locked drive. At the 30th second the resistance to motion of the rear left wheel RL decreased steeply and that of the rear front wheel increased. This caused an abrupt reduction in the velocities of the rear wheels, RL and RR (see the time interval from 30 to 35 s). Then the gripping conditions of the rear right wheel were made worse as the force RR was steeply reduced. Here the left wheel that previously caused to rotate continued spinning (see the interval of 35–60 s).

As seen from Figure 8.38, all that happened with the rear wheels and was caused by the properties of the open differential and the rear axle had no effect on the front wheels. During all this time (0–60 s) the front wheels had the same velocities since their gripping conditions were simulated as unchanged. However, after the 60th second the gripping conditions of both front wheels were made worse, but not simultaneously (see the steep and nonsimultaneous reduction in forces of FR and FL over the time interval between 60 and 70 s). As a result, the front left wheel, that started spinning before the gripping conditions of the front right wheel deteriorated, and continued spinning even after the resistance under the front right wheel decreased.

It is interesting to note that, in spite of the fact that the gripping conditions of all of the car's wheels at the 70–90 s interval are simulated as being approximately the same, the rolls (the car's wheels) have, as before, different speeds: the right-side wheels virtually stopped and the left-side wheels continued spinning. This stems from the inertia of the driveline, the rotating masses of which prevent instantaneous changes in parameters in accordance with the properties of the open differential. Only at the 90th second, when the gripping conditions of the rear right wheel deteriorated steeply, whereas the resistance at the rear left wheel increased, did the speeds of the rear rolls (rear-axle wheels) changed. Now the rear right wheel that found itself on ''ice'' slips, whereas the rear left wheel stopped.

The stand shown in Figure 8.34 can be used also for other investigations, for example, to determine certain properties of the tires. Consider a method and results of investigating parameters contained in formula (1.20) that relate the wheel torque T_w and its rolling radius r_w in the driving mode—this is the tangential elasticity factor λ_w and rolling radius in the driven mode r_w^0. Before becoming familiar with the method and results, the reader might want to return to Section 1.3.2 and refresh certain concepts associated with the wheel's rolling radius and its functional relationships with the torque and forces applied to the wheel.

Figure 8.39 presents a picture of an SUV on the Dynamometer and the Kistler wheel force sensors installed on the rear wheels.

The wheel force sensor outputs directly the following signals:

- Force components F_w, F_l, W_w
- Moment components M_x, T_w, M_z
- Sine and cosine of the angular position of the wheel

These components are used for determining the force, torque, and kinematic parameters of the wheel. Experiments were conducted at a constant vehicle speed of 6.7 m/s (15 mph). This constant speed was maintained by controlling the throttle position. The inflation pressure p_w was assigned as 0.21 MPa (31 psi) and 0.19 MPa (27 psi). The load applied to the rear rolls of the Vehicle Chassis Dynamometer was incrementally changed from its minimum to maximum values during the experiments.

The experiment procedure included the following steps. After the first value of the load was applied to the rear rolls (step 1), a 1 min time interval was kept in order to place the



FIGURE 8.39
4×4 vehicle chassis dynamometer with SUV.

vehicle wheels to steady motion with the above-specified speed of 15 mph (step 2). Some sensor signals of the rear wheels and the Vehicle Chassis Dynamometer were then recorded during another 1 min time interval (step 3). The rear rolls of the Vehicle Chassis Dynamometer were unloaded during the next step of the experiment, and then the test was stopped to allow the tire temperature to drop to the temperature of the surroundings (step 4). These four steps were repeated as many times as the many values of the roll load were assigned.

The following parameters were determined at the experiments: the wheel torque T_w, (N-m); the wheel net tractive force, F_w, (N); the wheel normal force, W_w, (N); the wheel angular speed ω_w, (rad/s); the roll torque, T_r, (N-m); the roll angular speed, ω_r, (rad/s). As proved by statistical analysis, these parameters have normal distributions. The means and the standard deviations of these parameters were also calculated by a statistical analysis.

Based on the above-mentioned statistical characteristics, the following parameters were computed:

- The number of the wheel revolutions

$$n_w = (\omega_w/(2\pi))t, \text{ (rev)}; \tag{8.6}$$

  here, t is the duration of the experiment; $t = 60$ s;
- The number of the roll revolutions

$$n_r = (\omega_r/(2\pi))t, \text{ (rev)}; \tag{8.7}$$

- The wheel travel (see Figure 1.50), S_w, (m)

$$S_w = 2\pi r_r n_r \tag{8.8}$$

  here, r_r, (m) is the roll radius;

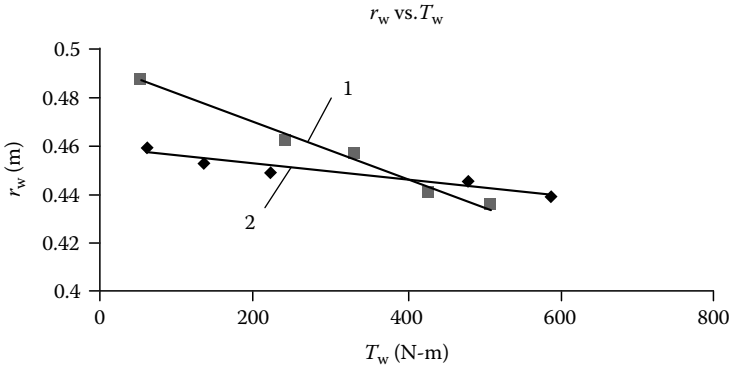


FIGURE 8.40
Experimental data.

- The effective rolling radius of the tire, r_w, (m)

$$r_w = S_w/(2\pi n_w) \tag{8.9}$$

Figure 8.40 presents experimentally obtained values of the effective rolling radius in the drive mode, r_w, vs. the wheel torque, T_w for the P265/70R17 tire.

As seen, when the torque increases, the effective rolling radius decreases differently for different inflation pressures. Statistical analysis has shown that there is a linear regression between the radius r_w and the torque T_w:

$$r_w = b_0 - b_1 T_w \tag{8.10}$$

here, the regression coefficients are

$$\begin{aligned} b_0 &= \frac{\sum_{i=1}^{n} T_{wi} \sum_{i=1}^{n} r_{wi}^2 - \sum_{i=1}^{n} r_{wi} T_{wi} \sum_{i=1}^{n} r_{wi}}{n \sum_{i=1}^{n} T_{wi}^2 - \left(\sum_{i=1}^{n} T_{wi}\right)^2} \\ b_1 &= \frac{n \sum_{i=1}^{n} r_{wi} T_{wi} - \sum_{i=1}^{n} T_{wi} \sum_{i=1}^{n} r_{wi}}{n \sum_{i=1}^{n} T_{wi}^2 - \left(\sum_{i=1}^{n} T_{wi}\right)^2} \end{aligned} \tag{8.11}$$

It is clear from the formulae (8.10) and (1.20), that $r_w = b_0$ when $T_w = 0$. From this the following comes:

$$r_w^0 = b_0 \tag{8.12}$$

Based on the result given by the formula (8.12), one may conclude that it is not necessary to conduct an experiment to determine the effective rolling radius in the driven mode. Its value automatically comes from the statistical development of the above-mentioned test data of a tire in the drive mode.

Another regression coefficient b_1 represents the slope of the function (8.10) as shown in Figure 8.41:

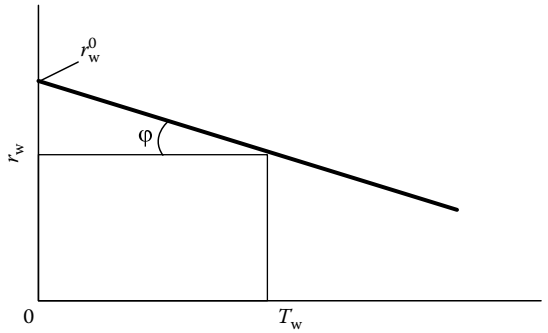


FIGURE 8.41
Linear function analysis.

$$b_1 = \tan \varphi = \frac{r_w^0 - r_w}{T_w - 0} = \frac{\Delta r_w}{\Delta T_w} \tag{8.13}$$

The ratio of $\Delta r_w / \Delta T_w$ may be characterized as the tire longitudinal elasticity coefficient:

$$\lambda_w = \frac{\Delta r_w}{\Delta T_w} \tag{8.14}$$

Once again, it is not necessary to conduct a separate experiment to determine the longitudinal elasticity of a tire. Its value automatically comes from the regression coefficient b_1 (see formulae (8.13) and (8.14)):

$$\lambda_w = b_1 \tag{8.15}$$

Finally, taking into consideration the formulae (8.12) and (8.15), Equation 8.10 may follow in the form given by formula (1.20) in which, the tire parameters r_w^0 and λ_w may be determined based on the experimental data obtained using the above-described procedure and formulae (8.11), (8.12), and (8.15). For the P265/70R17 tire, the effective rolling radius in the driven mode, r_w^0, and the longitudinal elasticity, λ_w, determined using the experimental data are presented in Table 8.11.

As seen from Table 8.11, different inflation pressure results in different values of the effective rolling radius in the driven mode. Obviously, the radius will become bigger with increasing inflation pressure.

The longitudinal elasticity, λ_w, is also different for different inflation pressure (see Table 8.11). It should be noticed here, that the longitudinal elasticity does not depend uniquely on the inflation pressure. When the tire normal load, W_w, is less than a specific value W_w^*, that is, $W_w < W_w^*$, an increase in inflation pressure leads to an increase in the longitudinal elasticity. When $W_w > W_w^*$, bigger inflation pressures bring less values of the longitudinal elasticity. The experimental data from Figure 8.40 corresponds to $W_w < W_w^*$.

TABLE 8.11
Tire Experimental Factors

No	p_w, (MPa)	r_w^0, (m)	λ_w, (m/N-m)
1	0.21	0.4929	0.000116
2	0.19	0.4585	0.000031

8.5 Field and Road Tests of Wheeled Vehicles

Field and road tests of vehicles are an obligatory component of the development of wheel driveline systems and designing power dividing units. The results of such tests make it possible to verify analytically obtained results and draw final conclusions in favor of a given driveline system. In certain cases, field and road tests may also be used instead of analytic investigations, if the developer does not have pertinent mathematical models. Certain properties of units and systems can be determined only on the vehicle itself.

Usually field and road tests are subdivided into the following kinds:

1. Proving ground tests that serve for investigating the effect of the driveline system on one of several operational properties of the vehicle(s). These tests are performed on specially constructed road or off-road sections.
2. Proving ground tests known as standard when the vehicle(s) are tested on certain specially selected route comprising of a set of different road and off-road sections. Such tests make it possible to provide a comprehensive assessment of the effect of the driveline system on the dynamics and performance of the vehicle(s).
3. Operational testing, which are usually performed by extended operation of the vehicles.

Figure 8.42 shows an example of testing grounds for testing the mobility of vehicles in modes (i).

Figure 8.43 shows examples of four (1–4) standard routes for testing the mobility of off-road vehicles. The sections of the routes represent obstacle objects and tracts: fiord, steep ascends and descends, ditches, segments with highly differing gripping conditions for wheels of the left and right sides of the vehicle, and other natural and man-made obstacles.

Testing routes also include broken down road sections, cart roads, and asphaltic concrete-covered parts of road. In addition to standard, obstacle-containing routes, the testing

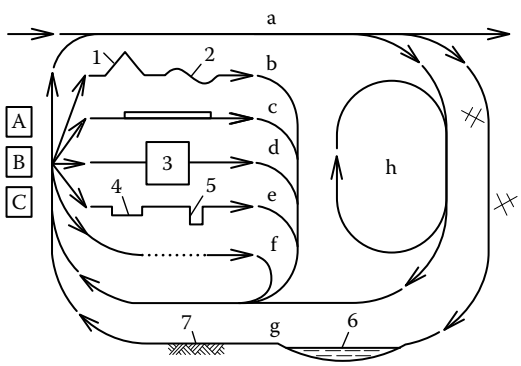


FIGURE 8.42
Schematic diagram of proving grounds with standard routes and special areas for mobility and service life testing of vehicles: (a) paved road; (b) dirt road with steep ascends and descends 1 and ruts 2; (c) concrete road; (d) slippery road (pavilion 3 with ice field); (e) road with square pits 4 of different height and narrow (narrower than the wheel diameter) ditches 5; (f) sand road; (g) forest road with fords 6 and swamps 7; (h) track. (A) Administration and service personnel building; (B) maintenance and repair station; (C) fueling station.

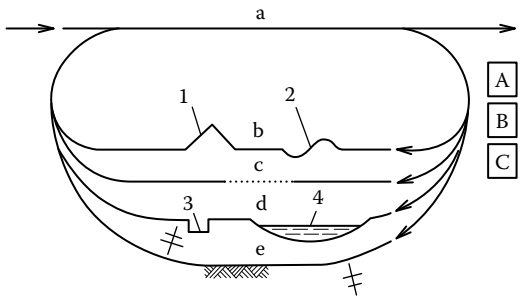


FIGURE 8.43
Schematic diagram of testing grounds with standard routes and special areas for mobility and service life testing of vehicles: (a) paved road; (b) dirt road with steep ascends and descends 1 and ruts 2; (c) concrete road; (d) slippery road (pavilion 3 with ice field); (e) road with square pits 4 of different height and narrow (narrower than the wheel diameter) ditches 5; (f) sand road; (g) forest road with fords 6 and swamps 7; (h) track. (A) Administration and service personnel building; (B) maintenance and repair station; (C) fueling station.

grounds must have sections for investigating the turnability, stability of motion and handling of vehicles, acceleration performance, drive smoothness, and other vehicle properties. It is important to maintain all the parts of the test routes in a state that would make them suitable for vehicle testing during different seasons.

The kind and number of parameters being measured depends on the purpose of the tests. The most typical parameters measured in investigating vehicles with different driveline systems include angular velocities of the wheels, vehicle speed, longitudinal and lateral acceleration, yaw rate (angular velocity of the vehicle about the vertical axis), vertical longitudinal and lateral forces on the wheel axles, wheel torques, wheel slippage, wheel turning and slip angles, and angle of deviation of the longitudinal axis of the vehicle from the specified direction. The need to experimentally determine the fuel consumption of vehicles as a function of the characteristics of their driveline system must be particularly emphasized. Other parameters measured in the course of tests include the travel path of the vehicles and the turning radii and the displacement of the center of turn. As an illustration, Figure 8.44 shows a method for determining the shift E of the center of turn of the vehicle in circular motion.

The method is based on determining the location of the actual center of turn based on the actual radius R''_{a2} of turn of the inner rear wheel, and of the straight line that forms an angle of 90° with the longitudinal axis of the vehicle and passing along the axis of the rear wheels.

In certain tests, particularly, in the winter, the temperature of the oil in axle housings and transfer cases in which power dividing units are located and the pressure in the hydraulic and pneumatic drive controls are also measured.

Consider certain specifics of preparing vehicles for tests, associated with investing the effect of driveline systems on the vehicle performance. Attention must be paid in the first place to determining the real dimensions of the wheelbase and of the distances between axles of multiwheel drive vehicles, wheel tread, and maximum turning angles of steered wheels in both directions. The possibility of more precise determination of the kinematic properties of wheels is of particular importance.

The static curb weight on the wheels of all the axles must be attained before the tests start. The air pressure in tires should conform to specifications. After the first runs of the vehicle and wearing out the flashes on the tire treads, it is necessary to measure the circumferences of the tire treads of all the wheels by removing the load from them. This

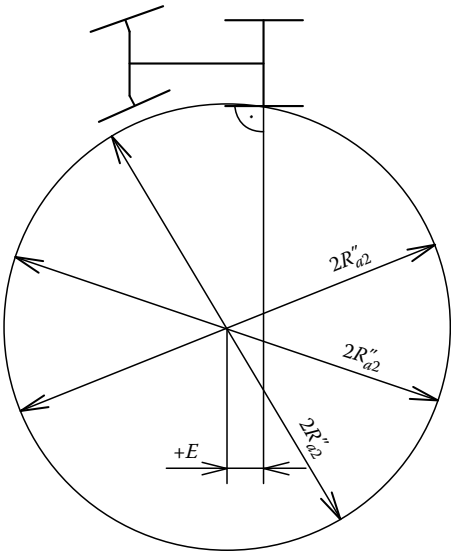


FIGURE 8.44
Schematic diagram for determining the shift of center of turn E.

will then allow calculating the free wheel radii r. Then all the tires should be numbered and the location of each tire should be documented. After this, it is necessary to determine the static radii r_s of the wheels of the vehicle with no payload and of the vehicle with full load. Assuming that the static radius is equal to the dynamic radius (this was discussed in Section 1.3.2), it is then possible to calculate the rolling radii r_w^f of the wheels in the free mode using formula (1.17).

The rolling radii r_w^0 of the wheels in the driven mode can be determined either under laboratory conditions (see Section 8.4) or on testing grounds in the following manner. In the ideal case, the wheels should be fully disconnected from the driveline system. Actually, however, this cannot be done. For this reason, it is necessary in the first place, to disassemble the driveshafts, which will thus separate the drive axles and eliminate the effect of friction in the driveline system on the rolling resistance of the wheels. The locked units should be unlocked, limited slip differentials should be removed from the axles. Straight-line towing of the vehicle should be implemented on a level asphalt or concrete road segment. The speed is constant and approximately equal to 10 km/h. The number of rotations of each wheel should be determined over a road segment at least 200 m long and the actual paths traversed by the wheel centers should be measured precisely. The rolling radii r_w^0 of wheels in the driven mode are calculated from formula (7.2). The values of the radii can also be determined for different tire air pressures. The values of r_w^0 are needed for determining the kinematic discrepancy in the locked drive and also for determining the kinematic and power parameters of the wheels and for investigating the power distribution between the vehicle's wheels.

While investigating the power distribution among the wheels it is advisable to measure not only the torques of the wheels and their angular velocities (the product of which gives the values of the power supplied to the wheels), but also the torque and angular velocity of the shaft from which the power distribution starts, for example, on the input shaft of the vehicle's transfer case. In addition, it is of interest to measure the torques and the angular velocities (i.e., powers) at the output shafts of the interaxle power dividing units. Such a distribution of sensors makes it possible to asses the power losses in the driveline system as a whole and in its individual parts (branches).

In investigating the effect of the driveline system on the fuel consumption of a transportation vehicle, it is advisable to determine the mean fuel consumption per 100 km of travel (or the number of miles per gallon of fuel). The fuel consumption of traction vehicles is usually measured in kilogram/hour. The tests should be performed at horizontal segments of the road and country, without shifting gears and with the torque converter (if the vehicle has) locked. The speeds of multiwheel drive vehicles are constant and usually amount to 50 km/h on asphalt and up to 30 km/h under off-road conditions. The above method makes it possible to determine the effect of different driveline systems on the vehicle's fuel consumption, by eliminating to a large extent the effect of the remaining systems of the vehicle.

Consider now the results of certain tests that may be of interest for further improvement of driveline systems.

The kinematic discrepancy in a locked interaxle drive and its effect on the vehicle's properties were examined in detail in Chapter 3. This chapter also presents experimentally determined numerical values of the kinematic discrepancy factors. Additional experimental results on the effect of different sizes of tires on the fuel economy of a 4×4 farm tractor with locked interaxle drive are presented in the following text. This means that these tests were concerned with the comprehensive effect of the kinematic discrepancy, rolling resistance of the wheels and their traction capabilities that are different for different sets of tires, on the fuel consumption. Table 8.12 lists data on the tractor that was tested.

The tests were performed in a straight-line uniform motion on stubble and on a field prepared for sowing upon total fuel feed. A loading tractor produced the traction load by having it driven at a speed different from that of the tested tractor.

It was established that at moderate traction loads ($F_d = 4$–8 kN) on stubble the 16.0-20/18.R38 set gives a reduction in the specific drawbar fuel consumption g_d of 8.0% on the average (Figure 8.45 and Table 8.13) as compared with the 11.2-20/15R38 set.

Over the nominal drawbar force range ($F_d = 12$–14 kN) the fuel consumption reduction is already 11.4%–18.2%. The minimum specific drawbar fuel consumption of the tractor with 11.2-20/15.5R38 tires is $g_d = 0.57$ kg/kWh ($F_d = 12$ kN), whereas for the 16.0-20/18.4R38 set it is 0.49 kg/kWh ($F_d = 13.6$ kN). At close values of kinematic discrepancy, these tire sets exert a different effect on the fuel consumption. The wider tires of set #3 reduce the generalized slippage of the tractor and improve the fuel economy.

Analysis of results of traction tests on stubble of the tractor with 13.6-20/16.9R38 tires showed their advantage also in comparison with the use of the 11.2-20/15.5R38 set. Thus at

TABLE 8.12

Specifications of a 4×4 Tractor

№	Tire Sets Front / Rear	Mass (kg), Devolving upon		Design Kinematic Discrepancy Factor, m_{ru}
		Front Axle	Rear Axle	
1	11.2−20 / 15.5R38	1480	2320	0.017
2	13.6−20 / 16.9R38	1528	2410	0.011
3	16.0−20 / 18.4R38	1550	2482	0.016
4	11.2−20 / 15.5R38	1480	2320	0.017

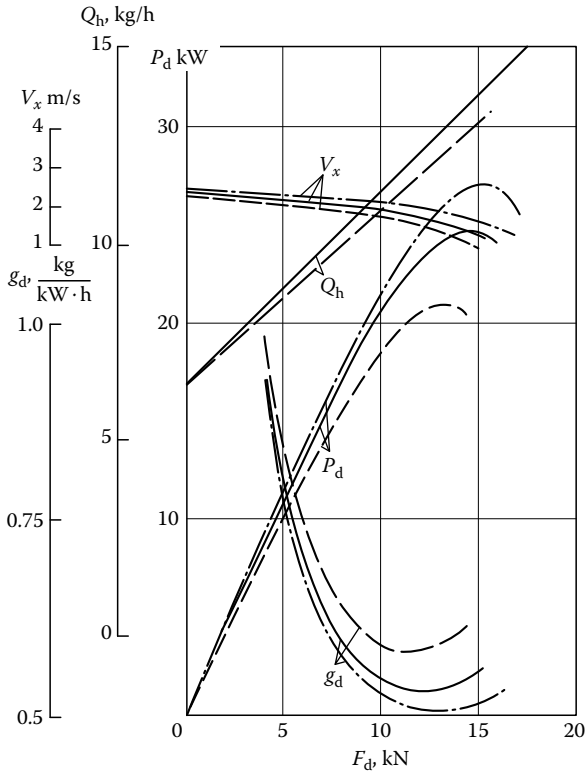


FIGURE 8.45
Performance of a 4 × 4 tractor on stubble with tire sets: – – –, #1 (11.2–20/15.5R38); ——, #2 (13.6–20/16.9R38); – · –, #3 (16.0–20/18.4R38).

TABLE 8.13

Effect of Tires Used on a 4×4 Tractor on the Specific Drawbar Fuel Consumption

Tires: Front / Rear	Specific Drawbar Fuel Consumption, g_d, kg/kWh at F_d, kN				Surface of Motion
	8	10	12	14	
11.2-20 / 15.5R38	0.642	0.582	0.568	0.602	Stubble
13.6-20 / 16.9R38	0.601	0.546	0.520	0.523	Stubble
16.0-20 / 18.4R38	0.587	0.531	0.503	0.492	Stubble
16.0-20 / 16.9R38	0.615	0.553	0.519	0.514	Stubble
11.2-20 / 15.5R38	0.675	0.626	0.630	—	Field ready for sowing
13.6-20 / 16.9R38	0.632	0.575	0.560	0.625	Field ready for sowing
16.0-20 / 18.4R38	0.615	0.551	0.530	0.541	Field ready for sowing
16.0-20 / 16.9R38	0.629	0.570	0.552	0.615	Field ready for sowing

$F_d = 12$–14 kN the specific fuel consumption decreases by 8.5%–13.1%. The minimum of g_d for the tractor with 13.6-20/16.9R38 tires is 0.54 kg/kWh. In this case the fuel saving is attributable not only to the greater width of the tire (that reduces the generalized slippage), but also to the lesser kinematic discrepancy.

Analysis of the results of testing the tractor on a field ready for sowing shows that the best fuel economy is provided by 16.0-20/18.4R38 tires (Figure 8.46 and Table 8.13).

The reduction in the specific drawbar fuel consumption as compared with the use of the 11.2-20/15.5R38 set is 15.8% at $F_d = 12$ kN, being 11.1% for the 13.6-20/16.9R38 set. These data are similar to those obtained on stubble and show a fuel consumption reduction of 3% on the average. The minimum of g_d for the tractor on a field ready for sowing with 11.2-20/15.5R38 is 0.62 kg/kWh ($F_d = 10.4$ kN) being 0.56 kg/kWh with 13.6-20/16.9R38 tires ($F_d = 11.8$ kN) and 0.54 kg/kWh ($F_d = 12.6$ kN) with 16.0-20/18.4R38 tires. Depending on the drawbar load F_d, the fuel economy of the tractor with 13.6-20/16.9R38 tires and with 16.0-20/18.4R38 tires is correspondingly 8%–11% and 9%–16% better than when using the 11.2-20/15.5R38 tires.

Table 8.14 reflects the effect of the air pressure p_{w2} in tires of rear wheels on the fuel economy of the 4×4 tractor under consideration. Variations in p_{w2} change the design kinematic discrepancy m_{ru}, which shall be then reflected on the values of the specific drawbar fuel consumption g_d. Note that a variation in the drawbar load between 6 and 11 kN causes a redistribution of the weight loads between the axles, which is reflected in the rolling radius of the front and rear wheels in the driven mode and modifies the value of the kinematic discrepancy m_{ru} listed in Table 8.14. Hence the change in g_d is different

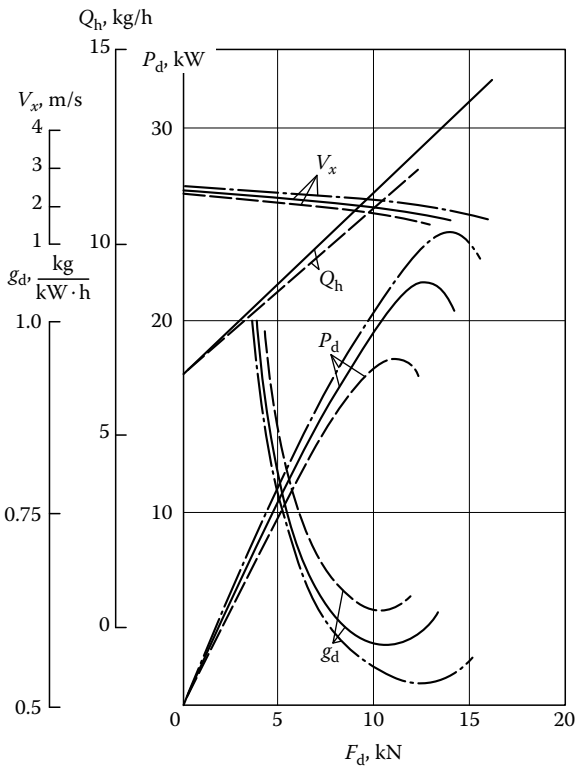


FIGURE 8.46
Performance of a 4×4 tractor on a field ready for sowing with tire sets: – – –, #1 (11.2–20/15.5R38); ——, #2 (13.6–20/16.9R38); –·–, #3 (16.0–20/ 18.4R38).

TABLE 8.14

Effect of Rear Tire Pressure in Rear-Wheel Tires on the Specific Drawbar Fuel Consumption of a 4×4 Tractor

Tires Pressure in Rear Tires Design Kinematic Discrepancy	Specific Drawbar Fuel Consumption, g_d, kg/kWh at F_d, kN				Variation in g_d, % as Compared with a Tire with $p_{w2} = 0.10$ MPa	Surface of Motion
	6	8	10	11		
11.2-20 15.5R38 $p_{w2} = 0.06$ MPa $m_{ru} = 0.011$	0.735	0.624	0.560	0.551	−2.1	Stubble
11.2-20 15.5R38 $p_{w2} = 0.1$ MPa $m_{ru} = 0.016$	0.750	0.638	0.582	0.575	—	Stubble
11.2-20 15.5R38 $p_{w2} = 0.14$ MPa $m_{ru} = 0.021$	0.762	0.651	0.601	0.594	+2.0	Stubble
11.2-20 15.5R38 $p_{w2} = 0.06$ MPa $m_{ru} = 0.011$	0761	0.654	0.598	0.597	−3.1	Field ready for sowing
11.2-20 15.5R38 $p_{w2} = 0.1$ MPa $m_{ru} = 0.016$	0.782	0.675	0.626	0.631	—	Field ready for sowing
11.2-20 15.5R38 $p_{w2} = 0.14$ MPa $m_{ru} = 0.021$	0.791	0.689	0.648	0.679	+2.0	Field ready for sowing

upon increasing F_d and Table 8.14 shows in a separate column the mean variations in g_d (in percent).

It should be reemphasized that a change in kinematic discrepancy m_{ru} causes a redistribution of power between the tractor's axles and, accordingly, changes in the power losses in the axle drives and power lost in wheel slippage (the slippage of the front and rear wheels changes). This in turn changes the running gear efficiency η_x^t and the traction efficiency η_t of the tractor, which is reflected in the specific drawbar fuel consumption. The above is illustrated in Figure 8.47 that shows the slippage curves $s_{\delta a2}$ and the running gear efficiency η_x^t of the 4×4 tractor with different models of the front-wheel tires. The graphs show the range of variations in the kinematic discrepancy brought about by increasing the drawbar load F_d from 0 to 38 kN. The values of η_x^t were computed from experimental data using formulae listed in Chapter 3.

The kinematic discrepancy in a locked interaxle drive depends on the distribution of normal loads between the axles. The results of testing of an off-road three-axle truck are

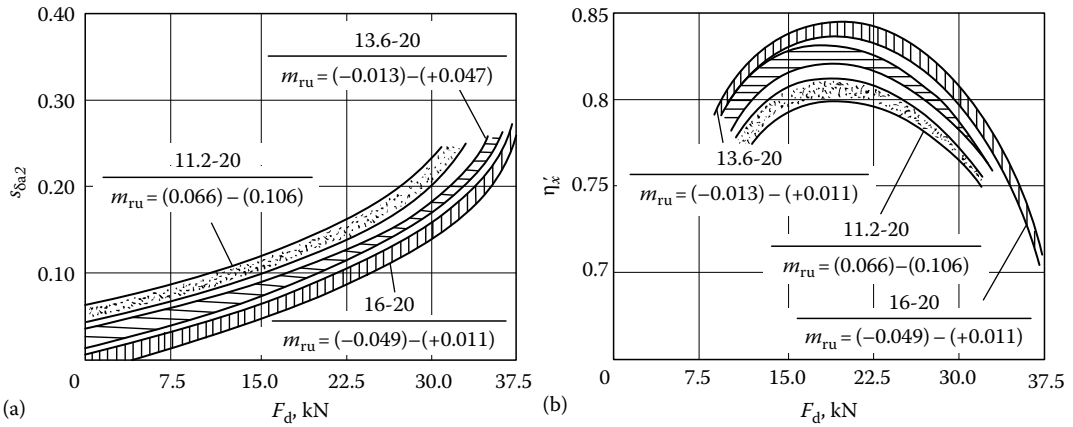


FIGURE 8.47
Generalized slippage $s_{\delta a2}$ of the rear wheels (a) and running-gear efficiency η_x^t (b) of a 4×4 tractor on stubble as a function of the drawbar load F_d and models of the front-wheel tires; the rear-wheel tires are 16.9R38.

demonstrative in this respect. In straight-line motion over asphalt pavement with the front axle disconnected from the drive and positively locked forward rear and rear axles the rear-axle torque amounted to 60%–75% of the torque of the forward rear axle. The appearance of kinematic discrepancy in the running gear, something that changed the torque of the axles, was caused by redistribution of normal loads. These loads changed as the vehicle traveled because of the sloping of the reaction suspension arms. If these are placed horizontally, then there will be no weight redistribution. However, the sloping of the arms makes possible obtaining driveshaft slopes that are more favorable for the driveline dynamics. The design engineer in this case must arrive at some kind of a comprise. For example, he/she may use an interaxle differential with a locker between the middle and rear axles.

A similar engineering problem arose in designing the interaxle drive of the rear tandem of one modification of an 8×8 off-road vehicle. It became possible to simplify the driveline system design after changes in the design of the suspension enabled obtaining equal normal reactions of the wheels of both axles of the tandem. This is made possible by using a permanently locked drive instead of a free-running interaxle differential. Other reasons for not using a free-running differential in the drive of this modification were discussed in Section 5.2.

The effect of the type of the interaxle driveline system on turnability is satisfactorily illustrated by the following example. A 4×4 off-road truck with a body-held payload of 4.5 ton and loaded by a trailer with a total mass of 9.5 ton was tested for motion in a circle under a variety of road conditions. The tests were performed with an unlocked and locked interaxle differential with gear ratio $u_d = 2$. The interwheel differentials were of the open type. The results listed in Table 8.15 show that with a positively engaged interaxle drive the minimum turning radius increases by 15%–25%.

For an explanation of these results the reader should refer to Sections 2.8.3 and 3.5.2 in which the effect of the interaxle drive on the vehicle's turnability is analyzed. In the given example, the locking of the interaxle differential causes a major kinematic discrepancy in the course of turning that brings about a parasitic power circulation between the axles (the circumferential force F_{x1} of the front wheels becomes negative). As a result, the lateral

TABLE 8.15

Test Results of a 4×4 Off-Road Truck

Surface	Direction of Motion	Turn Radius (m)		
		Unlocked Differential	Locked Differential	Increase in Radius (%)
Dry asphalt	Right	7.75/8.00[a]	9.75/10.00	26/25
	Left	8.75/9.00	11.25/11.25	28/25
Sandy soil	Right	7.75	9.25	19
	Left	9.00	10.25	14

[a] Numerator: truck without trailer; denominator: truck with trailer.

force in formula (2.393) changes to the opposite direction and increases highly in magnitude increasing the slip angles of the front wheels and the vehicle's turning radius. With the interaxle differential unlocked the lateral force F_{l1} decreases substantially, since the circumferential force F_{x1} of the front wheels is positive (see formula (2.393)). The slight difference between the radii of turning to the left and right is not associated with the effect of the interaxle differential and is attributed to the nonequal maximum turning angles of the front wheels when turning to the left and right.

An 8×8 off-road vehicle with two steered front axles and approximately the same distribution of weight between the axles was subjected to similar rests. The first test was performed on an even surface covered by 15–20 cm of snow. The vehicle moved in a circle with a diameter of about 30 m at 5 km/h both with a locked and unlocked symmetrical differential of the transfer case. The increase in the vehicle's turning radius under these conditions and the locked differential was 4%–5%. The second test of the 8×8 vehicle was carried out under the same conditions but on an asphalt-paved area with 5–7 cm deep and compacted snow-cover. In this case, the increase in the turning radius with the locked drive did not exceed 3%.

Field and road tests make it possible to investigate the effect of various types of interwheel power dividing units on the operational properties of multiwheel drive vehicles. It should be emphasized that this effect is not always unequivocal. Certain examples are considered here.

Locking the interwheel differentials and the use of limited slip differentials in the drive axles make possible a perceptible improvement of the mobility of vehicles on broken up, snow-covered cart roads and when moving over moderately deep (0.15–0.20 m) snow-covered soil. Such mechanisms make it possible for the vehicle to negotiate ditches and other natural and man-made obstacles, particularly when the gripping conditions of the left and right wheels of the vehicle are not the same.

If, however, the vehicle moves over wet meadowland, over sand (over a rather flat area), over the pressed-snow roads, that is, when the wheels of the vehicle's sides are gripping the surface in approximately the same manner, positive engagement of the interwheel differentials does not provide a perceptible improvement in the vehicle's mobility as compared with open differentials. Moreover, locking the interwheel differentials under these conditions may cause a reduction in mobility when making a turn. The inner wheels with significantly larger circumferential force may tear off the soft-top layer of the meadowland and sink into the soil.

The results of testing a 6×6 vehicle with a total mass of 12.7 ton with worm gear interwheel differentials in the forward rear and rear axles are rather interesting. The locking

coefficients of the differentials ranged between 6 and 10. The tests were performed on primitive and dirt roads and under off-road conditions during the spring thaw, over loose sand and under other road and climatic conditions. It was clarified as a result that a vehicle with worm gear differentials possesses a definitely better mobility than one with open bevel gear differentials. It was noted that a vehicle with worm-gear differentials in the forward rear and rear axles moves more effectively over snow and thawed soil, and its traction performance and velocity under these road conditions increased 10%–30% on the average.

A comparison of the results obtained from testing of vehicles with worm-gear and other differentials with locking coefficient 3–4 shows that they are identical with respect to mobility, but far from being identical in turnability. Cases were noted when a vehicle with worm gear differentials ($K_d = 6–10$) moving over ice-crusted ground could not travel over a close circle and continued moving forward while the front steered wheels were turned as far as they would go. The turning radius of the vehicle with worm-gear differentials on loose sand increased by 21%. It follows from this that the use of differentials with locking coefficients of 3–4 is preferable.

Free-running differentials were tested on 6×4 vehicles. Two vehicles equipped with such differentials completed a run of 25,000 km, of which 6,000 km with constant body load of 6 ton. During the test, the free-running differentials operated properly. Their use improved the mobility of the vehicles over difficult roads. However, in turns in the case of snow- and ice-crust covered road their turnability deteriorated, in the same manner as in vehicle with other locking differentials.

In straight-line travel over ground covered by 0.5–0.6 m deep and more snow, the interwheel power dividing units should have a sufficient locking performance. This was shown by comparative tests of two off-road vehicles with locked interaxle drive and identical 15.00-20 tires. A 6×6 vehicle with a total mass of 19.5 ton had open differentials in all three axles. A 4×4 vehicle with a total mass of 11.9 ton had an open differential in the front axle and a free-running differential in the rear axle. The load on the axles of both vehicles was approximately the same. The 6×6 vehicle traveled 400 m over snow-covered ground and was stuck, whereas the 4×4 vehicle traveled 550 m until it stopped entirely. When the 6×6 vehicle came to a full stop, three of its wheels slipped (one wheel per each axle), whereas the others did not move. When the 4×4 vehicle was stuck, both rear wheels and one front wheel slipped. The free-running differential markedly improved the mobility of the 4×4 vehicle. Replacing it by an open differential reduced the mobility of the 4×4 vehicle as compared with the 6×6 vehicle.

Data that can serve for a valid comparison are those obtained in testing under the same conditions of vehicles of the same type with different differentials in the drive gear. Reference here is made to tests that were performed on two identical 4×4 trucks with a total mass of 11.9 ton with 15.00-20 tires. One of them had a free-running differential on the rear axle and the other had an open bevel gear differential. The transfer cases and the front axles used differentials that were standard for this type of vehicle—an asymmetrical differential in the transfer case and an open symmetrical differential in the front axle. The tests were performed under the same road conditions and with maximum permissible loads. Both vehicles traveled 15,000 km over different roads in the Ukraine and Belarus under a variety of weather conditions. These tests showed that the truck with the free-running differential exhibits a better mobility. The mobility advantage was perceptible particularly when driving over ditches and gutters at an angle other than 90°, when moving over rugged terrain, over muddy and snow-covered roads, as well as in cases when the gripping conditions of the left and right sides of the road were not the same or the weight between the right and left wheels of the rear axles became redistributed.

The turnability of the vehicle with the free-running differential in the rear axle did not perceptibly differ from that with the open differential in the rear axle.

A multiple number of other tests of 4×2 and 4×4 vehicles and tests of multiwheel drive vehicles with larger number of axles confirm that the use of free-running differentials improves the mobility of the vehicles without a perceptible detriment to their turnability. Thus, when testing 8×8 vehicles with differentials between the axles on uneven sandy terrain, slip of both wheels of a single axle was observed because of the redistribution of the load between the axles and the tandems. This shortcoming was eliminated by replacing the open differentials in the rear-tandem axles by free-running differentials and by using limited slip differentials in the front-tandem axles.

For a quantitative assessment of the slippage of the left and right drive wheels under different gripping conditions, the results of testing a 3.7 ton 4×4 tractor with different front and rear wheels are considered, moving with one of its sides in a furrow and by its other side over stubble with drawbar load produced by a loading tractor (a simulation of the operation of tractor when plowing). The furrow was 0.25–0.30 m deep. The interaxle drive was positively locked; the rear-axle differential was unlocked. The front axle used a limited slip differential (see Figure 4.13). This differential was constructed in two versions that differed by the locking coefficient K_d—one was 2.6 and the other 3.14. It was established experimentally (see Figure 8.48a) that at drawbar pull of 10 kN and higher the slippages of the front wheels coupled by the differential with $K_d = 2.6$ are different (note that when plowing, the load on this tractor is usually $F_d = 12-13$ kN). Comparison of the records of angular velocities of the front wheels showed that these wheels rolled partially at equal and partially at different angular velocities. As a whole this brought about inequality of their slippages, $s'_{\delta 1} \neq s''_{\delta 1}$. Table 8.16 lists the mean values X of torques at the wheels and the traction forces, their standard deviations σ and variation factors ν. It can be concluded from Table 8.16 and Figure 8.48a that at certain values of F_d the difference between the torques of the front wheels becomes significant (the torque variation factors may be as high as 30%); as a result of this, the differential is actuated and does not cause wheel locking.

Using a limited slip differential with locking coefficient $K_d = 3.14$ causes the front-wheel slippage to be the same over the entire range of F_d, in spite of the high (more than 30%) variation factors of the front-wheel torques (Figure 8.48b and Table 8.17). This is attributed to the higher locking properties of the front-axle differential.

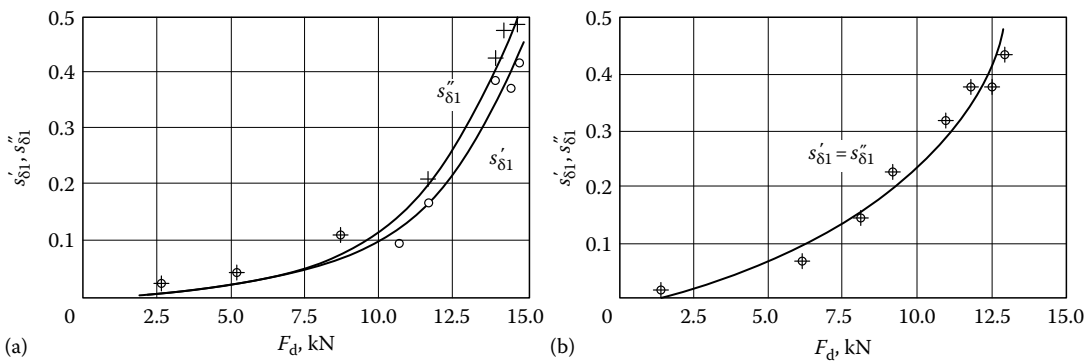


FIGURE 8.48
Slippage of front wheels of a 4×4 tractor. K_d: (a) 2.6; (b) 3.14.

TABLE 8.16

Statistical Characteristics of Torques and Drawbar Force ($K_d = 2.6$)

Drawbar Force, F_d			Front Left Torque, T'_{w1}, kN-m			Front Right Torque, T''_{w1}			Rear Left Torque, T'_{w2},			Rear Right Torque, T''_{w2}		
X, kN	σ, kN	v, %	X'_1, kN-m	σ'_1, kN-m	v'_1, %	X''_1, kN-m	σ''_1, kN-m	v''_1, %	X'_2, kN-m	σ'_2, kN-m	v'_2, %	X''_2, kN-m	σ''_2, kN-m	v''_2,%
2.65	1.37	51.70	0.19	0.04	21.05	0.15	0.03	20	3.5	0.57	16.29	3.31	0.53	16
14.04	1.61	11.46	1.03	0.28	27.68	0.91	0.26	28.46	8.44	0.61	7.23	8.28	0.64	7.73
14.33	1.09	7.61	1.27	0.23	18.06	0.75	0.16	21.3	8.83	0.78	8.83	8.55	0.87	10.18
14.77	1.89	12.8	1.31	0.28	21.37	0.99	0.24	23.92	8.90	0.65	7.3	8.85	0.68	7.68

TABLE 8.17

Statistical Characteristics of Torques and Drawbar Force ($K_d = 3.14$)

Drawbar Force, F_d			Front Right Torque, T'_{w1}			Right Front Torque, T''_{w1}			Rear Left Torque, T'_{w2}			Rear Right Torque, T''_{w2}		
X, kN	σ, kN	v, %	X'_1, kN-m	σ'_1, kN-m	v'_1, %	X''_1, kN m	σ''_1, kN-m	v''_1, %	X'_2, kN-m	σ'_2, kN-m	v'_2, %	X''_2, kN-m	σ''_2, kN-m	v''_2, %
7.45	0.741	9.94	0.715	0.227	31.8	0.662	0.227	34.2	5.23	0.51	9.8	5.05	0.479	9.49
7.76	0.762	9.82	0.726	0.183	25.2	0.675	0.185	27.4	5.71	0.42	7.4	5.45	0.38	6.92
10.84	0.712	6.57	0.827	0.232	28.1	0.628	0.223	35.5	7.24	0.613	8.47	7.2	0.598	9.53
11.00	0.902	8.22	0.909	0.262	28.8	0.649	0.194	29.9	7.68	0.942	12.3	7.51	0.979	11.96
11.82	0.790	6.68	0.914	0.243	26.6	0.773	0.247	31.9	7.97	0.511	7.2	7.8	0.60	11.08
12.26	0.723	5.89	0.931	0.257	27.6	0.903	0.219	24.3	8.24	0.57	6.9	8.19	0.424	5.65

TABLE 8.18

Minimum Turning Radii R''_{a2} of a 3.7 ton Tractor

4×2 with Disengaged Front Axle	4×4 Locked Axle Drive with Design Kinematic Discrepancy		4×2 with Disengaged Rear Axle	
	$K_d = 2.6$	$K_d = 3.14$	$K_d = 2.6$	$K_d = 3.14$
	Turning radius R''_{a2}, m			
3.70	4.50	4.55	3.34	3.40

Consider now the effect of both limited slip differentials of the front axle ($K_d = 2.6$ and 3.14) on the tractor's turnability. The experiments were performed with no load circular-path travel in the second gear on an asphalt-paved road at fully opened throttle. The steering wheel was turned as far as it went to the left. The turning radius R''_{a2} of the inner rear wheel was determined as the mean arithmetic value of the halves of three diameters of the circles produced by the tires on the road. The results are shown in Table 8.18.

The difference in the turning radii of tractors with different differentials in the front axle ranges between 1.06% and 1.09%. These data allow the conclusion that, in spite of the greater locking properties of one of differentials (something that causes a slightly larger resistance to the tractor's turning) both mechanisms exert virtually the same effect on the minimum turning radius of the tractor both in the 4 × 2 and 4 × 4 version with the rear axle uncoupled.

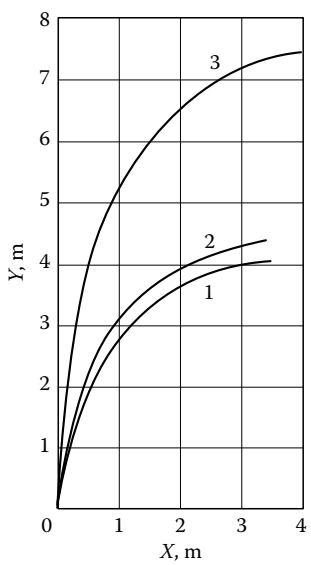


FIGURE 8.49
Paths of the rear inner wheel of a 4 × 4 tractor; rear-axle differential modes: 1, unlocked; 2, automatic locking and unlocking; 3, locked.

It is seen from Table 8.18 that the turning radius of the 4 × 4 tractor is 16.2%–18.7% larger than the turning radius of a tractor with uncoupled rear axle. This is attributed to high lateral forces at the front wheels of the 4 × 4 tractor that arise at high turning angles of the steered wheels, when the circumferential force of the front axle is negative (by virtue of the large design kinematic discrepancy and discrepancy caused by the difference in path traveled by front and rear wheels in turning). These lateral forces induce additional slippage of the front wheels and increase the turning radius.

The effect on the turnability of locking the rear-axle differential is illustrated by the results of testing of a 5.6 ton 4 × 4 tractor with locked interaxle drive and differently sized front and rear tires. The front axle had a limited slip differential with the locking coefficient $K_d = 2.6$. The rear-axle differential was locked with the possibility of automatic unlocking upon attaining a certain difference in the torques at the output shafts. In addition, this differential may be either always locked or always unlocked by the driver. Figure 8.49 shows the path of the rear inner wheel of the tractor when turning with a trailer ($F_d = 6$ kN) on a field ready for sowing. The rate of turning of the front steered wheels was 10°/s. As expected, timely automatic unlocking of the rear differential markedly improved the tractor's turnability.

At the same time, automatic locking of the rear-axle differential improves the traction performance of the tractor.

TABLE 8.19

Statistical Characteristics of Torques and Drawbar Force

Furrow Depth (m)	Drawbar Force (F_d)			Rear Left Torque (T'_{w2})			Rear Right Torque (T''_{w2})		
	X, kN	σ, kN	v, %	X'_2, kN-m	σ'_2, kN-m	v'_2, %	X''_2, kN-m	σ''_2, kN-m	v''_2, %
0.20–0.25	10.84	1.09	10.12	7.22	0.75	10.38	10.51	1.01	9.61
0.27–0.30	12.69	1.03	8.15	12.46	1.21	9.71	14.22	1.22	8.58

For this, the oil pressure in the disk-type locking clutch should ensure locking of the output shafts of the differential when working at high drawbar loads. In the course of testing the tractor with drawbar load between 0 and 23 kN moving by one side in two different furrows that were 0.20–0.25 and 0.27–0.3 m deep the pressure in the rear-axle differential locking clutch was ranged from 0.2 to 0.8 MPa at 0.05 MPa increments. At oil pressures up to 0.45 MPa, motion segments were observed when the automatic unlocking device could cause the axle's wheels to lock and they were subject to short-term separate slippage. Starting with a pressure of 0.45 MPa the automatic unlocking device did not actuate at all and both the rear-axle wheels turned rigorously at the same rpm, which was seen from the manner of the torque variation and the rpm of the wheels over the same time interval. The statistical characteristics of the torques at the rear wheels corresponding to their identical slippage are listed in Table 8.19.

It was shown analytically in Section 3.5.2 (see Figure 3.55) that when the drive axle with a locked differential makes a turn, a situation may arise when a higher torque is transmitted to the outer wheel (this wheel develops a greater circumferential force). This happens when the outer wheel moves over a dense soil and the inner wheel over a relatively less dense soil (it can also be stated that the inner wheel is subject to poor road conditions). This analytic result was verified as follows. A 3.7 ton tractor with the rear axle uncoupled moved with the front wheel turned to the left, the turn angle of the left front wheel was 4°. The inner left front wheel moved over a field and the right front outer wheel over stubble. The front wheel employed a limited slip differential with a locking coefficient $K_d = 3.14$. Note that the rear axle was uncoupled in order to highly increase the traction load on the front wheels, for which reason at high loads the traction load typically, increases at the outer wheel (see Figure 3.55). It follows from this experiment that the rpm of the front wheels were the same, that is, the differential was locked. It turned out that the torque T''_{w1} at the inner wheel was 0.679 kN-m, whereas that at the outer wheel was $T'_{w1} = 0.977$ kN-m. The experiment thus confirmed that under the above travel conditions locking the differential causes an increase in the circumferential force at the outer wheel and reduction at the inner wheel. The difference in these forces generates a torque at the plane of the road that promotes the tractor's turning, that is, causes oversteering. This points to the importance of incorporating the recognition of road conditions to which the wheels are subjected in real time into the design of contemporary mechatronic systems for controlling the locking/unlocking modes of differentials and in developing other power distributing units between the wheels.

This imparts particular importance to specially organized tests of vehicles under radically different wheel gripping conditions, the so-called μ-split conditions. As an illustration, consider the results of testing of a 4×4 off-road truck with a total mass of 11.9 ton. The front axle used an open bevel gear differential where the transfer case employed an asymmetrical spur-gear differential. The rear axle had a limited slip differential designed

as per Figure 4.13 with four steel disks in each clutch. All the differentials were run in on stands before being installed in the vehicle. At the first stage, the vehicle was tested on an asphalt-paved test area with one of the rear wheels placed on a smooth steel sheet copiously flooded with water. The vehicle itself was fastened by means of a hooking device to an unmovable support by a cable with a dynamometer device. During the tests, torque was applied to the wheels from the engine through the lower gears of the transmission and of the transfer case. When a drawbar load produced by a cable fastened to the support attained the value of 22–30 kN (range of readings for eight test runs) the rear wheel located on the water flooded steel sheet broke off its place. Following this jerk, this wheel started turning uniformly, slipping on the steel sheet. The remaining wheels remained stationary. This caused the drawbar load to drop to 12–13 kN, that is, 1.7-fold on the average. The drop in the drawbar load is attributed to the fact that, when the rear wheel slipped, the torques at both rear wheels were controlled by the static friction coefficients in disks of the limited slip differential and of the tire at the steel sheet, and at the time of slippage by the sliding friction coefficients. The results of this test are listed in Table 8.20.

The value of K_d of the rear limited slip differential being tested was obtained by dividing the torques of the left half axle by the torques of its right half axle (of the slipping wheel). It was found from eight test runs that it ranges between 1.54 and 2.03 with a mean of 1.8, which is virtually identical with the results of stand tests.

Table 8.21 lists the results of testing of the same vehicle, but with an open differential in the rear axle.

Since the rear-axle differential was run in before the experiments, its locking coefficient was found to be 1.07.

TABLE 8.20

Test Results of a 4 × 4 Truck with a Total Mass of 11.9 ton and Limited Slip Differential in the Rear Axle

№	Torque at Wheels, kN-m				$\sum_{i=1}^{2} T'^{(\prime\prime)}_{wi}$ kN-m	Drawbar Force, F_d, kN
	T'_{w1}	T''_{w1}	T'_{w2}	T''_{w2}		
1	2.02	2.02	2.74	3.98	10.76	22
	1.81	1.41	1.43	2.84	7.49	12–14
2	2.08	2.27	3.13	4.22	11.70	22
	1.35	1.49	1.67	2.88	7.39	12–13
3	2.08	2.17	2.67	4.05	10.97	22
	1.40	1.43	1.30	2.63	6.76	12–13
4	2.70	2.94	4.21	5.50	15.35	32
	1.70	1.78	2.28	3.58	9.34	13–14
5	2.64	2.94	3.57	5.63	13.78	28
	1.30	1.45	1.82	2.83	7.40	12–13
6	2.31	2.59	3.20	4.90	13.00	20
	1.55	1.67	1.67	3.34	8.23	12–13
7	2.70	4.70	3.37	5.50	16.27	32
	1.46	1.62	1.70	2.86	7.64	12–14
8	2.14	2.35	2.88	4.22	12.19	20
	1.40	1.43	1.87	2.88	7.58	12–14

TABLE 8.21

Test Results of a 4×4 Truck with a Total Mass of 11.9 ton and Open Differential in the Rear Axle

№	Torque at Wheels, kN-m				$\sum_{i=1}^{2} T_{wi}^{\prime(\prime\prime)}$ kN-m	Drawbar Force, F_d, kN
	T'_{w1}	T''_{w1}	T'_{w2}	T''_{w2}		
Interaxle differential unlocked						
1	2.25	2.18	3.74	3.75	11.92	25
	1.73	1.67	2.40	2.53	8.33	19
2	1.75	1.57	2.99	3.09	9.40	20
	1.59	1.51	2.34	2.43	7.87	16
Interaxle differential locked						
3	6.75	6.05	3.75	3.83	20.38	40
	6.00	5.72	3.29	3.38	18.39	36
4	6.93	6.60	3.75	3.82	21.10	45
	6.30	6.25	3.39	3.67	19.61	37

The data presented in Tables 8.20 and 8.21 demonstrate the extent of the increase in the total torque at the wheels when using a limited slip differential in the rear axle instead of an open differential. Dividing sum $\sum_{j=1}^{8}\left(\sum_{i=1}^{2} T_{wi}^{\prime(\prime\prime)}\right)_j$ of torques of the eight test runs by the sum of the torques $\sum_{j=1}^{8} T'_{w2j}$ (Table 8.20, second row of experimental data)

$$\frac{\sum_{j=1}^{8}\left(\sum_{i=1}^{2} T_{wi}^{\prime(\prime\prime)}\right)_j}{\sum_{j=1}^{8} T'_{w2j}} = \frac{61.83}{13.74} = 4.5$$

Then the same is done for the values of torque from Table 8.21 (second row of experimental data, interaxle differential uncoupled):

$$\frac{\sum_{j=1}^{2}\left(\sum_{i=1}^{2} T_{wi}^{\prime(\prime\prime)}\right)_j}{\sum_{j=1}^{2} T'_{w2j}} = \frac{16.20}{4.74} = 3.4$$

The ratio $4.5/3.4 = 1.33$ gives a measure of the increase in the total torque of the vehicle with the limited slip differential relative to the same vehicle with an open differential, that is, 33%.

The second stage of testing of the same vehicle (4×4 wheel formula, total mass 11.9 ton) with a limited slip differential in the rear axle was performed in order to investigate its mobility. The tests were performed under different conditions both in the winter (deep snow) and summer (dry asphalt pavement) times. When moving over soft soil and snow, including turns, the torques at all the half axles were positive. At the same time, when moving on a dry asphalt pavement with the interaxle differential locked the torques at the wheels of the front axle were negative, that is, they found themselves in the braking mode, whereas the torques on the wheels of the rear axle were positive, but with higher absolute values. Moreover, when making a turn on a dry asphalt pavement the magnitude of the torque at the wheel of the front steered axle that was external relative to the center of turn

turned out to be higher than on the inner wheel. This is confirmed by the expressions given below. When making a turn, when the front-axle wheels develop positive traction, one can have

$$T''_{w1} = 0.5(T_{01} + T_{r1})$$
$$T'_{w1} = 0.5(T_{01} - T_{r1}), \quad T''_{w1} > T'_{w1}$$

where, T_{01} if the torque at the front-axle differential case, whereas, T_{r1} is the friction torque in the front-axle differential.

In turning, when the front axle develops a negative thrust, the torque T_{01} has a minus sign, that is

$$T''_{w1} = 0.5(-T_{01} + T_{r1})$$
$$T'_{w1} = 0.5(-T_{01} - T_{r1})$$

and, accordingly, the relationship between the absolute values of torques has the form $T''_{w1} < T'_{w1}$. Hence when a vehicle makes a turn in the parasitic power mode (the interaxle differential is locked and the front-axle wheel torque is negative) the locking coefficient of the front-axle differential can be determined by dividing the torque of the outer wheel by that of the inner wheel.

Consider still another method of experimental determination of the locking coefficient K_d in vehicle testing. A 4×2 RWD truck with a total mass of 5.8 ton and a cam-plunger differential (see Figure 4.21) is fastened by a cable through a dynamometer device to an unmovable support (wall). One driving wheel was placed on a platform (plate on rollers) that was free to move, whereas the other driving wheel was placed on a nonmovable platform. Both these platforms were placed at the same level. The wheel located on the movable platform was rotated by the engine's crankshaft with the low gear engaged in transmission. The other wheel, that was located on the nonmovable platform, remained stationary. Here the total drawbar load was determined from the dynamometer readings. Then these two platforms were rotated in location under the wheels, and the wheel on the movable platform was rotated as before and the dynamometer readings were taken again. In the end, both wheels were placed on movable platforms. The engine was rotated as before and the vehicle's drawbar was again determined from dynamometer readings. This time both drive wheels rotated simultaneously.

When both wheels rotated on two movable platforms, which corresponds to the travel of the vehicle with slippage of both drive-axle wheels, the mean value of F_d was 4.24 kN. This means that each slipping wheel is subjected to a force of $0.5F_d = 2.12$ kN. Upon rotation (slippage) of one of the drive wheels located on the movable platform, the average value of the drawbar load was 6.95 kN. This means that the nonslipping wheels develop a traction force equal to $(6.95 - 2.12) = 4.83$ kN. From this the locking coefficient can be defined as $K_d = 4.83/2.12 = 2.3$.

The properties of the power dividing units of multiwheel drive vehicles exert a perceptible effect on the stability of motion, particularly under off-road conditions and on slippery roads. Vehicles with locked interwheel differentials (for example, with locking differentials or with limited slip differentials with a high locking coefficient) exhibit a greater tendency toward skidding then vehicles with open interwheel differentials. Thus, each of the two 6×6 vehicles with a total mass of 13.175 ton, one with open interwheel differentials and the other with worm-gear differentials, was observed to skid on slippery

roads. The same driver drove the vehicles one by one over a measuring road section. The vehicle with the open differentials skidded 13 times over the measured length, whereas the vehicle with the worm-gear differentials skidded 25 times. The reasons for this are obvious—the wheels of the vehicle with the worm-gear differentials with locking coefficients of 6–8 utilize the gripping conditions better for developing traction forces, and for this reason, have a poorer capability in taking up lateral loads. In addition, the vehicle with the worm-gear differentials is subjected in the plane of the road to a torque that arises from the inequality of the circumferential forces of the wheels, which tends to turn the vehicle about the vertical axis. This is the manner in which yawing of the vehicle starts. It decreases with reduction of the locking coefficient to 3–4 without any negative consequences for the vehicle's mobility.

It can be noted while investigating the stability of the passenger cars with open differentials in their axles, which move over roads with solid pavements, that both the body and the axles of the vehicle are subjected to transverse oscillations when an irregularity in the road causes one of the drive wheels to separate from the road. This reduction in stability is caused by the fact that the wheel that left the road starts spinning and when it reestablishes contact with the road this causes unequal longitudinal reactions of the left and right wheels (with allowance for inertia forces). The use of interwheel limited slip differentials makes it possible to reduce the spinning of the wheel that became detached from the road, which reduces the transverse oscillations and improves the vehicle's stability in a straight-line motion.

Cases are observed in operating vehicles (in particular of farm vehicles) that the resultant of the outer forces is shifted laterally from the vehicle's longitudinal axis. This generates a deflecting moment that tends to turn the vehicle about its vertical axis. To maintain the vehicle's rectilinear motion, the steered wheels must be constantly turned. In such cases, it is preferable to use a locked interwheel drive or locking differentials in the drive axles. Thus, tests of a farm tractor with a locking differential, intended for operation with a reaper showed the following. To maintain rectilinear motion upon the appearance of an external yaw moment in the plane of the road, the maximum angle of deviation of the steered wheels was about $\pm 6°$ and when using an open differential, $\pm 10°$.

The properties of driveline systems also affect vehicle handling. In particular, this effect is brought about by the steering system. It was noticed during road tests of vehicles with locked differentials in steered drive wheels that the load in the steering systems frequently changes, perceptibly in one or other direction. There is a reason for this. The wheel traction forces, F'_w and F''_w, in rectilinear motion of a vehicle generate moments about the turning center of kingpins at lever arm l (see Figure 8.50).

When $F'_w = F''_w$, the moments are also equal and they are mutually balanced by links a and transverse link b. In this case, the link c is not under load. When the traction forces are positive, the transverse link is subjected to tension forces and when they are negative (parasitic force circulation mode) it is subjected to compression. When the vehicle turns, forces F'_w and F''_w are not equal to one another. In connection with this, the force arising in the longitudinal link c of the steering system increases. This should be taken into account in investigating vehicles for handling.

It is a known fact that the use of locking differentials inevitably increases the load on the vehicle driveline components. The theory, verified by practical experience shows that when one of the wheels of an axle slips under conditions when the difference in the conditions of gripping the road is steep, the differential becomes the protector of the lagging half axle, the load on which does not exceed that on the half axle of the slipping wheel. However, this slows down the vehicle because of insufficient traction and may

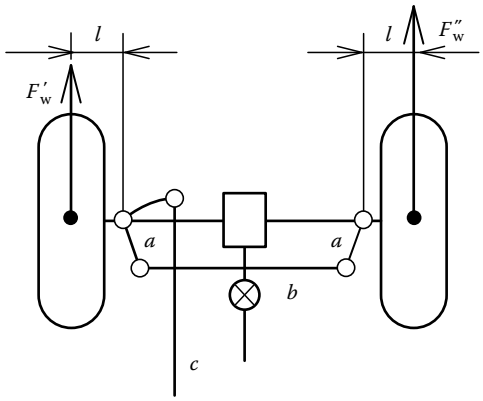


FIGURE 8.50
Schematic diagram of steered drive axle.

cause it to stop. Any attempt at increasing the traction at that time by improving the gripping of the road by the nonslipping wheel will inevitably increase the load on the half axle to which it is connected. Hence, in fact, the mobility of the vehicle is improved by increasing the load on the driveline system gear components. This load increase is particularly perceptible when a vehicle with a free-running differential travels over roads with a solid pavement. As is known, when the load is redistributed, the free-running differential transfers its entire traction to one wheel or one axle. Does such traction redistribution cause the driveline gear components to become overloaded? This question can be best resolved by specially designed tests. Such tests were performed in the course of road-testing grounds tests of a 4×2 vehicle with a totals mass of 11 ton with a free-running differential in the drive axle under different road conditions. Tests on roads with solid pavement showed that approximately each one-third of the route that was traveled was passed with two coupled half axles, with one or the other axle uncoupled while the other was coupled. But even under such unfavorable conditions of motion the traction mode of the driveline system was not too high, that is, the torques at the half axles were much lower than predicted. The results showed that the loads on the half axles increase and decrease smoothly and there are no impact loads in the driveline system when the free-running differential is actuated.

Prolonged road tests of this 4×2 vehicle and the experience in operating 8×8 terrain vehicles with free-running differentials show that the half axles, driveline components and tires have virtually the same service life of the components of the same vehicles equipped with nonlocking differentials.

The loads that act on driveline components were investigated in testing a 6×6 vehicle with a total mass of 8.69 ton with positively locked interaxle drive and with a locked and differential interwheel drive of the tandem's axles. The results of these tests showed that in rectilinear motion with approximately the same conditions of gripping of the road by the wheels, the loading modes of the right and left half axles with the differential and locked drive gear are also approximately equal and the torques at the half axles do not exceed their design values. The situation changed when different driving wheels were subjected to different road-gripping conditions. In these cases with the interwheel differentials of the tandem locked, the torques at individual half axles increased to up to 24% above their design values. The design torques of the half axles were calculated from the maximum engine torque and the largest gear ratio in the transmission.

It was also established while testing the vehicle that, if the locking clutches of the slipping axles of the tandem are locked when the vehicle stops, then this causes an impact load in the drivelines of these axles, that is, a steep short-time rise in torque occurs. When the vehicle moved over rugged terrain with the tandems' axles locked, the torques at the half axles of these axles were frequently 8%–10% higher than their design value. Consideration was also given to the case when one of the axle's wheels lost contact with the road. In these cases, when the tandem uses a differential, its traction torque is transmitted only to the two wheels of the other axles, and the torques at its half axles exceed their design value by up to 8%. On the other hand, with the tandem's driveline locked, the torque is transmitted to three wheels of the two axles, and the torques at their half axles are lower than their design value.

The greatest load distribution that at times causes the torques at certain half axles to be negative was attained when driving over roads with a solid pavement, with a high kinematic discrepancy in the driveline that was obtained by changing the air pressure in the tires. This also caused the highest excesses of design loads in the driveline system.

The loads on the half axles were also investigated on a 4×2 vehicle equipped either with an open bevel gear or with a free-running differential. The torques at the half axles were determined at the highest loading conditions, for example, such as an abrupt start from rest. The torques at the half axles of the differential increased insignificantly. The same was observed when using other locking differentials in the axles of this vehicle.

When a 4×2 vehicle equipped with a free-running differential took a turn when traveling on a solid-pavement road, the driving wheel that is external to the center of turn, that is, the outer half axle became unlocked each time. Then the entire load was transmitted to the inner half axle. The locking/unlocking of the outer half axle occurred smoothly without jerks or impacts, and the load on the other half axle increased only by 20%–45%. The same was observed when the vehicle started from rest with one of its half axle uncoupled. In this case the dynamic loads in the remaining components of the driveline system were 30%–35% lower than the loads under ordinary conditions.

The data obtained in testing vehicles with locking differentials thus allow the conclusion that the use of locking differentials increases the dynamic loads on the driveline components under certain operating conditions. However, the magnitudes of these overloads only rarely exceed the permissible design loads and do not cause, as previously assumed, breakage of driveline components or even to a perceptible wear of the latter. Under conditions that are standard for high-mobility vehicles, no significant changes occur in the loading modes of their driveline components. The loads on the drive gear components of these vehicles increase perceptibly when they are used on paved roads. However, these operating conditions are not natural for high-mobility vehicles. As to the service life of tires, when using locking differentials they wear less, since they slip less than when using open differentials.

Problems and Questions

Chapter 1

1.1 What kind of driveline system was used in the first wheeled motor vehicles of the nineteenth century?

1.2 Why should the wheels of one of the vehicle's axle be able to roll at different angular velocities (different rpm) even on a straight road section?

1.3 What happened to the wheels of the locked axles of the first motor vehicles in rectilinear motion?

1.4 What mechanism makes it possible for the left and right wheels of the drive axle to roll at different angular velocities?

1.5 Who in Europe was the first to invent and construct the first differential and when did this happen?

1.6 What are the kinematic and dynamic properties of an open differential?

1.7 What is the negative effect of the open differential on the mobility of a vehicle when the gripping conditions of the left and right wheels are not the same?

1.8 What design measures make it possible to increase the gripping of the support surface by the drive wheels?

1.9 Give some examples of driveline mechanisms that are employed to improve vehicle mobility.

1.10 Which differentials are known as locking differentials?

1.11 Define a limited slip differential.

1.12 How are differentials classified based on their location within the driveline system?

1.13 Describe the driveline system as a component part of the powertrain. Of what elements is the driveline system of a vehicle with (a) two drive axles and a transfer case, (b) three drive axles, in which the two rear axles form a tandem (the forward rear axle has a pass-through design), (c) a single rear drive axle, and (d) a single front drive axle composed?

1.14 What is the principal purpose of the driveline system?

1.15 Define the simple, combined, and integrated driveline systems.

1.16 Define the concept of a vehicle's wheel formula. How are vehicles with different wheel formulae designated? List examples of wheel formulae.

1.17 What is meant by the term drive formula? Present examples.

1.18 What is meant by the term axle formula? Present examples.

1.19 What is meant by the term steering formula of a vehicle with steered wheels? Present examples.

1.20 Explain the steering formula $0^{\underline{s}}0$.

1.21 What is meant by the term power-dividing unit? Present examples.

1.22 What is the number of power-dividing units of a vehicle with a single engine and number of drive axles equal to n? How many power-dividing units do vehicles with wheel formulae 4×4, 8×8, 12×12, and 16×16 have?

1.23 What are the principal power-loading modes of a wheel with a pneumatic tire?

1.24 Define the static and dynamic radii of a wheel with an elastic tire.

1.25 Define the effective rolling radius of a wheel. Clarify the physical substance of this radius. Why is the effective rolling radius of a wheel in the driven mode larger than the rolling radii of a wheel in the driving mode?

1.26 What is the value of the effective rolling radius of a wheel when its linear velocity is equal to zero and the angular velocity of the wheel is not equal to zero? Where is the instantaneous center of zero velocity located?

1.27 What is the value of the effective rolling radius of a wheel when its angular velocity is equal to zero and the linear velocity of the wheel is not equal to zero? Where is the instantaneous center of zero velocity located?

1.28 Define the slippage of a wheel and clarify its physical substance. What are the limits of variation of the slip ratio?

1.29 What is the slippage of the wheel if the instantaneous center of zero velocity is located on the axis of rotation of the wheel?

1.30 Answer YES or NO to the following four questions. Does wheel slippage depend on the following factors?

a. Wheel torque

b. Wheel normal load

c. Tire inflation pressure

d. Longitudinal tire-soil elasticity

1.31 The circumferential wheel force is equal to the torque divided by the radius. Which wheel radius should be used for determining the circumferential wheel force based on its torque?

1.32 What definitions of peak friction coefficient are encountered in engineering literature?

1.33 Explain the physical substance of wheel slippage power loss.

1.34 What energy efficiency factors assess the power loss of a vehicle in rolling in the tractive, transportation and transportation-tractive modes?

1.35 Given. A wheel with 16.00-20 tire is moving in the driving mode on a soft soil at constant speed. The rolling resistance coefficient is $f_1 = 0.08$. Inflation pressure is 0.14 MPa.

Determine. The slip efficiency, the rolling resistance efficiency, and the wheel tractive efficiency as functions of the net tractive force and of the number of passages over the same track if

- The normal load is of 10 kN
- The net tractive force is $0.5 \leq F_{\mathrm{w}} \leq 5$ kN
- The total number of passages over the same track is $n_k = 4$

Plot the efficiency factors $\eta_{\mathrm{fw}} = f(F_{\mathrm{w}}, n_k)$, $\eta_{\delta \mathrm{w}} = f(F_{\mathrm{w}}, n_k)$, $\eta_{\mathrm{w}}^{t} = f(F_{\mathrm{w}}, n_k)$. Analyze the results.

Hints: Assume that function $F_x = f(s_\delta)$ is exponential (see Formula 1.26), where $\mu_{px1} = 0.611$ and $k_1 = 4.095$.

Factors μ_{px} and k for any passage other than the first are as follows:

$$\mu_{px2} = 1.04\mu_{px1}; \quad \mu_{px3} = 1.02\mu_{px2}; \quad \mu_{px4} = \mu_{px3};$$

$$k_2 = 1.08k_1; \quad k_3 = 1.02k_2; \quad k_4 = k_3.$$

The rolling resistance factor is $f = R_x/W_w$.

The rolling resistance coefficient depends on the number of wheel passages over the same track $f_i = f_1(1 - 0.85 \log_{10} i)$, $i = 1, n_k$

1.36 Does the rolling radius in the driven mode change with an increase in the tire slip angle?

1.37 Why does wheel slippage increase upon appearance of sideslip and increase in the sideslip angle?

1.38 What happens to the slip resistance factor K_y when a torque is applied to the wheel? How is this reflected in the wheel slip angle if a constant lateral force is applied to it?

1.39 What are the three principal types into which ground vehicles can be subdivided and, accordingly, what vehicle motion modes are known as a function of the useful work performed by the vehicles. Present examples of vehicles and modes.

1.40 What are the two main forms of mechanical power losses in driveline systems? Clarify the physical nature of these losses.

1.41 What is the substance of the effect of the driveline system on power losses in the wheel system of vehicles?

1.42 Define the term vehicle mobility. What is meant by the topographical (geometric) and support-surface mobility?

1.43 Define the turnability of a vehicle. Clarify the manner in which design parameters and operating factors affect turnability.

1.44 Define the *static turnability* of a vehicle.

1.45 Define the *dynamic turnability* of a vehicle.

1.46 Define the *stability of motion* of a vehicle.

1.47 Define the *handling* of a vehicle.

1.48 Clarify the principles of driveline system design.

Chapter 2

2.1 What is meant by the gear ratio of an open differential? What is the gear ratio of a symmetrical differential? Answer YES or NO: Is the gear ratio of a differential the parameter that determines the distribution of torques between the front and rear wheels of a 4×4 vehicle with a positively engaged interaxle drive? Answer YES or NO to the question and explain your answer: If one wheel of a driving axle with an open differential does not turn, then does the second wheel turns three times as a fast as the differential's case?

2.2 Consider a 4×4 vehicle with an open symmetrical differential in the transfer case. The front wheels are on asphalt and the rear wheels are on an icy road. What answer (a, b, or c) is correct?

a. The torque of the front wheels is equal to the torque of the rear wheels

b. The slip of the front wheels is equal to the slip of the rear wheels

c. The front/rear wheel torque ratio is larger than two

2.3 Consider a 4×4 vehicle with an open asymmetrical interaxle differential. The front and rear wheels have different tires $\left(r_{a1}^0 \neq r_{a2}^0\right)$, and driveline gear ratios from that differential to the front wheels and to the rear wheels are not equal to each other $(u_1 \neq u_2)$. Are the circumferential forces of the front and rear wheels equal to each other under any road conditions?

2.4 Consider a driving axle with an open symmetrical differential (the inertial properties of the wheels and the driveline system and the elasticity of the driveline system are neglected)

a. Are the wheel torques equal to one another when the right wheel is subject to poor road condition and the left wheel is on asphalt?

b. Are the circumferential wheel forces equal to one another under the above road conditions if the normal loads of the wheels are different?

2.5 What is the sensible relation of the number of teeth of the side gear and pinion in a two-pinion and four-pinion bevel gear symmetrical differential to be assumed in the design in order to reduce the fluctuations of the axial forces in the mechanism, reduce vibrations, and increase the service life of the mechanism?

2.6 What design modifications can be utilized for controlling the strength and stiffness of a component?

2.7 What is the designation of the design of the drive half axles, in which design modifications transfer some loads from one component to another?

2.8 What loads on the screwed and riveted connections of the differential's case and of the bevel driven gear of the final drive can be eliminated by design means?

2.9 Why is it not advisable to use spring washers for fixing screwed connections in closed housings and cases with geared transmissions?

2.10 What design elements must be provided on the components of a bearing set for the disassembly of bearings?

2.11 When may the manufacturability of a shaft be improved (the cost of its manufacture reduced) by making slots of the same size for the same Woodruff keys on shaft segments having different diameters?

2.12 Define the energy-loading factor of a differential. Clarify the physical substance of this parameter.

2.13 The drive axle of a 4×2 pickup truck was equipped by a wheel-hub gear set and the differential of the axle was modified in a manner that the pressure on the rubbing surfaces in the new design of the differential remained approximately the same as on the rubbing surfaces of the previous design. If the vehicle's other units and systems were not modified, then clarify how the velocity modes of the differential's operation were affected? What will happen to the relative sliding velocities of the mechanism's rubbing surfaces?

2.14 List the principal types of lubrication systems of differentials employed in vehicles.

2.15 What types of gears are, as a rule, employed in asymmetrical differentials of transfer cases and why?

2.16 What is the principal design feature of the supports of intermediate shafts of pass-through axles of multiwheel drive vehicles?

2.17 What main requirements are put to lubricating oils and how do they affect the design of lubrication systems employed in vehicle driveline system?

2.18 What is done to prevent complete air tightness of the driveline lubrication systems and why?

2.19 What are the elements comprising the universal joint (Hooke's joint) drive?

2.20 For what purposes are universal joint drives used?

2.21 What types of universal joints are used in driveline system?

2.22 For what purpose and in what cases are flexible universal joints used?

2.23 At the same values of torques on the moving (in the axial direction) and nonmoving splined ends of the universal joint the specific load on the splines of the former (moving end) should be 2–3-fold lower than on the splines of the latter (nonmoving end)?

2.24 The splined telescopic joint of a drive shaft and the splined connection of the shaft of the final drive pinion transmit the same torque, but have different dimensions. Which splines are made larger and why?

2.25 Why must the drive shaft be movable and telescopic and have two universal joints at the ends?

2.26 Why does one of the yokes in a double universal joint of the steered drive axle must have a moving splined translational joint (e.g., a moving telescopic joint)?

2.27 Why should the moving (in the axial direction) splined shaft of the universal joint have a torsional moment resistance that is 1.5–2-fold higher than that of the non-moving shaft?

2.28 In what manner must the universal joint yokes at the ends of the drive shaft be positioned?

2.29 What should be done in order to attain complete equality of the speeds of rotation of two shafts connected by a universal joint?

2.30 What are the permissible installation angles of drive shafts in general and in tandems of multiaxle vehicles in particular?

2.31 Why is installing drive shafts at zero angles not recommended?

2.32 What is the feature of universal joint yokes that is specific in use in tandems of multiaxle vehicles?

2.33 What is the purpose of intermediate supports in drive shafts?

2.34 Why do the steered drive axles employ, as a rule, equal angular velocity joints?

2.35 What requirement must be satisfied in designing the turning device of the steered drive wheel with a constant angular velocity joint?

2.36 Of what are the tandems of drive axles of multiwheel drive vehicles comprised?

2.37 What roles do the balancing tandems of drive axles play in respect to the drive wheels and the vehicle as such?

2.38 Consider a 4×4 vehicle with an interaxle differential in the transfer case. The vehicle travels in a straight path at constant velocity. The gear ratio u_{d} of the interaxle differential is given.

The gear ratio from the transfer case to the front wheels and the gear ratio from the transfer case to the rear wheels are equal to one another: $u_1 = u_2 = u_f$.

The radii in the driven mode are different due to the different normal load on the front and rear wheels: $r_{a1}^0 \neq r_{a2}^0$.

The value of the total circumferential force is known and equal to $F_{x\Sigma}$.

Determine: the circumferential forces, F_{x1} and F_{x2}, of the front and rear wheels (neglect the power loss in the driveline system).

2.39 Why should triple-supported shafts be avoided?

2.40 Consider a 4×4 vehicle with a symmetric central differential making a turn. Does the lateral force on the rear wheels change its magnitude, or direction, or both when the differential gear ratio changes from 1 to 2.5?

2.41 Consider a 4×4 SUV with a symmetric interaxle differential in its transfer case.

Curb mass is of 1150 kg. Static curb weight W_{c} distribution is $W_{c1}/W_{c2} = 1.68$.

Full mass is of 1550 kg. Static full weight W_{a} distribution is $W_1/W_2 = 0.93$.

The wheelbase is $l_2 = 2.2\,\mathrm{m}$.

The vehicle starts moving at an acceleration of $a_{x\,\max} = 2.6\,\mathrm{m/s^2}$.

The rolling resistance coefficient of the front wheel is $f_1 = 0.10$.

The function $F_x = f(s_\delta)$ is exponential (see Formula (1.26)). Coefficients μ_{px} and k depend on the number of passages in the same track:

Front wheels—$\mu_{px1} = 0.6,\ k_1 = 7$.

Rear wheels—$\mu_{px2} = 1.04\mu_{px1},\ k_2 = 1.08k_1$.

Determine.

- The normal loads for the empty and fully loaded SUV.
- The circumferential forces and slip ratios of the front and rear wheels for the empty and fully loaded vehicle when moving at a given acceleration.
- The slip energy efficiency of the empty and fully loaded SUV.
- The interaxle differential ratio to provide the fully loaded SUV with the maximum slip energy efficiency.

Hints:

- The rolling resistance factor is $f = R_x/W_{\mathrm{w}}$.
- The rolling resistance factor depends on the number of wheel passages in the same track $f_i = f_1(1 - 0.85\,\log_{10} i),\ i = 1, 2$.
- Use the weight distribution ratios and wheelbase length to determine the coordinates of the center of gravity for the empty and fully loaded SUV.
- Apply the inertia force F_{a} in the center of gravity and determine the front/rear dynamic normal reactions for the empty and fully loaded SUV in motion.

- Use the dynamic normal reactions of the SUV in motion for computing the slip coefficients and the circumferential force distributions.
- Recall that the slip efficiency is maximized when the slip coefficients of the front and rear wheels are equal to one another.
- Neglect the offset displacement of the normal reaction from the wheel axis.
- Assume $r_{a1}^0 = r_{a2}^0$.
- To determine the height coordinate h of the center of gravity use the following formula:

$$h = \left((W_2'/W_{(c)a})l_2 - l_a\right)/\tan\alpha$$
$$\alpha = 7^\circ,$$

For the empty SUV $W_2' = 0.4095W_c$; for the fully loaded SUV $W_2' = 0.5504W_a$.

Chapter 3

3.1 How is the ratio of angular velocities of the output shafts of a locked power-dividing unit defined?

3.2 Describe a double-side action-overrunning clutch.

3.3 Define the theoretical velocity of a wheel. Why can theoretical velocities of the driving wheels of a 4×4 vehicle with positive engagement of the drive axles differ from each other?

3.4 Is the kinematic discrepancy a parameter that determines the power distribution to the front and rear wheels of a 4×4 vehicle with an open differential in the transfer case?

3.5 Define the kinematic discrepancy factor of a 4×4 vehicle with a locked interaxle driveline system. What is meant by design kinematic discrepancy и by operational-manufacturing kinematic discrepancy?

3.6 In what positively engaged driveline system is the design kinematic discrepancy set?

3.7 What operating conditions may bring about the appearance of operational-manufacturing kinematic discrepancy in a positively engaged driveline system?

3.8 What is the reason for the appearance of kinematic discrepancy in a positive interaxle engagement of a 4×4 vehicle with steered front wheels when making a turn?

3.9 How is the kinematic discrepancy factor in a positively engaged driveline system of a vehicle with any arbitrary number of drive axles determined?

3.10 What will happen to the energy efficiency if a negative torque appears in at least one of the drive wheels/axles of a vehicle?

3.11 Two drive wheels coupled to a single frame with a positively locked driveline system move one after the other over a solid road without a traction load. The diameter of the

rear wheel is by an amount Δ larger than the diameter of the front wheel. Describe the processes occurring with the rolling radii of both wheels.

3.12 How do locked and differential interaxle drivelines affect the fuel consumption when moving over hard-surfaced roads?

3.13 What is the preferable arrangement (a or b in Figure P3.13) of the intermediate gear from the point of view of loads on the bearings of this gear? Solve in general form, introducing any designations of forces and dimensions, at a given T_1. What clearances in the meshing of the gear teeth should be regarded as optimal in each of the arrangements? To solve the problem it is suggested to separately depict each arrangement and draw vectors of tangential and radial forces in the gear teeth meshing.

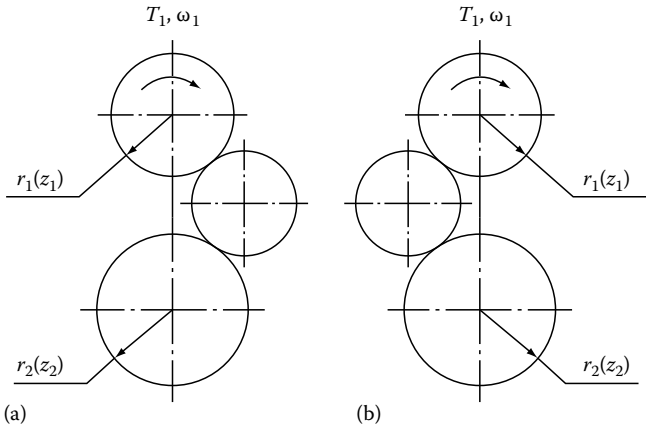


FIGURE P3.13
Diagrams of gear sets.

3.14 Consider a 4×4 vehicle with a positive locking engagement of the drive axles. Are the slip factors of the front and rear tires equal to one another if the design and operational-manufacturing kinematic discrepancy is zero? Provide a mathematically substantiated explanation.

3.15 Consider a 4×4 articulated loader with positive engagement of the front and rear axles. The normal loads and the inflation pressure of the front and rear tires are identically the same. The driveline gear ratio from the transfer case to the front wheels is equal to the gear ratio from the transfer case to the rear wheels. The center turning joint is located in the middle of the wheelbase. Hence, the length of the front frame and the length of the rear frame are the same. Interwheel differentials are open. The loader is in a turn. Road conditions are the same for all the wheels. Are the slip factors of the front and rear wheels equal to each other, or are they different? Explain.

3.16 Consider a 4×4 vehicle with positive locking engagement of the drive axles in straight-line motion.

The front and rear tires are 15.00-20.

The normal loads on the front and rear wheels vary within the range: $10 \leq W_w \leq 35$ kN.

The inflation pressure in the front and rear tires varies within the range: $0.15 \leq p_w \leq 0.45$ MPa.

Calculate and plot the kinematic discrepancy coefficient of the vehicle as a function of the normal load and inflation pressure. Analyze results.

Hints:

The gear ratios u_1 and u_2 are equal to each other.

Use the following formula from Petrushov (1975) $r_w^0 = r\dfrac{rp_w + \upsilon_1 W_w}{rp_w + \upsilon_2 W_w}$

here

$$\upsilon_1 = 0.04310\,\text{cm}^{-1} = 0.0004310\,\text{m}^{-1}$$

$$\upsilon_2 = 0.04965\,\text{cm}^{-1} = 0.0004965\,\text{m}^{-1}$$

3.17 Consider a 4×4 vehicle with the front steered wheels and positive engagement of the drive axles in turn. The interwheel differentials are open. The total circumferential force of the vehicle is $F_{x\Sigma} = 2$ kN. The steering angle is $\delta = 30°$.

Determine the front and rear slip coefficients, $s_{\delta a1}$ and $s_{\delta a2}$, and the circumferential wheel forces of the front and rear axles, F_{x1} and F_{x2}, if

- The longitudinal stiffness factors are $K_{a1} = 1.2$ kN and $K_{a2} = 1.8$ kN.
- The longitudinal stiffness factors are $K_{a1} = 1.8$ kN and $K_{a2} = 1.2$ kN.

Assume a linear relationship between the circumferential force F_x and the slip coefficient s_δ of the wheel.

3.18 How is the effect of the operational-manufacturing kinematic discrepancy in a positively engaged interaxle driveline system of a 4×4 vehicle reflected in the selection of the design kinematic discrepancy?

3.19 Why is the interwheel differential of a farm tractor working in fields usually locked, whereas it is unlocked when making a turn?

3.20 How do the circumferential forces of the two wheels of the drive axle of a 4×2 vehicle with a locked interwheel drive moving on soil change with a reduction in the turning radius? How does the total circumferential force of the vehicle affect this situation?

3.21 Consider a 4×4 vehicle with an overrunning clutch that provides for automatic positive locking engagement/disengagement of the front axle. The rolling radii are $r_{a1}^0 = 0.55$ m and $r_{a2}^0 = 0.75$ m. The gear ratios from the transfer case to the front and rear wheels are $u_1 = 22$ and $u_2 = 27.9$. In the course of designing this overrunning clutch it became necessary to provide for engagement of the front axle by the driver from the cabin. The question is, what design kinematic discrepancy factor should be provided upon ''manual'' engagement of the front axle? Calculate the gear ratio u_1, at which this value of kinematic discrepancy is attained.

3.22 Consider a 4×4 vehicle with positive locking engagement of the drive axles. The design kinematic discrepancy is zero when the vehicle travels at a constant speed. The final drive gear ratio is $u_f = 4.3$. Then the vehicle is accelerating. The weight distribution between the axles during the acceleration being about the following radii in the driven

mode $r_{a1}^0 = 286$ mm; $r_{a2}^0 = 278$ mm. What is the value of the kinematic discrepancy factor at this point in time? In which axle should the final drive gear ratio be changed to impart to the vehicle a zero design kinematic discrepancy: in the front axle, rear axle, or in both? Calculate the value of that final drive gear ratio.

3.23 Consider a 4×4 vehicle with front steered wheels and with positive locking engagement of the drive axles. The vehicle has zero kinematic discrepancy:

- The effective kinematic radii of the front and rear wheels in the driven mode are identical;
- The gear ratio from the transfer case to the front wheels is equal to the gear ratio to the rear wheels.

Calculate and plot the kinematic discrepancy factor of the vehicle in a turn as a function of the steering angle δ_1 of the front wheels. Does the kinematic discrepancy depend on the wheelbase size or any other vehicle parameters? Are the same values of the kinematic discrepancy obtained for any vehicles with positive locking axle engagement and front steering system?

3.24 Derive a formula to calculate the kinematic discrepancy factor for a 4×4 vehicle with positive locking engagement of its axles and both, the front and rear wheels, steered (Figure 2.13 helps understand the front and rear angles, δ_1 and δ_2, and also other geometric features of a turning vehicle).

Does this factor depend on a relation between the dimensions a and b, e.g., on the position of point C on line O_1O_2? If yes, calculate the kinematic discrepancy factor as a function of angle δ_1 and of ratio $RR = O_1C/O_1O_2$ when the ratio changes from 0 to 1. Plot and analyze the results.

Hint: To solve the problem, you have to determine the angle δ_2 as a function of δ_1.

Chapter 4

4.1 Does the reduced internal slip (e.g., the increased internal friction) in the limited slip differential have a marked effect on power losses in this mechanism?

4.2 Define the locking coefficient (or torque bias) of a limited slip differential under relative motion of its output shafts. What does it represent?

4.3 What does the static locking coefficient represent?

4.4 Consider a 4×2 vehicle with a limited slip differential in the drive axle. The torque bias of the limited slip differential is $K_d = 4$. What is the percentage of the road conditions in which the vehicle can develop maximum traction? Assume that the minimum and maximum friction factors are $\mu_{px\,min} = 0.1$ and $\mu_{px\,max} = 0.8$.

4.5 Consider a limited slip differential with a constant torque bias K_d and with no additional locking devices. Assume that you are changing the material for the plate disks. As a result, the friction coefficient in the differential μ has increased from 0.1 to 0.14. What do you have to do with the differential geometric parameter A from formula (4.28) to keep the same value of the torque bias K_d? Options: increase A; decrease A; keep A the same. If option 1 or 2 is used then name some ways to change A when designing the differential.

4.6 See formula (4.32) for the torque bias ratio of a limited slip differential with a constant torque bias K_d and with no additional locking devices.

As can be seen, the limited slip differential can be fully locked and never get actuated, that is, the output shafts will never get relative rotation, if relationship between the geometric parameter P_1 and the friction coefficient μ is incorrect. What is the value of the torque bias when the above incorrect relationship takes place? Derive a formula to describe the incorrect relationship between P_1 and μ mathematically.

4.7 Why is the locking coefficient of differentials with constant friction torque not constant, but rather decreases with increased applied torque?

4.8 What is the essence of limited slip differentials with both variable friction torque and torque bias?

4.9 What is the design feature specific to the worm-gear differential? Is its locking coefficient constant if $\mu = \text{const}$?

4.10 Describe a conceptual design of a cam-plunger limited slip differential.

4.11 What is the feature specific to a differential with hydraulic resistance?

4.12 Consider a limited slip differential with a constant torque bias K_d installed in the rear axle of a 4×4 vehicle with front steered wheels and positive engagement of two axles (design kinematic discrepancy is zero) and an open front differential. The vehicle is making a turn and the rear wheels have different angular velocities. Is the resisting yaw moment generated by the limited slip differential in the rear axle becoming bigger when the steering angle is increasing? Explain.

4.13 Consider a 4×2 vehicle with total circumferential force of 30 kN moving in a straight line. The limited slip differential in the rear drive axle is still locked. The rear tires are identically the same. Normal loads on the rear wheels are the same. The wheelbase is 4.2 m; the tread is 1.8 m. The road conditions are different for the rear wheels: the longitudinal stiffness coefficients are $K'_x = 100$ kN and $K''_x = 200$ kN.

Determine

a. The circumferential forces of the rear wheels, F'_{x2} and F''_{x2};

b. The yaw moment M_{ZR};

c. The lateral forces, F^{w}_{l1} and F^{w}_{l2}, generated by the yaw moment on the front and rear wheels

4.14 Consider a drive axle with the tread equal to $t_B = 2.2$ m. This axle has a limited slip differential with a decreasing friction moment. One of the geometric parameters of the differential is $A = 4.5$.

The friction coefficient of the plate disks is $\mu = 0.1$. The correction factor to adjust the torque bias is $K_{pu} = 1.18$. The longitudinal stiffness of the tire is $K_x = 140150$ N. The radius of the wheel in the driven mode is $r^0_w = 0.685$ m. The gear ratio of the wheel-hub gear set is given as $u_k = 3$ in linking the input torque T_0 with the wheel torque and, accordingly, with the wheel circumferential force F_x.

Determine the value of the additional geometric parameter H needed to provide the differential with a torque bias of $K_d = 3.0$ when the differential input torque T_0 is 3200 N-m.

Calculate the turn radius R_d of the axle at which the limited slip differential loaded with $T_0 = 3200$ N-m gets actuated.

Calculate changes in the radius of turn R_d if

- The input torque T_0 became reduced by 20%;
- The geometric parameter H was increased by 20% (the input torque is still $T_0 = 3200$ N-m).

4.15 Consider a nonsteered drive axle with a tread of $t_B = 2.0$ m. This axle has a limited slip differential with constant torque bias. The geometric parameter of the differential is of $P_1 = 4.5$. The rolling radius of the wheels in the driven mode is $r_w^0 = 0.44$ m. The longitudinal stiffness of each tire is $K_x = 150{,}000$ N.

Determine the value of torque bias if the friction coefficient in the differential is $\mu = 0.12$;

Calculate the turn radius R_d of the axle at which the limited slip differential loaded with $T_0 = 3{,}200$ N-m gets actuated.

4.16 The locking coefficient K_d of limited slip differentials with decreasing internal friction torque and with constant internal friction torque exhibit similar behavior as a function of the torque T_0. How do these limited slip differentials affect the turnability of a vehicle when they are installed in the drive axles?

Chapter 5

5.1 What is another name for a free-running differential?

5.2 Explain the conceptual principle of the operation of a free-running differential.

5.3 What is the principal drive element of the free-running differential?

5.4 What is the ordinary number of power teeth in each of the two gear rings of the drive clutch of a free-running differential and how are they arranged relative to one another?

5.5 What elements of the free-running differential are involved in disengaging the advancing wheel of the drive axle when the vehicle turns?

5.6 How is the noiseless operation of modern free-running differentials achieved?

5.7 Which differential's conceptual design has become the basis for designing currently produced free-running differentials?

5.8 What is the number of kinematic links into which the free-running differential becomes separated in the course of change of direction of the vehicle (forward–reverse and *vice versa*) when moving in a straight line in the traction mode?

5.9 What elements of the free-running differential make up link A and link B into which the differential is separated when the vehicle is moving in a straight line in the traction mode?

5.10 What happens in a free-running differential when a vehicle moving forward or in reverse in a straight line is braked?

5.11 What is the number of kinematic links into which the free-running differential is separated when the vehicle makes a turn?

5.12 What elements of the free-running differential make up link A' and link B'?

5.13 Which of the wheels of the drive axle of a vehicle with a free-running differential becomes disengaged when turning in the traction mode (wheel gripping conditions are the same)?

5.14 Which of the drive wheels of a drive axle of a vehicle with a free-running differential becomes disengaged when the turning vehicle is braked by the engine (wheel gripping conditions are the same)?

5.15 Which of the drive wheels of a drive axle with a free-running differential may become disengaged when the vehicle turns while it is coasting?

5.16 What is the reason for the fact that when a vehicle turns while coasting either of the wheels of the drive axle with a free-running differential may disengage? What should be done to ensure that one of the wheels of a drive axle with a free-running differential should definitely disengage and why must this be done?

5.17 What is the reason that when a vehicle turns in the traction mode neither the left nor the right wheel of a drive axle with a free-running differential may become disengaged, as it occurs when the vehicle turns while coasting?

5.18 How should springs for free-running differentials be selected?

5.19 What should be the height of the power teeth of the drive clutch and of the driven half clutches, as compared with the height of the trapezoidal teeth of the center ring in order to provide for a precise disengagement of one of the driven half clutches of the free-running differential at the proper moment?

5.20 What should be the height of the trapezoidal teeth of split-spring lock rings as compared with the height of the trapezoidal teeth of the driven half clutches of the free-running differential for the precise disengagement of the latter?

5.21 What should be done to prevent the trapezoidal teeth of the driven half clutch of a free-running differential from sliding off the ends of the teeth of the center ring earlier than the teeth of the split spring lock ring?

5.22 How should the split-spring ring be installed in the driven half clutch of a free-running differential in order not to weaken its coupling with the half clutch due to the centrifugal force exerted on it?

5.23 To what should the width of the slot in the lock (slit) of the split ring lock ring placed in the driven half clutch of a free-running differential be equal?

5.24 Is it permissible to modify the design of free-running differentials and their elements in a manner that would entirely change their layout?

5.25 In what types of vehicles are free-running differentials used?

5.26 In what are free-running differentials used as vehicular power-dividing units?

5.27 Are free-running differentials used in front steered axles of multiwheel drive vehicles?

5.28 Is it possible to use a roller-type overrunning (free-running) clutch instead of a free-running differential in the interaxle driveline of a 4×4 vehicle and what adjustment in the interaxle driveline of the drive axles of the vehicle must be made?

5.29 Can free-running differentials operate in the interaxle driveline without kinematic discrepancy between the drive axles?

Chapter 6

6.1 Rank driveline systems on the basis of their effect on the range of distribution of circumferential forces between the wheels of a multiwheel drive vehicle when making a turn: fully differential, fully locked, driveline system containing open differentials and free-running differentials.

6.2 Will the motion of an 8×8 vehicle making a turn be stable, if the gripping-force utilization factor $K_{\mu i}$ of the wheels of three axles is smaller than 0.5, and that of the rear axle is 0.6?

6.3 Why is the turning radius of a 4×4 vehicle with a positively engaged interaxle driveline system larger than that of the same vehicle, but with an open interaxle differential?

6.4 Is the optimization of the distribution of power between the wheels of a multicriterion or a single-criterion problem? Explain your answer.

6.5 In what does modeling of vehicle dynamics as an inverse vehicle dynamics consist in the course of optimizing the power distribution between the vehicle's wheels?

6.6 Compile a set of equations, the solution of which would provide for the optimal distribution of power in the acceleration of a 6×6 vehicle. Use solely the information in Section 6.3.

6.7 When the relationship between the circumferential force of a wheel and its slippage (see formula (1.26)) is nonlinear, are the optimum slippages of the vehicle's wheels corresponding to the maximum slippage efficiency and maximum running gear efficiency equal to one another if the gripping factors of all the wheels are the same or different?

6.8 Is it advisable to make an allowance for the difference in the optimum slippages of wheels corresponding to the maximum slippage efficiency and to the maximum running gear efficiency of a vehicle in the case of a nonlinear relationship between the circumferential force of the wheel and its slippage when designing automatic driveline system control?

6.9 Why is the optimization of power distribution between the wheels of a loader (see Section 6.4) based on the motion mode of scooping up of the material into the bucket?

6.10 Do constraints (6.19) in optimizing the distribution of power between the left and right wheels of each of the vehicle's axles change if the interaxle drive has been specified?

6.11 What is the manner in which the properties of the interwheel driveline are incorporated in optimizing the power distribution between the left and right wheels of each axle of the vehicle in the case when the interaxle power-dividing units are assumed to be specified?

6.12 When optimizing the power distribution between the wheels of a loader (Section 6.4) the maximum efficiency is attained when (1) the slippages of the left and right wheels of the front axle and the slippages of the left and right wheel of the rear axle are equal or in the case (2) when slippages of the left and right wheels of each axle are not equal?

6.13 In optimizing the power distribution between the wheels of a loader (Section 6.4) will the generalized slippage of the front axle equal to the generalized slippage of the rear axle?

6.14 Why does the rolling resistance of the loader's wheel increase when scooping up the material into the bucket?

6.15 Why does the total force, resisting the rolling of wheels over pliant soil increases more when the front and middle wheels are located close to one another than when the middle wheels are closer to the rear ones when the center of gravity of a 6×6 vehicle is shifted toward the rear wheels (see Figure 6.21)?

6.16 From the point of view of improving the traction efficiency of the running gear of a 6×6 vehicle, which arrangement of the middle wheels along the base is best?

6.17 Why in a 6×6 traction vehicle with the middle wheels close to the front or located in the middle of the base it is advisable, to design a driveline system in which the engine power is first divided between the rear axle on the one side and the front and middle axles on the other, and only then is the power supplied to the front and middle axles distributed between them. Use Figure 6.33 to explain your answer.

6.18 Why is it important to formulate the problem of optimal distribution of power between the wheels of an off-road multiwheel drive vehicle as a probabilistic problem? What principal operational factors should be regarded as random?

6.19 How is it possible to analytically compare the running gear efficiency of a vehicle that corresponds to optimal distribution of power between the wheels and the running gear efficiency of the same vehicle with its driveline system?

6.20 Is the difference between the efficiency of a vehicle corresponding to optimal distribution of power between the wheels and the efficiency of the running gear of the same vehicle with its existing driveline system significant? Give an example using material from Chapter 6.

6.21 What should be the criterion for accepting a solution upon statistical determination of the factors representing the optimal distribution of torques between the wheels?

6.22 Explain why the factor of optimal distribution of torque between the drive tandems of an 8×8 terrain vehicle with virtually equal normal wheel loads turns out to be higher than unity.

Chapter 7

7.1 Define a simple and a combined mechatronic driveline system.

7.2 Define an integrated mechatronic driveline system.

7.3 Present examples of the effects of mechatronic vs. mechanical driveline systems on passenger car dynamics.

7.4 Explain the substance of algorithms of control of the force parameters of a wheel constructed based on the inverse wheel dynamics approach.

7.5 What capabilities are provided by introducing into the wheel dynamics control algorithm of elements associated with the control of the rolling radius in the driving mode, in addition to the control of the rotational speed of the wheel?

7.6 What two main problems associated with the proactive assessment of terrain conditions are usually investigated and solved?

7.7 What study approaches are being developed for the proactive assessment of terrain conditions?

7.8 Why does the change of the rolling radius in the drive mode, referred to (that is divided by) the change in the wheel's torque ($\Delta r_w/\Delta T_w$) make it possible to asses variations in the wheel's gripping conditions?

7.9 Explain the practical value of the data in Figure 7.13 for synthesizing mechatronic systems for controlling the distribution of power between the vehicle's axles.

7.10 Define the planetary-transmission design parameter K. For what purpose is this parameter introduced? What is its value in a symmetrical bevel-gear differential?

7.11 What is the shortcoming of the open bevel-gear differential, when used as the turning mechanism in a tracked vehicle?

7.12 Will the shortcoming of the open bevel-gear differential discussed in Problem 7.11 manifest itself when used as an interwheel differential in a wheeled vehicle with a traction control system?

7.13 Does the ratio of angular velocities of the output shafts of an open bevel-gear interwheel differential depend on the angular velocity of its case, that is, on the vehicle's velocity?

7.14 Why is it advantageous in working out an algorithm of control of an interwheel differential in which the mechanism is locked upon sensing a difference between the rpm of output shafts to use the ratio of the angular velocities of the output shafts as the locking input signal, rather than the difference in the angular velocities of the output shafts?

7.15 Can a 4×2 vehicle with an open bevel-gear differential in the rear drive axle perform a turn about its inner wheel if the latter is braked?

7.16 Does a double differential cause an increase in the load on the engine in the same manner as an open differential when one of the gears of the outer differential is braked?

7.17 Can a 4×2 vehicle with a double bevel-gear differential in the rear drive axle perform a turn about its inner wheel if the inner gear of the outward differential is fully stopped?

7.18 Is it possible to change the design of a double differential in a manner that will increase its energy effectiveness at small turning radii?

7.19 A locking system of the differential of the drive axle of a 4×2 vehicle is being designed. The engineering idea here consists in locking the differential in the case when the ratio of the angular velocities of its output shafts would attain some threshold value. How is it possible to analytically—by mathematical simulation of the vehicle's motion—determine this threshold value while retaining a sufficiently high-energy efficiency of the vehicle under the specified conditions of motion? To resolve this matter, refer to Section 7.5.

7.20 Why is it so important to monitor wheel slippage during the first seconds when the vehicle starts moving from rest?

Chapter 8

8.1 What is the purpose of testing batch-produced power-dividing units for some time now?

8.2 Under what conditions are batch-produced power-dividing units tested? Are they subjected to indoor tests on stands or outdoor tests as a part of a vehicle?

8.3 What types of stands should be designed and used for testing power-dividing units that have been in production for some time now, newly designed, and improved power-dividing units: general purpose or specific purpose stands?

8.4 Are original (special purpose) power-dividing unit stands used in addition to general-purpose stands? Present examples, among them an example from Chapter 8.

8.5 What properties and parameters of newly designed limited slip differentials are the first to be investigated on stands?

8.6 What method is used for determining the torque bias of limited slip differentials on the stand shown in Figures 8.1 and 8.2?

8.7 What do braking torques applied to output shafts of differentials when tested on the stand of Figures 8.1 and 8.2 simulate?

8.8 What are the design parameters and operating factors, the effects of which on the locking performance of differentials, are investigated on the stand from Figures 8.1 and 8.2?

8.9 In addition to investigating the locking performance, to what other stand tests are power-dividing units subjected?

8.10 What are the main purposes of stand testing of differential lubrication systems?

8.11 What processes occur in differentials in which the lubrication device consists of oil scoops, but does not have oil-removal ports in the differential's halves?

8.12 What properties should be exhibited by a differential's lubrication system to prevent products of wear from plugging up access to friction surfaces?

8.13 How can the effectiveness of the flow-through lubrication system be visually ascertained?

8.14 What factors affect the flowage of oil through the differential?

8.15 What are the differential's rpm at which its flow-through lubrication system operates poorly or breaks down entirely?

8.16 What are the advantages of gear pumps?

8.17 What are the shortcomings of gear pumps?

8.18 Where and how should the gear pump be located within the lubrication system in order for it to operate stably?

8.19 Can a gear pump operate with air-permeated oil?

8.20 What is the recommended fluid flow velocity in the intake cavity of a gear pump in order to avoid a steep reduction in its output because of centrifugal forces at the rotor teeth?

8.21 What is meant by the term standard test route?

8.22 What is caused by the presence of kinematic discrepancy in the tandem of a 6×6 truck?

8.23 Under which road-gripping conditions do the locking differentials perceptibly not affect the mobility of a vehicle as compared with open differentials and what is the reason for this?

8.24 Under what conditions of gripping of the wheels and surface may complete locking of the differential or the use of limited slip differentials with high locking coefficients become detrimental to the mobility of a wheeled vehicle?

8.25 What is indicated by the fact that the mobility of a 4×2 vehicle with locking differential in the drive axle may turn out to be better than the mobility of a 6×6 vehicle with open differentials in the axles (at the same weight loads on the axles)?

8.26 How does the free-running differential compete with other locking differentials with respect to its effect on the vehicle's mobility?

8.27 What may be the shortcoming of a free-running differential when a vehicle makes a turn and how does it affect its turnability?

8.28 The turnability of which type of vehicle is least affected by the free-running differential?

8.29 How does increasing the locking coefficient of an interwheel limited slip differential affect the turn resisting moment and the turnability of an off-road vehicle?

8.30 Under what vehicle road conditions are the components of a locked drive and of a drive with locking differentials subjected to the highest loads?

8.31 What design features in the driveline system allow reducing the loads on its components when operating multiwheel drive vehicles on roads with high-grade pavement?

Bibliography

Ageikin, Y. S., *Mobility of Automobiles*, Mashinostroenie Publishing House, Moscow, Russia, 1981 (in Russian).

Aksenov, P. V., *Multi-Axle Automobiles*, 2nd edn., Mashinostroenie Publishing House, Moscow, Russia, 1989 (in Russian).

Aksenov, P. V., Belousov, B. N., Starikov, A. F., Fundamental principles of analysis and synthesis of transmission layouts of multi-axle vehicles, News of M.S.T.U. named after Bauman Publishing House, N 4, 1998 (in Russian).

Aleksandrov, E. B., Trikoz, A. A., Shemetov, S. V., Contemporary power diving mechanisms in the transmissions of contemporary vehicles, Survey Information, II. Cars and Buses, Central Research Institute of Information and Engineering Research of the Automobile Industry, Moscow, Russia, 1989 (in Russian).

Alekseeva, S. V. et al., *Power Transmissions of Transport Vehicles*, Mashinostroenie Publishing House, Leningrad, Russia, 1982 (in Russian).

Alexander, D., Separated at birth, Automotive Engineering, July, pp. 18, 20, 2005.

Alvarez, L., Yi, J., Horowitz, R., Olmos, L., Dynamic friction model-based tire-road friction estimation and emergency braking control, *Journal of Dynamic Systems, Measurements, and Control*, 127, 22–32, March 2005.

Ando, H., Murakami, T., AWD vehicle simulation with the intelligent torque controlled coupling as a fully controllable AWD system, SAE Paper No. 2005-01-0552, Society of Automotive Engineers, Warrendale, PA, 2005.

Andreev, A. F., Atamanov, Y. Ye., Bud′ko, V. V., Boikov, V. P., Vasilev, V. T., Kabanau, V. I., Lefarov, A. Kh., Masyuk, S. K., *Tractors: Senior Design Projects*, Visheishaya Shkola Publishing House, Minsk, Russia, 1985 (in Russian).

Andreev, A. F., Vantsevich, V. V., Lefarov, A.Kh., *Differentials of Wheeled Vehicles*, Mashinostroenie Publishing House, Moscow, Russia, 1987 (in Russian).

Anilovich, V. Ya., Vodolazhchenko, Y. T., *Calculations and Design of Agriculture Tractors Handbook*, 2nd edn., Mashinostroenie Publishing House, Moscow, Russia, 1976 (in Russian).

Antonov, A. S., *Complex Power Transmissions. Theory of Power Flow and Design of Transmission Systems*, Mashinostroenie Publishing House, Leningrad, 1981 (in Russian).

Antonov, D. A., *Theory of Stability of Motion of Multi-Axle Automobiles*, Mashinostroenie Publishing House, Moscow, Russia, 1978 (in Russian).

Anufriev, V. A., Bezverhij, S. F., Kutenev, V. F., Industry brunch system of automotive vehicles, *Avtomobil′naya Promishlennost′* (Automobile Industry), No. 3, pp. 1–4, 1983 (in Russian).

Arnett, M., Rizzoni, G., Heydinger, G. J., Guenther, D. A., Salaani, M. K., Implementation of an electric all-wheel drive (eAWD) system, SAE Paper, No. 2008-01-0599, Society of Automotive Engineers, Warrendale, PA, 2008.

Artobolevskij, I. I., *Theory of Mechanisms*, Nauka Publishing House, Moscow, Russia, 1967 (in Russian).

Asgari, J., Hrovat, D., On-demand four wheel-drive transfer case modeling, SAE Paper, No. 970969, Society of Automotive Engineers, Warrendale, PA, 1997.

Bahmutov, S. V., To problem of choosing torque bias values of an interwheel differential of a passenger car, *Avtomobil′naya Promishlennost′* (Automobile Industry), No. 10, pp. 15–17, 1979 (in Russian).

Barskij, I. B., *Design and Calculations of Tractors*, Mashinostroenie Publishing House, Moscow, Russia, 1980 (in Russian).

Bartsch, C., VW Golfsyncro und die Technik des allradantriebes, Krafthand. Dad Wokishofen, BRD, 58, 23, 1909–1913, 1985.

Bartus, Ch., Overrunning bi-directional clutch (ORBDC) unit manufactured by cold-forming process, SAE International AWD Vehicle Symposium, East Liberty, OH, August 21–24, 2006.

Barykin, A. Yu., Viscous clutches. Control of characteristics, *Avtomobil'naya Promyshlennost* (Automotive Industry), No. 2, pp. 18–20, 2002 (in Russian).

Barykin, A. Yu., The nature of self-locking in viscous clutch, *Vestnik Mashinostroeniya* (News of Machinebuilding), No. 7, pp. 12–14, 2001 (in Russian).

Bekker, M. G., *Introduction to Terrain-Vehicle Systems*, The University of Michigan Press, Ann Arbor, MI, 1969.

Belousov, B. N., Popov, S. D., *Wheeled Transport Super-Duty Vehicles*, M.S.T.U. named after Bauman Publishing House, 2006 (in Russian).

Boikov, P. I., Belov, S. M., Venzel L. I., Study of reliability and durability of differential of Belarus tractor, *Traktori I selhozmashini* (Tractors and Agriculture Implements), No. 2, pp. 6–9, 1969 (in Russian).

Boikov, V. P., Vantsevich, V. V., Lefarov, A. Kh., Striguniv, S. I., Traction characteristics of tires for agricultural tractors of 1.4 and 2.0 classes, *Traktori I selhozmashini* (Tractors and Agriculture Implements), No. 1, pp. 10–14, 1986 (in Russian).

Boikov, V. P., Sologub, A. M., Zhdanovich, C. I., Zelenij, P. V., *Unification and Building-Block Design of Tractors*, Adukaciya i Vyhavanne Publishing House, Minsk, Russia, 2003 (in Russian).

Brugel, E., Klein, H., Taureg, H., Williebald, K., Die visco-kupplung als bauelement in antriebssystemen, *Automobiltechnische Zeitschrift*, 88(12), 671–676.

Bryanskij, Y. A., *Handling of Heavy-Duty Automobiles*, Mashinostroenie Publishing House, Moscow, Russia, 1983 (in Russian).

Bud'ko, V. V., Study of optimal distribution of traction forces between the drive axles of a 4×4 tractor, *Auto- and Tractor Engineering*, No. 12, pp. 20–23, 1979 (in Russian).

Bussien, P., *Automotive Handbook*, Mashgiz Publishing House, Moscow, Russia, 1959 (translated from German, in Russian).

Cheok, K. C., Hoogterp, F. B., Fales, W. K., Kobayashi, K., Scaccia, S., Fuzzy logic approach to traction control design, SAE Paper No. 960957, Society of Automotive Engineers, Warrendale, PA, 1996.

Chudakov, E. A., *Rolling of Automobile Wheel*, Mashgiz Publishing House, Moscow, Russia, 1946.

Chudakov, E. A., *Circulation of Parasitic Power in Non-Differential Vehicle*, Mashgiz Publishing House, Moscow, Russia, 1950a (in Russian).

Chudakov, E. A., *Theory of Automobile*, State Publishing House of Machine-Building Literature, Moscow, Russia, 1950b (in Russian).

Chudakov, E. A. (Ed.), *Vehicle Engineering Handbook*, 3 volumes, Gosnauchtechizdat Publishing House, Moscow, Russia, 1951 (in Russian).

Chudakov, D. A., *Fundamentals of Theory and Calculations of Tractor and Automobile*, Kolos Publishing House, Moscow, Russia, 1972 (in Russian).

Claeys, X., Yi, J., Alvarez, L., Horowitz, R., Canudas de Wit, C., A new 3D dynamic tire/road friction model for vehicle control and simulation, IMECE2001/DSC-24528, New York, 2001.

Dick, W. M., All-wheel and four-wheel-drive vehicle systems, SAE publication, SP-1063 (952600), 69 p., 1995.

Divakov, I. V., Levin, I. A., Reasonable drives to the forward rear and reward rear axles of a 6×6 automobile, *Avtomobil'naya Promishlennost'* (Automobile Industry), No. 8, 1962 (in Russian).

Dixon, J. C., *Tires, Suspension and Handling*, 2nd edn., SAE Press, Warrendale, PA, 1996.

Draguniv, G. D., Semendyaev, K. N., A new transfer case for all-wheel drive vehicles, *Avtomobil'naya Promishlennost'* (Automobile Industry), No. 8, pp. 14–15, 2000 (in Russian).

Drakunov, S., Ozguner, U., Dix, P., Ashrafi, B., Variable structure control in automobile control systems. In: *Mechatronic Systems Techniques and Applications*, Vol. 2. *Transportation and Vehicular Systems*, Gordon & Breach, New York, pp. 387–410, 2000.

Echeistov, Yu.A., Selifonov, V. V., Impact of reactive arms' kinematics on traction force distribution among the tandem axles of a 3-axle automobile with positive engagement, *Avtomobil'naya Promishlennost'* (Automobile Industry), No. 4, pp. 24–25, 1967 (in Russian).

Esmailzadeh, E., Goodarzi, A., Vossoughi, G. R., Optimal yaw moment control law for improved vehicle handling, *Mechatronics*, No. 13, pp. 659–675, 2003.

Fal'kevich, B. S., *Theory of Automobile*, State Publishing House of Machine-Building Literature, Moscow, Russia, 1963 (in Russian).

Fancher, P, Winkler, C., Directional performance issues in evaluation and design of articulated heavy vehicles, *Vehicle System Dynamics*, 45, 7–8, 607–647, 2007.

Farobin, Y. E., *Theory of Transport Vehicles in Turn*, Mashinostroenie Publishing House, Moscow, Russia, 1970 (in Russian).

Farobin, Y. E., Shuplyakov, V. S., *Evaluation of Operational Properties of Vehicular Trains for International Transportation*, Transport Publishing House, Moscow, Russia, 1983 (in Russian).

Farobin, Y. E., Yakobashvili, A. M., Ivanov, A. M., Olitskij, V. S., Samoilenko, Y. A., *Three-Link Vehicular Trains*, Mashinostroenie Publishing House, Moscow, Russia, 1993 (in Russian).

Feltman, J., Ganley, J., Hamilton, S., Gradu, M., Mechatronic torque vectoring system with enhanced controllability for augmenting the vehicle agility and safety, SAE Paper No. 2006-01-0579, Society of Automotive Engineers, Warrendale, PA, 2006.

Feng, M., Ono, K., Mimura, K., Mixed EHL analysis of the variable torque slipping clutch with skewed rollers, *Journal of Tribology*, 125, 756–769, October 2003.

Filushkin, A. V., Bocharov, N. F., Pugin, P. P., Semenov, B. M., Influence of driveline system on fuel consumption of 3-axle automobile on a firm surface of motion, *Automobil'naya Promishlennost'* (Automobile Industry), No. 1, pp. 14–17, 1966.

Filushkin, A. V., Bocharov, N. F., Semenov, V. M., To unequal torque distribution among the axles of a 6×6 automobile, *Avtomobil'naya Promishlennost'* (Automobile Industry), No. 7, 1968 (in Russian).

Francis, Ph., Haselton, D., Pritchard, L., Pre-emptive torque management™ (PTM)™, SAE Paper No. 2006-01-0817, Society of Automotive Engineers, Warrendale, PA, 2006.

Frere, P., Historical survey of four-wheel drive, The Institution of Mechanical Engineers. International Conference All-Wheel Drive. *Proceedings of the Institution of Mechanical Engineers*,. London, U.K., No. 2, pp. 25–34, 1986.

Furunzhiev, R. I., Ostanin, A. N., *Control of Multi-Wheel Vehicle Vibrations*, Mashinostroenie Publishing House, Moscow, Russia, 1984 (in Russian).

Gao, X., Yu, Z., Xu, T., Longitudinal velocity estimation of electric vehicle with 4 in-wheel motors, SAE Paper No. 2008-01-0605, Society of Automotive Engineers, Warrendale, PA, 2008.

Gavrilenko, V. A., *Fundamentals of Involute Gearings*, Mashinostroenie Publishing House, Moscow, Russia, 1969 (in Russian).

Gee-Clough, D., Evernden, D. W., The empirical prediction of tractor implement field performance, *Journal of Terramechanics*, 15(2), 81–94, 1978.

Genta, G., *Motor Vehicle Dynamics: Modeling and Simulation*, World Scientific, Singapore, 1997.

Gillespie, T. D., *Fundamentals of Vehicle Dynamics*, SAE Press, Warrendale, PA, 1999.

Ginther, B., Kovalsky, Ch., Development of an AWD coupling and controls for a high performance sports car, SAE International AWD Vehicle Symposium, East Liberty, OH, August 21–24, 2006.

Glassmann, T., Barlage, J. A., Electronic torque manager (ETM®): An adaptive driveline torque management systems, SAE Paper No. 2004-01-0866, Society of Automotive Engineers, Warrendale, PA, 2004.

Gold, B. B., *Design of Automobiles*, Mashgiz Publishing House, Moscow, Russia, 1956 (in Russian).

Govindswamy, K., D'Anna, Th., Overcoming driveline noise, *Engine Technology International*, pp. 59–60, March 2004.

Gradu, M., Torque bias coupling for AWD applications, SAE Paper No. 2003-01-0676, Society of Automotive Engineers, Warrendale, PA, 2003.

Gradu, M., Harty, D., New mechatronic module for improved all wheel drive safety and dynamics, SAE International AWD Vehicle Symposium, East Liberty, OH, August 21–24, 2006.

Grecenko, A., Nove vysledky teorie rovinneho pohybu kola, *Zemedelska Technika*, 21 (XLVIII)(2), 507–524, 1979.

Grinchenko, I. V. et al., *High-Terrain Wheeled Automobiles*, Mashinostroenie Publishing House, Moscow, Russia, 1967 (in Russian).

Grishkevich, A. I. et al., *Design of Automobile Transmissions*, Handbook, Mashinostroenie Publishing House, Moscow, Russia, 1984 (in Russian).

Guskov, V. V. Making the 4WD more competitive: Some theoretical aspects of the performance vis a vis the 2WD, *Farm Machine Design Engineering*, pp. 42–48, December 1968.

Guskov, V. V. et al., *Tractors: Theory*, Mashinostroenie Publishing House, Moscow, Russia, 1988 (in Russian).

Guskov, V. V., Buimov, L. N., Theoretical issues of choosing a kinematic discrepancy and a driveline system for a 4 × 4 tractor with identical tires, *Proceedings of TsNIIMESH*, Minsk, Vol. VI, pp. 40–46, 1969 (in Russian).

Gustafsson, F., Monitoring tire-road friction using the wheel slip, *IEEE Control Systems*, pp. 42–49, August 1998.

Hall, L. C., The influence of limited slip differentials on torque distribution and steady state handling of four-wheel drive military vehicles, *International Conference All-Wheel Drive Vehicles*, London, U.K., pp. 59–66, March 5–6, 1986.

Hancock, M. J., Williams, R. A., Fina, E., Best, M. C., Yaw motion control via active differentials, *Transactions of the Institute of Measurement and Control*, 29(2), 137–157, 2007.

Harned, J. L., Johnston, L. E., Scharpf, G., Measurement of tire brake force characteristics as related to wheel slip (Antilock) control system design, SAE Paper No. 690214, Society of Automotive Engineers, Warrendale, PA, 1969.

Heinke, Raffinierter Allradantrieb, Kraftfahrzeugtechnik, BKD, 35(9), 282, 1985.

Heravi, O., An improved method for measuring the impact for axle-disconnect system on vehicle fuel economy, SAE International AWD Vehicle Symposium, East Liberty, OH, August 21–24, 2006.

Heravi, O., Fogelberg, M., Methodology to predict fuel economy benefits of secondary axle disconnects on four-wheel-drive/all-wheel-drive vehicles, SAE Paper No. 2005-01-0550, Society of Automotive Engineers, Warrendale, PA, 2005.

Higashimata, A., Adachi, K., Segawa, S., Kurugo, N., Waki, H., Development of a slip control system for a lock-up clutch, SAE Paper No. 2004-01-1227, Society of Automotive Engineers, Warrendale, PA, 2004.

Hoeck, M., Contribution of active torque management to vehicle safety and agility on the example of a front wheel drive MINI Cooper S in comparison of different driveline configurations, SAE International AWD Vehicle Symposium, East Liberty, OH, August 21–24, 2006.

Hoeck, M., Gasch, Ch., The influence of various 4WD driveline configurations on handling and traction on law friction surfaces, SAE Paper No. 1999-01-0743, Society of Automotive Engineers, Warrendale, PA, 1999.

Hohl, G. H., Military terrain vehicles, *Journal of Terramechanics*, 44(1), 23–34, 2007.

Horiuchi, Sh., Okada, K., Nohtomi, Sh., Improvement of vehicle handling by nonlinear integrated control of four wheel steering and four wheel torque, *JSAE Review*, 20, 459–464, 1999.

Huchtkoetter, H., Gassmann, Th., Vehicle dynamics and torque management devices, SAE Paper No. 2004-01-1058, Society of Automotive Engineers, Warrendale, PA, 2004.

Huchtkotter, H., Taureg, H., The effect of a viscous coupling used as a front-wheel drive limited-slip differential on vehicle traction and handling, SAE Paper No. 940875, Society of Automotive Engineers, Warrendale, PA, 1994.

Ivanovic, V., Herold, Z., Deur, J., Hancock, M., Assadian, F., Experimental setups for active limited slip differential dynamics research, SAE Paper No. 2008-01-0302, Society of Automotive Engineers, Warrendale, PA, 2008.

Ivens, J., Official fuel economy testing some practical aspects of dynamometer matching of the vehicle road load, SAE Paper No. 910038, Society of Automotive Engineers, Warrendale, PA, 1991.

Izvozchikov, V. S., Smirnov, G. A., Determination of power loss in units of drivetrain of 4-axle automobile, *Avtomobil'naya Promishlennost* (Automotive Industry), Moscow, Russia, No. 11, pp. 11–12, 1971 (in Russian).

Jackson, A., Brown, M., Crolla, D., Woodhouse, A., Parsons, M., Utilizing the potential of individual wheel control on a 6 × 6 off-road vehicle, IMECE2001/DE-23279, New York, 2001.

Jalali, K., Bode, K., Lambert, S., McPhee, J., Design of an advanced traction controller for an electric vehicle equipped with four direct driven in-wheel motors, SAE Paper No. 2008-01-0589, Society of Automotive Engineers, Warrendale, PA, 2008.

Jaskiewicz, Z., *Driving Axles*, Mashinostroenie Publishing House, Moscow, Russia, 1985 (in Russian).

Johansen, T., Petersen, I., Kalkkuhl, J., Ludermann, J., Gain-scheduled wheel slip control in automotive brake systems, *IEEE Transactions on Control Systems Technology*, 11(6), November 2003.

Johansson, R., Rantzer, A. (Eds.), *Nonlinear and Hybrid Systems in Automotive Control*, Springer-Verlag, London, U.K., 2003.

Karnopp, D., *Vehicle Stability*, Marcel Dekker, Inc., New York, 2004.

Karuzin, O. I., Selifonov, V. V., Bahmutov, S. V., *Influence of a Self-Locking Differential on Vehicle Rolling Resistance*, Safety and Reliability of Automobile, Moscow, Russia, pp. 44–54, 1980 (in Russian).

Katsigin, V. V., Gorin, G. S., Zenkovich, A. A., Kidalinskaya, G. V., Neverov, A. I., Orda, A. N., *Perspective Mobile Energy Vehicles for Agriculture*, Nauka i Technika Publishing House, Minsk, Russia, 1982a (in Russian).

Katsigin, V. V., Krinko, M. S., Melnikov, E. S., *Increasing Efficiency of Use of Tractor and Agriculture Implement Fleet*, Uradzhai Publishing House, Minsk, Russia, 1982b (in Russian).

Kelley, W., New technology for the management and distribution of torque in modern automotive drivetrains, SAE Paper No. 2005-01-0630, Society of Automotive Engineers, Warrendale, PA, 2005.

Kiencke, U., Nielsen, L., *Automotive Control Systems*, Springer and SAE, Warrandale, PA, 2000.

Klier, W., Reim, A., Stapel, D., Robust estimation of vehicle sideslip angle—An approach w/o vehicle and tire models, SAE Paper No. 2008-01-0582, Society of Automotive Engineers, Warrendale, PA, 2008.

Kochnev, E. D., *Encyclopedia of Military Automobiles, 1769-2006*, Za Rulem Publishing House, Moscow, Russia, 2006 (in Russian).

Komandi, G., Soil vehicle relationship: Tire peripheral force, *Journal of Terramechanics*, 43, 213–223, 2006.

Koo, J.-M., Choi, C. H., Huh, Y., Seok, C.-S., Development of a hydraulic limited slip differential system using a pressure generator, *International Journal of Automotive Technology*, 9(3), 323–327, 2008.

Korotonoshko, N. I., *Automobiles with Positively Locked and Differential Driveline Systems*, Mashgiz Publishing House, Moscow, Russia, 1948 (in Russian).

Korshunov, G. V., Shuklin, S. A., Influence of design parameters of interaxle differentials on their internal friction, *Avtomobil'naya Promishlennost'* (Automotive Industry), No. 9, pp. 15–18, 1982 (in Russian).

Kotte, G., Allradantrieb fur nutzfahrzeuge und baumaschinen auf reifenfahrwezeuge im gelandeschwereinsatz, *Baugewerbe*, 59(24), 34–35, 1979.

Krick, G., Behaviour of tires driven in soft ground with side slip, *Journal of Terramechanics*, 9(4), 9–30, 1973.

Krut'ko, P. D., *Control of Robot Actuators*, Science Publishing House, Moscow, Russia, 1991.

Krut'ko, P. D., *Inverse Dynamics Problems in Theory of Automation Control*, Mashinostroenie Publishing House, Moscow, Russia, 2004 (in Russian).

Ksenevich, I. P., Solonskij, A. S., Voichinskij, S. M., *Designing Farm Tractors*, Nauka i Technika Publishing House, Minsk, Russia, 1980 (in Russian).

Lavrinovich, M. F., Shusternyak, M. M., *Improvement of Resistance to Wear of Automobile Components*, Belarus Publishing House, Minsk, Russia, 1985 (in Russian).

Lee, H., Tomizuka, M., Adaptive vehicle traction force control for intelligent vehicle highway systems (IVHSs), *IEEE Transactions on Industrial Electronics*, 50(1), 37–47, February 2003.

Lee, Ch., Hedrick, K., Yi, K., Real-time slip-based estimation of maximum tire-road friction coefficient, *IEEE/ASME Transactions on Mechatronics*, 9(2), June 2004.

Lefarov, A. Kh., New locking differentials, *Avtomobil'naya Promishlennost* (Automotive Industry), No. 12, 1960 (in Russian).

Lefarov, A. Kh., Fuel efficiency of the truck MAZ-501 with an interaxle differential, *Avtomobil'naya Promishlennost'* (Automotive Industry), No. 8, pp. 19–21, 1966 (in Russian).

Lefarov, A. Kh., *Differentials of Automobiles and Trucks*, Mashinostroenie Publishing House, Moscow, Russia, 1972 (in Russian).

Lefarov, A. Kh., Power loss of an automobile with positive interaxle engagement, *Avtomobil'naya Promishlennost'* (Automobile Industry), No. 5, pp. 14–15, 1979 (in Russian).

Lefarov, A. Kh., Andreev, A. F., Study of locking differentials with frictional dick clutches, *Avtomobil'naya Promishlennost'* (Automobile Industry), No. 10, 1969 (in Russian).

Lefarov, A. Kh., Atamanov, Yu.E., Influence of the interaxle driveline system on stability of motion 4×4 automobile in turn, *Avtomobil'naya Promishlennost'* (Automobile Industry), No. 2, 1972 (in Russian).

Lefarov, A. Kh., Kabanau, V. I., Slip power loss in a 4×4 tractor with positive engagement of the axles, *Tractory i Selhozmashiny* (Tractors and Agriculture Machines), No. 12, 1971, (in Russian).

Lefarov, A. Kh., Kabanau, V. I., Slip power loss in a 4×4 tractor with positively engaged interaxle drive, *Tractory I Selkhozmashiny* (Tractors and Agriculture Machines), No. 12, pp. 16–18, 1975 (in Russian).

Lefarov, A. Kh., Andreev, A. F., Vasil'ev, V. T., Kabanau, V. I., Symmetrical locking differential and its properties, *Tractory i Selhozmashiny* (Tractors and Agriculture Machines), No. 9, 1967, (in Russian).

Lefarov, A. Kh., Kabanau, V. I., Strigunov, S. I., To problem of tire slip power loss of a 4×4 wheeled tractor, *Traktory I Sel'hozmashiny* (Tractors and Agriculture Machines), No. 7, pp. 9–11, 1979 (in Russian).

Lefarov, A. Kh., Vantsevich, V. V., Andreev, A. F., Atamanov, Yu.E., Research of turnability of multi-wheel drive vehicles, Technical Report, 1297/81, Belarusian National Technical University, Minsk, Russia, 1984 (in Russian).

Lefarov, A. Kh., Vantsevich, V. V., Andreev, A. F., Atamanov, Yu.E., Bud'ko, V. V., Kabanau, V. I., Development, research and implementation of complex methods for advancing designs of multi-wheel drive tractors and trucks with the purpose of improving their productivity, fuel efficiency, and handling, Technical Report, GB 81-15, Belarusian National Technical University, Minsk, Russia, 1986 (in Russian).

Lefarov, A. Kh., Vantsevich, V. V., Kabanau, V. I., Valyuzhenich, G. A., Ignatovich, A. I., Development and implementation in production of designs and computational methods of differential mechanisms with improved life service and reliability for heavy-duty and super heavy-duty automobiles, Technical Report, 515/86, Belarusian National Technical University, Minsk, Russia, 1988 (in Russian).

Lefarov, A. Kh., Vantsevich, V. V., Kabanau, V. I., Valyuzhenich, G. A., Ignatovich, A. I., Research of internal working processes of the interaxle differential of 6×4 MAZ-6422 and development of recommendations on improving its service life, Technical Report, 946/88, Belarusian National Technical University, Minsk, Russia, 1990a (in Russian).

Lefarov, A. Kh., Vantsevich, V. V., Andreev, A. F., Atamanov, Yu.E., Bud'ko, V. V., Traction properties, fuel efficiency, and turnability of tractors of 1.4-2.0 traction class and of power-module driven vehicular trains. Driveline influence, Technical Report, GB 86-03, Belarusian National Technical University, Minsk, Russia, 1990b (in Russian).

Lefarov, A. Kh., Vysotski, M. S., Vantsevich, V. V., Kabanau, V. I., *Energy Loading and Reliability of Differentials of Transport and Traction Vehicles*, Nauka i Technika Publishing House, Minsk, Russia, 1991 (in Russian).

Levin, M. A., Fufaev, N. A., *Theory of Rolling of Deformable Wheel*, Science Publishing House, Moscow, Russia, 1989 (in Russian).

Lew, J., Piyabongkarn, D., Grogg, J., Minimizing dynamic rollover prosperity with electronic limited slip differentials, SAE Paper No. 2006-01-1279, Society of Automotive Engineers, Warrendale, PA, 2006.

Lewis, R. P., O'Brien, L. J., Limited slip differentials, *SAE Transactions*, 67, pp. 203–212, 1959.

Li, L., Wang, F.-Y., Zhou, Q., Integrated longitudinal and lateral tire/road friction modeling and monitoring for vehicle motion control, *IEEE transactions on Intelligent Transportation Systems*, 7(1), 1–19, March 2006.

Li, K., Misener, J. A., Hedrick, K., On-board road condition monitoring system using slip-based tire-road friction estimation and wheel speed signal analysis, *Journal of Multi-body Dynamics*, Part K, 221(Special Issue), 129–146, 2007.

Lintinov, A. S., *Handling and Stability of Automobile*, Mashinostroenie Publishing House, Moscow, Russia, 1971 (in Russian).

Lisov, M. I., *Cardan Mechanisms*, Mashgiz Publishing House, Moscow, Russia, 1945 (in Russian).

Litvinov, A. S., Farobin, Y. E., *Automobile: Theory of Operational Properties*, Mashinostroenie Publishing House, Moscow, Russia, 1989 (in Russian).

Liu, Ch.-S, Monkaba, V., Tan, H., McKenzie, C., Lee, H., Suo, S., Driveline torque-bias-management modelling for vehicle stability control, SAE Paper No. 2002-01-1584, Society of Automotive Engineers, Warrendale, PA, 2002.

Lur'e, Z.Ya., Saenko, V. P., Operational volume of gerotor hydraulic machines, *Vestnik Mashinostroenia* (News of Machinebuilding), No. 2, pp. 11–13, 2002 (in Russian).

Maki, R. et al., Limited slip wet clutch transmission fluid for AWD differentials; Part 1: System requirements and evaluation methods, SAE Paper No. 2003-01-1980, Society of Automotive Engineers, Warrendale, PA, 2003.

Maki, R. et al., Measurement and characterization of anti-shudder properties in wet clutch applications, SAE Paper No. 2005-01-0878, Society of Automotive Engineers, Warrendale, PA, 2005.

Margolis, S. Ya., *Axles of Automobiles and Vehicular Trains*, Mashinostroenie Publishing House, Moscow, Russia, 1983 (in Russian).

Margolis, D. L., Frank, A. A., Morimoto, K., Directional stability augmentation for all wheel drive vehicles, SAE Paper No. 880701, Society of Automotive Engineers, Warrendale, PA, 1988.

McCann, M. K., All wheel drive increases payload, *Automotive Industries*, 162(2), 19, 21, 1982.

Milliken, W. F., Milliken, D. L., *Race Car Vehicle Dynamics*, SAE Press, Warrendale, PA, 1995.

Mohan, S., Comprehensive theory of viscous coupling operation, SAE Paper No. 2004-01-0867, Society of Automotive Engineers, Warrendale, PA, 2004.

Mohan, S., Four wheel steering and vehicle stability enhancement, International CTI Forum, Nurtingen, Germany, October 22–23, 2007.

Mohan, S., Ramarao, B., A comprehensive study of self-induced torque amplification in rotary viscous couplings, *Journal of Tribology*, 125, 110–120, January 2003.

Mohan, S., Williams, R. C., A survey of 4WD traction control systems and strategies, SAE Paper No. 952644, Society of Automotive Engineers, Warrendale, PA, 1995.

Mortimer, J., Torque vectoring for improved vehicle dynamics and responsiveness, *Autotechnology*, No. 1, pp. 30–32, 2002.

Mudrov, A. G., Kazan's school of theory of mechanisms and machines, *Vestnik Mashinostroenia* (News of Machinebuilding), No. 2, pp. 73–77, 2002 (in Russian).

Muller, S., Uchanski, M., Hedrick, K., Estimation of the maximum tire-road friction coefficient, *Journal of Dynamic Systems, Measurements, and Control*, 125, 607–617, December 2003.

Murillo-Soto, F., Smith, J. L., Traction efficiency of 4WD tractors, *ASAE Transactions*, 21(6), 1051–1053, 1978.

Muro, T., O'Brien, J., *Terramechanics: Land Locomotion Mechanics*, A. A. Balkema Publishers, Tokyo, Japan, 2004.

Mutoh, N., Saitoh, T., Sasaki, Y., Driving force control method to perform slip control in cooperation with the front and rear wheels for front-and-rear wheel-independent-drive-type EVs (*FRID EVs*), Proceedings of the 11th International IEEE Conference on Intelligent Transportation Systems, Beijing, China, October 12–15, 2008.

Newton, I., *Mathematical Principles of Natural Philosophy*, Vol. 1, University of California Press, Berkeley and Los Angeles, CA, 1962.

Ohba, M., Suzuki, H., Yamamoto, T., Development of a new electronically controlled 4WD system: Toyota active torque control 4WD, SAE Paper No. 1999-01-0744, Society of Automotive Engineers, Warrendale, PA, 1999.

Okcuoglu, M. N., A descriptive analysis of gerodisc type limited slip differentials and all wheel drive couplings, SAE Paper No. 952642, Society of Automotive Engineers, Warrendale, PA, 1995.

Olley, M., Stable and unstable steering, General Motors (Report), 1934.
Olley, M., Road manners of the modern car, *Proceedings of the Institution of Automobile Engineers*, Vol. 32, 1937–1938.
Opeiko, F. A., *Wheeled and Track Systems*, Publishing House of Belarus Academy of Sciences, Minsk, Russia, 1960 (in Russian).
Osborn, R., Shim, T., Independent control of all-wheel-drive torque distribution, SAE Paper No. 2004-01-2052, Society of Automotive Engineers, Warrendale, PA, 2004.
Ostrovtsev, A. N., *Fundamentals of Automobile Design*, Mashinostroenie Publishing House, Moscow, Russia, 1968 (in Russian).
Pacejka, H. B., *Tire and Vehicle Dynamics*, SAE Press, Warrendale, PA, 2002.
Paul, M., Pelchen, Ch., Rosemeier, Th., Networking of driveline and chassis, *AutoTechnology*, No. 2, pp. 56–59, 2005.
Pelchen, Ch., Granzow, C., Kubalczyk, R., Peter. R., Enhancement of vehicle agility and safety by means of wheel torque based driving, SAE International AWD Vehicle Symposium, East Liberty, OH, August 21–24, 2006.
Petrushov, V. A., Generalized method to evaluate rolling resistance of automobiles and vehicular trains with different driveline systems, *Avtomobil'naya Promishlennost'* (Automobile Industry), No. 7, 1965 (in Russian).
Petrushov, V. A., Shuklin, S. A., Moskovkin, V. V., *Rolling Resistance of Automobiles and Trucks*, Mashinostroenie Publishing House, Moscow, Russia, 1975 (in Russian).
Pirkovskij, Ju. V., Some issues in automobile wheel rolling, *Avtomobil'naya Promishlennost'* (Automobile Industry), No. 12, pp. 26–29, 1965 (in Russian).
Pirkovskij, Ju. V., General formula of rolling resistance power of an all-wheel drive automobile, *Avtomobil'naya Promishlennost'* (Automobile Industry), No. 1, pp. 34–35, 1973 (in Russian).
Pirkovskij, Y. V., Shukhman, S. B., *Theory of Motion of Multi-Wheel Drive Automobile*, 2nd edn., UNITY and ELIT Publishing House, Moscow, Russia, 2001 (in Russian).
Pirkovskij, Ju. V., Plisko, V. A., Shuklin, S. A., Capabilities in optimization of vehicle design parameters, *Avtomobil'naya Promishlennost'* (Automobile Industry), No. 9, 1980 (in Russian).
Platonov, V. F., *All-Wheel Drive Automobiles*, 2nd edn., Mashinostroenie Publishing House, Moscow, Russia, 1989 (in Russian).
Poletaev, A. F., *Fundamentals of Rolling Resistance and Traction of a Rigid Wheel on a Deformable Surface*, MAMI Press, Moscow, Russia, 1967.
Polungian, A. A. et al., *Design of All-Wheel Drive Vehicles*, Publishing House of M.S.T.U. named after Bauman, vol. 1–3, 2008 (in Russian).
Polungian, A. A. et al., Determination of rolling resistance torque of the drive wheel when an automobile is overcoming a single bump, *Avtomobil'naya Promishlennost'* (Automobile Industry), No. 4, pp. 12–14, 1980 (in Russian).
Post, B., Kang, X., Klaus, Th., The influence of direct yaw control awd systems on vehicle stability and response in all driving conditions, SAE Paper No. 2008-01-0591, Society of Automotive Engineers, Warrendale, PA, 2008.
Preukschat, A., *Fahrwerktechnik: Antriebsarten*, Vogel-Buchverlag, Wurzuburg, 1985.
Reece, A. R., Principles of soil-vehicle mechanics, *Proceedings of the Institutions of Mechanical Engineers*, vol. 180, part 2A, 1965–66.
Reimers, A. P., *Fundamentals of Machine Design*. Handbook, Mashinostroenie Publishing House, Moscow, Russia, 1962 (in Russian).
Reshetov, D. N., *Components of Machines*, Mashinostroenie Publishing House, Moscow, Russia, 1974 (in Russian).
Richter, R., Hoffman, B., Probleme des einsatres von fahrzeugen auf landwirtschaftlich genutztem boden, *Agrartechnik*, 31(9), 419–421, 1981.
Rompe, K., Prinzipieler vergleich moderner konzepte fur den allradantrieb von PKW, AFO/GU/VU. *Verkehrsunfall und Fahrzeugtechnik*, 24(11), 313–319, 1986.

Sawase, K., Inoue, K., Classification and characteristic analysis of right-and-left torque vectoring mechanisms based on velocity diagram, 11th International DVI Congress, Tires-Chassis-Road 2007, Hanover, Germany, October 23–24, 2007.

Sawase, K., Sano, Y., Application of active yaw control to vehicle dynamics by utilizing driving/braking force. *JSAE Review*, 20, 289–95, 1999.

Sawase, K., Ushiroda, Yu., Miura, T., Left-right torque vectoring technology as the core of super all wheel control (S-AWC), Mitsubishi Motors, Technical Review, No. 18, pp. 16–23, 2006.

Scarlett, M., Awesome foursome, Vehicle Dynamics International, No. 1, p. 34–36, 2006.

Schuler, O. E., Mehr zugleistung durch allradantrieb mit selbsperrdiffeential, *Zandtechn*, 30(2), 138–140, 1979.

Segel, L., Force and moment response of pneumatic tires to lateral motion inputs, *Transactions of ASME-Engineering for Industry*, pp. 37–44, February 1966.

Selifonov, V. V., Karuzin, O. I., To problem of choosing rational locking degree of a passenger car differential, *Avtomobil'naya Promishlennost'* (Automobile Industry), No. 8, pp. 20–22, 1975 (in Russian).

Shabarov, A. A., Some issues of steady rolling of a pneumatic drive wheel, Study of Wheeled Tractors' Running Gears (Works of NATI), No. 212, pp. 3–30, 1971 (in Russian).

Shalyagin, V. N., *Transport and Transport-Technological Vehicles of Improved Mobility*, Agropromizdat Publishing House, 1986, (in Russian).

Shetty, R. R., Arnold, L. B., Eriksen, A., Progressive traction control for automotive differentials, SAE Paper No. 2000-01-3465, Society of Automotive Engineers, Warrendale, PA, 2000.

Shibly, H., Iagnemma, K., Dubowsky, S., An equivalent soil mechanics formulation for rigid wheels in deformable terrain, with application to planetary exploration rovers, *Journal of Terramechanics*, 42, 1–13, 2005.

Shih, Sh., Bowerman, W., An evaluation of torque bias and efficiency of torsen differential, SAE Paper No. 2002-01-1046, Society of Automotive Engineers, Warrendale, PA, 2002.

Shishkarev, M. P., Distribution of load in N. D. Verner's clutch and its parameter choice, *Vestnik Mashinostrieniya* (News of Machinebuilding), No. 6, pp. 8–11, 2001a (in Russian).

Shishkarev, M. P., Limitations for choosing parameters of some adaptive frictional clutches, *Vestnik Mashinostrieniya* (News of Machinebuilding), No. 7, pp. 8–11, 2001b (in Russian).

Showalter, D., Development of a compact torque vectoring axle for primary or secondary axles, SAE Paper No. 2008-01-0305, Society of Automotive Engineers, Warrendale, PA.

Shukhman, S. B., Solov'ev, V. I., Prochko, E. I., *Theory of Power Drive to Wheels of Off-Road Automobiles*, S. B. Shukhman (Ed.), Agrobusiness Publishing House, Moscow, Russia, 2007 (in Russian).

Shuklin, S. A., To problem of choosing toque bias for interwheel differentials of high mobility automobiles, Proceedings of NAMI, No. 181, pp. 62–72, 1980 (in Russian).

Shyrokau, B. N., Happawana, G. S., Vantsevich V. V., Generalized model and computational algorithm for modeling passive driveline systems of AWD automobiles, ASME Congress, Boston, October 31–November 6, 2008.

Sigl, A., Demel, H., ABS-traction control, state of the art and some prospects, SAE Paper No. 900204, Society of Automotive Engineers, Warrendale, PA, 1990.

Sistem ital design di trazione integrale con differenziale intermedio, *ATA Ingegneria Automotoristica*, 34(11–12), 701–702, 1981.

Skoibeda, A. T., *Automation of Vehicle Running Gears*, Nauka i Techinika Publishing House, Minsk, Russia, 1979 (in Russian).

Smirnov, G. A., *Theory of Motion of Ground Vehicles*, Mashinostroenie Publishing House, Moscow, Russia, 1990 (in Russian).

Smirnov, G. A., Lelikov, O. P., Distribution of torques between wheels of a four-axle automobile moving on deformable grounds, *Avtomobil'naya Promishlennost'* (Automobile Industry), No. 4, pp. 19–21, 1970 (in Russian).

Smirnov, V. I., Artyushenko, A. D., Mitropan, D. M., Prokhorov, V. P., To the problem of torque redistribution among the axle wheels, *Vestnik XPI*, 3(120), 55–58, 1976 (in Russian).

Smirnov, G. A., Kupreyanov, A. A., Guchkov, D. K., Ignatushkin, A. P., Popov, S. D., Choosing rational transmission–wheels systems, *Avtomobil'naya Promishlennost'* (Automobile Industry), No. 5, pp. 15–17, 1984 (in Russian).

Society of Automotive Engineers, *All-Wheel Drive Systems Classification*, SAE J1952, Warrendale, PA, November 2003.

Society of Automotive Engineers, *Vehicle Dynamics Terminology*, SAE J670e, Warrendale, PA, 1976.

Steiner, M., Analyse, synthese und berechnungs methoden der friebkraft-schlupfkurve der luftreifen auf nachgiebigem boden, Technische Universitat, Munchen, 177 p., 1979.

Steinkampf, H., Die auswirkungen un terschiedlicher umfangsgeschwidigkeiten der rader eines allradschleppers auf seine zugfahigkeit, Grundlagen der Landtechnik, Bd. 22, No. 16, pp. 166–170, 1972.

Stepaniuk, P. N., Izrailevich, L. S., Study of symmetry of locking performance of an interwheel limited differential with disk friction clutch, *Tractory I Selkhozmashini* (Tractors and Farm Implements), No. 2, 1979 (in Russian).

Stepanova, E. A., Lefarov, A. Kh., *Locking Differentials of Trucks*, State Publishing House of Machine-Building Literature, Moscow, Russia, 1960 (in Russian).

Strigunov, S. I., Computing velocity of a 4×4 tractor with differential driveline system, *Automobile and Tractor Building*, No. 19, pp. 93–97, 1984 (in Russian).

Strigunov, S. I., Krivitskij, A. M., Kinematic discrepancy in tractors' interaxle driveline, *Design and operation of Automobiles and Tractors*, No. 3, pp. 74–76, 1988 (in Russian).

Strigunov, S. I., Vantsevich, V. V., Lefarov, A. Kh., Evaluation of mobility of wheeled tractors, Vehicle Mobility Issues, Blagoveshcensk, pp. 123–128, 1987 (in Russian).

Taborek, J. J., Mechanics of vehicle–1 through 14, Machine Design, May through December, 1957.

Takemura, T., Niikura, Y., An analysis of viscous coupling torque transmission characteristics and hump phenomenon, SAE Paper No. 900558, Society of Automotive Engineers, Warrendale, PA.

Teraoka, M., Development of the electro-magnetic controlled limited slip differential unit (EMCD), SAE Paper No. 931023, Society of Automotive Engineers, Warrendale, PA.

Tokarev, A. A., *Fuel Efficiency and Traction and Velocity Properties of Automobile*, Mashinostroenie Publishing House, Moscow, Russia, 1982 (in Russian).

Transmissions, Transfer cases, Power take offs, Catalog, TsNIITEIAutoprom, 1998 (in Russian).

Trucks and Buses, *AvtoRevyu*, No 22, p. 126, December 2006 (in Russian).

Tsitovich, I. S., Algin, V. B., *Dynamics of Automobile*, Nauka i Technika Publishing House, Minsk, Russia, 1981 (in Russian).

Tsitovich, I. S., Kanonik, I. V., Vavulo, V. A., *Automobile Transmissions*, Nauka i Technika Publishing House, Minsk, Russia, 1979 (in Russian).

Ul'yanov, N. A., *Wheel Systems of Earth-Moving and Road Vehicles*, Mashinostroenie Publishing House, Moscow, Russia, 1982 (in Russian).

Usui, H., Nishikura, Sh., Takematsu, K., Analysis of part-time four-wheel drive vehicle, SAE Paper No. 820743, Society of Automotive Engineers, Warrendale, PA, 1982.

Vakhrushev, Yu. M., Kalashnik, V. T., Self-locking differentials with hydraulic resistance, *Avtomobil'naya Promishlennost'* (Automobile Industry), No. 1, 1966 (in Russian).

Valeev, D. Kh., Kozadaev, A. I., Kuznetsov, V. Ya., Smirnov, I. G., New units of KamAZ trucks, *Avtomobil'naya Promishlennost'* (Automobile Industry), No. 4, pp. 11–17, 1997 (in Russian).

Vantsevich, V. V., Synthesis of driveline systems for multi-wheel drive vehicles, DSc dissertation in Automotive Engineering, The Higher Awarding Committee of the Russian Federation, 1992 (in Russian).

Vantsevich, V. V., A new effective research direction in the field of actuating systems for multi-drive vehicles, *International Journal of Vehicle Design* (UK), 15(3/4/5), 337–347, 1994.

Vantsevich, V. V., Mathematical fundamentals for vehicle performance control, *Proceedings of 2004 Global Congress on Powertrain*, pp. 60–63, Dearborn, September 28–30, 2004a.

Vantsevich, V. V., All-wheel drive vehicle energy efficiency evaluation. SAE Paper No. 2004-01-0864, Society of Automotive Engineers, Warrendale, PA, 2004b.

Vantsevich, V. V., All-wheel driveline mechatronic systems: principles of wheel power management, SAE Paper No. 2006-01-0580, Society of Automotive Engineers, Warrendale, PA, 2006a.

Vantsevich, V. V., Inverse wheel dynamics, IMECE Paper No. 2006-13787, *ASME Congress*, Chicago, IL, November 5–10, 2006b.

Vantsevich, V. V., Multi-wheel drive vehicle energy/fuel efficiency and traction performance: Objective function analysis, *Journal of Terramechanics*, 44(3), 239–353, 2007.

Vantsevich, V. V., Power losses and energy efficiency of multi-wheel drive vehicles: A method for evaluation, *Journal of Terramechanics*, 45(3), 89–101, 2008.

Vantsevich, V. V., Amani, L., Control of the vehicle's running abilities is a pre-condition for designing wheel drive systems, *ASME Annual Congress*, New York, 2001.

Vantsevich, V. V., Stuart, Ch., Probabilistic interaction between vehicle and surroundings: Modelling for control, IMECE2007-44071, ASME Congress, Seattle, WA, November 10–16, 2007.

Vantsevich, V. V., Lefarov, A. Kh., Kabanau, V. I., Pupeiko, A. I., Development of limited slip differentials for 4×4 loaders of 95.7 kW and of computer software for automated computation of traction performance, Technical Report, 574, Belarusian National Technical University, Minsk, Russia, 1989 (in Russian).

Vantsevich, V. V., Lefarov, A.Kh., Kabanau, V. I., Voiteshonok, V. S., Pupeiko, A. I., Research and development of interaxle differentials with improved performance for KrAZ-6437 truck, Technical Report, 2299/90, Belarusian National Technical University, Minsk, Russia, 1993 (in Russian).

Vantsevich, V. V., Vysotski, M. S., Zakevskij, A. D., Control of differentials of multi-wheel trucks, Scientific Center for Machine Mechanics Problems, National Academy of Sciences of Belarus, Minsk, Russia, 1994 (in Russian).

Vantsevich, V. V., Vysotski, M. S., Gileles, L. Kh., Kharytonchyk S. V., Development of theory and computational methodologies of mobile machines on the basis of identification of critical conditions of dynamic systems/designs, and computer and hardware simulation of the surroundings and internal dynamics, Technical Report: Optimization of mass and geometric parameters of mobile machines for traction and acceleration performance control, National Academy of Science of Belarus, Research Program 37 ''Mechanics,'' 1996 (in Russian).

Vantsevich, V. V., Andreev, A. F., Kabanau, V. I., Voiteshonok, V. S., Kharytonchyk, S. V., Improving traction and energy efficiency of an 8×8 vehicle by developing limited slip differentials with universal characteristics and by developing a computer imitator of a traction force control system, Technical Report, 21/95, Belarusian National Technical University, Minsk, Russia, 1997a (in Russian).

Vantsevich, V. V., Vysotski, M. S., Gileles, L. Kh., Kharytonchyk S. V., Development of theory and computational methodologies of mobile machines on the basis of identification of critical conditions of dynamic systems/designs, and computer and hardware simulation of the surroundings and internal dynamics, Technical Report: Math modeling, computational algorithms and computer software products for controlling traction and acceleration performance of mobile machines on the basis of synthesis of optimal mass and geometric parameters, National Academy of Science of Belarus, Research Program 37 ''Mechanics,'' 1997b (in Russian).

Vantsevich, V. V., Kharytonchyk, S. V., Happawana, G. S., Nwokah, O. D. I., Basis for logical control of circumferential wheel forces of highway trucks for improved traction and fuel efficiency, SAE Paper No. 980790, Society of Automotive Engineers, Warrendale, PA, 1998a.

Vantsevich, V. V., Vysotski, M. S., Gileles, L. Kh., *Mobile Transport Machines: Interaction with the Environment*, Belaruskaya Navuka Publishing House, Minsk, 1998b (in Russian).

Vantsevich, V. V., Vysotski, M. S., Gileles, L. Kh., A new direction in the development of the theory of motion of mobile machines, *Avtomobil'naya Promishlennost* (Automotive Industry), Moscow, Russia, No. 3, pp. 6–8, 1998c (in Russian).

Vantsevich, V. V., Vysotski, M. S., Kharytonchyk S. V., Control of wheel dynamics, *SAE 1998 Transactions*. SAE Paper No. 980242, 1998d.

Vantsevich, V. V. Vysotski, M. S., Gileles, L. Kh., Control of Traction and Velocity Performance of Automobiles: Optimization of Mass and Geometric Parameters, Belaruskaya Navuka Publishing House, Minsk, 1998e (in Russian).

Vantsevich, V. V., Vysotski, M. S., Gileles, L. Kh., Kharytonchyk S. V., Doubovik, D. A., Develop methodologies and technical designs for optimal distribution of traction forces for a 8 × 8 vehicle for improving its mobility and traction performance, Technical Reports: Development of a limited slip differential, National Academy of Science of Belarus, BelAutoTractorBuilding Research Program, 1999–2000 (in Russian).

Vantsevich, V. V. et al., Vehicle dynamics as the second dynamics problem, *International Journal of Vehicle Design* (UK), 25(3), 164–169, 2001.

Vantsevich, V. V., Howell, S. K., Vysotski, M. S., Kharytonchyk, S. V., An integrated approach to autonomous vehicle systems: Theory and implementation, *International Journal of Vehicle Autonomous Systems* (UK), Special Issue, pp. 271– 279, 2003a. (Guest Editor, V. Vantsevich).

Vantsevich, V. V., Lomako, G., Opeiko, A. F., 2003, Interaction between autonomous vehicles and road surface, *International Journal of Vehicle Autonomous Systems* (UK), 1(3/4), 291–308, Special Issue, 2003b (Guest Editor, V. V. Vantsevich).

Vantsevich, V. V., Vysotski, M. S., Doubovik, D. A., Wheel power control as a tool to control vehicle dynamics, *Avtomobil'naya Promishlennost* (Automotive Industry), No. 1, 2004 (in Russian).

Vantsevich, V. V., Barz, D., Kubler, J., Schumacher, A., Tire longitudinal elasticity and effective rolling radii: Experimental method and data. SAE Paper No. 2005-01-1823, Society of Automotive Engineers, Warrendale, PA, 2005.

Vantsevich, V. V., Zakrevskij, A. D., Kharytonchyk, S. V., Heavy-duty truck: Inverse dynamics and performance control, IMECE2007-42659, *ASME Congress*, Seattle, WA, November 10–16, 2007.

Vantsevich, V. V., Henke, S., Modeling and simulation of direct/inverse dynamics of a wheel, 11th Mechatronics Forum-Conference, IMechE and University of Limerick, Ireland, June 23–25, 2008a.

Vantsevich, V. V., Shyrokau, B. N., Autonomously operated power-dividing unit for driveline modeling and AWD vehicle dynamics control, 1st Annual ASME Dynamic Systems and Control Conference, University of Michigan, Ann Arbor, MI, October 20–22, 2008b.

Vantsevich, V. V., Vysotski, M. S., Doubovik, D. A., Control of the wheel driving forces as the basis for controlling off-road vehicle dynamics, *SAE 2002 Transactions–Journal of Commercial Vehicles*, pp. 452–459.

Virabov, R. V., *Traction Performance of Friction Transmissions*, Mashinostroenie Publishing House, Moscow, Russia, 1982 (in Russian).

Voiteshonok, V. S., Transfer case for all-wheel drive tractors belarus, *Design and Operation of Automobiles and Tractors*, No. 4, pp. 51–54, 1989 (in Russian).

Vysotski, M. S., Belenkij, U. Uy., Moskovkin, V. V., *Fuel Efficiency of Automobiles and Vehicular Trains*, Nauka i Tehnika Publishing House, Minsk, Russia, 1984 (in Russian).

Vysotski, M. S., Gileles, L. Kh., Khersonskij, S. G., *Lorry Trucks*, 2nd edn., Mashinostroenie Publishing House, Moscow, Russia, 1995 (in Russian).

Watanabe, K., Yamakawa, J., Saaki, T., Turning characteristics of multi-axle vehicles, *Journal of Terramechanics*, 44(1), 81–87, 2007.

Weber, R., Beitrag zum ubertragundsverhalten zwischen achlupf und reifenfuhrungskraften, *Automobil Industrie*, 26(4), 449–458, 1981.

West, R. S., Haselton, D., Approaches to achieving AWD torque accuracy, SAE Paper No. 2008-01-0303, Society of Automotive Engineers, Warrendale, PA, 2008.

Wheals, J. C., Baker. H., Ramsey, K., Turner, W., Torque vectoring AWD driveline: Design, simulation, capabilities and control, SAE Paper No. 2004-01-0863, Society of Automotive Engineers, Warrendale, PA, 2004.

Williams, B., Active mate?, *Vehicle Dynamics International*, No. 2, p. 54, 2005.

Williams, R. C., 4WD market trends in vehicle & the adaptations of new technology in the international automotive community, SAE Paper No. 1999-01-1264, Society of Automotive Engineers, Warrendale, PA, 1999.

Williams, R. C., 4WD—AWD market trends in vehicles and technology differences and similarities, from 1997 to 2004 primarily in the US market, and also some global comparisons, SAE Paper No. 2006-01-0822, Society of Automotive Engineers, Warrendale, PA, 2006.

Williams, R. C., Socin, R. J., Varma, S. K., A building block approach for understanding four wheel drive systems: past-present-future, SAE Paper No. 1999-01-1264, Society of Automotive Engineers, Warrendale, PA, 1995.

Wilson, R., A Foray of 4Matics, *Automotive Industries*, February, pp. 53–54, 2003.

Wong, J. Y., Optimization of the tractive performance of four-wheel-drive off-road vehicles, *SAE Transactions*, 79, 2238–2244, 1970.

Wong, J. Y., *Theory of Ground Vehicles*, 3rd edn., Wiley, New York, 2001.

Wong, J. Y., McLaughlin, N. B., Knezevic, Z., Burtt, S., Optimization of the tractive performance of four-wheel-drive tractors—Theoretical analysis and experimental substantiation, *Journal of Automobile Engineering*, *Proceedings of the Institution of Mechanical Engineers, Part D*, 212(D4), 285–297, 1998.

Wong, J. Y., Zhao, Z., Li, J., McLaughlin, N. B., Burtt, S., Optimization of the tractive performance of the four-wheel-drive tractors—Correlation between analytical predictions and experimental data, SAE Paper No. 2000-01-2596, Society of Automotive Engineers, Warrendale, PA, 2000.

Yamada, M., Oshima, T., Ueda, K., Horiba, I., Yamamoto, Sh., A study of the road surface condition detection technique for deployment on a vehicle, *JSAE Review*, 24, 183–188, 2003.

Yamakawa, J., Watanabe, K., A method of optimal wheel torque determination for individual wheel drive vehicles, *Journal of Terramechanics*, 43, 269–285, 2006.

Yatsenko, N. N., *Forced Proving Ground Tests of Trucks*, Mashinostroenie Publishing House, Moscow, Russia, 1984 (in Russian).

You, S.-S., Chai, Y.-H., Multi-objective control synthesis: An application to 4WS passenger vehicles, *Mechatronics*, No. 9, pp. 363–390, 1999.

Zakrevskij, A. D., Pottosin, Ju. V., Cheremisinova, L. D., *Logical Foundation of Discrete Devices Design*, Fizmatlit Publishing House, Moscow, Russia, 2007 (in Russian).

Zakrevskij, A. D., *Logical Synthesis of Cascade Circuits*, Nauka Publishing House, Moscow, Russia, 1981 (in Russian).

Zakrevskij, A. D., *Parallel Logical Control Algorithms*, 2nd edn., URSS Publishing House, Moscow, Russia, 2003 (in Russian).

Zaslavskiy, O. Ya., Structural and combinatory method of designing a driveline system for a multi-axle vehicle, *Avtomobil'naya Promishlennost'* (Automotive Industry), Moscow, Russia, No. 2, pp. 25–26, 1985 (in Russian).

Zaslavskiy, O. Ya., Evaluation of quality of technical decisions, *Avtomobil'naya Promishlennost'* (Automotive Industry), Moscow, Russia, No. 3, 1997 (in Russian).

Zaslavskiy, O. Ya., Ankinovich, G. G., Commercial automobile in the USA, *Avtomobil'naya Promish-lennost'* (Automotive Industry), Moscow, Russia, No. 1, 1998 (in Russian).

Zhukovsky, N. E., *Theory of a Device Designed by Dipl.-Eng. Romeiko-Gurko*, 1905. Also published in Prof. Zhukovsky's Complete Works, Vol. 8, Moscow, Russia, 1937 (in Russian).

Zimelev, G. V., *Theory of Automobile*, 2nd edn., Military Publishing House, Moscow, Russia, 1957 (in Russian).

Zomotor, A., Leiber, S., Neundorf, K., Richter, K. H., Buechle, K. H., Mercedec-Benz 4MATIC, an electronically controlled four-wheel drive system for improved active safety, SAE Paper No. 861371, Society of Automotive Engineers, Warrendale, PA, 1986.

Zyat'kov, N., Reliable unit—Reliable automobile, *Avtomobil'nij Transport* (Automobile Transport), No. 4, pp. 35–36, 1989 (in Russian).

Index

A

Advanced hybrid-hydraulic driveline system
  electronic control unit (ECU), 639
  Gidrohod-49061 vehicle, 630–631
  hydraulic drive efficiency, 633
  hydraulic-motor-pump drive, 630
  hydraulic motor shaft torque, 632
  hydraulic pump, 639
  hydrostatic full-flow drives (HD) advantages, 628–630
  hydrostatic power train advantages, 627–628
  kinematic and power coupling, 632
  schematic diagrams, 626–627
  version III vehicular HD, 633–634
  version IV vehicular HD, 634–635
  version V vehicular HD, 635–636
  version VI vehicular HD, 637–638
  version VII vehicular HD, 638–639
Articulated timber carriers
  energy loading factors, 191, 198
  estimated parameters, 191, 197
  Mercedes-Benz vehicles, 191
Articulated vehicles
  circumferential force, 490
  generalized slippage, 491
  lateral reactions, 489
  power-module driven vehicular train, 488
  two-mass model, 487–488
Audi-200 Turbo Quattro, 27

B

Bendix–Trakta joint, 14
Bendix–Weiss joint, 14
Benz automobile, 6
Bevel-gear differentials, tooth forces
  axial forces, pinion-side gear mesh
    angle α_k, 143–144
    angle υ_c, 144–145
    arm size determination, 142
    diameter, addendum circle, 143
    even tooth number, 144–145
    four-and two-pinion differential formula, 142
    mating bevel gear, 139–140
    MTZ 102 tractor, 145–146
    spur mating gears, 141
    straight-line segment, 144
  experimental results, 157, 159
  force evaluation
    coefficients, 155–156, 158
    MAZ 64277 interwheel differential, 157, 159
    two-pinion differentials, 154
  summation, axial forces, 160
  total axial forces
    determination, graphical approach, 151
    developed forms, gear sets, 146–147
    four groups, 146–147
    interwheel differentials, 147–148
    line segment, 147, 151
    MTZ 102 tractor, 148–151
    pinion, even tooth number, 152–153
    pinion, odd tooth number, 150, 152–153
    rear axle differential, 153–155
    T 150K tractor, 153, 156–157
    turn angles correlation, 148–149
Brunton's locomotive, 3
Bugatti-type53 machines, 15

C

Cam-plunger differentials
  cam sprockets, 413–414
  differential's kinematics, 413
  law of cosines, 416
  law of sines, 415
  locking coefficient, 417
  off-road trucks, 413
  plunger shape, 415
  shapes of cams, 414–415
  three-axle trucks, 417
Combined automated mechanical driveline systems
  interaxle power-dividing unit properties
    axles normal reactions distribution, 520–521, 524
    axle torque distribution, 522–523, 526–527
    geometric parameters, 519
    limited slip differentials, 529–530
    locking coefficients, 530
    maximum traction running gear efficiency, 521–522, 526
    total rolling resistance, 521, 524–525
    traction vehicle computational model, 519

interwheel power-dividing unit properties
circumferential forces, 512
digging force, 511
interwheel drives, 510
kinematics discrepancy factor, 518
loader parameters, 513–514
locking coefficient, 518
optimal energy and force characteristics, 515–516
optimal locking, 510
optimal torques distribution factor, 495, 513–514
pressure force, 511
running gear efficiency, 516–517
three-dimensional computational model, 510–511
traction-gripping performance, 512
unified limited slip differentials, 515–516
mathematical model
circumferential force, 532
computational model, 531
friction coefficient, 537
kinematic parameters, 532–533
micro-and macro-topographic features, 534
micro profiles, roads and terrain, 535
optimal distribution factors, 538
power train, 532
roads and terrain, macro-profiles, 536
rolling resistance, 536
second-order Lagrange equation, 533
statistical assessment methods, 539
third-order polynomial, 535
objective function analysis
Chudakov's analysis, 497
circumferential force, 499, 507–508
gear and slip efficiency, 498
implicit function, 507
Lagrange function, 501, 505
mathematical analysis, 496
nonlinear function, 498
power distribution control, 496
running gear efficiency and slip ratios, 507–509
slip coefficient, 499, 506
slip factors, 497
operational properties, 475
optimal properties
Bayes–Laplace criterion, 544
concrete highway and Belgian paved road, 540
engineering-economy efficiency, 553
flat and poor dry dirt road, 541, 544
locking coefficients, 545, 547, 549–550
meadow, level terrain, 542–543
optimal torque biases, 547–548
optimum locking coefficient, 552
optimum torque distribution factors, 546
rear and front tandem, 551
running gear efficiency, 539
snow-covered terrain, 542, 544
technical and economic evaluation, 553
steered wheels
Appel's equations, 475
chassis design, 485
circumferential force, 490
generalized slippage, 491
gripping force utilization factor, 481, 484–485
kinematic discrepancy, 486
KL database, 479–480
lateral reactions, 489
locked/engaged mechanism, 478
motion turnability and stability, 481
nonlinear theory, 478
power-module driven vehicular train, 488
quasi-velocities, 476
tandem axles, 483
two-mass model, 487–488
wheel slippage, 478–479
synthesis, optimal properties
distribution factors, 495
multiwheel drive vehicles, 492
optimal wheel power distribution, 493–494
statistical data analysis, 493
timber carrier characteristics, 492
transportation-traction vehicles, 495
turnability and stability criteria *vs.* constraints, 495
Cornering stiffness, 270
Cugnot's chariot, 1–2

D

Daimler car, 6
Diagonal driveline system, 55
Differential locking mode, 622–623
Disk differentials
cam lockers
bushing-spider friction couple, 396
disk clutches, 395
equilibrium equation, 392–393
free-body diagram, 392
friction clutches, 397
locking coefficient, 391, 394, 396
torque bias factor, 398

force fluctuations
axial forces, 437–439
bevel gear meshing, 436
cyclical sliding, 438
dampers, 442–443
extremal pressure, 440
friction torque, 441
locking coefficient, 436–437, 441
maximum and minimum pressure, 439
nonprecompressed plate springs, 442
premature wear and scuffing, 435
torque of friction clutches, 436
V-lockers
asymmetry factor, 403–404
axial forces, 400–401
balance equation, 405
equilibrium equation, 400
friction torques, 400–401
locking coefficient, 399–400, 405
nonperpendicularity, 403–404
nonuniformity, 402
quantitative assessment, 403
separate floating pinion pins, 399
side gears, 405
symmetrical locking properties, 402
torque bias factor, 401–402
total circumferential forces, 400, 402
without additional lockers
correction factor, 391
dimensionless geometric parameter, 387
dimensionless parameter, 388
free-body diagrams, 385–386
friction torque, 385, 387–388
locking coefficient, 385
locking factor, 389–390
primary friction, 390
static locking coefficient, 389
total circumferential force, 386
Driveline systems
axle, drive, wheel and steering formula
4×4 agricultural tractors, 35
all-wheel drive trucks, 48–49
definition, 35
farm and forestry tractors, 45
integrated mechatronic systems, 54
4×4 passenger cars, 53
passenger cars and SUVs, 52
power-module driven vehicular trains, 46
single-axle and multiaxle drive trucks, 47–48
Brunton's locomotive, 3
constant-velocity joints, 12–14
Cugnot's chariot, 1–2
design and vehicle performance
stability of motion, 110–112
system characteristics *vs.* vehicle properties, 103
traction and velocity properties, 103–106
turnability, 107–110
vehicle handling, 112–114
vehicle mobility, 106–107
vehicle properties *vs.* vehicle systems, 102
design principles
acceleration performance analysis, 116
general algorithm, 118
inverse dynamics, 115
power vectoring/power management, 117
diagonal driveline system, 55
differential transmissions
Benz automobile, 6
Daimler car, 6
La Manselle, 5
Panhard–Levassor automobile, 6
Renault automobile, 7
front-wheel drive (FWD) automobile, 7–8
Gordon's three-wheeled stagecoach, 3
Herney's steamer, 2
hybrid cars and all-wheel drive vehicles, 7
kinematic power train layout
K-710 tractor, 43
MTZ-82 tractor, 44
T-150K tractor, 43
12×12 vehicle, 51
mechanical four-wheel drives, 8–9
multiwheel drive trucks and passenger car
agricultural tractors, 24
Audi-200 Turbo Quattro, 27
Bugatti-type53 machines, 15
Ferguson clutches, 25
Ford GPV and GAZ-67, 17
KrAZ-260D, 10×10, 22
Kubelwagen, 17
Matra sports car, 26
MAZ-501, 18
MAZ-537, 12×12, 21
MAZ-7310, 8×8, 21
pail-car, 15–16
Semex-Tatra 4727OL pipe carrier, 19
statistical analysis, 21
T3 Rover, 16–17
truck mass parameters, 20
ZF A-95 transfer case, 26
Oructur Amphiblus, 3–4
part time interaxle system, 50
pneumatic tire invention
high-mobility tire treads, 12

Russo-Balt automobile, 10
snowmobile, 11
power dividing units
agricultural tractors, 32
in driving axles, 32
major types, 37
overrunning self-locking differentials, 30
symbols of mechanisms, 38
Tornton power lock self-locking differential, 30–31
viscous clutch, 28–29
power transfer units
elements for kinematic diagrams, 40–41
symbols of, 39
simple, combined, and integrated system, 39
steering system types, 36
6×6 vehicular train, 47
Driving tandems
high-mobility design, 232
6×4 highway tractor, 227–229
leakproof case, 232
lubricating rubbing surface, 230
oil flow, 227–228
tandem interaxle differential design, 231
temperature, 232

E

Energy efficiency
running gear, 92, 94, 95, 277, 336, 493
total, 73, 96, 258, 647, 648
traction, 57, 58, 73, 75, 76, 79, 80, 81, 85, 249, 257, 258, 338, 354, 493
transportation, 80, 81, 86, 90–94, 96, 101, 258, 259, 499
vehicle, 56–103, 249–264, 274, 277, 282, 301, 327, 329–355, 357, 370, 371, 373, 493, 496, 499, 507, 559, 681

F

Farm tractors
assessment criteria, 201–202
drawbar pull (traction load), 195–196
estimated parameters, 198–200
evaluation criteria, interwheel open differentials, 198, 201–202
rolling resistance factor, 196
total circumferential force, 196
Ferguson clutches, 25
Forced circulation systems, 203
Free-running differentials
applications
current production methods, 465
heavy-duty wheeled farm tractors, 464
interaxle drives, 464–465
interwheel free-running differential, 464
MAZ and ZIL automobiles, 466
reliability, 463
self-disengagement, 465
design and operating principles
assembled driving clutch, 455
centrifugal forces, 462
deceleration, 458–459
driven clutch half disengagement, 460
driving-clutch tooth, 463
inner clutch half disengagement, 458
kinematic coupling, 453
multi-pull differential, 455
NoSPIN differential, 455–456
power coupling, 453
radial apertures, 454
radial rectangular teeth, 453
rattle-like noise, 461
reactive forces, 459
second half-axle gear, 457
slit-spring lock ring, 454, 457, 461–462
Thornton-Tandem free-running differential, 455
traction mode, 456–457
Friction and gripping coefficients, 67, 68, 129, 142, 241, 264, 265, 282, 300, 382–384, 389, 402, 474, 483, 499, 537, 569, 570, 571, 606, 652, 654, 655, 658, 659, 661–667, 704
Front-steered wheels
angular velocity, 133–134, 138–139
center of gravity, 136–137
linear velocity, 133, 137
turn, vehicle, 133, 137
4×4 vehicles, 135
vehicle's longitudinal axis, 136–137
weight loads, 137
ω_{01} *vs.* ω_{02}, 135
Fuel supply reduction mode, 622–623
Full-flow driveline system, 626–627

G

Gear ratio concept
control principles
characteristics, interaxle differentials, 288
circumferential force, 275–276, 280
data analysis, 286

efficiency, 277–278
electrical signal, 285
generalized slippage, 278
gripping conditions, 274, 280
higher-rating truck design, 282–283
main frame, 285–286
normal loading factor, 275
optimal differential gear ratios, 283
planetary-type, 283–284
probabilistic properties, 282
slippage power losses, 278–279
static distribution, gross weight, 276
4×4 tractor, 281, 285–287
values calculation, 276–277
velocity, 278–279
weight loads adjustment, 285
kinematics and dynamics
angular velocity, 122–123, 130–131
bevel-gear and spur-gear differentials, 119–120
circumferential forces, 127–129
compliance, 130–131
definition, 121
driving wheels, 123
dynamic diagrams, 130
moments of inertia, 130–131
pinion *vs.* steering angle, 125–126
planetary-gear set characteristics, 122
power-dividing unit, 119–120
power transmission, link, 121
rear wheel drive vehicle, 124
torques, 127, 131
truck's differential, 132
turn angle, 121
two-axle tandem, 126–127
velocity ratios, 122, 131
Gordon's three-wheeled stagecoach, 3

H

Herney's steamer, 2
Highway heavy-duty trucks
average operating speed, 189–190
circumferential force and power, 190
energy loading factors, 191, 195
estimated parameters, 191–193
evaluation criteria, interwheel open differentials, 191, 194
hypothetical velocity, 190
linear sliding velocities, 191, 196
mileage wear factor, 190–191, 195
pinions and spider pins, 191, 196
Hooke's double joint, 14
Hydraulic-mechanical driveline (HMD) system, 626–627
Hydraulic resistance, 432–435
Hydraulic unit design selection
axial-plunger pumps, 639–640
duplex axial-plunger hydraulic machine, 641
dynamic factor, 642
maximum and minimum working volume, 643
maximum design torque, 642
maximum flow rate, 644–645

I

Integrated mechatronic systems, 54
Interaxle power-dividing unit properties
axles normal reactions distribution, 520–521, 524
axle torque distribution, 522–523, 526–527
geometric parameters, 519
limited slip differentials, 529–530
locking coefficients, 530
maximum traction running gear efficiency, 521–522, 526
total rolling resistance, 521, 524–525
traction vehicle computational model, 519
International Society for Terrain-Vehicle Systems (ISTVS), 34
Interwheel and interaxle differentials
bevel-gear differentials, tooth forces
axial forces, pinion-side gear mesh, 139–146
experimental results, 157, 159
force evaluation, 153–157
summation, axial forces, 160
total axial forces, 146–153
control principles, gear ratios
characteristics, interaxle differentials, 288
circumferential force, 275–276, 280
data analysis, 286
efficiency, 277–278
electrical signal, 285
generalized slippage, 278
gripping conditions, 274, 280
higher-rating truck design, 282–283
main frame, 285–286
normal loading factor, 275
optimal differential gear ratios, 283
planetary-type, 283–284
probabilistic properties, 282
slippage power losses, 278–279
static distribution, gross weight, 276

4×4 tractor, 281, 285–287
values calculation, 276–277
velocity, 278–279
weight loads adjustment, 285
differential geometry
accumulated-mileage wear factor, 222
angular and linear velocity, 188
articulated timber carriers, 191, 194, 196
circumferential force and pressure, 189
conditional cross-sectional area, 186–187
energy-loading factor, 186, 219, 226
evaluation criteria, 222
farm tractors, 195–196, 198–202
friction work, 187
geometric parameters, 219, 221
highway heavy-duty trains MAZ, 219–220
highway heavy-duty trucks, 189–191
KamAZ differential, 224
load forces, 186
Mercedes-Benz differentials, 225
mileage wear factor, 187
thrust washer, axial force and pressure, 189
6×4 timber-carrier tractor, 223, 225
6×6 timber-carrier tractor, 223–224, 226
vehicle velocity, 187
front-steered wheels
angular velocity, 133–134
center of gravity, 136–137
linear velocity, 133
turning vehicle, 133
4×4 vehicles, 135
vehicle's longitudinal axis, 136–137
weight loads, 137
ω_{01} *vs.* ω_{02}, 135
gear-ratio concept, kinematics and dynamics
angular velocity, 122–123, 130–131
bevel-gear and spur-gear differentials, 119–120
circumferential forces, 127–129
compliance, 130–131
definition, 121
driving wheels, 123
dynamic diagrams, 130
moments of inertia, 130–131
pinion *vs.* steering angle, 125–126
planetary-gear set characteristics, 122
power-dividing unit, 119–120
power transmission, link, 121
rear wheel drive vehicle, 124
torques, 127, 131
truck's differential, 132
turn angle, 121
two-axle tandem, 126–127
velocity ratios, 122, 131
general engineering issues and solutions
bearings pretensioning, 177
bevel-gear differential, 214–216
cantilevered and three-support shafts, 217
cantilevered placement, final drive pinion, 171–172
4×4 car, 217–218
central reduction gear, driving axle, 176
component design, 169
component durability, 178–179
contact patch location, 177
corrosion, 179
design manufacturability, 179
differential housing, 183
double planetary transmission, 185
drive-gear unit with bearings, 177–178
driven-gear fastening bolts, 173
drive sheave location, shaft, 169–170
driving axles design, 171
fastening methods, 172–173
final drive gear fastening nuts, 174
final-drive wheel fastening, 180–181
free-running mechanisms, 216–217
gripping device, 178
helical gears design, 175–176
hub design, wheel's drum, 169–170
hypoid final drive design, 177
hypoid-gear final drive, 215
open spur-gear differential, 183–184
oval nut, 174
principal and control elements, 210
rolled-up bronze bushing, 182
roller bearing, 182
shaft design, key slots, 179–180
spring support bracket design, 174–175
spur-gear interwheel differential, truck, 183–184
strength and stiffness, 169
structural limitations, 180–181
symmetrical spur-gear differential, 216
three-link planetary mechanism, 213
4×4 timber truck, 210, 212
torque, 218–219
transfer case design, 211, 213
transfer case kinematic layouts, 210–212, 214
locking devices design
cam-type clutch engagement, 242–243
clutches layouts, 243–244
engagement angle, 243
engagement force, 245

frictional pairs, 248
geometry, 246–248
hydraulic locking cam clutch differential, 248–249
jaw-type (cam-type) locking clutches, 240–241
locking differentials layout, 238–239
pin clutch, 240, 242
probability, 244–245
rectangular and trapezoidal cams, 240, 242
second type, 240, 242
torques, 239–240
oil lubrication systems
automobile axle, final drive, 203–204
classification, 203
driving tandems, 227–232
heavy-duty truck, 205–207
pumping bearing, 206
round and flat scoops, 208–209
slots shape and location, thrust washer, 208
splash oiling, rubbing surface, 203
transfer cases, 233–238
truck differential, 203–205
rear-and front-steered wheels
angular velocities, 138–139
linear velocities, 137
turn, vehicle, 137
robustness
axial shift, 166
cracks, 162
error factors, 165–166
fatigue and abrasive pitting, 162
fretting corrosion, 164
galling, 161, 164
highway heavy-duty trucks, 168
hole ellipticity, housing, 166
inverse friction pair, 163
lubricant circulation, 163–164
nonuniform distribution, 164
pinion axes, errors Δ_1 and Δ_2, 165
profound analysis, 167
rubbing elements, 163–164
sealing collar—differential-housing shaft pair, 163
side play, 165
spherical and flat pinion washer, 167
spider—housing contact, 164
typical breakdowns, 161
uniform distribution, 165
wear resistance, 162
wheel power distribution
angular velocity, 251, 261, 263
circumferential forces, 256–257
driving axle, 249–250
efficiency, 257
generalized rolling radius, 251, 253
generalized slippage, 251, 254, 263–264
linear velocity, 250–251
multiwheel drive vehicles, 254–255, 258–259
power supply, 257
slip efficiency, 4×4 truck, 260–261
theoretical velocity, 250
time force, 250
4-ton farm tractor, 258, 260
transportation efficiency, running gear, 258, 260–261
turnability and stability of motion, 268–274
two axles, turn, 262
4×4 vehicle, asymmetrical interaxle differential, 252
vehicle tractive and velocity properties, 264–268
wheel torques, 250
Interwheel power-dividing unit properties
circumferential forces, 512
digging force, 511
interwheel drives, 510
kinematic discrepancy factor, 518
loader parameters, 513–514
locking coefficient, 518
optimal energy and force characteristics, 515–516
optimal locking, 510
optimal torques distribution factor, 495, 513–514
pressure force, 511
running gear efficiency, 516–517
three-dimensional computational model, 510–511
traction-gripping performance, 512
unified limited slip differentials, 515–516
Inverse vehicle dynamics, 118, 532,

K

Kinematic discrepancy and generalized vehicle parameters
2m×2n wheel formula
articulated vehicles, 306
curvilinear motion, 309–312
interwheel positive engagement, 317–318
rectilinear motion, 306–309
steered wheels, 312–317
theoretical velocity, 30
4×4 wheel formula

equivalent layout, 301–302
gear ratios, 303
kinematic agreement, 303–304
kinematic consistency, 301
rolling radii, 304
transforming expression, 305
wheel-hub gear set, 302–303
wheel travel paths, 301
Kinematic power train layout
K-710 tractor, 43
MTZ-82 tractor, 44
T-150K tractor, 43
12×12 vehicle, 51
Kinematics and dynamics, mechanical subsystem
double differentials
angular velocity, 582, 587
bevel-gear and spur-gear differentials, 580
brake side gear, 582
braking power, 585
braking torque, 587
circumferential force, 586
double pinion equilibrium, 584
gear ratio, 583
linear velocity, 581
power recuperation, 586
principal axis of rotation, 580
steering system, 581
torque balance, 583–584
torque equilibrium equation, 584
velocity polygon, 581
open differential
axle turning radius, 578
circumferential force, 579
differential locking algorithm, 578
force analysis, 579
rear-driving axle, 577–578
slipping wheel braking algorithm, 578
traction and stability control system, 577
yaw moment, 579–580
single-row planetary mechanism, mating pinions
angular velocity, 593
coupling torque, 596
friction torque, 593–594
gear ratio, 591
kinematic coupling equation, 592
limited-slip differential, 595
step-up and step-down transmission, 591
step-up coupling c2, 592
three-link planetary rows (TPM)
angular velocity, 588
dry asphalt road, 591
energy loss, 590
friction elements, 589
kinematic coupling equation, 588
symmetrical bevel-gear differential, 587
symmetrical differential design parameter, 589
torque balance equation, 589

L

La Manselle, 5
Limited slip differentials
asymmetrical interaxle differentials
bevel-gear interaxle differential, 448
friction torque, 450
locking performance curve, 451–452
locking properties, 448, 450
stepped performance curve, 451
4×4 timber-carrier truck, 451
torque bias factor, 449
tractive efficiency, 452
cam-plunger differentials
cam sprockets, 413–414
differential's kinematics, 413
law of cosines, 416
law of sines, 415
locking coefficient, 417
off-road trucks, 413
plunger shape, 415
shapes of cams, 414–415
three-axle trucks, 417
disk differentials
cam lockers, 391–398
force fluctuations, 435–443
V-lockers, 399–405
without additional lockers, 385–391
geometrical parameters, 382, 387, 389, 393, 419, 420, 427, 490, 658
speed sensitive differentials
locking coefficient, 433–434
plunger-type rotary pump, 432
pressure difference, 433
pump capacity, 433
pump's resistance torque, 434
pump's working volume, 435
relative angular velocity, 434
torque bias, 33, 401, 402, 411, 417, 437, 449, 478, 508, 510, 514–516, 529, 649
torque biasing and locking performance
braking torque, 379
constant and variable locking coefficient, 385
efficiency, 380–381
gripping factor, 384

internal friction torque, 381
locking coefficient, 381–382
probability, 384–385
reduction gear, 379–380
relative angular velocity, 380
relative friction torque, 382
sliding (dynamic) friction coefficient, 384
static friction coefficient, 383–384
static locking coefficient, 383
torque sensitive differentials
bevel-gear meshing, 430
constant friction torque, 423–425
cylindrical springs, 427
disk-type friction clutches, 418–419
geometric parameters, 419–420
interwheel limited slip differential, 427, 430
locking properties, 427, 431–432
maximum friction torque, 419
mixed-type differential, 425–426
mode of motion, 421
plate-type springs, 427
principal operation mode, 421–422
road-gripping condition, 423
spring forces, 425
spur-gear couple, 424
tractive and velocity properties, 422
unified limited slip differentials, 427–429
vehicle's turnability, 425
tractive performance and drive axle yaw moment
bevel-gear differential, 443
friction moment, 447–448
gripping condition, 444–445
maximum circumferential force, 444
positive engagement, 446
resistance moment, 446–447
slippage efficiency, 445
slippage power loss, 446
uniform rectilinear motion, 443
worm-gear differentials
efficiency, 408, 410
equilibrium equation, 408–410
friction forces, 407
friction losses, 411
friction torque, 409–410
gear ratio, 412–413
helical-gear differential, 405, 411–412
Locking devices design
cam-type clutch engagement, 242–243
clutches layouts, 243–244
engagement angle, 243
engagement force, 245
frictional pairs, 248
geometry, 246–248
hydraulic locking cam clutch differential, 248–249
jaw-type (cam-type) locking clutches, 240–241
locking differentials layout, 238–239
pin clutch, 240, 242
probability, 244–245
rectangular and trapezoidal cams, 240, 242
second type, 240, 242
torques, 239–240
Longitudinal elasticity and stiffness, 67, 364

M

Matra sports car, 26
Mechanical power losses
driveline systems
front and rear axle, 340
generalized slippage, 340
parasitic power circulation mode, 341
rolling resistance factor, 341
second-order infinitesimals, 340–341
total circumferential force, 341
traction load, 342
fuel consumption
actual velocity, 345
braking power, 343
energy efficiency, 351–352
equivalent computational model, 343
linear velocity, 344
mechanical efficiency, 346
multiwheel drive vehicles, 352–353
negative and positive kinematic discrepancy, 349
overrunning clutch, 354–355
payload-conveying vehicle, 352
poser losses *vs.* generalized slippage, 348
poser losses *vs.* tractive load, 347–348
slippage efficiency, 344
slippage power, 345–346
sowing-ready field, 350
3.7-ton and 5.6-ton tractor, 350–351
towing mode, 4×4 truck, 347
traction efficiency, 352, 354
transportation efficiency, 352
wheel systems
automatic engagement/disengagement, 334
drawbar pull *vs.* kinematic discrepancy, 336
energy efficiency, 334, 336
generalized slippages, 331
gripping conditions, 332–333
interaxle drive, 335

linear acceleration, 336
longitudinal deformation, 330
longitudinal stiffness factor, 333
multiwheel drive vehicles, 338–339
parasitic power circulation, 333
positive engagement, 335–336
rear-axle engagement clutch, 336–337
slippage efficiency, 333, 338
4×4 SUV, 337
total mass, 4×4 truck, 331
traction and transportation efficiency, 338
Mechatronic driveline systems
acceleration-slip-regulation (ASR), 558
electromechanical and electronic device, 555
force and kinematic parameter, 559
hybrid driveline systems
axial-plunger pumps, 639–640
duplex axial-plunger hydraulic machine, 641
dynamic factor, 642
electronic control unit (ECU), 639
Gidrohod-49061 vehicle, 630–631
hydraulic drive efficiency, 633
hydraulic-motor-pump drive, 630
hydraulic motor shaft torque, 632
hydraulic pump, 639
hydrostatic full-flow drives (HD) advantages, 628–630
hydrostatic power train advantages, 627–628
kinematic and power coupling, 632
maximum and minimum working volume, 643
maximum design torque, 642
maximum flow rate, 644–645
schematic diagrams, 626–627
version III vehicular HD, 633–634
version IV vehicular HD, 634–635
version V vehicular HD, 635–636
version VI vehicular HD, 637–638
version VII vehicular HD, 638–639
hybrid drives, 560
integrated driveline system design
analytical results, 619
automatic control implementation, 623
braking mechanism, 612, 620
braking mode, 622–623
circumferential force and slippage, 609–610
conditional circumferential force, 611
control algorithm implementation circuit, 624–626
deforming surface time segment, 620
differential locking control algorithm, 617
differential locking mode, 622–623
energy intensity factor, 612
fuel supply reduction mode, 622–623
Lagrange multiplier, 607
locking mechanism, 614
logical control languages, 620–621
macro-and micro-topographic features, 606
manual control and sensor signal processing mode, 622–623
optimum circumferential force, 618
optimum torque distribution coefficient, 609
optimum wheel torque distribution factor, 614
pertinent logical and Boolean variable, 621
power and kinematic parameter, 610
probabilistic function, 609
rectilinear accelerated motion, 606–607
rolling resistance factor, 608
running gear efficiency, 607
slippage ratio, 615
specific friction work, 616
sprung and unsprung mass, 608
traction control, 605, 613, 615
tractor wheel slippage, 613
triggers and Boolean variables, 623
12-wheel heavy-duty highway vehicular train, 605–606
inverse wheel dynamics and control
acceleration loop, 565
angular acceleration, 564
angular velocity, 562
closed-loop system, 566
force and kinematic parameter control, 560
kinematic law of variation, 564
linear and angular velocity control, 563
mathematical treatment, 561
nonlinear function, 563
rigid wheel cycloid, 561
slip power, 563
torque *vs.* rolling radius, 562
tracking control loop, 565
transient process, 566–568
uncertain mathematical analytical function, 565
wheel angular velocity control algorithm, 568
wheel power balance equation, 560
kinematics and dynamics, mechanical subsystem
asymmetrical differentials, 576–577
automotive differentials, 576

differential turning mechanism, 574
double differentials, 580–587
engine torque, 574
open differential, 577–580
planetary gear drives, 575
planetary transmission design parameter, 575
single-row planetary mechanism, mating pinions, 591–596
three-link planetary rows (TPM), 587–591
three-link planetary transmission, 575
4MATIC system, 556–557
proactive assessment, terrain condition
Chudakov's linear equation, 571
current friction factors-slip ratio, 569
longitudinal elasticity factor, 571
measured slippage *vs.* rolling resistance factor, 568
peak friction (gripping) coefficient determination, 569
piecewise-linear approximation, 572
specifications, 570
time delay, 573
torque, 572–573
tractive/brake force slope determination, 569
simple and combined driveline system design
circumferential force, 598, 604
generalized slippage, 598–599
interaxle and interwheel drives, 596
lateral acceleration, 603
locking control system, 599
locking/unlocking differential modes, 603
logical Boolean variable, 604–605
optimal torque distribution factor, 600
probability function, 599
programmable logic device, 596
rapid prototyping, 597
running gear system efficiency, 601–602
slippage, 602
torque distribution factor, 597
wheel slippage, 598
slippage determination, 557
torque vectoring and management, 556
traction control (TC) system, 558
yaw rate, 559
Multiwheel drive trucks and passenger car
agricultural tractors, 24
Audi-200 Turbo Quattro, 27
Bugatti-type53 machines, 15
Ferguson clutches, 25
Ford GPV and GAZ-67, 17
KrAZ-260D, 10×10, 22
Kubelwagen, 17
Matra sports car, 26
MAZ-501, 18
MAZ-537, 12×12, 21
MAZ-7310, 8×8, 21
pail-car, 15–16
Semex-Tatra 4727OL pipe carrier, 19
statistical analysis, 21
T3 Rover, 16–17
truck mass parameters, 20
ZF A-95 transfer case, 26
Multiwheel drive vehicle testing
differential friction clutches
friction torque, 663–665
second-power polynomial, 666
sliding friction coefficient, 662–663, 665–667
wear-resistant material, 667
differential locking performance
alloy steel, 652
asymmetry factor, 660
balancing-braking device, 649–650
braking torque, 651
Cardan shaft, 650
dynamic friction coefficient, 658
friction disk sets, 653–654
interaxle cam-plunger differential, 661–662
internal force determination, 649
limited slip differential torque, 651–652
locking coefficients, 652, 655, 657, 661
locking-factor ratio, 655
open-type multipurpose stand, 649–650
parameters, 653
sensor-equipped pinion pin, 653–654
sliding rate, 657
sliding velocity, 658
stability, 659–661
static friction coefficient, 658–659
torque and axial force, 654–655
differential lubrication system
AU oil flow rate, 672
discharge port, 678
drive driven gear, 672
drive tandem, 678
electric motor shaft, 669
elements, 677
heavy-duty highway vehicular train, 668
interwheel differential, 668–670
lubricating oil, 673
MT-16P oil, 671

oil conduit production, 676
oil flow capacity, 678
oil flow rate, 670
oil temperature, 675
oil trap and collection, 677
operation, 670–671
plugged-up discharge port, 676
quantitative estimation, 678
reduction gear search, 676
TSp-15K oil flow rate, 673–675
vehicle chassis dynamometer, individual roll control
experiment procedure, 686
linear function analysis, 689
longitudinal elasticity coefficient, 689
main and auxiliary screen, 682–683
medium-class SUV, 685–686
Mustang dynamometer, 680
parameter computation, 687–688
power distribution, 681
power dividing unit (PDU), 679
probabilistic rolling resistance force, 684
random load value generation, 684
regression coefficient, 688
resistance torque and velocity, 684–685
test modes, 682–683
tire experiment factors, 689
torque and angular velocity, 680
turnability and stability, 682
4×4 vehicle specification, 682
4×2 vehicle stand, 679
wheel force sensor, 686
wheeled vehicles, field and road test
air pressure effects, 695–696
circumferential force, 698
disk-type locking clutch, 703
drive-axle wheels, 706
free-running differentials, 699–700, 708
front-axle wheel, 706
front-wheel slippage, 700
interaxle drive, 697
kinematic discrepancy factor, 693
location determination, 691
maximum engine torque, 708
minimum turning radii, 702
mobility and service life testing, 690–691
μ-split condition, 703
4×4 off-road truck, 698
parameter measurement, 691
power distribution, 692
rear-axle differential modes, 702
rear axle, open differential, 704–705
4×2 RWD truck, 706
sliding friction coefficient, 704
solid-pavement road, 709
specific drawbar fuel consumption, 693–695
static radii determination, 692
statistical characteristics, 701, 703
steered drive axle, 707–708
total torque, 705
traction torque, 709
4×4 tractor specification, 693
turnability, 697
types, 690
wheel slippage, 696–697
worm-gear differentials, 699, 707

O

Objective function analysis
Chudakov's analysis, 497
circumferential force, 499, 507–508
gear and slip efficiency, 498
implicit function, 507
Lagrange function, 501, 505
mathematical analysis, 496
nonlinear function, 498
power distribution control, 496
running gear efficiency and slip ratios, 507–509
slip coefficient, 499, 506
slip factors, 497
Oil lubrication systems
automobile axle, final drive, 203–204
classification, 203
driving tandems, 227–232
heavy-duty truck, 205–207
pumping bearing, 206
round and flat scoops, 208–209
slots shape and location, thrust washer, 208
splash oiling, rubbing surface, 203
transfer cases, 233–238
truck differential, 203–205
Oructur Amphiblus, 3–4

P

Panhard–Levassor automobile, 6
Parallel control algorithm
logical control algorithm
automatic control implementation, 623
braking mode, 622–623
implementation circuit, 624

manual control and sensor signal processing mode, 622–623
pertinent logical and Boolean variable, 621
triggers and Boolean variables, 623
logical control languages, 620–621
Power-dividing units
designs
actual friction coefficient, 300
angular velocities, 289
automatic clutch, 295–296
axle engagement, 294
controlled clutch, 298
disconnect devices and systems, 292
double free-running clutch, 292, 294
drag torque, 294
electromagnetic solenoid, 297
free-running clutch, 292–293
free-wheel clutch, 291
friction torque, 295
gear-type clutch, 292
hydraulic clutch, 297
interaxle drive of tandem, 289–290
kinematic layouts, 291–292
oil-filled housing, 299
on-demand systems, 295–297
plane-parallel transfer, 300
power transfer unit, 297–298
roller-type clutch, 292, 294
mechanical power losses
driveline systems, 338–343
fuel consumption, 343–355
wheel systems, 330–338
$2m \times 2n$ vehicles
force intensity, 330
generalized rolling radii, 329
generalized slippage, 326, 329
positive circumferential forces, 328
positive engagement, 327–328
6×6 power-module driven vehicular train, 327–328
principal equation, 329
theoretical axle velocities, 327
$2m \times 2n$ wheel formula
articulated vehicles, 306
curvilinear motion, 309–312
interwheel positive engagement, 317–318
rectilinear motion, 306–309
steered wheels, 312–317
optimal and reasonable kinematic discrepancy
automatic and manual modes, 373–374
automatic engagement/disengagement, 368, 373
axle weight load changes, 369
circumferential forces, 371–372
front axle engagement mode, 374
gear ratios, 376–377
inflation pressure changes, 369–370
manufacturing tolerance, 370–371
operational-manufacturing discrepancy, 368, 370
outer-diameter tolerance, 371
overrunning clutch, 372–373
parasitic power circulation, 376
ratio of angular velocities, 318
4×4 vehicles
generalized slippage, 319–320, 324
graphical interpretation, 323–324
kinematic inconsistency, 320
locked interaxle differentials, 319
longitudinal stiffness coefficient, 324
mechanical power losses, 322
negative slippages, 321
on-demand systems, 325
overrunning clutch, 323–325
parasitic power circulation, 321–322
torque distribution factor, 325
traction dynamics, 319
vehicle complex models, 326
vehicle tractive and velocity operational properties
overrunning clutch, 357
slippage efficiency, 355
total circumferential force, 356
traction load, 358
vehicle velocity variation factor, 356
vehicle turnability and motion stability
circumferential forces, 359–361
computational model, 358
gripping conditions, 361
interwheel and interaxle differentials, 367
interwheel powerdividing unit, 365
mathematical multi-body models, 368
positively engaged interaxle drive, 364–365
tire slippage, 362
5.6-ton tractor, loop-less turn, 367
total moment of resistance, 362
turning radius variation factor, 362–363, 366
turning resistance moment, 364
4×4 wheel formula
equivalent layout, 301–302
gear ratios, 303
kinematic agreement, 303–304
kinematic consistency, 301

rolling radii, 304
transforming expression, 305
wheel-hub gear set, 302–303
wheel travel paths, 301
Power dividing units (PDU)
agricultural tractors, 32
driving axles, 32
major types, 37
overrunning self-locking differentials, 30
symbols of mechanisms, 38
Tornton power lock self-locking differential, 30–31
viscous clutch, 28–29
Power transfer units (PTU)
elements for kinematic diagrams, 40–41
symbols of, 39
PRALU language, 621
Programmable logical matrix (PLM), 624

R

Renault automobile, 7
Rolling resistance power loss, 101, 278, 347
Russo-Balt automobile, 10
Rzeppa's joint, 14

S

Slip power loss, 71, 74, 100, 101, 274, 331, 332, 334, 348
Snowmobile, 11
Speed sensitive differentials
locking coefficient, 433–434
plunger-type rotary pump, 432
pressure difference, 433
pump capacity, 433
pump's resistance torque, 434
pump's working volume, 435
relative angular velocity, 434
Statistical assessments
concrete highway and Belgian paved road, 540
flat and poor dry dirt road, 541, 544
meadow on level terrain, 542–543
snow-covered terrain, 542, 544
Steered wheels
Appel's equations, 475
chassis design, 485
circumferential force, 490
generalized slippage, 491
gripping force utilization factor, 481, 484–485
kinematic discrepancy, 486
KL database, 479–480
lateral reactions, 489
locked/engaged mechanism, 478
motion turnability and stability, 481
nonlinear theory, 478
power-module driven vehicular train, 488
quasi-velocities, 476
tandem axles, 483
two-mass model, 487–488
wheel slippage, 478–479
Steering system types, 36

T

Torque sensitive differentials
bevel-gear meshing, 430
constant friction torque, 423–425
cylindrical springs, 427
disk-type friction clutches, 418–419
geometric parameters, 419–420
interwheel limited slip differential, 427, 430
locking properties, 427, 431–432
maximum friction torque, 419
mixed-type differential, 425–426
mode of motion, 421
plate-type springs, 427
principal operation mode, 421–422
road-gripping condition, 423
spring forces, 425
spur-gear couple, 424
tractive and velocity properties, 422
unified limited slip differentials, 427–429
vehicle's turnability, 425
Torque transmission, 471–474
Trakta vehicle, 13
Transfer cases, lubrication systems
angles, 238
combined systems, 233
critical angular velocity, 238
critical rpm, 238–239
improved gear pump, 234–235
internally coupled gear pump, 234
journal cross pins, brinelling, 238
linear motion, 236–237
multifunction wheeled vehicle chassis, 235–236
multiwheel drive vehicle, 233–234
power takeoff, 236–237
splined telescope joint, 236–237
yokes, driveshaft, 237–238
T3 Rover, 16–17

V

Vehicle chassis dynamometer, individual roll control
  experiment procedure, 686
  individual roll control, 681
  linear function analysis, 689
  longitudinal elasticity coefficient, 689
  main and auxiliary screen, 682–683
  medium-class SUV, 685–686
  Mustang dynamometer, 680
  parameter computation, 687–688
  power distribution, 681
  power dividing unit (PDU), 679
  probabilistic rolling resistance force, 684
  random load value generation, 684
  regression coefficient, 688
  resistance torque and velocity, 684–685
  test modes, 682–683
  tire experiment factors, 689
  torque and angular velocity, 680
  turnability and stability, 682
  4×4 vehicle specification, 682
  4×2 vehicle stand, 679
  wheel force sensor, 686
Vehicle energy/fuel efficiency
  mechanical power losses, driveline systems, 82–86
  modes of vehicle operation, 80
  multiwheel drive vehicles, 96–101
  vehicle power balance, 81
  wheel systems, mechanical power losses
    combined operating mode, 94–96
    tractive operating mode, 86–90
    transportation operating mode, 90–94
Vehicle properties
  traction and velocity properties, 103–106
  turnability, 107–110
  vehicle handling, 112–114
  vehicle mobility, 106–107
  vs. system characteristics, 103
  vs. vehicle systems, 102
Viscous clutches, 28–29, 466–474
  classical fluid dynamics, 474
  disk surfaces, 472
  equalization, 470
  hump mode, 473–474
  lower clutch filling factor, 473
  lower limiting, 468
  non-Newtonian fluids, 466–467
  normal stress, 470
  organosilicon—polymethylsiloxane fluid, 466
  shear stress, 468
  test-stand curve, 469
  thixotropy, 469
  trouble-free operation, 472

W

Weight
  adhesive, 23, 264, 265, 276, 384, 444
  curb, 19, 72, 91, 101, 278, 282, 691
  gross, 28, 219, 260, 275, 276, 282, 435
Wheel dynamics and energy efficiency
  kinematic and force factors
    effective rolling radius and slip ratio, 61–66
    under sideslip, 77–79
    wheel force and torque factors, 66–70
  longitudinal and lateral force interaction, 75–77
  power and force balance
    nonsteady planar motion, 74
    power-consuming system, 70
    tractive efficiency, 72
    transportation efficiency, 73
  power-loading modes
    axle with NoSPIN, 60
    bicycle model, 4×4 vehicle, 59
    driven rolling mode, 56
    driving mode, 57
    free-body diagrams, front and rear wheels, 58
    free mode, 56
    front and rear torques, 59
    neutral mode, 56
    torque–net tractive force diagram, 58
Wheel power distributions
  mechanical power losses
    driveline systems, 338–343
    fuel consumption, 343–355
    wheel systems, 330–338
  turnability and stability of motion
    axle's lateral slip resistance factor, 270
    circumferential force, 273
    driving axle, right turn, 268
    force couple, 269
    FWD truck, 271–272
    interaxle drive effect, 270
    lateral force, front wheels, 270
    RWD vehicle, 268–269, 271
    4×4 vehicle, 270–271, 274
    weight distribution factor, 272
    yaw moment, road, 268

vehicle parameters and energy/fuel efficiency
  angular velocity, 251, 261, 263
  circumferential forces, 256–257
  driving axle, 249–250
  efficiency, 257
  generalized rolling radius, 251, 253
  generalized slippage, 251, 254, 263–264
  linear velocity, 250–251
  multiwheel drive vehicles, 254–255, 258–259
  power supply, 257
  slip efficiency, 4×4 truck, 260–261
  theoretical velocity, 250
  time force, 250
  4-ton farm tractor, 258, 260
  transportation efficiency, running gear, 258, 260–261
  two axles, turn, 262
  4×4 vehicle, asymmetrical interaxle differential, 252
  wheel torques, 250
vehicle tractive and velocity properties
  adhesive weight redistribution, 265
  circumferential force, 265–266
  6×6 farm tractor, 265–267
  generalized slippage, 267
  maximum traction torque, 264–265
  overrunning clutch, 357
  slippage efficiency, 355
  total circumferential force, 356
  traction load, 358
  vehicle velocity variation factor, 356
vehicle turnability and motion stability
  circumferential forces, 359–361
  computational model, 358
  gripping conditions, 361
  interwheel and interaxle differentials, 367
  interwheel powerdividing unit, 365
  mathematical multi-body models, 368
  positively engaged interaxle drive, 364–365
  tire slippage, 362
  5.6-ton tractor, loop-less turn, 367
  total moment of resistance, 362
  turning radius variation factor, 362–363, 366
  turning resistance moment, 364
Wheel slips and circumferential wheel forces
  $2m \times 2n$ vehicles
    force intensity, 330
    generalized rolling radii, 329
    generalized slippage, 326, 329
    positive circumferential forces, 328
    positive engagement, 327–328
    6×6 power-module driven vehicular train, 327–328
    principal equation, 329
    theoretical axle velocities, 327
  ratio of angular velocities, 318
  4×4 vehicles
    generalized slippage, 319–320, 324
    graphical interpretation, 323–324
    kinematic inconsistency, 320
    locked interaxle differentials, 319
    longitudinal stiffness coefficient, 324
    mechanical power losses, 322
    negative slippages, 321
    on-demand systems, 325
    overrunning clutch, 323–325
    parasitic power circulation, 321–322
    torque distribution factor, 325
    traction dynamics, 319
    vehicle complex models, 326
Woodruf key slots, 179–180
Worm-gear differentials
  efficiency, 408, 410
  equilibrium equation, 408–410
  friction forces, 407
  friction losses, 411
  friction torque, 409–410
  gear ratio, 412–413
  helical-gear differential, 405, 411–412

MECHANICAL ENGINEERING

Ground Vehicle Engineering Series

Driveline Systems of Ground Vehicles

Theory and Design

"With this book, Prof. Dr. Vantsevich and his coauthors bring a tremendous contribution to the field of Automotive Transmission and Driveline Engineering, including his innovative methods for optimum driveline synthesis, as well as his experience with the development of various hardware solutions, from the basic limited slip differentials to the most sophisticated mechatronic systems."

—Dr.-Ing. Mircea Gradu
Director, Transmission and Driveline Engineering
Head, Virtual Analysis Tools
Chrysler Group LLC

Now that vehicles with four and more driving wheels are firmly ensconced in the consumer market, they must provide energy/fuel-saving benefits and improved operational quality including terrain mobility, traction and velocity properties, turnability, and stability of motion. A first-of-its-kind resource, ***Driveline Systems of Ground Vehicles: Theory and Design*** presents a comprehensive and analytical treatment of driveline research, design, and tests based on energy efficiency, vehicle dynamics, and operational properties requirements.

This volume addresses fundamental engineering problems including how to investigate the effect of different driveline systems on the properties of vehicles and how to determined the optimal characteristics of the driveline system and its power-dividing units (PDUs) and design it for a specific vehicle to ensure high levels of vehicle dynamics, energy efficiency, and performance. The authors develop an analytical apparatus for math modeling of driveline systems that can be compiled from different types of PDUs. They also introduce methodologies for the synthesis of optimal characteristics of PDUs for different types of vehicles.

Structured to be useful to engineers of all levels of experience, university professors and graduate students, the book is based on the R&D projects conducted by the authors. It explores intriguing engineering dilemmas such as how to achieve higher energy and fuel efficiency by driving either all the wheels or not all the wheels, solve oversteering issues by managing wheel power distribution, and many other technical problems.

K10894

CRC Press
Taylor & Francis Group
an Informa business
www.crcpress.com

6000 Broken Sound Parkway, NW
Suite 300, Boca Raton, FL 33487
270 Madison Avenue
New York, NY 10016
2 Park Square, Milton Park
Abingdon, Oxon OX14 4RN, UK

ISBN: 978-1-4398-1727-8
90000
9 781439 817278